

RIKEN Accelerator Progress Report

2009

vol. **43**

BOOK & CD-ROM

独立行政法人理化学研究所 仁科加速器研究センター
RIKEN Nishina Center for Accelerator-Based Science



RIKEN Accelerator Progress Report 2009

vol. **43**

BOOK & CD-ROM

独立行政法人理化学研究所 仁科加速器研究センター
RIKEN Nishina Center for Accelerator-Based Science
Wako, Saitama, 351-0198 JAPAN

Chairperson of the Editorial Committee

O. Kamigaito

Editorial Committee

H. Okuno	K. Yoneda
S. Nishimura	K. Morimoto
H. Haba	A. Kohama
M. Wada	N. Inabe
S. Yokkaichi	Y. Kobayashi
T. Tada	T. Kambara
T. Abe	Y. Uwamino
K. Yazaki	K. Ishida
T. Ichihara	T. Gunji
Y. Sakata	Y. Sato

All rights reserved. This report or any part thereof may not be reproduced in any form (including photostatic or microfilm form) without written permission from the publisher.

All reports are written on authors' responsibility and thus the editors are not liable for the contents of the report.

GRAVURES & HIGHLIGHTS OF THE YEAR

M. Wakasugi <i>et al.</i>	i
Construction of electron accelerators	
G. Watanabe <i>et al.</i>	iii
Formation of Nuclear “Pasta” in Supernovae	
I. Kishimoto and T. Takahashi	v
Numerical evaluation of gauge invariants for a -gauge solutions in open string field theory	
K. Takagi <i>et al.</i>	vii
Localization of γ H2AX Fluorescence along Tracks of Argon Beams	
M. Asai <i>et al.</i>	ix
α -fine structure spectroscopy for ^{257}Lr and ^{259}Lr	
P. Doornenbal <i>et al.</i>	x
In-beam gamma-ray Spectroscopy of ^{32}Ne	
K. Sekiguchi <i>et al.</i>	xi
Complete Set of Deuteron Analyzing Powers for dp Elastic Scattering at 250 MeV/nucleon and Three-Nucleon Forces	
K. Yoshida.	xii
Negative-parity excitations unique in deformed neutron-rich nuclei close to the drip line	
H. Nemura for HAL QCD Collaboration,	xiii
Lattice QCD study of Lambda N interaction	
K. Karatsu from the PHENIX Collaboration	xiv
W- Boson Production in Polarized p+p Collision at $\sqrt{s} = 500\text{GeV}$	
Y. Sato <i>et al.</i>	xv
Application of a Pair of Solenoid Magnets in Beam Transport Line	
H. Kuboki <i>et al.</i>	xvii
Measurement of charge-state distribution of uranium and xenon beams with a gas charge stripper	
T. Suzuki <i>et al.</i>	xix
Pressure-induced new magnetic phase in $\text{Tl}(\text{Cu}_{0.985}\text{Mg}_{0.015})\text{C}_{13}$ probed by muon spin rotation	
K. Yokoyama, K. Nagamine <i>et al.</i>	xx
Characterization of Spin-Dependent Response of Negative Muonium (Mu^-) to Laser Induced Polarized Electrons in n-type GaAs under Zero Field	

《Selection process of gravures and highlights》

Gravures and highlights will be selected in two-steps process. In the first step, referee will recommend manuscript for gravure or highlight. With the above recommendation, the editors will then give secondary recommendation.

After the following 1 and 2 are comprehensively considered, the editor-in-chief will draft a manuscript idea which will be thoroughly discussed by the editors for the final decision:

1. Approval based on the editor's judgment as an expert/non-expert in the field (there by agreeing with the referee's recommendation)
2. Additional recommendation based on the editor's expertise.

Construction of electron accelerators

M. Wakasugi, Y. Miyashita, H. Takehara,^{*1} H. Takahashi,^{*2} M. Togasaki,^{*2} T. Hori, M. Hara, K. Kurita^{*2} and T. Suda

An electron accelerators system, which consists of a microtron type of accelerator and a synchrotron storage ring, is now under construction in RIKEN Nishina Center aiming for electron scattering experiments for short-lived unstable nuclei using the SCRIT technique^{1,2)}. These accelerators are reuse of the synchrotron storage ring (AURORA-2S)³⁾ and the racetrack microtron (RTM)⁴⁾, which were developed and operated at Sumitomo Heavy Industry Co. Ltd.

These electron accelerators have been transferred from Sumitomo Heavy Industry Co. Ltd. in last summer. In the first half of this year, infrastructures required for the accelerator system and the experimental system have been constructed in the E21 experimental room at the RIBF. Reconstruction of the accelerators has been started at middle of September in this year. Since the AURORA-2S has been developed as the most compact synchrotron light source and there is no free straight section, it was remodeled to the AURORA-2D⁵⁾ type of the ring, which provides 2.15-m length straight sections for insertion of the SCRIT device. This revised storage ring is renamed to be SR2 (SCRIT-equipped Riken Storage Ring).

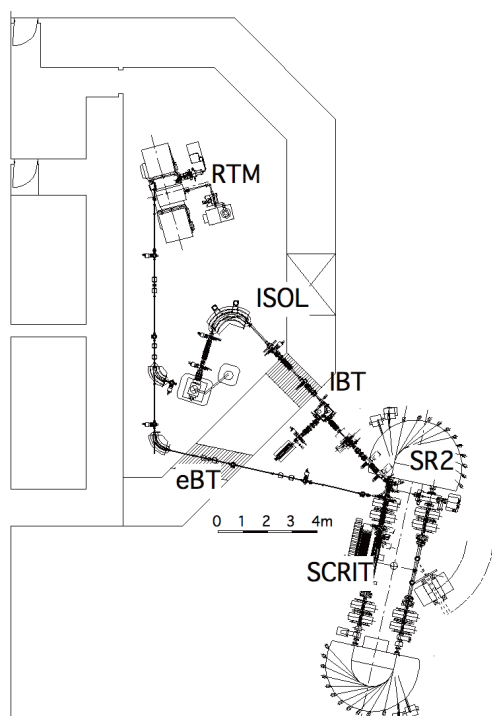


Fig. 1 Layout of electron accelerators. The RTM is placed in shielded room and the SR2 is outside. The SCRIT devices will be installed in a straight section of the SR2, and the ions of unstable nuclei will be supplied by ISOL system, which is planned to be constructed in the shielded room.

Layout of the accelerators is shown in Fig. 1. The RTM is placed in the small room surrounded by 2-m thick concrete wall for radiation shield. The RTM is connected to the SR2 placed outside the shielded room with 16-m long beam transport line (eBT) consisting of four quadrupole doublets and a 77.8-degree bending magnet.

Specifications of the RTM and the SR2 is shown in Table 1 and 2, respectively. The RTM has a S-band standing wave type of linac providing the energy gain of 6 MeV, which is driven by a 2-MW (peak) pulse klystron. The electron beam injected from the electron gun with the energy of 80 keV passes through the linac by 25 times and the final energy is 150 MeV. The RTM has another function as a driver for RI production via photo-fissions of Uranium target put in the ion source of the ISOL system.

Table 1. RTM specifications

Beam energy	(MeV)	150
Injection energy	(keV)	80
Peak current	(mA)	2-10
Pulse width	(μ s)	0.2-2
Repetition rate	(Hz)	100 (max.)
Energy resolution	(%)	± 0.1 (1σ)
Emittance	(π mm mrad)	0.5
Number of turns		25
RF frequency	(MHz)	2856
RF peak power	MW	2 (beam loading)
Energy gain	MeV/turn	6

Table 2. SR2 specifications

Circumference	(m)	21.95
Beam energy	(MeV)	150-700
Magnetic field	(T)	0.6-2.7
Bending radius	(m)	0.87
Betatron tune	(h/v)	1.72 / 1.84
RF frequency	(MHz)	191.244
Harmonic number		14
RF power	(kW)	30
RF voltage	(kV)	220
Stored current	(mA)	300 (expected)
Beam emittance	(π mm mrad)	0.4

The SR2 is a racetrack type of storage ring. The lattice structure is defined by two 180-degree-bending magnets and four quadrupole doublets. Electron beam from the RTM is injected into the SR2 through a 90-degree inflection pulse magnet. The SR2 accepts 150-MeV electron beam and it can accelerate the beam up to 700 MeV by lamping up the magnetic field. The maximum magnetic field in the 180-degree bending magnet is 2.7 T. The RF frequency is

191.244 MHz and the power of 30 kW in the cavity is required at the energy of 700 MeV.

□ Mechanical assembly of both accelerators has been almost completed by the end of 2009. Figure 2 shows photographs of the RTM and the SR2. Each component in the SR2 and the operating system are now undergoing testing. Commissioning of the RTM was performed at the end of 2009. We succeeded in acceleration of the electron beam up to 150 MeV and extraction of the beam from the RTM at Dec. 24 in 2009. Figure 3 (A) shows synchrotron radiation coming out the RTM during the acceleration. Light points corresponding to every electron beam orbits in the RTM were observed. Because only the beam getting energy gain of 6 MeV from the linac in every turn can circulate along the design orbit which is well defined by the magnetic field and small beam tubes, we could confirm the acceleration up to 150 MeV by counting the number of the light points. Accelerated electron beam was extracted from the RTM, and it was observed by a screen monitor as shown in Fig. 3 (B). The peak current of the first beam from the RTM was 1.5 mA, the pulse width was 1 μ s, and the repetition rate was 2 Hz.



Fig. 2. Photographs of the RTM (a) and the SR2 (b).

The SR2 will be commissioned within this fiscal year, and we will spend more half years for tuning of these machines. In next fiscal year, the SCRIT system will be installed into the SR2 after making the SR2 ready for experiments. Figure

4 shows a photograph of the SCRIT device. It consists of three electrodes providing trapping potential, ion injection and extraction channels, scraper-type beam position monitors, and nondestructive button-electrode-type beam position monitors. These components will be put in a 2-m long vacuum chamber and installed at the straight section of the SR2. Since this is a high-impedance device, careful tuning procedure of the SR2 after the installation will be required for stable accumulation of high-current electron beams.

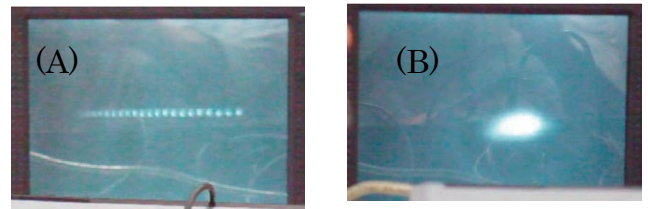


Fig. 3. Photographs of (A) the synchrotron radiations coming out from the RTM, and (B) the beam spot on the screen monitor at the exit of the RTM.



Fig. 4. Photograph of the SCRIT device, which will be installed in the SR2.

The SR2 will be operated not only for the SCRIT experiment but also for utilizing the synchrotron radiations. We will provide several light beam ports around the bending magnet. The energy of accumulated electron beams for synchrotron radiation use is required to be 700 MeV, while that will be 300 MeV or less for the SCRIT experiment. We will establish plural operation patterns for a responsibility to the users. Operation for synchrotron light use will be ready in 2011.

References

- 1) M. Wakasugi et al., Phys. Rev. Lett. 100, 164801 (2008).
- 2) T. Suda et al., Phys. Rev. Lett. 102, 102501 (2009).
- 3) H. Miyade et al., Proc. EPAC98, Stockholm, (1998) p.2413.
- 4) T. Hori et al., Proc. PAC91, San Francisco, (1991) p.2877.
- 5) T. Takayama et al., Proc., EPAC96, Barcelona, (1996) p.709.

Formation of Nuclear “Pasta” in Supernovae[†]

G. Watanabe^{*1,*2}, H. Sonoda,^{*1,*3} T. Maruyama,^{*4} K. Sato,^{*3,*5} K. Yasuoka,^{*6} and T. Ebisuzaki^{*1}

[Supernova explosions, nuclear pasta phases, quantum molecular dynamics]

The mechanism of collapse driven supernova explosions²⁾ has been one of the central mysteries in astrophysics for more than 40 years³⁾. Matter in supernova cores is also yet to be understood and these issues are closely connected. In collapsing supernova cores, while matter consists of bcc lattice of spherical nuclei at lower densities, “pasta” nuclei such as “spaghetti”-like columnar nuclei and “lasagna”-like planar nuclei, etc. are expected to be formed^{4,5)} at higher densities and they amount to more than 20% of the total mass of the cores just before the bounce⁶⁾. Since neutrino scattering property is very different between pasta nuclei and spherical ones^{7,8)}, pasta phases can have a significant influence on the dynamics of explosions.

However, most of the previous works about the pasta phases are based on assuming the shape of nuclei within a static framework. Therefore, a fundamental problem whether or not the pasta phases are actually formed in collapsing cores has been still unclear. Since formation of the pasta phases from spherical nuclei is accompanied by dynamical and drastic changes of the nuclear structure, an *ab-initio* approach is called for. In the present work, using a dynamical framework called quantum molecular dynamics (QMD)^{9,10)}, we have solved this question by demonstrating that a lattice of rod-like nuclei is formed from a bcc lattice by compression. Our result establishes that the pasta phases can be formed in collapsing supernova cores.

A generally accepted conjecture¹¹⁾ based on the Bohr-Wheeler condition for fission predicts that the formation of the pasta phases are triggered by the fission instability with respect to the quadrupolar deformation of spherical nuclei. Then all the nuclei are supposed to elongate in the same direction and they join up to form straight rod-like nuclei. The essential physics of the fission instability is that, at higher densities, the effect of the Coulomb repulsion between protons in nuclei, which tends to make a nucleus deform, becomes dominant over the effect of the surface tension of the nuclei, which favors a spherical nucleus. However, the Bohr-Wheeler condition is derived for isolated nuclei, and actually, several works have pointed

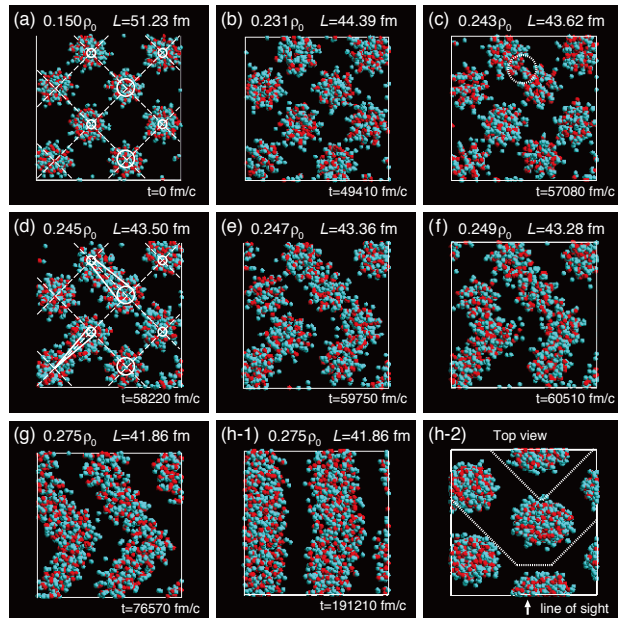


Fig. 1. Snapshots of the transition process from the bcc lattice of spherical nuclei to the pasta phase with rod-like nuclei obtained by our QMD simulation. The red particles show protons and the green ones neutrons. In panels (a)-(g) and (h-1), nucleons in a limited region [surrounded by the dotted lines in panel (h-2)] are shown for visibility. The vertices of the dashed lines in panels (a) and (d) show the equilibrium positions of nuclei in the bcc lattice and their positions in the direction of the line of sight are indicated by the size of the circles: vertices with a large circle, with a small circle, and those without a circle are in the first, second, and third lattice plane, respectively. The solid lines in panel (d) represent the direction of the two elongated nuclei: they take zigzag configuration. This figure is taken from Ref.¹⁾.

out that the background electrons, which have been ignored in the above prediction, suppress the effect of the Coulomb repulsion between protons in nuclei and the fission barrier never vanishes in the relevant density region^{12,13)}. This puzzle has been also solved by our present work.

In Fig. 1, we show the snapshots of the formation process of the pasta phase in adiabatic compression. Here, we start from initial condition at the density $\rho = 0.15\rho_0$ and the temperature $T = 0.25$ MeV [Fig. 1(a)]. At $\rho \simeq 0.243\rho_0$ [Fig. 1(c)], the first pair of two nearest-neighbor nuclei start to touch and fuse (dot-

[†] Condensed from Ref.¹⁾. In this work, we used MDGRAPE-2 and -3 of the RIKEN Super Combined Cluster System. This work is featured by the APS Physical Review Focus Synopsis and by RIKEN Research (issue of January 2010).

*1 RIKEN

*2 Asia Pacific Center for Theoretical Physics (APCTP)

*3 Department of Physics, University of Tokyo

*4 ASRC, Japan Atomic Energy Agency

*5 IPMU, University of Tokyo

*6 Department of Mechanical Engineering, Keio University

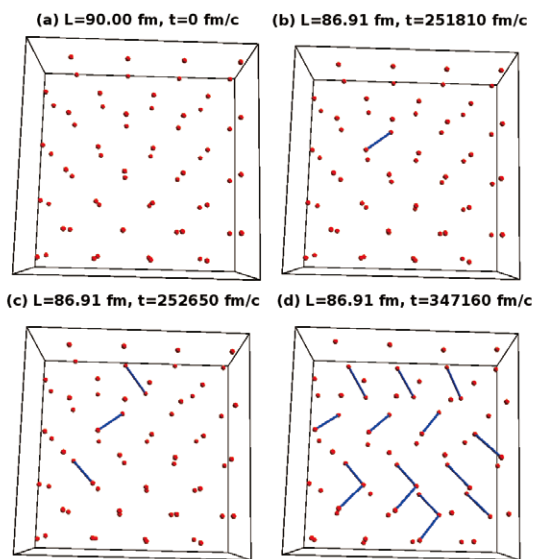


Fig. 2. Snapshots of the simulation of compression at $T < 0.01$ MeV using the simplified model. The red particles show the centers of mass of nuclei and the nuclei within the distance less than $0.89r_{nn}^{(0)}$ are connected by a blue line. Nuclei and connections within only two lattice planes normal to the line of sight are shown. This figure is taken from Ref.¹⁾.

ted circle), and then form an elongated nucleus. After multiple pairs of nuclei become such elongated nuclei, we observe zigzag structure [Fig. 1(d)]. Then these elongated nuclei stick together [see Figs. 1(e) and (f)], and all the nuclei fuse to form rod-like nuclei as shown in Fig. 1(g). Finally, we obtain a triangular lattice of rod-like nuclei after relaxation [Figs. 1(h-1) and (h-2)].

Note that before nuclei deform to be elongated due to the fission instability, they stick together keeping their spherical shape [see Fig. 1(c)]. Our simulation shows that the pasta phase can be formed even though there is no fission instability. Besides, in the middle of the transition process, pair of spherical nuclei get closer to fuse in a way such that the resulting elongated nuclei take a zigzag configuration and then they further connect to form wavy rod-like nuclei. This process is very different from the above mentioned generally accepted scenario.

We also examine the zigzag structure in the QMD simulation for a larger system using a simplified model. Since nuclei start to connect before they are deformed, it is reasonable to treat a nucleus as a sphere and incorporate only its center-of-mass degree of freedom. On the other hand, when the nearest neighbor nuclei are so close that the tails of their density profile overlap with each other, net attractive interaction between these nuclei starts to act. We thus consider the following minimal model in which each nucleus is

treated as a point charged particle interacting through the Coulomb potential and the potential of the Woods-Saxon form which describes the finite size of nuclei and models the internuclear attraction.

With this model, we perform compression of a bcc lattice with 128 nuclei ^{208}Pb , which corresponds to 8 times larger system than that of the QMD simulation. We show the snapshots of this simulation in Fig. 2. In the situation of Fig. 2(b), the first pair of nuclei starts to get closer and then we stop the compression and relax the system. We observe pairings in a zigzag configuration around the first pair [Fig. 2(c)] and finally we obtain a zigzag structure [Fig. 2(d)]. This result shows that the internuclear attraction leads to the spontaneous breaking of the bcc lattice and supports the formation of the zigzag structure observed in the QMD simulation.

In summary, we have shown that the pasta phase can be formed by the compression of matter in collapsing supernova cores. We have found that the formation process is very different from a generally accepted scenario based on the fission instability. Our QMD simulation has shown that a pair of the nearest neighbor nuclei start to connect before they deform due to the fission instability. This spontaneous breaking of the bcc structure is due to an internuclear attraction caused by the overlap of the tails of nucleon distribution of neighboring nuclei. We have also discovered that, in the transition process, the system takes a zigzag configuration of elongated nuclei, which are formed by a fusion of original two spherical nuclei.

References

- 1) G. Watanabe, H. Sonoda, T. Maruyama, K. Sato, K. Yasuoka, and T. Ebisuzaki, *Phys. Rev. Lett.* **103**, 121101 (2009).
- 2) H. A. Bethe, *Rev. Mod. Phys.* **62**, 801 (1990).
- 3) S. A. Colgate and R. H. White, *Astrophys. J.* **143**, 626 (1966).
- 4) D. G. Ravenhall, C. J. Pethick and J. R. Wilson, *Phys. Rev. Lett.* **50**, 2066 (1983).
- 5) M. Hashimoto, H. Seki, and M. Yamada, *Prog. Theor. Phys.* **71**, 320 (1984).
- 6) H. Sonoda, G. Watanabe, K. Sato, T. Takiwaki, K. Yasuoka, and T. Ebisuzaki, *Phys. Rev. C* **75**, 042801(R) (2007).
- 7) G. Watanabe, K. Iida, and K. Sato, *Nucl. Phys.* **A687**, 512 (2001).
- 8) C. J. Horowitz, M. A. Pérez-García, and J. Piekarewicz, *Phys. Rev. C* **69**, 045804 (2004).
- 9) J. Aichelin, *Phys. Rep.* **202**, 233 (1991).
- 10) T. Maruyama, K. Niita, K. Oyamatsu, T. Maruyama, S. Chiba, and A. Iwamoto, *Phys. Rev. C* **57**, 655 (1998).
- 11) C. J. Pethick and D. G. Ravenhall, *Annu. Rev. Nucl. Part. Sci.* **45** (1995) 429.
- 12) S. Brandt, Master thesis, Copenhagen Univ. (1985).
- 13) T. J. Bürvenich, I. N. Mishustin, and W. Greiner, *Phys. Rev. C* **76** (2007), 034310.

Numerical evaluation of gauge invariants for a -gauge solutions in open string field theory[†]

I. Kishimoto and T. Takahashi*¹

[Nonperturbative techniques, string field theory, D branes]

We evaluate the gauge invariants, action and gauge invariant overlap, for numerical solutions for tachyon condensation in the a -gauge in cubic bosonic open string field theory. With an increase in the truncation level, the values of the gauge invariants for various values of a approach those of Schnabl analytic solution¹⁾ for tachyon condensation. This is consistent with the expectation that these numerical solutions are gauge equivalent to the Schnabl analytic solution.

The a -gauge given by Asano and Kato²⁾ is a consistent linear gauge and includes a real parameter a . It can be regarded as an extension of the conventional Siegel gauge. It can be precisely expressed as

$$(b_0M + ab_0c_0\tilde{Q})\Psi = 0 \quad (1)$$

for a classical open string field Ψ . Here, the operators M and \tilde{Q} can be expressed by expanding the Kato-Ogawa BRST operator Q_B with respect to ghost zero modes (i.e., b_0 and c_0) as

$$Q_B = \tilde{Q} + c_0L_0 + b_0M. \quad (2)$$

By expanding the massless part of the action of the free string field theory in the a -gauge, one can find that the parameter a corresponds to the gauge parameter α of the ordinary gauge theory; the relationship between them is given by $\alpha = (a - 1)^{-2}$.

We construct numerical solutions³⁾ for tachyon condensation to the equation of motion of the cubic string field theory

$$Q_B\Psi + \Psi * \Psi = 0 \quad (3)$$

in the a -gauge using an iterative algorithm as follows. Using the initial configuration $\Psi_{(0)}$, which is the non-trivial solution in the lowest-level approximation, string fields $\Psi_{(1)}, \Psi_{(2)}, \Psi_{(3)}, \dots$ can be computed by solving the following linear equations for $\Psi_{(n+1)}$ ($n = 0, 1, 2, \dots$) in $(L, 2L)$ or $(L, 3L)$ truncation:

$$\mathcal{O}_{GF}\Psi_{(n+1)} = 0, \quad (4)$$

$$c_0b_0(Q_{\Psi_{(n)}}\Psi_{(n+1)} - \Psi_{(n)} * \Psi_{(n)}) = 0. \quad (5)$$

Here, (4) imposes the a -gauge condition, i.e.,

$$\mathcal{O}_{GF} = b_0M + ab_0c_0\tilde{Q} \quad (|a| < \infty) \quad (6)$$

or

[†] Condensed from the article in Prog. Theor. Phys. **121**, 695 (2009)

*¹ Department of Physics, Nara Women's University

$$\mathcal{O}_{GF} = b_0c_0\tilde{Q} \quad (a = \infty). \quad (7)$$

Further, $Q_{\Psi_{(n)}}$ is an operator that can be expressed as

$$Q_{\Psi_{(n)}}\phi = Q_B\phi + \Psi_{(n)} * \phi - (-1)^{|\phi|}\phi * \Psi_{(n)} \quad (8)$$

for any string field ϕ . If the configuration $\Psi_{(n)}$ obtained by the above iterations converges in the limit $n \rightarrow \infty$, a projected part of the equation of motion given by

$$c_0b_0(Q_B\Phi_{(\infty)} + \Phi_{(\infty)} * \Phi_{(\infty)}) = 0, \quad (9)$$

is satisfied in the a -gauge. In order to confirm the complete equation of motion for the converged configuration $\Psi_{(\infty)}$, we have numerically evaluated the remaining part that is given by

$$b_0c_0(Q_B\Phi_{(\infty)} + \Phi_{(\infty)} * \Phi_{(\infty)}) = 0. \quad (10)$$

For each numerical solution $\Phi_{(\infty)}$ obtained in the a -gauge, we computed the values of the action and the gauge invariant overlap. The results for the action $S(\Psi)$, where

$$S(\Psi) = -\frac{1}{g^2} \left(\frac{1}{2} \langle \Psi, Q_B\Psi \rangle + \frac{1}{3} \langle \Psi, \Psi * \Psi \rangle \right), \quad (11)$$

in the $(L, 3L)$ truncation are plotted in Fig. 1. The

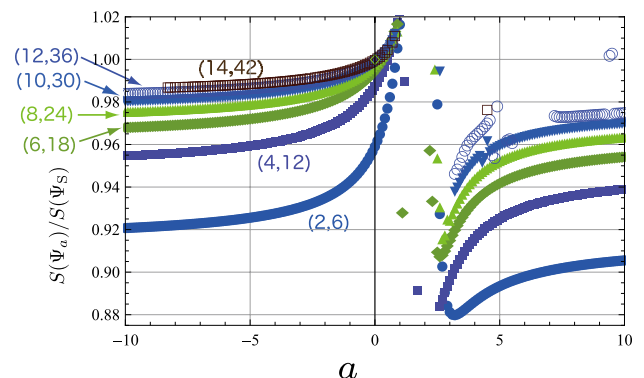


Fig. 1. Plots of the action for various a -gauge solutions Ψ_a in the $(L, 3L)$ truncation. The horizontal axis denotes the value of a and the vertical one denotes the normalized action $S(\Psi_a)/S(\Psi_S)$, where Ψ_S is the Schnabl solution. The label $(L, 3L)$ for each “curve” denotes the truncation level.

results for the gauge invariant overlap⁴⁾ $\mathcal{O}_\eta(\Psi)$, where

$$\mathcal{O}_\eta(\Psi) = \langle \hat{\gamma}(1_c, 2) | \Phi_\eta \rangle_{1_c} | \Psi \rangle_2, \quad (12)$$

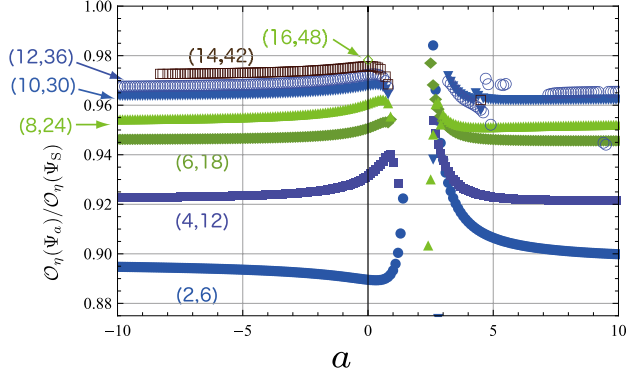


Fig. 2. Plots of the gauge invariant overlap for various a -gauge solutions Ψ_a in the $(L, 3L)$ truncation. The horizontal axis denotes the value of a and the vertical one denotes the normalized gauge invariant overlap $\mathcal{O}_\eta(\Psi_a)/\mathcal{O}_\eta(\Psi_S)$.

in the $(L, 3L)$ truncation are plotted in Fig. 2. We display plots of the action and overlap for various a including $a = \infty$ in Fig. 3. Table 1 shows the values of gauge invariants for the numerical solution in the ($a = 0$)-gauge, which is equivalent to the Siegel gauge.^{a)}

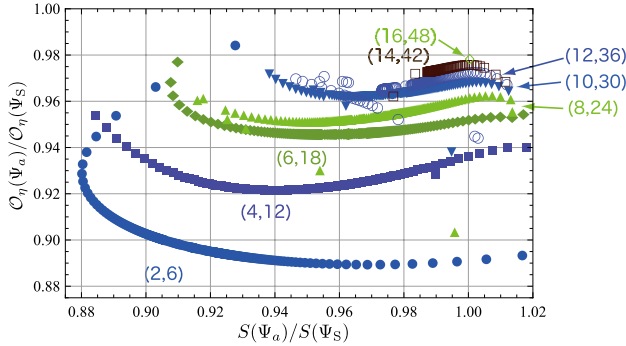


Fig. 3. Plots of gauge invariants for various a -gauge solutions Ψ_a in the $(L, 3L)$ truncation. The horizontal axis denotes the ratio of the action $S(\Psi_a)/S(\Psi_S)$ and the vertical one denotes that of the gauge invariant overlap $\mathcal{O}_\eta(\Psi_a)/\mathcal{O}_\eta(\Psi_S)$. Each point denotes $(S(\Psi_a)/S(\Psi_S), \mathcal{O}_\eta(\Psi_a)/\mathcal{O}_\eta(\Psi_S))$ for different values of a . The left part of the “curve” for each level corresponds to $4 \lesssim a < +\infty$ and the right part corresponds to $-\infty < a \lesssim 1/2$. The plots for $a \rightarrow +\infty$ and $a \rightarrow -\infty$ are continuously connected at that of the Landau gauge ($a = \infty$)-gauge).

a) The action for the numerical solution in the Siegel gauge was evaluated in the earlier literature⁵⁾ up to level (18, 54). The gauge invariant overlap for the solution was evaluated in our previous paper⁴⁾ up to level (10, 30) using our *Mathematica* program. Here, we made the new record of the truncation level up to (24, 72)⁶⁾. Calculations for higher truncation levels ($L \geq 18$) in Table 1 were performed by our C++ and Fortran program using our PC cluster in Nara Women’s

$(L, 3L)$	$S(\Psi_{a=0})/S(\Psi_S)$	$\mathcal{O}_\eta(\Psi_{a=0})/\mathcal{O}_\eta(\Psi_S)$
(0,0)	0.6846162	0.7165627
(2,6)	0.9593766	0.8898618
(4,12)	0.9878218	0.9319524
(6,18)	0.9951771	0.9510789
(8,24)	0.9979301	0.9611748
(10,30)	0.9991825	0.9681148
(12,36)	0.9998223	0.9725595
(14,42)	1.0001737	0.9761715
(16,48)	1.0003755	0.9786768
(18,54)	1.0004937	0.9809045
(20,60)	1.0005630	0.9825168
(22,66)	1.0006023	0.9840334
(24,72)	1.0006227	0.9851603

Table 1. The value of the action and the gauge invariant overlap for the numerical solution with $(L, 3L)$ truncation in the Siegel gauge ($a = 0$ -gauge). The values are normalized by the analytic result for Schnabl’s solution. If we use the fitting function⁵⁾ $F_N(L) = \sum_{n=0}^N \frac{a_n}{(L+1)^n}$ using data for $L = 0, 2, \dots, 24$ ($N = 13$), we obtain the extrapolated value of the action: 1.0000075 for $L = \infty$.

Except for the region at approximately $a = 1$, where the a -gauge condition is ill defined perturbatively and the iterations given by (4) and (5) do not converge in the limit $n \rightarrow \infty$, the values of both gauge invariants approach those of the Schnabl solution as truncation level increases. The same tendency is observed in the level $(L, 2L)$ calculation.

The calculated values of the gauge invariants are numerically stable and almost equal to those of Schnabl solution in the region where the gauge parameter a is well defined. These results provide further evidence of the gauge equivalence of various numerical and analytical solutions. It may further imply that the nonperturbative vacuum in bosonic open string field theory, where the original D-brane vanishes, is unique.

References

- 1) M. Schnabl: Adv. Theor. Math. Phys. **10**, 433 (2006).
- 2) M. Asano and M. Kato: Prog. Theor. Phys. **117**, 569 (2007), Nucl. Phys. B **807**, 348 (2009).
- 3) M. Asano and M. Kato: JHEP **0701**, 028 (2007).
- 4) T. Kawano, I. Kishimoto and T. Takahashi: Nucl. Phys. B **803**, 135 (2008).
- 5) D. Gaiotto and L. Rastelli: JHEP **0308**, 048 (2003).
- 6) I. Kishimoto: Talk at *APCTP Focus Program on Current Trends in String Field Theory*, Pohang, Korea, December 11, 2009.

University, the Computer Facility of the Yukawa Institute for Theoretical Physics in Kyoto University and the RIKEN Integrated Cluster of Clusters (RICC). In our computation for the level (22, 66) and (24, 72), we have used the $su(1, 1)$ -singlet basis, which is a consistent truncation in the Siegel gauge.

Localization of γ H2AX Fluorescence along Tracks of Argon Beams

K. Takagi*¹, T. Tsukada, M. Izumi, Y. Kazama, Y. Hayashi, and T. Abe
 [γ H2AX, DSB, heavy ion]

Mutations are generated through lesions in DNA and their inappropriate repair. Therefore, it is important to investigate the process of DNA damage for studying effects of heavy-ion beams on mutagenesis.

H2AX is one of the subtypes of the histone 2 family. When a DNA double strand break (DSB) occurs in a cell nucleus, H2AXs near the DSB site are phosphorylated at a serine residue near its carboxy terminal to form a cluster of phosphorylated H2AX (γ H2AX), the so-called γ H2AX "focus"¹⁾. Therefore, one can predict locations of DSB sites in cell nuclei by detecting γ H2AX foci.

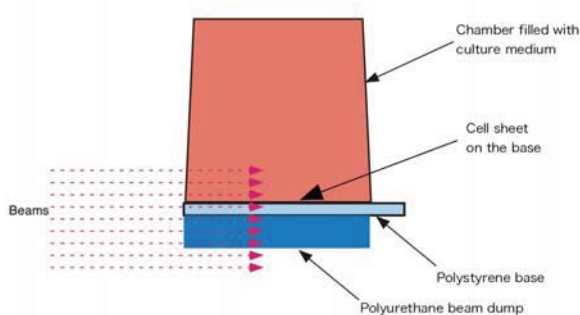


Fig. 1. Cell culture chamber for the irradiation

For studying the effects of argon beams on DSB formation along their flight paths, a confluent cell layer of BALB-3T3 mouse fibroblast cell line was placed parallel to the beam axis, as indicated in Fig.1, and $^{40}\text{Ar}^{17+}$ beams (95 MeV/nucleon) radiated on the cell layer at an initial fluence of 1 particle per $100 \mu\text{m}^2$. The cell layer was fixed 30 min after the irradiation, and γ H2AX was detected by means of immunofluorescent microscopy using an antibody raised against γ H2AX.

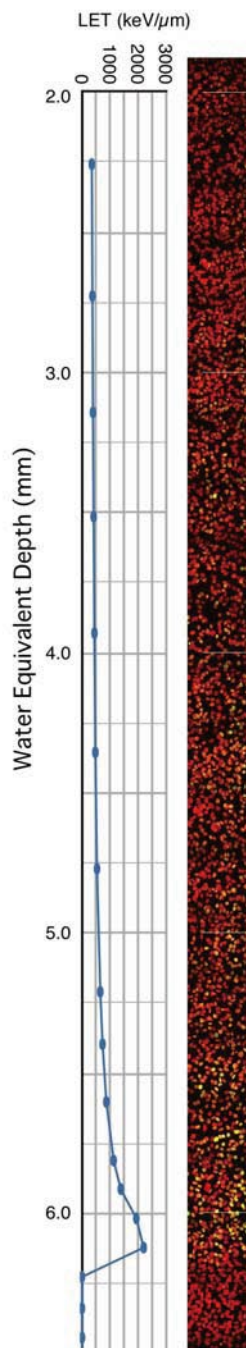


Fig. 2. LET change and corresponding γ H2AX foci localization

Red color in the photograph indicates cellular nuclei, and yellow color indicates immunofluorescence of γ H2AX.

*1 The Wakasa Wan Energy Research Center

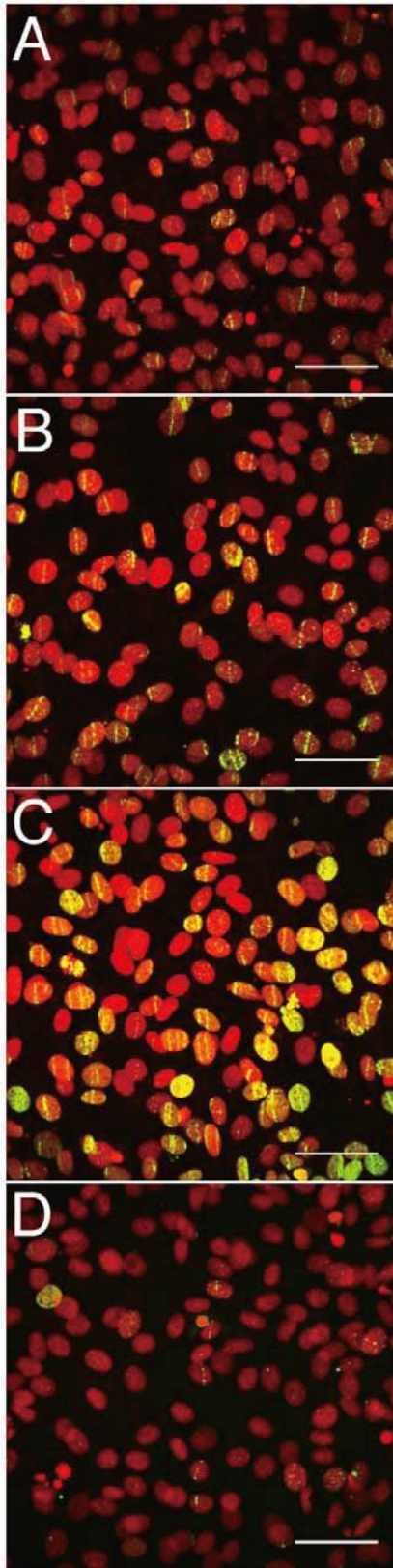


Fig. 3. Localization of γ H2AX foci at the different depth
 Panel A-D indicates the photograph at the depth of 2
 (A), 4 (B), 6 (C), and 12.5 mm (D), respectively. Each
 scale bar in panels indicates a length of 50 μ m.

Figure 2 shows depth dependent changes in the LET, and γ H2AX fluorescence in the corresponding region. The fluorescence intensity was increased with the increase of LET, and it almost disappeared corresponding to the abrupt decrease of LET. The photographs in Figs. 3A-D indicate the localization of γ H2AX at depth of 2, 4, 6, and 12.5 mm, respectively. At the depth of 2 mm (Fig. 3A), γ H2AX fluorescence revealed straight lines, implying that the DSBs were so dense along a particle track that each focus was indistinguishable. Figure 3C shows cells at the depth of 6 mm. This position is near the peak of LET. The γ H2AX fluorescence intensity increased, and extended to the entire cellular nuclear area in some cells. Interestingly, there seem to be more lines of γ H2AX fluorescence in Fig.3C than in Fig. 3A and B, and some lines appear as dotted lines, suggesting the existence of particles, having lower LET than the original argon ions had. These observations might be the result of nuclear fragmentation. Figure 3D depicts cells at the depth of 12.5 mm, where was apparently out of the range of the argon ions. A γ H2AX fluorescence line can be seen at the center of a photograph. The fluorescence suggests the presence of a fragmentation-derived particle that had lower LET than the original argon ion at shallower region had.

In the present study, we observed a straight line of γ H2AX fluorescence parallel to the beam axis. The fluorescence intensity gradually increased as the LET of particles increased, and it almost disappeared in regions beyond the range of the argon ions. These results imply that argon ions cause dense DSB along their flight path.

Further, the present study shows some behaviors of heavy ions in living tissues. Tracks of the projectile were visualized as lines of γ H2AX fluorescence, and some signs of nuclear fragmentation were inferred from dotted lines of fluorescence. Those results are probably the first visual evidence of nuclear fragmentation in cellular nuclei.

Reference

- 1) E. Rogakou et al.: J. Biol. Chem. **273**, 5858 (1998).

α -fine structure spectroscopy for ^{257}Lr and ^{259}Lr

M. Asai,^{*1} H. Haba, Y. Kasamatsu, N. Sato,^{*1} K. Tsukada,^{*1} and T.K. Sato,^{*1}[Nuclear structure, ^{257}Lr , ^{259}Lr , α decay]

Energy spacings and order of single-particle orbitals are sensitive probes to investigating shell structure of superheavy nuclei. In particular, energies of the proton orbitals around $Z = 101$, 103, and 105 (Md, Lr, and Db) are interesting because one orbital, $1/2^- [521]$, which originally lies just above the $Z = 114$ gap in a spherical nucleus comes down to the Fermi level in deformed nuclei around $Z = 101$ –105. Experimental assignments of the deformed proton orbitals around $Z = 101$ –105 thus give us valuable information on the spherical shell gap energy around $Z = 114$.

Experimental data on the single-particle states in odd-mass Md, Lr, and Db isotopes are, however, very scarce because spectroscopy of such heavy nuclei are extremely difficult. There is no firm information on excitation energies, spin-parities, and proton configurations of ground- as well as excited states in odd-mass Md, Lr, and Db isotopes except for the ground-state configurations of some Md isotopes.¹⁾

Recently, Chatillon *et al.*²⁾ studied the α decay of ^{255}Lr using a recoil separator and a cold fusion reaction of $^{209}\text{Bi}(^{48}\text{Ca}, 2n)^{255}\text{Lr}$. They found an α -decaying isomer in ^{255}Lr and proposed proton configurations of $1/2^- [521]$ and $7/2^- [514]$ for ^{255g}Lr and ^{255m}Lr , respectively. To definitely identify the spin-parities and configurations, spectroscopic data for α - or γ transitions are indispensable. However, in the α decay of $^{255g,m}\text{Lr}$, no γ ray was observed in coincidence with α particles,²⁾ because those α transitions would directly populate the $7/2^- [514]$ ground state or the $1/2^- [521]$ isomer in ^{251}Md . The same situation is expected in the α decay of other odd-mass Lr isotopes, which makes it impossible to assign spin-parities of the Lr isotopes through γ -ray spectroscopy. To study such nuclei, we proposed high-resolution α -fine structure spectroscopy which allows us to identify single-particle configurations only by measuring an α -singles spectrum. In the present work, we applied this technique to studying the α decay of ^{257}Lr and ^{259}Lr .

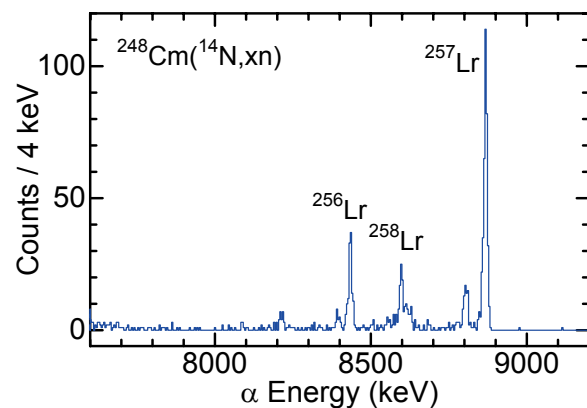
The nuclei ^{257}Lr and ^{259}Lr were produced in the $^{248}\text{Cm}(^{14}\text{N}, 5n)^{257}\text{Lr}$ and $^{248}\text{Cm}(^{15}\text{N}, 4n)^{259}\text{Lr}$ reactions using the RIKEN AVF cyclotron. Reaction products were transported through a 10-m long capillary with a He/KCl jet into a rotating-wheel α -detection system, and deposited on a thin foil forty of which were set on the rotating wheel. The wheel periodically rotated to move the deposited sources to seven consecutive detector stations each of which was equipped

with two Si detectors. To achieve a good α -energy resolution and to reduce a low-energy tail of α peaks, Si detectors were set at the distance with a solid angle of 13% of 4π . This setup also reduces energy sum between α particles and subsequently emitted conversion electrons, Auger electrons, and low-energy X rays which considerably distorts the measured α -energy spectrum. This energy sum becomes significant when α sources are implanted into a Si detector by a recoil separator like Ref. 2, which makes it impossible to observe α fine structure and to determine α energies and intensities precisely. The present setup using a gas-jet transport system and a rotating wheel system is of great advantage to observing α fine structure precisely.

Figure 1 shows a measured α energy spectrum for ^{257}Lr . The α energy resolution of ~ 12 keV FWHM was achieved. We can clearly see a weak α line at energy by 62 keV lower than that of the most intense α line of ^{257}Lr . These α lines are considered to be the transitions to the rotational band members of the one-quasiparticle state whose configuration is the same as that of the ground state of ^{257}Lr . Taking into account energy difference and intensity ratio of α transitions to rotational band members, we can assign a single-particle configuration of the ground state of the parent nucleus as well as the populated levels in the daughter. The energy difference of 62 keV agrees well with that between the $7/2^-$ bandhead and the $9/2^-$ member of the $7/2^- [514]$ band in neighboring nuclei. A similar result was obtained for the α decay of ^{259}Lr .

References

- 1) F.P. Heßberger *et al.*: Eur. Phys. J. A **26**, 233 (2005).
- 2) A. Chatillon *et al.*: Eur. Phys. J. A **30**, 397 (2006).

Fig. 1. Measured α energy spectrum for ^{257}Lr .

^{*1} Advanced Science Research Center, Japan Atomic Energy Agency

In-beam γ -ray spectroscopy of $^{32}\text{Ne}^\dagger$

P. Doornenbal, H. Scheit,¹ N. Aoi, S. Takeuchi, K. Li,¹ E. Takeshita, H. Wang,¹ H. Baba, S. Deguchi,² N. Fukuda, H. Geissel,³ R. Gernhäuser,⁴ J. Gibelin,⁵ I. Hachiuma,⁶ Y. Hara,⁷ C. Hinke,⁴ N. Inabe, K. Itahashi, S. Itoh,⁸ D. Kameda, S. Kanno, Y. Kawada,² N. Kobayashi,² Y. Kondo, R. Krücken,⁴ T. Kubo, T. Kuboki,⁶ K. Kusaka, M. Lantz, S. Michimasa,⁹ T. Motobayashi, T. Nakamura,² T. Nakao,⁸ K. Namihira,⁶ S. Nishimura, T. Ohnishi, M. Ohtake, N. Orr,⁵ H. Otsu, K. Ozeki, Y. Satou,² S. Shimoura,⁹ T. Sumikama,¹⁰ H. Takeda, K. N. Tanaka,² K. Tanaka, Y. Togano, M. Winkler,³ Y. Yanagisawa, K. Yoneda, A. Yoshida, K. Yoshida and H. Sakurai,

[Nuclear structure, Island of Inversion, neutron-rich nuclei, in-beam γ -ray spectroscopy]

The region around neutron-rich $N = 20$ nuclei has drawn strong theoretical and experimental attraction in the last few decades, as it was discovered that the well-known magic numbers are not global over the Segré chart and assuming only magic regions, i.e., regions in which a certain set of magic numbers is valid, seems more appropriate. Despite grand efforts, the exact dimension of the region of the “Island of Inversion”, a region in which the $N = 20$ shell closure disappears, are not established experimentally. In particular, data for neutron rich Ne isotopes are very scarce.

Here, we report on the first in-beam γ -ray spectroscopic study performed at the Radioactive Ion Beam Facility, aiming for the determination of the first excited state of ^{32}Ne . Its value provides a measure if the $N = 20$ shell is closed in this nucleus or not. A ^{48}Ca primary beam of 120 pA average intensity impinged at an energy of 345 MeV/u on a 20 mm rotating Be target mounted at the focus F0 of the fragment separator BigRIPS¹⁾. The secondary beams were separated and selected in the first stage of BigRIPS, employing the $B\rho$ - ΔE - $B\rho$ method with a 15 mm thick Al wedge degrader at the dispersive focus F1.

The particles were identified in the second stage of BigRIPS based on the ΔE -TOF- $B\rho$ method. The energy loss (ΔE) was measured with an ion-chamber²⁾ located at the focus F7, the time-of-flight (TOF) was deduced from two plastic scintillators located at the foci F3 and F7, while the $B\rho$ was obtained from position measurements with parallel plate avalanche counters³⁾ at the foci F3 and F5.

The main constituents of the secondary beam were ^{33}Na (26 pps) and ^{32}Ne (6 pps), which were transported to the focus F8 and incident on a 2.54 g/cm²

thick (natural) carbon target at mid-target energies of 245 and 226 MeV/u, respectively. After the secondary target, the particle spectrometer ZeroDegree was employed to select and identify the reaction residues by the same methods as described for BigRIPS.

To detect γ -rays emitted from excited states in ^{32}Ne , the secondary target was surrounded by 180 large volume NaI(Tl) crystals, the DALI2 array⁴⁾. After less than eight hours measuring time, γ -ray transitions were seen in the inelastically scattered ^{32}Ne and the one-proton removal reaction from ^{33}Na , which we assigned to the $2_1^+ \rightarrow 0_{\text{gs}}^+$ decay. The spectra are shown in Fig. 1, revealing a single γ -ray peak at 722(9) keV for the sum spectrum of both reaction channels.

A comparison with shell-model calculations by Utsuno *et al.*⁵⁾ and Caurier *et al.*⁶⁾ showed that this low excitation energy accords with the original perception about the dimension of the “Island of Inversion”, i.e., it extends at least to the neutron number $N = 22$ for the Ne isotopes.

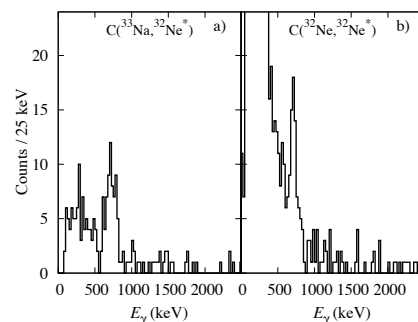


Fig. 1. Doppler corrected γ -ray spectra from DALI2 following one-proton removal of ^{33}Na (a) and inelastically scattered ^{32}Ne (b).

[†] Condensed from the article in Phys. Rev. Lett. **103**, 032501 (2009)

*1 Peking University, China

*2 Department of physics, Tokyo Institute of Technology

*3 GSI, Darmstadt, Germany

*4 Tech. Univ. München, Germany

*5 LPC Caen, France

*6 Department of Physics, Saitama University

*7 Department of Physics, Rikkyo University

*8 Department of Physics, University of Tokyo

*9 Center for Nuclear Study, The Univ. of Tokyo

*10 Tokyo University of Science

References

- 1) T. Kubo *et al.*, Nucl. Instr. Meth. B 204, 97 (2003).
- 2) H. Otsu *et al.*, RIKEN Accel. Prog. Rep. 42, 163 (2009).
- 3) T. Ohnishi *et al.*, J. Phys. Soc. Jpn. 77, 083201 (2008).
- 4) S. Takeuchi *et al.*, RIKEN Accel. Prog. Rep. 36, 148 (2003).
- 5) Y. Utsuno *et al.*, Phys. Rev. C 60, 054315 (1999).
- 6) E. Caurier *et al.*, Nucl. Phys. A693, 374 (2001).

Complete Set of Deuteron Analyzing Powers for dp Elastic Scattering at 250 MeV/nucleon and Three-Nucleon Forces

K. Sekiguchi, H. Okamura,^{*1} N. Sakamoto, H. Suzuki,^{*2} M. Dozono,^{*3} Y. Maeda,^{*4} T. Saito,^{*4} S. Sakaguchi, H. Sakai,^{*5} M. Sasano, Y. Shimizu, T. Wakasa,^{*3} and K. Yako,^{*5}

The study of three-nucleon forces (3NFs) is important for clarifying nuclear phenomena. The first signature of the 3NF was found in the binding energies of the ${}^3\text{H}$ and ${}^3\text{He}$, and the significance of 3NFs has recently been pointed out in providing descriptions of discrete states in higher mass nuclei. The study of three-nucleon scattering at intermediate energies ($E/A \sim 200$ MeV) is a promising approach for investigating the dynamical aspects of 3NFs, such as momentum and/or spin dependence. The experimental studies by polarized deuterons beams at intermediate energies are being carried out at the RIKEN RI Beam Factory with the aim of clarifying roles of the 3NFs in nuclei. As the first step, we have measured a complete set of deuteron analyzing powers (iT_{11} , T_{20} , T_{21} , and T_{22}) for deuteron–proton (dp) elastic scattering at 250 MeV/nucleon.

A schematic diagram of the experimental setup has been provided in Ref. (1). First vector- and tensor- polarized deuteron beams were accelerated by the injector cyclotrons AVF and RRC up to 90 MeV/nucleon; subsequently; they were accelerated up to 250 MeV/nucleon by the new superconducting cyclotron SRC. The polarization axis of each beam was rotated by using a Wien filter system prior to their acceleration²⁾. Therefore, single-turn extraction of the beams from all three cyclotrons, AVF, RRC, and SRC was required in order to maintain the polarization amplitudes during acceleration. The typical values of the beam polarizations determined by the experiment were 80% of the theoretical maximum values. Note that the beam polarizations were monitored continuously by using a beam line polarimeter, Dpol, prior to acceleration by the SRC. The dp elastic scattering was performed by using a detector system, BigDpol, which was installed at the extraction beam line of the SRC. Polyethylene (CH_2) with a thickness of 330 mg/cm^2 was used as the hydrogen target. In BigDpol, four pairs of plastic scintillators coupled with photo-multiplier tubes were placed symmetrically in the directions of azimuthal angles to the left, right, up and down. Scattered deuterons and recoil protons were detected in kinematical coincidence condition by each pair of detectors. The angles ($\theta_{\text{c.m.}}$) measured in the center-of-mass system are in the range 40° – 162° . In the experiment,

the deuteron beams were stopped in the Faraday cup which was installed at the focal plane F0 of the BiGRIPS spectrometer.

Angular distributions of all deuteron analyzing powers iT_{11} , T_{20} , T_{21} , and T_{22} represented by open circles in Fig. 1. The statistical errors are also shown. The dark (light) shaded bands in the figure represent the Faddeev calculations with (w/o) the Tucson-Melbourne99 3NF³⁾ based on modern NN potentials, namely CDBonn⁵⁾, AV18⁶⁾, and Nijmegen I and II⁷⁾. The solid lines represent the results of the calculations with the Urbana IX 3NF⁴⁾ based on the AV18 potential. Good agreements between the data and the calculations with the 3NFs are obtained at forward angles given by $\theta_{\text{c.m.}} \leq 120^\circ$; however, at backward angles, good agreements are not observed even when 3NFs are included. These results are quite similar to those obtained for the cross section and proton analyzing power for pd/nd elastic scattering at 250 MeV/nucleon^{8,9)}.

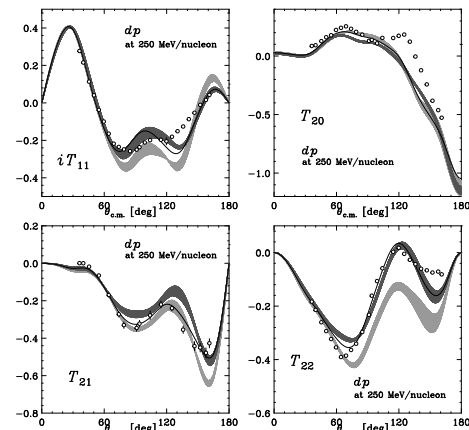


Fig. 1. Deuteron analyzing powers iT_{11} , T_{20} , T_{21} , and T_{22} for dp elastic scattering at 250 MeV/nucleon.

References

- 1) K. Sekiguchi et al.: RIKEN Accel. Prog. Rep. **42**, 27 (2009).
- 2) H. Okamura et al.: AIP Conf. Proc. **343**, 123 (1995).
- 3) S. A. Coon and H. K. Han: Few Body Syst. **30**, 131 (2001).
- 4) B. S. Pudliner et al.: Phys. Rev. C **56**, 1720 (1997).
- 5) R. Machleidt: Phys. Rev. C **63**, 024001 (2001).
- 6) R. B. Wiringa et al.: Phys. Rev. C **51**, 38 (1995).
- 7) V. G. J. Stoks et al.: Phys. Rev. C **49**, 2950 (1994).
- 8) K. Hatanaka et al.: Phys. Rev. C **66**, 044002 (2002).
- 9) Y. Maeda et al.: Phys. Rev. C **76**, 014004 (2007).

^{*1} RCNP, Osaka University

^{*2} University of Tsukuba

^{*3} Kyushu University

^{*4} Miyazaki University

^{*5} University of Tokyo

Negative-parity excitations unique in deformed neutron-rich nuclei close to the drip line[†]

Kenichi Yoshida

[Nuclear structure, Density functional theory, Unstable nuclei]

Study of the multipole responses in unstable nuclei is of considerable interest because the multipole responses can provide information on novel features of collective modes of excitation in extreme environments. The surface structure of neutron-rich nuclei is quite different from that of stable nuclei, because of the presence of the loosely bound neutrons. One of the unique features of neutron-rich nuclei is the presence of a neutron skin. Since collective excitations are sensitive to the surface structure, we can expect new kinds of exotic excitation modes associated with the neutron skin to appear in neutron-rich nuclei. An example of such an exotic excitation mode is the soft dipole mode or the pygmy dipole resonance (PDR).

The structure and collectivity of the PDR has been studied on the basis of mean-field calculations performed by many groups¹⁾. These studies, however, have been largely restricted to spherical systems. Recently the low-lying dipole excitation in neutron-rich Ne²⁾ and Sn isotopes³⁾ have been investigated by using deformed quasiparticle-random-phase approximation (QRPA),

In the present study, low-lying negative-parity excitation modes are investigated using the deformed QRPA on the basis of Skyrme-Hartree-Fock-Bogoliubov (HFB) mean field⁴⁾. The HFB calculations reveal that Mg isotopes under investigation are

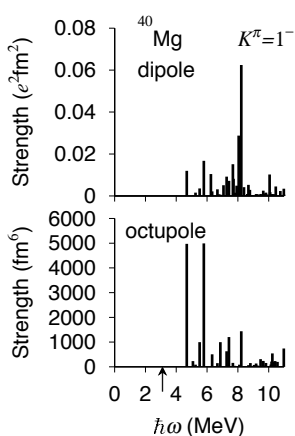


Fig. 1. Transition strengths for the $K^\pi = 1^-$ isovector (IV) dipole (upper) and isoscalar (IS) octupole (lower) excitations in ^{40}Mg . The arrow indicates the neutron-emission threshold energy.

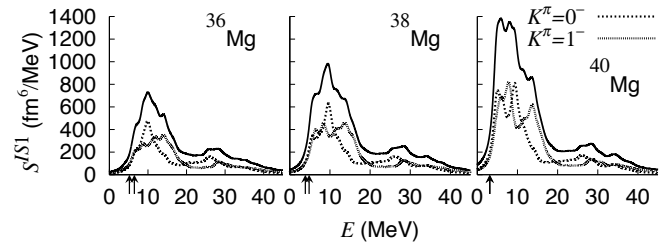


Fig. 2. IS dipole strength distribution in $^{36,38,40}\text{Mg}$. The transition strengths are smeared by a Lorentzian function with a width of $\Gamma = 2$ MeV.

prolately deformed and that they have neutron skins; the neutron-skin thickness of ^{36}Mg , ^{38}Mg and ^{40}Mg are 0.41 fm, 0.47 fm, and 0.54 fm, respectively.

The low-lying part of the isovector (IV) dipole strengths are shown in the upper panel of Fig. 1. We can see a prominent peak at around 8 MeV. The transition density to this state shows the following characteristic feature of PDR: Inside the nucleus and at the surface of the nucleus, protons and neutrons oscillate coherently, while outside the nucleus, only the neutrons oscillate, and the oscillations of the internal core and the neutron outside are out of phase. This corresponds to the classical picture of oscillation of the neutron skin against the isoscalar core along the ρ -axis, which is the axis perpendicular to the symmetry axis. It is also found that in PDR there is significant coupling between the dipole and octupole excitation modes because of the nuclear deformation, as shown in the lower panel of Fig. 1.

Figure 2 shows the transition strengths for the IS compressional dipole operator. When the drip line is approached, we can see a significant enhancement of the transition strengths occurring above the neutron-emission threshold energy; the transition strengths increase up to ~ 15 MeV. Since such an enhancement of the transition strengths in the lower-energy region is not observed in stable nuclei, we can conclude that it is one of the unique features of drip-line nuclei, and it occurs due to the strong mixing between the IS and IV modes and due to the presence of the neutron skin.

References

- 1) N. Paar et al.: Rep. Prog. Phys. **70**, 691 (2007).
- 2) K. Yoshida et al.: Phys. Rev. C **78**, 014305 (2008).
- 3) D. P. Arteaga et al.: Phys. Rev. C **79**, 034311 (2009).
- 4) K. Yoshida et al.: Phys. Rev. C **78**, 064316 (2008).

[†] Condensed from article in Phys. Rev. C **80**, 044324 (2009).

Lattice QCD study of ΛN interaction [†]

H. Nemura, for HAL QCD Collaboration,

[Lattice QCD, Hyperon-Nucleon interaction, Nuclear forces, Hypernuclei]

Baryon-baryon interaction is one of the important topics in nuclear physics. For the sector with strangeness $S = 0$, modern nucleon-nucleon (NN) potentials provide a good description of the NN scattering data at low energies. These NN potentials together with three-nucleon (NNN) forces have been considered for precision calculations in normal light nuclei²⁾. In contrast, hyperon-nucleon (YN) and hyperon-hyperon (YY) interactions involve large uncertainties because the scattering experiments are either difficult or impossible due to the short lifetimes of hyperons. The present phenomenological YN and YY interaction models are not well constrained by experimental data. The characteristics of the YN and YY interactions are important for studying the composition of hyperonic matter in neutron stars. For example, according to recent experimental and theoretical studies on Σ hypernuclei, Σ -nucleus interaction appears to be repulsive. Therefore, a Λ particle, instead of Σ^- , would be the first strange baryon to appear in the cores of neutron stars. Moreover, the quantitative information of the YY (e.g., $\Lambda\Lambda$) interaction could help to clarify the cooling mechanism of neutron stars.

Lattice QCD is a valuable theoretical tool for the first-principle calculation of baryon-baryon interactions. Recently, a new approach has been proposed to study the NN interaction using lattice QCD^{3,4)}. We study the ΛN potential by adopting this approach. In this article, the results of quenched QCD calculation performed by utilizing the plaquette gauge action and the Wilson quark action at $\beta = 5.7$ on a $32^3 \times 48$ lattice are presented. The lattice spacing at the physical point is determined as $a \approx 0.14$ fm from the ρ -meson mass. The spatial lattice volume is approximately $(4.5 \text{ fm})^3$. Figures 1 and 2 show the ΛN potentials obtained by the quenched QCD calculation. For the channel with angular momentum and parity $J^\pi = 1^+$, the central (V_C) and the tensor (V_T) potentials are shown in the Fig. 1, while V_C for the channel with $J^\pi = 0^+$ is shown in Fig. 2. To compare the strengths of the repulsive cores for two quark masses, the central potential multiplied by volume factor, i.e., $r^2 V_C(r)$, is shown in the left panel of each figure; the normal $V(r)$ is shown in the right panel of each figure. These figures present results for $(m_\pi, m_K) \approx (512, 606)$ and $(407, 565)$ MeV. As evident in both figures, the attractive well of the central potential slightly moves to outer direction as the u and d quark masses decrease, whereas the depth of these attractive pockets do not change considerably.

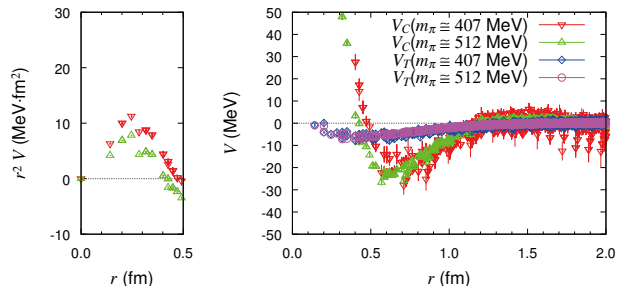


Fig. 1. The central and the tensor potentials in ${}^3S_1 - {}^3D_1$ channel of ΛN system in quenched QCD at $m_\pi \simeq 407$ MeV (downward-triangle and diamond) and 512 MeV (upward-triangle and circle).

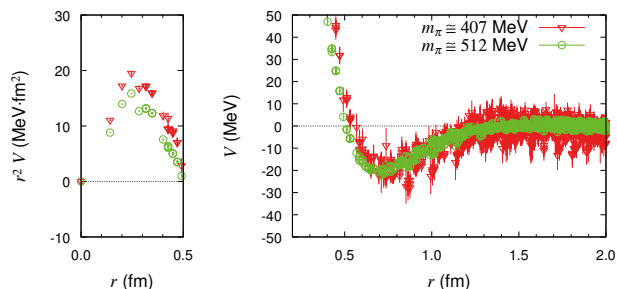


Fig. 2. The central potential in 1S_0 channel of ΛN system in quenched QCD at $m_\pi \simeq 407$ MeV (downward triangle) and 512 MeV (circle).

The present results show that the tensor force is weaker than the NN interaction, and the dependence of the tensor force on quark mass appears to be small. Both of the repulsive and attractive parts increase in magnitude as the u and d quark masses decrease. Calculations involving $2 + 1$ flavor full QCD gauge configurations that are generated by PACS-CS collaboration⁵⁾ are also in progress.

References

- 1) H. Nemura, for HAL QCD Collaboration: *Proceedings of the 10th International Conference on Hypernuclear and Strange Particle Physics (Hyp-X)*, Nucl. Phys. A **835**, 176 (2010).
- 2) S. C. Pieper, Riv. Nuovo Cim. **031**, 709 (2008) [arXiv:0711.1500 [nucl-th]].
- 3) N. Ishii, S. Aoki, T. Hatsuda: Phys. Rev. Lett. **99**, 022001 (2007).
- 4) S. Aoki, T. Hatsuda and N. Ishii: Prog. Theor. Phys. **123**, 89 (2010), arXiv:0909.5585 [hep-lat].
- 5) S. Aoki *et al.* [PACS-CS Collaboration]: Phys. Rev. D **79**, 034503 (2009), arXiv:0807.1661 [hep-lat].

[†] Condensed from the previously published article¹⁾.

W-Boson Production by Polarized p+p Collisions at $\sqrt{s} = 500$ GeV

K. Karatsu^{*1} from the PHENIX Collaboration

[nucleon spin, W-boson, polarized parton distribution]

Although the polarizations of valence quarks have been determined well by DIS (Deep Inelastic Scattering) and Semi-Inclusive DIS¹⁾, large uncertainty about the polarization of sea quarks still exists. One of the main objectives at RHIC involving polarized p+p collisions is to measure the polarization of sea quarks by producing W bosons²⁾. The single-spin asymmetry (A_L) in W -boson production is a clear indication of the polarization of sea quarks since the chirality of the interacting quarks is conserved in the V-A coupling. It is also possible to identify the flavor of the sea quarks by the charge-separated measurement of W^+/W^- ³⁾.

PHENIX⁴⁾ is a detector system that is capable of measuring leptons produced by W decay at midrapidity ($|\eta| < 0.35$, PHENIX central arms) and forward rapidity ($1.2 < |\eta| < 2.4$, PHENIX muon arms).

The run held in 2009 at RHIC (RHIC Run9) is the first collisions with $\sqrt{s} = 500$ GeV. This was also the first opportunity for PHENIX to measure significant amounts of W bosons. The first attempt to measure electrons produced by W decay was made using the PHENIX central arms, which are capable of good tracking and rejection of hadron background, along with drift chambers (DC) and electromagnetic calorimeters (EMCal).

In W decay, although the yields of pions (π^+ and π^-) exceed the yield of the electrons at the same p_T , as shown in Fig. 1²⁾, on the basis of the ratio of the deposited energy in the EMCal to the observed particle momentum (E/p cut), the pions are expected to be rejected by a factor of 100 since only a fraction of the total deposited energy is contributed by the pions. Additionally, an electron isolation cut, which requires no jet activity in the vicinity of the electron, is expected to reduce the pion background by a factor of 3 to 10. As a result of these two types of pion rejections, the electrons produced by W decay in the PHENIX central arms can be measured.

Fig. 2 shows the p_T spectra of raw yields obtained from RHIC Run9 data. The left plot shows the spectrum obtained without applying the isolation cut and the right shows the spectrum obtained by applying the isolation cut. These plots show that as expected, the isolation cut enhances the signal to background ratio of the W -decay electrons by reducing the hadron background by a factor of 3 to 5 (the E/p cut has been applied in both plots).

^{*1} Kyoto University, Kitashirakawa Oiwake-cho, Sakyo-ku, Kyoto 606-8502, Japan

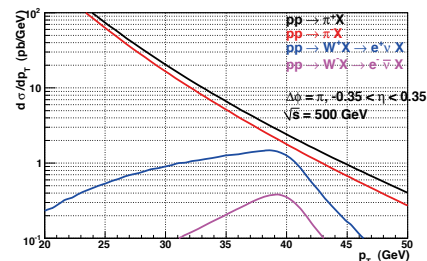


Fig. 1. Expected yields in the PHENIX central arms; e^- (purple) and e^+ (blue) are produced by W decay (data obtained using RHICBOS⁵⁾). π^+ (black) and π^- (red) are produced by other processes (data obtained by pQCD calculation). No particle identification was performed.

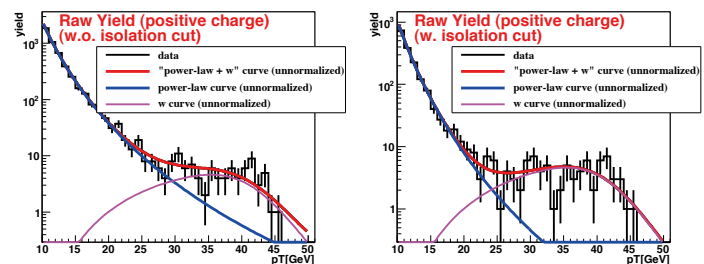


Fig. 2. Spectrum of raw yields of positively charged particles in high- p_T events ($p_T > 10$ GeV) (Left: without isolation cut, Right: isolation cut applied). The E/p cut has been applied in both plots. A power-law function (blue) and W curve from RHICBOS⁵⁾ (purple) are overlaid (unnormalized; curve obtained from RHICBOS is smeared).

Further analysis to calculate the cross section and the single-spin asymmetry of W -boson production is currently underway, and the results will provide the first direct measurement of sea-quark polarization.

References

- 1) D. de Florian, R. Sassot, M. Stratmann, and W. Vogelsang: Phys. Rev. Lett. 101:072001, (2008).
- 2) 2008 RHIC Spin Plan Report
- 3) G. Bunce, N. Saito, J. Soffer, and W. Vogelsang: Ann. Rev. Nucl. Part. Sci. **50**, 525 (2000).
- 4) PHENIX collaboration: Nucl. Instrum. Meth. **A 499**, 469 (2003).
- 5) P. M. Nadolsky and C. P. Yuan: Nucl. Phys. **B 666**, 31 (2003); hep-ph/0304002.

Application of a Pair of Solenoid Magnets in Beam Transport Line

Yoichi Sato,*¹ Jun-ichi Ohnishi, Nobuhisa Fukunishi, Akira Goto, and Hiroki Okuno

Solenoid pairs can be used to independently determine the rotation and focusing functions. In beam transport, a solenoid acts as a focusing and rotating lens element. A series of solenoid magnets, with drift spaces, can be used to cancel the rotation effect produced by these magnets, if their integrated magnetic flux is zero in the beam line. The beam emittance through these solenoids is decoupled horizontally and vertically. Such decoupling can be used in the muon-collider cooling channel¹⁻⁵). In addition to decoupling, multiple solenoids can be used to control transversely isotropic focusing without changing the total rotational angle. The use of multiple solenoids is convenient for a short transport line, and multiple solenoids can be used not only for the muon-collider but also for other types of beam lines, such as low energy beam transport (LEBT). In this paper, a very simple technique of using multiple solenoids, i.e., the use of a pair of identical solenoids is described; this technique is used in the design of LEBT for RIKEN's Radioisotope Beam Factory (RIBF) project. For a given injected beam, a pair of solenoids at a specific position has smaller bore diameters than a series of quadrupoles at the same position.

The 6×6 transfer matrix of a solenoid lens is the product of a rotation matrix and a focusing matrix, which are interchangeable. The rotation matrix and drift matrix are also interchangeable. Therefore, the transfer matrix of a series of two solenoids can be expressed as the product of a rotation matrix and a complex of a focusing matrix, a drift matrix, and a focusing matrix in series, as shown by the first-order transfer matrix of the series of two solenoids connected with drift space.

$$\begin{aligned}
 & R_{B,\text{sol}}(B_{B,\text{sol}}, L_{B,\text{eff}}) \otimes R_{\text{drift}} \otimes R_{A,\text{sol}}(B_{A,\text{sol}}, L_{A,\text{eff}}) \\
 &= (R_{B,\text{rot}} \otimes R_{A,\text{rot}}) \otimes (R_{B,\text{focus}} \otimes R_{\text{drift}} \otimes R_{A,\text{focus}}) \\
 &= R_{\text{rot}}(\theta_{\text{AB}}) \\
 &\otimes \begin{pmatrix} R_{11} & R_{12} & 0 & 0 & 0 & 0 \\ R_{21} & R_{22} & 0 & 0 & 0 & 0 \\ 0 & 0 & R_{33} & R_{34} & 0 & 0 \\ 0 & 0 & R_{43} & R_{44} & 0 & 0 \\ 0 & 0 & 0 & 0 & 1 & L_{\text{tot}}/\gamma^2 \\ 0 & 0 & 0 & 0 & 0 & 1 \end{pmatrix}, \quad (1)
 \end{aligned}$$

where $R_{\text{sol}}(B_{\text{sol}}, L_{\text{eff}}) = R_{\text{rot}} \otimes R_{\text{focus}} = R_{\text{focus}} \otimes R_{\text{rot}}$ is the solenoid matrix of magnetic field B_{sol} and effective length L_{eff} . R_{rot} and R_{focus} are the rotational component and focusing component, respectively, of the solenoid. The total rotational angle is $\theta_{\text{AB}} = K_A L_{A,\text{eff}} + K_B L_{B,\text{eff}}$, where $K_A = B_{A,\text{sol}}/(2B\rho_0)$,

$K_B = B_{B,\text{sol}}/(2B\rho_0)$, and $B\rho_0$ is the momentum rigidity of a beam. $L_{\text{tot}} = L_{A,\text{eff}} + L + L_{B,\text{eff}}$, where L is the drift space of R_{drift} . γ is the Lorentz factor. If $K_A K_B < 0$ and constant θ_{AB} , we can use the solenoids on a beam line as a focusing lens set with a fixed rotational angle around the beam axis. For example, a series of two identical solenoids, i.e., *pair solenoids*, with equal current in opposite directions has no rotational components, and the horizontal and vertical directions are decoupled since $B_{A,\text{sol}} = -B_{B,\text{sol}} = B_{\text{sol}}$ and $L_{A,\text{eff}} = L_{B,\text{eff}} = L_{\text{eff}}$ owing to which $\theta_{\text{AB}} = 0$.

The new injector of the RIBF project, RILAC2, is under construction and is designed to produce high-intensity uranium ion beam by late 2010⁶⁻⁸). The LEBT of RILAC2 is the beam transport line from the 28 GHz superconducting electron cyclotron resonance ion source (ECRIS) to the entrance of the radio-frequency quadrupole (RFQ), and this beam transport line has been designed to include two sets of pair solenoids. In Fig. 1, SOL12 and SOL34 are the pair solenoids. Figure 2 shows their layouts. The pair solenoids are used to reduce the beam diameter as the beam passes from SOL12 to the RFQ. In each solenoid pair, the two solenoids have equal current with opposite directions: this helps in the decoupling of beam emittances. The decoupling feature enables us to control the downstream elements on the basis of the projected diagnostics, as measured upstream of the pair solenoids. The four quadrupoles between SOL12 and SOL34 are used only for matching the beam with RFQ acceptance. In LEBT, the only horizontal and vertical coupling lens elements are the solenoids of the ECRIS and the solenoid SOL0 following the ion source.

In addition to decoupling feature for emittance, pair solenoids can be used to achieve a smaller beam radii in the magnets than that achieved by using the quadrupoles. Figure 3 shows the beam envelopes for a pair solenoids and quadrupole magnets under identical initial conditions in the RILAC2 LEBT design. The quadrupoles are needed to match the beam emittances with the acceptance of the RFQ and the buncher. The beam radii are reduced to half by introducing another pair of solenoids. For beam matching, the pair solenoids can be substituted by a series of quadrupoles, but these quadrupoles require large bore diameters, thereby, increasing the cost. Moreover, merely increasing the number of quadrupoles cannot help reduce the beam radii effectively. In general, for a quadrupole, the beam size in its defocusing direction is larger than that for a solenoid pair.

The aberration produced by the pair solenoids in the RILAC2 LEBT is simulated by 3D tracking calcu-

*1 yoichi.sato@j-parc.jp, yoichisato@riken.jp

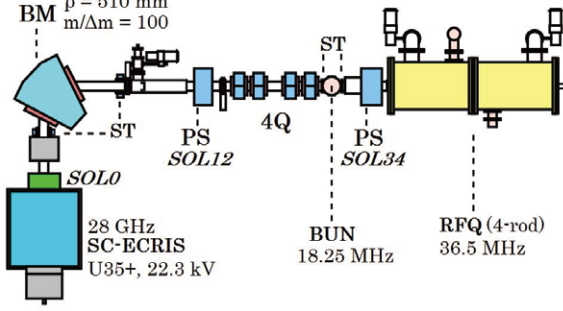


Fig. 1. Layout of RILAC2 LEPT. The 28 GHz superconducting ECRIS produces U^{35+} ions with an accelerating voltage of 22.3 kV. *SOL0* is a single solenoid right after the exit of the ECRIS. *SOL12* is the first set of pair solenoids, and *SOL34* is the second set of pair solenoids. There is a diagnostics chamber in front of each set. The abbreviations BM, PS, ST, 4Q, BUN, and RFQ represent the analyzing bending magnet, a set of pair solenoids, a steering magnet, a series of four quadrupoles, a buncher first harmonic: 18.25 MHz, and an RFQ second harmonic: 36.5 MHz.

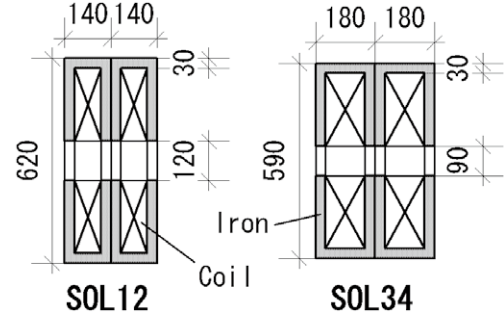


Fig. 2. Layout of pair solenoids. SOL12 has a 120 mm bore diameter, and SOL34 has a 90 mm bore diameter.

lations. SOL12 may produce a 6% emittance growth, but this value is acceptable in the design of RILAC2 LEPT. SOL34 may not produce any substantial aberration.

In the LEPT design, it is suitable to use the pair solenoids downstream a long drift space, e.g., a series of diagnostics, for operating downstream lens elements with small apertures. In the RILAC2, a strongly focused beam is required at the entrance of the RFQ. The RFQ and following linac line have 45° inclined quadrupoles. By setting SOL34 between the 45° inclined diagnostics and the RFQ, the linac can be controlled easily.

We express special thanks to M. Fujimaki, Dr. Y. Higurashi, E. Ikezawa, Dr. O. Kamigaito, M. Kase, Dr. T. Nakagawa, H. Watanabe, Dr. Y. Watanabe, and S. Yokouchi.

References

- 1) J. Gallardo et al.: Proc. the 1999 Particle Accelerator Conf., New York, USA, 1999, p. 3032.
- 2) H. Kirk: Presented at the Mini-Workshop on Ionization Cooling, 1998.
- 3) R. Fernow: Proc. the 1999 Particle Accelerator Conf., New York, USA, 1999, p. 3020.
- 4) V. Balbekov et al.: MUCOOL Note 125 (2000).
- 5) D. Neuffer: Nucl. Instr. and Meth. A **532**, 26 (2004).
- 6) O. Kamigaito et al.: Proc. PASJ6, Tokai, Japan, 2009, p. 38.
- 7) T. Nakagawa et al.: Presented at International Conference on Ion Sources, Gatlinburg, USA, 2009.
- 8) Y. Sato et al.: Proc. PASJ6, Tokai, Japan, 2009, p. 801.

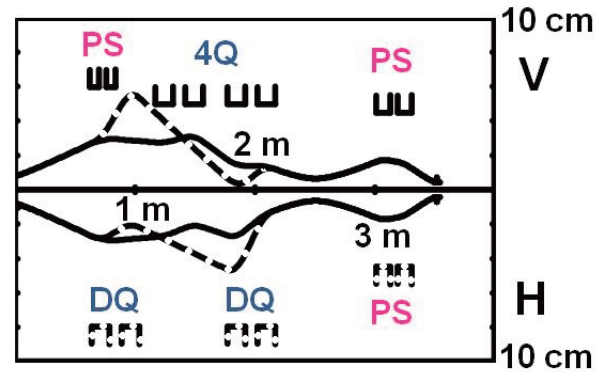


Fig. 3. Beam envelopes from the analyzing slit to the RFQ entrance in RILAC2 LEPT. The upper half shows vertical beam envelopes, and the lower half shows horizontal beam envelopes. The beam comprises U^{35+} ions, the acceleration voltage is 22.3 kV, and the horizontal and vertical emittance values are 200π mm·mrad. The solid lines indicate the beam envelopes for the case in which pair solenoids are placed right after the slit. The effective length and bore diameter of the lens elements are indicated by the solid marks in the upper half. The dashed lines indicate the beam envelopes for the case in which four quadrupole magnets are placed right after the slit. The effective length and bore diameter of the lens elements are indicated by the dashed marks in the lower half. In both cases, pair solenoids are used in front of the RFQ entrance. The beam envelopes for both cases are superposed.

Measurement of charge-state distribution of uranium and xenon beams with a gas charge stripper

H. Kuboki, H. Okuno, S. Yokouchi, T. Kishida, H. Hasebe, N. Fukunishi, O. Kamigaito, M. Kase, A. Goto, and Y. Yano

Charge strippers are essential components in a heavy-ion accelerator complex such as the RIKEN RI Beam Factory (RIBF)¹ since heavy ions in a high charge state can be efficiently accelerated at a small facility. At the RIBF, two strippers are used for the acceleration of uranium (^{238}U) ions with energies up to 345 MeV/nucleon². The first and second strippers, which are carbon foils with thicknesses of 0.3 mg/cm² and 17 mg/cm²³, are located downstream of the RRC and fRC, respectively. The energies of ^{238}U ions incident on each stripper are 10.75 and 51 MeV/nucleon. It should be noted that there are two serious problems associated with the first stripper. One is its short lifetime that is a consequence of the heat load during irradiation, and the other is the energy spread resulting from the nonuniformity of the foil thickness⁴.

We have developed a gas stripper that is a candidate for a long-lifetime stripper with uniform thickness. However, we could not predict whether the charge states obtained with a gas stripper would be acceptable for the fRC since charge states of heavy ions like ^{238}U or xenon (^{136}Xe) in gaseous media have not been studied well at energies around 10 MeV/nucleon. Therefore, the charge-state distributions of ^{238}U and ^{136}Xe ions with an energy of 10.75 MeV/nucleon in a gas stripper were measured as functions of the gas pressure up to its equilibrium charge-state distribution. The use of a differential pumping system with a target cell and five pumping stages^{4,5} made it possible to enhance the nitrogen (N_2) gas thickness up to 0.9 mg/cm², which was considered to be sufficient to obtain equilibrium charge states, taking into account that the carbon foil thickness for equilibrium is ~ 0.5 mg/cm²². The thickness of the gas stripper was calculated from the measured gas pressure in the target cell by assuming the longitudinal length of the gaseous medium to be equal to the cell length (10 cm).

The charge-state distribution measurements were carried out as follows: ^{238}U and ^{136}Xe ion beams with charge states of 35+ and 20+ were obtained from the 18 GHz ECR ion source and accelerated up to 10.75 MeV/nucleon with the RILAC and RRC. The beams were transported to the gas stripper located upstream of the fRC, as shown in Fig. 1. The beam currents incident on the gas stripper were measured at Faraday cup D16 (FC-D16) and were typically 300~500 enA (9~14 particle nA) for ^{238}U and 500~600 enA (25~30 particle nA) for ^{136}Xe . The spot diameter was about 6 mm, which was comparable to the orifice at the gas stripper entrance. Beams in dif-

ferent charge states emerged from the gas stripper. A beam in one charge state was selected and channeled downstream of the dipole magnets DAD4 and DMD4, and the magnetic fields were corrected for the energy loss in the gas. Beam currents of ^{238}U or ^{136}Xe in the selected charge state were measured with Faraday cup F41 (FC-F41) downstream of DMD4.

The fraction $F(q_i)$ of a charge state q_i is defined

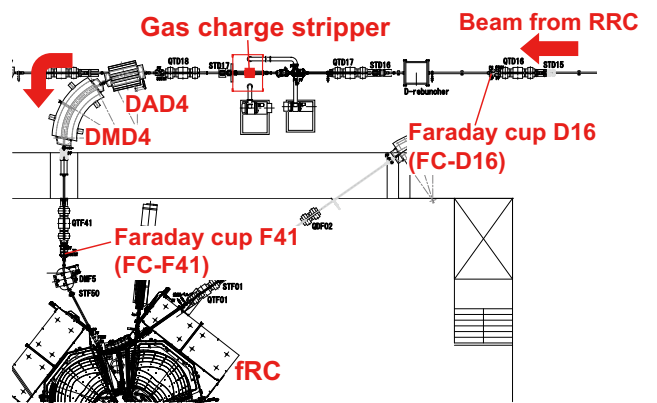


Fig. 1. Schematic view of the charge-state distribution measurement. Please see the text for details.

as $F(q_i) = \frac{I_{F41}/q_i}{I_{D16}/q_{ini}}$, where I_{F41} , I_{D16} , and q_{ini} denote the beam currents at FC-F41 and FC-D16, and the charge state of the beam obtained from the ion source, respectively.

The charge-state distributions of ^{238}U and ^{136}Xe

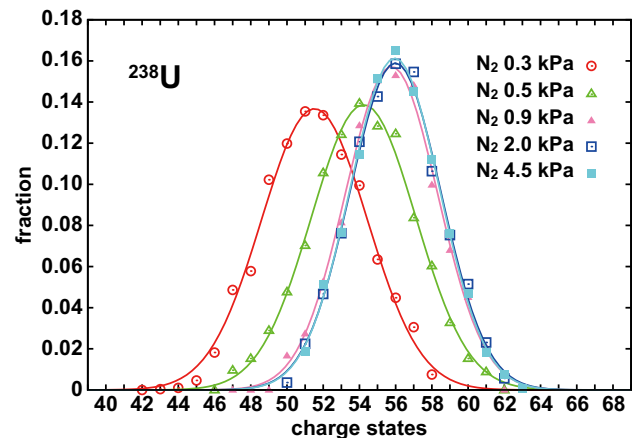


Fig. 2. Charge-state distribution of ^{238}U . The data obtained for gas pressures of 0.3, 0.5, 0.9, 2.0, and 4.5 kPa are denoted by open circles, open triangles, solid triangles, open squares, and solid squares, respectively.

Table 1. Obtained parameters of ^{238}U (left) and ^{136}Xe (right) charge-state distributions. The gas species is N_2 .

^{238}U				^{136}Xe			
pressure (kPa)	peak height	center	σ	pressure (kPa)	peak height	center	σ
0.3	0.137	51.52	2.92	0.3	0.189	35.74	2.11
0.5	0.139	54.23	2.87	0.3	0.178	36.10	2.24
0.9	0.158	55.76	2.53	0.5	0.184	38.48	2.16
2.0	0.159	55.99	2.51	0.9	0.199	40.07	2.01
4.5	0.161	55.95	2.47	2.0	0.207	40.59	1.93
				4.5	0.209	40.51	1.91

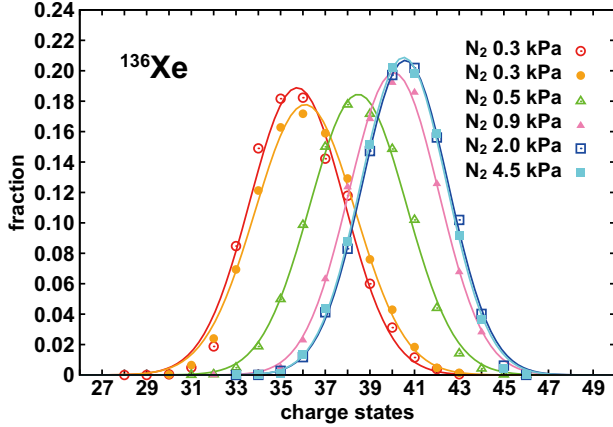


Fig. 3. Charge-state distribution of ^{136}Xe . The data obtained for gas pressures of 0.3, 0.5, 0.9, 2.0, and 4.5 kPa are denoted by open circles, solid circles, open triangles, solid triangles, open squares, and solid squares, respectively.

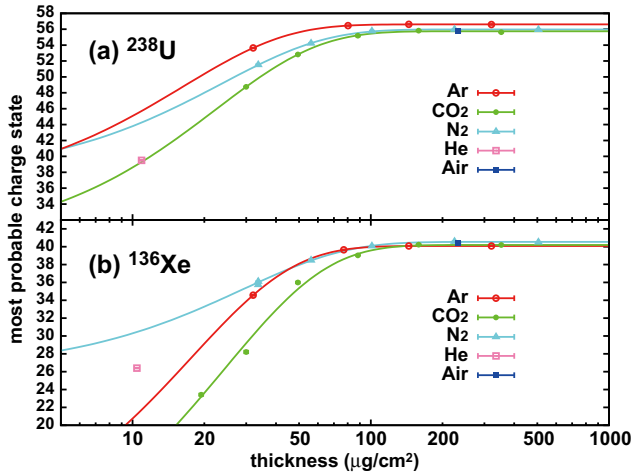


Fig. 4. Most probable charge states are plotted as a function of the gas thickness. Panels (a) and (b) present data of ^{238}U and ^{136}Xe , respectively.

obtained by changing the gas pressure in the target cell are shown in Figs. 2 and 3, respectively. The charge-state distribution data are fitted by a Gaussian function. The most probable charge state is defined

as the center value of the Gaussian function. All fitted parameters are tabulated in Table 1. The most probable charge states with values of 56.0 and 40.5 correspond to the equilibrium charge states for ^{238}U and ^{136}Xe , respectively. It is noticeable that the equilibrium charge states of ^{136}Xe obtained with the gas stripper are acceptable for fRC acceleration. The most probable charge states are plotted as a function of the gas thickness in Fig. 4. The data of Ar, CO_2 , He, and air are plotted together with those of N_2 . We have one datum for He and air. The data are fitted by the function $f(t) = a - b \exp(-ct)$, where t is the gas thickness and a , b , and c are parameters to be determined. The thickness necessary for equilibrium is calculated by using $f(t)$ and is found to be 59, 86, and 83 $\mu\text{g}/\text{cm}^2$ in the case of Ar, CO_2 , and N_2 , respectively. As for ^{136}Xe , the thicknesses necessary for equilibrium are 78, 111, and 104 $\mu\text{g}/\text{cm}^2$. These values are far less than that of carbon foil. This fact indicates that there are differences in the physical process of charge-stripping between a gas stripper and a solid stripper. Investigation of these differences is currently in progress.

We plan to measure the charge-state distributions of ^{238}U at different energies in the near future.

References

- 1) Y. Yano: Nucl. Instr. Meth. B **261**, 1009 (2007).
- 2) H. Ryuto, H. Hasebe, S. Yokouchi, N. Fukunishi, A. Goto, M. Kase, and Y. Yano: Proc. of 18th Int. Conf. on Cyclotrons and Their Applications, Catania, Italy, 2007, p. 314.
- 3) H. Hasebe, H. Ryuto, N. Fukunishi, A. Goto, M. Kase, Y. Yano: Nucl. Instr. Meth. A **590**, 13 (2008).
- 4) H. Kuboki, H. Okuno, S. Yokouchi, T. Kishida, H. Hasebe, N. Fukunishi, O. Kamigaito, H. Ryuto, M. Kase, A. Goto, Y. Yano: RIKEN Accel. Prog. Rep. **42**, 135 (2009).
- 5) T. Kishida, Y. Gono, M. Shibata, H. Watanabe, T. Tsutsumi, S. Motomura, E. Ideguchi, X.H. Zhou, T. Morikawa, T. Kubo, M. Ishihara: Nucl. Instr. Meth. A **438**, 70 (1999).

Pressure-induced new magnetic phase in $\text{Tl}(\text{Cu}_{0.985}\text{Mg}_{0.015})\text{Cl}_3$ probed by muon spin rotation

T. Suzuki, I. Watanabe, F. Yamada,*¹ M. Yamada,*¹ Y. Ishii, T. Kawamata, T. Goto,*² and H. Tanaka,*¹

[spin gap, impurity, crossover, magnetic order, pressure]

In impurity-introduced spin gap system $\text{Tl}(\text{Cu}_{1-x}\text{Mg}_x)$ the magnetic phase transition to an ordered state is observed by magnetization and specific heat measurements; neutron elastic scattering measurements identified that this impurity-induced ordered state is an antiferromagnetically ordered state in which the magnetic structure is the same as that in the case of the field-induced phase in TlCuCl_3 ¹). The inelastic neutron scattering measurement revealed that a finite spin gap still remains below the transition temperature²). Imamura *et al.* reported a pressure-induced magnetically ordered phase by magnetization measurements for $x = 0.012$, and concluded that the change from the impurity-induced phase to the pressure-induced phase is a crossover³). The purpose of this study is to investigate the microscopic properties of the pressure-induced phase in the impurity-doped spin gap system by zero-field muon spin rotation (ZF- μ SR).

Single crystals were grown from a melt by the Bridgman method. μ SR measurements in hydrostatic pressures were carried out using a spin-polarized double-pulsed positive decay-muon beam with an incident muon momentum of 90 MeV/c. The samples were pressurized by ⁴He gas pressure in a CuBe cell using the newly installed gas-pressurized μ SR setup of the RIKEN-RAL Muon Facility⁴).

Figure 1(a) shows the temperature dependence of the ZF- μ SR time spectra in a hydrostatic pressure of 3.1 kbar. Measurements were carried out with decreasing temperature. Below 8 K, the spontaneous muon-spin-precession is observed, which indicates the existence of a coherent long-range magnetically ordered state. The observed transition temperature in the pressure of 3.1 kbar is consistent with the temperature reported in the same pressure for the case of $x = 0.012$ deduced from the magnetization measurement³). In order to discuss the development of the internal static magnetic field at the muon sites which corresponds to the ordered Cu-3d magnetic moment, all spectra are analyzed using the two components function as follows: $A(t) = A_1 e^{-\lambda_1 t} \cos(\omega t + \theta) + A_2 e^{-\lambda_2 t} G_z(\Delta, t)$. The first term is the signal from the magnetically ordered region of samples, and the second term is that from the large pressure cell and the spin-fluctuating region of samples. λ_1 and λ_2 are the muon-spin-relaxation rate of each component, and ω is the muon-spin-rotation frequency.

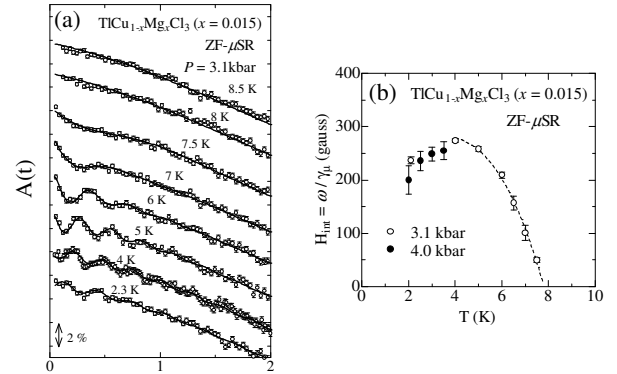


Fig. 1. (a) Time spectra of the ZF- μ SR in the hydrostatic pressure of 3.1 kbar. Solid lines are fitted results. Each plot is shifted consecutively for clarity. (b) Temperature dependence of H_{int} at 3.1 kbar and at 4.0 kbar. Dashed line is a guide for the eye.

$G_z(\Delta, t)$ is the static Kubo-Toyabe function. Fitted results are shown in Fig.1(a) as solid lines. From the fitted result, the internal static magnetic field H_{int} at the muon sites is deduced using the relation of $\omega = \gamma_\mu H_{\text{int}}$ because implanted muon spins precess around the total magnetic field, including the internal field and the external field, at the muon sites. The deduced internal static magnetic field $H_{\text{int}} = \omega/\gamma_\mu$ at the muon sites are summarized in Fig.1(b). With decreasing temperature at 3.1 kbar, H_{int} increases monotonously, and tends to saturate to 280 gauss around 4 K. However, H_{int} decreases to 240 gauss at 2.3 K. Similar decrease of H_{int} below 4 K is observed at 4.0 kbar. The decrease of H_{int} suggests an orientation of the ordered moments, because the change of the magnetic structure leads to the modification of dipole fields at the muon sites. Thus, we speculate that a spin-reorientation phase transition occurs and that an oblique antiferromagnetic phase, which is observed at the pressure of 14 kbar in pure TlCuCl_3 ⁵), appears in the Mg-doped system. In the case of Mg-doped system, it is expected that the pressure-induced new phase would appear at a pressure lower than that at which it appears in the case of pure system, because the spin gap has already partially collapsed in space due to the Mg doping.

References

- 1) M. Fujisawa *et al.*, J. Phys. Soc. Jpn. **75** (2006) 033702.
- 2) A. Oosawa *et al.*, Phys. Rev. B **67** (2003) 184424.
- 3) H. Imamura *et al.*, Phys. Rev. B **74** (2006) 064423.
- 4) I. Watanabe *et al.*, Physica B **404** (2009) 993.
- 5) F. Yamada *et al.*, Phys. Rev. B **78** (2008) 224405.

† Condensed from the proceedings of ASR2009

*¹ Department of Physics, Tokyo Institute of Technology

*² Faculty of Science and Technology, Sophia University

Characterization of Spin-Dependent Response of Negative Muonium (Mu^-) to Laser Induced Polarized Electrons in n -Type GaAs under Zero Field

K. Yokoyama¹, K. Nagamine^{1,2}, K. Shimomura², H.W.K. Tom¹, R. Kawakami¹, P. Bakule³,
Y. Matsuda⁴, K. Ishida, K. Ohishi, F.L. Pratt³, I. Shiraki⁵ and E. Torikai⁵

In the field of the spintronics, the consideration of spin-dependent exchange scattering of a polarized electron in ortho-muonium (ortho- Mu , μ^+e^- , a bound state of a positive muon and an electron with the spins aligned in the same direction) has been proposed to detect the conduction electron spin polarization (CESP) in semiconductors [1]. Recently, a feasibility study of this muon method was successfully carried out in strain-free n -type GaAs containing $3 \times 10^{16} \text{ cm}^{-3}$ Si by measuring the change in the μ^+ polarization corresponding to a change in the polarization direction under both longitudinal fields (LF) and zero field (ZF) [2]. In the study, CESP was induced by circularly polarized (CP) lasers.

The muon states in doped GaAs have been studied. The existence and properties of Mu^- ($\mu^+e^-e^-$, a diamagnetic bound state of μ^+ that contains two singlet electrons) in n -type GaAs with Si doping higher than 10^{16} are known [3].

Following a report [2], the present measurement was conducted at Port 2 of the RIKEN-RAL by using a pulsed 4-MeV positive muon beam. Tunable laser light of a wavelength of around 831 nm and a repetition frequency of 25 Hz was generated using a widely tunable OPO system. The linearly polarized laser output light was converted to CP light to illuminate the sample. A Pockel's cell (PC) was used for pulse-to-pulse switching between right-hand CP light ("Anti") and left-hand CP light ("Para"). A 10 ns laser pulse was irradiated at 0.9 μs after the muon pulse.

Asymmetry amplitudes of the ZF "Off" at 15 K are known to correspond mainly to Mu^- state with Gaussian relaxation (5.7%). Due to spin exchange reactions with doped electrons in n -GaAs, the 1/6 component of BC-Mu (Mu at body-center site, nearly 1.0%) shows exponential relaxation (rate; 1 μs) and that of T-Mu (Mu at tetrahedral site, nearly 1.0%) shows a rapid relaxation (within 1 ns).

In the ZF "Para-Anti" effect (Fig. 1), the major characteristic of the Mu^- state changes with a change of CP of the laser irradiation, while the BC-Mu is insensitive to the laser irradiation. To study the Mu^- response to laser-induced CESP, the followings were investigated: 1) the laser wavelength dependence, 2) laser-power dependence of the response and 3) the time-delay characteristic of the muon response.

A clear wavelength dependence reflecting the bandgap characteristics was found (Fig. 1), suggesting that the Mu^- response was due to the laser-induced CESP.

As seen in Fig. 2, an inverse power dependence was seen in "Para-Anti"/"Off-On", which is consistent with the spin lifetime measured in optical measurement [4]. Precise time spectrum measurement showed a slow (33(13) ns) "Para" response, in contrast to a fast (5.5(2.6) ns) "Anti" one.

In order to understand the observed spin-dependent Mu^- response, in addition to a possible multistep process, the admixture of the d-states due to symmetry of the interstitial site of the Mu^- state should be studied theoretically [5]. Work on this line is currently in progress.

[1] E. Torikai *et al.*, *Physica B* **289-290** (2000) 558-562.

[2] K. Yokoyama *et al.*, *RIKEN-APR* **42** (2008) 234-235.

[3] K.H. Chow *et al.* *Semicon. and Semimetals* **51a** (1997)137.

[4] J.M. Kikkawa *et al.*, *Phys. Rev. Lett.* **80** (1998) 4313-4316.

[5] S. Maekawa, *private communication* (2009).

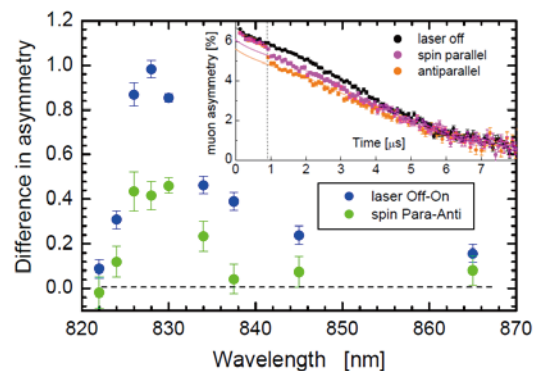


Fig.1. Laser wavelength dependence of the "Off-On" and "Para-Anti" effects with the μSR amplitude at $t = 0$. A typical time spectrum is shown in the inset.

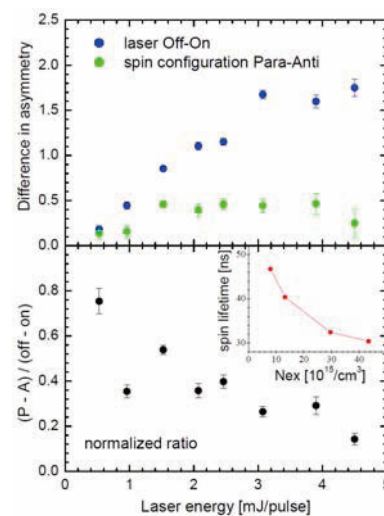


Fig. 2 (Upper) Laser power dependence of the "Off-On" and "Para-Anti" effects. (Lower) Laser power dependence of normalized "Para-Anti" and "Off-On" effects

¹Physics & Astronomy, University of California, Riverside

²Muon Science Laboratory, IMSS, KEK

³ISIS, Rutherford Appleton Laboratory

⁴Arts and Science, University of Tokyo

⁵Medicine and Engineering, University of Yamanashi

C O N T E N T S

Page

GRAVURES & HIGHLIGHTS OF THE YEAR

Construction of electron accelerators	i
Formation of Nuclear “Pasta” in Supernovae	iii
Numerical evaluation of gauge invariants for a-gauge solutions in open string field theory	v
Localization of γ H2AX Fluorescence along Tracks of Argon Beams	vii
α -fine structure spectroscopy for ^{257}Lr and ^{259}Lr	ix
In-beam γ -ray spectroscopy of ^{32}Ne	x
Complete Set of Deuteron Analyzing Powers for dp Elastic Scattering at 250 MeV/nucleon and Three-Nucleon Forces	xi
Negative-parity excitations unique in deformed neutron-rich nuclei close to the drip line	xii
Lattice QCD study of ΛN interaction	xiii
W -Boson Production by Polarized p+p Collisions at $\sqrt{s} = 500$ GeV	xiv
Application of a Pair of Solenoid Magnets in Beam Transport Line	xv
Measurement of charge-state distribution of uranium and xenon beams with a gas charge stripper	xvii
Pressure-induced new magnetic phase in $\text{Tl}(\text{Cu}_{0.985}\text{Mg}_{0.015})\text{Cl}_3$ probed by muon spin rotation	xix
Characterization of Spin-Dependent Response of Negative Muonium (Mu^-) to Laser Induced Polarized Electrons in n -Type GaAs under Zero Field	xx
I. PREFACE	1
II. RESEARCH ACTIVITIES I (Nuclear-Particle Physics)	
1. Nuclear Physics	
Measurement of interaction cross sections of Ne Isotopes	3
Inelastic scattering of ^{32}Mg at RIBF beam energies on various targets	4
Rates of production of fission fragments from a ^{238}U beam at 345 MeV/nucleon	5
Study on the isomer ratios of fission products of 345 MeV/u ^{238}U	6
Measurement of the $(t, ^3\text{He})$ reaction at 300 MeV/nucleon	7
Angular distribution for the $^8\text{He}(d,t)^7\text{He}_{g.s.}$ reaction	8
Breakdown of the $Z = 8$ shell closure in unbound ^{12}O	9
Measurement of unbound excited states of ^{24}O	10
Beta decay of the proton-rich nucleus ^{24}Si and its mirror asymmetry	11
Measurement on proton-proton correlation of the excited ^{23}Al	12

Persistent decoupling of valence neutrons toward the drip line: Study of ^{20}C by γ spectroscopy	13
Spin-Orbit Potentials of Neutron-Rich Helium Isotopes	14
Elastic scattering for 60MeV ^{17}F on ^{12}C target	15
Experiment to determine the g -factor of neutron-rich S isotope	16
Coulomb excitation of ^{36}Ca	17
Experimental investigation of stellar $^{30}\text{S}(p,\gamma)^{31}\text{Cl}$ reaction by Coulomb dissociation method	18
Branching ratio of γ to particle decay in 1.6-MeV state of ^{23}Al	19
Precision measurement of the hyperfine constant of $^{11}\text{Be}^+ \text{-II}$	20
Determination of nuclear charge radii of Be isotopes by precision optical spectroscopy of trapped ions	21
Development of CDCC program and its use to calculate momentum distribution in elastic breakup reaction	22
Measurement of reaction cross section for ^{11}Li using solid hydrogen target	23
The change about the number of trapped ions in the SCRIT experiment	24
Proton elastic scattering by ^9C beam with E/u of 290 MeV	25
Energy Dependence of π^-/π^+ Ratio Observed in $\text{In}+^{28}\text{Si}$ Reaction	26
Study of time-reversal symmetry in $^8\vec{\text{Li}}$ using tracking detector	27
New neutron-deficient actinide isotopes of ^{234}Bk and ^{230}Am	28
First Quantitative Study of Resonance Scattering of α -particles Using a ^{21}Na Radioisotope Beam	29
Progress in ^{30}S Beam Development for a Measurement of $^4\text{He}(^{30}\text{S},p)$	30
New measurement of resonance scattering of alpha particles on ^7Li	31

2. Nuclear Physics (Theory)

Subsystem correlations in Coulomb breakup reaction of ^6He	33
One-neutron removal strength of ^7He into ^6He using the complex scaling method	34
Five-body resonances of ^8He using the complex scaling method	35
Gamow-Teller transitions from $^{9,11}\text{Li}$ to $^{9,11}\text{Be}$	36
Systematic study of adiabatic-energy surfaces of Be isotopes	37
Study of $A = 7$ isotiplet Λ hypernuclei with the four-body cluster model	38
Shell-model study of Σ -mixing in hypernuclear isotopes	39
Complex-scaled CDCC method for nuclear breakup reactions	40
Long-Range Correlations and the Quenching of Spectroscopic Factors	41

Contribution of core polarization for electric quadrupole moments of neutron-rich nuclei in the island of inversion	42
Clustering and superdeformation in <i>sd</i> -shell region	43
Examination of non-monotonic shell evolution beyond $N = 28$ on the basis of the β -decay of K isotopes	44
Shell-model description of $N=Z$ pfg-shell nuclei	45
Newly developed program for the Monte Carlo shell model	46
Microscopic description of oblate-prolate shape mixing in proton-rich Se isotopes	47
Effects of Oblate-Prolate Symmetry Breaking on Triaxial Deformation Dynamics	48
Analysis of ^{78}Ge by generator coordinate method	49
Simple-model analysis of doublet bands in doubly odd nuclei	50
Linear Response Calculation Using Canonical-basis TDHFB with a Schematic Pairing Functional	51
Finite Amplitude Method for QRPA	52
Chemical potential beyond quasiparticle mean field	53
Canonical ensemble treatments of pairing in nite systems	54
Top-on-top mechanism for TSD bands in even mass nuclei	55
SU(3) symmetry in anisotropic harmonic oscillator	56
Investigation of <i>t</i> -band in ^{182}Os by GCM	57
Global fitting of pairing density functional	58
Mass-number dependence of total reaction cross sections in the black-sphere approximation	59
Holographic Nuclei	60
Critical velocity of superfluid flow through single barrier and periodic potentials	61
Contribution of Nuclear Reaction Data Centre to RIKEN Nishina Center	62

3. Hadron Physics

Gluon-Spin Contribution to the Proton Spin from the Double-Helicity Asymmetry in Inclusive π^0 Production in Polarized $p + p$ Collisions at $\sqrt{s} = 200$ GeV	63
Measurements of transverse single-spin asymmetry of single electrons from open heavy flavor decays in polarized $p + p$ collisions at $\sqrt{s} = 200$ GeV at PHENIX	64
Measurement of direct photon using virtual photon method in $\sqrt{s} = 200$ GeV d+Au collisions at RHIC-PHENIX	65
Azimuthal angle dependence of neutral pion suppression in $\sqrt{s_{NN}} = 200$ GeV Au+Au collisions at RHIC-PHENIX	66

Systematic Measurement of ω Mesons in p+p, d+Au, and A+A Collisions at $\sqrt{s_{NN}} = 200$ GeV at RHIC-PHENIX	67
Measurement of J/ψ production in ultra-peripheral Au+Au collisions at $\sqrt{s_{NN}} = 200$ GeV during RHIC RUN-7	68
Neutron asymmetry measurement with $\sqrt{s}=500$ GeV polarized proton collision at RHIC-PHENIX	69
Cosmic-ray background in PHENIX detector	70
Vernier Scan Method to Reduce Relative Luminosity Uncertainties	71
Method For Determining Relative Luminosity From Detection Probabilities	72
Installation and Tests of the PHENIX Muon Trigger RPCs	73
Upgrade of PHENIX Muon Tracker Performance and Trigger Capability for Sea Quark Polarization Measurement at RHIC	75
Performance evaluation of MuTRG for upgrading PHENIX muon trigger	76
Measurement of the interference fragmentation function in e^+e^-	77
Precision Measurements of Charged Hadron Multiplicities in e^+e^- Annihilation at BELLE	78
Photoproduction of $\Lambda(1405)$ and $\Sigma^0(1385)$ on the proton at $E_\gamma=1.5-3.0$ GeV at SPring-8/LEPS	79
E906 Drell-Yan experiment at Fermilab	80
A proposal to study medium mass modification of ϕ -mesons using ϕ -meson bound state in nucleus	81
Simulation study for the multiplicity Measurement in the Proton-Proton Collisions at the LHC	82
4. Hadron Physics (Theory)	
Nuclear Force from String Theory	83
Quark fragmentation functions in the NJL-jet model	84
Nucleon structure functions in 2+1-flavor dynamical DWF QCD	85
A first principles calculation of proton decay matrix elements	86
Quark masses from lattice QCD and QED	87
QCD phase structure in three-avor random matrix theory	88
Imaginary part of the real-time static potential at strong coupling	89
5. Particle Physics	
Tenth-order QED contributions to lepton $g - 2$	91
Color Magnetic Flux Tubes in Dense QCD	92
Scattering of Giant Magnons in CP^3	93

Gravitational Dual of Tachyon Condensation	94
Eschenburg space as gravity dual of avored $N=4$ Chern-Simons-matter theory	95
Genus-one correction to asymptotically free Seiberg-Witten prepotential from Dijkgraaf-Vafa matrix model	96
New Gauged Linear Sigma Models for 8D HyperKahler Manifolds and Calabi-Yau Crystals	97
Light-cone gauge string field theory in noncritical dimensions	98
Light-cone gauge NSR strings in noncritical dimensions	99
Light-cone gauge superstring field theory and dimensional regularization	100
Vacuum structure around identity-based solutions	101
Lattice formulation of 2D $N = (2, 2)$ SQCD based on B-model twist	102
SUSY WT identity in a lattice formulation of 2D $N = (2, 2)$ SYM	103

6. Accelerator

Conversion of RFQ linac for new RIBF injector	105
Design and construction of drift-tube linac no.1 for RILAC2	107
Design and Construction of Drift Tube Linac Cavities No. 2 and 3 for RILAC2	109
Construction of a new cavity for the double-rebuncher system for RRC	111
Construction of the RILAC2 (RIKE heavy-ion Linac 2) line	112
Production of highly charged U and Au ions from new RIKEN superconducting ECR ion source with sputtering method	114
Status of the new superconducting ECR ion source for RIKEN RIBF	116
Installation of new superconducting ECR ion source in the Cockcroft-Walton high- voltage terminal	117
Design of Low Energy Beam Transport in New RIKEN Injector	119
Design of Medium Energy Beam Transport for 127 kV U^{35+}	121
Construction of MEBT (Middle-Energy Beam Transport) line and acceleration test	123
Fabrication of thicker carbon foils with longer lifetime	125
Renovation of the central region of RIKEN AVF cyclotron and results of beam acceleration test	127
Possibility of formation of round beams in RIBF cyclotrons	129
Measurement of Magnetic Field of fRC Sector Magnets	131
Construction of Client System for 28GHz SC-ECRIS	133
Improvement of beam energy and longitudinal beam profile measurement system	135

Consistency in measurement of beam phase and beam intensity using lock-in amplifier and oscilloscope systems	136
Radiation monitoring in the RRC and the beam distribution corridor using ionization chambers.....	138
Water Cooling System in Accelerator for RIBF.....	140
Utilities in the RIBF experimental building	142
Calculation of Minimum Emittance in SR2	144
Capability of SR2 as a compact synchrotron radiation source	145
Magnetic plasma confinement for laser ion source	146
Effect of plasma drift distance on high current beam production in DPIS.....	147
Particle simulation for direct plasma injection in an RFQ matching section	148
Design research of laser ion source for RHIC-EBIS	149
Laser Beam Recycler with Asymmetric Confocal Cavity	150

7. Instrumentation

Status of the BigRIPS and ZeroDegree Project	151
Upgrading the BigRIPS target chamber	153
Status of the Control system of BigRIPS	155
Testing of Beam Viewer at BigRIPS	156
Measurement of field maps of superconducting quadrupole and sextupole magnets	157
Radiation-shielding system between the high-power beam dump and the second superconducting quadrupole triplet in the first stage of BigRIPS	159
Pillow seal around the beam dump of the BigRIPS	161
Radiation measurement around the BigRIPS	163
Separation of RI beams using two-stage separation method in BigRIPS	165
CCJ Operation in 2008-2009	167
SHARAQ Project: Progress in 2009	169
Construction of high resolution beam line for the SHARAQ spectrometer	171
Focus tuning method of the high-resolution beam line for the SHARAQ spectrometer.....	172
Focal Plane Detector System of SHARAQ Spectrometer	174
Development of Beamline Detectors for BigRIPS and High-Resolution Beamline.....	176
Current status of SAMURAI	178
Design of large-gap superconducting dipole magnet for SAMURAI spectrometer.....	180

Front-End Electronics for SAMURAI Si Detectors	182
Design study of equipment in Rare-RI Ring	184
Simulation of Particle Trajectories for RIKEN Rare-RI Ring	186
Second Report on Progress of the Portable Multi-Reflection Time-of-Flight Mass Spectrograph for SLOWRI	188
Status of the resonance ionization laser ion source at SLOWRI	190
Test report on primary beam dispersion matching at RIBF.....	191
Performance evaluation of Low-Pressure Multi-Wire Drift Chamber for RI beam	192
Development of ionization chamber for superheavy elements	194
Power spectrum detected by ion beam core monitor	195
Lithium doped Glass Scintillators for Low Energy Neutron Detection.....	196
Pulse structure dependence of the proton polarization rate	197
New method of pulse shape analysis for segmented Ge detectors by using moments	199
PHENIX silicon vertex tracker project	201
Silicon Pixel Detector for PHENIX Vertex Tracker	202
QA test bench for the PHENIX silicon pixel detector	204
Development of wire bonding electrical-short checker for silicon pixel ladder in the PHENIX vertex tracker	206
Quality assurance test of silicon pixel ladder for RHIC-PHENIX.....	208
Use of time-domain reflectometry for impedance measurement of fine-pitch and low-material-budget readout bus of the PHENIX pixel detector	210
GEM detectors for the experiment to measure the mass modification of vector mesons in nuclei at J-PARC	212
Development of a thick-GEM TPC for the J-PARC E15 experiment.....	214
Development of Cylindrical Detector System (CDS) for J-PARC E15 Experiment	215
Development of a Cylindrical Drift Chamber for an experimental search for K^-pp bound states at J-PARC	216
Development of a Hadron Blind Detector for the J-PARC E16 Experiment	217
Design and Construction of Station-3 Drift Chamber for FNAL-E906 Experiment	219
Computing and Network Environment at RIKEN Nishina Center	221
Time-Stamping System for RIBF experiments.....	222
Development of data acquisition system for short-time decay by using Flash ADC	224
Simple multichannel DAC, ADC, and interface for remote control from multiple computers	226

Installation of MuTRG-MRG and DCMIF and Confirmation of Stable Operation during Data Acquisition.....	228
III. RESEARCH ACTIVITIES II (Material Science and Biology)	
1. Atomic and Solid State Physics (ions)	
Single-Event Transient Test Results of Control IC of Point-of-Load DC/DC Converter	229
Feasibility of RI-beam-based wear analysis for industrial materials	230
In-beam Mössbauer experiment on stress-induced iron diffusion in silicon	231
Improvement in sensitivity of sensors for H ₂ and toxic-gas detection by using ePTFE irradiated with 5-MeV/nucleon ¹⁴ N beam	232
Irradiation-Induced Site Change of Hydrogen in Niobium	233
Simple simulation method for characterization of ion Coulomb crystals in a linear Paul trap.....	234
Excitation spectrum of Au atoms in superfluid helium	235
2. Atomic and Solid State Physics (muon)	
Installation and beam commissioning of new multi-channel μ SR spectrometer "CHRONUS" and beam commissioning at RIKEN-RAL	237
Data Acquisition System for μ SR Experiment at Port-4 of RIKEN-RAL Muon Facility	238
Development of a new Lyman- α laser for generation of ultraslow muons	239
Studies on Muon Spin Relaxation of n-Si Conduction Electrons Produced in <i>p</i> -GaAs Overlayer by Lasers and Injected by Electrical Method.....	240
New Measurements of the Chemical Reaction Rate of Muonium with Stimulated Raman-Pumped H ₂ [*] ($\nu=1$)	241
Study on the pressure-induced charge-transfer phase transition in (C ₅ H ₁₁) ₄ N[F _e ^{II} F _e ^{III} (C ₂ S ₂ O ₂) ₃] by means of μ SR spectroscopy.....	242
Investigating the role of protons in the unusual muon-spin relaxation of single molecule magnets	243
Muon-spin rotation and relaxation on the one-dimensional coordination polymer magnet [Co(hfac) ₂ •HNN] (HNN = hydro nitronyl nitroxide).....	244
Zero-Field and Longitudinal-Field μ SR Studies of Quasi-One-Dimensional Organic Conductor, TMTTF ₂ PF ₆	245
High-Pressure μ SR Study of an Organic Spin-Peierls Material MEM-[TCNQ] ₂	246
μ SR study on the spin-singlet state in cluster magnet GaNb ₄ S ₈	247
Magnetic order of the frustrated triangular lattice antiferromagnet HCrO ₂	248

μ SR Study of Ordered Phases in Triangular Ising-like Antiferromagnets CsCoCl ₃ and CsCoBr ₃	249
μ SR Studies of the 2D Triangular-lattice Spin-liquid System κ -ET ₂ Cu ₂ (CN) ₃	250
μ SR study around a quantum critical point in heavy-fermion compounds Ce ₂ RhIn _{8-χ} Sn _{χ}	251
Precise investigation and re-examination of magnetism and superconductivity of high-quality Fe-based superconductor, LaFeAsO _{1-χ} F _{χ}	252
Effect of Pressure on the Stripe Dynamics in La _{2-x} Sr _{x} Cu _{1-y} Zn _{y} O ₄ with $x = 0.13$	253
μ SR study of iron-substitution effects on the Cu-spin dynamics in the overdoped regime of La _{2-χ} Sr _{χ} Cu _{1-y} Fe _{y} O ₄	254
μ SR study of the impurity-induced development of magnetic correlation in the Bi-2201 high- T_c superconductor	255
μ SR study of the vortex state above T_c in high- T_c superconductors	256
μ SR study of the Heusler compound Ru _{1.9} Fe _{0.1} CrSi	257
ALC- μ SR Investigation of Model Porphyrins	258
μ SR study of structure-dependent electron radical dynamics in polythiophene and its derivatives	259
Study of dynamics of amorphous polymer by performing μ SR measurements	260
Diffusion of muon in hydrogen tungsten bronze	261
Measurement of the Mössbauer γ -rays from exotic Fe atoms produced by μ^- capture reactions	262
Muon Transfer Studies in Solid D ₂ with Implanted Rare-Earth Ions	263
Progress in the analysis of muon beam density enhancement effect observed when using tapered tubes	264

3. Radiochemistry and Nuclear Chemistry

Production of an isomeric state of ²⁶¹ Rf by the ²⁴⁸ Cm(¹⁸ O,5n) ²⁶¹ Rf reaction	265
Experiment on electrochemical oxidation of nobelium using a microchannel-electrode chip	266
Liquid scintillation counting of ²⁶¹ Rf produced in ²⁴⁸ Cm(¹⁸ O,xn) reaction and pre-separated using RIKEN GARIS/gas-jet system	267
Anionic fluoro complex of element 105, Db	268
Electrochemical reduction of Europium on a tracer scale as a model experiment for the reduction of Mendeleevium	269
Hydroxide coprecipitation of Zr and Hf with Sm: Model experiment for the chemical study of Rf	270
Study of the reversed-phase chromatography of element 104, rutherfordium (Rf) with TIOA or TTA extractant	271

Use of solvent-extraction apparatus with microchemical chip in heavy-element chemistry	272
Basic study of solvent extraction system with FIA for superheavy element chemistry	273
Mutual separation of short-lived lanthanides by capillary electrophoresis	274
4. Radiation Chemistry and Biology	
The effects of trichostatin A on DNA damage response after X-ray irradiation in human cells	275
Cell-killing effect of low dose of high-LET heavy ions (III)	276
Comparison of mutations of <i>Neurospora crassa</i> DSB repair-deficient mutants induced by carbon-ion beam	277
Chronic effects of ion-beam irradiation on protonemal cells in the moss <i>Funaria hygrometrica</i>	278
Seed hypoplasia induced by heavy-ion beam irradiation of pollen grains in dioecious plant <i>Silene latifolia</i>	279
Effect of X-ray irradiation on the expression of DNA repair related genes in rice	280
Characterization of temperature-sensitive chlorotic mutant induced by ion beam irradiation	281
Identification of mutated gene induced by heavy ion beam irradiation in rice	282
Identification of heavy-ion-beam induced DNA mutation by genetic mapping in <i>Arabidopsis</i> mutant	283
LET-dependent effect of heavy-ion-beam mutagenesis on deletion size	284
C-ion-induced DNA mutations in variegated mutant <i>Arabidopsis</i>	285
Early-flowering mutants developed by heavy-ion-beam irradiation in soybean	286
Induction of high-formaldehyde-absorption mutant by heavy-ion-beam irradiation in <i>Murraya paniculata</i>	287
Development of early-flowering mutant of strawberry cultivar "Satsumaotome" by C-ion irradiation	288
IV. OPERATION RECORDS	
1. Operation of RIBF	
Operations of RIBF ring cyclotrons	289
RILAC operation	291
AVF cyclotron operation	293
Beam time statistics for user experiments	295

PAC Meetings for Nuclear Physics, and Material and Life Science	296
Radiation Safety Management at RIBF	297
Fee-based distribution of radioisotopes produced at AVF cyclotron	299
Operation of SRC cryogenic system	300
Present status of the BigRIPS cryogenic plant	302
Present Status of Liquid-Helium Supply and Recovery System	304
Improvement made to couplers used for liquid-helium supply and recovery lines (1)	306
V. RECORDS OF LABORATORIES, GROUPS, AND TEAMS (Activities and members)	
Events in Nishina Center from January 2009 to March 2010	309
Theoretical Research Division	
Theoretical Physics Laboratory	310
Theoretical Nuclear Physics Laboratory	314
Strangeness Nuclear Physics Laboratory	320
Sub Nuclear System Research Division	
Radiation Laboratory	322
Advanced Meson Science Laboratory	329
RIKEN BNL Research Center	
Theory Group	339
Experimental Group	342
RIBF Research Division	
Heavy Ion Nuclear Physics Laboratory	346
Radioactive Isotope Physics Laboratory	356
Superheavy Element Laboratory	360
Accelerator Group	
Accelerator R&D Team	363
Ion Source Team	365
RILAC Team	366
Cyclotron Team	367
Beam Dynamics & Diagnostics Team	368
Cryogenic Technology Team	370
Instrumentation Development Group	
SLOWRI Team	371
Polarized RI Beam Team	375
Rare RI-ring Team	378

SCRIT Team	380
Research Instruments Group	
GARIS Team	382
BigRIPS Team	383
SAMURAI Team	385
Computing and Network Team	386
Detector Team	388
Accelerator Applications Research Group	
Radiation Biology Team	390
RI Applications Team	394
User Liaison and Industrial cooperation Group	
User Support Office	396
Industrial Cooperation Team	397
Safety Management Group	398
CNS (Center for Nuclear Study, Graduate School of Science, University of Tokyo)	400
TORIJIN (Todai-RIKEN Joint International Program for Nuclear Physics)	405
VI . LIST OF PUBLICATIONS & PRESENTATION	407
VII . LIST OF PREPRINTS	491
VIII . LIST OF SYMPOSIA	493
IX . LIST OF SEMINAR	495
X . AUTHOR INDEX	503

I. PREFACE

Preface

RIKEN Accelerator Progress Report (APR) compiles the yearly research activities conducted by the laboratories and the groups of RIKEN Nishina Center for Accelerator-Based Science, or simply RIKEN Nishina Center (RNC). It also contains progress reports submitted by the users of RI Beam Factory (RIBF) and RIKEN Muon Facility at Rutherford Appleton Laboratory in UK. This volume is No. 42 of APR containing our major research activities conducted in 2009.

In 2009, significant changes took place in the Nishina Center Administration. In October 2009, Hideto En'yo was appointed as the new director of RIKEN Nishina Center. As a chief scientist of RIKEN since 2001, he has spearheaded the international collaboration between RIKEN and Brookhaven National Laboratory, and is now in charge of all research activities at Nishina Center. The former director, Yasushige Yano has completed the world's largest cyclotron at the heart of RIBF; the new director is committed to open up this newly-born facility for the world wide users and to produce world-class research results.

To achieve this, Walter Henning was invited to join RIKEN Nishina Center as Associate Director from the 1st of April, 2010. With his distinguished career as the leader of GSI (Gesellschaft für Schwerionenforschung) in Germany, Argonne National Laboratory in USA, and as the Chair of Nuclear Physics Program Advisory Committee of Nishina Center, he is expected to further promote scientific activities at RIBF and help Nishina Center grow as a truly internationalized synergetic-use laboratory.

On the same date, we also invited Hideyuki Sakai, former Professor of the University of Tokyo and the chair of Japanese Experimental Nuclear Physics Community, as the head of User Liaison and Industrial Cooperation Group. He is asked to lead the user interface function of Nishina Center from the community's perspective, not RIKEN's.

Moreover, we have promoted many young researchers to the heads of the teams to support and develop the infrastructures and experimental equipments of RIBF. With these major administrative changes, Nishina Center is committed to metamorphose itself into a synergetic-use laboratory open to the world's nuclear-physics community. Your support and encouragements are most appreciated.

With regard to the scientific progress of Nishina Center, outstanding achievements have been made last year. The construction of basic experimental apparatuses is in progress toward a full scale completion of the facility,

while many experiments are ongoing with the existing apparatuses using the world's most powerful heavy ion beams. One of the major news is on the electron storage ring for SCRIT (Self-Confining RI Ion Target) experiment. The ring was kindly donated from Sumitomo Heavy Industry. Previously known as AURORA, it is now renamed as SR², ScRit-equipped Storage Ring. The ring was modified to have longer straight sections for the SCRIT application, and electrons were successfully stored in December 2009. The physics experiment is scheduled for 2010, and in the meanwhile, we will be promoting the use of synchrotron radiations from SR².

The new superconducting ECR ion source and Linear Accelerator RILAC-II were set up in 2009 from which we expect much higher beam intensity of uranium. An independent operation of RILAC-I for super-heavy element search and other low energy applications is being actively promoted as well.

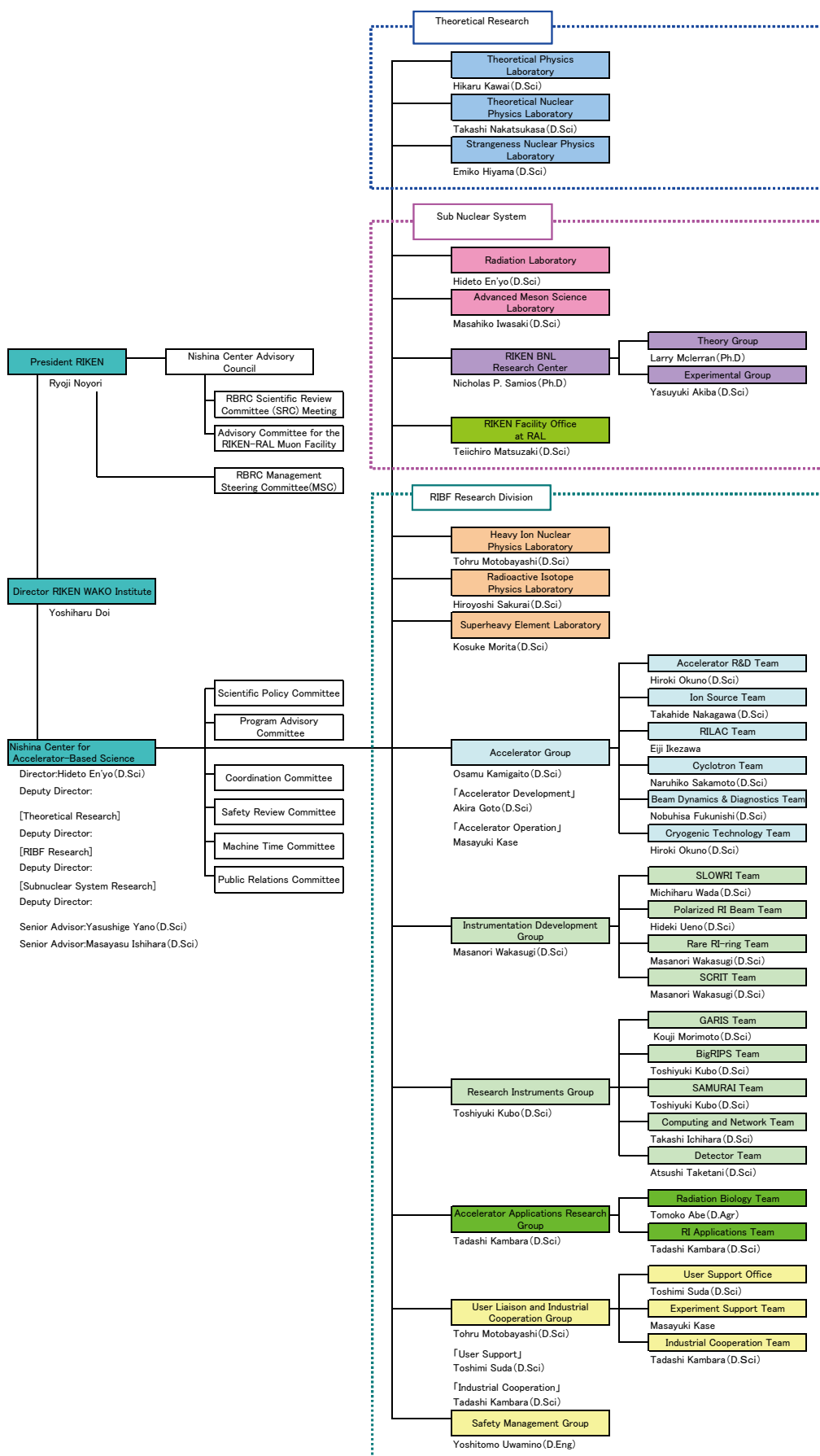
The construction of SAMURAI, multiple-particle spectrometer with a large acceptance, has been proceeding smoothly. T. Motobayashi, who retired as chief scientist, became the head of the construction team to enhance the collaborative work among all who are interested in this project.

Significant scientific achievements of the last year are selected by the editorial committee of RIKEN Accelerator Progress Report, and presented in "Frontispiece" and "Highlights of the Year". Of all these achievements, special attention should be given to the work on a gas charge stripper by Kuboki *et al.* This work may well be a key to solve a long-standing problem of charge stripper in accelerating uranium and other heavy elements. The power of the ⁴⁸Ca beam was again demonstrated by the in-beam γ -ray spectroscopy of ³²Ne by Doornenbal *et al.* utilizing the BigRips isotope separator, the Zero-Degree Spectrometer and the NaI(Tl) crystal array, DALI2. A special campaign for many experiments inline using ⁴⁸Ca beam is scheduled for 2010 with an endorsement by the Program Advisory Committee.

Other works covering a wide range of research from super string theory to accelerator applications are compiled in this volume. We believe such diversity and the strategic focus on the RIBF science are and will continue to be the source of strength of Nishina Center for Accelerator-Based Science.

Hideto En'yo
Director,
RIKEN Nishina Center for Accelerator-Based Science

Organization Chart of Nishina Center for Accelerator-Based Science



II. RESEARCH ACTIVITIES I

(Nuclear-Particle Physics)

1. Nuclear Physics

Measurement of interaction cross sections of Ne Isotopes

T. Ohtsubo^{*1}, M. Takechi, M. Fukuda^{*2}, T. Kuboki^{*3}, T. Moriguchi^{*4}, D.Q. Fang^{*5}, H. Geissel^{*6},
 R. Chen, N. Fukuda, I. Hachiuma^{*3}, N. Inabe, Y. Ishibashi^{*4}, Y. Ito^{*4}, D. Kameda, Y. Kikuchi^{*3}, M. Lantz, Y.G. Ma^{*5},
 M. Mihara^{*2}, D. Nagae^{*4}, M. Nagashima^{*1}, H. Nakazato^{*3}, K. Namihira^{*3}, D. Nishimura^{*2}, T. Ohnishi, H. Ooishi^{*4},
 A. Ozawa^{*4}, K. Sakuma^{*3}, T. Suda, H. Suzuki^{*4}, T. Suzuki^{*3}, H. Takeda, K. Tanaka, T. Yamaguchi^{*3}, and T. Kubo
 [BigRIPS, reaction cross section, nuclear structure, unstable nuclei]

Last year, we measured interaction cross sections (σ_I) of neutron-rich neon isotopes ${}^A\text{Ne}$ ($A:28\sim32$) to determine the root mean square radii $\langle r_m^2 \rangle^{1/2}$ of these nuclei¹⁾. An enhancement of radii in these nuclei compared to the systematics of stable isotope nuclei was suggested²⁾.

This short note reports the successive measurements on ${}^A\text{Ne}$ ($A:20\sim28$), in addition to the previous measurements with the aim of comparing the $\langle r_m^2 \rangle^{1/2}$ values of ${}^A\text{Ne}$ with those of the nuclei in the "island of inversion". The formation of a neutron halo in heavier Ne isotopes was expected, and a level inversion of the $1f$ and $2p$ orbitals was predicted³⁾, and the evidence supporting the existence of the neutron halo in ${}^{31}\text{Ne}$ has been recently reported⁴⁾.

The experiment was performed at the Big-RIPS facility⁵⁾, which is a part of the RI beam factory operated by the RIKEN Nishina Center and CNS at the University of Tokyo. A schematic drawing of the experimental setup is shown in Fig. 1. The experimental setup is essentially the same as that used in the previous measurement¹⁾. We employed a transmission method to measure σ_I . A ${}^{48}\text{Ca}$ primary beam with an energy of 345 MeV/nucleon bombarded a Be production target at F0. The intensity of the primary beam was optimized for each isotope on the basis of the counting rate recorded by the data acquisition system. The fragments produced at an energy of around 250 MeV/nucleon were pre-separated at the first stage of BigRIPS. The Al wedge-shaped degrader was placed at F1. A carbon target with a thickness 1.8 g/cm² or 3.6 g/cm² was located at F5. The incident and outgoing secondary beams were identified at the first (F3-F5) and second (F5-F7) halves of the second stage of BigRIPS, respectively; using the $B\rho\text{-}\Delta E\text{-TOF}$ method. We used the standard detectors⁶⁾ at F3, F5, and F7 to identify the beams. We used the ion chamber (IC) at F3 for the energy loss (ΔE) measurement of the incident beam. We replaced the standard plastic scintillators at F5 and F7 with wider ones (240×100 mm) having a thickness of 1 mm and 3 mm, respectively. These scintillation detectors provided information on both TOF and ΔE .

An example of a particle identification plot is shown in Fig. 2. We accumulated the data on the σ_I values of all Ne isotopes; the accuracy of the data was 1 %. Data analysis to determine σ_I is now underway.

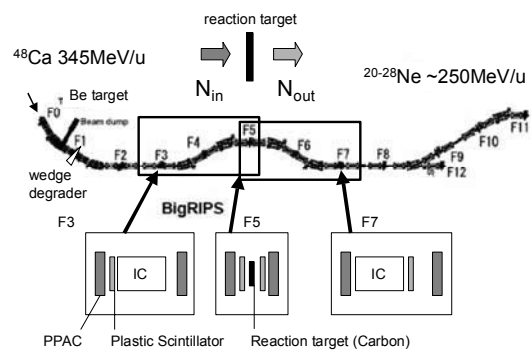


Fig. 1 Experimental setup at BigRIPS. The incident and outgoing particles were identified by the particle detectors at F3, F5, and F7 using the $B\rho\text{-}\Delta E\text{-TOF}$ method.

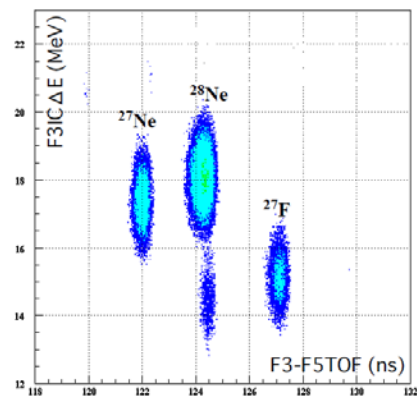


Fig. 2 Typical TOF- ΔE spectrum for the first stage of BigRIPS.

References

- 1) T. Ohtsubo *et al.*: RIKEN Accel. Prog. Rep. **42**, 5 (2008).
- 2) M. Takechi *et al.*: Nucl. Phys. A **834**, 412c (2010).
- 3) W. Pöschl, D. Vretenar *et al.*: Phys. Rev. Lett. **79**, 3841 (1996).
- 4) T. Nakamura *et al.*: Phys. Rev. Lett. **103**, 262501 (2009).
- 5) T. Kubo *et al.*: Nucl. Instr. & Meth. in Phys. Res. **B 204**, 97 (2003).
- 6) T. Ohnishi *et al.*: J. Phys. Soc. Japan **77**, 083201 (2008).

^{*1} Graduate School of Science, Niigata University
^{*2} Department of Physics, Osaka University
^{*3} Department of Physics, Saitama University
^{*4} Institute of Physics, University of Tsukuba
^{*5} SINAP
^{*6} GSI, Germany

Inelastic scattering of ^{32}Mg at RIBF beam energies on various targets

H. Scheit, K. Li,¹ N. Aoi, H. Baba, P. Doornenbal, Y. Kondo, T. Motobayashi, S. Nishimura, H. Sakurai, S. Takeuchi, Y. Togano, H. Wang,¹ and K. Yoneda,

[Nuclear structure, Island of Inversion, neutron-rich nuclei, in-beam γ -ray spectroscopy]

In-beam γ -ray spectroscopy of exotic nuclei produced in projectile fragmentation reactions at intermediate beam energies is an important tool for nuclear structure studies and is routinely applied at major radioactive ion beam facilities worldwide. Various experimental methods depend or benefit from it, such as Coulomb excitation, few-nucleon removal reactions, direct reactions on light targets, in-elastic scattering, secondary fragmentation, and lifetime measurements (RDM, DSAM, recoil-shadow method). With the commissioning of the RIBF not only has the intensity of available radioactive beams been increased enormously, but also the energies of the secondary beams are much higher. Typically, secondary beam energies were in the range from about 30 MeV/ u to 100 MeV/ u at the RIPS facility, while at the RIBF beam energies above 200 MeV/ u are common for light secondary beams with, say $A \leq 50$.

At this high beam energy, not only will the atomic background increase dramatically, but also standard analysis tools used at lower beam energies should be tested and possibly adapted. For instance, the Coulomb excitation cross section to populate a collective 2+ state drops by about a factor of 4 when going from 50 to 200 MeV/ u , while the nuclear excitation cross section stays nearly constant. Thus, Coulomb-nuclear interference effects are expected to be much more enhanced at the higher beam energies, possibly limiting the precision of the extracted transition probabilities.

In order to study the background conditions for in-beam γ -ray spectroscopy at the RIBF and to test currently employed analysis techniques a high statistics measurement of elastic and inelastic scattering of ^{32}Mg on several targets was performed.

A primary ^{48}Ca beam with an average intensity of about 10 particle nA and an energy of 345 MeV/ u was impinging on a 20 mm (3.7 g/cm²) thick rotating Be target located at the F0 focus of the BigRIPS¹⁾ fragment separator. The produced secondary beams were separated using the standard $B\rho$ - ΔE - $B\rho$ method employing a 15 mm thick wedge shaped Al degrader at the F1 dispersive focus of the BigRIPS separator. The momentum acceptance was $\pm 3\%$. The beam particles were identified event-by-event using the standard ΔE -TOF- $B\rho$ method. The time of flight (TOF) was measured between two thin plastic scintillators located at the F3 and F7 achromatic foci (separated by a flight

path of about 47 m), the energy-loss was determined with an ion-chamber² also located at the F7 achromatic focus and the $B\rho$ was deduced from a position measurement at the dispersive F5 focus of BigRIPS.

These secondary beams were then transported to the F8 secondary target position. To induce inelastic excitations a 14.1 mm (2.54 g/cm²) thick (natural) carbon target was used. Furthermore, plastic (CH₂) and Pb targets, resulting in about the same energy loss as for the carbon target, were employed. The secondary ^{32}Mg beam with an intensity of about 1000 particles/s had an energy of about 220 MeV/ u at the center of the secondary target. The emitted de-excitation γ rays were detected by the DALI2 γ spectrometer² with a full energy peak efficiency of about 20% and an expected resolution after correcting the large Doppler shift of about 10% for a 1 MeV γ transition. For the particle identification and track reconstruction after the secondary target the spectrometer ZeroDegree was employed. As before, the ΔE -TOF- $B\rho$ method was applied to unambiguously identify the particles event by event.

The data taking times for the Pb, CH₂ and the C targets were about 5, 3, and 2 hours, respectively, which allowed us to collect several thousand counts in the 885 keV peak, corresponding to the $2_1^+ \rightarrow 0_{gs}^+$ transition in ^{32}Mg . For the C and CH₂ targets several transitions above 885 keV could be observed. In particular a comparison to similar data obtained at the lower beam energy of about 50 MeV/ u at the RIPS facility³⁾ will be of interest.

The data are currently under analysis.

- 1) T. Kubo *et al.*, Nucl. Instr. Meth. B 204, 97 (2003)
- 2) S. Takeuchi *et al.*, RIKEN Acc. Rep. 36, 148 (2003)
- 3) S. Takeuchi *et al.*, PRC 79, 054319 (2009)

^{*1} Peking University, China

Rates of production of fission fragments from a ^{238}U beam at 345 MeV/nucleon

T. Ohnishi, T. Kubo, K. Kusaka, A. Yoshida, K. Yoshida, M. Ohtake, N. Fukuda, H. Takeda, D. Kameda, K. Tanaka, N. Inabe, Y. Yanagisawa, Y. Gono, H. Watanabe, H. Otsu, H. Baba, T. Ichihara, Y. Yamaguchi, M. Takechi, S. Nishimura, H. Ueno, A. Yoshimi, H. Sakurai, T. Motobayashi, T. Nakao ^{*1}, Y. Mizoi ^{*2}, M. Matsushita ^{*3}, K. Ieki ^{*3}, N. Kobayashi ^{*4}, K. N. Tanaka ^{*4}, Y. Kawada ^{*4}, N. Tanaka ^{*4}, S. Deguchi ^{*4}, Y. Satou ^{*4}, Y. Kondo ^{*4}, T. Nakamura ^{*4}, K. Yoshinaga ^{*5}, C. Ishii ^{*5}, H. Yoshii ^{*5}, Y. Miyashita ^{*5}, N. Uematsu ^{*5}, Y. Shiraki ^{*5}, T. Sumikama ^{*5}, J. Chiba ^{*5}, E. Ideguchi ^{*6}, A. Saito ^{*6}, T. Yamaguchi ^{*7}, I. Hachimura ^{*7}, T. Suzuki ^{*7}, T. Moriguchi ^{*8}, A. Ozawa ^{*8}, T. Ohtsubo ^{*9}, M. A. Famiano ^{*10}, H. Geissel ^{*11}, A. S. Nettleton ^{*12}, B. M. Sherrill ^{*12}, S. Manikonda ^{*13}, and J. A. Nolen ^{*13}

[Unstable Nuclei, In-flight fission, nuclear reactions $\text{Be}(^{238}\text{U}, x) E = 345 \text{ MeV/nucleon}$,
nuclear reactions $\text{Pb}(^{238}\text{U}, x) E = 345 \text{ MeV/nucleon}$]

The production rates of fission fragments from fisible beams provide important information about the reaction mechanism in fission processes. In addition, they can be used to evaluate the performance of the RI beam separator. In this report, we present the rates of production of fission fragments produced by the in-flight fission of ^{238}U beam at 345 MeV/nucleon; these rates were obtained during experiments performed in 2008 for finding new isotopes.¹⁾

The 2008 experiment was performed using a primary ^{238}U beam at an energy of 345 MeV/nucleon and an average intensity of 0.22 pnA. Fission fragments emitted at an angle of around 0° were collected and analyzed using the BigRIPS separator.²⁾ The particles were identified using the magnetic rigidity, energy loss, and time of flight values measured in the second stage of the BigRIPS separator. Details of the particle identification are presented in Ref. 1. In this experiment, three different settings of the separator, namely, G1, G2, and G3, were used to search for new neutron-rich isotopes with atomic numbers (Z) of ~ 30 , ~ 40 , and ~ 50 , respectively. The production targets were 5-mm Be at G1, 3-mm Be at G2, and 1-mm Pb at G3. Other settings are described in Ref. 1.

Figure 1 shows the production rates of fission fragments with Z ranging from 25 to 54. These fragments were fully stripped. The upper and lower panels in Fig. 1 show the results of the U + Be and the U + Pb

reactions, respectively. For example, the measured production rates of ^{78}Ni and ^{132}Sn are 4×10^{-3} and 1×10^3 count/s/pnA, respectively. These rates were measured at a $B\rho$ value that was almost 10% higher than the $B\rho$ value required for maximum yield. In case of U beam with an intensity of 1 μA , the expected count rates of ^{78}Ni and ^{132}Sn are several counts/s and 10^7 counts/s, respectively.

The solid lines in Fig. 1 indicate the predictions with the LISE++ simulation.³⁾ The production cross sections of the fission fragments were calculated using the LISE++ code for abrasion fission and Coulomb fission calculations. A comparison of the measured and predicted production rates showed that the measured data were fairly well reproduced. Detailed analysis is described in Ref. 1.

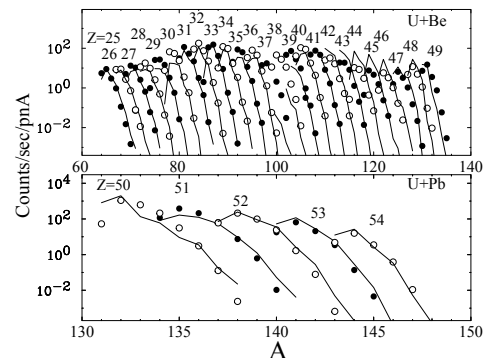


Fig. 1. Measured production rates, shown along with the predictions from the LISE++ simulation (solid lines). The upper and lower panels show the results of the U + Be and U + Pb reactions, respectively. The measured data for fragments with Z ranging from 25 to 37 are obtained at G1, while those for fragments with Z ranging from 38 to 49 are obtained at G2. The closed and open circles denote even and odd Z values, respectively.

References

- 1) T. Ohnishi et al.: J. Phys. Soc. Jpn. **79**, 073201 (2010).
- 2) T. Kubo et al.: Nucl. Instr. and Meth. **B 204**, 97 (2003).
- 3) O. B. Tarasov and D. Bazin: Nucl. Instr. and Meth. **B 266**, 4657 (2008).

^{*1} Department of Physics, The University of Tokyo
^{*2} Department of Engineering Science, Osaka Electro-Communication University
^{*3} Department of Physics, Rikkyo University
^{*4} Department of Physics, Tokyo Institute of Technology
^{*5} Department of Physics, Tokyo University of Science
^{*6} Center for Nuclear Study, The University of Tokyo
^{*7} Department of Physics, Saitama University
^{*8} Institute of Physics, University of Tsukuba
^{*9} Department of Physics, Niigata University
^{*10} Department of Physics, Western Michigan University
^{*11} Gesellschaft fuer Schwerionenforschung mbH
^{*12} National Superconducting Cyclotron Laboratory, Michigan State University
^{*13} Argonne National Laboratory

Study on the isomer ratios of fission products of 345 MeV/u ^{238}U

D. Kameda, T. Nakao,^{*1} T. Kubo, T. Ohnishi, K. Kusaka, A. Yoshida, K. Yoshida, M. Ohtake, N. Fukuda, H. Takeda, K. Tanaka, N. Inabe, Y. Yanagisawa, H. Watanabe, H. Otsu, Y. Kondo, Y. Gono, H. Sakurai, T. Motobayashi, H. Baba, T. Ichihara, Y. Yamaguchi, M. Takechi, S. Nishimura, H. Ueno, A. Yoshimi, M. Matsushita,^{*2} K. Ieki,^{*2} N. Kobayashi,^{*3} K. Tanaka,^{*3} Y. Kawada,^{*3} N. Tanaka,^{*3} S. Deguchi,^{*3} Y. Sato,^{*3} T. Nakamura,^{*3} K. Yoshinaga,^{*4} C. Ishii,^{*4} H. Yoshii,^{*4} N. Uematsu,^{*4} Y. Shiraki,^{*4} Y. Miyashita,^{*4} T. Sumikama,^{*4} J. Chiba,^{*4} E. Ideguchi,^{*5} A. Saito,^{*5} T. Yamaguchi,^{*6} I. Hachiuma,^{*6} T. Suzuki,^{*6} T. Moriguchi,^{*7} A. Ozawa,^{*7} T. Ohtsubo,^{*8} M. A. Famiano,^{*9} A. Nettleton,^{*10} B. Sherrill,^{*10} S. Manikonda,^{*11} and J. Nolen^{*11}

[in-flight fission, short-lived isomer, isomer ratio]

Techniques based on in-flight separation and identification of nuclear reaction products at intermediate energies provide us with a unique opportunity to study the metastable states, i.e., isomers. The systematic data of the isomer ratio F , defined as the ratio of the yield of an isomer to the total yield of the product, is useful information not only for designing experiments involving the isomer but also for understanding the mechanism of production reaction¹⁾. A new-isotope search utilizing the in-flight fission of 345 MeV/u ^{238}U was conducted in 2008²⁾, here, we observed a number of known isomers along with more than ten new isomers³⁾. In this paper, the isomer ratios for several of the known isomers are reported.

The isomer ratio can be expressed as $F = N_m D / N_p$. N_p denotes the total number of particles implanted into a aluminum stopper. For particle identification, the mass-to-charge ratio A/Q and the atomic number Z were evaluated using the measured magnetic rigidity ($B\rho$) and time of flight in BigRIPS and the energy loss in the ionization chamber which was located 1-m upstream of the stopper. The reaction loss in the stopper was estimated to be as large as 30% for the isotopes with $Z \sim 30$. N_m denotes the population of the isomeric state that was derived from the γ -photo-peak counts by taking into account the detection efficiency⁴⁾ and the total internal conversion ratio reported in the γ -decay scheme. The isomeric γ -detection efficiency ε_γ , in particular for the low energy γ rays, depends on the position at which the particles were implanted in the stopper due to the γ -ray attenuation effect. We performed Monte-Carlo simulations (GEANT3) for evaluating this effect on the basis of the measured $B\rho$ value and the observed beam profile at the stopper. In addition, the ε_γ decreased by 22 %

Table 1. Isomer ratios for the known isomers. E^* and I^π denote the excitation energy and the spin and parity of the isomeric state, respectively. F and σ_f indicate the isomer ratio and spin cutoff parameter estimated from the obtained isomer ratio, respectively.

Nuclide	E^* (keV)	I^π	F (%)	σ_f (\hbar)
^{78}Zn	2673	(8 ⁺)	7.9(16)	3.7
^{95}Kr	196	(7/2 ⁺)	39(10)	2.9
^{128}Cd	2714	(10 ⁺)	3.0(5)	4.0
^{130}Cd	2130	(8 ⁺)	10(3)	4.0
^{132}Sn	4849	(8 ⁺)	3.2(8)	3.2

in the worst case from the value calibrated offline; this was due to the prompt γ events prior to isomeric γ -decay events. D is a correction factor of the in-flight decay occurring between the production target and the stopper. The $B\rho$ settings allowed only the isomers of the high-momentum side to be observed.

Table 1 shows several isomer ratios along with the spin cut-off parameter σ_f . The parameter σ_f represents the width of the angular-momentum distribution $P(J)$ of the prefragments; the distribution is expressed as $P(J) \propto (2J+1) \exp(-J(J+1)/2\sigma_f^2)$ ⁵⁾. The loss of the angular momentum of the fragment in the subsequent particle evaporation and γ emission is assumed to be negligibly small. Then, σ_f is tentatively estimated using the obtained isomer ratio on the basis of the sharp cutoff model in which the value of F corresponds to the population of states with spin, higher than the isomeric spin I^1 . The obtained values of σ_f are somewhat smaller than those reported in the case of α -induced fission of ^{238}U ⁵⁾, although more detailed evaluation of σ_f is needed. Further systematic investigation is currently in progress.

^{*1} Department of Physics, The University of Tokyo
^{*2} Department of Physics, Rikkyo University
^{*3} Department of Physics, Tokyo Institute of Technology
^{*4} Department of Physics, Tokyo University of Science
^{*5} Center for Nuclear Study, The University of Tokyo
^{*6} Department of Physics, Saitama University
^{*7} Institute of Physics, University of Tsukuba
^{*8} Department of Physics, Niigata University
^{*9} Physics Department, Western Michigan University
^{*10} Michigan State University
^{*11} Argonne National Laboratory

References

- 1) J.M. Daugas et al.: Phys. Rev. C **63**, 064609 (2001).
- 2) T. Ohnishi et al.: RIKEN Accel. Prog. Rep. **42**, viii (2009).
- 3) D. Kameda et al.: RIKEN Accel. Prog. Rep. **42**, xv (2009).
- 4) T. Nakao et al.: RIKEN Accel. Prog. Rep. **42**, 29 (2009).
- 5) H. Naik et al.: Nucl. Phys. A **648**, 45 (1999).

Measurement of the ($t, {}^3\text{He}$) reaction at 300 MeV/nucleon

K. Miki,^{*1,*3} H. Sakai,^{*1} T. Uesaka,^{*2} H. Baba,^{*3} G.P.A. Berg,^{*4} N. Fukuda,^{*3} D. Kameda,^{*3} T. Kawabata,^{*5} S. Kawase,^{*2} T. Kubo,^{*3} K. Kusaka,^{*3} S. Michimasa,^{*2} H. Miya,^{*2} S. Noji,^{*1} T. Ohnishi,^{*3} S. Ota,^{*2} A. Saito,^{*2} Y. Sasamoto,^{*2,*3} M. Sasano,^{*1} S. Shimoura,^{*2} H. Takeda,^{*3} H. Tokieda,^{*2} K. Yako,^{*1} Y. Yanagisawa,^{*3} A. Yoshida,^{*3} K. Yoshida,^{*3} and R.G.T. Zegers.^{*6}

[SHARAQ, giant resonance, charge exchange reaction]

The isovector spin monopole resonance (IVSMR) has been an important topic of interest in the study of spin-isospin responses in nuclei¹⁾. Since the IVSMR is a breathing mode with spin and isospin flips, it can be related to the nuclear matter compressibility with spin and isospin degrees of freedom. In spite of the importance of the IVSMR, it has not been clearly identified, especially for the β^+ side. In order to identify the IVSMR(β^+), we measured the ${}^{208}\text{Pb}(t, {}^3\text{He})$ and ${}^{90}\text{Zr}(t, {}^3\text{He})$ reactions at 300 MeV/nucleon. This was the first physics experiment performed with the newly constructed SHARAQ spectrometer²⁾.

The experiment was performed at the RIBF facility at RIKEN. A primary α beam of 320 MeV/nucleon was bombarded onto a ${}^9\text{Be}$ production target (thickness: $d = 4$ cm) installed at BigRIPS-F0. The produced tritons of 300 MeV/nucleon were achromatically^{a)} transported along the high-resolution beam line to the secondary target installed at the pivot of the SHARAQ spectrometer. The intensities were typically 300 particle nA for the primary beam and 1×10^7 cps for the secondary tritons. The purity of the triton beam was 100%, since no other particle has the same momentum-to-charge ratio ($p/Q = 2.4$ GeV/c) at the energy, because of kinematic restrictions.

The secondary targets used were ${}^{208}\text{Pb}$ ($d = 0.35$ mm) and ${}^{90}\text{Zr}$ ($d = 0.46$ mm) foils for the IVSMR measurements and a CH_2 ($d = 0.5$ mm) foil for calibrations. The ${}^3\text{He}$ particles in the reaction products were momentum analyzed by the SHARAQ spectrometer and counted by cathode-readout drift chambers installed in the final focal plane of the SHARAQ spectrometer. The differential cross sections were measured at an excitation energy of $0 \leq E_x \leq 70$ MeV and scattering angles of $0^\circ \leq \theta \leq 3^\circ$.

Figure 1 shows the measured $\text{CH}_2(t, {}^3\text{He})$ spectra. The left panel shows the XY spectrum measured in the focal plane of the SHARAQ spectrometer. X_{FP} and Y_{FP} are proportional to the momentum and the vertical scattering angle of the ${}^3\text{He}$ particles, respectively. Two main loci can be identified in the figure; these are

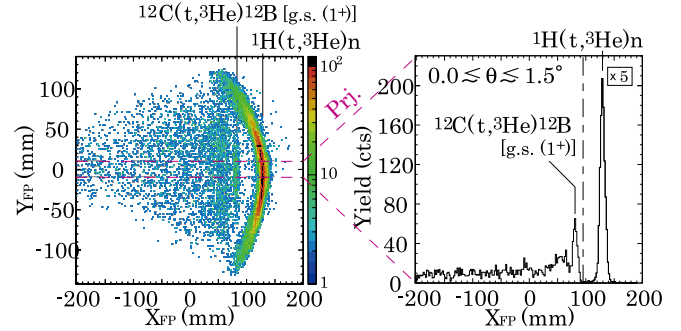


Fig. 1. The obtained image at the SHARAQ focal plane for the $\text{CH}_2(t, {}^3\text{He})$ reaction [left] and its projection [right].

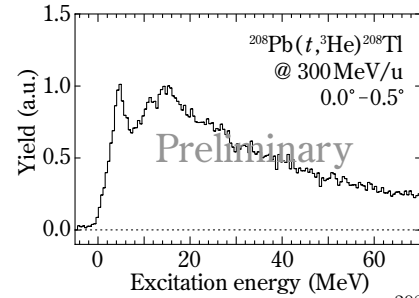


Fig. 2. Excitation energy spectrum for the ${}^{208}\text{Pb}(t, {}^3\text{He})$ reaction (preliminary). See text for details.

attributed to the ${}^1\text{H}(t, {}^3\text{He})$ and ${}^{12}\text{C}(t, {}^3\text{He}){}^{12}\text{B}$ [g.s.] reactions. A kinematic correlation due to the recoil of target protons is nicely observed for the ${}^1\text{H}(t, {}^3\text{He})$ reaction. A projection of this picture is shown in the right panel. From the distance between the two observed peaks, the dispersion of the SHARAQ spectrometer is determined to be 5.85 m, which is in agreement with the design value of 5.86 m. The energy resolution obtained from the ${}^{12}\text{C}(t, {}^3\text{He}){}^{12}\text{B}$ [g.s.] peak is about 2 MeV (FWHM).

Figure 2 shows the ${}^{208}\text{Pb}(t, {}^3\text{He})$ spectrum at a scattering angle of 0° . Two peaks are observed around 5 MeV and 15 MeV. Although the latter is close to the predicted position for the IVSMR, the isovector spin quadrupole excitations are also expected to give a significant cross section in this region. Therefore, it is crucial to perform the multipole decomposition (MD) analysis by using the obtained angular distributions. The data reduction for the precise MD analysis is currently in progress.

References

- 1) I. Hamamoto and H. Sagawa: Phys. Rev. C **62**, 024319 (2000).
- 2) T. Uesaka *et al.*: RIKEN Accel. Prog. Rep. **43** (2010).

*1 Department of Physics, University of Tokyo

*2 CNS, University of Tokyo

*3 RIKEN Nishina Center

*4 JINA, Department of Physics, University of Notre Dame

*5 Department of Physics, Kyoto University

*6 NSCL, Michigan State University

a) The SHARAQ facility was not operated in the high-resolution dispersive mode because of the requirement for the large amount of statistics.

Angular distribution for the ${}^8\text{He}(d,t){}^7\text{He}_{g.s.}$ reaction

E. Yu. Nikolskii,^{*1} A. S. Denikin,^{*2,*3} A. A. Korshennikov, H. Otsu, H. Suzuki,^{*4} K. Yoneda, H. Baba, K. Yamada, Y. Kondo,^{*5} N. Aoi, M. S. Golovkov,^{*2} A. S. Fomichev,^{*2} S. A. Krupko,^{*2} M. Kurokawa, E. A. Kuzmin,^{*6} I. Martel,^{*7} W. Mittig,^{*8} T. Motobayashi, T. Nakamura,^{*4} M. Niikura,^{*9} S. Nishimura, A. A. Ogloblin,^{*6} P. Roussel-Chomaz,^{*8} A. Sanchez-Benitez,^{*7} Y. Satou,^{*5} S. I. Sidorchuk,^{*2} T. Suda, S. Takeuchi, K. Tanaka, G. M. Ter-Akopian,^{*2} Y. Togano,^{*10} and M. Yamaguchi

[Nuclear reactions, $d({}^8\text{He},t){}^7\text{He}$, unstable nuclei]

Previously, we have reported on the measurement of the excitation energy spectrum of ${}^7\text{He}$ nucleus in the one-neutron $d({}^8\text{He},t){}^7\text{He}$ transfer reaction at the RIPS facility. The reaction was studied at forward laboratory angles $\theta_{lab} \approx (11^\circ\text{--}22^\circ)$ using the ${}^8\text{He}$ 42 MeV/ u beam and a deuteron target.¹⁾ In the spectrum of tritons, a strong peak corresponding to the ground state (g.s.) of ${}^7\text{He}$ was observed. Figure 1 shows the angular distribution for the ${}^7\text{He}_{g.s.}$ state extracted from the experimental data.

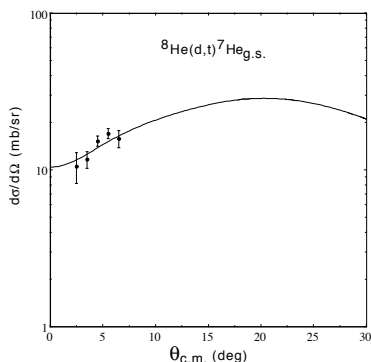


Fig. 1. The angular distribution for the ${}^8\text{He}(d,t){}^7\text{He}_{g.s.}$ reaction. The error bars are statistical only. The curve is the DWBA calculation.

The differential cross sections were analyzed with the DWBA approach using the code DWUCK5.²⁾ The initial parameters of Woods-Saxon optical model potentials (OP) were obtained in two steps: (i) we performed optical model fitting of the elastic scattering data from the ${}^8\text{He}(p,p)$ reaction at $E_{lab} = 15, 26, 32.5, 66,$ and 72 MeV/ u ³⁾ and obtained OP parameters for $E_{lab} = 42$ MeV/ u by linear interpolation; (ii) by analyzing the ${}^6\text{Li}(p,p)$, ${}^6\text{Li}(d,d)$ and ${}^6\text{Li}({}^3\text{He},{}^3\text{He})$ scattering data⁴⁾ at 25 MeV/ u , we determined the tendency

of changes in OP under projectile variation and applied it to the case of the deuteron-induced reaction. For the final $t-{}^7\text{He}$ channel, the OP for the ${}^6\text{Li}({}^3\text{He},{}^3\text{He})$ system was used. Taking the spectroscopic factors (SF) $SF[t = n + d] = 1.5^{5)}$ and $SF[{}^8\text{He} = n + {}^7\text{He}] = 4$ (assuming 4 neutrons in $p_{3/2}$ state, see also⁶⁾), we obtained a good description of the angular distribution with the normalization factor of 1.4–1.5. We found that no normalization was needed when the parameters for the imaginary part in the exit channel were slightly varied (within less than 10%) to fit to the absolute cross section. The result of the corresponding calculation is shown in Fig. 1 by a solid line, and the optical parameters are given in Table 1. The obtained OP were used to estimate the DWBA cross section for the $d({}^8\text{He},{}^3\text{He}){}^7\text{H}$ reaction which was simultaneously measured in this experiment.⁷⁾

Table 1. Optical potential parameters.

$$U(r) = -V_0 f(r, r_V, a_V) + 4a_W W_D \frac{d}{dr} f(r, r_W, a_W),$$

$$f(r, r_i, a_i) = \{1 + \exp[(r - r_i A^{1/3})/a_i]\}^{-1}$$

	V_0 (MeV)	r_V (fm)	a_V (fm)	W_D (MeV)	r_W (fm)	a_W (fm)
$d+{}^8\text{He}$	97.2	1.11	0.817	10.5	2.33	0.45
$t+{}^7\text{He}$	89.7	1.03	0.790	8.8	1.50	0.70
$n+{}^7\text{He}$	*)	1.30	0.750	–	–	–
$n+d$	*)	1.25	0.600	–	–	–

*) varied to reproduce the experimental separation energy.

References

- 1) E. Yu. Nikolskii et al.: RIKEN Accel. Prog. Rep. **41**, 14 (2008).
- 2) P. D. Kunz: Computer code DWUCK5 (1980), <http://spot.colorado.edu/~kunz/DWBA.html>.
- 3) A. A. Korshennikov et al.: Phys. Lett. B **316**, 38 (1993); Phys. Lett. B **343**, 53 (1995); Phys. Rev. C **53**, R537 (1996); R. Wolski et al.: Nucl. Phys. A **701**, 29c (2002); F. Skaza et al.: Phys. Lett. B **619**, 82 (2005).
- 4) D. Gupta et al.: Nucl. Phys. A **674**, 77 (2000); M. Avrigeanu et al.: Nucl. Phys. A **759**, 327 (2005); T. Sinha et al.: Phys. Rev. C **47**, 2994 (1993).
- 5) O. F. Nemets et al.: *Nucleon Associations in Atomic Nuclei and Many-Nucleon Transfer Reactions* (Naukova Dumka, Kiev, 1988) [in Russian].
- 6) F. Skaza et al.: Phys. Rev. C **73**, 044301 (2006).
- 7) E. Yu. Nikolskii et al.: RIKEN Accel. Prog. Rep. **41**, 15 (2008).

*1 On leave from Kurchatov Institute, Russia

*2 Joint Institute for Nuclear Research, Russia

*3 International University "Dubna", Russia

*4 Department of Physics, University of Tokyo

*5 Department of Physics, Tokyo Institute of Technology

*6 Kurchatov Institute, Russia

*7 Departamento de Fisica Aplicada, Universidad de Huelva, Spain

*8 GANIL, Caen Cedex, France

*9 Center for Nuclear Study, University of Tokyo

*10 Department of Physics, Rikkyo University

Breakdown of the $Z = 8$ shell closure in unbound $^{12}\text{O}^\dagger$

D. Suzuki,^{*1,*2} H. Iwasaki,^{*1,*2} D. Beaumel,^{*2} L. Nalpas,^{*3} E. Pollacco,^{*3} M. Assié,^{*2} H. Baba,
Y. Blumenfeld,^{*2} N. De Séréville,^{*2} A. Drouart,^{*3} S. Franchoo,^{*2} A. Gillibert,^{*3} J. Guillot,^{*2} F. Hammache,^{*2}
N. Keeley,^{*4} V. Lapoux,^{*3} F. Maréchal,^{*2} S. Michimasa,^{*5} X. Mougeot,^{*3} I. Mukha,^{*6} H. Okamura,^{*7} H. Otsu,
A. Ramus,^{*2} P. Roussel-Chomaz,^{*8} H. Sakurai, J. -A. Scarpaci,^{*2} O. Sorlin,^{*8} I. Stefan,^{*2} and M. Takechi

[Nuclear structure, unstable nuclei, missing-mass spectroscopy]

We report on the missing-mass spectroscopy of unbound ^{12}O in the $^{14}\text{O}(p,t)$ reaction at 51 AMeV.

Mirror symmetry is a fundamental feature of atomic nuclei. Recent experimental studies have shown that the conventional magic numbers disappear in neutron-rich regions at $N = 8, 20,$ and 28 . Theoretical studies point to various underlying mechanisms. The validity of the mirror symmetry of these effects under extreme conditions of isospin and binding energies remains an open question, limiting predictions for very proton-rich nuclei. We experimentally investigated the mirror symmetry in the shell quenching phenomena between $^{12}_8\text{O}_4$ and its mirror partner $^{12}_4\text{Be}_8$.

The systematics of the low-lying excited states in even-even nuclei provides a sensitive probe to study the evolution of the shell structure. The anomalously lowered excited states in $^{12}\text{Be}^{1-3}$ are known to be a manifestation of the breakdown of the $N = 8$ shell closure. However, experimental difficulties have hampered the determination of a level scheme for ^{12}O . The advantage of the (p,t) reaction is that the angular distributions are sensitive to the transferred angular momentum. Observations of the characteristic distributions provide a firm confirmation of a new state and enable a reliable determination of its spin-parity.

In missing-mass studies using RI beams, the measurement of the energies and angles of the recoiling particles is essential to identify the excited states of interest and to determine the scattering angles for the reaction. The recoiling ions generally have low energies, and this results in a severe constraint on the possible target thickness. However, in the present reaction, which has a highly negative Q value (-31.7 MeV), the momentum of the incoming ^{14}O that yields ^{12}O is greatly reduced; this results in a relatively large momentum being imparted to the recoiling triton that is emitted in the forward direction. This enables us to use a 1-mm-thick solid hydrogen target⁴⁾ to increase the experimental yield.

The experiment was performed at the GANIL facility. The secondary ^{14}O beam at 51 AMeV was produced in the SISSI device⁵⁾ and delivered to the hydrogen target located in the scattering chamber of the SPEG spectrometer.⁶⁾ The incident position and incident angle on the target were monitored by two sets of multiwire low pressure chambers, CATS.⁷⁾ The purity (intensity) of ^{14}O was around 40% (6×10^4 pps). The ejectiles were detected by SPEG or a Si ΔE - E telescope provided by RIKEN. The energies and angles of the recoiling tritons were measured by an array of four MUST2 telescopes⁸⁾ located 30 cm downstream of the target. Each telescope, with an active area of 10×10 cm², consisted of a 0.3-mm-thick double-sided Si strip detector and a 4-cm-thick 16-fold CsI calorimeter.

The excitation energy (E_x) spectrum was made from the total kinetic energy and the laboratory scattering angle of the recoiling tritons. We observed a peak at an E_x of 1.8(4) MeV, which indicates a new excited state of ^{12}O . The spin-parity of the state was determined to be 0^+ or 2^+ by comparing the measured differential cross sections with distorted-wave calculations.

The E_x of the ^{12}O excited state is remarkably smaller compared to the second 0^+ and first 2^+ states of $^{14,16}\text{O}$ ($E_x \sim 6$ MeV) with a firm shell closure at $Z = 8$. On the other hand, it is close to the states of ^{12}Be ($E_x \sim 2$ MeV) with significant neutron sd -shell configurations. Thus, the lowered excited state indicates that the proton shell closure at $Z = 8$ is diminishing in ^{12}O . This demonstrates the persistence of mirror symmetry in the disappearance of the magic number 8 between ^{12}O and ^{12}Be . Implications for the shell quenching mechanism were discussed in terms of the shell model and the cluster model.

References

- 1) D. E. Alburger et al.: Phys. Rev. C **17**, 1525 (1978).
- 2) H. Iwasaki et al.: Phys. Lett. B **491**, 8 (2000).
- 3) S. Shimoura et al.: Phys. Lett. B **560**, 31 (2003).
- 4) P. Dolégiéviez et al.: Nucl. Instrum. Methods A **564**, 32 (2006).
- 5) A. Joubert et al.: Proceedings of the Second Conference of the IEEE Particle Accelerator p. 594 (1991).
- 6) L. Bianchi et al.: Nucl. Instrum. Methods A **276**, 509 (1989).
- 7) S. Ottini-Hustache et al.: Nucl. Instrum. Methods A **431**, 476 (1999).
- 8) E. Pollacco et al.: Eur. Phys. J. A **25**, 287 (2005).

[†] Condensed from the article in Phys. Rev. Lett. **103**, 152503 (2009)

^{*1} Department of Physics, University of Tokyo

^{*2} Institut de Physique Nucléaire, IN2P3-CNRS, France

^{*3} CEA-Saclay, DSM/IRFU SPhN, France

^{*4} The Andrzej Sołtan Institute for Nuclear Studies, Poland

^{*5} CNS, University of Tokyo

^{*6} Universidad de Sevilla, Spain

^{*7} RCNP, Osaka University

^{*8} GANIL, CEA/DSM-CNRS/IN2P3, France

Measurement of unbound excited states of ^{24}O

K. Tshoo,^{*1} Y. Satou,^{*1} T. Nakamura,^{*2} N. Aoi, H.C. Bhang,^{*1} S. Choi,^{*1} S. Deguchi,^{*2} F. Delaunay,^{*3} J. Gibelin,^{*3} T. Honda,^{*4} M. Ishihara, Y. Kawada,^{*2} Y. Kondo,^{*2} T. Kobayashi,^{*5} N. Kobayashi,^{*2} F.M. Marques,^{*3} M. Matsushita,^{*4} Y. Miyashita,^{*6} T. Motobayashi, Y. Nakayama,^{*2} N.A. Orr,^{*3} H. Otsu, H. Sakurai, S. Shimoura,^{*7} D. Sohler,^{*8} T. Sumikama,^{*6} S. Takeuchi, K.N. Tanaka,^{*2} N. Tanaka,^{*2} Y. Togano, K. Yoneda, K. Yoshinaga,^{*6} T. Zheng,^{*9} Z.H. Li, Z.X. Cao,^{*9}

[Nuclear structure, Neutron-rich nuclei, Magic number, Shell structure]

Changes in the magic number and shell structure that accompany an increase in neutron or proton numbers are important factors that indicate the structures of nuclei close to drip lines. Oxygen isotopes are the heaviest nuclei for which the neutron drip line has been experimentally established.¹⁾ While the γ -rays from the bound excited states of ^{20}O , ^{21}O , and ^{22}O ($N = 12\sim 14$) have been identified at GANIL,²⁾ those emitted from $^{23-24}\text{O}$ have not been observed. It implies that the first excited states of $^{23-24}\text{O}$ lie above the neutron threshold. Recently, the unbound excited states of ^{23}O have been determined by the invariant mass method at RIKEN and MSU.^{3,4)} The first 2^+ excited state of the most neutron rich oxygen isotope, ^{24}O , was studied by Hoffman *et al.*⁵⁾ However, the excited state was not clearly identified. Since the position of the first 2^+ excited state is one of the indicators of a magic nucleus, unambiguous identification of this state is essential to confirm that ^{24}O is a doubly magic nucleus. In the present experiment, we investigated the unbound excited states of ^{24}O using the $^{24}\text{O}(p,p')^{24}\text{O}^* \rightarrow ^{23}\text{O}+n$ reaction in inverse kinematics. The 2^+ excited state can be identified in the invariant mass spectrum of $^{23}\text{O}+n$. The experiment was performed at the RIPS facility operated by the RIKEN Nishina Center. A 63 MeV/nucleon secondary beam of ^{24}O was produced in a beryllium production target by the fragmentation of a 95 MeV/nucleon ^{40}Ar primary beam. The secondary beam was selected by magnetic analysis in the fragment separator, RIPS, and the ^{24}O beam with an intensity of ~ 4 ions/s was directed towards a liquid-hydrogen target. The target thickness was ~ 160 mg/cm². Background measurements were performed using an empty target cell. A schematic of the experimental setup is shown in Fig.1. The trajec-

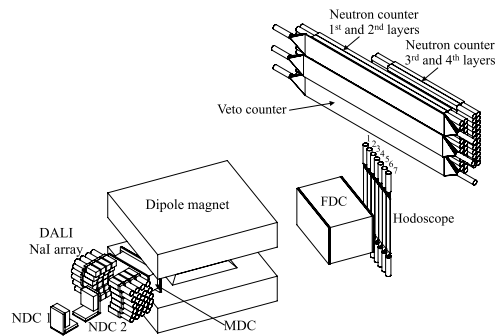


Fig. 1. Schematic view of the experimental setup.

tories of the charged fragments originating from the target were measured using two drift chambers, MDC (Middle Drift Chamber) and FDC (Fragment Drift Chamber), placed before and after a dipole magnet. The nuclear charge of the fragments was determined from the energy loss in the hodoscope placed just after the FDC. The neutrons emitted during the decay of $^{24}\text{O}^*$ were detected by a neutron-counter array placed ~ 4.5 m downstream from the target. The momentum vector of the neutrons were determined from the hit position in the neutron-counter array and the time of flight. A preliminary decay energy spectrum obtained

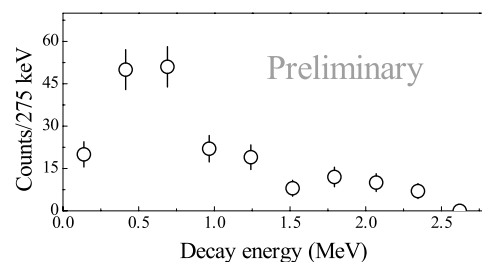


Fig. 2. Preliminary decay energy spectrum of $^{23}\text{O}+n$.

from the invariant mass of $^{23}\text{O}+n$ is shown by the open circles in Fig. 2. The first 2^+ excited state of ^{24}O is expected to be identified.

References

- 1) M. Thoennessen: Rep. Prog. Phys. **67**, 1187 (2004).
- 2) M. Stanoiu *et al.*: Phys. Rev. C **69**, 034312 (2004).
- 3) Z. Elekes *et al.*: Phys. Rev. Lett. **98**, 102502 (2007).
- 4) A. Schiller *et al.*: Phys. Rev. Lett. **99**, 112501 (2007).
- 5) C. R. Hoffman *et al.*: Phys. Lett. B **672**, 17 (2009).

^{*1} Department of Physics and Astronomy, Seoul National University, Korea.

^{*2} Department of Physics, Tokyo Institute of Technology, Japan.

^{*3} LPC Caen, ENSICAEN, Université de Caen, CNRS/IN2P3, Caen, France.

^{*4} Department of Physics, Rikkyo University, Japan.

^{*5} Department of Physics, Tohoku University, Japan.

^{*6} Department of Physics, Tokyo University of Science, Japan.

^{*7} Department of Physics, The University of Tokyo, Japan.

^{*8} Institute of Nuclear Physics (ATOMKI), Debrecen, Hungary.

^{*9} School of Physics and State Key Laboratory of Nuclear Physics and Technology, Peking University, Beijing, China.

Beta decay of the proton-rich nucleus ^{24}Si and its mirror asymmetry[†]

Y. Ichikawa, T. K. Onishi,^{*1} D. Suzuki,^{*1} H. Iwasaki,^{*1} T. Kubo, V. Naik,^{*2} A. Chakrabarti,^{*2} N. Aoi, B. A. Brown,^{*3} N. Fukuda, S. Kubono,^{*4} T. Motobayashi, T. Nakabayashi,^{*5} T. Nakamura,^{*5} T. Nakao,^{*1} T. Okumura,^{*5} H. J. Ong,^{*6} H. Suzuki, M. K. Suzuki, T. Teranishi,^{*7} K. N. Yamada, H. Yamaguchi,^{*4} and H. Sakurai

[Nuclear structure, Proton rich, Beta decay]

We performed β -decay spectroscopy on ^{24}Si to investigate the characteristic structure of proton-rich nuclei containing a weakly bound proton. We focused on the mirror asymmetry of the Gamow-Teller transition strength $B(\text{GT})$. The asymmetry of $B(\text{GT})$ reflects changes in the configuration of the wave function, induced by the Thomas-Ehrman (TE) shift^{1,2)} of the weakly bound s -wave proton. The spectroscopy included measurements of delayed γ rays, which had not been measured previously, as well as delayed protons^{3,4)} using a ΔE - E method.

The experiment was performed at RIPS⁵⁾. The secondary beam of ^{24}Si was produced by projectile fragmentation of a 100-MeV/nucleon ^{28}Si beam. For the γ -ray measurement, 0.72-mm-thick ^{nat}Ni was used as the primary target to improve beam purity, while for the proton measurement, 3.0-mm-thick ^9Be was used as the target to obtain a high yield of ^{24}Si . The total intensity of the secondary beam and the purity of ^{24}Si were 20 (4) kcps and 1.5 (4.1) %, respectively, in the case of the ^9Be (^{nat}Ni) target. To measure the half-lives of the detected particles, the beam was pulsed with a duty cycle of 500 ms/500 ms (beam on/off).

The measurements of delayed γ rays and protons were carried out using separate setups. In the γ -ray measurement, the beam was stopped by an active stopper made of a plastic scintillator to determine the implantation number of ^{24}Si . The emitted γ rays were detected using a clover-type Ge detector equipped with BGO Compton suppressors and a plastic β veto counter. For the proton measurement, the ΔE - E method, using telescopes composed of a gas ΔE detector and silicon E detectors, was employed in order to distinguish protons from β rays. To use the gas detector, all the setups were contained in a chamber filled with 20-Torr P10 (Ar 90% + CH_4 10%) gas.

By combining the results of the two measurements, the entire decay scheme of ^{24}Si was reconstructed. We observed two β branches to the bound 1_1^+ and 1_2^+ states

in ^{24}Al for the first time. The observation of the allowed transition firmly established the spin-parity assignment for the 1_2^+ state. The branching ratios to the 1_1^+ and 1_2^+ states were determined to be 31(4)% and 23.9(15)%, respectively. For obtaining the branching ratio to the 1_1^+ state, we assumed a reference value of the γ -decay ratio, $I_\gamma(^{24}\text{Al}^m) = 0.82(3)$ ⁶⁾. The branching ratios to three unbound states in ^{24}Al , including a new level at 6.735 MeV, were also determined for the first time. From the half-life measurement, the previously observed proton peaks^{3,4)} were confirmed to originate from ^{24}Si .

$B(\text{GT})$ of ^{24}Si was deduced for the observed allowed transitions. Focusing on the low-lying bound states, $B(\text{GT})$ values were determined to be 0.13(1) and 0.14(1) for the 1_1^+ and 1_2^+ states, which were smaller than its mirror counterparts⁷⁾ by 22(11)% and 10(8)%, respectively. The asymmetry observed of $B(\text{GT})$ in the 1_2^+ state and the 1_1^+ state indicated changes in the configuration of the wave function, induced by the TE shift. To clarify the mechanism of the asymmetry from a microscopic perspective, the experimental values of $B(\text{GT})$ were compared with theoretical estimates obtained using the shell model. The asymmetry of $B(\text{GT})$ was reproduced by the shell-model calculation with the USD Hamiltonian⁸⁾ and effects of the weak binding energy, where the single-particle energy of the proton $1s_{1/2}$ orbital was lowered by 500 keV to reproduce the TE shift for the 1_2^+ state in ^{24}Al . The applicability of the calculation was confirmed in terms of the overall $B(\text{GT})$ distribution over the unbound states in ^{24}Al . The calculation indicated the asymmetry of $B(\text{GT})$ in the 1_1^+ state could be attributed to the changes in the configuration of the wave function, accompanying the lowering of the $1s_{1/2}$ orbital. As for the 1_2^+ state, changes in some amplitudes are canceled, and in these cases, the asymmetry is not significant.

References

- 1) R. G. Thomas: Phys. Rev. **88**, 1109 (1952).
- 2) J. B. Ehrman: Phys. Rev. **81**, 412 (1951).
- 3) S. Czajkowski *et al.*: Nucl. Phys. **A628**, 537 (1998).
- 4) V. Banerjee *et al.*: Phys. Rev. C **63**, 024307 (2001).
- 5) T. Kubo *et al.*: Nucl. Instrum. Meth. **B70**, 309 (1992).
- 6) J. Honkanen *et al.*: Phys. Scr. **19**, 239 (1979).
- 7) R. E. McDonald *et al.*: Phys. Rev. **181**, 1631 (1969).
- 8) B. A. Brown and B. H. Wildenthal: Ann. Rev. of Nucl. Part. Sci. **38**, 29 (1988).

[†] Condensed from the article in Phys. Rev. C **80**, 044302 (2009)

^{*1} Department of Physics, University of Tokyo

^{*2} Variable Energy Cyclotron Centre, India

^{*3} Department of Physics and Astronomy, and NSCL, Michigan State University, USA

^{*4} Center for Nuclear Study, University of Tokyo

^{*5} Department of Physics, Tokyo Institute of Technology

^{*6} Research Center for Nuclear Physics, Osaka University

^{*7} Department of Physics, Kyushu University

Measurement on proton-proton correlation of the excited ^{23}Al

Y. G. Ma,^{*1} D. Q. Fang,^{*1} P. Zhou^{*1,*2} X. Z. Cai,^{*1} J. G. Chen,^{*1} W. Guo,^{*1} X. Y. Sun^{*1,*2} W. D. Tian,^{*1} H. W. Wang,^{*1} G. Q. Zhang^{*1,*2} X. G. Cao^{*1,*2} Y. Fu^{*1,*2} Z. G. Hu,^{*3} J. S. Wang,^{*3} M. Wang,^{*3} Y. Togano, N. Aoi, H. Baba, Y. Hara,^{*4} T. Honda,^{*4} K. Ieki,^{*4} Y. Ishibashi,^{*5} Y. Itou,^{*5} N. Iwasa,^{*6} S. Kanno, T. Kawabata,^{*7} H. Kimura,^{*8} Y. Kondo, K. Kurita,^{*4} M. Kurokawa, T. Moriguchi,^{*5} H. Murakami, H. Oishi,^{*5} K. Okada,^{*4} S. Ota,^{*7} A. Ozawa,^{*5} H. Sakurai, S. Shimoura,^{*7} R. Shioda,^{*4} E. Takeshita, S. Takeuchi, K. Yamada, Y. Yamada,^{*4} Y. Yasuda,^{*5} K. Yoneda, and T. Motobayashi

[$C(^{23}\text{Al}, p+p+^{21}\text{Na})C$, two-proton emission, momentum correlation]

For the proton-rich nuclei, the proton decay mechanism is complicated, especially for two-protons radioactivity¹⁾. Considering the proton-rich nucleus ^{23}Al is of very interesting in many aspects²⁻⁵⁾, we measured the relative momentum and opening angle of the two protons emitted from the excited state in ^{23}Al . A radioactive isotope beam of ^{23}Al was produced and selected using RIPS facility in RIKEN Nishina Center. The secondary ^{23}Al beam with an incident energy of 72 AMeV were generated by the projectile fragmentation of a 135 A MeV ^{28}Si primary beam on a ^9Be production target and then transported to a ^{12}C reaction target. Five layers of silicon detector were arranged in the downstream, of which the first two layers of Si-strip (5mm width) detectors located 62 cm downstream of the ^{12}C target were used to measure the emitted angle of the fragment and protons. Each Si-strip layer consists of 5×5 matrix without detectors in the four corners. Three layers of element Si detectors were used as the ΔE - E detectors for the fragment. The plastic hodoscopes located 2.95 m downstream of the target were used as ΔE , E and TOF detectors for protons. Most of the protons stopped before the third layer. The particle identification of ^{23}Al before the reaction target was done by means of $B\rho$ - ΔE -TOF method. After the reaction target, the heavy fragments were identified by five layers silicon detectors combination through the ΔE - E technique. Both the emitted angle and energy loss can be obtained for the fragments. The total energy of heavy fragments can be obtained by summing over the energy loss of the five layers silicon detectors.

Clear particle identification was got and the ($^{21}\text{Na} + p + p$) reaction channel was picked. By the full reconstruction of ^{23}Al three-body decay channel, we can reconstruct the excitation energy of ^{23}Al based on the invariant mass analysis. Preliminary results of relative momentum spectrum and opening angle of the two protons in the rest frame of three-body decay system of

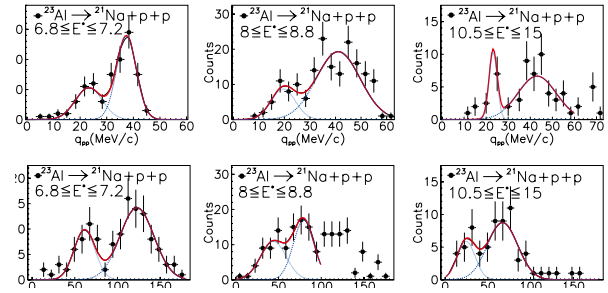


Fig. 1. Preliminary results of the relative momentum spectrum of two protons for ^{23}Al decays into two protons and ^{21}Na (upper panel) and of the opening angle between two protons in the center of mass of decaying system (lower panel) in different excitation energy windows.

$p+p+^{21}\text{Na}$ are presented in Fig. 1, respectively, under some excitation energy windows. From the left to the right, it corresponds to the windows of $6.8 \leq E^* \leq 7.2$, $8.0 \leq E^* \leq 8.8$ and $10.5 \leq E^* \leq 15$, respectively. Two Gaussian fits are plotted in the spectra. A peak in relative momentum q_{pp} around 20 MeV/c is observed which dominantly corresponds to a peak in smaller opening angular θ_{pp} around 30-60° in those excitation windows. In the same time, another peak is observed around $q_{pp} \sim 40$ MeV/c which dominantly corresponds to larger θ_{pp} . Physically, the peak at 20 MeV/c of q_{pp} and small opening angle is consistent with the diproton emission mechanism. In contrary, the peak at larger q_{pp} and θ_{pp} may correspond to sequential proton decay or three body democratic decay. More details on the analysis are in progress.

References

- 1) V. I. Goldansky: Nucl. Phys. 19, 482 (1960).
- 2) X. Z. Cai et al.: Phys. Rev. C 65, 024610 (2002).
- 3) T. Gomi et al.: Nucl Phys. A 758, 761c (2005).
- 4) A. Ozawa et al.: Phys. Rev. C 74, 021301(R) (2006).
- 5) D. Q. Fang et al.: Phys. Rev. C 76, 031601(R) (2007).

^{*1} Shanghai Institute of Applied Physics, CAS, Shanghai 201800, China

^{*2} Graduate School of the CAS, Beijing 100039, China

^{*3} Institute of Modern Physics, CAS, Lanzhou 730000, China

^{*4} Department of Physics, Rikkyo University, Japan

^{*5} Institute of Physics, University of Tsukuba, Ibaraki, Japan

^{*6} Department of Physics, Tohoku University, Japan

^{*7} Department of Physics, Kyoto University, Japan

^{*8} Department of Physics, University of Tokyo, Japan

Persistent decoupling of valence neutrons toward the drip line: Study of ^{20}C by γ spectroscopy[†]

Z. Elekes, *¹ Zs. Dombrádi, *¹ T. Aiba, *² N. Aoi, H. Baba, D. Bemmerer, *³ B. A. Brown, *⁴ T. Furumoto, *⁵
Zs. Fülöp, *¹ N. Iwasa, *⁶ Á. Kiss, *⁷ K. Kobayashi, *¹⁰ Y. Kondo, *⁸ T. Motobayashi, T. Nakabayashi, *⁸
T. Nannichi, *⁸ Y. Sakuragi, *⁵ H. Sakurai, D. Sohler, *¹ M. Takashina, *⁹ S. Takeuchi, K. Tanaka, Y. Togano,
K. Yamada, M. Yamaguchi, and K. Yoneda

[nuclear structure, unstable nuclei, inelastic scattering]

A few years ago, the decoupling of strongly bound neutrons in heavy carbon and boron isotopes was reported¹⁻⁴; the decoupling was observed as a reduction in the quadrupole polarization charge of the neutrons. This suppression of the polarization charge was associated with the extended distribution of the valence neutrons⁵⁻⁷ detected in reaction cross-section measurements⁸. This might also be accompanied by a change in the structure of the giant quadrupole resonance in neutron rich nuclei^{5,6,9}.

Recently, the lifetime of the 2_1^+ state in ^{16}C has been remeasured, and the decoupling phenomenon has been reviewed¹⁰. However, another recent work suggests the existence of this decoupling effect¹¹. Here, we report a study on neutron and proton transition strengths and polarization charges, as investigated by inelastic scattering processes in the heavy carbon isotope ^{20}C , lying next to ^{19}C in the chart of nuclides, which shows halo characteristics in its ground state. Our aim is to provide further evidence that the decoupling phenomenon occurs in the carbon isotopic chain.

The experiment was carried out at RIKEN Nishina Center, where a ^{20}C beam with an intensity of 10 particle/s (pps) was provided by the RIPS fragment separator. The beam was transmitted to secondary targets of ^{208}Pb and liquid hydrogen with thicknesses of 1445 mg/cm² and 190 mg/cm², respectively. The reaction occurred at a mean energy of 37.6 MeV/nucleon (middle of the target) in the Pb run and 41.4 MeV/nucleon in the ^1H run. A stack of 160 NaI(Tl) crystals, called DALI2, surrounded the target; thus the de-excitation γ rays emitted by the inelastically scattered nuclei could be detected. From the experimental γ ray spectra, we determined the cross sections at $\sigma^{Pb}(0_{gs}^+ \rightarrow 2_1^+) = 35 \pm 8$ mb and

$\sigma^{pp}(0_{gs}^+ \rightarrow 2_1^+) = 24 \pm 4$ mb for the runs involving Pb and liquid hydrogen targets, respectively. The results were analyzed in the framework of the coupled channel code ECIS97. This code uses standard collective form factors to calculate the inelastic cross sections. In this manner, the neutron and proton deformation lengths were determined as $\delta_n = 1.57 \pm 0.14$ (stat) fm, $\delta_p = 0.60 \pm 0.32$ (stat) fm. The corresponding multipole proton and neutron transition matrix elements (M_p^2, M_n^2) could then be calculated as $M_p^2 = 7.8 \pm_{-6.1}^{+10.6}$ (stat) fm⁴ and $M_n^2 = 292 \pm 52$ (stat) fm⁴, respectively. The validity of the phenomenological approach was further examined by performing microscopic coupled-channels (MCC) calculations involving the use of folding model interactions along with the AMD transition density¹²; the results of this calculation agreed well with those of phenomenological analysis. In order to analyze the effective charges, the transition probabilities were calculated within the shell model. A reduction in the value of the normal polarization charges by a factor of about 0.4 was needed to reproduce the experimental trend in carbon isotopes. The fact that the polarization charges have decreased to less than half of the standard values indicates that the coupling of the valence neutrons to the core has become weaker; or in other words, the valence neutrons decoupled to some extent from the nuclear core. These decreased values of polarization charges could be attributed to the extended valence neutron distribution.

References

- 1) H. Ogawa et al.: Phys. Rev. C **67**, 064308 (2003).
- 2) Zs. Dombrádi et al.: Phys. Lett. B **621**, 81 (2005).
- 3) N. Imai et al.: Phys. Rev. Lett. **92**, 062501 (2004).
- 4) Z. Elekes et al.: Phys. Lett. B **586**, 34 (2004).
- 5) H. Sagawa et al.: Phys. Rev. C **63**, 064310 (2001).
- 6) H. Sagawa et al.: Eur. Phys. J. A **13**, 87 (2002).
- 7) Y. Suzuki et al.: Phys. Rev. C **70**, 051302 (2004).
- 8) A. Ozawa et al.: Nucl. Phys. A **691**, 599 (2001).
- 9) H. Sagawa et al.: Phys. Rev. C **65**, 064314 (2002).
- 10) M. Wiedeking et al.: Phys. Rev. Lett. **100**, 152501 (2008).
- 11) H. J. Ong et al.: Phys. Rev. C **78**, 014308 (2008).
- 12) Y. Kanada-En'yo et al.: Phys. Rev. C **71**, 014310 (2005).

[†] Condensed from the article in Phys. Rev. C **79**, 011302(R) (2009)

*¹ Institute of Nuclear Research of the Hungarian Academy of Sciences, Hungary

*² Niigata University, Japan

*³ Forschungszentrum Dresden-Rossendorf, Germany

*⁴ Michigan State University, USA

*⁵ Osaka City University, Japan

*⁶ Tohoku University, Japan

*⁷ Eötvös Loránd University, Hungary

*⁸ Tokyo Institute of Technology, Japan

*⁹ RCNP, Osaka University, Japan

*¹⁰ Saitama University, Japan

Spin-Orbit Potentials of Neutron-Rich Helium Isotopes[†]

S. Sakaguchi, T. Uesaka,^{*1} T. Kawabata,^{*1} T. Wakui,^{*2} N. Aoi, Y. Hashimoto,^{*3} Y. Ichikawa, K. Itoh,^{*5} M. Itoh,^{*2} H. Iwasaki,^{*4} T. Kawahara,^{*6} Y. Kondo,^{*3} H. Kuboki, Y. Maeda,^{*7} K. Miki,^{*4} T. Nakamura,^{*3} T. Nakao,^{*4} Y. Nakayama,^{*3} S. Noji,^{*4} H. Okamura,^{*8} H. Sakai,^{*4} Y. Sasamoto,^{*1} M. Sasano, Y. Satou,^{*3} K. Sekiguchi, T. Shimamura,^{*3} Y. Shimizu, M. Shinohara,^{*3} K. Suda, D. Suzuki,^{*4} Y. Takahashi,^{*4} A. Tamii,^{*8} K. Yako,^{*4} and M. Yamaguchi

[Nuclear reactions, Polarized proton, Elastic scattering, Helium isotope]

Recently, much interest has been focused on spin-dependent interactions in unstable nuclei. In order to investigate the spin-dependent interactions between protons and neutron-rich He isotopes, we measured the vector analyzing power of the proton elastic scattering from ⁶He and ⁸He at 71 MeV/A. The experiment was carried out using the RIKEN Projectile-Fragment Separator (RIPS). We used a solid polarized proton target as a secondary target; this target was specially constructed for radioactive-ion-beam experiments^{1,2}). The target was a 1-mm-thick single crystal of naphthalene. The average target polarization was $11.0 \pm 2.5\%$. Recoil protons and scattered particles were both detected. The measured differential cross sections $d\sigma/d\Omega$ and analyzing powers A_y are indicated by closed circles in Fig. 1. The values of $d\sigma/d\Omega$ are consistent with the previous data³), which are indicated by open circles.

In order to extract the global nature of \vec{p} -^{6,8}He interactions, our experimental data were phenomenologically analyzed by using optical model potentials. We assumed the central and spin-orbit terms as functions similar to Woods-Saxon function and Thomas type function, respectively. We used fitting code ECIS79 to determine a parameter set that reproduces the

data. The parameter set for \vec{p} -⁶Li elastic scattering at 72 MeV/A⁴) was used as the initial potential. The dashed lines in Fig. 1 indicate the calculation performed using the initial parameters. Results obtained using the best-fit parameters are represented by the solid curves. Except at backward angles, the $d\sigma/d\Omega$ and A_y data are well reproduced.

Next, we focus on the radius and the amplitude of the peak of the spin-orbit potential; we call the former as “LS radius” and the latter as “LS amplitude”. Since the spin-orbit potential is approximated by the radial derivative of density distribution, LS radius and LS amplitude should be closely related to the radius and the gradient, respectively, of the density distribution. The LS radii and LS amplitudes of ⁶He and ⁸He are indicated by closed squares in Fig. 2. Those of neighboring even-even stable nuclei^{5,6}) and the global optical potential⁷) are indicated by closed and open circles, respectively. It is apparent that the LS amplitudes of ⁶He and ⁸He are much smaller than those of stable nuclei. Thus, the neutron-rich helium isotopes are characterized by remarkably shallow spin-orbit potentials. This feature can be intuitively explained from the diffused density distribution of ⁶He and ⁸He, whose density gradient is less than half that of ⁴He.

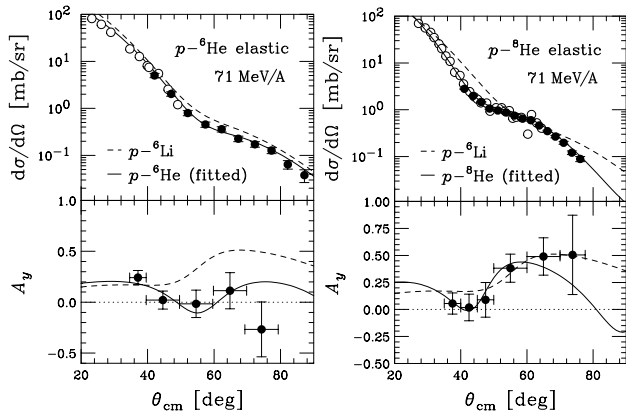


Fig. 1. Differential cross sections and vector analyzing powers of the \vec{p} -^{6,8}He elastic scattering at 71 MeV/A.

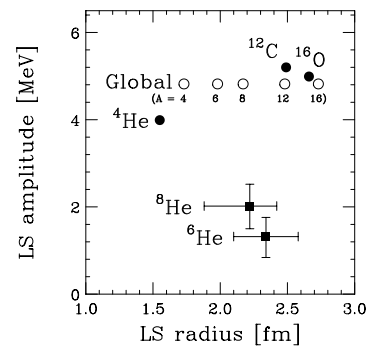


Fig. 2. LS radii and LS amplitudes of even-even nuclei.

^{*1} Center for Nuclear Study, University of Tokyo
^{*2} Cyclotron and Radioisotope Center, Tohoku University
^{*3} Department of Physics, Tokyo Institute of Technology
^{*4} Department of Physics, University of Tokyo
^{*5} Department of Physics, Saitama University
^{*6} Department of Physics, Toho University
^{*7} Department of Physics, Kyushu University
^{*8} Research Center for Nuclear Physics, Osaka University

References

- 1) T. Wakui et al.: Nucl. Instr. Meth. **550**, 521 (2005).
- 2) T. Uesaka et al.: Nucl. Instr. Meth. **526**, 186 (2004).
- 3) A. Korshennikov et al.: Nucl. Phys. A **617**, 45 (1997).
- 4) R. Henneck et al.: Nucl. Phys. A **571**, 541 (1994).
- 5) Y. Iseri et al.: Genshikaku Kenkyu **49** No.4, 53 (2005).
- 6) H. Sakaguchi et al.: Phys. Rev. C **26**, 944 (1982).
- 7) B.A. Watson et al.: Phys. Rev. **182**, 977 (1969).

Elastic scattering for 60MeV ^{17}F on ^{12}C target[†]

G. L. Zhang,^{*1} K. J. Liu,^{*1} H. Q. Zhang,^{*2} C. J. Lin,^{*2} C. L. Zhang,^{*2} G. P. An,^{*2} Z. D. Wu,^{*2} H. M. Jia,^{*2} X. X. Xu,^{*2} F. Yang,^{*2} Z. H. Liu,^{*2} S. Kubono,^{*3} H. Yamaguchi,^{*3} S. Hayakawa,^{*3} D. N. Binh,^{*3} Y. K. Kwon,^{*4} and N. Iwasa^{*5}

[Elastic scattering, optical potential, proton drip line]

Our knowledge of nuclei comes mainly from the experiments with nuclei in the valley of the stability. Experiments with nuclei far from the stability-line are expected to provide tests of current nuclear structure models. In particular, light nuclei locating near the drip line may exhibit exotic phenomena, such as manifestations of halo/skin structure. Information on the nuclear structure can be extracted from the reaction data. Among many nuclear reactions, the elastic scattering is a major channel and will provide rich information on reaction mechanism and structures of the nuclei. It is also used to determine optical potentials which are important inputs for any reaction studies. However, elastic scattering data for light exotic nuclei are extremely scarce, which raises questions about accuracy and reliability of nuclear structure information extracted from the reaction studies. Because of halo/skin structures and the small binding energy of the last nucleon(s), the light exotic nuclei may behave differently from stable, well-bound nuclei in reactions and reliability of simple-minded extrapolation from the systematics in stable nuclei is open to doubt. Thus, studies of elastic scattering induced by light exotic nuclei are of particular interest.

Study of the ^{17}F elastic scattering is motivated by our interest described above. The study of this nucleus is quite interesting for three reasons: (i) Because of its small binding energy of 601keV, the rms radius could be significantly larger than that of ^{16}O core. (ii) It has only one bound state below the breakup threshold, (iii) its first excited state has a halo structure.^{1,2)} Many experiments have been performed to explore its structure and reaction mechanisms in recent years. Elastic scattering of $^{17}\text{F}+^{208}\text{Pb}$ was measured at 10MeV/nucleon,³⁾ 98MeV and 120 MeV,⁴⁾ 90.4MeV,⁵⁾ respectively. Precise data have been obtained for the elastic scattering of ^{17}F on ^{12}C and ^{14}N at 10MeV/nucleon.⁶⁾ In most of the above cases, the data are taken for the ^{208}Pb target. The experimental data on light targets are hardly found, except for the data on ^{12}C and ^{14}N at the energy of 10MeV/nucleon.⁶⁾ Therefore the experiment was planned to extract the optical potential of the elastic scattering for ^{17}F on light target at energies near Coulomb barrier.

In order to obtain the elastic scattering data at energy near Coulomb barrier, 60MeV $^{17}\text{F}+^{12}\text{C}$ reaction was studied at CNS Radioactive Ion Beam separator (CRIB). The beam intensity on the target was about 4×10^5 pps. A $435\mu\text{g}/\text{cm}^2$ -thick ^{12}C target was used. Projectile ^{17}F was identified by the time of flight (TOF) method. The Position of ^{17}F on ^{12}C target was determined by using infor-

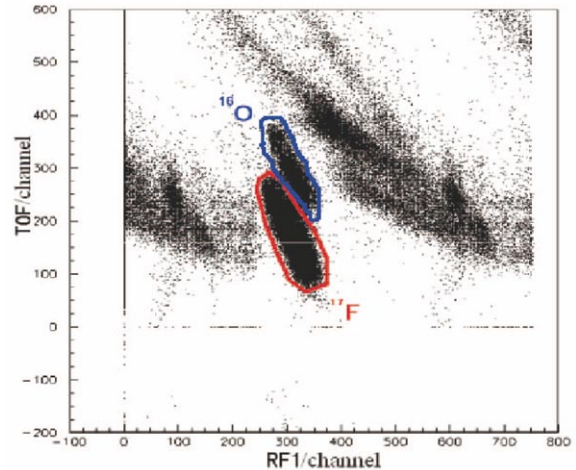


Fig. 1. The particle identification before target.

mation from two position-sensitive PPACs (Parallel Plate Avalanche Counters) set in the beam line. Six sets of ΔE -E detector telescopes were composed of double sided Silicon strip detectors (50mm \times 50mm in area) (DSSD) and silicon detectors without strips (SSD), and covered angle range $\theta_{lab} = 5^\circ - 80^\circ$. They were symmetrically positioned around the beam axis in order to measure efficiently the events of ^{17}F elastic scattering. The distance from the target center to the strip detectors are 145 mm, 115 mm and 85 mm depending on the three angle settings. Thin ΔE detectors (DSSD, 65 μm thickness) were placed in front of 300 μm -thick E detectors (SSD). Such detector configuration allowed identification of the atomic number Z of the scattered charged particles. The emission angle of ^{17}F can be determined precisely by the silicon strip detectors. We will be able to extract precisely the angular distribution of elastic scattering for 60MeV $^{17}\text{F}+^{12}\text{C}$.

Figure 1 shows the particle identification before target. RF1 the time when the beam particle arrives at a PPAC relative to the radiofrequency signal from the cyclotron resonator. TOF is obtained by using the time signals of two PPACs before target. It is shown that ^{17}F particles can be identified clearly from the primary ^{16}O beam with a high intensity. More detailed analysis of elastic scattering for 60MeV $^{17}\text{F}+^{12}\text{C}$ are being done.

References

- 1) R. Morlock et al.: Phys. Rev. Lett. **79**, 3837 (1997).
- 2) M. J. Borge et al.: Phys. Lett. B. **217**, 25 (1993).
- 3) J. F. Liang et al.: Phys. Rev. C **65**, 051603 (2002).
- 4) J. F. Liang et al.: Phys. Rev. C **67**, 044603 (2003).
- 5) M. Romoli et al.: Phys. Rev. C **69**, 064614 (2004).
- 6) J. C. Blackmon et al.: Phys. Rev. C **72**, 034606 (2005).

*1 School of Physics and Nuclear Energy Engineering, Beihang University, Beijing 100191, China

*2 China Institute of Atomic Energy, Beijing 102413, China

*3 Center of Nuclear Study, University of Tokyo, Japan

*4 Department of Physics, Chung-Ang University, Seoul 156-756, South Korea

*5 Department of Physics, Tohoku University, Aoba, Sendai, Miyagi 980-8578, Japan

Experiment to determine the g -factor of neutron-rich S isotope

A. Yoshimi, H. Ueno, Y. Hasama,^{*1} H. Iijima,^{*1} Y. Ishii,^{*1} Y. Ichikawa, K. Tajiri,^{*2} T. Furukawa,^{*1}
 Y. Ishibashi,^{*3} D. Nagae,^{*3} K. Suzuki,^{*1} T. Inoue,^{*1} M. Tsuchiya,^{*1} H. Hayashi,^{*1}
 M. Uchida,^{*1} H. Kawamura,^{*4} and K. Asahi^{*1}

[Nuclear structure, magnetic moment, unstable nuclei]

The nuclear moments of neutron-rich $^{30-33}\text{Al}$ were determined¹⁻³⁾ using the β -NMR method that involves spin-polarized radioactive-isotope beams. We have recently started measuring the nuclear moments of neutron-rich nuclei with neutron number N around 28; several interesting phenomena indicating the disappearance of the $N = 28$ shell gap in Si and S isotopes were reported from γ -spectroscopy experiments⁴⁾. The measurement of magnetic moments is important in order to precisely understand the nuclear wave function.

The first experiment for ^{41}S was carried out at the RIKEN Accelerator Research Facility in January 2010. A beam of ^{41}S was produced by the fragmentation of ^{48}Ca projectiles at an energy $E = 63 \text{ A MeV}$ impinging on a ^9Be target having a thickness of 139 mg/cm^2 . The beam current of ^{48}Ca impinging on the Be target was typically $100 - 200$ particle nA. The isotope-separation of the ^{41}S beam was carried out using a projectile-fragment separator RIPS (RIKEN Projectile Separator), in which the emission angle θ_F and momentum p_F of the fragment were selected so as to obtain spin-polarized secondary beam. Under the condition of $p_F = p_0 \times (1.035 \pm 0.030)$ and $\theta_F > 0.5^\circ$ with a primary beam of 100 particle nA, ^{41}S beam from RIPS with a purity of 44% and an intensity of 3.8×10^3 particles/s was obtained. Here, p_0 represents the central momentum of the fragment.

The ^{41}S beam was then transported to the final focus and implanted into a 0.7-mm-thick CaS (Calcium Sulfide) multi-crystal stopper in the β -NMR apparatus. A static magnetic field $B_0 = 500 \text{ mT}$ was applied to the stopper in order to preserve the spin polarization. A radio-frequency oscillating field B_1 of around 1 mT was applied to the stopper in the direction perpendicular to B_0 . From the results of solid-state NMR measurements for the stable isotope ^{33}S , it was observed that the relaxation time of ^{33}S in CaS was longer than in other materials⁵⁾; hence, CaS was as the material for the stopper.

The search of the g -factor of ^{41}S was performed using the β -NMR technique. In this technique, resonance is detected by the change in the β -ray up/down ratio R , which is measured using plastic scintillator telescopes located above and below the stopper. On the basis of a double ratio R/R_0 , where R_0 is the β -ray up/down

ratio when the oscillating magnetic field B_1 is not applied, the resonance frequency is derived from the measured β -NMR spectrum. Since the ground-state spin and parity of ^{41}S have not been determined, the shell model predicts the ^{41}S g -factor to be in the wide range $0.25 - 1.25$. For this experiment, we have developed a fast-switching LCR circuit⁶⁾ in order to realize the quick and sequential application of the NMR B_1 field with frequencies over a wide range. This technique makes it possible to efficiently scan the frequencies over a wide range for g -factor in the range $0.25 - 1.25$. The g -factor search in the range $g = 0.25 - 1.25$ was performed for two kinds of stopper materials CaS and Si. The analysis of the NMR spectrum is now in progress.

References

- 1) D. Nagae et al.: Phys. Rev. C **79**, 027301 (2009).
- 2) H. Ueno et al.: RIKEN Accel. Prog. Rep. 42 (2009).
- 3) M. De Rydt et al.: Phys. Lett. B **678**, 344 (2009).
- 4) J. Fridmann et al.: Nature **435**, 922 (2006).
- 5) T.A. Wagler et al., J. Mag. Res. **161**, 191 (2003).
- 6) K. Minamisono et al., Nucl. Inst. Meth. in Phys. Res. A **589**, 185 (2008).

^{*1} Department of Physics, Tokyo Institute of Technology

^{*2} Department of Physics, Osaka University

^{*3} Department of Physics, University of Tsukuba

^{*4} Department of Physics, Rikkyo University

Coulomb excitation of ^{36}Ca

N. Iwasa,^{*1} N. Kume,^{*1} Y. Togano, N. Aoi, H. Baba, S. Bishop, X. Cai,^{*2} P. Doornenbal, D. Fang,^{*2} T. Furukawa, Y. Hara,^{*3} T. Honda,^{*3} K. Ieki,^{*3} S. Kanno, T. Kawabata,^{*4} N. Kobayashi,^{*5} Y. Kondo, T. Kuboki,^{*6} K. Kurita,^{*3} M. Kurokawa, K. Li, Y.G. Ma,^{*2} M. Matsushita,^{*3} S. Michimasa,^{*4} H. Murakami, T. Nakamura,^{*5} K. Okada,^{*3} S. Ota,^{*4} Y. Satou,^{*5} H. Scheit, S. Shimoura,^{*4} R. Shioda,^{*3} T. Suzuki,^{*6} S. Takeuchi, K.N. Tanaka,^{*5} K. Tanaka, W. Tian,^{*2} H. Wang,^{*2} J. Wang,^{*7} K. Yamada, Y. Yamada,^{*3} K. Yoneda, and T. Motobayashi

[NUCLEAR REACTIONS: $\text{Pb}(^{36}\text{Ca}, ^{35}\text{K} p)$, Coulomb excitation]

The Coulomb excitation of the proton-rich nucleus of ^{36}Ca was studied to determine the reduced transition probability $B(E2)$ and the ratio of neutron-to-proton multipole matrix elements M_n/M_p for the $0_{\text{gs}}^+ \rightarrow 2_1^+$ transition in ^{36}Ca . Recently, the 2_1^+ excitation energy of ^{36}Ca was determined to be $3.015(16)$ MeV¹, which is 0.44 MeV higher than the proton separation energy and 0.28 MeV lower than the excitation energy of the mirror nucleus ^{36}S . The extremely large mirror energy difference was discussed in the framework of the shell model by considering an ^{16}O core, the sd -shell isospin-symmetric interaction USD, and the experimental single particle energies of ^{17}F and ^{16}O ¹. To obtain further information on the nuclear structure of ^{36}Ca , the experimental determination of $B(E2)$ and M_n/M_p is desirable.

An experiment was carried out using a part of the RIBF accelerator complex operated by the RIKEN Nishina Center and Center for Nuclear Study, University of Tokyo. A lead target with a thickness of 244 mg/cm² was bombarded by a radioactive ^{36}Ca beam; the beam was produced by the fragmentation of a ^{40}Ca beam at 100 A MeV on a 1-mm-thick Be target and separated by RIPS and the RF deflector². The average beam energy in the target was 58 A MeV. The typical ^{36}Ca beam intensity was 100 cps and the purity of the beam was 4.3%.

Scattering angles of reaction products, ^{36}Ca , ^{35}K , and protons were measured by an array of 21 position-sensitive silicon telescopes arranged in a 5×5 matrix and placed 0.62 m downstream of the target. Since ^{36}Ca and ^{35}K particles were stopped in the telescopes, particle identification was performed by the ΔE - E method. Protons penetrated the telescopes and were detected by a plastic scintillator hodoscope consisting of 5-mm-thick ΔE and 60-mm-thick E layers that were placed 2.95 m downstream of the target. De-excitation γ rays from the reaction products were detected using 160 NaI (Tl) scintillators (DALI2)³ surrounding the

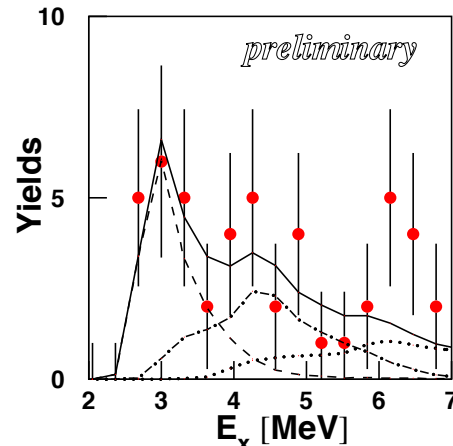


Fig. 1. Yields of breakup events plotted as a function of the excitation energy of ^{36}Ca . The solid curve represents the best fit; simulated response functions at $E_x = 3.0$, 4.3, and 6.0 MeV are also shown (dashed, dot-dashed, and dotted curves, respectively).

target. Experimental results relating to the γ channel have previously been reported⁴.

The p - ^{35}K coincidence yields are shown in Fig. 1 as a function of the excitation energy of ^{36}Ca which is calculated from the measured scattering angles and energies of ^{35}K and proton. A peak corresponding to the 2_1^+ excited state is clearly seen at 3.0 MeV, and two new peaks are observed around 4.3 MeV and 6.0 MeV. The spectrum is well reproduced by response functions calculated by Monte Carlo simulations using GEANT3⁵. In the calculation of the response function, theoretical angular distributions calculated with the coupled channel code ECIS97⁶ were used. Further analysis of the data is in progress.

References

- 1) P. Doornenbal et al.: Phys. Lett. B **647**, 237 (2007).
- 2) K. Yamada et al.: Nucl. Phys. A **746**, 156c (2004).
- 3) S. Takeuchi et al.: RIKEN Accel. Prog. Rep. **36**, 148 (2003).
- 4) N. Iwasa et al.: RIKEN Accel. Prog. Rep. **42**, 14 (2009).
- 5) Detector description and simulation tool developed by CERN, Geneva, Switzerland.
- 6) J. Raynal, coupled channel code ECIS97, unpublished.

*1 Department of Physics, Tohoku University
 *2 Shanghai Institute of Applied Physics, China
 *3 Department of Physics, Rikkyo University
 *4 CNS, University of Tokyo
 *5 Department of Physics, Tokyo Institute of Technology
 *6 Department of Physics, Saitama University
 *7 Institute of Modern Physics, China

Experimental investigation of stellar $^{30}\text{S}(p, \gamma)^{31}\text{Cl}$ reaction by Coulomb dissociation method

Y. Togano, T. Motobayashi, N. Aoi, H. Baba, S. Bishop, X. Cai,^{*1} P. Doornenbal, D. Fang,^{*1} T. Furukawa, K. Ieki,^{*2} N. Iwasa,^{*3} T. Kawabata,^{*4} S. Kanno, N. Kobayashi,^{*5} Y. Kondo, T. Kuboki,^{*6} N. Kume,^{*3} K. Kurita,^{*2} M. Kurokawa, Y. G. Ma,^{*1} Y. Matsuo, H. Murakami, M. Matsushita,^{*2} T. Nakamura,^{*5} K. Okada,^{*2} S. Ota,^{*4} Y. Satou,^{*5} S. Shimoura,^{*4} R. Shioda,^{*2} K. N. Tanaka,^{*5} S. Takeuchi, W. Tian,^{*1} H. Wang,^{*1} J. Wang,^{*7} K. Yamada, Y. Yamada,^{*2} and K. Yoneda

[$^{208}\text{Pb}(^{31}\text{Cl}, p\ ^{30}\text{S})^{208}\text{Pb}$, nuclear astrophysics, Coulomb dissociation]

The stellar reaction $^{30}\text{S}(p, \gamma)^{31}\text{Cl}$ was studied by Coulomb dissociation method. This reaction occurs during the rapid proton (*rp*) capture process of hydrogen burning on an accreting neutron star.¹⁾ The ^{30}S nucleus is a candidate for the waiting point, at which the reaction flow temporarily stops, in the *rp* process.²⁾ As the $^{30}\text{S}(p, \gamma)^{31}\text{Cl}$ reaction proceeds, the amount of ^{30}S decreases and thus, the reaction flow in the *rp* process is speeded up. Therefore, the strength of this reaction affects the resultant abundance of heavy elements and energy production in the *rp* process. ^{31}Cl formation in the *rp* process mainly depends on the cross section of resonance capture to the first excited state in ^{31}Cl (energy: 0.75 MeV).³⁾ Thus far, direct measurements have not been made on the $^{30}\text{S}(p, \gamma)^{31}\text{Cl}$ reaction because of the short lifetime of ^{30}S and the small reaction cross section. We overcome this difficulty by employing the Coulomb dissociation method.⁴⁾ With this method, one can determine the cross section of the relevant stellar reaction at a relatively low beam intensity. The aim of the present study is to determine the rate of resonance capture in $^{30}\text{S}(p, \gamma)^{31}\text{Cl}$, which leads to the first excited state in ^{31}Cl .

The experiment was performed using the RIKEN Projectile Fragmentation Separator RIPS at the RIKEN Nishina Center. A ^{31}Cl beam with an energy of 58 MeV/nucleon was produced by the fragmentation of a 115-MeV/nucleon ^{36}Ar beam. The ^{31}Cl beam bombarded a ^{208}Pb target whose thickness was 104 mg/cm². The momentum vectors of the reaction products, i.e., the ^{30}S nucleus and protons, were obtained using the detectors located downstream of the target. The energy of ^{30}S and the positions of ^{30}S and the protons were measured by the silicon telescope located 62 cm downstream of the target. The time of flight of the protons, which penetrate the silicon telescope, was measured by the plastic scintillator hodoscope located 2.95 m downstream of the target. Details of the experimental setup are provided in Ref. 5.

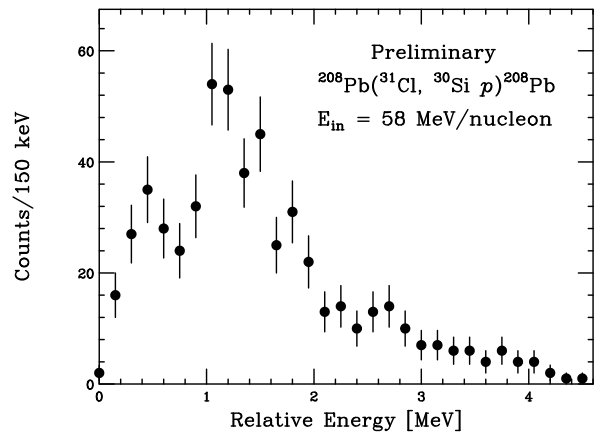


Fig. 1. Preliminary relative energy spectrum between ^{30}S and proton in the Coulomb dissociation reaction of ^{31}Cl . The peak at 0.45 MeV corresponds to the first excited state in ^{31}Cl at 0.75 MeV.

The relative energy between ^{30}S nucleus and the protons was calculated from the momentum vectors.

Fig. 1 shows the preliminary relative energy spectrum. The peaks at 0.45 MeV and 1.1 MeV, respectively correspond to the known first and second excited states in ^{31}Cl ⁶⁾ at 0.75 MeV and 1.4 MeV. The Coulomb dissociation cross section for the first excited state in ^{31}Cl is found preliminarily to be 7 mb by assuming the detection efficiency of the $^{31}\text{Cl} \rightarrow ^{30}\text{S} + p$ channel to be 45%. This value is consistent with that estimated using the known lifetime of the ^{31}Si mirror level⁷⁾. The angular distribution of the scattered ^{31}Cl is currently being analyzed to determine the multipolarity of the excitation.

References

- 1) H. Schatz et al.: Phys. Rev. Lett. **86**, 3471 (2001).
- 2) J. L. Fisker et al.: Astrrophys. J. **608**, L61 (2004).
- 3) C. Iliadis et al.: Astrophys. J. Suppl. Ser. **134**, 151 (2001).
- 4) G. Baur et al.: Nucl. Phys. **A458**, 188 (1986).
- 5) Y. Togano et al.: RIKEN Accel. Prog. Rep. **42**, 11 (2009).
- 6) L. Axelsson et al: Nucl. Phys. **A634**, 475 (1998).
- 7) C. Iliadis et al: Astrphys. J. Suppl. Ser. **134**, 151 (2001).

^{*1} Shanghai Institute of Applied Physics, CAS

^{*2} Department of Physics, Rikkyo University

^{*3} Department of Physics, Tohoku University

^{*4} Center for Nuclear Study (CNS), University of Tokyo

^{*5} Department of Physics, TITECH

^{*6} Department of Physics, Saitama University

^{*7} Institute of Modern Physics, CAS

Branching ratio of γ to particle decay in 1.6-MeV state of ^{23}Al

T. Honda,^{*1} Y. Togano, K. Okada,^{*1} Y. G. Ma,^{*2} N. Aoi, H. Baba, X. Cai,^{*2} J. Chen,^{*2} D. Fang,^{*2} W. Guo,^{*2} Y. Hara,^{*1} Z. Hu,^{*3} K. Ieki,^{*1} Y. Ishibashi,^{*4} Y. Itou,^{*4} N. Iwasa,^{*5} S. Kanno, T. Kawabata,^{*6} H. Kimura,^{*7} Y. Kondo, K. Kurita,^{*1} M. Kurokawa, T. Moriguchi,^{*4} H. Murakami, H. Oishi,^{*4} S. Ota,^{*6} A. Ozawa,^{*4} H. Sakurai, S. Shimoura,^{*6} R. Shioda,^{*1} E. Takeshita, S. Takeuchi, W. Tian,^{*2} K. Yamada, Y. Yamada,^{*1} H. Wang,^{*2} J. Wang,^{*7} K. Yoneda and T. Motobayashi,

[C($^{23}\text{Al},p$ ^{22}Mg)C, nuclear structure]

We carried out the inelastic scattering of ^{23}Al on a C target to investigate the structure of the excited state in ^{23}Al . Emission of 1618-keV γ rays was observed from the $7/2^+$ state in ^{23}Al ; the energy of these γ rays was 1.5 MeV higher than the one-proton separation energy of ^{23}Al (141 keV²). On the basis of the shell-model calculations, Gade *et al.* suggested that the $7/2^+$ state of ^{23}Al consists of $^{22}\text{Mg}(2^+)$ and a $d_{5/2}$ proton and estimated the branching ratio between the γ decay to the ^{23}Al ground state and the particle decay to $^{22}\text{Mg}(2^+)$ and proton (Γ_γ/Γ_p) to be 20¹. The aim of the present study is to determine the branching ratio between the γ decay and the particle decay in the 1618-keV state of ^{23}Al .

Experiments were performed using the RIKEN Projectile Fragmentation Separator RIPS at the RIKEN Nishina Center. The present study was carried out as a by-product of the experiment performed to determine the momentum correlation function for $^{23}\text{Al}^3$. A secondary ^{23}Al beam at 72 MeV/nucleon was produced by the fragmentation of a 135-MeV/nucleon ^{28}Si beam on a ^9Be target. The ^{23}Al beam was made to bombard a 355-mg/cm² C target. The momentum vectors of the reaction products, ^{22}Mg nuclei and protons, were measured by the silicon telescope and plastic scintillator hodoscope located downstream of the target. The energy of the de-excitation γ -rays emitted from ^{22}Mg was measured using DALI2⁴. Details of the experimental setup are described in Ref. 5. The relative energy between ^{22}Mg and the proton was obtained by using the invariant mass method.

Figure 1 shows the relative energy spectrum of ^{22}Mg and the proton coincident with the de-excitation γ ray from the first 2^+ state in ^{22}Mg at 1274 keV. The Doppler-corrected γ -ray energy spectrum obtained for ^{22}Mg is given in the inset. In the γ -ray spectrum, de-excitation of the γ ray from the 2^+ state at 1274 keV to the ground state and from 4^+ state at 3308 keV to the 2^+ state was observed. The relative energy spectrum was obtained by gating the 1274-keV peak. In the rel-

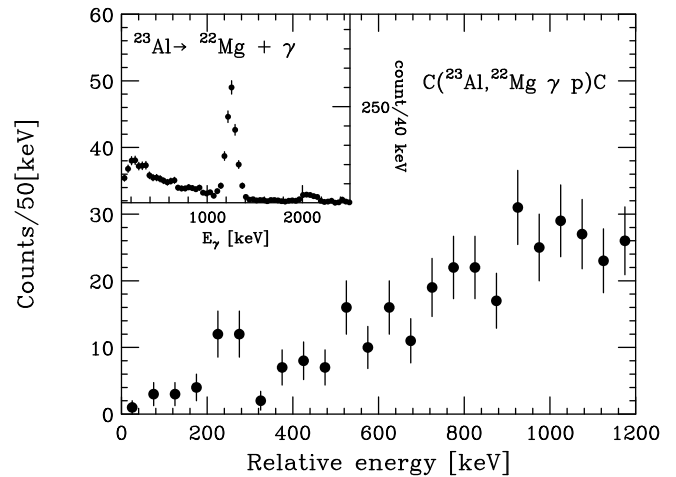


Fig. 1. Relative energy spectrum between ^{22}Mg and proton coincident with the de-excitation γ ray from the first 2^+ state of ^{22}Mg at 1274 keV. The Doppler-corrected γ -ray energy spectrum of ^{22}Mg is shown in the inset.

ative energy spectrum, a peak at around 250 keV was observed; this peak corresponded to the $^{23}\text{Al}(7/2^+) \rightarrow ^{22}\text{Mg}(2^+) + p$ channel. The cross section of this channel was preliminarily calculated to be 0.1 mb, by assuming the detection efficiencies of DALI2 and the breakup event to be 16.6% and 50%, respectively. By combining the cross section of the γ decay channel from the $7/2^+$ state to the ground state⁶), we determined the branching ratio Γ_γ/Γ_p to be 23. This value was consistent with that predicted theoretically by Gade *et al.* Further analysis for the branching ratio is now in progress.

References

- 1) A. Gade et al.: Phys. Lett. B **666**, 218 (2008).
- 2) A. Saastamoenen et al.: Phys. Rev. C **80**, 044330 (2009).
- 3) Y. G. Ma et al.: RIKEN Accel. Prog. Rep. **43**, (2010).
- 4) S. Takeuchi et al.: RIKEN Accel. Prog. Rep. **39**, 63 (2006).
- 5) T. Honda et al.: RIKEN Accel. Prog. Rep. **42**, 12 (2009).
- 6) K. Okada: Master thesis, Rikkyo University, 2009.

*1 Department of Physics, Rikkyo University

*2 Shanghai Institute of Applied Physics, CAS

*3 Institute of Modern Physics, CAS

*4 Department of Physics, Tsuba University

*5 Department of Physics, Tohoku University

*6 Center for Nuclear Study (CNS), University of Tokyo

*7 Department of Physics, University of Tokyo

Precision measurement of the hyperfine constant of $^{11}\text{Be}^+$ -II

A. Takamine, M. Wada, K. Okada^{*1}, T. Nakamura, T. Sonoda, P. Schury^{*2}, H. Iimura^{*3}, Y. Yamazaki, Y. Kanai, T. M. Kojima, T. Kubo, S. Ohtani^{*4}, I. Katayama^{*5}, H. Wollnik^{*6}, and H. A. Schuessler^{*7}

[neutron halo, magnetization radius, laser spectroscopy]

To study the electromagnetic properties of the one-neutron halo nucleus ^{11}Be by using the nuclear-model-independent probe of optical spectroscopy, we have measured the hyperfine constants of radioactive Be isotope ions in an on-line ion trap. The purpose of the study, the method used in the study, and part of the results have been described elsewhere.¹⁻³⁾ Here, we report recently obtained results of the precision measurement of the ground-state hyperfine constant of $^{11}\text{Be}^+$; this measurement is 30 times more accurate than our previous measurement.³⁾

A unique feature of $^{11}\text{Be}^+$ in comparison with $^7\text{Be}^+$ and $^9\text{Be}^+$ is that the upper hyperfine structure (hfs) level ($F = 0$) does not split because the nuclear spin I is $1/2$. If one can accommodate a fraction in the $F = 0$ state, one can measure the frequency of the transition $(F, m_F) = (0, 0) \leftrightarrow (1, 0)$, a 0-0 transition that is field independent to the first order. We evaluated the population of the ground-state hfs levels of Be isotopes using incompletely polarized radiation, σ^+ with a small percentage of σ^- . We observed that only in the case of $^{11}\text{Be}^+$ a noticeable fraction of the population was in the $(F, m_F) = (0, 0)$ state even with a small mixture of depolarized-radiation. Under this pumping condition, resonant microwave radiation at ν^0 induces the 0-0 transition, and resonance can be detected from an increase in the fluorescence intensity.

A typical microwave resonance spectrum of the 0-0 transition of $^{11}\text{Be}^+$ obtained by considering the fluorescence intensity as a function of the applied microwave frequency is shown in Fig. 1. The Rabi oscillation observed in this spectrum can be attributed to 76- μs pulsed microwave radiation. The transition frequency was determined by a least-square fit to the Rabi transition probability function.

Table 1. Resonance frequencies ν^0 for different magnetic fields.

I_{coil} [A]	B [mT]	ν^0 [MHz]
5	0.23813(16)	2677.31134(12)
14	0.69627(26)	2677.37430(10)
30	1.504448(18)	2677.63430(13)

^{*1} Department of Physics, Sophia University

^{*2} Institute of Physics, Tsukuba University

^{*3} Japan Atomic Energy Research Association

^{*4} ILS, University of Electro-Communications

^{*5} Institute of Particle and Nuclear Studies, KEK

^{*6} II. Physikalisches Institute, Justus-Liebig-Universitaet

^{*7} Department of Physics, Texas A&M University

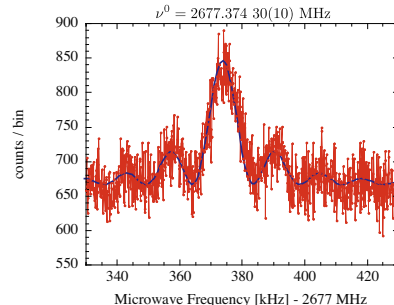


Fig. 1. Typical laser-microwave double resonance spectrum of the ground state hfs transition $(F, m_F) = (0, 0) \rightarrow (1, 0)$ for $^{11}\text{Be}^+$ for a magnetic field B of 0.69627(26) mT.

The field-independent 0-0 transition still shows a small quadratic dependence on the magnetic field, as indicated by the Breit-Rabi formula, which can be written as follows:

$$\nu^0(B) = \sqrt{A^2 + B^2 g_J^2 \mu_B^2 (1 - \gamma)^2}, \quad (1)$$

where A is the magnetic hfs constant; B , the magnetic field strength; g_J , the atomic g -factor; μ_B , the Bohr magneton; and γ , the g -factor ratio. We measured ν^0 for three different magnetic fields, as listed in Table 1. The field strengths were determined from the hyperfine splittings of $^9\text{Be}^+$ ions under the same conditions. The resonance frequencies were fitted to Eq. (1), and the hyperfine constant was determined to be $A_{11} = 2677.302988(72)$ MHz.

The present study provides important data for the study of the magnetization radius of the one-neutron halo nucleus ^{11}Be by taking into consideration the Bohr-Weisskopf effect.⁴⁻⁶⁾ We need *high-precision* nuclear g -factor data for all odd Be isotopes to complete the study. A unique method to determine the nuclear g -factors of odd Be isotopes is to measure the Zeeman splittings of the hfs for a high magnetic field. We have demonstrated the measurement method for stable $^9\text{Be}^+$ ions⁷⁾ and are preparing to apply it to radioactive isotopes.

References

- 1) K. Okada *et al.*: Phys. Rev. Lett. **101**, 212502 (2008).
- 2) A. Takamine *et al.*: Eur. Phys. J. A **42**, 369 (2009).
- 3) M. Wada *et al.*: RIKEN Accel. Prog. Rep. **42**, 17 (2009).
- 4) A. Bohr and V. F. Weisskopf: Phys. Rev. **77**, 94 (1950).
- 5) T. Fujita *et al.*: Phys. Rev. C **59**, 210 (1999).
- 6) Y. Parfenova and Ch. Leclercq-Willaim: Phys. Rev. C **72**, 024312 (2005).
- 7) T. Nakamura *et al.*: Opt. Comm. **205**, (2002) 329.

Determination of nuclear charge radii of Be isotopes by precision optical spectroscopy of trapped ions

A. Takamine, M. Wada, T. Sonoda, T. Nakamura, K. Okada^{*1}, P. Schury^{*2}, H. Imura^{*3}, Y. Yamazaki, Y. Kanai, T. M. Kojima, T. Kubo, S. Ohtani^{*4}, I. Katayama^{*5}, H. Wollnik^{*6}, and H. A. Schuessler^{*7}

[neutron halo, charge radius, laser spectroscopy, ion trap]

Precision optical spectroscopy experiments for trapped ions have been performed at the prototype SLOWRI facility of RIKEN¹⁻⁵) with the aim of studying the nuclear charge radii of Be isotopes. The isotope shifts of optical transition frequencies have been used to determine the nuclear charge radii of radioactive nuclei in a nuclear-model-independent manner⁶). However, for very light elements such as Be, the shift due to the nuclear volume is as small as 10 MHz, whereas the optical transition energy is about 10^9 MHz and the effect due to the different mass is about 10^3 MHz. We need precise theoretical results⁷) to subtract the mass-dependent contribution from the isotope shifts as well as to measure the absolute transition frequencies with a relative accuracies of over 10^{-9} .

In previous reports,^{3,4}) we presented the measurement results for the $2s^2S_{1/2}$ (smaller F)- $2p^2P_{3/2}$ transition frequencies obtained by the optical-optical double resonance spectroscopy with the $2^2S_{1/2}$ (largest F)- $2^2P_{3/2}$ transition for cooling and detection of the resonance. However, in this study, we noticed that there are several possible transitions for the probe transition due to the occurrence of Zeeman splitting, and further, that the probability of each transition strongly depends on the optical-pumping condition. We observed noticeable fluctuation in the transition frequencies in systematic measurements.

In order to avoid such ambiguities, the same transition as the cooling transition was measured using a weak probe laser ($0.2 \mu\text{W}$) for a short period of $14 \mu\text{s}$, while a strong cooling laser ($170 \mu\text{W}$) was used to irradiate for $5.6 \mu\text{s}$ so that the ion temperature remains low. Fast and sharp switching of the cooling laser was carried out by an AOM device. The probe-laser frequency was measured simultaneously with the photon-counting data using a frequency comb system and a beat frequency counting system, which was constructed in-house.⁸) The resonance frequencies were determined from the thus obtained Lorentzian shape spectra (Fig. 1), and the frequencies at the center of the gravity in case of the $2s^2S_{1/2} \rightarrow 2p^2P_{3/2}$ transition were deduced after taking into account the com-

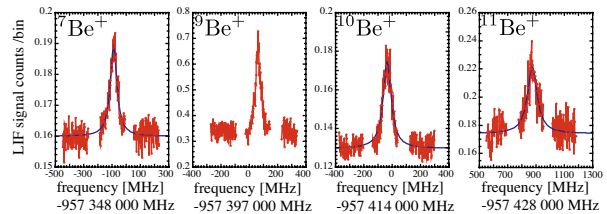


Fig. 1. Spectra of the probe transition for Be isotopes.

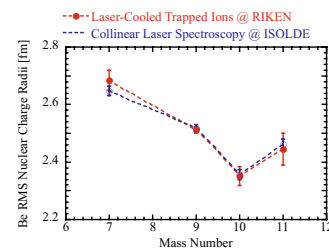


Fig. 2. Preliminary evaluated charge radii of Be isotopes.

pensation required for due the hyperfine and Zeeman splittings. The results for $^{7,9,10,11}\text{Be}^+$ were 957 347 372.0(1.2) MHz, 957 396 618.7(0.6) MHz, 957 413 945.1(0.9) MHz, and 957 428 188.9(2.9) MHz, respectively. The large discrepancy between the results for $^{11}\text{Be}^+$ obtained in the present study and that obtained in a previous one³) is mainly attributed to the incomplete cooling condition as a results of the large hyperfine splitting of $^{11}\text{Be}^+$.

Although the analysis is still in progress, the charge radii of Be isotopes obtained from preliminary evaluation are shown in Fig. 2 along with the results of the collinear-laser spectroscopy experiment performed by the COLLAPS group at ISOLDE⁹). There are noticeable discrepancies between our results of the absolute frequencies and those obtained by the COLLAPS group. However, the values of isotope shifts agree within the margin of errors.

References

- 1) T. Nakamura *et al.*: Phys. Rev. A **74**, 052503 (2006).
- 2) K. Okada *et al.*: Phys. Rev. Lett. **101**, 212502 (2008).
- 3) A. Takamine *et al.*: RIKEN Accel. Prog. Rep. **42**, xiv (2009).
- 4) A. Takamine *et al.*: Eur. Phys. J. A **42**, 369 (2009).
- 5) M. Wada *et al.*: Hyp. Int. **196**, 43 (2010).
- 6) E. W. Otten: in Treatise on heavy-ion science, D. A. Bromley (Ed.), **8**, 517 (1989).
- 7) Z. -C. Yan *et al.*: Phys. Rev. Lett. **100**, 243002 (2008)
- 8) M. Wada *et al.*: RIKEN Accel. Rep. **42** 191 (2009).
- 9) W. Nöertershäuser *et al.*: Phys. Rev. Lett. **102**, 062503 (2009).

^{*1} Department of Physics, Sophia University

^{*2} Institute of Physics, Tsukuba University

^{*3} Japan Atomic Energy Research Association

^{*4} ILS, University of Electro-Communications

^{*5} Institute of Particle and Nuclear Studies, KEK

^{*6} II. Physikalisches Institute, Justus-Liebig-Universitaet

^{*7} Department of Physics, Texas A&M University

Development of CDCC program and its use to calculate momentum distribution in elastic breakup reaction

Yasuo Aoki, Tohru Motobayashi, and Akira. Ozawa,*¹

A computer program `hctak.f`, which is based on the continuum discretized coupled channels(CDCC)¹⁾ idea, was developed. It aims at calculating S matrix elements of a scattering process involving loosely bound projectile and a hard target. The whole system is assumed to composed of three particles and are named as 1, 2 and 3. The Hamiltonian H of the system is written as,

$$H = T_{12} + T_{(1+2)-3} + V_{12} + V_{13} + V_{23}.$$

T 's in the above expression are kinetic energies and V 's are interaction potentials among particles, which are specified by the suffices. Optical potentials are assumed for these potentials.

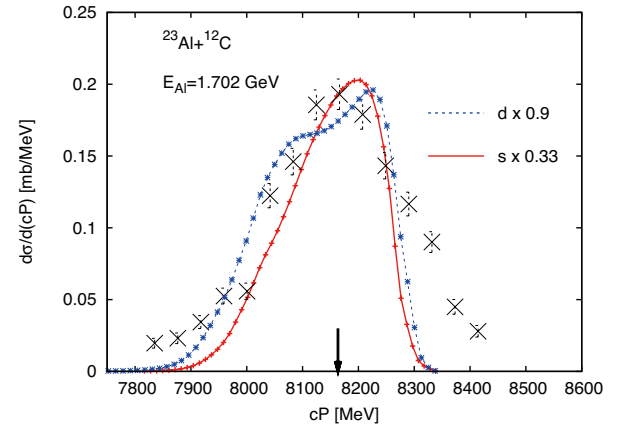
The function of the program are 1) calculate bound and scattering state wave functions of 1-2 system, whose Hamiltonian is given by $T_{12} + V_{12}$, 2) expand the potentials $V_{13} + V_{23}$ into multipoles and evaluate the matrix elements of these potentials, 3) construct a set of coupled equation for given angular momentum and parity, and solve this coupled equation with proper boundary conditions, and 4) calculate S matrix elements corresponding to elastic scattering and many break up channels.

Resulting S matrix elements may be used to evaluate many physical observable, like differential cross sections of elastic scattering, double and triple differential cross sections of break up processes, momentum distribution in the fragmentation reaction.

The reaction $^{23}\text{Al}+^{12}\text{C}$ with $E_{Al} = 1.702 \text{ GeV}$ ²⁾ was taken as the first case to apply this newly developed analysis method. The projectile ^{23}Al is assumed to consists of a proton and a ^{22}Mg . The binding energy is reported to be 125 keV, and the spin and parity J^π of the system is reported³⁾ to be $5/2^+$. To save cpu time, intrinsic spin of nucleons are suppressed. To see the structure dependence of the projectile, two calculations are performed, one with d -state and the other with s -state as the ground state wave function. Scattering states of proton- ^{22}Mg system(1-2 system) are generated by assuming a real central potential, which reproduce the bound state energy and a resonant s -state located about 500 keV above the ground state. These scattering states are truncated to have orbital angular momenta of s , p , d , f and g waves and the maximum wave numbers of 2.0 fm^{-1} . This wave number span is divided into 20 bins. Interaction potentials between proton and ^{12}C , V_{13} , is taken from the literature⁴⁾, while that of ^{22}Mg and ^{12}C , V_{23} is the set F

of the work by Beunerd et al.,⁵⁾. Nucleon optical potential is well established, but that of heavy ions are under developing stage.

The following figure compares ^{22}Mg momentum distribution measured at 0° . Dots are the experimental ones, red and blue curves are due to s (d)-state ground state wave functions.



d -state wave function reproduces the experimental width better than that of the s -state. Absolute magnitude of the calculated results are scaled to fit into the figure. Total reaction cross section is reported²⁾ to be 1609 mb, while the present calculation predicts 1271(1305) mb for $d(s)$ -state of the ^{22}Mg . We can adjust the relatively ambiguous optical potential of $^{22}\text{Mg}+^{12}\text{C}$ to reproduce the magnitude of total reaction cross section, at the cost of reduced intensity of the momentum spectrum. From this experience, improved optical potential is highly requested.

Many thanks are due to computation services offered by riken integrated cluster of clusters(ricc).

References

- 1) M. Kamimura, et al., Prog. Theor. Phys. Jpn. Suppl. **89**(1986) 1
- 2) D. Q. Fang et al., Phys. Rev. **C76**,031601(R)(2007)
- 3) A. Ozawa et al., Phys. Rev. **C74**,021301(R)(2006)
- 4) B. A. Watson, P. P. Singh and R. E. Segel, Phys. Rev. **182**, 977(1969)
- 5) M. Beunerd et al., Nucl. Phys. **A424**, 313(1984)

*¹ Department of Physics, Tsukuba University

Measurement of reaction cross section for ^{11}Li using solid hydrogen target

T. Moriguchi,^{*1} A. Ozawa,^{*1} H. Suzuki,^{*1} Y. Ito,^{*1} H. Ooishi,^{*1} Y. Ishibashi,^{*1} Y. Abe,^{*1} S. Ishimoto,^{*2} T. Suzuki,^{*3} T. Yamaguchi,^{*3} T. Kuboki,^{*3} I. Hachiuma,^{*3} K. Namihira,^{*3} M. Fukuda,^{*4} D. Nishimura,^{*4} T. Suda, M. Takechi, M. Lantz, K. Tanaka, and T. Ohtsubo^{*5}

[reaction cross section, nuclear structure, unstable nuclei, solid hydrogen target]

The reaction cross section (σ_R) for ^{11}Li has been measured by using a solid hydrogen target (SHT). The purpose of this experiment is to deduce the skin thickness by combining the σ_R value with the carbon target¹⁾ without directly measuring of the charge radius by optical isotope shift measurements. If this new method is successful, it can be used to deduce the skin thickness of nuclei such as ^{78}Ni , on which optical isotope shift measurements cannot be performed. In this method, we performed the σ_R measurements on hydrogen and carbon targets, which have different sensitivities to the densities of protons and neutrons. We have previously developed a thick SHT for use in the σ_R measurement of unstable nuclei²⁾.

The experiment was performed using the RIKEN Projectile Fragment Separator (RIPS). A primary beam of ^{18}O was accelerated up to 100 MeV/nucleon in the RIKEN Ring Cyclotron. A secondary beam was produced by bombardment of the ^{18}O beam on a Be target (10 mm^t). ^{11}Li particles with an energy of 45 MeV/nucleon were separated by the RIPS. In the dispersive focal plane (F1), an energy degrader of 2683 mg/cm² Al was installed, and a horizontal slit defined the momentum acceptance as $\pm 0.5\%$. Figure 1 shows the experimental setup in the final focal plane (F3). Identification of the incident particles before the reaction target was performed by the $B\rho$ -TOF- ΔE method (Fig. 2), where $B\rho$, TOF, and ΔE refer to the magnetic rigidity, time of flight, and energy loss. The TOF between the achromatic focal plane (F2) and F3 was measured by 0.5-mm-thick plastic scintillators. ΔE was measured by a 150- μm -thick silicon detector (SSD) placed in F3. The typical yield and purity of ^{11}Li were 800 cps and 60%, respectively. The position of the beam at the target surface was determined by three sets of parallel-plate avalanche counters (PPACs) placed upstream of the target. High efficiency was achieved even for low-Z nuclei such as ^{11}Li by employing a charge division readout instead of the delay-line readout that is normally used in the RIPS.

The volume of the SHT in this experiment was $\phi 50$ mm \times 30 mm^t, which corresponded to approximately

0.26 g/cm². A Kapton foil with a thickness of 25 μm was used at the entrance and exit windows of the SHT cell. The entrance of the cell, which was in a vacuum chamber connected to the exit of the F3 chamber, was located 1741 mm downstream of the end of the triplet Q-magnet in F3. A 127- μm -thick Mylar foil was used for the vacuum window, downstream of the SHT. ΔE and the total kinetic energy (E) of the particles ejected from the reaction target were detected by two silicon detectors (100 \times 100 \times 0.3 mm³) and a NaI(Tl) detector ($\phi 5'' \times 60$ mm^t), respectively. The ΔE - E method was used for the identification of the outgoing particles. We also performed an experiment using a carbon target and an empty cell and compared the obtained result with the earlier result¹⁾. In this case, the carbon target (0.505 g/cm²) was installed immediately after the vacuum window in air. σ_R can be deduced from the ratio of the number of incident particles to the number of outgoing particles. The analysis to deduce σ_R is now in progress.

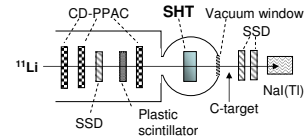


Fig. 1. Experimental setup at F3.

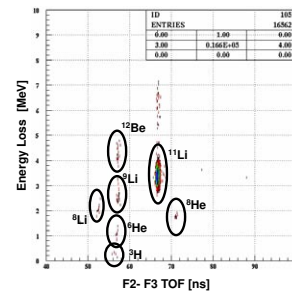


Fig. 2. Identification of the incident particles before the reaction target by the $B\rho$ -TOF- ΔE method.

*1 Institute of Physics, University of Tsukuba
 *2 High Energy Accelerator Research Organization
 *3 Department of Physics, Saitama University
 *4 Department of Physics, Osaka University
 *5 Graduate School of Science, Niigata University

References

- 1) Inabe et al.: RIKEN Accel. Prog. Rep. **24**, 9 (1990).
- 2) T. Moriguchi et al.: RIKEN Accel. Prog. Rep. **42**, 185 (2008).

The change about the number of trapped ions in the SCRIT experiment

S. Wang, T. Suda, T. Emoto, K. Kurita¹, T. Tamae², M. Wakasugi and Y. Yano

In the SCRIT experiment, ions trapped by an electron beam in an electron storage ring are used as nuclear target for electron scattering experiment. In the R&D experiment using ¹³³Cs ions, the number of trapped ions and their charge-to-mass ratio were measured by an analyzer^[1], which consists of an electrode, a magnet and nine channeltrons, as shown in Fig.1. Luminosity of ion-electron scattering was determined from a luminosity monitor^[2] by measuring small scattering angle electrons.

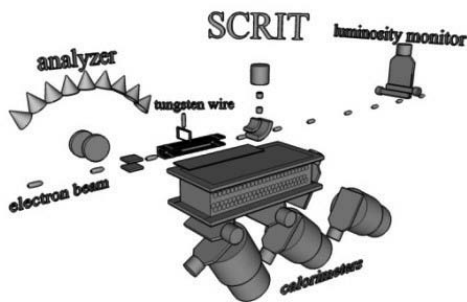


Fig.1 Position of analyzer and luminosity monitor.

The luminosity determined by luminosity monitor and the number of trapped ions at different beam currents are shown in Fig.2. Both of them increase with beam currents from 40 mA. This may cause by deeper trapping potential of the electron beam at larger beam current.

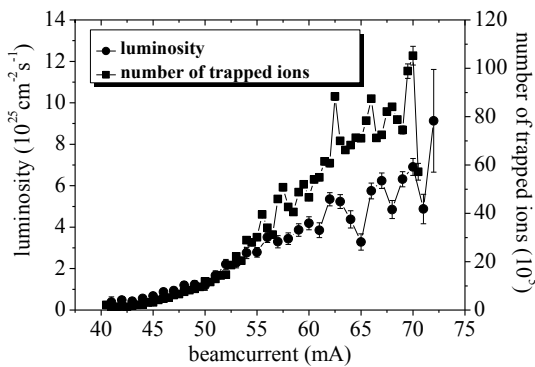


Fig.2: Luminosity and the number of trapped ions at different beam currents.

Electron beam was injected into storage ring every 4 seconds in order to keep a large beam current at 80 mA and the measurement started at 2 seconds after beam injection. During the 2 seconds measurement, ions were injected, trapped for 50

microseconds and extracted^[3], as shown in Fig.3. The background measurement was done for the successive 50 microseconds without ion injection. Those 18 cycles are defined as cycle number from 1 to 18. Each cycle included with and without Cs ions injection.

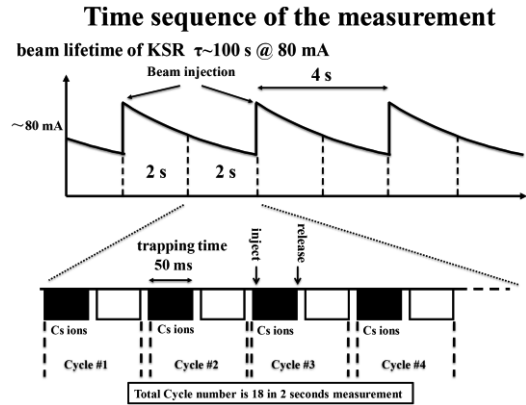


Fig. 3: Time sequence of the measurement.

During the 2 seconds measurement, the luminosity and the number of trapped ions were increased at small cycle numbers and became stable at large cycle numbers, as shown in Fig.4. Due to radiation damping, electron beam shrunk to small size gradually and became stable, after being injected into storage ring. This mechanism can be thought to cause larger luminosity and the higher number of trapped ions at large cycle numbers. In Fig.4, the electron beam seemed to become stable around cycle number 10. Therefore, we can use similar figure like fig.4 to select the optimum measurement period in the future SCRIT experiment.

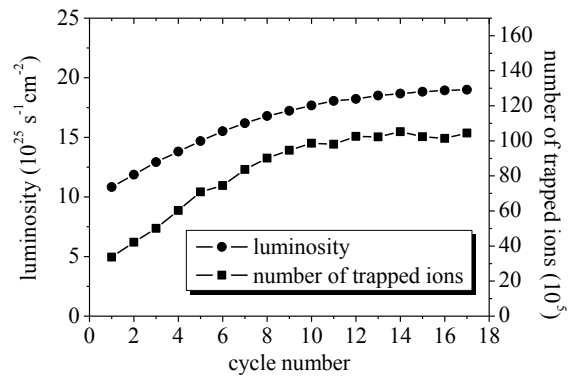


Fig.4: Luminosity and the number of trapped ions at different cycle numbers.

*1 Rikkyo University
*2 Tohoku University

1) M. Wakasugi, et al.: Phys. Rev. Lett. 100, 164801 (2008).
2) S. Wang, et al.: RIKEN Accel. Prog. Rep. 41 (2008).
3) T. Suda, et al.: Phys. Rev. Lett. 102, 102501 (2009).

Proton elastic scattering by ${}^9\text{C}$ beam with E/u of 290 MeV

Y. Matsuda,*¹ T. Kobayashi,*¹ S. Terashima,*² H. Sakaguchi,*³ J. Zenihiro,*³ H. Takeda, H. Otsu, K. Yoneda, K. Ozeki, Y. Satou,*⁴ T. Murakami,*⁵ and M. Kanazawa*⁶

[Nuclear structure, Proton elastic scattering, Unstable nuclei]

Size and density distribution are the fundamental properties of nuclei and have been experimentally and theoretically studied. Proton elastic scattering at intermediate energies can be used to study these properties and has been analyzed for medium-heavy stable nuclei by using relativistic impulse approximation (RIA).¹⁾ However, experimental data available on the proton elastic scattering of unstable nuclei are limited because of the experimental difficulties.

In order to confirm the substantial variation in the matter distribution in carbon isotopes that has been predicted by various theoretical models, we studied for the first time the proton elastic scattering at intermediate energies using a ${}^9\text{C}$ beam with E/u of 290 MeV which was extracted from the HIMAC synchrotron at NIRS.²⁾ Since ${}^9\text{C}$ has no bound excited states, proton elastic scattering by the ${}^9\text{C}$ beam can be feasibly studied by using a 5 mm thick solid-hydrogen target, drift chambers, plastic scintillators, and NaI(Tl) calorimeters. In addition, due to the large difference between the proton number (6) and the neutron number (3) of ${}^9\text{C}$, we can expect ${}^9\text{C}$ to have a large proton skin.

In Fig. 1, we show the experimentally observed angular distribution of proton elastic scattering from ${}^9\text{C}$ represented by circles along with that from ${}^{12}\text{C}$ represented by squares, which is considered to be the reference data.³⁾ The diffraction pattern obtained for ${}^9\text{C}$ is smoother than that for ${}^{12}\text{C}$.

Since in the case of light nuclei, the RIA cannot give a precise explanation of the scattering process, and therefore, it becomes difficult to deduce the nuclear matter density, we compared the qualitatively calculated results of scattering for different density distributions. In Fig. 1, the solid and the dashed lines show the results obtained for the density distributions given by the relativistic mean field (RMF) theory¹⁾ and by the antisymmetrized molecular dynamics (AMD)⁴⁾, respectively. Since the RIA tends to underestimate the scattering at backward angles, a comparatively smoother diffraction pattern is reproduced for the density distributions given by the RMF theory than for those given by the AMD. Figure 2 shows the density distributions. The solid and the dashed lines show the

proton and neutron density distributions for the RMF, respectively, while the long dashed-dotted and the dotted lines show those for the AMD. The proton and neutron density distributions calculated by using the RMF theory and the AMD were found to be different of the surface of the solid-hydrogen target. The RMF density distribution suggests that there might be a large difference between the proton and neutron radii, which are 2.58 fm and 2.06 fm, respectively. In conclusion, the obtained data indicates that ${}^9\text{C}$ has a proton skin.

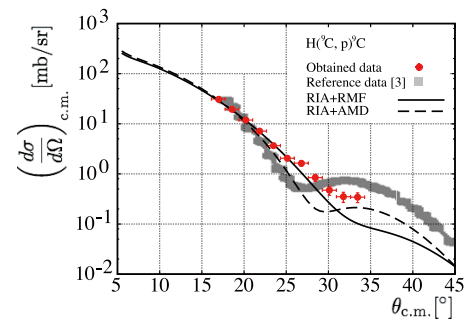


Fig. 1. The differential cross sections for $\text{H}({}^9\text{C},\text{p})\text{C}$ reaction compared with ${}^{12}\text{C}$ data. Results of the theoretical calculations (described in the text) are also plotted.

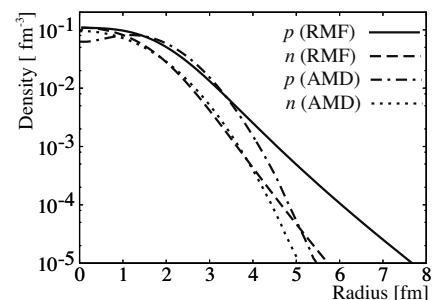


Fig. 2. Proton and neutron density distributions of ${}^9\text{C}$ calculated by using the RMF theory and the AMD.

References

- 1) C. J. Horowitz et al.: *in Computational Nuclear Physics 1*, edited by Steven E. Koonin (Springer-Verlag, Berlin, 1991), Chapter 7.
- 2) S. Terashima et al.: RIKEN Accel. Prog. Rep. **40**, 18 (2007).
- 3) H. O. Meyer et al.: Phys. Rev. C **37**, 544 (1988).
- 4) Y. Kanada-En'yo and H. Horiuchi: Prog. Theor. Phys. Suppl. **142**, 647 (2001).

*¹ Department of Physics, Tohoku University

*² GSI, Darmstadt, Germany

*³ Department of Physics, Osaka University

*⁴ Department of Physics and Astronomy, Seoul National University, Korea

*⁵ Department of Physics, Kyoto University

*⁶ Department of Accelerator and Medical Physics, NIRS, Chiba, Japan

Energy Dependence of π^-/π^+ Ratio Observed in $\text{In}+^{28}\text{Si}$ Reaction

T. Murakami,^{*1} Y. Ichikawa,^{*1} S. Imajo,^{*1} M. Sako,^{*1} R. Sameshima,^{*1} E. Takada,^{*2} K. Ieki,^{*3}
M. Matsushita,^{*3} J. Murata,^{*3} Y. Nakai, S. Nishimura, and H. Sakurai

[Symmetry energy, pion ratio, high density]

The density dependence of nuclear symmetry energy $E_{\text{sym}}(\rho)$ is one of the hottest topics not only in both nuclear physics but also in astrophysics. It is predicted that detailed studies of $Y(\pi^-)/Y(\pi^+)$ yield ratios in central nucleus-nucleus collisions at intermediate energies would provide significant constraints on the $E_{\text{sym}}(\rho)$ at high densities $\rho > \rho_0$ ¹. For last three years we have been developing a compact centrality filter and a pion range counter in order to measure the $Y(\pi^-)/Y(\pi^+)$ yield ratios. This year we have modified our pion range counter by inserting additional two 5 mm thick plastic scintillators and a 10 mm thick one in between the second (2 mm) and third (15 mm) elements of its 2008's version². By this addition we could improve its identification-power for low energy pions.

Following the successful application of both the centrality filter and the range counter to the $\text{In}(^{132}\text{Xe}, \pi^\pm)$ reaction at $E/A = 400$ MeV last year³, we have performed a series of experiments using 400, 600, and 800 MeV/nucleon ^{28}Si beams accelerated at HIMAC. A typical intensity was 5×10^6 ppp and a target thickness was 330 mg/cm². Using the range counter π^+ events were clearly identified by selecting double pulse signals corresponding to $\pi^+ \rightarrow \mu^+ + \nu_\mu$ decays after stop at one of its elements. Since most of negative pions are captured by carbon atoms in the scintillator to trigger an instantaneous disintegration of a carbon nucleus, only positive pions generate double pulse. A total number of charged pions was, then, estimated by using $\Delta E_i - \Delta E_j$ correlations empirically determined for π^+ events. It turned out that four or more ΔE detectors are needed to sufficiently suppress the background arising from protons. Signals from the range counter were processed by a FPGA module, QDC's and multi-hit TDC's and then accumulated by a Linux PC. A charged particle multiplicity from the centrality filter was also recorded by event by event basis.

Figure 1 shows π^+ energy spectra obtained for $\text{In}+^{28}\text{Si}$ reaction at $E/A = 400$ MeV. They have been corrected for various effects; decay in flight, nuclear reactions of pions in the range counter, and multiple Coulomb scattering. Currently only statistical errors are included though we expect 10% order overall uncertainties for the absolute values. Only smooth change in shape was observed as a function of the angle. We have not yet finalized π^- energy spectra since we still

need to work out the efficiency of $\Delta E_i - \Delta E_j$ correlation gates for the charged pion extraction.

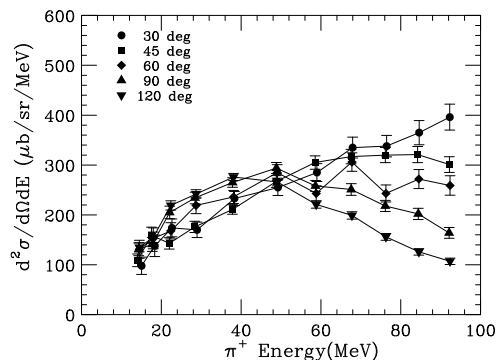


Fig. 1. Double differential cross section for π^+ productions with 400A MeV ^{28}Si on In.

Preliminary results of $Y(\pi^-)/Y(\pi^+)$ yield ratios estimated for the pions at 90° in the laboratory system are shown as a function of transverse momentum of pions in Fig.2. The three ratios for three different incident beam energies are almost identical at this angle despite we expected to see some increase of the ratio as the incident energy approaches to the pion threshold energy. Further analysis of the data is in progress.

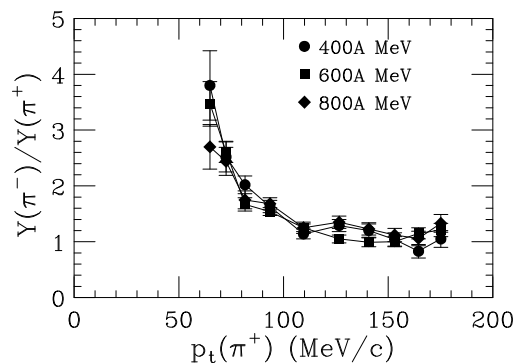


Fig. 2. Preliminary results of $Y(\pi^-)/Y(\pi^+)$ yield ratios at 90° in the laboratory system for $\text{In}+^{28}\text{Si}$ collisions at various incident energy/nucleon.

References

- 1) Bao-An Li, Gao-Chan Yong, and Wei Zuo, Phys. Rev. C **71** (2005) 014608.
- 2) T. Murakami et al., RIKEN Accel. Prog. Rep. **41** (2009) 28.
- 3) T. Murakami et al., Nucl. Phys. A **834** (2010) 593c-595c (NN2009 proceedings).

^{*1} Department of Physics, Kyoto University, Kyoto, Japan

^{*2} Department of Accelerator and Medical Physics, NIRS, Chiba, Japan

^{*3} Department of Physics, Rikkyo University, Tokyo, Japan

Study of time-reversal symmetry in $^8\vec{\text{Li}}$ using tracking detector

H. Kawamura,^{*1} T. Akiyama,^{*1} J.A. Behr,^{*2} M. Hata,^{*1} Y. Hirayama,^{*3} Y. Ikeda,^{*1} T. Ishii,^{*4} D. Kameda, P. Levy,^{*2} S. Mitsuoka,^{*4} N. Miyahara,^{*1} H. Miyatake,^{*3} Y. Nakaya,^{*1} D. Nagae,^{*5} K. Ninomiya,^{*1} M. Nitta,^{*1} N. Ogawa,^{*1} J. Onishi,^{*1} M. Pearson,^{*2} E. Seitabashi,^{*1} T. Toyoda,^{*1} K. Tsukada,^{*1} Y.X. Watanabe,^{*3} and J. Murata^{*1}

A new experimental project, MTV (Mott polarimetry for T-Violation), that aims to test the time-reversal symmetry in nuclear β -decay with high precision has been launched at TRIUMF. Our aim is to measure the R -parameter (defined below) with a precision of 0.01%; currently, at PSI, it is being measured with a precision of 0.2%¹⁾. The leptokuark model predicts a significant T-violating effect around 0.01% level when the leptokuark mass is about 1 TeV¹⁾. The R -parameter is defined in the β -decay rate function as²⁾

$$W \propto 1 + A \frac{\langle \vec{J} \rangle}{J} \cdot \frac{\vec{p}}{E} + R \frac{\langle \vec{J} \rangle}{J} \cdot \left(\frac{\vec{p} \times \vec{\sigma}}{E} \right) \dots,$$

where \vec{J} is the nuclear polarization, and E , \vec{p} , and $\vec{\sigma}$ are the energy, momentum and spin of the electron, respectively. The R -correlation term represents a transversely polarized electron emitted from polarized nuclei that violates time reversal as well as parity conservation. The transverse polarization of electron is measured by Mott scattering. The up-down asymmetry of electrons scattered from a thin metal foil is determined using the incident and scattered tracks. In the present study, a drift chamber has been used in the Mott polarimeter for the first time in order to nullify the major background and systematic effects. The drift chamber is located between a ^8Li beam stopper and the metal foil in order to measure the backward scattered tracks; the maximum figure of merit of the polarimeter is expected at this location.

A physics experiment RNB08K04 was performed at KEK-TRIAC in September 2008 using an 8% vertically polarized ^8Li beam at 178 keV/u and 10^5 pps³⁾. Fig. 1 shows the Mott-scattering angular distribution obtained by electron-tracking analysis. The R -parameter is determined using the effective analyzing power in the Mott scattering as follows:

$$R = -0.020 \pm 0.41(\text{stat}) \pm 0.024(\text{syst}) (1\sigma).$$

We confirmed that our detector setup worked well. In order to achieve a higher precision, we had proposed that the next set of experiments be conducted at TRIUMF-ISAC by using an 80% polarized ^8Li beam with very high intensity, which could help us to measure the R -parameter with a precision of 0.01%. The proposal was accepted, and the experiment number is

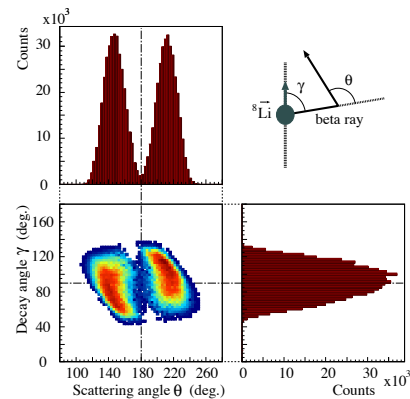


Fig. 1. Two-dimensional histogram for the decay angle γ and the scattering angle θ of the Mott-scattering events.

S1183.

We performed the first commissioning run at TRIUMF in November 2009. The entire experimental equipment was shipped from KEK-TRIAC to TRIUMF in July 2009. In the test run, some technical problems were encountered in studies on beam-intensity dependence of the event trigger rate. Two major problems pertained to the space-charge effect and DAQ bandwidth. The space-charge effect observed in the gas is not negligible in a 10^7 -pps beam environment. We have started R&D for obtaining an optimum chamber gas; we have taken isobutane and CF₄ into consideration instead of P10, which is being used currently. The current DAQ is not capable of acquiring data for all the triggered events at the highest intensity. Therefore, DAQ is being modified to utilize the buffering mode instead of the event-by-event mode, which is being used currently.

A physics run is scheduled for November 2010 with the aim of reaching a precision of at least 0.1% precision, which is the value for the final-state interaction predicted by the standard model. We are also evaluating how to distinguish between the standard-model effects and the new physics signals, which are expected to have nonzero values, using electron-momentum dependence. Precise measurement of the R -correlation using a high-pitch cylindrical drift chamber will be performed subsequently; the drift chamber is currently under construction.

References

- 1) R. Huber et al.: Phys. Rev. Lett. **90**, 202301 (2003).
- 2) J.D. Jackson et al.: Nucl. Phys. **4**, 206 (1957).
- 3) H. Kawamura: Ph. D. Thesis, Rikkyo University, Tokyo (2010).

*1 Rikkyo University

*2 TRIUMF

*3 KEK

*4 JAEA

*5 University of Tsukuba

New neutron-deficient actinide isotopes of ^{234}Bk and ^{230}Am

D. Kaji, H. Haba, Y. Kasamatsu, Y. Kudou, K. Morimoto, K. Ozeki, T. Sumita,*¹ A. Yoneda, H. Koura,*² N. Sato,*² S. Goto,*³ H. Murayama,*⁴ F. Tokanai,*⁵ K. Mayama,*⁵ S. Namai,*⁵ M. Takeyama,*⁵ and K. Morita

[^{234}Bk , ^{230}Am , new isotope, GARIS]

Two neutron-deficient actinide isotopes, ^{234}Bk and its decay product ^{230}Am , were newly identified via a $^{197}\text{Au}(^{40}\text{Ar},3\text{n})$ reaction using the gas-filled recoil ion separator (GARIS).

The decay properties of neutron-deficient actinides provide information on the nuclear mass surface close to the proton drip line, nuclear structure of large deformed heavy nuclei, and fission properties far from nuclear stability line via the electron-capture (EC) delayed fission. In this region, the detailed information is not available because of their low production rates and decay properties, such as EC-decay or spontaneous fission.

Projectiles of ^{40}Ar with the charge state 11^+ were extracted from the 18-GHz ECR ion source and accelerated by RILAC (RIKEN Linear Accelerator). An ^{40}Ar beam with an energy of 189.5 MeV was extracted from RILAC. The absolute accuracy in the beam energy was ± 0.3 MeV. The typical beam intensities at the target were $1.5 \times 10^{13} \text{ s}^{-1}$ (corresponding to 2.5 μA). The target was prepared by the vacuum evaporation of metallic ^{197}Au on a 30- $\mu\text{g}/\text{cm}^2$ carbon backing foil. The target thicknesses were 513 $\mu\text{g}/\text{cm}^2$. Sixteen targets were mounted on a $\phi 30$ cm wheel, which rotated at 3000 rpm, so that they could withstand the irradiation by high-intensity beams. The reaction products of interest were separated in flight from the beams and the majority of the nuclear transfer products by GARIS, and were guided into a gas-jet chamber (i.d.: 100 mm; depth: 20 mm) through a 0.7 μm -thick Mylar window, which was supported by a circular-hole grid with 84% transparency. The separator was filled with helium gas at a pressure of 67 Pa. The magnetic rigidity for ^{234}Bk measurement was set to $B\rho = 1.92$ Tm. In the gas-jet chamber, the reaction products were stopped in He gas, attached to KCl aerosols, and continuously transported through a Teflon capillary (i.d.: 2.0 mm; length: 10 m) to a rotating wheel system, MANON, in order to perform α -spectrometry. The He flow rate was 2.0 L min^{-1} , and the pressure inside the chamber was 46 kPa. In MANON, the aerosols were deposited on 0.5 μm -thick Mylar foils placed at the periphery of

a stainless steel wheel of diameter 420 mm. After the aerosol collection, the wheel was moved in steps at 30-s intervals to position the foils between seven pairs of Si PIN photodiodes (Hamamatsu S3204-09). The products was identified basis of the genetic correlations of mother and daughter nuclei.

Total of 119 decay chains were assigned to subsequent decays from ^{234}Bk . The α (mother)- α (daughter) correlation plot is shown in Fig. 1. The ^{234}Bk had the following decay modes: alpha decay, spontaneous fission, and electron capture. The ^{234}Bk was connected to ^{230}Pu through two routes : [1] $^{234}\text{Bk}(\alpha) \rightarrow ^{230}\text{Am}(\text{EC}) \rightarrow ^{230}\text{Pu}$ and [2] $^{234}\text{Bk}(\text{EC}) \rightarrow ^{234}\text{Cm}(\alpha) \rightarrow ^{230}\text{Pu}$. Then, ^{230}Pu underwent subsequent decays of $^{230}\text{Pu} \rightarrow ^{226}\text{U} \rightarrow ^{222}\text{Th} \rightarrow ^{218}\text{Ra} \rightarrow ^{214}\text{Rn}$.

Three groups of α -decay energies for ^{234}Bk were identified. The mean α -decay energies for the three groups were 7.95, 7.87, and 7.75 MeV. The half-life of ^{234}Bk was determined to be 10 s. No α decay due to ^{230}Am was detected in measurements that followed the alpha decay of ^{234}Bk , but four SF events of ^{230}Am were observed. The half-life of ^{230}Am was determined to be 31 s. The decay properties of ^{234}Cm agree well with those indicated by reference values¹⁾. Detailed analysis is in progress.

References

- 1) P. Cagada et al.: GSI Sci. Rep. 2001, 15 (2002).

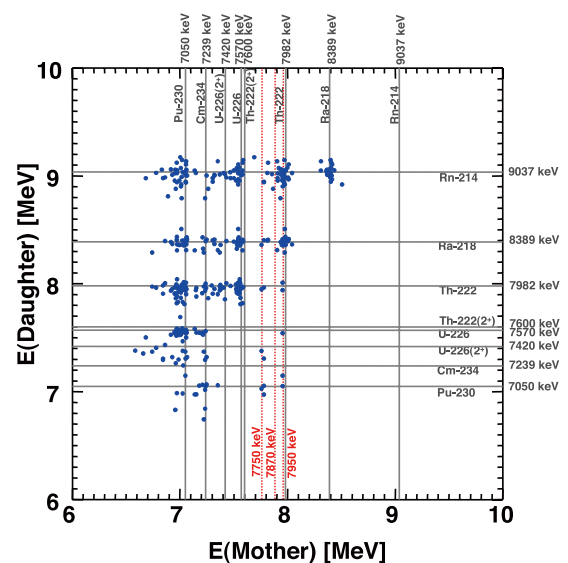


Fig. 1. A lot of α (mother)- α (daughter) correlation for subsequent decays from ^{234}Bk (see text).

*1 Faculty of Science and Technology, Tokyo University of Science

*2 Advanced Science Research Center, Japan Atomic Energy Agency

*3 Center for Instrumental Analysis, Niigata University

*4 Faculty of Science, Niigata University

*5 Department of Physics, Faculty of Science, Yamagata University

First Quantitative Study of Resonance Scattering of α -particles Using a ^{21}Na Radioisotope Beam[†]

D. N. Binh,^{*1} L. H. Khiem,^{*2} N. T. Tho,^{*2} H. Yamaguchi,^{*1} Y. Wakabayashi,^{*1} S. Hayakawa,^{*1} T. Hashimoto,^{*1} T. Teranishi,^{*3} N. Iwasa,^{*4} N. Kume,^{*4} N. Kato,^{*5} and S. Kubono^{*1}

[RI beam, Novae, X-ray burst]

Nucleosynthesis of ^{22}Na is an interesting subject because of possible γ -ray observation and the presence of isotopic anomalies in the presolar grains^{1,2}. ^{22}Na should be mainly produced in the NeNa cycle. It is a long-lived radioisotope with a half-life of 2.6 years; its β -decay leads to the first excited state which promptly followed by the emission of an 1.275 MeV γ -ray³. This γ -ray is a candidate to detect by satellite observatories to understand stellar events. At high temperatures, the $^{21}\text{Na}(\alpha, p)^{24}\text{Mg}$ reaction could play a significant role in the NeNa cycle progressing to the MgAl cycle and beyond. Clearly, the $^{21}\text{Na}(\alpha, p)^{24}\text{Mg}$ stellar reaction would make a branching reaction on ^{21}Na and bypass ^{22}Na , resulting in a reduction in ^{22}Na production. Therefore, it could be directly related to the 1.275 MeV galactic γ -ray observation and the Ne-E problem⁴. It could be also important in understanding the early stage of the rp-process⁵. Resonances observed by the resonance scattering of α -particles on ^{21}Na and their resonant parameters are very important for calculating the stellar reaction rate of the $^{21}\text{Na}(\alpha, p)^{24}\text{Mg}$ reaction.

Measurement of the resonance scattering of α -particles using a low energy ^{21}Na radioisotope (RI) beam in inverse kinematics was performed for the first time by the thick target method. The beam was produced at the CNS Radio Isotope Beam separator (CRIB) of the University of Tokyo⁶. The ^{21}Na particles were produced by the (d,n) reaction in inverse kinematics; a ^{20}Ne primary beam accelerated up to 6.2 MeV/u by the RIKEN-AFV cyclotron was used. The ^{21}Na beam was selected and purified by the CRIB facility, and finally, at the scattering chamber containing the experimental setup, we obtained a 39.5-MeV beam with of about 93% purity. Energies and positions of both proton and α -particles were measured in the $\alpha + ^{21}\text{Na}$ scattering by three ΔE -E telescopes mounted at three different angles (6° , 16° , and 26°) with respect to the beam line. Each telescope consisted of a Micron double-sided silicon detector (MDSSD), a Hamamatsu position sensitive silicon detector (HPSSD), and two solid state silicon detectors (SSD). Protons and α -particles were clearly identified

by the ΔE -E method. The alpha scattering data were analyzed to obtain the excitation function. Five resonances were observed, as shown in Fig. 1. The gap at around $E_{cm} = 3.5$ MeV in the figure is due to the dead layer of the MDSSD. A combination of spins and par-

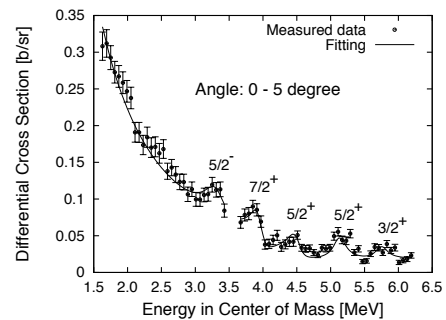


Fig. 1. Excitation function of resonance scattering of α -particles on ^{21}Na .

ities has been deduced successfully so far by applying the R-matrix method. The best fit of this combination is shown in Fig. 1, and the result of the R-matrix analysis is presented in Table 1.

Table 1. R-matrix analysis result

E_r (MeV)	Γ (MeV)	J^π	ℓ
3.390 ± 0.305	0.523 ± 0.052	$5/2^-$	3
3.983 ± 0.279	0.217 ± 0.017	$7/2^+$	2
4.516 ± 0.135	0.231 ± 0.009	$5/2^+$	2
5.214 ± 0.260	0.371 ± 0.022	$5/2^+$	2
5.760 ± 0.058	0.233 ± 0.005	$3/2^+$	2

The analysis is still in progress. We are investigating other possible combinations of spins and parities for which the R-matrix fit gives reasonable χ^2 values (within the standard deviation).

References

- 1) P. Jean *et al.*: “Search for a Galactic 1275 KeV Line Emission with SPI/INTEGRAL”, Proc. 5th INTEGRAL Workshop, Munich, Germany, 2004.
- 2) M. Aliotta: Eur. Phys. J. Special Topics **150**, 201 (2007).
- 3) D. D. Clayton and F. Hoyle, Astro. J. **101**, 187 (1974).
- 4) M. Arnould and H. Norgaard: Astro. Astrophys. **64**, 195 (1978).
- 5) S. Kubono: Nucl. Phys A **558**, 305 (1995).
- 6) S. Kubono *et al.*: Eur. Phys. J. A **13**, 217 (2002).

^{*1} Center for Nuclear Study, Graduate School of Science, University of Tokyo

^{*2} Institute of Physics, Vietnamese Academy of Science and Technology

^{*3} Department of Physics, Kyushu University

^{*4} Department of Physics, Tohoku University

^{*5} Department of Physics, Yamagata University

Progress in ^{30}S Beam Development for a Measurement of $^4\text{He}(^{30}\text{S},\text{p})$

D. Kahl,^{*1} A. A. Chen,^{*2} S. Kubono,^{*1} D. N. Binh,^{*1} J. Chen,^{*2} T. Hashimoto,^{*1} S. Hayakawa,^{*1} D. Kaji,^{*4} A. Kim,^{*4} Y. Kurihara,^{*1} N. H. Lee,^{*4} S. Michimasa,^{*1} S. Nishimura,^{*4} Y. Ohshiro,^{*1} K. Setoodeh nia,^{*2} Y. Wakabayashi,^{*1,*5} and H. Yamaguchi,^{*1}

[Unstable nuclei, astrophysics]

We performed a third and final low-energy ^{30}S RI beam development test in preparation for a future measurement of the $^4\text{He}(^{30}\text{S},\text{p})$ cross section. Our July 2009 experiment, reported here, was a follow-up to our previous beam tests in December 2006⁽¹⁾ and May 2008⁽²⁾. This work is performed at the low-energy Center for Nuclear Study (CNS) radioactive ion beam (CRIB) separator facility^(3,4) of the University of Tokyo and located at the Nishina Center of RIKEN. In 2010, we will perform the first-ever direct measurement of the $^4\text{He}(^{30}\text{S},\text{p})$ cross-section at astrophysical energies relevant to Type I X-Ray Bursts. The $^{30}\text{S}(\alpha,\text{p})$ reaction rate is important to the overall energy generation of X-Ray Bursts⁽⁵⁾, influences the neutron star crustal composition⁽⁶⁾, and may explain the bolometric double-peaked nature of some rare X-Ray Bursts⁽⁷⁾.

We produce ^{30}S via the $^3\text{He}(^{28}\text{Si},^{30}\text{S})\text{n}$ reaction by bombarding a cryogenic gas target^(8,9) of ^3He at 90 K with beams of ^{28}Si . By placing a $2.5\ \mu\text{m}$ Be foil after the production target, we are able to increase the population of the $^{30}\text{S}^{16+}$ species (compared to the charge-state distribution of the gas-cell Havar exit window), which is easier to purify from beam contaminates. Although the $^{30}\text{S}^{14+}$ species is more preferentially populated at the achromatic focal plane F2, as shown in Fig. 1, it is difficult to separate and purify. The beam purity at the target focal plane F3 is improved compared to Fig. 1 by passing the beam through a Wien (velocity) filter after F2.

We successfully developed a $^{30}\text{S}^{16+}$ RI beam of 10^4 pps of 25% purity and $E_{\text{beam}} = 30 \pm 3$ MeV on target normalized to a 7.4 MeV/u $^{28}\text{Si}^{9+}$ primary beam at $1.3\ \text{e}\mu\text{A}$; the primary beam intensity is limited by the maximum heat deposit of 2 W in the $2.5\ \mu\text{m}$ Havar exit window of the production target. The improvement compared to our previous work can mainly be attributed to recent upgrades to the practical K value of the Nishina Center AVF cyclotron. Consistent with predictions from the ion-optic modeling program MO-CADI, our transmission efficiency is primarily limited by energy straggling in the production target, and

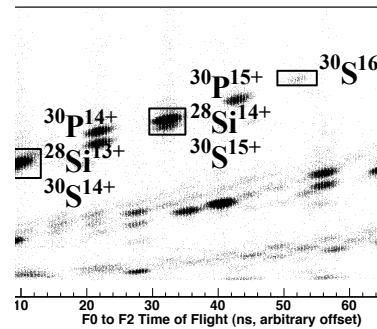


Fig. 1. ToF-E spectrum using a delay-line PPAC and SSD at F2. $^{30}\text{S}^{16+}$ is clearly separated.

thus the ability to accelerate a $^{28}\text{Si}^{9+}$ beam up to 7.4 MeV/u is a considerable improvement for ^{30}S beams at CRIB. If we normalize our previous results to the higher primary beam current used in this work, use of the Be foil only increased the production of $^{30}\text{S}^{16+}$ by a factor of two, where as we expected this increase to be a factor of ten from previous work with carbon foils and the predictions of LISE++; this discrepancy can be somewhat accounted for by the fact that the Be foil was partially broken.

In September 2010, we will measure the $^4\text{He}(^{30}\text{S},\text{p})$ cross section on an event-by-event basis using an active target method using the thick-target method in inverse-kinematics⁽¹⁰⁾. It is critical that we may get a $^{28}\text{Si}^{9+}$ beam at $1.3\ \text{e}\mu\text{A}$ with long-term current-stability delivered to the primary beam focal point of CRIB for the future experiment using the ^{30}S beam developed and detailed in this report.

References

- 1) D. Kahl *et al.*: ASPC **393** (2008) 219.
- 2) D. Kahl *et al.*: PoS NIC **X** (2008) 171.
- 3) S. Kubono *et al.*: Eur. Phys. J. A **13** (2002) 217.
- 4) Y. Yanagisawa *et al.*: Nucl. Instr. Meth. **A539** (2005) 74.
- 5) A. Parikh *et al.*: ApJS **178** (2008) 110.
- 6) H. Schatz and K. E. Rehm: Nucl. Instr. Meth. **A777** (2006) 601.
- 7) J. L. Fisker, F.-K. Thielemann and M. Wiescher: ApJ **608** (2004) L61.
- 8) H. Yamaguchi *et al.*: Nucl. Instr. Meth. **A589** (2008) 150.
- 9) G. Amadio *et al.*: Nucl. Instr. Meth. **A590** (2008) 191.
- 10) K. P. Artemov *et al.*: Soviet J. Nucl. Phys. **52** (1990) 408.

^{*1} Center for Nuclear Study, University of Tokyo

^{*2} Department of Physics & Astronomy, McMaster University, Canada

^{*3} RIKEN (the Institute of Physical and Chemical Research)

^{*4} Department of Physics, Ewha Womans University, Korea

^{*5} Advanced Science Research Center, Japan Atomic Energy Agency (JAEA), Japan

New measurement of resonance scattering of alpha particles on ${}^7\text{Li}$

H. Yamaguchi,^{*1} T. Hashimoto,^{*1} D.N. Binh,^{*1} D. Kahl,^{*1} S. Hayakawa,^{*1} Y. Wakabayashi,^{*2} T. Kawabata,^{*3}
and T. Teranishi^{*4}

[Nuclear astrophysics, Nuclear cluster structure, unstable nuclei]

In recent years, the exotic cluster structures in ${}^{11}\text{B}$ and ${}^{11}\text{C}$ nuclei have attracted considerable attention¹⁾. The $3/2_3^-$ state of ${}^{11}\text{B}$ at the excitation energy $E_{\text{ex}}=8.11$ MeV is considered to be a dilute cluster state²⁾, in which two alpha particles and ${}^3\text{He}$ are weakly interacting. In particular, the α -cluster structure in ${}^{11}\text{B}$ was studied by measuring its isoscalar monopole and quadrupole strengths in the ${}^{11}\text{B}(d, d')$ reaction. The studies indicated that the mirror state of the 8.11-MeV state has a dilute cluster structure.^{3,4)} In the present study, we used ${}^7\text{Li}+\alpha$ resonant elastic scattering to investigate the cluster structures. The strengths of the resonances are expected to provide information about the α -cluster structure. The ${}^7\text{Li}+\alpha$ system is also related to the astrophysical reaction ${}^7\text{Li}(\alpha, \gamma){}^{11}\text{B}$. The study of resonance parameters carried out in the present work should contribute to the precise determination of the ${}^7\text{Li}(\alpha, \gamma){}^{11}\text{B}$ reaction rate at high temperatures ($T_9 > 1$).

The measurement of the ${}^7\text{Li}+\alpha$ elastic scattering was performed at CRIB^{5,6)} using the thick-target in inverse-kinematics method^{7,8)} to determine the excitation function when the excitation energy of ${}^{11}\text{B}$ is 10–13 MeV. The excited states of ${}^{11}\text{B}$ in this energy region have been studied by ${}^7\text{Li}+\alpha$ elastic scattering and other methods⁹⁾; however, some of the resonance parameters are still unclear. In particular, the alpha widths were not accurately determined. Using inverse kinematics, the excitation function at 180 deg in the center-of-mass system, where potential scattering is minimum and the resonances can be observed most clearly, was measured for the first time.

The ${}^7\text{Li}$ beam was accelerated in the AVF cyclotron and transported to the final focal plane (F3) of CRIB. The beam had an energy of 13.7 MeV, and was collimated by a 3×3 -mm aperture at F3. A helium-gas target consisting of a 50-mm-diameter duct and a small chamber was used in the measurement. α particles recoiling at forward angles were detected and identified by the “ ΔE - E counter”. The counter consisting of 20- μm - and 480- μm -thick silicon detectors was placed in the small chamber. Measurements for 2.9×10^{10} particles of ${}^7\text{Li}$ injected into a helium-gas target were performed for 2.5 days. Most of the particles measured was α particles from the elastic scattering, and only a

small number of protons and tritons, which are possibly from ${}^7\text{Li}(\alpha, p)$ reaction and from the break up of ${}^7\text{Li}$, were observed in the measurement.

The obtained energy spectrum of α particles is shown in Fig. 1. The spectrum had peaks consistent with those observed in previous measurements^{10,11)}. A low-background measurement was successfully performed, and it was demonstrated that the thick-target inverse-kinematics method can be adopted for measurements involving light beams and target particles with the minimum atomic number difference ($\Delta Z = 1$). The calculation of the kinematics by taking into account the energy loss in the gas target can provide the excitation energy of ${}^{11}\text{B}$ from the measured energy of the alpha particle. Thus, the excitation function for the ${}^7\text{Li}+\alpha$ elastic scattering will be obtained.

References

- 1) Y. Kanada-En'yo: Phys. Rev. C **75**, 024302 (2007).
- 2) A. Tohsaki *et al.*: Phys. Rev. Lett. **87**, 192501 (2001).
- 3) T. Kawabata *et al.*: Phys. Rev. C **70**, 034318 (2004).
- 4) T. Kawabata *et al.*: Phys. Lett. B **646**, 6 (2007).
- 5) S. Kubono *et al.*: Eur. Phys. J. A **13**, 217 (2002).
- 6) Y. Yanagisawa *et al.*: Nucl. Instrum. Methods Phys. Res., Sect. A **539**, 74 (2005).
- 7) K. Artemov *et al.*: Sov. J. Nucl. Phys. **52**, 408 (1990).
- 8) H. Yamaguchi *et al.*: Phys. Lett. B **672**, 230–234 (2009).
- 9) F. Ajzenberg-Selove, Nucl. Phys. A **506**, 1 (1990).
- 10) R.Y. Cusson *et al.*: Nucl. Phys. **86**, 481–508 (1966).
- 11) N. Soić *et al.*: Nucl. Phys. A **742**, 271–290 (2004).

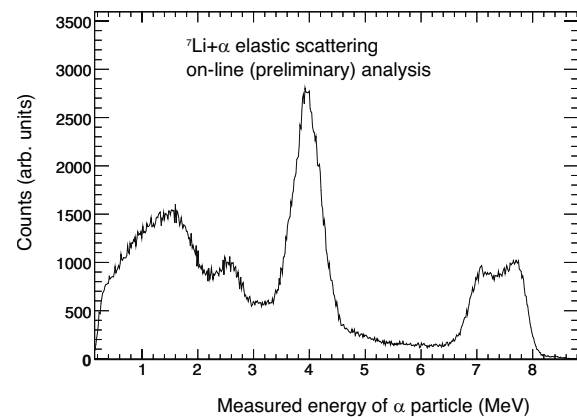


Fig. 1. Energy spectrum of the α particles in the measurement. The α particles are mostly from ${}^7\text{Li}+p$ elastic scattering.

^{*1} Center for Nuclear Study, Graduate School of Science, University of Tokyo

^{*2} Advanced Science Research Center, JAEA

^{*3} Department of Physics, Kyoto University

^{*4} Department of Physics, Kyushu University

2. Nuclear Physics (Theory)

Subsystem correlations in Coulomb breakup reaction of ${}^6\text{He}$

Y. Kikuchi,^{*1} T. Myo,^{*2,*4} M. Takashina,^{*3,*4} K. Katō,^{*1} and K. Ikeda

[NUCLEAR REACTIONS: Halo nuclei, Coulomb breakup]

The purpose of our study is to understand the structures of two-neutron halo nuclei such as ${}^6\text{He}$ and ${}^{11}\text{Li}$ via the Coulomb breakup reactions. Here, we focus on the correlations of the binary subsystems of core- n and n - n in two-neutron halo nuclei. We clarify the relationship between E1 excitations and the correlations in halo nuclei. In this study, we investigate the breakup of ${}^6\text{He}$ into $\alpha + n + n$ three-body continuum states.

To describe the subsystem correlations in three-body breakups, we use complex-scaled solutions of the Lippmann-Schwinger equation (CSLS)¹. In the CSLS, the formal solution of the Lippmann-Schwinger equation is combined with the complex scaling method. CSLS makes it possible to evaluate the physical quantities as functions of the relative energies of subsystems. As a result of this advantage, we can directly discuss the subsystem correlations if the breakup observables are known. We calculate the invariant mass spectra of the Coulomb breakup cross section of ${}^6\text{He}$ for both subsystems of α - n and n - n .

Figure 1 shows the calculated invariant mass spectra and the one obtained from the experiments²). The results obtained using the CSLS for the α - n and n - n subsystems reproduce the observed spectra well. In Fig. 1(a), it is found that the spectrum has a peak at around $E_{\alpha-n} \sim 0.7$ MeV, which corresponds to ${}^5\text{He}(3/2^-)$ resonance energy. This result indicates the importance of the sequential decay via the ${}^5\text{He}(3/2^-)$ resonance in the Coulomb breakup reaction of ${}^6\text{He}$. In the invariant mass spectrum shown in Fig. 1(b), a higher number of the cross section is seen near zero-energy region. This behavior can be understood as the effect of the n - n virtual state in the final states.

To estimate the ground-state correlation in the invariant mass spectra, we also show the results for the breakup components obtained for the transition from the ground state to the non-interacting continuum states. This components correspond to the Fourier transformation of the ground state and are shown as dashed lines in Fig. 1. In both panels, we can see that the spectra for the direct breakup have no clear peaks. By comparing the original and direct breakup results, we conclude that it is difficult to obtain the informa-

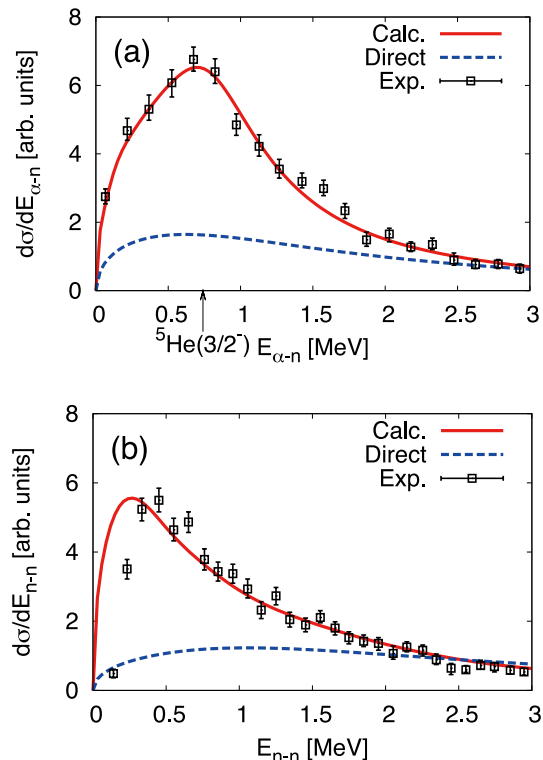


Fig. 1. Invariant mass spectra given in arbitrary units. The panels (a) and (b) show results with respect to the α - n and n - n subsystem energies, respectively. The solid lines represent the original results obtained using CSLS, in which all the final-state interactions are taken into account, and the dashed lines represent the results for the direct breakup components obtained for the transition from the ground state to the non-interacting three-body continuum states. The open squares with error bars denote experimental data²). The arrow in panel (a) indicates the resonance energy of ${}^5\text{He}(3/2^-)$.

tion on the ground-state correlation directly from the Coulomb breakup. This fact indicates the strong influence of the final state interactions on the breakup cross section.

References

- 1) Y. Kikuchi, T. Myo, M. Takashina, K. Katō, and K. Ikeda: Prog. Theor. Phys. **122**, 499 (2009), Y. Kikuchi, K. Katō, T. Myo, M. Takashina, and K. Ikeda: Phys. Rev. C **81**, 044308 (2010).
- 2) T. Aumann et al.: Phys. Rev. C **59**, 1252 (1999).

^{*1} Division of Physics, Graduate School of Science, Hokkaido University

^{*2} General Education, Faculty of Engineering, Osaka Institute of Technology

^{*3} Department of Medical Physics and Engineering, Graduate School of Medicine, Osaka University

^{*4} Research Center for Nuclear Physics (RCNP), Osaka University

One-neutron removal strength of ${}^7\text{He}$ into ${}^6\text{He}$ using the complex scaling method

T. Myo,^{1,2} R. Ando,³ and K. Kato,³

[Nuclear structure, Unstable nuclei, Cluster model, Resonance]

In recent times, many experiments on the unbound nucleus ${}^7\text{He}$, have been reported¹⁾. However, there are still contradictions in the observed energy levels, in particular, in the excited states. Experiments suggest that the excited states of ${}^7\text{He}$ appear as four-body resonances above ${}^4\text{He}+n+n+n$ threshold energy.

Theoretically, when we discuss the structures of ${}^7\text{He}$, it is important to consider its many-body decays to the channels ${}^6\text{He}+n$, ${}^5\text{He}+2n$, and ${}^4\text{He}+3n$. The purpose of this study is to investigate the resonance structures of ${}^7\text{He}$ by imposing the accurate boundary conditions of many-body decays. We employed the cluster-orbital shell model of the ${}^4\text{He}+n+n+n$ system, in which the open channel effects of the multineutron emissions are explicitly taken into account. We will describe the many-body resonances under the correct boundary conditions using the complex scaling method. We employed the Hamiltonian to obtain the ${}^4\text{He}-n$ scattering data and the ${}^6\text{He}$ energies²⁾.

We obtained five resonances of ${}^7\text{He}$ as shown in Table 1. Further, we investigated the spectroscopic factors (S factors) of the ${}^6\text{He}-n$ component, which are important to understand the coupling between ${}^6\text{He}$ and the additional neutron in ${}^7\text{He}$. It was found that the ${}^6\text{He}(2_1^+)$ state contributed largely in several ${}^7\text{He}$ states. Only in the case of the $1/2^-$ state, the ${}^6\text{He}(0_1^+)$ component was dominant and close to unity. This result indicates that the $1/2^-$ resonance can be considered to be a single particle resonance of the $p_{1/2}$ neutron surrounding the halo state of ${}^6\text{He}$.

In Fig. 1, we show the one-neutron removal strength $S(E)$ from the ${}^7\text{He}$ ground state into ${}^6\text{He}$; this strength is determined by taking into account the three-body continuum components of ${}^6\text{He}$ in the final states as well as the 2_1^+ resonance shown in Table 1. From Fig. 1 (a), it is found that the contribution of ${}^6\text{He}(2_1^+)$ is considerably large, resulting in the peak value at the resonance energy of 2_1^+ . The ${}^6\text{He}(0_1^+)$ contribution of 0.61 agrees with the recent observation of 0.64 ± 0.09 ³⁾. The strengths of other spin states made small contributions, as shown in Fig. 1 (b). The peak values for these states was observed at approximately 1 MeV. This structure is a threshold effect of the ${}^5\text{He}(3/2^-)+n$ two-body decay, which starts at

Table 1. Energies and widths of the ${}^7\text{He}$ resonances measured from ${}^4\text{He}+3n$ threshold in MeV, and the corresponding S factors of the ${}^6\text{He}-n$ components.

	Energy	Width	${}^6\text{He}(0_1^+)-n$	${}^6\text{He}(2_1^+)-n$
$3/2_1^-$	-0.790	0.014	$0.64 + i0.06$	$1.55 - i0.31$
$3/2_2^-$	2.58	1.95	$0.005 + i0.01$	$0.95 + i0.02$
$3/2_3^-$	4.53	5.77	$0.003 + i0.0002$	$0.02 - i0.004$
$1/2^-$	0.26	2.19	$1.00 - i0.13$	$0.10 - i0.05$
$5/2^-$	2.46	1.50	$0.00 + i0.00$	$0.95 + i0.02$

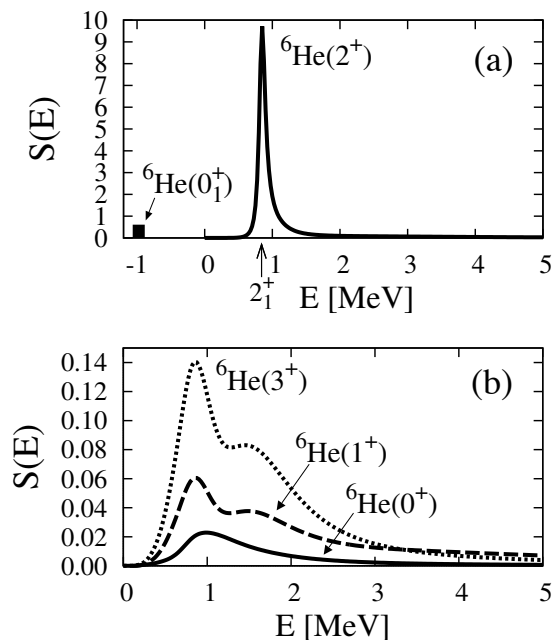


Fig. 1. One-neutron removal strength of ${}^7\text{He}$ to ${}^6\text{He}(J^\pi, E)$ states measured from the ${}^4\text{He}+n+n$ threshold energy. The vertical arrow in (a) indicates the resonance energy of ${}^6\text{He}(2_1^+)$.

0.74 MeV. From these results, it is concluded that the contribution of the ${}^6\text{He}(2_1^+)$ is maximum in the one-neutron removal strength of ${}^7\text{He}$ above the ${}^4\text{He}+n+n$ threshold energy.

References

- 1) F. Skaza et al.: Phys. Rev. **C73**, 044301 (2006), and references therein.
- 2) T. Myo, K. Kato, K. Ikeda: Phys. Rev. **C76**, 054309 (2007).
- 3) F. Beck et al.: Phys. Lett. **B645**, 128 (2007).

[†] Condensed from the article in Phys. Rev. **C80**, 014315 (2009)

¹ General Education, Faculty of Engineering, Osaka Institute of Technology

² Research Center for Nuclear Physics, Osaka University

³ Graduate School of Science, Hokkaido University

Five-body resonances of ${}^8\text{He}$ using the complex scaling method

T. Myo,^{1, 2} R. Ando,³ and K. Kato,³

[Nuclear structure, Unstable nuclei, Cluster model, Resonance]

Recently, many experiments on ${}^8\text{He}$ have been reported. Most of the excited states of ${}^8\text{He}$ are located above the ${}^4\text{He}+4n$ threshold energy¹⁾. This indicates that the observed resonances of ${}^8\text{He}$ can decay into the channels of ${}^7\text{He}+n$, ${}^6\text{He}+2n$, ${}^5\text{He}+3n$, and ${}^4\text{He}+4n$. This multiparticle decay of ${}^8\text{He}$ makes it difficult to observe its excited states.

The purpose of this study is to carry out the resonance spectroscopy of ${}^8\text{He}$ by imposing the accurate boundary conditions of many-body decays. We employ the cluster-orbital shell model of the five-body effects of the multineutron emissions are taken into account explicitly. We describe the many-body resonances under the correct boundary conditions by using the complex scaling method (CSM). It is a challenge to describe the five-body nuclear resonances by using CSM. We employ the Hamiltonian, which reproduces the ${}^4\text{He}$ - n scattering data and the ${}^6\text{He}$ energies²⁾.

Figure 1 shows the obtained energy spectra of He isotopes. We can observe a good agreement between theory and experiment. The matter and charge radii of ${}^6\text{He}$ and ${}^8\text{He}$ nicely reproduce the experiments, as listed in Table 1. We also successfully predict 0_2^+ of ${}^8\text{He}$ as a five-body resonance in CSM; the excitation energy and decay width of this resonance are 6.21 MeV with 3.19 MeV, respectively.

We calculate the pair number of four valence neutrons in ${}^8\text{He}$; the pair number is defined by the matrix element of the operator $\sum_{\leq\beta} A_{J\pi}^\dagger(\beta) A_{J\pi}(\beta)$. Here, α and β represent the single-particle orbits of neutrons, and $A_{J\pi}^\dagger$ ($A_{J\pi}$) is the creation (annihilation) operator of a neutron pair with spin-parity J^π . This quantity helps us to understand the pair coupling structures of four neutrons. Figure. 2 shows the pair numbers for ${}^8\text{He}$ ($0_{1,2}^+$). In the 0_1^+ state, the 2^+ neutron pair is close to unity and the 0^+ pair is almost unity. This result was obtained from a main configuration of $(p_{3/2})^4$ with the probability of 86% using the CFP decomposition (1 and 5 for 0^+ and 2^+ , respectively). The 0_2^+ state has almost two 0^+ neutron pairs in addition to the 2^+ pairs. This is consistent with the $(p_{3/2})^2(p_{1/2})^2$ configuration with a probability of 96%; this configuration is decomposed into the pairs of 0^+ , 1^+ and 2^+ with occupations of 2, 1.5, and 2.5, respectively. In summary, by using CSM, we have successfully obtained the 0_2^+ state as a five-body reso-

Table 1. Matter (R_m) and charge (R_{ch}) radii of ${}^{6,8}\text{He}$ compared with the experiments; a⁴⁾, b⁵⁾, c⁶⁾, d³⁾.

	Present [fm]	Experiments [fm]
${}^6\text{He}$	R_m	2.33(4) ^a 2.30(7) ^b 2.37(5) ^c
	R_{ch}	2.068(11) ^d
${}^8\text{He}$	R_m	2.49(4) ^a 2.45(7) ^b 2.49(4) ^c
	R_{ch}	1.929(26) ^d

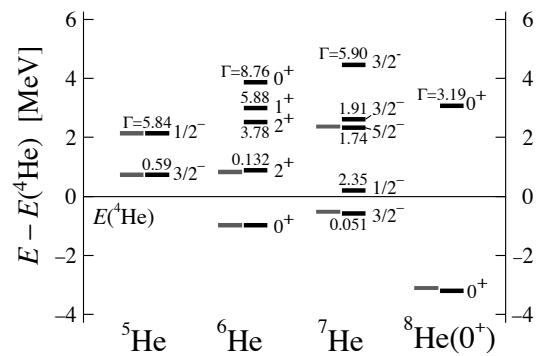


Fig. 1. Energy levels of He isotopes. Small numbers are decay widths. Black and gray lines represent theory and experiments, respectively.

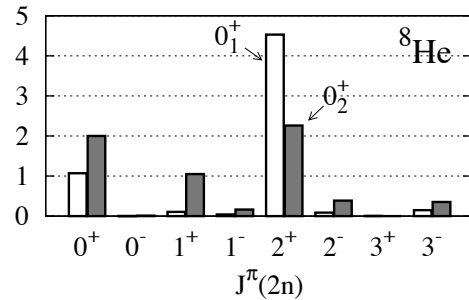


Fig. 2. Pair numbers of the $0_{1,2}^+$ states of ${}^8\text{He}$.

nance, which has two 0^+ pairs of neutrons.

References

- 1) F. Skaza *et al.*: Nucl. Phys. A **788**, 260c (2007), and references therein.
- 2) T. Myo, R. Ando and K. Kato: Phys. Rev. C **80**, 014315 (2009).
- 3) P. Mueller *et al.*: Phys. Rev. Lett. **99**, 252501 (2007).
- 4) I. Tanihata *et al.*: Phys. Lett. B **289**, 261 (1992).
- 5) G. D. Alkharov *et al.*: Phys. Rev. Lett. **78**, 2313 (1997).
- 6) O. A. Kiselev *et al.*: Eur. Phys. J. A **25**, Suppl. 1, 215 (2005).

¹ General Education, Faculty of Engineering, Osaka Institute of Technology

² Research Center for Nuclear Physics, Osaka University

³ Graduate School of Science, Hokkaido University

Gamow-Teller transitions from ${}^9,{}^{11}\text{Li}$ to ${}^9,{}^{11}\text{Be}$ Y. Kanada-En'yo^{*1}

Experimental studies of the β decays from unstable nuclei near drip lines are currently progressing due to recent advances in experimental techniques. In recent years, the β decays of ${}^9\text{Li}$ and ${}^{11}\text{Li}$ have been measured in several experiments, e.g., at the ISOLDE facility in CERN. They provide information on new states in ${}^9\text{Be}$ and ${}^{11}\text{Be}$ such as their excitation energies, spins, and $B(GT)$ values. In the β decay of ${}^9\text{Li}$, the GT transitions to the low-lying ${}^9\text{Be}$ states at $E_x \leq 10$ MeV are weak, while strong transitions have been reported to the 11.81 MeV state¹⁻³⁾ which give an abnormal large $B(GT)$ value as a few factor large as the theoretical value calculated by a shell model⁴⁾. The β decay has also been measured experimentally for the drip-line nucleus, ${}^{11}\text{Li}$ ⁵⁻⁸⁾, and many excited states of ${}^{11}\text{Be}$ were observed in the low energy region.

In this paper, we investigate the GT transition strengths of the β decays, ${}^9\text{Li} \rightarrow {}^9\text{Be}$ and ${}^{11}\text{Li} \rightarrow {}^{11}\text{Be}$, with a theoretical method of antisymmetrized molecular dynamics(AMD)^{9,10)}. The distribution of the $B(GT)$ values is analyzed for each spin of final states.

$B(GT)$ distribution for the decays ${}^9\text{Li} \rightarrow {}^9\text{Be}$ and ${}^{11}\text{Li} \rightarrow {}^{11}\text{Be}$ is shown in Fig. 1. The calculated $B(GT)$ values are small for transitions to low-lying states of Be isotopes because of the 2α -core structures in the final states. Significant strengths are found in the $B(GT)$ distribution to non-cluster states of ${}^9\text{Be}$ in the $E_x \geq 10$ MeV region. Also in ${}^{11}\text{Li} \rightarrow {}^{11}\text{Be}$ decays, relatively large $B(GT)$ values are found for excited states at excitation energy $E_x \geq 10$ MeV.

Particular attention was paid to the strong β -transition from ${}^9\text{Li}$ to ${}^9\text{Be}(5/2^-)$ state at 11.8 MeV which was reported experimentally¹⁻³⁾. The present results are inconsistent with the strong GT transition to the $5/2^-$ state which shows a large fraction of the Ikeda sum rule value. Also in terms of the sum rule, the experimental value $B(GT) = 8.9$ for the $5/2^-$ state seems too large to be described by theoretical calculations if the ${}^9\text{Li}$ ground state has an ordinary structure.

This work is the first in which the AMD method was applied to the study of GT transitions to highly excited states. One advantage of the present method is that one can describe various final states in the daughter nucleus(Be), such as low-lying cluster states and high-lying non-cluster states. Although the present model space is not a complete basis, it exhausts the GT transition strengths exactly.

References

- 1) G. Nyman *et al.* [ISOLDE Collaboration], Nucl. Phys. A **510**, 189 (1990).

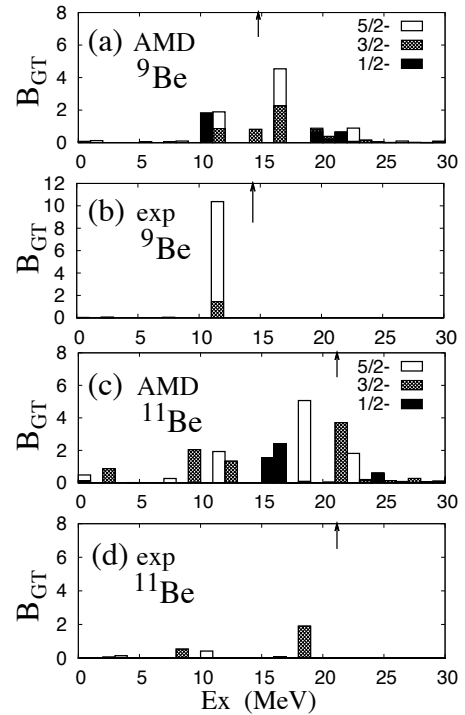


Fig. 1. $B(GT)$ distribution for the decays ${}^9\text{Li} \rightarrow {}^9\text{Be}$ and ${}^{11}\text{Li} \rightarrow {}^{11}\text{Be}$. The $B(GT)$ values to $1/2^-$, $3/2^-$, and $5/2^-$ states of ${}^9,{}^{11}\text{Be}$ are piled up. An arrow in each panel indicates the energy of the IAS state. The value $(g_A/g_V)^2$ is taken to be 1.26^2 . The theoretical values are calculated by using the MV1 force and the G3RS spin-orbit force with parameters, $b = h = 0.15$, $m = 0.62$ and $u_I = -u_{II} = 3000$ MeV.

- 2) W. T. Chou, E. K. Warburton and B. A. Brown, Phys. Rev. C **47**, 163 (1993).
- 3) Y. Prezado *et al.*, Phys. Lett. **B576**, 55 (2003).
- 4) D.J. Millener, Eur. Phys. J. A **25**, s01, 97 (2005).
- 5) N. Aoi *et al.*, Nucl. Phys. **A616**, 181c (1997).
- 6) H.O.U. Fynbo *et al.*, Nucl. Phys. **A736**, 39 (2004).
- 7) Y. Hirayama *et al.*, Phys. Lett. **B611**, 239 (2005).
- 8) M. Madurga *et al.*, Phys. Lett. B **677**, 255 (2009).
- 9) Y. Kanada-En'yo, H. Horiuchi and A. Ono, Phys. Rev. C **52**, 628 (1995); Y. Kanada-En'yo and H. Horiuchi, Phys. Rev. C **52**, 647 (1995).
- 10) Y. Kanada-En'yo and H. Horiuchi, Prog. Theor. Phys. Suppl. **142**, 205 (2001).

^{*1} Department of Physics, Kyoto University, Japan

Systematic study of adiabatic-energy surfaces of Be isotopes †

M. Ito,*¹

[Nuclear structure, cluster model, chemical bonding]

In the last two decades, experiments performed using a secondary RI beam significantly improved our understanding of light neutron-rich nuclei. In particular, substantial efforts have been devoted to the study of the molecular structure of Be isotopes. These isotopes are typical examples of two-center superdeformed systems, which build on ^8Be with an $\alpha+\alpha$ rotor. Like the covalent electrons of molecules, low-lying states of these systems are characterized by the formation of molecular orbitals (MOs) such as π^- and σ^+ orbitals¹⁾.

Furthermore, recent experiments on ^{12}Be have revealed the existence of many resonant states with small energy spacings of less than 1 MeV^{2,3)}. The observed resonances decay strongly into $^6\text{He}_{g.s.}+^6\text{He}_{g.s.}$ and $\alpha+^8\text{He}_{g.s.}$. Similar resonances, which decay into He isotopes, have also been observed in ^{10}Be ²⁾ and ^{14}Be ³⁾. The observed resonances are the candidates for the $^X\text{He}+^Y\text{He}$ molecular resonances ($X, Y = 4, 6, 8$) analog to atomic orbital (AO) configurations.

We have attempted to unify the studies on the nuclear structures of $^{10,12}\text{Be}$ and the nuclear reactions of $\alpha+^{6,8}\text{He}^{4-6)$ by applying the generalized two-center cluster model (GTCM). In this model, various AO configurations with excess neutrons can be considered around the $\alpha+\alpha$ cores, and the eigenvalue problem is solved using the basis functions of the constructed AO configurations. We found that the characteristic structural change from MOs to AOs is as the function of excitation energy, and many resonances with small energy intervals are reproduced well.

Recently, we have extended our studies to include the neutron drip-line systems $^{14,16}\text{Be} = \alpha+\alpha+Xn$ ($X = 6, 8$) In this report, we present the adiabatic energy surfaces (AESs) calculated using the GTCM and discuss the possible appearance of $^X\text{He}+^Y\text{He}$ structures in heavier Be isotopes. The adiabatic states can be determined by solving the eigenvalue problem for a fixed $\alpha-\alpha$ distance. The AESs are obtained by connecting a series of adiabatic states, as shown by the two curves in Fig. 1.

Two deep minima are observed in the lowest two AESs of ^{14}Be . When the $\alpha-\alpha$ distance becomes large, the energies of the AESs increase, and AESs A and B are smoothly connected to the asymptotic channels of $^6\text{He}_{g.s.}+^8\text{He}_{g.s.}$ and $^6\text{He}(2_1^+)+^8\text{He}_{g.s.}$, respectively. This means that the adiabatic states on the rising part of the energy curve (shown by the dotted lines with an arrow) have an enhanced component of the respective asymptotic channels. Previous calculation of the en-

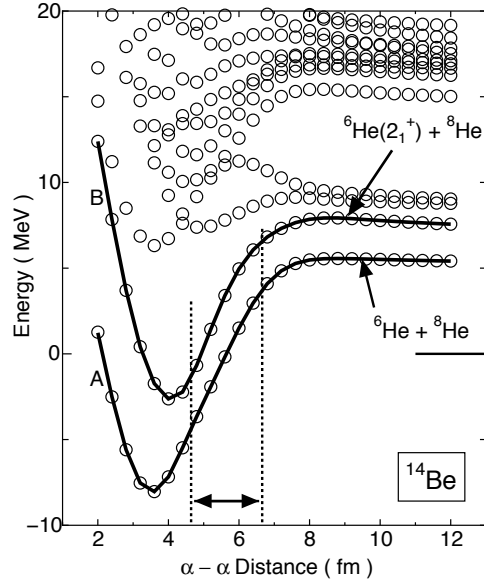


Fig. 1. Adiabatic energy surfaces (AESs) of ^{14}Be . The circles and curves represent the adiabatic states and the AESs, respectively. The origin of the energy axis is taken to be the threshold energy for $^6\text{He}+^8\text{He}$.

ergy levels on the basis of the adiabatic states indicate that the adiabatic states of $^{10,12}\text{Be}^{4-6)$ are stabilized as the resonant states. Therefore, the present calculation results strongly suggest the possible appearance of the $^6\text{He}_{g.s.}+^8\text{He}_{g.s.}$ and $^6\text{He}(2_1^+)+^8\text{He}_{g.s.}$ structures in the excited state of ^{14}Be . We can expect $^8\text{He}_{g.s.}+^8\text{He}_{g.s.}$ structures in ^{16}Be because there appears a connection between the local minimum and the asymptotic channels in AES. We should calculate the energy spectra to investigate the possibility of the formation of $^6\text{He}+^8\text{He}$ and $^8\text{He}+^8\text{He}$. The calculation of energy level is now under progress.

References

- 1) N. Itagaki and S. Okabe: Phys. Rev. C **61**, 044306 (2000).
- 2) M. Freer et al.: Phys. Rev. C **63**, 034301 (2001).
- 3) A. Saito et al.: Suppl. Prog. Theor. Phys. **146**, 615 (2003).
- 4) M. Ito, K. Kato and K. Ikeda: Phys. Lett. B **588**, 43 (2004); I. Mod. Phys. Lett. A **18**, 178 (2003).
- 5) Makoto Ito: Phys. Lett. B **636**, 293 (2006); I. Mod. Phys. Lett. A **21**, 2429 (2006).
- 6) M. Ito, N. Itagaki, H. Sakurai, and K. Ikeda: Phys. Rev. Lett. **100**, 182502 (2008); M. Ito and N. Itagaki: Phys. Rev. C **78**, 011602(R) (2008).

*¹ Department of Pure and Applied Physics, Kansai University

Study of $A = 7$ isotriplet Λ hypernuclei with the four-body cluster model[†]

E. Hiyama¹, Y. Yamamoto,^{*1} T. Motoba,^{*2} and M. Kamimura^{*3}

[hypernuclei, cluster model, hyperon-nucleon interaction]

This study is focus on the structure of a multiplet of Λ hypernuclei such as ${}^7_{\Lambda}\text{He}$, ${}^7_{\Lambda}\text{Li}$ and ${}^7_{\Lambda}\text{Be}$; this multiplet is specified by an isospin T . An important subject related to the isospin multiplet of Λ hypernuclei is the charge symmetry breaking (CSB) component in ΛN interactions. The most reliable evidence of the CSB interaction appears in the Λ binding energies B_{Λ} of the $A = 4$ members with $T = 1/2$ (${}^4_{\Lambda}\text{He}$ and ${}^4_{\Lambda}\text{H}$). The CSB effects are attributed to the difference $\Delta_{CSB} = B_{\Lambda}({}^4_{\Lambda}\text{He}) - B_{\Lambda}({}^4_{\Lambda}\text{H})$; the experimental values of Δ_{CSB} are 0.35 ± 0.06 MeV and 0.24 ± 0.06 MeV for the ground (0^+) and excited (1^+) states, respectively. In the p -shell region, there exist mirror hypernuclei such as the $T = 1$ multiplet with $A = 7$ (${}^7_{\Lambda}\text{He}$, ${}^7_{\Lambda}\text{Li}^*$, and ${}^7_{\Lambda}\text{Be}$). Historically, some authors mentioned CSB effects in these p -shell Λ hypernuclei^{1,2)}. However, there is no microscopic calculation of these hypernuclei taking account of the CSB interaction.

In this study, we investigate $A = 7$ hypernuclei within the framework of an $\alpha + \Lambda + N + N$ four-body model so as to take account of the full correlations between all the constituent baryons. Two-body interactions among constituent particles are chosen so as to reproduce all the existing binding energies of the subsystems (αN , $\alpha \Lambda N$, $\alpha \Lambda$, etc). Our analysis is performed systematically for ground and excited states of $\alpha \Lambda NN$ systems with no more adjustable parameters in this stage, so that these predictions offer important guidance for the interpretation of the upcoming hypernucleus experiments such as the ${}^7\text{Li}(e, e'K^+){}^7_{\Lambda}\text{He}$ reaction at Jlab.

First, in Fig. 1, we show the energy spectra of $A = 7$ hypernuclei without the CSB interaction. The ground-state energy of ${}^7_{\Lambda}\text{He}$ is -6.39 MeV with the respect to the $\alpha + n + n + \Lambda$ four-body breakup threshold. From ${}^7_{\Lambda}\text{Li}$ to ${}^7_{\Lambda}\text{Be}$, as the number of protons increases, the Coulomb repulsion becomes more and more effective. Recently in KEK-E419 experiment³⁾, they produced the $T = 1$, $1/2^+$ state of ${}^7_{\Lambda}\text{Li}$. The observed value of $B_{\Lambda}=5.26$ MeV is in good agreement with our calculated value 5.28 MeV. In the case of ${}^7_{\Lambda}\text{Be}$, there are the old emulsion data giving $B_{\Lambda}=5.16$ MeV. This value should be compared with our obtained value 5.21 MeV. Then, the B_{Λ} value in the ground $1/2^+$ state of ${}^7_{\Lambda}\text{He}$

is predicted to be 5.36 MeV without taking the CSB effect into account.

Next, let us consider the CSB effect in $A = 7$ isotriplet hypernuclei. In the case of ${}^7_{\Lambda}\text{Li}$, the calculated B_{Λ} is 5.29 MeV, to which the CSB interaction brings about almost no contribution, because there is one proton and one neutron outside the α core and the Λn and Λp CSB interactions cancel each other out.

The calculated B_{Λ} s are 5.16 MeV and 5.44 MeV for ${}^7_{\Lambda}\text{He}$ and ${}^7_{\Lambda}\text{Be}$, respectively. The CSB interaction works repulsively (+0.20 MeV) and attractively (-0.20 MeV) in the ${}^7_{\Lambda}\text{He}$ and ${}^7_{\Lambda}\text{Be}$ cases, respectively. Therefore, our result indicates that if the experimental energy resolution is as good enough as less than 0.2 MeV, the CSB effect could be observed in these cases.

References

- 1) A. Gal, Adv. Nucl. Sci. **8**, 1 (1977).
- 2) B. F. Gibson and E. V. Hungerford III, Phys. Rep. **257**, 349 (1995).
- 3) H. Tamura *et al.*, Phys. Rev. Lett. **84** 5963 (2000).

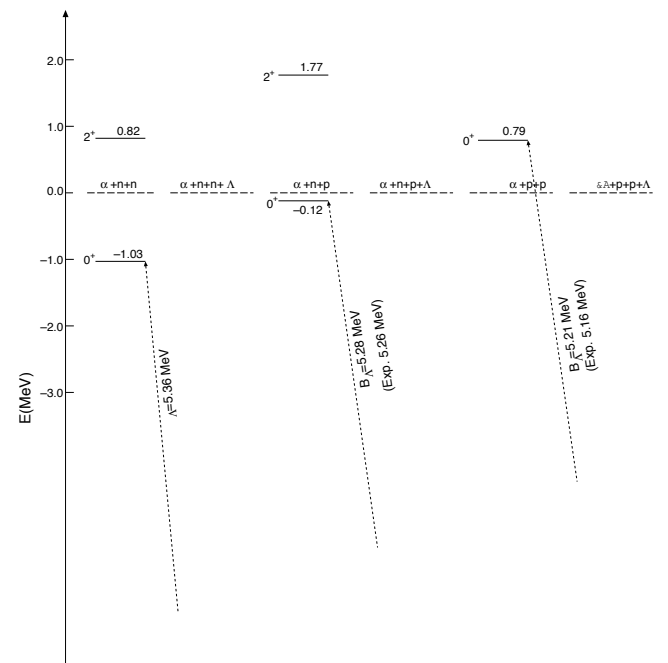


Fig. 1. The calculated energy levels of ${}^6\text{He}$, ${}^7_{\Lambda}\text{He}$, ${}^6\text{Li}^*$, ${}^7_{\Lambda}\text{Li}$, ${}^6\text{Be}$ and ${}^7_{\Lambda}\text{Be}$ with spin-spin and spin-orbit ΛN interactions. The CSB potential is not included in the calculated energies of $A = 7$ hypernuclei.

[†] Condensed from the article in Phys. Rev. C. **80**, 054321(2009)

^{*1} Physics Section, Tsuru University

^{*2} Laboratory of Physics, Osaka Electro-Communication University

^{*3} Department of Physics, Kyushu University

Shell-model study of Σ -mixing in hypernuclear isotopes

A. Umeya and T. Harada ¹

[Nuclear structure, shell model, hypernuclei]

One of the important subjects in strangeness nuclear physics is neutron-rich Λ hypernuclei.¹⁾ It is expected that a Λ hyperon acts as a glue in the nuclei that are beyond the neutron drip line, and knowledge of the behavior of hyperons in an environment with excess neutrons will significantly influence our understanding of neutron stars because the addition of hyperons softens the Equation of State.²⁾ Recently, Akaishi *et al.*^{3,4)} suggested that coherent ΛN - ΣN coupling was important in light Λ hypernuclei, and a shell-model study⁵⁾ showed that the Σ -mixing probability and the energy shift due to the ΛN - ΣN coupling in the $^{10}_{\Lambda}\text{Li}$ ground state are higher than those in $^7_{\Lambda}\text{Li}$. The purpose of our study is to theoretically clarify the structure of neutron-rich Λ hypernuclei by using a shell model. In this study, we investigate the structure of $_{\Lambda}\text{Li}$ hypernuclei in which A is in the range 7–10 by focusing on the Σ -mixing probabilities and energy shifts in shell-model calculations for which the ΛN - ΣN coupling effect is taken into consideration.

In the configuration space for Λ hypernuclei in which ΛN - ΣN coupling exists, the Hamiltonian is given as $H = H_{\Lambda} + H_{\Sigma} + V_{\Lambda\Sigma}$, where H_{Λ} and H_{Σ} are the Hamiltonians in the Λ and Σ configuration spaces, respectively. $V_{\Lambda\Sigma}$ denotes the two-body ΛN - ΣN coupling interaction. We can write a $_{\Lambda}\text{Li}$ eigenstate as

$$|_{\Lambda}\text{Li}\rangle = \sum_{\nu} C_{\nu} |\psi_{\nu}^{\Lambda}\rangle + \sum_{\mu} D_{\mu} |\psi_{\mu}^{\Sigma}\rangle, \quad (1)$$

where $|\psi_{\nu}^{\Lambda}\rangle$ and $|\psi_{\mu}^{\Sigma}\rangle$ are eigenstates of H_{Λ} and H_{Σ} , respectively. We construct wave functions in the p -shell model space for the nucleon part and the s -shell model space for the hyperon part. In the case of NN effective interaction, we consider the Cohen-Kurath (8–16) 2BME.⁶⁾ We use radial integrals⁵⁾ in the case of YN effective interaction, which is given in Refs.^{7,8)} and is based on the NSC97e,f potentials.⁹⁾

Table 1 lists the calculated values of Σ -mixing probabilities and energy shifts for the $_{\Lambda}\text{Li}$ hypernuclei. We observe that the Σ -mixing probabilities and energy shifts are of the order of $10^{-1}\%$ and 10^{-1} MeV, respectively, and increase with the neutron number. The Σ -mixing probability is approximately 0.35% and the energy shift is approximately 0.28 MeV for the neutron-rich $^{10}_{\Lambda}\text{Li}$ ground state; these values are about three times those of $^7_{\Lambda}\text{Li}$.

Figure 1 shows the calculated values of the strength $|D_{\mu}|^2$ of the ΛN - ΣN coupling between the Σ -nuclear

Table 1. Calculated values of Σ -mixing probability P_{Σ} and energy shift $\Delta\epsilon$ for $_{\Lambda}\text{Li}$ isotopes.

	J^{π}	T	Z	N	P_{Σ} (%)	$\Delta\epsilon$ (MeV)
$^7_{\Lambda}\text{Li}$	$\frac{1}{2}^{+}$	0	3	3	0.098	0.085
$^8_{\Lambda}\text{Li}$	1	$\frac{1}{2}$	3	4	0.172	0.139
$^9_{\Lambda}\text{Li}$	$\frac{3}{2}^{+}$	1	3	5	0.211	0.172
$^{10}_{\Lambda}\text{Li}$	1	$\frac{3}{2}$	3	6	0.345	0.280

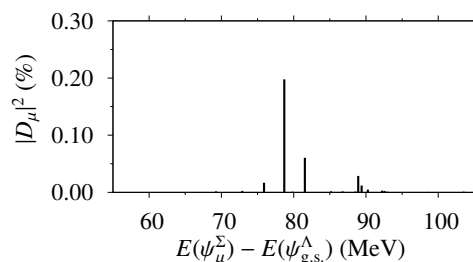


Fig. 1. ΛN - ΣN coupling strength $|D_{\mu}|^2$ of the Σ -nuclear states in the ground state of $^{10}_{\Lambda}\text{Li}$.

eigenstates $|\psi_{\mu}^{\Sigma}\rangle$ and the Λ -nuclear ground state $|\psi_{\text{g.s.}}^{\Lambda}\rangle$. Several Σ excited states considerably contribute to the Σ -mixing. These contributions are coherently enhanced by configuration mixing, which is caused by the ΣN interaction, leading to the enhancement of the Σ -mixing probability. It is shown that the nature of the Σ -nuclear states plays an important role in the ΛN - ΣN coupling. Such a Σ admixture is required in a DWIA calculation¹⁰⁾ to explain the (π^{-}, K^{+}) spectrum of $^{10}_{\Lambda}\text{Li}$ on a ^{10}B target at 1.2 GeV/ c .¹¹⁾

References

- 1) L. Majling: Nucl. Phys. A **585**, 211c (1995).
- 2) M. Baldo, G. F. Burgio, and H.-J. Schulze: Phys. Rev. C **61**, 055801 (2000).
- 3) Khin Swe Myint, T. Harada, S. Shinmura, and Y. Akaishi: Few-Body Syst. Suppl. **12**, 383 (2000).
- 4) Y. Akaishi, T. Harada, S. Shinmura, and Khin Swe Myint: Phys. Rev. Lett. **84**, 3539 (2000).
- 5) A. Umeya and T. Harada: Phys. Rev. C **79**, 024315 (2009).
- 6) S. Cohen and D. Kurath: Nucl. Phys. **73**, 1 (1965).
- 7) D. J. Millener: Lect. Notes. Phys. **724**, 31 (2007); Nucl. Phys. A **804**, 84 (2008).
- 8) D. J. Millener (private communication).
- 9) Th. A. Rijken, V. G. J. Stoks, and Y. Yamamoto: Phys. Rev. C **59**, 21 (1999).
- 10) T. Harada, A. Umeya, and Y. Hirabayashi: Phys. Rev. C **79**, 014603 (2009).
- 11) P. K. Saha *et al.*: Phys. Rev. Lett. **94**, 052502 (2005).

¹ Research Center for Physics and Mathematics, Osaka Electro-Communication University

Complex-scaled CDCC method for nuclear breakup reactions

M. Takashina,^{*1,*2} T. Myo,^{*3,*2} Y. Kikuchi,^{*4} Y. Hirabayashi,^{*5} and K. Kato^{*4}

[Complex scaling method, CDCC, breakup reaction]

Nuclear-reaction experiments have revealed various exotic phenomena of unstable nuclei. The study of the nuclear-breakup process is very important in the case of reactions induced by light unstable nuclei because of the weak binding nature of these nuclei. When the projectile nucleus breaks up to form a two-body or a three-body system, it is necessary to solve the three-body or the four-body scattering problem, respectively, including the target nucleus. Although it is difficult to accurately solve the three- and four-body scattering problems, many authors have attempted to describe breakup reactions.

The continuum-discretized coupled-channel (CDCC) method is known to be useful in analyzing the nuclear breakup processes¹⁾. In CDCC, the breakup continuum states of the projectile nucleus are discretized in an appropriate manner. Recently, pseudo-state (PS) CDCC method was developed; using this method the continuous S-matrix elements can be calculated by introducing a *smoothing function* when the projectile breaks up and forms a two-body system²⁾. It also becomes possible to include the three-body breakup effects of projectile like ${}^6\text{He}$ in analysis of elastic scattering³⁾. More recently, several new methods for obtaining *smoothing functions* have been developed⁴⁾; these methods can be used to study three-body breakup.

In the present study, we propose another approach. We consider applying the complex-scaling method⁵⁾ to the CDCC [complex-scaled (CS) CDCC] method such that only the internal coordinate and the momentum of the projectile are complex-scaled. The expected advantages of CS-CDCC are as follows: (1) In spite of the discretization, exact continuum level density can be obtained⁷⁾, and then, the continuous S-matrix elements can also be calculated without introducing any *smoothing function*. (2) In the complex-scaling method, the three-body scattering problem can be properly solved⁶⁾. (3) The resonance state is strictly separated from the continuum states; as a result, the CS-CDCC method is more advantageous for investigating the reaction mechanism than the ordinary CDCC method⁵⁾.

We derive the CS-CDCC equation for the breakup reaction $d \rightarrow p + n$ on a ${}^{58}\text{Ni}$ target at an inci-

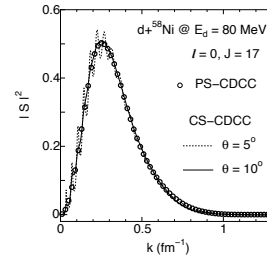


Fig. 1. Squared modulus of S-matrix elements as a function of k .

dent energy of $E_d=80$ MeV. The potential parameters are taken from Ref.2. For simplicity, we neglect the deuteron states corresponding to $\ell=2$, the Coulomb potential between the proton in deuteron and ${}^{58}\text{Ni}$, and the imaginary potentials of the p - ${}^{58}\text{Ni}$ and n - ${}^{58}\text{Ni}$ systems. Further theoretical study is necessary to account for the imaginary potentials. The CS-CDCC equation is solved by applying the proper boundary condition. Since the calculated S-matrix elements are complex-scaled, they are projected onto the real-energy axis, as in the calculation of the strength function in Ref.6.

Figure 1 shows the calculated S-matrix element for total angular momentum $J=17$ as a function of the relative momentum k between the proton and the neutron in a deuteron. The open circles represent the result of the ordinary PS-CDCC calculation, and the solid and dotted curves represent the results of the CS-CDCC calculations at the scaling angles θ of 10° and 5° , respectively. It is found that the results of the CS-CDCC calculations at a scaling angle of 10° are almost equivalent to those of PS-CDCC. As expected, the dotted curve exhibits oscillatory behavior. This result indicates that CS-CDCC can be used for analyzing the nuclear breakup reactions. It should be noted that the exact S-matrix elements can be obtained using CS-CDCC without the need for any *smoothing function*.

References

- 1) M. Kamimura et al.: Prog. Theor. Phys. Suppl. **89**, 1 (1986).
- 2) T. Matsumoto et al.: Phys. Rev. **C 68**, 064607 (2003).
- 3) T. Matsumoto et al.: Phys. Rev. **C 70**, 061601 (2004).
- 4) T. Matsumoto et al.: Prog. Theor. Phys. **121**, 885 (2009).
- 5) J. Aguilar and J. M. Combes: Commun. Math. Phys. **22**, 269 (1971); E. Balslev and J. M. Combes: *ibid.* **22**, 280 (1971).
- 6) S. Aoyama et al.: Prog. Theor. Phys. **116**, 1 (2001).
- 7) R. Suzuki et al.: Prog. Theor. Phys. **113**, 1273 (2005).

*1 Graduate School of Medicine, Osaka University

*2 RCNP, Osaka University

*3 General Education, Faculty of Engineering, Osaka Institute of Technology

*4 Division of Physics, Graduate School of Science, Hokkaido University

*5 Information Initiative Center, Hokkaido University

Long-Range Correlations and the Quenching of Spectroscopic Factors

C. Barbieri,*

This work considered the valence orbits around the closed-shell ^{56}Ni isotope and investigated how different types of correlations quench their spectroscopic factors (SFs). The single-particle Green's function¹⁾ was calculated in Refs.^{2,3)} within a large basis, including up to 10 oscillator shells. This space is large enough to include long-range correlations (LRC) effects directly. Short-range correlations (SRC) from outside this space were accounted for by using a G-matrix.

The LRC were treated in the Faddeev random phase approximation (FRPA), which includes particle-vibration coupling in all possible channels. This leads to the spectral function depicted in Fig. 1 where the single particle states of the valence orbits in the pf shell are evident. Their SFs are obtained from

$$Z_\alpha = \frac{1}{1 - \frac{\partial \Sigma_{\hat{\alpha}\hat{\alpha}}^*(\omega)}{\partial \omega}} \Bigg|_{\omega=\pm(E_\alpha^{\pm 1} - E_0^A)}, \quad (1)$$

where $\Sigma_{\hat{\alpha}\hat{\alpha}}^*(\omega) \equiv \langle \hat{\psi}_\alpha | \Sigma^*(\omega) | \hat{\psi}_\alpha \rangle$ is the matrix element of the self-energy calculated for the overlap function itself but normalized to unity ($\int d\mathbf{r} |\hat{\psi}_\alpha(\mathbf{r})|^2 = 1$).

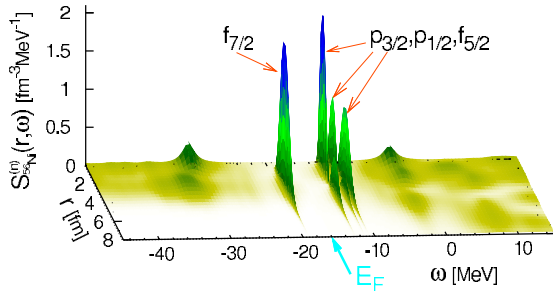


Fig. 1. Single-particle spectral distribution for neutrons in ^{56}Ni ^{2,3)}. Energies above (below) E_F are for transitions to excited states of ^{57}Ni (^{55}Ni). The quasiparticle states close to the Fermi surface are clearly visible.

The formalism of Ref.²⁾ allows to separate the contributions of SRC and LRC to the derivative in Eq. (1). The SFs obtained for neutron orbits are given in the first two columns of Tab. 1 for the chiral N3LO interaction⁴⁾: LRC are responsible for most of the quenching. In order to investigate the importance of configuration mixing near the Fermi surface (not included in the FRPA formalism), both shell-model (SM) and FRPA were also calculated in the sole pf shell model space. Tab. 2 shows that the correction due to extra correlations in the SM is almost negligible in this case. The total results after adding this correction is given Tab. 1

† Condensed from the article in Ref.³⁾

* Theoretical Nuclear Physics Laboratory, RIKEN Nishina Center, Japan

		10 osc. shells			Exp. ⁵⁾
		SRC	S+LRC	FRPA+ ΔZ_α	
^{57}Ni :	$\nu 1p_{1/2}$	0.96	0.63	0.61	0.58(11)
	$\nu 0f_{5/2}$	0.95	0.59	0.55	
	$\nu 1p_{3/2}$	0.95	0.65	0.62	
^{55}Ni :	$\nu 0f_{7/2}$	0.95	0.72	0.69	

Table 1. Quenching of neutron SFs around ^{56}Ni , as obtained in a large space with up to 10 oscillator shells. The column ‘‘SRC’’ includes only SRC effects in calculating Eq. (1). ‘‘S+LRC’’ is the full FRPA result with both SRC and LRC from particle-vibration couplings. The column ‘‘FRPA+ ΔZ_α ’’ includes the correction for additional configuration mixing estimated in Tab 2.

		pf space		
		FRPA	SM	ΔZ_α
^{57}Ni :	$\nu 1p_{1/2}$	0.79	0.77	-0.02
	$\nu 0f_{5/2}$	0.79	0.75	-0.04
	$\nu 1p_{3/2}$	0.82	0.79	-0.03
^{55}Ni :	$\nu 0f_{7/2}$	0.89	0.86	-0.03

Table 2. Comparison of SFs obtained with the FRPA and the SM (up to 6p6h configurations), for the pf model space. The differences (ΔZ_α) estimate the importance of configuration mixing beyond 2p1h and 2h1p.

and nicely agree with the experiment. Similar conclusions were obtained for ^{48}Ca as well³⁾.

It remains clear that configuration mixing (that is, SM) effects have an important impact on open shell nuclei where they can determine the relative SFs (i.e., the fragmentation pattern at low energy)⁶⁾. On the other hand, the overall quenching of absolute SFs requires the coupling to collective modes at higher energies which cannot be approached by standard SM calculations. For valence orbits around shell closures, particle-vibration coupling was found to be the main mechanism. Proper calculations of this effect may pave a new way for understanding effective charges and interactions in the SM.

References

- 1) W. H. Dickhoff and D. Van Neck, *Many-Body Theory Exposed!* (World Scientific, Singapore, 2005).
- 2) C. Barbieri and M. Hjorth-Jensen, *Phys. Rev. C* **79**, 064313 (2009).
- 3) C. Barbieri, *Phys. Rev. Lett.* **103**, 202502 (2009).
- 4) D. R. Entem *et al.*, *Phys. Rev. C* **68**, 041001(R) (2003).
- 5) K. L. Yurkewicz *et al.*, *Phys. Rev. C* **74**, 024304 (2006).
- 6) M. B. Tsang *et al.*, *Phys. Rev. Lett.* **102**, 062501 (2009).

Contribution of core polarization for electric quadrupole moments of neutron-rich nuclei in the island of inversion[†]

Kenichi Yoshida

[Nuclear structure, Density functional theory, Unstable nuclei]

At present, the small excitation energy of the first 2^+ state and striking enhancement of $B(E2; 0_1^+ \rightarrow 2_1^+)$ in $^{32}\text{Mg}^{1)}$ are being actively studied with reference to the onset of the quadrupole deformation and the disappearance of the spherical magic number $N = 20$. The electric quadrupole moment (Q moment) represents the deviation from a sphere. The Q moment is directly related to the deformation property of the nucleus, and hence it is desirable to experimentally and theoretically investigate the Q moment of neutron-rich nuclei around $N = 20^{2)}$. Recently, the Q moment of ^{33}Al was measured at GANIL^{3)}.}

In order to study the Q moments of neutron-rich Al isotopes in the vicinity of the “island of inversion,” we carry out particle-vibration coupling (PVC) calculation on the basis of the Skyrme energy-density functional; the self-consistent HFB + quasiparticle-RPA (QRPA) that was developed recently^{4)}.}

The wave functions of the odd- A system,

$$|\phi\rangle = \sum_i c_i^0 \hat{\beta}_i^\dagger |0\rangle + \sum_{\lambda_j} c_{\lambda_j}^1 \hat{B}_\lambda^\dagger \hat{\beta}_j^\dagger |0\rangle, \quad (1)$$

are obtained by diagonalizing the Hamiltonian

$$\hat{H} = \sum_i E_i \hat{\beta}_i^\dagger \hat{\beta}_i + \sum_{\lambda} \hbar\omega_\lambda \hat{B}_\lambda^\dagger \hat{B}_\lambda + \hat{H}_{\text{couple}}. \quad (2)$$

Here, $\hat{\beta}_i^\dagger$ and \hat{B}_λ^\dagger are creation operators of the Bogoliubov quasiparticles and the QRPA phonons respectively. The Bogoliubov quasiparticles have excitation energy of E_i . The QRPA phonons with excitation energy $\hbar\omega_\lambda$ represent the collective vibrations, including low-lying states and giant resonances. The vacuum $|0\rangle$ represents the ground state of the neighboring even system.

In the present calculation, ^{31}Al , ^{33}Al , and ^{35}Al are described as a proton single-hole state $(\pi d_{5/2})^{-1}$ coupled to a ^{32}Si , ^{34}Si , and ^{36}Si core to form $I^\pi = 5/2^+$. Figure 1 shows the ground-state Q moments of Al isotopes. The calculated Q moment of ^{31}Al agrees well with the new experimental value^{5)}, which is denoted as exp(2) in the figure. The difference between the values denoted by filled squares and diamonds represents the core polarization effect.}

The predicted Q -moment of ^{33}Al also agrees well with the experimental value^{3)}. The difference between the value denoted as GR by the filled circle and the value denoted by the diamond represents the core polarization effect originated from the coupling to the}

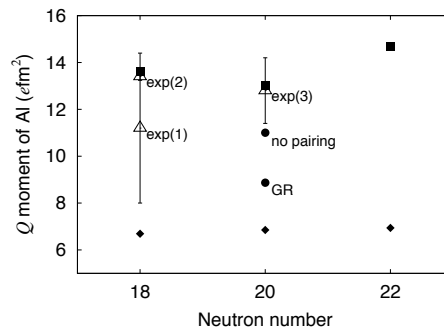


Fig. 1. Comparison of Q moments of $^{31,33,35}\text{Al}$ determined from experiments (open triangles) and by calculations with/without pair correlation (filled squares/circles). The calculation that includes only the giant quadrupole resonance (GR) is also shown. Filled diamonds represent the Q moment of the proton $1d_{5/2}^{-1}$ state. The experimental values, exp(1), exp(2), and exp(3), are obtained from Ref.^{2)}, Ref.^{5)} and Ref.^{3)}, respectively.}}}

giant quadrupole resonance only. This is about 70% of the observed value. Hence, the further enhancement is required to explain the experimental Q -moment. The coupling to the low-lying 2^+ state brings about this enhancement.

Note that calculations indicate the core nucleus to be spherical. However, the narrowing of the $N = 20$ shell gap as shown in Fig. 2 in Ref.^{6)}, and the neutron pairing across $N = 20$ that results in a neutron $2p-2h$ configuration admixture, play a crucial role in explaining the experimental value. When the neutron pairing is not considered, the enhancement of the Q moment resulting from the coupling to the low-lying 2^+ state is about half as shown in Fig. 1 (the filled circle denoted as “no pairing”).}

The results of the calculation indicate the weakening of the $N = 20$ magicity in ^{33}Al . However, this weakening is insufficient to drive permanent nuclear deformation. Therefore, we consider that ^{33}Al is located on the border of the “island of inversion.”

References

- 1) T. Motobayashi et al: Phys. Lett. B **346**, 9 (1995).
- 2) D. Nagae et al: Phys. Rev. C **79**, 027301 (2009).
- 3) T. Nagatomo et al: Eur. Phys. J. A **42**, 383 (2009).
- 4) K. Yoshida et al: Phys. Rev. C **78**, 064316 (2008).
- 5) M. De Rydt et al: Phys. Lett. B **678**, 344 (2009).
- 6) M. Yamagami et al: Phys. Rev. C **69**, 034301 (2004).

[†] Condensed from article in Phys. Rev. C **79**, 054303 (2009).

Clustering and superdeformation in *sd*-shell region

Y. Taniguchi

[nuclear structure, clustering, superdeformation]

Studies on the structures in ^{28}Si and ^{40}Ar have been focused on superdeformation and clustering; deformed-basis antisymmetrized molecular dynamics (AMD) and the generator coordinate method (GCM) have been used in these studies.

A deformed-basis AMD wave function is a Slater determinant of triaxially deformed Gaussian wave packets. By varying the energy while applying constraints, the wave functions of various structures were obtained. Parity and angular momentum before and after energy variation, respectively, were projected. By superposing those obtained wave functions after parity and angular momentum projections, Hamiltonian and norm matrices were diagonalized (GCM).

1 α clustering and superdeformation in ^{28}Si

It was proposed to develop α - ^{24}Mg cluster structures by carrying out the $^{24}\text{Mg}(^6\text{Li}, d)$ reaction¹⁾.

By applying constraints to the cluster distance and quadrupole deformation during variational calculation, GCM basis wave functions with various structures such as α - ^{24}Mg and ^{12}C - ^{16}O cluster structures and deformed structures are obtained. The superposition of these basis wave functions yields an oblate ground state band, a β vibration band, a normal-deformed prolate band (ND), and a superdeformed band (SD). The ND and SD bands correspond to a high percentage of the ^{12}C - ^{16}O and α - ^{24}Mg cluster components, respectively. The results also suggest the presence of two excited bands with the developed α - ^{24}Mg cluster structure; the intercluster motion and the ^{24}Mg -cluster deformation play important roles in this cluster structure.

The details of this work is reported in Ref. 2. This was a collaborative study by Y. Taniguchi of RIKEN, Y. Kanada-En'yo of Kyoto University, and M. Kimura of Hokkaido University.

2 Triaxial superdeformed states in ^{40}Ar

Very recently, the presence of an SD band corresponding to the $J^\pi = 0_2^+$ state (2.12 MeV) was experimentally confirmed up to the $J^\pi = (12^+)$ state³⁾, but theoretical studies on the SD states have not been conducted. GCM basis wave functions were obtained by considering the energy variation by applying a constraint on the quadrupole deformation parameter β , and other quantities such as the triaxiality γ were optimized by energy variation. By performing the GCM calculation, an SD band just above the

ground state band was determined. This SD band includes a $K^\pi = 2^+$ sideband due to the triaxiality. The calculated values of the quadrupole electric transition strength of the SD band agree well with the experimental values. The present results suggest that the experimentally observed $J^\pi = 2_5^+$ (3.92 MeV), 3^+ (4.23 MeV), and $(2, 3, 4)^+$ (5.17 MeV) states are members of the $K^\pi = 2^+$ SD band. It is important to consider triaxiality in order to understand deformations in low-lying states.

The details of this work is reported in Ref. 4. This was a collaborative study by Y. Taniguchi of RIKEN, M. Kimura of Hokkaido University, Y. Kanada-En'yo of Kyoto University, K. Ikeda of RIKEN, H. Horiuchi of Osaka University, and E. Ideguchi of the University of Tokyo.

References

- 1) K. P. Artemov, M. S. Golovkov, V. Z. Goldberg, V. I. Dukhanov, I. B. Mazurov, V. V. Pankratov, V. V. Paramonov, V. P. Rudakov, I. N. Serikov, V. A. Solovov, and V.A. Timofeev: *Sov. J. Nucl. Phys.* **51**, 777 (1990).
- 2) Y. Taniguchi, Y. Kanada-En'yo, and M. Kimura: *Phys. Rev. C* **80**, 044316 (2009).
- 3) E. Ideguchi, S. Ota, T. Morikawa, M. Oshima, M. Koizumi, Y. Toh, A. Kimura, H. Harada, K. Furutaka, S. Nakamura, F. Kitatani, Y. Hatsukawa, T. Shizuma, M. Sugawara, H. Miyatake, Y.X. Watanabe, Y. Hirayama, and M. Oi: *Phys. Lett. B* **686**, **18** (2010).
- 4) Y. Taniguchi, Y. Kanada-En'yo, M. Kimura, K. Ikeda, H. Horiuchi, and E. Ideguchi: arXiv:1002.4495 (2010).

Examination of non-monotonic shell evolution beyond $N = 28$ on the basis of the β -decay of K isotopes

Y. Utsuno,^{*1} T. Otsuka,^{*2*3} B.A. Brown,^{*4*3} M. Honma,^{*5} and T. Mizusaki^{*6}

[Nuclear structure, shell model, unstable nuclei]

One-body potentials such as the Woods-Saxon potential have been successful in describing the shell structure of near-stable nuclei. The one-body picture always gives a smooth and monotonic change in the shell structure as the number of nucleons varies. On the other hand, it has recently been pointed out that the monopole interaction, an angular-momentum-averaged interaction between two orbits, could cause a different behavior in very neutron-rich regions.¹⁾ It is thus of great interest to find such a manifestation of shell evolution.

In this study, we explore the proton shell structure; we perform shell-model calculations using a monopole-based universal interaction picture proposed recently.²⁾ Many cases of single-particle evolution in exotic nuclei have been successfully explained by considering a simple force consisting of a Gaussian force as the central force and a $\pi + \rho$ meson-exchange force as the tensor force.²⁾ In the present study, the parameters in expression for the central force given in Ref. 2 are modified to better fit to the central part of the GXPF1 interaction.³⁾ Part of the work was carried out as a RIKEN-CNS collaborative project on large-scale nuclear structure calculations.

The shell-model interaction considered in this study predicts the proton shell evolution to be quite different from that predicted by the potential picture, as shown in Fig. 1. The $1s_{1/2}$ orbit moves above $0d_{3/2}$ at $N = 28$, and it goes down below $0d_{3/2}$ at $N = 32$, where $1p_{3/2}$ is fully filled. This is an example of non-monotonic shell evolution, which is never given by the one-body picture.

If non-monotonic shell evolution occurs, the ground state of ^{51}K must be $3/2^+$. Although there is no direct measurement of the spin/parity of ^{51}K , we have found that it is highly likely that the ground state is $3/2^+$. Our finding is supported by the good agreement between the β -decay properties observed experimentally and those obtained theoretically (Fig. 2). The experimental decay pattern cannot be explained from the $1/2^+$ state of ^{51}K .

References

- ^{*1} Advanced Science Research Center, Japan Atomic Energy Agency
^{*2} Department of Physics and Center for Nuclear Study, University of Tokyo
^{*3} National Superconducting Cyclotron Laboratory, Michigan State University
^{*4} Department of Physics and Astronomy, Michigan State Uni-

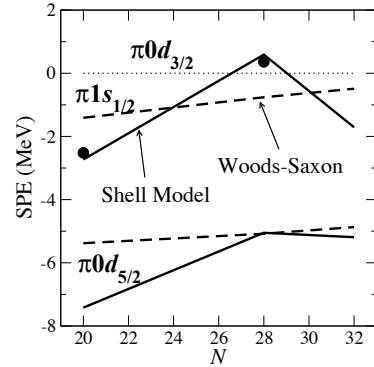


Fig. 1. Proton single-particle energies of $1s_{1/2}$ and $0d_{5/2}$ measured from $0d_{3/2}$ as a function of the neutron number. Solid lines and dashed lines represent the shell-model and Woods-Saxon potential, respectively. Filled circles denote experimentally observed single-hole states in corresponding K isotopes.

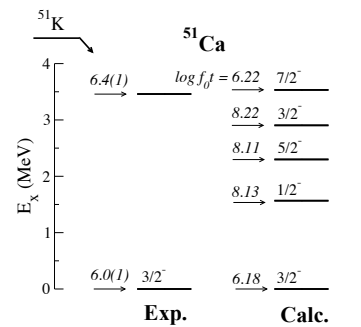


Fig. 2. Comparison of $\log f_0t$ values of β decay from ^{51}K to ^{51}Ca obtained experimentally⁴⁾ and by shell-model calculations in which the ground state of ^{51}K is assumed to be $3/2^+$.

- 1) T. Otsuka, R. Fujimoto, Y. Utsuno, B.A. Brown, M. Honma, and T. Mizusaki: Phys. Rev. Lett. **87**, 082502 (2001).
 2) T. Otsuka, T. Suzuki, M. Honma, Y. Utsuno, N. Tsunoda, K. Tsukiyama and M. Hjorth-Jensen, Phys. Rev. Lett. **104**, 012501 (2010).
 3) M. Honma, T. Otsuka, B.A. Brown and T. Mizusaki: Phys. Rev. C **69**, 034335 (2004).
 4) F. Perrot et al.: Phys. Rev. C **74**, 014313 (2006).

versity
^{*5} Center for Mathematical Sciences, University of Aizu
^{*6} Institute of Natural Sciences, Senshu University

Shell-model description of $N=Z$ pfg-shell nuclei

M. Honma,^{*1} T. Otsuka,^{*2,*3} T. Mizusaki,^{*3} and M. Hjorth-Jensen^{*4}

[NUCLEAR STRUCTURE, shell model]

In upper pf-shell nuclei, various interesting phenomena have been discovered recently, such as the development of nuclear deformation, the coexistence of different shapes near the ground state, the formation of isomeric states, the double β decay, and so on. In neutron-rich nuclei, the shell structure can be different from that of the stable nuclei, which reveals a new aspect of the nuclear tensor force¹. For deeper understanding and reliable predictions of these phenomena, a unified theoretical framework has been desired.

We have developed an effective interaction JUN45 for shell-model calculations in the model space consisting of valence orbits $1p_{3/2}$, $0f_{5/2}$, $1p_{1/2}$ and $0g_{9/2}$ assuming an inert ^{56}Ni core (f5pg9-shell). Here, we modified a realistic interaction (renormalized G-matrix²) derived from the Bonn-C potential) through the iterative fitting calculations to a body of experimental energy data as we did in the derivation of the GXPF1 interaction for the pf-shell³. In the latest iteration, we have attained the rms error of 185 keV for 400 data taken from 87 nuclei with masses $A=63$ -96.

In $N=Z$ nuclei, since protons and neutrons occupy the same orbit, the strong proton-neutron interaction works efficiently, which can develop significant collectivity. In the derivation of the JUN45 interaction, we excluded the experimental data of nuclei around $N\sim Z\sim 40$ region for the fit in order to avoid possible difficulties for describing such collectivity due to the limited model space. Therefore, it is interesting to examine to what extent we can explore this region with the f5pg9-shell space.

As an example, we consider ^{68}Se ($N=Z=34$), for which the shape coexistence has been predicted by the deformed potential model. Experimental observation^{5,6} is in fact consistent with the oblate ground state band, which is crossed by an excited band with prolate shape at around the spin $J\sim 8$. As shown in Fig.1, we have obtained two low-lying bands on top of the 0_1^+ and the 0_2^+ states. The calculated quadrupole moment for the 2_1^+ is $+44\text{efm}^2$, and that for the 2_2^+ state is -41efm^2 . This indicates that the ground band shows the oblate shape, while the excited band is prolate, which is consistent with the experimental findings. However, the calculated moment of inertia is

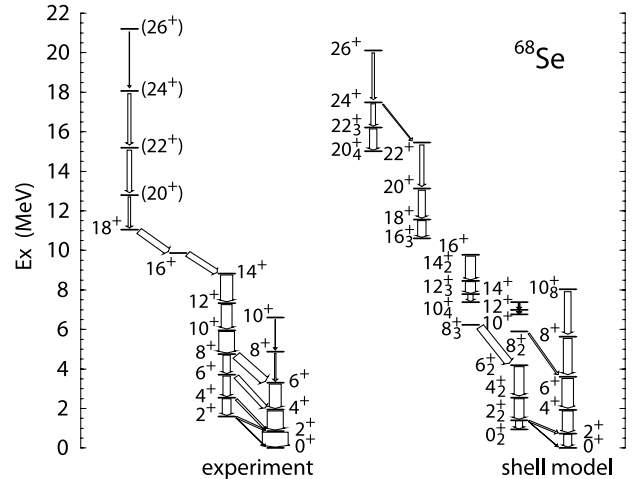


Fig. 1. Comparison of energy levels between the experimental data and the shell-model results for ^{68}Se . The width of the arrow drawn in the experimental part corresponds to the relative γ -ray intensity, while it stands for the relative $B(E2)$ values in the theoretical part. Experimental data are taken from Refs.^{5,6}. The shell-model results are obtained by using the efficient shell-model code MSHELL⁴.

somewhat too small especially in the prolate band. As a result, the crossing with the oblate band never occurs. This indicates the insufficient collectivity for the prolate deformation within the present model space.

The calculated occupation number of the $g_{9/2}$ orbit is almost constant within each band. It is about 1.0, 2.3, and 4.1 for the low spin ($J=0\sim 8$), intermediate spin ($J=10\sim 14$), and high spin ($J=16\sim 22$) band, respectively. Thus, the higher spin bands are generated by successive promotions of nucleons into the $g_{9/2}$ orbit. Considering the reasonable overall agreement between the experimental data and the shell-model results, we can expect that the JUN45 successfully describes the single-particle properties related to the $g_{9/2}$ orbit in the deformed mean potential.

References

- 1) T. Otsuka, et al.: Phys. Rev. Lett. **95**, 232502 (2005).
- 2) M. Hjorth-Jensen et al.: Phys. Rep. **261**, 125 (1995).
- 3) M. Honma, et al.: Phys. Rev. C **65**, 061301(R) (2002); Phys. Rev. C **69**, 034335 (2004).
- 4) T. Mizusaki: RIKEN Accel. Prog. Rep. **33**, 14 (2000).
- 5) S. M. Fischer *et al.*: Phys. Rev. Lett. **84**, 4064 (2000).
- 6) S. M. Fischer *et al.*: Phys. Rev. C **67**, 064318 (2003).

† Condensed from the article in Phys. Rev. C **80**, 064323/1-36 (2009)

*1 Center for Mathematical Sciences, University of Aizu

*2 Department of Physics and Center for Nuclear Studies, University of Tokyo

*3 Institute of Natural Sciences, Senshu University

*4 Department of Physics and Center of Mathematics for Applications, University of Oslo

Newly developed program for the Monte Carlo shell model

N. Shimizu,¹ Y. Utsuno,² T. Abe,¹ and T. Otsuka^{1, 3}

[nuclear structure, shell model, computational physics]

The Monte Carlo shell model method (MCSM) has been developed since 1995¹⁾ in order to avoid the difficulty of diagonalizing the Hamiltonian matrix which has very large dimensions in the nuclear shell model. The MCSM has been successfully applied in the nuclear-structure study up to the medium-heavy nuclei, including exotic nuclei²⁾ by using the powerful Alphleet-1 and Alphleet-2 computer clusters.

As its applicability is enlarged, the MCSM code has been extended accordingly. For instance, the MCSM was recently used to perform *ab initio* calculations. Nevertheless, the original MCSM code has some limitations that restrict its use in more up-to-date nuclear-structure calculations. In particular, it can handle only isospin-conserving interactions. In most *ab initio* calculations, the isospin symmetry is not assumed to be conserved. If we consider the portability of the code, the original code is not expected to run on most state-of-the-art supercomputers because the Parallel Virtual Machine (PVM)³⁾, which is decreasing in popularity, is used for parallel computing. It is not easy to overcome these limitations by locally modifying the existing code. This is partly because the original MCSM code was coded in Fortran 77, in which it becomes increasingly difficult to develop well-structured code as the size of the code increases.

In order to overcome these limitations and fully utilize modern computational technologies, we initiated a project to write a novel MCSM code from scratch. The new MCSM code is equipped with the following features:

- (1) The code is written in modern Fortran 95.
- (2) Hybrid parallel computing based on Message Passing Interface library (MPI)⁴⁾ and OpenMP is used.
- (3) It can handle isospin-breaking interaction.
- (4) It can evaluate many physical quantities which are important in *ab initio* calculations (*e.g.* root-mean-square radius).
- (5) The code incorporates a new algorithm for the calculation of the Hamiltonian matrix elements.

At the present stage, the new code can calculate the Hamiltonian matrix elements using the angular-momentum and parity projection for any Slater determinant basis, and the eigenvalue of the Hamiltonian can be obtained with those matrix elements. The code for generating and selecting bases is to be developed.

Since calculating the Hamiltonian matrix element is the most time-consuming part in MCSM, it is worth examining its computing performance by comparing with the original code. As a benchmark calculation, the eigenvalue of the Hamiltonian for the 0^+ of ^{56}Ni in *pf*-shell is computed with given *ve* Slater determinants. Angular momentum is fully projected by performing three-dimensional ($25 \times 25 \times 25$) integration. Table 1 shows the computation time on a system with an Intel Xeon E5430 2.66-GHz processor and an Intel Fortran compiler version 11.1 was used. In Table 1, codes “orig.”, (A), (B) represent the original MCSM code, newly developed code without feature (5), and newly developed code with feature (5), respectively. Although the new code (A) has the same algorithm as the original one, its performance is 25% better than that of the original code because of feature (1).

code	orig.	(A)	(B)
computation time [sec.]	61.1	46.0	30.5

Table 1. Result of the benchmark test for ^{56}Ni in the *pf*-shell. See the text for more details.

We wrote the new code (B) so that the Hamiltonian matrix elements of the two-body interaction are computed by matrix multiplication; here, we exploit the symmetries of the two-body interaction to reduce the computation time. Table 1 indicates that this algorithm results in an improvement of 50% in the performance, and, consequently, the performance of the new code (B) is superior to that of the original one by a factor of two.

This newly developed code and state-of-the-art supercomputers will enable us to attack *p*-shell nuclei and its beyond through *ab initio* calculations. In addition, the good maintainability of the code makes it easy for us to incorporate useful functions, for example, a quasi-particle vacuum can be adopted as a basis wave function⁵⁾.

This study is a part of the RIKEN-CNS joint project for large-scale nuclear-structure calculations.

References

- 1) M. Honma, T. Mizusaki, and T. Otsuka: Phys. Rev. Lett. **75**, 1284 (1995).
- 2) T. Otsuka, M. Honma, T. Mizusaki, N. Shimizu, and Y. Utsuno: Prog. Part. Nucl. Phys. **46**, 319 (2001).
- 3) <http://www.csm.ornl.gov/pvm/>
- 4) <http://www.mcs.anl.gov/research/projects/mpi/>
- 5) N. Shimizu, T. Otsuka, T. Mizusaki, and M. Honma: Phys. Rev. Lett. **86**, 1171 (2001).

¹ Department of Physics, University of Tokyo

² Japan Atomic Energy Agency

³ Center for Nuclear Study, University of Tokyo

Microscopic description of oblate-prolate shape mixing in proton-rich Se isotopes

N. Hinohara, T. Nakatsukasa, M. Matsuo¹ and K. Matsuyanagi²

[Nuclear structure, large-amplitude collective motion]

Recent experimental data¹⁾ for ^{70}Se and ^{72}Se indicate that there is a gradual change in the character of the ground rotational band from oblate to prolate with an increase in the angular momentum. The data also suggest considerable mixing of the oblate and prolate shapes in the low-lying states of ^{70}Se and ^{72}Se . Since shape mixing is caused by large-amplitude collective motion connecting different shapes, it cannot be theoretically described within the static mean-field approximation or the small-amplitude fluctuations about equilibrium shapes.

We investigate the shape coexistence/mixing dynamics in ^{68}Se , ^{70}Se , and ^{72}Se by the adiabatic self-consistent collective coordinate (ASCC) method²⁾; this method enables us to extract the collective degrees of freedom (collective path) that provide information on the dynamics of large-amplitude shape mixing. As to the microscopic Hamiltonian, we use the pairing-plus-quadrupole model that takes into consideration the quadrupole-pairing force.

The one-dimensional collective path and the collective Hamiltonian describing the large-amplitude shape vibration are derived fully microscopically. It is found that the collective path almost follows the triaxial potential valley, indicating the importance of the triaxial degree of freedom in these isotopes.

The excitation spectra, $B(E2)$, and spectroscopic quadrupole moments are calculated by requantizing the collective Hamiltonian and solving the collective Schrödinger equation. The basic properties of the two coexisting rotational bands in the above-mentioned nuclei are found to be well reproduced. In the case of ^{68}Se , the energy of the calculated 0_2^+ state is located above that of 2_2^+ state, suggesting that the low-lying states in ^{68}Se are in an intermediate situation between oblate-prolate shape coexistence and the Wilets-Jean γ -unstable model. This γ -unstable nature is also found from the calculated interband $E2$ -transition probabilities. In the case of ^{70}Se , we found cross-talks of the $E2$ transitions between the 2^+ and 4^+ states associated with a significant change in the localization properties of the wave functions. In the case of ^{72}Se , the 0_1^+ wave function has the maximum value at the oblate deformation, while the prolate character develops in the ground rotational band with an increase in the angular

momentum.

The results of calculations show that oblate-prolate shape mixing becomes weak as the rotational angular momentum increases, and this is a common feature of all the three isotopes. We have analyzed the dynamical origin of this trend and found that the rotational energy plays a crucial role in determining the degree of localization of the collective wave function in the (β, γ) plane. The rotational effect causing the localization of the collective wave function may be called “rotational hindrance of shape mixing.”

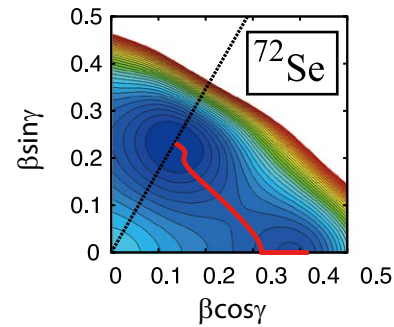


Fig. 1. Collective path for ^{72}Se obtained by the ASCC method. The collective path projected onto the (β, γ) plane is indicated by the solid line on the potential energy surface.

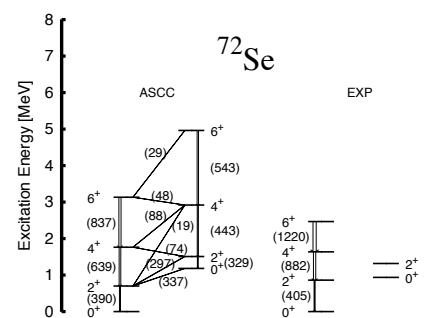


Fig. 2. Theoretical and experimental excitation spectra and $B(E2)$ values for low-lying states in ^{72}Se . The values of the $B(E2)$ are shown in units of $e^2 \text{fm}^4$.

References

- 1) J. Ljungvall, et al.: Phys. Rev. Lett. **100**, 102502 (2008).
- 2) M. Matsuo, T. Nakatsukasa and K. Matsuyanagi: Prog. Theor. Phys. **103**, 959 (2000).

[†] Condensed from the article in Phys. Rev. C **80**, 014305 (2009)

¹ Department of Physics, Faculty of Science, Niigata University

² Yukawa Institute for Theoretical Physics, Kyoto University

Effects of Oblate-Prolate Symmetry Breaking on Triaxial Deformation Dynamics[†]

K. Sato,^{*1} N. Hinohara, T. Nakatsukasa, M. Matsuo,^{*2} and K. Matsuyanagi^{*3}

[Nuclear structure, large-amplitude collective motion, shape coexistence]

In recent years, experimental data suggesting the coexistence of a ground-state rotational band with an oblate shape and an excited band with a prolate shape in proton-rich unstable nuclei have been obtained. These observations along with the variety of shape coexistence phenomena observed in various regions of the nuclear chart stimulate the development of a nuclear structure theory capable of describing large-amplitude collective phenomena.

In this study, from the viewpoint of oblate-prolate symmetry and its breaking, we propose a simple model based on the quadrupole collective Hamiltonian in order to study the dynamics of triaxial deformation in shape coexistence phenomena. Our model can describe the axially symmetric rotor model, the γ -unstable model, the rigid triaxial rotor model, an ideal situation for the oblate-prolate shape coexistence, and the intermediate situations between them by varying a few parameters. It is derived from the well-known five-dimensional quadrupole collective Hamiltonian¹⁾ by fixing the β degree of freedom, and thus, it is (1+3) dimensional^{a)} (one dimension for γ vibration and three dimensions for rotation). Using this model, we first analyze the properties of low-lying states in the case where the collective masses possess the oblate-prolate symmetry; this is done by varying the parameters of the collective potential. Then, we investigate how the properties of the low-lying states change when the oblate-prolate symmetry is broken in the collective masses. We also evaluate the validity of the (1+3)D model by liberating the β degree of freedom, i.e., by using the (2+3)D model, for the case involving the intermediate situation between the γ -unstable and ideal oblate-prolate shape-coexistence limits; we are particularly interested in the intermediate situation.

Figure 1 shows the excitation spectra and $B(E2)$ values of the (1+3)D and (2+3)D models for the intermediate situation mentioned above, where the oblate-prolate symmetry is broken both in the collective potential and the inertial mass functions; here, the collective potential has an oblate local minimum, and the prolate local minimum is slightly higher than the oblate one. The moments of inertia are larger on the oblate side than on the prolate side. The essential fea-

tures of the excitation spectrum in the (1+3)D model are identical to those in the (2+3)D model. In particular, the ordering of these eigenstates in the calculations based on the two models is identical. One can also see that in both the models, the interband transitions between the initial and final states having equal angular momentum become weaker with increasing angular momentum. This is caused by the oblate-prolate asymmetry in the moments of inertia. These observations indicate that the β - γ coupling plays only a secondary role and that the major feature of the excitation spectrum is determined by the triaxial deformation dynamics. The γ -dependence of the collective masses and the collective potential also play an important role.

We performed numerical calculations for the triaxial deformation dynamics using this model. The results of the calculations revealed the following: (1) The relative energy of the excited 0^+ state can indicate the potential shape along the γ direction. (2) Specific $E2$ transition probabilities are sensitive to the breaking of the oblate-prolate symmetry. (3) Nuclear rotation may induce the localization of collective wave functions in the (β, γ) deformation space.

References

- 1) A. Bohr and B. R. Mottelson, *Nuclear Structure*, Vol. II (W. A. Benjamin Inc., 1975; World Scientific, 1998).

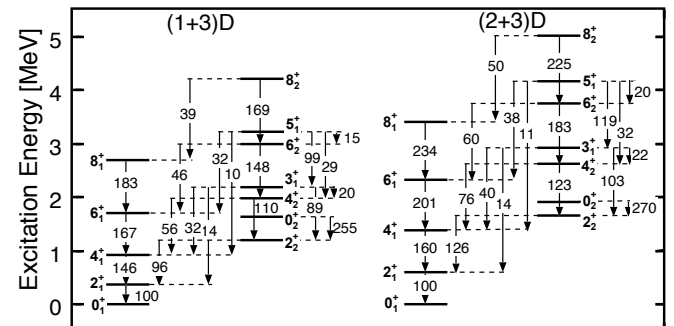


Fig. 1. Comparison of the excitation spectra and $E2$ -transition properties in the (1+3)D model (left) with those in the (2+3)D model (right); the $B(E2)$ values are written on the transition arrows, with $B(E2; 2_1^+ \rightarrow 0_1^+)$ normalized to 100.

[†] Condensed from the article in Prog. Theor. Phys. **123** (2010), 129.

^{*1} Department of Physics, Kyoto University

^{*2} Department of Physics, Niigata University

^{*3} Yukawa Institute for Theoretical Physics, Kyoto University

^{a)} Therefore, we call it the (1+3)D model.

Analysis of ^{78}Ge by generator coordinate method

K. Higashiyama*¹ and N. Yoshinaga*²

[Nuclear structure, generator coordinate method]

The intriguing properties of the even-even Se and Ge isotopes in the mass region $A \sim 80$ have been investigated in a number of previous experimental and theoretical studies¹. These isotopes belong to a typical transitional region that lies between spherical and deformed regions. The structure of their low-lying states can be attributed to the interplay of rotational and vibrational collective motions. For high-spin states, γ -ray spectroscopy of the near-yrast states in the $N = 44$ and 46 isotones of Se ($^{80,82}\text{Se}$) was carried out for deep-inelastic reactions². Recently, full-fledged shell-model calculations have been performed on the even-even and odd-mass nuclei in this mass region³. The shell model calculations well reproduce the experimental energy levels and electromagnetic transition rates for the low-lying and high-spin states.

In the present study, we apply the quantum-number-projected generator coordinate method (PGCM) to ^{78}Ge under the same interaction as used in previous shell model studies³. All the four orbitals $g_{9/2}$, $p_{1/2}$, $p_{3/2}$, and $f_{5/2}$ in the major shell of $28 \leq N(Z) \leq 50$ are considered, and the valence neutrons (protons) are treated as holes (particles).

In the present scheme, the spins of the neutron and proton systems (I_ν and I_π) are projected separately, and the total spin is constructed by angular momentum coupling. To generate functions for the PGCM, we employ the intrinsic Nilsson states $|\Phi_\tau(\beta, \gamma)\rangle$ for the neutron or proton systems ($\tau = \nu$ or π), where (β, γ) denotes the deformation parameters. The PGCM wavefunction for the ρ th state of a spin I_τ in neutron or proton spaces is given by

$$|\Psi_{I_\tau M_\tau \rho}^{(\tau)}\rangle = \sum_i \sum_{K_\tau = -I_\tau}^{I_\tau} \mathcal{F}_{K_\tau \rho}^{I_\tau i} \hat{P}_{M_\tau K_\tau}^{I_\tau} |\Phi_\tau(\beta_i, \gamma_i)\rangle, \quad (1)$$

where $\hat{P}_{M_\tau K_\tau}^{I_\tau}$ is the spin projection operator, $\mathcal{F}_{K_\tau \rho}^{I_\tau i}$ is the weight function to be determined by the PGCM, and i stands for a representative point of deformation (β, γ) . Then, the many-body wavefunction for an even-even nucleus can be written as

$$|\Psi_{IM}(I_\nu \rho I_\pi \sigma)\rangle = [|\Psi_{I_\nu \rho}^{(\nu)}\rangle \otimes |\Psi_{I_\pi \sigma}^{(\pi)}\rangle]_M^{(I)}, \quad (2)$$

where I is the total spin and M is its projection. PGCM calculations are carried out for two cases: (i) triaxial deformations with $\beta = 0.2, 0.6, 1.0$ and $\gamma = 10^\circ, 20^\circ, 30^\circ, 40^\circ, \text{ and } 50^\circ$ (15 points); (ii) only axial deformations with $\beta = 0.0, 0.2, \dots, 2.0, 3.0, \text{ and } 4.0$ and $\gamma = 0^\circ, 60^\circ$ (25 points).

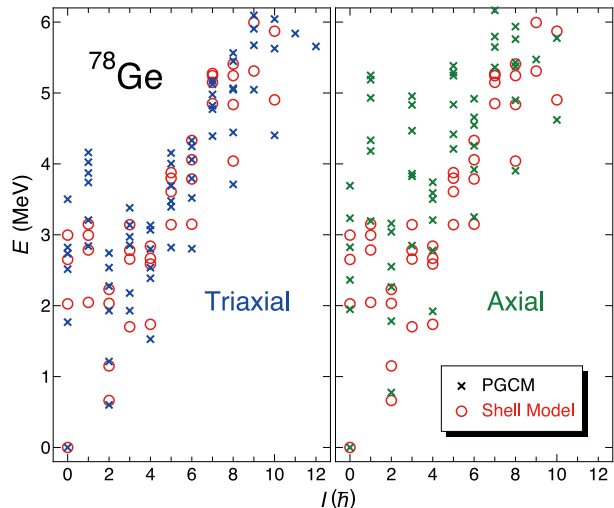


Fig. 1. Excitation energies calculated using the shell model states (open circles) and the PGCM (crosses) as a function of spin I in ^{78}Ge .

In Fig.1, energy levels calculated with the shell model are compared with those calculated by the PGCM for ^{78}Ge . The PGCM results for triaxial and axial deformations are shown in the left and right panels, respectively. In both cases, the PGCM reproduces the energy levels of the even-spin yrast band well. In the case of the other excited states, the PGCM calculations performed by assuming triaxial deformation are in good agreement with the shell model results, especially for the 2_2^+ , 3_1^+ , 4_2^+ , and 5_1^+ states, which are members of the γ -band. However, the energy levels calculated by assuming only axial deformation for the 2_2^+ , 3_1^+ , and 5_1^+ states are higher than those calculated using the shell model. Apparently, the description of the 2_2^+ , 3_1^+ , 4_2^+ , and 5_1^+ states is not satisfactory when assuming only axially symmetric shape. The triaxial components play an essential role in the description of these states.

References

- 1) K.-H. Speidel et al.: Phys. Rev. C **57**, 2181 (1998), and references therein.
- 2) G. A. Jones et al.: Phys. Rev. C **76**, 054317 (2007).
- 3) N. Yoshinaga, K. Higashiyama, and P. H. Regan: Phys. Rev. C **78**, 044320 (2008).

*¹ Department of Physics, Chiba Institute of Technology

*² Department of Physics, Saitama University

Simple-model analysis of doublet bands in doubly odd nuclei

N. Yoshinaga*¹ and K. Higashiyama*²

[Nuclear structure, quadrupole coupling model, chopsticks configuration]

Recently, the study of $\Delta I = 1$ doublet bands become one of the most interesting subjects in nuclear physics. Such pairs of bands arising from the high- j orbitals of a neutron and a proton have been experimentally found in many doubly odd nuclei. In order to characterize the doublet bands in a simple and consistent manner, we developed the quadrupole coupling model (QCM)¹⁻³, in which the collective core representing the even-even part of the nucleus couples with a neutron and a proton in intruder orbitals via quadrupole-quadrupole interactions.

We applied this model to the doublet bands built on the $\nu h_{11/2} \otimes \pi g_{9/2}$ configuration for the doubly odd nuclei with a mass of approximately 100³. With this approach, the experimental energy levels and electromagnetic ratios $B(M1; I \rightarrow I-1)/B(E2; I \rightarrow I-2)$ have been successfully reproduced. Analysis of the wave functions revealed a new band structure, which resulted from the ‘‘chopsticks configuration’’ of the unpaired neutron in the $0h_{11/2}$ orbital and the unpaired proton in the $0g_{9/2}$ orbital, weakly coupled with the quadrupole collective excitations of the even-even core. In this study, we extend the QCM to include multipole interactions for the neutron $0h_{11/2}$ orbital and the proton in the $0g_{9/2}$ orbital.

In Fig. 1, the experimental energy levels based on the $\nu h_{11/2} \otimes \pi g_{9/2}$ configuration are compared with

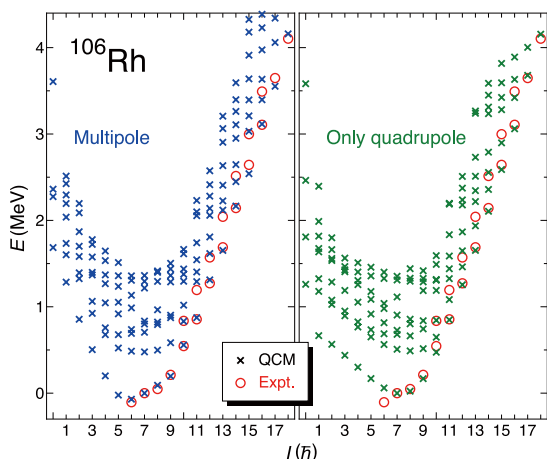


Fig. 1. Calculated energy levels (crosses) and experimental data (open circles) as a function of spin I for the states with $\nu h_{11/2} \otimes \pi g_{9/2}$ configuration in ^{106}Rh .

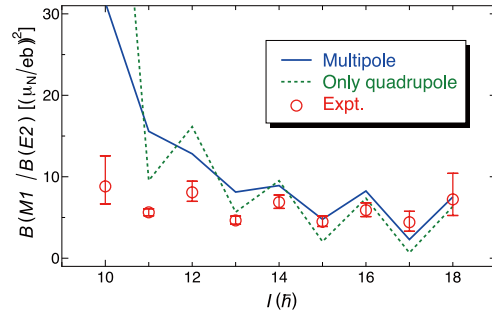


Fig. 2. Comparison of $B(M1; I \rightarrow I-1)/B(E2; I \rightarrow I-2)$ ratios in the QCM with the experimental data (expt.). Solid and dotted lines show the results obtained when considering multipole interactions and those obtained when considering only quadrupole interactions, respectively.

those calculated using the QCM for ^{106}Rh . The current results obtained by considering the multipole interactions and those obtained by considering only the quadrupole interactions³) are shown in the left and right panels, respectively. In our previous study³), we failed to reproduce the bandhead state; experimentally, the 6_1^- state was lower in energy than the 7_1^- state, while theoretical studies indicated that the 6_1^- state was higher in energy than the 8_1^- state. In the present analysis, however, we succeeded in reproducing the bandhead energy of the 6_1^- state. Moreover, the energies of the 10_1^- and 10_2^- states were considerably improved.

In Fig. 2, we compare the theoretical ratios $B(M1; I \rightarrow I-1)/B(E2; I \rightarrow I-2)$ for the yrast states with the experimental values. The theoretical result gives a successful description of the large-amplitude staggering of the $B(M1)/B(E2)$ ratios. The mechanism underlying this even-odd staggering has been discussed in detail within our present model³). In the present study, we also found that while neutron and proton quadrupole interactions are dominant among other interactions, octupole and hexadecapole interactions are more important for reproducing the bandhead energies.

References

- 1) N. Yoshinaga and K. Higashiyama: Eur. Phys. J. A **30**, 343 (2006); **31**, 395 (2007).
- 2) K. Higashiyama and N. Yoshinaga: Eur. Phys. J. A **33**, 355 (2007).
- 3) K. Higashiyama and N. Yoshinaga: Prog. Theor. Phys. **120**, 525 (2008).

*¹ Department of Physics, Saitama University

*² Department of Physics, Chiba Institute of Technology

Linear Response Calculation Using Canonical-basis TDHFB with a Schematic Pairing Functional

S. Ebata,¹ T. Nakatsukasa T. Inakura,^{1, 2} Y. Hashimoto,² and K. Yabana^{1, 2}

[Nuclear structure, unstable nuclei]

The recent progress at radioactive facilities such as RIBF in RIKEN has resulted in a strong demand for theoretical frameworks that can analyze and predict the properties of unknown nuclei. Such a framework should include the effects of nuclear deformation and pairing correlation, and should be capable of calculating properties of not only the ground state but also the excited state. A combination of the Hartree-Fock-Bogoliubov method and quasiparticle-random-phase approximation (HFB+QRPA) is a candidate for such a framework, and it is applicable to a wide range of light and heavy nuclei. However, in this framework, considerable efforts are required for coding the programs, and significant computational resources are necessary. The HFB+QRPA for deformed nuclei is currently still in the preliminary stage.

We proposed the canonical-basis time-dependent Hartree-Fock-Bogoliubov (CbTDHFB) in the three-dimensional coordinate-space representation, which can take into account the effect of nuclear deformation without symmetry-restriction while treating the pairing correlation in the BCS-like approximation. We reported in brief the derivation and conservation rules of the CbTDHFB equations¹⁾.

We derived the CbTDHFB equations using the time-dependent variational principle; they can be achieved only if we choose a special pairing functional $E_{\text{pair}} = -G|\sum_{l>0} u_l(t)v_l(t)|^2$. Here, u_l and v_l correspond to the time-dependent BCS factors for the canonical pair of states $\phi_l(\mathbf{r}, t)$ and $\phi_{\bar{l}}(\mathbf{r}, t)$. Note that the state l is not necessarily the time-reversed state of the state l .

This year, we use the modified pairing functional, $E'_{\text{pair}} = -\tilde{G}|\sum_{l>0} f(\varepsilon_l)u_l(t)v_l(t)|^2$, to treat a wide range of nuclei. Here, $f(\varepsilon)$ is a cut-off function, and ε_l are the single-particle energies of the ground state. In the present calculation, $f(\varepsilon_l)$ are fixed during the time evolution. The parameter \tilde{G} and the function $f(\varepsilon)$ are the same as those given in Ref.²⁾ When we choose the pairing functional E'_{pair} , the CbTDHFB equations are written as

$$\begin{cases} i\hbar\dot{\phi}_l(\mathbf{r}, t) = (\hat{h}[\rho(t)] - \varepsilon_l(t))\phi_l(\mathbf{r}, t), \\ i\hbar\dot{\rho}_l(t) = f(\varepsilon_l)(\Delta(t)K_l(t) - \Delta(t)K_{\bar{l}}(t)), \\ i\hbar\dot{K}_l(t) = K_l(t)(\varepsilon_l(t) + \varepsilon_{\bar{l}}(t)) + f(\varepsilon_l)\Delta(t)(2\rho_l(t) - 1), \end{cases}$$

where $\rho_l \equiv |v_l|^2$ are the occupation probabilities, and $K_l \equiv u_l v_l$ are the pair densities; $\Delta \equiv \tilde{G}\sum_{l>0} f(\varepsilon_l)K_l(t)$

is the gap energy, and $\varepsilon_l(t) \equiv \langle \phi_l(t) | \hat{h}[\rho(t)] | \phi_l(t) \rangle$. These equations obey the same conservation rules as do the original CbTDHFB equations¹⁾.

We solve the CbTDHFB equations in real time and calculate the linear response of the nuclei. In the linear-response calculation, we consider an external field $\hat{V}_{\text{ext}}(\mathbf{r}, t)$ which is weak and instantaneous in time, $\hat{V}_{\text{ext}}(\mathbf{r}, t) \equiv -k\hat{F}\delta(t)$; $k \ll 1$. \hat{F} is a one-body operator, for example, the isoscalar quadrupole operator, $\hat{Q}_{20} = r^2 Y_{20}$. We calculate the time evolution of the expectation value of \hat{F} and obtain the strength function $S(\hat{F}; E)$ by Fourier transformation¹⁾.

Figure 1 shows the isoscalar quadrupole strength functions ($K = 0$) for magnesium isotopes, calculated using the SkM^{*} parameter set. In this calculation, the ground states of these isotopes are found to be deformed into a prolate. These calculations employ a schematic pairing functional and a very good approximation of the HFB+QRPA using a realistic pairing functional.

Currently, we are developing a CbTDHFB code for parallel computing to facilitate the calculation for heavy nuclei. With this new code, we plan to carry out a systematic investigation of nuclear responses.

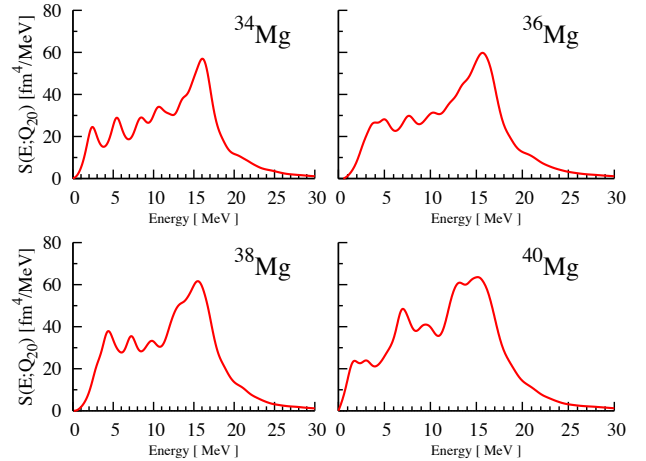


Fig. 1. The quadrupole strength functions ($K = 0$) for $^{34,36,38,40}\text{Mg}$ calculated using the Skyrme functional of the SkM^{*} parameter set. The smoothing parameter $\Gamma = 2$ MeV is used.

References

- 1) S. Ebata *et al.*: RIKEN Accel. Prog. Rep. **42**, 49 (2009).
- 2) N. Tajima *et al.*: Nucl. Phys. **A 603**, 23 (1996).

¹ Graduate School of Pure and Applied Sciences, University of Tsukuba

² Center for Computational Science, University of Tsukuba

Finite Amplitude Method for QRPA

P. Avogadro, T. Nakatsukasa

The aim of this research is to generalize the finite amplitude method (FAM)¹⁾ for the purpose of making it applicable to superfluid systems. In practice we aim to develop a quasiparticle random phase approximation (QRPA) code from a Hartree Fock Bogoliubov (HFB) code. The QRPA formalism can be used to determine the structure and energy of low-lying excited states of nuclei in which pairing correlations play an important role; thus, the formalism is useful for the study of exotic nuclei. Generally it is difficult to use this formalism because of two main reasons. The first reason is that the “construction” of the QRPA matrix is difficult; the analytic derivation of the nuclear Hamiltonian in some cases (especially in deformed systems) is extremely complicated, and some parts of the Hamiltonian have to be neglected, leading to a loss of full self-consistency. The second reason is that the QRPA matrix is usually large, and hence, the diagonalization procedure is time consuming. The FAM helps to overcome the first difficulty. The QRPA equations in the standard formulation are as follows:

$$\begin{pmatrix} A & B \\ B^* & A^* \end{pmatrix} \begin{pmatrix} X \\ Y \end{pmatrix} = \omega \begin{pmatrix} X \\ -Y \end{pmatrix}. \quad (1)$$

These equations are equivalent to the TDHFB equations in the small-amplitude limit²⁾; in order to prove this equivalence we write the quasiparticle annihilation operator as the sum of the HFB operator and a time dependent-perturbation:

$$a_\mu(t) = (a_\mu + \delta a_\mu(t)) e^{-iE_\mu t}. \quad (2)$$

By substituting Eq. (2) in the quasiparticle annihilation operator equation of motion and by expressing the TDHFB Hamiltonian as the sum of the HFB Hamiltonian term and a small perturbation, we obtain:

$$i \frac{\partial \delta a(t)}{\partial t} = E_\mu \delta a_\mu(t) + [H_{HFB}, \delta a_\mu(t)] + [\delta H(t), a_\mu]. \quad (3)$$

By Fourier expansion, we obtain a set of equations that is equivalent to Eq. (1):

$$\begin{cases} (E_\mu + E_\nu) X_{\nu\mu} + \delta H_{\mu\nu}^A(\omega) = \omega X_{\nu\mu} \\ (E_\mu + E_\nu) Y_{\nu\mu}^* + \delta \tilde{H}_{\nu\mu}^{A\dagger}(\omega) = -\omega Y_{\nu\mu}^* \end{cases}, \quad (4)$$

where E_ν and E_μ represent the quasiparticle energies, and δH^A and $\delta H^{A\dagger}$ are defined as follows:

$$\delta H^A(\omega) = U^\dagger \delta h(\omega) V^* - V^\dagger \delta \tilde{\Delta}^*(\omega) V^* + U^\dagger \delta \Delta(\omega) U^* - V^\dagger \delta h^T U^*, \quad (5)$$

$$\delta H^{A\dagger}(\omega) = U^\dagger \delta h^\dagger(\omega) V^* - V^\dagger \delta \Delta^*(\omega) V^* + U^\dagger \delta \tilde{\Delta}(\omega) U^* - V^\dagger \delta h^* U^*. \quad (6)$$

Here, U and V represent the quasiparticle amplitudes

obtained from HFB calculation. In general, the calculation of the matrix elements of Eq. (4) is not easier than Eq. (1). The FAM facilitates the calculation of Eq. (5) and Eq. (6), which are the terms of Eq. (4) that are difficult to calculate. In order to understand the FAM clearly, we emphasize that in the TDHFB approximation, self-consistency is maintained always. When a nucleus is excited, density perturbations with respect to the ground state (i.e. the HFB state) are present. In the small-amplitude limit, the fields (h and Δ) can be expanded linearly as functions of the densities: $\delta h = \delta h(\delta\rho)$ and $\delta\Delta = \delta\Delta(\delta\kappa)$, on the other hand, the transition densities in the QRPA formalism are functions of the X and Y amplitudes thus the residual fields can be written as follows: $\delta h = \delta h(X, Y)$ and $\delta\Delta = \delta\Delta(X, Y)$. In practice, $\delta h(\omega)$ and $\delta\Delta(\omega)$ are calculated using numerical derivatives; in the case in which the pairing interaction depends only on the abnormal density, FAM gives:

$$\begin{aligned} \delta h(\omega) &= \frac{h[(V^* + \eta UX)(V^T + \eta Y^T U^\dagger) - h[\rho_0]]}{\eta}, \\ \delta h^\dagger(\omega) &= \frac{h[(V^* + \eta UY^*)(V^T + \eta X^T U^\dagger) - h[\rho_0]]}{\eta}, \\ \delta\Delta(\omega) &= \frac{\Delta[(V^* + \eta UX)(U^T + \eta Y^T V^\dagger) - \Delta[\rho_0]]}{\eta}, \\ \delta\tilde{\Delta}(\omega) &= \frac{\Delta[(V^* + \eta UY^*)(U^T + \eta X^T V^\dagger) - \Delta[\rho_0]]}{\eta}. \end{aligned}$$

The small parameter η has been introduced for numerical differentiation. The FAM procedure needs the X and Y QRPA amplitudes; however these quantities are the solutions that we aim to obtain. Hence we carry out iterative procedures such as the conjugate gradient method. The algorithm starts with a guess for the solution (X and Y in this case) and returns a new value that is closer to the exact solution; the process can then be repeated till convergence is attained. A QRPA code obtained by the FAM is fully self-consistent. All the terms in the single-particle Hamiltonian present in the original HFB code are automatically taken into account through numerical derivatives; moreover, the application of the FAM is not restricted to systems with spherical symmetry. This technique can thus be a very useful tool to obtain a fully self-consistent deformed QRPA code.

References

- 1) T. Nakatsukasa, T. Inakura and K. Yabana: Phys. Rev. C 76, 024318 (2007)
- 2) P. Ring and P. Shuck: *The Nuclear Many Body Problem*, Springer-Verlag, Berlin (1980).

Chemical potential beyond quasiparticle mean field*

N. Dinh Dang, N. Quang Hung

NUCLEAR STRUCTURE, pairing, superfluid-normal phase transition, BCS theory, modified BCS theory, selfconsistent quasiparticle RPA, Lipkin-Nogami method, grand canonical ensemble, canonical ensemble, exact solution of pairing problem, chemical potential, quantal and thermal fluctuations

The results of a considerable number of theoretical studies have shown that fluctuations in small systems indeed lead to significant modifications of quantities, which are defined within the mean field and/or thermal equilibrium, where the effects of fluctuations are ignored. Among the two unknowns, which are defined by solving the BCS equations, namely the pairing gap and chemical potential, much attention has been devoted so far to the study of the first one, the pairing gap. It has been shown, for instance, that removing quantal fluctuations by using various methods of particle-number projection (PNP) significantly improves the agreement between the theoretical predictions and experimental data on pairing energies. The PNP also eliminates the shortcoming of the BCS theory, which breaks down at small values $G \leq G_c$ of the pairing interaction parameter, where the BCS equations have only trivial solutions. At finite temperature ($T \neq 0$), the results of theoretical studies in the last three decades have also shown that thermal fluctuations smooth out the sharp transition between the superfluid phase to the normal one (the SN phase transition) in nuclei.

The second quantity, the chemical potential, describes the change in the energy when one particle is added to the system at constant entropy and volume. In nuclear physics, the vanishing of chemical potential indicates the vicinity of the nucleon drip line. In the study of Bose-Einstein condensation (BEC), one expects the system to undergo the BEC into a single quantum state with zero total momentum when the chemical potential of the bound pair of fermions reaches the bottom of the bound state band. The present article studies the effects due to quantal and thermal fluctuations beyond the BCS quasiparticle mean field on the chemical potential within a model, which consists of N particles distributed amongst Ω doubly folded equidistant levels interacting via a pairing force with parameter G . The results obtained at zero and finite temperatures T within several approaches such as the BCS, Lipkin-Nogami (LN) particle-number projection (PNP), selfconsistent quasiparticle RPA plus LN-PNP (LNSCQRPA)¹, and modified BCS (MBCS) (See, e.g.,²) theories are compared with the exact results, whenever the latter are available. The analysis of the numerical results show that the chemical potential within this model remains

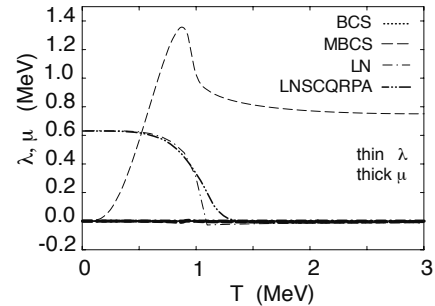


Fig. 1. Chemical potentials μ and λ as functions of T for $\Omega = N = 50$ at $G = 0.3$ MeV. The thin lines show the parameter λ , whereas the thick lines are the corresponding thermodynamic chemical potentials $\mu = \partial F / \partial N$ with the Helmholtz free energy F .

a constant in the middle of the spectrum only in the half-filled case within the mean-field approximation that neglects the self-energy corrections to the single-particle energies. Beyond the quasiparticle mean field, quantal and thermal fluctuations significantly alter the chemical potential as a function of G and/or T (Fig. 1). As the result, the quantity that corresponds to the chemical potential but includes the effects due to particle (quasiparticle)-number fluctuations, such as the parameter $\lambda_{LN} = \lambda_1 + 2\lambda_2(N+1)$ within the LN method or λ within the MBCS theory, gradually loses its strict physical meaning as a chemical potential with increasing T , and as the approximate PNP approaches the exact one, where all particle-number fluctuations are eliminated.

In the study of BCS-BEC transition in finite systems, we have shown that the system in the strong coupling regime can approach the BEC limit only in the strongly underfilled case ($N \ll \Omega$) at $T = 0$. Even if it can take place, increasing T will drive the system out of the BEC limit. However, this conclusion is obtained here within a simple one-dimensional model. How this feature is modified in realistic nuclei remains a question to be answered in the future studies.

References

- 1) N. Quang Hung and N. Dinh Dang, Phys. Rev. C **76**, 054302 (2007); Ibid **77** 029905(E); Ibid **77**, 064315 (2008).
- 2) N. Dinh Dang, Nucl. Phys. A **784**, 147 (2007).

* Condensed from Phys. Rev. C **81**, 034301 (2010).

Canonical ensemble treatments of pairing in finite systems

N. Quang Hung and N. Dinh Dang

[NUCLEAR STRUCTURE, pairing, canonical ensemble, BCS theory, quasiparticle RPA.]

As the atomic nucleus is a system with a fixed number of particles, the thermodynamic averages of the exact solutions of the pairing problem are usually carried out within the canonical ensemble (CE), and the results are compared with theoretical predictions, which are however obtained within the grand canonical ensemble (GCE). The latter consists of identical systems in thermal equilibrium, each of them exchanges its energy and particle number with an external reservoir. The systems of the CE exchange only their energy, whereas the particle number is fixed, remaining the same for all systems. Moreover, although the pairing problem can be solved exactly, the exact diagonalization of the pairing Hamiltonian is impracticable for large particle numbers ($N > 14$) in the case of half-filled model $N = \Omega$ (Ω is number of single-particle levels)^{a)}. It is therefore highly desirable to construct an approach based on the CE, which can offers results in good agreement with the exact CE ones for any value of the particle number. Such approach is proposed in the present study.

The main idea of present study is to embed the solutions of the pairing Hamiltonian obtained within the BCS and selfconsistent quasiparticle RPA (SCQRPA)¹⁾ combined with the Lipkin-Nogami particle-number projection for each total seniority or number of unpair particles $S = 0, 2, \dots, \Omega$ at zero temperature into the CE. These approaches are called the CE-BCS and CE-SCQRPA, respectively, whereas the GCE-BCS stands for the conventional finite-temperature BCS. In this way, the number of eigenstates and computational time are much reduced within the present approaches. The proposed approaches are tested within a schematic model as well as for a realistic nucleus. For the schematic model, we employ the doubly-degenerated multilevel pairing model whose single-particle energy are chosen as $\epsilon_j = 0, 1, \dots, \Omega - 1$. The model is half-filled, i.e. $N = \Omega$. As for the realistic nucleus, we employ the same Woods-Saxon single-particle spectrum from Table I of Ref²⁾ for neutron in $pf + sdg$ shell of ^{56}Fe so that we can compare the results obtained within our approaches with the predictions by the finite-temperature quantum Monte-Carlo (FTQMC) method²⁾. The analysis of numerical calculations for the total energy \mathcal{E} , pairing gap Δ and heat capacity C shows that the CE-SCQRPA offers the best fits to the exact results as well as those obtained within the FTQMC calculations (See e.g. Fig. 1). The CE-BCS

^{a)} This is true only for nonzero T because one has to construct the partition function with all excited states.

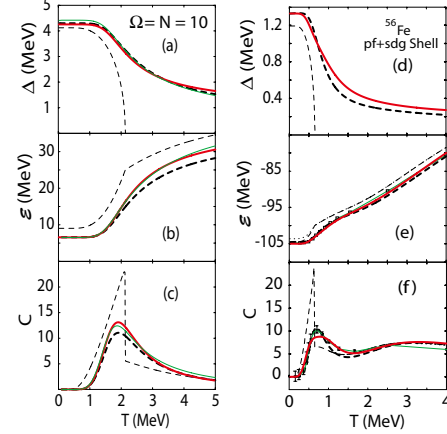


Fig. 1. Pairing gaps Δ , total energies \mathcal{E} and heat capacities C as function of temperature T (MeV) obtained for $N = 10$ (left panels) with interaction parameter $G = 1$ MeV and for neutrons in ^{56}Fe with $G = 16/A$ MeV ($A = 56$). The thin dashed, thick dashed, and thick lines denote the results obtained within the GCE-BCS, CE-BCS and CE-SCQRPA, respectively. The thin lines in the left panels stand for the exact CE, whereas those in the right panels depict the FTQMC calculations.

results are a little bit off from the exact ones but still offer much better agreement with the exact solutions than the predictions by the GCE-BCS. The most interesting feature here is that neither the pairing gaps obtained within the CE-BCS nor those obtained within the CE-SCQRPA collapse at a critical temperature T_C as predicted by the GCE-BCS, but they monotonously decrease with increasing T [See e.g. Fig. 1 (a) and (d)]. As the result, the superfluid-normal phase transition is smoothed out even within the CE-BCS calculations due to the effects of quantal and thermal fluctuations. This feature suggests that any exact particle-number projection method at finite temperature, which could bring a GCE-BCS to CE-BCS, should have the same feature as presented here with a nonvanishing gap. Since present approaches do not involve any matrix diagonalization, its merit resides in its simplicity and its application to larger finite systems, where the exact solution is impracticable, whereas the FTQMC is time consuming.

References

- 1) N.Q. Hung and N.D. Dang: Phys. Rev. C **76**, 054302 (2007).
- 2) S. Rombouts, K. Heyde, and N. Jachowicz: Phys. Rev. C **58**, 3295 (1998).

Top-on-top mechanism for TSD bands in even mass nuclei[†]

K. Tanabe,^{*1,*2} and K. Sugawara-Tanabe^{*1,*3}

[TSD bands, Particle-rotor model, D_2 -invariance]

The algebraic solution to the particle-rotor model with high j nucleon coupled to a triaxially deformed core, $H = H_{\text{rot}} + H_{\text{sp}}$,^{1,2)} successfully takes into account the Coriolis term, $\vec{I} \cdot \vec{j}$, which mediates strong correlation between two tops, i.e., the rotating core with $\vec{R} = \vec{I} - \vec{j}$ and the single-particle top with \vec{j} . This makes a big difference from the wobbling model.³⁾ We have demonstrated that such a “top-on-top mechanism” not only reproduces the energy level scheme,¹⁾ but also gives the approximate selection rules for the $E2$ and $M1$ transitions among TSD bands²⁾ in the odd mass Lu isotopes. The TSD bands are classified in terms of two quantum numbers, (n_α, n_β) , describing the precession of total angular momentum \vec{I} and of the single-particle angular momentum \vec{j} , respectively. Invariance of the nuclear states under D_2 symmetry restricts the range of n_α and n_β depending on $I - j$. We have estimated the overlap, $G_{n_\alpha n_\beta; n_\alpha n_\beta}^{Ij}$, between the eigenstates of H expressed by boson numbers n_α and n_β , and the original Holstein-Primakoff boson numbers n_a and n_b .

In extending the above scheme to the TSD bands in even-even nuclei, the angular momentum j is assumed to be a sum of two single particle angular momenta as $j = j_1 + j_2$, and the magnitude of integer j is kept as a constant over a certain range of I . Then, the transition rates gain a factor of $G_{0000}G_{1010} \propto (\frac{I-j}{I})^3$ both for $E2$ - and $M1$ -transitions with $\Delta I = 1$ among the favored (0,0) and the unfavored (1,0) bands. The value of $I - j$ is smaller for even- A case than odd- A case, which makes the observation of the other partner band in even mass nuclei difficult. This explains the situation that no linking transition between the (0,0) and the (1,0) bands has been found for the TSD bands in Hf isotopes and ¹⁶⁴Lu.

References

- 1) K. Tanabe and K. Sugawara-Tanabe: Phys. Rev. C **73**, 034305 (2006); *ibid.* **75**, 059903(E) (2007).
- 2) K. Tanabe and K. Sugawara-Tanabe: Phys. Rev. C **77**, 064318 (2008).
- 3) A. Bohr and B. R. Mottelson: *Nuclear Structure* (Benjamin, Reading, MA, 1975), Vol. II.

[†] Based on the article in Bull. Am. Phys. Soc. **54**, No. 10, 69 (2009)

^{*1} Theoretical Nuclear Physics Laboratory, RIKEN Nishina Center, Wako, Saitama 351-0198

^{*2} Department of Physics, Saitama University, Sakura-Ku, Saitama 338-8570

^{*3} Otsuma Women's University, Tama, Tokyo 206-8540

SU(3) symmetry in anisotropic harmonic oscillator[†]

K. Sugawara-Tanabe,^{*1,*2} K. Tanabe,^{*1,*3} A. Arima,^{*4} and B. Gruber^{*5}

[Triaxially deformed harmonic oscillator, SU(3) invariance, New magic numbers]

In this paper we propose a new boson transformation by which all the oscillator states for an anisotropic case can be embedded in the SU(3) bases.¹⁾ We start from an anisotropic harmonic oscillator Hamiltonian without spin-orbit interaction, whose oscillator frequencies ω_x , ω_y and ω_z are related to the deformation parameters β and γ . Suppose that three oscillator frequencies have an integral rational ratio $a : b : c$, i.e., $\omega_x = a\omega_{\text{sh}}$, $\omega_y = b\omega_{\text{sh}}$ and $\omega_z = c\omega_{\text{sh}}$. Then, the eigenvalues and eigenfunctions of H are described by a set of quantum numbers (n_x, n_y, n_z) , $H|n_x, n_y, n_z\rangle = \hbar\omega_{\text{sh}}(N_{\text{sh}} + \frac{a+b+c}{2})|n_x, n_y, n_z\rangle$. Here the n_k is the eigenvalue of the number operator $\hat{n}_k = c_k^\dagger c_k$, with the harmonic oscillator boson operator c_k ($k = x, y, z$), and $N_{\text{sh}} = an_x + bn_y + cn_z$. In order to rewrite H in a SU(3)-invariant form, we express c_k ($k = x, y, z$) in terms of an m -fold product of new bosons s_m ($m = a, b, c$), by requiring $s_m^\dagger s_m = mc_k^\dagger c_k$, and $[s_m, s_m^\dagger] = 1$. The new bosons s_m are introduced for any positive integer m by the non-linear transformation, i.e. $c_k = \left[m \prod_{r=1}^{m-1} (\hat{n}_m + r) \right]^{-1/2} (s_m)^m = \left[\frac{\Gamma(\hat{n}_m+1)}{m\Gamma(\hat{n}_m+m)} \right]^{1/2} (s_m)^m$, where $\hat{n}_m = s_m^\dagger s_m$. Thus, we have $\hat{N}_{\text{sh}} = s_a^\dagger s_a + s_b^\dagger s_b + s_c^\dagger s_c$. In dealing with many boson states, the projection operator, $P_m = \frac{1}{m} \sum_{k=0}^{m-1} e^{i\frac{2\pi k}{m}\hat{n}_m}$ ($m = a, b, c$), may be useful to eliminate unphysical states other than the eigenstates of the original Hamiltonian. We can classify the single-particle states in terms of three quantum numbers, i.e., two diagonal operators expressed by number operators together with a Casimir operator. The single-particle level given by N_{sh} provides new magic numbers for the case of triaxially deformed harmonic oscillator.

References

- 1) K. Sugawara-Tanabe, K. Tanabe, A. Arima and B. Gruber: Phys. Rev. C **80**, 044307 (2009).

[†] Condensed from the article in Phys. Rev. C **80**, 044307 (2009)

^{*1} Theoretical Nuclear Physics Laboratory, RIKEN Nishina Center, Wako, Saitama 351-0198

^{*2} Otsuma Women's University, Tama, Tokyo 206-8540

^{*3} Department of Physics, Saitama University, Sakura-Ku, Saitama 338-8570

^{*4} Science Museum, Japan Science Foundation, Tokyo 102-0091

^{*5} College of Science, Southern Illinois University, Carbondale, Illinois 62901, USA

Investigation of t -band in ^{182}Os by GCM

Y. Hashimoto,*¹ and T. Horibata *²

When the axial symmetry in a nuclear mean field is lost, a general type of nuclear rotational motion occurs, in which the rotational axis is not parallel to the principal axis (PA) with the largest moment of inertia.^{1,2)}

From a theoretical viewpoint, an even more general type of rotation is expected, where the rotational axis is located away from any of the principal axes.^{3,4)} This is called tilted-axis rotation (TAR).⁵⁾ The three-dimensional (3D) cranking model plays a central role in the study of wobbling motion and TAR.

Experimental data that support the theoretical assumption of the occurrence of the general type of nuclear rotational motion have been accumulated.^{6,7)}

With the purpose of studying the microscopic mechanism of TAR, we performed 3D cranked Hartree-Fock-Bogoliubov (3D-CHFB) calculations for ^{182}Os . We introduce the tilt angle ψ measured with respect to the x-axis, which is perpendicular to the symmetry axis (z-axis) along the prime meridian. The wave function $|\Phi(\psi)\rangle$ that includes the tilt angle ψ is obtained by solving the 3D-CHFB equation with the pairing-plus-quadrupole Hamiltonian.

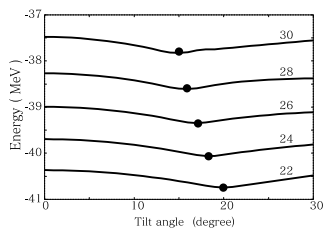


Fig. 1. Energy determined from cranked-HFB versus tilt angle. The angular momentum ranges from $J = 22\hbar$ to $J = 30\hbar$. The filled circles indicate the positions of TAR states.

Fig. 1 shows some examples of the 3D-CHFB solutions plotted against the tilt angle for the angular momentum values from $J = 22\hbar$ to $30\hbar$. Each of the *branches* has a local minimum structure called the TAR state and is connected with an unstable state in the *s*-band.⁸⁾ A similar local minimum structure is found in the branch with an angular momentum $J \geq 16\hbar$.⁸⁾ The TAR states are expected to be members of a band with $K = 8$.⁹⁾ The band structure that includes the ground state band is presented in Ref. 9).

We believe that a new band structure of TAR states may support Walker's long-standing prediction that

the t -band is responsible for the occurrence of the back-bending in the region corresponding to $A \sim 180$ ⁶⁾. In the t -band, the signature splitting phenomena between the group of states with even angular momentum values and that with odd values are observed. The signature splitting phenomena are attributed to a purely quantum mechanical effect, namely, the tunneling effect between the two TAR states in the northern and southern hemispheres of the angular momentum space.¹⁰⁾

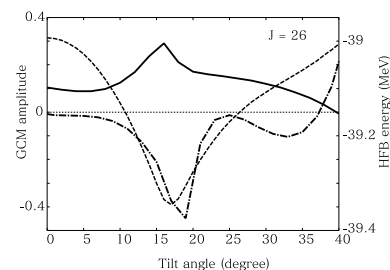


Fig. 2. GCM amplitudes with even (solid curve) and odd (dash-dotted curve) symmetries for an angular momentum $J = 26\hbar$. The CHFB energy is also shown (dashed curve).

We are now studying the signature splitting in the t -band by using the generator coordinate method (GCM). Fig. 2 shows an example of a pair of GCM solutions with even and odd symmetries for $J = 26\hbar$. We see the amplitudes are large around the TAR state. The energy splitting in this case is 252 keV, which is consistent with the results obtained by Walker.⁶⁾ The investigation of the t -band structure for an angular momentum $J \leq 16\hbar$ is in progress.

References

- 1) A. Bohr and B. R. Mottelson: *Nuclear Structure*, Vol.II (Benjamin, Reading, MA, 1975).
- 2) S. Frauendorf: *Rev. Mod. Phys.* **73**, 463-514 (2001).
- 3) A. K. Kerman and N. Onishi: *Nucl. Phys. A* **361**, 179-191 (1981).
- 4) N. Onishi: *Nucl. Phys. A* **456**, 279-297 (1986).
- 5) T. Horibata and N. Onishi: *Nucl. Phys. A* **596**, 251-284 (1996).
- 6) P. M. Walker et al.: *Phys. Lett. B* **309**, 17-22 (1993).
- 7) S.W. Ødegård et al.: *Phys. Rev. Lett.* **86**, 5866-5869 (2001).
- 8) Y. Hashimoto and T. Horibata: *Phys. Rev. C* **74**, 017301 (2006).
- 9) Y. Hashimoto and T. Horibata: *Eur. Phys. J. A* **42**, 571-575 (2009).
- 10) T. Horibata, M. Oi, N. Onishi and A. Ansari: *Nucl. Phys. A* **646**, 277-295(1999); **A 651**, 435-436 (1999).

*¹ Graduate School of Pure and Applied Sciences, University of Tsukuba, Tsukuba 305-8571, Japan

*² Faculty of Software and Information Technology, Aomori University, Aomori, Aomori 030-0943, Japan

Global fitting of pairing density functional[†]

M. Yamagami^{*1}, Y. R. Shimizu^{*2}, and T. Nakatsukasa

We have developed a density functional for the global description of pairing correlations by focusing on the neutron-excess dependence. The accurate pairing density functional (pair-DF) is indispensable for predicting pairing-sensitive properties (for example, low-energy dynamics) in reaction networks of r-process nucleosynthesis and nuclear reactors, and also for predicting the superfluidity in neutron-star matter.

We demonstrated that the pair-DF should include the isovector density ($\rho_1 = \rho_n - \rho_p$) dependence, since the standard pair-DF with only isoscalar density ($\rho = \rho_n + \rho_p$) terms fails to reproduce the α -dependence ($\alpha = (N - Z)/A$) of the pairing correlations. To demonstrate this, we examined the pair-DF $\tilde{h}_\tau(\mathbf{r}) = \frac{1}{2}V_0 g_\tau(\mathbf{r}) \tilde{\rho}_\tau(\mathbf{r})$, where

$$g_\tau(\mathbf{r}) = 1 - \eta_0 \frac{\rho(\mathbf{r})}{\rho_0} - \eta_1 \frac{\tau_3 \rho_1(\mathbf{r})}{\rho_0} - \eta_2 \left(\frac{\rho_1(\mathbf{r})}{\rho_0} \right)^2.$$

Here, $\tau_3 = 1(-1)$ for $\tau = n$ ($\tau = p$) and $\rho_0 = 0.16 \text{ fm}^{-3}$. We determined the optimal set of (η_0, η_1, η_2) by minimizing the r.m.s. deviation $\sigma_{tot}(\eta_0, \eta_1, \eta_2)$ between the experimental and calculated pairing gaps. For this purpose, we performed the Skyrme-Hartree-Fock-Bogoliubov calculation for 156 nuclei with A in the range 118-196 and $\alpha < 0.25$. During the calculation, the strength V_0 was constrained so as to reproduce the neutron-pairing gap of ^{156}Dy for each set of (η_0, η_1, η_2) .

Fig. 1 shows that σ_{tot} increases sharply as a function of η_0 for the case in which $\eta_1 = \eta_2 = 0$. We provide

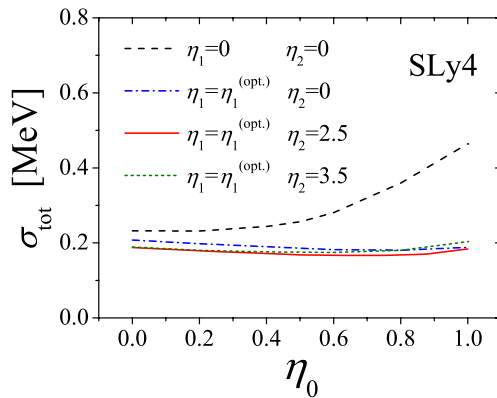


Fig. 1. The r.m.s. deviation σ_{tot} for different values of η_1 and η_2 is shown as a function of η_0 . See text for details.

[†] Condensed from the article in Phys. Rev. C, Vol.80, 064301 (2009)

^{*1} Department of Computer Science and Engineering, University of Aizu

^{*2} Department of Physics, Kyushu University

the two reasons for this behavior: the artificial quenching of proton pairing due to the poor overlap between $g_p(\mathbf{r}) = 1 - \eta_0 \rho(\mathbf{r})/\rho_0$ and $\tilde{\rho}_p(\mathbf{r})$ in $\tilde{h}_p(\mathbf{r})$ for nuclei with neutron skin, and the difference between the ρ_1 dependence of the pair-DF and that of the effective mass. In the Skyrme density functional (Skyrme-DF), the effective mass is given by

$$\frac{\hbar^2}{2m_\tau^*(\mathbf{r})} = \frac{\hbar^2}{2m} \left[\frac{m}{m_s^*} + \tau_3 I \left(\frac{m}{m_s^*} - \frac{m}{m_v^*} \right) \right]$$

where $I(\mathbf{r}) = \rho_1/\rho$. Here the m_s^* (m_v^*) is the isoscalar (isovector) effective mass. The neutron-proton effective mass splitting is controlled by the enhancement factor κ of the Thomas-Reiche-Kuhn sum rule ($m/m_v^* = 1 + \kappa$).

The effects of the neutron skin and the effective-mass splitting can be taken into account in the pair-DF as the linear ρ_1 term. Fig. 1 shows σ_{tot} for $\eta_1 = \eta_1^{(opt.)}$ and $\eta_2 = 0$. Here, the optimal value of η_1 (we call $\eta_1^{(opt.)}$) is determined so as to minimize σ_{tot} for each (η_0, η_2) . The resultant σ_{tot} remains almost constant, and it is drastically improved compared to that with $\eta_1 = \eta_2 = 0$.

The improvement in σ_{tot} observed when $\eta_2 > 0$ is small, although the σ_{tot} with $\eta_1 = \eta_1^{(opt.)}$ and $\eta_2 = 2.5$ is minimum along the η_0 direction.

To clarify the relation between the pair-DF and the effective mass, the $\eta_1^{(opt.)}$ at $(\eta_0, \eta_2) = (0.5, 2.5)$ for 12 standard Skyrme parameters are shown in Fig. 2. The linear correlation between $\eta_1^{(opt.)}$ and $m/m_v^* = 1 + \kappa$ is obvious. The value of κ remains uncertain in Skyrme-DF, and its accurate determination will enable us to effectively determine the effective mass and pairing properties in neutron-rich nuclei consistently.

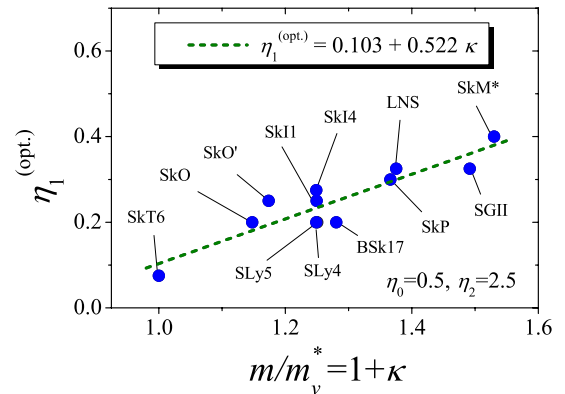


Fig. 2. The optimal value $\eta_1^{(opt.)}$ at $(\eta_0, \eta_2) = (0.5, 2.5)$ for 12 Skyrme forces.

Mass-number dependence of total reaction cross sections in the black-sphere approximation

A. Kohama, K. Iida,^{*1} and K. Oyamatsu^{*2}

[Nuclear reaction, reaction cross section, nuclear radius]

Neutron-rich unstable nuclei often exhibit exotic properties, such as “unexpectedly” large interaction cross sections. In order to quantify these properties, we have to pay attention to the deviation from, for example, total reaction cross sections that are carefully calculated on the basis of our sound knowledge of *stable* nuclei. Systematic understanding of the mass-number (A) and energy dependence is indispensable for clarifying the non-exotic behavior of the cross sections.

Recently, we have developed a formula for a proton-nucleus total reaction cross section σ_R as a function of the mass and the neutron excess of the target nucleus and the proton incident energy T_p in a way free from any adjustable T_p -dependent parameters.¹⁾ We deduce the dependence of σ_R on T_p on the basis of the nuclear “optical” depth to the projectile within the framework of a black-sphere (BS) approximation of nuclei. We call the formula the BS cross-section formula. The scale of the formula is set by the BS radius a , which is determined by fitting the angle of the first elastic diffraction peak calculated for proton diffraction by a circular black disk of radius a to the measured value.²⁾ The energy dependence of the formula is driven by that of proton-nucleon total cross sections. For stable nuclei, this formula reproduces the empirical T_p dependence of σ_R at $T_p = 100$ –1000 MeV remarkably without requiring any adjustable T_p -dependent parameters. Due to its suitability in systematic calculations, the present formula is being incorporated into the Particle and Heavy Ion Transport code System (PHITS).

In this work, we examine the A -dependence of the BS cross-section formula. We analytically find that our formula includes $A^{1/6}$ -dependence in addition to $A^{2/3}$ -dependence. The former dependence, which is due to the optical depth, is one of the characteristic features of our formula. In Fig. 1, we compare our numerical results with those obtained by the Carlson formula,³⁾ which is an example of a formula based on geometrical arguments and is given by $\sigma_R = \pi(R_p + r_0 A^{1/3})^2$, where R_p and r_0 are parameters obtained by fitting to the empirical data.³⁾ The difference between the two is remarkable in the energy range between 100 MeV and 600 MeV, but it is still unclear whether or not such a difference is due to the different A -dependence of each formula. Further work is currently in progress.

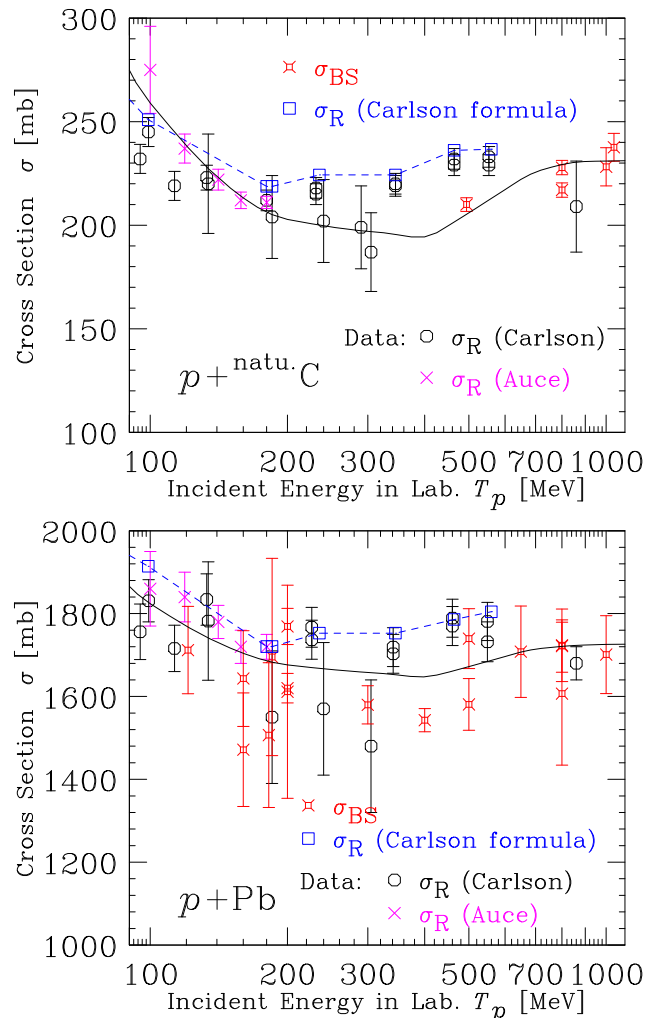


Fig. 1. Comparison of the numerical results of $\sigma_R(p + \text{natu.C})$ (upper) and $\sigma_R(p + \text{Pb})$ (lower) obtained by the BS cross-section formula (solid curve) with those by the Carlson formula (\square on dashed line). We adopt the BS radii at 800 MeV as 2.7 fm for carbon and 5.7 fm for lead. We also plot the empirical data, which were presented by Carlson (\circ)³⁾ and by Auce *et al.* (\times)⁴⁾ $\sigma_{BS}(\equiv \pi a^2)$, which is represented by squares with cross, is consistent with measured σ_R .

References

- 1) K. Iida *et al.*: J. Phys. Soc. Japan **76**, 044201 (2007).
- 2) A. Kohama *et al.*: Phys. Rev. **C 72**, 024602 (2005).
- 3) R.F. Carlson: At. Data Nucl. Data Tables **63**, 93 (1996).
- 4) A. Auce *et al.*: Phys. Rev. **C 71**, 064606 (2005).

^{*1} Department of Natural Science, Kochi University

^{*2} Department of Library and Information Science, Faculty of Letters, Aichi Shukutoku University

Holographic Nuclei[†]

K. Hashimoto^{*1}

[Giant resonances, Superstring theory, AdS/CFT correspondence]

We provide a dual gravity description of heavy atomic nuclei, via AdS/CFT correspondence. In holographic QCD such as Sakai-Sugimoto model, baryons are D-branes wrapping a sphere in 10 dimensional curved spacetime, so any nucleus is a collection of A such D-branes where A is mass number of the nucleus. Quantum theory on the nucleus is ADHM-like $U(A)$ Yang-Mills-Higgs theory on the sphere. Taking a large A limit (corresponding to heavy nuclei) leads to a dual gravity describing collective excitations of constituent nucleons of the heavy nucleus. This dual gravity computes spectra of the heavy nucleus, and gives discrete states whose gap roughly agrees with experimental nuclear data.

Application of a superstring technique, the AdS/CFT correspondence¹⁾, to low energy QCD has provided quite remarkable progress on hadron physics. This subject called holographic QCD has grown up to be a major research arena of string theory. Dual gravity description has revealed various aspects of low energy QCD which were unreachable by conventional analytic methods because of notorious strong coupling. They include spectra of glueballs, mesons and baryons, and interactions among them, and even phase transitions at finite temperature/density. However, almost all of the results are on hadron physics, not really nuclear physics, dare to mention. In this paper, we take a first step toward nuclear physics: we provide a dual gravity description of *heavy nuclei*.

The essence of the gauge/gravity correspondence is the large N limit, where N refers to the rank of the gauge group $U(N)$ of the gauge theory living on N coincident D-branes. This limit, together with large λ ('tHooft coupling) limit, allows a dual, holographic, equivalent gravity theory on a near horizon geometry of black brane solutions created by the N D-branes.

Baryons in QCD-like gauge theories are described, in the dual gravity description, by in fact additionally put D-branes wrapping a higher dimensional sphere in 10 dimensional curved spacetime. Any nucleus is a collection of baryons (nucleons), so in holographic QCD the nucleus is a collection of D-branes. Therefore, heavy nuclei with large mass number A can have a dual gravity description provided by a near horizon geometry of those “baryonic” A D-branes, in large A limit. In this paper we pursue and realize this idea. We describe a possible dual geometry, check its validity as a limit of string theory, and provide a comparison with nuclear

data.

For the D-brane configuration for the baryons in QCD at strong coupling, we use the D4-D8 model²⁾. We distribute the baryonic D4-branes into the shape of a ball to mimic the spherical nucleus. The nuclear saturation property is assumed. Then we calculate the near-horizon back-reacted geometry of these D4-branes, and compute fluctuation spectrum of scalar field in the background. It is finally given by

$$E_n \sim \frac{N^{2/3}}{A^{1/3}\sqrt{\lambda}} M_{\text{KK}} n \quad (n = 1, 2, \dots) \quad (1)$$

We ignored all the numerical factors. This (1) is the excitation spectrum of heavy nuclei with mass number A , as a result of AdS/CFT correspondence. The coefficient is naively evaluated as $N^{2/3}M_{\text{KK}}/\sqrt{\lambda} \sim \mathcal{O}(10^2)$ [MeV], but this is just for order of magnitude.

It is surprising that this formula is actually consistent with the experimental data of heavy nuclei, as follows. It is known from experiments that heavy nuclei have coherent excitations (phonons) of constituent nucleons, called giant resonances,^{a)} $E_n = \omega(A)n$, ($n = 1, 2, \dots$). Excitations with lower n have been analysed in detail experimentally. Phenomenological models, including liquid drop model of heavy nuclei, indicates consistent harmonic behaviour in n . Experimental results for giant resonance of heavy nuclei with $A > 60$ shows an empirical formula, $E \sim 80A^{-1/3}$ [MeV], for the first gap of 0^+ isoscalar excitation. Our result (1) is not so much different from the nuclear data, and in particular, we reproduced the A dependence of the resonance excitations.

In this paper, we have given a dual gravity description of heavy atomic nuclei, by applying the gauge/string duality (AdS/CFT correspondence). We took a large mass number limit $A \rightarrow \infty$. Dual gravity description is valid in this limit, and we obtained a near horizon geometry corresponding to the heavy nucleus. The corresponding supergravity solution has discrete fluctuation spectra, and we compared them with nuclear experimental data.

References

- 1) J. M. Maldacena, Adv. Theor. Math. Phys. **2**, 231 (1998).
- 2) T. Sakai and S. Sugimoto, Prog. Theor. Phys. **113**, 843 (2005), Prog. Theor. Phys. **114**, 1083 (2005).

[†] Condensed from the article in Prog. Theor. Phys. **121** (2009) 241

^{*1} Theoretical Physics Laboratory, RIKEN

^{a)} The author is indebted to T. Nakatsukasa for invaluable discussions on this correspondence, and also to T. Matsui for his helpful explanations.

Critical velocity of superfluid flow through single barrier and periodic potentials[†]

G. Watanabe,^{*1,*2,*3} F. Dalfovo,^{*3} F. Piazza,^{*3} L. P. Pitaevskii^{*3,*4}, and S. Stringari^{*2}

Ultracold gases in optical lattices provide a new exciting frontier of research. In a recent experiment with Fermi superfluids in one-dimensional (1D) optical lattices, the critical velocity along the BCS-BEC crossover has been measured and the result of this measurement has revealed that superfluidity is particularly robust at unitarity²⁾. The critical velocity of superfluid flow is a fundamental issue in the physics of quantum fluids. A mechanism for the onset of dissipation is provided by Landau instability: if the excitation spectrum satisfies suitable criteria, there exists a critical flow velocity above which the kinetic energy of the superfluid can be dissipated *via* the creation of excitations.

Motivated by the above experiment, we study the problem of an ultracold atomic gas in the superfluid phase flowing in the presence of a potential barrier or a periodic potential^{1,4)}. Using a hydrodynamic scheme in the local density approximation (LDA), we obtain an analytic expression for the critical current j_c as a function of the barrier height or the lattice intensity, which applies to both Bose and Fermi superfluids¹⁾. We compare this prediction with the results of the numerical solutions of the Gross-Pitaevskii (GP)¹⁾ and Bogoliubov-de Gennes (BdG) equations^{1,3)}.

In Fig. 1, we show the critical velocity v_c in the case of the single rectangular barrier (top panel) and the periodic potential (bottom panel). In both cases, one clearly sees that the results of the BdG equations approach the LDA prediction when the width of the barrier (the half of the lattice spacing) L is much larger than the healing length $\xi \sim 1/k_F$, where $k_F = (3\pi^2 n)^{1/3}$ is the Fermi momentum of a uniform non-interacting Fermi gas of density n . The way of approach is, however, different. In the case of the periodic potential, v_c exhibits a plateau for $Lk_F \lesssim 1$ and small maximum V_{\max} of the external potential; the plateau is instead absent in the case of the single barrier.

Our results allow one to identify three limiting cases: i) a regime of hydrodynamic flow in the LDA (close to the thick solid lines in Fig. 1); ii) a regime of macroscopic flow through thin and weak barriers, where the LDA is not applicable, i.e., for $Lk_F \lesssim 1$ and $V_{\max}/\mu < 1$; iii) a regime of weakly coupled superfluids separated by thin and strong barriers, i.e., for $Lk_F \lesssim 1$ but $V_{\max}/\mu \gg 1$.

[†] Condensed from Ref.¹⁾. This work is also selected for the Virtual Journal of Atomic Quantum Fluids, **1** (2009).

^{*1} RIKEN

^{*2} Asia Pacific Center for Theoretical Physics (APCTP)

^{*3} CNR INFM-BEC and Department of Physics, University of Trento

^{*4} Kapitza Institute for Physical Problems

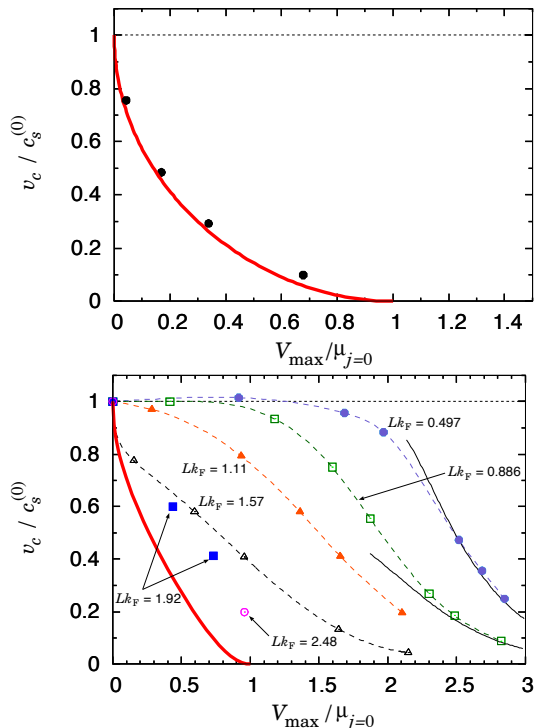


Fig. 1. Critical velocity for energetic instability of a superfluid of dilute fermions at unitarity subject to a 1D external potential. The critical velocity v_c is given in units of the sound velocity of a uniform gas, $c_s^{(0)}$, and is plotted as a function of the maximum of the external potential in units of the chemical potential $\mu_{j=0}$ of the superfluid at rest. Top panel: the case of a single potential barrier. Bottom panel: the case of a periodic potential. Thick solid lines: prediction of the LDA hydrodynamic theory. Symbols in the top panel: BdG results of Ref.³⁾ with $Lk_F = 4$. Symbols in the bottom panel represent our BdG results for a periodic lattice. The thinner black solid lines are the tight-binding prediction. Dashed lines are guides to the eye. This figure is taken from Ref.¹⁾.

We finally discuss the relevance of these results in the context of current experiments with ultracold gases.

References

- 1) G. Watanabe *et al.*, Phys. Rev. A **80**, 053602 (2009).
- 2) D. E. Miller *et al.*, Phys. Rev. Lett. **99**, 070402 (2007).
- 3) A. Spuntarelli, P. Pieri, and G. C. Strinati, Phys. Rev. Lett. **99**, 040401 (2007).
- 4) G. Watanabe *et al.*, Phys. Rev. A **78**, 063619 (2008).

Contribution of Nuclear Reaction Data Centre to RIKEN Nishina Center

K. Kato,^{*1} M. Kimura,^{*2} N. Otuka,^{*3} T. Asano,^{*4} N. Furutachi,^{*4} A. Makinaga,^{*4} T. Matsumoto,^{*4}
T. Togashi,^{*1} and K. Tsubakihara^{*4}

[Nuclear reaction, database, NRDF, EXFOR]

The development of a nuclear reaction database is very important not only in nuclear physics but also in astrophysics and nuclear power engineering. The “Nuclear Reaction Data Centre” (JCPRG) was established on April 1, 2007, for compiling own nuclear database, NRDF. The center was approved as a branch of Faculty of Science at Hokkaido University, and it took over nuclear database activities carried out by Japan Charged-Particle Nuclear Reaction Data Group. Furthermore, another important task of the center as a member of International Network of Nuclear Reaction Data Centers is to cooperate on EXFOR nuclear database compilation. The members of JCPRG have been devoting themselves to the following activities:

- (1) Compilation of reaction data (NRDF and Experimental Nuclear Reaction Data, EXFOR)
- (2) Development of a new nuclear reaction database for astrophysical evaluation (NRDF/A)
- (3) Conversion of old data from NRDF format to EXFOR format
- (4) Bibliography compilation (CINDA)
- (5) Database maintenance and development (NRDF, EXFOR/ENDF, and CINDA)
- (6) Development of a digitization system (GSYS).

In particular, we adopt a strategy where the reaction data obtained from domestic institutes is compiled in a domestic nuclear database, since frequent communication with authors will be helpful for quickly and precisely compiling the given reaction data. For this purpose, we have been compiling the experimental data obtained from Japanese facilities. These results can be accessed through our web site¹⁾.

In Table 1, we list the number of papers that were selected for compilation in NRDF and for conversion into the EXFOR format in 2009. We also list the number of compiled papers in which the reaction data obtained from RIKEN facilities were used. This table shows that the papers reporting RIKEN experiments²⁻¹²⁾ appear to constitute a majority of NRDF entries and the entries converted to the EXFOR format. These data can be accessed in the EXFOR database¹³⁾ with the

E-numbers shown in the References.

In addition to cooperating with IAEA-NDS, we have to provide domestic experimental data to the international nuclear physics community with easy access, in the form of original tasks of NRDF. Recently, the center established a research contract with the RIKEN Nishina Center in order to compile efficiently the reaction data obtained by using beams of unstable nuclei at the RIKEN Nishina Center, RIBF. We are now discussing the extension of the NRDF format in order to compile new experimental data that will be obtained from RIBF. In the future, in cooperation with experimentalists, it will be important to develop the domestic database, NRDF, to compile all data obtained from RIKEN and other Japanese institutes.

Table 1. The number of papers chosen for compilation in NRDF and for conversion from the NRDF format to the EXFOR format in 2009. All entries are obtained from the papers published in 2008 and 2009.

	RIKEN	Total
NRDF entries	17	51
Entries converted to EXFOR	11	32

References

- 1) <http://www.jcprg.org/>
- 2) J. J. He *et al.*: Eur. Phys. J. A **36**, 1 (2008); E2107 in EXFOR.
- 3) T. Ohnishi *et al.*: J. Phys. Soc. Jpn. **77**, 083201 (2008); E2116 in EXFOR.
- 4) S. Ota *et al.*: Phys. Lett. B **666**, 311 (2008); E2120 in EXFOR.
- 5) H. Iwasaki *et al.*: Phys. Rev. C **78**, 021304(R) (2008); E2122 in EXFOR.
- 6) A. Ozawa *et al.*: Phys. Rev. C **78**, 054313 (2008); E2124 in EXFOR.
- 7) M. Janek *et al.*: Phys. of At. Nucl. **71**, 1495 (2008); E2125 in EXFOR.
- 8) J. Gibelin *et al.*: Phys. Rev. Lett. **101**, 212503 (2008); E2127 in EXFOR.
- 9) Y. Kondo *et al.*: Phys. Rev. C **79**, 014602 (2009); E2132 in EXFOR.
- 10) H. Yamaguchi *et al.*: Phys. Lett. B **672**, 230 (2009); E2133 in EXFOR.
- 11) D. Kaji *et al.*: J. Phys. Soc. Jpn. **78**, 035003 (2009); E2137 in EXFOR.
- 12) T. Nakamura *et al.*: Phys. Rev. C **79**, 035805 (2009); E2139 in EXFOR.
- 13) <http://www.jcprg.org/exfor/>

^{*1} Department of Physics, Faculty of Science, Hokkaido University

^{*2} Creative Research Institution, Sosei Research Department, Hokkaido University

^{*3} IAEA Nuclear Data Section

^{*4} Nuclear Reaction Data Centre (JCPRG), Faculty of Science, Hokkaido University

3. Hadron Physics

Gluon-Spin Contribution to the Proton Spin from the Double-Helicity Asymmetry in Inclusive π^0 Production in Polarized $p + p$ Collisions at $\sqrt{s} = 200 \text{ GeV}^\dagger$

K. Boyle^{*1} and S. Taneja^{*2} for the PHENIX Collaboration

[Gluon Spin, Helicity Asymmetry, PHENIX]

Polarized Deep Inelastic Scattering (DIS) data have shown the spin of the quarks only contributes about $\sim 25\%$ of the proton spin^{2,3)}, implying that the remainder of spin is either from the gluon spin contribution, ΔG , or the orbital angular momentum of the quarks and gluons.

ΔG can be accessed in polarized proton collisions by measuring the double helicity asymmetry, A_{LL} , which is defined as

$$A_{LL} = \frac{1}{P_1 P_2} \frac{N_{++} - RN_{+-}}{N_{++} + RN_{+-}}, R = \frac{L_{++}}{L_{+-}} \quad (1)$$

where $N_{++(+)}$ is the yield in the same (opposite) helicity collisions, L is the luminosity, R is the relative luminosity and P is the polarization. At $\sqrt{s} = 200 \text{ GeV}$, we sample the gluon momentum fraction range of $0.02 < x < 0.3$, and so we write $\Delta G^{[0.02,0.3]}$.

Results for A_{LL} in π^0 production in the 2005¹⁾ and 2006 RHIC runs are plotted as a function of transverse momentum, p_T in Fig. 1a. The systematic uncertainty (not shown) in A_{LL} from the relative luminosity determination is 5×10^{-4} in the combined result. A scaling uncertainties from polarization of 6.8% is not shown. The data are plotted along with expectations based on different fits to the DIS data.

The different fits to DIS have significantly distinct shapes as a function of x . By varying the size of the gluon polarization in the different DIS fit results, a set of A_{LL} expectations for each fit is produced. χ^2 is calculated for different values of ΔG and the results are plotted in Figure 1b. At $\Delta\chi^2 = 9$ ($\sim 3\sigma$), a consistent constraint of $-0.7 < \Delta G^{[0.02,0.3]} < 0.5$ is found.

Using one fit to the DIS data, GRSV³⁾, the impact of the systematic uncertainties are shown in Fig. 2 when the polarization and relative luminosity uncertainties are varied by $\pm 1\sigma$. It is clear that while the polarization uncertainty has little effect, there is about a ± 0.1 uncertainty in $\Delta G^{[0.02,0.3]}$ due to relative luminosity.

The π^0 cross section measured at PHENIX¹⁾ agrees with theory expectations within the theoretical scale uncertainty. This theoretical scale uncertainty was included in the expectation for A_{LL} in the GRSV fit, and it's impact on the $\Delta G^{[0.02,0.3]}$ was similarly evaluated. This led to a sizeable uncertainty for negative values of ΔG .

$A_{LL}^{\pi^0}$ results from 2005 and 2006 significantly constrain the gluon spin contribution to the proton spin. We find $\Delta G^{[0.02,0.3]} = 0.2 \pm 0.1(stat) \pm 0.1(syst)_{-0.4}^{+0.0}(shape) \pm 0.1(scale)$, and a consistent constraint at $\sim 3\sigma$. Additional data from the Run9 RHIC run will further constraint $\Delta G^{[0.02,0.3]}$, while the first measurements at $\sqrt{s} = 500 \text{ GeV}$ will allow access to a lower x range.

References

- 1) A. Adare, et al. Phys. Rev. D 76, 051106 (2007)
- 2) D. de Florian, R. Sassot, M. Stratmann, and W. Vogelsang, Phys. Rev. Lett. 101, 072001 (2008).
- 3) M. Glück, E. Reya, M. Stratmann, and W. Vogelsang, Phys. Rev. D 63, 094005 (2001).

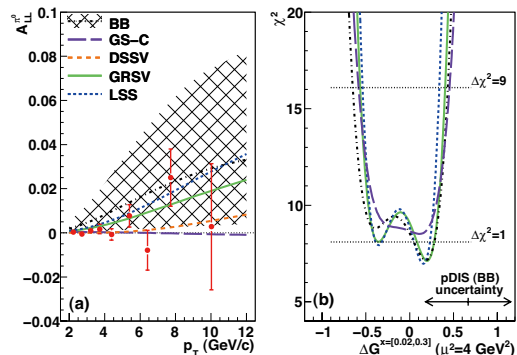


Fig. 1. (a) $A_{LL}^{\pi^0}$ vs. p_T compared with different expectations based on fits to DIS data. (b) Constraint on $\Delta G^{[0.02,0.3]}$ based on the different fits.

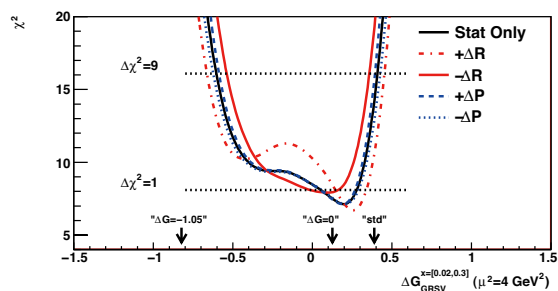


Fig. 2. Constraint on $\Delta G^{[0.02,0.3]}$ using the GRSV fit result to DIS data. Impact of two primary systematic errors are shown.

[†] Condensed from the article in PRL, Vol.103, 012003 (2009)

^{*1} RIKEN BNL Research Center

^{*2} Stony Brook University

Measurements of transverse single-spin asymmetry of single electrons from open heavy flavor decays in polarized $p + p$ collisions at $\sqrt{s} = 200$ GeV at PHENIX[†]

S. Dairaku*¹ for the PHENIX Collaboration

[Transverse Spin, Asymmetry, PHENIX]

Using the PHENIX detector at the Relativistic Heavy Ion Collider (RHIC), we measured the transverse single-spin asymmetry (A_N) of single electrons from open heavy flavor decays. The preliminary results of A_N measurements at mid-rapidity at PHENIX are presented here.

A number of mechanisms based on quantum chromodynamics have been proposed for explaining the obtained A_N , and measurements in different processes have played complementary and important roles in the attempt to understand A_N . At RHIC energy, A_N in open charm production was suggested to probe the gluon Sivers function¹, which includes the correlation between the transverse momentum of an unpolarized parton in a transversely polarized nucleon and the nucleon polarization vector. Because open charm production is dominated by the gluon fusion process at RHIC energy and the gluon's transversity is zero, there is no significant contribution to A_N in open charm production from the Collins function, which describes the correlation between the transverse spin of a fragmenting quark and the transverse momentum of the produced hadron. Therefore, the measurement of A_N in open charm production at RHIC can help in probing of the gluon Sivers function.

A_N is determined using the following equation:

$$A_N \equiv \frac{\sigma_{\uparrow} - \sigma_{\downarrow}}{\sigma_{\uparrow} + \sigma_{\downarrow}} = \frac{1}{P} \frac{\sqrt{N_L^{\uparrow} N_R^{\downarrow}} - \sqrt{N_L^{\downarrow} N_R^{\uparrow}}}{\sqrt{N_L^{\uparrow} N_R^{\downarrow}} + \sqrt{N_L^{\downarrow} N_R^{\uparrow}}}, \quad (1)$$

where P is the absolute polarization value measured by the RHIC polarimeters, and $N_{L(R)}^{\uparrow(\downarrow)}$ is the number of electrons scattered to the left (right) when the direction of beam polarization is vertically upwards (downwards). The detected electrons used for the calculation of A_N include electrons from background processes, because of which the measured inclusive asymmetry can be diluted. We can extract the asymmetry in heavy flavor production (A_N^{HF}) from the measured inclusive asymmetry (A_N^{incl}) as follows:

$$A_N^{HF} = \frac{A_N^{incl} - r A_N^{bg}}{1 - r}, \quad (2)$$

where A_N^{bg} is the background asymmetry and r is the background fraction defined as $r = \sigma_{background}/\sigma_{inclusive}$.

*¹ Department of Physics, Kyoto University, Japan

The dominant background source in this measurement is π^0 ²). Some previous results have indicated that A_N in π^0 production at mid-rapidity at PHENIX is zero³). Therefore, we assumed that A_N^{bg} is zero in this study. The background fraction (r) is determined by using a *cocktail* of the contributions from background processes²) and by the *converter* technique, in which the electron spectra measured with an additional photon converter introduced into the acceptance region are compared with those recorded without the converter²).

Measurements have been carried out on a data sample with an integrated luminosity of 2.7 pb^{-1} in transversely polarized $p + p$ collisions at a center-of-mass energy $\sqrt{s} = 200$ GeV in 2006. The results for the A_N^{HF} of single electrons from open heavy flavor decays are shown in Fig. 1. The left and right plots show the A_N^{HF} values for positive charge: $p + p \rightarrow e^+ + X$ and for negative charge: $p + p \rightarrow e^- + X$, respectively. The observed A_N^{HF} of the single electrons from heavy flavor decays are significantly smaller than those predicted theoretically for D -meson production with a maximum gluon Sivers function¹, which is greater than 10% in the kinematic region of our measurements ($x_F \sim 0$). Therefore, the obtained results could reject the maximum gluon Sivers function¹).

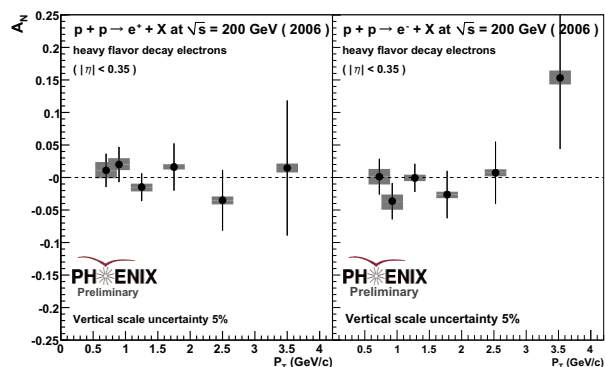


Fig. 1. A_N^{HF} of single electrons from heavy flavor decays as a function of p_T .

References

- 1) M. Anselmino, M. Boglione, U. D'Alesio, E. Leader, and F. Murgia: Phys. Rev. D **70**, 074025 (2004).
- 2) S. S. Adler et al.: Phys. Rev. Lett. **96**, 032001 (2006).
- 3) S. S. Adler et al.: Phys. Rev. Lett. **95**, 202001 (2005).

Measurement of direct photon using virtual photon method in $\sqrt{s} = 200$ GeV d+Au collisions at RHIC-PHENIX

Y.L. Yamaguchi,^{*1} Y. Akiba, T. Gunji,^{*1} and H. Hamagaki,^{*1}[Direct photon, virtual photon method, Low p_T]

Direct photons are one of the most important probes to investigate properties of the matter created by heavy ion collisions since they leave the medium without strong interaction. Thermal photons from the Quark Gluon Plasma (QGP) are considered to be the primary contributor in $1.0 < p_T < 5.0$ GeV/ c ¹ and are of special interest.

In the PHENIX experiment, two different analysis methods, namely, a “real” photon method and a “virtual” photon method, have been developed. The real photon method using an electromagnetic calorimeter has been used successfully for $p_T > 4.0$ GeV/ c and the virtual photon method is employed for $1.0 < p_T < 5.0$ GeV/ c . Direct photon spectra both in p+p and Au+Au collisions have been successfully measured using the real and virtual photon methods, as shown in Fig 1. A clear excess over the binary scaled p+p result

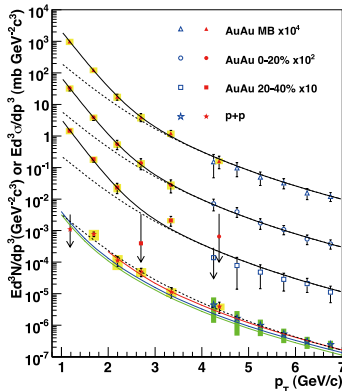


Fig. 1. Direct photon spectra in p+p and Au+Au collisions as a function of p_T .

(shown by the dotted line) is seen in Au+Au collisions for $1.0 < p_T < 3.0$ GeV/ c . However, the observed excess cannot be concluded to be of thermal origin at this moment. Data on d+Au collisions are needed to evaluate nuclear effects such as the Cronin effect and nuclear shadowing since nuclear effects may increase or decrease the photon yield in low p_T region. Efforts are being made to measure the low- p_T direct photons in d+Au collisions using the virtual photon method. The current status of the analysis in 200GeV d+Au collisions are reported in this report.

All combinations of electrons and positrons in a same event are considered. The obtained e^+e^- pair

mass distribution contains several components from different sources, which are listed below.

- Virtual direct photon decays
- Hadron decays
- Photon conversions
- Combinatorial background
- Cross pairs from $\pi^0, \eta \rightarrow 2\gamma$ (or γe^+e^-) $\rightarrow e^+e^-e^+e^-$

The pairs from photon conversions are removed by a cut on the orientation of the pair in the magnetic field²). The combinatorial background is computed using a mixed-event technique. Cross pairs are evaluated by comparing the like-sign pair distributions between the real and simulated distributions. Finally, the correlated e^+e^- pair mass distribution that consists of pairs from known hadron decays and virtual photon decays is obtained after background subtraction.

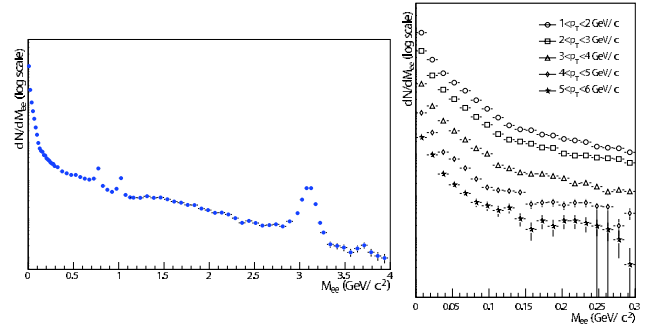


Fig. 2. Correlated e^+e^- pair mass distribution in d+Au collisions for $p_T > 1.0$ GeV/ c (left) and the p_T -sliced e^+e^- pair mass distributions for $M_{ee} < 300$ MeV/ c^2 and $1.0 < p_T < 6.0$ GeV/ c (right).

The left panel in Fig. 2 shows the correlated e^+e^- pair mass distribution in d+Au collisions for $p_T > 1.0$ GeV/ c . The d+Au data has abundant statistics so that even Ψ' is clearly visible around 3.7 GeV/ c^2 . The right panel in Fig. 2 shows the p_T -sliced e^+e^- pair mass distributions for $M_{ee} < 300$ MeV/ c^2 and $1.0 < p_T < 6.0$ GeV/ c , which are suitable for virtual direct photon measurements. The results up to 6.0 GeV/ c are expected to be obtained for d+Au collisions. Although some corrections should be made in order to obtain the direct photon spectrum in d+Au collisions, the d+Au result is promising.

References

- 1) S. Turbide, et al.: Phys. Rev. C **69**, 014903 (2004).
- 2) A. Toia: arXiv:0711.2118 [nucl-ex] (2007).

^{*1} Center for Nuclear Study (CNS), University of Tokyo

Azimuthal angle dependence of neutral pion suppression in $\sqrt{s_{NN}} = 200$ GeV Au+Au collisions at RHIC-PHENIX

Y. Aramaki*

[Quark Gluon Plasma, Jet quenching, Parton energy loss]

It has been observed in central Au+Au collisions at Relativistic Heavy Ion Collider (RHIC) that the yield of neutral pion at high transverse momentum ($p_T > 5$ GeV/c) is strongly suppressed compared to the one expected from $p + p$ collisions scaled by the number of binary collisions. This suppression is considered to be due to the energy lost by hard scattered partons in the medium (jet quenching), which results in a decrease of the yield at a given p_T . Many theoretical models have been proposed to understand the parton energy loss mechanism. GLV method¹⁾ is one of the calculations that predicts that the magnitude of energy loss is proportional to square of the path length. Studying the path length dependence of energy loss should help in understanding of energy loss process.

The Muon piston calorimeter (MPC) to determine the reaction plane is used for measuring the azimuthal anisotropy of neutral pion at PHENIX. MPC is made of PbWO₄. Even though MPC is similar rapidity coverage to the detector which is used in the previous measurement, the reaction plane determination is expected to be improved due to good energy resolution. Figure 1 shows the azimuthal anisotropy of neutral pion as a function of p_T for each centrality class. The nuclear modification factor (R_{AA}) for each azimuthal angle is calculated by using them.

Recently theoretical models (ASW²⁾, HT³⁾ and AMY⁴⁾) to describe parton energy loss mechanism which involve the time-evolution of the medium produced at RHIC have been proposed. These models succeeded in reproducing the centrality dependence of $R_{AA}(p_T)$ ⁵⁾. The measured R_{AA} is compared with one model (ASW) of them. Figure 2 show the R_{AA} as a function of p_T and azimuthal angle for centrality 20-30 % and ASW model. Closed and open points show the measured R_{AA} for in-plane and out-of-plane, respectively. Since the produced medium after the collisions is assumed to be almond shape, the in-plane path length is shorter than out-of-plane. This difference of the path length is reflected in the R_{AA} for each azimuthal angle. Solid and dashed lines show the theoretical curve for ASW model of in-plane and out-of-plane, respectively. The central big band shows the p_T correlated systematic uncertainty on the azimuthal angle integrated R_{AA} . The right and the left small bands show the number of collisions uncertainty from Glauber calculation and $p + p$ normalization uncer-

tainty, respectively. The bands on the measured points show p_T correlated systematic uncertainties on the measurement of the azimuthal anisotropy of in-plane and out-of-plane, respectively. As shown in Fig. 2, even though ASW reproduce the in-plane R_{AA} has slightly difference at lower p_T .

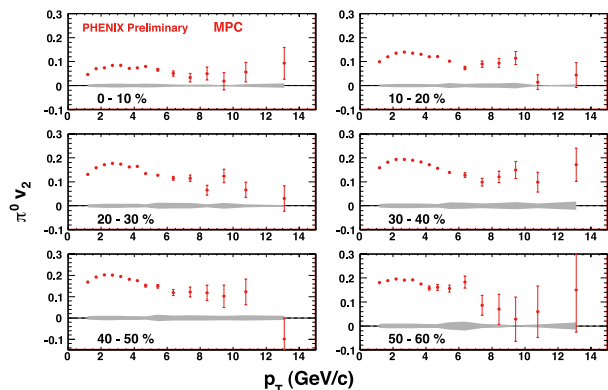


Fig. 1. Azimuthal anisotropy of neutral pion v_2 with MPC for each 10% centrality classes.

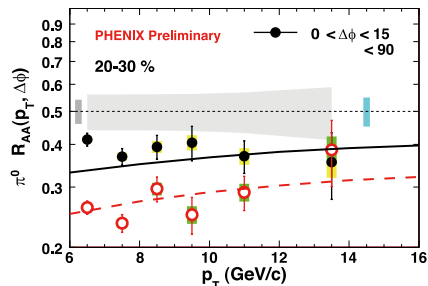


Fig. 2. The R_{AA} as a function of p_T and azimuthal angle from the reaction plane for centrality 20-30 % and ASW.

We can also estimate the averaged path length by measuring the azimuthal angle from reaction plane and mapping it into the shape of the participant region, which can be calculated by Glauber model for each impact parameter (centrality).

References

- 1) M. Gyulassy *et al.*: Phys. Lett. **B538**, 282 (2002).
- 2) T. Renk *et al.*: Phys. Rev. **C75** 031902 (2007).
- 3) A. Majumder *et al.*: Phys. Rev. **C76** 041902 (2007).
- 4) G-Y. Qin *et al.*: Phys. Rev. **C76** 064907 (2007).
- 5) S.A. Bass *et al.*: J. Phys. **G35** 104064 (2008).

* Center for Nuclear Study, Graduate School of Science, University of Tokyo, Japan

Systematic Measurement of ω Mesons in p+p, d+Au, and A+A Collisions at $\sqrt{s_{NN}} = 200$ GeV at RHIC-PHENIX

M.Ouchida*¹ D.Sharma² K.M.Kijima¹ V.Riabov³ Y.Tsuchimoto⁴ Y.Riabov³ Y.Nakamiya¹

The measurement of hadrons under extreme conditions created by relativistic heavy-ion collisions is part of an interesting study being carried out as a part of the quest to observe the QCD phase transition to quark gluon plasma (QGP).

The ω meson that has vector properties and both lepton and hadron decay modes serves as a useful probe in the study of the mechanism of particle production in the collision. We measured ω mesons in p+p, d+Au, and A+A collisions in both leptonic and hadronic decay modes. The systematic measurement can be carried out over a wide kinematic range since low p_T values can be included in the leptonic decay mode and high p_T values can be included in the hadronic decay mode.

The dielectron decay mode, $\omega \rightarrow e^+e^-$ is reconstructed in a Crenkov detector that can identify electrons and positrons. In an event, the source of any electron or positron is unknown, and therefore, all electrons and positrons are combined into pairs. This results in a large combinatorial background, especially in central Au+Au collisions because of their high multiplicity. The background is computed by a mixed event technique, which combines tracks from different events with similar event topology.

The first step for both hadronic and photonic analysis based on the $\omega \rightarrow \pi^+\pi^-\pi^0$ and $\omega \rightarrow \pi^0\gamma$ is to reconstruct π^0 candidates by combining photons pairs and applying a p_T -dependent cut around the mass of the π^0 . Candidates (included in the combinatorial background) are combined with a third photon for $\omega \rightarrow \pi^0\gamma$ or with two unidentified charged tracks (assumed to be π mesons) for $\omega \rightarrow \pi^+\pi^-\pi^0$. Owing to the high multiplicity and low S/B associated with it, cut optimization was performed in the case of A+A analysis. For p+p and d+Au analysis, raw yields were extracted by fitting the p_T slices of the invariant mass distribution, as shown in the figures. In A+A analysis, the background is subtracted by estimating correlated and uncorrelated backgrounds from two combinations of a mixed event technique.

Fig.1. shows the obtained invariant cross section for ω production in p+p collisions and minimum bias d+Au at $\sqrt{s_{NN}} = 200$ GeV as a function of p_T . The results indicate a good agreement among different decay channels. Fig.2. shows the spectra corresponding to Au+Au collisions, as measured in the two decay

mode, e^+e^- for the low p_T region in a minimum-bias event, and $\pi^0\gamma$ for the high p_T region in three centrality values (the value used to characterize the heavy-ion collisions), namely, 0-20%, 20-60%, and 60-92%. The lines represent estimated yields from p+p collisions, after scaling by the number of collisions in which there was no a nuclear matter effect. If data points lie below the lines for higher centrality values, we can suggest that the invariant yield is suppressed in the high p_T region for higher centrality values; this, in turn, implies that some jets from hard collisions are quenched when they pass through the dense and hot medium created by heavy-ion collisions.

We are preparing a publication on this result. The target date for submission is in summer 2010.

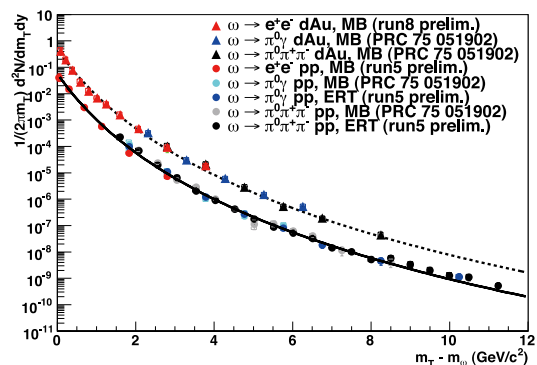


Fig. 1. The m_T spectra corresponding to p+p (circle points) and d+Au (triangle points) collisions. The solid line and dotted line represent the fitted Levy function for p+p and d+Au.

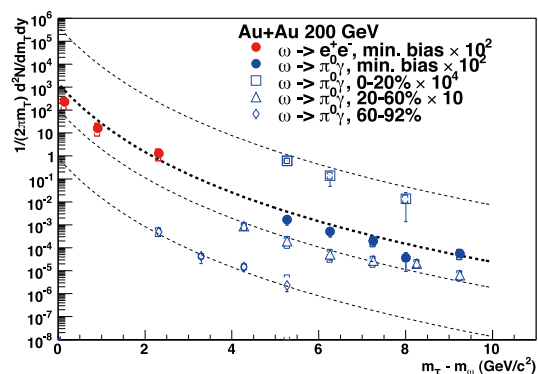


Fig. 2. The m_T spectra corresponding to Au+Au for different centrality value. The centrality increases from bottom to top. The lines represent estimated yields from p+p collisions, after scaling by the number of collisions.

*1 Hiroshima University

*2 Weizmann Institute, Israel

*3 PNPI, Petersburg Nuclear Physics Institute, Russia

*4 Center for Nuclear Study, University of Tokyo

Measurement of J/ψ production in ultra-peripheral Au+Au collisions at $\sqrt{s_{NN}} = 200$ GeV during RHIC RUN-7[†]

A. Takahara*¹

[Nuclear structure]

In this paper, we present the RHIC RUN-7 measurements of the photoproduction of J/ψ and of the two-photon production of high-mass e^+e^- pairs in ultra-peripheral nucleus-nucleus interactions of Au nuclei at $\sqrt{s_{NN}} = 200$ GeV. Ultra-peripheral collision(UPC) refers to a collision in which impact distance is greater than the sum of the nuclear radii with no nuclear overlap. The proposed use of UPCs to study photoproduction at hadron colliders has attracted considerable interest in recent years¹⁻³. UPCs can be used for determining gluon density at low x . Similar measurements performed in RHIC RUN-4 have been reported in⁴.

UPC events are tagged by the emission of forward neutrons instead the Coulomb excitation of one or both Au* nuclei.

The event triggers have the following requirements; 1) There should be no coincident signals from the beam-beam counters; 2) a 2x2 tile EMCal trigger ERT with a trigger threshold of 0.8 GeV is needed; 3) the energy of the beams to the ZDCs should be a minimum of 30 GeV. Further, the offline requirements are $Z_{vertex} \leq 30$ cm, only two charged particles, EMCal cluster with no dead or noisy towers within 2×2 tile, and EMCal cluster energy of over 1 GeV/c for one member of the pair. The UPC J/ψ measurement is based on mainly purely electromagnetic process. The high-mass e^+e^- pairs distribution will be combination of exponential and Gaussian(J/ψ) distribution. In this report, the exponential curve was plotted on the basis of the RUN-4 simulations⁴ since RUN-7 simulation have not been performed yet.

The mass distribution is shown in Fig. 1. There are 17 e^+e^- pairs between 2.8 GeV/c and 3.2 GeV/c. In RUN-4 there were 12 e^+e^- pairs RUN 4⁴. Fig. 2 is the dN/dpT distribution of the pairs.

The squared form factor of a Au nucleus is represented as

$$|F_{Au}(p_T^2)|^2 = \left| 3 \frac{\sin(Rp_T) - Rp_T \cos(Rp_T)}{(Rp_T)^3(1 + (ap_T)^2)} \right|^2 \quad (1)$$

In this case, $R = 6.7$ fm and $\alpha = 0.7$ fm⁵. Please note that the function is not calculated on the bias of any properties of the detector.

The high-mass distribution of e^+e^- pairs analysed in RHIC RUN-7 UPC. However, the exponential curve may not be accurate. We may find differences between

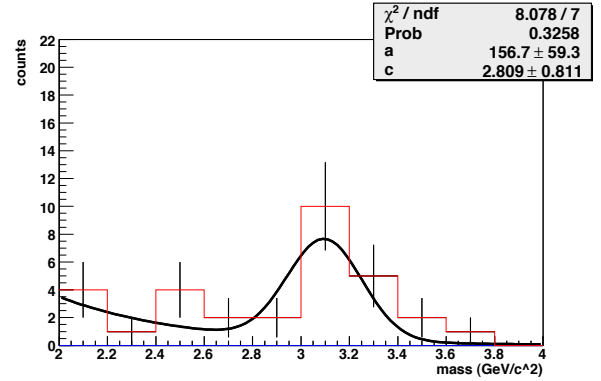


Fig. 1. Invariant mass distribution of e^+e^- pairs fitted to the combination of a dielectron continuum (exponential distribution) and a J/ψ (Gaussian) signal. Exponential curve is fixed by RUN 4 simulation.

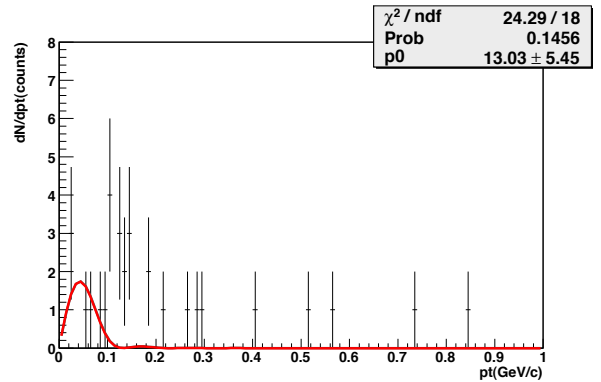


Fig. 2. dN/dpT distribution of the pairs with $m_{e^+e^-} \geq 2$ GeV/c² fitted to the (truncated) Au nuclear form factor

RUN-7 and RUN-4 continuum curves because a new detector HBD was installed in RUN7.

References

- 1) G. Baur, K. Hencken, D. Trautmann, S. Sadovsky, and Y. Kharlov: Phys. Rept. B, 359 (2002).
- 2) C. A. Bertulani, and S. R. Klein, J. Nystrand, Ann. Rev. Nucl. Part. Sci. B, 271 (2005).
- 3) A. Baltz et al.: Phys. Rept. B 171 (2008).
- 4) S. Afanasiev PHENIX Collaboration: Phys. Lett. B 321(2009).
- 5) K. T. R. Davies and J. R. Nix: Phys. Rev. B 1977 (1976).

[†] Department of Physics, University of Tokyo

Neutron asymmetry measurement with $\sqrt{s}=500$ GeV polarized proton collision at RHIC-PHENIX

M. Togawa, Y. Goto, and S. Dairaku*¹ for the PHENIX collaboration

One of the main programs at the Relativistic Heavy Ion Collider (RHIC) is the measurement of polarized gluon distribution function in the proton by using longitudinally polarized proton collisions at $\sqrt{s} = 200$ GeV¹⁾. In the RHIC ring, vertical polarization is stable. The spin rotator magnets located around the experimental area rotate the spin vector by 90° to enable longitudinal collisions at the PHENIX interaction point. The PHENIX local polarimeter system is used to confirm that protons are longitudinally polarized at the interaction point during a run, by measuring a remaining transverse neutron asymmetry²⁾.

The local polarimeter system consists of a Zero-Degree Calorimeter (ZDC) and a position-sensitive Shower-Max Detector (SMD)^{3,4)}. The ZDC and SMD cover the forward and backward directions with a maximum angle of 2.8 mrad., including zero degree⁴⁾. In the 2009 run at RHIC, an experiment was carried out using polarized proton collisions at $\sqrt{s} = 500$ GeV for the first time. It was observed that the neutron asymmetry remains finite at this high energy. Figure 1 shows the ϕ -dependent asymmetries observed in transverse and longitudinal runs. It is clear that the asymmetry is finite in the transverse run and almost zero in the longitudinal run.

Thus far, the asymmetry was calculated from the raw data recorded using the standard PHENIX DAQ and therefore the statistical precision was limited by the DAQ bandwidth. In this run, we implemented the scalar mode, in which we recorded the number of hit counts in the right and left parts of the SMD. Figure 2 shows the left-right asymmetry as a function of RHIC beam bunch ID obtained from the counts in 5 min. This figure demonstrates that precise bunch-by-bunch asymmetry can be achieved within such a short time. Presently, calculation of asymmetry using the scalar data is carried out by the standard PHENIX online monitor system, and the results are sent to the accelerator database. The data are used for accelerator tuning in the 2009 run.

In such forward kinematics, information on the p_T dependence of asymmetry may be obtained from the results at different colliding energies, where p_T is calculated using the relation of $p_T \sim E_n \sin(\theta)$. Figure 3 shows the asymmetry as a function of neutron p_T evaluated using a full detector simulation. The amplitude increases with \sqrt{s} . This new data will help us to understand the production mechanism of neutron asymmetry.

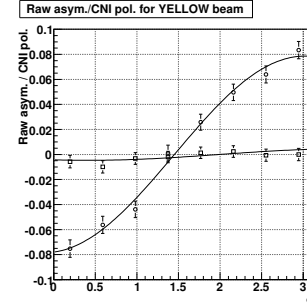


Fig. 1. ϕ -dependent asymmetries for transverse (open circle) and longitudinal (open square) runs.

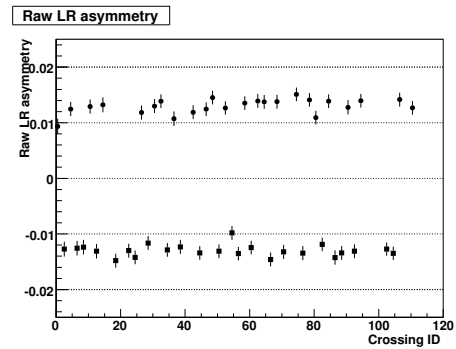


Fig. 2. Raw LR asymmetry ($= (N_L - N_R) / (N_L + N_R)$) as a function of RHIC beam bunch ID. Circles and squares indicate spin down and up, respectively, as determined by accelerator database.

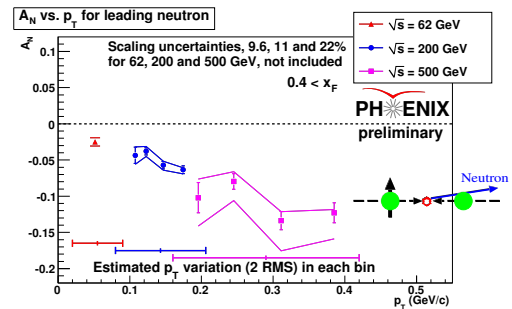


Fig. 3. Single transverse spin asymmetry as a function of neutron p_T , evaluated by a full simulation. The asymmetry increases with \sqrt{s} and possible from the p_T dependence.

References

- 1) G. Bunce et al.: Ann. Rev. Nucl. Part. Sci. **50**, 525 (2000).
- 2) Y. Fukao and M. Togawa et al.: Phys. Lett. **B650**, 325 (2007).
- 3) C. Adler et al.: Nucl. Instr. & Meth. **A470**, 488 (2001).
- 4) A. Deshpande et al.: RIKEN Accel. Prog. Rep. **37**, 246 (2004).

*¹ Department of Physics, Kyoto University

Cosmic-ray background in PHENIX detector

D.S. Blau,*¹ and K. Okada

High-energy photons are important probes in the field of nuclear physics. They provide early-stage information on nuclear collisions. At PHENIX¹, photons are detected by the electromagnetic calorimeters (EMCals). One problem is a cosmic-ray event can be identified as a direct photon event. Fig. 1 shows two examples of cluster shapes in EMCals made by cosmic-rays. The clusters with the shape shown in Fig. 1(a) can be easily eliminated; however, those with the shape shown in fig.1(b) are retained. Competition exists between the rates of the real signal and the cosmic event. Since the signal rate is considerably lesser in $p+p$ collisions, the contribution of cosmic-rays is a more serious problem in $p+p$ collisions than in $Au+Au$ collisions.

In 2007, control data were obtained when there was no activity in the accelerator for a total period of about 20,000 s. Fig. 2 shows the energy spectra of this data set. The EMCal miscalculates the energy deposit of cosmic-ray hits because it is calibrated for photons coming from the collision.

Fig. 3 shows the energy spectra for a total of 6.5×10^{10} events triggered by $p+p$ (at $\sqrt{s} = 200$ GeV) collisions. The thick line represents all the clusters, the dashed line represents the clusters with $|ToF| < 5$ ns, and the thin line represents the clusters with $|ToF| > 5$ ns. Since the beam crossing interval is about 100 ns, a reduction in background by a factor of 10 is expected in the case of $|ToF| < 5$ ns. The background is dominant in the high-energy region.

Two plots (Figs. 2 and 3) are compared by multiplying a factor calculated using the data-accumulation period and the probability of having collisions in coincidence. The factor is obtained using the following formula:

$$T_1 \cdot \frac{1}{T_0} \cdot \frac{R}{R_{cross}} = \frac{6.5 \times 10^{10}}{R} \cdot \frac{1}{20300} \cdot \frac{R}{10 \times 10^6} = 0.32,$$

*¹ Russian Research Center "Kurchatov Institute", Moscow, Russia

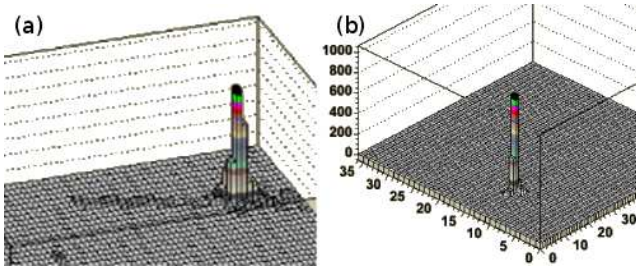


Fig. 1. Cosmic ray cluster examples. Each square corresponds to a EMCal tower. The height is proportional to the pulse height.

where T_0 and T_1 are data-accumulation periods, and R (R_{cross}) is the rate of collisions (accelerator crossings). With this factor, the rate of cosmic-ray (Fig. 2) and the background rate in the collision data (Fig. 3) are consistent.

In this report, the background component in $p+p$ collisions at $\sqrt{s} = 200$ GeV identified using ToF information is explained by cosmic-ray contribution. At a high center-of-mass energy (e.g., 500 GeV), we need to handle rarer signals. The ToF information is essential to reduce cosmic-ray background.

References

- 1) K. Adcox et al.: Nucl. Inst. Meth. A **499**, 469 (2003).

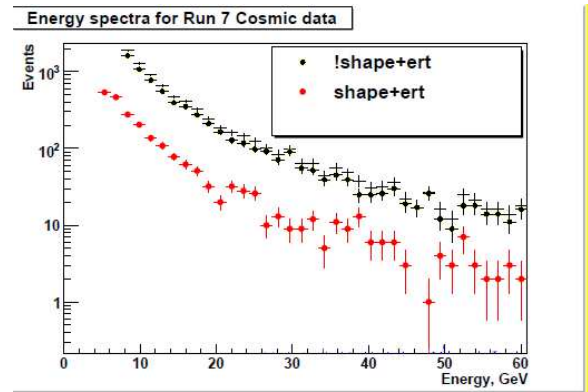


Fig. 2. Energy distribution of cosmic-ray data obtained over 20,000 s. The clusters (the top histogram) are divided into two groups by the shape cut. The bottom histogram shows good shape clusters.

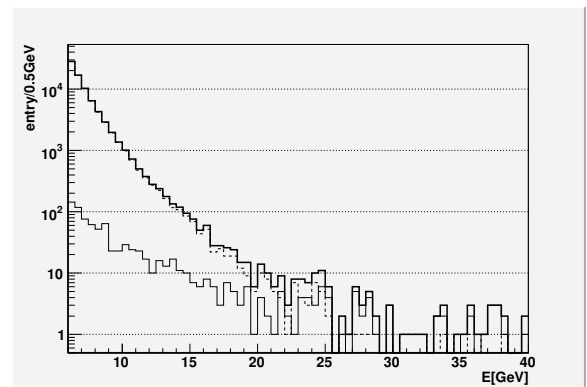


Fig. 3. Spectra of photon-like clusters with 6.5×10^{10} minimum bias collision triggered data (RHIC Run5pp). The thin-line histogram is for clusters out of collision timing ($|ToF| > 5$ ns).

Vernier Scan Method to Reduce Relative Luminosity Uncertainties[†]

D. Kawal, ^{*1,*2}

Introduction

The PHENIX experiment at the Relativistic Heavy Ion Collider (RHIC) has measured the asymmetry, A_{LL} , in inclusive π^0 production from collisions of longitudinally polarized protons beams at $\sqrt{s} = 200$ GeV¹. The asymmetry is defined as :

$$A_{LL} = \frac{1}{P_1 P_2} \frac{N_{++} - R N_{+-}}{N_{++} + R N_{+-}}, \quad \text{where } R = \frac{L_{++}}{L_{+-}} \quad (1)$$

and N_{++} is the π^0 yield from collisions of protons in helicity states $++$, and N_{+-} is for $+-$, P_1, P_2 are beam polarizations and L_{++} and L_{+-} are the corresponding beam luminosities. The asymmetries are of great physics interest because of their leading-order sensitivity to the contribution of gluon spin, Δg , to the spin of the proton^{2,3}.

Determining the asymmetry in cross-section requires a measurement of the relative luminosity of the colliding beams, $R = L_{++}/L_{+-}$, to higher precision than the expected asymmetries in particle production. The measurement of R has become increasingly important for several reasons. First, a comprehensive global fit to polarized deep-inelastic scattering data and A_{LL} measurements of jets and π^0 at RHIC, indicate that Δg is small ($\int_0^1 \Delta g(x, Q^2) dx \approx -0.084$ at $Q^2 = 10$ GeV²), and the expected asymmetries are small³. For instance, $A_{LL}^{\pi} < 5 \times 10^{-3}$ for $p_T^{\pi} < 20$ GeV at $\sqrt{s} = 500$ GeV³. Reducing the uncertainty on Δg will thus require measurements of R at the level of a few $\times 10^{-4}$. We also note that the greatest uncertainty on Δg comes from the low- x region, which is accessed primarily from low p_T^{π} where the predicted asymmetries are very small. Second, at the design luminosity of RHIC, $\mathcal{L} = 10^{32}$ cm⁻²s⁻¹, there will be $> 25\%$ chance of two or more collisions per bunch crossing. Currently PHENIX measures the beam luminosity by counting coincidences between two Beam-Beam Counters (BBCs), located on either side of the interaction region, which detect pp collision by-products⁴. They count at most 1 event per bunch crossing, and so become nonlinear at high rates. The amount of non-linearity can be modeled by measuring the BBC efficiency for detecting pp collisions. In this technique, the machine luminosity, \mathcal{L} , is measured during a vernier scan⁵, as is the peak rate \dot{N} observed in the BBC. We then extract an effective cross-section for the BBC, σ_{BBC} from the relation $\dot{N} = \mathcal{L}\sigma_{BBC}$. Knowing the pp inelastic cross-section allows us to extract the BBC efficiency. The disadvantage of this approach is that

σ_{BBC} is seldom determined to better than 10% due to the uncertainty on some collider parameters such as the focusing β^* , which is required to calculate the machine luminosity, and which is only known to about 10%. Still, event-generator⁶ plus detector simulations suggest we can determine R to $\leq 10^{-3}$ at design luminosity with these techniques.

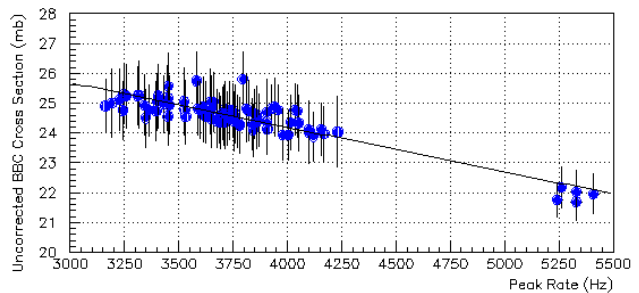


Fig. 1. Effective BBC cross-section in millibarns versus collision rate in Hz.

Vernier Scan Approach

To do better, we note that σ_{BBC} should be a constant, dependent primarily on the BBC coverage in η and ϕ , and in particular it should be independent of the rate. Now consider what happens when we extract $\sigma_{BBC} = \dot{N}/\mathcal{L}$ from vernier scans performed at low rate and high rate. At low rate, \dot{N} is linear in the “true” rate, and the value extracted for σ_{BBC} is reasonable. At high rate, \dot{N} under-counts. The denominator, \mathcal{L} , comes from measuring the transverse sizes of the colliding bunches, and is *largely independent* of rate effects. Taking the ratio at high rate then leads to a smaller value of σ_{BBC} as seen in Fig. 1 from a vernier scan at $\sqrt{s} = 500$ GeV at PHENIX. The fractional difference observed in σ_{BBC} is equal to the fractional correction required on the rate. This method is *independent* of poorly known collider parameters, which cancel when calculating the fractional changes. The new method should reduce the uncertainty δR by at least a factor two compared to the approach above.

References

- 1) A. Adare *et al.*, Phys. Rev. Lett. **103**, 012003 (2009).
- 2) G. Bunce *et al.*, Ann. Rev. Nucl. Part. Sci. **50**, 525 (2000).
- 3) D. de Florian *et al.*, Phys. Rev. D **80**, 034030 (2009).
- 4) M. Allen *et al.*, Nucl. Instr. and Meth. A **499**, 549 (2003).
- 5) S. van der Meer, CERN ISR-PO/68-31, KEK68-64 (1968).
- 6) PYTHIA 6.4, T. Sjostrand, S. Renna and P. Skands, JHEP 0605:026 (2006).

^{*1} RIKEN-BNL Research Center, Brookhaven National Laboratory, Upton, NY, USA

^{*2} Department of Physics, University of Massachusetts, Amherst, MA, USA

Method For Determining Relative Luminosity From Detection Probabilities

A. Manion,^{*1} K. Boyle,^{*2} and A. Deshpande^{*1}

Measurement of ΔG , the gluon contribution to the proton spin, is an important part of the spin program at RHIC¹. In particular, it can be accessed through measurements of double longitudinal spin asymmetries in polarized proton collisions:

$$A_{LL} = \frac{1}{P_B P_Y} \frac{N_{++} - RN_{+-}}{N_{++} + RN_{+-}}, \quad (1)$$

where P_B, P_Y are the polarizations of the beams, N' represent yields in collisions with same ($++$) and opposite ($+-$) beam helicities, and R is the relative luminosity, defined by $R = \frac{L_{++}}{L_{+-}}$. Here L_{++} and L_{+-} are the beam luminosities for the different spins. R is typically measured by counting coincidences in the Beam-Beam Counters (BBCs), detectors that trigger on low energy particles in a pseudo-rapidity range $\Delta\eta = (3.1-3.9)$ on the North and South sides of the interaction point. It is usually assumed that the number of BBC coincidences is proportional to the number of collisions, a convenient assumption because the BBCs do not collect enough information to accurately count collisions. This is justified when the number of collisions per beam crossing averages much less than 1, but breaks down at high luminosities when multiple collisions become common, resulting in under-counting.

One possible solution to this counting problem is to use the probability of measuring zero in the BBCs. Actually, three probabilities are required: the probability of measuring zero in the North detector, $P^N(0) = e^{-\epsilon_N(\lambda+\lambda_N)}$, the South detector, $P^S(0) = e^{-\epsilon_S(\lambda+\lambda_S)}$, and zero in *both* detectors,

$$\begin{aligned} P^{N,S}(0) &= [P^N(0)][P^S(0)|N=0] \\ &= [e^{-\epsilon_N\lambda} e^{-\epsilon_N\lambda_N}] [e^{-\epsilon_S(1-\epsilon_N)\lambda} e^{-\epsilon_S\lambda_S}] \\ &= e^{\epsilon_S\epsilon_N\lambda - \epsilon_S(\lambda+\lambda_S) - \epsilon_N(\lambda+\lambda_N)}. \end{aligned}$$

The definitions in the above equations are as follows: λ_N and λ_S are the true rates of events capable of triggering only the North or only the South BBC, although they are allowed in principle to cause an accidental coincidence. λ is the true rate of events capable of causing a real coincidence, although they may not. The ϵ 's are the efficiencies of the detectors, assumed to be constant over the sample in which R is being calculated. These equations can be solved for the quantity

$$\epsilon_N\epsilon_S\lambda = \ln(P^{N,S}(0)) - \ln(P^S(0)) - \ln(P^N(0)), \quad (2)$$

which can be used in a new definition of R . Experimentally, the probabilities involved can be measured

using the ratio of events to beam crossings, for example, $P^S(0) = 1 - (N_S/N_{\text{crossings}})$.

When checking for systematic uncertainties in R , the typical procedure is to take the ratio of coincidences with another set of North and South detectors, the Zero Degree Calorimeters. These cover $\Delta\eta = \pm(6, \infty)$ and trigger on forward neutral particles. This means they sample an independent class of physics, and thus any asymmetry seen there gives an estimate of the systematic uncertainty in using the BBC to determine R . Figures 1 and 2 show the results of the typical method and the one outlined here applied to this procedure. The typical method obviously suffers from rate effects, while the new method is relatively stable. The new-method calculation here used only recorded data, but in the future all live trigger data will be available which will significantly reduce the uncertainty.

References

- 1) A. Adare, et al. PRL, Vol. 103, 012003 (2009)

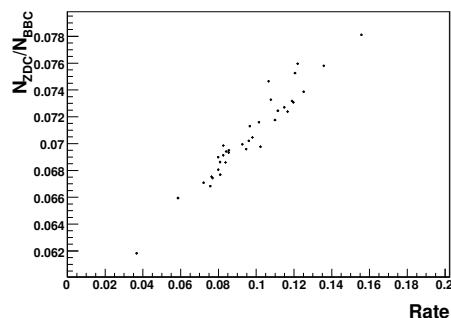


Fig. 1. ZDC counts over BBC counts vs. a collision Rate proxy (ZDC “N or S” triggers normalized to time).

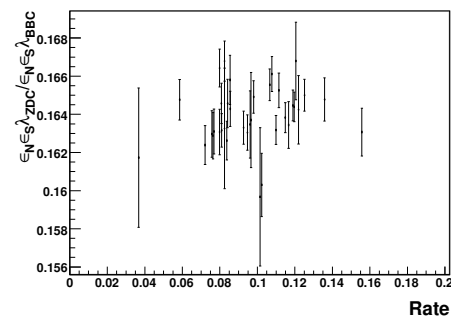


Fig. 2. A ZDC to BBC ratio using the new definition vs. a Rate proxy.

^{*1} State University of New York at Stony Brook

^{*2} RIKEN BNL Research Center

Installation and Tests of the PHENIX Muon Trigger RPCs[†]

M. Grosse Perdekamp^{*1}, Anselm Vossen^{*1} and R. Seidl^{*2} for the PHENIX Muon Trigger Upgrade Group.

[Proton Spin Structure, W-Boson, Muon Trigger, RPCs]

The PHENIX collaboration at Brookhaven National Laboratory (BNL) prepares measurements of the proton quark- and anti-quark-helicity distributions through the observation of parity violating single spin asymmetries between muon yields from W-production in polarized proton-proton collisions at RHIC. The measurements will be carried out at a center of mass energy of $\sqrt{s} = 500$ GeV and p - p collisions rates reaching up to 10 MHz.

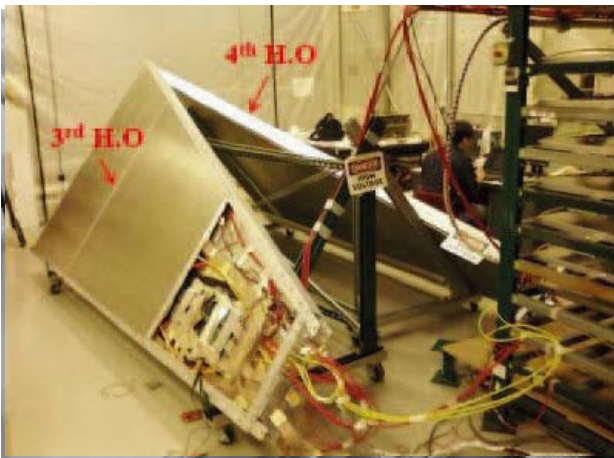


Fig. 1. Noise and high voltage test of two RPC-3 north half octants in the RPC assembly laboratory at BNL.

The high rates require a two-component upgrade of the PHENIX first level muon trigger with the goal to increase the rejection power of the existing muon trigger by a factor 50: (1) New front end electronics for the existing muon tracking chambers has been developed that transfers muon tracking information to fast FPGA based trigger processor boards. The new front end electronics was funded through the JSPS and was successfully developed and installed by the Los Alamos, KEK, Kyoto, RIKEN Rikkyo and UNM groups in PHENIX. (2) New dedicated muon trigger Resistive Plate Chamber (RPC) stations were developed for insertion in the two existing PHENIX muon spectrometers. The RPCs provide additional tracking information and the timing information required for the rejection of beam backgrounds on-line and cosmic ray background off-line. The RPC timing information will be also used to connect events at high rates to the correct collision and polarization information.

The RPCs, their front end electronics and the level one trigger processors have been funded through the

NSF and are being developed and built by a group of PHENIX collaborators from ACU, CIAE, Columbia, Colorado, GSU, ISU, Hanyang University, Korea University, Morgan State, Muhlenberg, PKU, RBRC, UCR and UIUC.



Fig. 2. Pre-assembly of 16 RPC-3 half octants at UIUC.



Fig. 3. Fully installed RPC-3 north detector stations seen from the RHIC accelerator tunnel in November 2009.

The RPC technology used was developed originally for the muon trigger detectors of the CMS experiment at the LHC. The PHENIX trigger RPC design follows closely the design of the endcap muon trigger RPCs in CMS¹⁾. The bakelite RPC gas gaps for PHENIX have been manufactured by the CMS RPC detector laboratory at Korea University (KODEL) and delivered for assembly to BNL. Figure (1) shows two PHENIX RPC half octants during high voltage and noise testing in the RPC assembly facility at BNL and figure (2) shows the pre-assembly of 16 RPC-3 half octant shells at the

^{*1} University of Illinois, Urbana Champaign, USA.

^{*2} Riken BNL Research Center, Upton, USA.

nuclear physics laboratory at UIUC.

For the RHIC data taking in 2009 with polarized p - p collisions at $\sqrt{s} = 200$ GeV and at $\sqrt{s} = 500$ GeV two full size RPC half octant prototypes were installed in the south PHENIX muon spectrometer. In November 2009 the installation of the first full RPC-3 detector station was completed in the north muon spectrometer. RPC-3 north is shown in figure (3) after installation.

During detector assembly the muon trigger RPCs are carefully tested for possible gas leaks, high voltage stability and their performance with regards to detection efficiency, timing resolution and cluster size. This tests are carried out with the help of dedicated test stations for high voltage and gas leak testing and in a cosmic ray test stand. The cosmic ray test stand holds up to 10 RPC detector modules and allows a detailed evaluation of the RPC performance. Figure (4) shows results for the detection efficiency versus RPC high voltage for an RPC-3 north detector module. As can be seen from the figure the efficiency reaches 95% for a broad range of thresholds and high voltages of 9.5 kV or larger.

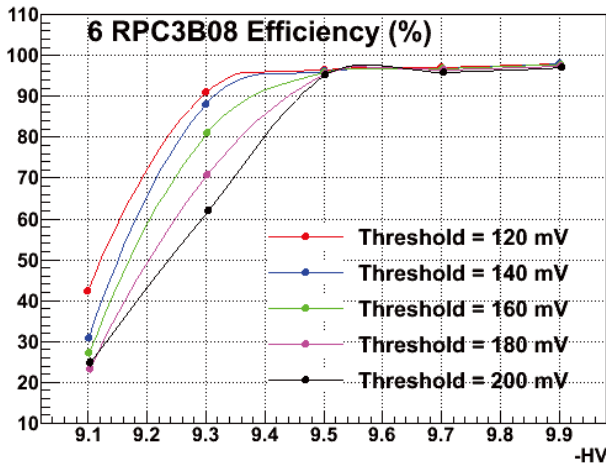


Fig. 4. RPC efficiencies for different discriminator thresholds versus high voltage.

The assembly of the RPC-3 south RPC half octants will be completed by April 2010 and RPC-3 south will be installed during the RHIC summer shutdown 2010. It is also expected that the assembly of the smaller upstream RPC trigger stations, RPC-1 south and north will be completed during the summer of 2010. A first long RHIC run for W-physics at $\sqrt{s} = 500$ GeV is scheduled for 2011.

Prototype Performance in RHIC Run 2009

During the 2009 RHIC run two full size half-octant prototypes with similar layout and nearly identical dimensions to the final RPC design were installed in PHENIX. One prototype, RPC2, was located downstream of the south muon magnet in front of the MUID gap 0, the second prototype, RPC3, was located in

the south tunnel at the same z-position as the RPC3 South location. The prototypes were integrated in the PHENIX data acquisition and slow control during the run and their performance was found to be quite stable and reliable.

Initially, the LV cable to the RPC2 did pick up high frequency electronics noise, which resulted in high noise rates in most of the RPC2 area. After installing an additional low pass filter, the noise rates dropped and RPC2 became useable. Apart from a few noisy readout strips, the noise rates stayed below the target noise rate of 10 Hz/cm^2 which will allow us to use this detector for triggering.

The readout of the data shows that the collision related particles can be nicely seen in the time distributions as shown in Fig. 5 for all non-noisy strips. Fitting them with a Gaussian distribution shows, that these peaks can be described well with widths of only a few ns.

The observed timing resolution is consistent with expected contributions from the RPC-TDC resolution and variations in hit position and cable lengths.

In fact it was found that for trigger operation a timing window shorter than the design value of 20 ns can be used. The timing resolution is sufficient to reject beam backgrounds and to connect the triggered event to the correct polarization information.

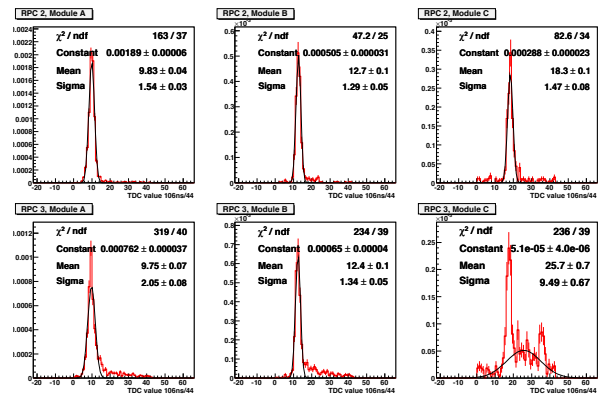


Fig. 5. Raw TDC distributions in the two detectors for the three radial segments. The red distribution shows muon candidate tracks passing in the vicinity of the RPC prototype volumes. The muon candidate events are fit with a Gaussian whose fit parameters are also displayed.

In addition, an offline time window of 20 ns or less will also allow to reduce the cosmic muon background by at least a factor of 5 compared to the present time gate defined by the muon identifier streamer tube stations.

References

- 1) S.H. Ahn *et al.* : Nucl. Instrum. Meth. A 469 (2001).

Upgrade of PHENIX Muon Tracker Performance and Trigger Capability for Sea Quark Polarization Measurement at RHIC

I. Nakagawa, T. Mibe,^{*1} N. Saito,^{*1} I. Ichikawa,^{*2} K. Karatsu,^{*2} T. Murakami,^{*2} K. Nakamura,^{*2} R. Sameshima,^{*2} Y. Fukao, Y. Ikeda,^{*3} J. Murata,^{*3} N. Ogawa,^{*3} K. Ninomiya,^{*3} J. Onishi,^{*3} and S. Hirota,^{*4}

[nucleon spin, W-boson, polarized parton distribution, Electronics, trigger]

Several decades have passed since the parity-violating production of the W boson was pointed out to be the ideal probe for sea quark polarization measurement; this claim is based on almost fixed flavors and fragmentation-function-free interpretation of observed asymmetry¹⁾. Such measurement has just begun at RHIC using longitudinally polarized proton beams at a collision energy of 500 GeV. The W program is the highlight of the RHIC spin project, which will continue over the next 5 years; thus, the following projects have been proposed to upgrade the PHENIX muon arms in order to carry out the rare probe measurement under conditions in which the background rate is high.

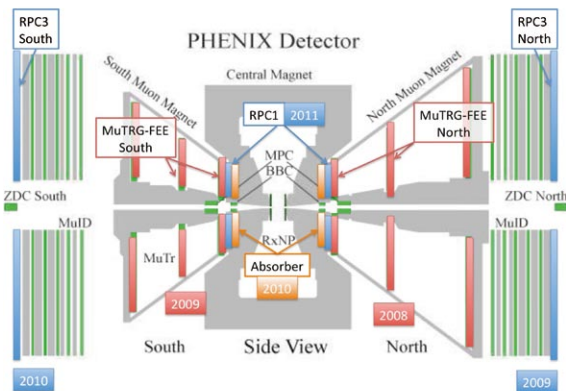


Fig. 1. Installation schedule of PHENIX muon arm upgrade projects. Year in solid square is the scheduled year of installation.

New front-end electronics (MuTRG-ADTX boards³⁾ were developed and produced to add the trigger capability to existing PHENIX muon tracker (MuTr) detectors. The installation in the North muon arm was completed during the 2008 shutdown period; back-end electronics (MuTRG-MRG and MuTRG-DCMIF) boards⁵⁾ that serve as an interface between MuTRG-ADTX and local-level-one (LL1) trigger boards and data collection modules (DCM) were also installed. The newly installed trigger electronics chain was commissioned during the engineering run of the first 500

GeV polarized proton-proton collision in Run9. The observed performance has been discussed elsewhere^{6,7)}. The installation of MuTRG-ADTX boards in the South muon arm began during the shutdown period that followed Run09 and was completed by the end of 2009. These newly installed boards were commissioned along with Au-Au beams in Run10.

As a result of the project being carried out to upgrade the PHENIX muon arms, the performance of the muon detection system will be improved as shown in Fig.1. Another project aimed at upgrading; Resistive Plate Chambers²⁾ production is also being carried out. The additional hadron absorbers will be installed in Run11, where the first production run of polarized proton-proton collision at 500 GeV is scheduled. Thus, trigger upgrade projects are running on schedule. Efforts to improve the performance of existing detectors are also underway. The momentum resolution of MuTr is a major concern since only resolutions that are lower than its intrinsic resolution ($100\mu\text{m}$) by a factor of 2 - 3 have been demonstrated in the past. It has been proposed that the motion of MuTr chambers on a daily basis deteriorates the alignment precision. The relative alignment between MuTr chambers is carried out using straight particle trajectories with magnet field off of MuTr. We observed chamber movement of the order of $100\mu\text{m}$ over the course of a few months during Run9 by using an optical alignment system (OASys) implemented in MuTr chamber frames. The OASys consists of light sources, lenses, and CCD cameras attached to chambers in Station1, Station2, and Station3, respectively, and it tracks the relative motion of the chambers by continuously monitoring the light spot in the CCD camera⁸⁾. The chamber displacement predicted by the OASys can be verified by the zero field data that are obtained at intervals of months. This consistency analysis is now in progress.

References

- 1) C. Burrell and J. Soffer, Phys. Lett. **B314**, 132 (1993).
- 2) CDR for a Fast Muon Trigger (2007).
- 3) TDR on Amplifier-Discriminator board and Data Transfer board for the MuTr FEE upgrade (2008).
- 4) Y. Fukao *et. al.*, RIKEN Accel. Prog. Rep. **42** (2009).
- 5) T. Mibe *et. al.* RIKEN Accel. Prog. Rep. **42** (2009).
- 6) Y. Fukao *et. al.*, RIKEN Accel. Prog. Rep. **43** (2010).
- 7) K. Nakamura *et. al.*, RIKEN Accel. Prog. Rep. **43** (2010).
- 8) H. Akikawa *et. al.*, NIM **A499** 537 (2003).

^{*1} KEK, Tsukuba, Ibaraki, 305-08011 Japan

^{*2} Kyoto University, Kitashirakawa-Oiwakecho, Kyoto, 606-8502 Japan

^{*3} Rikkyo University, Rikkyo, 3-34-1, Nishi-Ikebukuro, Tokyo, 171-8501 Japan

^{*4} University of Tokyo, 7-3-1 Hongo, Bunkyo-ku, Tokyo 113-0033 Japan

Performance evaluation of MuTRG for upgrading PHENIX muon trigger

Y. Fukao for the PHENIX MuTr FEE Upgrade Group

[nucleon spin, W boson, polarized parton distribution, electronics, trigger]

The PHENIX experiment aims to directly probe the contribution of sea quarks to proton spin by performing measurements of single helicity asymmetry in W boson production. In order to record the W production events effectively, we are developing a new trigger system for the PHENIX muon arm.¹⁾ The trigger is designed to sort out events with high momentum tracks, which are expected to be muons resulting from W decays, by performing rough momentum measurements online. An overview of the trigger system is provided elsewhere.²⁾ In 2008, additional electronic component (MuTRG) were installed in the north PHENIX muon trackers (MuTr) to provide readouts of fast signals to the trigger. The MuTRG was commissioned in the 2009 run with the first polarized pp collisions at the center-of-mass energy of 500 GeV. This paper describes the preliminary results of the MuTRG commissioning tests. Related articles are provided in this reports.^{3,4)}

The MuTRG has several optional parameters such as the threshold of the deposit charge in MuTr, clustering, and sagitta acceptance Δs ^{a)} that can be adjusted to ensure optimal performance. Figure 1 shows MuTRG efficiency as a function of particle momentum measured by MuTr. The efficiency achieved at the plateau is ~ 0.9 . The turn-on point of the trigger is improved from 2.0 GeV/c to 12.2 GeV/c when $\Delta s = 0$ and to 8.5 GeV/c when $\Delta s \leq 1$. Figure 2 shows the relation between the efficiency at the plateau and the trigger rejection power. The rejection power is defined as the number of collisions divided by the number of events accepted by the MuTRG. Although tight cuts improve the rejection power, they decrease the efficiency.

The installation of the MuTRG in the south muon arm was completed after the 2009 run and its commissioning is ongoing in the 2010 run with heavy-ion beams. The signal from MuTRG is finally combined with the signal from resistive plate chambers (RPC) which is another trigger detector. More improvement in the trigger rejection power is expected with the use of RPCs. In the polarized pp physics run to be performed in 2011, it is estimated that a trigger rejection power of 4500 will be required with a DAQ bandwidth of 2 kHz. A combined analysis of MuTRG and RPC is

^{a)} Sagitta is defined as the distance between a hit strip in the MuTr 2nd station and the linearly interpolated positions of hit strips in the 1st and 3rd station. Hits are required in a strip at the 2nd station on the linear interpolation when $\Delta s = 0$. Hits are required in ± 1 strips in the 2nd station around the linear interpolation when $\Delta s \leq 1$.

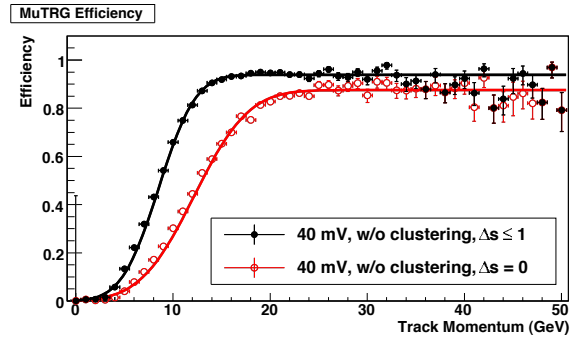


Fig. 1. Efficiency of MuTRG as a function of track momentum. A threshold voltage of 40 mV is applied and clustering is not applied. The black closed circles represent the efficiencies when $\Delta s \leq 1$ and those with red open circles represent the efficiencies when $\Delta s = 0$.

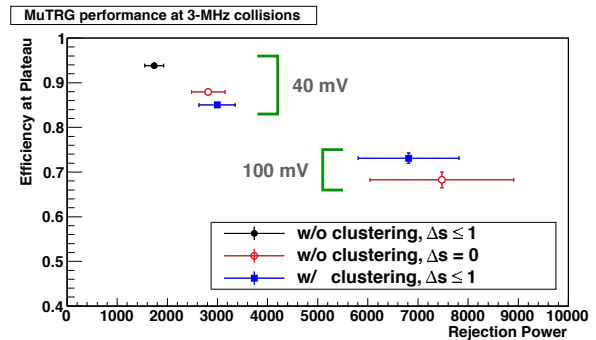


Fig. 2. Relation between efficiency and rejection power. The black closed circles and blue closed squares represent the case when $\Delta s \leq 1$, while the red open circles represent the case when $\Delta s = 0$. Clustering of hits is applied in each station in the case represented by the blue closed squares. Threshold voltage of 40 mV and 100 mV is set for the points where the rejection power is less than and greater than 5000, respectively.

being carried out to evaluate the final performance and determine the parameters for optimal performance of the MuTRG.

References

- 1) PHENIX collaboration: Nucl. Instrum. Meth. **A 499**, 537 (2003).
- 2) I. Nakagawa et al.: RIKEN Accel. Prog. Rep. **42** (2009).
- 3) I. Nakagawa et al.: RIKEN Accel. Prog. Rep. **43** (2010).
- 4) K. Nakamura et al.: RIKEN Accel. Prog. Rep. **43** (2010).

Measurement of the interference fragmentation function in e^+e^-

R. Seidl,^{*1} A. Vossen,^{*2} M. Grosse-Perdekamp,^{*2} A. Ogawa,^{*3}, M. Leitgab,^{*2} and P. Francisconi,^{*2}

[spin dependent fragmentation, transverse spin]

The interference fragmentation function IFF is a chiral-odd fragmentation function suggested by Collins¹⁾ which can act as an analyzer of transverse quark spin. In contrast to the Collins function⁴⁾, previously also measured in e^+e^- by us^{2,3)}, the IFF does not require a transverse momentum dependence and collinear factorization can be applied. This allows a model independent extraction of the quark transversity from SIDIS and pp data using the known collinear evolution⁵⁾. Following Boer⁶⁾, the measurement relies on extracting an azimuthal correlation of the planes spanned by two charge ordered $\pi^+\pi^-$ pairs relative to the reaction plane defined by the incoming leptons and the formed quark-antiquark pair approximated by the thrust axis. The planes and angular definitions are displayed in Fig. 1. The results are obtained from a 672fb^{-1} data sample that contains 711×10^6 $\pi^+\pi^-$ pairs and was collected near the $\Upsilon(4S)$ resonance, with the Belle detector at the KEKB asymmetric energy e^+e^- collider. In events with a clear two-jet like topology as defined by a thrust value larger than 0.8 a $\pi^+\pi^-$ pair is selected in each hemisphere. The azimuthal angular yield of these pairs is then normalized by the average yield and fit by several azimuthal modulations. The $\cos(\phi_1 + \phi_2)$ modulation (a_{12}) is proportional to the product of the interference function $H_1^\perp(z, m)$ on the quark side times the interference function on the antiquark side, normalized by the corresponding unpolarized functions, where $z = E_{\text{pair}}/E_{\text{quark}}$ is the fractional energy of the hadron pair and m its invariant mass. Preliminary results were first shown this year⁷⁾

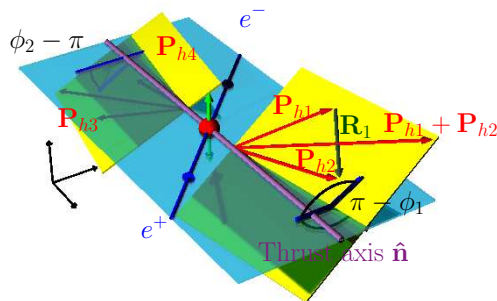


Fig. 1. Azimuthal angle definitions for ϕ_1 and ϕ_2 as defined relative to the thrust axis.

^{*1} Riken BNL Research Center, Upton, USA.

^{*2} University of Illinois, Urbana Champaign, USA.

^{*3} Brookhaven National Laboratory, Upton, USA.

and the publication of the final results is in progress. We observe large asymmetries which are rising with the fractional energy, as can be seen in Fig. 2. Since the product to two interference fragmentation functions is measured, the effect of each individual function rises up to more than 30% at highest z . The asymmetries are also rising with the invariant mass of the pion pair which is not shown here due to space limitations. It is important to note, that this mass behavior favors model calculations by Radici⁹⁾ over those by Jaffe⁸⁾ which have predicted a sign change at the ρ meson mass.

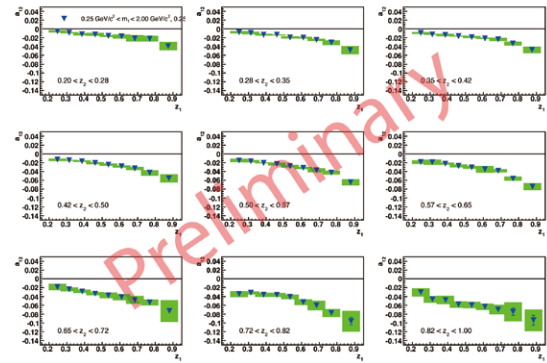


Fig. 2. a_{12} modulations for the 9×9 z_1, z_2 binning as a function of z_2 for the z_1 bins, where 1, 2 stands for the hemisphere.

The analysis for the extraction of the interference function for other hadron combinations is ongoing.

References

- 1) J. C. Collins, S. F. Heppelmann and G. A. Ladinsky, Nucl. Phys. B **420**, 565 (1994) [arXiv:hep-ph/9305309].
- 2) R. Seidl *et al.* [Belle Collaboration], Phys. Rev. Lett. **96** (2006) 232002 [arXiv:hep-ex/0507063].
- 3) R. Seidl *et al.* [Belle Collaboration], Phys. Rev. D **78**, 032011 (2008) [arXiv:0805.2975 [hep-ex]].
- 4) J. C. Collins, Nucl. Phys. B **396**, 161 (1993) [arXiv:hep-ph/9208213].
- 5) F. A. Ceccopieri, M. Radici and A. Bacchetta, Phys. Lett. B **650**, 81 (2007) [arXiv:hep-ph/0703265].
- 6) D. Boer, R. Jakob and M. Radici, Phys. Rev. D **67** (2003) 094003 [arXiv:hep-ph/0302232].
- 7) A. Vossen, R. Seidl, M. Grosse-Perdekamp, M. Leitgab, A. Ogawa and K. Boyle, to appear in the proceedings of the Dubna Spin workshop 2009, arXiv:0912.0353 [hep-ex].
- 8) Jaffe, R.L. and Jin, X. and Tang, J., Phys. Rev. Lett. **80**, 1166, (1998)
- 9) Bacchetta, A. and Radici, M., Phys. Rev., **D74**, 114007 (2006)

Precision Measurements of Charged Hadron Multiplicities in e^+e^- Annihilation at BELLE

M. Leitgab,^{*1} M. Grosse Perdekamp,^{*1} R. Seidl,^{*2} A. Ogawa,^{*3} A. Vossen,^{*1} K. Boyle^{*2} and P. Francisconi^{*1}

[Precision hadron multiplicities, fragmentation functions, BELLE, particle identification]

1 Measurement Description

This paper summarizes the status of precision measurements of $\pi^{+,-}$ and $K^{+,-}$ (in the following, resolving all particle charges is implied) multiplicities in e^+e^- annihilation at a center of mass energy of 10.52 GeV at the BELLE experiment at KEK, Japan¹⁾. The hadron multiplicities are measured as a function of z which is the hadron energy relative to half of the center-of-mass energy in electron-positron annihilation into quark-antiquark pairs. The measured multiplicity distributions are corrected for particle misidentification and acceptance effects.

2 Motivation

Multiplicity measurements at Belle are motivated by two recent studies on the extraction of unpolarized fragmentation functions^{2),3)}. Fragmentation functions describe hadron production from a final-state quark or gluon in processes such as hadron collisions, electron-positron annihilation and deep inelastic scattering of leptons on protons or nuclei. The present measurement is intended to provide high precision datasets as an input to the extraction of fragmentation functions, and thereby significantly lower the uncertainties of these. Precise knowledge of fragmentation functions is required for the extraction of the gluon helicity distribution from spin asymmetries measured in hadron collisions at the Relativistic Heavy Ion Collider⁴⁾.

3 Measurement Status and Outlook

For charged hadrons, experimental particle yields need to be corrected for particle misidentification. In an analysis test-run this correction has been found to change the measured charged particle distributions at the order of 5 to 10% for pions and 10 to 35% for kaons. The correction is performed through an unfolding technique based on inverse 4x4 particle identification (PID) probability matrices. To not rely on the GEANT-based⁵⁾ Monte Carlo modelling of the BELLE PID performance, the elements of the probability matrices are obtained from reconstructing unstable particles in experimental data with purely kinematical means, forming samples of tracks with known 'real/physical'

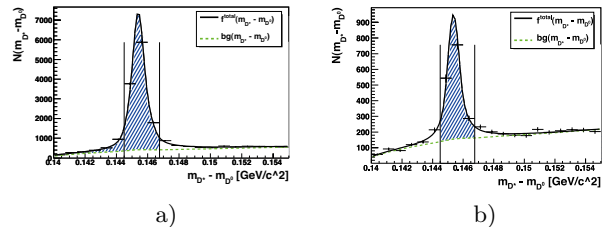


Fig. 1. Fits of experimental data invariant mass distributions on a reconstructed sample of the decay $D^* \rightarrow \pi(D^0 \rightarrow K\pi)$. Figures a) and b) show distributions without and with an additional PID likelihood cut to select particles of species $j = \pi$. Extracting the PID probability $p_{(K^- \rightarrow \pi^-)}$ from the ratio of the hatched areas yields 0.111 ± 0.004 for negatively charged kaons with laboratory frame momentum in [1.4; 1.6] GeV/c and laboratory azimuthal angle θ in [77.9; 89.0] degrees.

species $i = \{e/\mu, \pi, K, p\}$. PID probabilities $p_{(i \rightarrow j)}$ can be calculated by additionally applying PID likelihood cuts to select particles of species j from the reconstructed samples and forming ratios of the yields obtained with and without PID cuts. Decays of D^* , Λ and J/ψ particles are analyzed. Figure 1 shows fits of experimental data distributions from the reconstructed decay $D^* \rightarrow \pi(D^0 \rightarrow K\pi)$ which allow to extract the PID probability $p_{(K^- \rightarrow \pi^-)}$.

Eventually, the measurement of hadron multiplicities against their normalized energy z will be performed from about 0.2 to close to 1.0 in z . The systematic uncertainty analysis for PID, momentum smearing and acceptance effects will be finalized. The leading uncertainty is expected to arise from the systematic uncertainties connected with the PID correction. The overall systematic uncertainties are expected to remain below 3% (5%) for π (K) spectra for $z < 0.6$, and to increase with z up to 5% (17%) for π (K) spectra, respectively.

References

- 1) A. Abashian *et al.*; Nucl. Instrum. Methods **A** 479, (2002), pp. 117-232.
- 2) M. Hirai, S. Kumano, T.-H. Nagai, K. Sudoh; Phys. Rev. D 75, 114010 (2007).
- 3) D. de Florian, R. Sassot, M. Stratmann; Phys. Rev. D 75, 094009 (2007).
- 4) A. Adare *et al.*; Phys. Rev. Lett. 103, 012003 (2009).
- 5) Geant 4 Collaboration; Nucl. Instrum. Methods **A** 506, (2003), pp. 250-303.

^{*1} University of Illinois at Urbana-Champaign (UIUC), USA

^{*2} RIKEN BNL Research Center (RBRC), USA

^{*3} Brookhaven National Laboratory (BNL), USA

Photoproduction of $\Lambda(1405)$ and $\Sigma^0(1385)$ on the proton at $E_\gamma = 1.5\text{-}3.0$ GeV at SPring-8/LEPS

Y. Nakatsugawa for LEPS collaboration

[photoproduction, $\Lambda(1405)$]

In a quark model, $\Lambda(1405)$ is a p -wave q^3 baryon. However, it is also suggested that $\Lambda(1405)$ has a non- q^3 structure such as a meson-baryon molecular state. In some theoretical studies, chiral Lagrangian and coupled unitary model were used to predict the line shape of $\Lambda(1405)$ as $\pi\Sigma^0$ and $\bar{K}N$.¹⁾ The two-pole structure of $\Lambda(1405)$ was also suggested.²⁾ The contribution of the second pole might be extracted by treating K and K^* exchange reaction separately, and information about exchanged particles can be obtained from photon beam asymmetry. Therefore, it is of interest to obtain the mass spectrum of $\Lambda(1405)$ and determine the photon beam asymmetry. On the other hand, it has been firmly established that $\Sigma^0(1385)$ is a q^3 baryon. The difference between the internal structures of $\Lambda(1405)$ and $\Sigma^0(1385)$ may appear in the photoproduction cross sections and/or photon beam asymmetries. Recently, differential cross sections for $\gamma p \rightarrow K^+\Lambda(1405)$ and $\gamma p \rightarrow K^+\Sigma^0(1385)$ reactions were measured by LEPS collaboration.³⁾ However, the statistics were limited. A new experiment was carried out at SPring-8/LEPS using a liquid hydrogen target and a linearly polarized photon beam. In order to detect the decay products of hadrons, a time projection chamber (TPC) surrounding the target was used along with the LEPS spectrometer. Detailed information on the differential cross sections of $\gamma p \rightarrow K^+\Lambda(1405)$ and $\gamma p \rightarrow K^+\Sigma^0(1385)$ and the line shapes of $\Lambda(1405)$ will be obtained from new data. The photon beam asymmetries will be also investigated.

The analysis of new data is still underway. The present status of the analysis and very preliminary results are reported in this article.

In order to obtain the spectra of $\Lambda(1405)$ and $\Sigma^0(1385)$ separately, we selected the following two reactions and imposed certain cut conditions:

- (1) $\gamma p \rightarrow K^+\Sigma^0(1385) \rightarrow K^+\Lambda\pi^0 \rightarrow K^+p\pi^-\pi^0$
- (2) $\gamma p \rightarrow K^+\Lambda(1405) \rightarrow K^+\Sigma^\pm\pi^\mp \rightarrow K^+n\pi^+\pi^-$

The spectrum of $\Sigma^0(1385)$ was obtained by observing reaction (1) under the following cut conditions: (i) K^+ was detected in the forward spectrometer, (ii) a proton and a π^- were detected in the TPC, and (iii) a $\Lambda(1116)$ was identified on the basis of the invariant mass of $p\pi^-$. In Fig.1(a), a bump corresponding to $\Sigma^0(1385)$ can be seen. Owing to isospin conservation, $\Lambda(1405)$ does not decay into $\Lambda\pi^0$, hence the yield of $\Sigma^0(1385)$ can be estimated from its decay branching ratios. The spectrum of $\Lambda(1405)$ was obtained by observing reaction (2) under the following cut conditions:

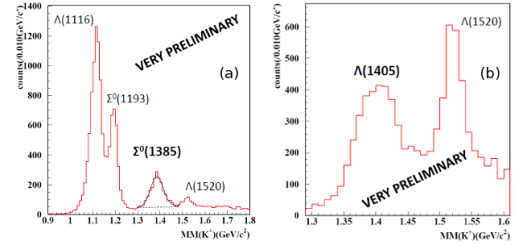


Fig. 1. Missing mass spectrum of $\gamma p \rightarrow K^+X$: (a) Selection cuts (i), (ii), and (iii) were applied. (b) Selection cuts (iv), (v), and (vi) were applied.

(iv) K^+ was detected in the forward spectrometer, (v) a π^+ and a π^- were detected in the TPC, and (vi) a neutron was identified on the basis of the missing mass of $\gamma p \rightarrow K^+\pi^+\pi^-X$. The bump around 1.4 GeV in Fig. 1(b) corresponds to $\Lambda(1405)$. Since $\Sigma^0(1385)$ can decay into $\Sigma\pi$, the contribution of the contamination should be subtracted from the spectrum in order to estimate the yield of $\Lambda(1405)$. However, this has not yet been done because the acceptance calculation is yet to be completed. In the future, the differential cross sections of $\gamma p \rightarrow K^+\Sigma^0(1385)$ and $\gamma p \rightarrow K^+\Lambda(1405)$ will be determined, and the E_γ dependence of the cross sections and line shape of $\Lambda(1405)$ will be investigated. In this study, photon beam asymmetries were also measured for $\gamma p \rightarrow K^+\Sigma^0(1385)$ and $\gamma p \rightarrow K^+\Lambda(1405)$ reactions. The error is large because only one quarter of all data was used for the analysis of photon beam asymmetries. More precise results will be reported as final results.

References

- 1) J. C. Nacher, E. Oset, H. Toki, and A. Ramos: Phys. Lett. B **455**, 55 (1999).
- 2) D. Jido, J. A. Oller, E. Oset, A. Ramos, and U.-G. Meissner: Nucl. Phys. A **755**, 669 (2005).
- 3) M. Niiyama *et al.*: Phys. Rev. C **78**, 035202(2008).

E906 Drell-Yan experiment at Fermilab

Y. Goto, Y. Fukao, K. Imai,^{*1} Y. Miyachi,^{*2} S. Miyasaka,^{*3} S. Mizugashira,^{*3} T. Nagae,^{*1} K. Nakano, S. Sawada,^{*4} T.-A. Shibata,^{*3} A. Taketani, and M. Togawa for the Fermilab E906/SeaQuest Collaboration

Flavor symmetry violation of antiquark distributions was first observed by the New Muon Collaboration in muon deep inelastic scattering (DIS) experiments.¹⁾ The Drell-Yan process provides a complementary way to select only the antiquark distributions and it is an ideal process for flavor asymmetry measurement. In leading order, the ratio of the proton-proton to proton-deuterium Drell-Yan yields can be expressed as

$$\frac{\sigma_{pd}}{2\sigma_{pp}} \Big|_{x_1 \gg x_2} = \frac{1}{2} \left[1 + \frac{\bar{d}(x_2)}{\bar{u}(x_2)} \right],$$

assuming that $x_1 \gg x_2$ and the $u\bar{u}$ annihilation term is dominant; x_1 and x_2 are the momentum fractions of a quark or an antiquark in the beam proton and target proton, respectively. The Fermilab E866 experiment determined the x -dependence of the \bar{d}/\bar{u} ratio in this way,²⁾ as shown in Fig.1, with an 800 GeV/ c proton beam from the Fermilab Tevatron incident on hydrogen and deuterium targets. At moderate values of x , the data show an excess of \bar{d} over \bar{u} by more than 60%, but this excess disappears and the antiquark distributions appear to be symmetric at high x values. The ratio of \bar{d} to \bar{u} quarks determines whether there is competition between perturbative QCD gluon dissociation and non-perturbative contributions. Calculations have shown that perturbative processes create flavor-symmetric antiquark distributions, while non-perturbative approaches such as the use of meson cloud models, chiral perturbation theory, or instantons can explain a large asymmetry, but not the return to symmetric distributions seen as $x \rightarrow 0.3$. None of the models predicts an excess of \bar{u} over \bar{d} , as shown by the CTEQ6 global parton distribution fit³⁾ in Fig.1. Many of these models relate the flavor asymmetry to the intrinsic spin carried by the antiquark. The Fermilab E906 experiment will use a 120 GeV proton beam extracted from the Fermilab Main Injector to study flavor symmetry violation at high values of $x > 0.45$.

The E906 experiment will also measure the Drell-Yan yields from nuclear targets. The nuclear target data can be used to constrain partonic energy loss in cold nuclear matter. This is a necessary step in understanding models that also predict partonic energy loss in the hot nuclear matter used at the RHIC. In addition, the data will allow us to observe modifications of the antiquark distributions in nuclei relative to the nucleon. The distribution of partons in a free nucleon is different from that in a bound nucleon, an

effect first discovered by the European Muon Collaboration from muon DIS experiments in 1983.⁴⁾ Although many models of nuclear binding involve virtual meson exchange, which modifies the antiquark distributions of the nuclei, present data suggest that the antiquark distributions are not modified.⁵⁾ The E906 experiment will either observe the modifications predicted by these models or invalidate many of the models.

The collaboration expects to begin data collection in the summer of 2010. Japanese groups (RIKEN, KEK, Kyoto Univ., Tokyo Tech., and Yamagata Univ.) are in charge of one of the drift-chamber stations. The station is currently under construction in Japan, and it will be shipped to Fermilab in the spring of 2010.⁶⁾

References

- 1) P. Amaudruz *et al.*: Phys. Rev. Lett. **66**, 2712 (1991); M. Arneodo *et al.*: Phys. Rev. D **50**, R1 (1994).
- 2) R. S. Towell *et al.*: Phys. Rev. D **64**, 052002 (2001).
- 3) J. Pumplin *et al.*: JHEP **0207**, 012 (2002).
- 4) J. J. Aubert *et al.*: Phys. Lett. B **123**, 275 (1983).
- 5) D. M. Alde *et al.*: Phys. Rev. Lett. **64**, 2479 (1990).
- 6) K. Nakano *et al.*: RIKEN. Accel. Prog. Rep. **43**, xxx (2010).

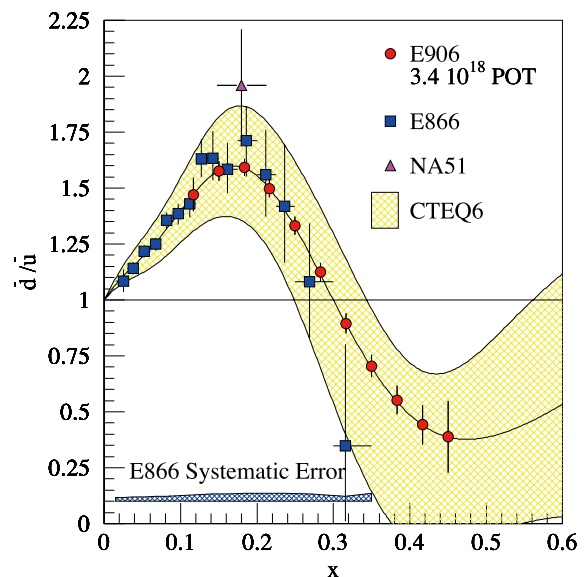


Fig. 1. The ratio \bar{d}/\bar{u} as determined in the E866 (blue squares) and NA51 (pink triangle) experiments. The central curve in the band shows the \bar{d}/\bar{u} ratio and uncertainty in the CTEQ6 fit, which includes the E866 data. The red circles represent the expected statistical uncertainties in the E906 data. The expected systematic uncertainty is approximately 1%.

^{*1} Kyoto University

^{*2} Yamagata University

^{*3} Tokyo Institute of Technology

^{*4} KEK

A proposal to study medium mass modification of ϕ -mesons using ϕ -meson bound state in nucleus[†]

H. Ohnishi*¹ and K. Tsukada*¹

[Spontaneous breaking of Chiral symmetry, meson bound state]

A proton is composed of two "Up" quarks and one "Down" quark and has a mass of 938 MeV/c². On the other hand, the mass of bear quark, *i.e.* "Up" and "Down" quark is known to be a few MeV/c². Therefore, the contribution of the constituent quarks to the mass of a proton is very less. We must now identify a process by which more than 90 % of the proton mass can be generated from vacuum. This mechanism is now known to involve spontaneous breaking of chiral symmetry, and it generates a non-zero quark antiquark condensate $\langle \bar{q}q \rangle$ in vacuum. This quark-antiquark condensate $\langle \bar{q}q \rangle$ is the major contributor to the mass of low-lying hadrons such as protons, neutrons and pions. In the theoretical framework, the quark-antiquark condensate $\langle \bar{q}q \rangle$ (chiral order parameter) is a function of temperature and chemical potential (density).

In this study we focus on the ϕ -mesons in a nucleus. According to an experimental study of the invariant mass spectra of ϕ -mesons in the pA reaction, the ϕ -meson mass shift in medium heavy nuclei (Cu) is approximately about 3.4% and the natural width broadening of $\Gamma_\phi/\Gamma_\phi^{free}$ is ≈ 3.6 ¹⁾. We are attending to understand the meaning of the mass reduction of 3.4% (= 35 MeV/c²) observed for the ϕ -mesons in a nucleus. A possible clue can be obtained from the kaon in nucleus. Reference²⁾ shows that the mass of the K^- will be reduced in nuclear matter owing to the strong attractive potential between the K^- and the nucleon. This theoretical prediction indicates that the mass reduction of ϕ -mesons in a nucleus is directly related to the possible existence of an attractive potential between the ϕ meson and the nucleus. The depth of the potential well is expected to be on the same order as measured mass reduction. Therefore, we adopted an experimental approach to measure the ϕ -meson properties in nuclear media, by studying formation of a ϕ -meson bound state. The most interesting ϕ -meson formation channel that could be ideal for the formation of a ϕ -meson bound state is the $\bar{p} + p \rightarrow \phi + \phi$ channel. One striking outcome of this reaction is the rather large $\phi\phi$ production cross section near the production threshold (~ 0.9 GeV/c), namely, an incident \bar{p} momentum of 1.3 \sim 1.4 GeV/c. The most distinguishable feature of this reaction channel is its *fully background-free* nature. The yield of the processes, $\phi K^+ K^-$ and $K^+ K^- K^+ K^-$, are considerably

smaller than those of the double ϕ production channel when the incident \bar{p} momentum is selected below 1.4 GeV/c³⁾. Another unique feature of this reaction is that all the particles we observe, including those emitted in the forward $\phi \rightarrow K^+ K^-$ decay, are labeled with strangeness so that they be clearly distinguish from the particles formed in other processes. This ensures that the process is free process of any accidental background. In addition to strangeness tagging by forward-going kaons, the background can be considerably reduced in missing-mass spectra by using a combination of (\bar{p}, ϕ) spectroscopy together measurements and $K^+ \Lambda$ tagging for this reaction; this ensures that strange quarks are actually embedded in the nucleus. From the missing mass and invariant mass study of the sub-threshold energy region, one can independently deduce the mass-shift information. A systematic study of several nuclear targets will help in the unique, definitive, and precise determination of the in-medium mass modification of the vector meson $\phi(s\bar{s})$. Despite of the low cross section of the $p(\bar{p}, \phi)\phi$ reaction, we can expect an excellent ground-state-formation rate of 240 per month when using a \bar{p} beam with an intensity of 2×10^6 particles per *spill* on a carbon target. The conceptual design for the spectrometer be used in (\bar{p}, ϕ) spectroscopy is shown in Figure 1.

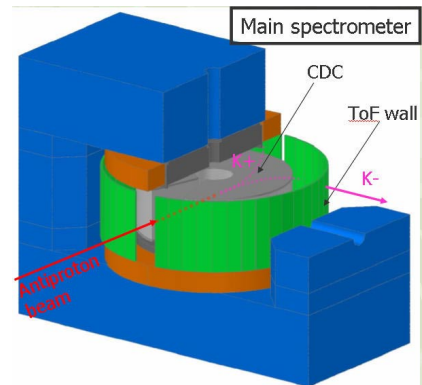


Fig. 1. conceptual design for the spectrometer.

The experimental proposal has been submitted to the J-PARC Program Advisory Committee, and detail status and R&D activities for the detector are currently underway.

References

- 1) R. Muto *et al.*; Phys. Rev. Lett. **98**,042501 (2007).
- 2) T. Waas *et al.*; Nucl.Phys.**A617**, 449(1997)
- 3) C. Evangelista *et al.*; Phys. Rev. D**57** 5370(1996).

[†] Condensed from the experimental proposal submitted to J-PARC (P29)

*¹ RIKEN Nishina Center

Simulation study for the multiplicity Measurement in the Proton-Proton Collisions at the LHC[†]

S. Sano,^{*1} H. Hamagaki,^{*1} T. Gunji,^{*1} C. Garabatos² M. Ivanov² and J. Wiechula²

[Multiplicity, Color Glass Condensate (CGC), LHC]

Parton density grows rapidly with decrease of fractional momentum x , but eventually tends to saturate, as a consequence of self-interaction of gluons, which is an intrinsic property of non-Abelian gauge theory. Such saturated state may be described with a classical field theory such as Color Glass Condensate (CGC)^{1,2}. An investigation of gluon saturation is important to decide the initial condition for high-energy heavy-ion collisions. CGC effects may be seen even at mid-rapidity through the measurement of pseudo-rapidity distribution of charged particles $dN/d\eta$ in $\sqrt{s_{NN}} = 10$ TeV $p + p$ collisions and $\sqrt{s_{NN}} = 5.5$ TeV Pb+Pb collisions at LHC³. This report describes the status of a preparation for the measurement of $dN/d\eta$.

Simulation study for $dN/d\eta$ was done, and the correction factor was evaluated. $dN/d\eta$ can be measured using the ALICE Time Projection Chamber (TPC), which is the main detector for tracking in the central barrel⁴. AliRoot, the ALICE software package, can provide event generation, simulation of the detector response, and reconstruction. The reconstructed tracks are recorded as ESD (Event Summary Data) tracks which have labels corresponding to the ID number of generated particles. Therefore, the reconstruction efficiency can be evaluated from the comparison between generated particles (MC particles) and ESD tracks using labels. PYTHIA 6 event generator was adopted, and 277,500 events of minimum-bias $p + p$ collisions at $\sqrt{s} = 10$ TeV were used.

The detection efficiency is assumed to depend on pseudo-rapidity, and transverse momentum. Therefore, $dN/d\eta$ is calculated as

$$\frac{dN}{d\eta} \Big|_{\eta=\eta'} = \int_{p_{T1}}^{p_{T2}} C(\eta', p_T) \left(\frac{dN}{dp_T d\eta} \right)_{\text{ESD}} dp_T \times C'_{p_{T\text{cut}}}(\eta') \quad (1)$$

where the integration is executed for the available region of p_T . $C(\eta', p_T)$ is the correction factor obtained as $C(\eta, p_T) = \frac{N_{\text{gen}}(\eta, p_T)}{N_{\text{acc}}(\eta, p_T)}$. $N_{\text{acc}}(\eta, p_T)$ and $N_{\text{gen}}(\eta, p_T)$ are the numbers of charged particles accepted and generated, respectively. $C'_{p_{T\text{cut}}}(\eta')$ is the correction factor due to the p_T cutoff. In this analysis, particles of $p_T < 0.3$ GeV are cut.

Figure 1 shows the projections of $1/C(\eta, p_T)$ to η and p_T , which corresponds to the reconstruction efficiency of the TPC for charged particles, where any feed-down

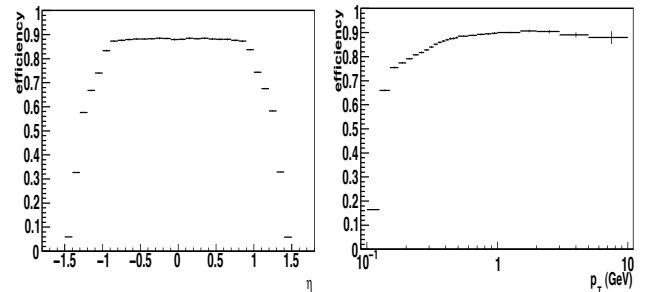


Fig. 1. The reconstruction efficiencies for charged particles as a function of η and p_T . These are the projections of $1/C(\eta, p_T)$ to η and p_T .

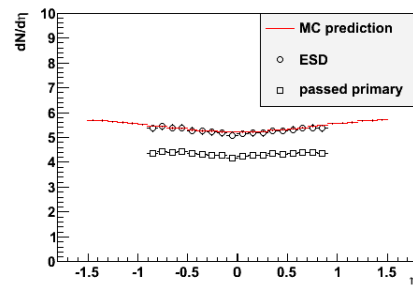


Fig. 2. Comparison of $dN/d\eta$ between MC prediction and ESD. Circles show the result of ESD analysis and squares show the plots for only primary particles passed the cut of ESD analysis.

correction is not applied.

Figure 2 shows the comparison of $dN/d\eta$ between MC prediction (lines) and this analysis with the correction according to Eq. 1. (circles). The result of this analysis (circles) includes both primary particles and secondary particles which passed the cut of this analysis. Squares in Fig. 2 show the plots for only primary particles. The ratio of the true primary particles to ESD plots (circles) of Fig. 2 is about $82 \pm 2\%$ at $|\eta| < 0.5$.

References

- 1) L.V. Gribov, E.M. Levin, M.G. Ryskin, Phys. Rep.100 (1983) 1.
- 2) L. McLerran, R. Venugopalan, Phys. Rev. D49 (1994) 2233.
- 3) D. Kharzeev, E. Levin, M. Nardi, Nucl Phys A 747 (2005) 609.
- 4) ALICE Collaboration. "ALICE TPC Technical Design Report". CERN/LHCC 2000-001.

^{*1} Center for Nuclear Study (CNS), University of Tokyo, Japan

^{*2} Gesellschaft für Schwerionenforschung (GSI), Germany

4. Hadron Physics (Theory)

Nuclear Force from String Theory[†]

K. Hashimoto,^{*1} T. Sakai,^{*2} and S. Sugimoto^{*3}

[Nuclear force, Superstring theory]

We compute nuclear force in a holographic model of QCD on the basis of a D4-D8 brane configuration in type IIA string theory. Repulsive core of nucleons is quite important in nuclear physics, but its origin has not been well-understood in strongly-coupled QCD. We find that string theory via gauge/string duality deduces this repulsive core at short distance between nucleons. Since baryons in the model are realized as solitons given by Yang-Mills instanton configuration on flavor D8-branes, ADHM construction of two instantons probes well the nucleon interaction at short scale, which provides the nuclear force quantitatively. We obtain, as well as a tensor force, a central force which is strongly repulsive as suggested in experiments and lattice results. In particular, the nucleon-nucleon potential $V(r)$ (as a function of the distance) scales as r^{-2} , which is peculiar to the holographic model. We compare our results with one-boson exchange model using the nucleon-nucleon-meson coupling obtained in our previous paper²⁾.

Nuclear force, the force between nucleons, exhibits a repulsive core of nucleons at short distances. This repulsive core is quite important for large varieties of physics of nuclei and nuclear matter. For example, the well-known presence of nuclear saturation density is essentially due to this repulsive core. However, from the viewpoint of strongly coupled QCD, the physical origin of this repulsive core has not been well-understood. In spite of the long history of the problem, it was rather recent that lattice QCD could reach the problem, and of course any understanding of it based on analytic computations is quite helpful for revealing basic nature of nuclear and hadron physics.

Recent rapid progress in applying gauge/string duality to QCD, holographic QCD, is really surprising. Now it has been made possible to compute various observables in hadron physics such as spectra of mesons/baryons/glueballs and interactions among them. Although most of the works rely on the supergravity approximation that works for large N_c and large 't Hooft coupling λ , it turned out that the holographic QCD reproduces quite well the properties of hadrons not only qualitatively but also quantitatively.

We apply this gauge/string duality to the problem of nuclear force. In our previous paper²⁾, we computed

nucleon-nucleon-meson couplings, by using the holographic QCD based on a D4-D8 brane configuration in type IIA string theory¹⁾, which incorporates chiral quark dynamics. This amounts in principle to computing the large distance behavior of nuclear force, as the potential between two nucleons can be understood as exchange of mesons among them. In this paper, we make one step further: by directly solving the two-nucleon system in the D4-D8 model of the holographic QCD, we find shorter distance scale of the nuclear force.

In fact, we find the repulsive core of nucleons. Our computation shows the following result for the central and tensor forces,

$$V_C(|\vec{r}|) = \pi \left(\frac{27}{2} + \frac{32}{5} (I_1^a I_2^a) (J_1^b J_2^b) \right) \frac{N_c}{\lambda} \frac{1}{|\vec{r}|^2}, \quad (1)$$

$$V_T(|\vec{r}|) = \frac{8\pi}{5} I_1^a I_2^a \frac{N_c}{\lambda} \frac{1}{|\vec{r}|^2}. \quad (2)$$

This is, first of all, repulsive, and second, has $1/r^2$ dependence. The r -dependence is peculiar to the four-dimensional space, not the three-dimensional harmonic potential. The appearance of the $1/r^2$ potential is due to the extra holographic dimension, thus typical in holographic description. Physically speaking, the Kaluza-Klein summation of all the meson states in the tower produces this new behavior.

The main reason why the force is repulsive is as follows. In holographic QCD, global symmetries of QCD are upgraded to local ones via the correspondence, and so baryon number carried by the baryon is coupled to local gauge fields in higher dimensions. This produces the repulsive force. The Kaluza-Klein decomposition of the higher-dimensional gauge fields provides a mass tower starting with ω meson as the lightest vector meson¹⁾, and so, our computation shows that the repulsive force is partly due to the ω meson exchange. Not only the ω meson but also the whole massive mesons participate in the nuclear force, and resultantly, the nucleon-nucleon potential becomes $1/r^2$.

It would be very interesting if our results can be consistently compared with lattice results or empirically known potentials used in “ab-initio” calculations of nuclear spectra.

References

- 1) T. Sakai and S. Sugimoto, Prog. Theor. Phys. **113**, 843 (2005), Prog. Theor. Phys. **114**, 1083 (2005).
- 2) K. Hashimoto, T. Sakai and S. Sugimoto, Prog. Theor. Phys. **120**, 1093 (2008).

[†] Condensed from the article in Prog. Theor. Phys. **122**, 427 (2009)

^{*1} Theoretical Physics Laboratory, RIKEN

^{*2} Department of Physics, Ibaraki University

^{*3} Institute for the Physics and Mathematics of the Universe, University of Tokyo

Quark fragmentation functions in the NJL-jet model[†]

W. Bentz,^{*1} T. Ito,^{*1} I. C. Cloët,^{*2} A. W. Thomas,^{*3} and K. Yazaki^{*4}

[QUARK FRAGMENTATION FUNCTIONS, Semi-inclusive pion production, Deep inelastic scattering]

Quark distribution and fragmentation functions are the basic nonperturbative ingredients for a QCD-based analysis of hard scattering processes. In this paper we show the results of recent calculations of fragmentation functions in the NJL-jet model¹⁾.

The spin-independent fragmentation function for the process $q \rightarrow h$ is defined by

$$D_q^h(z) = \frac{z}{12} \int \frac{d\omega^-}{2\pi} e^{ip-\omega^-/z} \sum_n \langle p(h), p_n | \bar{\psi}(0) | 0 \rangle \gamma^+ \langle 0 | \psi(\omega^-) | p(h), p_n \rangle.$$

The field operators refer to a quark of flavour q , the symbol $p(h)$ refers to a hadron h with momentum p , and p_n labels the spectator state. The light-cone components of a 4-vector a^μ are defined by $a^\pm = a_\mp = (a^0 \pm a^3)/\sqrt{2}$. From this definition one can derive the expression

$$D_q^h(z) dz = \frac{1}{6} dp_- \int d^2 p_\perp \sum_\alpha \frac{\langle k(\alpha) | a_h^\dagger(p) a_h(p) | k(\alpha) \rangle}{\langle k(\alpha) | k(\alpha) \rangle},$$

where the creation and annihilation operators refer to the hadron h , $k(\alpha)$ labels a quark state of flavour q with momentum k and spin-color α , and $p_- = zk_-$ for some fixed $k_- > 0$. The above result can be interpreted as the light-cone momentum distribution of the hadron h in the quark q .

The momentum and isospin sum rules obtained from the above formula are

$$\sum_h \int_0^1 dz z D_q^h(z) = 1, \quad \sum_h \int_0^1 dz t_h D_q^h(z) = t_q.$$

The condition which lies at the basis of these sum rules is that the initial quark state is an eigenstate of the momentum and isospin operators, expressed solely in terms of hadrons. Their physical content is that 100% of the initial quark light-cone momentum (k_-) and isospin (t_q) are transferred to the hadrons. (Note that the definition of the fragmentation function implies an average over the isospin of the soft quark remainder of a fragmentation chain.)

In order to satisfy the momentum and isospin sum

rules, it is necessary to take into account the possibility that the fragmenting quark produces a cascade of mesons. In order to describe these multi-fragmentation processes, we use the ideas of the quark jet model of Field and Feynman²⁾. Assuming that the fragmenting quark can produce a maximum of N mesons, we make a product ansatz to express the total fragmentation function as a product of N elementary splitting functions. Because only in the limit $N \rightarrow \infty$ it becomes possible to transfer 100% of the initial quark momentum and isospin to the mesons, we take this limit in the final results. The details of this product ansatz can be found in Ref.¹⁾.

In the numerical calculations we take into account the fragmentation to pions only. The results for the “favored” fragmentation process $u \rightarrow \pi^+$ are shown in Fig. 1. This figure demonstrates the tremendous enhancement of the fragmentation function arising from the cascade-type multi-fragmentation processes. In order to improve the agreement with the empirical fragmentation function, one should perform the Q^2 evolution in next-to-leading order, and include the effects of fragmentation processes to other hadrons, mainly the nucleons, antinucleons and kaons.

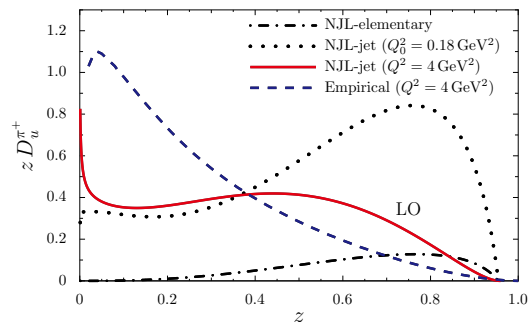


Fig. 1. Fragmentation function $zD_u^{\pi^+}(z)$. The dash-dotted line is the elementary fragmentation function, and the dotted line is the full fragmentation function in the NJL-jet model. The solid line is the result after LO evolution to $Q^2 = 4 \text{ GeV}^2$, and the dashed line is the empirical NLO result of Ref.³⁾, evolved to $Q^2 = 4 \text{ GeV}^2$.

[†] Condensed from an article by T. Ito, W. Bentz, I.C. Cloët, A.W. Thomas and K. Yazaki, Phys. Rev. D **80** (2009) 074008.

^{*1} Department of Physics, Tokai University, Kanagawa, Japan

^{*2} Department of Physics, University of Washington, Seattle, WA, U.S.A.

^{*3} University of Adelaide, Adelaide, Australia

^{*4} Radiation Laboratory, RIKEN, Saitama, Japan

References

- 1) T. Ito, W. Bentz, I.C. Cloët, A.W. Thomas, K. Yazaki, Phys. Rev. D **80**, 074008 (2009).
- 2) R. D. Field and R. P. Feynman, Phys. Rev. D **15**, 2590 (1977).
- 3) M. Hirai, S. Kumano, T. H. Nagai and K. Sudoh, Phys. Rev. D **75**, 094009 (2007).

Nucleon structure functions in 2+1-flavor dynamical DWF QCD[†]

S. Ohta,^{*1*2*3} for RBC and UKQCD Collaborations

[Quantum Chromodynamics, Hadron Physics, Nucleon Structure]

Nucleon structure functions were first measured by lepton deep-inelastic scattering off nucleon¹. The RHIC Spin experiments², of which RIKEN Nishina Center is a major participant through RIKEN-BNL Research Center, plan to measure some new types of the structure functions such as transverse-polarized spin structure function, as well as more conventional unpolarized or longitudinally polarized ones.

RIKEN-BNL-Columbia (RBC) collaboration worked on numerical lattice-QCD theoretical calculations of moments of these structure functions^{3,4}, as well as nucleon elastic form factors^{4,5}. More recently the UKQCD collaboration joined the effort: Based on our realistic 2+1-flavor dynamical domain-wall quark lattice-QCD numerical ensembles⁶, we reported an unexpectedly huge finite-size effect on axialvector-current form factors of nucleon^{7,8}. It appears a lattice spatial volume larger than $(\sim 7 \times m_\pi^{-1})^3$, or $(\sim 10\text{fm})^3$ at the physics point, would be necessary to accurately calculating these form factors to within 1% accuracy, in contrast the volumes of $(\sim 4 \times m_\pi^{-1})^3$, or $(\sim 3\text{fm})^3$ at unphysical $m_\pi \sim 300\text{MeV}$, presently used in our state-of-the-art calculations.

A question thus arises whether such small volumes presently used are sufficient for the structure function calculations. Small volumes may indeed be sufficient as the structure functions are measured in deeply inelastic processes, in contrast to the elastic form factors. During the past year the RBC and UKQCD collaborations tested if our present volumes are sufficient by comparing the calculations on two volumes, the smaller $(\sim 1.8\text{fm})^3$ and the larger $(\sim 2.7\text{fm})^3$, of the lowest moments, the isovector quark momentum fraction, $\langle x \rangle_{u-d}$, the first moment of the unpolarized structure function, and the isovector quark helicity fraction, $\langle x \rangle_{\Delta u-\Delta d}$, the first moment of the polarized⁹.

The ratio, $\langle x \rangle_{u-d}/\langle x \rangle_{\Delta u-\Delta d}$, of these two moments is summarized in Fig. 1: no discernible volume nor mass dependence can be observed while agreement with experiment is excellent. This is in clear contrast to a similarly naturally renormalized ratio of isovector axial and vector charges, g_A/g_V , which deviates away from experiment because of the huge finite-size effect^{7,8} that becomes severe in the region where a parameter $m_\pi L$, the product of pion mass m_π and lattice linear extent L , is below 7. The absolute values of the quark momentum and helicity fractions also do not show any volume dependence, but show encouraging

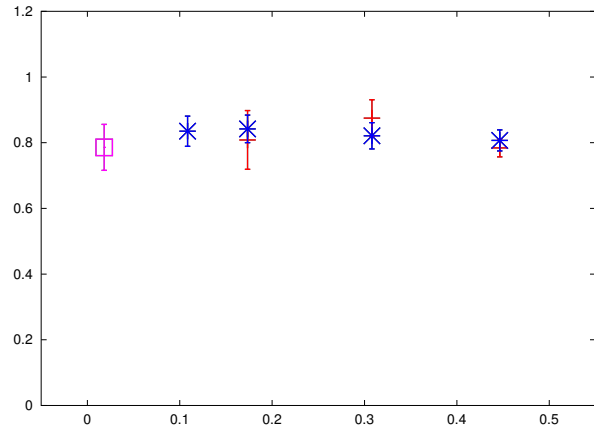


Fig. 1. Ratio of the quark momentum and helicity fractions, plotted against pion mass squared, m_π^2 , in GeV^2 : \times 's denote results from larger $(2.7\text{fm})^3$ volume, $+$'s from the smaller $(1.8\text{fm})^3$, and \square the experiment.

trending toward experiments at low quark mass. These results suggest low moments of nucleon structure functions in general can be calculated on a relatively small lattice volume, as small as $(\sim 3 \times m_\pi^{-1})^3$, or $(\sim 5\text{fm})^3$ at the physical pion mass, in contrast to axialvector form factors that require much larger volume^{7,8}.

I thank the RBC and UKQCD Collaborations. RIKEN, Brookhaven National Laboratory and the US DOE, Edinburgh University and the UK PPARC provided the facilities essential for this work.

References

- 1) J.I. Friedman, H.W. Kendall and R.E. Taylor, Rev. Mod. Phys. **63**, 629 (1991); J.I. Friedman, *ibid.* 615; H.W. Kendall, *ibid.* 597; R.E. Taylor, *ibid.* 573.
- 2) G. Bunce *et al.*, [RHIC Spin], (2008), http://spin.riken.bnl.gov/rsc/report/spinplan_2008/spinplan08.pdf.
- 3) K. Orginos *et al.*, [RBC], Phys. Rev. D **73**, 094503 (2006) [arXiv:hep-lat/0505024].
- 4) H.W. Lin *et al.*, [RBC], Phys. Rev. D **78**, 014505 (2008) [arXiv:0802.0863 [hep-lat]].
- 5) S. Sasaki *et al.*, [RBC], Phys. Rev. D **68**, 054509 (2003) [arXiv:hep-lat/0306007].
- 6) C. Allton *et al.*, [RBC+UKQCD], Phys. Rev. D **78**, 114509 (2008).
- 7) T. Yamazaki *et al.*, [RBC+UKQCD], Phys. Rev. Lett. **100**, 171602 (2008) [arXiv:0801.4016 [hep-lat]].
- 8) T. Yamazaki *et al.*, [RBC+UKQCD], Phys. Rev. D **79**, 114505 (2009) [arXiv:0904.2039 [hep-lat]].
- 9) S. Ohta, [RBC+UKQCD], PoS (LAT2009) 131 (2010) [arXiv:0910.5686 [hep-lat]].

^{*1} Institute of Particle and Nuclear Studies, KEK

^{*2} SOKENDAI Graduate University of Advanced Studies

^{*3} RIKEN BNL Research Center

A first principles calculation of proton decay matrix elements

Y. Aoki*¹ [RBC and UKQCD collaborations]

[Lattice QCD, grand unified theories]

Proton decay, once observed, is a smoking gun evidence of the physics beyond the standard model. It naturally happens under (SUSY) GUT. On-going deep mine experiments, though yet to observe an event, are pushing up the lower bound of the proton lifetime, excluding GUT models which allow protons decay more frequently. Hadronic matrix elements, especially the relevant form factor W_0 of the proton decay are essential ingredients in estimating lifetime of proton. Lattice QCD provides the most reliable estimate for such low energy hadronic quantities.

A partial decay width, e. g. for $p \rightarrow \pi^0 + e^+$, reads

$$\Gamma(p \rightarrow \pi^0 + e^+) \propto |C \cdot W_0(p \rightarrow \pi^0)|^2,$$

where C depends mass spectrum of underlying (SUSY) GUT theory (X boson mass, sfermion masses \dots). $W_0(p \rightarrow \text{meson})$ is the relevant form factor of the proton to meson transition with a certain three-quark baryon number violating operator. The partial lifetime is given by $\tau = 1/\Gamma$.

The form factor W_0 of one body decay ($p \rightarrow \text{meson}$), which are process and operator dependent, can be directly calculated through a combination of three- and two-point functions on the lattice. There is also a method to calculate the matrix element by using an approximation through chiral perturbation theory reduction, where two low-energy constants need to be calculated on the lattice. Since the former (direct method) requires many types of quark correlation functions, it is more demanding (typically factor 10 computer time) than latter (indirect method).

In our first attempt¹⁾ to calculate the matrix elements, we have used the domain-wall lattice fermion formulation, which preserves the chiral symmetry in a precision sufficient to protect the operator mixing due to lattice artifact. The direct calculation was performed using the quenched approximation where all the sea quark effects were neglected by hand. We also performed the indirect calculation, where we have checked that 1) the systematic error on the low energy constants from the finite lattice spacing is negligible, and 2) those from the quenching appeared to be small by comparing quench (dynamical number of flavor $n_f = 0$) and $n_f = 2$ computations. We also have developed the non-perturbative renormalization (NPR) scheme for the baryon number violating three quark operators, which helped to reduce the systematic error compared to the perturbative renormalization scheme employed in all lattice calculations performed by then. An important outcome of this pilot

study is that the indirect approximation always underestimates the magnitude of the matrix elements, thus, is unjustifiably generous for any (SUSY) GUTs. Although the indirect method is good to an order-of-magnitude precision, the more demanding, direct calculation must be performed for more accuracy.

We now can perform a first principles calculation of the proton decay form factors, using the $n_f = 3$ domain-wall fermion simulation to take into account all the light sea quark effects. As the pilot study indicate, the use of chiral fermion formulation with our NPR help keep the systematic error under control. First we have looked at the the low energy constants α and β^2 . They appeared to be consistent with the $n_f = 0$ and 2. We are now calculating the all possible $p \rightarrow$ pseudoscalar meson form factors. The preliminary result is given in Fig. 1.

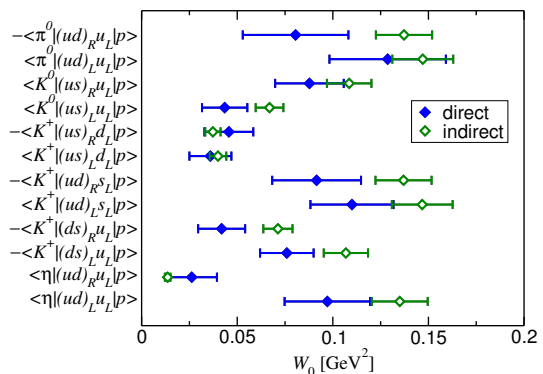


Fig. 1. Preliminary result of relevant form factors W_0 of the proton decay matrix elements in the full dynamical domain-wall quark calculation. Operators have been matched to $\overline{\text{MS}}$, NDR at $\mu = 2$ GeV, using NPR.

For the current precision the results are consistent with the quenched ones¹⁾. Results from the proper direct calculation pose more stringent constraint to (SUSY) GUTs than the indirect calculation. They are closer to the lower bound of the various phenomenological estimates, which had been used for the conservative estimate of the proton lifetime. Improvement of this result is underway by increasing the statistics. and through more elaborate analysis.

This project is supported in part by US DOE through USQCD collaboration, Japanese MEXT grant Kakenhi No. 21540289.

References

- 1) Y. Aoki et al., Phys. Rev. D75 (2007) 014507.
- 2) Y. Aoki et al., Phys. Rev. D78 (2008) 054505.

*¹ RIKEN-BNL Research Center

Quark masses from lattice QCD and QED[†]

T. Izubuchi^{*1*2} and T. Ishikawa,^{*2*3} for RBC and UKQCD Collaborations

Lattice QCD+QED determination of the most basic parameter, the masses of up, down, and strange quarks, is presented. We take into account the isospin (and $SU(3)_F$) breaking effect due to different masses and electric charges among up, down and strange quarks based on dynamical lattice QCD simulation including electromagnetic (QED) effects, which are needed for accurate hadron mass analysis. This is the the world first determination of quark masses directly addressing the two sources of isospin breaking using lattice chiral quarks with $N_F = 2 + 1$ dynamical quark effects.

We perform the lattice QCD with photon coupled to electromagnetic (EM) charge of quarks following the pioneering work¹⁾. The photon field, $A_{em,\mu}(x)$, in its non-compact implementation, is generated in the Feynman gauge with eliminating the diverging zero modes. The gluon field ensembles are generated by RBC and UKQCD collaborations²⁾ using the domain-wall fermions (DWF) as lattice quarks. The detail settings and parameters of the simulation are in 3). Since the photon field is not confined, it propagates for longer distances than the gluon field. Results from two lattice volumes, $V = (16a = 1.84\text{fm})^3$ and $(24a = 2.75\text{fm})^3$, are compared to each other to check the finite volume effects. We found that averaging over meson propagators of positive (+e) and negative QED charges (-e) is very useful to reduce the statistical noise⁴⁾ since its $\mathcal{O}(e)$ contribution to the noise is explicitly cancelled in the average keeping the physical signal, which is $\mathcal{O}(e^2)$.

We fit the psuedosclar mass $M_{PS}(m_1, q_1, m_3, q_3; m_i)$, made of quark pairs $\psi_1(x)$ and $\psi_3(x)$, each pair of whose charge and mass is (m_i, q_i) with $i = 1, 3$ using both of $SU(3) + \gamma$ chiral perturbation theory (ChPT) and $SU(2) + \text{Kaon} + \gamma$ ChPT. The latter is derived by ourselves for the first time and is preliminary. From the fit, we obtained the physical quark masses by solving the three equations of ChPT meson mass formula for π^\pm (139.57018(35) MeV), K^\pm (493.677(13) MeV), and K^0 (497.614(24) MeV) treating the three quark masses $m_{\text{up}}, m_{\text{down}}, m_{\text{strange}}$ as unknown variables. The preliminary results are shown in Table 1. The disconnected quark loops, needed for π^0 , is not calculated in our simulation, so we refrain from using π^0 mass in this work.

We will reduce the discretization error using finer lattice ensemble, and the chiral extrapolation error us-

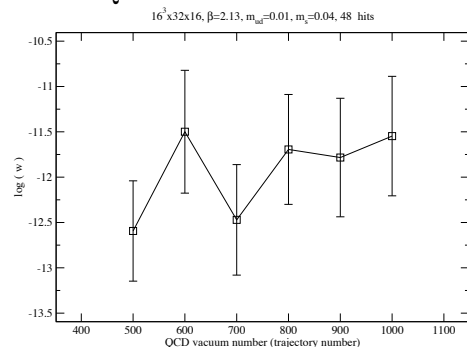


Fig. 1. $\log(w)$ for several QCD vacuum.

Fit, V	m_{cut}	m_{up}	m_{down}	m_{strange}
SU(3), (2.7 fm) ³	40	2.76(26)	4.80(46)	95(9)
SU(3), (2.7 fm) ³	70	2.55(23)	4.78(46)	95(9)
SU(3), (1.8 fm) ³	70	2.93(19)	4.85(29)	95(5)
SU(3) δm_{res} , (2.7 fm) ³	40	2.52(24)	4.74(45)	95(9)
SU(2) (2.7 fm) ³	70	2.24(16)	4.62(24)	101(5)

Table 1. Preliminary determinations of quark masses in MeV in $\overline{\text{MS}}(\text{NDR})$ at $\mu = 2$ GeV using SU(3) ChPT+ γ fit. Errors are only statistical. The last two rows are the fit results with an alternative treatment for residual chiral symmetry breaking and the results from SU(2) fit.

ing lighter quark mass simulations. Other sources of systematic error include the dynamical EM charge effects. The correction for the missing EM charge of sea quark in the above results can be calculated by the reweighting factor, which is the ratio of the sea quark's Dirac determinants between with and without the EM charges:

$$w = \det \mathcal{D}(m_{ud}, m_s, e) / \det \mathcal{D}(m_{ud}, m_s, e = 0)$$

In Figure 1, $\log(w)$ for a few QCD vacuum is plotted. We found fluctuation among vacuum is under control: typical fluctuation for $\log(w)$ is less than three for this volume, which is an encouraging result for eliminating the error of the sea quark charges omission.

In Reference 3), we also presented preliminary results for the mass difference between Nucleon and Proton, which is an important necessary condition for the stability of the proton in this nature, as well as the break-up of the charge splitting of Kaon mass into the part coming from up, down quark mass difference and that from electromagnetic effects.

References

- 1) A. Duncan, *et. al.*, *Phys. Rev. Lett.* **76** (1996) 3894.
- 2) **RBC-UKQCD** Collaboration, C. Allton *et. al.*, *Phys. Rev.* **D78** (2008) 114509.
- 3) T. Izubuchi, in KAON09 Proceedings (2009).
- 4) T. Doi, *et. al.* *PoS LAT2006* (2006) 174.

[†] Condensed from Reference 3)

^{*1} Brookhaven National Laboratory, USA

^{*2} RIKEN-BNL Research Center, USA

^{*3} Physics Department, University of Connecticut, USA

^{*} We thank RIKEN, Brookhaven National Laboratory and US DOE, University of Edinburgh and UK PPARC for providing the facilities essential for the completion of this work.

QCD phase structure in three-flavor random matrix theory[†]

R. Arai*¹ and N. Yoshinaga*¹

[QCD, phase transition]

In hadron physics, the study of quantum chromodynamics (QCD) at finite temperatures and nonzero baryon densities is fascinating. Therefore, experimental studies on heavy ion collisions have been actively performed.

At zero temperature, for high isospin chemical potential $\mu_I \geq m_\pi/2$, pion condensation occurs. This is also predicted by chiral perturbation theories¹⁾ and has been observed in lattice QCD simulations²⁾. The extension of two-flavor analyses to the three-flavor case indicates that kaon condensation occurs in the region of high strangeness chemical potential $\mu_S \geq m_K$ ^{3,4)}. The kaon condensation is also expected to occur in high density nuclear matter such as neutron stars⁵⁾.

In a previous study, we constructed a three-flavor random matrix model with nonzero quark chemical potentials at a finite temperature⁶⁾. We found that QCD phase structure in the three-flavor random matrix model qualitatively agrees with that in chiral perturbation theory³⁾ and the three-flavor Nambu-Jona-Lasinio (NJL) model⁴⁾ at zero temperature.

In this report, we study the QCD phase diagram at a finite temperature and for a nonzero baryon number, nonzero isospin, and nonzero strangeness chemical potentials using the three-flavor random matrix model. In the case of zero baryon number chemical potential ($\mu_B = 0$), our model qualitatively agrees with QCD phase diagrams of the three-flavor NJL model⁴⁾.

A phase diagram in the (μ_B, T) plane for light quark masses m_u and m_d with $m_u = m_d = 0.01$ and the s quark mass $m_s = 0.25$ at finite isospin and finite strangeness chemical potentials is shown in Fig.1. Below the threshold values of pion and kaon condensation, the nonzero μ_I breaks the flavor symmetry for the light quarks and separates the lines of first-order phase transitions which coincide with each other for u and d quarks for $\mu_I = 0$. This observation agrees with the two-flavor random matrix model⁷⁾. Regarding the phase transition for s quarks, the line of first-order phase transition is in the regime of large baryon number chemical potential even if $\mu_S = 0$. The nonzero value of μ_S shifts the phase transition line toward larger baryon number chemical potentials. However, the critical temperature is not affected at all by the isospin and strangeness chemical potentials.

Our analysis gives very important results relating to actual instances where μ_B , μ_I , and μ_S are nonzero, such as the interior of neutron stars or relativistic

heavy ion collisions. An increase in μ_I results in the critical end point for u quarks being shifted toward smaller values of μ_B , as described for the two-flavor random matrix model⁷⁾. Consequently, reaching the critical end point for u quarks might become easier through relativistic heavy ion collision experiments. Similarly, an increase in μ_S results in the critical end point for s quarks being shifted toward larger values of μ_B . Thus, the critical phenomenon for s quarks is not expected to occur in heavy ion collision experiments, but only in the central interior region of neutron stars.

References

- 1) D.T. Son and M.A. Stephanov: Phys. Rev. Lett. **86**, 592 (2001).
- 2) J.B. Kogut and D.K. Sinclair: Phys. Rev. D **66**, 014508 (2002).
- 3) J.B. Kogut and D. Toublan: Phys. Rev. D **64**, 034007 (2001).
- 4) A. Barducci, R. Casalbuoni, G. Pettini, and L. Ravagli: Phys. Rev. D **71**, 016011 (2005).
- 5) N.K. Glendenning and J. Schaffner-Bielich: Phys. Rev. Lett. **81**, 4564 (1998).
- 6) R. Arai and N. Yoshinaga: Phys. Rev. D **78**, 094014 (2008).
- 7) B. Klein, D. Toublan, and J.J.M. Verbaarschot: Phys. Rev. D **68**, 014009 (2003).

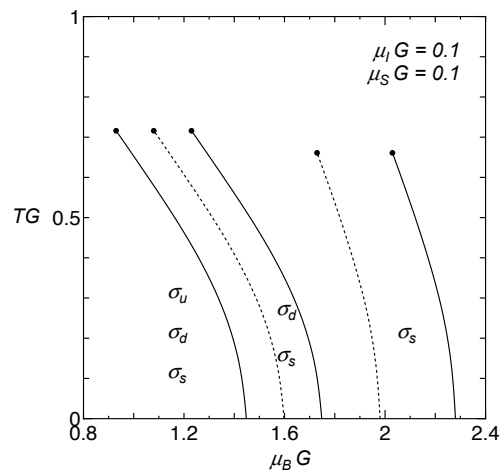


Fig. 1. Phase diagram in the (μ_B, T) plane with $m_u = m_d = 0.01$ and $m_s = 0.25$ for $\mu_I = \mu_S = 0.1$. The solid lines indicate lines of first-order phase transition for each flavor. The dotted lines indicate lines of first-order phase transition for $\mu_I = \mu_S = 0$. σ_u , σ_d , and σ_s represent chiral condensates for u , d , and s quarks, respectively.

[†] Condensed from the article in Phys. Rev. D **85**, 017501 (2009)

*¹ Department of Physics, Saitama University

Imaginary part of the real-time static potential at strong coupling[†]

A. Dumitru^{*1}

[QCD, AdS/CFT correspondence, Quarkonium, Quark-Gluon Plasma]

Consider the potential at finite temperature between static sources in a color singlet state defined via the expectation value of a Wilson loop

$$\exp[-it\mathcal{V}(r, T)] \equiv \langle W(C) \rangle . \quad (1)$$

The rectangular contour C extends over a spatial distance r and over a time $t \rightarrow \infty$. The expectation value $\langle W(C) \rangle$ could also be calculated as a function of Euclidean time τ but then requires analytic continuation, $\tau \rightarrow it$, before the limit $t \rightarrow \infty$ is taken¹. This makes it rather difficult to evaluate $\mathcal{V}(r, T)$ within non-perturbative lattice-QCD approaches.

At weak coupling the potential $\mathcal{V}(r, T)$ can be obtained directly from the Fourier transform of the physical “11” component of the resummed propagator for static gluons in the real-time (Schwinger-Keldysh) formalism of thermal field theory². Due to Landau damping of the exchanged gluon the resulting potential exhibits an imaginary part: for $rT \ll 1$, in the leading-logarithmic approximation it is proportional to $\text{Im } \mathcal{V} \sim -\alpha_s^2 C_F N_c T (rT)^2 \log(rT)^{-1}$. This translates into a width of the Υ state which is on the order of tens of MeV (at $T = 300$ MeV) and may lead to significant suppression of the $\Upsilon \rightarrow \ell^+ \ell^-$ process in heavy-ion collisions at RHIC and LHC³. We emphasize that this is not due to Debye screening of the *real* part of $\mathcal{V}(r, T)$ which indeed is weak at $rT < 1$.

The expectation value of $W(C)$ can also be calculated for $\mathcal{N} = 4$ SYM at large t’Hooft coupling, $\lambda = g^2 N_c \gg 1$, which at $N_c \rightarrow \infty$ admits a weakly coupled dual gravity description on $\text{AdS}_5 \times S_5$. The conformal $\mathcal{N} = 4$ SYM theory is used here as a toy model for the deconfined phase of QCD. An infinitely massive excitation in the fundamental representation of $SU(N_c)$ in the CFT is dual to a classical string in the bulk hanging down from a probe brane⁴. The configuration which minimizes the action of a static $Q\bar{Q}$ pair is a U-shaped curve that connects the string endpoints at the boundary and has a minimum at some U_* in AdS_5 . At finite temperature, the dual description of the gauge theory involves a near-extremal black brane in the bulk. The horizon is located at $U_h = \pi R^2 T$, where R denotes the radius of AdS_5 .

In the gravity description the imaginary part of the static potential is due to fluctuations about the extremal solution $U_c(x)$ ³. When the bottom of the string is sufficiently close to the horizon,

classical worldsheet fluctuations $\delta U(x)$ can generate an imaginary contribution to the action $S_{\text{NG}} \sim \int dx \sqrt{U'^2 + V(U)}$ when both $U_c'^2$ and $V(U_c)$ are small; i.e. near the bottom of the extremal string. This gives³

$$\text{Im } \mathcal{V}_{Q\bar{Q}} = -\frac{\pi}{24\sqrt{2}} \sqrt{\lambda} T \frac{3\zeta^4 - 1}{\zeta} \Theta(\zeta - 3^{-1/4}) \quad (2)$$

where $\zeta \equiv U_h/U_* < 1$. At small LT it follows from the zero-temperature solution⁴ that $LT = b\zeta$ with $b = 2\Gamma(3/4)/\sqrt{\pi}\Gamma(1/4)$.

The imaginary part of the potential shifts the Bohr energy level obtained from the Coulomb-like vacuum potential, $E_0 \rightarrow E_0 - i\Gamma$. For the ground state of the $\sim \sqrt{\lambda}/r$ potential, this shift amounts to

$$\Gamma_{Q\bar{Q}} = \frac{\pi\sqrt{\lambda}}{48\sqrt{2}} \frac{b}{a_0} \left[45 \left(\frac{a_0 T}{b} \right)^4 - 2 \right] , \quad (3)$$

where $a_0 = \Gamma(1/4)^4/2\pi^2\sqrt{\lambda}m_Q$ is the Bohr radius. The width decreases with the quark mass and with the t’Hooft coupling, approximately as $\Gamma_{Q\bar{Q}} \sim 1/\lambda m_Q^3$; it increases rapidly with the temperature, $\sim T^4$. For $m_Q = 4.7$ GeV, $T = 0.3$ GeV, $\sqrt{\lambda} = 3$ we obtain $\Gamma_\Upsilon \simeq 48$ MeV. This thermal width is small compared to the binding energy of the Υ but large compared to its electromagnetic decay width. Thus, a suppression of $\Upsilon \rightarrow \ell^+ \ell^-$ decays in heavy-ion collisions is expected,

$$R_{AA}(\Upsilon \rightarrow \ell^+ \ell^-) \simeq e^{-\bar{\Gamma}t} < 1 . \quad (4)$$

Here, $\bar{\Gamma}$ denotes an average of the decay rate over the life time t of the high-temperature phase. The experimental analysis of this process in heavy-ion collisions at RHIC is currently in progress⁵.

References

- 1) M. Laine, O. Philipsen, P. Romatschke and M. Tassler, *JHEP* **0703**, 054 (2007).
- 2) N. Brambilla, J. Ghiglieri, A. Vairo and P. Petreczky, *Phys. Rev. D* **78**, 014017 (2008); A. Dumitru, Y. Guo and M. Strickland, *Phys. Lett. B* **662**, 37 (2008); *Phys. Rev. D* **79**, 114003 (2009); O. Philipsen and M. Tassler, arXiv:0908.1746 [hep-ph].
- 3) J. Noronha and A. Dumitru, *Phys. Rev. Lett.* **103**, 152304 (2009).
- 4) J. M. Maldacena, *Phys. Rev. Lett.* **80**, 4859 (1998); S. J. Rey and J. T. Yee, *Eur. Phys. J. C* **22**, 379 (2001).
- 5) E. T. Atomssa [PHENIX Collaboration], *Nucl. Phys. A* **830**, 331C (2009).

^{*1} Department of Natural Sciences, Baruch College (CUNY), New York and RIKEN-BNL Research Center (RIKEN fellow)

5. Particle Physics

Tenth-order QED contributions to lepton $g-2$

T. Aoyama,^{*1} K. Asano,^{*2} M. Hayakawa,^{*2} T. Kinoshita,^{*3} M. Nio, and N. Watanabe^{*2}

[QED, anomalous magnetic moment, electron, muon]

The anomalous magnetic moment of electron, called $g-2$, plays a central role in testing the validity of quantum electrodynamics (QED). A Harvard team recently reported an astonishing result regarding a newly measured value of the electron anomaly $a_e = (g-2)/2^1$

$$a_e = 1\,159\,652\,180.73 (0.28) \times 10^{-12} (0.24 \text{ ppb}). \quad (1)$$

To match the experimental precision, the theory should take into consideration the QED contributions up to the tenth order of the perturbation theory. The largest uncertainty in the current theoretical value comes from the yet-uncalculated tenth-order contribution. There are 12672 vertex Feynman diagrams that contribute to the tenth-order $g-2$. They are further divided into 32 gauge-invariant sets, as shown in Fig. 1. The contributions from 17 sets, sets I(a-f), II(a,b), II(f), VI(a-c), VI(e,f), and VI(i-k), were previously determined by us.²⁾ In this article, we report our progress on the evaluation of the remaining 15 sets.

The first automation system we developed is *GENCODEN*, which deals with Feynman diagrams without fermion loops.³⁾ Given one-line information specifying a diagram, *GENCODEN* generates a set of FORTRAN programs that can be used for numerical evaluation. With the help of *GENCODEN*, we generated programs for sets III(a,b), IV, and V. The numerical evaluation of the sets III(a,b) and IV was relatively easy and we determined anomaly contributions from these sets. Set V consists of 6354 diagrams; its numerical evaluation is very difficult and requires large computational resources. For several years, RIKEN's Super-Combined Cluster System(RICC) had been used for the evaluation of set V. Since fall 2009, a new computer RIKEN's Integrated Cluster of Clusters(RICC) is being used for the numerical evaluation of set V. The evaluation is still in progress.

The second automation system, *GENCODEVPN*, deals with vacuum-polarization diagrams consisting of single lepton loops. This enables us to rapidly evaluate sets I(g,h), I(i), and II(c,d).⁴⁾

The last automation system, *GENCODELBLN*, deals with diagrams that include light-by-light scattering subdiagrams. The anomaly contributions from Sets IV(d,g,h) were then determined.

Sets II(e) and III(c) also include light-by-light scattering subdiagrams, but unlike in sets IV(d,g,h), none

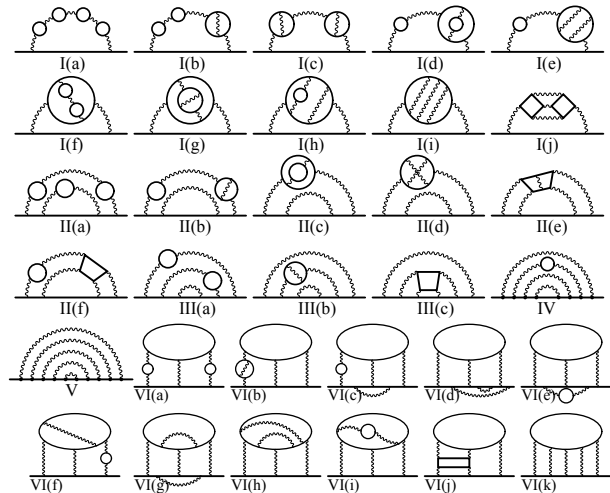


Fig. 1. Feynman diagrams contributing to the tenth-order lepton $g-2$. Typical diagrams from 32 gauge-invariant sets are shown. An external photon vertex is omitted for simplicity. There are 12672 vertex diagrams in total.

of the photon legs of a light-by-light scattering loop is an external magnetic field. Such a diagram requires a delicate treatment because a light-by-light scattering loop causes ultraviolet divergence. Nagoya group of the present authors investigated these diagrams, and the results they obtained were confirmed by an independent check by the rest of us.⁵⁾

The investigation of set I(j), which has a very different structure from other diagrams, was also dominated by the Nagoya Group. The result has been published.⁶⁾

At present, all the 32 gauge-invariant sets of the tenth-order diagrams has been investigated. Furthermore, we have computed the contributions to the muon $g-2$ from the diagrams involving fermion loops. We will soon determine the entire contributions of the tenth-order term to both electron and muon.

References

- 1) D. Hanneke, S. Fogwell, and G. Gabrielse: Phys. Rev. Lett. **100**, 120801 (2008).
- 2) T. Kinoshita and M. Nio: Phys. Rev. D **73**, 053007 (2006).
- 3) T. Aoyama, M. Hayakawa, T. Kinoshita, and M. Nio: Nucl. Phys. B **740**, 138 (2006); *ibid* **796**, 184 (2008).
- 4) T. Aoyama, M. Hayakawa, T. Kinoshita, and M. Nio: Phys. Rev. D **78**, 113006 (2008).
- 5) T. Aoyama, K. Asano, M. Hayakawa, T. Kinoshita, M. Nio, and N. Watanabe: Phys. Rev. D **81**, 053009 (2010).
- 6) T. Aoyama, M. Hayakawa, T. Kinoshita, M. Nio, and N. Watanabe: Phys. Rev. D **78**, 053005 (2008).

^{*1} Institute of Particle and Nuclear Studies, High Energy Accelerator Research Organization (KEK)

^{*2} Department of Physics, Nagoya University

^{*3} Laboratory for Elementary-Particle Physics, Cornell University

Color Magnetic Flux Tubes in Dense QCD[†]

M. Eto, E. Nakano,^{*1} and M. Nitta^{*2}

[High density QCD, Color superconductivity, Topological soliton]

Theoretical studies suggests that a color superconducting phase exists in the high-density, low-temperature region of the QCD phase diagram¹⁾. Such a state of matter is considered to occur in the core of compact stars. To capture their signatures, it is necessary to determine the various properties of color superconductivity.

In the three-flavor case, which we are interested in, and in higher-density regions where the effects of quark masses can be ignored and the three-flavor symmetry effectively holds, the color-flavor locking (CFL) phase would be generated with the order parameter

$$\Phi_{k\gamma}^{L(R)} = \epsilon_{ijk}\epsilon_{\alpha\beta\gamma}\langle q_{i\alpha}^{L(R)} C q_{j\beta}^{L(R)} \rangle \propto \delta_{k\gamma},$$

where i, j , and k and α, β , and γ are flavor and color indices, respectively. This diagonal configuration that locks flavor and color minimizes the free energy²⁾. In the CFL phase, the symmetry $G \simeq SU(3)_C \times SU(3)_L \times SU(3)_R \times U(1)_B$ breaks down to the diagonal symmetry $H \simeq SU(3)_{C+L+R} \equiv SU(3)_{C+F}$; here we consider the case where all the quarks are massless, and the left- and right-handed quarks are separated.

When a symmetry of a system is spontaneously broken in the ground state, various kinds of topological defects occur; these defects correspond to a non-trivial topology of the order parameter space. In this study, we investigate the vortices in the CFL phase^{4)–8)}. One might expect that stable vortices associated with breaking of the $U(1)_B$ symmetry, but this is only true for the confining phase such as a hadronic matter. Each of the vortices is unstable and decays into three non-Abelian vortices³⁾, which are found in color magnetic flux tubes⁷⁾. In the core of rotating stars, the generated non-Abelian vortices might form a vortex lattice, similar to the case of superfluid vortices in a helium superfluid or a Bose-Einstein condensate. The lattice structure of vortices can be determined from the details on vortex-vortex interaction.

The most significant features of the non-Abelian vortices are the additional NG zero modes associated with the additional breaking of symmetry that appear around the vortex string because of the creation of the vortex: $H = SU(3)_{C+F} \rightarrow K = [U(1) \times SU(2)]_{C+F}$. These modes parametrize the complex projective space $H/K = \mathbf{CP}^{23}$, and they are called orientational zero modes. Points in \mathbf{CP}^2 have a one-to-one correspon-

dence with the color degrees of freedom of the vortex.

In the study⁸⁾, we have obtained full numerical solutions for the semi-superfluid non-Abelian vortices for a wide range of parameters. We have analytically shown that both the scalar and gauge fields asymptotically behave as e^{-mr} , where $m = \min(m_G, m_\chi)$ and m_G and m_χ are the masses of the gluons and the traceless part of the scalar fields, respectively. We have also numerically evaluated the width of the color flux and found that it is not always equal to the penetration depth, which is the Compton wave length m_G^{-1} . When the gluon mass is smaller than the scalar masses, the width cannot exceed certain values that are determined on the basis of the masses of other fields; hence, we found that the color flux is confined to the scalar core.

In the study¹⁰⁾, we have explicitly shown the normalizability of the orientational zero modes and derived the low-energy effective world-sheet theory of a non-Abelian semi-superfluid vortex. To this end, we have generalized the derivation of the effective action of the BPS non-Abelian vortex string; the derivation was presented by Gorsky, Shifman and Yung⁹⁾. They found the decay constant (overall constant) in the \mathbf{CP}^{N-1} model to be $4\pi/g_s^2$ where g_s is a gauge coupling constant. In the present case of a non-Abelian vortex in the CFL phase, we have found that the decay constant in the \mathbf{CP}^2 model is not equal to $4\pi/g_s^2$ as in the BPS case. The decay constant can be greater or smaller depending on the parameter regions. Our study will be the first step in the investigation of the dynamics of semi-superfluid non-Abelian vortex strings, which will be relevant, for instance, in neutron star physics.

References

- 1) K. Rajagopal and F. Wilczek, arXiv:hep-ph/0011333.
- 2) M. G. Alford, K. Rajagopal, and F. Wilczek; Nucl. Phys. B **537**, 443 (1999)
- 3) E. Nakano, M. Nitta, and T. Matsuura; Phys. Rev. D **78**, 045002 (2008) Prog. Theor. Phys. Suppl. **174**, 254 (2008)
- 4) I. Giannakis and H. c. Ren; Phys. Rev. D **65**, 054017 (2002)
- 5) K. Iida and G. Baym; Phys. Rev. D **66**, 014015 (2002)
- 6) M. M. Forbes and A. R. Zhitnitsky; Phys. Rev. D **65**, 085009 (2002)
- 7) A. P. Balachandran, S. Dugal, and T. Matsuura; Phys. Rev. D **73**, 074009 (2006)
- 8) M. Eto and M. Nitta; Phys. Rev. D **80**, 125007 (2009)
- 9) A. Gorsky, M. Shifman, and A. Yung; Phys. Rev. D **71**, 045010 (2005)
- 10) M. Eto, E. Nakano, and M. Nitta; Phys. Rev. D **80**, 125011 (2009)

[†] Condensed from the article in Phys.Rev.D80:125007,(2009) and Phys.Rev.D80:125011(2009)

^{*1} Extreme Matter Institute, GSI, Darmstadt, Germany

^{*2} Department of Physics, and Research and Education Center for Natural Sciences, Keio University,

Scattering of Giant Magnons in $\mathbf{CP}^{3\dagger}$

Y. Hatsuda and H. Tanaka^{*1}

[AdS/CFT correspondence, Integrability, Solitons]

The gauge/gravity duality helps us to understand strongly coupled dynamics in gauge theory. The AdS/CFT correspondence¹⁾ is a useful tool to study this duality. Recently, Aharony, Bergman, Jafferis, and Maldacena (ABJM) proposed a three-dimensional $\mathcal{N} = 6$ superconformal Chern-Simons theory with the $U(N) \times U(N)$ gauge group.²⁾ This theory is used to describe the low-energy effective theory of multiple M2-branes. The ABJM model has another interesting feature. It provides a new example of the AdS/CFT correspondence. The dual string theory is the type IIA superstring theory on the $\text{AdS}_4 \times \mathbf{CP}^3$ background. Hereafter, we refer to this duality as the $\text{AdS}_4/\text{CFT}_3$ duality.

In the well-known duality between the four-dimensional $\mathcal{N} = 4$ super Yang-Mills and the type IIB superstrings on $\text{AdS}_5 \times \text{S}^5$, both theories have the integrable structures that play a key role in understanding the spectrum on both sides. The $\text{AdS}_4/\text{CFT}_3$ duality also has a similar integrable structure. The spectral problem for the ABJM model is converted to that for an alternating spin-chain model. Once the vacuum of the model is determined, the excitations over the vacuum, which are called magnons, are classified on the basis of the residual $SU(2|2)$ global symmetry. Each magnon bound-state has the following dispersion relation:

$$\epsilon_Q(P) = \sqrt{\frac{Q^2}{4} + 4h^2(\lambda) \sin^2\left(\frac{P}{2}\right)}, \quad (1)$$

where P is the total momentum, and the integer Q is the number of magnons. The function $h(\lambda)$ of the 't Hooft coupling λ behaves under weak or strong coupling as follows:

$$h(\lambda) = \begin{cases} \lambda + \mathcal{O}(\lambda^3) & (\lambda \ll 1), \\ \sqrt{\lambda/2} + \mathcal{O}(1) & (\lambda \gg 1). \end{cases} \quad (2)$$

The string duals of such magnon bound-states are known as dyonic giant magnons; these were originally discovered by Hofman and Maldacena.³⁾ In the $\text{AdS}_4/\text{CFT}_3$ duality, there are two kinds of dyonic giant magnons: one exists in the \mathbf{CP}^2 subspace of \mathbf{CP}^3 , and the other in \mathbf{RP}^3 .

The purpose of this study is to investigate the scattering of two \mathbf{CP}^2 dyonic giant magnons. The scattering matrix is a fundamental tool to study the AdS/CFT spectrum in the large R -charge/spin sector.

The S -matrix is also important for studying the finite-size effects by applying the Lüscher corrections in both string and gauge theories. The exact S -matrix of the $\text{AdS}_4/\text{CFT}_3$ duality has already been conjectured by Ahn and Nepomechie.⁴⁾ Since the \mathbf{CP}^2 dyonic giant magnons are new solutions, which do not exist in the case of $\text{AdS}_5 \times \text{S}^5$, it is important to investigate their scattering. This will be useful for understanding the spectral problem in the $\text{AdS}_4/\text{CFT}_3$ duality.

We computed the classical phase shift for the scattering of two \mathbf{CP}^2 dyonic magnons, and compared it with the conjectured S -matrix of two magnon bound-states in the large 't Hooft coupling limit. To compute the classical phase shift, we first constructed the general two-soliton solutions in the \mathbf{CP}^3 sigma-model. We used the dressing method, which is a useful technique to obtain multi-soliton solutions, for developing the $SU(4)/U(3)$ coset model. Next we evaluated the classical time delay from these two-soliton solutions. The phase shift was finally obtained by integrating the time delay with respect to the energy of one of two solitons.

Our computation shows that the classical scattering phase of \mathbf{CP}^2 dyonic giant magnons agrees with that of magnon bound-states in the ABJM model up to the gauge-dependent term. In the ABJM model, there are two types of excitations, that is, the odd-site excitations and even-site excitations. Our result shows two polarizations of dyonic giant magnons that correspond to these two kinds of excitations in the alternating spin-chain.

In this work, we focused on the classical aspects of the scattering phase. It is interesting to consider quantum (α') corrections of the scattering phase in the future work.

References

- 1) J. M. Maldacena: Adv. Theor. Math. Phys. **2**, 231 (1998) [Int. J. Theor. Phys. **38**, 1113 (1999)].
- 2) O. Aharony, O. Bergman, D. L. Jafferis, and J. Maldacena: JHEP **0810**, 091 (2008).
- 3) D. M. Hofman and J. M. Maldacena: J. Phys. A **39**, 13095 (2006).
- 4) C. Ahn and R. I. Nepomechie: JHEP **0809**, 010 (2008).

[†] Condensed from the article in JHEP **1002**, 085 (2010)

^{*1} Department of Physics, University of Tokyo

Gravitational Dual of Tachyon Condensation[†]

G. W. Gibbons,^{*1} K. Hashimoto,^{*2} and S. Hirano^{*3}

[Superstring theory, D-brane, Tachyon Condensation]

There has been considerable progress in understanding non-perturbative aspects of string theory with or without supersymmetries. These developments culminated in the gauge/string duality primarily in supersymmetric cases¹⁾, which would define string theory itself non-perturbatively, using conventional gauge theories in 4 spacetime dimensions. Meanwhile, in non-supersymmetric cases one of the most remarkable progress is the open string tachyon condensation²⁾. This describes pair-annihilation of D-branes and anti-D-branes, and should be incorporated in any kind of non-perturbative definition of string theory.

However, these two developments have been rather orthogonal to each other, except for two-dimensional string theories. In this note we study an open string tachyon condensation in the gauge/string duality and provide an example in which these two connect at the quantitative level.

In formulating tachyon condensations in the gauge/string duality, one immediate obstacle is that the mass squared of open string tachyons is of order $\mathcal{O}(1/\alpha')$ which may not be visible in the field theory limit $\alpha' \rightarrow 0$. However, there exist systems in which the open string tachyon mass remains of order $\mathcal{O}(1)$ (in an appropriate unit) in the limit $\alpha' \rightarrow 0$. One such example is a system of intersecting branes at angles. The mass squared of open string tachyons stretched between intersecting branes is proportional to θ/α' where θ is an angle. In this case we can take the $\alpha' \rightarrow 0$ limit, keeping θ/α' fixed finite. This type of open string tachyons manifest themselves as unstable modes in the gauge theory in the low energy $\alpha' \rightarrow 0$ limit of intersecting D-branes³⁾. In the present paper we consider a T-dual version of the system studied in³⁾ in the 't Hooft limit, $N \rightarrow \infty$ and $g_{YM} \rightarrow 0$ with $\lambda = g_{YM}^2 N$ fixed finite.

One of the most important aspects of open string tachyon condensation is that unstable D-branes which support open string tachyons disappear after the tachyons are condensed. Accordingly, Sen's conjecture states that the height of the tachyon potential equals the tension (energy density) of unstable D-branes²⁾. Hence the height of the tachyon potential is one of the most important and unambiguous quantities in the open string tachyon condensation. The main objective

of this paper is to compute the height of the tachyon potential both in the gauge theory and the dual AdS gravity for a large N D3-brane configuration and to see if they agree. We indeed find an exact agreement in the large N limit, thus providing an example of gravitational duals of open string tachyon condensation.

We consider a brane configuration of a D3-D1 bound state parallel to coincident N D3-branes at some distance. The low energy description of this system is given by $\mathcal{N} = 4 U(N+1)$ super Yang-Mills (SYM) theory. A D1-brane on D3-branes is represented by a magnetic flux. Our brane configuration is thus described by the following gauge and adjoint scalar fields

$$F_{23} = \text{diag}(B, 0, 0, \dots), \Phi = \text{diag}(\phi, 0, 0, \dots), \quad (1)$$

There appears a tachyonic instability in this background, and the endpoint of the tachyon condensation is a bound state of $N+1$ D3-branes and D1-branes. The field configuration of the end point is

$$F_{23} = \text{diag}\left(\frac{B}{N+1}, \frac{B}{N+1}, \dots, \frac{B}{N+1}\right), \Phi = 0. \quad (2)$$

If we compute the energy difference of these two configurations by using the classical SYM hamiltonian, at large N , the difference of the energy yields

$$\mathcal{E}|_{\phi=\infty} - \mathcal{E}|_{\phi=0} = \frac{NB^2}{2\lambda} + \mathcal{O}(1). \quad (3)$$

This is the height of the tachyon potential at weak coupling.

At the strong coupling, if we use the AdS/CFT, we obtain an effective action

$$S = \frac{-1}{(2\pi)^3 g_s} \int d^4x \frac{U^4}{2\lambda} \left[\sqrt{1 + \frac{2(2\pi)^2 \lambda B^2}{U^4}} - 1 \right]. \quad (4)$$

where U directly corresponds to ϕ . Using this action, we can show that the energy difference between $U = \infty$ and $U = 0$ is precisely given by (3). We thus find an exact agreement.

In this note we provide an example of open string tachyon condensations in the gauge/string duality. The idea is to consider a brane configuration in which open string tachyons survive in the field theory $\alpha' \rightarrow 0$ limit. One can explore various similar brane set-ups by generalising the example we presented.

References

- 1) J. M. Maldacena, Adv. Theor. Math. Phys. **2**, 231 (1998).
- 2) A. Sen, JHEP **9808** (1998) 012; Int. J. Mod. Phys. **A14** (1999) 4061; JHEP **9912** (1999) 027.
- 3) A. Hashimoto and W. I. Taylor, Nucl. Phys. **B503** (1997) 193.

[†] Condensed from the article in JHEP **0909** (2009) 100

^{*1} DAMTP, University of Cambridge, Wilberforce Rd, Cambridge CB30WA, U.K.

^{*2} Theoretical Physics Laboratory, RIKEN

^{*3} The Niels Bohr Institute, Blegdamsvej 17, DK-2100, Copenhagen, Denmark

Eschenburg space as gravity dual of flavored $\mathcal{N}=4$ Chern-Simons-matter theory[†]

M. Fujita*¹ and T. -S. Tai*²

[String theory, Gravity/gauge correspondence]

The program towards studying gauge/gravity correspondence in the context of AdS_4/CFT_3 ¹⁾ becomes concrete owing to the pioneering work²⁾ by Aharony, Bergman, Jafferis and Maldacena last year. They found that constructing a much higher supersymmetric conformal field theory (SCFT) of Chern-Simons-matter (CSM) type is possible due to an elliptic brane setup in Type IIB string theory. Through T-duality and M-theory lift, one obtains N M2-branes filling (012) transverse to a 8D cone: $Cone(\mathcal{B}_7)$ ($\mathcal{B}_7 = S^7/\mathbf{Z}_k$) along (345678910). The corresponding gravity dual is thus a solution of 11D supergravity $AdS_4 \times \mathcal{B}_7$ after N M2-branes backreact.

Later on, generalizing their idea to yield elliptic $\mathcal{N} \geq 3$ SCFTs is done by attaching various kinds of $(1, k_i)5$ -branes on a stack of circular D3-branes. The resulting field theory at infra-red (IR) fixed point ($g_{YM} \rightarrow \infty$) is still of quiver CSM type with product gauge group $\prod_I U(N)_I$. Its Lagrangian is so rigid, i.e. CS level k_I w.r.t. I -th gauge factor is determined by two adjacent D5-brane charges $k_I = k_i - k_{i-1}$, while the superpotential is obtained by integrating out non-dynamical massive adjoint Φ_I (\subset vector multiplet) coupled to hypermultiplets in a typical manner.

Among many kinds of elliptic $\mathcal{N} \geq 3$ SCFTs, we will focus on a specific type of $\mathcal{N}=4$ SCFT which is constructed via IIB N circular D3- (0126), p NS5- (012345) and q $(1, k)5$ - (012[3, 7] _{θ} [4, 8] _{θ} [5, 9] _{θ}) branes. Note that θ (twisted angle) and $g_{YM}^2 k/4\pi$ (adjoint mass) are related to each other by (L : segment length on x^6)

$$\frac{\tan \theta}{L} = g_{YM}^2 k, \quad \frac{1}{g_{YM}^2} = \frac{L}{g_s}.$$

Taking IR limit implies naturally a strongly coupled M-theory picture. Its 11D gravity dual $AdS_4 \times \mathcal{M}_7$ parameterized by (k, p, q) is explicitly known³⁾ and this is the main reason why we study this kind of SCFT here.

In this note, motivated by works on the flavored $\mathcal{N}=6$ ABJM theory, we construct a new $\mathcal{N}=3$ SCFT by adding N_F massless fundamental flavors and study its gravity dual. From Type IIB picture, adding flavor corresponds to further attaching N_F D5-branes (012789) on the circle x^6 and results in a less supersymmetric $\mathcal{N}=3$ SCFT. This construction is by definition

an elliptic one, so in M-theory to have N M2-branes probing a 8D cone may thus be expected due to conformality.

We find that this turns out to be true and the dual geometry is now $AdS_4 \times \mathcal{M}_7$ parameterized by three natural numbers $(t_1, t_2, t_3) = (qN_F, pN_F, kpq)$ without any common factor. In fact, many properties of $\mathcal{M}_7(t_1, t_2, t_3)$ (modulo common factor) known as Eschenburg space have been explored by mathematicians. For example, $Cone(\mathcal{M}_7)$ is Ricci-flat with special $Sp(2)$ holonomy. Namely, it is hyperKähler and the base \mathcal{M}_7 must be tri-Sasakian (which preserves a fraction 3/16 of 32 SUSY). Moreover, the cone is available through applying a hyperKähler quotient to a 3D (flat) quaternionic space. The equivalence between two descriptions seems straightforward because three moment maps $\mu_Q = \sum_{i=1}^3 t_i \mu_i$, $p\mu_1 + q\mu_2$ and $kq\mu_2 + N_F\mu_3$ are linearly independent.

On the geometry side, we are led to compute the volume of 7-cycle of Eschenburg space by taking advantage of a formula given in⁵⁾. Also, the on-shell action of IIA probe D6-branes is taken care of. The correct embedding of D6-branes can be found by performing a further hyperKähler quotient to $Cone(\mathcal{M}_7)$. One obtains a 4D Taub-NUT space thereof over which flavor probes should wrap after doing KK reduction to IIA theory. In addition, we consider 5-cycles among \mathcal{M}_7 because M5-branes wrapped over them correspond to baryonic operators in the field theory.

References

- 1) J. M. Maldacena, Adv. Theor. Math. Phys. **2** (1998) 231
- 2) O. Aharony, O. Bergman, D. L. Jafferis and J. Maldacena, JHEP **0810** (2008) 091
- 3) Y. Imamura and K. Kimura, Prog. Theor. Phys. **120** (2008) 509
- 4) D. L. Jafferis and A. Tomasiello, JHEP **0810** (2008) 101
- 5) K. M. Lee and H. U. Yee, JHEP **0703** (2007) 012

[†] Condensed from the article in JHEP **062**, 0909 (2009)

*¹ Department of Physics, Kyoto University

*² Nishina Ctr., RIKEN

Genus-one correction to asymptotically free Seiberg-Witten prepotential from Dijkgraaf-Vafa matrix model[†]

M. Fujita^{*1}, Y. Hatsuda^{*2} and T. -S. Tai^{*2}

[Seiberg-Witten theory, Matrix model]

Recently, owing to a milestone discovery made by Alday, Gaiotto and Tachikawa,¹⁾ there have been lots of publications and research related to their work. In particular, Dijkgraaf and Vafa²⁾ proposed a Penner type matrix model whose classical spectral curve can reproduce the so-called Gaiotto curve \mathcal{G} .³⁾ Note that \mathcal{G} consists of a punctured Riemann surface $C_{g,n}$ whose moduli space $\mathcal{M}_{g,n}$ (g : genus, n : puncture) is referred to as a Teichmüller space. Surprisingly, $\mathcal{M}_{g,n}$ boils down to the space of exactly marginal gauge couplings of a large family of 4D $\mathcal{N} = 2$ superconformal gauge theories whose weakly-coupled *cusps* correspond to various patterns of colliding punctures on $C_{g,n}$. In addition, when $(g, n) = (0, 6)$ there appear *generalized* quiver SCFTs in contrast to known linear quiver SCFTs. Because \mathcal{G} is a rewritten Seiberg-Witten curve which emerges by taking a thermodynamic limit of Nekrasov's partition function $Z_{\text{Nekrasov}} = Z_{\text{classical}} Z_{1\text{-loop}} Z_{\text{inst}}$, attempts towards proving an equivalence between both sides are naturally expected.

At the level of \mathcal{F}_0 (tree-level free energy), Eguchi and Maruyoshi⁴⁾ showed that \mathcal{F}_0 (including asymptotically free cases) coincides with the original Seiberg-Witten prepotential. Moreover, all-genus proofs in certain restricted cases are presented by executing exact matrix integrals and comparing them with Z_{Nekrasov} .^{5,6)}

Motivated by these works, in this work we showed agreements between matrix model and field theoretical results on the genus-one free energy \mathcal{F}_1 of $\mathcal{N} = 2$ $SU(2)$ Seiberg-Witten theory with $N_f = 2, 3$.

On field theory side, the genus-one free energy is computed by the following formula:

$$\mathcal{F}_1 = b(u) - \frac{2}{3}c(u), \quad (1)$$

with

$$b(u) = \frac{1}{2} \log \left(\frac{du}{da} \right), \quad c(u) = \frac{1}{8} \log(\Delta_{SW}). \quad (2)$$

Here u stands for the gauge- and monodromy-invariant coordinate of the complex one-dimensional Coulomb branch, a is the electric period integral of the corresponding Seiberg-Witten curve, and Δ_{SW} denotes its discriminant. We evaluated $b(u)$ in terms of a large- u expansion (weak coupling expansion) for the $N_f = 2$ and 3 cases. For $N_f = 2$, we obtain

$$b(u) = \frac{3}{4} \log 2 - \frac{1}{4} \log \zeta - \frac{3\Lambda^2}{2048} (\Lambda^2 + 6m_1 m_2) \zeta^2 + \mathcal{O}(\zeta^3), \quad (3)$$

and for $N_f = 3$,

$$b(u) = \frac{1}{2} \log 2 - \frac{1}{4} \log \zeta - \frac{\Lambda^2}{2048} \zeta - \frac{\Lambda}{8388608} (7\Lambda^3 + 12288(m_1^2 + m_2^2 + m_3^2)\Lambda + 786432m_1 m_2 m_3) \zeta^2 + \mathcal{O}(\zeta^3), \quad (4)$$

where $\zeta = 1/u$, and we have denoted flavor bare masses and the dynamical scale by m_i 's and Λ respectively.

On matrix model side, if we consider two-cut solutions, the genus-one free energy is given by a universal form

$$\mathcal{F}_1 = -\frac{1}{24} \sum_{i=1}^4 \log M_i - \frac{1}{12} \log \Delta - \frac{1}{2} \log |K(\ell)| + \frac{1}{4} \log |(x_1 - x_3)(x_2 - x_4)|, \quad (5)$$

where x_i ($i = 1, \dots, 4$) are four branch points of two cuts, $\ell^2 = (x_1 - x_4)(x_2 - x_3)/(x_1 - x_3)(x_2 - x_4)$, $\Delta = \prod_{i < j} (x_i - x_j)^2$, and $K(\ell)$ is the complete elliptic integral of the first kind. The first term of the right hand side in Eq. (5) is an irrelevant term and can be omitted. We confirmed that the second term is equal to $-2c(u)/3$ while the last two terms just agree with $b(u)$ in the field theoretical computation.

In summary, we provided further evidence on the equivalence between a recently proposed Dijkgraaf-Vafa matrix model and low-energy dynamics of $\mathcal{N} = 2$ asymptotically free $SU(2)$ Yang-Mills theory with $N_f = 2, 3$ at the level of \mathcal{F}_1 . Showing perfect agreements with the field theoretical result, we thus extended the equivalence of Z_{DV} and Z_{Nekrasov} at next-to-leading order non-trivially.

References

- 1) L. F. Alday, D. Gaiotto and Y. Tachikawa, arXiv:0906.3219 [hep-th].
- 2) R. Dijkgraaf and C. Vafa, arXiv:0909.2453 [hep-th].
- 3) D. Gaiotto, arXiv:0904.2715 [hep-th].
- 4) T. Eguchi and K. Maruyoshi, arXiv:0911.4797 [hep-th].
- 5) R. Schiappa and N. Wyllard, arXiv:0911.5337 [hep-th].
- 6) A. Mironov, A. Morozov and S. Shakirov, arXiv:0911.5721 [hep-th].

[†] Condensed from the article in e-Print: arXiv:0912.2988 [hep-th]

^{*1} Department of Physics, Kyoto University

^{*2} Nishina Ctr., RIKEN

New Gauged Linear Sigma Models for 8D HyperKähler Manifolds and Calabi-Yau Crystals[†]

Y. Baba^{*1} and T. -S. Tai^{*1}

[String theory, 2D Sigma model]

A gauged linear sigma model (GLSM) in two dimensions¹⁾ is capable of describing a curved geometry (typically a symplectic or Kähler quotient space) through gauge theory language. More precisely, the isometry of the transverse internal space gets partially gauged and chiral multiplets on the worldsheet are coupled to corresponding gauge fields. Then, the curved geometry $\mathbf{C}^n//G$ arises as the supersymmetric vacuum (moduli space) of the 2D gauge theory. Note that $G = \mathbf{C}^{*r}$ stands for r complexified $U(1)$'s with moment maps

$$\mu : \mathbf{C}^n \rightarrow \mathbf{R}^r, \quad \mu^a = \sum_{i=1}^n Q_i^a |\phi_i|^2 - \rho^a, \quad a = 1, \dots, r$$

under the charge assignment Q_i^a . $\{\phi_i\}$ parameterizing \mathbf{C}^n represents the lowest component of $\mathcal{N}=(2,2)$ chiral superfield $\{\Phi_i\}$. μ^a 's are called Fayet-Iliopoulos (FI) parameters and correspond to bringing in r Kähler classes. Eq. (1) modulo the following gauge symmetry

$$\phi_i \sim \phi_i e^{i \sum_a Q_i^a \lambda^a}, \quad \lambda^a \in \mathbf{R}$$

is exactly the vacuum manifold denoted as $\mathbf{C}^n//G$ or $\mu^{-1}(0)/U(1)^r$.

Similarly, a hyperKähler quotient space is defined by $\mathbf{H}^n//\mathcal{G}$ ($\mathbf{H}^n \cong \mathbf{R}^{4n}$) where \mathcal{G} (\subset triholomorphic isometry) is generated by vector fields K 's with $\mathcal{L}_K g = 0$ (g : metric) and $\mathcal{L}_K I^\alpha = 0$. The 2-form complex structure I^α ($\alpha = 1, 2, 3$) is associated with each \mathbf{H} described by $ds^2 = |dq|^2 + |d\tilde{q}|^2$ ($q, \tilde{q} \in \mathbf{C}$) and transforms as a triplet under $SU(2)$. A quaternion $y + \mathbf{y}$ ($\mathbf{y} \in \mathbf{H}$ with a pure imaginary $\mathbf{y} = ui + vj + wk$ ($u, v, w \in \mathbf{R}$)) consists of two complex numbers: $q + \tilde{q}j$. For n quaternions, r moment maps associated with \mathcal{G} under a charge matrix Q_i^a will read

$$\sum_{i=1}^n Q_i^a (|q_i|^2 - |\tilde{q}_i|^2) = \xi^{3a}, \quad \sum_{i=1}^n Q_i^a 2q_i \tilde{q}_i = \xi^{1a} - i\xi^{2a}.$$

Here, triplets ξ 's are given level sets. By definition $\mathbf{H}^n//\mathcal{G}$ has real $4(n-r)$ dimensions.

In this note, we propose two kinds of GLSMs which have, respectively, 8D hyperKähler manifolds and Calabi-Yau (CY) 4-folds as their moduli spaces. Moreover, taking an infra-red (IR) limit leads to frozen kinetic terms of vector-multiplets. By integrating them out, a nonlinear sigma model (NL σ M) can be realized in the Higgs branch where its kinetic term pulls back the quotient space metric. The latter case is an $\mathcal{N}=(2,2)$ model whose Higgs branch realizes instead a CY 4-fold at IR. It is not Witten's one¹⁾ executing a symplectic quotient because it possesses key features of newly found 3D $\mathcal{N}=2$ Chern-Simons-matter theories on M2-branes probing toric CY 4-folds. That is,

usually F-term conditions (defining a master space) and D-term ones as a whole give a CY 3-fold just as the story in 4D $\mathcal{N}=1$ SCFT. However, because of one *dualized photon* appearing in the theory, the D-term associated with it becomes redundant due to *dynamical* Fayet-Iliopoulos (FI) parameters, then a 4-fold emerges thereof. Remarkably, we find these properties definitely show up in our model. The Lagrangian under consideration is $\mathcal{L} = \mathcal{L}_D + \mathcal{L}_F$ where

$$\begin{aligned} \mathcal{L}_D &= \int d^4\theta \frac{1}{2g^2} (P^\dagger + P + \mathbf{k} \cdot g^2 \sqrt{2}\mathbf{V})^2 - \sum_{a=1}^r \frac{1}{e_a^2} \Sigma_a^\dagger \Sigma_a \\ &+ \sum_i \mathcal{H}_i^\dagger e^{2V_{h(i)}} \mathcal{H}_i e^{-2V_{t(i)}} + \sum_{a=1}^r \Phi_a^\dagger e^{2V_a} \Phi_a, \\ \mathcal{L}_F &= \int d\theta^+ d\theta^- \mathcal{W} + c.c., \quad \mathbf{k} = (k_1, \dots, k_r). \end{aligned}$$

Note that \mathcal{W} denotes some generic superpotential. Taking $(e_a^2, g^2) \rightarrow \infty$, what we are left with are (bosonic part only)

1. Kinetic terms of (h_i, ϕ_a) (bosonic component of (\mathcal{H}_i, Φ_a))
2. A rennant:

$$-g^2(\partial\gamma + \mathbf{k} \cdot \mathbf{A})^2$$

3. A potential:

$$\begin{aligned} V_{pot} &= \sum_i |h_i|^2 |Q_i^{h(i)} \sigma_{h(i)} - Q_i^{t(i)} \sigma_{t(i)}|^2 + \sum_a 2|\sigma_a|^2 |\phi_a|^2 \\ &+ \sum_a g^2 |k_a \sigma_a|^2 + \sum_i \left| \frac{\partial \mathcal{W}}{\partial h_i} \right|^2 + \sum_a \left| \frac{\partial \mathcal{W}}{\partial \phi_a} \right|^2 + V_D, \end{aligned}$$

where

$$\begin{aligned} V_D &= \sum_a \frac{e_a^2}{2} \left(\sum_i (\delta_{h(i)}^a Q_i^a - \delta_{t(i)}^a Q_i^a) |h_i|^2 + |\phi_a|^2 - k_a x \right)^2 \\ &= \sum_a \frac{e_a^2}{2} D_a^2 \end{aligned}$$

The vacuum manifold \mathcal{M} is determined by $\sigma_a = \phi_a = 0$, $D_a = 0$, $d\mathcal{W} = 0$. We have only $(r-2)$ linearly independent D-term conditions:

$$\sum_a \ell_a D_a = 0, \quad \ell \in \text{Ker}(\mathbf{k}), \quad \ell \neq (1, \dots, 1).$$

This fact is consistent with that we have a dualized \mathcal{A} and leads naturally to a CY 4-fold by definition emerging from a 3-fold. Namely, $\mathcal{M} = \{d\mathcal{W} = 0\}/C^{*r-1}$ is a CY 3-fold because its derivation is just the same with that of 4D $\mathcal{N}=1$ SCFTs on a bunch of D3-branes probing CY₃ cones.

References

- 1) E. Witten, Nucl. Phys. B **403**, 159 (1993) [arXiv:hep-th/9301042].

[†] JHEP02,006(2010)

^{*1} Nishina Ctr., RIKEN

Light-cone gauge string field theory in noncritical dimensions[†]

Y. Baba, N. Ishibashi,^{*1} and K. Murakami

[String field theory, Conformal field theory, BRST symmetry]

Light-cone gauge string field theory is useful for defining string theories. From the action, it is possible to define the amplitudes and calculate them perturbatively, although we should check if they are well defined. Since it is a gauge-fixed theory, a light-cone gauge string theory can be considered in noncritical space-time dimensions. As it is noncritical, it does not possess the space-time Lorentz invariance and corresponds to a string theory in a Lorentz noninvariant background. In other words, we should be able to find a BRST invariant worldsheet theory containing a non-standard X^\pm part.

In this paper, we study the theory for X^\pm variables, since it can be used to regularize the string field theory. Dimensional regularization is one of the most powerful regularizations in quantum field theory of particles. It may also be useful in string theory. In particular, in the light-cone gauge superstring field theory, unwanted divergences occur even at the tree level because of the transverse supercurrent inserted at the interaction points of the vertices. In order to deal with these divergences, in a previous paper¹⁾, we have proposed a dimensional regularization scheme, in which we consider the number of space-time dimensions d to be a large negative value. We have checked that the results of the first quantized formalism are reproduced without any counterterms in the four-point case. In order to proceed further, we need to show that dimensional regularization preserves the important symmetries of the theory. If the light-cone gauge string field theory corresponds to a BRST invariant formulation even in noncritical dimensions, it means that the dimensional regularization preserves the BRST symmetry.

This study is confined to the case of closed bosonic string field theory in order to avoid technical difficulties involved in the superstring theory and focus on the tree-level amplitudes.

The theory for X^\pm variables that we propose is a CFT with the action

$$\begin{aligned}
 S_{X^\pm} &= -\frac{1}{2\pi} \int d^2z (\partial X^+ \bar{\partial} X^- + \bar{\partial} X^+ \partial X^-) \\
 &\quad + \frac{d-26}{24} \Gamma [\ln(-4\partial X^+ \bar{\partial} X^+)] , \\
 \Gamma[\phi] &= -\frac{24}{24\pi} \int d^2z \partial \phi \bar{\partial} \phi .
 \end{aligned} \tag{1}$$

The energy-momentum tensor $T_{X^\pm}(z)$ obtained from the action in eq.(1) is

$$T_{X^\pm}(z) = \partial X^+ \partial X^- - \frac{d-26}{12} \{X^+, z\} , \tag{2}$$

where $\{X^+, z\} \equiv \frac{\partial^3 X^+}{\partial X^+} - \frac{3}{2} \frac{\partial^2 X^+}{\partial X^+}^2$ denotes the Schwarzian derivative. Since the action in eq.(1) contains the terms proportional to $1/\partial X^+$, ∂X^+ should have a nonvanishing expectation value in order that the theory be well defined. For this purpose, we always consider this theory in the presence of the insertions of the vertex operators $e^{-ip_r^+ X^-}(Z_r, \bar{Z}_r)$ ($r = 1, \dots, N$) with $\sum_{r=1}^N p_r^+ = 0$. For functionals $F[X^+]$ that do not depend on X^- , it is possible to perform the path integral which gives

$$\begin{aligned}
 &\left\langle F[X^+] \prod_{r=1}^N e^{-ip_r^+ X^-}(Z_r, \bar{Z}_r) \right\rangle \\
 &\sim F \left[-\frac{i}{2}(\rho + \bar{\rho}) \right] \exp \left[-\frac{d-26}{24} \Gamma [\ln(\partial \rho \bar{\partial} \bar{\rho})] \right] ,
 \end{aligned} \tag{3}$$

where $\rho(z) = \sum_{r=1}^N 2p_r^+ \ln(z - Z_r)$ is the Mandelstam mapping. Roughly speaking, by differentiating this equation with respect to p_N^+ and then setting $p_N^+ = 0$, we obtain

$$\left\langle F[X^+] X^-(Z_N, \bar{Z}_N) \prod_{r=1}^{N-1} e^{-ip_r^+ X^-}(Z_r, \bar{Z}_r) \right\rangle . \tag{4}$$

In this way, we can, in principle, obtain arbitrary correlation functions by considering the right hand side of eq.(3) to be a generating functional, although the momentum conservation condition somewhat complicates this procedure.

From the correlation functions thus obtained, we can obtain the OPEs for the CFT for X^\pm variables and find that T_{X^\pm} satisfies the OPE for the Virasoro algebra with a central charge of $28 - d$. This implies that by combining the theories for the $d - 2$ transverse coordinates X^i and the bc -ghosts with this system, we can construct a nilpotent BRST charge. Thus, we formulate a BRST invariant worldsheet theory that corresponds to the light-cone gauge string theory in d ($d \neq 26$) space-time dimensions. We can also show that the tree amplitudes of the light-cone gauge bosonic string field theory can be recast into a BRST invariant form by using the CFT for X^\pm variables formulated here.

We shall report the supersymmetric generalization of the present analyses in a separate paper.

References

- 1) Y. Baba, N. Ishibashi and K. Murakami: JHEP **10** (2009) 035.

[†] Condensed from the article in JHEP **12** (2009) 010

^{*1} Institute of Physics, University of Tsukuba

Light-cone gauge NSR strings in noncritical dimensions[†]

Y. Baba, N. Ishibashi,^{*1} and K. Murakami

[Conformal field theory, String field theory, Superstring theory]

In the light-cone gauge formulation of string theory, the theory can be considered in noncritical space-time dimensions. Since the Lorentz invariance is broken in such dimensions, this theory describes a string in a Lorentz noninvariant background. In a previous paper¹⁾, we considered the bosonic string theory and identified the worldsheet CFT for the longitudinal variables x^\pm that corresponds to such a background.

In this paper, we carry out the supersymmetrization of the results of Ref. 1). We propose a superconformal field theory for the longitudinal variables x^\pm , ψ^\pm and $\tilde{\psi}^\pm$, which correspond to the longitudinal part of the light-cone gauge NSR string in d ($d \neq 10$) dimensions. We show that the Virasoro central charge of the superconformal field theory is $\hat{c} = 12 - d$ and that we can therefore construct a nilpotent BRST charge with the transverse variables and ghosts combined.

In order to supersymmetrize the results of Ref. 1), it is convenient to use the superfield formalism on the worldsheet. We introduce the supercoordinate $\mathbf{z} \equiv (z, \theta)$ and the superfields $X^\pm(\mathbf{z}, \bar{\mathbf{z}})$ which can be expanded as

$$X^\pm(\mathbf{z}, \bar{\mathbf{z}}) = x^\pm + i\theta\psi^\pm + i\bar{\theta}\tilde{\psi}^\pm + i\theta\bar{\theta}F^\pm. \quad (1)$$

We propose that the supersymmetric generalization of the action for the x^\pm CFT¹⁾ takes the form

$$\begin{aligned} S_{X^\pm} &= -\frac{1}{2\pi} \int d^2\mathbf{z} (\bar{D}X^+D^- + \bar{D}X^-DX^+) \\ &\quad + \frac{d-10}{8} \Gamma_{\text{super}}[\Phi], \\ \Gamma_{\text{super}}[\Phi] &= -\frac{8}{16\pi} \int d^2\mathbf{z} \bar{D}\Phi D\Phi, \end{aligned} \quad (2)$$

where D and \bar{D} denote the supercovariant derivatives, and the superfield $\Phi(\mathbf{z}, \bar{\mathbf{z}})$ is defined as

$$\Phi = \ln(-4(D\Theta^+)^2(\bar{D}\bar{\Theta}^+)^2), \quad \Theta^+ = \frac{DX^+}{(\partial X^+)^{\frac{1}{2}}}. \quad (3)$$

The super energy-momentum tensor derived from the action S_{X^\pm} in eq.(2) becomes

$$\begin{aligned} T_{X^\pm}(\mathbf{z}) &= \frac{1}{2} (DX^+ \partial X^- + DX^- \partial X^+) \\ &\quad - \frac{d-10}{4} S(\mathbf{z}, \mathbf{X}_L^+). \end{aligned} \quad (4)$$

Here $S(\mathbf{z}, \mathbf{X}_L^+) \equiv \frac{D^4\Theta^+}{D\Theta^+} - 2\frac{D^3\Theta^+D^2\Theta^+}{(D\Theta^+)^2}$ denotes the super Schwarzian derivative for the superconformal mapping $\mathbf{z} = (z, \theta) \mapsto \mathbf{X}_L^+ = (X_L^+(\mathbf{z}), \Theta^+(\mathbf{z}))$, where

[†] Condensed from the article in JHEP 01 (2010) 119

^{*1} Institute of Physics, University of Tsukuba

$X_L^+(\mathbf{z})$ denotes the holomorphic part of the superfield $X^+(\mathbf{z}, \bar{\mathbf{z}})$.

In order to make the theory well-defined, e^Φ should have a non zero expectation value. As in the bosonic case¹⁾, we always consider the theory in the presence of the insertion $e^{-ip_r^+ X^-}(\mathbf{Z}_r, \bar{\mathbf{Z}}_r)$ ($r = 1, \dots, N$), with $\sum_{r=1}^N p_r^+ = 0$. For the functionals $F[X^+]$ which are independent of X^- , one can obtain

$$\begin{aligned} &\left\langle F[X^+] \prod_{r=1}^N e^{-ip_r^+ X^-}(\mathbf{Z}_r, \bar{\mathbf{Z}}_r) \right\rangle \\ &\sim F \left[-\frac{i}{2}(\rho + \bar{\rho}) \right] e^{-\frac{d-10}{8} \Gamma_{\text{super}}[\ln((D\xi)^2(\bar{D}^2\bar{\xi}))]}, \end{aligned} \quad (5)$$

where

$$\rho(\mathbf{z}) = \sum_{r=1}^N 2p_r^+ \ln(\mathbf{z} - \mathbf{Z}_r), \quad \xi(\mathbf{z}) = \frac{D\rho}{(\partial\rho)^{\frac{1}{2}}}(\mathbf{z}). \quad (6)$$

Roughly speaking, we obtain

$$\left\langle F[X^+] X^-(\mathbf{Z}_N, \bar{\mathbf{Z}}_N) \prod_{r=1}^{N-1} e^{-ip_r^+ X^-}(\mathbf{Z}_r, \bar{\mathbf{Z}}_r) \right\rangle \quad (7)$$

by differentiating eq.(5) with respect to p_N^+ and then setting $p_N^+ = 0$. More precisely, we have to take into account the momentum conservation condition. In this way, we can, in principle, derive all the correlation functions by considering the right hand side of eq.(5) as a generating functional. From the correlation functions thus obtained, we can deduce the OPEs of the superconformal field theory for X^\pm variables. Using them, we find that $T_{X^\pm}(\mathbf{z})$ satisfies the OPE for the super Virasoro algebra with central charge $\hat{c} = 12 - d$. By taking into account the transverse variables $X^i(\mathbf{z}, \bar{\mathbf{z}})$ ($i = 1, \dots, d-2$), the total central charge of the system becomes $\hat{c} = 10$. This implies that it is possible to construct a nilpotent BRST charge, with the ghost superfields $B(\mathbf{z}) = \beta(z) + \theta b(z)$ and $C(\mathbf{z}) = c(z) + \theta\gamma(z)$.

Thus, we formulate a BRST invariant superconformal field theory that corresponds to the light-cone gauge NSR superstring theory in d ($d \neq 10$) space-time dimensions. We will report the application of this theory to the dimensional regularization of the light-cone gauge string field theory^{2,3)} in a separate paper.

References

- 1) Y. Baba, N. Ishibashi and K. Murakami: JHEP **12** (2009) 010.
- 2) Y. Baba, N. Ishibashi and K. Murakami: JHEP **10** (2009) 035.
- 3) Y. Baba, N. Ishibashi and K. Murakami: arXiv:0912.4811.

Light-cone gauge superstring field theory and dimensional regularization[†]

Y. Baba, N. Ishibashi,^{*1} and K. Murakami

[String field theory, Superstring, Conformal symmetry]

In the light-cone gauge NSR superstring field theory^{1,2)}, perturbative expansion of amplitudes involves divergences even at the tree level. Transverse supercurrents T_F^{LC} are inserted at the interaction points z_I of the joining-splitting interaction, and divergences arise when these supercurrents are close to each other. Similar divergences exist in other superstring field theories.

In a previous paper³⁾, we proposed a dimensional regularization scheme to deal with these divergences. In the light-cone gauge, one can define the theory in d ($d \neq 10$) dimensions. By considering d to be largely negative, we can make the tree-level amplitudes finite. By defining the amplitudes for such d , one can obtain the amplitudes for $d = 10$ by analytic continuation. Since what matters is the Virasoro central charge on the worldsheet, d can also be effectively changed by adding a superconformal field theory to that for the transverse variables X^i , ψ^i and $\tilde{\psi}^i$. In Ref. 3), we proposed one such scheme and showed that the results of the first quantized formulation can be reproduced by such a procedure in the case of four-string amplitudes.

In order for the dimensional regularization scheme to be effective, it should preserve as many symmetries of the theory as possible. In Refs. 4) and 5), we showed that the light-cone gauge string field theory in non-critical spacetime dimensions corresponds to a BRST invariant worldsheet theory with the longitudinal variables and the ghosts. Since the BRST symmetry on the worldsheet is supposed to be related to the gauge symmetry of the string field theory, these results imply that the dimensional regularization can be carried out with the gauge symmetry preserved.

In this paper, we would like to propose a dimensional regularization scheme for the light-cone gauge NSR superstring field theory, in which the results of Ref. 5) can be used. We just formulate the theory in d dimensions and define the amplitudes as analytic functions of d . In this paper, we deal with closed string field theory and restrict ourselves to amplitudes with only the (NS,NS) external lines. We show that the tree amplitudes can be recast into a BRST invariant form using the superconformal field theory proposed in Ref. 5).

The light-cone gauge superstring field theory can be defined even for $d \neq 10$. Starting with the definition, the N -string tree amplitudes can be calculated perturbatively. The results can be expressed by using the worldsheet field theory for the transverse variables on

the complex z -plane. Using the superconformal field theory for the longitudinal variables, we can recast the amplitude into the form

$$\begin{aligned} \mathcal{A}_N \sim & \int [dX d\psi d\tilde{\psi} d(\text{ghost})] e^{-S} \\ & \times \int \prod_{I=1}^{N-3} d^2\mathcal{T}_I \left(\prod_{I=1}^{N-3} \left[\oint_{C_I} \frac{dz}{2\pi i} \frac{b}{\partial\rho}(z) \oint_{C_I} \frac{d\bar{z}}{2\pi i} \frac{\tilde{b}}{\bar{\partial}\rho}(\bar{z}) \right] \right) \\ & \times \prod_{r=1}^N \left[c\tilde{c} e^{-\phi-\tilde{\phi}} V_r^{\text{DDF}}(Z_r, \bar{Z}_r) \right] \prod_{I=1}^{N-2} \left[X(z_I) \tilde{X}(\bar{z}_I) \right] \\ & \times \prod_{r=1}^N \oint_{z_I^{(r)}} \frac{dz}{2\pi i} D\Phi(\mathbf{z}) \oint_{\bar{z}_I^{(r)}} \frac{d\bar{z}}{2\pi i} \bar{D}\Phi(\bar{\mathbf{z}}) \\ & \times e^{\frac{d-10}{16} \frac{i}{p_r^+} X^+}(\mathbf{z}, \bar{\mathbf{z}}) . \end{aligned} \quad (1)$$

Here S denotes the action of the total system. $\rho(z) = \sum_{r=1}^N \alpha_r \ln(z - Z_r)$ is the Mandelstam mapping for the light-cone string diagram. The integration contour C_I lies around the propagator between the consecutive interaction points $\rho(z_{I+1})$ and $\rho(z_I)$, and $\mathcal{T}_I = \rho(z_{I+1}) - \rho(z_I)$ denote the $N - 3$ complex moduli parameters of the light-cone string diagram. V_r^{DDF} is the DDF vertex operator for string r . $X(z)$ denotes the picture-changing operator, and $\Phi(\mathbf{z})$ is a superfield defined in Ref. 5).

We can show that the amplitude (1) is BRST invariant when d is considered to have a sufficiently large negative value. By following the standard procedure, we can change the positions of the picture-changing operators to the insertion points of the vertex operators. The resultant amplitudes reproduce the results of the first quantized formulation in the analytic continuation $d \rightarrow 10$ without adding any contact interaction terms as counterterms.

References

- 1) S. Mandelstam: Nucl. Phys. **B69** (1974) 77.
- 2) S.-J. Sin: Nucl. Phys. **B281** (1987) 269.
- 3) Y. Baba, N. Ishibashi and K. Murakami: JHEP **10** (2009) 035.
- 4) Y. Baba, N. Ishibashi and K. Murakami: JHEP **12** (2009) 010.
- 5) Y. Baba, N. Ishibashi and K. Murakami: JHEP **01** (2010) 119.

[†] Condensed from the article in arXiv:0911.3704

^{*1} Institute of Physics, University of Tsukuba

Vacuum structure around identity-based solutions[†]

I. Kishimoto and T. Takahashi*¹

[Nonperturbative techniques, string field theory, D branes]

We construct numerical solutions of the theory around Takahashi-Tanimoto's analytic solution¹⁾ (TT solution) with a parameter a ($\geq -1/2$) in open bosonic string field theory and evaluate gauge invariants, the potential height and the gauge invariant overlap, for the numerical solutions. Our result provides further quantitative evidence that for $a > -1/2$, the TT solution is pure gauge and that for $a = -1/2$, it represents a nonperturbative vacuum where a D-brane vanishes.²⁾

The TT solution Ψ_a is of the form^{a)}

$$\Psi_a = Q_L(e^h - 1)\mathcal{I} - C_L((\partial h)^2 e^h)\mathcal{I}, \quad (1)$$

where \mathcal{I} is the identity state and h is a function with the parameter a ($\geq -1/2$). Expanding around Ψ_a , we have the action

$$S_a[\Phi] = -\frac{1}{g^2} \left(\frac{1}{2} \langle \Phi, Q' \Phi \rangle + \frac{1}{3} \langle \Phi, \Phi * \Phi \rangle \right), \quad (2)$$

where the new BRST operator $Q' = Q_B + \text{ad}_{\Psi_a}$ can be computed explicitly. Let us consider the equation of motion for $S_a[\Phi]$, namely, $Q' \Phi + \Phi * \Phi = 0$. We solve it under the Siegel gauge condition $b_0 \Phi = 0$. By multiplying the equation of motion by b_0 , we have

$$L(a)\Phi + b_0(\Phi * \Phi) = 0, \quad (3)$$

where $L(a) = \{b_0, Q'\}$, and we construct numerical solutions to this equation by an iterative approach with the level $(L, 3L)$ truncation approximation.

We have constructed two types of solutions. One, denoted as Φ_1 , is obtained by smoothly varying a from $a = 0$. The other, denoted as Φ_2 , is obtained by smoothly varying a from $a = -1/2$. At $a = 0$, Φ_1 is the conventional tachyon vacuum solution because $Q' = Q_B$. At $a = -1/2$, Φ_2 can be constructed by iteration, beginning with the initial configuration, which is given by the nontrivial solution for the lowest truncation. For the obtained configurations, we have computed the potential height $f_a(\Phi)$ ($\equiv -2\pi g^2 S_a[\Phi]/V_{26}$) and the gauge invariant overlap.

For Φ_1 , the result of our numerical calculations is plotted in Fig. 1. For $L \rightarrow \infty$, the figure suggests that $f_{a=-1/2}(\Phi_1) = 0$ and $f_{a>-1/2}(\Phi_1) = -1$. This implies that there exists a nonperturbative stable vacuum where a D-brane vanishes, except for $a = -1/2$. On the other hand, for Φ_2 , our result is depicted as

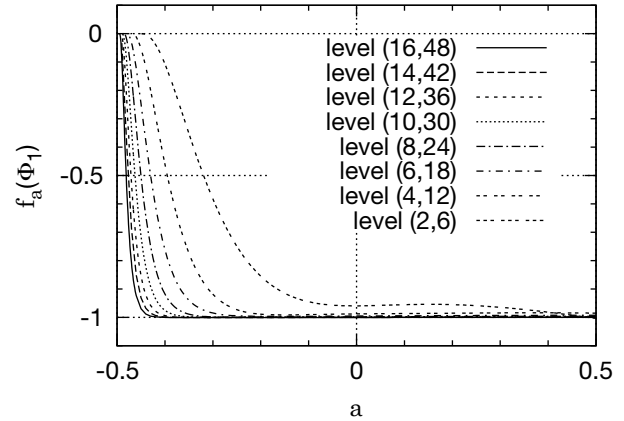


Fig. 1. Plots of the potential height $f_a(\Phi_1)$ for $a \geq -1/2$.

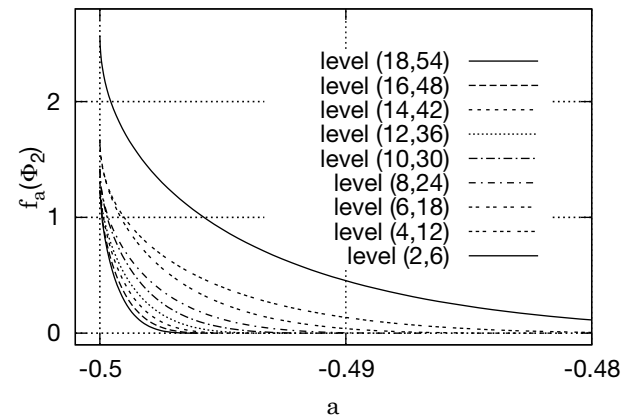


Fig. 2. Plots of the potential height $f_a(\Phi_2)$ for $a \geq -1/2$.

Note that the range of a is much narrower than that of Fig. 1.

in Fig. 2. For $L \rightarrow \infty$, the figure suggests that $f_{a=-1/2}(\Phi_2) = 1$ and $f_{a>-1/2}(\Phi_2) = 0$, which implies that there exists a nonperturbative unstable vacuum corresponding to the perturbative vacuum only for $a = -1/2$. The behavior of the gauge invariant overlap is similar to that of the potential height. These results are consistent with the expectation that the TT solution for $a = -1/2$ represents the nonperturbative vacuum where a D-brane vanishes.

References

- 1) T. Takahashi and S. Tanimoto: JHEP **0203**, 033 (2002).
- 2) I. Kishimoto and T. Takahashi: Prog. Theor. Phys. **108**, 591 (2002).

[†] Condensed from the article in Prog. Theor. Phys. **122**, 385 (2009)

*¹ Department of Physics, Nara Women's University

^{a)} It is difficult to evaluate gauge invariants for this type of "identity-based" solutions directly. Therefore, we investigated the theory around the TT solution.

Lattice formulation of 2D $\mathcal{N} = (2, 2)$ SQCD based on B-model twist[†]

D. Kadoh, F. Sugino,^{*1} and H. Suzuki

[Supersymmetry, lattice gauge theory]

After a seminal study by Kaplan et al.,^{1,2)} various lattice formulations of extended supersymmetric gauge theories have recently been proposed (see Ref. 3 for a review). A common feature of these lattice formulations is that at least one fermionic symmetry Q , which is a linear combination of supersymmetry charges, is manifestly preserved even in the case of finite lattice spacings. This could be possible if Q is nilpotent, $Q^2 = 0$, and the continuum action S is Q -exact as $S = QX$. Thus, such a Q is naturally identified with a BRST supercharge of topological field theory.⁴⁾ In lower-dimensional models, because of this exact fermionic symmetry Q , one may expect that full supersymmetry is restored in the continuum limit without (or with a little) fine tuning. Recently, the occurrence of expected supersymmetry restoration in a lattice formulation⁵⁾ of two-dimensional (2D) $\mathcal{N} = (2, 2)$ supersymmetric Yang–Mills theory (SYM) was clearly confirmed⁶⁾ by means of a Monte Carlo simulation.

From an extended supersymmetric theory, one can construct a topological field theory by a procedure called *topological twist*; this procedure involves defining a new rotational group (twisted rotation) by considering a particular combination of the original spacetime rotation and an internal R -symmetry. The above BRST charge Q transforms as a scalar under the twisted rotation. However, if one does not regard the twisted rotation as a real spacetime rotation, which is the standpoint we adopt here, the topological twist is merely the simple relabeling of dynamical variables in the original supersymmetric action in a flat spacetime. Nevertheless this procedure is useful to determine the above Q transformation and a Q -exact form of the action in the continuum theory.

In this paper, we present a new lattice formulation of 2D $\mathcal{N} = (2, 2)$ $U(k)$ supersymmetric QCD (SQCD) with N matter multiplets in the fundamental representation (and no antifundamental multiplet). In 2D $\mathcal{N} = (2, 2)$ theories, a topological twist can be performed in two ways.⁷⁾ One is the so-called A-model twist, in which the twisted rotation is defined as a diagonal $U(1)$ subgroup of the product of the original 2D rotation, $SO(2) \simeq U(1)$, and the internal $U(1)_V$ symmetry. The other is the B-model twist, in which one considers the diagonal $U(1)$ part of the product of the 2D rotation $U(1)$ and the internal $U(1)_A$ symmetry. Here, our objective is to construct a *simple* lattice formulation. For this purpose, we adopt the *B-*

model twist picture in which, under Q , left- and right-handed components of the fundamental fermions are symmetrically transformed. This property of the B-model twist helps to obtain a lattice action that is relatively simple compared with the action in the existing lattice formulations^{8,9)} of 2D $\mathcal{N} = (2, 2)$ $U(k)$ SQCD, which are based on the A-model twist.^{a)}

It has been discussed that a 2D $\mathcal{N} = (2, 2)$ $U(k)$ SQCD with N fundamental matter multiplets possesses rich physical contents. The low-energy effective theory would be given by the Grassmannian $G(k, N)$ supersymmetric nonlinear sigma model, in which one expects the spontaneous chiral symmetry breaking $\mathbb{Z}_{2N} \rightarrow \mathbb{Z}_2$ (the $U(1)_A$ symmetry is anomalous and broken to \mathbb{Z}_{2N}) and the dynamical generation of a mass gap. In the near future, we hope to use the present lattice formulation to investigate the physical behavior of in 2D $\mathcal{N} = (2, 2)$ $U(k)$ SQCD with N fundamental multiplets, as has been done for 2D $\mathcal{N} = (2, 2)$ SYM in Refs. 10–13.

References

- 1) D. B. Kaplan, E. Katz, and M. Ünsal: JHEP **0305**, 037 (2003) [arXiv:hep-lat/0206019].
- 2) A. G. Cohen, D. B. Kaplan, E. Katz, and M. Ünsal: JHEP **0308**, 024 (2003) [arXiv:hep-lat/0302017].
- 3) J. Giedt: PoS **LAT2006**, 008 (2006) [arXiv:hep-lat/0701006].
- 4) E. Witten: Int. J. Mod. Phys. **A 6**, 2775 (1991).
- 5) F. Sugino: JHEP **0403**, 067 (2004) [arXiv:hep-lat/0401017].
- 6) I. Kanamori and H. Suzuki: Nucl. Phys. **B 811**, 420 (2009) [arXiv:0809.2856 [hep-lat]].
- 7) E. Witten: Nucl. Phys. **B 403**, 159 (1993) [arXiv:hep-th/9301042].
- 8) F. Sugino: Nucl. Phys. **B 808**, 292 (2009) [arXiv:0807.2683 [hep-lat]].
- 9) Y. Kikukawa and F. Sugino: Nucl. Phys. **B 819**, 76 (2009) [arXiv:0811.0916 [hep-lat]].
- 10) I. Kanamori, H. Suzuki, and F. Sugino: Phys. Rev. **D 77**, 091502 (2008) [arXiv:0711.2099 [hep-lat]].
- 11) I. Kanamori, F. Sugino, and H. Suzuki: Prog. Theor. Phys. **119**, 797 (2008) [arXiv:0711.2132 [hep-lat]].
- 12) I. Kanamori and H. Suzuki: Phys. Lett. **B 672**, 307 (2009) [arXiv:0811.2851 [hep-lat]].
- 13) I. Kanamori: Phys. Rev. **D 79**, 115015 (2009) [arXiv:0902.2876 [hep-lat]].

[†] Condensed from the article in Nucl. Phys. **B 820**, 99 (2009)

^{*1} Okayama Institute for Quantum Physics

^{a)} We could not find a lattice discretization of the superpotential that is invariant under our lattice Q transformation. This restricts the applicability of our lattice formulation.

SUSY WT identity in a lattice formulation of 2D $\mathcal{N} = (2, 2)$ SYM[†]

D. Kadoh and H. Suzuki

[Supersymmetry, lattice gauge theory]

In this study, we clarify some issues related to supersymmetric (SUSY) Ward–Takahashi (WT) identities in Sugino’s lattice formulation of two-dimensional (2D) $\mathcal{N} = (2, 2)$ $SU(k)$ supersymmetric Yang–Mills theory (SYM).^{1,2)} This study is important, because determining whether SUSY is restored in the continuum limit is the most fundamental issue in non-perturbative lattice formulation of SUSY theories and the best way to observe the SUSY restoration in the continuum limit would be to confirm SUSY WT identities.

In this study, we first clarify how to derive lattice identities in Sugino’s formulation that would become SUSY WT identities in the target 2D $\mathcal{N} = (2, 2)$ SYM in the continuum limit. For this purpose, we devise an ingenious method to define a lattice counterpart of the supercurrent—the Noether current associated with SUSY—such that its covariance under the global $U(1)_A$ -symmetry can be manifested. Then, on the basis of the formal perturbation theory, we address the renormalization and mixing of composite operators appearing in the identities. The study of the composite operators is quite similar in principle to the standard analysis of the chiral symmetry on the lattice.³⁾ We can in fact argue that the lattice identities reproduce the SUSY WT identities of the continuum target theory in the continuum limit without any operator renormalization/mixing and tuning of lattice parameters. This conclusion is consistent with the expected SUSY restoration in the effective action of elementary fields without any fine-tuning, which has been discussed within the perturbation theory in Ref. 1. That consideration on the SUSY restoration in Ref. 1 implies the restoration of the SUSY WT identities in the continuum limit was claimed in Ref. 4 only intuitively. The present analysis remedies this gap.

Our argumentation up to this stage is standard but formal to some extent. To partially substantiate our formal argument, we carried out a one-loop calculation that confirmed the SUSY WT identities in the first nontrivial order of a semi-perturbative expansion (that is similar to the expansion proposed in Ref. 5) which was justified for small volume lattices. This result is also complementary with the non-perturbative numerical confirmation of the SUSY WT identities reported in Ref. 4.

As an interesting application of the lattice SUSY WT identities, we show that a prescription for the hamiltonian density in this lattice formulation, advocated by Kanamori, Sugino, and Suzuki^{6,7)} in the con-

text of spontaneous SUSY breaking, can be justified by using “current algebra” involving supercurrents and the hamiltonian density. We have

$$\partial_\mu^* \langle (s_\mu)_{i=4}(x) (s'_0)_{i=1}(y) \rangle = i \frac{1}{a^2} \delta_{x,y} \langle Q (s'_0)_{i=1}(x) \rangle, \quad (1)$$

where ∂_μ^* denotes the lattice backward difference, $s_\mu(x)$ is the lattice supercurrent defined above, $s'_\mu(y)$ is another appropriately-chosen supercurrent, and a is the lattice spacing. The subscript i refers to the spinor index, and the ($i = 4$) component of the supercurrent corresponds to a fermionic transformation Q and ($i = 1$) to a fermionic transformation $Q^{(0)}$. In the target continuum theory, the Q transformation of the time component of the Noether current associated with the $Q^{(0)}$ transformation is the hamiltonian density, $Q(s'_0)_{i=1}(x) = 2\mathcal{H}(x)$, as is consistent with the SUSY algebra, $\{Q, Q^{(0)}\} = -2i\partial_0 + (\text{gauge transf.})$. Therefore, it is quite natural to regard the right-hand side of Eq. (1) as the expectation value of the hamiltonian density in quantum theory:

$$\langle Q (s'_0)_{i=1}(x) \rangle \equiv 2 \langle \mathcal{H}(x) \rangle. \quad (2)$$

This is precisely the prescription advocated in Refs. 6 and 7 for the hamiltonian density in the present lattice formulation. Note that Eqs. (2) and (1) show that $\langle \mathcal{H}(x) \rangle$ is precisely the order parameter of SUSY breaking; this means that its non-zero (positive) value implies the massless Nambu–Goldstone fermion in the channel of the left-hand side of Eq. (1). In Ref. 8, the vacuum energy density of 2D $\mathcal{N} = (2, 2)$ SYM has numerically been studied on the basis of this prescription, indicating no SUSY breaking in this system, contrary to theoretical conjecture.

References

- 1) F. Sugino: JHEP **0401**, 015 (2004) [arXiv:hep-lat/0311021].
- 2) F. Sugino: JHEP **0403**, 067 (2004) [arXiv:hep-lat/0401017].
- 3) M. Bochicchio, L. Maiani, G. Martinelli, G. C. Rossi, and M. Testa: Nucl. Phys. **B 262**, 331 (1985).
- 4) I. Kanamori and H. Suzuki: Nucl. Phys. **B 811**, 420 (2009) [arXiv:0809.2856 [hep-lat]].
- 5) T. Onogi and T. Takimi: Phys. Rev. **D 72**, 074504 (2005) [arXiv:hep-lat/0506014].
- 6) I. Kanamori, H. Suzuki, and F. Sugino: Phys. Rev. **D 77**, 091502 (2008) [arXiv:0711.2099 [hep-lat]].
- 7) I. Kanamori, F. Sugino, and H. Suzuki: Prog. Theor. Phys. **119**, 797 (2008) [arXiv:0711.2132 [hep-lat]].
- 8) I. Kanamori: Phys. Rev. **D 79**, 115015 (2009) [arXiv:0902.2876 [hep-lat]].

[†] Condensed from the article in Phys. Lett. B **682**, 466 (2010)

6. Accelerator

Conversion of RFQ linac for new RIBF injector

K. Yamada, S. Arai, H. Fujisawa, E. Ikezawa, M. Kase, H. Okuno, N. Sakamoto, K. Suda, Y. Watanabe, and O. Kamigaito

A new injector (RILAC2)¹⁾ has been constructed at RIKEN Nishina Center for performing independent RIBF experiments and super-heavy-element synthesis. RILAC2 consists of a 28-GHz superconducting ECR ion source²⁾, a low-energy beam transport with a pre-buncher, a four-rod RFQ linac, three drift-tube linac tanks (DTL1-3)^{3,4)}, a rebuncher between the RFQ and DTL1, and strong quadrupole magnets between the rf resonators for transverse focusing. Very heavy ions with an m/q of 7, such as $^{136}\text{Xe}^{20+}$ and $^{238}\text{U}^{35+}$, can be accelerated up to 680 keV/u in the cw mode and injected to the RIKEN Ring Cyclotron without charge stripping. To save construction costs, the RFQ linac provided by Kyoto University is modified and used for RILAC2.

The original RFQ linac was developed by Nissin Electric Co., Ltd. in 1993 for ion implantation⁵⁾. Since the termination of its acceleration tests in the company, the system has been maintained by the Advanced Research Center for Beam Science, Kyoto University, for several years. The RFQ linac can accelerate heavy ions with an m/q of 16 up to 84 keV/u in the cw mode with an rf frequency of 33.3 MHz. The maximum rf input power was adjusted to be 50 kW(cw). If the RFQ resonator is so modified to have a resonant frequency of 36.5 MHz, ions with an m/q of 7 can be accelerated to 100 keV/u for RILAC2 without changing the vane electrodes. The intervane voltage required for RILAC2 is 42 kV, which is less than the originally designed value of 55 kV. The basic parameters corresponding to the RFQ linac after the conversion are listed in Table 1; the parameter values were obtained by scaling the original values.

Table 1. Basic parameters corresponding to RFQ linac

Frequency (MHz)	36.5
Duty (%)	100
m/q ratio	7
Input energy (keV/u)	3.28
Output energy (keV/u)	100.3
Input emittance (mm·mrad)	200 π
Vane length (cm)	225.6
Intervane voltage (kV)	42.0
Mean aperture (r_0 :mm)	8.0
Max. modulation (m)	2.35
Focusing strength (B)	6.785
Final synchronous phase (deg.)	-29.6
Unloaded Q	4500 (MWS)
Shunt impedance (k Ω)	63 (MWS)
Required rf power (kW)	17.5 (80%-Q)

For modification of the resonant frequency, we in-

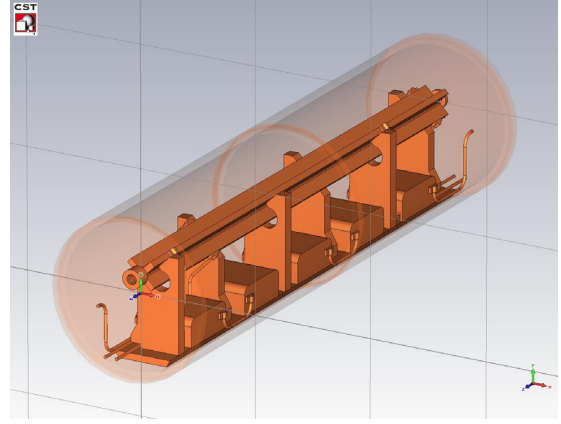


Fig. 1. A 3D model of MWS calculation for RFQ with block tuner.

serted a block tuner into the gaps between the posts supporting the vane electrodes. The block reduces magnetic flux, and consequently, the resonant frequency increases. The size of the block tuner was optimized by 3D electromagnetic calculations using the computer code Microwave Studio 2009 (MWS) and rf measurements using cold-model test pieces made of aluminum. Figure 1 shows a 3D model of the MWS calculation. The block dimensions were determined to be 240 mm \times 260 mm \times 114 mm. The rf power required to excite the intervane voltage of 42 kV was evaluated to be 17.5 kW by taking into account 80% derating of the shunt impedance (63 k Ω) determined by the MWS calculation. The maximum output power (40 kW) of the final amplifier was sufficient for operating the modified RFQ resonator. Note that the shunt impedance and unloaded quality factor of the original

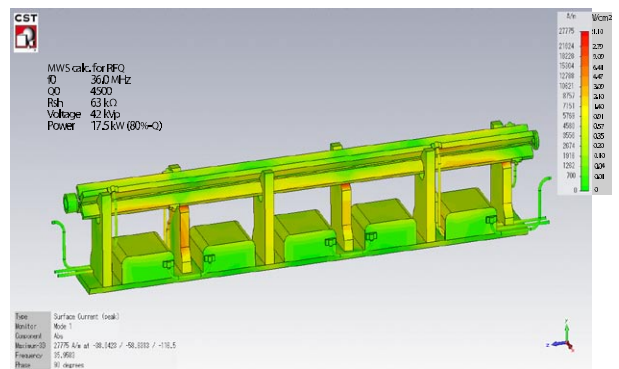


Fig. 2. Distribution of heat load at an input power of 17.5 kW.

RFQ linac were $77.9 \text{ k}\Omega^6$) and 5300, respectively.

The heat load distribution was also evaluated by MWS calculations to decide the cooling conditions. Figure 2 shows the distribution scaled to an rf input of 17.5 kW. The maximum current density in the block was 32 A/cm, which was very small. The total heat load estimated for the five blocks was approximately 2.1 kW. The size of the cooling water channel was so chosen that the flow rate of water was approximately 16 L/min; at this flow rate, the water temperature increases only by 2 °C. The cooling capacity was found to be sufficiently high if the value of the shunt impedance degraded to 70%.

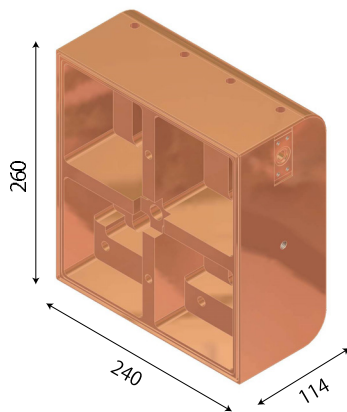


Fig. 3. 3D view of block tuner.



Fig. 4. 3D view of a part of the water inlet for the block tuner.

The block tuner was made of oxygen-free copper; three types of blocks were required by the mounting position. Intricate cutting was carried out on the block in order to reduce the weight of block to half the original value. The caps of the water channel was sealed by electron beam welding. Figures 3 and 4 show the 3D view of the block tuner and water inlet, respectively. The bottom view of the corresponding block is shown in Fig. 5. The blocks were mounted on a base with

an rf contact provided by coil springs (bal seal). The water channels in the blocks were connected in series by copper pipes. Figure 6 shows the internal structure of the RFQ linac after mounting the block tuner and water pipe. Although the equipments were successfully assembled, apparent leaks were found in the water channels in some of the blocks, by using a leak hunt. The leak points were repaired in a factory.



Fig. 5. Bottom view of the block tuner.

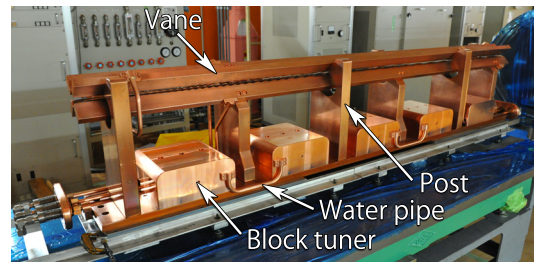


Fig. 6. Internal structure of RFQ after mounting the block tuner.

After the repair, all the equipments were re-assembled in February 2010. A low-power test was performed to evaluate the rf characteristics, and the resonant frequency was found to be changed to 36.5 MHz successfully. Rf amplifiers, low-level circuits, and a control system for RILAC2 were installed at the appropriate positions in February 2010. The main body of the RFQ has been moved to the AVF cyclotron vault in May 2010. Immediately after preparing the cooling water, vacuum pumps, and electric cables on the RFQ resonator, a high-power test will be performed.

References

- 1) O. Kamigaito et al., PASJ3-LAM31, Sendai, Aug. 2006, WP78, p502 (2006).
- 2) T. Nakagawa et al., Rev. Sci. Instrum. **79**, 02A327 (2008).
- 3) K. Yamada et al., in this report.
- 4) K. Suda et al., in this report.
- 5) H. Fujisawa, Nucl. Instrum. Meth. A **345**, 23 (1994).
- 6) H. Fujisawa et al., Proc. 7th Int. Symp. on Advanced Energy Research, Takasaki, Mar. 1996, p.436 (1996).

Design and construction of drift-tube linac no.1 for RILAC2

K. Yamada, K. Suda, N. Sakamoto, S. Arai, E. Ikezawa, M. Kase, H. Okuno, and O. Kamigaito

A new additional injector (RILAC2)¹⁾ has been constructed at the RIKEN Nishina Center so that RIBF experiments and synthesis of super-heavy element can be carried out independently. The RILAC2 consists of a 28-GHz superconducting electron-cyclotron-resonance ion source (ECRIS)²⁾, a low-energy beam transport (LEBT) with a pre-buncher, a four-rod radio-frequency quadrupole (RFQ) linac^{3,4)}, three drift-tube linac tanks (DTL1-3), a rebuncher between the RFQ and DTL1, and strong quadrupole magnets that were placed between the rf resonators for the transverse focusing. Very heavy ions with mass-to-charge ratio (m/q) of 7, such as $^{136}\text{Xe}^{20+}$ and $^{238}\text{U}^{35+}$, are accelerated up to an energy of 680 keV/u in the cw mode and injected into the RIKEN Ring Cyclotron without charge stripping. This report describes the design and construction of DTL1.

The DTL1 consists of a quarter-wavelength coaxial-cavity resonator, which has nine drift tubes with stems and two drift tubes at the end (10 gaps). The aperture of the drift tube has a radius of 17.5 mm, and the gap length is 20 mm. The DTL1 is operated at a gap voltage of 110 kV with a radio frequency of 36.5 MHz and it can accelerate ions from 100 keV/u to 220 keV/u. In order to optimize the rf characteristics and to determine the cavity dimensions, 3D electromagnetic calculation was performed using the computer code Microwave Studio 2009 (MWS). Figure 1 shows a DTL1 model used in the 3D electromagnetic calculation. The length of the stem was optimized to reduce the asymmetry of the electric field distribution between the gaps. The distribution of rf-power dissipation in the cavity was also evaluated by the MWS calculation to determine the amount of cooling required. The basic properties of DTL1 are listed in Table 1.

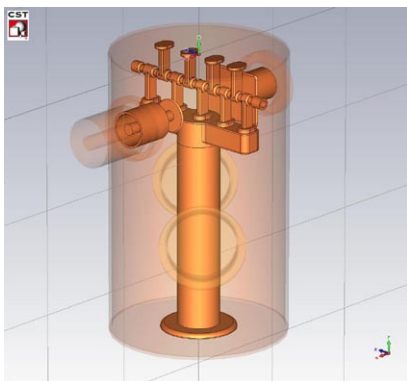


Fig. 1. A DTL1 model used in the 3D electromagnetic calculation; the model includes a tuner and coupler.

In order to reduce the construction cost and the space occupied by the equipments, a direct coupling

Table 1. Basic properties of DTL1

	DTL1
Frequency (MHz)	36.5
Duty (%)	100
m/q ratio	7
Input energy (keV/u)	100
Output energy (keV/u)	220
Cavity diameter (m)	0.8
Cavity height (m)	1.32
Gap number	10
Gap length (mm)	20
Gap voltage (kV)	110
Drift-tube aperture radius (mm)	17.5
Peak surface field (MV/m)	8.2
Synchronous phase (deg.)	-25
Max. power of amp. (kW)	25

scheme was adopted for the rf amplifier. A plate electrode of a 4CW50000E vacuum tube was directly connected to the capacitive coupler, which was mounted on the cavity. The load impedance of the vacuum tube can be adjusted by changing the position of the coupler electrode. When the coupler and vacuum tube were mounted on the cavity, the resonant frequency decreased because of their series/parallel capacitance. Thus, we had to set the target frequency of the cavity such that this decrease in the resonant frequency was compensated. The decrease in the resonant frequency was estimated by comparing the result of MWS calculation with the measurement results obtained using DTL3⁵⁾ with a 50- Ω coupler. Since the DTL3 was obtained by modifying a decelerator resonator that was developed for a Charge-State-Multiplier system⁶⁾, we were able to use it for the comparison. Finally, the cavity length of DTL1 was determined to actualize the target frequency of 36.725 MHz.

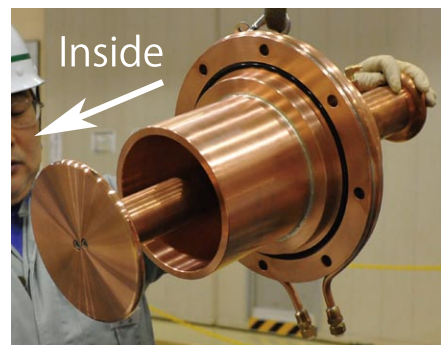


Fig. 2. Capacitive coupler for DTL1. ϕ 170 mm electrode is attached.

The coupler of DTL1 was designed such that the

load impedance could be adjusted to approximately $1000 + j0 \Omega$ with using vacuum tube. The default position and radius of the coupler electrode were determined by the MWS calculation using a frequency-domain solver. The coupler for DTL1 is shown in Fig. 2.

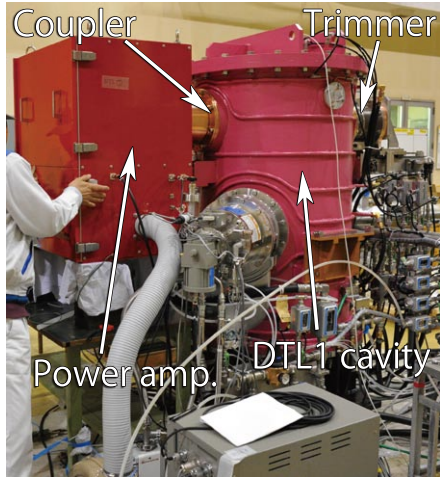


Fig. 3. Exterior of DTL1

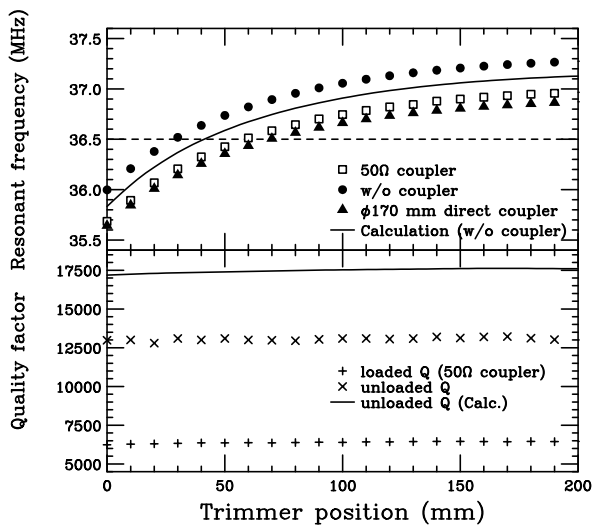


Fig. 4. Frequency response of DTL1 as a function of trimmer position.

The construction of the DTL1 was completed in January 2010, and low-power and high-power tests were performed immediately. Figure 3 shows the exterior of DTL1 used in test measurements. The results of the low-power test measurements carried out using a network analyzer are indicated in Fig. 4. The frequency response as a function of trimmer position is plotted in the upper panel of Fig. 4. The lower panel presents the quality factors. As shown in the figure, an operation frequency of 36.5 MHz was achieved at the trimmer position of 68 mm by using a ϕ 170 mm direct coupler. The load impedance can be adjusted from 600 to

1300 Ω by moving the coupler electrode over a distance of 40-mm.

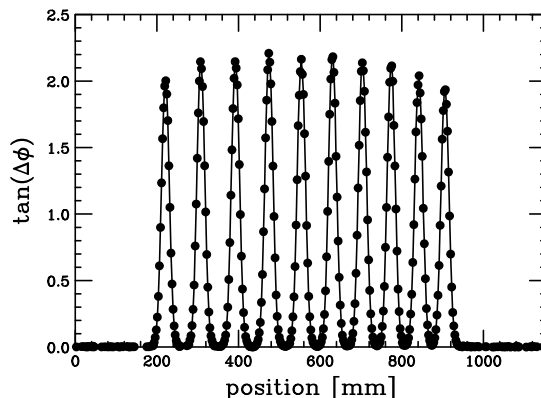


Fig. 5. Electric-field distribution of DTL1 along the beam axis.

The electric-field distribution along the beam axis was measured using a ϕ 12 mm TiO_2 bead by the perturbation method. The results of phase variations are plotted in Fig. 5. The shunt impedance was evaluated from the integral of the result, and the required rf power was determined. The rf characteristics of DTL1 are listed in Table 2.

A high-power test was performed with a load impedance setting of 1000 Ω . After one day of conditioning, the rated voltage of 110 kV was successfully achieved.

The DTL1 was installed in the AVF cyclotron vault in February 2010. Further conditioning and tests is now in progress.

Table 2. Rf characteristics of DTL1

	Calculated	Measured
Frequency (MHz)	35.83–37.13	35.64–36.87
Unloaded Q	17500	13000
Shunt impedance (M Ω)	1.13	0.94
Effective shunt imp. (M Ω /m)	163	135
Required rf power (kW)	5.3	6.5

References

- 1) O. Kamigaito et al.: PASJ3-LAM31, Sendai, Aug. 2006, WP78, p. 502.
- 2) T. Nakagawa et al.: Rev. Sci. Instrum. **79**, 02A327 (2008).
- 3) H. Fujisawa: Nucl. Instrum. Meth. **A 345**, 23 (1994).
- 4) K. Yamada et al.: in this report.
- 5) K. Suda et al.: in this report.
- 6) O. Kamigaito et al.: Rev. Sci. Instrum. **76**, 013306 (2005).

Design and Construction of Drift Tube Linac Cavities No. 2 and 3 for RILAC2

K. Suda, S. Arai, Y. Chiba, O. Kamigaito, M. Kase, N. Sakamoto, and K. Yamada

A new injector RILAC2 for RIKEN RI-Beam Factory is under construction¹⁾ (Fig. 1). The injector is

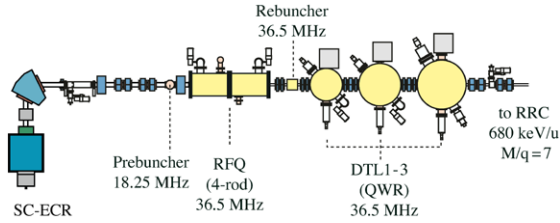


Fig. 1. Schematic view of the new injector RILAC2.

designed to accelerate very heavy ions such as $^{238}\text{U}^{35+}$ and $^{136}\text{Xe}^{20+}$ up to 680 keV/u for injection to the RIKEN Ring Cyclotron. The injector consists of a superconducting ECR ion source, a low-energy beam transport line, an RFQ linac, three drift tube linac (DTL) tanks, and a high-energy beam transport line. The structure of the DTL tanks is based on that of a quarter-wavelength resonator. The inner diameter ranges from 0.8 to 1.3 m. The DTL tanks are designed to be operated at a fixed RF frequency of 36.5 MHz. The design parameters are shown in Table 1. The

Table 1. Design parameters for DTL2 and DTL3.

Resonator	DTL2	DTL3
Frequency (MHz)	36.5	36.5
Duty (%)	100	100
Mass-to-charge ratio	7	7
Input energy (keV/u)	220	450
Output energy (keV/u)	450	680
Diameter (m)	1.1	1.3
Height (m)	1.429	1.890
Gap number	10	8
Gap length (mm)	50	65
Gap Voltage (kV)	210	260
Drift tube aperture (mm)	17.5	17.5
Peak surface field (MV/m)	9.4	9.7
Synchronous phase ($^{\circ}$)	-25	-25
Input power (100% Q: kW)	13.4	15.4
Power amp. (Maximum: kW)	40	40

first two tanks (DTL1 and DTL2) have been newly constructed while the decelerator tank developed for Charge-State-Multiplier system²⁾ (CSM-D1) is modified to obtain the third tank DTL3. For the purpose to simplify and minimize the size of a final RF amplifier and to reduce construction cost, the amplifier was directly coupled to the tank. In this report, we describe the design and construction of DTL2 and DTL3. The schematic view of DTL3 is shown in Fig. 2.

First, DTL3 was designed. DTL3 has eleven drift

tubes, a non-50 Ω capacitive coupler, and a trimmer (fine frequency tuner). The modification of CSM-D1 to DTL3 was performed as follows. Firstly, the original drift tubes and stems were replaced with those specifically designed for DTL3. The frequency of CSM-D1

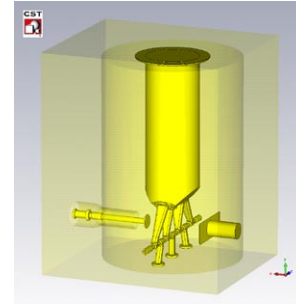


Fig. 2. Schematic view of DTL3. It has eleven drift tubes, a non-50 Ω capacitive coupler, and a trimmer.

can be varied from 36 to 76.4 MHz by changing the position of a movable shorting plate. In order to install the modified tank in the AVF hall, it was necessary to reduce the tank height by removing the shorting plate as well as its drive mechanism, cutting the inner and outer cylinders, and attaching a new fixed top plate with a flange which supports inner cylinder. Therefore, low-power tests were performed in order to estimate the decrease in the resonant frequency due to the directly coupled amplifier and to determine the tank height. The 50- Ω coupler originally attached to CSM-D1 was used for this measurement. The length of the coaxial line was 1700 mm. Coupler plate of two sizes (ϕ 115 and 210 mm) were used. The optimum input impedance to the tank was estimated to be 700 Ω on the basis of the analysis of the operation of the tetrode 4CW50000E, which was used in the final power amplifier. This impedance needs to be matched when the tetrode is connected in parallel, the capacitance of which is approximately 55 pF. In the case of the coupler plate of ϕ 115 mm, the input impedance was matched to 50 Ω when the coupler was at a position of 456.2 mm from the center of the tank. When the coupler plate of ϕ 210 mm was used, matching condition for 50 Ω was not found within the stroke of the coupler. The coupling condition for direct coupler was estimated by transforming the measured data using f-matrix calculations to the case of a shorter 50 Ω coaxial line (529.8 mm), which matches the geometry of the direct coupler. According to the estimation, the impedance will be matched to 700 Ω at the coupler position of around 300 mm from the cen-

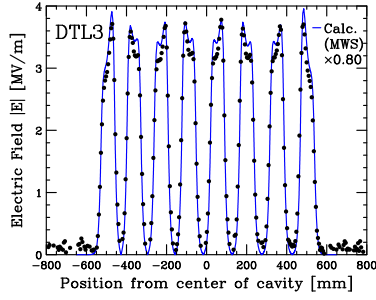


Fig. 3. Electric field distribution of DTL3. The data are plotted as solid circles. A calculation result by MWS is shown as a solid line.

ter of the tank, and the decrease in frequency is within a range of 175 kHz and 275 kHz (average 225 kHz). On the other hand, the flange below the top plate increases the frequency by +125 kHz from the calculation of the Eigenmode solver of the CST Microwave Studio (MWS). Therefore, the target frequency was fixed at 36.6 MHz ($= 36.5 + 0.225 - 0.125$). Then, the tank height was determined to be 1.890 m. Figure 3 shows the measured electric-field distribution of DTL3. The deduced shunt impedance is 1.72 M Ω , which is 80% of the value calculated using MWS. An average gap voltage of 260 kV can be obtained if an input power of 19.6 kW is fed.

After the tank height was determined, a capacitive coupler was designed. This coupler consists of a non-50 Ω coaxial cylinder and a plate at the end of an inner cylinder. The position of the inner cylinder can be adjusted manually to ± 20 mm in order to tune the input impedance. The maximum diameter of the coupler plate has to be less than 213 mm because of the size of the flange. In order to be able to adjust the input impedance by changing the diameter of the plate, the coupler position was set to be 250 mm from the center of the tank (50 mm lesser than previous position). The diameter of the coupler plate was then determined to be 130 mm from calculations using MWS. However, when the coupler and tetrode were attached, the input impedance was found to be lower than expected. Therefore, the actual diameter of plate was increased to 135 mm. The frequency of the tank was decreased by 288 kHz (Fig. 4). The cooling powers needed for the tank and coupler were determined by taking into consideration the calculated thermal distribution on the condition of the maximum output of the amplifier.

Based on the experience of designing DTL3, DTL2 was designed by only calculations. Figure 5 shows a schematic view of DTL2. The length of stems was changed from 200 mm (original) to 150 mm in order to improve the deviation of gap voltages³⁾. The deviation was reduced from 6.4% to 4.6%. The tank height was determined, as in the case of DTL3, by taking into account the change in frequency, but without that due

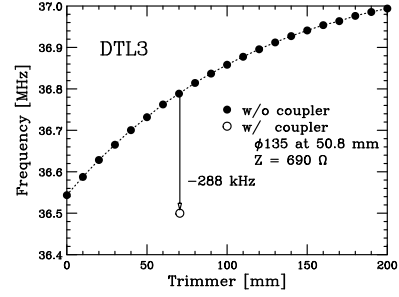


Fig. 4. Resonant frequency of DTL3. The measured values without and with coupler are denoted by closed and open circles, respectively. The decrease in the frequency was 288 kHz.

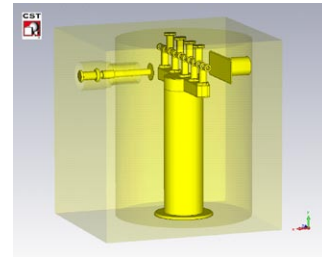


Fig. 5. Schematic view of DTL2. It has nine drift tubes, a non-50 Ω capacitive coupler, and a trimmer. The shorting end is placed in the vertically down direction, which is the opposite of the case of DTL3, owing to a shorter height of cavity and a deeper (+40 cm) floor level.

to the flange. This is because the flange was taken into account in the calculations using MWS. Therefore, the target frequency was set to be 36.725 MHz ($= 36.5 + 0.225$), and the tank height was determined to be 1.429 m. The coupler position was determined as follows. At first, the coupler position which results in an impedance of 50 Ω was determined. When a plate of ϕ 115 mm was used, and the actual Q-value was assumed to be 70% of that obtained by calculations, the position was estimated to be 420 mm from the center of the tank. Then, as in the case of DTL3, this position was changed to obtain an impedance of 700 Ω . The diameter of the plate was determined to be 140 mm by a low-power test.

A high-power test of DTL3 and DTL2 were performed in December 2009 and January 2010, respectively, and the desired gap voltages were successfully obtained. These tanks as well as DTL1 will be installed in the AVF hall in February 2010.

References

- 1) O. Kamigaito et al.: Proc. PASJ6 (2009), p. 38.
- 2) O. Kamigaito et al.: Proc. LINAC'98 (1998), p. 603; O. Kamigaito et al.: Rev. Sci. Instrum. **76**, 013306 (2005).
- 3) K. Yamada et al.: In this report.

Construction of a new cavity for the double-rebuncher system for RRC

N. Sakamoto, K. Suda, K. Yamada, M. Kase, and O. Kamigaito

A new cavity has been designed and built to replace one of the cavities of the double rebuncher system for RRC (RIKEN Ring Cyclotron). The present S6 cavity¹⁾, which is located close to RRC, was originally used as the third harmonic rebuncher for the harmonic 5 operation (i.e. the rf frequency of the RRC is the fifth harmonic of beam revolution frequency) in the case of AVF injection. Therefore its frequency band of 60 to 90 MHz does not match to the beams from RILAC whose frequency is 18 to 38 MHz.

The specifications of the new cavity are summarized in Table.1. The range of frequencies from 36.5 to 76.4 MHz is the second harmonic of the beam frequency from the injector RILAC. A peak voltage of 20 kV at 36.5 MHz is set in order to achieve point-to-point conversion from the exit of the RILAC to the injection point of the RRC in the operation of $^{238}\text{U}^{35+}$ beam acceleration with a final energy of 345 MeV/u.

Table 1. Specifications of new rebuncher.

frequency	36.5~76.4 MHz
$\beta \cdot \lambda/2$	156 mm
gap	20 mm
no. of gap	4
cavity	$\lambda/2$
voltage	20 kV/gap(36.5 MHz)
amplifier	1 kW
trimmer	$\frac{\Delta f}{f} = \pm 0.5\%$

The structure of the cavity (Fig.1) has been optimized by using a 3D electromagnetic-field-calculation codes MWS. The present cavity is a $\lambda/2$ cavity whose res-

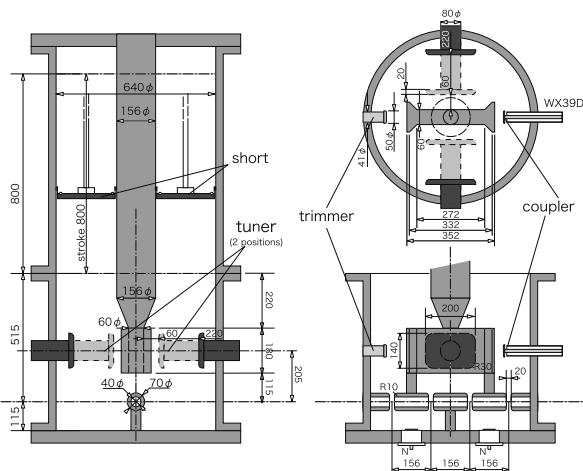


Fig. 1. Schematic of new rebuncher cavity. The scale is presented in the unit of mm.

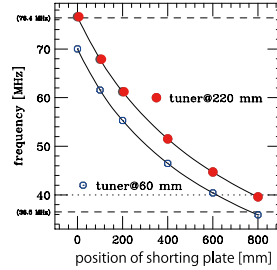


Fig. 2. Resonant frequency as a function of the position of the shorting plate is plotted for two tuner positions.

onant frequency can be varied by moving a shorting plate. In order to achieve wide frequency range, for a low frequencies between 36.5 and 40 MHz, a pair of capacitive tuners is used to make the resonant frequency lower as shown in Fig. 2. The rf power is fed to the cavity by a 50 Ω coaxial waveguide of WX39D. The coupling is a capacitive one and the coupling β can be varied by changing the position so as to the impedance is matched to 50 Ω . A capacitive trimmer installed at the opposite side of the coupler changes the resonant frequency by $\pm 0.5\%$. The parallel shunt impedance

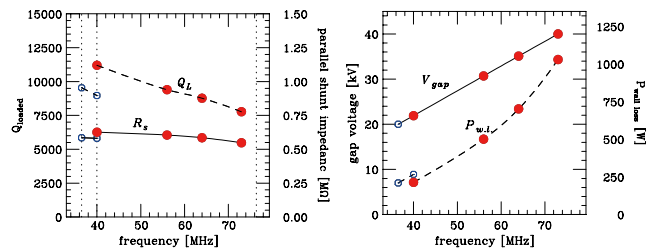


Fig. 3. Results of low-power tests. The open and closed circles represent the results obtained when the tuner was 220 mm from the drift tube support, respectively.

(R_s) was measured by using a perturbation method. The perturbation bead was a ceramic ball (K-140 Kyocera, $\epsilon_r = 138$) with a diameter of 12 mm, which gives a maximum phase shift of 74° . The measured Q, R_s , and wall loss of the cavity are plotted in Fig.3. The Q values are 60~80% of the calculated values.

A Power test is underway and the installation of the cavity is planned in February 2010.

References

- 1) A. Goto et al.:RIKEN Accel. Prog. Rep. **23**(1989).

Construction of the RILAC2 (RIKEN heavy-ion Linac 2) line[†]

Yutaka Watanabe, Eiji Ikezawa, Yoichi Sato, Hiroki Okuno, Takahide Nakagawa, Yoshihide Higurashi, Jun-ichi Ohnishi, Masaki Fujimaki, Nobuhisa Fukunishi, Naruhiko Sakamoto, Kenji Suda, Kazunari Yamada, Keiko Kumagai, Takeshi Maie, Shigeru Yokouchi, Misaki Komiyama, Tadashi Fujinawa, Hiroshi Watanabe, Shigeaki Arai, Hideyuki Yamazawa, Masayuki Kase, Akira Goto and Osamu Kamigaito

A new superconducting ECR ion source (SC- ECRIS)¹⁻⁴⁾ with an operational frequency of 28 GHz has been constructed with the aim of increasing the intensity of uranium beams. A 28-GHz SC-ECRIS was installed in the high-voltage terminal by the end of 2008, and commissioning, beam tests, and machine studies were successfully performed with the new mode “28-GHz SC-ECRIS – Low-Energy Beam Transport (LEBT) line - Middle-Energy Beam Transport (MEBT) line – RILAC” in 2009^{1), 5)}.

On the basis of the results of the abovementioned tests a new injector RILAC 2 has been designed for use in heavy-ion acceleration⁶⁻⁸⁾. RILAC2 mainly consists of the 28-GHz SC-ECRIS, a radio frequency quadrupole (RFQ) linac based on the four rod structure, the LEBT line between the source extraction system and the entrance to the RFQ, a drift-tube linac (DTL) based on three quarter-wavelength resonators (QWR), and the High-Energy Beam Transport (HEBT) line.

Figure 1 shows the schematic layout of the RILAC2 line for the 28-GHz SC-ECRIS. The RFQ, DTL, magnets, and buncher/rebuncher are installed at optimal positions where the beam spot size is minimum. The devices used in the RILAC2 are as follows:

- (1) RFQ; RFQ [modified], Amplifier [new]
- (2) DTL; DTL1 and DTL2 [new], DTL3 [modified, charge-state multiplier system (CMS-D1) from small irradiation room]
- (3) Buncher; Buncher [modified, used in the MEBT line]
- (4) Rebuncher; REB-B21 and B71 [modified], REB-3 [new, switching to REB-3 from S6-rebuncher]
- (5) BM; DMB6 and 7 [new], DMC2 [modified]
- (6) QM; QQB12abcd [from the CNS], QDB21ab - QTB41abc [new], QTB51abc-QDB71ab [from the CNS]
- (7) ST; SHB/SVB12ab, 21ab [used in an old line]
- (8) Chambers; U10 - B41 [new, stainless steel], B51 - B71 [undecided]
- (9) GV; GV-U10 - B50 [new]
- (10) Ducts; Stainless-steel duct [new, from GV-U11 to buncher], aluminum duct [new, from DTL3 to DMC2]

We have been preparing and making some arrangements and certain tasks before the construction of the RILAC2 line:

- (1) Outdoor plumbing and construction of a new SC-ECR ion source room.
- (2) Construction of mezzanine in the E6 room (RIPS vault) for some control panels and amplifiers.

- (3) Construction of a water cooling system on the roof of the SC-ECR ion source room.
- (4) Boring of holes in the wall and floor for the construction of the LEBT line and installation of cables [SC-ECR ion source room - AVF vault, AVF vault – E6 room, SC-ECR ion source room - E6 room, Second stage – third stage in the AVF vault, etc.].
- (5) Setting of control panels [second stage in AVF vault, PS room (substation in LINAC lab.)].

The RILAC2 line will finally be installed by the end of October 2010, as shown in Figure 1. The main outline of the future plan is as follows:

- February 2010, construction of the SC-ECR ion source room
- March 2010, (1) construction of DTL [from B20 to DTL3], panels [E6 room, polarized ion source room, PS room (substation in LINAC lab.)], and water cooling system, (2) individual tests on the devices (DTL1-3, RFQ, QM, etc.).
- May 2010, (1) construction of LEBT line [from U10 to SOB13ab, excepting QQB12abcd], (2) construction of SC-ECRIS in New room.
- June to October 2010, (1) construction of LEBT and HEBT line (including circulation of cooling water and compressed air, installation of cables and a power supply), (2) operation of SC-ECRIS.
- November 2010, (1) commissioning of SC-ECRIS and RILAC2 line, (2) beam tests and machine studies.

References

- 1) O. Kamigaito, S. Arai et al., Proc. PASJ6 (2009), Tokai, Aug. 5_7, 38_41 (2009).
- 2) J. Ohnishi, T. Nakagawa et al.: RIKEN Accel. Prog. Rep. **42**, 115_116 (2008).
- 3) T. Nakagawa, Y. Higurashi et al., RIKEN Accel. Prog. Rep. **42**, ix_x (2008).
- 4) Y. Higurashi, O. Kamigaito et al., Proc. PASJ6 (2009), Tokai, Aug. 5_7, 375_377 (2009).
- 5) Y. Watanabe, E. Ikezawa et al., Proc. PASJ6 (2009), Tokai, Aug. 5_7, 608_610 (2009).
- 6) Y. Sato, E. Ikezawa et al. Proc. PASJ6 (2009), Tokai, Aug. 5-7, 801_804 (2009).
- 7) H. Okuno, T. Fujinawa et al., RIKEN Accel. Prog. Rep. **42**, 150_151 (2008).
- 8) K. Yamada, O. Kamigaito et al., Proc. PASJ6 (2009), Tokai, Aug. 5_7, 1030_1034 (2009).

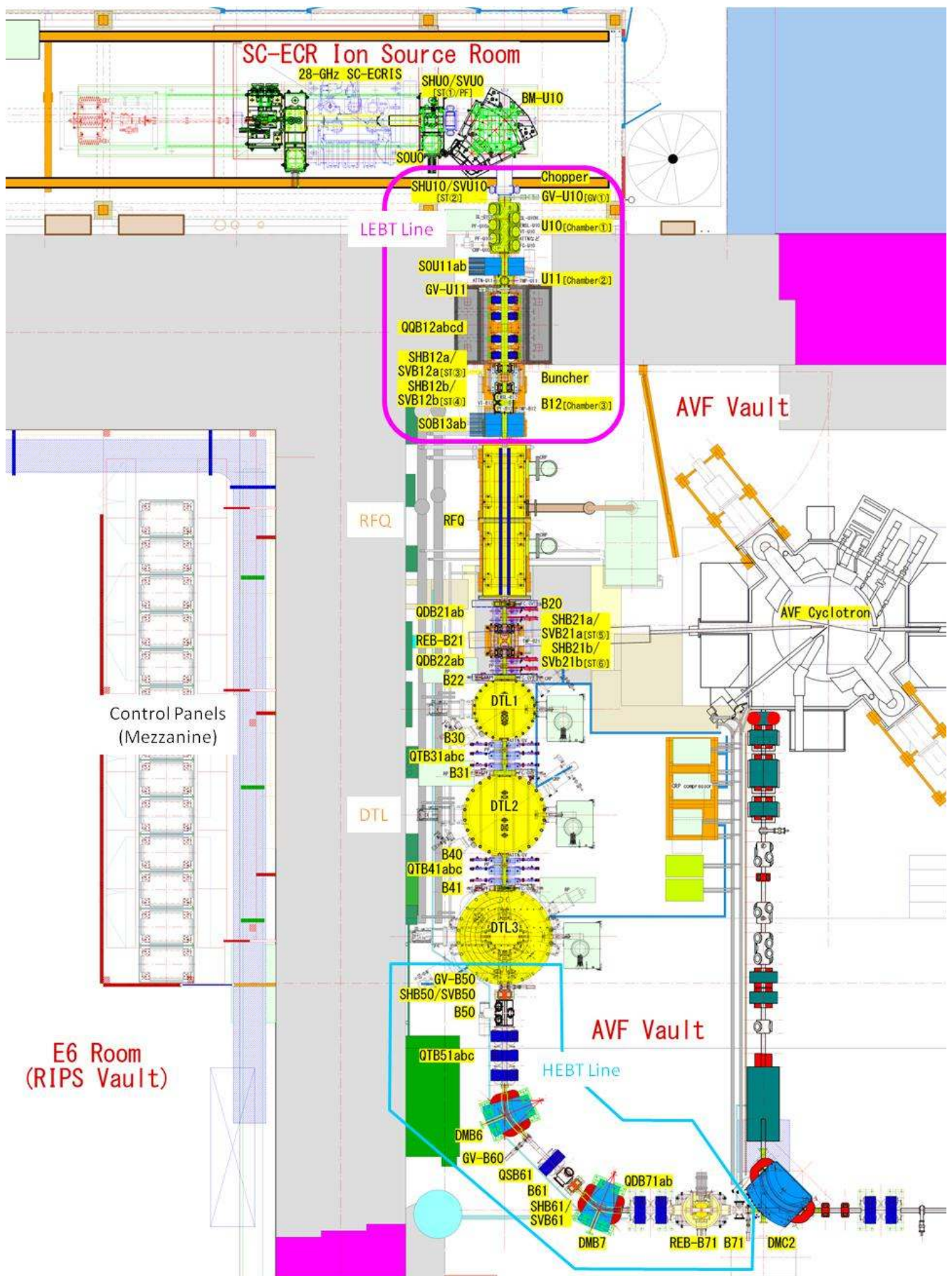


Fig. 1. Schematic layout of the RILAC2 line.

Production of highly charged U and Au ions from new RIKEN superconducting ECR ion source with sputtering method

Y. Higurashi, J. Ohnishi, T. Nakagawa, T. Aihara*, M. Tamura*

In the autumn of 2009, it was required to produce few ten of microamperes of U^{35+} beam from the new superconducting ECR ion source in order to increase the U beam intensity for producing radioisotope beams. To meet this requirement, we performed a test experiment before the production of the U beam from the new RIKEN superconducting ECR ion source^{1,2)} with sputtering method. Figure 1 shows a photograph of the RF injection side of the ion source used in the sputtering method. As shown in this figure, we set a metal rod at the tip of a support rod. The position of the metal rod was remotely controlled with an accuracy of 0.5 mm. For sputtering, the metal rod was supplied with high negative voltage (~several kV). Oxygen gas was used as the ionized gas.

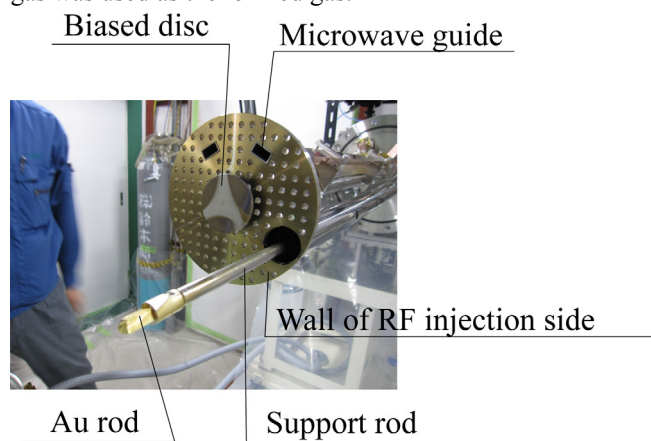


Fig.1. Photograph of RF injection side of the ion source used in sputtering method.

Before producing the U beam, we performed a test experiment in which highly charged Au ions were produced from a Au rod. Figure 2 shows the charge-state distribution of the Au ions. The ion source was tuned to produce Au^{30+} ions. The maximum magnetic field strength at the RF injection side (B_{inj}), the minimum strength of mirror the magnetic field (B_{min}), the maximum magnetic field strength at the beam extraction side (B_{ext}), the radial magnetic field strength at the inner surface of the plasma chamber wall (B_r), gas pressure, RF power (18 GHz), and extraction voltage (V_{ext}) are listed in the figure. Figures 3a) and 3b) show beam intensity as a function of the rod position and bias disc voltage, Rod position is defined as the distance between the metal rod and the wall of the RF injection side (see Fig.1). Using this sputtering method, we produced Au^{30+} ion beam with beam intensity $\sim 30 e\mu A$.

* SHI Accelerator Service Ltd.

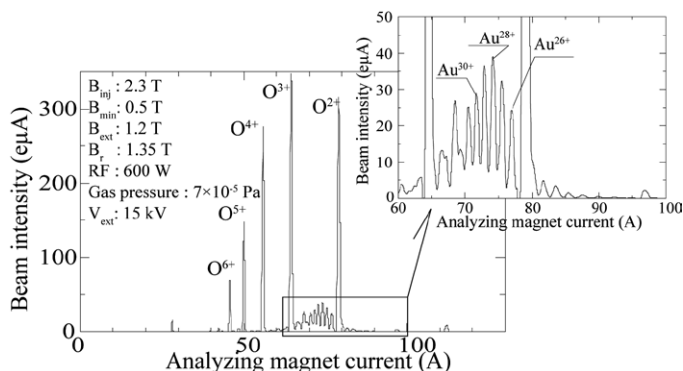


Fig. 2. Charge-state distribution of Au ions. Ion source was tuned to produce Au^{30+} ions.

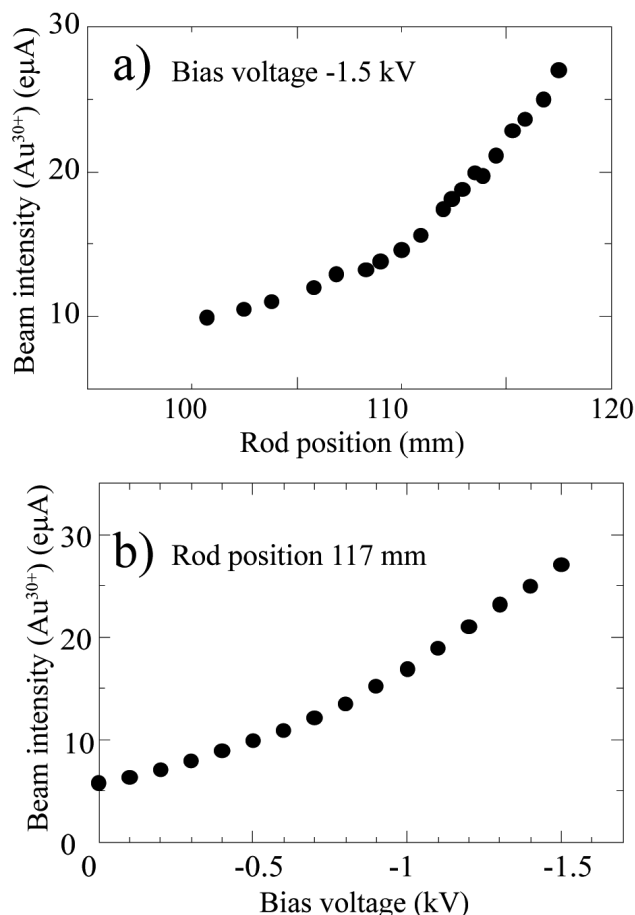


Fig. 3. Beam intensity as a function of a) rod position and b) bias disc voltage.

After successful Au beam production, we tried to produce highly charged U ions by using the same method. Figure 4

shows the charge-state distribution of the U ions. The ion-source conditions are listed in Fig. 4. The ion source was tuned to produce U^{35+} ion beam. The maximum beam intensity of $15 \text{ e}\mu\text{A}$ was obtained on the RF power of 850 W (18 GHz). Using this method, we provided a continuous supply of U^{35+} beam (average beam intensity; $12 \text{ e}\mu\text{A}$) for the experiments for one month.

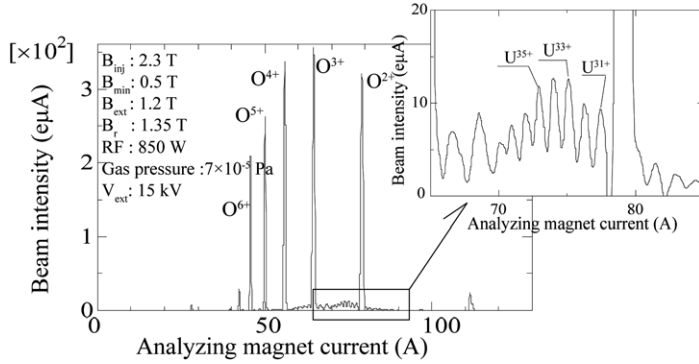


Fig. 4. Charge-state distribution of U ions.

References

- 1) T. Nakagawa et al.: Rev. Sc. Instrum. 79, 02A327 (2008)
- 2) T. Nakagawa et al.: accepted for publication in Rev. Sci. Instrum.

Status of the new superconducting ECR ion source for RIKEN RIBF

Y. Higurashi, J. Ohnishi, T. Nakagawa, T. Aihara*, M. Tamura*, A. Uchiyama*, H. Okuno, K. Kusaka, M. Kidera, E. Ikezawa, M. Fujimaki, Y. Sato, Y. Watanabe, M. Komiyama, M. Kase, A. Goto, O. Kamigaito, and Y. Yano

Since the middle 1990s, RIKEN has undertaken the construction of a new accelerator facility called the Radio Isotope Beam Factory (RIBF)¹⁾ and successfully produced 345 MeV/u U beam (~ 0.4 pA on target) in 2007.²⁾ For the RIBF, a primary beam intensity of 1 pA on target is required; hence, we have to increase the beam intensity. Hence, in the summer of 2007, we started the construction of a new superconducting ECR ion source (SC-ECRIS) with the optimum magnetic field strength to achieve an operational microwave frequency of 28 GHz. In the end of 2008, we achieved a magnetic field strength value that was 102% of the designed value.³⁾ In the spring of 2009, the SC-ECRIS produced the first beam with 18 GHz microwaves. After obtaining the first beam from the ion source, we performed various test experiments using 18 GHz microwaves, the experiments were aimed at increasing the beam intensity of highly charged heavy ions

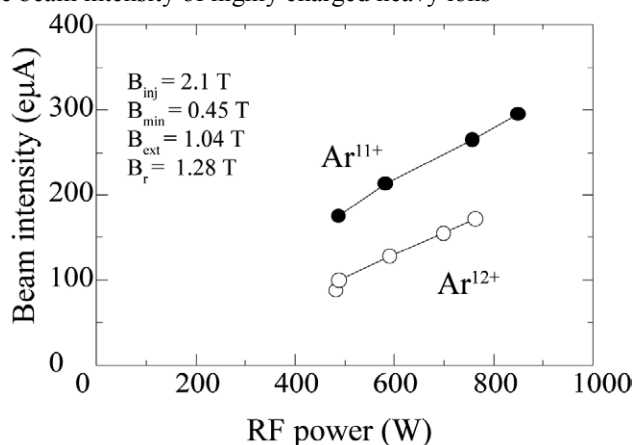


Fig. 1. Beam intensity of Ar¹¹⁺ and Ar¹²⁺ beam as a function of RF power

The detailed structure of the ion source is described in ref.4. Figure 1 shows the beam intensity of Ar¹¹⁺ and Ar¹²⁺ beams as a function of RF power. The maximum magnetic field strength at RF injection side (B_{inj}) and beam-extraction side (B_{ext}) and the minimum strength of the mirror magnetic field (B_{min}) are listed in this figure. The magnetic field strength at the surface of the plasma chamber (B_r) is also shown. We obtained ~ 300 eμA of Ar¹¹⁺ beam and 180 eμA of Ar¹²⁺ beam at an RF power of ~ 800 W.

The unique feature of this ion source compared to the other superconducting ECR ion sources is that it has six solenoids that are used to produce the axial mirror magnetic field. Using the six solenoids system, we can change the magnetic field gradient in the resonance zone and the ECR surface size independently. From model calculations⁵⁾, it is predicted that the magnetic field gradient in the resonance

zone and ECR surface size strongly affect the beam intensity of highly charged heavy ions; however, the effect of the field gradient and ECR surface size on beam intensity has not yet been verified experimentally. To clarify the effect of these two factors on beam intensity, we measured the beam intensity of highly charged heavy ions as a function of the magnetic field gradient for several ECR surface sizes. Figure 2 shows the beam intensity of Xe²⁴⁺ beam as a function of the average magnetic field gradient in the ECR zone for several ECR surface sizes. The average field gradients were calculated by using the OPERA 3D code. The extraction voltage and RF power were fixed at 15 kV and 600 W, respectively. The main magnetic field parameters are listed in Fig. 2. It is apparent that the beam intensity increases as the field gradient decreases and the ECR surface size increases. A detailed analysis is in progress

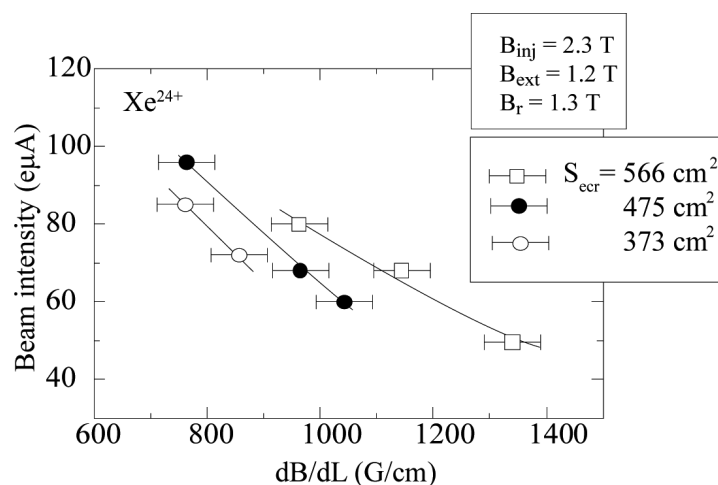


Fig. 2. Beam intensity of Xe²⁴⁺ beam as a function of average magnetic field gradient in the resonance zone for several ECR surface sizes

References

- 1) Y. Yano.: Nucl. Instrum. Methods **B261**1009(2007)
- 2) N. Fukunishi et al.: Proc. PAC'09 in press
- 3) J. Ohnishi et al.: RIKEN. Prog. Rep. **42** 115(2009)
- 4) T. Nakagawa et al.: Accepted for publication in Rev. Sci. Instrum.
- 5) A. Girard et al.: Rev. Sci. Instrum. **751** 381(2004)

* SHI Accelerator Service Ltd.

Installation of new superconducting ECR ion source in the Cockcroft-Walton high-voltage terminal

J. Ohnishi, Y. Higurashi, T. Nakagawa, T. Aihara,*¹ M. Tamura,*¹ and O. Kamigaito

A 28-GHz ECR ion source is currently being constructed at the RIBF in order to obtain high-intensity beams of highly charged ions like U^{35+} .¹⁾ One of the most important elements of the ECR ion source is its superconducting magnet. This magnet consists of six solenoids and a set of sextupole coils. Its design and construction was difficult because of its complex structure and high magnetic fields. Its construction began in October 2007 and was completed successfully in December 2008.²⁾ It was planned that an ion source that uses this superconducting magnet will be assembled and tested by using two existing 18-GHz microwave sources because a 28-GHz source had not been constructed in 2009. Nevertheless, the new source was expected to generate currents that would be ten times-higher than the current generated by the existing 18-GHz ECR ion source because of its strong magnetic field and large plasma volume. Therefore, it was decided that the new ECR ion source will be installed as a RILAC source and uranium beams will be supplied to the RIBF.³⁾

For this purpose, we planned to install the new ion source onto the Cockcroft-Walton high voltage terminal that was used previously and inject the uranium beams into the

RILAC at the energy of 127 kV per charge but not via the RFQ linac. The main reason for this was that the extraction voltage of the ion source needs to be increased from the present considerably low value of 5.6 kV in order to be injected into the RFQ.

We built an additional stage for the high-voltage terminal in order to increase its area from 16 m² to 31 m². On the other hand, the insulation distance to the wall was decreased from 2.5 m to 0.5 m because the new terminal voltage is lower than the previous value which was 450 kV. Although the old terminal was supported on nine double-layer porcelain insulators with a length of 1150 mm, for the new terminal, the support structure was altered such that it consisted of 17 single-layer insulators; this was done because the total load on the terminal exceeds 15 t when the terminal voltage is low. Further, we constructed a simple room in the terminal in order to limit the area where uranium may scatter.

Figure 1 shows the plan view of the high-voltage terminal. The magnetic elements in the low energy beam transport (LEBT) on the terminal⁴⁾ include a solenoid, an analyzing bending magnet (BM), and two steering magnets

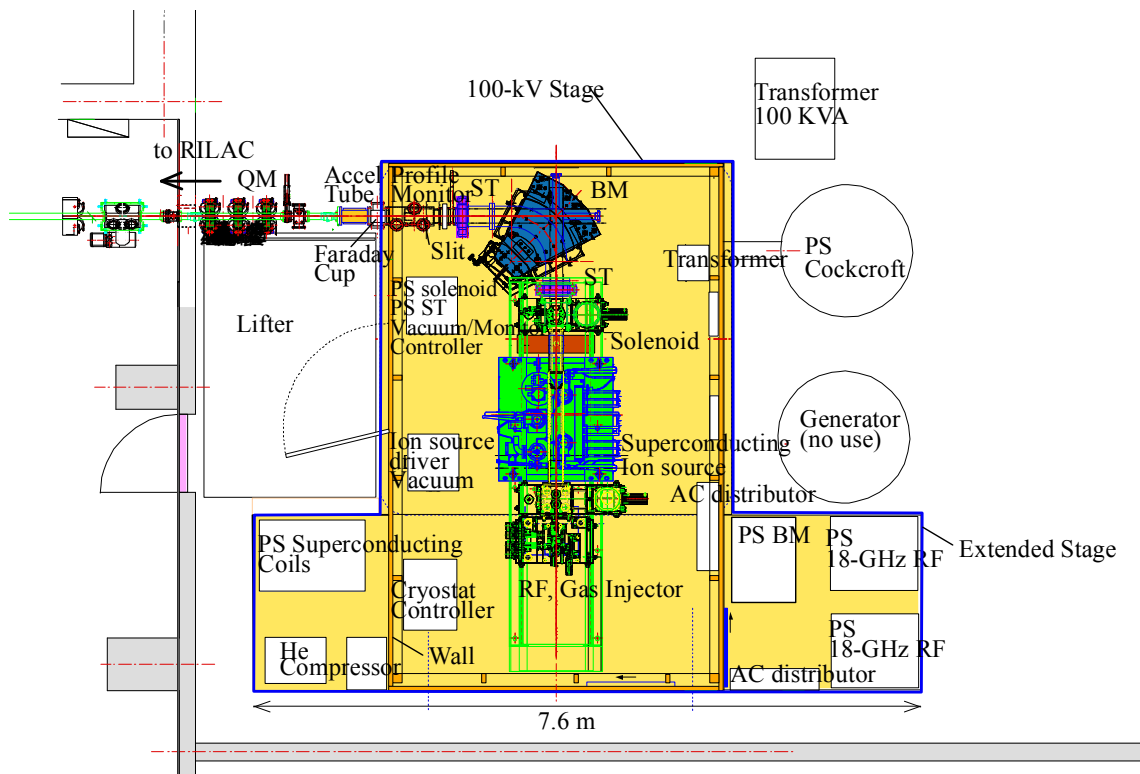


Fig. 1. Plan view of the Cockcroft-Walton high-voltage terminal.

*¹ SHI Accelerator Service Ltd

(ST) for horizontal and vertical directions. The analyzing magnet, whose design is the same as that in the 28-GHz superconducting ion source VENUS at LBL, has sextupole field components to reduce the aberration generated by that the magnet has a large aperture.⁵⁾ The beam optics is a double-focus system and the focus point is 1.0 m downstream of the exit point of the BM. A horizontal slit is located at the focus point and beam profile monitors are located 0.1 m and 0.3 m downstream of the slit. A Faraday cup is placed immediately before an accelerating tube.

Electric power and cooling water for the devices on the high-voltage terminal are listed in Table 1. The electric power is supplied only through a 100-KVA insulated transformer. The total power shown in the table exceeds the capacity of the transformer because each value is given by the full power. Cooling water at 100 L/min is supplied through rubber hoses with a size of 32A for electric insulation from the existing cooling water system.

After the superconducting magnet was installed in the high-voltage terminal in December 2008, the construction of the simple room, alignment of the beam line, cabling and piping were carried out in January and February 2009. The application test of the high-voltage terminal was performed on February 18. Initially, some arcs were observed; this was because an iron plate placed temporary on the ceiling and AC lines floated electrically from the terminal floor. The arcs disappeared as soon as the plate and AC lines were grounded to the floor. Further, some coronas were observed at some corners of the building; these were ignored since they did not seem to affect the beam operation. The leakage current was 1.7~2.0 mA at 110 kV and its major cause was presumed to be the electric conduction through the water hoses.

Precooling of the superconducting coils and filling of liquid helium in the cryostat was carried out in March. During precooling, the magnet was cooled using evaporated nitrogen gas at a low temperature before liquid nitrogen was poured over it; this was done to reduce the thermal stresses due to the large difference between the temperature of the magnet and that of liquid nitrogen. This precooling was carried out for four days (no operation were performed at night), and 1200 L of liquid nitrogen were used. After the precooling, 700 L of liquid helium was poured and its 330 L was stored. The stored liquid helium is maintained by three helium GM refrigerators.⁶⁾ Two of these can cool up to 10 K (SUMITOMO RDK408S), while the other can cool up to 4 K (RDK408D2). Further GM-JT refrigerator (V316SLCR, 4 W @ 4 K) is equipped to cool the heat load due to bremsstrahlung from ion-source plasma. The superconducting magnet was excited successfully at 90% of the design current on March 17. This current level is sufficient for an 18-GHz operation. Subsequently, the chambers, a vacuum system, an rf system and beam monitors were assembled, and the first beam of oxygen was extracted from the ion source on May 11. Then, the aging and the investigation of the ion source began. The operation of the ion source is described in another report.⁷⁾ The first acceleration test in the RILAC was performed using Xe²⁰⁺

Table 1. Summary of electric power and cooling water required for the devices in the high-voltage terminal.

	Number	Electric Power (kW)	Cooling Water (L/min)
18GHz RF source	2	30	
Superconducting magnet		12	
Analyzing magnet	1	20	15
Solenoid coil	1	15	15
Steering magnet	4	2	
He refrigerator/compressor	4	40	40
Ion source body		1	15
Vacuum system		3	
Beam Diagnostic		1	5
Cryostat controller		1	
Total		125	90

beam on July 26.

The ion source generated much stronger bremsstrahlung when compared to that generated by the old one. This reason seems to be because the electron temperature of the plasma is higher than that in the old one. We had to decrease the X-ray leakage to the outside of the RILAC building. The distances from the ion source are approximately 5 m to the east and west wall, 7.5 m to the north wall, and 5 m to the roof. In order to maintain the leakage within the allowed limit (2.5 μ SV/h), 36 lead blocks each with a thickness of 100 mm were laid on the axis and two layers of lead plates each with a thickness of 5 mm were fixed on the north side of the yoke. The total weight was approximately 1.5 t. Further, the roof area was set to a controlled area.

In October, a production test of Au ions was carried out after preparation for the sputtering method. We received approval for handling nuclear fuels on October 30, and uranium beams were produced successfully on November 2. The U³⁵⁺ beam current was approximately 10 μ A. The U³⁵⁺ beams were accelerated in the RILAC on November 13 and supplied to RIBF experimenters from November 26. The beam current from the new ion source was approximately five-times higher than that from the old one.

The construction of the 28-GHz microwave source was completed in March 2010. Furthermore, a new injector called RILAC II which consists of an RFQ linac and DTLs is also under construction. Therefore, we are planning to move the ion source to a newly constructing building and provide it upon completion of its construction as the 28-GHz ECR ion source for the RILAC II in 2010.

References

- 1) T. Nakagawa et al.: RIKEN Accel. Prog. Rep. **42**, ix (2009).
- 2) J. Ohnishi et al.: RIKEN Accel. Prog. Rep. **42**, 155 (2009).
- 3) O. Kamigaito et al.: Proc. the 11th Int. Conf. Heavy Ion Accel. Technology 21 (2009).
- 4) Y. Sato et al.: RIKEN Accel. Prog. Rep. **42**, 148 (2009).
- 5) C. M. Lyneis et al.: AIP Conf. Proc. **600**, 219 (2001).
- 6) J. Ohnishi et al.: Proc. 2009 ann. Meet. Particle Accel. Soc. Jpn. 635 (2009).
- 7) Y. Higurashi et al.: in this report.

Design of Low Energy Beam Transport in New RIKEN Injector

Y. Sato,*¹ M. Fujimaki, N. Fukunishi, A. Goto, Y. Higurashi, E. Ikezawa, O. Kamigaito, M. Kase, T. Nakagawa, J. Ohnishi, H. Okuno, H. Watanabe, Y. Watanabe, and S. Yokouchi

The RIBF project needs high-intensity uranium-ion beams. We are constructing a new injector RILAC2, which would provide beams with several hundred times higher intensity¹⁾. The RILAC2 consists of an electron cyclotron resonance ion source (ECRIS), an analyzing bending magnet (BM), a buncher, a radio frequency quadrupole (RFQ), a re-buncher, and 3 DTLs²⁾ (Fig. 1). The 28 GHz superconducting ECRIS³⁾ and the DTLs have been newly developed⁴⁾. Improvements were made to the RFQ, which was originally being operated at the Kyoto University. The buncher will be operated at the first harmonic, 18.25 MHz. The RFQ, the re-buncher, and the 3 DTLs will be operated at the second harmonic, 36.5 MHz. The RILAC2 will be operational in winter 2010.

As a part of the RILAC2, we designed a low energy beam transport (LEBT) from the ECRIS to the RFQ entrance (Fig. 2). In this paper, we present the requirements of the LEBT and the challenges faced in its design, and also our final design to overcome these challenges. The LEBT is now under construction based on this design. We assumed the beam properties since we had to design the LEBT before testing the newly developed ECRIS. The main requirements of the LEBT are summarized in Table 1.

Table 1. The main requirements of RILAC2 LEBT.

Total length (ECRIS to RFQ)	6.8 m
Beam	$^{238}\text{U}^{35+}$
Acceleration voltage	22.3 kV
Estimated emittance	$\sim 150 \pi \text{ mm}\cdot\text{mrad}$
$B\rho$	0.056 Tm
Energy per nucleon	3.28 keV
90° analyzing bending magnet	
Bending radius	510 mm
Resolution	100
RFQ Acceptance	
ϵ_x, ϵ_y	$150 \pi \text{ mm}\cdot\text{mrad}$
$x_{\text{max}}, y_{\text{max}}$	4.47 mm
$x'_{\text{max}}, y'_{\text{max}}$	49.0 mrad
r_{12}, r_{34}	-0.410

The U^{35+} beam emittance in the region beyond the analyzing bending magnet was estimated from the results of experiments performed using the Versatile ECRIS for Nuclear Science (VENUS) at the Lawrence Berkeley National Laboratory⁵⁾. The design of the analyzing bending magnet is the same as that of the VENUS system in which sextupole compensation has been achieved on its yoke.

The beam condition strongly depends on the degree

*1 yoichi.sato@j-parc.jp, yoichisato@riken.jp

of space-charge (SC) compensation. The maximum expected U^{35+} current would be 0.5 emA. However, since oxygen is used as a supporting gas at the ECRIS, the ECRIS produces not only U^{35+} but also U ions with other charge states and O ions. Therefore, the total produced ion current may be over 10 emA. The SC effect of the ions increases the beam emittance and influences the beam properties of U^{35+} in the low energy region. In order to compensate the SC effect of the ions, we keep and use the electrons within the LEBT. The electrons are originally produced due to residual-gas ionization or beam scratching on beam chamber. We installed a double-layered extraction system at ECRIS. This system produces a mirror electric field to keep the electrons within the LEBT. Only magnetic lenses are used as the lens elements in the LEBT so that the electrons within the LEBT are not absorbed. The compensation ratio was estimated to be 80~99%⁵⁾⁶⁾. In our design, we consider that the LEBT consists of three sections described as follows. Section 1 is around the extraction electrode of the ECRIS. Section 2 is from the ECRIS to the analyzing bending magnet. Section 3 is downstream of the analyzing bending magnet. The assumptions adopted in the simulation for each section are listed in Table 2. We performed cylindrical simulations of multiple-ion beams in section 1 using IGUN. We compared two different simulations in section 2. One was the simulation of multiple-ion beams using KOBRA, and the other was the simulation of single-ion beams using TRANSPORT. The emittance figures of U^{35+} ions in both simulations are similar. However, the KOBRA simulation showed non-normalized emittance of around 600 $\pi \text{ mm}\cdot\text{mrad}$, which was four times larger than the emittance estimated using VENUS. In section 3, by taking into consideration the RFQ acceptance, we adopt an initial condition based on the results at the end of the section 2 in phase space obtained using KOBRA, and an emittance of 200 $\pi \text{ mm}\cdot\text{mrad}$.

Table 2. Assumptions in the design of RILAC2 LEBT.

Section	SC ratio	Current	Ions	Code
1	100%	10 emA	O, U	IGUN ⁷⁾
2	10%	0.1~1 emA	O, U	KOBRA ⁸⁾
2	10%	0.1~1 emA	U^{35+}	TRANSPORT ⁹⁾
			upstream of the analyzing BM	
2	0~100%	0~0.5 emA	U^{35+}	TRANSPORT
			inside the analyzing BM	
3	0~100%	0~0.5 emA	U^{35+}	TRANSPORT

The transverse real space distribution of ions had not been clearly understood. Therefore, the simula-

tions in section 3 were performed by adopting several initial conditions with different horizontal and vertical waist positions. The LEBT was designed for as many different beam conditions as possible. We required lens elements having large acceptance and an accurate diagnostics system in the LEBT.

The RFQ is a four-rod RFQ having four vanes whose planes are inclined both horizontally and vertically at an angle of 45° ¹⁰⁾. It will be operated at a frequency of 36.5 MHz. It requires 22.3 kV for $^{238}\text{U}^{35+}$ and cylindrical strong-focus acceptance. We need a minimum degree of freedom of four for the LEBT lens elements for good matching. A buncher of 18.25 MHz is required upstream of the RFQ. The buncher is a two-gap system having 64.5 mm gaps, 150 mm total length, and 40 mm inner diameter. The buncher should be located within 1 m of the RFQ in order to ensure that the required voltage is obtained. The beam diameter through the buncher should be less than 25 mm in order to obtain the required electric-field distribution. These requirements are necessary to ensure a transmission of over 75% through the RFQ¹¹⁾.

There are two diagnostic systems. The first diagnostic system is located downstream of the analyzing bending magnet. It includes an analyzing slit, a vertical slit, emittance slits, two profile monitors, a viewing target monitor, a Faraday cup, and a vacuum pump. Its emittance monitor is expected to have 10% accuracy. The chamber length of the first diagnostics system is about 1 m. If we install a quadrupole lens immediately following the chamber, the beam diameter would be over 100 mm. The second diagnostic system is located upstream of the RFQ. It has an emittance monitor, two profile monitors, a viewing target monitor, and a vacuum pump. Its emittance monitor should measure emittances inclined at 45° to operate skewed quadrupoles between the RFQ and the DTLs. In each diagnostic system, the two profile monitors will be used to adjust the beam axis using steerers.

The final RILAC2 LEBT design is shown in Fig. 2. Figure 3 is the U^{35+} beam profile in LEBT simulated using TRANSPORT. The transverse lens elements are a single solenoid that is placed right after the ECRIS extraction, the 90° analyzing bending magnet, a pair of solenoids, four quadrupoles, and another pair of solenoids. The bending magnet is between two steerers. The buncher is between two steerers. The quadrupoles have 100 mm diameter. The paired solenoids are identical but will be operated to generate magnetic fields in directions opposite to each other¹²⁾. This operation of the paired solenoids prevents the rotation of a solenoid if only one is used. The paired solenoids can be used as decoupled isotropic focusing elements. A diagnostic chamber is present in front of each pair of solenoids. The paired solenoids enabled us to reduce the beam size in the lens elements following the solenoids, to decouple horizontal and vertical

emittances, and to ensure that a long drift space exists before the diagnostic chambers.

References

- 1) O. Kamigaito et al.: Proc. PASJ6, Tokai, Japan, 2009.
- 2) Y. Watanabe et al: in this report.
- 3) Y. Higurashi et al: in this report.
- 4) K. Suda et al.: in this report; K. Yamada et al.: in this report.
- 5) D. Leitner et al.: PAC 05, 179 (2005); D. Todd et al.: ECRIS08, Chicago, USA, 2008.
- 6) P. Spaedtke et al.: ECRIS08, Chicago, USA, 2008.
- 7) R. Becker et al.: Rev. Sci. Instrum. **63**, 2756 (1992).
- 8) P. Spaedtke et al.: Rev. Sci. Instrum. **71**, 820 (2000).
- 9) U. Rohrer, (<http://pc532.psi.ch/trans.htm>).
- 10) H. Fujisawa, NIM A **345**, 23 (1994).
- 11) H. Okuno et al.: Proc. PASJ6, Tokai, Japan, 2009.
- 12) Y. Sato, et al.: in this report.

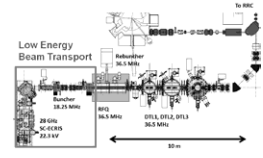


Fig. 1. The layout of the RILAC2.

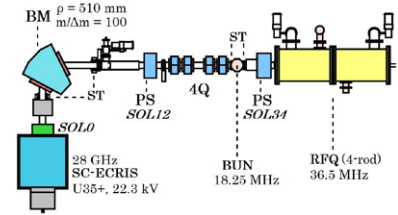


Fig. 2. The RILAC2 LEBT design. The abbreviations BM, PS, ST, 4Q, BUN represent the analyzing bending magnet, a set of paired solenoids, a steering magnet, a series of four quadrupoles, and a buncher.

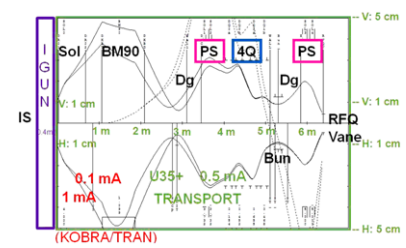


Fig. 3. The beam profiles in the RILAC2 LEBT simulated using TRANSPORT. The abbreviations Sol and Dg represent a single solenoid and a diagnostics chamber. The upper half shows vertical beam envelopes and the lower half shows horizontal beam envelopes. The larger and smaller envelopes are for ions with a current of 1 mA and of 0.1 mA, respectively, in section 2. The ions in section 3 have a current of 0.5 mA.

Design of Medium Energy Beam Transport for 127 kV U³⁵⁺

Y. Sato,*¹ M. Fujimaki, N. Fukunishi, A. Goto, Y. Higurashi, E. Ikezawa, O. Kamigaito, M. Kase, T. Nakagawa, J. Ohnishi, H. Okuno, H. Watanabe, Y. Watanabe, and S. Yokouchi

As a part of the RI beam factory (RIBF) project, we developed a new preinjector line, namely, the medium energy beam transport (MEBT) line for 127 kV uranium U³⁵⁺ beams in order to produce intense uranium-ion beams. This MEBT line is intended for temporary operation from 2009 to 2010. It will be dismantled for the construction of RIKEN's future linac (RILAC2). A newly developed superconducting ECR ion source (ECRIS), which was originally developed for RILAC2, was set on a high-voltage Cockcroft terminal. The MEBT line extends from the terminal to the entrance of the RIKEN linac (RILAC) (Fig. 1).

U³⁵⁺ beams were extracted from the ECRIS, whose voltage was higher than that of the Cockcroft terminal by 15~17 kV. The beams were transported from the terminal to the MEBT line through an acceleration tube. The voltage of the Cockcroft terminal was controlled to obtain a beam energy of 127 kV in the MEBT line. After passing through the 13.6 m long MEBT line, the 127 kV U³⁵⁺ beams were directly injected, without using a radio-frequency quadrupole (RFQ), into the RILAC at RIKEN. In this paper, we present the design of the MEBT line and the results obtained using this line.

The MEBT optics are set in the following order: the acceleration tube, triplet quadrupoles (TQ), doublet quadrupoles (DQ), buncher, DQ, 60° bending dipole (BM), 2 DQs, -60° BM, and DQ. The MEBT line was designed by performing simulations of the acceleration tube and the optics downstream of the tube. We had to design the MEBT before testing the newly developed ECRIS. Therefore, we needed to assume the beam properties for low energy beam transport (LEBT)¹⁾ using the Cockcroft terminal. We assumed that the U³⁵⁺ beam had upright emittance of 150 π mm-mrad and a circular beam spot of 10~20 mm diameter at the LEBT slit position that is 0.5 m upstream of the acceleration tube entrance. The beam state greatly depends on the extent of space-charge compensation. The MEBT line was designed to operate under as many different beam conditions of the LEBT as possible.

The acceleration tube was originally designed for an acceleration voltage of 100 kV, but it can be used for up to a voltage of 120 kV. In fact, the acceleration tube was operated at 110~112 kV in 2009. To model the acceleration tube, we used KOBRA simulation code²⁾. The diameter of the acceleration tube was chosen so as to avoid aberration, and the chosen value was 100 mm. The longitudinal distance between the 100 kV electrode and ground electrode is 260 mm. By per-

forming the simulation, we chose the acceleration tube geometry such that the beam emittance and the ion-speed ratio were decreased appropriately during acceleration (Figs. 2, 3). In our model, the U³⁵⁺ beam induced a space-charge effect of 200 e μ A around the acceleration tube.

TRANSPORT code³⁾ was used to design the MEBT that extended from the acceleration tube exit to the RILAC entrance. A H-H' emittance diagram as the initial conditions for the TRANSPORT simulation was chosen to be similar figure obtained using the results of KOBRA simulation at the accelerator tube exit. The initial conditions corresponded to circular beam spots of 10 mm, 12 mm, 15mm, and 20 mm diameter at the slit in the LEBT and emittance value of 65.6 π mm-mrad downstream of the acceleration tube (Table 1).

Table 1. Initial conditions of simulations at accelerator tube exit for different beam diameter at LEBT slit.

at LEBT slit	At acceleration tube exit		
Diameter	x_{max}	x'_{max}	r_{12}
	Emittance = 65.6 π mm-mrad		
10 mm	14.9 mm	5.27 mrad	0.553
12 mm	13.0 mm	5.46 mrad	0.384
15 mm	10.9 mm	6.06 mrad	0.0859
20 mm	9.13 mm	7.55 mrad	-0.304

The beam-matching conditions at the surface of the connection flange of the RILAC entrance were based on the E014 data that was previously obtained at RIKEN⁴⁾: $x_{max} = 7.13$ mm, $x'_{max} = 14.2$ mrad, $r_{12} = -0.761$, $y_{max} = 12.5$ mm, $y'_{max} = 5.30$ mrad, $r_{34} = -0.134$, $\epsilon_x = \epsilon_y = 65.6 \pi$ mm-mrad.

The MEBT line was designed to be achromatic. The beam diameter was set to be ≤ 30 mm at the buncher and ≤ 50 mm for the entire beam line. Further, the MEBT line was designed to be stable even if the quadrupoles were misaligned or some adjustments that could affect achromaticity were performed. The results of the TRANSPORT simulations show that $\Delta p/p \leq 0.03\%$ has to be achieved at the acceleration tube exit. This restriction is based on the longitudinal acceptance of the RILAC and it determines the LEBT specifications. The MEBT line was aligned to satisfy these conditions, a variety of initial conditions, and a space-charge effect of 0~500 e μ A (Figs. 4, 5).

On the basis of this design, the MEBT line was constructed, and the line was ready for operation in July 2009⁵⁾. The commissioning of the MEBT was performed from July to September 2009. Beams of ¹³⁶Xe²⁰⁺ ions, which have the same mass-to-charge

*1 yoichi.sato@j-parc.jp, yoichisato@riken.jp

ratio as $^{238}\text{U}^{35+}$ ions, were used in this commissioning. $^{238}\text{U}^{35+}$ beams were used in the operation of the MEBT line from November to December 2009. The currents measured in these operations are listed in Table 2. Here, FC represents a Faraday cup. $\text{FC}_{\text{H}0}$ is downstream of the analyzing bending magnet in the LEBT, $\text{FC}_{\text{e}014}$ is the exit of the MEBT, and $\text{FC}_{\text{e}11}$ is downstream of the analyzing bending magnet right after the RILAC. The MEBT magnets were optimized to improve the RILAC transmission rather than to maximize the $\text{FC}_{\text{e}014}$ current.

Table 2. The currents measured at LEBT, MEBT, and RILAC.

Date	Beam	$\text{FC}_{\text{H}0}$	$\text{FC}_{\text{e}014}$	$\text{FC}_{\text{e}11}$
2009/9/11	$^{136}\text{Xe}^{20+}$	24 μA	17 μA	8.4 μA
2009/11/13	$^{238}\text{U}^{35+}$	10.3 μA	8.0 μA	N/A
2009/11/16	$^{238}\text{U}^{35+}$	10.0 μA	6.2 μA	2.7 μA

For $^{238}\text{U}^{35+}$, the value of emittance that includes only current greater than 1/3 of the peak current in MEBT may be $\epsilon_x \cong \epsilon_y \cong 30 \sim 40 \text{ mm}\cdot\text{mrad}$ at 127 kV; this emittance value was estimated from the data obtained using a profile monitor by tuning a quadrupole.

References

- 1) Y. Sato et al.: RIKEN Accel. Prog. Rep. **42**, 148 (2009).
- 2) P. Spaedtke, C. Muhle: Rev. Sci. Instrum. **71**, 820 (2000).

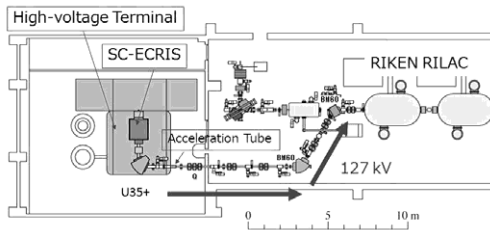


Fig. 1. The MEBT line. The transverse lens elements between the acceleration tube and the RILAC entrance are two 60° bending magnets and 13 quadrupoles.

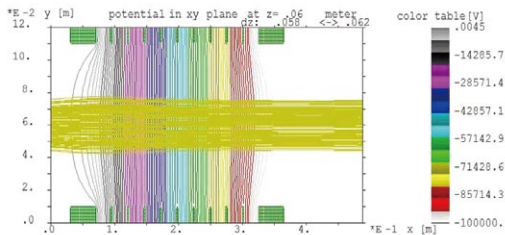


Fig. 2. Potential distribution in the 100 kV acceleration tube.

- 3) U. Rohrer: In *Graphic Transport Framework* (<http://pc532.psi.ch/trans.htm>).
- 4) O. Kamigaito, A. Goto et al.: RIKEN Accel. Prog. Rep. **30**, 191 (1997). M. Tonuma et al.: RIKEN IPCR **51**, 53 (1975). A. Goto et al.: Unpublished.
- 5) Y. Watanabe et al.: in this report.

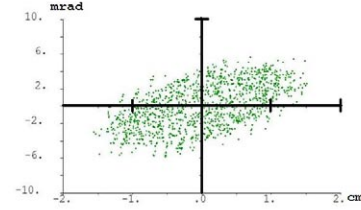


Fig. 3. The H-H' diagrams of U^{35+} for the acceleration tube exit. Emittance at the accelerate tube entrance is $150 \pi \text{ mmomrad}$.

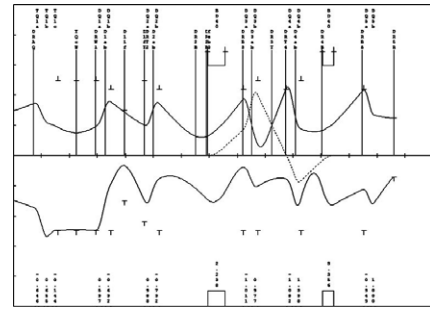


Fig. 4. The MEBT beam profiles of the 127 kV U^{35+} beams with zero-current space charge. The upper line is the vertical profile; the lower line, the horizontal profile; and the dashed line, R16. The transverse profile is in cm; the longitudinal, in m; and R16, in cm/percent.

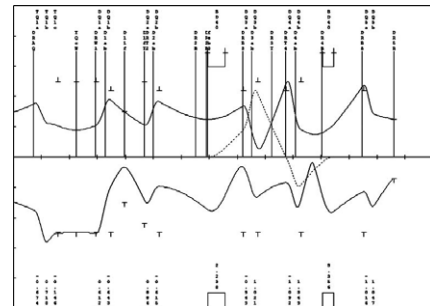


Fig. 5. The MEBT beam profiles of the 127 kV U^{35+} beams with 500 μA space charge. The upper line is the vertical profile; the lower line, the horizontal profile; and the dashed line, R16. The transverse profile is in cm; the longitudinal, in m; and R16, in cm/percent.

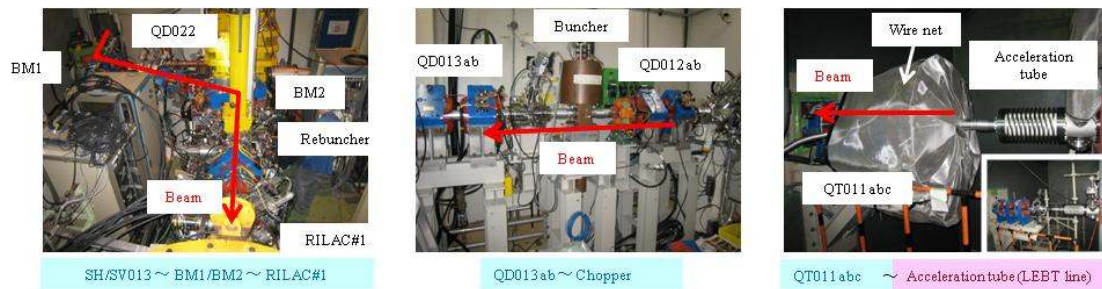


Fig. 2. Photographs of the MEBT line after construction.

the devices and bases.

The following four points related to the construction of the MEBT line are worth mentioning:

- (1) To achieve high vacuum in the MEBT line, all the chambers and ducts were subjected to a wet surface treatment (chemical polishing and precision cleaning), and two cryogenic pumps (CRP) were installed.
- (2) QT011abc was covered with a wire net to prevent electrical discharge from the high-voltage terminal, as shown in Figure 2.
- (3) Because of switching between the MEBT line and existing line, BM2 in the MEBT line and QDN2-1,2 in the existing line could be easily exchanged by using a plate for positioning.
- (4) The devices, bases, and ducts in the existing or old line were used wherever possible, so that these devices, bases, and ducts need not be newly manufactured.

Commissioning of the MEBT line was performed between the end of July and September 2009. First, $^{136}\text{Xe}^{20+}$ beams whose M/Q value was identical to that of (6.8), were used $^{238}\text{U}^{35+}$ beams. Figure 3 shows an example of the beam properties measured by profile monitors (PF). Some of the magnets in the MEBT line were adjusted, and appropriate vacuum baking was performed on the basis of the result of

the first beam test.

Then, the second round of commissioning was successfully completed, and $^{136}\text{Xe}^{20+}$ beams with a beam current 8.4 euA were detected by FC-e11. Then, beam acceleration and experiments were performed using a $^{238}\text{U}^{35+}$ beam between November and December 2009. Acceleration of the $^{238}\text{U}^{35+}$ beam and commissioning of the MEBT line were successfully performed using the $^{136}\text{Xe}^{20+}$ beam (Table 1). We are planning to conduct beam acceleration tests using uranium beams again in April 2010.

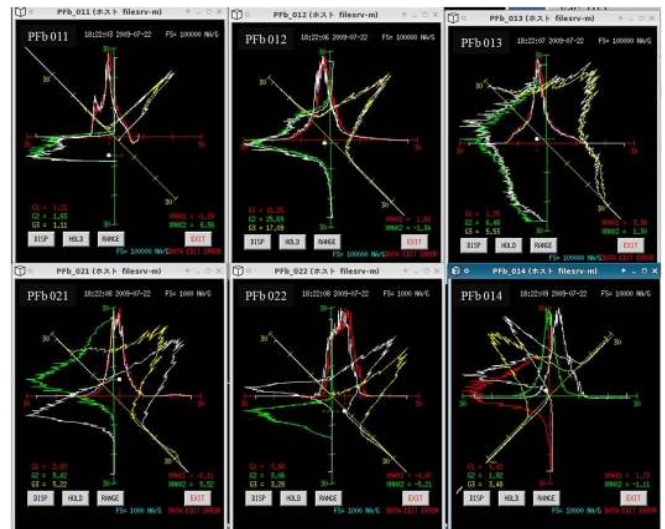


Fig. 3. Example of beam properties measured by profile monitors.

Table 1 Summary of beam acceleration tests.

July 22, 2009	First beam test from MEBT line to the end of the RILAC line using $^{136}\text{Xe}^{20+}$
September 11, 2009	$^{136}\text{Xe}^{20+}$: 127 kV extraction from SC- ECRIS, HV 110 kV [FC-H0; 24 euA, FC-e11; 8.4 euA]
November 13, 2009	Beam acceleration and tuning
November 13, 2009	$^{238}\text{U}^{35+}$: 15-kV extraction from ECRIS, HV 112 kV, Vacuum level in MEBT $\sim 2 \times 10^{-5}$ Pa [FC-H0; 10.3 euA, FC-e11; 8.0 euA]
November 16, 2009	$^{238}\text{U}^{35+}$: To optimize transport through RILAC, some magnets in the MEBT line were adjusted and appropriate vacuum baking was performed [FC-H0; 10 euA, FC-e11; 2.7 euA]
November 26 to December 13, 2009	Experiments at BigRIPS

References

- 1) O. Kamigaito, S. Arai et al., Proc. PASJ6 (2009), Tokai, Aug. 5_7, 38_41 (2009).
- 2) J. Ohnishi, T. Nakagawa et al.: RIKEN Accel. Prog. Rep. **42**, 115_116 (2008).
- 3) T. Nakagawa, Y. Higurashi et al., RIKEN Accel. Prog. Rep. **42**, ix_x (2008).
- 4) Y. Higurashi, O. Kamigaito et al., Proc. PASJ6 (2009), Tokai, Aug. 5_7, 375_377 (2009).
- 5) Y. Sato, M Fujimaki et al.: RIKEN Accel. Prog. Rep. **42**, 148_149 (2008).
- 6) Y. Watanabe, E. Ikezawa et al., Proc. PASJ6 (2009), Tokai, Aug. 5_7, 608_610 (2009).
- 7) Y. Sato et al., in this report.
- 8) E. Ikezawa et al., in this report.

Fabrication of thicker carbon foils with longer lifetime

H. Hasebe, H. Okuno, H. Kuboki, N. Fukunishi, O. Kamigaito A. Goto, M. Kase, and Y. Yano

A carbon foil (C-foil) is commonly used as a charge stripper in a heavy-ion accelerator such as RIKEN RIBF. However, the decrease in their lifetime when they are exposed to high-intensity heavy-ion beams is a serious disadvantage. Since 1999¹⁾, we have been developing C-foils that would have a long life even when exposed to the high-intensity and high-energy beams of the RIBF. The RIBF is continuously improved and the beam intensity is increased day by day. Since 2005, we have been fabricating polymer-coated carbon foils (PCC-foils) using a magnetron sputtering source by a polymer-coating technique with the aim of fabricating larger and thicker C-foils.^{2,3)} However, C-foils with adequately high quality and long lifetime have not been fabricated yet using this method.



Fig.1. High-vacuum evaporation system (SH-350 by ULVAC).

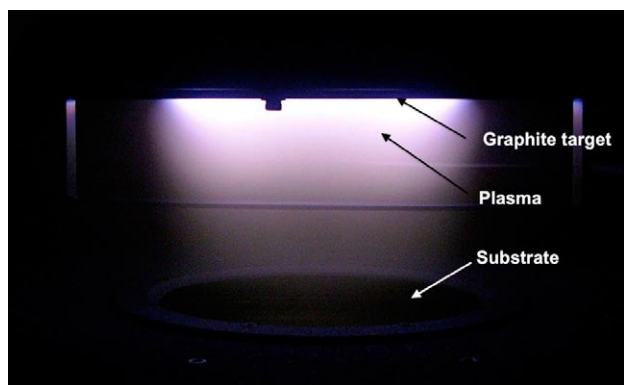


Fig.2. A state of the evaporation.

We installed a high-vacuum evaporation system (SH-350 by ULVAC⁴⁾) at the RILAC building in August 2009 (Fig. 1). The system has a vacuum chamber with a diameter of 500 mm and a height of 300 mm. It also has a oil-sealed pump and a 1800 L/s turbomolecular pump. A magnetron sputtering source is installed in the upper part of the evaporation chamber. The target of the magnetron sputtering source is a graphite plate with 6 inches diameter. A substrate is placed in the lower part of the evaporation chamber and is rotated during evaporation to ensure that the film thickness remains uniform. The substrate is 5 inches in diameter. A silicon wafer or glass material is used as the substrate. The substrate can be heated up to 250 °C. The distance between the substrate and a magnetron sputtering source can be adjusted from 35 mm to 85 mm. Figure 2 shows a photograph taken during the evaporation. The plasma is produced by the input of DC or RF (radio frequency) power into the evaporation chamber. Argon gas is circulated in the chamber and the flow rate of the gas is regulated using a mass flow meter. A vacuum of about 0.6 kPa exists during the evaporation. The relationship between thickness of carbon evaporated in one hour and the DC power of the magnetron sputtering source is shown in Fig. 3. The thickness of the C-foil was determined by dividing the measured mass of the C-foil (g) by the area (cm²). The deviation in the C-foil thickness was within 10%. The glass substrate on which the evaporated carbon was deposited looked like a mirror surface, as shown in Fig. 4. The C-foil removed from the substrate also appeared like a mirror.

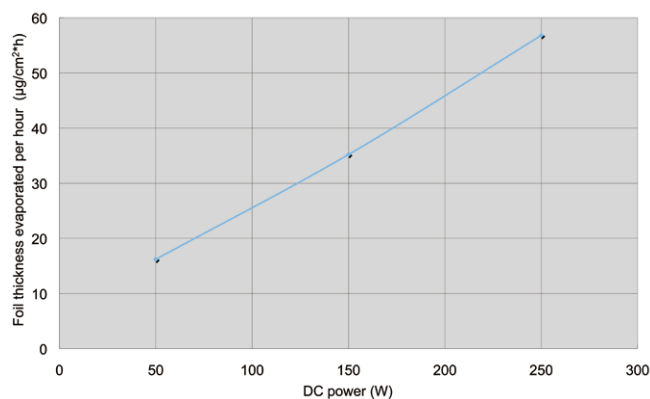


Fig.3. Thickness of carbon evaporated in one hour as a function of the DC power of the magnetron sputtering source.



Fig.4. The glass substrate on which evaporated carbon was deposited.

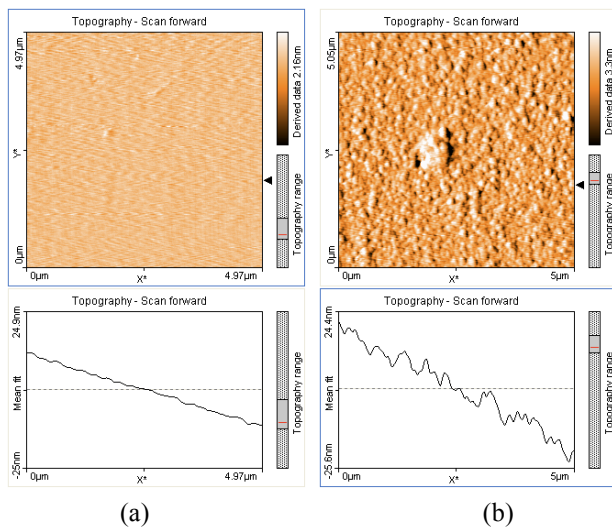


Fig.5. (a) is the C-foil surface on the side of the substrate, and (b) is C-foil surface on the side of the magnetron sputtering source (AFM images).

Figure 5 shows the images of the C-foil surfaces obtained using an atomic force microscope (AFM⁵). The surface area shown in the image is $5\ \mu\text{m} \times 5\ \mu\text{m}$. Figure 5 (a) shows the surface on the side of the substrate, while Fig. 5 (b) shows that on the side of the magnetron sputtering source. As seen in Fig. 5 (a), the surface is almost smooth. The other surface is slightly rough, as shown in Fig. 5 (b). However, the deviation in the thickness is about several nanometers, which is considerably lesser than that in case of PCC-foils or commercially available C-foils. We succeeded in fabricating C-foils with thickness from 0.2 to $1.5\ \text{mg}/\text{cm}^2$ by this method. Previously, $0.5\ \text{mg}/\text{cm}^2$ was the maximum thickness obtained. Carbon foils with a thickness of $0.3\ \text{mg}/\text{cm}^2$ were attached to a fixed holder having a hole of size $14\ \text{mm} \times 23\ \text{mm}$ and were used as a practical charge stripper during the beam time in December 2009. The carbon foils were irradiated with a $11\text{-MeV}/u\ ^{238}\text{U}^{35+}$ beam having an intensity of about $2\sim 3\ \text{e}\mu\text{A}$ which was obtained from the RIKEN ring cyclotron (RRC). The beam spot size was approximately $5\ \text{mm}$ in diameter. At first, the C-foil broke immediately within a short time even when the foil

was irradiated by a beam with low intensity. The C-foil was irradiated with strobe light⁶) to remove mechanical stress on the foil and to produce a wrinkle on the foil. After that, we did not observe the immediate cracking of the C-foils and they were used for about $5\sim 9$ hours. A beam irradiation test using a C-foil with a large area attached on a rotating cylindrical stripper device⁷) will be performed in the near future.

References

- 1) H. Hasebe, M. Kase, H. Ryuto, and Y. Yano: Proc. The 17th International Conference on Cyclotrons and their Applications (Cyclotrons 2004), Tokyo, Japan, October 2004, p. 313.
- 2) H. Hasebe, H. Ryuto, N. Fukunishi, A. Goto, M. Kase, and Y. Yano: Nucl. Instr. and Meth. **A 590**, 13 (2008).
- 3) H. Hasebe, H. Okuno, H. Kuboki, N. Fukunishi, O. Kamigaito, A. Goto, M. Kase, and Y. Yano: RIKEN Accel. Prog. Rep. **42**, 133 (2009).
- 4) ULVAC, Inc. URL: <<http://www.ulvac.co.jp/>>
- 5) Nanosurf AG, URL: <<http://www.nanosurf.com/>>
- 6) H. Hasebe, M. Kase, E. Ikezawa, Y. Miyazawa, M. Hemmi, T. Aihara, T. Ohki, and H. Yamauchi: Proc. The 24th Linear Accelerator Meeting in Japan, Sapporo, Japan, July 1999, p. 287.
- 7) H. Ryuto, H. Hasebe, N. Fukunishi, S. Yokouchi, A. Goto, M. Kase, and Y. Yano: Nucl. Instr. and Meth. **A 569**, 697 (2006).

Renovation of the central region of RIKEN AVF cyclotron and results of beam acceleration test

A. Goto, S. B. Vorozhtsov,^{*1} E. E. Perepelkin,^{*1} A. S. Vorozhtsov,^{*1} S. Watanabe,^{*2} S. Kubono,^{*2} and M. Kase

In order to increase the maximum available energies of $^{16}\text{O}^{7+}$ and $^6\text{Li}^{3+}$ ion beams to 12 MeV/nucleon (see Fig. 1), we renovated the central region of the AVF cyclotron in August 2009 on the basis of beam simulations. We then performed an acceleration test in September 2009 by using the $^4\text{He}^{2+}$ ion beam, which is equivalent to a $^6\text{Li}^{3+}$ ion beam, with the new central region geometry.

Fig. 1 shows the performance of the AVF cyclotron. The shaded pentagon-shaped region indicates the region where ion beams are designed to be available. The inclined line

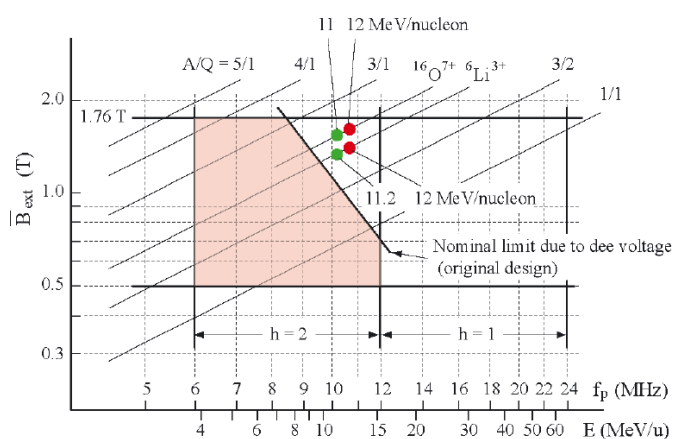


Fig. 1. Acceleration performance of the AVF cyclotron. See the text for details.

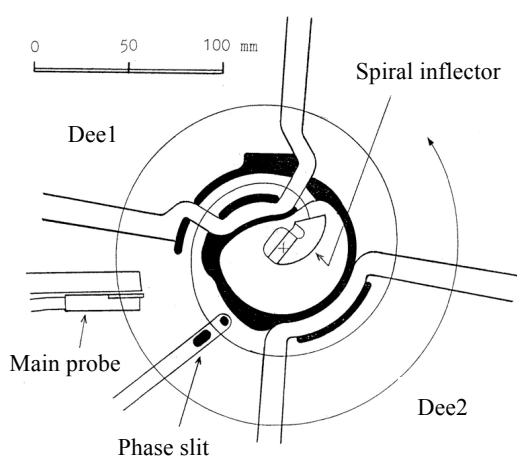


Fig. 2. Original geometry of the central region of the AVF cyclotron.

shows the limit determined for the original design on the basis of the central region geometry (see Fig. 2) and the frequency characteristics of the available dee voltage. If the beam is allowed to pass through (not necessarily along the center of) the aperture of the channel at the inner tip of the first dee electrode, Dee1, the maximum beam energy may increase to some extent even with this geometry. In addition, beam simulations performed using the 3D electric fields^{1,2,3,4} calculated for the central region revealed that the original design underestimated the limit. Actually, a 11 MeV/nucleon $^{16}\text{O}^{7+}$ ion beam and a 11.2 MeV/nucleon $^6\text{Li}^{3+}$ ion beam were accelerated successfully in December 2008. To further increase the beam energies, however, the geometry of the central region had to be modified.

The renovation process involved the following steps: 1) replacement of the RF shield accommodating the spiral inflector as well as the inner tips of Dee1 and Dee2 with new ones (see Fig. 3) and 2) elongation of the inflector electrode by attaching 2-mm-thick copper plates to the end surfaces of the inflector entrance and exit (see Fig. 4). The aim of the first step was to bring the side walls of the dee-electrodes and the wall of the RF shield as close to the cyclotron center as possible, as shown by the white curves in Fig. 3. 3D beam simulations performed with the new geometry confirmed that the beam energy can be increased to 12 MeV/nucleon while ensuring the beam quality is as good as that with the old geometry. The second step was necessary since previous 3D beam simulations showed that reduction of the inflector-electrode length by cutting off a 4-mm (half of the electrode gap) pieces from each end contributed to overcorrection.

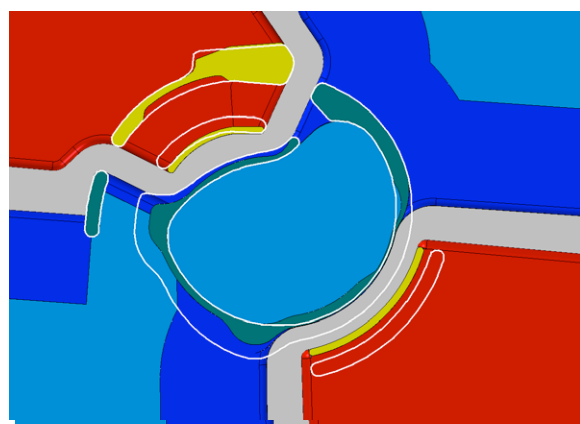


Fig. 3. Renovation of the central region. White line: old geometry; shaded part: new geometry.

^{*1} Joint Institute for Nuclear Research, Russia

^{*2} Center for Nuclear Study, University of Tokyo

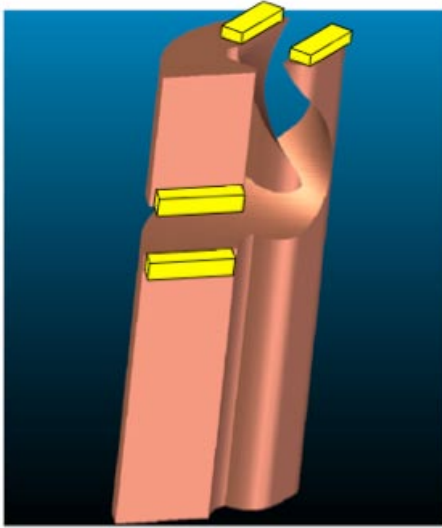


Fig. 4. Renovation of the spiral inflector. The inflector electrode was elongated by attaching 2-mm-thick copper plates to the end surfaces of the inflector entrance and exit.

In the beam test performed in September 2009, we focused on the injection, acceleration, and extraction of a 11.2 MeV/nucleon ${}^4\text{He}^{2+}$ ion beam. The acceleration to 12 MeV/nucleon, which had been previously planned, had to be canceled owing to machine trouble. Fig. 5 shows the beam transmission through the AVF cyclotron along with that observed in December 2008. The injection efficiency (the ratio of the beam intensity at I36 and $R = 74$ mm) for the new geometry was approximately 50 %, which was five times that obtained for the old geometry. This high efficiency was obtained when the Dee1 voltage was 37 kV, which was lower than that applied in the previous test (41 kV). The extraction efficiency, on the other hand, was very poor, because of which there was no notable improvement in the total transmission efficiency (approximately 10 %). From the performance achieved thus far, we speculated that the operational parameters for the extraction system, including those for the harmonic coils, were not optimal. The performance can be improved with careful tuning of the aforementioned parameters for future extractions.

The 3D beam simulation results show that the dee voltage required for the 12 MeV/nucleon ${}^{16}\text{O}^{7+}$ ion beam is

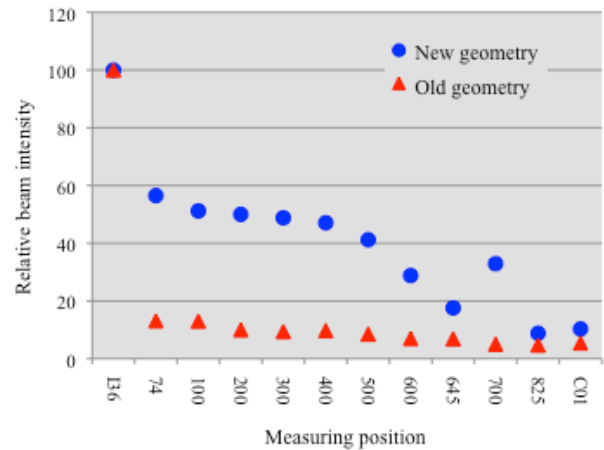


Fig. 5. Comparison of beam currents (relative values) obtained with the old and new central-region geometries. I36 and C01 denote Faraday cups placed immediately before and after the AVF cyclotron, respectively. The numbers with mm units denote the radial positions of the main probe: 825 mm denotes the position after the extraction system. The beam current is staggered at 500 mm-700 mm because the main probe fails to detect the entire beam current when the beam is not aligned appropriately with the probe; this is because of off-centered beam oscillations.

49 kV, which is close to the presently available maximum voltage. Furthermore, it has been found in the present test that the experimentally optimized dee voltage for Dee1 is slightly lower than the required voltage determined by the 3D beam simulation. Therefore, it can be concluded that acceleration of the 12 MeV/nucleon ${}^{16}\text{O}^{7+}$ ion beam (as well as the ${}^6\text{Li}^{3+}$ ion beam) is possible with the new central region geometry.

References

- 1) A. S. Vorozhtsov et al.: RIKEN-NC-AC-2.
- 2) E. E. Perepelkin et al.: Proc. RuPAC 2008, p.40.
- 3) S. B. Vorozhtsov et al.: Proc. RuPAC 2008, p.51.
- 4) S. B. Vorozhtsov et al.: Proc. 6th Annual Meeting of Particle Accelerator Society of Japan, Tokai, Japan, August 5-7, 2009, p.240.

Possibility of formation of round beams in RIBF cyclotrons

H. Okuno, A. Adelman,^{*1} and J.J. Yang^{*2}

[Cyclotron, Space charge]

The increase in the intensity of uranium beam in the RIBF accelerator complex motivated us to study the vortex motions in cyclotrons. Longitudinal space-charge force causes an increase in the acceleration of head particles and deceleration of tail particles. The accelerated or decelerated particles move to higher or lower radii because of the isochronous condition in cyclotron, which causes a rotation of the ion bunch. The nonlinearity of the space-charge force leads to a spiral-shaped halo of the bunch, which finally turns into a rotating sphere. These vortex-motion phenomena were theoretically studied as shown in the reference¹⁾ and experimentally verified at the PSI Injector II.

In his thesis²⁾, Pozdeyev described that the effects of the space-charge force on the bunches of similar lengths approximately scale as

$$\frac{qI}{\gamma^5 m h \omega^3}, \quad (1)$$

where I is the total beam current, h is the harmonic number, and the momentum is $m\gamma R\omega$. Table 1 lists the values of the parameter described above in the case of Injector II, RRC, fRC, IRC, and SRC, indicating that the effects of the space-charge force observed in RRC is approximately same as that observed in the Injector II, while the effects observed in the other three cyclotrons are small. Therefore, our beam dynamics study focused on the RRC, which is a low-energy cyclotron.

OPAL-cycl³⁾ is one of the flavours of the Object Oriented Parallel Accelerator Library (OPAL) framework. It is a new 3D PIC-based self-consistent numerical simulation code that takes into account neighboring bunch effects. The self-consistency of the code is clarified in electrostatic approximation. A more detailed description of the OPAL framework and OPAL-cycl code can be found in the User's Reference Guide⁴⁾.

The RRC consists of four sector magnets and two double-gap rf resonators. Simulations performed using OPAL-cycl require an accurate isochronous field map and radial distribution of rf voltage at the gaps. A highly accurate field map of the isochronous field was calculated using ANSYS⁵⁾. Radial distribution of rf voltage was assumed to be constant since radial distribution of the resonator of the RRC remains constant at 18.25 MHz.

Single-particle tracking using OPAL-cycl is necessary to check the isochronism of the field map, the validity of the initial condition, and the matching phase

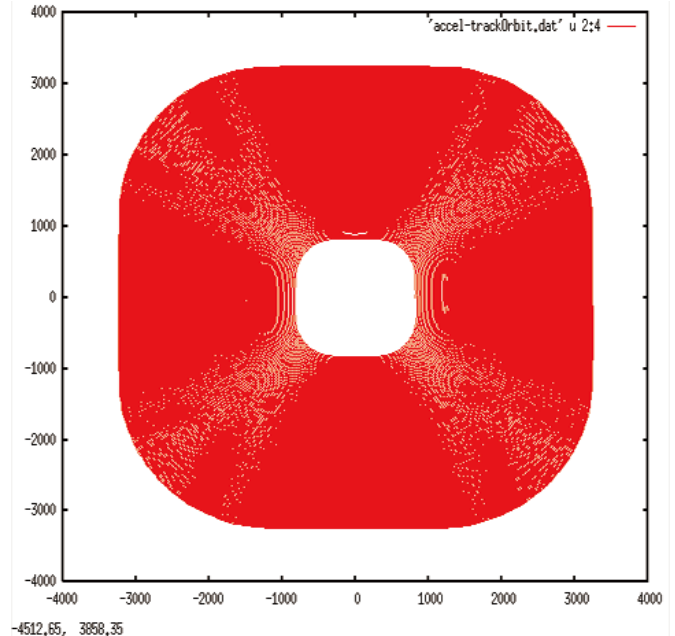


Fig. 1. Top view of single-particle tracking of the reference particle up to the final turn in RRC.

ellipse before multi-particle tracking including space-charge forces. Figure 1 shows the single-particle tracking of a reference particle accelerated up to its final turn. It took about 296 turns for the particle to attain a final energy of the cyclotron. The phase slip at the rf-gap crossing, which is shown in Fig. 2, indicating that the used field map is sufficiently isochronous. Single-particle tracking was carried out with initial offsets of $r(z) = 5.0$ mm and $pr(pz) = 0.0$ mrad from the static equilibrium orbit at injection energy in order to obtain eigen ellipses in the radial and vertical directions. The results (Fig. 3) show that the ratios of the semi-major axis to semi-minor axis are 5.0/4.2 and 5.0/2.5 mm/mrad in the radial and vertical directions, respectively. These ellipses were used as the initial conditions for multi-particle tracking.

Multi-particle tracking taking into account space charge forces was carried out at a beam current of 0.5 mA using the initial conditions obtained from the

Table 1. List the value of the parameter of (1) in the text.

PSI Inj. II	RRC	fRC	IRC	SRC
1	0.644	0.096	0.031	0.016

^{*1} Paul Sherrer Institute

^{*2} CIAE and Tsinghua University

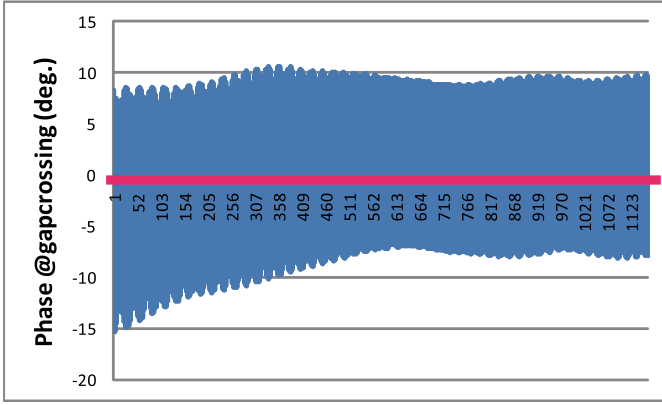


Fig. 2. The blue lines show phase slip at the gap crossing in RRC while the red line shows 0° at gap crossing. The horizontal axis shows the total number of the gap crossing.

single-particle tracking studies. We performed simulations of the acceleration in the first 10 turns after injection because we are mainly interested in the behaviour of the bunches just after beam injection. Initial transverse rms emittance was assumed to be 2.5π mm mrad on the basis of operational experience. The initial rms bunch length was assumed to be 2° or 4° in order to study how the bunch length impacts on the vortex motions. Figure 4 shows the results of the simulations. The results for both 2.0° and 4.0° clearly indicate vortex motions of bunches toward stationary circular distributions. The bunch in the case of 2.0° has smaller tails and rotates faster than that in the case of 4.0° . More detailed simulations up to the final turns taking into account the space-charge effects from neighbouring turns are in progress.

References

- 1) S. Adam: IEEE Trans. On Nuclear Science 32, 2507 (1985).
- 2) E. Pozdeyev: Ph. D. Thesis, MSU, USA (2003).
- 3) J. Yang, A. Adelmann, M. Humbel, et. al.: Proc. of HB2008, in press, August 2008, Nashville.
- 4) A. Adelmann, et. al.: Tech. Rep. PSI-PR-09-05, Paul Scherrer Institut (2009).
- 5) L. Stingelin: private communication

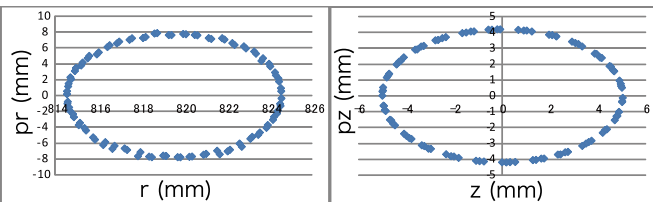


Fig. 3. Eigen ellipses at the first turn of RRC in the radial and vertical directions.

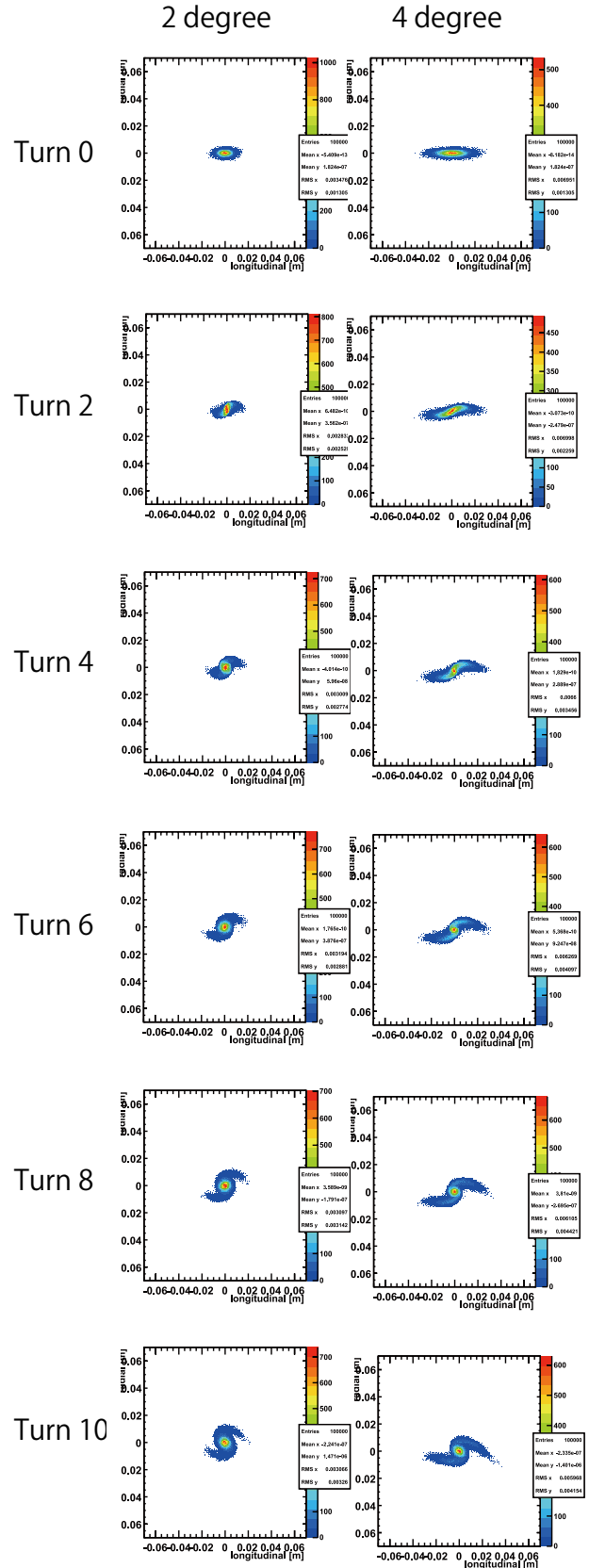


Fig. 4. Results of multi-particle tracking. The turn numbers are given on the left of the contour plots. The rms value of the initial bunch length is mentioned at the top of the contours.

Measurement of Magnetic Field of fRC Sector Magnets

K. Kumagai and N. Fukunishi

The fixed frequency ring cyclotron (fRC) accelerates uranium beams with a charge state of $71+$ ^{1,2}. These U^{71+} ions are converted from U^{35+} at the charge stripper located downstream of RIKEN Ring Cyclotron (RRC). The thickness of the carbon film used in the charge stripper is about $300 \mu\text{g}/\text{cm}^2$. On the basis of the result of the measurements, the energy spread of the uranium beam passing through the film is estimated to increase by 0.4 - 0.5% and this increase causes the beam losses. Since the energy spread is proportional to the film thickness, the use of a thinner film is desirable but it decreases the charge state of the product with maximum yield. When we use a film with a thickness of $200 \mu\text{g}/\text{cm}^2$, the maximum yield is in U^{69+} . Therefore it was necessary to perform the measurement of the magnetic field of the fRC to confirm whether or not the U^{69+} ions can be accelerated. We developed a magnetic-field measuring system capable of measuring the one-dimensional magnetic field along the centerline of sector magnets.

The fRC consists of four sector magnets, namely, NE, SE, NW, and SW, whose pole gaps are 50 mm, ten trim coils are attached to the upper and lower pole surfaces. The maximum current of the main coil is 650 A, and the maximum magnetic field at the magnet center is about 1.75 T.

Figure 1 shows a field measuring system. Square pipes, which are 4-m long, are installed in the beam chamber from backside of the magnet yoke along the centerlines of the sector magnet. The measurement devices are placed within the pipes that are at atmospheric pressure. Two measuring apparatus with the same specifications were assembled. First, two sector magnets on the east side were measured, and then, the two on the west side were measured. The beam chamber was evacuated during the measurements.



Fig. 1. Photograph of the magnetic field measuring system. The left of figure is a backside of the magnet yoke.

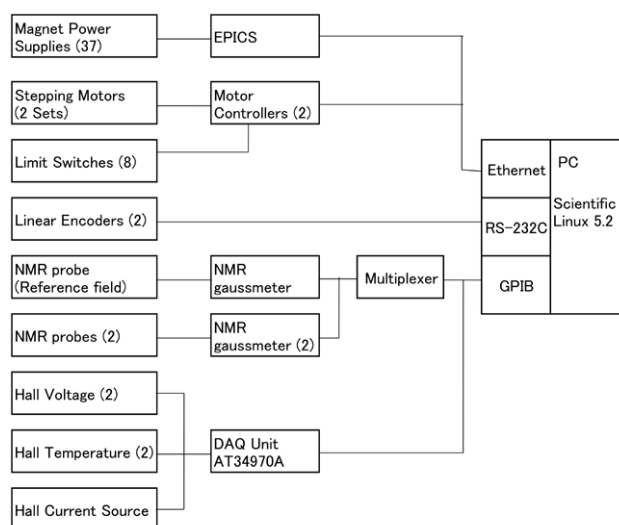


Fig. 2. Block diagram of the measurement and control system.

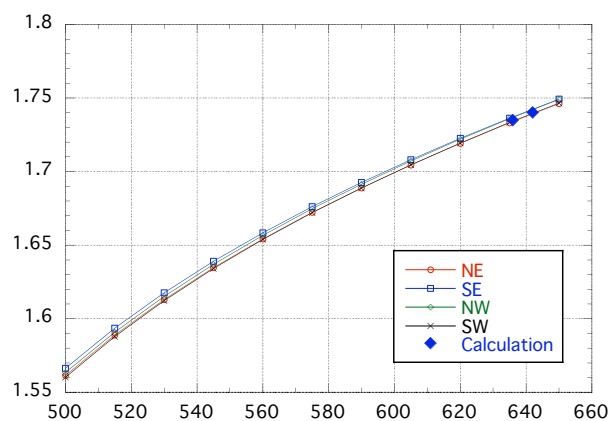


Fig. 3. Excitation curves of the four sector magnets observed at $R = 2600 \text{ mm}$ and calculated strength by TOSCA-3D.

Figure 2 shows a block diagram of the measurement system. Most of the driving devices such as stepping motors, linear encoders and limit switches were recycled from the magnetic-field measuring equipments of the SRC. NMR measuring instrument (Echo Electric Co., Ltd, EFS-800S) and high linearity Hall-effect sensors (F.W. BELL Products; BHT-900 series) were used as measuring probes. The fields were measured using both the NMR and Hall sensors in the region where the magnetic field was uniform and by Hall sensors in the region where the magnetic gradient was strong. The Hall sensors were fixed on a block where the temperature was controlled to within $30 \pm 0.2 \text{ }^\circ\text{C}$ for accurate measurement. As several years had passed since

the Hall sensors had been calibrated, they were recalibrated with the NMR measured in the uniform field area. The variation in the measurements of the Hall sensors between several years ago and the current were about 10 gauss. A program for the field measurement was written in Python using VISA (Virtual Instrument Software Architecture). The magnet power supplies were controlled using EPICS.

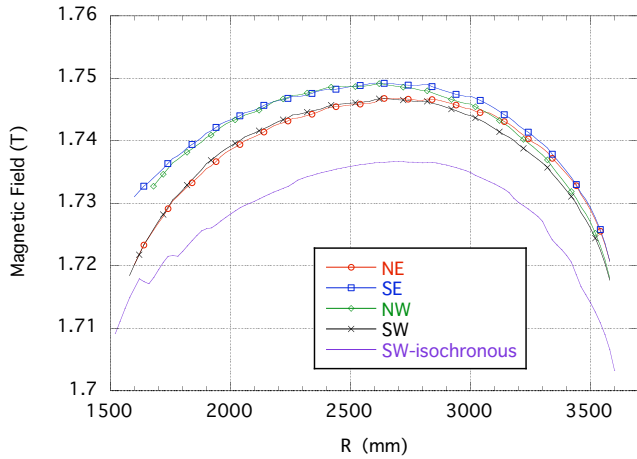


Fig. 4. Difference in the magnetic field distributions of four sector magnets at a main coil current of 650 A and a calculated isochronous field distribution for U^{69+} acceleration.

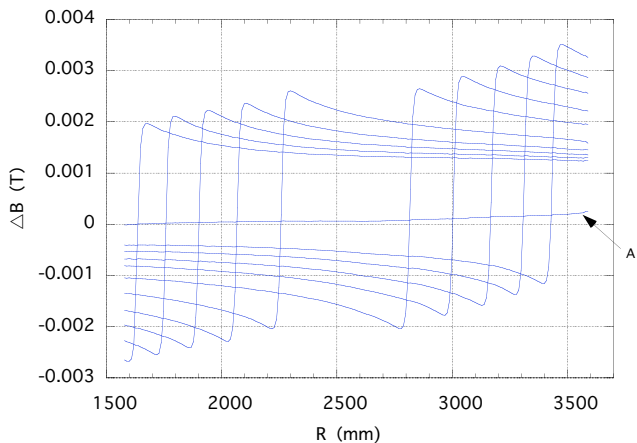


Fig. 5. Trim-coil field distributions at a main-coil current of 650 A. The currents are +100 A for each trim coil. A indicates the distribution after the ten trim coils are excited one by one and then returned to their initial states.

The magnetic fields were measured at main-coil current between 500 and 650 A; the current was raised by 15 A for consecutive measurement. On the other hand, the trim coil currents were increased by 50 A for consecutive measurements. The interval between measurement was 20 mm for main coil and was 10 mm for trim coil. The magnet was initialized before each measurement of the main-coil field.

Excitation curves of the four sector magnets at a radius

of 2600 mm on the sector centerlines are shown in Fig. 3. The calculation results by TOSCA-3D at 636 A and 642 A are also shown. The measured results are in good agreement with the calculated values.

Figure 4 shows the magnetic field distributions along the centerline of the four sector magnets at a main coil current of 650 A. The field distributions of the NE sector and the SW sector are about 30 gauss smaller than those of NW and SE sectors. These discrepancies can be corrected by 30-A bypass power supplies of the main coils and ± 200 A trim-coil power supplies which exist individually by each sector. The calculated isochronous magnetic field distribution for U^{69+} acceleration is also shown in Fig. 4. Since the measured distributions were significantly larger than the calculated distribution, we can conclude that it is possible to obtain the isochronous field distribution that is required for U^{69+} acceleration.

An example of the magnetic field distribution produced by trim coils is shown in Fig. 5. The current of each of the main coils and the trim coils to generate the isochronous magnetic field can be determined by precisely fitting these measurement results.

Furthermore, in order to accelerate U^{69+} beam we need to increase the maximum currents of injection and extraction magnet power supplies (EBM, MIC2, MDC1). After the improvement for magnet power supplies, we will be planning to accelerate U^{69+} beam.

References

- 1) N. Fukunishi et al.: RIKEN Accel. Prog. Rep. **41**, 79, 81 (2008).
- 2) N. Fukunishi et al.: RIKEN Accel. Prog. Rep. **42**, 105 (2009).

Construction of Client System for 28GHz SC-ECRIS

A. Uchiyama,^{*1} M. Kobayashi-Komiyama, M. Fujimaki, Y. Higurashi, M. Tamura,^{*1} and T. Nakagawa

To increase the intensity of the Uranium ion beam used in the RIKEN RI beam factory project, a new RIKEN 28GHz superconducting ECR ion source (28GHz-ECRIS) was constructed in 2009.¹⁾ For effective and stable operation of the 28GHz-ECRIS, the client system should have a user-friendly user interface (UI) in the control system. For this reason, we constructed a new client system with a graphical user interface (GUI), a web interface and a data acquisition system (DAQ). In this paper, we report the system and its status in detail.

To control the 28GHz-ECRIS, the system incorporated with several types of distributed systems for remote control along with Ethernet. For the control of main devices such as gas valves and the rod position in 28GHz-ECRIS, a combination of a Yokogawa F3RP61-2L module that acts an EPICS input/output controller (IOC) and FA-M3 programmable logic controllers (PLCs) is adopted with the embedded EPICS technology.^{2,3)} A vacuum control system and a beam diagnostic system are constructed by EPICS using Linux-based IOCs connected with N-DIMs via Ethernet. The bending magnet control system and steering magnet control system comprise a VME-based IOC that communicates with NIOs.³⁾ To facilitate information exchange among different types of controllers, the protocol for the abovementioned controllers should be unified by a channel access (CA) protocol from the client's point of view. The 28GHz-ECRIS control system, however, includes not only an EPICS-based system but also a standalone system that uses Melsec PLCs for controlling superconducting magnet. The client system for the Melsec PLCs has been constructed by using SoftGOT1000, and it can be run on a Microsoft Windows XP PC. Therefore, our main work is to construct the client system for 28GHz-ECRIS operation with exception of the superconducting magnet. The requirements for the client system are as follows:

- Useful GUI application for main control
- XY plotter
- Beam current monitor
- Log notebook
- Water leak alert
- Data acquisition system

For the 28GHz-ECRIS client system, two Microsoft Windows XP PCs are used in the RILAC control room (see Fig. 1). The X Window System with Cygwin is installed on the PCs; the system has six displays based on multiple-display environment. A main GUI panel for controlling the gas valves, RF power supplies, magnets power supplies, and beam extraction devices has been developed by using EDM. EDM is one of the motif-based display managers provided by the EPICS collaboration for developing a client system with a GUI. Before construction

of 28GHz-ECRIS client system, the many GUI applications in RIKEN RIBF control system were developed by using MEDM. Since EDM has following advantages over MEDM, we adopted the former for development of GUI applications in 28GHz-ECRIS client.

1) The EDM has rich component for GUI objects. For example, the mouse-operated up-down button in EDM is suitable for the operations of the magnet power supply because separate functions can be allocated by right click and left click.

2) In the X window system, it is available to set the window at the required position. EDM has a high degree of usability in multiple displays with wide area.

3) It is possible to output the calculated values to the GUI application without the need for maintaining any calculation records into the EPICS database. Therefore, it is possible to simplify source code and reduce the number of programs.

As an example, a constructed XY plotter chart is shown in Figure 2.



Figure 1. Client PCs with Microsoft Windows XP in RILAC control room.

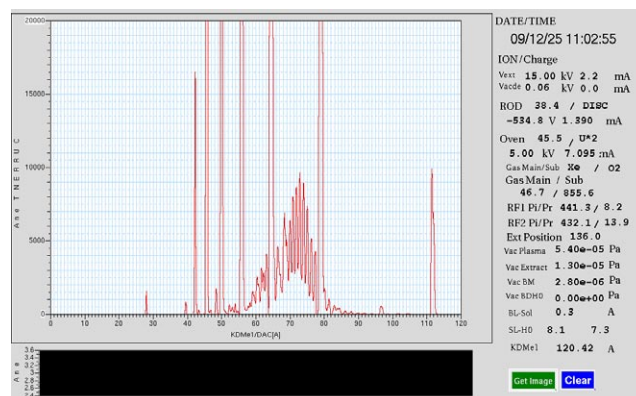


Figure 2. XY plotter chart developed by using EDM in 28GHz-ECRIS operation

For monitoring the 28GHz-ECRIS beam current, a GUI application is developed by using EDM. On the other hand, the beam current for another ion source, RIKEN 18GHz-ECRIS, was regularly monitored by the operators with the help of a picoammeter for beam tuning. Comparison of both methods revealed the picoammeter was more suitable for beam tuning. Therefore, in the future, we plan to develop a new GUI meter that is ergonomically better than the picoammeter for beam current monitoring.

Since there are numerous parameters related to the 28GHz-ECRIS operation, maintaining records in a paper notebook is not feasible. To save the 28GHz-ECRIS parameters in an effective manner, we plan to construct a paperless log system by using Wiki (See Fig. 3). Wiki is a system that can edit and create hypertext documents on the web server by using the web browser; HTML knowledge is not required in this case. Currently, various types of Wiki are being used because of the increase in the rate of Internet access around the world. In our system, an open-source PukiWiki⁴⁾ is installed in the server. Simultaneously, we have developed a program for the client; this program dumps image files from the GUI clients and automatically pastes the image file inset the PukiWiki page. The procedure for saving the 28GHz-ECRIS parameters is as follows.

1. Click the icon on the GUI to dump the image file.
2. Edit the Wiki page that has the image file, if needed.



Figure 3. Wiki page with an image dump file for 28GHz-ECRIS main control GUI panel

In the main panel, vacuum monitor and XY plotter chart provide the above-mentioned function in cooperation with Wiki. In this manner, operators can record the parameters easily quickly and accurately many times during an experiment. In the actual 28GHz-ECRIS operation, operators obtain the parameter log every 3h. The Wiki page often contains important information when an operator informs others of the trouble status. In addition, this Wiki-based system has a log management function that carries out a search by the keyword method for automatically inserted EPICS record values and manually

inputted comments. Therefore, it is easy to find a parameter log from a large number of the page. Thus, we confirmed that this Wiki-based system is more useful for recording the parameters than is a paper log notebook.

In the case of a water leak, the accelerator operators are alerted by the hardware buzzer. In our system, water leak in the 28GHz-ECRIS room is triggered by an alarm system by using the EPICS sequencer on F3RP61-2L. As a client for embedded EPICS on F3RP61-2L, a hardware alarm that use a PIC network interface card (PICNIC) is implemented in the control room.⁵⁾ On the other hand, the EPICS collaboration provides Alarm Handler as a standard software for the same purpose. However, for Alarm Handler to provide the desired service, the operating application and X Window System must be continuously run on the PC equipped with speakers. For this reason, the real emergency alarm function should be active at all times with the hardware alarm.

By MyDAQ2⁶⁾ developed at JASRI/Spring-8 as the DAQ in the 28GHz-ECRIS, we record EPICS values such as vacuum, extraction current, and RF power in the MySQL database. In our system, we developed an EPICS CA client for data collection. Data are added to the MySQL database every 10 second via a socket connection to the server that runs MyDAQ2. Since the graph and text can be easily displayed on web browsers, the web applications have a user-friendly UI as well as a Wiki-based system. The DAQ based on MyDAQ2 can be used for reducing the turnaround time during system construction.

One of the authors (A. U) wishes to thank Ms. T. Hirono, JASRI/Spring-8, for assistance in the construction of the MyDAQ2 system.

References

- 1) Y. Higurashi et al.: in this report.
- 2) J. Odagiri et al.: Proc. ICALEPCS09, Kobe, Japan, 2009.
- 3) M. Komiyama et al.: Proc. ICALEPCS09, Kobe, Japan, 2009.
- 4) <http://pukiwiki.sourceforge.jp/>
- 5) A. Uchiyama et al.: Proc. ICALEPCS09, Kobe, Japan, 2009.
- 6) T. Hirono et al.: Proc. PCaPAC08, Ljubljana, Slovenia, 2008, p.55.

Improvement of beam energy and longitudinal beam profile measurement system

T. Watanabe, N. Fukunishi, K. Yamada, M. Kase, M. Wakasugi, M. Fujimaki, N. Sakamoto, K. Suda, H. Kuboki, R. Koyama, and O. Kamigaito

Plastic scintillation monitors (scintillation monitors) have been fabricated to evaluate the energy and longitudinal profiles of heavy-ion beams at the RIKEN RI beam factory (RIBF)^{1,2}. Four sets of scintillation monitors (8 monitors) were installed in the transport lines of the RIKEN heavy-ion linac (RILAC), RIKEN ring cyclotron (RRC), fixed-frequency ring cyclotron (fRC), and intermediate-stage ring cyclotron (IRC) to measure the time of flight (TOF), namely the acceleration energy, of the heavy-ion beams. Furthermore, a total of six scintillation monitors were installed in the transport line, upstream of the injection points and downstream of the extraction points of these accelerators, to optimize the phase between the RF cavities and the beam. The improvements made to the scintillation monitor system are reported in this article.

Figure 1 shows a block diagram of the system. The plastic scintillator is pneumatically inserted into the beam transport chamber by the pneumatic rotary feeder when the measurement process is started. When a scintillation material is bombarded by a charged particle, fluorescence photons are produced. Then, these photons are amplified by a photomultiplier that has extremely high sensitivity. Longitudinal beam profiles are obtained using a time-to-digital converter (TDC), which digitizes the time lag between the start pulse (detected signal) and the stop pulse (bunch clock). The energy of the beam can be calculated from the measured TOF of the beam by using a longitudinal profile monitor set. For data acquisition and control

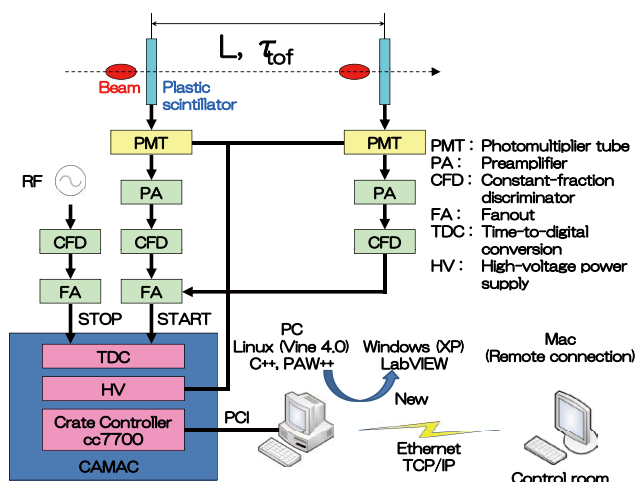


Fig. 1. Block diagram of beam energy and longitudinal beam profile measurement system.

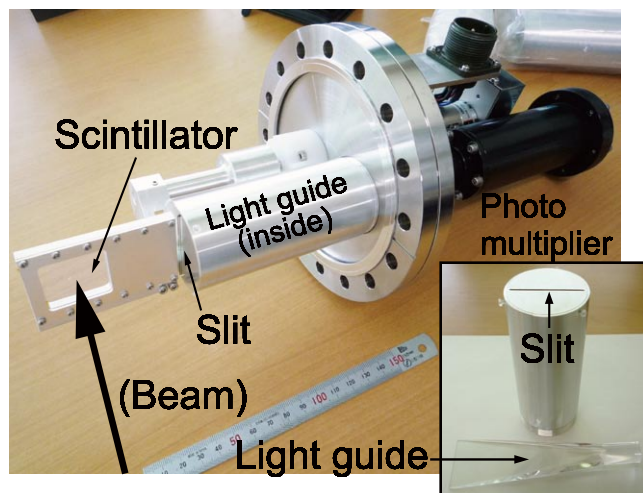


Fig. 2. Photo of scintillation monitor with slit and light guide.

of the scintillation monitors, the CAMAC system with Linux-based PCs is used. These PCs are connected to a laptop in the main control room located 200 m from the RRC hall by using Ethernet and remote connection. The measured results are displayed by PAW++ based on several components of the CERN Program Library. The driving control and status monitoring of the plastic scintillator are controlled by the EPICS system. These programs are written in C language using PAW++ macros and are run on the Linux (Vine 4.0) operation system. This year, to help users operate the system more easily, a new embedded controller with a higher-performance CPU has been introduced and new programs have been written in LabVIEW³, these programs run on the Windows 7 operation system. A device driver for the TDC (TOYO CC/7700) and LabVIEW's call library function nodes using dynamic link libraries (DLLs) have been newly developed. Currently, programs for driving control, data acquisition, and result display have been developed, and work on integrating these programs is in progress.

In order to improve the time resolution, a slit and a light guide have been newly fabricated. Figure 2 shows the scintillation monitor with the slit and light guide. Since the unnecessary light is cut off, the resolution of the TOF is enhanced, namely, the resolution of the beam energy is improved.

References

- 1) T. Watanabe et al.: RIKEN Accel. Rep. **39**, 241 (2006).
- 2) T. Watanabe et al.: RIKEN Accel. Rep. **40**, 131 (2007).
- 3) National Instruments Co., Ltd.

Consistency in measurement of beam phase and beam intensity using lock-in amplifier and oscilloscope systems

R. Koyama*¹, M. Fujimaki, N. Fukunishi, A. Goto, M. Hemmi, M. Kase, N. Sakamoto, T. Watanabe, K. Yamada, and O. Kamigaito

The RIKEN RI beam factory (RIBF) consists of four ring cyclotrons (RRC, fRC, IRC, and SRC) and two injectors (RILAC and AVF) which are all connected in cascade. RILAC, AVF, and RRC began operation in the 1980s, and fRC, IRC, and SRC were installed in 2006. Phase probes (PPs) are installed in all cyclotrons and beam transport lines of RIBF, and the beam-bunch signals that are detected nondestructively by these PPs are used for tuning of isochronous magnetic field of cyclotrons and for monitoring the beam phase and beam intensity (Fig. 1). We mainly use a newly developed system that incorporates a lock-in amplifier (LIA; SR844, SRS) for those tuning and monitoring;¹⁾ however, in AVF and RRC, a conventional measurement method using an oscilloscope system (OSC; DSO6052A, Agilent) is used. In this study, we investigated the consistency in the measurements carried out using LIA and OSC systems.

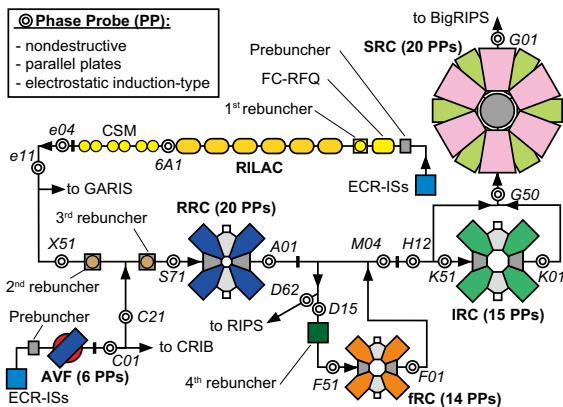


Fig. 1. Schematic layout of RIBF.

The block diagram of the measurement system is shown in Fig. 2. The beam-bunch signals from PPs are divided by a power divider and transported to the LIA and OSC and measured by them simultaneously. Using these measured data, the beam phase and the beam intensity are analyzed automatically by the LabVIEW program.²⁾

The comparison of the isochronism of SRC ($^{14}\text{N}^{7+}$ beam, Energy: 250 MeV/u, Frequency: 27.4 MHz) that was evaluated on the basis of the results of three measurement methods is shown in Fig. 3. This figure shows the relative beam phase observed by 20 PPs, which are radially mounted in the orbital region of SRC. Here, “LIA-3f” is the beam phase measured using LIA with the third harmonic of acceleration RF as its

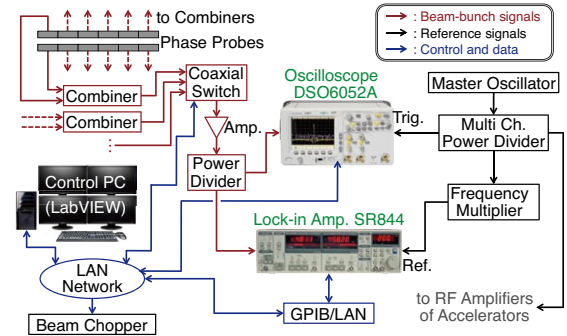


Fig. 2. Block diagram of measurement system.

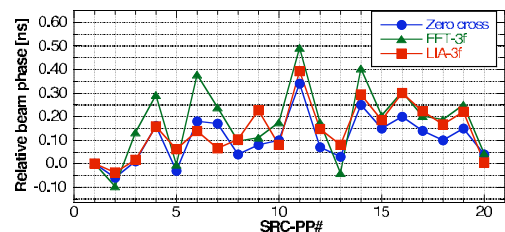


Fig. 3. Comparison of isochronism of SRC on the basis of three measurement methods.

reference signal, “FFT-3f” is the third frequency component (3f) of FFT-analyzed phase of the beam-bunch signal measured using OSC, and “Zero cross” is the zero-cross points of the beam-bunch shape observed using OSC (conventional method).²⁾ We measured the 3f component of the beam-bunch signal because it had good S/N ratio (approximately +5 dB). It was observed that the phase differences between the three measurement methods are less than 0.2 ns (approximately 2° at fundamental acceleration RF).

Figure 4 shows the FFT-analyzed phase up to the 10f component of the beam-bunch signal measured using OSC, together with “LIA-3f” and “Zero cross”. Since in the LIA system, we can basically measure only one frequency component of the beam-bunch signal,²⁾ we need to investigate the other frequency components. However, from the measurements carried out in our work, it was found that the phase differences between ten frequency components are less than 0.5 ns (approximately 5° at fundamental acceleration RF).

Figure 5 shows the beam phase and the beam intensity of a 0.669-MeV/u $^{136}\text{Xe}^{20+}$ beam (RF: 18.25 MHz) detected by PP-S71 (see Fig. 1) over a 4-h period. In this case, the 5f component of the beam-bunch signal had good S/N ratio (approximately +20 dB). The correlation diagrams of the LIA and OSC data presented in Fig. 5 are shown in Fig. 6, and a certain degree of linearity is observed between them.

*¹ SHI Accelerator Service, Ltd.

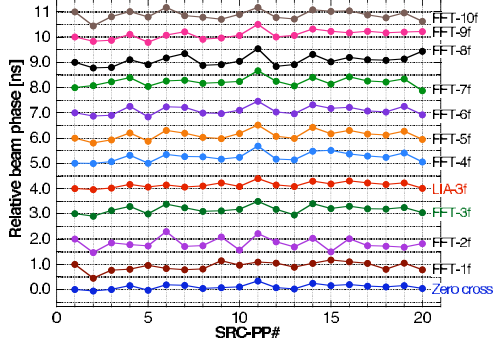


Fig. 4. Comparison of isochronism of SRC for 1st to 10th frequency components (1f–10f) of FFT-analyzed phase.

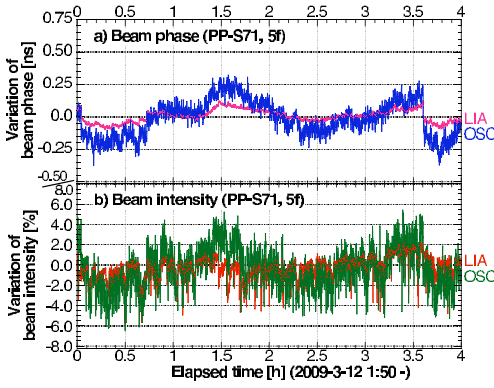


Fig. 5. Beam phase and beam Intensity at PP-S71 measured using LIA and OSC systems.

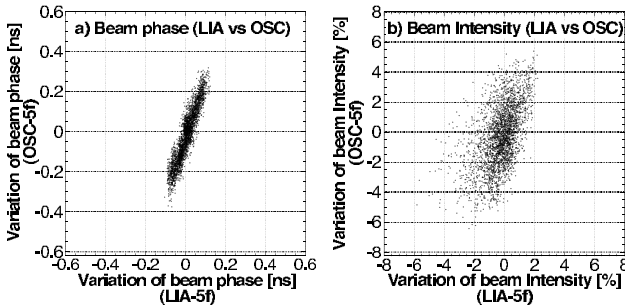


Fig. 6. Correlation diagrams for LIA and OSC data presented in Fig. 5.

Since the fluctuation ranges of both the beam phase and the beam intensity measured using OSC are slightly larger than those of the beam phase and the beam intensity measured using LIA, we investigated the voltage and phase resolution of the LIA and OSC using a function generator (AFG3252, Tektronix). Figure 7a shows the phase and voltage variation measured using the LIA and OSC when the input phase and voltage from AFG3252 to them are varied by 0.01–0.10° and 0.01–0.10%, respectively, after 90 s (frequency: 18.25 MHz). Figure 7b shows 90-s average of the phase and voltage variations plotted in Fig. 7a as a function of the total increment in the input phase and voltage from AFG3252. Here, the error bars in Fig. 7b are

standard deviation for measurements performed after 90 s each ($\pm 1 \sigma$), and they represent the measurement uncertainty. We consider the voltage and phase variations, which are obtained irrespective of the error bars, as the resolution. The error margins for LIA in Fig. 7b are insignificant (smaller than the symbols), indicating low measurement uncertainty in the case of LIA. The resolution and measurement uncertainty of LIA and OSC are summarized in Table 1.

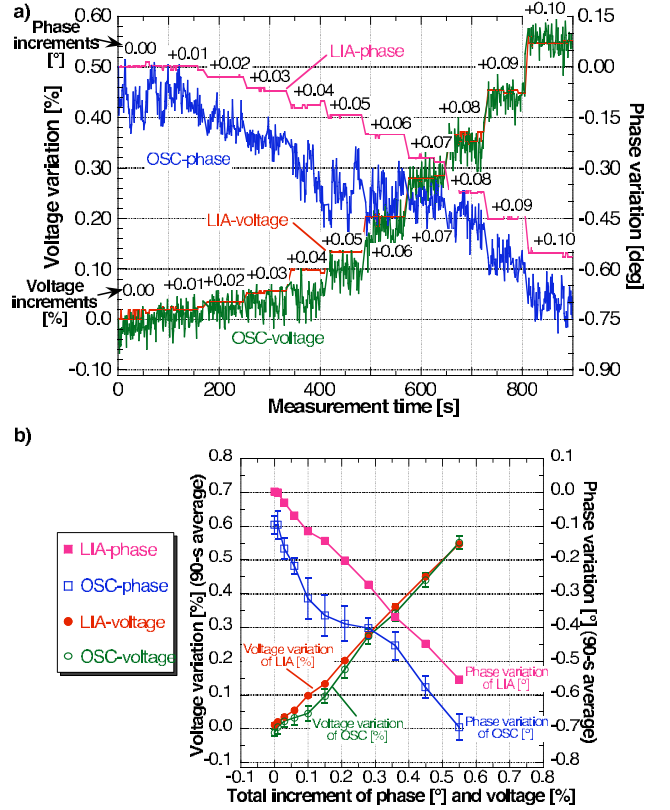


Fig. 7. Phase and voltage resolution of LIA and OSC using AFG3252.

Table 1. Estimated measurement accuracy of LIA and OSC systems.

system	phase [°] ([ps])		voltage [%]	
	resolution	uncertainty	resolution	uncertainty
LIA	0.02 (3)	± 0.007 (1)	0.02	± 0.009
OSC	0.09 (14)	± 0.06 (9)	0.05	± 0.025

As conclusion, the consistency in the measurement results of LIA and OSC is confirmed, as shown in Figures 3–6, and it was observed that LIA has a higher measurement accuracy than OSC, as summarized in Table 1.

References

- 1) R. Koyama et al.: RIKEN Accel. Prog. Rep. **42**, pp. xviii–xix (2009).
- 2) R. Koyama et al.: Proc. of PASJ6, Tokai-mura, Ibaraki, August 2009, WOOPB03, pp. 25–29.

Radiation monitoring in the RRC and the beam distribution corridor using ionization chambers

M. Nakamura, H. Watanabe, H. Okuno and M. Kase

Recently, many experiments have been successfully performed by using the RIBF. However, beam losses in accelerators continue to pose serious problems. To detect beam loss, we constructed an ionization chamber that could be used to monitor radiation from the electrostatic deflection channel (EDC) of the SRC.¹⁾ In this paper, we discuss a trial performed to detect radiations from the RRC and the beam line connected to RIPS in the beam distribution corridor. The RRC and the beam distribution corridor are expected to be quite frequently used during RIBF operations of this year. For the trial, we positioned four ionization chambers at suitable positions and simultaneously measured the signals from these chambers.

The positions of the ionization chambers are shown in Fig. 1. The first chamber was set near the EDC of the RRC, as shown by circle a. The second chamber was set near the phase probe (PP) in the beam distribution corridor, as shown by circle b. The third chamber was set near the target for beam fragmentation (circle c). The fourth chamber was set near the exit of the beam to the RIPS, as shown by circle d.

The size of each ionization chamber was $400 \text{ mm} \times 250 \text{ mm} \times 100 \text{ mm}$. The two electrodes in the chamber were constructed using Al plates that were 1.5 mm thick. The dimensions of the electrodes and the distance between them in the chambers at a) and d) were $360 \text{ mm} \times 200 \text{ mm}$ and

50 mm , respectively. Before the measurements, quite strong signals were observed in the chambers at b) and c), and these signals could not be quantified by our system. Therefore, to decrease the signal intensity, we reduced the sensitive region by remodeling the electrodes and decreasing the gap between the electrodes. Thus, the size of the electrodes and the distance between the electrodes in the chambers at b) and c) were set to be $160 \text{ mm} \times 90 \text{ mm}$ and 25 mm , respectively. This change decreased the sensitivity of these chambers to a value ten times smaller than that of the chambers at a) and d). All these chambers were filled with air at atmospheric pressure.¹⁾

We used two amplifiers (AMPs) to detect the signals from the ionization chambers. The resistances of the AMPs were $1 \text{ G}\Omega$. FLUKE 415 B and Matsusada HEL-4RO.3x2-R were used to supply power to the HV electrodes of the ionization chambers. A GRAPHTEC GL800 data logger was used for recording signals from the AMPs. Data were recorded every 5 s. We monitored radiations during the operation of the RIBF from January 5 to 11, 2010. During this period, $^{48}\text{Ca}^{17+}$ was accelerated to 63 MeV/nucleon. A Be target was used for beam fragmentation. During the period of operation, the voltage supplied to the HV electrodes of the ionization chambers was 2 kV.

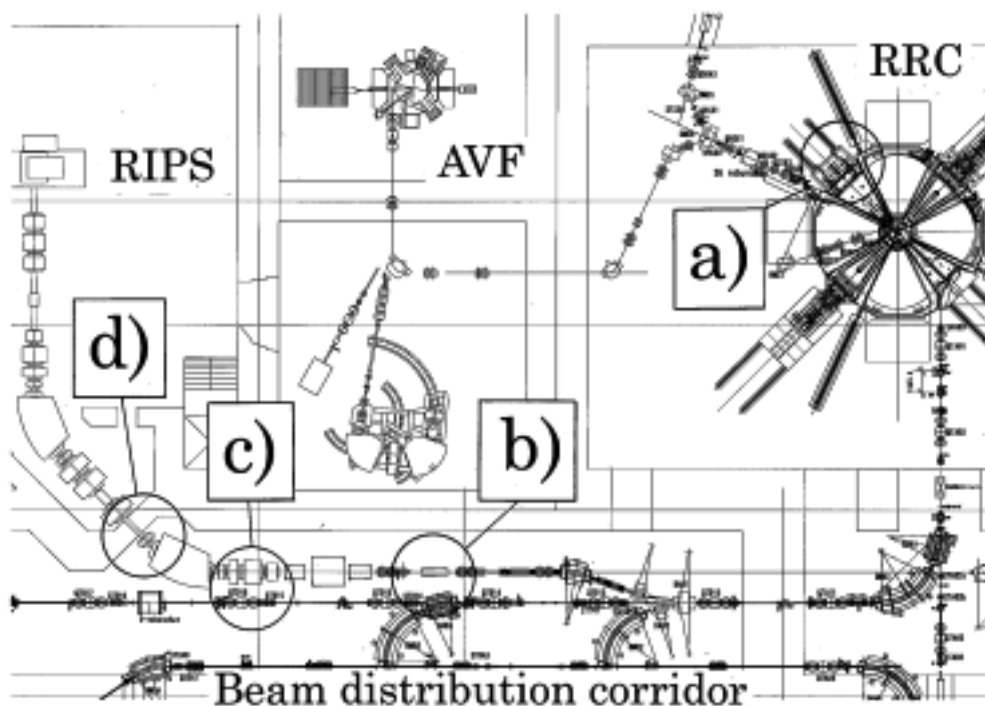


Fig. 1. Positions of ion chambers in the RRC and beam distribution corridor.

Figures 2 a), b), c), and d) show the data recorded during 2010/1/8 9:00 to 2010/1/9 9:00 as typical examples of recorded data. In Figs 2 a), b), and d), the maximum value of the vertical axis was set to 2 V for facilitating easy comparison. In the case of Fig. 2 c), the signal was so strong that the maximum value of the vertical axis was set to 16 V. In these figures, we can clearly recognize the signals corresponding to secondary radiations produced by the $^{48}\text{Ca}^{17+}$ beam. On the other hand, we observe no signals in each figure when the ion beam is stopped. The signal at position a) was between 0.5 V and 1.5 V. We could adjust the EDC so as to minimize this signal and extract an ion beam with the maximum intensity from the RRC. As shown in Fig. 2 b), the signal from position b) was between 0.5 V and 1.5 V. However, considering the size of electrodes and the distance between them, which was described above, radiations from the PP were about ten times more intense than those from the EDC of the RRC. The strongest signal was observed at position c) and was in the range 12–13 V, as shown in Fig. 2 c). Considering that the resistance of the AMPs was $1\text{ G}\Omega$, the current obtained

by this ion chamber was estimated to be 12–13 nA. As shown in Fig. 2 d), the signals at position d) were near 0.5 V. This value was the smallest among the values at the four positions.

In this trial, we performed simultaneous measurements of beam loss at four positions. If we analyze a more detailed time profile of these four signals, we can determine the detailed conditions during the extraction, transport, and focusing of the ion beam, apart from many other factors. By positioning many ionization chambers at suitable places in the facility, we can infer the distribution of ion beam loss in the entire RIBF. We can use such data to make changes to the operation of the RIBF and adjust the important parts of accelerators so as to ensure the best conditions. Furthermore, if the signals corresponding to beam loss become too large, we can stop the accelerator operations and protect the accelerators from serious damage.

Reference

- 1) M. Nakamura, et al.: RIKEN Accel. Prog. Rep. 42, 141 (2008).

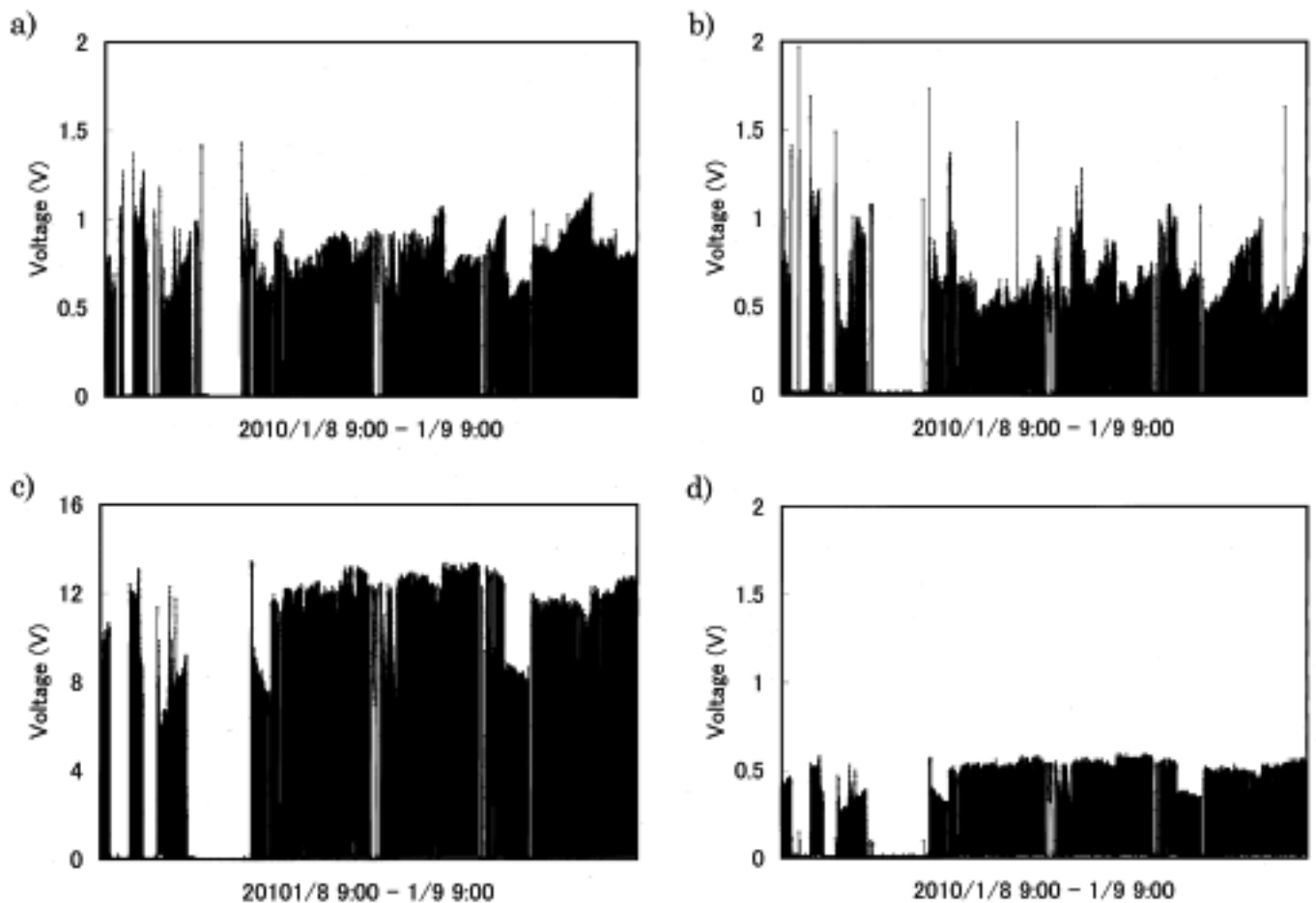


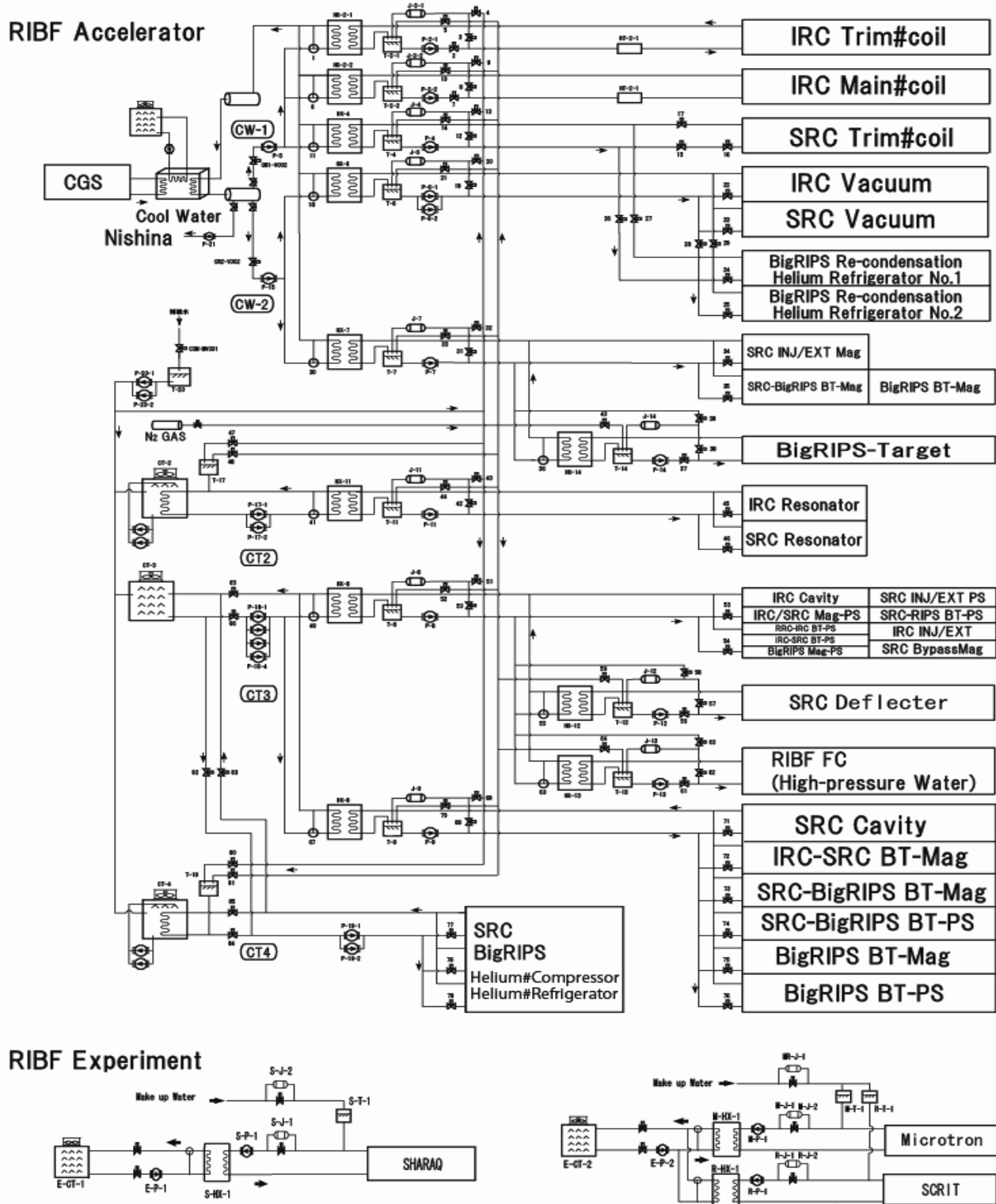
Fig. 2. Observations of signals from ionization chambers during the commissioning of the RIBF with a 63 MeV/u $^{48}\text{Ca}^{17+}$ beam.

The label of each figure (a, b, c, or d) is identical to the location of the ionization chamber (see Fig. 1) from which the signals shown in the figure were obtained.

Water Cooling System in Accelerator for RIBF

T. Maie, K. Kusaka, T. Kageyama, E. Ikezawa, Y. Watanabe, H. Okuno and M. Kase

Water Cooling System in Accelerator for RIBF



RRC: RIKEN RING Cyclotron, fRC: Fixed-frequency Ring Cyclotron, IRC: Intermediate-stage Ring Cyclotron,

SRC: Superconducting Ring Cyclotron, INJ/EXT: Injection/Extraction, FC: Faraday Cup,

BT-Mag: Beam Transport Magnet, CGS: Cogeneration System

Fig. 1. Water-cooling system for RIBF.

The water-cooling system for the RI Beam Factory (RIBF) was newly constructed in 2004.

A schematic diagram and photograph of the water-cooling system are shown in Figure 1 and Figure 2, respectively. On the other hand, the Spectroscopy with High-resolution Analyzer and Radio Active Quantum beams (SHARAQ) water-cooling system was constructed in 2008, and its operation began in 2008, and Fig.2 The SHARAQ cooling system was constructed in 2008. The SCRIT water-cooling system was constructed and its operation began in 2009.

The total operation time of the water-cooling system in fiscal year 2009 was 130 days. In December, during the beam time, the FC faction water pump (P-13) in the sub

system stopped twice because of a failure in its control circuit, consequently, the accelerator operation was effected.



Fig. 2. Photograph of the cooling-water pump on the first floor and the SHARAQ water-cooling system.

Piping for Cool Water in Nishina Building

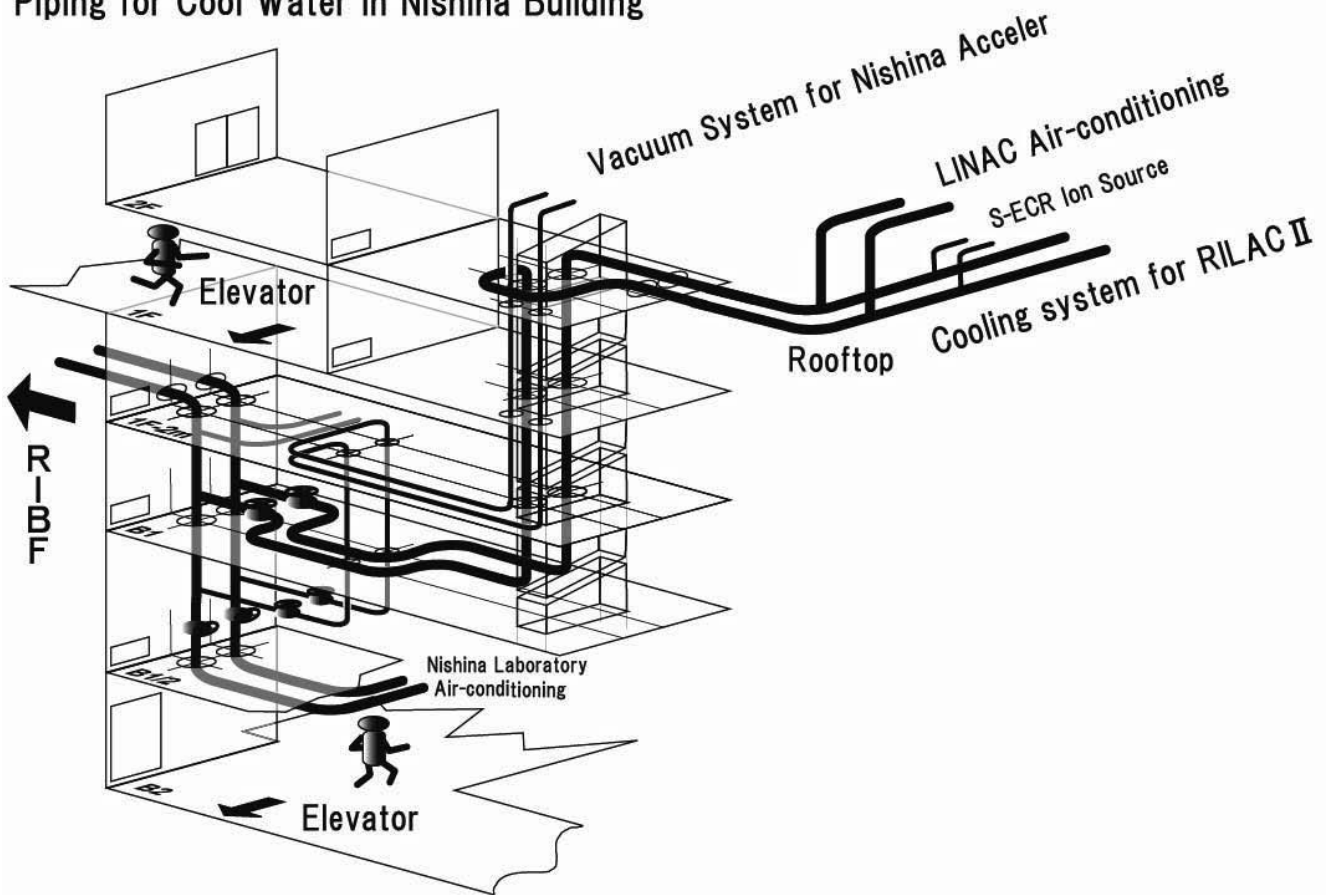


Fig. 3. Usage of cool water in Nishina Building.

The cool water, which is produced by the CGS, is sent to the Nishina and Linac buildings for various purposes, in particular, the water is supplied not only for air-conditioning but also for accelerator operation. In addition, the cool water from the CGS will be used in the water-cooling system of the new injector (RILAC2) in 2010. Figure 3 shows the usage of the cool water produced by the CGS in the Nishina building.

Utilities in the RIBF experimental building

T. Fujinawa and K. Shiraishi*

1. Cranes in E20 and E21 rooms

In each experimental area in RI Beam factory, considerably heavy instruments are present and these are to be moved using cranes. In 2008, we installed cranes for maintenance activities in a SHARAQ room E20. The main crane installed is called "hoist type overhead traveling" crane. The crane was originally designed to move from east to west. However, since it was found that the movement in this direction was not convenient for the maintenance work required in SHARAQ experiments, the traveling direction of the crane was changed so that it moved from north to south and vice versa. For this purpose, new anchor bolts were embedded in the ceiling for adjusting the layout for this modification. All the sophisticated components¹⁾ such as wireless systems, inverter operation systems and other systems are the

same as those in the RIBF building. All the cranes were installed by Sanko Setsubi Co. Ltd.

RIKEN and Kanaden Corporation made a contract on Crane for SCRIT in the E21 room. Called the "Overhead Traveling Crane with shuttle girder", it works asymmetrically according to the layout of SR2. SR2 is the main accelerator of SCRIT and is a modified version of AURORA. This crane is designed such that it can be used to carry instruments as well as be used to in the construction and maintenance activities for an accelerator and a water cooling system. The crane and a chain block were installed in August 2009. They are currently in service.

Specifications of the cranes are shown in Table 1.

Crane No.	Crane 2E1 SHARAQ Room E20	Crane 2E2 SHARAQ Room E20	Crane 2E3 SHARAQ Room E20	Crane 2E4 SHARAQ Room E20	Crane 2F1 SCRIT Room E21	Crane 2F2 SCRIT Room E21
Type	§ 2 OTC	§ 1 JIB	§ 1 JIB	§ 1 JIB	§ 3 OTC-SG	§ 4 TELPH
Rated Load (t)	2.8 t	1 t	1 t	1 t	2.8 t	2 t
Span (m)	7	-	-	-	5.3	10.5
Lift (m)	12	6	7	5.7	4.1	7
Operation	Wireless ※2	Pendant/Manual	※1 Manual	※1 Manual	Wireless	Manual
Rated Speed						
Main Hoist (m/min)	1.1/10	3.9	Manual	Manual	1.1/10	Manual
Traverse (m/min)	2.5/25	10	Manual	Manual	2.5/20	Manual
Travel (m/min)	0/21	Turning	Turning	Turning	2.4/24	-
Travel Rail	I-250 x 125 x 10	Jib Crane	Jib Crane	Jib Crane	I-250 x 125 x 10/19	I-250 x 125 x 7.5/12.5
Electric Power	AC 200 V 50 Hz 3 ph	AC 200 V 50 Hz 3 ph	-	-	AC 200 V 50 Hz 3 ph	-

§ 1: Jib Crane

§ 2: Overhead travelling crane

§ 3: Overhead travelling crane with shuttle girder

§ 4: Telferage

※1: Hoisting/Traversing: Hand Chain

Turning: Pushed by Hand type

※2: Hoisting/Traversing: Pendant

Turning: Pushed by Hand type



Mitsubishi Electric FA Industrial Products Corporation

Table 1 Crane specification

*Mitsubishi Electric FA Industrial Products Corporation

2. Water cooling system

The general plans for the water cooling system for experimental facilities such as SHARAQ, SCRIT and Rare-RI ring were prepared by taking into account the estimation that each facility requires 1 MW. The cooling system is being constructed in three stages. Flow diagrams are shown in Fig.1.

In the first stage, a secondary pipeline with a water pump (37kW) that can carry 8,000 L/min (equivalent of 3 MW) were installed. However, the capacity of the cooling tower was only 1 MW, and the pipe length from the experimental building's basement to the roof was more than 40 m. The primary cooling water pump has a capacity of 30 kW with a water pressure of 0.5 MPa.

The second stage of construction is commenced in 2009 with the installation of two primary pumps. One of the pumps with a

capacity of 37 kW (800 L/min) is used for SR2. The other pump with a capacity of 11 kW (250 L/min) is used for a microtron, which acts as an injector for SR2. The water pressure in both pumps is of 0.8 MPa. An extra 37 kW pump with a 1 MW cooling tower has been installed in non-radioactive area. All electrical motors used have a high efficiency, and all motor starters are direct connecting type²⁾ enabling a quick start and an efficient restart. They also save more “monergy” at the time of initial installment and operation compared with inverter starter system or star- delta starter system.

The primary water cooling line is a closed pipeline; this ensures that the water will never evaporate. The system has a makeup water alarm which goes off in the event of a leakage.

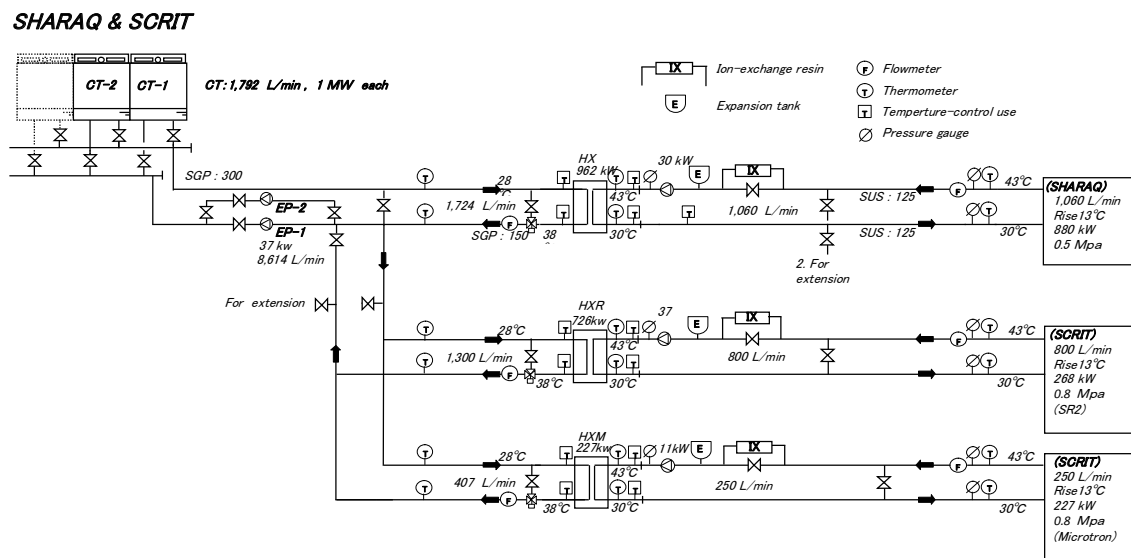


Fig. 1 Flow diagram

Reference

- 1) T. Fujinawa et al: RIKEN Accel. Prog. Rep. 37 (2004) p.289-290.
- 2) T. Fujinawa: JOURNAL OF CIT NIHON Univ. Vol.41 No.2 (2008) ISSN 0385-4442 p.91-97.

Calculation of Minimum Emittance in SR2

M. Hara, T. Hori, and M. Wakasugi

[minimum emittance, electron storage ring, Chasman-Green lattice]

An electron accelerator system is under construction at the RIKEN Nishina Center. This accelerator system is composed of the TRM (racetrack microtron), the ISOL (Isotope Separator On-Line), and the SR2 (SCRIT-equipped RIKEN Storage Ring)¹⁾. The electron synchrotron storage ring SR2 has the same magnetic structure as HiSOR²⁾. Two long, magnet-free straight sections of the SR2 are prepared to insert SCRIT devices and used for electron scattering off radioactive isotopes. The layout and specifications of the RTM and SR2 are described in another report¹⁾. SR2 is operated with an electron energy of 300 MeV to conduct electron scattering experiments using SCRIT in the straight section. Furthermore, when the ring is operated with an electron energy of 700 MeV, it serves as a very valuable light source in the VUV to soft X-ray region.

The theoretical minimum emittance in an electron storage ring and that for the Chasman-Green lattice are derived.

The amplitude of the betatron oscillation (emittance) is determined by the equilibrium process of photon emission and the rf acceleration which compensates the energy loss of the synchrotron radiation. The horizontal emittance is expressed as

$$\varepsilon_x = C_q \gamma^2 \frac{\langle H \rangle_{dipole}}{J_x \rho} \quad (1)$$

where $C_q = 3.84 \times 10^{-13}$ m, $J_x \approx 1$ is the damping partition number, γ is the Lorentz factor, ρ is the bending radius, and $\langle H \rangle$ is the average of the following function over the dipole

$$\langle H(s) \rangle_{dipole} = \frac{1}{l_B} \int_0^{l_B} (\gamma_x \eta_x^2 + 2\alpha_x \eta_x \eta_x' + \beta_x \eta_x'^2) ds \quad (2)$$

The dispersion function is generally expressed as

$$\eta(s) = \rho(1 - a \cos \frac{s}{\rho} + b \sin \frac{s}{\rho}) \quad (3)$$

The betatron function is generally expressed as,

$$\beta_x(s) = \beta_0 \cos^2 \frac{s - s_0}{\rho} + \frac{\rho^2}{\beta_0} \sin^2 \frac{s - s_0}{\rho} \quad (4)$$

The betatron function is assumed to have a minimum value β_0 at $s = s_0$ in the bending magnet. The other functions, namely, η_x , γ_x and α are derived and equation (2) can be estimated. The $\langle H \rangle_{dipole}$ can be expressed as a quadratic equation using ρ , l_B , θ , s_0 , a , b , and β_0 . For given ρ , l_B , and θ , the minimum condition gives $a = \sin \theta / \theta$ and $b = (\cos \theta - 1) / \theta$. With this condition, β_0 for is determined for any θ_0 ($\theta_0 = s_0 / l_B$). Among these θ_0 values, $\theta_0 = \theta / 2$ gives minimum emittance.

and
$$\beta_0 = \rho \sqrt{\frac{1 - (\frac{2}{\theta} \sin \frac{\theta}{2})^2 - ((\frac{2}{\theta} \sin \frac{\theta}{2})^2 - \frac{\sin \theta}{\theta})}{1 - (\frac{2}{\theta} \sin \frac{\theta}{2})^2 + ((\frac{2}{\theta} \sin \frac{\theta}{2})^2 - \frac{\sin \theta}{\theta})}} \quad (5)$$

$$\langle H(s) \rangle_{min} = \rho \sqrt{\left(1 - (\frac{2}{\theta} \sin \frac{\theta}{2})^2 + ((\frac{2}{\theta} \sin \frac{\theta}{2})^2 - \frac{\sin \theta}{\theta})\right) \left(1 - (\frac{2}{\theta} \sin \frac{\theta}{2})^2 - ((\frac{2}{\theta} \sin \frac{\theta}{2})^2 - \frac{\sin \theta}{\theta})\right)} \quad (6)$$

when $\theta \ll 1$, the minimum emittance is expressed as $\varepsilon = C_q \gamma^2 \theta^3 / 12\sqrt{15}$, where $\beta_0 = \rho \theta / 2\sqrt{15}$.

For SR2 ($\theta = \pi$), $a = 0$, $b = -\pi/2$, $\theta_0 = \pi/2$, and $\beta_0 = 0.38$ m gives the minimum emittance of $\varepsilon = 0.4 \pi$ mm•mrad. In Fig. 1, the dispersion and betatron functions in the dipole calculated using these parameters are compared with the HiSOR parameters. Both functions are very similar, and HiSOR and SR2 are designed to achieve emittance minimum.

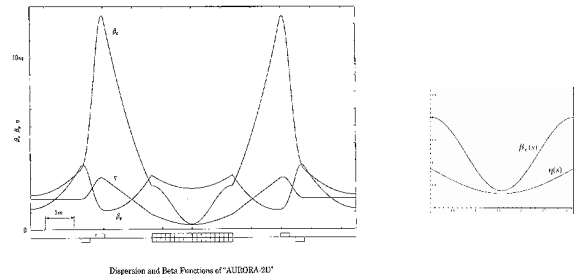


Fig. 1 Betatron and dispersion function of Aurora II-D (left) and of minimum emittance lattice in dipole.

The Chasman-Green (Double Bend Achromat) lattice is used in many electron storage rings²⁾. The lattice provides dispersion-free section outside the pair of bending magnets. Usually, insertion devices such as wiggler or undulators are installed. The minimum emittance condition for the Chasman-Green lattice is also derived and applied for SR2, which can have only one cell. Double-bend achromat condition gives $a = 1$ and $b = 0$ in the eq. (4).

$$\langle H(s) \rangle_{CGmin} = \beta_0 \left(1 - \frac{\sin \theta}{\theta} - \frac{1}{4} \frac{\sin(2\theta - 2\theta_0) + \sin 2\theta_0}{\theta} - \frac{1}{2} \cos 2\theta_0 + \frac{\sin(\theta - 2\theta_0) + \sin 2\theta_0}{\theta} \right) + \frac{\rho^2}{\beta_0} \left(1 - \frac{\sin \theta}{\theta} + \frac{1}{4} \frac{\sin(2\theta - 2\theta_0) + \sin 2\theta_0}{\theta} + \frac{1}{2} \cos 2\theta_0 - \frac{\sin(\theta - 2\theta_0) + \sin 2\theta_0}{\theta} \right) \quad (7)$$

When θ is π , minimum emittance condition gives θ_0 of a little smaller than $3\theta/8$.

When $\theta \ll 1$, as is well known, minimum condition gives $\theta_0 = 3\theta/8$ and $\varepsilon = C_q \gamma^2 \theta^3 / 4\sqrt{15}$ where $\beta_0 = \rho \theta \sqrt{3} / 8\sqrt{15}$. Minimum emittance value becomes three times larger by the additional condition of zero dispersion.

References

- 1) M. Wakasugi et al.: in this Accelerator Progress Report.
- 2) R. Chasman et al.* IEEE Trans. Nucl. Sci. NS-22, 1765(1975).
S.Y. Lee et al.: Proc. of 1991 PAC, p. 2679.

Capability of SR2 as a compact synchrotron radiation source

T. Hori, M. Hara and M. Wakasugi

An electron accelerator system which consists of 150 MeV racetrack microtron injector and 700 MeV compact storage ring is under construction at E21 experimental room of RIBF as SR2 (SCRIT-equipped Riken Storage Ring) aiming at electron scattering experiments for short-lived unstable nuclei using the SCRIT technique¹⁾. In the past the system was developed and operated at Tanashi Works of Sumitomo Heavy Industries, Co. Ltd. (SHI) as AURORA-2S²⁾ (A2S) having a racetrack orbit of 11 m circumference with a Q-singlet in each straight section. A2S was transferred from SHI to RIKEN last summer after modified to AURORA-2D³⁾ (A2D) as 22 m circumference with two Q-doublets in each extended straight section, where a free space of 2 m in length is reserved for inserting various devices.

In addition to the major purpose mentioned above, SR2 is to play another role at Nishina Center as a compact synchrotron radiation (SR) light source in VUV~ soft X-ray region. The basic configuration of SR2 is the same as the SR light source HiSOR⁴⁾ in Hiroshima University, except for the insertion devices of two undulators which are mainly used for high-resolved photo emission spectroscopy (PES). Therefore, SR2 is applicable to the similar research activities as HiSOR, namely, in solid state physics, in photo chemistry, in molecular biology, etc. However, A2S had originally been designed as a light source for X-ray lithography, thus the SR2 system might be much suitable for developing micro/nano fabrication technology. The SR spectra from SR2 bendings are shown below (Fig. 1), where the critical photon energy 0.87 keV (1.24 nm wavelength).

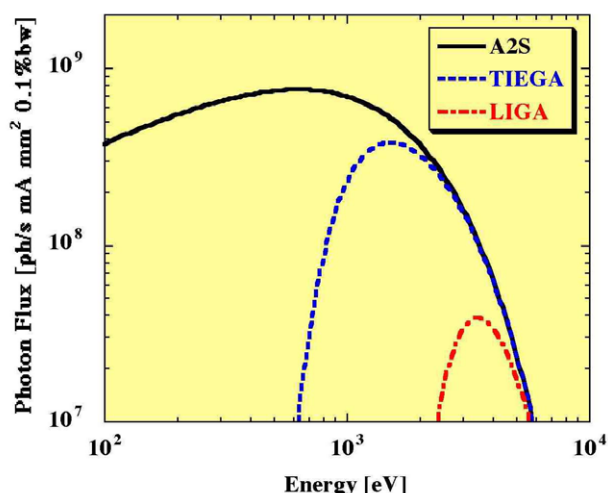


Fig. 1. SR spectra from bending magnets of SR2.

While transferring A2S, beam lines (BLs) for LIGA (Lithographie, Galvanoformung, Abformung)⁵⁾ and TIEGA (Teflon Induced Etching and Galvanicforming)⁶⁾ were moved simultaneously from SHI to RIKEN. These BLs are

rather short, a few meters, compared with those for basic researches like PES, etc. The following picture shows these BLs connected to A2S in SHI's Tanashi Works (Fig. 2). Some of them are planned to be re-joined to SR2 in the next fiscal year.

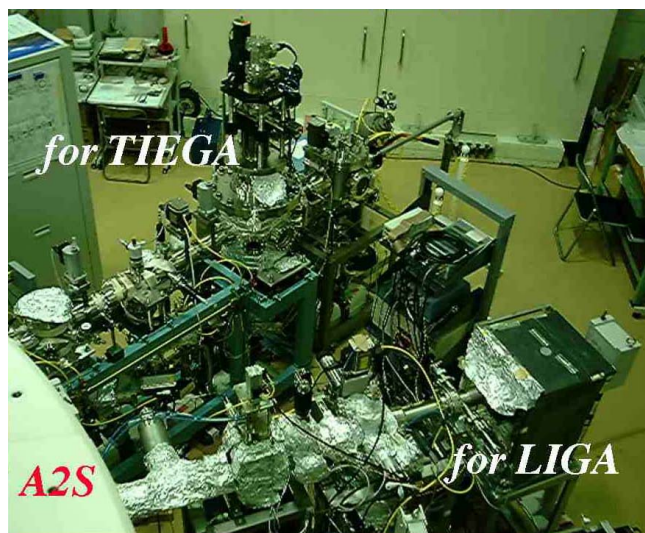


Fig. 2. Photo of micro/nano fabrication BLs at Tanashi.

As for SR2, each bending magnet provides 10 connection ports for BLs, besides the extraction port from the straight section. There is a thick pillar, however, in front of a bending magnet called M2. Only SR emitted from the other bending M1 is available for conjunction to user's BLs. Right now 4 ports are reserved for such BLs as the SR from M1 with more than 10-m length of alignment space for BL components. A few ports will be available in addition with much shorter spaces (~5m) for BL settings. These optional ports might be adequate for BLs LIGA/TIEGA.

In the next fiscal year, the SCRIT system will be installed into one straight section. Another straight section would be vacant for subsequent several years. It means that there is a possibility to develop insertion devices to improve SR from the compact ring by exploiting this time interval. Routine operation of SR2 for SR users with the designed intensity, which means 300 mA stored beam, will be ready in 2011.

References

- 1) M. Wakasugi et al., Phys. Rev. Lett. 100, 164801 (2008).
- 2) D. Amano et al., Proc. EPAC2000, Vienna (2000) p.604.
- 3) T. Hori et al., Proc. 11th Symp. on Accel. Sci. & Tech., Hyogo, (1997) p.534.
- 4) <http://www.hsrc.hiroshima-u.ac.jp/hisor.htm>
- 5) S. Sugiyama et al., Microsystem Technol. 4, 61 (1998).
- 6) T. Katoh et al., J. Synchrotron Rad. 5, 1153 (1998).

Magnetic plasma confinement for laser ion source†

M. Okamura*¹, T. Kanesue*², and K. Kondo*³

The direct plasma injection scheme (DPIS), which uses a laser ion source (LIS) and a radio frequency quadrupole linear accelerator (RFQ), was recently developed to accelerate intense heavy ions. In this scheme, a high-power laser is focused onto a solid-state target to produce dense plasma, which contains highly charged ions. The laser-produced plasma expands in a direction perpendicular to the target surface, and this expansion causes an increase in the plasma pulse width and a decrease in the current density. Since the plasma spreads three dimensionally, the plasma pulse length is proportional to the drift distance L and the ion current density is proportional to L^{-3} . After drifting, the ions are extracted from the plasma at the entrance of the RFQ and are accelerated to the design energy. We have already accelerated aluminum and carbon beams with currents greater than 60 mA using the DPIS¹⁾. Although the peak current is high, the pulse width of the beam is too small for some applications, for example, as a beam provider for a large synchrotron. We can easily increase the pulse width by increasing the plasma drift distance; however, the current injected to the RFQ becomes very small. To prevent this reduction in the current, the use of solenoidal magnetic confinement was tested. The presence of an axial magnetic field decreases the transverse expansion of the plasma and thereby leads to a high density during the expansion^{2,3)}.

To verify this scheme, a simple coil comprising a 2-mm-diameter wire directly wound on a beam pipe was considered. The inner diameter and the length of the coil were 76 mm and 480 mm, respectively.

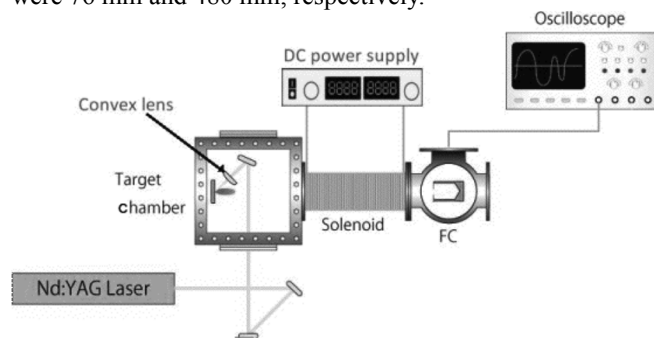


Fig. 1 Experimental setup

To observe the effect of the solenoid, a graphite target and other equipment were assembled. A suppressor mesh was placed before the Faraday cup to distinguish the ions from the laser plasma. The laser power and laser pulse duration were 0.9 J and 7 ns (FWHM), respectively.

† Condensed from the article in Review of Sci. Instr., 81, 1 (2010)

*¹ Brookhaven National Laboratory

*² Department of Applied Quantum Physics and Nuclear Engineering, Kyushu University

*³ Department of Energy Science, Tokyo Institute of Technology

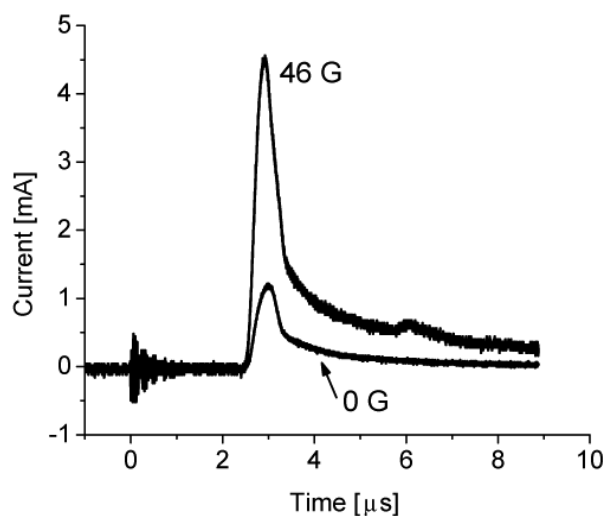


Fig. 2 Enhanced current in the case of a multi-charged carbon beam.

The effect of the solenoid was clearly seen when the solenoid current was increased. A typical current waveform taken by the Faraday cup is shown in Fig. 2. The charge states vary from 3+ to 6+, with the highest yield of charge state being 4+. To avoid a discharge between the suppression mesh and the Faraday cup, a collimator with an opening diameter of 1.55 mm was installed at a distance of 803 mm from the target. Above 50 G, the plasma current density became too high to pass through the biased mesh, which was connected to a voltage source of -4.5 kV. This shows that the ions and the electrons are not separated, and the space-charge repulsion force can still be compensated in the presence of the axial magnetic field. We might be able to apply a longer solenoid field in order to extend the beam pulse duration. It was seen that a 46-G field increased the peak value by approximately four times.

It was confirmed that a solenoid can effectively enhance the ion density, and the technique can be used in the DPIS. Further, the solenoid may improve any LISs. By applying a programmable pulsed power supply to the solenoid, we might be able to control the current shape by changing the solenoid current.

References

- 1) M. Okamura, T. Takeuchi, R. A. Jameson, S. Kondrashev, H. Kashiwagi, K. Sakakibara, T. Kanesue, and J. Tamura, Rev. Sci. Instrum. 79, 02B314 (2008)
- 2) J. Wolowski, J. Badziak, I. Ivanova-Stanik, P. Parys, W. Stepniowski, and E. Woryna, Rev. Sci. Instrum. 75, 1356 (2004)
- 3) Y. Y. Tsui, D. Vich, and R. Fedosejevs, Appl. Phys. Lett. 70 (15), 14 (1997)

Effect of plasma drift distance on high current beam production in DPIS†

T. Kanetsue, *¹ M. Okamura, *² K. Kondo, *³ J. Tamura, *³ and H. Kashiwagi, *⁴

The Direct Plasma Injection Scheme (DPIS) is a scheme to produce and accelerate a high current, highly charged heavy ion beam using a laser ion source and a Radio Frequency Quadrupole (RFQ) linac.^{1), 2)} A laser ion source produces plasma that contains highly charged, heavy ions from any species of solid state target using a pulsed high-power laser. The initial velocity of the plasma is towards the normal to the target and the plasma simultaneously expands three dimensionally. With the expansion, the ion current density and ion pulse width change according to the following equation.

$$\Delta t \propto L \quad (1)$$

$$j \propto L^{-3} \quad (2)$$

where Δt is the ion pulse width and j is the ion current density at a distance of L from the target.³⁾

In the DPIS, the laser ion source is directly attached to the RFQ linac. Ions are extracted at the entrance of the RFQ linac and captured by the RF focusing field immediately, and an intense heavy ion beam can be produced. However, a simulation study has indicated that the injection efficiency decreases when the ion current density in an ion extraction region is extremely high because of the mismatched between the emittance of the extracted beam and acceptance of the RFQ linac.⁴⁾ We studied the beam loss due to the mismatch for three different ion currents in the ion extraction region; by changing the plasma drift distance.

A Nd:YAG laser with a wavelength of 1064 nm (0.91 J/7.1 ns) was used. A graphite target plate was placed inside a target cage that was isolated from the ground potential. Plasma expanded through a pipe, which had the same potential as the target cage, into a RFQ linac. We used a RFQ dedicated to the DPIS. Plasma drift distances of 30, 62.5, 91 cm were considered in this experiment. The ion current was measured by a current transformer (CT) at the exit of the RFQ linac. The charge state distribution was determined using a cylindrical, 90° electrostatic ion analyzer (EIA) and a Faraday cup.

Figure 1 shows that total beam current after the RFQ linac. The results of an analysis showed that about 90% of the accelerated beam was C⁶⁺. Signals measured for the plasma drift distance of 62.5 and 91 cm were scaled to those for the plasma drift distance of 30 cm using Eq. (1) and (2) so as to compare the measured signals. Figure 2 shows the converted and measured signals. A beam current of 100 mA

was expected on the basis of the scaled signals, as seen in Fig.2. However, the measured current of 30 mA was much lower than that corresponding to the scaled signals. This can be explained by considering a strong space charge effect. At high values of the beam current, the divergence of the extracted beam increases with the beam current. This causes the mismatch.

As discussed above, the beam current accelerated by the RFQ linac is determined by the balance between the input current and the injection and acceleration efficiency in the RFQ linac, and therefore the plasma drift distance, which controls the ion current at the extraction point, should be selected carefully to achieve the maximum accelerated ion yield.

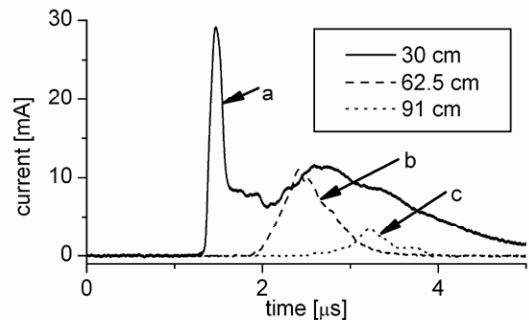


FIG. 1. Total beam current after the RFQ linac for plasma drift distances of (a) 30 cm, (b) 62.5 cm, and (c) 91 cm.

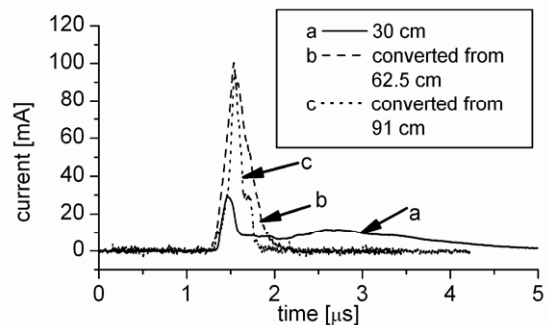


FIG. 2. Measured signal for the 30 cm plasma drift distance (a) and signals expected on the basis of signals obtained for plasma drift distances of 62.5 cm (b) and 91 cm (c), determined using the Eq. (1) and (2).

† Condensed from the article in B25, ICIS2009

*¹ Department of Applied Quantum Physics and Nuclear Engineering, Kyushu University

*² Collider Accelerator Department, Brookhaven National Laboratory

*³ Department of Energy Sciences, Tokyo Institute of Technology

*⁴ Takasaki Advanced Radiation Research Institute, Japan Atomic Energy Agency

References

- 1) H. Kashiwagi et al.: Rev. Sci. Instrum. **77**, 03B305 (2006).
- 2) M. Okamura et al.: Rev. Sci. Instrum. **77**, 03B303 (2006).
- 3) B. Sharkov and S. Kondrashev: Proc. PAC96, Barcelona, 1996, p. 1550.
- 4) H. Kashiwagi et al.: Rev. Sci. Instrum. **81**, 02B724 (2010)

Particle simulation for direct plasma injection in an RFQ matching section [†]

J. Tamura,^{*1,*2} T. Hattori,^{*1} N. Hayashizaki,^{*1} T. Ishibashi,^{*1} T. Kanesue,^{*3} H. Kashiwagi,^{*4} K. Kondo,^{*1} and M. Okamura^{*5}

The Direct Plasma Injection Scheme (DPIS) has been used in radio frequency quadrupole (RFQ) linacs, and high-intensity heavy-ion beams have been generated and accelerated.¹⁾ By using the DPIS, a C^{6+} beam with a maximum beam current greater than 10 mA has been accelerated from 20 keV/nucleon to 100 keV/nucleon.²⁾ One of the most unique features of the DPIS is that the ions are extracted from plasma at the RFQ entrance. This means that in the RFQ radial matching (RM) section, ions are forced by both the electrostatic field generated by the extraction electrode and the RF electric field generated by the RFQ electrode. On the other hand, in the conventional beam injection scheme used in RFQ linacs, ions are forced only by the latter field. To describe the evolution of the beam extracted from the laser plasma in the RM section, we performed particle tracking simulation using a three-dimensional particle-in-cell method.^{3,4)} In this simulation, we made the following assumptions,

- The extracted beam comprises only C^{6+} ions.
- The plasma sheath is flat and perpendicular to the beam axis.
- Initially, the beam is axisymmetric and uniformly distributed in real space.

As mentioned above, the external field in the RM section consists of both the electrostatic field and the RF electric field. The potential maps for these fields were obtained using KOBRA3-INP.⁵⁾ The quadrupole symmetry is maintained throughout the RM section.

Particles of different beam currents of 6 mA, 30 mA, 60 mA, and 90 mA are tracked. Figure 1 shows the particle distribution in the $x = 0$ plane for the beam current of 6 mA. To visualize the geometry clearly, particles that satisfy the condition $x^2 + y^2 > (\text{aperture radius of the RFQ electrode})^2$ are not displayed. The transmission efficiency to the adjacent normal RFQ cell is about 37%, 29%, 24%, and 19% for the beam currents of 6 mA, 30 mA, 60 mA, and 90 mA, respectively. Even in the case of the relatively low beam current of 6 mA, ions are not captured by the RFQ. The reason they are not captured is that the electrostatic field generated by the extraction electrode has a divergent component. To avoid this divergent component, the beam has to be focused initially. Figure 2 shows an example of an initially convergent beam in the DPIS.

From these simulations, so as to avoid the radial defocusing force which is particular force in DPIS we found

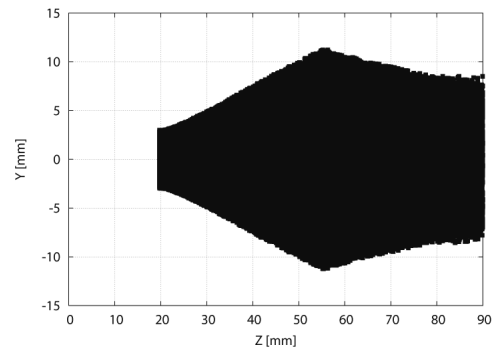


Fig. 1. Particle distribution for the beam current of 6 mA ($x = 0$ plane).

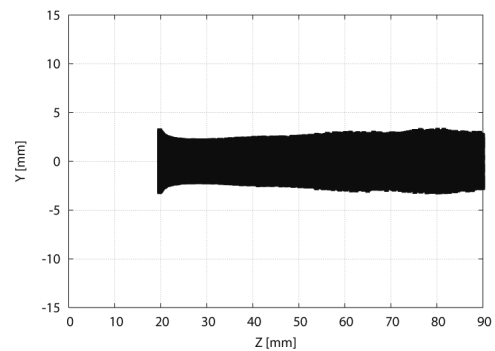


Fig. 2. Particle distribution for the beam current of 6 mA ($x = 0$ plane) when the beam is initially focused.

that it is necessary to provide a more convergent beam in the DPIS than usual RFQ injection. The initial condition of the extracted beam is decided by the shape of the plasma sheath which mainly depends on the plasma density. The plasma density can be varied by changing the plasma drift length.⁶⁾ The longer the laser plasma drifts, the lower is the density of plasma injected into the RFQ. In the DPIS, we need to optimize the plasma density to realize a concave ion-emitting surface which produces a convergent beam.

References

- 1) M. Okamura et al.: Rev. Sci. Instrum. **79**, 02B314 (2008).
- 2) H. Kashiwagi et al.: Rev. Sci. Instrum. **77**, 03B305 (2006).
- 3) R. W. Hockney and J. W. Eastwood: *Computer Simulation Using Particles* (Taylor & Francis Group, New York, 1988).
- 4) C. K. Birdsall and A. B. Langdon: *Plasma Physics via Computer Simulation* (Taylor & Francis Group, New York, 2005).
- 5) P. Spädtke: KOBRA3-INP USER MANUAL WINDOWS-VERSION 4.43 (INP).
- 6) T. Kanesue et al.: Rev. Sci. Instrum. **81**, 02B723 (2010).

[†] Condensed from the article in Rev. Sci. Instrum. **81**, 02B726 (2010)

^{*1} Tokyo Institute of Technology, Japan

^{*2} RIKEN, Japan

^{*3} Kyushu University, Japan

^{*4} Japan Atomic Energy Agency, Japan

^{*5} Brookhaven National Laboratory, United States

Design research of laser ion source for RHIC-EBIS[†]

K. Kondo,¹ T. Kanosue,² J. Tamura,¹ and M. Okamura³

[Laser ion source, Electron-beam ion source, Relativistic heavy-ion collider]

At present, it is not feasible to use the Laser Ion Source (LIS) as a primary ion source for Relativistic Heavy Ion Collier-Electron Beam Ion Source (RHIC-EBIS)¹⁾ because the requirements of both limited low current for Low-Energy Beam Transport (LEBT) and injection of a sufficient number of 1+ ions, cannot be satisfied at the same time. However, the results of LIS experiments in which a solenoid is used show that the beam current and total ion yield are enhanced²⁾. We derive an appropriate condition for RHIC-EBIS with a solenoid.

In the LIS, the following relationships hold.

$$j \propto L^{-3}, \quad (1)$$

$$t \propto L, \quad (2)$$

$$N \propto L^{-2}, \quad (3)$$

where j , L , t and N are current density, plasma drift length, beam pulse duration and particle number, respectively. To satisfy the requirements of limited low current for LEBT and sufficient particle number for RHIC-EBIS, we use the solenoid to enhance the beam current and total ion yield. For an enhancement factor α , we can rewrite Eqs (1) and (3) as follows:

$$j \propto \alpha L^{-3}, \quad (4)$$

$$N \propto \alpha L^{-2}. \quad (5)$$

The relationship between t and L does not depend on the solenoid field; no significant change was observed in t in the presence or absence of the solenoid²⁾.

We assume that for a realistic design of the LIS, L , the distance between solid target and extraction point is 5 m and laser power density is 2.0×10^8 W/cm². Peak current, pulse width, and particle number at $L = 5$ m in the absence of the solenoid can be derived from the experimental results³⁾⁴⁾ corresponding to $L = 1$ m by using Eqs (1), (2), and (3). The number of 1+ charged ions, N_0 , injected by using the solenoid is determined by considering the value of α at $L = 5$ m; the value of α can be fixed so that the requirement of limited current for LEBT is satisfied. The overall efficiency β , which is defined as the required ratio of the net ion number before and after RHIC-EBIS, is determined by considering the ratio of the minimum

number of singly charged ions, N_{\min} , to N_0 . Table 1 lists the beam properties at $L = 5$ m for ve ion species: Al, Si, Fe, Ta, and Au; these are the typically species required for National Aeronautics and Space Administration Space Radiation Laboratory (NSRL) science programs and Au ions collision in RHIC.

It is desirable that LIS optics be located far away from the vacuum target chamber to prevent damage to the optics by laser ablation. A galvano mirror with an operation time of a few hundred microseconds is used for changing the direction of laser irradiation to obtain different ion species. In Fig.1, we show a sketch of LIS, which is a primary ion source for RHIC-EBIS, with its optics arrangement and the solenoid.

The solenoid in the LIS is useful since it helps satisfy the requirements of both low peak current and sufficient particle number. It is suitable to use this LIS system, with optics as shown in the figure, as the primary ion source of a singly charged ion beam.

Table 1. Beam properties for RHIC-EBIS.

Ion species	Al	Si	Fe	Ta	Au
Pulse length t [μ s]	190	180	220	280	430
Enhancement factor α	11	15	6.6	116	3.6
N_0 ($\times 10^{10}$)	6.1	6.5	5.2	5.2	5.3
Overall efficiency β %	75	66	46	35	32

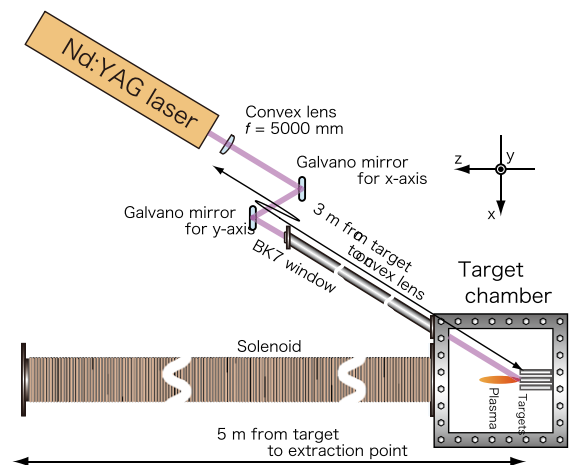


Fig. 1. Sketch of LIS for RHIC-EBIS.

[†] Condensed from the article in Rev. Sci. Instrum. **81**, 02A511 (2010)

¹ Department of Energy Sciences, Tokyo Institute of Technology

² Department of Applied Quantum Physics and Nuclear Engineering, Kyushu University

³ Collider-Accelerator Department, Brookhaven National Laboratory

References

- 1) J. Alessi *et al.*: Proc. of LINAC 2006, P.385.
- 2) M. Okamura *et al.*: Rev. Sci. Instrum. **81**, 02A510 (2010).
- 3) T. Kanosue *et al.*: Proc. of EPAC 08, P.421.
- 4) T. Kanosue *et al.*: Rev. Sci. Instrum. **79**, 02B102 (2008).

Laser Beam Recycler with Asymmetric Confocal Cavity

I. Yamane, M. Nakamura, and H. Okuno

[ion beam, charge-exchange, laser stripping]

Against the background of rapid progress of laser technology, there is considerable expectation that laser beams may be applied for ion-beam stripping. As described in the reference¹⁾, calculations based on Gaussian beam optics suggest that for a high-power laser beam, beam stacking can be achieved at the confocal point of an asymmetric confocal cavity. Although similar geometrical-optics-based studies^{2,3)} were performed on beam stacking in an asymmetric confocal cavity, in these experiments, the enhancement of beam intensity by stacking was not observed. The experiment described in this paper was performed in order to examine the results of calculations based on Gaussian beam optics.

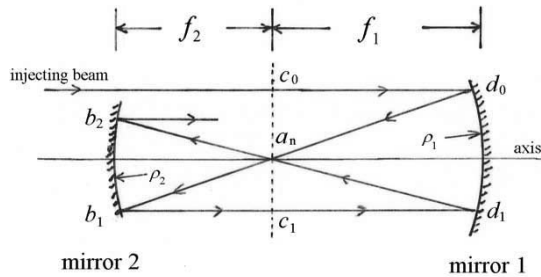


Fig. 1, Asymmetric confocal cavity and beam path

When a laser beam is injected into an asymmetric confocal cavity such that the beam is parallel to the axis of the cavity, as shown in Fig. 1, it repeatedly follows the triangular path, $a \rightarrow b_n \rightarrow c_n \rightarrow d_n \rightarrow a$, in the cavity and returns to the confocal point a after every loop.

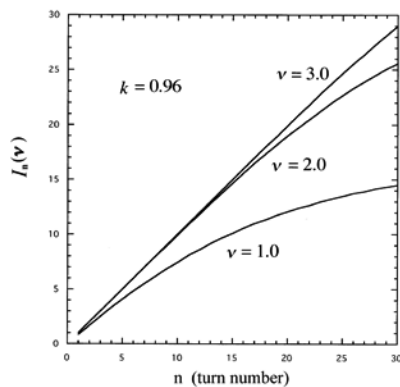


Fig. 2, Evolution of beam intensity with beam radius ν (= radius/ w_{c0}). The unit of the stacked-beam intensity is the injected-beam intensity. k is the ratio f_2/f_1 .

If the path of the injected beam is sufficiently closed to the axis of the cavity, the repetition period remains almost

constant. Therefore, when a continuous or pulsed beam with a period equal to its repetition period in the cavity is injected, all reflected laser beams in the cavity converge at a at the same time, and the beam intensity increases considerably. We call such a cavity as a “laser-beam recycler”. As described in the reference¹⁾, when a Gaussian beam with a waist at c_0 , and Rayleigh range f_1 , that is, $\pi w_{c0}^2/\lambda = f_1$, is injected, the beam returns to a as a waist every time, and the beam intensity stacks up. Here, w_{c0} is the half width at $1/e^2$ of the peak at c_0 , and λ is the wavelength of the injected laser beam. However, because the beam size at a gradually increases with the number of turns, the beam intensity for the given useful beam diameter increases and reaches a saturation level. As is shown in Fig. 2, the intensity of a beam of radius of $2w_{c0}$ may be 25 or more times of the injected-beam intensity. This high intensity makes the laser beam useful in various applications such as in a laser neutralizer for high-energy H^- beam substitute for the magnetic neutralizer used in beam splitting⁴⁾.

As the first step of the experiment, we measured the evolution of the half width at $1/e^2$ of the peak to clarify whether the laser beam is Gaussian. As is shown in Fig. 3, the M^2 factor of the laser beam is estimated to be 1.04, and the beam is confirmed to be nearly Gaussian.

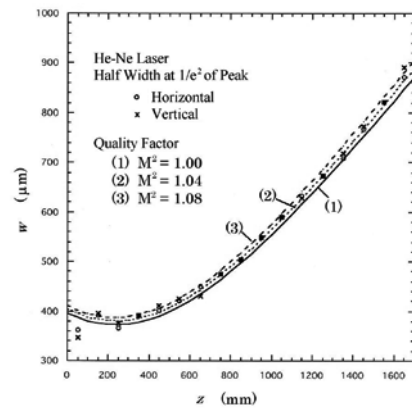


Fig. 3, Measured and calculated evolution of the half width at $1/e^2$ of the peak.

References

- 1) I. Yamane and H. Okuno: KEK Report **2009-9**, November 2009.
- 2) S. Amano and T. Mochizuki: Jpn. J. Appl. Phys. **40**, 654 (2001).
- 3) A. J. Rollason, X. Fang, D. E. Dugdale: Nucl. Instr. Meth. In Phys. Res. A **526**, 560 (2004).
- 4) A. Facco, R. Paparella, D. Berkovits, I. Yamane: PRST-Accelerators and Beams **10**, 091001 (2007).

7. Instrumentation

Status of the BigRIPS and ZeroDegree Project

T. Kubo, K. Kusaka, T. Ohnishi, K. Yoshida, A. Yoshida, N. Fukuda, M. Ohtake, Y. Yanagisawa, H. Takeda, N. Inabe, D. Kameda, and K. Tanaka

The status of the major research instruments in the RI beam factory (RIBF), such as the BigRIPS in-flight separator,^{1,2)} the ZeroDegree spectrometer,³⁾ and the high-resolution beamline for the SHARAQ spectrometer,⁴⁾ is presented in this report. A schematic layout of the major research instruments is shown in Fig. 1 along with the cyclotrons at RIBF.

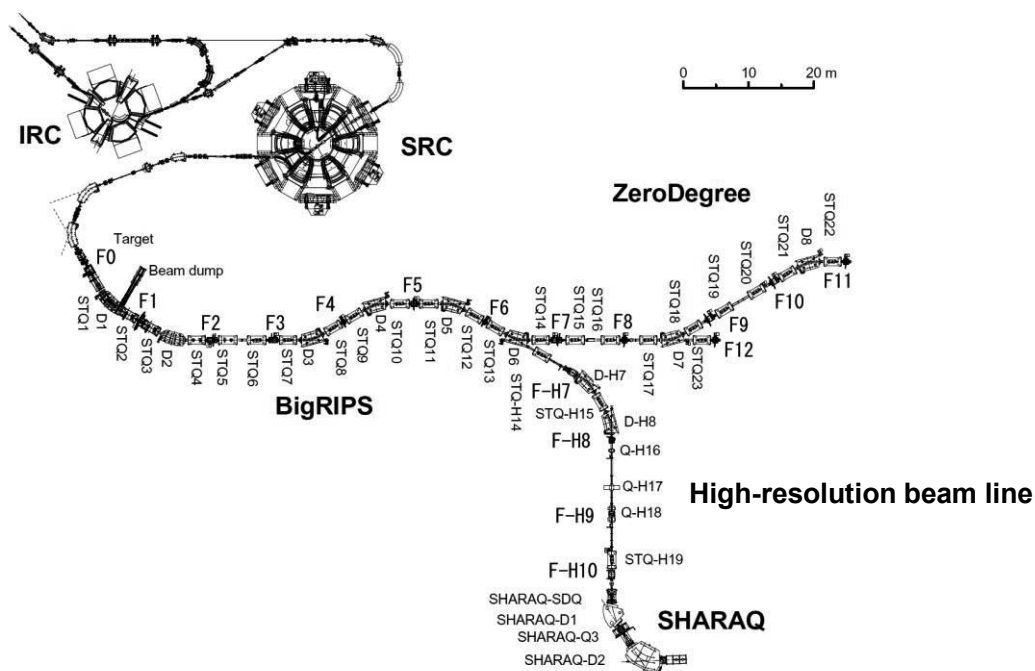
The BigRIPS separator is composed of fourteen superconducting triplet quadrupoles having large apertures (STQ1–14) and six room-temperature dipoles (D1–6). There are seven focuses (F1–7). One of the important features of BigRIPS is its large acceptance, which results in efficient production of RI beams by not only projectile fragmentation of various heavy-ion beams but also in-flight fission of a uranium beam. This feature was achieved by using the large-aperture superconducting quadrupoles.

Another important feature is its two-stage structure. The first stage consists of the components between the production target (F0) and F2, while the second stage consists of those from F3 to F7. The section from F2 to F3 acts as an ion-optical matching section between them. This feature allows a separator-spectrometer mode as well as a two-stage separation mode. In the former mode, RI beams are separated using an energy degrader in the first stage, while the second stage works as a spectrometer to identify the RI beams. The second stage is designed to have good

momentum resolution so that RI beams can be identified without having to measure total kinetic energies even though ions are not fully stripped at the RIBF energies. In the two-stage separation mode, an energy degrader is used at both stages to purify the RI beams further.

There is a focal-plane chamber in each focus that accommodates various beam-line devices and detectors used for diagnostics and particle identification (PID). The PID scheme is based on the ΔE -TOF-B ρ method in which trajectory reconstruction is used to improve momentum resolution. The primary beams stops at a high-power beam dump located at the first dipole D1. A water-cooled rotating-disk target is used to cope with high-power beams. The first stage is surrounded by concrete radiation shields that weigh about 7000 tons.

The RI-beam delivery line that follows the BigRIPS is designed not only for the transportation of RI beams to experimental setups but also for use as a forward spectrometer that has been named ZeroDegree. The delivery line consists of nine STQs (STQ15–23), two dipoles (D7–8), and five focuses (F8–12). The section from F8 to F11 forms the ZeroDegree spectrometer, while that from F7 to F8 is acts as an ion-optical matching section between the BigRIPS and ZeroDegree. The magnets of ZeroDegree have the same design as those of BigRIPS. There is a focal-plane chamber in each focus to accommodate various beam-line



devices and detectors used for diagnostics and PID, as in the BigRIPS separator. A secondary target is placed at F8 when the delivery line is used as the ZeroDegree spectrometer for reaction experiments with RI beams. The ZeroDegree is used to analyze and identify projectile reaction residues often in coincidence with γ -rays that are measured by an array detector surrounding the target. The ZeroDegree can be operated in different optics modes depending on the experimental requirements.

The high-resolution beamline extends from F3 to D6 (the existing part) and from D6 to the SHARAQ target position (the new part). The new part is composed of three STQs (STQH14–15, STQH19), three room-temperature quadrupoles (QH16–18), two dipoles (DH7–8), and four focuses (FH7–10). The beamline can be operated in a high-resolution dispersive mode so that the dispersion matching conditions can be attained at the SHARAQ focal plane, thus allowing high-resolution measurements using the SHARAQ spectrometer.

The BigRIPS and the ZeroDegree became operational in May 2007 and November 2008, respectively. The high-resolution beam line was commissioned in March 2009 together with the SHARAQ spectrometer.

In December 2009, the BigRIPS and the ZeroDegree were used for experiments using a ^{238}U beam and a ^{48}Ca beam at 345 MeV/u. In-beam γ -ray spectroscopy for neutron-rich exotic nuclei was performed using RI beams of $^{130-132}\text{Sn}$. β - γ spectroscopy was performed for several neutron-rich exotic nuclei around ^{106}Sr . These isotopes were produced via in-flight fission of the ^{238}U beam. Interaction cross sections were measured for a wide range of neutron-rich Ne isotopes that were produced by projectile fragmentation of the ^{48}Ca beam.

In the commissioning experiments for the high-resolution beam line and the SHARAQ spectrometer in March and May 2009, the dispersion matching was successfully tested using primary beams and RI beams. In November 2009, the first nuclear physics experiment at SHARAQ was carried out using a triton beam produced from a ^4He beam at 320 MeV/u. A ($t,^3\text{He}$) reaction was studied to investigate isovector spin-monopole excitation. Details of the SHARAQ experiments are presented elsewhere.

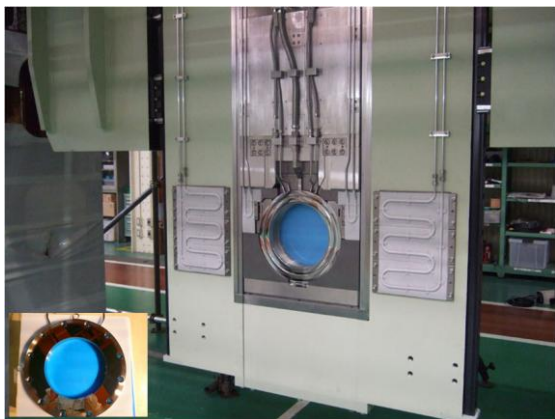


Fig. 2. Photograph of the beam-dump pillow seal with radiation shields that was installed between D1 and STQ2.

In order to cope with high-intensity primary beams, pillow seals and radiation shields have been installed around the beam dump and the production target in the first stage of the BigRIPS separator. The pillow seals allow remote disconnection of beam pipes and significantly facilitate the handling and maintenance of the devices under high residual radiation. The radiation shields are used to shield light charged particles and neutrons emitted from the beam dump and the target in order to protect the STQs against radiation damage and to reduce the radiation heat loads on them. Figure 2 shows a photograph of the beam-dump pillow seal that was installed between D1 and STQ2. The pillow seal is surrounded by the radiation shields made of heavy metal and steel. In summer 2009, some concrete shielding blocks were removed from the first stage, and the pillow seals and radiation shields were installed.

The operation of the BigRIPS cryogenic plant, which is used to cool STQ1–5, has been very stable as a result of the upgrade of the oil-removal unit of the compressor. The operation of the cryo-coolers, which are used to cool the rest of the STQs, has also been stable.

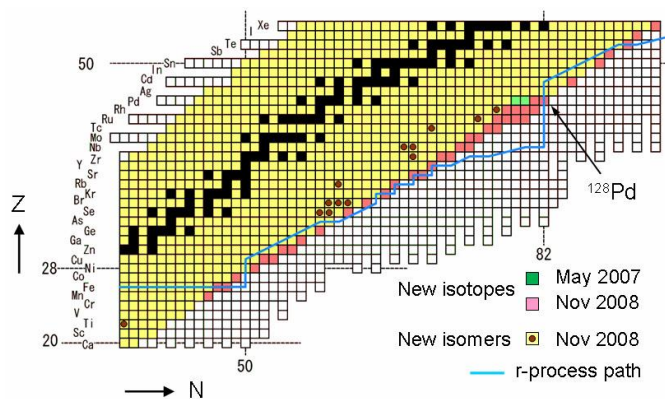


Fig. 3. Nuclear chart that shows new isotopes produced by in-flight fission of a ^{238}U beam at 345 MeV/u. New isomers observed in the same experiment and the r-process path are also shown.

The analysis of the new-isotope search experiment conducted in November 2008, which was performed using a ^{238}U beam at 345 MeV/u, has almost completed. We observed 42 new neutron-rich isotopes and 13 new isomers over a wide range of atomic numbers, as shown in Fig. 3.

More detailed reports on the project have been provided elsewhere in this progress report.

(Note that the number of observed new isotopes is 45 in our paper published recently.)

References

- 1) T. Kubo: Nucl. Instr. and Meth. **B 204**, 97 (2003).
- 2) T. Kubo et al.: IEEE Trans. Appl. Supercond. **17**, 1069 (2007).
- 3) Y. Mizoi et al.: RIKEN Accel. Prog. Rep. **38**, 297 (2005).
- 4) T. Kawabata et al.: RIKEN Accel. Prog. Rep. **41**, 129 (2008).
- 5) T. Ohnishi et al.: J. Phys. Soc. Japan **77**, 083201 (2008).

Upgrading the BigRIPS target chamber

Atsushi Yoshida, Tetsuya Ohnishi, Yoshiyuki Yanagisawa, Kensuke Kusaka and Toshiyuki Kubo

The target chamber for the production of RI beams in the projectile fragment separator (BigRIPS) has been upgraded for two reasons. Firstly, to facilitate chamber replacement, pillow seal devices were installed at the beam duct connection of the target chamber. Secondly, to reduce the heat load on an air-core-type superconducting triplet quadrupoles magnet¹⁾ (STQ1), a beam scraper was installed at the downstream wall of the target chamber.

The target chamber was designed such that it included a replaceable unit structure that facilitates maintenance under a high-radiation environment.²⁾ All the target system components assembled in the chamber can be replaced using a remote-handling maintenance cart. However, when a fatal malfunction occurs at the chamber itself or at the neighboring STQ1 magnet located downstream, it must be possible to disconnect the chamber from the beam line easily. The pillow seal device³⁾ consists of a seal-face flange, inflatable bellows, and inflatable thin metal diaphragms similar to a balloon pillow. A vacuum-tight duct connection is established by supplying air pressure to the device. Thus, a vacuum duct can be remotely disconnected without unscrewing bolts. Two pillow seal units⁴⁾ were installed at the beam duct connections of the chamber (Fig. 1). Pillow seals with inner diameters of 110 mm and 250 mm were mounted at locations up- and downstream of the beam duct, respectively. The downstream pillow seal has water ways inside the flanges to deal with the heat load from the target. Its operating air pressure is 0.35 MPa which is required to inflate both bellows and diaphragms. The measured vacuum leak rate for He gas was lower than the background level of 1×10^{-9} Pa·m³/sec.

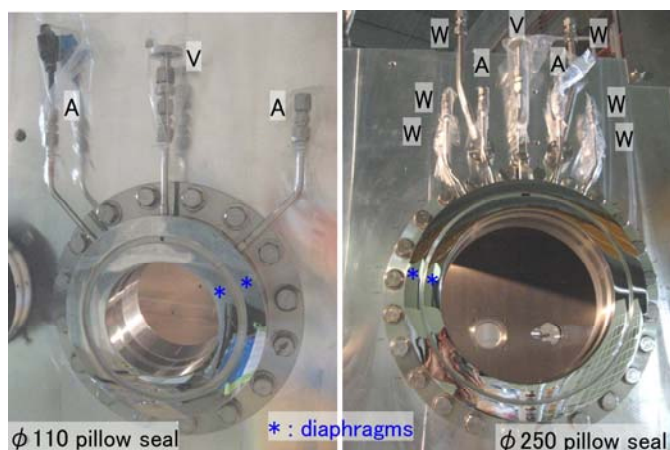


Fig. 1. Pillow seal devices installed at beam duct connections upstream (left) and downstream (right) on the target chamber. In the photos, A, W, and V represent utility pipes used to supply air pressure, to supply water for cooling, and to create vacuum for differential pumping, respectively.

At the target used for producing secondary RI beams, a large number of high-energy light-charged particles and neutrons are also produced. These undesired particles affect the heat load on the neighboring STQ1 magnet. To reduce the heat load, a beam collimator, the so-called “scraper”, was used to scrape off these particles from a bundle of the main secondary beam. A prototype scraper was designed (Fig. 2) considering the limited space between the walls of the target chamber and STQ1. A possible solution is to insert a cylindrical structure into the downstream pillow seal. The structure has a beam collimation hole with a diameter of 36 mm, which corresponds to $\pm 5^\circ$ (± 87 mrad) with respect to the target position. Note that this angle is sufficiently larger than the angular acceptance of the BigRIPS separator, which is ± 40 mrad and ± 50 mrad in the horizontal and vertical directions, respectively. The material of the scraper should be as heavy as possible in order to stop high-energy light-charged particles, mainly fragmented protons with a maximum energy of 350 AMeV. For the prototype, we used copper with a thickness of 126 mm, which is greater than the proton range of 110 mm.

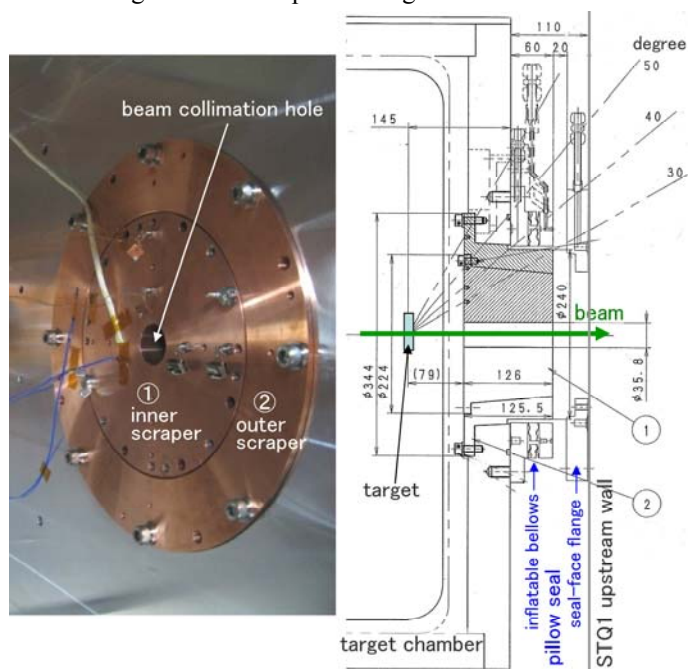


Fig. 2. Prototype scraper installed in the target chamber (left). Its typical dimensions are shown (right). It consists of inner (1) and outer (2) scraper blocks weighting 30 kg and 29 kg, respectively. The inner block will be disassembled using the remote-handling maintenance cart.

The heat load was estimated using PHITS⁵⁾ simulation code. The inner structure of STQ1 cryostat was modeled. The bombardment of a 15 mm thick beryllium target by an intense 1 μ A ⁴⁸Ca beam was simulated. Fig. 3 shows the

flux distribution of protons, neutrons and nuclei in horizontal cross sectional view. Here, the nuclei include various nuclei for which $1 < Z < 20$. Note that each flux includes secondary protons, neutrons, and nuclei produced in high-energy cascade processes. The bundle of secondary beams (Fig. 3a) passes through the beam hole of the scraper. The protons (Fig. 3c) emitted at the forward angle pass through the beam hole as well, whereas most of the protons emitted at angles with magnitude greater than 5° are stopped in the scraper or 6 cm-thick aluminum wall of the target chamber. It is clear that for high-energy neutrons (Fig. 3b), the limited thickness of the scraper is not effective.

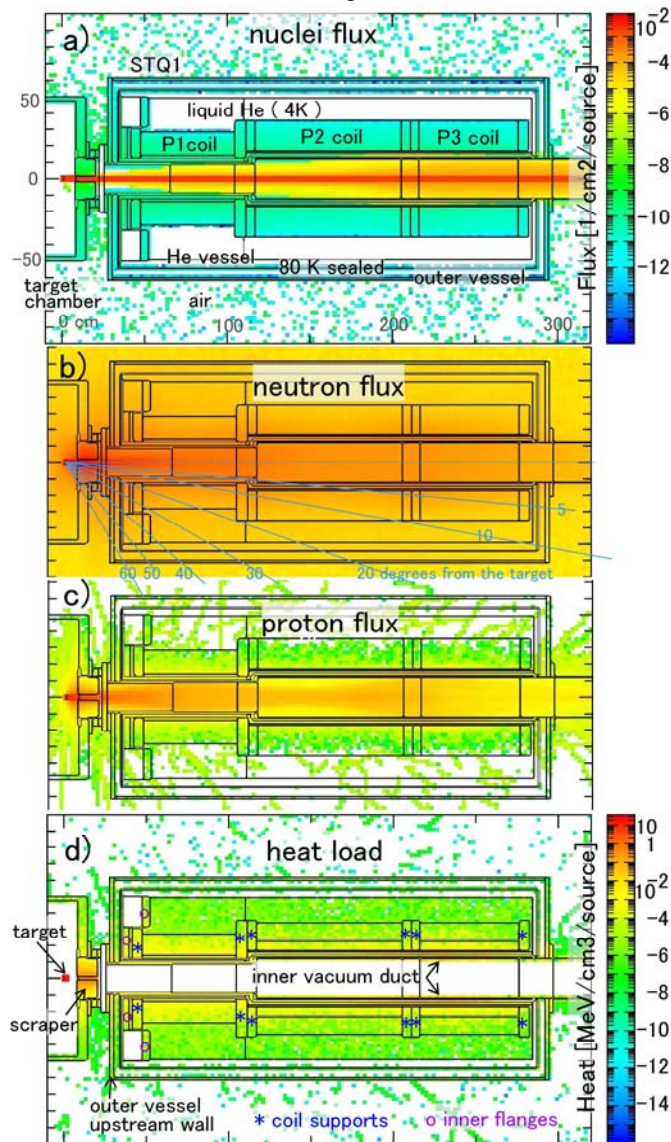


Fig. 3. Calculation results obtained using the PHITS code. The flux intensities of a) nuclei, b) neutrons, and c) protons are plotted in units of $[1/\text{cm}^2/\text{source}]$. The heat load intensity d) is plotted in units of $[\text{MeV}/\text{cm}^3/\text{source}]$. Here, the normalization factor “per source” means “caused by one nucleus of primary ^{48}Ca beam”.

The total heat load generated by all particles is plotted in Fig. 3d and listed in Table. 1. The largest heat load appears at the scraper. The next largest heat load appears at the

helium vessel and inner vacuum duct near the beam axis. In this simulation, the magnetic rigidity of STQ1 was optimized for a main secondary ^{31}Ne beam. Then, the trajectories of protons and light-charged particles, which have smaller magnetic rigidities, were over-focused in STQ1. This can be seen in Fig. 3c; some of these protons hit the inner vacuum duct.

The heat load calculated with and without the scraper are listed and compared in Table 1. The sub total of the heat load on the components assembled in the region at 4 K decreased from 460 W to 298 W because of the scraper. It has been reported⁶⁾ that the excess cooling capacities for the load at 4 K region in the BigRIPS cryogenic plant were measured as 322 W. This excess capacity should be shared by five STQ magnets, including STQ1, in the beam line. Although the main heat load sources are expected to be STQ1 and STQ2, the present heat load on STQ1 should be sufficiently smaller than the excess capacity. We are planning to measure the actual heat load during experiments by using an intense ^{48}Ca beam; we also plan to compare the values with the simulation results mentioned above. To optimize the final design of the scraper, we should decrease the diameter of the beam hole and use a heavier material like tungsten.

STQ1 components	Heat load [Watt]	
	Without Scraper	With Scraper
Liquid He	22.3	13.5
P1 coil	23.9	9.7
P2 coil	11.1	7.8
P3 coil	4.4	4.8
P1 coil support	123.0	41.9
P2 coil support	28.0	19.0
P3 coil support	16.7	17.8
Inner flanges	18.7	8.4
He vessel	211.0	175.0
(sub total in the region at 4 K)	(459.1)	(297.8)
80 K sealed vessel	43.0	39.2
Inner vacuum duct	88.5	111.0
Outer vessel (upstream wall)	21.2	7.1
Outer vessel (others)	8.8	6.4
Scraper	0.0	253.0

Table 1. Heat load calculated with and without the scraper for various inner components of STQ1 cryostat.

References

- 1) K. Kusaka et al.: RIKEN Accel. Prog. Rep. **37**, 297 (2004).
- 2) A. Yoshida et al.: RIKEN Accel. Prog. Rep. **41**, vii (2008).
- 3) Y. Yamanoi et al.: Proc. 2nd Annu. Meet. of Particle Accelerator Society of Japan and the 30th Linear Accelerator Meeting in Japan, Tosu, Japan, 2005-6, 736 (2005).
- 4) Fabricated by Mirapro Co. LTD. , <http://www.mirapro.co.jp/>
- 5) H. Iwase, K. Niita, and T. Nakamura; “Development of General Purpose Particle and Heavy Ion Transport Monte Carlo Code”, J.Nucl. Sci. Technol., **39**, 1142 (2002).
- 6) K. Kusaka et al.: RIKEN Accel. Prog. Rep. **41**, 244 (2008).

Status of the Control system of BigRIPS

K. Yoshida, T. Ohnishi, K. Kusaka, A. Yoshida, Y. Yanagisawa, N. Fukuda, M. Ohtake, H. Takeda, D. Kameda, N. Inabe, K. Tanaka, and T. Kubo

The control system of BigRIPS¹⁾ is based on the experimental physics and industrial control system (EPICS)²⁾; it was constructed in 2007 and has since been operated without any severe failures. The status of magnets, cryostats, beam diagnostic devices, and vacuum pumps is constantly recorded by the *channel archiver* utility through out the year, regardless of whether BigRIPS is in operation. Up to 13GB of data are archived in one year.

Over the last two years, two major modifications were made to the control system. First, the control of the high-resolution beam line for SHARAQ spectrometer is added to the control system. The high-resolution beam line consists of two dipole magnets, three superconducting quadrupole magnets (STQs), four normal-conducting quadrupole magnets, four focus chambers, and six vacuum pump stations. Each focus chamber is equipped with two beam diagnostic devices whose positions can be changed by pneumatic cylinder. Most of the elements have control interfaces that are identical to those in BigRIPS and ZeroDegree spectrometer. Therefore, the control system was easily modified by adding a new control record that is based on the same control routine as those in BigRIPS and ZeroDegree spectrometer. On the other hand, for the control of the STQ, STQ-H19, a new control routine was required since the power supply of STQ-H19 uses the general purpose interface bus (GPIB) for the control. The interface routine that issues and receives GPIB commands to and from the power supply was written by using the framework of "asyn-GPIB" utility in the EPICS. The routine was developed such that STQ-H19 would have a same user interface as other magnets.

The control logic of currents of the magnets was modified in order to improve the operativeness. A scaling factor was introduced into the calculation of the currents. Originally, the currents of the magnets were calculated using the central rigidity, the beam optics parameters, and the excitation function of the magnets.¹⁾ The central rigidity was converted to the strength magnetic fields of the magnets by using the beam optics parameters, and then, the current was calculated from the magnetic field using the excitation function. In the new control logic, the strength of the magnetic field is multiplied by the scaling factor before calculating the current. The current of the magnets is currently fine-tuned by changing the scaling factor instead of changing the current directly so that the correction will remain in the same ratio even if the central rigidities are changed. Furthermore, the

control system was modified such that it could detect the current drifts of the magnets.

In order to process simple I/O signals, the routines which handle IP Power 9212 (AVIOSYS International Inc.) and PICNIC (TriState Ltd.) were developed and included in the system. These devices are tiny boxes which control digital I/O through the Ethernet. PICNIC has the capability of the analog input also. The device support routine sends the command packet through Ethernet and receives response packets from them synchronously. The routine depends only on the standard EPICS libraries and does not require any device-specific libraries. Device support for Lock-In Amplifier SR844 (Stanford Research systems), which along with the fast current transformer is used for obtaining the beam current was also provided in similar manner. Data from the serial port (RS-232C) of SR844 are converted to the Ethernet packets by the serial device server NPort 5410 (MOXA Inc.), and the Ethernet packets are received by the support routine.

References

- 1) K. Yoshida et al.: RIKEN Accel. Prog. Rep. **41**, 127 (2008).
- 2) <http://www.aps.anl.gov/epics/>

Testing of Beam Viewer at BigRIPS

K. Yoshida, A. Yoshida, Y. Yanagisawa, T. Ohnishi, N. Fukuda, K. Kusaka, M. Ohtake, H. Takeda, D. Kameda, N. Inabe, K. Tanaka, and T. Kubo

A beam viewer composed of a video camera and a fluorescent plate is one of the popular beam diagnostic devices that evaluate beam characteristics such as the position, shape, and size of the beam from an accelerator. When a beam impinges on the fluorescent plate, the plate emits visible light which is detected by the video camera. The degree of lightening of the plate is a measure of the beam intensity. A vidicon camera or a charge coupled device (CCD) camera is commonly used as the detection camera. The sensitivity of beam viewers is rather low and hence, generally, only the profile of the primary beam from the accelerator is visible to the viewer. Recent enhancement of the sensitivity of CCD cameras, however, makes it possible to observe the profile of secondary beams which usually have very low intensity.¹⁾

The testing of the beam viewer was carried out in the F2 chamber of BigRIPS using the primary and secondary beams from SRC and BigRIPS. The detection camera used was an ultra high-sensitivity CCD camera (WAT-902H2 Ultimate, WATEC, minimum illumination: 0.0001 lx at f-number: 1.4) coupled with an LMVE-990A lens (KOWA, f-number: 1.8). Fluorescent plates made from three types of phosphors, $Y_2O_2S:Eu$ (NP1154-67RG, Nichia Corp.), $ZnS:Cu,Al$ (NP-1108-110RG, Nichia Corp.), and $Zn_2SiO_4:Mn$ (P1G1, Kasei Optonix) were examined. The camera was set at the top of the F2 chamber and could record the light emitted by the plate through the glass flange of the chamber. The fluorescent plates were mounted on the movable ladder of the F2 chamber. The plates were positioned perpendicular to the direction of the beam and the emitted light was observed in the direction of 60° relative to the beam direction. NTSC video signal from the camera was sent to a video-capture card of a computer.

The fluorescent plates were irradiated by a ^{14}N beam with an energy of 250 MeV/n and an intensity of less than 500 kcps. The largest signal was obtained from the plate made from $Y_2O_2S:Eu$ phosphor among the three phosphors tested. The plate made from $ZnS:Cu,Al$ phosphor gave a signal that was nearly the same as that given by the plate made from $Y_2O_2S:Eu$ phosphor. The $Zn_2SiO_4:Mn$ phosphor plate only gave a signal that was smaller than that of the $Y_2O_2S:Eu$ phosphor plate by a factor of 5.

Figure 1 shows the obtained image of the $Y_2O_2S:Eu$ phosphor plate irradiated by the ^{14}N primary beam and ^{12}B secondary beam which was produced from the ^{14}N beam. An oblong, white spot at the center of Fig. 1a represents the ^{14}N primary beam with an inten-

sity of 8 kcps. Small white dots scattered all over Fig. 1a are the noise from the amplifier inside the WAT-902H2. The noise can be eliminated by averaging a couple of images captured under the same conditions. Fig. 1b shows the average of 30 images which corresponds to the average of video signals during 1s. The noise is eliminated to a considerable extent, and the beam shape is clearly seen. As seen in Fig. 1c, a beam with an intensity as low as 1.5 kcps can be observed with this method. The ^{12}B secondary beam with an intensity of 150 kcps can be observed. Since the secondary beam has a large emittance, its beam size is much larger than that of the primary beam; hence, higher intensity is needed to observe its shape in similar brightness.

During this testing, the averaging of the recorded images was performed off-line. Therefore, we cannot observe the clear picture on-line. In order to observe the clear picture on-line, we are considering the use of a special video-capture card that provides the averaging function, or the use of a frame accumulation camera that has a slow shutter speed such as 1s.

References

- 1) J. W. Stetson: *Notes on NSCL Beam Viewplates, NSCL, Michigan State University, private communication.*

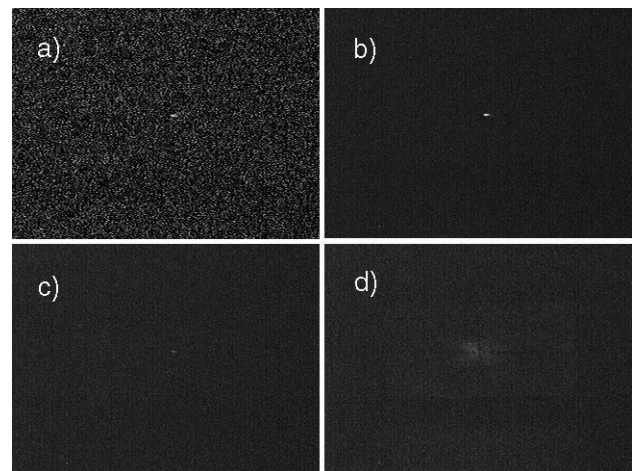


Fig. 1. Observed pictures of the beams. a) A ^{14}N primary beam with an intensity of 8 kcps. b) A ^{14}N primary beam with an intensity of 8 kcps (after averaging). c) A ^{14}N primary beam with an intensity of 1.5 kcps (after averaging). d) A ^{12}B secondary beam with an intensity of 150 kcps (after averaging).

Measurement of field maps of superconducting quadrupole and sextupole magnets

H. Takeda, T. Kubo, T. Ohnishi, N. Fukuda, M. Matsushita,*¹ H. Sato, K. Kusaka, and Y. Yanagisawa

BigRIPS¹⁾ is an in-flight RI beam separator at RIBF. Its operation is based on a two-stage separation scheme; energetic RI beams are produced and separated in the first stage and particle identification is performed in the second stage. The mass-to-charge ratio A/Q is one of the most important quantities in particle identifications because in the range of energies at RIBF, RI beams are produced in several charge states, especially in the case of heavy RI beams. Large acceptance is an important feature of BigRIPS that facilitates efficient transmission of RI beams even when the in-flight fission of uranium beams is carried out as a production reaction. Large-aperture superconducting triplet-quadrupole (STQ) magnets are used to realize large acceptance. Ion optical calculations with realistic magnetic field maps are necessary for achieving high resolution in A/Q .

We have already measured the field maps of the STQs at 20-A intervals of excitation currents from 20 A to 165 A²⁾. However, we found that these maps may not be satisfactory in the range of currents around 80 A, where the effective lengths vary on the order of 1% between the 20-A intervals used for measurement. The measurement of sextupole magnets, which are superimposed on some quadrupole magnets, was also unsatisfactory. It is already known that the field maps of the sextupole magnet were affected by the excitation of the corresponding quadrupole magnet; however, the measurements performed by exciting the quadrupole magnet have been limited to a few combinations of quad- and sextupole excitation currents. Thus, we also measured the field maps of quadrupole and sextupole magnets. Since STQ7, which has been used in the previous measurement, was installed in the BigRIPS beamline and was unavailable for the measurements, STQ22 was used. Since STQ22 is located at the end of the ZeroDegree spectrometer, a field-mapping device (Fig. 1) can be easily installed. The STQ22 consists of Q500, Q800, and Q500, where the nominal effective lengths of Q500 and Q800 are 500 mm and 800 mm, respectively. In the case of STQ22, the sextupole magnet is superimposed on the upstream Q500 magnet.

We measured the cylindrical field maps (B_r, B_θ, B_z) along the beam axis, where $B_r, B_\theta,$ and B_z are the field components along the radial, azimuthal, and beam axes, respectively. Three-axis Hall sensors (AXIS-3 AERPOC Ltd.) were mounted on an arm of the mapping device, as shown in Fig. 2. The axes of the sensors corresponded to the $r, \theta,$ and z directions described above. The center of the sensors was fixed on the arm

at radii r of 81, 94, and 107 mm from the beam axis. The arm was moved with a two-motion stage driven by stepping motors in the θ and z directions. The measurement was performed at 10-mm intervals in the z direction. At each z position, the arm was rotated 360° at steps of 3° when the sextupole magnet was excited. When quadrupole measurement was carried out without exciting the sextupole magnet, 9° steps were applied to save measurement time. The Hall voltages were measured by a digital multimeter (KEITHLEY 2700+7700) with a drive current of 10 mA supplied by a current source (Yokogawa 7651). Calibration data for each Hall sensor were obtained by using an NMR probe inside the SHARAQ D2 magnetic field in both directions. A cubic spline was used for interpolation of the calibration data. We also installed a thermocouple device near the Hall sensors to measure the temperature drift. The drift was less than ± 1 K throughout the measurement. The quadrupole and sextupole components of the field were extracted from the measured magnetic fields by applying a discrete Fourier trans-



Fig. 1. Field-mapping device (before installation inside the STQ)

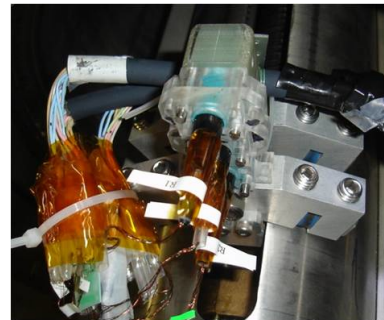


Fig. 2. Hall sensors are mounted on an arm of the field-mapping device.

*¹ Department of Physics, Rikkyo University

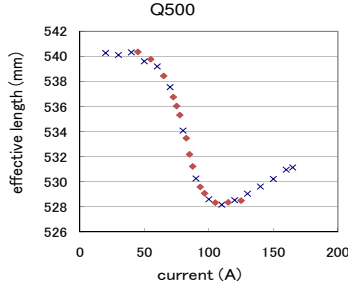


Fig. 3. Effective lengths of Q500

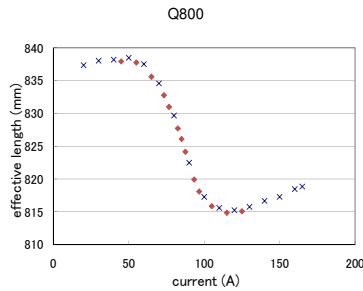


Fig. 4. Effective lengths of Q800

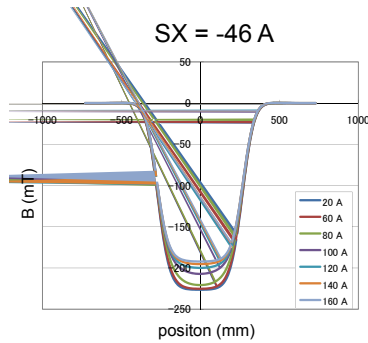


Fig. 5. Field maps of the sextupole magnet at -46 A. The corresponding quadrupole currents are changed.

formation. These distributions are implemented in the COSY ion optical calculation. Octupole and higher components are also obtained, but currently, they are not taken into account in the COSY calculation.

In order to check the agreement with previous measurements, the effective lengths of Q500 and Q800 are plotted as a function of excitation current in Figs. 3 and 4. We can see that the newly measured data (diamond marks) are consistent with previous data (cross marks). An example of the sextupole magnetic field distribution is shown in Fig. 5, where the sextupole components of the magnetic field at a warm bore radius of 120 mm are plotted as a function of z position along the beam axis. Note that the sign of the field is

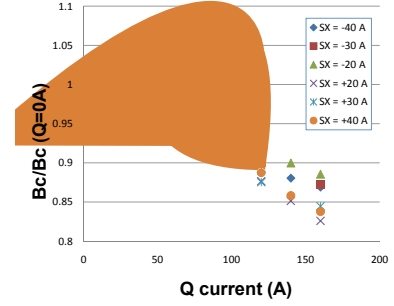


Fig. 6. The ratio of the field strength of the sextupole magnet at the magnet center under quadrupole excitation to that in the absence of quadrupole excitation is plotted.

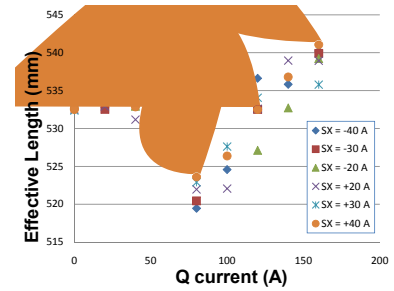


Fig. 7. Effective lengths of the sextupole magnet.

defined such that particles with positive x -values are driven toward or away from the optic axis under the influence of a positive or negative field, respectively. In this figure, the excitation current is fixed at -46 A for the sextupole magnet, whereas the corresponding quadrupole currents are changed. The field strengths decrease as the current of the quadrupole increases. The same features can be seen at all other sextupole currents in Fig. 6, in which the ratio of the sextupole field strength to the field strength in the absence of the quadrupole excitation at $z = 0$ (the center of the Q500 magnet) are plotted. The effective lengths of the sextupole magnet also vary according to the quadrupole currents, as shown in Fig. 7. These features seem to be related to the saturation of the magnet pole. Ion optical analysis using newly measured field maps is in progress.

References

- 1) T. Kubo: Nucl. Instr. and Meth. **B204**, 97 (2003).
- 2) Y. Yanagisawa *et al.*: RIKEN Acc. Prog. Rep. **41**, 125 (2008).

Radiation-shielding system between the high-power beam dump and the second superconducting quadrupole triplet in the first stage of BigRIPS

N. Inabe, K. Tanaka, K. Yoshida, M. Ohtake, N. Fukuda, D. Kameda, and T. Kubo

Production of RI beams using high-intensity (high-power) primary beams cause serious problems such as radiation damages, radiation heat loads, and high residual radiation in the devices and components in the first stage of the BigRIPS separator¹⁾ where the production target and beam dump are located. These problems arise because of the strong flux of neutrons and light charged particles emitted from the production target and beam dump, as well as the intense primary beam itself. Figure 1 shows a schematic layout of the first stage that includes the production target and the beam dump²⁾.

The intense primary beam stops at the beam dump. The target beam power is 83 kW, which is the same as that of a ²³⁸U beam at 345 MeV/u and 1 pμA. The resulting high residual radiation will prevent us from approaching a vacuum beam duct between the beam dump and the second superconducting quadrupole triplet (STQ2). This vacuum duct must be detached when maintenance work (or replacement) of the beam dump and the first dipole magnet (D1) that accommodates the beam-dump chamber is required. See Fig. 1 for details. Furthermore, the strong flux of neutrons and light charged particles emitted from the beam dump lead to heat loads and radiation damage of the STQ2. In order to find a solution to these problems, we have built and installed a radiation-shielding system in the small gap between the beam dump and STQ2.

Figure 2 shows a schematic drawing of the total system which consists of 4 parts. A base part, a guide part and a shield part compose the radiation-shielding system manufactured by Toshiba Co. Ltd. A pillow seal part,

manufactured by Mirapro Co. Ltd, is a vacuum duct which enables to detach the vacuum connection by remote handling. A detail description of the pillow seal is presented elsewhere in this progress report³⁾.

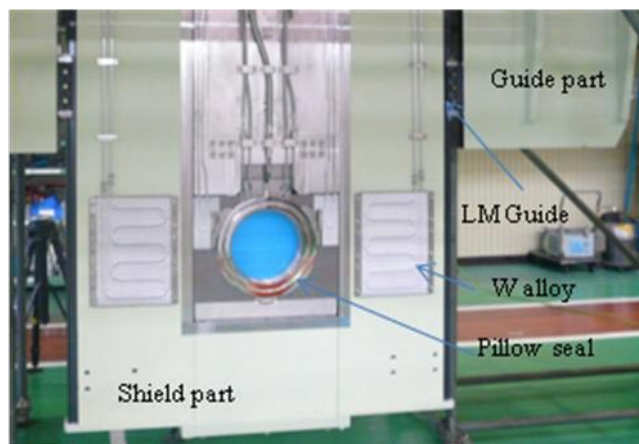
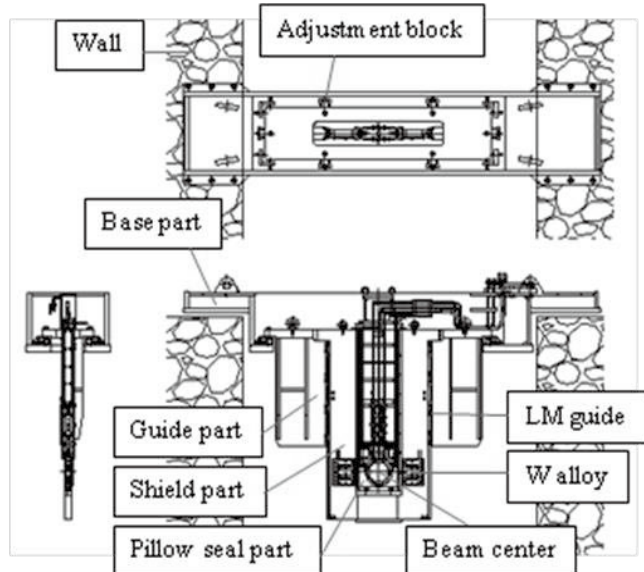


Fig. 2. Schematic drawing of the total system (above) and its photograph taken in Toshiba factory (below)

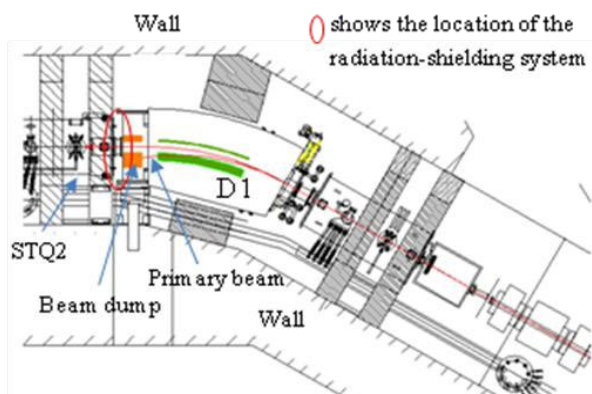


Fig. 1. Schematic layout (top view) of the first stage of BigRIPS around the production target and the beam dump. The radiation-shielding system has been installed in small gap between the beam dump chamber and STQ2.

The radiation-shielding system was designed by taking into account small clearances that are required between the devices so that the devices can be safely removed on for maintenance work. Oscillations occurring due to earthquakes were also taken into consideration in the design, assuming horizontal acceleration of 0.45 g. The system

was designed to have a robust structure so that the oscillation amplitude will be less than ± 2.5 mm, which is sufficiently small for the clearances.

The radiation-shielding system was mounted by placing the base part on top of the walls on both sides of the BigRIPS beam line, as shown in Fig. 2. The shield part was inserted downward into the beam line along the guide part, which is supported by the base part. The shield part was safely inserted using guide rails called LM guides, which are attached between the guide and the shield parts. The pillow seal was positioned by adjusting the position of the guide part. This adjustment was performed by using adjustment blocks in the base part. The alignment accuracy achieved was better than ± 1 mm. The radiation-shielding system including the base part must be removed when the maintenance of D1, STQ2, and beam dump is performed. Two knock pins are used in the base part in order to ensure that the alignment remains the same as before when the system is installed again.

The radiation-shielding system was constructed using iron (SS400) and tungsten (W) alloy (AN-1800 by Mitsubishi Material CMI Co. Ltd.). The total weight of the system was about 12.5 tons. The W alloy (heavy metal, 18.0 g/cm^3) was used near the axis of the primary beams (see Fig. 2 below) where the flux of the neutrons is strong because its shielding capability is about 1.5 times that of iron. Water-cooling channels were provided on the surface of the W-alloy part to reduce the effect of the radiation heat loads. The W-alloy part was coated with a thin layer of sprayed aluminum in order to ensure good heat transfer between the W-alloy part and the water channels. The thicknesses of the iron and the W-alloy parts are 100 mm and 110 mm respectively.

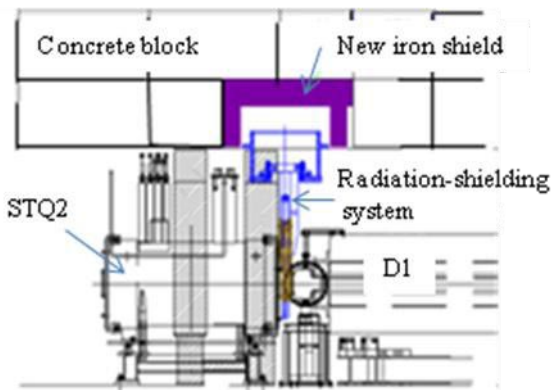


Fig. 3. Side view of the area where the radiation-shielding system is installed.

Figure 3 shows the side view of the area where the radiation-shielding system is installed. In order to install the radiation-shielding system, a concrete block of 1-m thickness, which was used to shield the ceiling of the first stage of BigRIPS⁴⁾ was replaced with a new iron shield. A schematic drawing of the iron shield is shown in Fig. 4. The iron shield was produced by OES Aqua Fuoco Co. Ltd.

The thickness of the new iron shield is 400 mm and its radiation-shielding capability is comparable to that of the concrete block of 1-m thickness. The upper iron plates were painted with an organic Zn-rich paint (Galber #400FC) in order to increase the friction between concrete blocks that are piled above them. The organic Zn-rich paint is resistant to radiation. The total weight of the iron shield is about 52 t.

The radiation-shielding system was installed in the middle of August 2009 and about one month was required to complete the installation. Prior to the installation of the radiation shield by Toshiba, we removed the concrete blocks of the ceiling and the beam duct between the beam-dump chamber and STQ2 and attached mirror flanges to the vacuum flanges of both the beam-dump chamber and STQ2. The diaphragm of the pillow seal was made to touch the mirror flange to maintain the vacuum. The removal of the beam duct and the mounting of the mirror flanges were performed in a very narrow space and under relatively high residual radiation. Therefore, prior to the actual removal and mounting, these actions were performed many times using a mock-up that simulated the system³⁾. After the installation, we carried out a vacuum test to confirm that vacuum was maintained well by the pillow seal. Finally, we replaced the concrete blocks with the new iron shield. All work related to the installation of the radiation-shielding system was completed by the middle of October.

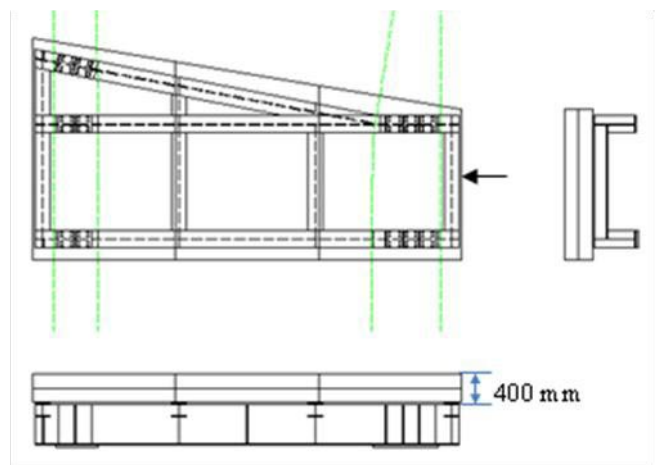


Fig. 4. Schematic drawing of the new iron shield. The black arrow points to the side shown in Fig. 3

References

- 1) T. Kubo: Nucl. Instr. Meth. **B 204**, 97 (2003).
- 2) N. Fukuda et al. RIKEN Accel. Prog. Rep. 41, 119 (2008).
- 3) K. Tanaka et al. in this progress report
- 4) K. Yoshida et al. RIKEN Accel. Prog. Rep. 37, 301 (2004).

Pillow seal around the beam dump of the BigRIPS

K. Tanaka, N. Inabe, N. Fukuda, D. Kameda, M. Ohtake, K. Yoshida, and T. Kubo

A pillow seal is a remotely operated vacuum duct utilized in high-radiation environments. The pillow-seal system was invented at the Paul Scherrer Institute and then improved by the High-Energy Accelerator Research Organization (KEK) hadron group¹. High-intensity primary beams cause a high neutron flux in the devices around the beam dump of the BigRIPS separator in the RI beam factory (RIBF)², thus causing high-radiation damage and residual radiation. This high residual radiation prevents us from approaching the devices around the beam dump that are in need of replacement or maintenance work. In order to overcome this problem, a pillow-seal system was installed to connect the chamber of the first room-temperature dipole (D1), which contains the beam dump, and the second superconducting triplet quadrupole magnet (STQ2) of the BigRIPS.

The pillow seal is remotely operated using compressed air in order to reduce personal exposure to residual radiation. Figure 1 shows the structure of a

pillow seal. The pillow seal consists of two flanges connected by dual bellows. The length of the pillow seal is decreased by evacuating the dual bellows and is increased by using compressed air.

Vacuum sealing is achieved using the pillow seal as follows: The seal surface is in contact with the special flange (seal-face flange), which faces the pillow seal once the bellows are extended. Diaphragms that can expand are utilized to remain in contact with the surface of the seal-face flanges. Compressed air is filled in the region between the flange and diaphragms to expand the diaphragm, as shown in the sectional side view in Fig. 1. The diaphragm surfaces are polished to obtain a mirror-like finish within 5-nm roughness to make the vacuum seals. The surfaces of the seal-face flanges are also polished to obtain a mirror-like finish. The mirror-like surface of the diaphragms get tightly stretched over the seal-face flange by extended bellows of the pillow seal. As a result, vacuum sealing of the metal surfaces in close contact is achieved without employing any radiation-sensitive gaskets, such as rubber O-rings. The reverse procedure is followed to detach the pillow seal. As shown in Fig. 1, the seal surfaces have a double structure. The intermediate region between two seal surfaces is vacuated to improve the seal performance¹.

Figure 2 shows the RIBF pillow-seal system. The RIBF pillow seal is present inside the radiation shield; the latter is also required in the narrow space between D1 and STQ2³. Three bearings on the side of the pillow-seal flanges remain in contact with the inner shield, as indicated in Fig. 2, in order to align the pillow seal. The bearings move the pillow-seal flanges smoothly along the beam axis to extend or shorten the pillow seal. The space where the RIBF pillow seal will be installed has a length of 100 mm, and the inner shield is 90-mm thick. In order to be mounted, the RIBF pillow seal is shortened to a length of 80 mm. The outer shield has guides to mount and dismount the RIBF pillow seal system. Two pivots and guides on the outer shield are used to align the inner shield with the pillow seal. The pillow seal in the inner shield is positioned within ± 1 mm relative to the center of the outer shield. The inner shield is made of an alloy of stainless steel, lead, and tungsten alloy (A1800 produced by Mitsubishi Material CMI Co. Ltd.). The tungsten alloy has 1.5 times better shielding capability than an alloy of stainless steel and lead. Therefore, it can be located near the pillow seal where the neutron flux is high. In order to reduce the radiation-heat load on the pillow seal, cooling water can be circulated in the channels within the flanges. 0.3-MPa N₂ gas is

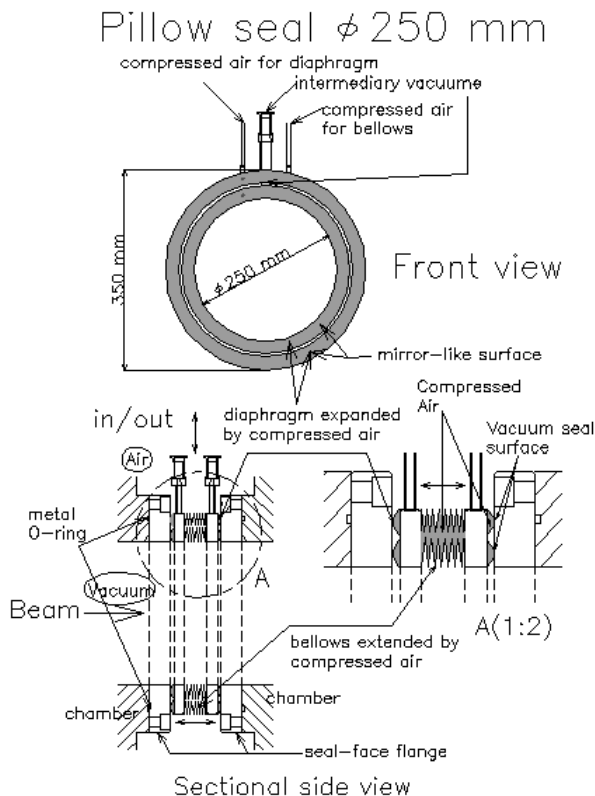


Fig. 1. Schematic view of a pillow seal. Three pipes are connected to the pillow-seal flanges. Two pipes are for compressed air and another is for vacuum. See text for details.

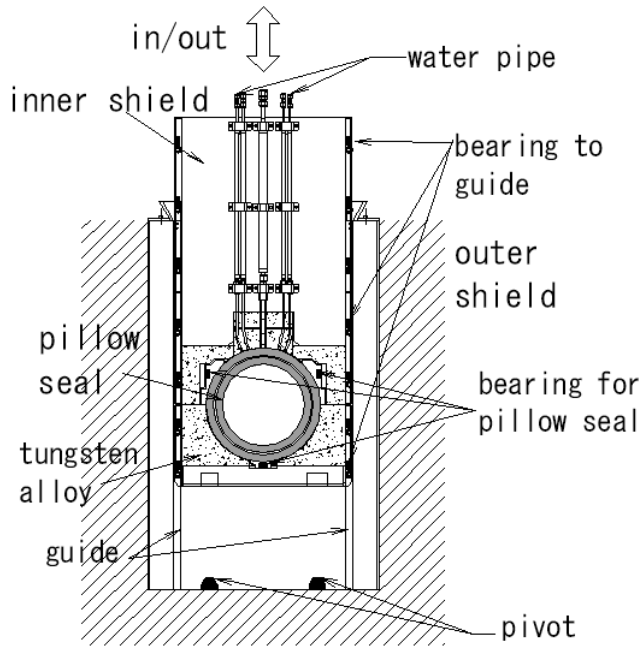


Fig. 2. Schematic view of the pillow seal mounted on the radiation shield. The pillow seal with three bearings is present in the inner shield. The inner shield is mounted in the guide on the outer shield with bearings attached on the inner shield. Unlike the pillow seal shown in Fig. 1, two pipes for cooling water are connected to the pillow-seal flange.

used to operate the pillow seal instead of compressed air because NO_x corrosion as a result of air ($\text{N}_2 + \text{O}_2$) activation is possible when air is used.

We developed a test bench to check the vacuum-sealing performance of the pillow seal before we design the pillow-seal system along with the radiation shield. Figure 3 schematically shows the test bench. The position and slope of the pillow seal with respect to the two seal-face flanges can be changed, and the leak rate was measured using helium under several conditions. The leak rate was lower than $10^{-9} \text{ Pa m}^3\text{s}^{-1}$ for a $\pm 2\text{-mm}$ difference in the position and a $\pm 10\text{-mrad}$ difference in the inclination of the pillow-seal flanges relative to the seal-face flange.

The detachment of an existing duct and the attachment of the two seal-face flanges will have to be carried out in a narrow space in the high-residual-radiation environment before installing the pillow-seal system in the BigRIPS. Radiation-hard metal O-rings (U-tight seal produced by Usui Kokusai Sangyo Co. Ltd.) were used as gaskets for the two seal-face flanges, where a high neutron flux is provided from the beam dump.

To reduce the radiation exposure as much as possible, mock-ups of D1 magnet, D1 chamber, and STQ2 magnet were built to improve the installation process and to practice completing the installation more

quickly and precisely. As a result, the time required for completing the installation process reduced by half, and the exposure was limited to less than $15 \mu\text{Sv}$ in a $\sim 100\text{-}\mu\text{Sv/h}$ environment⁴.

The radiation shield along with the RIBF pillow-seal system was installed after the seal-face flanges were installed, and then the pillow seal was connected to the BigRIPS setup. The leak rate was found to be over $10^{-9} \text{ Pa m}^3\text{s}^{-1}$ which is appropriate for the vacuum in the BigRIPS setups.

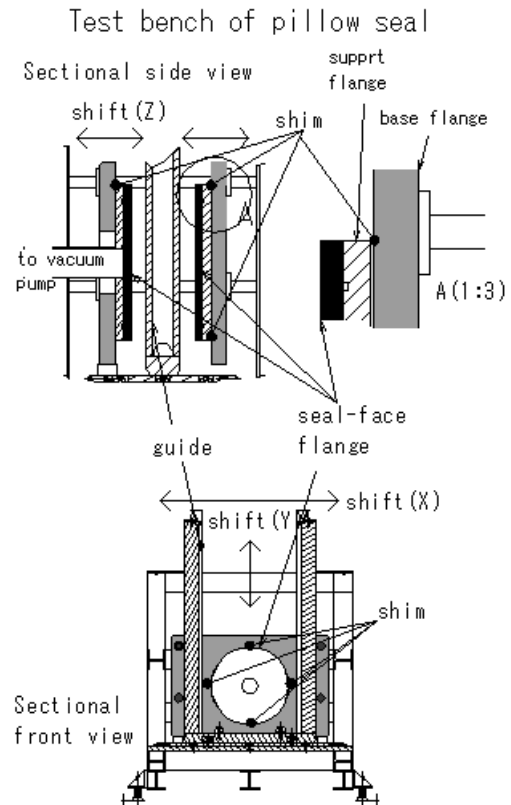


Fig. 3. Schematic view of the test bench. The pillow-seal system is mounted in the guide, as shown in this figure, which is similar to that of the outer shield shown in Fig. 2. To test the effects of any alignment changes, the the pillow seal in the guide can be shifted along the horizontal (X) and vertical (Y) direction. The seal-face flanges can shift along the beam-axis direction (Z) with the base flanges, and they can be declined using the shim between the support and base flanges.

References

- 1) Y. Yamanoi et al.: Proc. 2nd Annual Meeting of Particle Accelerator Society of Japan and the 30th Linear Accelerator Meeting in Japan, Tosu, Japan, 2005-6, p. 736.
- 2) T.Kubo: Nucl. Instr. and Meth. **B 204**, 97 (2003).
- 3) N. Inabe et al.: in this report.
- 4) K. Tanaka et al.: in this report.

Radiation measurement around the BigRIPS

K. Tanaka, N. Inabe, Y. Gono, and T. Kubo

Since the setup around the BigRIPS is being continuously modified and improved, it is necessary to predict the residual radioactivity in the region by taking into account the beam intensity and the beam cooling time in order to reduce exposure to residual radiation. Since the installation of a pillow-seal system around the beam dump of the BigRIPS where the radiation level was high was planned in the summer of 2009, a precise estimation of the radiation dose was necessary. Therefore, we measured the residual radioactivity at several places around the BigRIPS by using the Teletector 6112D GM survey meter, which can perform remote measurements, and we evaluated their time dependence. A γ -ray spectrum was also measured in the region of the beam dump with a Ge detector in order to identify the residual radionuclides and to predict future dose rates.

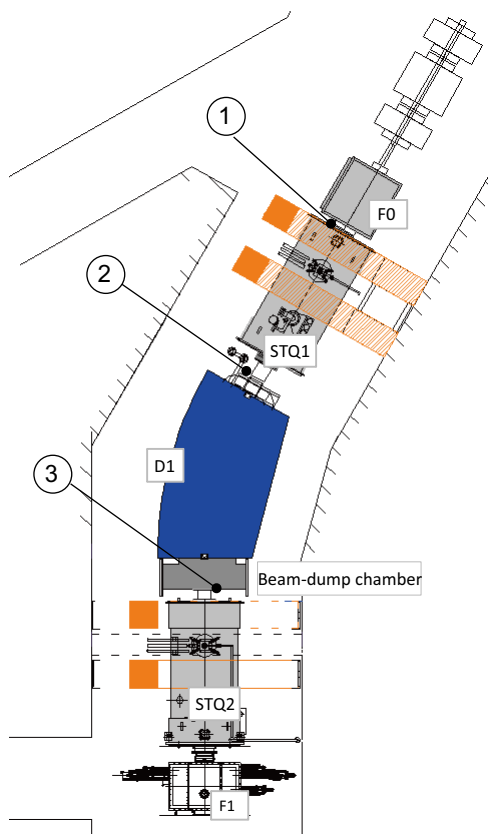


Fig. 1. Layout around the F0 and the beam-dump chamber of the BigRIPS.

The spots 1-3, which have been marked with solid circles in Fig. 1, denote the places around BigRIPS where high dose rates were observed. Figure 2 shows the time dependence of the measured radioactivity. Some unnatural variations in the plots shown in Fig. 2

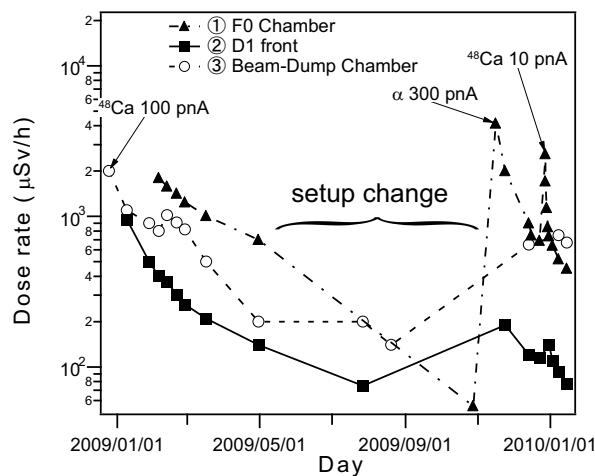


Fig. 2. Time dependence of the residual radioactivity. Spots of each plot are shown in Fig. 1. Owing to intense beams indicated in this figure, the radioactivities highly rose.

occurred as a result of the setup changes and beam irradiations, as indicated in the figure. From June to October 2009, the setup around the F0 production target and the beam-dump chamber were changed. In particular, the F0 chamber was replaced with a new one¹⁾ in June 2009, and then the dose rate decreased considerably.

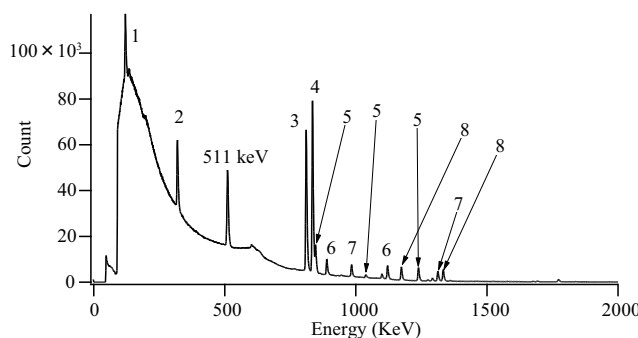


Fig. 3. Ge spectrum measured around the beam-dump chamber. The numbers in this figure indicate the nuclides listed in Table 1. Peaks with same numbers indicate the same nuclide.

In August 2009, the setup around the beam-dump chamber where the radiation was already high was changed²⁾. In order to precisely estimate the personal exposure during this work, and to prepare an efficient work plan, we measured a γ -ray spectrum (Fig. 3) near the beam-dump chamber with a Ge detector on March 2, 2009. The major material in the setup used around

Table 1. List of the nuclides and their properties measured using a Ge detector placed near the beam-dump chamber. Peak Nos. 1–8 indicate the peaks shown in Fig. 3, which were measured on March 2, 2009. The nuclides that mainly contributed to the radiation are listed in the table. The radiation due to the nuclides that was estimated in August 2009 is also listed.

Peak No.	Nuclide	Energy (keV)	Half life	Dose ratio (%)	
				March 2009 (measured)	⇒ August 2009 (estimated)
1	⁵⁷ Co	122	271 days	0.3	0.5
2	⁵¹ Mn	320	28 days	1.5	0.06
3	⁵⁸ Co	811	71 days	25	12
4	⁵⁴ Mn	835	312 days	27	47
5	⁵⁶ Co	846, 1037, 1238, 1772, 2598	79 days	17	10
6	⁴⁶ Sc	889	84 days	7.8	5.0
7	⁴⁸ V	984, 1037, 1312	16 days	8.1	0.01
8	⁶⁰ Co	1173, 1332	5.3 years	11	26
total				98	100
				Radioactivity (μ Sv/h)	
				230	⇒ 90 (estimated) 85 (measured)

the beam-dump chamber is stainless steel (SUS316). From the spectrum, we identified the nuclides that mainly contribute to the radiation dose near the beam-dump chamber; they were ⁵⁴Mn, ⁵⁶Co, ⁵⁸Co, and ⁶⁰Co. The radiation dose in August was estimated by taking into account the half lives of the nuclides. Table 1 shows the observed major nuclides and their radioactivity. In this table, the dose was relatively estimated using the photoelectric-peak count of the spectrum, the correction factor for the detector efficiency (ϵ), and the γ -ray energy, as

$$dose \propto (peak\ count)/\epsilon \times energy. \quad (1)$$

The dose ratio is the ratio of each nuclide dose to the sum of all nuclide doses. In August 2009, the dose ratios were estimated from the ratios obtained on March 2, 2009 by taking into account the half lives of the nuclides. The total dose was measured with the GM survey meter on March 2 and August 20 at the spot where the setup was changed²⁾. As shown in Table 1, the radiation doses estimated in August were accurate within ± 10 %.

References

- 1) A. Yoshida et al.: In this report.
- 2) K. Tanaka et al.: In this report.

Separation of RI beams using two-stage separation method in BigRIPS

N. Fukuda, T. Kubo, T. Ohnishi, N. Inabe, H. Takeda, D. Kameda,
and ZeroDegree commissioning collaboration

[In-flight fission, Particle identification]

One of the important characteristics of the BigRIPS in-flight separator¹⁾ is its two-stage structure (Fig. 1). The two-stage structure can be used for the delivery of tagged RI beams or as two separators in tandem with each other. The former is achieved in the tagging mode of the separator¹⁾ in which the first stage is used to produce and separate RI beams with a wedge-shaped degrader, while the second stage works as a spectrometer to analyze and identify those RI beams. The latter is achieved in the two-stage separation mode of the separator, where an additional energy degrader is used at the second stage to further purify the RI beams.

In the commissioning experiment of the ZeroDegree spectrometer conducted in November 2008, we tested the applicability of the two-stage isotope-separation method in separating the fission fragments produced in the $^{238}\text{U}+\text{Pb}$ reaction at 345 MeV/nucleon. The produced fission fragments have momentum spread over a large range; this is a characteristic of Uranium fission. Consequently, we detected more than 200 different isotopes having the same magnetic rigidity.

In this report, we present the experimental results and demonstrate the applicability of the two-stage separation method in the BigRIPS separator.

In the above experiment, a $^{238}\text{U}^{86+}$ beam bombarded a Pb target having a thickness of 1.5 mm at $E = 345$ MeV/nucleon. The magnetic rigidity ($B\rho$) of the first dipole magnet (D1) was set to 7.3940 Tm, which was kept constant during the measurement. The momentum slit was set to $\pm 3\%$ by suitably adjusting slits at the F1 dispersive focus located at the center of the first stage (F0–F2). In the two-stage separation method, the first wedge-shaped aluminum degrader having a thickness of 3 mm was installed at the F1 focal plane in the first stage, and the second curved aluminum degrader having a thickness of 1.8 mm was installed at the F5 dispersive focus located at the center of the second stage (F3–F7). The $B\rho$ values in the region following the F1 were set so as to obtain $^{140}\text{Te}^{52+}$ at the center of each focal plane and collect the isotopes with atomic numbers Z in the range of 50–55. The slit at F2 was set to ± 15 mm.

The second stage is designed to function as a spectrometer for particle identification (PID). The PID was performed by measuring the energy loss (ΔE), time of flight (TOF), and $B\rho$ of the fragments using the beamline detectors installed at the F3, F5, and F7 foci. The

ΔE was measured at F7, while the TOF measurement was performed between F3 and F7. The $B\rho$ was determined by tracking the trajectories of the fragments between F3 and F5, and those between F5 and F7. Since we use the $B\rho$ between F3 and F5 ($B\rho_{35}$) or the one between F5 and F7 ($B\rho_{57}$) for PID, we have to know the velocity between F3 and F5 ($\beta_{35}c$) or between F5 and F7 ($\beta_{57}c$). If the mass-to-charge ratio (A/Q) does not change at the F5 degrader, the β_{35} value can be deduced from the following relations:

$$\frac{B\rho_{35}}{B\rho_{57}} = \frac{(A/Q)_{35} \gamma_{35} \beta_{35}}{(A/Q)_{57} \gamma_{57} \beta_{57}}, \quad (1)$$

$$\text{TOF}_{37} = \frac{L_{35}}{\beta_{35}c} + \frac{L_{57}}{\beta_{57}c}, \quad (2)$$

where γ , L , and u denote Lorentz factor, the flight-path length, and atomic mass unit, respectively. In the data analysis, we reject the events whose A/Q changes at the F5 degrader by checking the correlation between the $B\rho_{35}$ and $B\rho_{57}$ values.

The experimental results are shown in Fig. 2, where the PID plots for three different cases were obtained by calculating the atomic number Z and the A/Q of each fragment from the measured ΔE , TOF, and $B\rho$ values. In Fig. 2 (a) (the PID plot obtained when no degrader is used) more than 200 isotopes with Z ranging from 30 to 55 are clearly identified. In order to collect the required isotopes with $Z = 50$ –55, the energy degrader was installed at F1. Figure 2 (b) shows the PID plot when the degrader is installed. The relative yield of the required isotopes increases up to approximately 40%, although some lighter isotopes ($Z = 30$ –45) that are contaminants may also be obtained. The contaminants are the isotopes that have different atomic charge state (H-like) between the F0 and the F1 degrader and

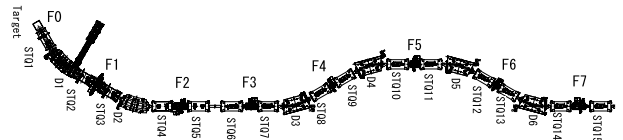


Fig. 1. Schematic layout of the BigRIPS separator. There are seven foci in the beamline that are denoted as F1–F7. The first stage includes the components from the production target-position (F0) to F2, while the second stage includes those from F3 to F7.

these are transported to the F2 focus as fully electron-stripped ions. The present identification of the variations in the charge state is confirmed by the position distribution at F3 in which the charge dispersion can be clearly seen as shown in Fig. 3.

In order to further purify the RI beams, another degrader was installed at F5. The PID plot obtained in this case is shown in Fig. 2 (c). The second degrader ensures a drastic purification of isotopes with $Z = 50$ – 55 by rejecting the lighter ions. The purity achieved is over 99%.

Finally, we describe another benefit of the two-stage separation method. The use of the second degrader reduces the amount of ions that are not completely stripped, as shown in Fig. 4. The figure represents the A/Q spectra of Sn ($Z = 50$) isotopes for the cases (a) without degrader, (b) with one degrader, and (c) with two degraders. The relative yield of $^{132}\text{Sn}^{49+}$ to $^{135}\text{Sn}^{50+}$ in the case of two-stage separation is negligible compared to those in the cases when no degrader or one degrader is used.

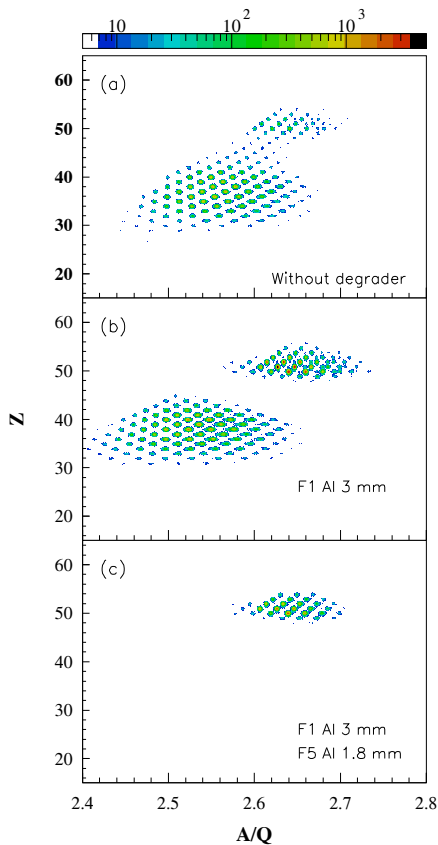


Fig. 2. Two-dimensional plots of Z versus A/Q for the fission fragments produced in the $^{238}\text{U}+\text{Pb}$ reaction obtained (a) without degrader, (b) with one degrader (F1) setup, and (c) with two degrader (F1 and F5) setup.

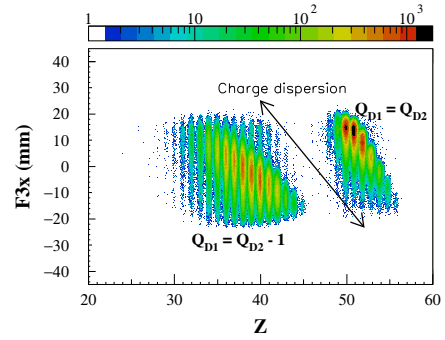


Fig. 3. Two-dimensional plot of the x -position at F3 ($F3x$) versus Z showing charge dispersion at the F3 focus. Two components of charge dispersion are seen. The isotopes with $Z = 50$ – 55 are transported from F0 to F3 as fully stripped ions, while those with $Z = 30$ – 45 are transported from F0 to the F1 degrader as H-like ions, then are transported from F1 to F3 as fully stripped ions.

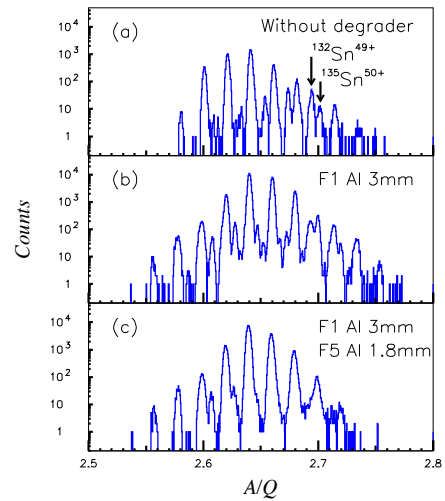


Fig. 4. A/Q spectra of the Sn ($Z = 50$) isotopes obtained for the cases (a) without degrader, (b) with one degrader (F1), and (c) with two degraders (F1 and F5). $^{135}\text{Sn}^{50+}$ and its contaminant $^{132}\text{Sn}^{49+}$ are indicated by arrows. The ratio of $^{132}\text{Sn}^{49+}$ to $^{135}\text{Sn}^{50+}$ for the two-stage separation case is negligible compared to those for the cases when no degrader or one degrader is used.

References

- 1) T. Kubo: Nucl. Instr. and Meth. **B 204**, 97 (2003).

CCJ Operation in 2008-2009

T. Nakamura, H. En'yo, Y. Goto, T. Ichihara, Y. Watanabe and S. Yokkaichi

1 Overview

The RIKEN Computing Center in Japan (CCJ)¹⁾ has been developed since April 1998 for analyzing the huge amounts of data collected in the PHENIX experiment at RHIC. Thus far, CCJ has been providing numerous services as Asia's regional computing center. For instance, CCJ maintains sufficient computing power by the PC cluster operated by Scientific Linux²⁾ for simulation and individual data analysis. The collected data are transferred through SINET3 with a 10 Gbps bandwidth, maintained by NII³⁾, from Brookhaven National Laboratory (BNL) by using GridFTP⁴⁾. The transferred data are once stored in High Performance Storage System (HPSS)⁵⁾ before starting the analysis. This HPSS is one of the joint operations with the RIKEN Integrated Cluster of Clusters (RICC) project. One of the most successful achievements of the CCJ operation up to now is the completion of more than 30 doctoral dissertations with the analysis results obtained using the computing resources at CCJ.

A summary of the basic configuration of the CCJ system has been published elsewhere⁶⁾. Since last year, several major hardware-level upgrades have been carried out. The center network switch has been replaced with Catalyst4900M, which has eight 10 Gbps ports, in July 2009. The operation of the HPSS was started with a new version 7.1 in January 2010. In February 2010, four sets of UPS were replaced by SANUPS ADS series (Sanyo Denki). The server (ccjnfs11) for Network File system (NFS), which managed a 6.8 TB FC-FC RAID box and a 8.9 TB FC-SATA RAID box, was ended the service to be upgraded in March 2010. Recently, effective use of the existing computing resources has become difficult owing to the rapid increase in the PHENIX data size. In this report, the details of several upgrades and developments made to the CCJ system in the 2008-2009 period are included.

2 PC cluster specification

Until early 2008, CCJ was operated by approximately 190 PC nodes, 166 nodes of which were used as calculation nodes for the simulation and PHENIX data analysis. In June 2008, 112 nodes were eliminated. The remaining 36 and 18 dual CPU nodes have Intel Pentium III (1.4 GHz) CPU and Intel Pentium 4 (2.0 GHz) CPU, respectively. Each calculation node has 1 GB memories.

In February 2009, 18 PC nodes (HP ProLiant DL180 G5) were newly introduced to compensate for the low total computing power. Each node has dual CPUs (Quad-Core Intel Xeon E5430 2.66 GHz) and 16 GB memories. These nodes have twelve 3.5 inch bays of

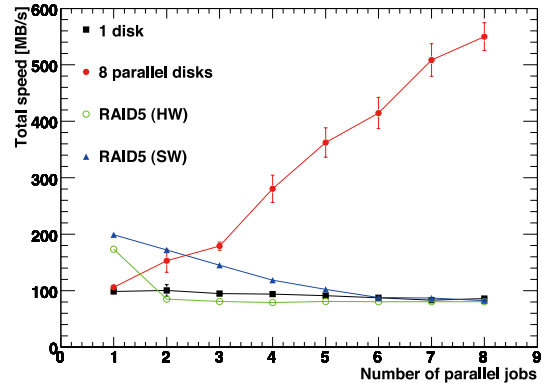


Fig. 1. Average total speed for reading 1 GB files in one disk (square), 8 parallel disks (filled circle), hardware RAID5 (open circle), and software RAID5 (triangle) as a function of number of parallel jobs.

HDD for each chassis. Two 146 GB SAS disks are mounted for the operating system and used by mirroring to reduce the down time originating from the troubles on the HDD. Initially, eight 1 TB SATA disks were mounted for local data storage. In December 2009, two additional 1 TB SATA disks were added to each node. Currently, local disks with a total capacity of 180 TB are available for the data storage. This specification is the key feature for I/O bound jobs, as will be described in the next section. Each node has a 1 Gbps network interface card, and all of the nodes are connected to a network switch (Dell PowerConnect 6224) mounted on the same rack. This network switch is up linked to the center network switch at CCJ (Catalyst 4900M) via a 10 Gbps connection. This new cluster has the capability to process a typical PHENIX analysis job approximately three times faster than the old PC nodes in a CPU core.

In October 2009, 20 PC nodes were setup as a cluster at RICC for the exclusive use of the CCJ users. Each node has dual CPUs (Quad-Core Intel Xeon X5570 2.93 GHz) and 12 GB memories and is operated by Scientific Linux 4.4 on VMware ESXi⁷⁾ so that it is dedicate to the PHENIX analysis environment. Condor⁸⁾ system is available as a batch job scheduler for this cluster.

Thus, a total of 412 CPU cores are presently available as calculation nodes for the CCJ users.

3 Development of job submission scheme

The PHENIX data stored once in the HPSS will be transferred to several RAID boxes for the analysis. Although users can access the data in the RAID boxes through the NFS servers, multiple access from numer-

Table 1. Summary of nDSTs in local disk.

Dataset	nDST type	Data amount
Run 9 $p + p$ 200 GeV	All type	65.4 TB
Run 9 $p + p$ 500 GeV	All type	31.2 TB
Run 8 $p + p$ 200 GeV	All type	21.2 TB
Run 6 $p + p$ 200 GeV	w/o detector	14.6 TB
Run 5 $p + p$ 200 GeV	w/o detector	9.9 TB

ous calculation nodes at the same time is not possible because of the decrease in the I/O speed. Therefore, users must transfer the data from the RAID boxes to the calculation node for each batch job. Since the size of PHENIX data is growing steadily, such data transfer becomes a bottleneck in data analysis. This problem is eliminated with the use of the newly introduced calculating nodes, which have large capacity local disks for storing the data a priori (see previous section). However, since these new calculating nodes have multi-core CPUs, which is predominant in the market, data analysis remains an I/O bound type job. Therefore, it is necessary to optimize the composition of the local HDD. We performed a benchmark test to evaluate the I/O performance for the new cluster. Figure 1 shows the average total speed for reading 1 GB files as a function of the number of parallel jobs. Originally, each HDD shows the I/O performance of 100 MB/s. However, the use of a multi-HDD is not advantageous with the RAID configuration, as shown by the open circles and triangles in Fig. 1. Since the RAID configuration gives us a single name space, maintaining the data location becomes easy. Nevertheless, we do not chose this configuration to maximize the I/O performance. In October 2009, approximately 96 TB Run 9 $p + p$ data, so-called nano-DST, were transferred from BNL as soon as data reconstruction was completed at the RHIC Computing Facility (RCF)⁹⁾. They were stored in local disks along with the previously stored data. Table 1 shows a summary of the dataset in the local disks accessible to users by the batch queuing system.

In the calculation nodes, users can process their own analysis code via the batch queuing system (LSF version 7.0¹⁰⁾) in the CCJ cluster. We have added some software modules to enable the user specify the nDSTs distributed to the local disks during job submission. Figure 2 shows a brief flowchart of the data-oriented job submission scheme. Since all the subsets of the PHENIX data have identical run numbers, the module first obtains the location of the nDST by the user-specified run number from a database. Then, the module submits the user jobs to the appropriate node by the LSF. To avoid multiple access for a local disk from several jobs, the module sets a lock file for exclusive access and grants permission only to the user by the Access Control List (ACL) method. As a result, each job dispatched to a calculating node exclusively handles a local disk. The advantage of this method is that the I/O performance is enhanced, as shown by

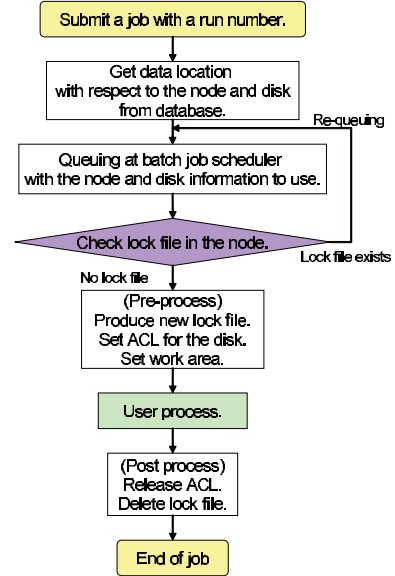


Fig. 2. Data-oriented job submission scheme.

the filled circles in Fig. 1. Further, a temporary work area for the job is assigned to the same disk with the data location. Therefore, this scheme is effective for eliminating the I/O bound problem in case of generic jobs as well *e.g.* simulation. Each job are able to save the processing time on the data transfer approximately 10 times as compared to the typical jobs in the pre-existing calculating nodes. An instruction is provided in this URL¹¹⁾ on how to access to the data stored in the local disks.

4 Summary

18 calculating nodes with 180 TB local disks were introduced for effectively analyzing huge amounts of PHENIX data. A data-oriented batch queuing system was developed as a wrapper of the LSF system to increase the total computing throughput. Indeed, the total throughput was improved by roughly 10 times as compared to that in the existing clusters; CPU power and I/O performance are increased threefold and tenfold, respectively. Thus, users can analyze data of several tens of terabytes within a few hours. This is one of the most significant developments made to the CCJ operation in 2009.

References

- 1) <http://ccjsun.riken.jp/ccj/>
- 2) <http://www.scientificlinux.org/>
- 3) <http://www.nii.ac.jp/>
- 4) <http://www.globus.org/grid/software/data/gridftp.php>
- 5) <http://www.hpss-collaboration.org/>
- 6) S. Yokkaichi et al., RIKEN APR **42**, 223 (2009).
- 7) <http://www.vmware.com/products/esxi/>
- 8) <http://www.cs.wisc.edu/condor/description.html>
- 9) <http://www.rhic.bnl.gov/RCF/>
- 10) <http://www.platform.com/products/LSF/>
- 11) <http://ccjsun.riken.go.jp/ccj/doc/LSF/lsf-wrapper.html>

SHARAQ Project: Progress in 2009

T. Uesaka,^{*1} S. Michimasa,^{*1} S. Ota,^{*1} A. Saito,^{*1} K. Nakanishi,^{*1} Y. Sasamoto,^{*1} H. Miya,^{*1} H. Tokieda,^{*1} S. Kawase,^{*1} Y. Shimizu,^{*1} S. Shimoura,^{*1} K. Miki,^{*2} S. Noji,^{*2} H. Sakai,^{*2} K. Yako,^{*2} S. Itoh,^{*2} H. Kurei,^{*1} N. Yamazaki,^{*1} A. Yoshino,^{*1} T. Kawabata,^{*4} Y. Yanagisawa,^{*3} T. Kubo,^{*3} T. Ohnishi,^{*3} H. Takeda,^{*3} D. Kameda,^{*3} N. Fukuda,^{*3} K. Tanaka,^{*3} K. Yoshida,^{*3} A. Yoshida,^{*3} N. Inabe,^{*3} K. Kusaka,^{*3} M. Ohtake,^{*3} M. Kurokawa,^{*3} M. Sasano,^{*3} K. Itahashi,^{*3} H. Baba,^{*3} T. Ichihara,^{*3} Y. Shimbara,^{*5} M. Nagashima,^{*5} G. P. A. Berg,^{*6} D. Bazin,^{*7} and P. Roussel-Chomaz,^{*8}

On March 23, 2009, the first beam was successfully transported to the final focal plane of the SHARAQ spectrometer. We investigated detector responses to heavy-ion beams and the ion optical properties of the SHARAQ spectrometer¹⁾ and the high-resolution beam line²⁾ in the subsequent commissioning runs and found that the system as a whole worked almost as per its design. The first physics run with the spectrometer was performed in November 2009. In this article, we review the progress in the SHARAQ project in 2009.

1 Last minutes of the construction

The construction of the spectrometer and the beam line was continued until the end of February 2009. Cathode read-out drift chambers (CRDC) were installed at the focal plane of the SHARAQ spectrometer in January 2009. The vacuum chambers and pumping systems of the spectrometer were built in February.



Fig. 1. Newly constructed beam line magnets: two normal-conducting dipole magnets (DH7 and DH8) and a superconducting triplet quadrupole magnet(STQ-H15).

Two normal conducting dipole magnets with a bending angle of 30° , vacuum chambers for beam line de-

tectors, and vacuum pumps were installed in the high-resolution beam line in February 2009³⁾. Figure 1 shows a photograph of the newly constructed beam-line magnets: two normal-conducting dipole magnets (DH7 and DH8) and a superconducting triplet quadrupole magnet(STQ-H15).

2 Commissioning runs

A primary ^{14}N beam accelerated up to 250 MeV in SRC was transported from F0 of BigRIPS to the focal plane of the SHARAQ spectrometer. This is the first time that a beam was accelerated without involving an IRC. The ion beam struck plastic scintillation counters placed downstream of the focal plane for the first time at 22:37 on March 23, 2009 (JST).

The beam-line detectors consisting of eight multi-wire drift chambers (MWDC) and the SHARAQ focal-plane CRDCs were irradiated by the ^{14}N beam and the secondary beams of ^{12}B , ^9Li , ^6He , and ^3H at 200A MeV. The detectors were operated at a low gas pressure of 10 kPa for the beam-line MWDCs and at 2 kPa for the CRDCs. Detection efficiencies were found to be almost 100% even for light ions with Z in the range 1–7^{6,7)}. We have also confirmed that position resolutions are high and amount to 200–300 μm FWHM, which meets the design requirements. A new data taking system was also found to function satisfactorily.

The ion-optical properties of the magnetic system were investigated by using beam trajectories determined by the tracking detectors described above. Momentum dispersions ($x|\delta$) at the dispersive focal planes F6 and FH7 and at the focal plane of the SHARAQ spectrometer were found to be 7.8 m, 7.5 m and 5.8 m, respectively. These values are consistent with the design values.

Beam-line tuning was carried out to achieve lateral and angular dispersion matching conditions and double focus conditions at the SHARAQ target position⁴⁾; the tuning was performed by adjusting the excitation currents of the four quadrupoles QH18, STQH19a, b, and c. During the tuning, the correlations between particle trajectories at the dispersive focal plane FH7 and at the focal plane of the SHARAQ spectrometer were used for diagnostics. The beam position at FH7, x_{FH7} , corresponds to the beam momentum, and thus, the correlation between x_{FH7} and the position in the

*1 Center for Nuclear Study (CNS), University of Tokyo

*2 Department of Physics, University of Tokyo

*3 RIKEN Nishina Center

*4 Kyoto University

*5 Niigata University

*6 University of Notre Dame

*7 National Superconducting Cyclotron Laboratory, Michigan State University

*8 GANIL

focal plane of the SHARAQ spectrometer, x_{FP} , provides a good measure of $(x|\delta)$ of the whole ion-optical system. The upper panel of Fig. 2 shows the correlation between x_{FH7} and x_{FP} . The upright correlation between x_{FH7} and x_{FP} in the figure clearly shows that the beam position at the focal plane of the SHARAQ spectrometer is independent of the beam momentum, which indicates the achievement of the lateral dispersion matching condition.

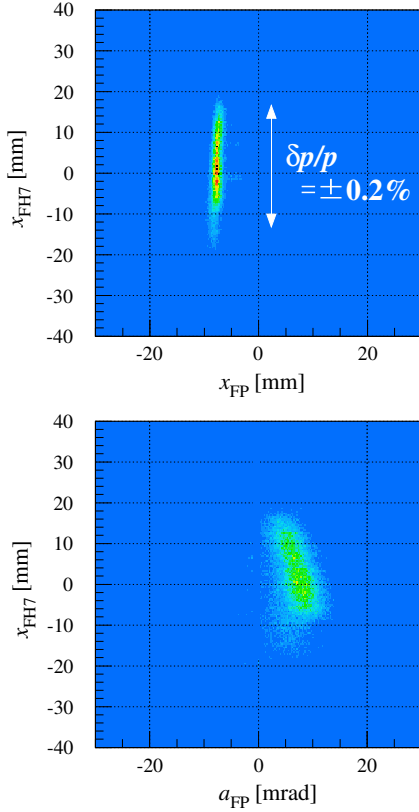


Fig. 2. Horizontal beam images at the final focal plane in the achromatic (upper panel) and the dispersion matching transport (lower panel).

Similarly, the correlation between x_{FH7} and the horizontal angle at the focal plane of the SHARAQ spectrometer, a_{FP} , that is shown in the lower panel of Fig. 2 is a good measure of the angular dispersion matching. After tuning, we succeeded in obtaining the lateral and angular dispersion matching conditions simultaneously.

Figure 3 shows the horizontal beam image at the focal plane of the SHARAQ spectrometer. Its width corresponds to the intrinsic momentum resolution of the ion-optical system. The upper panel presents the data obtained in the achromatic transport mode. In this mode, the resolution was limited by the momentum spread of the beam. After the dispersion matching condition was obtained by carrying out beam line tuning, the beam image was narrowed down considerably, as shown in the lower panel of Fig. 3.

The resulting momentum resolution $\delta p/p$ was found to be approximately 8100. Further studies to improve the momentum resolution are in progress. From the ion-optical studies, it is clearly demonstrated that tracking of the beam particles in the beam line facilitates beam line tuning that is required to obtain the dispersion matching conditions.

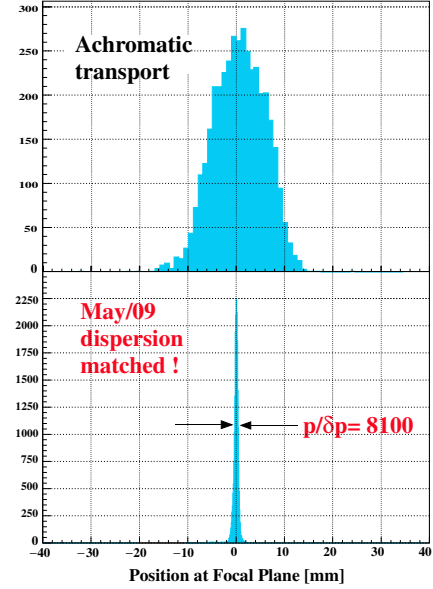


Fig. 3. Horizontal beam images at the final focal plane in the achromatic transport mode (upper panel) and in the dispersion matched transport mode (lower panel).

3 The (t , ^3He) Experiment

The first physics run with the SHARAQ spectrometer was performed to search for β^+ -type isovector spin monopole resonances in ^{90}Zr and ^{208}Pb . The (t , ^3He) reaction at 300 MeV/nucleon was used to extract β^+ strengths. An intense triton beam of 10^7 s^{-1} was produced by projectile fragmentation of a primary 320-MeV/nucleon ^4He beam, and the scattered ^3He ions were momentum-analyzed by the SHARAQ spectrometer. The details of the experiment are described in Ref. 8.

References

- 1) T. Uesaka et al.: Nucl. Instrum. Methods B **266**, 4218 (2008).
- 2) T. Kawabata et al.: Nucl. Instrum. Methods B **266**, 4201 (2008).
- 3) Y. Yanagisawa et al.: Bull. Amer. Phys. Soc. **54**, 48 (2009).
- 4) Y. Sasamoto et al.: RIKEN Acc. Prog. Rep. **43** (2010).
- 5) S. Michimasa et al.: RIKEN Acc. Prog. Rep. **43** (2010).
- 6) A. Saito et al.: RIKEN Acc. Prog. Rep. **43** (2010).
- 7) H. Miya et al.: RIKEN Acc. Prog. Rep. **43** (2010).
- 8) K. Miki et al.: RIKEN Acc. Prog. Rep. **43** (2010).

Construction of high resolution beam line for the SHARAQ spectrometer

Y. Yanagisawa, T. Kubo, K. Kusaka, M. Ohtake, K. Yoshida, T. Ohnishi, Y. Sasamoto, *¹

A. Saito, *¹ T. Uesaka, *¹ S. Shimoura, *¹ T. Kawabata, *² S. Noji, *³ and H. Sakai*³

High resolution beam line has been constructed for the SHARAQ spectrometer at RIBF in order to achieve dispersion matching that can facilitate high-resolution measurement at the focal plane of the spectrometer. This beam line is formed by the existing BigRIPS separator¹⁾ and a newly constructed beam line that diverges from BigRIPS and extends up to the target position of SHARAQ. The SHARAQ spectrometer is designed to achieve a high momentum resolution $\Delta p/p$ of 1/15000 for charged particles with a magnetic rigidity (Bp) of 6.8 Tm. The high resolution beam line is designed to satisfy the lateral and angular dispersion matching conditions; designing process involved the precise ion optical calculations²⁾.

The SHARAQ spectrometer is installed in the E20 room. Since the RI beam emitted from the production target at F0 is achromatically focused at F3 in the normal beam transport procedure for the BigRIPS, the starting point of the high-resolution transport²⁾ to the SHARAQ spectrometer is determined to be F3.

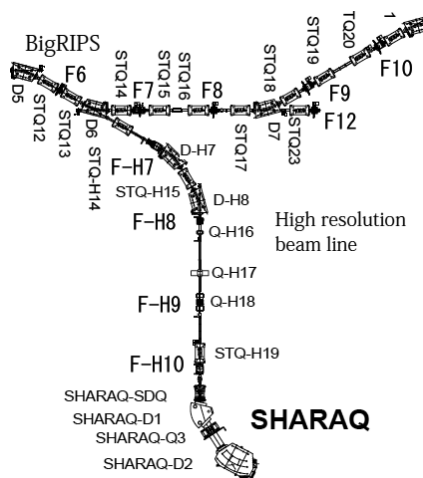


Fig. 1. Layout of the high resolution beam line.

Up to F6, the beam line shares the magnetic elements with the BigRIPS. After F6, the high resolution beam line branches from BigRIPS at the location of the E15 room and bends 60° toward the target. Since the layout of the magnetic elements of the BigRIPS separator has already been determined, the layout between the branching point and the target should be optimized to satisfy the dispersion matching conditions. The high resolution beam line consists

of two 30° bend dipoles (D-H7,D-H8), one quadrupole doublet (Q-H16,Q-H17), one quadrupole singlet (Q-H18-a,b), three superconducting triplet quadrupole magnets (STQ-H14,STQ-H15,STQ-H19), and four focal planes (F-H7,F-H8,F-H9,F-H10), as shown in Fig.1.

To reduce the cost of construction, normal conducting quadrupole magnets are used for the existing magnets. Magnets of Q-H16 and Q-H17 are identical to those of PQ3 and PQ2 in the used that were for the SMART spectrograph, respectively. The magnets of Q-H18-a and Q-H18-b reused redundant magnets in the E1 room. On the other hand, two dipoles are newly constructed with the same specifications as the dipole in the BigRIPS.

The maximum magnetic rigidity of the beam line is 8.5 Tm, which is limited by the maximum field gradient of the quadrupole doublets. The basic specifications of the magnetic elements are listed in Table 1.

STQ-H14, STQ-H15, STQ-H19
Pole length 500mm-800mm-500 mm
Pole tip radius 170 mm
Warm bore radius 120 mm
Max. field gradient 14.1 T/m
One hexapole coil is installed (STQ-H14)
D-H7, D-H8
Normal conducting
Pole gap 14 cm
Bending angle 30°
Mean orbit radius 6 m
Magnetic rigidity 9 Tm
Q-H16
Bohr radius 135 mm
Max. field gradient 3.3 T/m
Effective Length 400 mm
Q-H17
Bohr radius 185 mm
Max. field gradient 4.0 T/m
Effective Length 660 mm
Q-H18a,b
Bohr radius 90 mm
Max field gradient 8.1 T/m (a), 8.0 T/m (b)
Effective length 490 mm (a), 390 mm (b)

Table 1. Specifications of the magnetic elements

Construction of the high resolution beam line was completed in March 2009. Commissioning experiments and tests for verifying the proper functioning of the SHARAQ spectrometer were performed in March and May 2009. Results of the commissioning experiments are described in ref. 3.

References

- 1) T. Kubo et al.: Nucl. Instr. Meth. Phys. Res. B **204**, 97 (2003).
- 2) T. Kawabata et al.: Nucl. Instr. Meth. Phys. Res. B **266**, 4201 (2008).
- 3) Y. Sasamoto et al: RIKEN Accel. Prog. Rep. in this report.

*¹ Center for Nuclear Study, University of Tokyo

*² Department of Physics, Kyoto University

*³ Department of Physics, University of Tokyo

Focus tuning method of the high-resolution beam line for the SHARAQ spectrometer

Y. Sasamoto,^{*1} T. Uesaka,^{*1} S. Shimoura,^{*1} T. Kubo, Y. Yanagisawa, H. Takeda, H. Sakai,^{*2} S. Michimasa,^{*1}
A. Saito,^{*2} S. Ota,^{*1} S. Noji,^{*2} K. Miki,^{*2} H. Tokieda,^{*1} H. Miya,^{*1} S. Kawase,^{*1} T. Kawabata,^{*3}
G.P.A. Berg,^{*4} and SHARAQ team

New missing-mass spectroscopy involving RI beams will be conducted at the RIBF with the SHARAQ spectrometer¹⁾. The SHARAQ spectrometer is designed to achieve a resolving power of $p/\delta p = 1.5 \times 10^4$ and a high angular resolution $\delta\theta$ of 1 mrad for particles with a maximum magnetic rigidity $B\rho$ of 6.8 Tm. In order to avoid loss of energy resolution due to the momentum spread of the RI beams, the dispersion matching (DM) technique is applied in high resolution measurements²⁾.

A high-resolution beam line has been constructed³⁾ according to the ion optical design described in Ref. 2. Figure 1 shows the layout of the high-resolution beam line. The RI beam emitted from the production target at F0 is achromatically focused at F3. F3 is the ion-optical starting point of the high-resolution beam line. Beyond the starting point, the beam line consists of 30 superconducting quadrupole magnets, 4 normal conducting quadrupole magnets, and 5 dipoles. In order to reduce the tuning time for the beam line, the primary settings for each magnet were determined from the ion optical calculations performed on the basis of precise magnetic-field-measurements⁴⁾. Fine tuning is still needed for the high-resolution measurements. In this report, the tuning method that is used in the commissioning of the high-resolution beam line for the SHARAQ spectrometer⁵⁾ is described.

Measurement of the transfer matrix R , which relates the initial and final coordinate vectors X and X' as $X' = RX$, is required for fine-tuning. The elements of R are usually obtained from the correlations between phase-space variables of two focal planes. For example, in order to tune the focus condition for the matrix element $(x|a)_{if} = 0$, where each digit in the subscript denotes the corresponding focal plane, we use the correlation between the position x_f at the final point and the angle a_i at the initial point. The slope of the plot corresponds to the magnitude of $(x|a)_{if}$. Thus, for beam-tuning the high-resolution beam line for the SHARAQ spectrometer between F3 and F4 shown in Fig. 1, the correlation between the positions at F4 and the angles at F3 can be used. In this report, we call this method, which involves the use of the correlation between x_f and a_i , the standard focus-tuning method.

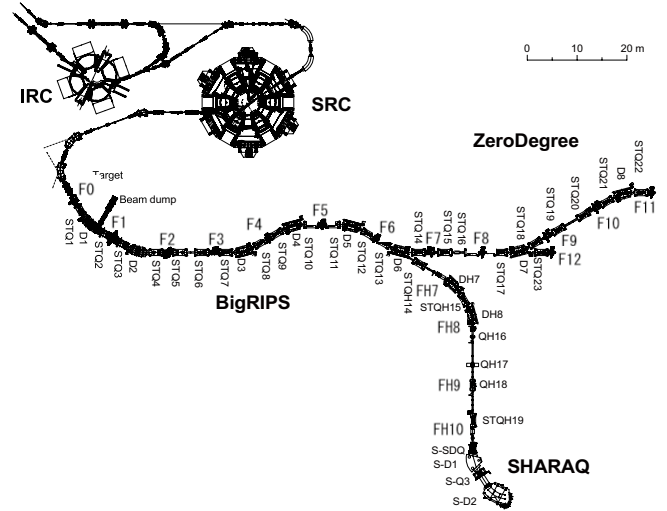


Fig. 1. Layout of the high-resolution beam line. It branches from BigRIPS after F6. F3 is the ion-optical starting point of the high-resolution beam line.

The use of correlations in the standard tuning method is not always effective in RI-beam experiments. Figure 2 shows the correlation between the angle at F3 and the position at F6 for a primary ^{14}N beam during the commissioning. The position and angle are determined experimentally by using multiwire drift chambers⁶⁾. The correlations shown in the left and right panels in the figure were obtained at different magnetic-field settings. Therefore, the slopes in the panels should be different. However, it is difficult to determine the difference.

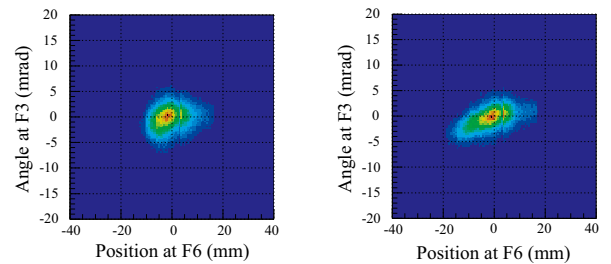


Fig. 2. Correlation between the angles at F3 and the positions at F6 for a primary ^{14}N beam under different field settings. The slope corresponds to the magnitude of $(x|a)_{36}$.

This difficulty is caused by the spread of the image at the focal plane, which result from the large dispersion and beam-energy spread. The dispersion at the focal

^{*1} Center for Nuclear Study, University of Tokyo

^{*2} Department of Physics, University of Tokyo

^{*3} Department of Physics, Kyoto University

^{*4} Department of Physics and Joint Institute for Nuclear Astrophysics, University of Notre Dame

planes in the DM mode are summarized in Table 1. When the primary beam with a momentum spread Δp of $\sim\pm 0.1\%$ is used, the horizontal beam image, for example, at F6, spreads by about ± 8 mm because of the dispersion. The beam spread smears the information for $(x|a)$. Even if momentum slits are used to reduce the beam momentum, the reduced momentum is almost on the same order as the momentum of the primary beam. The standard tuning method could be applied between F3 and F4 as described above because the spread caused by the dispersion is not considerably larger than that at other points.

Table 1. Design dispersion $(x|\delta)$ for the DM mode.

Focal plane	F4	F6	FH7	FH9	FH10
Design value	-19	76.7	-73.7	229	150
(mm/%)					

One of the methods to reduce the effect of the beam-energy spread involves the use of the measured beam momentum and the matrix elements. Although this method is simple and valid, a considerable amount of time is required to experimentally deduce both the beam momentum and the matrix elements, which are coupled to each other.

Another method, which we introduce, is to use quantities that do not depend on the beam momentum. In this report, we call this method the momentum-independent tuning method. This method is effective for tuning in the focal planes that exhibit a large dispersion. Let us consider focus tuning between F4 and FH7 for the purpose of achieving $(x|a)_{74} = 0$. The beam momentum δ could be assumed to be $x_7/(x|\delta)_{37}$ in the largely dispersive focal plane of FH7. Then, phase-space variables are related in first-order optics as

$$x_4 - \left((x|x)_{74} - \frac{(x|\delta)_{74}}{(x|\delta)_{37}} \right) x_7 = (x|a)_{74} a_7. \quad (1)$$

The term on the left-side of in Eq. (1) is independent of the beam momentum; by eliminating the spread due to the beam-energy spread at FH7.

Next, we will consider a simple example between F6 and FH7. In the following, the left-hand side is independent of the beam momentum:

$$x_6 - (x|x)_{76} x_7 = (x|a)_{76} a_7. \quad (2)$$

In this equation, the dispersive term is not included because there is no dipole magnet between F6 and FH7. In Eq. (2), the particles are assumed to be emitted from FH7 to F6. To evaluate the left-hand side of Eq. (2), the magnification $(x|x)_{76}$ should be experimentally deduced. Figures 3 and 4 show the correlation between F6 and FH7. Figure 3 shows the correlation of x_6 with x_7 and the slope of this corresponds to the magnification $(x|x)_{76}$. Figure 4 shows the correlation between

the terms on the left side of Eq. (2) and the angle at FH7, a_7 , under a different magnetic-field setting. In Fig. 4, it is clearly seen that the slope, which indicates the magnitude of $(x|a)_{76}$, is different. If the standard tuning method is applied using the correlation between x_6 and a_7 , the spread of the image caused by x_7 because of the large dispersion smear $(x|a)_{76}$ information. Fine-tuning is thus possible by momentum-independent focus tuning.

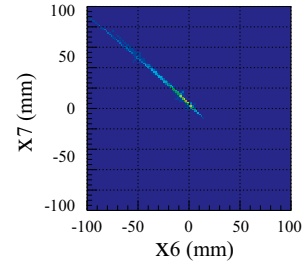


Fig. 3. Correlation between positions at F6 and FH7, which are represented as x_6 and x_7 , respectively. The slope corresponds to the magnification between F6 and FH7, namely $(x|x)_{67}$.

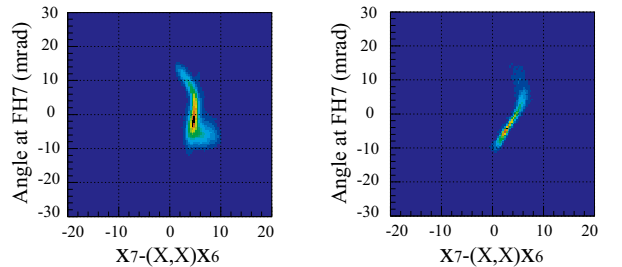


Fig. 4. Correlation between the term on the left side of Eq. (2) and the angle at FH7, a_7 , under different magnetic-field settings. It is clearly seen that the slope, which corresponds to the magnitude of $(x|a)_{67}$, is different.

This is an expeditious tuning method since it does not involve a complicated procedure. This method facilitates the quick optimization for the magnetic settings of the high-resolution beam line for the SHARAQ spectrometer. Quick beam tuning is important for beam lines with many focal planes.

References

- 1) T. Uesaka et al.: Nucl. Instrum. Meth. Phys. Res. B **266**, 4218 (2008).
- 2) T. Kawabata et al.: Nucl. Instrum. Meth. Phys. Res. B **266**, 4201 (2008).
- 3) Y. Yanagisawa et al.: Bull. Amer. Phys. Soc. **54**, 48 (2009).
- 4) H. Takeda et al.: Private correspondence.
- 5) T. Uesaka et al.: RIKEN Accel. Prog. Rep. **43**, (2010).
- 6) A. Saito et al.: RIKEN Accel. Prog. Rep. **43**, (2010).

Focal Plane Detector System of SHARAQ Spectrometer

S. Michimasa,¹ H. Tokieda,¹ S. Noji,² S. Ota,¹ S. Shimoura,¹ T. Uesaka,¹ H. Sakai,²
P. Roussel-Chomaz,³ J-F. Libin,³ P. Gangnant,³ and C. Spitaels³

[SHARAQ spectrometer, cathode-readout drift chamber]

The construction of the SHARAQ spectrometer¹⁾ and the high-resolution beam line²⁾ was completed at the RI Beam Factory (RIBF) at RIKEN in March 2009, and commissioning beam runs were performed in March and May 2009. During the beam runs, we examined dispersion-matching ion optics and evaluated the performance of the detectors installed in the focal planes of the beam line and that of the spectrometer. Valuable information on the basic performance of the high-resolution spectrometer system was obtained. This report describes the basic performance of the detector system installed in the final momentum-dispersive focal plane of the SHARAQ spectrometer.

Figure 1 shows the detector setup used in the commissioning runs. Two tracking detectors and two plastic scintillators were installed in the final focal plane of the SHARAQ spectrometer. The focal plane is located

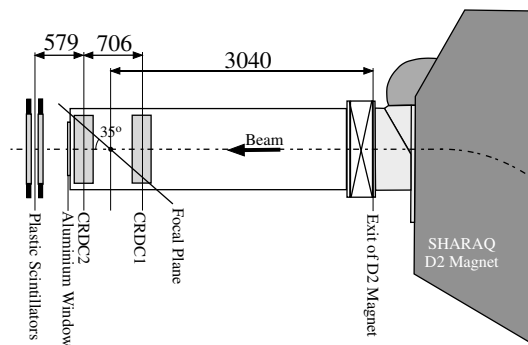


Fig. 1. Detector setup in the final focal plane of SHARAQ in the commissioning runs (top view). The detector system consists of two tracking detectors and two plastic scintillators.

3.04 m downstream from the exit of the SHARAQ D2 magnet and inclined at 35 degrees relative to the central orbit. The beam particles passed through the tracking detectors installed in vacuum and then passed into the air through a 10 mm-thick aluminum window. The plastic scintillators were placed downstream of the aluminum window.

The plastic scintillators were used to measure the timings of beam particles at the focal plane and to measure the energy deposits in them. The two-layer configuration of the scintillators was effective in rejecting cosmic-ray events. The measured results ob-

tained from each scintillator were read out by two photomultiplier tubes attached to the left and right of the scintillators. The size of the plastic scintillator was 1110 (H) \times 300 (V) \times 5 (T) mm³. Charge and timing data obtained from the scintillators were collected using charge-to-time converters (QTCs)³⁾ and multi-hit TDCs. We were able to identify ¹²N and ¹¹C particles with a separation of more than 5 σ .

The tracking of particles were performed using two cathode-readout drift chambers (CRDCs)^{4,5)}. The CRDCs have manufactured in January 2009 in collaboration with the detector developing group of GANIL. The structure of the CRDC is described in detail in Ref.⁵⁾. In the commissioning runs, the CRDCs were operated with isobutane gas at 15 or 30 torr for the detection of various light nuclei such as *t*, ⁶He, ⁹Li, ¹²B, and ^{12,14}N at around 200A–250A MeV.

The CRDC transmits two signals from the anode wires and two multiplexed signals from the cathode pads. The anode signals were used to deduce the drift time and the charge of secondary electrons. The preamplifiers for the anodes were charge sensitive; they had a gain of 0.9 V/pC and a time constant of 20 ns. The time reference for the measurement of the drift time was provided by the plastic scintillators. Since the anode signal is generated when an avalanche occurs around the anode wires, the drift times are determined by the difference between the anode timing signal and the timing signal of the plastic scintillator. We operated CRDCs with drift electric fields of 83.3 (140) V/cm using 15-(30-)torr isobutane. The drift velocity of the secondary electrons were 5.9 cm/μs at 15 torr and 5.3 cm/μs at 30 torr, respectively. These values are approximately equal to those evaluated by using the GARFIELD code⁶⁾. Under the above mentioned conditions, the vertical position resolution was approximately 0.9 mm (FWHM), which is inferior to the design value by a factor of 2. We are continuing data analysis in order to improve the position resolution.

Figure 2 shows the avalanche gain measured by CRDCs operated with 30-torr isobutane as a function of the voltage supplied to the anode wires. CRDC1 (CRDC2) corresponds to the upstream (downstream) tracking chamber in Fig. 1. The avalanche gain of CRDC2 was consistently smaller than that of CRDC1. This difference in the gains is considered to be due to the difference in their configurations. In CRDC1, potential wires are placed between anode wires, while CRDC2 has no potential wires; this has been schemati-

¹ Center for Nuclear Study, University of Tokyo

² Department of Physics, University of Tokyo

³ GANIL, France

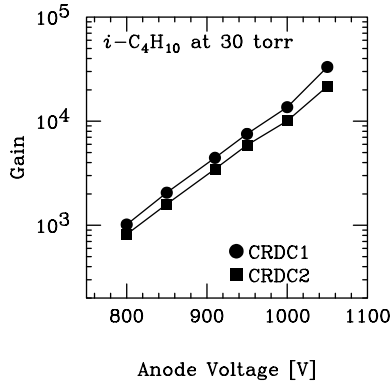


Fig. 2. Avalanche gain of CRDCs measured using isobutane gas at 30 torr. The definitions of CRDC1 and CRDC2 are described in the text.

cally depicted in Fig. 2 of Ref.⁵). However, we demonstrated that both the CRDCs achieved an avalanche gain higher than the required gain of 10^4 .

The detection efficiency of the CRDC is defined here as the ratio of the detection using the anode signal to the detection by the plastic scintillators. Figure 3 shows the detection efficiency of CRDC1 as a function of the supplied anode voltage. Fig. 3(a) shows the detection efficiency curves for ^{14}N ions at 250A MeV in the 15- and 30-torr operations, and Fig. 3(b) shows the detector efficiency for lighter particles at around 220A MeV in the 30-torr operation. It was confirmed

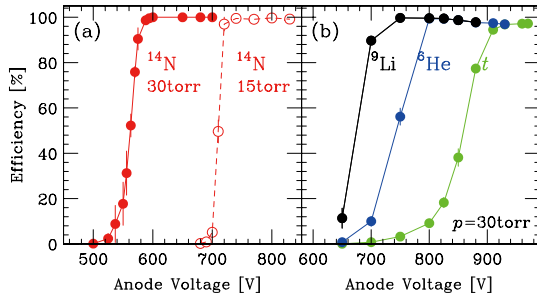


Fig. 3. (a) Detection efficiency for 250A-MeV ^{14}N ions with the 15- and 30-torr operations. (b) Detection efficiency for t , ^6He , ^9Li particles with the 15- and 30-torr operations.

that the CRDCs designed for SHARAQ will achieve detection efficiencies of approximately 100% for 200A-MeV tritons even when operated using 30-torr isobutane gas.

The horizontal position in the focal plane is determined by the charge distribution on the cathode pads. The charge signals from the cathode pads were read out by using GASSIPLEX chips⁷) and a CRAMS module⁸). The pedestals of the channels the GASSIPLEX chip ranged from 60 to 70 mV and were stable (< 2 mV) over the 10-day measurements. The track-and-hold signals were generated by the timing of the anode signal of the CRDC under the condition that two plastic scintillators and the anode were detected

simultaneously. In the commissioning run, we applied anode voltages that were 30 V higher than the voltages for which the detection efficiencies were 100%. At the supplied voltage, induced charges were distributed over approximately 10 cathode pads, and the maximum induced charge was present around the middle of the dynamic range of GASSIPLEX. The horizontal position was deduced by fittings of the charge distributions to a function

$$q(x) = a_1 \cdot \text{sech}^2 [\pi(x - a_2)/a_3],$$

where a_i ($i = 1, 2, 3$) are fitting parameters⁹). The horizontal position corresponds to a_2 . The typical resolutions of horizontal position were estimated to be 500 μm and 700 μm (FWHM) for ^{14}N at 250A-MeV and ^6He at 220A-MeV, respectively.

In summary, we examined the detector system installed in the focal plane of the SHARAQ spectrometer in the commissioning runs of the SHARAQ spectrometer by using light radioactive isotopes at 200A–250A MeV. All the detectors were operated successfully and the basic data on their performance were obtained. Identification of particles with atomic numbers Z of around 7 was performed by using plastic scintillators. Under the present conditions, the position resolution of CRDCs was estimated to be 0.9 mm (FWHM) in the horizontal direction and 0.7 mm (FWHM) in the vertical direction. In the first experiment¹⁰) that was performed in November 2009, the focal plane detector system was used, and the data on the ($t, ^3\text{He}$) reactions at 300A MeV were obtained. Further analysis is now in progress in order to optimize the detectors' parameters and to improve the data-analysis algorithm used in the detectors.

References

- 1) T. Uesaka et al.: Nucl. Instrum. Methods Phys. Res. B **266**, 4218 (2008).
- 2) T. Kawabata et al.: Nucl. Instrum. Methods Phys. Res. B **266**, 4201 (2008); Y. Yanagisawa et al.: Bull. Amer. Phys. Soc. **54**, 48 (2009).
- 3) H. Nishino et al.: Nucl. Instrum. Methods Phys. Res. A **610**, 710 (2009).
- 4) M.H. Tanaka et al.: Nucl. Instrum. Methods Phys. Res. A **362**, 521 (1995).
- 5) S. Michimasa et al.: CNS-REP-80, (2009) 55.
- 6) R. Veenhof, GARFIELD, CERN Program Library W5050.
- 7) The GASSIPLEX is a re-designed chip of the AMPLEX by J.C. Santiard of CERN. The AMPLEX is described in E. Beuville et al.: Nucl. Instrum. Methods Phys. Res. A **288**, 157 (1990).
- 8) V551 C.A.E.N sequencer User Guide, V550 C.A.E.N CRAMS User Guide.
- 9) K. Lau and J. Pyrlík: Nucl. Instrum. Methods Phys. Res. A **366**, 298 (1995).
- 10) K. Miki et al.: RIKEN Accel. Prog. Rep. **43**, (2010).

Development of Beamline Detectors for BigRIPS and High-Resolution Beamline

A. Saito,^{*1} S. Shimoura,^{*1} H. Miya,^{*1} K. Miki,^{*2} T. Yoshida,^{*3} T. Kawabata,^{*4} S. Itoh,^{*2} K. Itahashi M. Sasano Y. Shimizu,^{*1} Y. Shimbara,^{*5} S. Kawase,^{*1} H. Kurei,^{*1} S. Michimasa,^{*1} K. Nakanishi,^{*1} S. Noji,^{*2} S. Ota,^{*1} Y. Sasamoto,^{*1} H. Tokieda,^{*1} T. Uesaka,^{*1} and H. Sakai^{*2}

1 Introduction

We are developing low-pressure multiwire drift chambers (LP-MWDCs) and plastic scintillators to be used in BigRIPS and the high-resolution beamline (HRBL), for SHARAQ spectrometer experiments¹⁾.

Figure 1 shows a layout of BigRIPS, HRBL, and SHARAQ spectrometer. LP-MWDCs are installed at F3, F6, F-H7, F-H9, and F-H10. A list of the LP-MWDCs is shown in Table 1. Plastic scintillators are installed at F3, F-H7, F-H9, and F-H10. Herein, we report on the developments made to LP-MWDCs and the plastic scintillators as well as the commissioning performed in March, May, and November 2009.

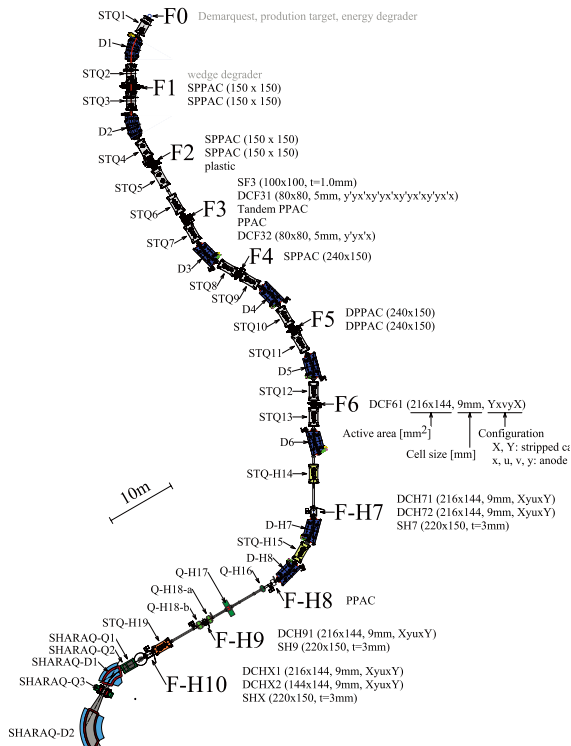


Fig. 1. LP-MWDCs and plastic scintillators in BigRIPS and HRBL.

The tracking detectors used must fulfill certain requirements. The thickness of the detectors should

^{*1} Center for Nuclear Study, University of Tokyo
^{*2} Department of Physics, University of Tokyo
^{*3} Department of Physics, Rikkyo University
^{*4} Department of Physics, Kyoto University
^{*5} Department of Physics, Niigata University

be very low, i.e. approximately 10^{-4} of the radiation length, so that multiple scattering in the detectors is reduced to approximately 0.1 mrad. The efficiency should be as high as possible even for light RI beams such as 200-MeV/nucleon ^8He beams. The position resolution is required to be less than $300 \mu\text{m}$ in FWHM. The maximum counting rate should be 1 MHz for the dispersive beam transport. Energy loss information should be obtained by the tracking detectors for particle identification of the RI beam and for rejecting in-flight β -decay events.

LP-MWDCs are being developed in order to achieve the above mentioned performance. Low-pressure operation at around 10 kPa must be carried out to reduce multiple scattering in the detector to 0.1 mrad.

Table 1. List of LP-MWDCs in BigRIPS and HRBL. X and Y are the stripped cathode with delay-line readout; x, u, and y are anode layers.

Focal Plane	Name	Active area [mm ²]	Cell size [mm]	Configuration
F3	DC31	80 × 80	5	xx'yy'xx'yy'
	DC32	80 × 80	5	xx'yy'
F6	DC61	216 × 144	9	XyuxY
F-H7	DC71	216 × 144	9	XyuxY
	DC72	216 × 144	9	XyuxY
F-H9	DC91	216 × 144	9	XyuxY
F-H10	DCX1	216 × 144	9	XyuxY
	DCX2	144 × 144	9	XyuxY

2 MWDCs at F6, F-H7, F-H9, and F-H10

Figure 2 shows a schematic view of DCX2, which includes three anode layers (x, u, and y) and two stripped cathodes (X and Y). The u wires are tilted by 30° with respect to the x wires. The cathodes on the outer side are stripped in the horizontal and vertical directions (X and Y). The stripped cathodes provide redundant position information and information about the energy loss of the RI beam for particle identification. The signals from the stripped cathodes are read out using delay lines (DL's). Three high voltages can be supplied individually to the stripped cathodes, other cathodes, and field wires. The signals from the DLs are amplified by a Kaizu 3356 preamplifier. The signals from the anode wires are amplified and discriminated by a REPIC RPA-130/131 64-channel preamplifier and discrimina-

tor cards. The timing signals from RPA-130/131 are digitized by CAEN V1190A/B multihit TDCs.

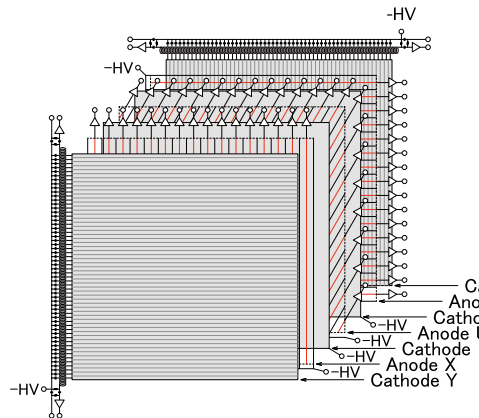


Fig. 2. Schematic of DCX2.

Figure 3 shows the detector setup at F-H10. Two LP-MWDCs are separated by a distance of 500 mm in order to track the RI beams with an angular resolution better than 1 mrad.

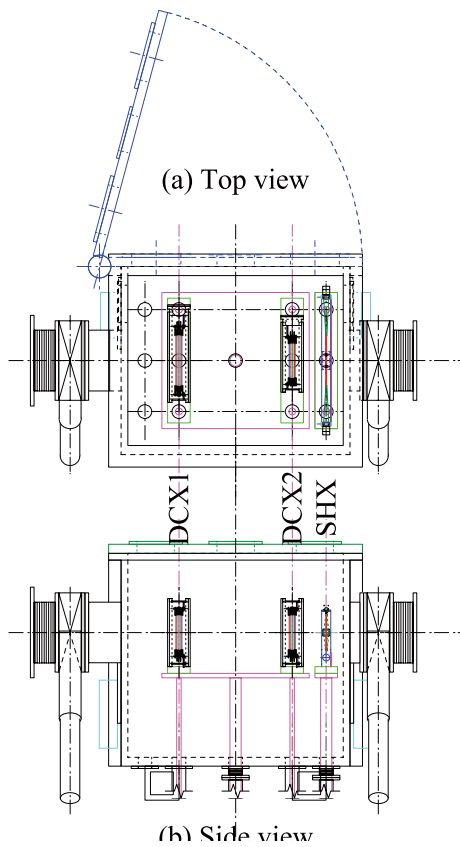


Fig. 3. Detector setup at F-H10.

3 Plastic scintillators

Plastic scintillators were installed at F3, F-H7, F-H9, and F-H10. Eljen Technology EJ-212 scintillators were used. The dimensions of SF3 and the others were $100 \times 100 \times 1 \text{ mm}^3$ and $220 \times 150 \times 3 \text{ mm}^3$, respectively. The scintillation light was read out by two Hamamatsu R7600 photomultiplier tubes with light guides attached to both ends of the scintillator.

4 Commissioning

Commissioning of HRBL and the SHARAQ spectrometer was performed in March, May, and November 2009. Eight LP-MWDCs listed in Table 1 were used in the commissioning. In March and May 2009, we evaluated the tracking efficiencies and resolutions of the LP-MWDCs at F6, F-H7, F-H9, and F-H10, at 10 kPa for the RI beams produced by fragmentation of the ^{14}N beam. We also evaluated the performances at 50 kPa for triton and ^3He beams, in November 2009. Details of the data analysis are described elsewhere⁷⁾.

References

- 1) T. Uesaka et al.: Nucl. Instrum. Meth. in Phys. Res. **B266**, 4218 (2008).
- 2) T. Kawabata et al.: Nucl. Instrum. Meth. in Phys. Res. **B266**, 4201 (2008).
- 3) K. Miki et al.: RIKEN Accel. Prog. Rep. **42**, 175 (2009); K. Miki et al.: CNS Ann. Rep. 2008 (2009).
- 4) H. Miya et al.: CNS Ann. Rep. 2007, 60 (2008); H. Miya et al.: RIKEN Accel. Prog. Rep. **42**, 173 (2009).
- 5) T. Yoshida et al.: CNS Ann. Rep. 2008 (2009).
- 6) H. Kumagai et al.: Nucl. Instrum. Meth. in Phys. Res. **A470**, 562 (2004).
- 7) H. Miya et al.: CNS Ann. Rep. 2008 (2009); H. Miya et al.: RIKEN Accel. Prog. Rep. **43**, (2010).

Current status of SAMURAI

K. Yoneda, N. Iwasa,^{*1} T. Kawabata,^{*2} T. Kobayashi,^{*1} Y. Kondo,^{*3} T. Kubo, K. Kusaka, T. Motobayashi, T. Murakami,^{*2} Y. Nakai, T. Nakamura,^{*3} J. Ohnishi, T. Ohnishi, H. Okuno, H. Otsu, H. Sakurai, H. Sato, Y. Satou,^{*4} K. Sekiguchi, and Y. Togano

This report describes the current status of construction of the experimental apparatus, SAMURAI. SAMURAI (Superconducting Analyzer for Multi-particles from Radio Isotope beam) is a large-acceptance multiparticle spectrometer to be constructed in RIBF. A schematic illustration of SAMURAI is shown in Fig. 1. The main component of SAMURAI is a large-gap (80 cm) superconducting dipole magnet with the maximum bending power of 7 Tm. This magnet will be used for the analysis of momentum of heavy projectile fragments and projectile-rapidity protons with large momentum and angular acceptance. The large gap also enables measurement of projectile-rapidity neutrons with large angular acceptance in coincidence with heavy projectile fragments.

SAMURAI can be used in a variety of applications in experiments with the RI beams provided by BigRIPS. When used in experiments on breakup of neutron-rich and proton-rich nuclei, SAMURAI's large acceptance enables efficient heavy ion(HI)-neutron and HI-proton coincidence measurements that are required for invariant-mass spectroscopy. SAMURAI is also suitable for use in missing-mass spectroscopy, in which measurement of charged particles after the reaction not only enables the tagging of the reaction channels but also provides knowledge of the decay modes; this is possible because of the multi-particle detection capability. SAMURAI is also used to scrutinize scattering reactions of light nuclei, such as polarized deuteron scattering on proton, in order to study fundamental nucleon-nucleon interactions, including three-nucleon force effects. We also plan to install a time projection chamber in the large gap of the SAMURAI magnet, which is used mainly for reaction studies such as investigation of density dependence of the asymmetry term in the nuclear equation of state.

The construction is funded for four years from fiscal year (FY) 2008. At present, designing and construction of the magnet and detectors are underway and are proceeding according to the schedule, and the first experiment will be performed in summer 2011.

The magnet is an H-type dipole with cylindrical poles of diameter 2 m. Each pole is surrounded by a superconducting coil that generates a magnetic field of about 3 T across the pole gap of 80 cm at the center of the magnet. The yoke and pole of the magnet have

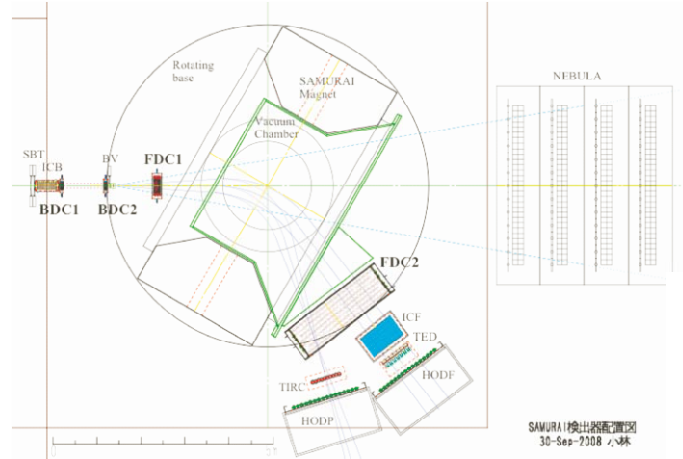


Fig. 1. Schematic image of SAMURAI system. SAMURAI consists of a large bending magnet that is surrounded by particle detectors. The magnet is a superconducting dipole magnet with the maximum bending power of 7 Tm and a large pole gap of 80 cm. Heavy-ion detectors, neutron detectors, and proton detectors, are installed around the magnet. The detector configuration is changed depending on experimental requirements.

been designed, and at present, the designs of the coil and cryogenic system are being finalized¹⁾.

In the following sections, an overview of the detectors to be prepared for SAMURAI is given. Three types of detectors, namely, heavy ion detectors, neutron detectors, and proton detectors, are to be prepared. The heavy ion detectors consist of 1) beam detectors, 2) tracking detectors that are placed before and after the magnet, 3) detectors used for particle identification (PI) and time-of-flight (TOF) measurement.

• Beam Detectors

The beam particles are detected in front of the target to obtain the information required for PI and the beam profiles, which is used to generate an important trigger signal.

The beam timing is measured by the plastic scintillators (SBT). Two sets of plastic scintillators, i.e., two 1-mm-thick scintillators and two 0.5-mm-thick scintillators are prepared. Each scintillator has an active area of 100 mm × 100 mm, and both ends of each scintillator are PMTs (HAMAMATSU H1949-50MODB). Plastic scintillators with a hole are prepared and are used as beam halo veto detectors (BV). Three BVs with a hole of diameter 20 mm, diameter 25 mm, and

^{*1} Department of Physics, Tohoku University

^{*2} Department of Physics, Kyoto University

^{*3} Department of Physics, Tokyo Institute of Technology

^{*4} Department of Physics and Astronomy, Seoul National University, Korea

diameter 30 mm, are prepared. These detectors are ready for use.

An ion chamber (ICB) is installed in the beamline to measure the energy loss of the beam particles. The ICB has an active area of 150 mm × 150 mm; it is 420-mm thick, and has multiple cathodes and anodes that are vertical to the beamline. An ICB performance test was performed.

Beam profiles are measured by two multiwire drift chambers (BDC1, BDC2) or two multiwire proportional chambers (BPC1, BPC2, not shown in the figure). The active areas of BDC and BPC are 80 mm (V) × 80 mm (H) and 150 mm (V) × 240 mm (H), respectively. BDC is designed to work at low gas pressure, so that the detector can be installed in the beamline. The performance of BDC at low pressure was tested. These detectors have already been fabricated.

- Tracking Detectors

The HI tracking detectors (FDC1, FDC2) that are to be set in front of and behind the magnet will be constructed. FDC1 will be installed between the target and magnet. It is expected that the beam particle density at FDC1 is high, and hence the operation rate should be high. For this purpose, FDC1 is designed to have a drift distance of 5 mm. FDC1 has an active area of 340 mm (V) × 620 mm (H) to allow projectile-rapidity neutrons to pass through the detector aperture. FDC1 has already been fabricated.

FDC2 is placed behind the magnet in order to measure HI tracks. Particles will spread in space behind the magnet, and hence FDC2 is designed to cover a large area (~810 mm (V) × 2230 mm (H)). FDC2 is being designed, and so far structural calculations have been performed. FDC2 will be constructed in FY2010.

- Detectors for PI and TOF measurement

Plastic scintillator hodoscopes (HODF, HODP) are used for TOF measurement. Each hodoscope consists of 16 plastic scintillators (1200 mm (V) × 100 mm (H), 10 mm thick). Both ends of the scintillators are coupled to the PMTs (HAMAMATSU H7195MODB). Velocity measurement can also be performed by using total internal-reflection-type Cherenkov detectors (TIRC).

An ion chamber for reaction fragments (ICF) is installed for measuring the energy loss of HIs. The ICF has an active area of approximately 400 mm (V) × 700 mm (H). Pure CsI scintillators are prepared for use as total energy detectors (TED). The crystal size is 100 mm × 100 mm × 50 mm, and the crystal is coupled to a PMT (HAMAMATSU R6233ASSY). The performances of TIRC and TED were tested. All these detectors are ready to be fabricated.

- Neutron Detectors

A neutron detector system, called NEBULA (NEutron Detection system for Breakup of Unstable Nuclei with Large Acceptance), is placed at forward angles. NEBULA consists of four sets of detector array, and each set consists of 60 neutron detection plastic scintillators (120 mm × 120 mm × 1800 mm), which are arranged in two layers and cover an area of 1800 mm (V) × 3600 mm (H), and 12 charged-particle-veto scintillators (320 mm × 10 mm × 1900 mm). Two PMTs (HAMAMATSU R7724ASSY) are coupled to both ends of each scintillator. The angular acceptance of NEBULA is ±5° (V) and ±10° (H), which corresponds to almost 100% coverage for breakup events with a relative energy of 3 MeV and about 40% for a relative energy of 10 MeV. Neutron detection efficiency with full volume is estimated to be about 60% for the projectile-rapidity neutrons. Half the required number of neutron detection scintillators and full veto detectors are ready for use.

- Proton Detectors

The TOF of protons is measured by the hodoscope, which has been described earlier. A tracking detector that is to be placed after the magnet (PDC, not shown in the figure) is prepared separately so that proton-HI coincidence measurement can be carried out. PDC will be fabricated by May 2011.

The tracking detector that is to be placed before the magnet should be capable of detecting protons even when both protons and HIs hit the detector; a gas detector cannot be used for this purpose. Therefore, layers of silicon strip detectors are installed between the target and magnet. Here, the detector should be capable of detecting protons as well as heavy ions, leading to the generation of signals ~2500 times larger than proton signals. Additionally, the number of channels is as high as ~2500. In order to overcome these difficulties, we started developing a new ASIC front-end circuits. The circuits are being designed and tested, and the results are reported by M. Kurokawa *et al.* ²⁾.

The magnet will be assembled in Room E21 in RIBF building in autumn 2010, and the assembling will be completed by early 2011. The detectors and electronics will be simultaneously developed. After some tests and commissionings, the first SAMURAI experiment is expected to be performed in early 2012.

References

- 1) H. Sato *et al.*: RIKEN Accel. Prog. Rep. **43**, 180 (2010).
- 2) M. Kurokawa *et al.*: RIKEN Accel. Prog. Rep. **43**, 182 (2010).

Design of large-gap superconducting dipole magnet for SAMURAI spectrometer

H. Sato, N. Iwasa,^{*1} T. Kawabata,^{*2} T. Kobayashi,^{*1} Y. Kondo,^{*3} T. Kubo, K. Kusaka, T. Motobayashi, T. Murakami,^{*2} T. Nakamura,^{*3} J. Ohnishi, T. Ohnishi, H. Okuno, H. Otsu, H. Sakurai, Y. Satou,^{*4} K. Sekiguchi,^{*1} Y. Togano, and K. Yoneda

A large-acceptance spectrometer named SAMURAI is under construction at the RIKEN RI Beam Factory (RIBF).^{1,2)} The SAMURAI spectrometer consists of a large-gap superconducting dipole magnet, heavy-ion detectors, neutron detectors, and proton detectors. The purpose of the spectrometer is to perform kinematically complete measurements of multiple particles emitted in reactions induced by RI beam. The superconducting dipole magnet is required to have a rigidity resolution of about 1/700 (rms) at $P/Z = 2.2$ GeV/c, which corresponds to a magnetic rigidity $B\rho$ of 7.3 Tm, where P is a momentum and Z is an atomic number. It should also be able to identify particles having mass numbers up to 100. The superconducting dipole magnet has been designed to satisfy these requirements on the basis of 3-dimensional magnetic field calculations performed using the code OPERA-3D/TOSCA.

Figure 1 shows the schematic view and the cross-sectional views of the dipole magnet. The magnet is an H-type dipole, having cylindrical poles with diameters of 2 m, a large pole gap of 880 mm, and circular superconducting coils. To change the experimental setup, the magnet can be rotated about the y-axis. The upper and lower superconducting coils are installed in their respective cryostat and cooled separately by a liquid helium bath. The maximum magnetomotive force is 1.9×10^6 AT/coil, which generates a magnetic field of about 3 T at the center of the poles in the median plane. The magnet is designed to have a maximum bending power (BL integral) of 7 Tm.

Figure 2(a) shows the excitation curves of the dipole magnet. The points on the solid line are the values calculated by using TOSCA, while the dotted straight line is obtained by assuming that the magnetic permeability of iron is infinity. The y component of the magnetic fields, $B_y(z)$, obtained with a magnetomotive force of 1.9×10^6 AT/coil is plotted along the z-axis in Fig. 2(b). Note that the schematic representation of the coordinates is given in Fig. 1. The integral of $B_y(z)$ for the region from $z = -2$ m to $z = +2$ m is calculated to be 7.05 Tm, which satisfies the design requirement for the bending power. The main parameters of the magnet are listed in Table 1.

Fig. 3(a) shows the $B_y(z)$ distribution calculated for

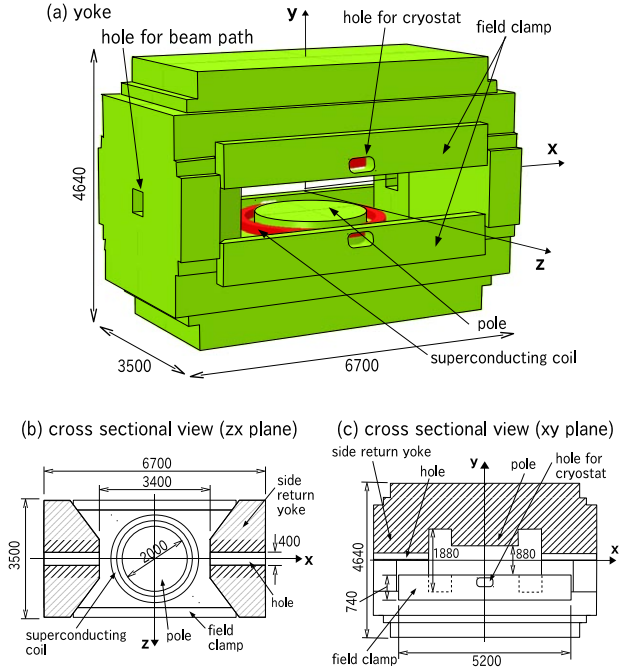


Fig. 1. Schematic view (a) and cross-sectional views (b)(c) of the superconducting dipole magnet.

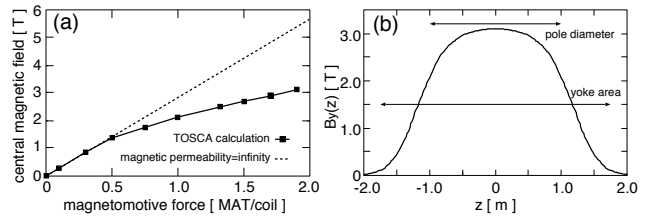


Fig. 2. (a) Excitation curve. (b) y component of magnetic field, $B_y(z)$, plotted along z-axis (1.9×10^6 AT/coil).

different central magnetic fields. In the case of the maximum magnetic field of 3.1 T, the peak value of the fringing fields was calculated to be -2.6×10^{-3} T. This value is acceptable for achieving the required magnetic rigidity resolution.

We checked the effects of two kinds of holes on the magnet (see Fig. 1). The first type of hole is a rectangular hole (490 mm \times 260 mm) that is located at the horizontal center of each field clamp. This hole is used for installing cryocoolers. The other hole serves as a beam path at each side yoke, whose cross-sectional size

^{*1} Department of Physics, Tohoku University

^{*2} Department of Physics, Kyoto University

^{*3} Department of Physics, Tokyo Institute of Technology

^{*4} Department of Physics and Astronomy, Seoul National University, Korea

Table 1. Parameters of the superconducting dipole magnet and the superconducting wire.

Magnet	
type	H-type, superconducting
number of turns	3411 turns/coil
current	560 A
magnetomotive force	1.9×10^6 AT/coil
current density of coil	66.0 A/mm ²
field at the pole center (median plane)	3.1 T
BL integral at 3.1 T	7.05 Tm
maximum magnetic field in a coil	5.26 T
inductance	212 H
stored energy	33 MJ
inner diameter of coil	2350 mm
outer diameter of coil	2710 mm
cross section of coil	180×160 mm ²
weight of coil	1783 kg/coil
pole shape	circular
pole gap	880 mm
pole diameter	2000 mm
pole height	500 mm
yoke width	6700 mm
yoke depth	3500 mm
yoke height	4640 mm
yoke weight	566140 kg
Superconducting wire	
material	NbTi/Cu
diameter	3 mm ϕ
Cu/SC ratio	5.0~6.0
insulation	PVF(≥ 40 μ m)
filament diameter	~ 28 μ m ϕ
number of filaments	~ 1760
twist pitch	~ 88 mm
RRR	≥ 100
critical current at 4.2 K	>4000 A at 3 T >3290 A at 4 T >2690 A at 5 T >2150 A at 6 T

is 400 mm \times 400 mm.

The $B_y(z)$ distribution when the field clamps did and did not have holes is shown in Fig. 3(b) by lines (iii) and (ii), respectively. Although some effects of the holes can be recognized in the figure, the effects only appear in a narrow region from $z = 2.25$ m to $z = 2.75$ m, and the BL obtained in the region of $2.2 \leq z \leq 5$ m decreases by 5%.

The influence of the beam paths on the side yokes is shown by line (iv) in Fig. 3(b). The presence of these holes increases the peak value of the fringing fields by 36% and also increases the BL by 30%.

Line (i) in Fig. 3(b) represents the $B_y(z)$ distribution when the holes are present in both the field clamps and

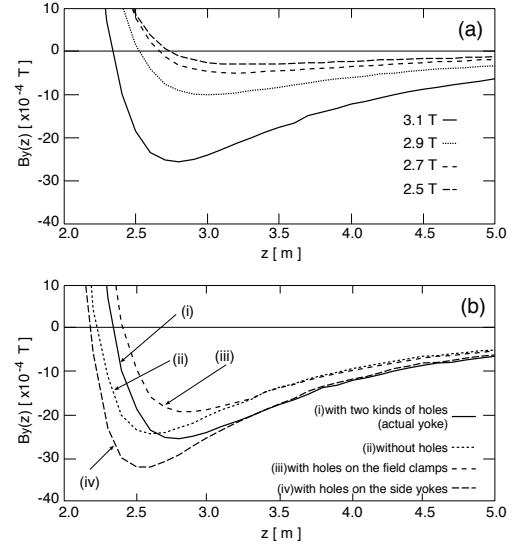


Fig. 3. Magnetic field distribution $B_y(z)$ in the fringing field region: (a) for different central magnetic fields and (b) with the holes in the field clamps and the side return yokes.

Table 2. List of the cryocoolers for one cryostat.

cryocooler	liquid-He vessel	thermal shield		current lead
	GM-JT $\times 2$	20 K	80 K	
cooling	3.5 W	5 W	45 W	60 W
power	@4.3 K	@20 K	@40 K	@40 K
heat load	4.11 W	4.96 W	78.22 W	53.94 W

the side yokes. It is observed that the effects of these two kinds of holes (see Fig 3(b,iii) and (b,iv)) cancel each other, and as a result, the total effect of the holes on the fringing fields becomes small (as indicated by the change from Fig 3(b,ii) to (b,i)). Thus, we conclude that the presence of these holes does not have a serious degrading influence upon the fringing fields.

The upper and lower superconducting coils are installed in separate cryostats and cooled by a small cryocooler system mounted on each cryostat. Thus, there are no superconducting links between the coils. Table 2 lists the cryocoolers for one cryostat. There are a total of 10 cryocoolers for this superconducting dipole magnet.

The assembly and installation of the superconducting dipole magnet will start at the RIBF site in autumn 2010 and will be completed by early 2011.

References

- 1) K. Yoneda *et al.*: RIKEN Accl. Prog. Rep. **42**, 26 (2009).
- 2) K. Yoneda *et al.*: RIKEN Accl. Prog. Rep. **43**, 178 (2010).

Front-End Electronics for SAMURAI Si Detectors

M. Kurokawa, Y. Aoki,^{*1} N. Iwasa,^{*2} M. Masuyama,^{*1} T. Motobayashi, H. Murakami, A. Taketani, M. Tanaka,^{*3} Y. Togano, and K. Yoneda

In an experiment performed to study the Coulomb breakup reaction of proton-rich nuclei,¹⁾ array of silicon strip detectors (SSDs) is installed between the secondary target and Superconducting Analyzer for Multi-particle from Radio Isotope beam (SAMURAI) for identifying the reaction products and measuring their scattering angles. The strip pitch is determined on the basis of the accuracy required in the angle measurement. Thus, a total of around 2500 strips are installed. We are going to employ the Application Specific Integrated Circuits (ASIC) technologies in the front-end circuits of the array to handle the enormous number of signal channels. The circuit must be able to provide a dynamic range of 2500 for the identification of charged particles from proton to Sn nucleus, whose atomic number is 50. In order to analyze the pile-up events of heavy charged particles, wider range is required. We are developing an ASIC so that the front-end circuit can provide a dynamic range of around 10,000. This article reports the specifications and the present status of the development of a prototype ASIC. This work is supported by the High Energy Accelerator Organization, for the promotion of collaborative research programs in universities.

The ASIC for a preamplifier was fabricated using a 0.5- μm CMOS process. Figure 1 shows the circuit diagram of the preamplifier in which the techniques described below are applied to increase the dynamic range.

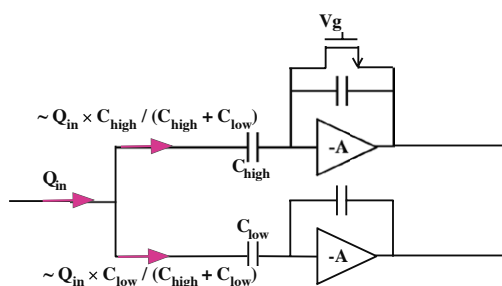


Fig. 1. A circuit diagram of the preamplifier under development. Q_{in} and V_g represent the input charge from a strip of SSDs and the gate bias voltage, respectively.

In the first stage of the circuit, the input charge Q_{in} is unsymmetrically divided into two channels in proportion to the capacitance ratio between the external

coupling condensers C_{high} and C_{low} , as in the case of Ref.²⁾. In the present case, the capacitance of the C_{high} ($= 5.6 \text{ nF}$) is ten times C_{low} ($= 560 \text{ pF}$), as shown in Table 1. The lower and upper detection limits given in the table are equal to the magnitude of Q_{in} . For the estimation, we assumed that the single-channel amplifier possesses a dynamic range of 1,000 and the lower and upper limits are 3.6 fC and 3.6 pC, respectively. For a system utilizing the both channels, the range will be 10,000 and the lower and upper limits will be 4.0 fC and 40 pC. Thus, we can increase the range by as much as the capacitance ratio by implementing the dual-channel system.

Here, saturation has to be avoided for the upper channel. The capacitive division of charge does not work correctly at saturation because the upper channel cannot absorb the divided charge completely for the case. Useful method to avoid saturation is the compensation of the charge at the input of the amplifier by making use of its charge sensitivity. For this purpose, an FET has been introduced in the feedback stage.³⁾ Depending on the saturation voltage of the amplifier, the gate bias voltage V_g is adjusted. The applicability of this method for saturation suppression has been established only in the case of discrete circuits^{4,5)} and not for in the case of highly integrated circuit. This novel technique will be examined with the present ASIC for the first time.

In a circuit based on the capacitive division, the open-loop gain of the amplifier is an important factor. Its value should be as large as possible, so that the capacitive division works correctly. We implemented the cascode connection of the current mirror, as seen in Ref.⁶⁾. A simulation was performed to confirm the increase in the open-loop gain. The gain was 54 dB for a basic mirror and 82 dB for the cascode connection.

The simulated response of the circuit is shown in Fig. 2. From Fig. 2(b), which represents the pulse shape for the upper channel, we can see that the saturation suppression is effective because the maximum pulse height for each signal is maintained at around a voltage of -2.1 V, which is below the saturation voltage of around -2.4 V. Steep peaks at the rising edges in the curves in Figs. 2(c) and 2(d) are due to the finite rise time of the amplifier. The effect of the peak is removed by a shaping amplifier with an integration time constant of around 1.0 μs . The simulated pulse shapes show that each channel is working correctly up to the upper limit given in Table 1. The measurement, which includes the determination of the upper and lower limits, will be performed after the comple-

^{*1} Tokyo Metropolitan College of Industrial Technology

^{*2} Department of Physics, Tohoku University

^{*3} Institute of Particle and Nuclear Studies, High Energy Accelerator Organization

Table 1. Summary of specifications of the preamplifier.

	upper channel ^(a)	lower channel ^(a)	dual channel
coupling capacitance	$C_{\text{high}} = 5.6 \text{ nF}$	$C_{\text{low}} = 560 \text{ pF}$	
lower limit	4.0 fC	40 fC	4.0 fC
upper limit	4.0 pC	40 pC	40 pC
dynamic range	1,000	1,000	10,000

(a) See Fig. 1.

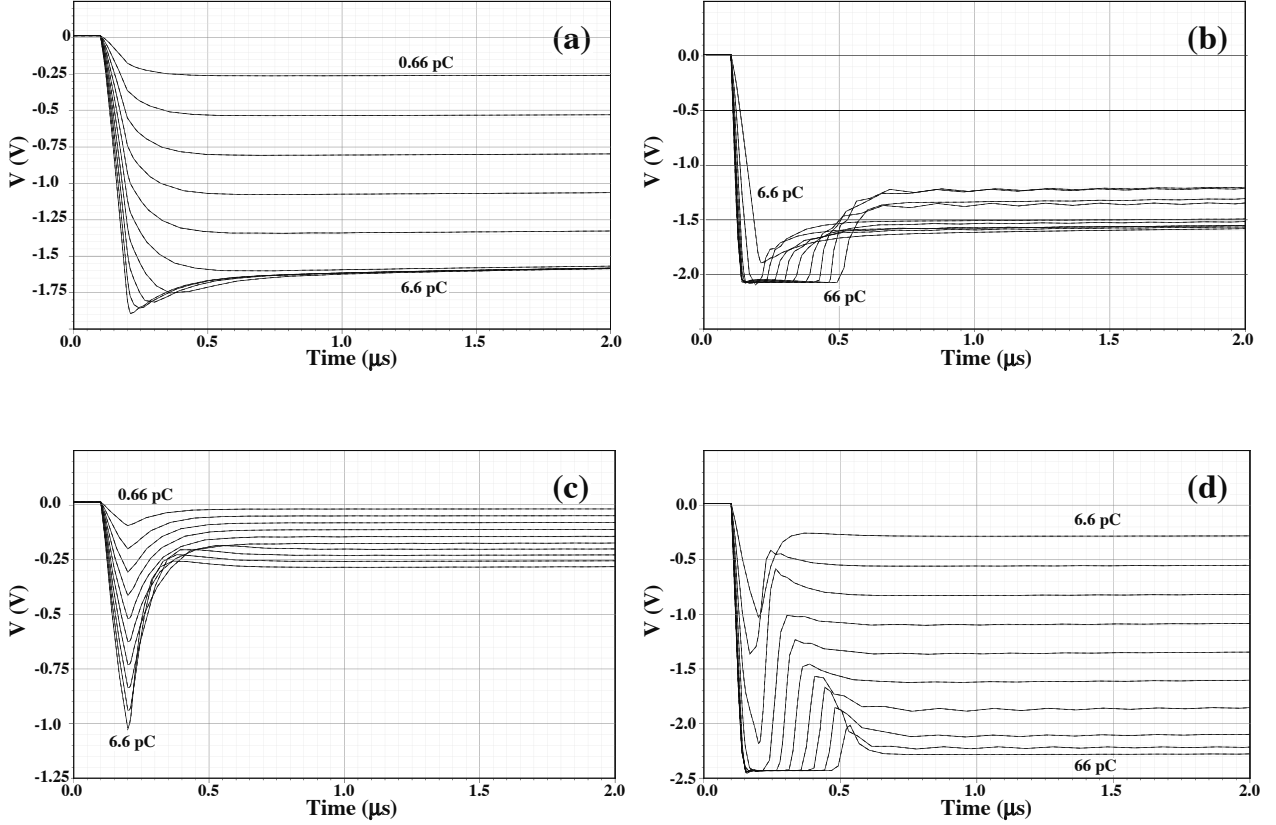


Fig. 2. Output signals obtained in the simulation are shown for the upper ((a) and (b)) and lower channels ((c) and (d)). In (a) and (c), the input charge varies from 0.66 pC to 6.6 pC, with a step size of 0.66 pC. In (b) and (d), the input charge varies from 6.6 pC to 66 pC, with a step size of 6.6 pC.

tion of the prototype ASIC.

References

- 1) K. Yoneda et al.: RIKEN Acc. Prog. Rep. **43** (2010).
- 2) N. Uematsu and S. Nishimura: RIKEN Acc. Prog. Rep. **41** (2008) 151.
- 3) H. Murakami, private communication.
- 4) T. Machida, Master thesis of Rikkyo Univ. 2007.
- 5) Y. Aoki and M. Masuyama, private communication.
- 6) G.L. Engel et al.: Nucl. Instrum. Meth. in Phys. Res. **A573** (2007) 418.

Design study of equipment in Rare-RI Ring

Y. Yamaguchi, I. Arai,^{*1} T. Fujinawa, N. Fukunishi, A. Goto, T. Kikuchi,^{*2} S. Kubono,^{*3} T. Moriguchi,^{*1} D. Nagae,^{*1} T. Ohnishi, T. Ohtsubo,^{*4} A. Ozawa,^{*1} H. Sakurai, H. Suzuki,^{*1} T. Suzuki,^{*5} M. Wakasugi, T. Yamaguchi,^{*5} and Y. Yano

We are continuing a design study on each piece of equipment in the rare-RI ring; the study is based on the conceptual design of the rare-RI ring¹⁾. The rare-RI ring consists of a long injection beam line²⁾ and a cyclotron-like storage ring. The cyclotron-like storage ring, which is a unique device that has features of both a cyclotron and a storage ring, is composed of a septum magnet, kicker system, RF cavity, and sector magnet. Because the sector magnet is an especially important device for our project, we mainly report on the design study of the sector magnet.

To determine the masses of short-lived rare nuclei with a precision on the order of 10^{-6} , we will measure the revolution time inside the ring with an accuracy of 10^{-6} , under the condition that an isochronicity is tuned with a precision of 10^{-6} in a certain momentum acceptance. The isochronicity of the ring is obtained by adjusting the magnetic field of each sector magnet. In a first-order γ -factor correction, the isochronous magnetic field is formed by the edge-angle of each sector magnet, which is designed for a fixed beam energy. An isochronous magnetic field can be generated with greater precision by using trim coils in each sector magnet.

To design the sector magnet with such components, a geometrical calculation was performed under the following conditions: edge angle, 8.7° in 200 MeV/nucleon; radius of curvature, 4.3 m. Figure 1 shows ideal radial distributions of the strength of the isochronous magnetic field. This magnetic field strength can be approximated well by a quadratic function of r ,

$$\frac{B(r)}{B_0} = 1 + 1.3159 \times 10^{-8} r^2; \quad (1)$$

here, B_0 is the magnetic field strength at the central orbit. The second component is very small compared to B_0 . This quantity is corrected by using trim coils.

For the sector magnet, two-dimensional field analysis was performed to optimize the geometry of the coils, iron poles, yokes, and iron shims. The pole gap was 110 mm, and the magnetomotive force was about 140,000 AT for the main coils. If the main coils are connected in series, compensation coils are required for adjusting the field homogeneity with a precision of

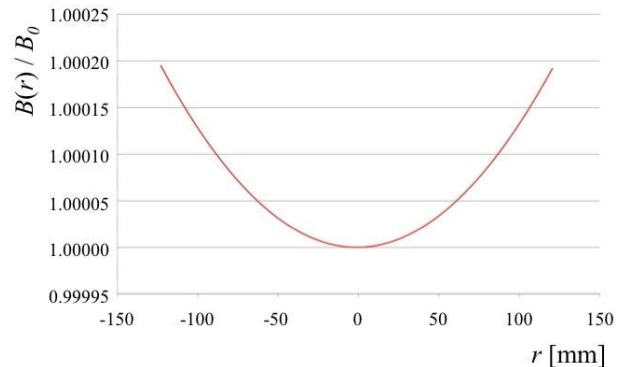


Fig. 1. Ideal radial distributions of the strength of the isochronous magnetic field, as determined by performing geometrical calculations.

10^{-4} for each sector magnet.

On the other hand, it is necessary to arrange the trim coils in order to efficiently make more precise corrections. To evaluate how the magnetic field can be brought close to the ideal isochronous magnetic field by using trim coils, a function was assumed to represent the error in the magnetic field caused by various factors (e.g., gap distortion, edge-angle error, and multipole components). As a result, it has been understood that the magnetic field can be made to match the isochronous magnetic field with a precision of greater than 10^{-6} by using appropriately arranged trim coils.

Three-dimensional field analysis was performed to evaluate an effective magnetic field length. In our concept, the magnetic field boundary should be same as the pole edge. As a result, because the influence of the leakage magnetic field on a circulating particle is strong, it is necessary to set up a field clamp or to shorten the pole length. We should consider the variation in the effective magnetic field length depending upon the radial distributions and the shape of the field clamp.

We conclude that there is no technical difficulty in building the sector magnet. However, how to treat the long-term fluctuations of temperature and current³⁾ and how to control the long-term stability of the ring, including the power supply, should still be considered. We are evaluating the behavior of a particle inside the ring by using the developed simulation code⁴⁾.

To inject a particle into the ring, we adopt a single-turn injection method with dispersion matching by using both the septum magnet and kicker system. The particle is bent by about 11° when the septum mag-

^{*1} Institute of Physics, University of Tsukuba

^{*2} Department of Electrical Engineering, Nagaoka University of Technology

^{*3} Center for Nuclear Study, University of Tokyo

^{*4} Department of Physics, Niigata University

^{*5} Department of Physics, Saitama University

net is used under the present condition. The septum magnet is divided into two magnets in order to reduce the load exerted on it. After the particle revolves about 1000 times in the equilibrium orbit, it is extracted from the ring by using a combination of the same kicker system and other septum magnets. The specification of the septum magnet for extraction is the same as that for injection. Therefore, it is necessary to design two kinds of septum magnets and one kicker system. Here, we explain only the important features of their design in this study.

Septum magnets, which are operated as DC magnets, are adjacent to a straight-section vacuum duct of the ring. The leakage magnetic field may affect the isochronicity of the ring, especially in the case of the septum magnet located downstream/upstream for injection/extraction. Three-dimensional field analysis indicated that it is necessary to take the leakage magnetic field into account when adjusting the isochronicity of the ring because the leakage magnetic field inside the duct is greater than 10^{-4} times B_0 , even if countermeasures to suppress the leakage magnetic field are implemented.

The kicker system, which is operated as a pulsed system, is arranged in a straight section of the ring. For the kicker magnet, in order to minimize the field rise-time, we adopt a distributed twin kicker type system⁵⁾. An elementary cell of the magnet consists of a C-shaped ferrite core and electrodes. The electrodes and the conductors are made of aluminum. To suppress electrical discharge, the aluminum surface is subjected to electro-polishing. As mentioned above, this kicker system is used not only for injection but also for extraction, and hence, a special power supply is required. For efficient injection and extraction, because the waveforms should be different from each other, two thyratrons must be installed in the power supply. We believe that a short pulse is suitable for injection and a trapezoidal pulse is suitable for extraction. Therefore, it is necessary to develop different pulse-forming networks respectively. Recently, we began a feasibility study on the power supply by using a prototype kicker system.

As the last piece of equipment, we briefly mention the RF cavity. It is used to accelerate/decelerate a reference particle of an well-known mass when adjusting the isochronicity in a certain region of the ring. We found that the strength of the RF magnetic field⁶⁾ is less than 10^{-7} times B_0 and that there is no technical difficulty in production.

References

- 1) Y. Yamaguchi et al.: Nucl. Instrum. Methods Phys. Res. B **266**, 4575 (2008).
- 2) Y. Yamaguchi et al.: RIKEN Accel. Prog. Rep. **41**, 137 (2007).
- 3) Y. Yasuda et al.: RIKEN Accel. Prog. Rep. **42**, 197

- (2009).
- 4) H. Suzuki et al.: RIKEN Accel. Prog. Rep. **43**, (2010); I. Arai et al.: Proceedings of STORI'08, **498** (2008).
- 5) T. Kawakubo: OHO'96.
- 6) W. Joho: Particle Accelerators **6**, 41 (1974).

Simulation of Particle Trajectories for RIKEN Rare-RI Ring

H. Suzuki^{*1}, I. Arai^{*1}, T. Fujinawa, N. Fukunishi, A. Goto, T. Kikuchi^{*2}, S. Kubono^{*3}, T. Moriguchi^{*1}, D. Nagae^{*1}, T. Ohnishi, T. Ohtsubo^{*4}, A. Ozawa^{*1}, H. Sakurai, T. Suzuki^{*5}, M. Wakasugi, T. Yamaguchi^{*5}, Y. Yamaguchi, and Y. Yano

Rare-RI Ring¹⁾, which can be used to determine the mass of unstable nuclei supplied by BigRIPS²⁾ with a precision on the order of 10^{-6} is currently being developed. The mass can be deduced by simply measuring the revolution time (TOF for 1000 turns) and the velocity (β_t) of even one particle in isochronous optics. In addition, since its measuring time would be less than 0.5 ms, this new device is suitable for mass measurements of short-lived rare nuclei, including the r -process nuclei.

This ring, which is 55.710 m in circumference, is a unique device having the features of both cyclotrons and storage rings. It consists of six straight sections (4.782 m) and six sector magnets each with a bending angle of 60° and a diameter of 4.300 m. This device has a large momentum acceptance ($\Delta P/P \sim \pm 1\%$) and can be used for measuring the mass of unstable nuclei supplied as a secondary beam.

The mass of the nuclei is measured as follows. First, an isochronous magnetic field inside the ring is adjusted with reference to the mass of a particle with known mass. The isochronous magnetic field is formed with precise edge angles (β) of each sector magnet and harmonic components (κ) of the magnetic field in the radial direction by using trim coils. Next, the revolution time (TOF for 1000 turns) and velocity β_t of a particle with unknown mass is measured. For a particle with unknown mass, the condition of isochronism is no longer fulfilled. The mass of the required nuclei can be deduced from the difference between the TOFs and the β_t values of the reference and this required nuclei. β_t is required because the velocities of these particles are relativistic.

In order to evaluate the magnetic field, we have developed a simulation program using a fourth-order Runge-Kutta algorithm in C language³⁾. The program includes the following five components: 1) main.c, 2) Ring.c, 3) ST.c, 4) DM.c, and 5) Eq.c. The program main.c evaluates the setup parameters for the desired ring. These parameters are velocity of the beam particle in the central orbit, charge-to-mass ratio of the beam particle, and correction factors for β and κ . The program Ring.c controls each element of the ring and revolves the beam particles 1000 times in their orbits. The program ST.c represents a straight section, and

DM.c, a magnetic sector. The dispersion of the ring is calculated by Eq.c.

In order to achieve a precision as high as possible, which is required for determining of the trajectory of a beam particle, we perform geometric tracking of the beam particles in the magnetic sector by assuming that the particles revolve in circular orbits within a small spatial segment. For this purpose, the magnetic sector is divided into 150 subsectors in order to use the rectangular (hard-edge) distributions of the magnetic fields. When divided into 150 subsectors, the calculated TOFs of particles converged. In each subsector, the magnetic field is represented as a function of radial direction for harmonic components. The beam trajectory at the exit of a subsector is evaluated from the entrance trajectory by using the Runge-Kutta method.

In the first-order Lorentz-factor correction, we considered the effects of the edge-angle of each sector magnet. When β was set as 8.7° , an isochronous magnetic field was formed with the accuracy of the isochronism being over 4×10^{-5} , which was determined by performing the simulation. Trim coils are used for further (second-order) tuning by generating the harmonic component of the magnetic field. The required isochronism is achieved with an accuracy of over 1×10^{-6} with the harmonic field.

Particle trajectories in the horizontal direction were calculated as shown in Fig. 1 (up). The trajectories for 10 turns are shown in this figure. In this simulation, three trajectories of particles having different momenta, i.e., central momentum, 1% higher than it, and 1% lower than it, are calculated. The starting positions of these particles at the injection point fulfilled the condition of dispersion matching. It is observed that the particles revolving around the ring are stable with a certain dispersion. Figure 1 (down) shows the trajectories in the vertical direction for 10 turns. In this figure, all particles have central momentums. The trajectories for particles with the injection points at the mid-plane height, 1 cm above it, and 1 cm below it, are shown. Betatron oscillation is seen in the vertical direction.

The emittance for an isochronism with a precision of 10^{-6} in Rare-RI Ring was also investigated by performing the simulations. Figure 2 shows the emittances for 1000 turns when isochronism maintained as functions of the position and angle at the injection point of the ring. From this result, the emittance of isochronism region with a precision of 10^{-6} is found to be 40π mm mrad and 45π mm mrad in the horizontal and vertical

^{*1} Institute of Physics, University of Tsukuba

^{*2} Department of Electrical Engineering, Nagaoka University of Technology

^{*3} Center for Nuclear Study, University of Tokyo

^{*4} Department of Physics, Niigata University

^{*5} Department of Physics, Saitama University

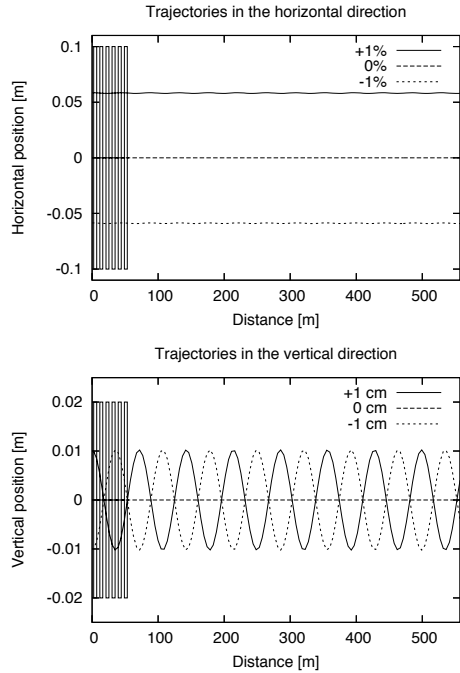


Fig. 1. Particle trajectories (10 turns) in the horizontal direction (up) and the vertical direction (down). The thin boxes represent the sector magnets for 1 turn. Up panel: Horizontal direction. In this simulation, three trajectories of particles that have different momenta are calculated, i.e., central momentum, 1% higher than it, and 1% lower than it. The starting positions of these particles at the entrance of the ring fulfill the dispersion matching condition. Down panel: Vertical direction. All particles have a central momentum. The trajectories for particles whose injection point is at the mid-plane height, 1 cm above it, and 1 cm below it are shown.

directions, respectively, for any momentum of the particle. This emittance is sufficient for the beam transported by the beamline between BigRIPS and Rare-RI Ring.

The effects of incorrect edge angle or misalignment of Rare-RI Ring on the isochronism of the ring were investigated by performing simulations. It was considered that either of these could adversely affect the isochronism of the ring. The limit of misalignment is determined on the basis of the TOFs of the particles with $\Delta P/P = \pm 1\%$, which exceeds that of the particles in the central orbit by 10^{-6} . A misalignment up to 2 mm and 6 mm in the radial and azimuthal directions of the ring, respectively, is allowed for each sector magnet. The rotation of the horizontal plane of each magnet is permissible up to 1 mrad. A deviation of β by 0.017° is permissible. The loss of isochronism caused by misalignment can be overcome by further adjustment of the magnetic field with the trim coils.

A simulation with soft-edge (fringe field) approxi-

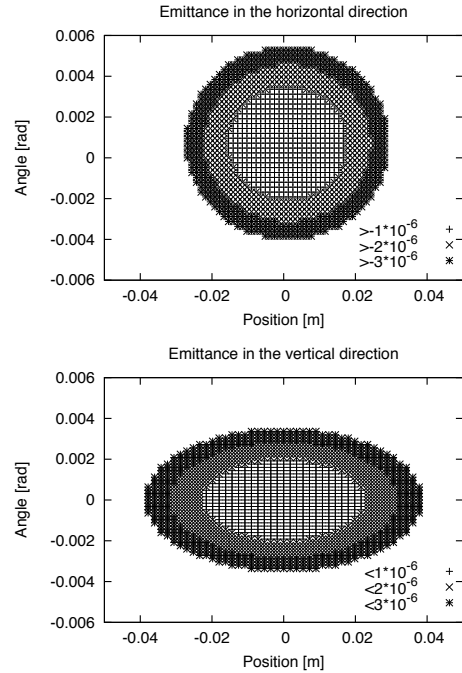


Fig. 2. Emittance in horizontal direction (up) and vertical direction (down) when isochronism of Rare-RI Ring is maintained. “+” represent the region for isochronism with a precision of 10^{-6} . The emittances are 40π mm mrad and 45π mm mrad in the horizontal and vertical directions, respectively.

mation of the magnetic distribution is currently being performed. The shape of the fringe field was obtained using the PEP magnet at SLAC⁴⁾, which was supplied as the “default” magnet, using the code COSY Infinity⁵⁾ developed at Michigan State University. The emittances for the isochronism with a precision of 10^{-6} do not change from those calculated using hard-edge approximation. In order to simulate the particle trajectories more precisely, the fringe shape should be determined by using the TOSCA program.

Rare-RI Ring is currently being designed using the simulation results. This device is expected to contribute significantly to the study of unstable nuclei with medium-to-high masses.

References

- 1) Y. Yamaguchi et al.: Nucl. Instrum. Methods Phys. Res. B **266**, 4575 (2008); Y. Yamaguchi et al.: RIKEN Accel. Prog. Rep. **43**, (2010).
- 2) T. Kubo: Nucl. Instrum. and Methods Phys. Res. B **204**, 97 (2003); T. Kubo et al.: IEEE Trans. Appl. Supercond. **17**, 1069 (2007).
- 3) I. Arai et al.: Proceedings of STORI’08, 498 (2008).
- 4) K. L. Brown and J. E. Spencer: IEEE Trans. on Nucl. Sci., **NS-28**, 3:2568 (1981).
- 5) K. Makino and M. Berz: Nucl. Instrum. Methods Phys. Res. A **427**, 338 (1999).

Second Report on Progress of the Portable Multi-Reflection Time-of-Flight Mass Spectrograph for SLOWRI†

P. Schury,*¹ K. Okada, V. A. Shchepunov.*² T. Sonoda, A. Takamine, M. Wada, and H. Wollnik*³

[Mass measurements, unstable nuclei, low energy beam]

We continue the development of a multi-reflection time-of-flight (MRTOF) mass spectrometer for use with radioactive ion (RI) beams at the future SlowRI facility. The MRTOF will initially be attached to its own dedicated gas stopping cell, allowing the system-as-designed to be portable and providing flexibility in commissioning the device by making it possible to use RI sources wherever available. Three of the main components for the MRTOF – the ion trap, reflection chamber and ppm-precision bias controller – have been built; preliminary testing is underway.

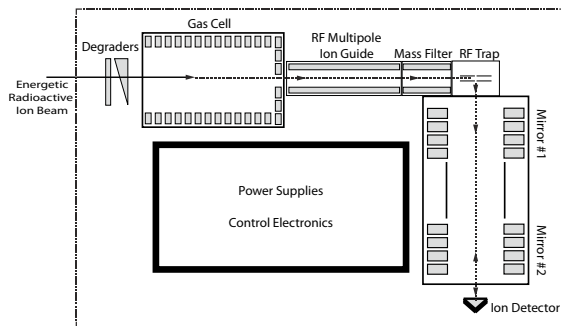


Fig. 1. Planned layout for the portable MRTOF system.

Figure 1 provides a sketch of the system. Energetic ions will be slowed in a solid degrader and thermalized in a helium-filled chamber. Thermalized ions are injected into a radio-frequency (RF) multipole ion beam guide to be transported through a differentially pumped region after being extracted from the gas cell using a proven RF-carpet technique¹⁾. An RF quadrupole mass filter will select for a specific ion mass number, removing non-isobaric ions. The isobaric ion ensemble will then be cooled in a low-pressure gas-filled RF ion trap before being injected into the MRTOF. The system is described in detail previously^{4,5)}.

Lessons learned from an early offline prototype²⁾ include the need to minimize both the emittance of the ion pulse and the amount of gas injected into the reflection chamber from the ion trap. Additionally, while the isochronicity of the mirrors is robust, temperature-dependent voltage drifts cause the center-time of the ion distribution to drift and make measurements with low intensity ions difficult. By paying attention to

these lessons, the new on-line system is expected to be able to achieve very-high resolving powers with a high efficiency. High-efficiency will result from reducing the emittance of ion pulses extracted from the trap and improving the vacuum level in the reflection chamber by using a sophisticated ion trap. High-resolving power will result from achieving extremely high-stability voltage supplies for the MRTOF electrodes and also reducing the energy and time spreads of ion pulses extracted from the ion trap.

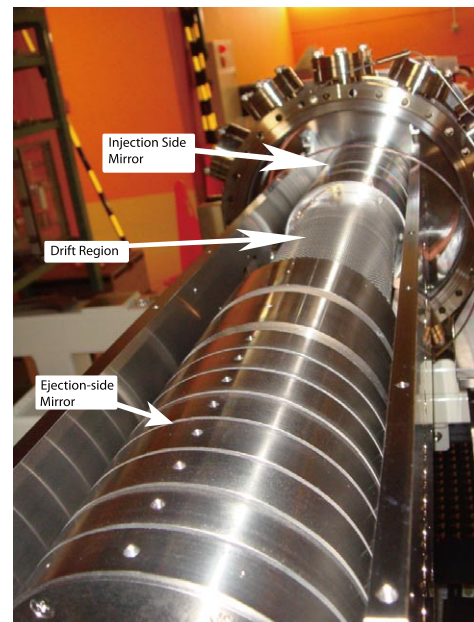


Fig. 2. Photograph of the MRTOF reflection chamber. The ion trap will be connected to the obscured flange at the top of the image. The gas cell will be placed to the left of the ion trap.

The ion trap and reflection chamber for the MRTOF have been constructed during the past year. Figure 2 shows a photograph of the reflection chamber electrodes, support structure and feedthroughs. All reflection chamber electrodes are connected to feedthroughs at the injection side of the reflection chamber. This allows for the vacuum chamber to be removed without the need to undo any connections, simplifying maintenance and troubleshooting.

Each of the annular electrodes is machined from Titanium and gold-plated on the inside to avoid patches. The electrodes are isolated from the Titanium support bracket by a pair of precision ceramic rods, not

*¹ Tsukuba University, Ibaraki, Japan

*² SRL, Manchester, England

*³ University of Gießen, Gießen, Germany

shown. Titanium's excellent vacuum properties will enhance the vacuum quality inside the reflection chamber; the similarity in thermal expansion coefficients of Titanium and the ceramic will allow for baking the system with minimal worry of dynamic misalignment.

As the total flight length may be as much as 1 km, the reflection chamber must be maintained at ultra-high vacuum to minimize deleterious effects of ion-neutral collisions, which would strongly affect both the efficiency of the system and the maximum resolving power. The reflection chamber has been vacuum tested using a single 300 l/s turbo-molecular pump, achieving a pressure of $8 \cdot 10^{-9}$ mbar.

To minimize gas loading of the reflection chamber with buffer gas from the ion trap, the trap makes use of an ejection hole of $200 \mu\text{m}$ diameter. The trap, shown in Fig. 3 is built from a pair of printed circuit boards, each consisting of three segmented strip electrodes. An RF signal applied to the outer electrodes creates a confining quadrupole pseudo-potential. The strips segmentation allows an axial potential well for ion trapping. The ions are introduced into the trap parallel to the electrodes; after cooling, the ions can be ejected perpendicular to the trap through a small ($r = 100 \mu\text{m}$) hole in the central electrode. The very low gas throughput of this geometry should produce very well-cooled ions without deleteriously affecting the vacuum in the reflection chamber, leading to highly efficient operation.

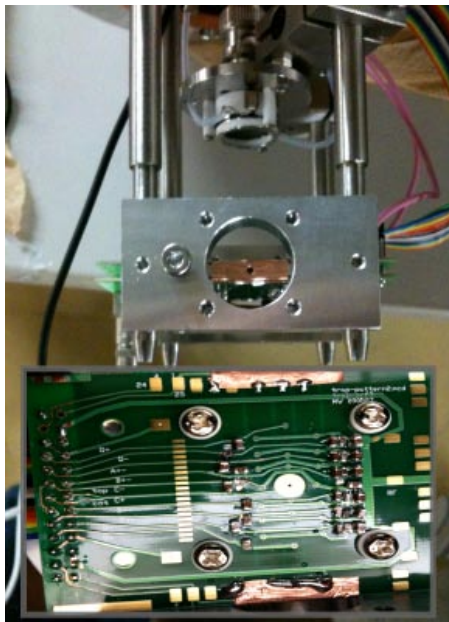


Fig. 3. Photograph showing the mounted ion trap. Above the trap an MCP detector has been placed for testing purposes. The inset photograph details the printed circuit board used to construct the trap.

In order to achieve the highest possible resolving power, the mirror electrodes' bias voltages must be

extremely stable. To achieve this, a thermally stabilized 24-bit DAC-ADC and voltage monitor system has been built (Fig. 4). It consists of a large voltage divider network built from Alpha Electronics' zero-TC resistors, a set of $\approx 1000:1$ precision dividers, a 24-bit ADC, an effective 24-bit DAC and a Peltier element inside a leak-tight plastic box. The DAC monitors all reflection chamber bias voltages via the dividers as well as the temperature inside the box. Using a digital PID algorithm, the temperature and all voltages can be maintained to great precision. The control software is still under development. In order to achieve the requisite ppm stability, the PID algorithm will need to maintain the biases to 4-bits precision in the 24-bit system, which is perfectly reasonable.

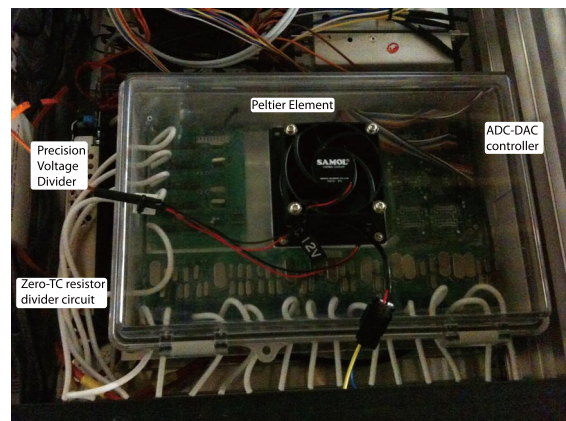


Fig. 4. Photograph of temperature controlled 24-bit ADC-DAC system. The system is intended to provide stabilization of the bias voltages on the ppm level.

Development work for the portable MRTOF-MS continues. The MRTOF electrodes and vacuum chamber have been assembled and ultra-high vacuum conditions have been achieved. The ion trap, required to prepare ions for injection into the MRTOF, has been assembled and testing is underway. A temperature stabilized 24-bit ADC-DAC has been constructed. Using a voltage-divider network constructed from very low temperature coefficient resistors, the ADC-DAC system will be the basis for a digital PID loop capable of maintaining all MRTOF voltages to $\delta V < 1$ ppm.

References

- 1) M. Wada et al., Nucl. Instrum. Methods **B204**, 570 (2003)
- 2) Y. Ishida, M. Wada and H. Wollnik: Nucl. Instrum. Methods and Phys. Res. **B241**, 982 (2005).
- 3) Y. Ishida, M. Wada and H. Wollnik: RIKEN Accel. Prog. Rep. **40**, 150 (2007)
- 4) P. Schury, et al., *Multi-Reflection Time-of-Flight Mass Spectrograph for Short-Lived Radioactive Ions*, Proceeding of the 5th Conference on Exotic Nuclei and Atomic Masses
- 5) P. Schury et al., RIKEN Accel. Prog. Rep. **42**, 189 (2009)

Status of the resonance ionization laser ion source at SLOWRI

T. Sonoda, T. Furukawa,^{*1} Y. Hirayama,^{*2} M. Huyse,^{*3} N. Imai,^{*2} H. Ishiyama,^{*2} S. Jeong,^{*2} I. Katayama,^{*2}
 T. Kubo, Yu. Kudryavtsev,^{*3} Y. Matsuo, H. Miyatake,^{*2} K. Okada,^{*4} P. Schury,^{*5} T. Shinozuka,^{*6}
 A. Takamine, H. Tomita,^{*7} P. Van Duppen,^{*3} T. Wakui,^{*6} Y. Watanabe,^{*2} and M. Wada

A new laser system for the resonance ionization laser ion source has been installed at SLOWRI facility in RIBF B1F, as shown in Fig. 1. This system is intended to be employed in various applications involving the use of the resonance ionization laser ion source^{1,2)} for producing pure beams of exotic nuclei.

We proposed a new scheme named Parasitic production of slow RI-beam from a projectile fragment separator by ion guide Laser Ion Source (PALIS).³⁻⁶⁾ This scheme can be adopted at the SLOWRI facility to provide low-energy RI beams for the comprehensive measurement of static properties of thousands of exotic nuclei. Because the expected beam time is very low in comparison with the demand, PALIS can help to obtain low-energy RI beams everyday, as long as the fragment separator BigRIPS is in operation. Most RI beams produced by projectile fragmentation or in-flight fission are abandoned at the first dipole magnet or in the slits in the first focal plane of the BigRIPS. A PALIS gas cell located in the vicinity of the first slit will *rescue* such RIs by capturing and neutralizing in high-pressure Ar gas and reionizing by resonance laser ionization at the exit of the cell. The selectively ionized RIs can be mass separated by a simple mass separator and transported to the SLOWRI experimental room.

In addition to PALIS, we plan to realize some more applications by using the laser system. One application is in-cell/in-gas-jet laser spectroscopy;^{7,8)} the aim

of this application is to increase the number of elements that can be considered in nuclear laser spectroscopy, which is so far limited to 50. Another application is the production of polarized RI beams during ionization.⁹⁾ These RI beams will be used in decay spectroscopy to measure nuclear moments. Another major development is the KEK Isotope Separator System (KISS) project, which is aimed at synthesizing r-process nuclides with N values around 126. Such exotic nuclei produced at very low rates can be efficiently collected and separated to achieve a high purity by using a high-pressure gas cell and adopting a resonance laser ionization scheme.

We borrowed many old laser components from TIARA-JAERI, IRCNMS, and other RIKEN laboratories; these components include two excimer XeCl lasers (Lambda Physik LPX240i) and seven pulsed dye lasers (Lambda Physik FL3001/3002 and Scanmate2E). We plan to use two-step two-color schemes for the resonance laser ionization of radioactive atoms. The first-step laser excites atoms into an intermediate state. By using the second-step laser, the excited atoms are made to undergo a transition into an auto ionizing state. In the first-step, we can use UV radiation generated by a second harmonic generator.

Although the laser components are about 15 years old and have not been used for eight years, we confirmed that the excimer lasers can fire with reasonable power after comprehensive maintenance. We have already done first test for the resonance ionization scheme of Ni atoms by using an off-line reference cell. We will build a test gas cell with a compact mass separator in order to carry out further off-line tests before constructing the on-line setups.

We would like to thank the original owners of the laser components, namely, Dr. Wakasugi of RIKEN, Dr. Koizumi of JAEA and Dr. Mitsugashira of IRCNMS for their kind support to our projects.

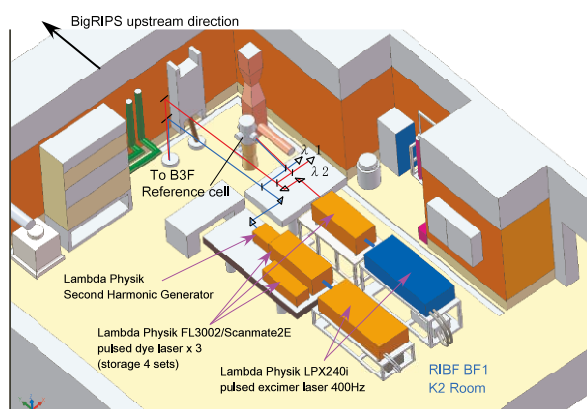


Fig. 1. Layout of new laser system at SLOWRI

^{*1} Department of Physics, Tokyo Institute and Technology
^{*2} High Energy Accelerator Research Organization (KEK)
^{*3} Nuclear Spectroscopy group, IKS, K.U. Leuven (Belgium)
^{*4} Department of Physics, Sophia University
^{*5} Department of Physics, Tsukuba University
^{*6} Cyclotron and Radioisotope Center, Tohoku University
^{*7} Faculty of Engering, Nagoya University

References

- 1) L. Vermeeren *et al.*: Phys. Rev. Lett. **73** 1935(1994).
- 2) Yu. Kudryavtsev *et al.*: Nucl. Phys. A **701** 465(2002).
- 3) T. Sonoda *et al.*: AIP Conf. Proc. **1104** 132 (2009).
- 4) M. Wada *et al.*: AIP Conf. Proc. **1104** 16 (2009).
- 5) T. Sonoda *et al.*: RIKEN Accel. Prog. Rep. **42** 187 (2008).
- 6) M. Wada *et al.*: Hyp. Int. (2010) DOI 10.1007/s10751-010-0162-y.
- 7) T. Sonoda *et al.*: Nucl. Inst. Meth. B **267** 2918 (2009).
- 8) T.E. Cocolios *et al.*: Phys. Rev. Lett. **103** 102501 (2009).
- 9) Y. Matsuo *et al.*: Phys. Rev. A **77** 063404 (2008).

Test report on primary beam dispersion matching at RIBF

S. Itoh,^{*1,*2} H. Baba,^{*2} G.P.A. Berg,^{*3} N. Fukunishi,^{*2} Y. Goto,^{*1} T. Hashimoto,^{*1} R.S. Hayano,^{*1} N. Inabe,^{*2} K. Itahashi,^{*2} D. Kameda,^{*2} P. Kienle,^{*4,*6} T. Kobayashi,^{*1} T. Kubo,^{*2} K. Kusaka,^{*2} K. Miki,^{*1} H. Miya,^{*5} T. Nishi,^{*1} T. Ohnishi,^{*2} A. Saito,^{*5} K. Suzuki,^{*6} H. Tatsuno,^{*1} K. Todoroki,^{*1} H. Takeda,^{*2} and T. Uesaka^{*5} for the pionic-atom factory collaboration.

[Pionic-atom, precision spectroscopy, dispersion matching]

We are planning to perform precision pionic-atom spectroscopy¹⁾ at the RI beam factory (RIBF). The objective of the experiment is to achieve the highest ever precision in the deeply bound-pionic-atom spectroscopy by exploiting the ($d,^3\text{He}$) reaction, and thus, to precisely determine the in-medium isovector interaction strength between the pion and the nucleus. By applying the dispersion matching technique²⁾ between the beam transfer line (from the SRC to the target) and the BigRIPS spectrometer³⁾ (from the target to the F5 focal plane), we expect to achieve an experimental resolution of 200 keV (FWHM), with which it is possible to simultaneously observe both the $1s$ and $2s$ states of the pionic Sn atom. In May 2009, we performed a test experiment to establish a method for realizing the dispersion matching and for measuring the resolution.

We used a ^{14}N beam with an energy of 250 MeV/nucleon; the beam was provided by the SRC. The beam energy was chosen such that the beam rigidity was identical to that of the deuteron beam for use in the pionic-atom spectroscopy. The beam positions and the directions in each focal plane were measured by using PPAC⁴⁾ detectors. The PPAC position resolution was estimated to be 1.5 mm (FWHM) on the basis of ray fitting of the incident beam. The beam emittance was measured to be 39 mm mrad (FWHM) and 22 mm mrad (FWHM) in the F3 achromatic focal plane in the horizontal and vertical directions, after subtracting the PPAC resolution.

The dispersion matching condition is described as

$$b_{16}s_{11} + b_{26}s_{12} + s_{16} = 0 \quad (1)$$

where b_{ij} and s_{ij} denote R -matrix elements for the beam transfer line and the BigRIPS spectrometer (F0-F5), respectively. The elements in the matching condition (1) were selected such that $b_{16} = 46$ mm/%, $b_{26} = 0.0$ mrad/%, $s_{11} = 0.69$, $s_{12} = 0.0$ mm/mrad, and $s_{16} = 32$ mm/%. We installed Al degraders in order to measure the dispersion values b_{16} and s_{16} . The measured dispersion values were consistent with the selected values.

Figure 1 shows the histograms of the horizontal position in the F5 focal plane before and after the dispersion matching was applied; the hatched and the unhatched histograms correspond to the position before and after the dispersion matching, respectively. The position resolution improved by a factor of two after the dispersion matching was applied. The obtained resolution was 0.83 mm (FWHM), after the PPAC resolution was subtracted. The resolving power of the BigRIPS was estimated to be 3860 (FWHM). The obtained resolving power yields an experimental resolution of 190 keV (FWHM) for the emitted ^3He at 365 MeV of the ($d,^3\text{He}$) reaction in the deeply bound-pionic-atom spectroscopy.

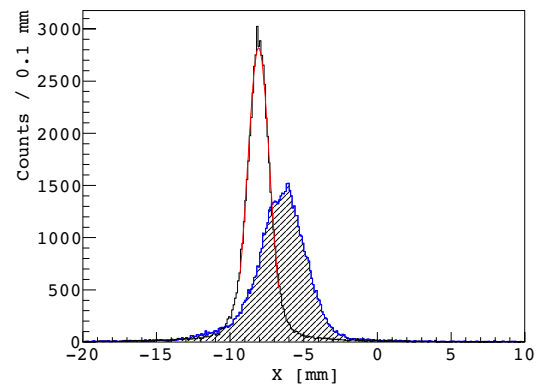


Fig. 1. The histograms of the position in the F5 focal plane before and after dispersion matching was applied. The hatched and the unhatched histograms correspond to the position before and after dispersion matching, respectively.

References

- 1) K. Itahashi *et al.*, RIBF proposal No.054 (2008).
- 2) T. Wakasa *et al.*, Nucl. Inst. Meth. A **482**, 79 (2002).
- 3) T. Kubo *et al.*, Nucl. Inst. Meth. B **204**, 97 (2003).
- 4) H. Kumagai *et al.*, Nucl. Inst. Meth. A **470**, 562 (2001).

*1 Department of Physics, University of Tokyo

*2 RIKEN Nishina Center, RIKEN

*3 JINA, University of Notre Dame

*4 Technische Universität München

*5 Center for Nuclear Study, University of Tokyo

*6 Stefan Meyer Institute

Performance evaluation of Low-Pressure Multi-Wire Drift Chamber for RI beam

H. Miya,¹ S. Shimoura,¹ A. Saito,¹ K. Miki,^{2,3} M. Sasano,³ K. Itahashi,⁴ S. Itoh,^{2,3} T. Kawabata,⁵ M. Nagashima,⁶ Y. Shimizu,³ Y. Shimbara,⁶ H. Baba,⁴ S. Kawase,¹ H. Kurei,¹ S. Michimasa,¹ K. Nakanishi,¹ S. Noji,² S. Ota,¹ Y. Sasamoto,¹ H. Tokieda,¹ K. Yako,² T. Uesaka,¹ and H. Sakai²

We are developing Low-Pressure Multi-Wire Drift Chambers (LP-MWDCs)¹⁻⁴ for light radioactive isotope (RI) beams with an energy of 100–300 MeV/nucleon. The LP-MWDCs are used in BigRIPS and High-Resolution Beamline (HRBL)⁵ at RI Beam Factory.

The LP-MWDCs have three anode layers (x, u, and y). Layer u is tilted at an angle of 30° with respect to x. The counter gas used is pure isobutane at a pressure of 10 kPa. By maintaining the gas pressure at a low value, the effect of multiple scattering can be diminished. Details of the structures and specifications of the LP-MWDCs are provided elsewhere¹⁻⁴.

In March, May, and November 2009, the performance of the LP-MWDCs, in which the gas pressure was 10 kPa and 50 kPa, was evaluated using RI beams with $z = 17$, in the commissioning of SHARAQ and HRBL. We report the position resolutions and tracking efficiencies for the RI beams as a function of the applied voltage.

In March and May, the primary beam used was ¹⁴N with an energy of 250 MeV/nucleon. RI beams of ³H, ⁶He, ⁹Li, ¹⁰B, ¹²Be, and ¹¹C were produced by a projectile-fragmentation reaction carried out using ¹⁴N and a primary target of ⁹Be. In November, the primary beam used was ⁴He with an energy of 320 MeV/nucleon. RI beams of ³H and ³He were produced by the reaction of ⁴He with the target. LP-MWDCs and plastic scintillators were placed in focal planes F3, F6, F-H7, F-H9, and F-H10 in BigRIPS and HRBL. The dimensions of the scintillator at F3 were 100 × 100 mm² and the scintillator thickness was 1 mm. The scintillator was used as a trigger counter. The dimensions of the scintillators at F-H7, F-H9, and F-H10 were 220 × 150 mm² and the thickness was 3 mm. Details of the experimental setup at each focal plane is provided in the ref².

The anode signals from the LP-MWDCs were read out, amplified, and discriminated by REPIC RPA-130/131. The timing of the leading and trailing edges was recorded by using CAEN V1190A/B multihit TDCs. The signals read out from the plastic scintillators were amplified and discriminated by IWATSU Charge to Time Converters (QTCs)⁷. Information

about the timing and energy loss was recorded by using the TDCs.

While the beam passes through the counter gas, γ -rays are generated because the electrons of the gas are kicked by the beam. The γ -rays trigger the electron avalanches in the cells through which the beam does not pass. To avoid incorrect tracking, the γ -ray signals must be discriminated from the beam signals.

In our experiments, pulse widths were obtained from RPA-130/131; these pulse widths were related to the pulse height of the analog signal³. Using the obtained pulse, we can discriminate between the beam signals and the γ -rays on the basis of the difference in the energy loss in these two cases. From the signals obtained for each layer and trigger event, we selected the beam signals with the maximum pulse width.

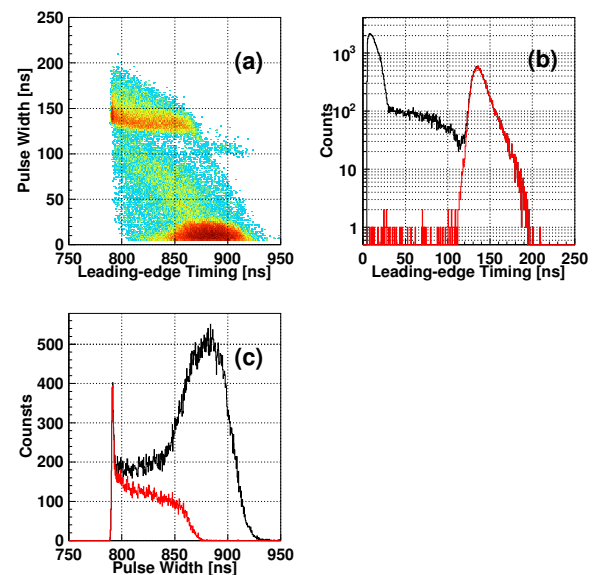


Fig. 1. (a) Relation between pulse width and leading-edge timing acquired from the wires in one plane (b) spectra of the pulse width and (c) spectra of the leading-edge timing obtained by selecting the pulse width at 1100 V and 10 kPa for ¹⁴N.

Figure 1(a) shows the relation between the pulse width and the leading-edge timing acquired from the wires in the x layer for ¹⁴N at 1100 V. Figure 1(b) shows the spectrum of the pulse width in x layer. The black and red peak denote the signals from the wires and those with the maximum pulse width selected from each trigger event, respectively. The leading-edge tim-

¹ Center for Nuclear Study, University of Tokyo

² Department of Physics, University of Tokyo

³ Riken Nishina center

⁴ Department of Physics, Kyoto University

⁵ Department of Physics, Niigata University

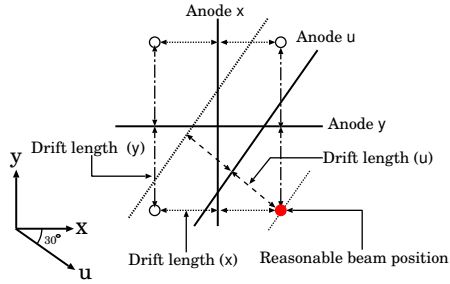


Fig. 2. The geometric con guration of the planes helps in accurate position determination.

ing spectrum is shown in Fig. 1(c). The spectra of the signals with the maximum pulse (red) width show a reasonable drift distribution. The pulse width of the beam can be discriminated from that of the γ -rays on the basis of the correlation between the maximum pulse width.

In order to estimate the position resolution, the distribution of $u_u - u_{xy}$ was investigated. Here, u_u is a hit position in the u layer, and u_{xy} is a hit position along the u axis and is calculated from the hit positions in layers x and y . The geometric con guration of the planes helps in accurate determination of the hit position u (see Fig. 2.) The position resolution is given by $\Delta_{u_u - u_{xy}}/\sqrt{2}$, where $\Delta_{u_u - u_{xy}}$ is the full width half maximum of the distribution of $u_u - u_{xy}$. Figure 3 shows the distribution of $u_u - u_{xy}$ at 1100 V and 10 kPa for ^{14}N . The beam size is 100 mm and 20 mm in the horizontal and vertical directions, respectively, at this F-H7 detectors. From the aforementioned distribution, the position resolution can be estimated.

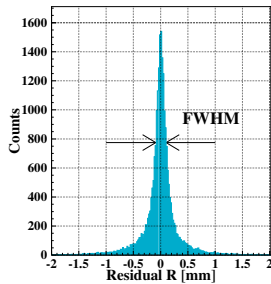


Fig. 3. Residual distribution of $u_u - u_{xy}$ at 1100 V and 10 kPa for ^{14}N .

Figure 4 shows the position resolutions as a function of the applied voltage, evaluated by the above-mentioned method at gas pressures of 10 kPa and 50 kPa. The position resolutions were 200–300 μm for the beam with $z = 2-7$ at 10 kPa and around 200–300 μm for the beam with $z = 1-2$ at 50 kPa. At 1100 V, the LP-MWDCs had a dynamic range of $z = 3-7$.

The tracking efficiency is defined as the ratio of the number of events satisfying 3σ of the residual distribution to the number of the beams counted by the plastic scintillator placed the downstream of the LP-MWDCs

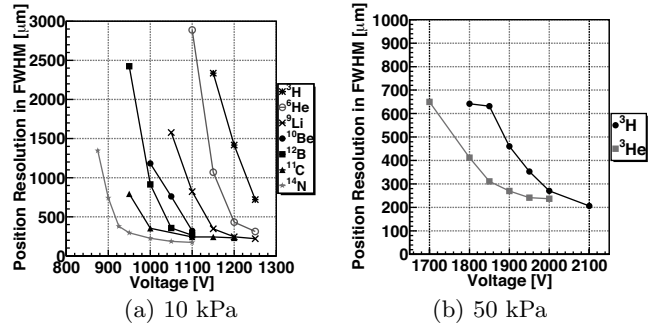


Fig. 4. Position resolution (FWHM) as a function of the applied voltage at 10 kPa and 50 kPa.

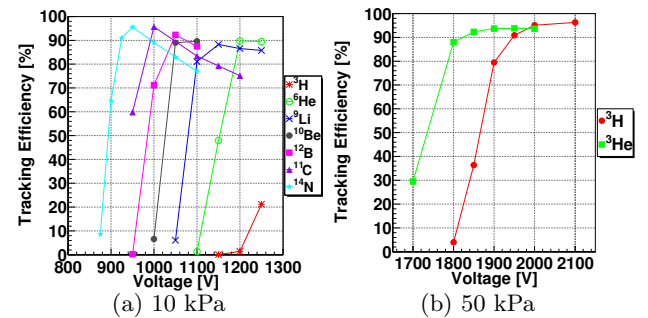


Fig. 5. Tracking efficiency as a function of applied voltage at 10 kPa and 50 kPa.

at gas pressures of 10 kPa and 50 kPa. Here, σ of a Gaussian distribution is derived from $\Delta_{u_u - u_{xy}}$. Figure 5 shows the tracking efficiencies as a function of the applied voltage. The tracking efficiencies approached 90% for the RI beams at 10 kPa and 50 kPa.

The position resolutions and tracking efficiencies of the LP-MWDCs were evaluated as a function of the applied voltage for the RI beam with $z = 1-7$ at 10 kPa and 50 kPa. The position resolutions were 200–300 μm (FWHM) for the beams with $z = 2-7$ at 10 kPa and 200–300 μm (FWHM) for the beams with $z = 1-2$ at 50 kPa. At 10 kPa and 1100 V, the LP-MWDCs had a dynamic range of $z = 3-7$. The tracking efficiencies reached around 90% for the beams at 10 kPa and 50 kPa.

References

- 1) H. Miya et al.: CNS Ann. Rep.2008 49 (2010).
- 2) A. Saito et al.: RIKEN Prog. Rep. **43** (2010).
A. Saito et al.: CNS Ann. Rep. 2008 47 (2010).
- 3) K. Miki et al.: CNS Ann. Rep. 2008 51 (2010).
- 4) T. Yoshida et al.: CNS Ann. Rep. 2008 53 (2010).
- 5) T. Kawabata et al.: Nucl. Instr. and Meth. B **266** 4201 (2008).
- 6) T. Uesaka et al.: Nucl. Instr. and Meth. B **266** 4218 (2008).
- 7) H. Nishino et al.: Nucl. Instr. and Meth. A **610** 710 (2009).

Development of ionization chamber for superheavy elements

K. Ozeki, T. Sumita,*¹ K. Morimoto, K. Morita, and A. Yoneda

In superheavy element laboratory, we have been developing an ionization chamber (IC) to determine Z and A of superheavy elements. This IC is intended to measure the kinetic energy less than 100 keV/nucleon. The anode electrode is segmented into six strips, which are labeled 1-6 from upstream to downstream, for the purpose of the measurement of dE/dx . A detailed configuration of the IC and the voltage applied to each component of the IC are described in ref. [1].

P10 gas was filled in the IC. Figure 1 shows the energy spectra of α particles emitted by ^{241}Am obtained under various pressures. The energy deposits in each segmented electrode and the summation of the energy deposits in each electrode (i.e., 1+2, 1+2+3, ...) are shown. The intrinsic energy spread in the case of an α particle with an energy of 4.763 MeV is 60 keV (rms).

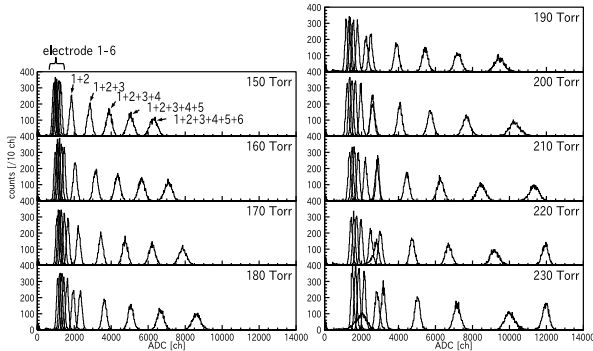


Fig. 1. Energy spectra of α particles.

The energy deposits in each segmented electrode were estimated using the Stopping and Range of Ions in Matter code²⁾. Figure 2 shows the correlation between estimated and measured energy loss. If the equipotential plane is deformed, dE/dx cannot be measured correctly because a part of ionization electrons escapes to another electrode than that corresponding to the region in which the electrons are originally ionized. The good linearity of the correlation between the estimated and measured energy loss, as shown in Fig. 2, suggests that the ionization electrons are collected at the corresponding electrodes by means of a successfully constructed parallel equipotential plane.

The operating characteristics were understood basically by α -particle measurement. Then, kinetic energy of ^{11}B beam from Pelletron³⁾ was measured. Beamline parameters were set to extract ^{11}B of 6.01 MeV; the terminal voltage was 1.50 MV and the charge of ^{11}B was varied from 1- to 3+. However, several kinds of particles were measured simultaneously; it was thought that these particles have different Z , A , or q . Among those particles, $^{11}\text{B}^{3+}$ -like events were analyzed. The incident energy was determined as 5.62 MeV by using

the calibration constant determined from a previous α -particle measurement.

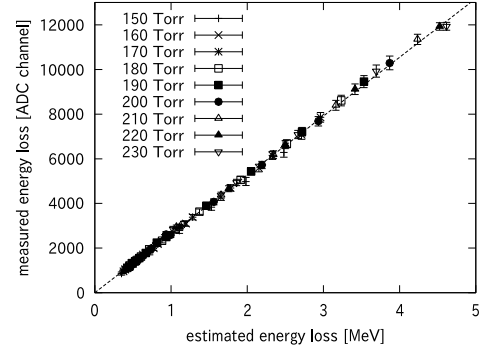


Fig. 2. Correlation between estimated and measured energy loss of α particles

Figure 3 shows the correlations between measured and estimated energy loss when the energy of ^{11}B is assumed to be 5.62 MeV and 6.01 MeV. The dashed lines show the correlation determined from α -particle measurement. Although the correlation determined by assuming the incident energy to be 6.01 MeV has better linearity than that determined by assuming the energy to be 5.62 MeV, the former is inconsistent with the measured value of total energy loss.

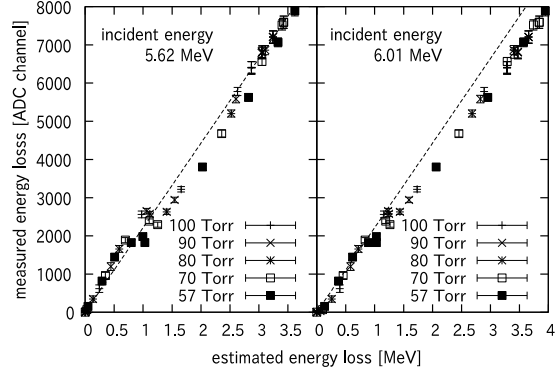


Fig. 3. Correlations between estimated and measured energy loss of ^{11}B .

Shifts in average ionization energy (W -value) of the gas depending on the nuclide and energy of the incident particle has been reported⁴⁾. The discrepancy on the incident energy measurement from the beamline setting may be caused by the W -value shift.

Further measurements are planned for heavier elements such as ^{197}Au . First, it is necessary to characterize the Pelletron and beamline in order to determine the nuclide and energy of the incident particle.

References

- 1) K. Ozeki *et al.*: RIKEN Accel. Prog. Rep. **42** (2009).
- 2) <http://www.srim.org>
- 3) <http://www.pelletron.com>
- 4) J. Rodriguez-Cossio *et al.*: GSI Scientific Report 2000

*¹ Faculty of Science and Technology, Tokyo Univ. of Science

Power spectrum detected by ion beam core monitor

H. Watanabe, S. Watanabe,¹ R. Koyama,² and M. Kase

A nondestructive ion beam core monitor has been developed to measure the intensity of a beam current from 2008.¹⁾ It is particularly useful if one can continuously monitor the ion beam current without interrupting the ion beam. The core monitor has been installed into the RIKEN Ring Cyclotron (RRC) output beamline to measure ion beams and background noise. The RRC is driven by the AVF cyclotron placed upstream of the RRC. The acceleration RF power supplied for both cyclotron of the AVF cyclotron and RRC was 14.5 MHz and 29.0 MHz, respectively. We report here the power spectrum detected by the ion beam core monitor.

We used a Fast Current Transformer (FCT) manufactured by BERGOZ Instrumentation. The transformer, model FCT-082-05:1-H-INS, consists of a toroidal core.

The RRC beam is equivalent to a single-turn coil on the primary side of the transformer which induces a magnetic flux in the toroidal core, resulting in an induced current in the secondary coil. The bandwidth of the FCT is 32 kHz – 700 MHz. The fast response of the detector allows us to observe the higher harmonics of the pulsed beam.

In order for the transformer to measure a current passing through its center, the wall current imaging the ion beam must be diverted around the outside of the device. The beam pipe is electrically isolated by a PEEK sleeve of 4 mm width and the FCT is mounted close to the gap. A SUS304 box cover forms the FCT electrostatic shielding as well as the electrical connection between the interrupted beam pipe outside the FCT. The signal from the FCT is sent to a low-noise preamplifier. The gain of the preamplifier is 20 dB. The signals obtained from the preamplifier were measured by a spectrum analyzer.

Since the bunch width of the RRC beam is very short, it generates many harmonics and the higher order harmonics have almost the same power as the fundamental one (14.5 MHz), shown in Fig. 1. Then the background noise consists mostly of 29 MHz signal and its harmonics, shown in Fig. 2. In Fig. 1, it is clear that the peaks of 14.5 MHz and its odd number harmonics originated from the ion beam. It is considered that the high-frequency noise current originated from RF power of RRC passing through FCT center. In the future, the noise current will be suppressed by the arrangement of a suitable insulator. •••

••

Reference

1) H. Watanabe, S. Watanabe, R. Koyama, and M. Kase: RIKEN Accel. Prog. Rep. **42**, 139 (2009).

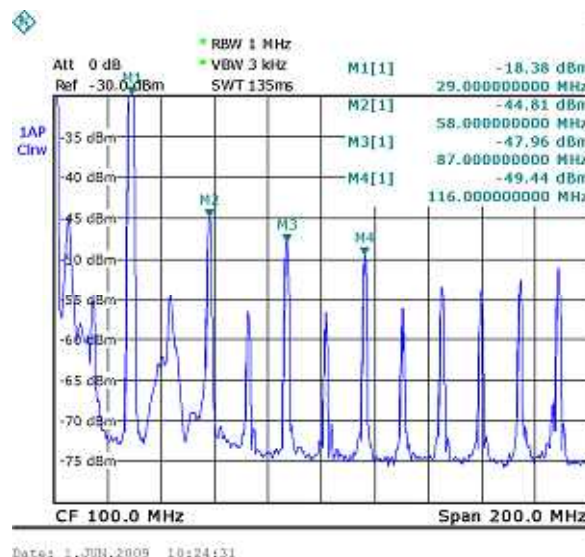


Fig.1 Power spectrum of ¹⁸O beam of 1.5 euA detected by the FCT. Many higher order harmonics peaks of the RRC (1f = 29.0 MHz) and the AVF cyclotron (1f = 14.5 MHz = 29.0 MHz / 2) were observed.

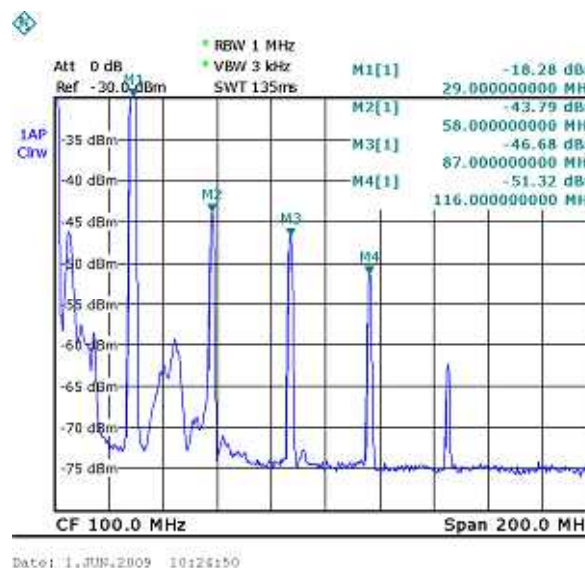


Fig.2 Power spectrum of background noise at beam off detected by the FCT. Many higher order harmonics peaks of the RRC (1f = 29.0 MHz) were observed. ••

¹ Center for Nuclear Study, University of Tokyo

² SHI Accelerator Service, Ltd

Lithium doped Glass Scintillators for Low Energy Neutron Detection

M. Furukawa,*¹ M. Kurata-Nishimura, H. Otsu, and H. Sakurai

The aim of this work is to test ⁶Li-doped glass (⁶Li-glass) and ⁷Li-doped glass scintillators (⁷Li-glass) for low energy neutron detection and γ /neutron discrimination. Neutron detection depends highly on the energy. For high energy neutrons (> 1 MeV), any hydrogenous material (i.e. plastic) can be used to detect the recoil proton in the (n, p) scattering reaction. For lower energy neutron (< 1 MeV) neutrons are detected through the (n, γ) or (n, α) reaction.

The ⁶Li-glass is one of the best candidates for the low energy neutron detector¹⁾ because of fast timing response and high cross section for the reaction: $n + {}^6\text{Li} \rightarrow \text{t} + \alpha + 4.78\text{MeV}$. A positive Q-value implies that very low energy neutrons can be detected. The only disadvantage is that ⁶Li is also sensitive to γ and β rays. However pulse height discrimination can be utilized to select neutrons from γ -ray background.

1 Experimental Setup and Data Acquisition

In this work, ⁶Li- and ⁷Li-doped glass scintillator (SAINT-GOBAIN Crystal: GS20 and GS30, respectively) were used. Its composition was SiO₂ (57%), MgO (4%), Al₂O₃ (18%), Ce₂O₃ (4%) and Li₂O (18%). The percentage weight of ⁶Li in GS20 is 95% and the percentage weight of ⁷Li in GS30 is 99.9%. The Li-glass have a diameter of 5cm and thickness of 1cm.

Three species of γ sources (²²Na, ¹³⁷Cs and ⁶⁰Co) and a neutron source (²⁵²Cf) were placed in front of the Li-glass attached to a photomultiplier tube (PMT). In order to confirm a neutron signal, a 2 cm lead brick was inserted between the ²⁵²Cf source and the Li-glass. A signal from the PMT was connected directly to the storage oscilloscope (Tektronix: 3034B). A linear amplifier for PMT (10 times gain) was used for low amplitude signals. Waveform data were acquired using tekXL on excel toolbar through network connection. Voltages and time information for each triggered event was stored event by event directly into an excel spreadsheet. An amplitude, a total charge, a charge in the tail area, rise time and trailing time were evaluated from the waveforms in csv format.

2 Results

Histograms of the amplitude distributions are plotted using ²²Na and ²⁵²Cf in Figs. 1. The pulse height distributions discriminate between neutron and γ source obviously. It is confirmed that the peak around 0.06V for the ²⁵²Cf is originated from neutrons by comparing the distributions with and without the

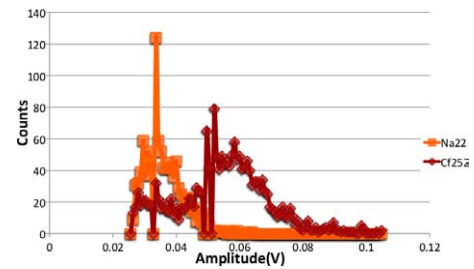


Fig. 1. Histogram of the amplitude distributions of signals from ⁶Li-glass using ²²Na γ source and ²⁵²Cf fission source.

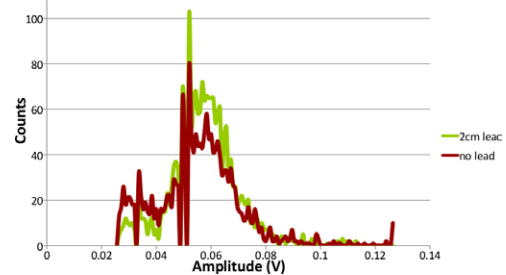


Fig. 2. Histogram of the amplitude distributions of signals from ⁶Li-glass using ²⁵²Cf with and without a 2 cm lead brick. The lead brick absorbs γ rays lowering γ ray counts and increasing neutron counts.

lead brick between the source and the detector as is shown in Figs. 2. Rising times were also calculated for an estimation of the time resolution and pulse shape discrimination. It is found that the typical rise time for neutron signal is less than 5 ns. Thus we can expect the sufficient time resolution for the neutron detection using ⁶Li-glass. For the pulse shape discrimination, further investigation is needed.

3 Conclusion

In this work, ⁶Li- and ⁷Li-doped glass were tested for a neutron detector. The waveforms were measured by the oscilloscope and recorded event by event automatically. By analyzing the waveform with a different aspects, separation of neutron from γ was studied. The pulse height distributions discriminate between neutron and γ source obviously for ⁶Li-glass while no clear difference is observed for ⁷Li-glass. It is expected that ⁶Li-glass can provide a sufficient time resolution for the neutron detection.

At the end, we would like to express special thanks to Prof. Shimoda in Osaka University, who kindly provides us the ⁶Li- and ⁷Li-doped glass scintillator for this work.

References

- 1) S. Schwarz, L. G. Strömberg and A. Bergström: Nucl. Phys. 63 593 (1965)

*¹ Department of Physics, McMaster University, Canada

Pulse structure dependence of the proton polarization rate

T. Kawahara,^{*1} T. Uesaka,^{*2} Y. Shimizu, S. Sakaguchi and T. Wakui,^{*4}

A polarized solid proton target for RI beam experiments has been developed at the Center for Nuclear Study, University of Tokyo¹⁾. Protons are polarized through the transfer of the electron population difference in the photoexcited triplet states of pentacene⁴⁾. By using this method, proton polarization of approximately 20% has been achieved at a low magnetic field of 0.1 T and at high temperatures of 100 K. Although this target has been successfully used in RI beam experiments^{2,3)}, further improvement of proton polarization is desirable for future applications. To enhance the photoexcitation power, we examined the pulse-structure dependence of the proton polarization rate.

For the optical excitation of pentacene molecules, an Ar ion laser (Coherent TSM25) with a wavelength range from 454.5 nm to 528.7 nm and a total maximum output power of 25 W is used. Since this laser is a continuous wave (CW) laser, light can be mechanically pulsed by using an optical chopper (Fig. 1). The duty factor can be easily varied by adjusting the degree of the overlap of two chopper blades. The frequency of the laser pulse can be changed by changing the rotating speed of the optical chopper.

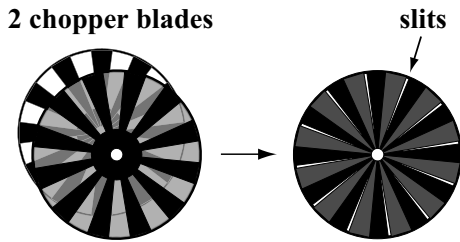


Fig. 1. Optical chopper blades

With the help of this optical system, we can change the duty factor from 5% to 50% and the repetition frequency from 0.75 to 10.5 kHz. The pulse width is determined from the duty factor and repetition frequency. These three parameters are related as

$$D = ft, \quad (1)$$

where D , f , and t are the duty factor, repetition frequency, and pulse width, respectively.

Measurements were carried out under the following conditions. The crystal used was 14 mm in diameter and 3 mm in thickness. Protons were polarized at 200 K in a magnetic field of approximately 60 mT.

Figure 2 shows a typical time chart of the polarization process. This process is repeated at a certain repetition

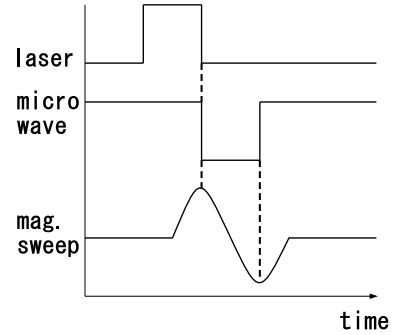


Fig. 2. Time chart of polarization. When the crystal is irradiated by the laser, the electron polarization occurs. Immediately after laser irradiation, microwave irradiation is effected, and the magnetic field strength is swept in order to transfer the electron polarization to the protons.

frequency. The magnitude of proton polarization after a 5-min buildup is defined as the proton polarization rate, which is measured by the pulsed NMR method.

The results are shown in Fig. 3, where the proton polarization rate is plotted as a function of repetition frequency.

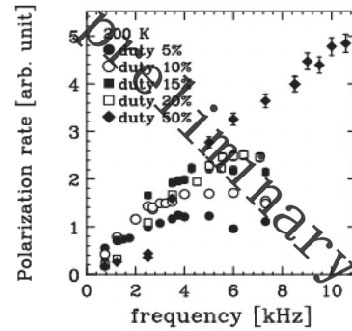


Fig. 3. Polarization rate measured by changing the duty factor and repetition frequency.

In a previous study¹⁾, the repetition frequency and duty factor were reported to be 2.5 kHz and 5%, respectively. The measured data are normalized by the previous data. At high frequency limits, the polarization rate is almost saturated and is proportional to the duty factor. In the present study, we found that the proton polarization rate takes the maximum value when the repetition frequency is 10.5 kHz and the duty factor is 50%. The polarization rate is improved by a factor of 5 as compared to that reported previously.

To estimate the polarization rate, we built a simple theoretical model of electron population. The polar-

^{*1} Department of Physics, Toho University

^{*2} Center for Nuclear Study, Graduate School of Science, University of Tokyo

^{*3} Cyclotron and Radioisotope Center, Tohoku University

ization process involves three steps: electron polarization, polarization transfer from electrons to protons, and relaxation of electron polarization. In this model, we assume that the efficiency of the polarization transfer from electrons to protons is 100%. Electron polarization is the electron population difference between the $m = 0$ and $m = -1$ states, which are the magnetic substates of the triplet state of pentacene.

In the first step, the electron population increases according to the buildup function during laser irradiation. The buildup function is given as

$$f_{b,i}(t) = A_i \tau_i \left\{ 1 - \exp\left(-\frac{t}{\tau_i}\right) \right\}, \quad (2)$$

where τ_i is the lifetime of the triplet state, A is the population rate and i is the magnetic substate of the triplet state. After laser irradiation, the electron population difference is transferred to the protons, and the electron population decreases according to the relaxation function. When the electron polarization is transferred, the number of electrons in the two magnetic substates is reversed by cross polarization³⁾. The relaxation function is given as

$$f_{r,i}(t) = \exp\left(-\frac{t}{\tau_i}\right). \quad (3)$$

Here, the lifetimes of the two substates used in the model are considered as free parameters.

The solid and dotted lines in Fig. 4 represent the time development of the electron population in the $m = 0$ and $m = -1$ states, respectively.

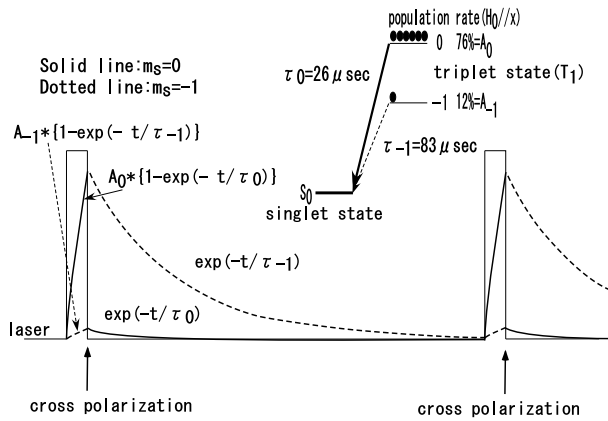


Fig. 4. Time development of electron polarization.

ρ_0 and ρ_- , the electron populations in the $m = 0$ and $m = -1$ states, respectively, are calculated by using equations (2) and (3). The proton polarization rate is derived as

$$\frac{dP_p}{dt} \propto \rho_0 - \rho_-. \quad (4)$$

The lifetimes τ_0 and τ_- are determined to be 26 μsec and 88 μsec , respectively, by using the measurement

result and the present calculation. In Ref. 4, the lifetimes at 100 K are $\tau_0=26 \mu\text{sec}$ and $\tau_-=83 \mu\text{sec}$. The lifetimes observed at 200 K are almost the same as those at 100 K. The proton polarization rate calculated by our simple model reproduces the measured data as shown in Fig. 5.

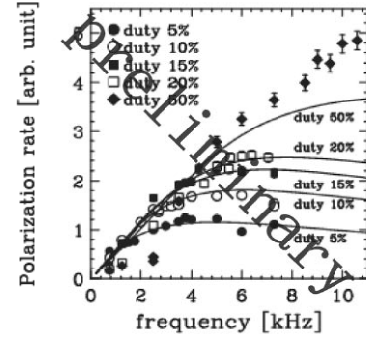


Fig. 5. Polarization rate calculated from our simple model (solid curves) and the measured polarization rate. The rates are calculated for duty factors of 5%, 10%, 15%, 20%, and 50%.

We have examined the pulse-structure dependence of proton polarization rate. We found that the proton polarization rate depends strongly on the pulse structure. At a duty factor of 50% and repetition frequency 10.5 kHz, the polarization rate is improved by a factor of 5. The pulse-width dependences are reproduced with a simple model, by assuming the life time of the triplet state at 200 K to be $\tau_0 = 26 \mu\text{sec}$ and $\tau_- = 83 \mu\text{sec}$. These values are almost equal to those measured at 100 K.

References

- 1) T. Wakui *et al.*, Nucl. Instr. Meth. A **550** (2005) 521.
- 2) M. Hatano *et al.*, Eur. Phys. J. A **25** (2005) 255.
- 3) S. Sakaguchi *et al.* Proceedings of ISPUN07, World Scientific (2009) 245.
- 4) M. Inuma. Ph. D thesis, Kyoto University, (1997).

New method of pulse shape analysis for segmented Ge detectors by using moments

S. Go,^{*1} S. Shimoura,^{*1} E. Ideguchi,^{*1} S. Ota,^{*1} H. Miya,^{*1} H. Baba^{*2}

We have been developing a position-sensitive Ge detector array, CNS GRAPE (Gamma-Ray detector Array with Position and Energy sensitivity). The array consists of 18 detectors, each of which contains two planer Ge crystals with an effective radius of 30 mm and thickness of 20 mm. Each detector has a common anode between two crystals and two 3×3 cathodes. Fig. 1 shows the definition of the coordinates. The interaction point of the γ -ray can be deduced by pulse shape analysis. Our group has developed a method for position extraction by using the analog pulse shape technique^{1,3)}.

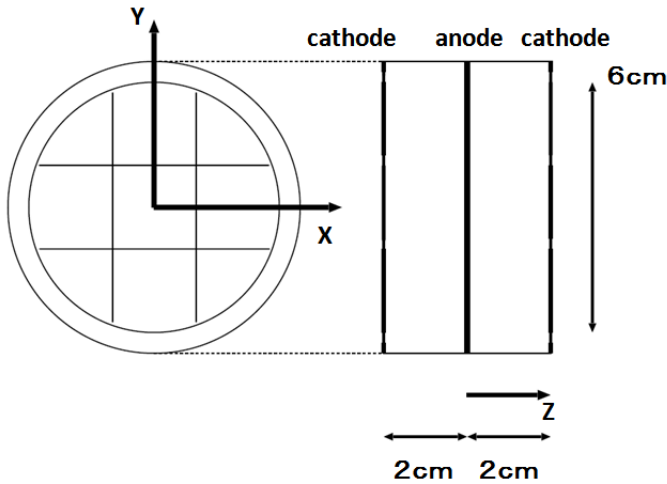


Fig. 1. Schematic view of detector.

In 2008, we started to upgrade the system by digital signal processing (DSP), where the outputs from the preamplifier are digitized by a 100-MHz flash ADC and processed by digital filtering methods such as trapezoidal shaping and constant-fraction time pick-off (Fig. 2).

In order to use the DSP system for position extraction, we are attempting to develop a simple algorithm for the digitized data. The moments of the digitized signals are introduced as candidates for developing such an algorithm²⁾. The n -th moment of the signal is expressed as

$$\langle t \rangle_n = \frac{\sum_i t_i^n \times f(t_i)}{\sum_i f(t_i)}, \quad f(t_i) = \frac{dQ(t_i)}{dt}, \quad (1)$$

where $Q(t_i)$ denotes the digitized data obtained from the charge sensitive preamplifier, and t_i denotes the



Fig. 2. DSP system consisting of two 9-ch ADCs and our daughter modules (TechnoAP, APU7110-A40).

digitized time. The first-order moment corresponds to the average of the pulse shape; the second to the RMS; the third to the skewness.

Fig. 3 demonstrates the correlation between the first moments from the measured data recorded by DSP. This dependence is result obtained using the analog pulse shape technique, where the z -value of the hit position can be extracted from the ordinate and abscissa³⁾.

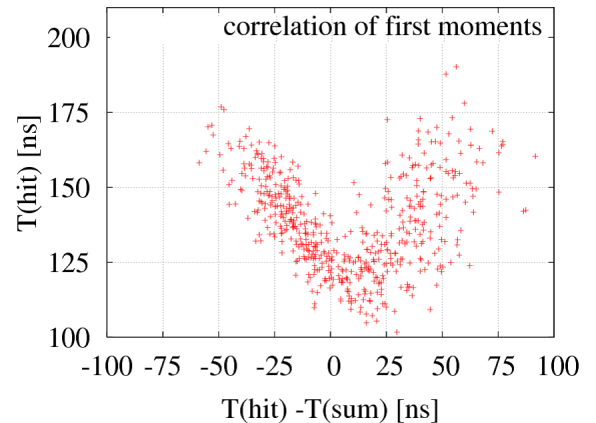


Fig. 3. Correlation between first moments, using a ^{22}Na source. The event near the cathode is selected when the moments are calculated.

In order to extract three-dimensional-position, detailed comparison of the pulse shapes and pulse simulation are important. The time evolution of induced charge signals on cathodes, pulse shapes, can be simulated by calculating the three-dimensional electric po-

^{*1} Center for Nuclear Physics, University of Tokyo

^{*2} RIKEN Nishina center

tential and by using the weighting potential proposed in the Schokley-Ramo theorem⁴⁾. Fig. 4 shows an example of the calculated weighting potential. On the basis of this theorem, the time evolution of the induced charge $Q(t_i)$ is expressed as follows:

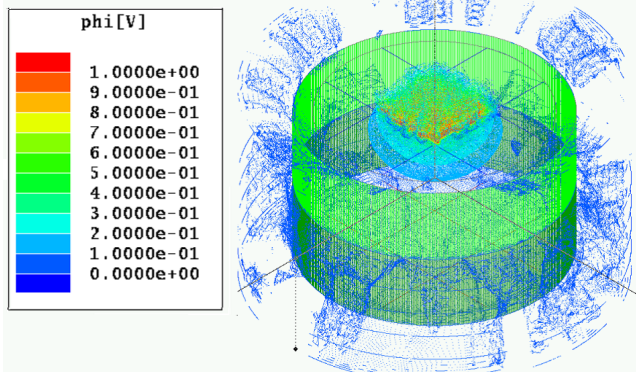


Fig. 4. Calculated weighting potential. In this case, a voltage of 1[V] is applied to the center electrode, and a voltage of 0[V] is applied to the boundary.

$$Q(t_i) = n_0 e (\phi_w(X_h(t_i), Y_h(t_i), Z_h(t_i)) - \phi_w(X_e(t_i), Y_e(t_i), Z_e(t_i))), \quad (2)$$

where n_0 denotes the number of carriers, and e is the elementary charge. The position of the carriers (electrons and holes) at time t_i is denoted by $(X(t_i), Y(t_i), Z(t_i))$, which is determined by the distribution of the static electric field, mobilities, and diffusion constants. ϕ_w is the weighting potential. Figure 5 shows the preliminary results obtained by assuming that the electron and hole move in the z -direction with constant velocities; in this case, the hit positions are $(0, 0, 5\text{mm})$ and $(0, 0, 15\text{mm})$.

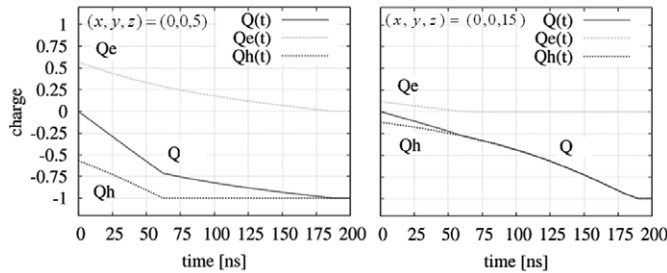


Fig. 5. Simulated charge signal induced in the cathode. The dashed curve shows the contribution of the holes and electrons. In this case, the γ -ray interacts at $(0, 0, 5\text{mm})$ and $(0, 0, 15\text{mm})$. The pulse heights are normalized to 1.

First, the extraction of the z -position will be carried out by using the correlation between the first moments from the simulated pulses. Extraction of the x - and y -positions will also be carried out using the simulated

pulse shapes of the non-hit segments. These extraction are currently underway.

References

- 1) S. Shimoura : Nucl. Instr. and Meth. A **525**, 188 (2004).
- 2) S. Go: Am. Phys. Soc. Vol **54**, 10, 119 (2009).
- 3) M. Kurokawa: IEEE **50** 1309 (2003).
- 4) Z. He: Nucl. Instr and Meth. A **463** 250 (2001).

PHENIX silicon vertex tracker project

Y. Akiba, S. Baumgart, N. Cassano,^{*1} S. Chollet,^{*2} V. Cianciolo,^{*3} A. Deshpande,^{*1,*4} O. Drapier,^{*2} A. Drees,^{*1} H. En'yo, K. Fujiwara,^{*5} F. Gastaldi,^{*2} Y. Haki,^{*6} K. Hashimoto,^{*6} R. Ichimiya, J. Kanaya, M. Kasai,^{*6} K. Kurita,^{*6} M. Kurosawa, A. Lebedev,^{*7} E. J. Mannel,^{*8} R. Nouicer,^{*9} C. Ogilvie,^{*7} Y. Onuki, R. Pak,^{*9} C. Pancake,^{*1} P. Riedler,^{*10} E. Shafto,^{*1} M. Sekimoto,^{*11} W. Sondheim,^{*12} M. Togawa, A. Taketani, and the PHENIX VTX group

We are constructing a silicon vertex tracker (VTX) for the PHENIX experiment at RHIC. The primary purpose of the detector is to carry out precise measurements of heavy-quark (charm and beauty quarks) production in $A + A$, $p(d) + A$, and polarized $p + p$ collisions. The main physics topics addressed by the VTX are as follows.

- Probing high-density partonic matter
 - Energy loss of heavy quarks (charm and bottom quarks) in dense matter
 - Elliptic flow of heavy quarks in dense matter
 - Open heavy-quark production
 - Medium induced modification of jets
- Measurement of the gluon spin polarization $\Delta G(x)$ of the nucleon
 - $\Delta G(x)$ with heavy-quark production
 - $\Delta G(x)$ with γ -jet measurement
- Nucleon structure in nuclei
 - Gluon shadowing over a broad x range

These are key measurements that are required for future RHIC programs, both for the study of Quark Gluon Plasma (QGP) in heavy-ion collisions and for the measurement of the nucleon spin-structure functions.

The VTX detector consists of two inner layers of silicon pixel detectors¹⁾ and two outer layers of silicon strip detectors. The detector covers $|\eta| < 1.2$ in pseudorapidity and $\Delta\phi \approx 2\pi$ in azimuth. The project is funded by RIKEN, the US DOE, and Ecole Polytechnique. The US side of the project commenced in US FY2007. The total budget is 4.7 M US dollars over four years (FY2007-FY2010).

The significant developments made this year are as follows.

- The second annual review of VTX was held at BNL in June 2009.
- The Q/A of the pixel sensor module is ongoing.
- The assembly of the pixel ladders is ongoing.²⁾
- An electronic checking system for pixel ladders is developed.³⁾
- The production of pixel staves (mechanical support + cooling) has been completed at LBNL.
- The production of pixel read-out boards (SPRIO) has been completed at Ecole Polytechnique.
- The production of pixel front-end-module (FEM) has been completed at Stony Brook University.
- Test bench system of pixel ladders has been developed.⁴⁾ One set of the system is installed at BNL.
- The Q/A of the strip sensors has been complete.
- The production of strip read-out card (ROC) is ongoing and to be completed soon.
- The assembly of strip silicon modules is ongoing.
- The first strip ladder has been assembled.
- The development of the read-out electronics chain for the strip system is nearing completion at ORNL. The production of the RCC boards is ongoing. The production of the LDTB boards, the strip buses, DIB, and CIB will start soon.
- The design of the mechanical support system and cooling of the VTX has been completed.
- The fabrication of mechanical support system of VTX is ongoing at LBNL and will be completed soon.
- On the software side the physics simulation of VTX^{?)} is ongoing.

References

- 1) A. Taketani et al.: RIKEN Accel. Prog. Rep. **43**, 202 (2010).
- 2) M. Kurosawa et al.: RIKEN Accel. Prog. Rep. **43**, 208 (2010).
- 3) Y. Haki et al.: RIKEN Accel. Prog. Rep. **43**, 206 (2010).
- 4) M. Kasai et al.: RIKEN Accel. Prog. Rep. **43**, 204 (2010).

^{*1} Stony Brook University, USA

^{*2} LLR, Ecole Polytechnique, CNRS-IN2P3, France

^{*3} Oak Ridge National Laboratory, USA

^{*4} RIKEN BNL Research Center, USA

^{*5} Tokyo Metropolitan Industrial Technology Research Institute, Japan

^{*6} Rikkyo University, Japan

^{*7} Iowa State University, USA

^{*8} Columbia University, USA

^{*9} Brookhaven National Laboratory, USA

^{*10} European Organization for Nuclear Research, Switzerland

^{*11} High Energy Accelerator Research Organization, Japan

^{*12} Los Alamos National Laboratory, USA

Silicon Pixel Detector for PHENIX Vertex Tracker[†]

A. Taketani, Y. Akiba, N. Apdula,^{*1} S. Baumgart, C. Biggs,^{*2} S. Chollet,^{*3} O. Drapier,^{*3} A. Dress,^{*1} H. En'yo, K. Fujiwara,^{*4} F. Gastaldi,^{*3} Y. Haki,^{*5} K. Hashimoto,^{*5} R. Ichimiya, Y. Ikegami, J. Kanaya, M. Kasai,^{*5} T. Kobayashi,^{*4} T. Kondo,^{*4} K. Kurita,^{*5} M. Kurosawa, J. LaBounty,^{*2} E. J. Mannel,^{*6} Y. Nomiyama, R. Nouicer, H. Ohnishi, Y. Onuki, R. Pak,^{*2} C. Pancake,^{*1} P. Riedler,^{*7} M. Sekimoto,^{*8} E. Shafto,^{*1} S. Shimoda, W. Sondheim,^{*9} M. Togawa, S. Watanabe,^{*10} Y. Yamada, and the PHENIX VTX group

PHENIX experiment at Relativistic Heavy Ion Collider (RHIC) will be upgraded with a silicon vertex tracker (VTX) in 2010. It will enhance physics capability in both spin and heavy-ion programs. The VTX covers $|\eta| \leq 1.2$ and $\Delta\phi \sim 2\pi$ with four layers of silicon sensors.¹⁾ It will be installed 2.5 cm away from the beam line, which is located just outside with a radius of 2 cm beam pipe. The VTX can be used to determine whether heavy quarks or light quarks are produced; this is possible since the VTX can track a displaced vertex corresponding to the long-lived charm and bottom mesons, whose $c\tau$ values are in the range of 100 to 400 μm . Further, the jet can be determined by measuring the momentum of the charged track within its large acceptance of the VTX.

In the VTX, pixel detectors are located on the two inner layers and strip detectors²⁾ are located on the two outer layers. We, the RIKEN group, are in charge of 30 pixel ladders, which is the smallest replaceable unit in the detector. This article describes the progress of the pixel ladders.

A pixel ladder consists of four sensor hybrids, a support stave, and two readout buses. The pixel size of the sensor is $50 \times 425 \mu\text{m}^2$. One sensor has $256 \times 32 \times 4$ pixels and is connected to four ALICELHCB1 chips by bump bonding. Signals from the sensor are converted to binary hit pattern data by using a preamplifier and a discriminator. These binary data are transmitted as digital signals to a silicon pixel readout (SPIRO) board via a pixel bus and an extender. The SPIRO board multiplexes data from eight ALICELHCB1 chips and transmits the data to a front end module (FEM) through 1.6 Gbps serial optical links.

The process of gluing the sensor hybrids, support stave, and readout buses in the ladder fabrication were improved; glue was dispensed by using a metal and a paddle instead of dispensing robot³⁾ in the previous years. The gaps between the hybrids and stave were carefully adjusted manually under a microscope during

the stacking process.

After the gluing process, the hybrids and readout buses were connected by wire bonding. In the initial stage test fabrication of the pixel ladder, a wire shorted between a bonding pad and the guard ring surrounding the pad; hence the signal could not be transmitted. Since it was not easy to visually detect the short, a wire-bonding checker was developed.⁴⁾ The checker can be used to measure the resistance between the pad, and the guard ring which is connected to the ground. When a short to the ground is detected, the associated wires are replaced.

We fabricated two pixel ladders as production version by the following improved gluing procedure. The ladders were electrically tested by performing charge injection tests, β -ray irradiation tests, and cosmic-ray tests by using SPIRO and FEM. Their functionality of the ladders was confirmed.⁵⁾

The ladders were operated in 0°C environment. A test bench box with a cooling system was developed. An interlock system that helps to prevent any accidental damage to the ladders destruction of ladders by accidents was developed.⁶⁾ The temperature and flow rate of the cooling liquid were monitored. Further, the humidity of the test bench box, which is filled with dry N₂ gas was measured. If these monitored values deviate from a specific value, the interlock system will shut off power supply to the ladder or close the valve for the cooling liquid.

In summary, we developed some tools for fabrication quality assurance (QA) and ladder-functionality QA processes. The fabrication of PHENIX pixel ladders has been commenced. They will be installed and will start operation in 2010.

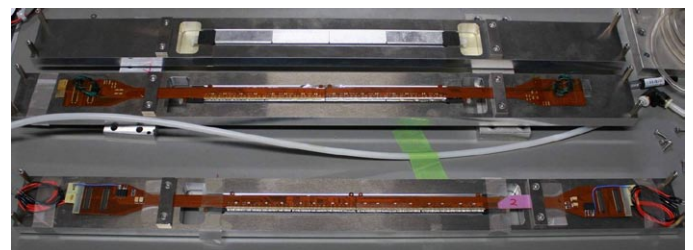


Fig. 1. Assembled pixel ladder, Top: Dummy assembly before gluing. Center: Dummy after gluing. Bottom: Fully assembled and functional ladder

*1 Stony Brook University, USA

*2 Brookhaven National Laboratory, USA

*3 LLR, Ecole Polytechnique, CNRS-IN2P3, France

*4 Tokyo Metropolitan Industrial Technology Research Institute, Japan

*5 Rikkyo University, Japan

*6 Columbia University, USA

*7 European Organization for Nuclear Research, Switzerland

*8 High Energy Accelerator Research Organization, Japan

*9 Los Alamos National Laboratory, USA

*10 Tokyo Metropolitan College of Industrial Technology, Japan

References

- 1) Y.Akiba et al.: RIKEN Accel. Prog. Rep. **43**, 201 (2010)
- 2) Z.Lee et al.: Nucl. Instr. Meth. A **466**, 366 (2001)
- 3) A.Taketani et al.: RIKEN Accel. Prog. Rep. **42**, 203 (2009)
- 4) Y.Haki et al.: RIKEN Accel. Prog. Rep. **43**, 206 (2010)
- 5) M.Kurosawa et al.: RIKEN Accel. Prog. Rep. **43**, 208 (2010)
- 6) M.Kasai et al.: RIKEN Accel. Prog. Rep. **43**, 204 (2010)

QA test bench for the PHENIX silicon pixel detector

M. Kasai,^{*1} A. Taketani, C. Biggs,^{*2} C. Pancake,^{*3} E. Mannel,^{*4} E. Shafto,^{*3} H. En'yo, J. LaBounty,^{*2} J. Kanaya, K. Kurita,^{*1} K. Hashimoto,^{*1} K. Fujiwara,^{*5} M. Kurosawa, M. Togawa, M. Sekimoto,^{*6} N. Apadula,^{*3} R. Nouicer,^{*2} R. Ichimiya, S. Baumgart, S. Shimoda,^{*7} Y. Akiba, Y. Nomiya,^{*7} Y. Onuki, Y. Haki,^{*1} Y. Ikegami,^{*7} Y. Yamada^{*7} and PHENIX VTX group.

A Silicon Vertex Tracker (VTX) will be installed for PHENIX experiment at RHIC in 2010. The VTX will enhance the physics capabilities of the PHENIX central arm spectrometers by providing precision measurements of heavy-quark (charm and beauty) production in A+A, p(d)+A and polarized p+p collisions.

The VTX consists of pixel detectors at inner 2 layers (10 ladders and 20 ladders) and strip detectors at outer 2 layers, which cover pseudo-rapidity of $|\eta| < 1.2$, and $\phi \sim 2\pi$ in azimuth. Japanese group including Rikkyo university, RIKEN and KEK is responsible for the pixel ladders.

We have started a mass production of the pixel ladder¹⁾²⁾³⁾ since last year. The assembled ladders have to go through quality assurance(QA) test at RIKEN and BNL. During QA test, there are possibilities of a serious damage for example, the glued parts of each material peel off and the coolant builds up condensation on the surface of the ladder, and so on. So we made an interlock system on the ladder test bench in order to prevent the serious damage on the ladder and to be within an acceptable level. In this report, we describe the interlock system for construction of ladder QA test bench.

Figure 1 shows a schematic view of QA test bench for the pixel ladder. The ladder was connected to a Silicon Pixel Interface Read Out (SPIRO) board which controls read-out chips and collects data and sends them to the FEM (Front End Module) via optical cables. The ladder is confined in a bench box filled with dry nitrogen gas. NOVEC, which is cooled to 0°C by a chiller to improve the resistance to radiation, flows into the ladder, and returns to the chiller through a control box. The control box is connected with three power supplies (High Voltage for sensor bias, Low Voltage for ladder, SPIRO⁴⁾) to operate the ladder. And pixel silicon sensor needs a reverse bias voltage (50V) to make it depleted. Low voltage (3.5V) is for operating read-out chips.

The bench box is made to be as compact as possible, and is attached by the connectors for NOVEC and nitrogen gas as shown Figure 2. A hygrometer is placed to a center of the bench box. In order to main-

tain air tightness of the test bench, extenders (Flexible printed circuits) are pressed by the silicon rubbers. In order to test the hermetic seal of the box, dry nitrogen gas whose humidity is 0% flowed into it at the rate of 0.03L/min. Then humidity in the box is maintained at 1.0%.

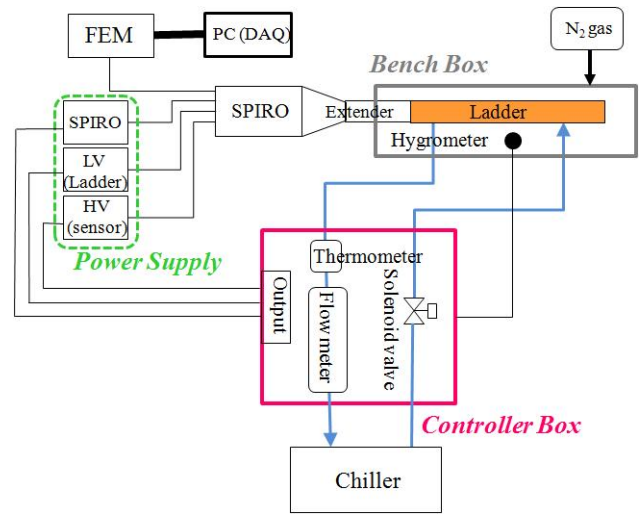


Fig. 1. A schematic view of ladder QA test bench.

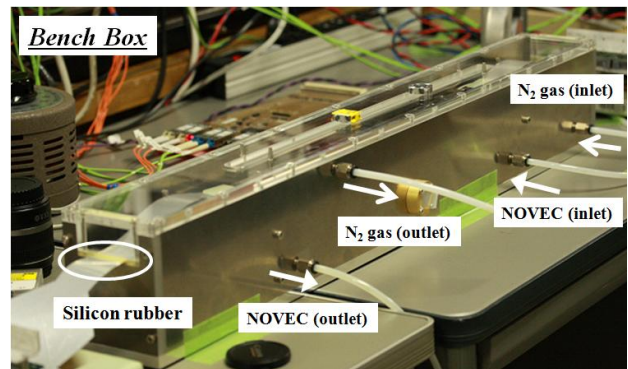


Fig. 2. A bench box with NOVEC and nitrogen gas connectors.

Figure 3 shows a front and rear panel side of the control box. A thermometer and temperature controller, a humidity controller, a flow meter and a solenoid valve are installed. We can monitor these values and set their thresholds.

- H [%] : Humidity in the bench box
- T [°C] : Temperature of NOVEC (outlet from the

*1 Department of Physics, Rikkyo University

*2 Brookhaven National Laboratory

*3 Stony Brook University, USA

*4 Nevis Labs Columbia University, USA

*5 Tokyo Metropolitan Industrial Technology Research Institute.

*6 KEK

*7 Advanced Technology Support Center in RIKEN

ladder)

- F [L/min] : Flow rate of NOVEC (outlet from the ladder)

The LED indicators display the status of the each interlock monitors. Green shows normal, and red shows the cause of the interlock.

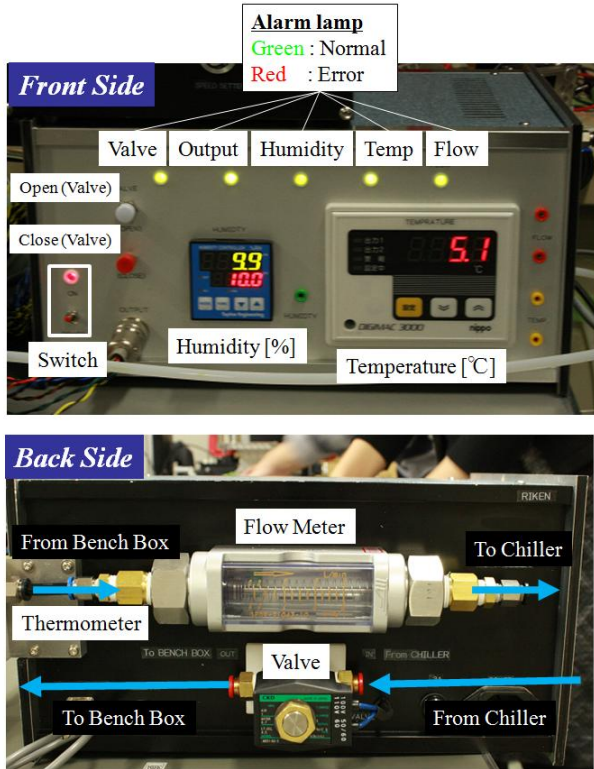


Fig. 3. A control box for the interlock system.

We set these threshold conditions on the control box.

- (1) H is lower than 5%.
- (2) T is lower than 5°C.
- (3) F is higher than 0.5L/min.

Before we start ladder QA test, firstly a power supply of the control box is turned on. Secondly, we flow dry nitrogen gas into the bench box. Thirdly, the chiller is operated at 0°C after H is lower than 5%. Finally, three power supplies are turned on and the ladder can work for QA test. If even one of the condition is not satisfied, the interlock system works and the prohibition signal is sent to all power supplies.

Now the test bench including the interlock system for ladder QA test has been completed and settled at BNL as shown in Figure 5. We confirmed that the interlock system operated correctly. We built a second test bench for RIKEN. Ladder QA test can be performed at RIKEN and BNL.

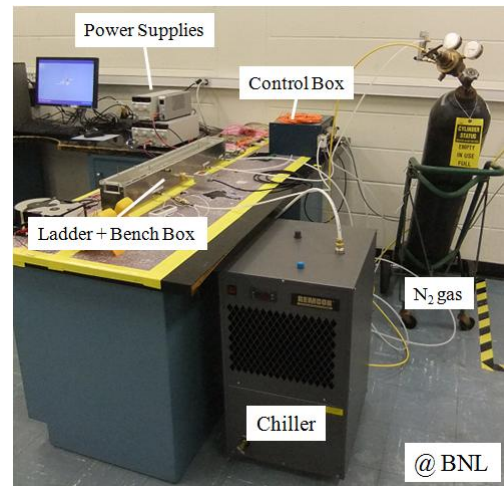


Fig. 4. Ladder QA test bench at BNL

References

- 1) Y. Onuki et al.: NIM A 606(2009)395-403 (2009)
- 2) M. Kurosawa: RIKEN Accel. Prog. Rep. 43, 208 (2010)
- 3) Y. Haki: RIKEN Accel. Prog. Rep. 43, 206 (2010)
- 4) R. Ichimiya: RIKEN Accel. Prog. Rep. 41, 171 (2007)

Development of wire bonding electrical-short checker for silicon pixel ladder in the PHENIX vertex tracker

Y. Haki^{*1}, M. Kurosawa, Y. Akiba, S. Baumgart, H. En'yo, K. Fujiwara^{*2}, A. Taketani, K. Hashimoto^{*1}, R. Ichimiya, K. Kurita^{*1}, M. Kasai^{*1}, J. Kanaya, Y. Onuki, C. Pancake^{*3}, M. Sekimoto^{*4}, E. Shafto^{*3}, M. Togawa and the PHENIX VTX group

The PHENIX detector at RHIC-BNL will be upgraded with a silicon vertex tracker (VTX) surrounding a beam pipe with four cylindrical layers¹. The inner two layers include silicon pixel detectors (SPDs), and the outer two layers include silicon strip detectors. The RIKEN-Rikkyo group is currently developing an SPD as part of the PHENIX VTX upgrade. The SPD is made up of 30 assembly units called ladders, each of which consists of a thermal plate, four sensor hybrids, and two pixel buses². A sensor hybrid is an assembly of a silicon pixel sensor and four readout chips (ALICE1LHCb), which are bonded to the sensor via bumps with a diameter of $20\ \mu\text{m}$. The readout chip has 8192 pixel cells arranged in 32 columns and 256 rows. The pixel size is $50\ \mu\text{m} \times 425\ \mu\text{m}$. The pixel bus is a copper-aluminum-polyimide base flexible printed circuit board. The signals from the silicon pixel sensor are read out through the readout chip and pixel bus, which are electrically connected by wire bonding, as shown in Fig. 1.

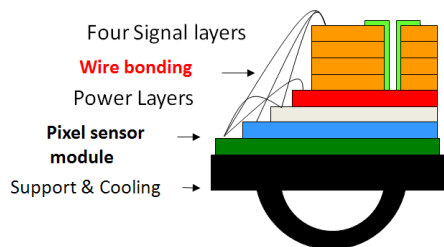


Fig. 1. Ladder cross section.

A pattern diagram and closeup image around the bonding pads of readout chip are shown in Fig. 2. A guard ring is located at top of the bonding pads. Sometimes, dust particles introduced during the quality assurance (QA) process performed hybrid sensor are retained on the bonding pad. Electrical short occurs if a wire is bonded to a dust-covered bonding pad and a guard ring. This electrical short causes failure of data transmission from the ladder. Therefore, an electrical-short checker must be used during the production of the ladder. Thus, we have developed a wire-bonding short checker (WBC) for the silicon pixel ladder.

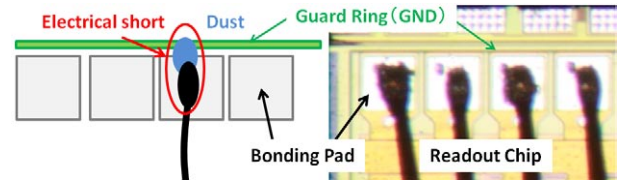


Fig. 2. Pattern diagram and closeup image for the region around the bonding pads of the readout chip.

A setup of the WBC is shown in Fig. 3. A half-ladder is connected to a switch system (7002 SWITCH SYSTEM) with a flexible printed circuit board (pixel bus and bus extender³) and a test card. The switch system changes the signal lines of the pixel bus, whose resistance is known. A digital multimeter (2000 MULTIMETER) measures the resistance between a signal line of the pixel bus and the guard ring (ground layer). A Visual Basic program controls the switch system and the digital multimeter via GPIB-to-USB interface (NI GPIB-USB-HS) in the Windows XP environment.

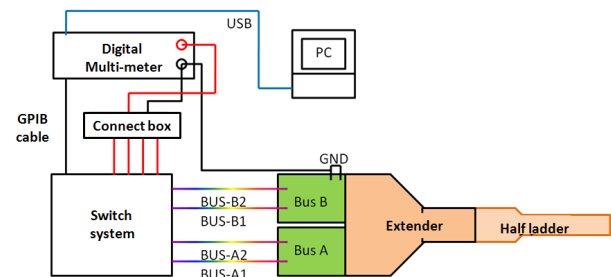


Fig. 3. Setup of wire-bonding short check system.

In the QA procedure, the criterion to be satisfied for the electrical short is that the resistance between a signal line of the pixel bus and the ground layer should be less than $100\ \Omega$. This is because the average resistance value of a signal line of pixel bus is $40\ \Omega$. The test voltage of the multimeter becomes as high as 10 V during high-resistance measurements under normal conditions. The dielectric withstanding voltage of a capacitor on the pixel bus is 6.3 V. In order to reduce the test voltage, a protection zener diode is added to the connection box. A characteristic curve obtained the zener diode and a circuit diagram of the connection box are shown in Fig. 4. If the test voltage exceeds the breakdown voltage (2.5 V in the present case), the current i_2 increases. Therefore, the voltage applied to the capacitor on the pixel bus is controlled to be less than 2.5 V.

^{*1} Department of Physics, Rikkyo University

^{*2} Tokyo Metropolitan Industry Technology Resrarch Institute

^{*3} Department of Physics and Astronomy, Stony Brook University, USA

^{*4} Institute of Particle and Nuclear Studies, KEK

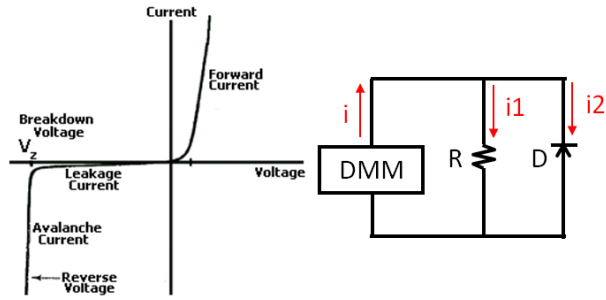


Fig. 4. A characteristic curve obtained for the zener diode and a circuit diagram of the connection box.

The switching rate of the switch system is 2 Hz, which is determined by the digital multimeter response rate. With this switching rates, it is possible to detect the occurrence of an electrical short between the bond wires in less than 2 min for a half ladder.

The pixel ladders, passing the WBC have been confirmed to be problem-free in a beta-ray irradiation test conducted in a subsequent QA cycle. Our wire-bonding electrical-short checker can check the quality of wire bonding within a short time and help achieve a steady production rate for a trouble-free pixel ladder.

References

- 1) Y. Akiba, et al.: RIKEN Accel. Prog. Rep. **43**, 201 (2010).
- 2) Y. Onuki, et al.: RIKEN Accel. Prog. Rep. **41**, 165 (2008).
- 3) K. Fujiwara, et al.: IEEE Trans. Nucl. Sci. **56**, 250 (2009).

Quality assurance test of silicon pixel ladder for RHIC-PHENIX

M. Kurosawa, Y. Akiba, H. En'yo, K. Fujiwara,^{*2} Y. Haki,^{*3} K. Hashimoto,^{*3} R. Ichimiya,^{*1} J. Kanaya, M. Kasai,^{*3} K. Kurita,^{*3} Y. Onuki,^{*1} C. Pancake,^{*4} R. Petra,^{*5} M. Sekimoto,^{*1} E. Shafto,^{*4} B. Stephen, M. Togawa,^{*6} and A. Taketani

PHENIX is an experiment aimed at studying the spin structure of nucleons and studying hot and dense matter at Relativistic Heavy Ion Collider (RHIC) at Brookhaven National Laboratory (BNL). The PHENIX detector will be upgraded with a silicon vertex tracker (VTX)¹ in order to enhance its physics capabilities for spin and heavy ion program. The VTX comprises a four-layer barrel detector built from two inner silicon pixel detectors and two outer silicon strip detectors. The main roles of the VTX are precision measurement of decay position of heavy-flavor decays and precision reconstruction of jet axis with its large acceptance.

A silicon pixel ladder is the basic component of a silicon pixel detector. The two inner layers of the silicon pixel detectors are made up of 30 silicon pixel ladders. Mass production of silicon pixel ladders started by the end of 2009. In order to ensure correct operation before the assembly of the silicon pixel detectors, quality assurance (QA) tests of the silicon pixel ladders need to be performed. This report presents the recent results of the QA test for the fabricated silicon pixel ladders.

The structure of a silicon pixel ladder is shown in Fig. 1. It consists of four silicon sensor modules, two

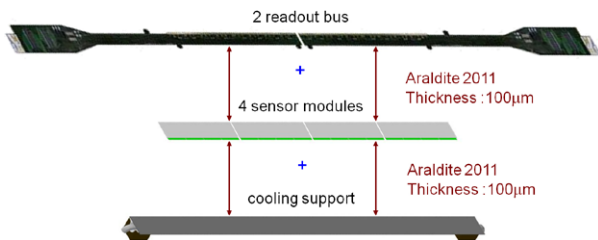


Fig. 1. The structure of silicon pixel ladder.

readout buses and a cooling support. Each component is glued with Araldite 2011. The silicon sensor module is an assembly of a silicon pixel sensor and four readout chips² (ALICE1LHCb) bump-bonded to the sensor (bonded by VTT^a) using bumps with diameters of 25 μm . The readout chip has 8192 pixel cells arranged in 32 columns and 256 rows. The pixel size is

50 $\mu\text{m} \times 425 \mu\text{m}$. Each pixel cell has an analog circuit and a digital circuit as shown in Fig. 2. The analog

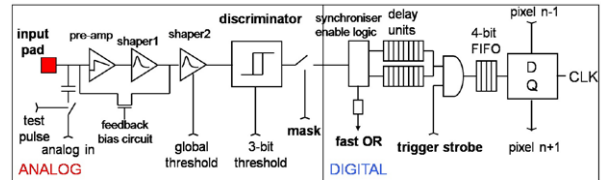


Fig. 2. An analog and digital circuit in a pixel cell.

circuit has a pre-amplifier followed by a shaper, a discriminator and a NAND gate to mask hot pixel. The digital circuit consists of a synchroniser to the clock, two digital delay units to store a hit for the duration of the trigger latency, and a four-event FIFO that acts as the multi-event buffer. The main test items are to check these components in order to ensure that they function correctly after assembling. The items to be evaluated in the test are as follows:

- (1) Current consumption.
 - The current consumption of the analog and the digital circuits of the readout chips are measured.
- (2) JTAG functionality.
 - It is confirmed whether the configuration settings in the chip can be read and written by using the Joint Test Action Group (JTAG) protocol.
- (3) Mask functionality.
 - The noisy pixels can be masked by a mask functionality.
- (4) Minimum threshold and noise level.
 - For all chips, the minimum threshold in all pixel matrices are determined.
- (5) Mean threshold and mean noise for the complete pixel matrix.
 - The test pulse from the pulsar inside the chip is transmitted to each pixel cell and the mean threshold and noise levels are determined.
- (6) Performance of the pixel ladder with the β source (^{90}Sr).
 - Faulty bump bonds and the maximum efficiency are evaluated by β -source measurement.

The setup of the QA-test system is shown in Fig. 3. The assembled sensor modules (ladder) are con-

^{*1} KEK

^{*2} Tokyo Metropolitan Industrial Technology Research Institute

^{*3} Department of Physics, Rikkyo University

^{*4} Department of Physics and Astronomy, Stony Brook University

^{*5} CERN

^{*6} Department of Physics, Osaka University

^{a)} VTT Electronics, Tekniikatie 17, Espoo, P.O. Box 1101, FIN-02044 Espoo, Finland

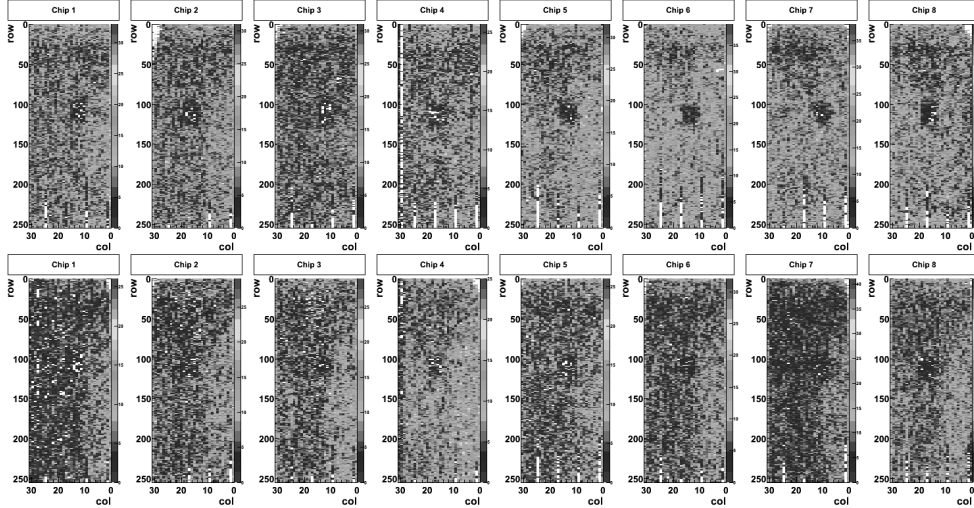


Fig. 5. Response of pixel ladder to a β source. The horizontal and vertical axes represent pixel position along the column and row directions, respectively. Low gray-levels represent low number of hits.

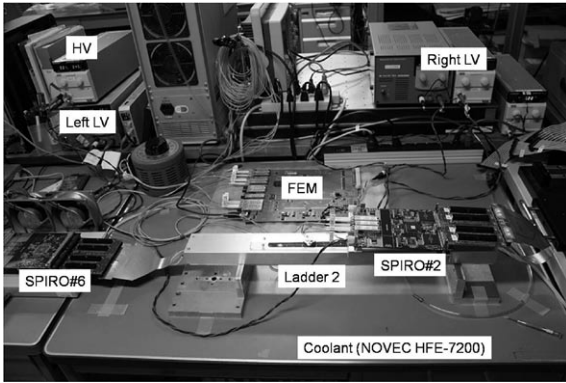


Fig. 3. Setup for QA test.

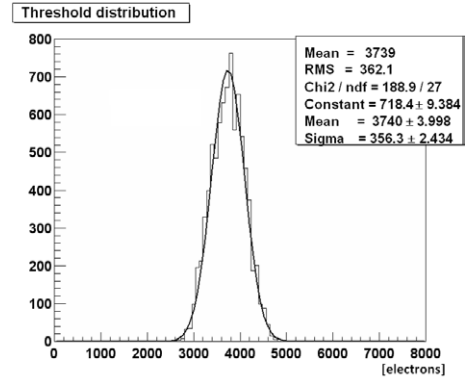


Fig. 4. Threshold distribution for a chip.

nected to Silicon Pixel Read-Out (SPIRO) modules. The SPIRO modules provide all electricity, control the readout chip of the sensor module and read out pixel data. The front-end module (FEM) is an interface between the SPIRO modules and the data acquisition system. The NOVEC HFE-7200 was used to the cool readout chips. In the QA test, the DAC values on each readout chip were optimized. These DACs provide a bias to the analog and digital circuits and are configured by using the JTAG interface. The minimum threshold level for each chip was determined and hot pixels were masked. In order to obtain a uniform pixel matrix, the efficiency of each pixel was measured using a test pulse by varying the amplitude of the pulse voltage. Then, the mean threshold level was determined. Finally, the performance test of a pixel ladder with β source was carried out.

So far, the QA tests of three pixel ladders have been completed and the correct operation of the ladders has

been confirmed. The threshold distribution for a chip is shown in Fig. 4. The measured mean threshold of 3,700 electrons was considerably low comparing with the 14,000 electrons of MIP. The typical response of the pixel ladder with 16 readout chips to the β source is shown in Fig. 5. The inefficient area at the bottom of columns 1, 9, 17, and 25 is attributed to the imperfect optimization of DACs.

In summary, QA tests of three assembled pixel ladders were carried out. The reference voltage for DACs were optimized, and the response of the pixel ladders to the β source were measured. The results confirmed that the three pixel ladders operate correctly.

References

- 1) Y. Akiba et al.: RIKEN Accel. Prog. Rep. **43**, 201 (2010).
- 2) K. Fujiwara et al.: RIKEN Accel. Prog. Rep. **39**, 207 (2005).

Use of time-domain reflectometry for impedance measurement of fine-pitch and low-material-budget readout bus of the PHENIX pixel detector

K. Fujiwara,^{*1} A. Taketani, T. Kobayashi,^{*1} T. Kondo,^{*1} Y. Akiba, Y. Haki,^{*2} S. Watanabe,^{*3} M. Kasai,^{*2} M. Kurosawa, H. En'yo, K. Kurita, M. Sekimoto, K. Hashimoto,^{*2} J. Kanaya, Y. Onuki, M. Togawa, S. Baumgart, R. Ichimiya, and the PHENIX VTX group

The PHENIX detector system at the relativistic heavy ion collider (RHIC) at the Brookhaven National Laboratory will be upgraded by installing a four-layer silicon vertex tracker (VTX) in 2010¹. The VTX consists of two inner silicon pixel detectors and two outer silicon strip detectors. It can enhance the capabilities of the PHENIX detector system, enabling the identification of heavy quarks via the measurement of the displacement of vertices. This will facilitate investigations of new hot and dense nuclear matter produced in heavy-ion collisions and the spin structure of nucleons produced in polarized proton-proton collisions at the RHIC¹. Our group is responsible for developing and fabricating the silicon pixel detectors. A new transmission line was introduced in the silicon pixel detector for studying the above-mentioned topics. The radiation length of the transmission line is 0.22%^{2,3}.

The charged-particle-induced signals in silicon pixel sensors are fed to dedicated bump-bonded readout chips and converted to binary data. One readout chip generates 32×256 -bit data, where 256 represents the depth of the data. The binary data are transferred to a SPIRO board⁴) via fine-pitch and low-material-budget pixel buses. The signals on the SPIRO board are converted to optical serial data and transmitted to the PHENIX DAQ system. The pixel bus has already been produced.

This report describes the measurement of the characteristic impedance of the pixel bus by using time-domain reflectometry (TDR); the measurement was performed at Tokyo Metropolitan Industrial Technology Research Institute (TIRI). A dedicated probe needle with a joystick was developed by NS Corporation.

The bus is fabricated using a flexible printed circuit (FPC) board with copper and aluminum conductors set on the polyimide insulators^{2,3}). Figure 1 shows a cross section of the pixel bus.

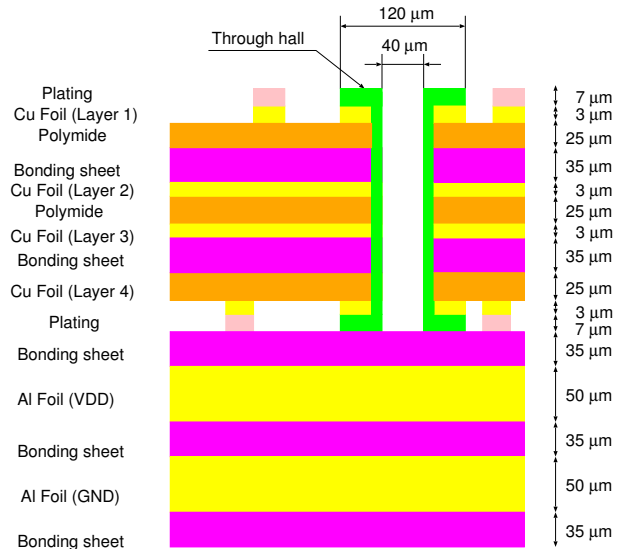


Fig. 1. Cross section of a pixel bus.

The bus has two signal layers made of copper, two copper layers for manufacturing purposes, and a power layer and a ground layer that are both made of aluminum to minimize the material budget. The production process involves (1) pattern etching, (2) layer stacking, (3) laser drilling, (4) through-hole plating, and (5) electrical continuity testing of each signal line. The outline of bus is shared for final shape. The bus contains 128 data lines and 60 control and peripheral lines in total. The area of the bus is $13.9 \times 250 \text{ mm}^2$. Hence, each signal and control line (copper line) is $30 \mu\text{m}$ wide and $3 \mu\text{m}$ thick; the minimum spacing between two such lines is $30 \mu\text{m}$ ^{2,3}).

The signal propagation behavior and impedance were predicted by HSPICE simulation. In this report, we compare the calculated impedance value with the value measured using the TDR system, Agilent 86100C Digital Communication Analyzer with a 54754A TDR module.

In general, the TDR system is used for the time-domain analysis of minute defects in coaxial cables or microstrip lines⁵). The TDR system consists of a high-speed pulser and an oscilloscope. A fast step-pulse is injected into a signal line, and the reflected signal is then observed on the scope. Changes in the characteristic impedance of the transmission line are explained by the superposition of the injected pulse and reflected

^{*1} Electronics Group, Tokyo Metropolitan Industrial Technology Research Institute

^{*2} Department of Physics, Rikkyo University

^{*3} Tokyo Metropolitan College of Industrial Technology

pulse in time domain.

Figure 2 shows a dedicated probe needle and a joystick-type actuator developed by NS Corporation, Musashino-shi, Tokyo. The needle has a tungsten contact for transmitting and receiving signals, a ground pad, and a semi rigid cable with an SMA female connector.

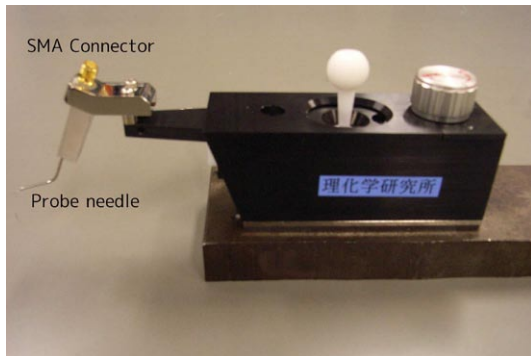


Fig. 2. Dedicated probe needle with a joystick-type actuator.

Figure 3 shows the changes in the characteristic impedance of a transmission line of a pixel bus as measured in time domain. The rise time of the injection pulse is 35 ps. The typical value of the impedance of the transmission line is approximately 120 Ω . The characteristic impedance calculated by HSPICE simulation is in the range 110–140 Ω ²⁾. Thus, it is confirmed that the calculated value agrees with the measured one.

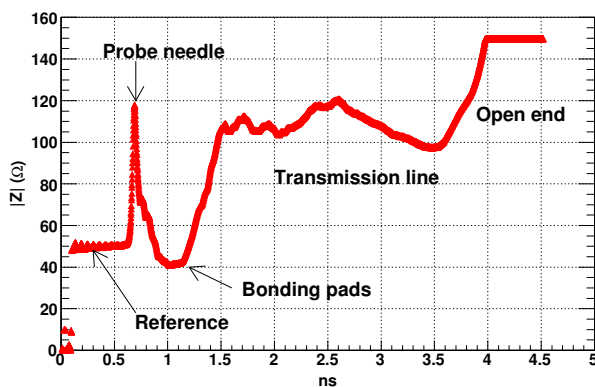


Fig. 3. Characteristic impedance measured by TDR.

We checked that the signals from the readout chips are transferred correctly during both measurement and simulation²⁾. Thus, we formulated a design procedure of FPC by using the HSPICE simulator and developed an impedance evaluation method using TDR.

Using TDR measurements, defects in vias (plated-through holes) can be detected after final sharing. We are continuing impedance measurement using TDR to

develop a new quality assurance procedure and to improve the yield rate of the plated-through hole making.

References

- 1) Y. Akiba: RIKEN Accel. Prog. Rep. **43** (2010).
- 2) K. Fujiwara: Development of a silicon pixel tracker for an experiment of high energy heavy ion and polarized proton collisions, Doctoral dissertation, Niigata University, 2007.
- 3) K. Fujiwara, et al.: IEEE Transactions on Nuclear Science 56, No.1 (2009).
- 4) R. Ichimiya: RIKEN Accel. Prog. Rep. **40** (2007).
- 5) J. R. Andrews: "TDR, Setp Response and "S" Parameter Measurements in the Time Domain," Picosecond Pulse Labs, Colorado, USA, Application Note AN-4, May 1989.

GEM detectors for the experiment to measure the mass modification of vector mesons in nuclei at J-PARC

S. Yokkaichi for the J-PARC E16 Collaboration

We proposed an experiment E16¹⁾ to measure the vector meson decays in nuclei in order to investigate the chiral symmetry restoration in dense matter. The experiment is planned to be performed at the J-PARC hadron experimental facility. The proposal of the experiment was granted scientific (“stage 1”) approval by the PAC^{a)} in March 2007. For full approval, we are required to show not only the experimental feasibility but also the prospects for acquiring sufficient funds and even the prospects for beam line construction.

The aim of experiment is to perform the systematic study of the mass modification of vector mesons, especially ϕ meson, in nuclei. The mass modification of vector mesons in hot and/or dense matter is predicted on the basis of the QCD; due to the restoration of chiral symmetry in such matter. On the other hand, taking only hadronic many-body effects into account, mass modifications in matter are also predicted. Many experimental studies have been conducted, and the mass modifications in hot/dense matter have been observed, including in KEK-PS E325²⁾, of which the author were one of the collaborators. However, the cause of the modification has not yet been confirmed; in other words, there is no consensus on the interpretations of the phenomena. To determine the cause, the systematic study of the modification is required in order to accurately compare the data with various theoretical predictions.

A goal of this experiment is to measure the ϕ meson decays in the e^+e^- channel with the statistics that are two orders of magnitude larger than those of the preceding experiment E325; namely, there are 1×10^5 to 2×10^5 events for each nuclear target, H, C, Cu, and Pb. Thus, we can deduce the dependences of the modification on the matter size and meson momentum, which have never been measured. At the same time, the e^+e^- decays of the ρ , ω , and J/ψ mesons can be measured. For the experiment, we will use a 10^{10} -Hz, 30-GeV proton beam at the high-momentum beam line, which will be constructed at J-PARC hadron experimental facility. To increase the statistics by a factor of 100, the beam intensity is changed to achieve a factor of 10, the acceptance of spectrometer is changed to achieve a factor of 5, and the production cross section is increased by increasing beam energy to achieve a factor of 2. To cope with the interaction rate at the target that has increased by a factor of 10, to 10^7 Hz, new spectrometer based on new technology should be built.

The development of detectors for the experiment has been performed. There are two key detectors in the experiment, both use the GEM (Gas electron multiplier) technology. One is the Hadron blind detector (HBD), which is to separate the electrons from the pions, and the other is the GEM tracker, which is used to cope with the high rate that is expected to reach 5 kHz/mm^2 at the most forward region of the proposed spectrometer. HBD is being developed at RIKEN and GEM Tracker is being developed at University of Tokyo, while a basic study on the GEM is being performed at both. The status of development of the GEM and GEM Tracker are reported in this article; the status of development of HBD is reported elsewhere³⁾ in this report. With lead-glass EM calorimeters, GEM Tracker and HBD compose an electron-ID detector module as shown in Fig. 1.

Typically, a GEM is a thin kapton foil that has thin copper electrodes on both sides and many small holes (typically $70 \mu\text{m}$ in diameter, aligned in a triangular lattice with a $140\text{-}\mu\text{m}$ pitch). The typical thicknesses of

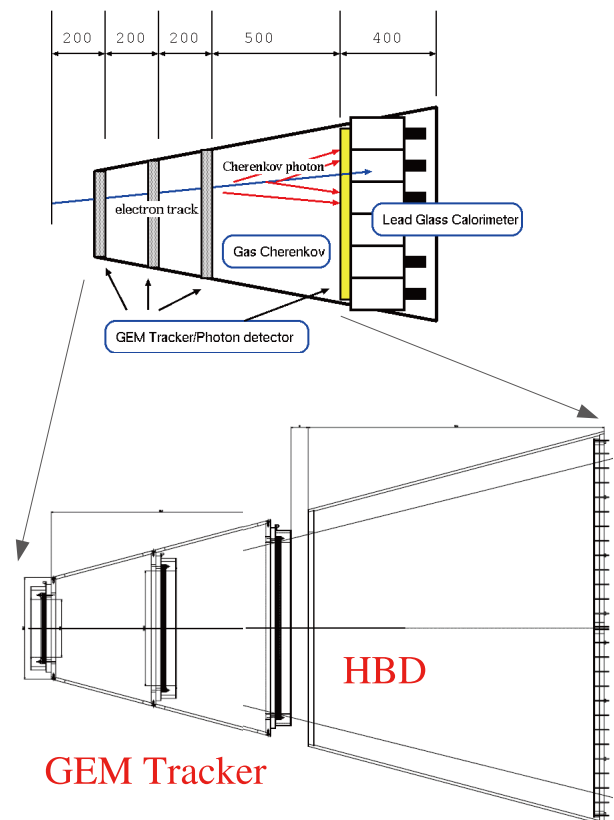


Fig. 1. The schematic view of the electron-ID detector module and drawings of GEM Tracker and HBD.

^{a)} Program Advisory Committee for Nuclear and Particle Physics Experiments at the J-PARC 50-GeV Proton Synchrotron

kapton and copper are 50 μm and 5 μm , respectively. The typical sensitive area is $100 \times 100 \text{ mm}^2$. Gas amplification occurs in the high electric field in the small holes. Typical gas gain is 20 for a foil with an electrode voltage of 340 V for such a typical 50- μm -thick GEM in P10 ^{b)} gas; in order to obtain a sufficient gain, three or four foils are stacked.

The GEM was originally developed at CERN⁴⁾, which was made using the chemical etching method. In Japan, the plasma and laser etching methods were adopted successfully to produce GEM at CNS, U-Tokyo and the RIKEN Cosmic radiation laboratory ^{5,6)}. Such domestic GEMs, especially 100 μm -thick liquid crystal polymer(LCP) foil, had greater stability and higher gain than that of the typical CERN-made GEM; however, the domestic GEMs were three times as expensive as the CERN-made. It should be noted that the cost of chemical etching in mass production is expected to be decreased, but the cost associated with the laser is proportional to the number of holes and number of GEMs; thus, the cost decrease due to the mass production cannot be expected. In our experiment, the tracker and HBD should cover the largest area among all existing GEM detectors in the world, and thus, the size and cost are serious concerns.

The trial production of some types of GEMs for our detectors was carried out by domestic companies. The first domestic production of a larger-size ($200 \times 200 \text{ mm}^2$ and $300 \times 300 \text{ mm}^2$) 50 μm -thick kapton GEM by chemical etching was carried out. The GEMs could operate but their gain was lower than expected. The control of the hole size in the etching process was not very good, and the larger size than expectation might have resulted in the lower gain.

Next, we successfully developed GEMs with a higher gain by chemical etching of 50- μm -thick kapton with smaller holes (diameters of holes are $45 \pm 5 \mu\text{m}$ for Kapton at the most narrow part, and $75 \pm 5 \mu\text{m}$ for Copper) and sizes of $100 \times 100 \text{ mm}^2$ and $200 \times 200 \text{ mm}^2$. By the end of June 2010, sample with a size of $300 \times 300 \text{ mm}^2$ and with identical hole size will be delivered and tested. When their successful operation is confirmed, GEM Tracker will be economically constructed.

The test indicated that the domestic 100 μm -thick LCP GEM made by laser-etching is suitable for the HBD. In CF_4 gas, which is required for the HBD³⁾, a higher voltage is required to achieve the same gain as that achieved in P10 gas. Thus, the stability requirement for HBD is more strict than that for the tracker. For reducing the cost and increasing the size, some trials to produce a 100- μm -thick LCP GEM based on a different technology are in progress. The chemical etching of LCP was one of the tested technology, and finally found to be unsuitable.

For the GEM Tracker, a thin read-out board with a double-sided fine-pitch strip was produced and tested for comparison with the above GEMs using an electron beam of momentum 670 MeV/c and 2 GeV/c at LNS-Tohoku and KEK, respectively. In electron measurement, reducing the amount of material is essential for reducing the radiative tail and the background from the γ -conversion. Three GEM chambers using the above GEMs and read-out boards, which consist of three tracking plane, will be placed in the tracking region; the total radiation length of the three chambers is less than 1.2%.

The read-out boards are made of 25- μm -thick kapton with 700- and 350- μm -pitch copper strip. We aim to achieve a position resolution of 100 μm in order to achieve a mass resolution of 5 MeV/ c^2 for ϕ mesons. The requirement is satisfied for the track injected the tracker vertically; using P10 gas and 700 μm -pitch strip read-out board with charge information of signals. On the other hand, for a tilted track, e.g., a track at 30° to the vertical, the resolution is deteriorated to 150 μm or more. Further investigation is being carried out by using timing information of signals, optimizing the GEM HV configuration and gas mixture, etc.

References

- 1) S. Yokkaichi; RIKEN Accel. Prog. Rep. **39**, 219 (2006), S. Yokkaichi *et al.*; J-PARC proposal No. 16 (http://j-parc.jp/NuclPart/pac_0606/pdf/p16-Yokkaichi_2.pdf), Lect. Notes Phys. **781** 161 (2009).
- 2) M. Naruki *et al.*; *Phys. Rev. Lett.* **96**, 092301 (2006), R. Muto *et al.*; *Phys. Rev. Lett.* **98**, 042501 (2007).
- 3) K. Aoki *et al.*; in this report.
- 4) F. Sauli, *Nucl. Instrum. Meth.* **386**, 531 (1997).
- 5) M. Inuzuka *et al.* *Nucl. Instrum. Meth.* **525**, 529 (2004).
- 6) T. Tamagawa *et al.* *Nucl. Instrum. Meth.* **560**, 418 (2006).

^{b)} Ar 90% + CH_4 10%

Development of a thick-GEM TPC for the J-PARC E15 experiment

F. Sakuma and M. Tokuda,*¹ members of the J-PARC E15 Collaboration

[thick-GEM, TPC, J-PARC E15]

The J-PARC E15 experiment aims to determine the simplest kaonic nuclear bound state K^-pp by in-flight ${}^3\text{He}(K^-, n)$ reaction¹. The dedicated detector system consists of a beam-line spectrometer, a Cylindrical Detector System (CDS), and a neutron TOF counter. The key point of such measurement is to accurately identify Λ and Σ decays in the CDS using their secondary vertex reconstruction because the expected decay modes of K^-pp are $p\Lambda/p\Sigma^0$ and $p\pi\Sigma$. In order to perform these measurements, we have been developing a Thick Gas Electron Multiplier (TGEM) Time Projection Chamber (TPC) as an inner tracker for the E15 upgrade. For the TPC, the spatial resolution in the Z direction should be less than 1 mm, and the material budget for detector acceptance should be minimized as much as possible.

The TPC is cylindrical in shape with an inner diameter of 170 mm and an outer diameter of 280 mm and is filled with P-10 gas at atmospheric pressure. The drift length is 30 cm with field cages of a double-sided Flexible Printed Circuits (FPC) having staggered strip electrodes. A photograph of the TPC is shown in Fig. 1. We use a double-TGEM structure for amplification, and signals are read out with 4-mm-long and 20-mm-wide pads on a standard PCB. The TGEM is economically constructed from double-clad 400- μm -thick FR4 plate using standard PCB techniques. It has mechanically drilled holes with diameters of 0.3 mm and chemically etched rims typically at 0.03 mm around each hole to prevent electrical discharges. The TPC with TGEM are advantageous because TGEM do not require support frames, which are essential when standard GEM foils having thickness of 50 μm are used²).

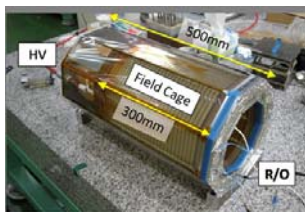


Fig. 1. A photograph of the TPC.

In order to study the performance of the TGEM, we used a prototype TGEM with an active area of $10 \times 10 \text{ cm}^2$ produced by REPIC Corp., Japan. Measurements were carried out with double-TGEM configuration using a test bench consisting of a gas chamber, the TGEMs operating in cascade, a voltage di-

vider with a resistive chain, and the read-out pad with a charge sensitive preamplifier. The required effective gain is about 10^4 , and the stability of the gain and energy resolution should be about 20% and 10%, respectively. Figure 2 shows the effective gain of the double TGEM measured with ${}^{55}\text{Fe}$ having four types of rim configurations, and Fig. 3 shows the stability of the gain and the energy resolution for the same configurations. All types of TGEM achieve an optimal effective gain of over 10^4 , but TGEMs with larger rims require a higher voltage. Moreover, TGEMs without any rims and those with small rims (30 μm) work rather stably; however, TGEMs with large rims (100 and 50 μm) are unstable. This instability of the large-rims TGEM is possibly caused by the charging up of the insulator that was not metalized, but this behavior is not yet understood well. Further studies of the basic TGEM behavior and performance are in currently progress.

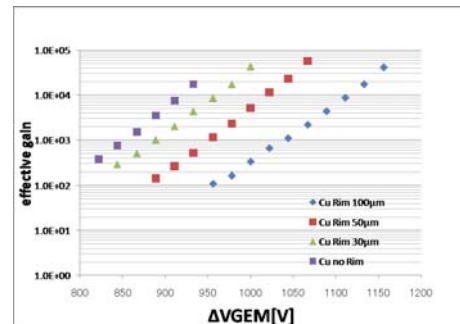


Fig. 2. The effective gain of the double TGEM.

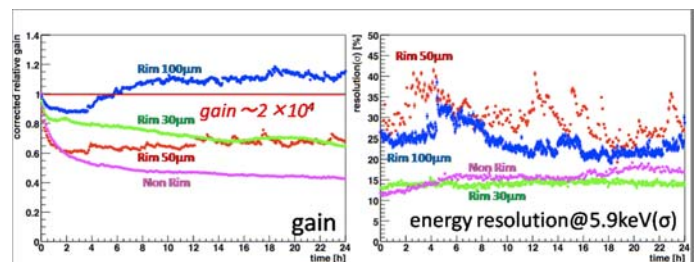


Fig. 3. The stability of the gain the and energy resolution of the double TGEM.

References

- 1) E15 proposal, http://j-parc.jp/NuclPart/pac_0606/pdf/p15-Iwasaki.pdf
- 2) F. Sauli, Nucl. Instrum. Meth. A **386**, 531 (1997).

*¹ Department of Physics, Tokyo Institute of Technology

Development of Cylindrical Detector System (CDS) for J-PARC E15 Experiment[†]

K. Tsukada for J-PARC E15 collaboration

[Nuclear physics, strangeness]

Recently, significant progress has been made to study on deeply bound kaonic nuclei. Although there are several experimental reports on the search for deeply bound kaonic nuclear states¹⁻⁶), results are still controversial because there is no conclusive evidence for the observation of such bound states. As has been found in experimental and theoretical studies the binding energy and decay width of the K^-pp state vary from a few 10 MeV to around 100 MeV.

To address this issue, the J-PARC E15 experiment was proposed. The aim of this experiment was to search for the simplest kaonic nuclear bound state, namely K^-pp , via the in-flight ${}^3\text{He}(K^-, n)$ reaction using a 1.0 GeV/c K^- beam⁷). This experiment is advantageous because it allows for the simultaneous measurement of the missing-mass spectra of the primary neutrons and the invariant-mass spectra of the expected decay particles, $K^-pp \rightarrow \Lambda p \rightarrow p\pi^-p$.

The E15 spectrometer has four components: a beam line spectrometer, a cylindrical detector system (CDS) with a liquid ${}^3\text{He}$ target, a beam sweeping magnet, and a neutron time-of-flight (TOF) wall. The decay particles from the expected decay $K^-pp \rightarrow \Lambda p \rightarrow p\pi^-p$ are detected by the CDS, forward neutrons whose flight length is approximately 15 m are detected by the TOF wall. Incident kaons that pass through the target are deflected by the beam sweeping magnet placed immediately after the CDS. By the assumption of the K^-pp binding energy to be 100 MeV/c², the expected spectrometer performance for the K^-pp measurement is 9.2 MeV/c² (σ) for the missing-mass resolution and 16 MeV/c² for the invariant-mass resolution. The CDS preparation status is described below.

In the CDS, all the detectors are configured cylindrically. The trajectory of the particles is reconstructed with the Cylindrical Drift Chamber (CDC) on a cylindrical drift chamber (CDC), which operates in a magnetic field of 0.5 T generated by a solenoid magnet. A cylindrical detector hodoscope (CDH) surrounds CDC and is used for the trigger counter and the particle identification hodoscope.. The solid angle of the CDS at the center is approximately 7.4 sr.

The CDC consists of two 200 mm thick aluminum end-plates, a carbon fiber reinforced plastics (CFRP) tube with a thickness of 1 mm as the inner wall, and six aluminum blocks placed outside the tracking region. The CDC uses gold-plated tungsten with a diameter of 30 μm as sense wires and gold-plated aluminum with a diameter of 100 μm as field and guard wires. The

total length along the beam axis of tracking volume is approximately 840 mm. A 50:50 mixture of Ar and ethane (1 atm) is used. The CDC has 15 layers of hexagonal cells with a typical drift length of 9 mm; the cells are grouped into 7 super layers (A1, U1, V1, A2, U2, V2, A3). Information of a longitudinal position along the beam axis is obtained by 8 stereo layers with a typical tilt angle of 3.5°. The number of readout channels is 1816, and the total number of wires in the CDC is 8064. Commissioning of the CDC is currently underway, and a typical spacial resolution of 200 μm is achieved by measuring trajectories of the cosmic rays in the absence of a magnetic field. The CDH consists of 36 segments, each of which is individually mounted on the inner wall of the solenoid magnet. Hamamatsu-type R7761 fine-mesh photomultipliers (PMTs) with a diameter of 1.5 inch are selected. The time resolution of the CDH measured using cosmic rays is typically 71 ps, which indicates that the design goal has been achieved. The CDC and CDH have been successfully installed in the solenoid magnet, as shown in Fig. 1. Excitation of the solenoid and evaluation of the CDC and CDH performance in the magnetic field will be carried out in the near future.

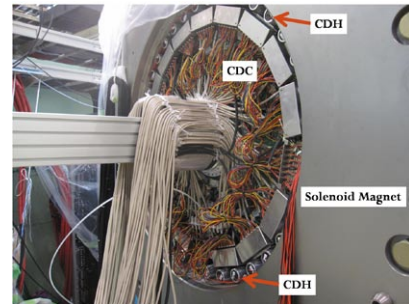


Fig. 1. Photograph of the CDS. The CDC and CDH are installed in the solenoid magnet.

References

- 1) M. Sato *et al.*: Phys. Lett. B **659**, 107 (2008).
- 2) T. Suzuki *et al.*: Mod. Phys. Lett. A **24**, 442-445 (2009).
- 3) T. Kishimoto *et al.*: Prog. Theor. Phys. **118**, 181 (2007).
- 4) M. Agnello *et al.*: Phys. Rev. Lett. **94**, 212303 (2005).
- 5) G. Bendiscioli *et al.*: Nucl. Phys.A **789**, 222 (2007).
- 6) T. Yamazaki *et al.*: arXiv:0810.5182 [nucl-ex].
- 7) M. Iwasaki *et al.*: Proposal of J-PARC 50-GeV PS “A search for deeply-bound kaonic nuclear states by in-flight ${}^3\text{He}(K^-, n)$ reaction” (2006).

Development of a Cylindrical Drift Chamber for an experimental search for K^-pp bound states at J-PARC

T. Hiraiwa,^{*1} Y. Fujiwara,^{*2} M. Iio,^{*3} K. Itahashi,^{*3} M. Iwasaki,^{*3,*4} H. Kou,^{*4} H. Ohnishi,^{*3} H. Outa,^{*3} F. Sakuma,^{*3} M. Tokuda,^{*4} D. Tomono,^{*3} K. Tsukada,^{*3} T. Yamazaki,^{*2,*3} and the J-PARC E15 Collaboration

1 Introduction

The J-PARC E15 experiment aims to search for K^-pp bound states using in-flight (K^-, n) reaction on $^3\text{He}^1$). In this experiment, we measure the missing mass in the in-flight (K^-, n) reactions and the invariant mass of the decay such as $K^-pp \rightarrow \Lambda p \rightarrow \pi^- p \pi^-$, simultaneously. We newly developed a Cylindrical Detector System (CDS) for the invariant mass study, which mainly consists of a large solenoid magnet, a Cylindrical Drift Chamber and hodoscope counters (See Fig. 1).

In this report, the design and current status of Cylindrical Drift Chamber are presented.

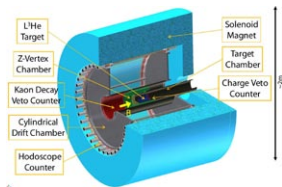


Fig. 1. A schematic view of Cylindrical Detector System (CDS).

2 Design for Cylindrical Drift Chamber

As shown in Fig. 2, a Cylindrical Drift Chamber (CDC) has an inner diameter of 150 mm and an outer diameter of 530 mm and the total length is 950 mm. CDC consists of two aluminum end-plates of 20 mm thickness, a 1 mm thick CFRP cylinder as an inner wall, and six aluminum posts which are placed outside a tracking volume. Gold-plated tungsten wires with $30 \mu\text{m}$ ϕ are used for sense wires and gold-plated aluminum wires with $100 \mu\text{m}$ ϕ for guard and field wires. All wires are supported by feedthroughs with a bushing inserted at the end. A tracking volume of CDC is filled with argon(50%)-ethan(50%) mixed gas at 1 atm. CDC has total 15 layers of hexagonal cells with typical drift length of 9mm, which corresponds to 7 super layers (A1 U1 V1 A2 U2 V2 A3). The number of the readout channels is 1816 and the total number of wires is 8064. A high voltage is applied to the field and guard wires and the sense wires are kept

at ground potential. The read-out electronics consist of an amplifier-shaper-discriminator (ASD), LVDS-ECL converter and a time-to-digital converter (TDC).

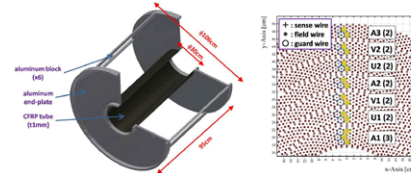


Fig. 2. A schematic view of the Cylindrical Drift Chamber (CDC). A left panel shows a frame structure of the CDC, and a right panel shows a cell configuration of the CDC.

3 Performance test of CDC

The development of the CDC, including read-out electronics, have been completed in mid-2009, and the commissioning of the CDC started at the J-PARC K1.8BR experimental area. Fig 3 shows a result of the cosmic ray test, together with results of simulations, assuming the intrinsic resolution of 150, 200 and 250 μm . By comparing with the results of simulations, the intrinsic resolution of 200 μm was achieved for straight tracks.

In March 2010, the excitation test of the solenoid magnet will be done, and the performance test of CDC in the magnetic field will start.

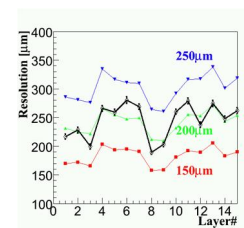


Fig. 3. Layer dependence of the CDC resolution. The black line shows a measured resolution from cosmic ray test. The red, green and blue lines corresponds to results of simulations, assuming intrinsic resolution of 150, 200 and 250 μm , respectively.

^{*1} Department of Physics, Kyoto University, Japan
^{*2} Department of Physics, The University of Tokyo, Japan
^{*3} RIKEN Nishina Center, RIKEN, Japan
^{*4} Department of Physics, Tokyo Institute of Technology, Japan

References

- 1) M. Iwasaki *et al.*, Proposal to the J-PARC 50 GeV Proton Synchrotron.

Development of a Hadron Blind Detector for the J-PARC E16 Experiment

K. Aoki, for the J-PARC E16 Collaboration

[HBD, GEM, Cherenkov detector, chiral symmetry, mass modification, vector meson]

1 Introduction

The J-PARC E16 experiment^{1,2)} was proposed to investigate the origin of hadron mass through the mass modification of vector mesons in nuclei. The vector mesons (ρ , ω , and ϕ) are produced in p+A reactions and the mass is reconstructed by using the e^+e^- decay. A Cherenkov detector with a large acceptance and fine segmentation is required for electron identification. The Hadron Blind Detector (HBD)³⁾, which is a mirrorless and windowless Cherenkov detector, is ideal for the purpose. It was originally developed for the PHENIX experiment.

The HBD is a box containing pure CF_4 , and the inner bottom surface is covered with photocathodes sensitive to Cherenkov light. A photocathode consists of a stack of Gas Electron Multipliers (GEMs) on top of which CsI is evaporated. CF_4 functions as an amplification gas and a Cherenkov radiator. The water and oxygen contamination levels should be kept at ~ 10 ppm since they absorb vacuum ultraviolet light, which is of interest. CsI is a deliquescent material.

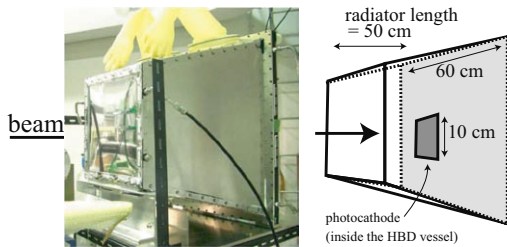


Fig. 1. Photograph of the HBD prototype for J-PARC E16.

2 HBD prototype for J-PARC E16

We have developed a prototype of the HBD for the J-PARC E16 experiment. Figure 1 shows a photograph of the prototype. The vessel has approximately the same size as a module of the planned detector, which consists of 26 modules. The length of the radiator is 50 cm. Figure 2 displays the photocathode that partially covers the inner bottom surface of the vessel. ^{a)} It is constructed with two layers of LCP-GEMs with a thickness of $100 \mu\text{m}$ with CsI on top of the layers. The Cherenkov photons are converted into photoelectrons by CsI. The photoelectrons are amplified

^{a)} In Fig. 1, the beam direction is left to right, while in Fig. 2, the direction is from top to bottom.

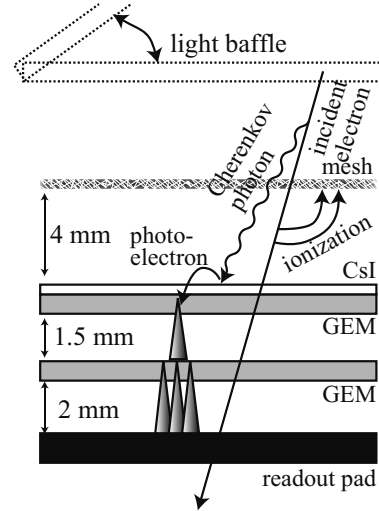


Fig. 2. Photocathode of the HBD prototype.

by the two layers of GEMs, and the amplified signal is then read out using the pads. A mesh is placed over the top GEM to manipulate the electric field above the top GEM. When a reverse bias field is applied between the mesh and the top GEM, electrons from energy loss (dE/dx) are mostly swept out while photoelectrons are not. Therefore, the HBD is sensitive to photoelectrons. The pad is hexagonally shaped and the radius of the circle circumscribing it is 16.9 mm, which is roughly equal to the size of a Cherenkov blob. The use of a thicker GEM leads to a larger gain (~ 500 with $400 \text{ V}/50 \mu\text{m}$) in the first stage and larger tolerance to sparks, unlike the regular $50 \mu\text{m}$ kapton-GEMs (~ 10 with $500 \text{ V}/50 \mu\text{m}$) used for the PHENIX experiment. A large gain in the first stage is important to obtain a sufficiently larger signal from Cherenkov photons than that from energy loss between the first and second GEMs.

A light baffle (an aluminum plate) was prepared to cover the photocathode to shield the Cherenkov photons. Therefore, the difference in the results obtained with and without the baffle would provide direct evidence of Cherenkov radiation.

The number of photoelectrons measured with the PHENIX HBD is ~ 22 . Although there are differences between the prototype and the PHENIX HBD, e.g., in the thickness of the GEM and the spacing between the GEMs, the differences are expected to be insensitive to the number of photoelectrons. A rejection factor of 100 can be achieved with a threshold at ~ 16 electrons.

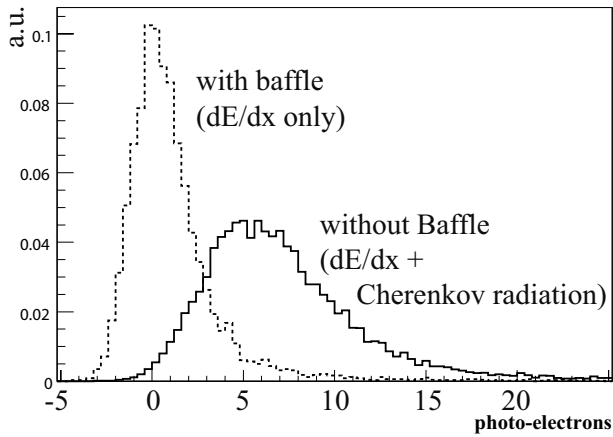


Fig. 3. Observed charge distribution with the baffle (dashed line) and without the baffle (solid line). The difference between these two distributions provides direct evidence of Cherenkov radiation.

3 Beam test

A beam test was performed using a positron beam with a momentum of 670 MeV/c at the Research Center for Electron Photon Science, at Tohoku University, in December 2009. The HBD was sandwiched between scintillators to confine the triggered incident electrons to an area of 1 cm \times 1 cm, which was small enough for the incident positron to hit a particular pad. Therefore, the target pad and six neighboring pads were read out and the values were summed to obtain the Cherenkov signal. The water contamination level was \sim 60 ppm and the oxygen contamination level was \sim 30 ppm. The contaminants were expected to absorb \sim 30 % of the Cherenkov photons.

Figure 3 shows the distribution of charge summed over seven pads, which were expected to be larger than the Cherenkov blob from triggered positrons. A reverse bias of 20 V/4 mm was applied. It is evident that the prototype successfully detect Cherenkov radiation from the positron beam. The number of photoelectrons was five or six. The prototype is the first to be made in Japan and can clearly detect Cherenkov radiation. However, it is not enough to achieve a rejection factor of 100 while keeping reasonable efficiency.

4 Discussions on improvement

The loss of 30% of Cherenkov photons is due to absorption by residual water vapor and oxygen. Therefore, in principle, the loss can be reduced by eliminating the contamination, and such an improvement is practically possible. However, it is difficult to achieve a contamination level of 10 ppm level for water in a short test experiment since materials absorb water vapor and hold it for a long time. It takes more than a month to achieve a level of \sim 10 ppm with dry gas flow

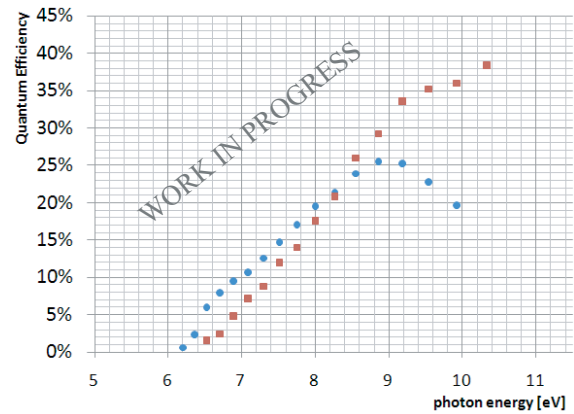


Fig. 4. Quantum efficiency vs photon energy for the prototype (circle) and the PHENIX HBD⁴⁾ (box)

and this is not possible in a short test experiment. In addition, a large amount of gas is needed. Therefore, a gas circulation system are required. Such a system is being developed for the E16 experiment.

To qualitatively understand the number of photoelectrons, the quantum efficiency (QE) of the photocathode is determined. The results are displayed in Fig. 4. Although CF₄ is transparent to photons up to 11.5 eV, it is difficult to measure the QE above an energy of 10 eV (120 nm). Therefore, extrapolation is needed to calculate the number of expected photoelectrons, which leads to a large systematic uncertainty. As far as the measured energy range is concerned, a difference in energy dependence is seen above 9 eV. This indicates that there is room for improving the QE of the prototype. A study is currently underway to determine the reason for the difference.

5 Summary

We have built a prototype of the HBD for the J-PARC E16 experiment. The prototype successfully detected Cherenkov radiation, and the number of photoelectrons was five or six. The QE of the photocathode was also measured and compared with that of the PHENIX HBD photocathode. A difference was seen in the energy dependence of the QE above 9 eV, and is the reason for this difference is currently being investigated. Improvement from QE and gas purity is expected.

References

- 1) S. Yokkaichi et al.: RIKEN Accel. Prog. Rep., this volume.
- 2) <http://rarfaxp.riken.go.jp/~yokkaich/paper/jparc-proposal-0604.pdf>
- 3) A. Kozlov et al.: Nucl. Instrum. Meth. **A 523**, 345 (2004).
- 4) B. Azmoun et al.: IEEE Trans. Nucl. Sci. **56**, 1544 (2009).

Design and Construction of Station-3 Drift Chamber for FNAL-E906 Experiment [†]

K. Nakano, Y. Goto, Y. Miyachi,^{*1} S. Miyasaka^{*2},
S. Mizugashira^{*2}, S. Sawada^{*3}, T.-A. Shibata^{*2}, and A. Taketani

1 Introduction

E906/SeaQuest is a fixed-target experiment for which preparations are being made at Fermilab, USA. In this experiment, a 120-GeV proton beam extracted from the Fermilab Main Injector is used to measure the cross section of the Drell-Yan process, $q\bar{q} \rightarrow \gamma^* \rightarrow \mu^+\mu^-$, in proton-nucleon reactions by detecting the final-state muon pair. The main goal of this experiment is to investigate the flavor asymmetry of the sea quarks (\bar{u} and \bar{d}) in protons¹⁾. In particular, we focus on the asymmetry of sea quarks at a large x_{Bj} ($\gtrsim 0.25$), where x_{Bj} is the fraction of the momentum carried by the scattered quarks.

The E906 detector should be capable of not only detecting the muon pairs produced in the Drell-Yan process but also eliminating the huge number of low-momentum charged particles, particularly the muons formed in the reaction $p + N \rightarrow \pi^\pm + X \rightarrow \mu^\pm + X'$. Figure 1 shows the E906 detector setup, where the proton beam comes from the left-hand side. The target used is liquid hydrogen or liquid deuterium stored in a cryogenic target cell. A focusing magnet labeled as “F Mag” in Fig. 1 condenses signal muons into the detector acceptance cone and sweeps out low-momentum background muons. A large iron block placed inside the focusing magnet acts as a hadron absorber and a beam dump. Stations 1, 2 and 3 are multi layer drift chambers (DCs). At these stations, the positions of the passing muons are detected, and the tracks and momenta of the muons are reconstructed with an analyzing magnet labeled as “K Mag” in Fig. 1; this magnet deflects the muons in the horizontal direction. Station 4 comprises alternate layers of drift tubes and iron absorbers. It identifies high-momentum muons by selecting the particles that penetrate the absorbers to a sufficient depth. Each station has one or two hodoscopes for triggering muon-pair events.

The proton beam becomes available in October 2010. Data will be recorded intermittently over a period of three years. We, the E906 Japanese group, take charge of the construction and operation of Station 3. This article reports the design and construction of a new drift chamber for Station 3.

2 Performance Requirements

To optimize the position and size of all the detectors, the expected signal statistics for various detector settings have been evaluated using a Monte Carlo program. The optimal conditions are as follows. Station 3 positioned 19 m away from the target, and the size of the acceptance of Station 3 is 3.2 m in the vertical direction and 2.2 m in the horizontal direction. The position resolution required at Station 3 is less than 400 μm . The expected background rate has been evaluated using the GEANT detector simulator²⁾. It is at maximum 5 kHz/cm² at Station 3; hence, at this station, the DC is required to detect muons up to this rate without loss of detection efficiency and gas amplification gain.

The DC at Station 3 consists of six layers called U, U', X, X', V and V'. For precise measurement of the muon track position in the bending (horizontal) direction, all the wires are aligned vertically, while U^(') and V^(') are tilted by 14°. A mixture of argon and ethane (50:50) is used because it is a standard gas mixture commonly used for other drift chambers.

3 Design

First, the entire structure of Station 3 is examined. Because the size of the Station 3 acceptance cone (3.2 m \times 2.2 m) is large, we decided to divide this station into two parts so that the design and construction could be completed within a given period (1.5 years).

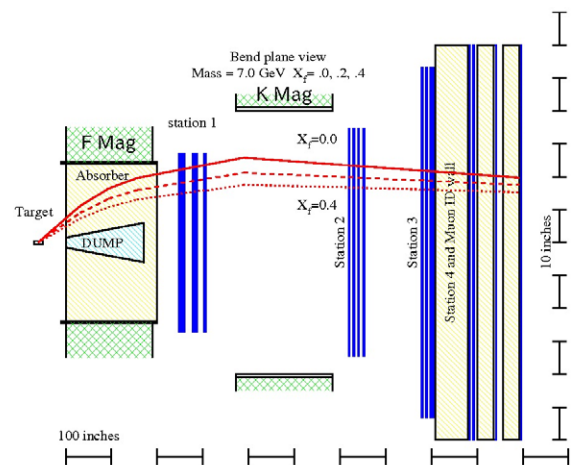


Fig. 1. Schematic of detector setup (top view).

^{*1} Yamagata University

^{*2} Tokyo Institute of Technology

^{*3} KEK

The top half is covered by the new DC that we constructed, and the bottom half is covered by the existing DC at Fermilab. In this configuration, the frame of the two chambers occupy a part of the Station 3 acceptance. We have confirmed that multiple scatterings of muons in the frame material are sufficiently small to satisfy the required momentum resolution.

On the basis of studies that will be described later, we adopted the cell structure shown in Fig. 2. The supposed HV values are -2.8 kV for the field and cathode wires and -1.4 kV for the guard wires. The gas amplification gain is expected to be $\mathcal{O}(10^5)$, as decided by studies performed using the Garfield gas-detector simulator³⁾. Two layers such as X and X' are staggered to one-half of their cell width so that the left-right ambiguity in the drift direction is eliminated. Since the HV values are common to all cathode wires, the two layers can share a cathode-wire plane so that the total number of wires and the amount of frame material used are reduced. The number of sense wires, and thus readout channels, is 768, and the number of field and guard wires is 4368.

Figure 3 shows the paths and contour lines of electron drift in one cell. Because the E -field strength is so adjusted that the electron drift velocity is almost constant (saturated), the drift length becomes proportional to the drift time. The drift-time deviation has also been evaluated using Garfield; it is ~ 2 ns or $100 \mu\text{m}$ (for a drift velocity of $50 \mu\text{m}/\text{ns}$), including the

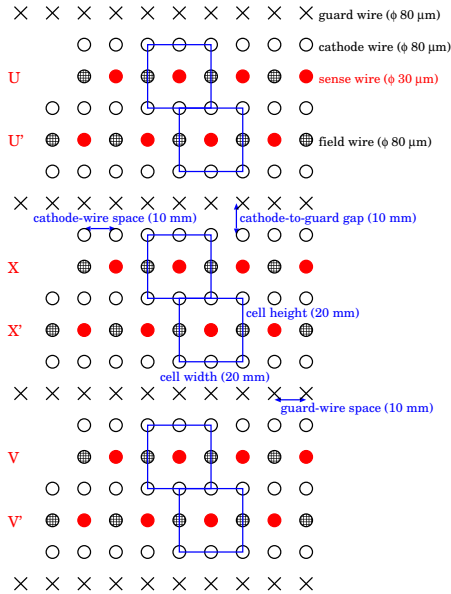


Fig. 2. Cell structure of new drift chamber for Station 3. X and X' wires run perpendicular to the plane of this paper, and U, U', V and V' wires are tilted by 14° . The distance between neighboring tilted wires is $10 \cos(14^\circ) = 9.7$ mm. Blue boxes represent unit drift cells.

effect of electron diffusion, which is well below the required overall position resolution of $400 \mu\text{m}$.

4 Construction

The drift chamber design was finalized in July 2009. Immediately after, construction work was commenced in Japan. The frame was completed by the end of September. All the wires were placed in late November, and the Mylar windows were closed. Figure 4 shows an image of the Station 3 DC recorded in January 2010. The argon-ethane mixture is flowed in order to perform various basic tests before the DC is transported to Fermilab. The DC will be installed in the experimental hall in July 2010, and tested with the first proton beam in October.

References

- 1) J. Arrington *et al.*, Proposal of E906 Experiment, <http://www.phy.anl.gov/mep/drell-yan/proposals/>.
- 2) CERNLIB Webpage, <http://cernlib.web.cern.ch/cernlib/>
- 3) CERNLIB Webpage, <http://garfield.web.cern.ch/garfield/>

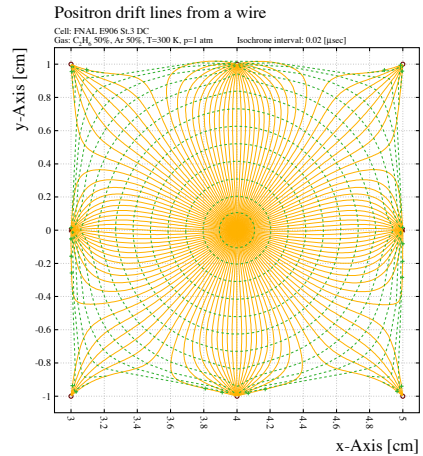


Fig. 3. Paths and contour lines of electron drift simulated with Garfield for X cell. This figure shows the unit cell for X, i.e., a sense wire is at the center and is surrounded by eight field/cathode wires.



Fig. 4. Photograph of new drift chamber for Station 3.

Computing and Network Environment at RIKEN Nishina Center

T. Ichihara, Y. Watanabe, and H. Baba

We have been operating Linux/Unix NIS/NFS cluster systems^{1,2)} at the RIKEN Nishina Center. The major part of the systems is installed in the 1F server room of the RIBF building that is equipped with emergency power supply and UPS systems, which ensure the non-stop operation of the computing system, even during power outages.

Figure 1 shows the current configuration of the Linux/Unix servers at the Nishina Center. We are adopting Scientific Linux³⁾ as the primary operating system; this operating system has been developed at the Fermi National Laboratory and is widely used at accelerator research facilities worldwide and by the nuclear physics and high-energy physics communities.

The host *RIBF* is used as the mail server, NFS server of the user home directory `/rarf/u/`, and NIS master server. Approximately 500 user accounts are registered on this server. fibre channel RAIDs with capacities of 10 TB and 5.6 TB with fibre channel hard disk drives `/rarf/w/` and `/rarf/d/` are connected to the *RIBF-DATA01* server for data analysis and raw data storage for the RIBF experiment. The host *RIBF00* is used as an ssh login server to provide access to users from the outside the Nishina Center; it is also used as a general-purpose computational server, printer server, and a gateway to the RIBF intranet. Public-key authentication is used for ssh login to improve security. New SSL server certificates have been installed in *RIBF* and *RIBFUSER* for secure encrypted communication.

Postfix is used as the mail transport software and Dovecot is used for IMAP and POP services. These software packages enable secure and reliable mail delivery. The hosts *RIBFSMTP1/2* are mail front-end servers, and they are used for tagging spam mails and isolating virus-infected mails. Sophos Email Security and Control (PMX) was installed on these servers in March 2008 and it has been working well and serving the intended purposes. The probability of being identified spam by PMX is approximately 99%.

An anonymous ftp server, *FTP.RIKEN.JP*, is managed and operated at the RIKEN Nishina Center. We have changed the hardware of the server from Sun Fire V40z to HP ProLiant DL380G6 to improve the IO performance. This server is has a speed of 10 Gbps and connected to the Local Area Network (LAN) using the dual-port 10GbE NIC with a PCI express interface. The average network transfer rate of this server is approximately 50 MBps, and it is one of the most heavily loaded server in RIKEN. A 26 TB SATA RAID system with quad-port 8 Gbps Fibre Channel interface has been added to this server. Major Linux distributions, which include Scientific Linux, CentOS, Ubuntu, Fe-

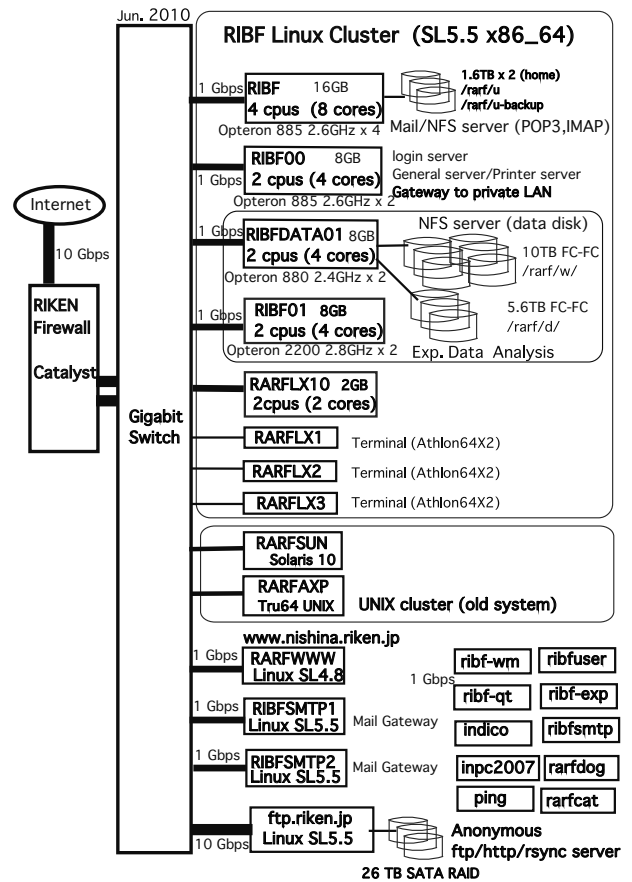


Fig. 1. Configuration of RIBF Linux cluster.

dora, Debian, OpenSUSE, Mandrake, Slackware, and Vine are mirrored daily at the ftp server for the convenience of the facilitating high-speed access to their users. Archives on the server are available via anonymous ftp, http, and rsync protocols.

The development of the RIBF Data Acquisition system (DAQ) is described elsewhere.⁴⁾

Most of the users of the Nishina Center have e-mail addresses of one of the following forms:

`username@ribf.riken.jp` and `username@riken.jp`.

The former represents an e-mail address of the mail server (*RIBF*) of the RIKEN Nishina Center, while the latter represents an e-mail address of the mail server (*POSTMAN*) of the RIKEN Advanced Center for Computing and Communication.

References

- 1) <http://ribf.riken.jp/>
- 2) T. Ichihara et al.: RIKEN Accel. Prog. Rep. 42, 198 (2009).
- 3) <https://www.scientificlinux.org/>
- 4) H. Baba et al.: In this report.

Time-Stamping System for RIBF experiments

H. Baba, T. Ichihara, T. Ohnishi, S. Takeuchi, K. Yoshida, Y. Watanabe, S. Ota,*¹ and S. Shimoura*¹

The development of time-stamp-based data acquisition (DAQ) systems is currently in progress at several accelerator facilities^{1,2)}. Today, time-stamping systems become one of the basic requirements in nuclear-physics experiments. They are required for complex triggering measurement and they facilitate the inter-connection between different DAQ systems. Here, we report the newly developed time-stamping system for RIBF experiments.

In this system, 48-bits-deep time stamps with a precision of 10 ns (100 MHz) are used. This time specification corresponds to a period of one month, which is sufficient to perform a series of experiments. The time-stamping system is installed in each sub-DAQ system, and all data are stored together with the time-stamp information. Once the data is stored, the data of the required events can be extracted in accordance with the coincidence condition. This facilitates the coincident measurement with individual triggers using several DAQ systems.

The configuration of the time-stamping DAQ system is shown in Fig. 1. The clock signal is transmitted to each sub-DAQ system. According to its trigger, each sub-DAQ accumulates data. The time-stamp-based event builder, which is newly developed, constructs complete event by using separately stored data obtained from each sub-DAQ system. Its coincidence condition is programmable. This time-stamping system is constructed by modifying the existing RIBF DAQ³⁾ system so that includes time-stamp information. The seamless integration of the individual trigger system and the common trigger system is achieved.

In order to manage the time-tamp information, Logic Unit for Programmable Operation (LUPO) modules are developed one with CAMAC and another with VME form. A LUPO module is a simple logic module based on Field Programmable Gate Array (FPGA) for general purposes. A user can implement customized circuits on the FPGA for functions other than the time stamping function, for example, for the input register, output register, interrupt register, coincidence register, scaler, rate divider, and gate and delay generator. Figures 2 and 3 show photographs of CAMAC LUPO and VME LUPO, respectively. The main components and specifications are listed below.

- Components

- User FPGA
- CAMAC/VME interface CPLD
- 50-MHz crystal oscillator
- 8 LED

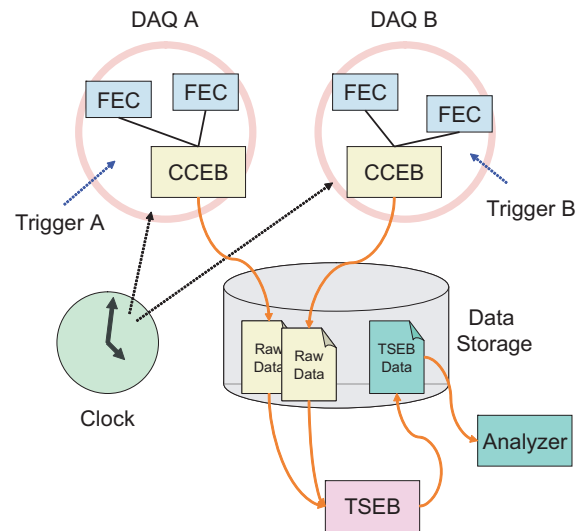


Fig. 1. The configuration of the time-stamp-based DAQ system. CCEB is the common trigger + common dead-time-based event builder. FEC is the front-end computer for CAMAC/VME. Details on CCEB and FEC are given in Ref 1. TSEB is the time-stamp-based event builder.

- 4 NIM inputs
- 4 NIM outputs
- 34-pin MIL connector for LVDS I/O and LVTTL I/O

- FPGA Specification

- Xilinx Spartan 3E (XC3S500E)
- 500-K system gate
- 73-Kbits distribute-RAM
- 350-Kbits block-RAM
- 4 digital clock managers (including DLL)

CPLD is installed as a interface for the CAMAC and VME buses to simplify the communication protocols. Because of this interface, the FPGA circuit can be constructed without taking into consideration the differences between CAMAC and VME. A 34-pin MIL connector is used for 16 LVDS I/O and 32 LVTTL I/O. The LVDS and LVTTL are selected on the basis of FPGA constraints. The FPGA has 4 digital clock managers including a delay-lock-loop (DLL) circuit. The DLL provides the functions of the clock-skew elimination and the frequency synthesis.

The time-stamping function is implemented on LUPO. The block diagram of the time-stamping circuit is shown in Fig. 4. The DLL circuit generates a 100-MHz clock signal from a 25-MHz external clock or a 50-MHz internal oscillator. Even if the internal

*¹ Center for Nuclear Study, University of Tokyo

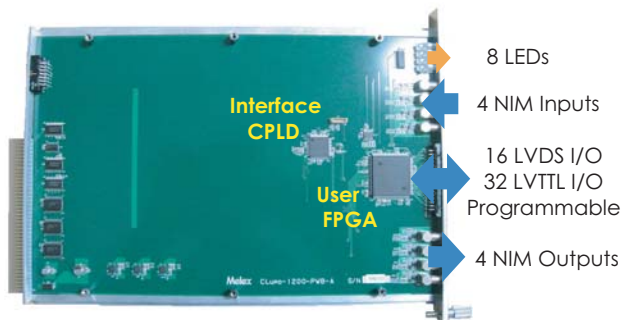


Fig. 2. CAMAC version of LUPU.

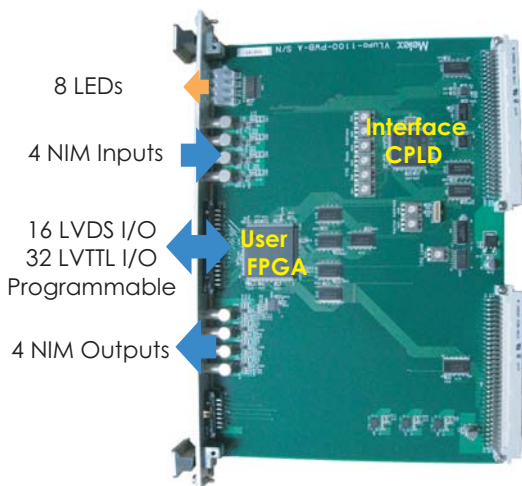


Fig. 3. VME version of LUPU.

oscillator is capable of achieving a frequency accuracy on the order of 10^{-6} , the clock-count difference between different modules will be 100 counts within 1 second. In order to obtain measurements that are coincident to within 10 ns, an external clock should be used to synchronize the modules. Usually a 25-MHz external clock is used to transmit the clock signal to generic NIM circuits; however, if the bandwidth of the transfer path is sufficiently high, a 100-MHz external clock without DLL can be used. Using the trigger signal, the counter value is determined and stored in the FIFO memory. The FIFO is constructed with built-in FPGA block RAM, and can store upto 1024 time stamps with 48-bits-deep. A clear signal is used as a timing reference, and it resets the counter value to 0. For the timing synchronization, two signal lines for the external clock and for the clear signal are required. The selection of the internal and external clock can be switched by a CAMAC/VME command.

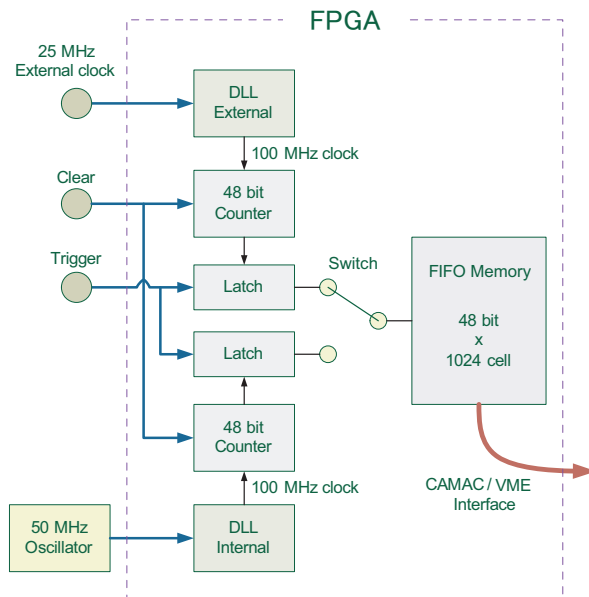


Fig. 4. The block diagram of the time-stamping circuit which is implemented in FPGA.

The developed time-stamping system was used in experiments held in November and December 2009. One of the experiments was for the measurement of the $(t, {}^3\text{He})$ transfer reaction⁴⁾ using the SHARAQ spectrometer. The other experiment was the β -decay measurement using the ZeroDegree spectrometer. These two experiments showed that the time-stamping system is very useful. This system is expected to be used in various experiments at RIBF in the future.

References

- 1) G. Wittwer et al.: 14th IEEE-NPSS Real Time Conference 2005.
- 2) P. Moritz: GSI Scientific Report, 64 (2006).
- 3) H. Baba et al.: RIKEN Accel. Prog. Rep. **41**, 155 (2008).
H. Baba et al.: IEEE Nuclear Science Symposium Conference Record 2008, 1384 (2008).
- 4) K. Miki et al.: in this report.

Development of data acquisition system for short-time decay by using Flash ADC

K. Morimoto, D. Kaji, H. Baba and F. Tokanai*¹

[GARIS, short life decay, DAQ, super heavy element, production and decay]

A data acquisition (DAQ) system has been upgraded for super heavy element research performed using the Gas-filled Recoil Ion Separator (GARIS). In order to measure the very short lives (0.1-10 μ s) of α decays and spontaneous fission, an additional signal digitizer has been installed in the original system.

Super heavy elements studied by using GARIS¹⁾ and GARIS-II²⁾, especially in the heaviest region on the nuclear chart, may have a very short life. The original GARIS readout electronics cannot separate sequential decays that occur at intervals shorter than 5 μ s because of the pileup in the shaping amplifier. The shaping time is set at 2.5 μ s in order to maintain good energy resolution. We modified the original readout system by using the Flash ADC (FADC) so that it can be used to detect shorter decay intervals.

Figure 1 shows the configuration of the system. The system consists of the original GARIS readout electronics and the newly added pulse shape acquisition (digitization) part. The original GARIS DAQ system consists of preamplifiers, shaping amplifiers, and peak-sensing ADCs, which are connected to the position-sensitive silicon strip detector (PSD) mounted in the focal plane of the GARIS. The front-side anode of the PSD comprises 16 resistive strips with a pitch of 3.75 mm. The hit position can be determined from the center of gravity of the pulse height in each strip. Preamplifiers and FADC (SIS-3301 100 MHz 14 bit) are added to the readout on the rear side of the PSD. The signal shapes obtained from the rear-side preamplifier are digitized over a period of 20 μ s at 50 ns intervals. The decay energies can be obtained from the pulse height E1 for mother nuclei and E2 for daughter, and the decay time δt can be obtained by analyzing the digitized pulse-shape data. The system can distinguish between two fast sequential decays if the time interval between them is longer than 0.1 μ s.

This system was used in experiments³⁾ to search for a new isotope ²³⁴Bk in the reaction ¹⁹⁷Au(⁴⁰Ar,3n). These experiments were performed by using (1) GARIS + PSD mounted on the focal plane and (2) a combination of GARIS, a gas jet, and MANON⁴⁾. A total of 119 decay chains were observed; all these decay chains were assigned to subsequent decays from ²³⁴Bk. ²¹⁸Ra and ²¹⁴Rn, which have very short life times (15.6 μ s and 0.27 μ s, respectively) were contained in the decay chains. Sequential fast decay of these isotopes was observed in the digitized preamplifier signal. Figure 2

shows an example of α decay of ²¹⁸Ra (E1) and ²¹⁴Rn (E2). The energies and decay times can be clearly seen in the obtained data. Detailed analysis of the system performance is in progress.

References

- 1) K. Morita et al.: Eur. Phys. J. **A21**, 257-263 (2004).
- 2) D. Kaji et al.: RIKEN Accel. Prog. Rep. **42**, 179 (2009).
- 3) D. Kaji et al.: RIKEN Accel. Prog. Rep. **43**, (2010).
- 4) H. Haba et al.: J. Nucl. radiochem. Sci. **8**, 55 (2007).

*¹ Department of Physics, Yamagata University

Signal processing diagram

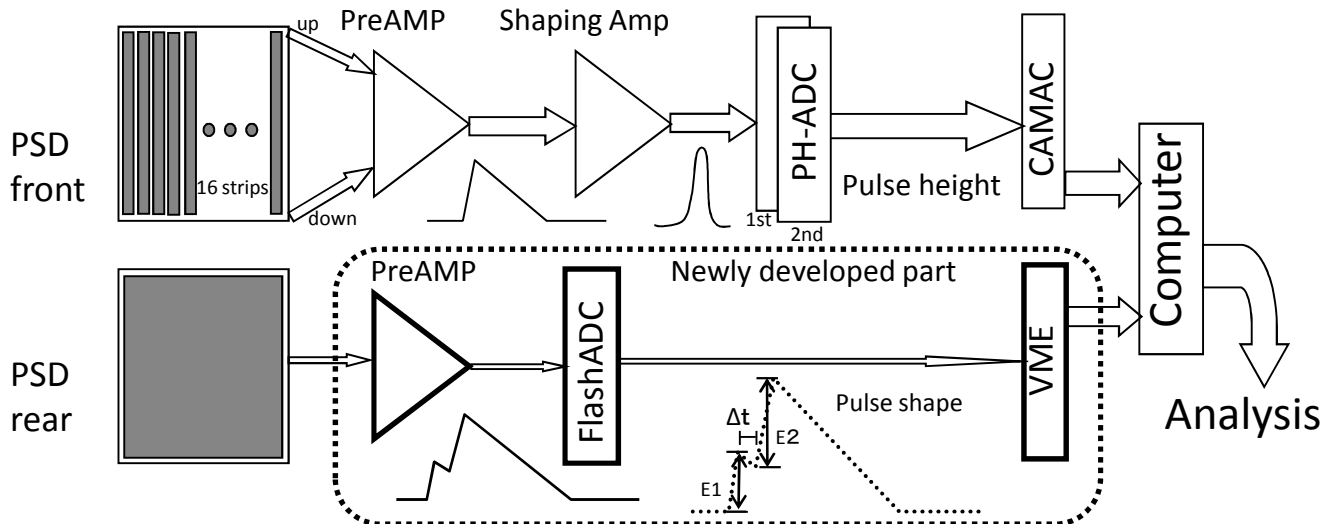


Fig. 1. Signal processing diagram of the newly developed GARIS data acquisition system.

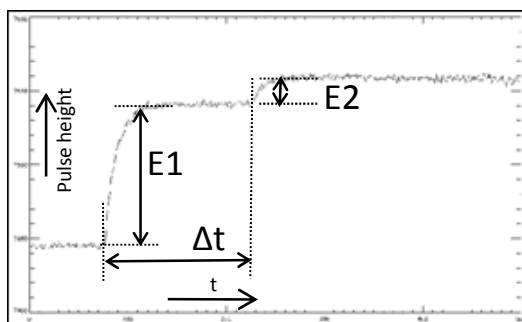


Fig. 2. Preamplifier signal for the sequential α decay of ^{218}Ra and ^{214}Rn

Simple multichannel DAC, ADC, and interface for remote control from multiple computers

M. Wada and P. Schury*¹

[DAC, ADC, Serial Peripheral Interface]

Physics experiments often require control of many devices and measurement of many experimental conditions. For example, in our multireflection time-of-flight mass spectrograph¹⁾, tens of independent high-precision high voltages have to be precisely controlled, and the actual voltages applied to the electrodes should be accurately measured in order to ensure a high performance of the spectrograph. Usually, such data are properly monitored and manipulated by computers by using analog-to-digital converters (ADC) and digital-to-analog converters (DAC) for sophisticated feedback control. We have been using commercial PCI-bus interface cards with an industrial PC running under a real-time Linux operating system as well as National Instruments interface cards which can be conveniently used with LabVIEW software, for our RF ion guide experiments²⁾. However, these commercial interface cards do not always satisfy our demands, especially when we need more input/output channels, lower costs, more compactness, or a higher performance that is better than that of commercially available solutions. Many low-cost discrete chips which can satisfy our experimental requirements, are readily available. Earlier, it was rather complicated to handle bulk chips in actual experiments; however, modern chips have standard interfaces such as Serial Peripheral Interface (SPI), in which all functions are integrated onto a single chip. Evaluation kits of these chips are often available that help us for developments.

Simple DAC, ADC, and isolated SPI distribution cards for general purpose use in experimental devices, which can be connected to host computers via tiny commercial SPI interface cards having ethernet or USB connections were developed in-house. Figure 1 shows a block diagram of the method.

The DAC card has a 32-channel 16-bit DAC chip (AD5372 from Analog Devices) and four 16-pin connectors for direct output. This output range is programmable within ± 10 V by software as well as by the reference voltage. The DAC board is also capable of summing two outputs to form a single output with different gain; this is done by a precision operational amplifier (OPA4117). Therefore, a virtual 23-bit DAC can be used, although its absolute accuracy is limited by the quality of the reference voltage and the noise and temperature dependence of the related circuits. The digital interface of the card is SPI and it requires power supplies of ± 12 V and +5 V.

The ADC card contains a 24-bit Σ - ADC chip (LTC2449 from Linear Technology) with eight differential input channels (or 16 common mode input channels) and a precision reference voltage chip (MAX6350 from Maxim Integrated Circuit). Voltages ranging from -0.3 V to +5.3 V are acceptable for all input pins of the ADC. To measure negative voltage inputs, two instrumentation amplifiers (LT1107 from Linear Technology) are mounted on this card. It also has some peripheral circuits for an on-board temperature sensor and two high voltage dividers. The card has on-board dropper voltage regulators (LM317, LM337) for stable- and low-noise power supplies for the precision ADC chip. During the test measurement of this card, the noise levels for the maximum acquisition period of 120 ms was found to be below $1 \mu\text{V}$ (Fig. 2).

The isolated SPI distribution card (Fig. 3) accepts a single SPI input and 3-bit digital inputs in order to deliver four independent SPI channels, which can be connected to the ADC and DAC cards. Each SPI output channel is electrically isolated by an ISO7241 digital isolator chip from Texas Instruments. In this way, all the DAC or ADC cards can be isolated from each other. Usually, the SPI bus is logically shared by multiple devices, and a CS (Chip Select) signal selects an active device on the bus. In the present design, all signals are gated by CS in order to avoid any noise propagating from the digital signals when other devices are active.

We use two types of interface cards for the SPI in-

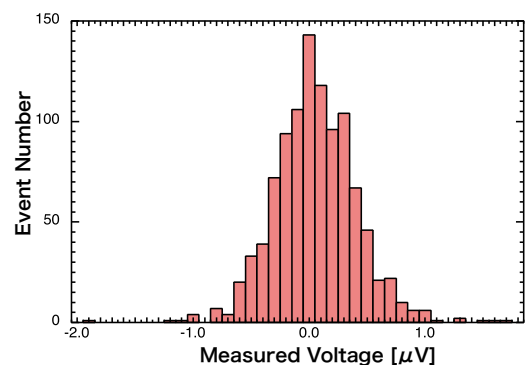


Fig. 2. Histogram of the data measured by LTC2449 ADC when a differential input pair was connected to the ground and the acquisition period was 120 ms. The standard deviation of the noise was deduced to be $0.34 \mu\text{V}$.

*¹ Institute of Physics, Tsukuba University

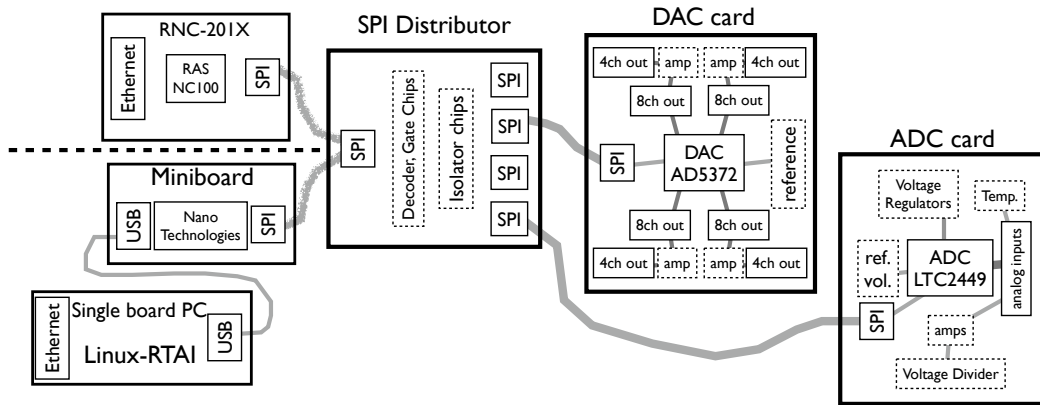


Fig. 1. Block diagram of the DAC, ADC, SPI interface cards, and peripheral devices. The thick boxes indicate in-house developments.

terface to a computer. One is an Ethernet-SPI interface card (RNC-201X from Sysmex-RC), which easily interfaces with a network device. Any host computers using the TCP/IP protocol can communicate with any SPI devices via this card. A simple combination of the DAC card and the RNC-201X acts as a networked multichannel DAC device. A drawback of this interface card is that the network capability is limited by the “protocol-on-a-chip” design. For example, only a single TCP connection is allowed at a time. If multiple host computers intend to connect to a device, it becomes difficult to arbitrate in an efficient manner. Another particular problem faced in the case of the RNC-201X card is that the SPI communication with an analog chip is half-duplex. Many ADC chips such as LTC2449 can be programmed while simultaneously reading the converted data if the SPI communication is full-duplex. Therefore, half-duplex operation could limit the maximum performance of the ADC.

The other SPI interface card we use is a USB-SPI interface card (Miniboard from Nano River Technology). It is a simple USB 1.1 device that can be connected to a variety of computers. The control program using

this USB device is based on the standard open-source library LibUSB and an upper-level Application Programming Interface (API) library written in C++ that is provided by the manufacturer. We can use this USB interface card directly from a host computer; however, we wish to use it as a network device. Therefore, we add one more interface layer between the device and the host computer by including a single-board industrial PC. The PC is operated by a variant of real-time Linux, Linux-RTAI. Using such a standard operating system ensures a versatile network capability.

The real-time Linux operating system has been used in our data-acquisition systems and remote-control systems for many years. Among numerous useful functions of the real-time operating system, we use the *semaphore* function for mutual exclusion of resources for the present purpose. A versatile network server program library described in the Stevens’ textbook³⁾ is used for the device. It permits multiple TCP connections from different processes or from different computers. In such cases, mutual exclusion is essential for hardware devices or critical data in order to avoid conflicts.

The analog interface cards and related commercial interface cards that were developed in-house allow us to build versatile control/monitor setups with very low cost-performance ratios, while building sophisticated feedback systems with relatively less effort. We will initially use these devices with the precision high voltage supplies of our mass spectrograph.

References

- 1) P. Schury et al.: RIKEN Accel. Prog. Rep. **42** 189 (2008).
- 2) K. Okada et al.: Phys. Rev. Lett. **101**, 212502 (2008).
- 3) W. R. Stevens: “Unix Network Programming”, Prentice Hall, New Jersey (1990).

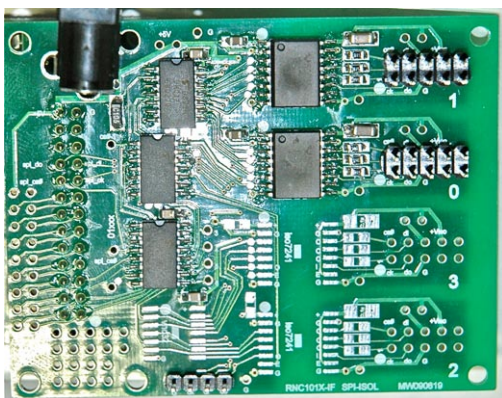


Fig. 3. Isolated SPI distribution card.

Installation of MuTRG-MRG and DCMIF and Confirmation of Stable Operation during Data Acquisition

K.R. Nakamura,^{*1} Y. Fukao, T. Mibe,^{*2} I. Nakagawa, N. Saito,^{*2} A. Taketani,
for the PHENIX MuTr FEE Upgrade Group

[nucleon spin, W-boson, polarized parton distribution, electronics, trigger]

For the study of the sea-quark polarization in a nucleon, measurement of the single-spin asymmetry in W boson production in a 500-GeV polarized proton-proton collision is planned at PHENIX¹⁾. A W boson is identified by the high-momentum muon from the decay. For the efficient detection of W bosons, the read-out electronics of the PHENIX muon tracking chamber (MuTr) must be upgraded so that a new trigger system can be mounted. This trigger system quickly measures the coarse radius of the track curvature by using the MuTr digitalized hit information and selects only the high-momentum track²⁾.

The key components in this upgrade are two back-end electronic devices: a data-merging board (MuTRG-MRG) and an interface board for the data-collection module (MuTRG-DCMIF). MuTRG-MRG receives the MuTr digitalized hit data from the front-end electronic device called amplifier-discriminator-transmission board (MuTRG-ADTX) and transmits reformatted data to Local Level-1 trigger board (LL1). MuTRG-DCMIF, on the other hand, receives the same data that MuTRG-MRG sends to LL1 when a trigger is fired and sends the data to the data-collection module (DCM). MuTRG-MRG also controls the MuTRG-ADTX remotely. The functions and requirements of MuTRG-MRG and MuTRG-DCMIF are described in detail elsewhere³⁾.

For the trigger system, 64 MuTRG-MRG boards and 8 MuTRG-DCMIF boards are necessary. These boards were developed and evaluated during 2007 and 2008⁴⁾, and they passed quality assurance tests at KEK.

During the 2009 RHIC collision period (from Feb to Jun 2009), half the number of MuTRG-MRG and MuTRG-DCMIF boards (32 + 4), corresponding to one half of the MuTr acceptance, were installed. These modules were set with a practical configuration, but it was ensured that the MuTr hit data was not sent to LL1, and data was acquired with the PHENIX DAQ system. In this long-range operation, instability was caused by a few minor errors. After careful investigations, we concluded these errors are mainly due to loose connection between the LAN cables and the connectors. Thus, we plan to improve the stability by replacing these connectors. The slow control system used for MuTRG-ADTX functioned appropriately during the

operation. The data accumulated by MuTRG-MRG and MuTRG-DCMIF were analyzed for evaluating the performance of the trigger system⁵⁾.

The rest of MuTRG-MRG and MuTRG-DCMIF boards were installed during the 2009 RHIC shut-down period. The stable operation of these modules was confirmed with the PHENIX stand-alone DAQ for MuTr. With this installation, the installation of MuTRG-MRG and MuTRG-DCMIF boards was completed. Figure 1 shows the complete setup of the back-end electronics. In addition to this installation, a GUI software for the steady and smooth control of MuTRG-MRG and MuTRG-DCMIF was also developed.

In summary, we have completed the installation of MuTRG-MRG and MuTRG-DCMIF for the new trigger system. These modules are ready for the next 500-GeV proton-proton collision in the RHIC.



Fig. 1. The installed MuTRG-MRG and MuTRG-DCMIF boards.

References

- 1) G. Bunce, N. Saito, J. Soffer, W. Vogelsang: *Ann. Rev. Nucl. Part. Sci.* **50**, 525 (2000).
- 2) I. Nakagawa et al.: *RIKEN Accel. Prog. Rep.* **43** (2010).
- 3) K.R. Nakamura et al.: *RIKEN Accel. Prog. Rep.* **41** (2008).
- 4) T. Mibe et al.: *RIKEN Accel. Prog. Rep.* **42** (2009).
- 5) Y. Fukao et al.: *RIKEN Accel. Prog. Rep.* **43** (2010).

^{*1} Kyoto University, Kitashirakawa-Oiwake, Sakyo, Kyoto, 606-8502, Japan

^{*2} KEK, Tsukuba, Ibaraki, 305-08011, Japan

III. RESEARCH ACTIVITIES II

(Material Science and Biology)

1. Atomic and Solid State Physics (ion)

Single-Event Transient Test Results of Control IC of Point-of-Load DC/DC Converter

Y. Yano^{*1}, N. Ikeda^{*1}, S. Kuboyama^{*1}, H. Ohzono^{*2}, O. Shimada^{*2}, H. Otomo^{*2}, H. Mutoh^{*2}, T. Kambara^{*3}, and M. Kase^{*3}

Recent space systems use high-speed and high-performance electronic devices such as a Micro Processing Unit (MPU) and Field Programmable Gate Array (FPGA). These devices require low-voltage and high-current input. When power is supplied through long wires, their resistance causes a voltage drop at the input of these devices. As a result, the input voltage could be below the specification limit. This problem can be solved by using a Point-of-Load (POL) DC/DC converter, which is installed near these devices. A POL converter consists of a control IC and several components, and the performance of the POL converter depends greatly on the control IC.

Figure 1 shows an example of the output voltage drop in a POL converter; this is due to a Single-Event Transient (SET) at the control IC. An SET is a temporal variation in the output voltage or current of the circuit due to a passage of a heavy ion from deep space through a sensitive device. A large change in voltage or current caused by SET could cause malfunction or data error to the connecting devices. Therefore, we performed heavy-ion irradiation test using the cyclotron at RIKEN to identify which part of the circuit is sensitive to SET. Kr ions were used; energy, Linear Transfer Energy (LET), and range of Kr ion in Si were 977 MeV, 29.2 MeV-cm²/mg and 124 μm, respectively.

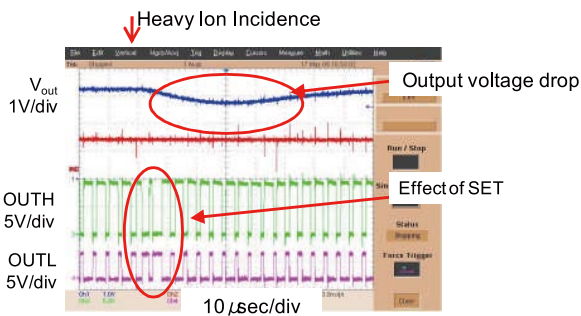


Fig.1 SET observed at the analog block of the control IC during Kr irradiation at RIKEN.

The control IC is composed of several blocks such as analog and logic circuits, shown in Figure 2. We covered a part of the block with a small piece of metal during heavy-ion irradiation. By covering different area and comparing the responses, we can identify the block that is sensitive to SET. SET cross section is calculated as the reciprocal of the average ion fluence in a single SET occurrence. This cross section corresponds to the size of the SET-sensitive area and is a good index that can be used to determine SET sensitivity.

First, we performed irradiation tests to find the most sensitive element in the IC. The result showed that the

smallest SET cross section was observed when the analog block was covered; this indicates that the element contained in the analog block is the most sensitive to SET.

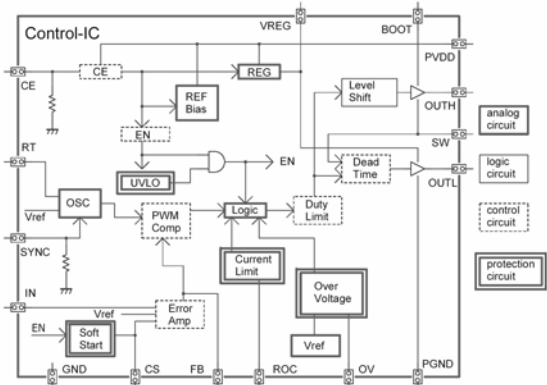


Fig.2 Block diagram of control IC

The cross section of the analog circuit was approximately 1,000 μm² under the irradiation condition for our study. This is a considerably large area, and a MOSFET in the voltage reference circuit (V_{ref}) is the only element that has such a large area. Therefore, we concluded that this MOSFET is the origin of the SET in most cases.

Then we considered how the output voltage drop shown in Figure 1, occurred. V_{ref} is a very important circuit that is connected to various circuits in the IC. Figure 3 shows the SET sensitive circuit in the analog block. We speculated that the process by which V_{ref} affects the output voltage drop is as follows (see Figure 4):

1. A heavy ion strikes the MOSFET in V_{ref}, and the V_{ref} voltage drops (Fig.3).
2. An error amplifier detects a change in the output voltage with reference to V_{ref}. The voltage drop in V_{ref} is also detected as an error, shown in Figure 4 as “V_{ER}”.
3. A Pulse-Width Modulation (PWM) signal is generated by comparing V_{ER} with Oscillator (OSC). Therefore, PWM duty temporarily decreases due to the V_{ER} drop.
4. The output voltage drops as a result of the temporary decrease in PWM duty.

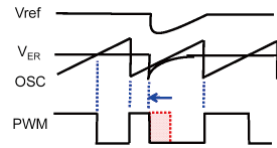
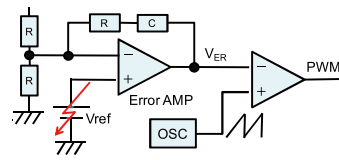


Fig.3 SET-sensitive circuit Fig.4 Effect of SET

We have clarified that the drop in the output voltage occurred in the V_{ref} circuit and that the MOSFET was the most SET-sensitive element. The results were considered for the redesign of the IC to achieve a better SET tolerance.

*1 Japan Aerospace Exploration Agency
 *2 Ryohei Technica Corporation
 *3 RIKEN

Feasibility of RI-beam-based wear analysis for industrial materials

T. Kambara, A. Yoshida, Y. Yanagisawa, N. Fukuda, D. Kameda, T. Kubo, H. Haba, A. Nagano,*¹
and R. Uemoto*¹

Parts of machines such as internal combustion engines are generally exposed to severe conditions such as harsh chemical environments, high temperature, and mechanical friction. Hence, the wear and corrosion of the material determine the reliability and lifetime of the parts. Recently, new materials and surface treatment techniques for such mechanical parts have been developed in industries for achieving better efficiency and safety, low energy consumption, and long product lifetime. For such developments, it is crucial to carry out real-time monitoring of the wear and corrosion of the mechanical parts of machines operating under various conditions. One method of wear analysis involves incorporation of radioisotopes (RIs) in the material and detection of the γ rays emitted from the mechanical parts or the wear particles mixed with the circulating lubricant; the analysis of the γ rays from the mechanical parts helps monitor the degradation of the material. A conventional method to produce RIs in a material involves irradiation of protons from an accelerator to induce nuclear reactions in the material. However, this method requires high-dose irradiation of the proton beam and hence causes radiation damage to the material, and for some elements, RIs with suitably long lifetimes and decay modes cannot be produced by such reactions.

An alternative method has been proposed¹⁾ to overcome this problem; in this method, RI nuclei are incorporated into the material from an external source as an RI beam, instead of activating the nuclei in the material by particle irradiations. In this case, a proper RI nuclide can be selected, irrespective of the composition of the material, and radiation damage is significantly reduced because the number of incident particles is small. The depth profile of the RI distribution can be controlled by controlling the energy of the RI beam.

We evaluated the feasibility of this method at RIKEN by performing an RI implantation experiment at the RIPS to measure the efficiency and depth profile of the implanted RI. We selected ^{22}Na ($T_{1/2} = 2.6$ y) as a tracer nuclide since its lifetime is suitable for wear analysis and it emits γ rays efficiently; ^{22}Na undergoes β^+ decay to afford two 511-keV γ rays, while a 1275-keV γ ray is emitted from the daughter ^{22}Ne .

In this experiment, a 63-MeV/nucleon ^{23}Na beam was accelerated by the RILAC and the RIKEN Ring Cyclotron and was led to the RIPS with a maximum intensity of 300 pA. The primary beam was made incident on a production target, a 1.5-mm-thick Be foil, and the secondary ^{22}Na beam was separated and

guided to the F3 target position. The purity of ^{22}Na in the beam was approximately 85%. At the F3 target position, the RI beam was made to pass through a set of energy degraders with adjustable and fixed thicknesses so that it could be stopped in a test sample, which was a stack of Al foils.

After 14 h of implantation with the primary beam having the maximum intensity, the γ rays emitted from the sample were analyzed using a Ge detector. Figure 1 shows the γ -ray spectrum recorded approximately 4.5 h after the implantation. The measured radioactivity of ^{22}Na was approximately 25 kBq, which corresponded to around 3×10^{12} nuclei in the sample. The yield efficiency of the implanted ^{22}Na was estimated to be around $2.8 \times 10^6/\text{s}$ per 10 pA of the primary ^{23}Na beam. This value was in good agreement with that calculated using the RI-beam production rate and the transportation efficiency of the RIPS. The depth distribution of ^{22}Na , estimated from the radioactivity measured at each Al foil in the stack, ranged between 50 μm and 150 μm , with the maximum at about 100 μm from the surface. The γ -ray spectrum also showed the presence of ^{24}Na ($T_{1/2} = 15$ h), whose radioactivity was 660 Bq; this nuclide was probably produced by nuclear reactions between the Al nuclei in the sample and the ^{22}Na beam.

The present results show that RI-beam implantation with the RIPS is feasible for wear analysis of mechanical parts. Technical and operational improvements must be carried out so that the radioactivity of the implanted ^{22}Na increases to 1 MBq.

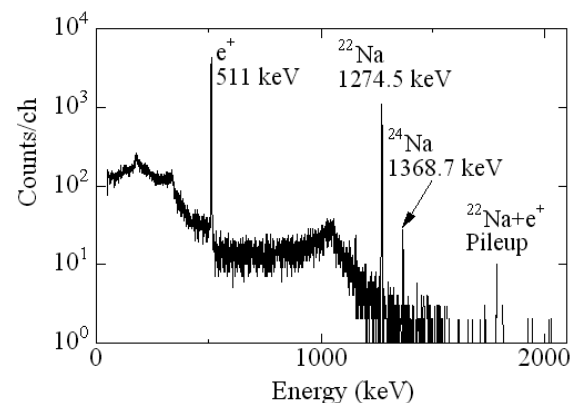


Fig. 1. γ -ray spectrum of the implanted sample.

References

- 1) P. Fehsenfeld, C. Eifrig, and R. Kubat: Nucl. Phys. A **701**, 235c (2002).

*¹ S.H.I. Examination & Inspection, LTD.

In-beam Mössbauer experiment on stress-induced iron diffusion in silicon

K. Suzuki,^{*1} Y. Yoshida,^{*2} Y. Kobayashi, H. Ueno, K. Yukihiro,^{*2} K. Hayakawa,^{*2} M. Mihara,^{*3} W. Sato,^{*4} A. Yoshimi, T. Nagatomo,^{*5} Y. Ichikawa, T. Furukawa,^{*1} T. Inoue,^{*1} Y. Hasama,^{*1} H. Iijima,^{*1} M. Tsuchiya,^{*1} H. Hayashi,^{*1} Y. Ishii,^{*1} T. Nanao,^{*1} and K. Asahi^{*1}

In-beam Mössbauer spectroscopy involving Coulomb-excitation and recoil-implantation techniques has previously been applied to the study of dynamical processes of impurity diffusion in metals and semiconductors^{1, 2)}. The final lattice locations of the probe atoms were determined by observing hyperfine interactions between the nuclear probes and the electrons surrounding them in solids. Furthermore, the jump frequencies corresponding to cage motion of interstitial ⁵⁷Fe in α -Zr¹⁾ and long-range diffusion of interstitial ⁵⁷Fe atoms in Si²⁾ were observed at 50 K and 600 K, respectively. Recently, at the RIKEN RI beam facility, in-beam Mössbauer experiments on ⁵⁷Mn/⁵⁷Fe impurities in silicon have been performed at temperatures up to 1200 K by using nuclear fragmentations and by applying the implantation technique^{3, 4)}. In these experiments, relaxation due to interstitial ⁵⁷Fe jumps and subsequent defect reactions with vacancies that result in the formation of substitutional ⁵⁷Fe atom have been directly observed and compared with a kinetic model that includes defects and the ⁵⁷Fe probes. The purpose of the present experiment is to study stress-induced diffusion of the iron atoms in silicon under an external stress.

An n-type float zone silicon wafer was cut into a rectangular disk of dimensions 20 × 10 × 0.53 mm and was fixed between a pair of ceramic blocks in a tensile testing machine. The tensile testing machine has been developed in order to apply external stresses of up to 20 MPa. By applying a compressive stress along the [011] direction, the Si wafer was bent, and this resulted in a tensile strain on one side of the wafer and compressive strains on the other side. A pulsed ⁴⁰Ar beam with an energy of 4 MeV/u and a period of 1 μ s was obtained from the AVF cyclotron and was transmitted to a thin ⁵⁷Fe target. The ⁵⁷Fe nucleus was Coulomb-excited into the levels at 137 keV, 367 keV, and 707 keV. The 14.4 keV isomers ^{57m}Fe that were populated through the de-excitation of these levels emerged from the target and were implanted into the Si wafer. The Mössbauer spectra of ⁵⁷Fe were acquired at room temperature by using a parallel plate avalanche counter (PPAC) when ^{57m}Fe was implanted in the tensile region.

The Mössbauer spectra obtained for ^{57m}Fe implanted in an n-type FZ-Si sample under external stress are shown in Fig. 1. The spectrum obtained before applying the external

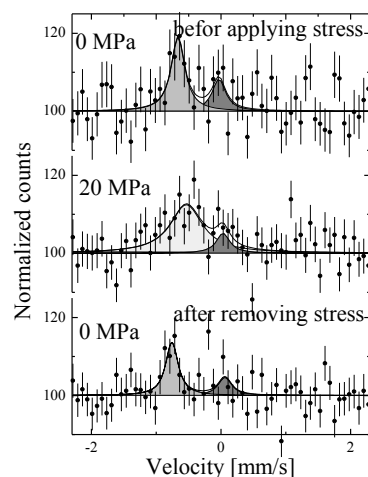


Fig. 1. Mössbauer spectra for isolated ⁵⁷Fe in silicon under the external stress after implantation. The singlet at the left-hand side corresponds to interstitial Fe⁺, and at right-hand side to substitutional Fe.

stress was well fitted by two sets of Lorentz functions representing the substitutional and interstitial Fe⁺, respectively. This spectrum is consistent with the previous result reported by P. Schwarbach²⁾. When an external stress of 20 MPa was applied, the shape of the spectrum changed into one presumably formed by a broad singlet and a sharp singlet. Although the statistical errors are not good enough for finer analyses, line broadening that suggests stress-induced diffusion of ⁵⁷Fe atoms. The diffusion coefficient corresponding to the observed line width is of the order of 10⁻⁹ cm²/s. This result is consistent with our previous results from the transmission Mössbauer experiments,⁵⁾ and the value is larger than that reported for relaxed Si by six orders of magnitude⁶⁾. Furthermore, the peak position of the interstitial line is shifted toward the substitutional line. This phenomenon is explained by motional averaging, which is considered to be due to exchange jumps of the ⁵⁷Fe probes between substitutional and interstitial sites within a time scale of the lifetime of ^{57m}Fe (~100 ns).

References

- 1) Y. Yoshida et al., Phys. Rev. Lett. 61 (1988) 195.
- 2) P. Schwarbach et al., Phys. Rev. Lett. 64 (1990) 1274.
- 3) Y. Yoshida et al., Physica B 376 (2006) 69.
- 4) Y. Yoshida et al., Physica B 401 (2007) 101.
- 5) K. Suzuki et al., Physica B 404 (2009) 4678.
- 6) E. R. Weber, Appl. Phys. A 30 (1983) 1-22.

*1 Tokyo Institute of Technology

*2 Shizuoka Institute of Science and Technology

*3 Osaka University

*4 Kanazawa University

*5 International Christian University

Improvement in sensitivity of sensors for H₂ and toxic-gas detection by using ePTFE irradiated with 5-MeV/nucleon ¹⁴N beam

Y Suzuki, T. Tanaka, T. Kobayashi, K. Takahashi, T. Kambara, F. Saito, *¹ T. Hyodo, *¹ Y. Nagashima, *² K. Okamura, *³ S. Uchikoshi, *³ N. Nakano, *³ A. Iwase, *⁴ D. Mano, *⁵ and Y. Shiga *⁵

Amperometric gas sensors have been widely used for various industrial purposes and in environmental monitoring for the detection of hydrogen, hydrogen sulfide, nitrogen oxides, and some other gases [1]. However, there is a constant demand for gas sensors having a superior sensitivity and selectivity. Expanded polytetrafluoroethylene (ePTFE) are used as electrodes in the sensors. In the present study, we attempted to improve the gas permeability characteristics of the ePTFE using an ion-beam irradiation technique. Ion-beam irradiation through the ePTFE membrane influences the permeability of gases [2]. To investigate the effectiveness of ion-beam irradiation in improving the characteristic of the ePTFE, the sensitivity of sensors for hydrogen and toxic gases were equipped with the ion-beam irradiated membranes was determined. A porous 30 mm square ePTFE electrode with a thickness of 0.2 mm was used. Its pore size was 0.3 μm in diameter and porosity was 34%. The membranes were irradiated with 5-MeV/nucleon N⁷⁺ ions with fluences ranging from 1×10^{12} to 3×10^{13} ions/cm² at room temperature; the N⁷⁺ ions were obtained from the AVF cyclotron. Au ion-plating (BMC800, SHINCRO, Japan) was carried out on the ion-beam irradiated ePTFE membrane surfaces in order to obtain gas-permeable electrodes. The plating rate was 0.1 nm/s under an Ar gas pressure of 2.3×10^{-2} Pa. The thickness of the Au ion layer was about 370 nm.

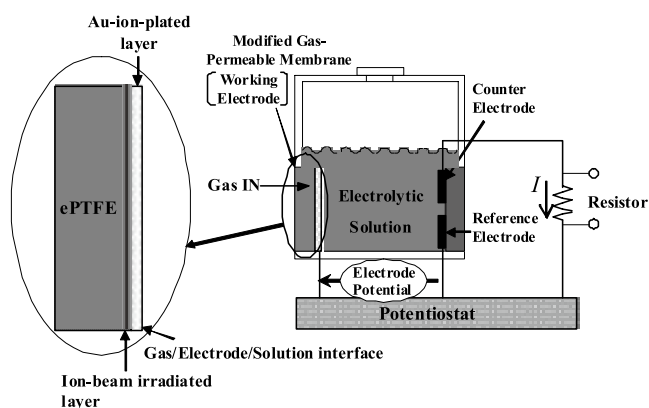


Fig. 1 Schematic diagrams of the electrochemical gas sensor and the ion-beam irradiated gas-permeable electrode.

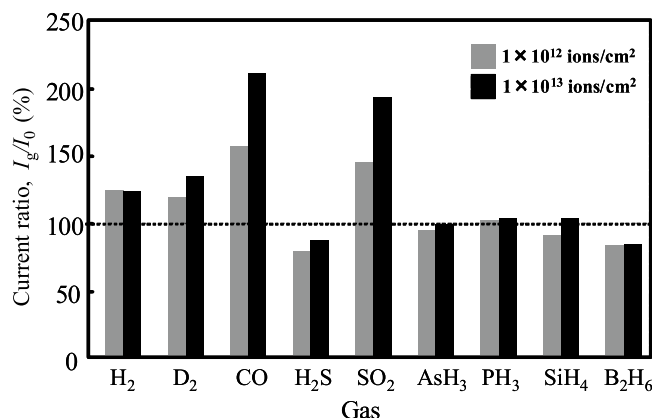


Fig. 2 Characteristic current ratio of ion-beam irradiated ePTFE (I_g) to that of non irradiated ePTFE (I_0) as a function of fluences of ions.

The sensor structure is shown in Fig. 1. The gas-permeable working electrode used was 28 mm in diameter. The counter electrode and the reference electrode were Au-black electrodes, and the electrolyte solution was 9 mol/dm³ H₂SO₄. The applied electrode potential was 50 mV. The flow rate of the sample gas was 0.25 dm³/min. The current-time curves were recorded using a pen recorder and the variation in the current two minutes after the introduction of the gas into the sensor was considered the characteristic current (I_g) for the sample gas. Figure 2 shows the relationship between the current ratio, I_g/I_0 , and the fluences of the ions. I_g and I_0 are the characteristic current of sensors equipped with the ion-beam irradiated ePTFE and that in the sensor equipped with non-irradiated ePTFE for the same gas species, respectively. From the figure, we can observe that the I_g for H₂, D₂, CO, and SO₂ increased with increase in the fluence of ions. The highest value of I_g/I_0 is approximately 212%; this suggests that the N⁷⁺ ion-beam irradiation of the ePTFE membrane is significantly effective in improving the sensitivity of sensors for CO gas detection.

References

- 1) T. Ishiji, T. Iijima, and K. Takahashi: *Denki Kagaku* **64**, 1304 (1996).
- 2) K. Okamura, T. Ishiji, M. Iwaki, Y. Suzuki, and K. Takahashi: *Surface & Coatings Technology* **201**, 8116 (2007).

*¹ University of Tokyo
 *² Tokyo University of Science
 *³ Riken Keiki Co.Ltd.
 *⁴ Osaka Prefecture University
 *⁵ Meiji University

Irradiation-Induced Site Change of Hydrogen in Niobium†

E. Yagi,^{*1} K. Sakuma,^{*2} N. Higami,^{*2} S. Hagiwara,^{*2} K. Mori,^{*2} M. Yoshii,^{*2} S. Koike,^{*3} T. Hayashi,^{*2} and K. Ogiwara

Hydrogen (deuterium)-defect interactions in metals have been important subjects as fundamental properties of hydrogen and also from the technological interest in the fusion reactor materials. On the atomistic state of hydrogen (deuterium) interacting with defects, a number of experiments have been performed on implanted deuterium, because implantation introduces deuterium and lattice defects simultaneously into specimens. As its lattice location, different types of sites displaced from a tetrahedral (*T*) site or an octahedral (*O*) site, which are equilibrium sites for dissolved deuterium, have been reported from channelling experiments and, for the occupancy of such displaced sites, different interpretations have been proposed; trapping of deuterium by vacancies or trapping in an anisotropically distorted lattice induced by implantation. Therefore, the state of deuterium is still in question. For hydrogen (H), recovery of H-doped metals irradiated at low temperatures has been investigated by electrical resistivity and the positron-lifetime measurements, but the lattice location has not been studied, because a channelling method to locate hydrogen was not available despite its usefulness.

Since the behaviour of hydrogen is not necessarily the same as that of deuterium as recognized in the difference of a phase diagram in the metal-H (D) systems, studies on hydrogen are indispensable. Therefore, in the present study, the effect of ion-irradiation on the lattice location of hydrogen dissolved in Nb, NbH_{0.023}, is studied by the channelling method utilizing a nuclear reaction ${}^1\text{H}({}^{11}\text{B}, \alpha)\alpha\alpha$ with a ${}^{11}\text{B}$ beam of about 2 MeV, which has been developed to locate hydrogen dissolved in metals.¹⁾ In this method, hydrogen can be detected by measuring emitted α particles, whose energy ranges from zero to about 5 MeV.

The specimen is a Nb single-crystal. Hydrogen was doped from the gas phase. The channelling analyses were performed at room temperature for $\langle 100 \rangle$, $\langle 110 \rangle$ and $\{100\}$ channels. The yield of ${}^{11}\text{B}$ ions backscattered by Nb atoms and the yield of emitted α particles were measured as a function of the incidence angle ψ (angular profiles) with respect to the channel direction in question by tilting the specimen (angular scan). The irradiation was made at room temperature with ${}^{11}\text{B}^+$ ions of 2.03 MeV up to a dose of about $1.4 \times 10^{16}/\text{cm}^2$ at a dose rate of about $3 \times 10^{11}/(\text{cm}^2 \cdot \text{sec})$ at an angle more than 3.5° off from the channelling direction in question, i.e., in the random direction. This irradiation produces only Frenkel defects in the near surface region shallower than $0.2 \mu\text{m}$, which is probed in the

channelling analysis, because the projected range of incident ${}^{11}\text{B}^+$ ions is $1.35 \mu\text{m}$.

Figure 1 shows the channelling angular profiles obtained after the irradiation. From the comparison with the profiles calculated for 5 different types of sites as in a previous paper,²⁾ the lattice location of hydrogen was determined to be a site displaced from an original *T* site by $0.45\text{--}0.55 \text{ \AA}$ towards its nearest neighbour lattice point (Fig. 2). Taking into account the results of electrical resistivity and positron-lifetime measurements hitherto made on the recovery of electron-irradiated H-doped Nb, it is concluded that this irradiation-induced site change of hydrogen from *T* sites is due to trapping of hydrogen by irradiation-introduced monovacancies. Hydrogen is located at a site displaced from one of the *T* sites attached to a vacancy towards that vacancy. This site is completely different from those proposed for implanted deuterium.

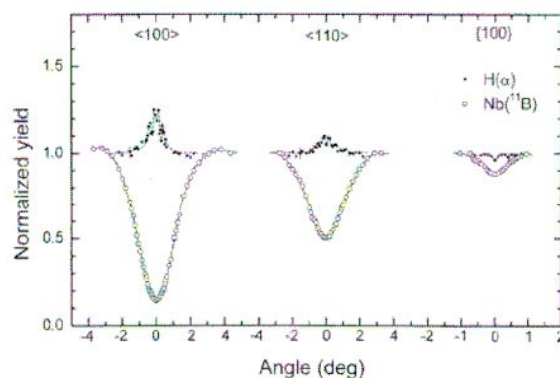


Fig. 1. Channelling angular profiles obtained at room temperature after irradiation with 2.03 MeV ${}^{11}\text{B}^+$ ions up to a dose of $1.4 \times 10^{16}/\text{cm}^2$.

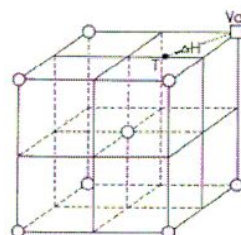


Fig. 2. Atomic configuration of hydrogen trapped by a monovacancy. Hydrogen (Δ) is located at a site displaced from one of the *T* sites (\bullet) attached to a vacancy (\square) by $0.45\text{--}0.55 \text{ \AA}$ towards that vacancy.

References

- 1) E. Yagi, T. Kobayashi, S. Nakamura, Y. Fukai, and K. Watanabe: J. Phys. Soc. Jpn. **52**, 3441 (1983).
- 2) E. Yagi, S. Koike, T. Matsumoto, T. Urai, N. Tajima, and K. Ogiwara: Phys. Rev. B **66**, 024206 (2002).

† Condensed from the article in J. Phys. Soc. Jpn. **77**, 124602 (2008)

*¹ RIKEN and The School of Sci. and Eng., Waseda University

*² The School of Sci. and Eng., Waseda University

*³ Department of Physics, Tokyo University of Science

Simple simulation method for characterization of ion Coulomb crystals in a linear Paul trap

K. Okada,^{*1} M. Wada, T. Takayanagi,^{*1} S. Ohtani,^{*2} H.A. Schessler,^{*3}

[Coulomb crystals, Ca^+ , laser cooling]

Coulomb crystals of laser-cooled ions are being increasingly used in various new research fields, for example in quantum calculations¹⁾ and high precision spectroscopy for the analysis of unstable nuclear ions²⁾. Moreover the sympathetic cooling method by laser cooled ions is suitable for cold ion-molecule chemistry³⁾ and for the spectroscopic analysis of unstable nuclear ions, which cannot be cooled by lasers.

We report a simple and fast method to simulate the observed images of ion Coulomb crystals in a linear Paul trap⁴⁾. In the present simulation, cold elastic collisions between Coulomb crystals and virtually light atoms with a mass of $M_{\text{ion}}/100$ are implemented in a molecular dynamics (MD) simulation code instead of using a radiation pressure force and a heating term such as *velocity kick*^{5,6)}. With such an approach, the *observed* images of Coulomb crystals can be reproduced by introducing a large number of cold collisions (typically 10^6). In actual, density plots of the statistics of existence of each ion are obtained for comparison with the observed ion images. Then, the major properties of Coulomb crystals, such as secular temperature, structure, and the number of ions are determined from CCD images with the help of the simulated images. Such information forms the basis for the aforementioned applications of ion Coulomb crystals.

This simple method is advantageous because the computation time is shorter than that of previous calculation methods⁶⁾. Not all forces are dependent on ion velocities, and hence the velocity Verlet algorithm, which is considerably faster than other algorithms, is used for numerically solving ordinary differential equations.

To demonstrate our simulation method, we determined the number of ions and the ion temperature from a selected CCD image. Figure 1 shows the CCD image of an ion crystal containing 290 Ca^+ ions. The number of ions was determined by comparing the volume of the simulated image to that of the CCD images⁴⁾. On the other hand, the temperature of the crystal was determined by comparing the clarity of simulated images, which were obtained at the assumed equilibrium temperatures. Since many single spots could be seen in the concentric ellipsoidal shells in the observed crystal in Fig. 1 (bottom), the temperature should be less than 7 mK but higher than 5 mK; that

is, the best fit temperature is 6 ± 1 mK. It is to be noted that the ion temperature determined from the CCD image normally gives an upper bound value because of the limited spatial resolution of the imaging optics. However, it is clear that the resolution of the present CCD images is sufficient for detecting temperature differences as small as 1 mK.

References

- 1) J. I. Cirac *et al.*: Phys. Rev. Lett. **74**, 4091 (1995).
- 2) K. Okada *et al.*: Phys. Rev. Lett. **101**, 212502 (2008).
- 3) S. Willitsch *et al.*: Phys. Rev. Lett. **100**, 043203 (2008).
- 4) K. Okada *et al.*: Phys. Rev. A **81**, 013420 (2010).
- 5) K. Okada *et al.*: Phys. Rev. A **75**, 033409 (2007).
- 6) C. B. Zhang *et al.*: Phys. Rev. A **76**, 012719 (2007).

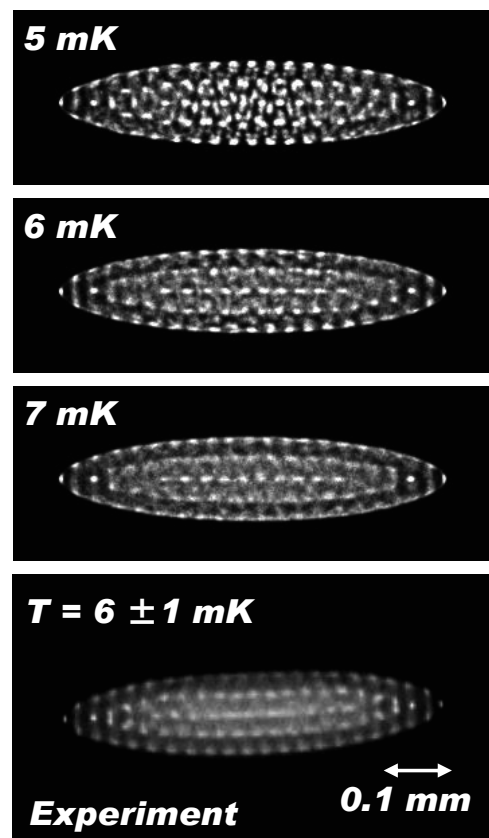


Fig. 1. Experimental (bottom) and simulated (upper) Coulomb crystal images with 290 Ca^+ ions.

^{*1} Department of Physics, Sophia University

^{*2} ILS, University of Electro-Communications

^{*3} Department of Physics, Texas A&M University

Excitation spectrum of Au atoms in superfluid helium

Y. Matsuura,^{*1} T. Furukawa, T. Kobayashi, A. Hatakeyama,^{*3} K. Fujikake,^{*1}
M. Tachikawa,^{*1} and Y. Matsuo

Superfluid helium (He II) is expected to be an effective environment for determining the nuclear spins and moments of short-lived unstable nuclei by using laser spectroscopic method¹⁾. We plan to measure Zeeman splittings and hyperfine structure splittings of atoms with unstable nuclei by the optical pumping and laser-radio frequency/microwave double resonance spectroscopy. Atoms implanted into He II show a blue-shifted and broadened excitation spectrum because of the atomic-bubble effect in He II²⁾. One can take advantage of this property for the optical pumping of a variety of atomic species because it is not necessary to fine-tune the laser frequency. The other advantage of using He II is that highly sensitive optical detection can be achieved since the emitted photons can be completely separated from the laser excitation light on the basis of their wavelength because of the large difference between the emission and excitation wavelengths. So far, we have succeeded in the optical pumping of alkali atoms Cs and Rb³⁾ and a group 11 element, Ag⁴⁾. In order to achieve efficient optical pumping, the wavelength of the laser should be at the peak position of the excitation spectrum in He II. Therefore, the excitation spectrum of Au atoms in He II has to be measured.

The experimental setup is shown in Fig.1. The apparatus consists of a cryostat chamber (Oxford) with quartz windows, an optical detection system, and three lasers. A Au sample is placed 1 cm above the quartz cell ($70 \times 70 \times 70 \text{ mm}^3$) that is filled with He II by transferring liquid he by exploiting the fountain effect.

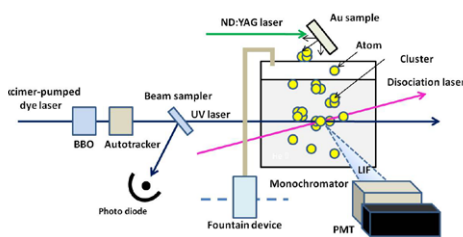


Fig. 1. Experimental setup.

At first, the solid Au sample was sputtered using Nd:YAG laser (wavelength: 532 nm, pulse energy: 3 mJ, repetition rate: 10 Hz, pulse width: 10 ns) to produce Au clusters. Next, the clusters are dissociated into atoms by using a femtosecond laser (wavelength:

800 nm, pulse energy: $150 \mu\text{J}$, repetition rate: 500 Hz, pulse width: 200 fs). The generated atoms are irradiated by a UV laser pulse, which is generated by the frequency doubling of a pulsed dye that is laser pumped by an excimer laser (wavelength: 308 nm, repetition rate: 10 Hz, pulse width: 18 ns); this frequency doubling is achieved using a BBO crystal. We observed laser-induced fluorescence (LIF) by sweeping the wavelength of the UV laser from 254 nm to 265 nm. In order to maintain the phase-matching condition of the frequency-doubling BBO crystal, we installed an autotracker (Inrad, Model: AT-II) along with the BBO crystal. LIF was detected by a photomultiplier tube (PMT) using a monochromator that was set to the Au emission wavelength of 267 nm, which is close to the S-P transition wavelength of Au in free space (267.594 nm). Additionally, we simultaneously monitored the power of the UV laser in order to normalize of the laser power because LIF intensity is proportional to the incident laser power. Figure 2 shows the normalized LIF intensity plotted against the UV-laser wavelength. The maximum excitation wavelength was observed to be around 263.5 nm, with a pulse width of 2 nm. We concluded that the most efficient optical pumping of Au atoms in He II would occur at a wavelength of 263.5 nm. In the near future, we plan to induce atomic polarization of Au atoms and determine their nuclear moments by the optical pumping with the laser of 263.5nm in near future.

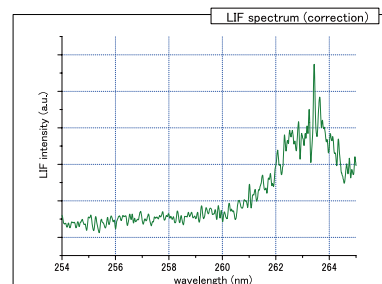


Fig. 2. Excitation spectrum of Au atoms.

References

- 1) T. Furukawa et al.: RIKEN Accel. Prog. Rep. **38**, 99 (2005).
- 2) B. Tabbert, H. Günther, and G. zu Putlitz: J. Low Temp. Phys. **109**, 653 (1997).
- 3) T. Furukawa et al.: Phys. Rev. Lett. **96**, 095301 (2006).
- 4) T. Furukawa et al.: RIKEN Accel. Prog. Rep. **42**, 194 (2009).

^{*1} Department of Physics, Graduate School of Science and Technology, Meiji University

^{*2} Department of Physics, Graduate School of Science and Technology, Tokyo Institute of Technology

^{*3} Institute of Physics, Graduate School of Arts and Sciences, The University of Tokyo

2. Atomic and Solid State Physics (muon)

Installation and beam commissioning of new multi-channel μ SR spectrometer “CHRONUS” and beam commissioning at RIKEN-RAL

D. Tomono, T. Kawamata, Y. Hirayama*¹, M. Iwasaki*¹, I. Watanabe, K. Ishida and T. Matsuzaki

A research project aimed at investigating various types of matters under several extreme conditions, such as high pressure, low temperature and laser irradiation by the μ SR technique¹⁾ has been underway; the high-intensity beam at the RIKEN-RAL muon facility is begin used in this project. In order to further promote the project, the multichannel spectrometer named CHRONUS (multi-CHannel Riken muON Universal Spectrometer) has been newly developed in the Port-4 area; this spectrometer enables us to perform experiments in parallel by dividing the double-pulsed muon beam between Port-2 and Port-4 using kicker magnets. On the basis of a performance feasibility test²⁻⁴⁾, we designed a spectrometer consisting of 606 decay positron counters, a counter mold and frame, fiber light guides, multianode photomultiplier tubes covered with magnetic field shields, and a new data acquisition system.

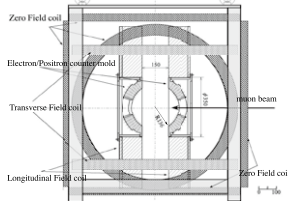


Fig. 1. Schematic illustration of the magnets and counter system in the spectrometer.

Figure 1 shows a vertical view of the spectrometer. All magnets had good homogeneity within a deviation of 0.1%. A pair of large longitudinal field coils were mounted coaxially along with the muon beam, transverse field coils were mounted on the top and bottom, and three pairs of zero-field coils were wound around the sample; all coils were fixed in a square aluminum frame. Fully polarized slow muons were implanted in the sample; the muons stop at specific sites and interact with the local magnetic field while undergoing spin precession at the Larmore frequencies. Since decay positrons are emitted preferentially in the direction of the instantaneous muon spin, an internal magnetic field in the sample can be measured by decay positron counters that are mounted coaxially inside of the bore of the longitudinal field magnet. The time evolution of the asymmetry $A(t)$ is written as

$$A(t) = \frac{N_F(t) - \alpha N_B(t)}{N_F(t) + \alpha N_B(t)},$$

where N_F and N_B are the instantaneous number of muon decays for a total of 303 forward and backward counter assemblies, respectively. The parameter α is a setup-dependent correction factor. The number of

*¹ also Department of Physics, Tokyo Institute of Technology

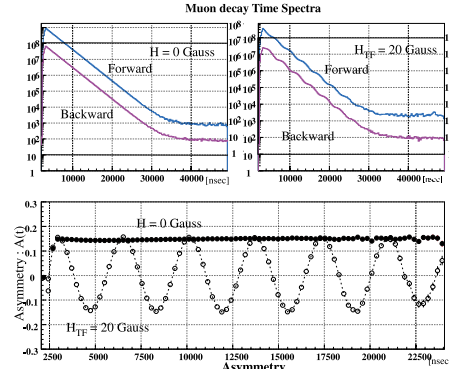


Fig. 2. Top: typical muon decay time spectra for forward and backward counters, as obtained by using a silver target at $H=0$ and $H_{TF}=20$ G; bottom: the corresponding asymmetry spectra for $H=0$ and $H_{TF}=20$ G, represented by closed and open circles, respectively. segments enables us to reduce distortion of the time spectrum caused by pile-up signals. In the period between June and the present, the above mentioned components have been assembled and installed, and a spectrometer has been commissioned using a muon beam. A silver plate with a diameter greater than the beam diameter was mounted at the center of the spectrometer. After an appropriate threshold level was set by the method explained in Ref.^{2,3)}, time spectra were measured under a transverse magnetic field of 20 G and under the zero field.

Figure 2 shows the preliminary time spectra for forward and backward counters as well as the corresponding asymmetry spectra obtained at room temperature. The background level is suppressed to less than 10^{-5} of the number of events at the time zero. The amplitudes of the asymmetry spectra are found to be approximately 15%; these amplitudes are smaller than those expected on the basis of the solid angle of the counters (20%). Further analysis is being carried out to increase the amplitude. In addition, muonium precession was measured using a SiO_2 plate in order to conduct homogeneity test on the Helmholtz coils. An oxygen-free copper target was used along with a helium low cryostat to observe the temperature dependence of the asymmetry spectra down to 5 K. These commissioning data is being analyzed in order to prove that the spectrometer can be used for practical μ SR measurement. A remote control system for various devices is being implemented and the operation of devices such as a cryostat system will begin.

References

- 1) I. Watanabe et al.: *Physica B* **404**, 993(2009).
- 2) Y. Hirayama et al.: *RIKEN Accel. Rep.* **41**, 195(2008).
- 3) D. Tomono et al.: *Nucl. Inst. Meth. A* **600**, 44(2009).
- 4) D. Tomono et al.: *RIKEN Accel. Rep.* **42**, 237(2009).

Data Acquisition System for μ SR Experiment at Port-4 of RIKEN-RAL Muon Facility

T. Kawamata, D. Tomono, I. Watanabe, K. Ishida, and T. Matsuzaki

[μ SR, data acquisition system]

Presently, muon spin rotation/relaxation/resonance (μ SR) experiments are carried out using a spectrometer named “ARGUS” at Port-2 of the RIKEN-RAL Muon Facility. ARGUS is equipped with 192 plastic scintillation counters for recording timing signals from decay positrons/electrons. The obtained signals are digitized by time-to-digital converters (TDCs) and saved as time histograms at each counter by the EXP software running on a Linux personal computer (PC)¹⁾. The data acquisition system (DAQ) used for ARGUS consists of CAMAC modules and MACS-EXP software running on a PC. The dead time of the DAQ is dominated by the low data transfer rate between CAMAC and the PC, because CAMAC and the PC are connected by the old SCSI technique. In μ SR experiments, the software MACS running on a Windows PC controls external conditions such as the temperature and magnetic field of the sample and controls EXP via a communication file. The obtained histogram data are converted to asymmetry data and analyzed using a software WiMDA²⁾ running on a Windows PC.

Recently, we have installed a new spectrometer named “CHRONUS” in Port-4 of the RIKEN-RAL Muon Facility, in order to perform μ SR experiments at a high data acquisition rate; a high-intensity muon beam is used for the experiments. CHRONUS has 606 small plastic scintillation counters to avoid counting losses for multiplex hits. A new DAQ system must be installed in CHRONUS for acquiring and analyzing large amounts of data from the 606 counters.

The hardware configuration of the DAQ system is such that the signals from 606 plastic scintillation counters are converted to digital signals by 38 16-channel VME discriminators (CAEN V895). Then, the digital signals are converted to time information by five 128-channel VME multihit TDCs (CAEN V1190). The data stored in the output buffers of the TDCs are transferred to a Linux PC via a VME-PCI optical link bridge (CAEN V2718). Data transfer can be completed before the next spill because of the high data transfer rate of V2718. Moreover, no beam loss occurs during data transfer because the output buffer of the TDCs can be read out independent of the data acquisition process. Two VME-USB2.0 bridges (CAEN V1718) are used to control the discriminators.

Because many users carry out μ SR experiments, it is necessary that the user interface of the DAQ system is the same as that of the DAQ system of ARGUS, to avoid confusion. Therefore, we replaced only

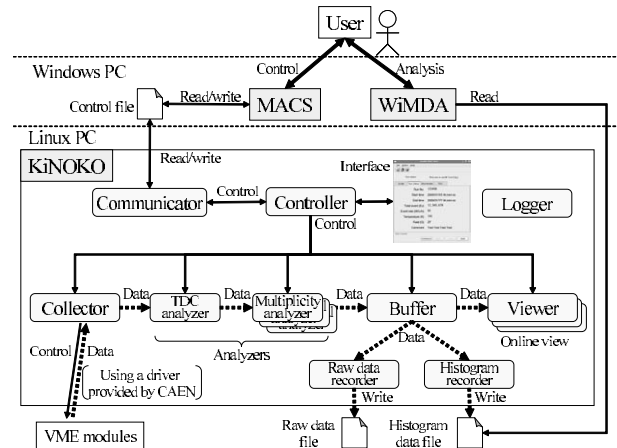


Fig. 1. Diagram showing the relation between the user and the software and processes in the new data acquisition system used for μ SR experiments. The rounded rectangles show the processes managed by the KiNOKO system.

EXP with a new DAQ system, KiNOKO,³⁾ which is a general-purpose DAQ system based on the distributed object technology and written in C++. Basically, the KiNOKO system consists of seven processes; controller, collector, analyzer, buffer, recorder, viewer, and logger. KiNOKO can be customized by the addition, removal, or realignment of these processes and/or customized processes. A customized process is built by the inheritance of the classes prepared by the KiNOKO system. Figure 1 shows the customized Kinoko system used for μ SR experiments. In this system, the raw data acquired by the collector from the TDCs are analyzed by the customized analyzers (TDC analyzer, multiplicity analyzer, etc.) and transferred to the buffer. The viewers and customized recorders (raw data recorder, histogram recorder, etc.) obtain data from the buffer for online display and data storage, respectively. Test experiments reveal that the DAQ system can successfully transfer data without data loss. We plan to add a new process communicator to facilitate remote operations from MACS via a communication file, similar to that used for EXP. We are debugging the communicator at present and are planning to complete the installation of this DAQ system in the near future.

References

- 1) S.N. Nakamura and M. Iwasaki: Nucl. Inst. and Meth. A **388**, 220 (1997).
- 2) F.L. Pratt: Physica B **289-290**, 710 (2000).
- 3) S. Enomoto: “KiNOKO - A General-Purpose Data Acquisition System”, <http://www.awa.tohoku.ac.jp/~sanshiro/kinoko-e/index.html> (28/Jan/2010).

Development of a new Lyman- α laser for generation of ultraslow muons

K. Yokoyama, N. Saito, O. A. Louchev,^{*1} K. Ishida, M. Iwasaki and S. Wada

Development of the high intensity, low energy muon ($LE\text{-}\mu^+$) source is of importance in various fields such as particle, atomic, and condensed matter physics because of its narrow energy spectrum and low temperature. Bakule et al. have been developing a pulsed $LE\text{-}\mu^+$ source at the RIKEN-RAL muon facility in UK by photo-ionizing muonium, and obtained an overall generation efficiency of 3×10^{-5} , generating $\sim 15 \mu^+$ /s, which may not be sufficient for practical uses¹⁾. To improve the yield, it is crucial to develop a high-intensity Lyman- α ($Ly\text{-}\alpha$) laser light (122 nm) for exciting muonium from the 1S to 2P state, before ionization by another UV light at 360 nm. We are currently developing a new $Ly\text{-}\alpha$ laser system that can generate $\sim 100 \mu\text{J}/\text{pulse}$, which is 100 times the energy generated by the existing laser system at RIKEN-RAL.

Since no optical crystals are transparent at the wavelength of the $Ly\text{-}\alpha$ line ($\omega_{Ly\text{-}\alpha}$), nonlinear optical processes in gaseous media have been used to generate vacuum UV light. Here, we use the two-photon resonant four-wave mixing process in Kr gas. As shown in Fig. 1, ω_1 (212.55 nm) excites a Kr atom through the two-photon absorption process, then ω_2 (815~850 nm) generates $\omega_{Ly\text{-}\alpha}$ by difference frequency generation. Since Kr has negative dispersion at $\omega_{Ly\text{-}\alpha}$, it is necessary to add Ar gas, which has positive dispersion at $\omega_{Ly\text{-}\alpha}$, so that the gas mixture satisfies the phase-matching condition. It is known that by this method, relatively high conversion efficiency ($\sim 10^{-4}$) and tunability (121.5~122.2 nm) can be achieved.

To achieve $\omega_{Ly\text{-}\alpha}$ with 100 $\mu\text{J}/\text{pulse}$, it is necessary to generate ω_1 with a pulse energy as high as 100 mJ because the conversion efficiency is proportional to $P_1^2 P_2$, where P_1 and P_2 are the laser power for ω_1 and ω_2 , respectively. For this purpose, we use the Nd:GdVO₄ crystal, which was recently developed by the authors²⁾. This crystal has a gain spectrum centered at 1062.9 nm with ~ 2 nm bandwidth, thus the crystal can be used as a gain medium at 1062.75 nm, for which the fifth-order harmonics is 212.55 nm. Therefore, the crystal is considered as an ideal gain medium for a fundamental wavelength of ω_1 . The seed laser for the fundamental wavelength is a distributed-feedback laser diode (DFB-LD) that gives narrow linewidth (~ 2 GHz),

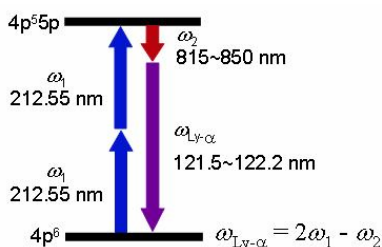


Fig. 1 Energy diagram of four-wave mixing process in Kr.

^{*1} MegaOpto Co., Ltd., Saitama, Japan

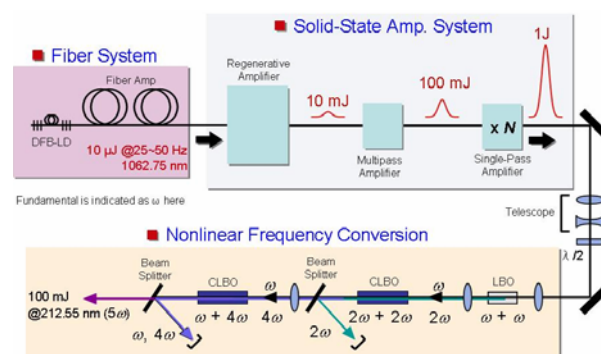


Fig. 2 Laser system for generation of ω_1 .

which is important because the energy of two-photon absorption of ω_1 is well defined. Since it is estimated that we require ~ 1 J/pulse of the fundamental wavelength to obtain ω_1 with 100 mJ/pulse (10 %), we have to build a couple of amplification stages, as shown in Fig. 2. The amplified fundamental is converted to ω_1 by a nonlinear frequency-conversion system. We use an LBO (lithium borate) crystal for the second harmonic generation and CLBO (Cesium lithium borate) crystals for the fourth and fifth order harmonic generation to achieve 10% conversion efficiency. The CLBO crystal has high conversion efficiency and relatively high damage threshold at ω_1 , making it an ideal crystal for long-term stable operation.

For the ω_2 laser, we use the DFB-LD as an oscillator in a manner similar to the case of ω_1 , and then we amplify it by optical parametric amplification using an LBO crystal. As in the case of ω_1 , our goal for ω_2 is also 100 mJ/pulse. This should not be very difficult because technologies are more established for the wavelength range unlike the case of ω_1 .

ω_1 and ω_2 are made collinear and focused on a gas cell containing the Kr/Ar mixture to generate $\omega_{Ly\text{-}\alpha}$. Unfortunately, there have been no systematic studies so far on the conversion efficiency of $\omega_{Ly\text{-}\alpha}$ as a function of parameters such as the ratio of partial pressures of the gases, absolute pressure, laser intensity, and laser spatial profile. We need to measure fundamental optical parameters such as the third-order susceptibility of Kr when the atom is in an excited state, to simulate the best conditions for generating $\omega_{Ly\text{-}\alpha}$. To generate $\sim 100 \mu\text{J}/\text{pulse}$ of $\omega_{Ly\text{-}\alpha}$ with 100 mJ/pulse of ω_1 and ω_2 , the conversion efficiency should be approximately $\sim 10^{-3}$, which makes this development itself already challenging. We have started building the laser system and performing simulations. We aim to achieve the above-mentioned goals during the second half of 2010 and install the $Ly\text{-}\alpha$ laser at RIKEN-RAL by early 2011 for the experiment on slow-muon production.

References

- 1) P. Bakule et al.: Nucl. Instr. Meth. B **266**, 335 (2008).
- 2) T. Ogawa et al.: Opt. Lett. **28**, 2333 (2003)

Studies on Muon Spin Relaxation of n-Si Conduction Electrons Produced in *p*-GaAs Overlayer by Lasers and Injected by Electrical Method

E. Torikai¹, K. Nagamine^{2,3}, I. Shiraki¹, K. Shimomura³, R. Kawakami², H.W.K. Tom², P. Bakule⁴, F.L. Pratt⁴, K. Ishida, K. Ohishi, K. Yokoyama², Y. Matsuda⁵, K. Takeda⁶, T. Ujihara⁶, T. Saka⁷, and T. Kato⁷

It has been proposed that spin-dependent exchange scattering of the polarized electron in ortho muonium (ortho-Mu, μ^+e^- , a bound state of a positive muon and an electron in which the spins of both particles aligned in the same direction) can help to detect the conduction electron spin polarization (CESP) in semiconductors [1]. Recently a proof-of-principle experiment on this muon method was successfully carried out in a strain-free *n*-type GaAs (containing $3 \times 10^{16} \text{ cm}^{-3}$ Si) by measuring the change in the μ^+ polarization corresponding to the change in the polarization direction under both longitudinal fields (LF) and zero field (ZF) [2, 3].

The production and detection of CESP in Si is known to be difficult because of an indirect band-gap and a small spin-orbit interaction. There exists only a limited knowledge on hot electron injection through ferromagnetic layer grown on Si [4, 5]. The proposed muon method is expected to be most effective for detecting CESP in Si. Here, the behavior of the un-polarized conduction electron (CE) found during the course of the CESP studies is reported.

The experiment was conducted at the RIKEN-RAL Muon facility located at ISIS of Rutherford Appleton Laboratory. A pulsed 4-MeV μ^+ beam was used. Tunable laser light with a wavelength of around 815 nm energy of 1.52 eV, and a repetition frequency of 25 Hz was generated by using an OPO system pumped by a 355-nm Nd:YAG laser. The linearly polarized laser output is converted to 100% circularly polarized (CP) light to illuminate the sample. The average power of the laser was nearly 1.5 mJ/pulse, which corresponds to $6 \times 10^{15} \text{ cm}^{-3}$ photons/pulse.

The sample used in the present measurement (Fig. 1) was the same as that used in the KEK experiment [1]. Here, laser excited CE in a *p*-GaAs (0.14 μm in thickness) layer was electrically injected into an *n*-Si substrate (290 μm in thickness) through a GaAsP buffer layer (2 μm in thickness) under the influence of the intrinsic electric field of the *pn* junction which had a strength of 20 V/300 μm (670 V/cm). Because of the sample thickness, most of the injected muons are stopped in the *n*-Si substrate, whose doping rate is estimated to be 10^{14} cm^{-3} on the basis of resistance data. There have been several experimental studies for the characterization of the muon states at low temperatures in this type of Si sample and the following observations were made [6]: 30% was Mu state located at BC-site (BC-Mu), 10% was in diamagnetic state and the missing fraction of muon polarization was 0.70.

From the “Off-On” effect observed in the LF decoupling data, we can conclude that the state in which response to laser is observed is BC-Mu because in the state in which response to the laser is observed, the Mu are decoupled by the LF by following a correct decoupling

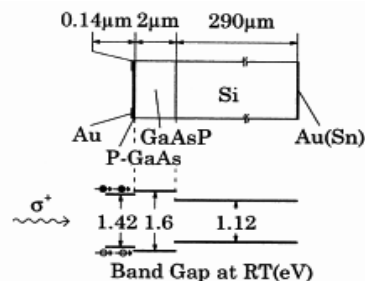


Fig. 1 The schematic structure (GaAs/GaAsP/Si) and band gaps of the sample used in the present experiment and in the KEK experiment [1].

procedure using a known hfs constant [6]. At the same time, the laser “On” effect can be considered to process the characteristic of time-delayed nucleation. Thus, the interaction between the lasers and BC-Mu can be considered to be due to the CE induced by lasers and transported through the Si substrate by the intrinsic *pn* junction voltage mentioned above.

In order to observe the diffusion length of the CE, measurements were carried out to determine the dependence of the “Off-On” effect on the position at which the muon stops. By changing the thickness of the range absorber, the muon energy can be adjusted and the position at which the muon stops in 200- μm thick *n*-Si substrate can be changed.

In the present measurement, the expected dependence on the position at which the muon stops was clearly observed. Within the current spatial resolution, the average time-delay of 300-ns was observed by changing stopping position by 100- μm ; this indicates average CE velocity of $10^{-6}c$ (c : light velocity).

In order to understand the nature of the CE produced at *p*-GaAs and transported into the *n*-Si substrate through the interfaces, the dependences on the laser timing with reference to the muon pulse was measured. It was found that the “Off-On” effect exists even for a negative timing of 3 μs ; the electron produced by lasers 3 μs before muon arrival does exist and interact with BC-Mu.

A trial was conducted to detect CESP, as in the *n*-GaAs experiment. By using 100% circularly polarized lasers with an energy of 1.5 mJ and a wavelength of 815 nm, a limited polarization effect was observed. The effect in terms of “Para-Anti”, which refers spins of Mu and CE parallel and anti-parallel, was 0.12(0.11)% out of -4.13(0.05)% “Off-On” effect.

In conclusion, the CEs in Si were optically produced in *p*-GaAs overlayer and electrically injected by intrinsic *p-n* voltage; CEs showed the following novel behaviors: a) the transport velocity is of the order of $10^{-6}c$, and b) a large fraction of CEs have a long life time of the order of μs .

¹Interdisciplinary Graduate School of Medicine and Engineering, University of Yamanashi

²Physics Department, University of California, Riverside

³Muon Science Laboratory, IMSS, KEK

⁴ISIS, Rutherford Appleton Laboratory

⁵Graduate School of Arts and Sciences, University of Tokyo

⁶Graduate School of Engineering, Nagoya University

⁷Daido Institute of Technology

[1] E. Torikai *et al.*: Physica **B 289-290**, 558 (2000).

[2] K. Yokoyama *et al.*: Physica **B 404**, 856 (2009).

[3] K. Yokoyama *et al.*: RIKEN-APR **42**, 234 (2008).

[4] I. Appelbaum *et al.*: Nature, **447**, 295 (2007).

[5] B. Huang *et al.*: Phys. Rev. Lett., **99**, 177209 (2007).

[6] K.H. Chow *et al.*: Phys. Rev. **B 50**, 8918 (1994).

New Measurements of the Chemical Reaction Rate of Muonium with Stimulated Raman-Pumped $\text{H}_2^*(v=1)$

D.G. Fleming,^{*1} P. Bakule,^{*2,*3} K. Ishida,^{*2} F.L. Pratt,^{*3} O. Sukhorukov,^{*4} T. Momose,^{*5} and Y. Matsuda,^{*6}

The goal of these experiments is to provide unique tests of reaction rate theory from accurate measurements of Mu rate constants from laser-pumped molecular vibrational states. Initial studies are on $\text{Mu} + \text{H}_2^*(v=1)$, an isotopomer of the fundamental H_3 reaction system¹⁻³). Stimulated Raman pumping from the Nd:YAG laser of the new laser- μSR facility at the RIKEN/RAL laboratory is used to produce H_2^* in its $v=1$ state. Details may be found in Ref.⁴).

The signal of interest is the difference in μSR spectra for *laserON-laserOFF*, defined by $S(t)$ in Ref.⁴). Most variables in $S(t)$ can be determined from fitting the *laserOFF* data, notably the muonium asymmetry, A_{Mu} , and background relaxation rate, λ_0 , so only the relaxation rate λ^* and the fraction 'x' of Mu atoms that overlap with the laser pumped $\text{H}_2^*(v=1)$ volume needs to be fit or otherwise determined. The key parameter is λ^* since this gives the rate constant of interest, from $\lambda^* = k_{\text{Mu}}[\text{H}_2^*]$ for the $\text{Mu} + \text{H}_2^* \rightarrow \text{MuH} + \text{H}$ reaction.

In our preliminary experiment reported in Refs.⁴⁾⁵⁾, we measured $\lambda^* = 0.085 \pm 0.051 \mu\text{s}^{-1}$, giving $k_{\text{Mu}} = 8.5 \pm 5.4 \times 10^{-13} \text{ cm}^3 \text{ molec}^{-1} \text{ s}^{-1}$. The difficulty in accurate determination of λ^* then was mainly due to the magnetic field inhomogeneity over the cell volume, giving rise to a large background relaxation $\lambda_0 \sim 0.5 \mu\text{s}^{-1}$. This, along with low statistics, contributed to the poor signal-to-noise seen. The experiment (R379) was repeated in a week of beam time in Nov. 2009, but prior to this a number of improvements were implemented: the magnetic field environment at the end of Port 2 was thoroughly mapped and all magnetic sources were removed, a high-stability Kepco supply was used to drive the TF left-right coils on the Argus spectrometer, and a magnetometer was used to provide a stable field ($\pm 2 \text{ mG}$).

These changes resulted in a *20-fold* improvement, to $\lambda_0 = 0.0261 \pm 0.0016 \mu\text{s}^{-1}$. The present fitted result for $S(t)$ for a total of 13.7×10^8 events, for 50 bar H_2 in a 2.1 G field, is shown in Fig. 1, giving a value of $\lambda^* = 0.286 \pm 0.039 \mu\text{s}^{-1}$, for $x A_{\text{Mu}} = 0.46\%$. The (larger) $[\text{H}_2^*] = 2.8 \pm 0.5 \times 10^{17} \text{ molec cm}^{-3}$ was determined from

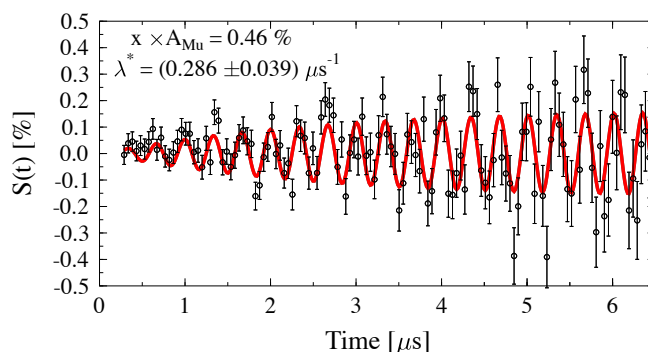


Fig. 1. The new laser difference signal, $S(t)$. (See text).

the (smaller) laser beam volume and the number of Raman-shifted photons measured. From these new values, $k_{\text{Mu}} = 10.3 \pm 2.4 \times 10^{-13} \text{ cm}^3 \text{ molec}^{-1} \text{ s}^{-1}$, in excellent agreement with theory, $k_{\text{Mu}}(\text{theory}) = 9.5 \times 10^{-13} \text{ cm}^3 \text{ molec}^{-1} \text{ s}^{-1}$ at RT⁴). The data analysis is still ongoing, hence the somewhat expanded experimental error bars here.

In order to provide a more definitive test of theory though, additional studies are needed:

- The relaxation rate, λ^* , depends crucially on both the overlap of the laser beam with the stopping distribution of Mu (x above) and on accurately knowing $[\text{H}_2^*]$. Improvements in the reproducibility of both are needed. Additional MC simulations using the *Geant-4* code, in comparison with measured range curves, will be used to better assess the overlap. Additional off-line measurements of $[\text{H}_2^*]$ using improved optics and detection schemes will also be carried out. See background in Ref.⁴).
- The present determination of k_{Mu} is from one value of $[\text{H}_2^*]$, only. Additional measurements of λ^* at different concentrations are needed, by varying the laser power, changing the laser optics or increasing the total pressure.
- The present measurements have only been carried out at RT. Additional studies at lower temperatures, down to $\sim 100 \text{ K}$, are desirable. This will necessitate changes to the target cell but would yield important results pertinent to the degree of quantum tunneling in the $\text{Mu} + \text{H}_2^*$ reaction.

References

- 1) S.L. Mielke et al.: Phys. Rev. Let. **91**, 6 (2003).
- 2) S.L. Mielke et al.: J. Chem. Phys. **122**, 22 (2005).
- 3) S.L. Mielke et al.: J. Chem. Phys. (2009).
- 4) P. Bakule et al.: Physica B **404**, 1013-1016 (2009).
- 5) D.G. Fleming et al.:RIKEN Accel. Prog. Rep. **432**, 236 (2009).

^{*1} TRIUMF and Department of Chemistry, University of British Columbia, Vancouver, Canada

^{*2} Advanced Meson Science Laboratory, RIKEN Nishina Center, Wako, Saitama 351-0198, Japan

^{*3} ISIS Muon Facility, Rutherford Appleton Laboratory, Didcot, OX11 0QX, United Kingdom

^{*4} Chemistry Dept., Univ. of Alberta, Edmonton, Canada

^{*5} Depts. of Chemistry and Physics, University of British Columbia, Vancouver, Canada

^{*6} Graduate school of Arts and Sciences, University of Tokyo, maba 3-8-1, Meguro, Tokyo 153-8902, Japan

Study of the pressure-induced charge-transfer phase transition in $(\text{C}_5\text{H}_{11})_4\text{N}[\text{Fe}^{\text{II}}\text{Fe}^{\text{III}}(\text{C}_2\text{O}_2\text{S}_2)_3]$ by μSR spectroscopy

M. Enomoto,^{*1} N. Kida,^{*1} I. Watanabe,^{*2} T. Suzuki,^{*2} Y. Ishii,^{*2} and N. Kojima^{*1}

We have previously investigated the magnetic properties of mixed-valence iron complexes, $(n\text{-C}_n\text{H}_{2n+1})_4\text{N}[\text{Fe}^{\text{II}}\text{Fe}^{\text{III}}(\text{dto})_3]$ ($\text{dto} = \text{C}_2\text{O}_2\text{S}_2$, $n = 3, 5$), in which both ferromagnetic transition and a novel charge-transfer phase transition (CTPT) take place.¹⁾ During the CTPT, an electron transfer coupled with spin transition between Fe^{II} and Fe^{III} occurs to minimize the free energy in the whole system. The spin states of the $[\text{Fe}^{\text{II}}\text{Fe}^{\text{III}}(\text{dto})_3]$ layer strongly depend on the size of an intercalated cation. On the basis of the magnetic-susceptibility and ^{57}Fe Mössbauer spectroscopy, it was determined that the CTPT takes place around 120 K in the complex with $n = 3$, while it does not take place between 2 and 300 K in the one with $n = 5$. The low-temperature phase (LTP) with Fe^{II} ($S = 0$) and Fe^{III} ($S = 5/2$) causes ferromagnetic transitions at $T_C = 7$ K in the complex with $n = 3$, while the high-temperature phase (HTP) with Fe^{II} ($S = 2$) and Fe^{III} ($S = 1/2$) gives rise to ferromagnetic transition at 19.5 K in the complex with $n = 5$.²⁾ In the case of the complex with $n = 5$, the CTPT with wide thermal hysteresis is observed in the temperature dependence of the magnetic susceptibility at pressures above 0.5 GPa.³⁾ Moreover, the Curie temperature shifts from 19.5 K to 7 K at 0.5 GPa, which implies that the LTP responsible for the low Curie temperature of 7 K appears above 0.5 GPa in the complex with $n = 5$. Recently, we have measured the muon spin relaxation (μSR) for the CTPT of the complex with $n = 3$. An anomalous increase in the dynamic temperature-dependent muon-spin depolarization rate with a thermal hysteresis loop is observed between 60 and 140 K; over this temperature range, a corresponding anomalous decrease in the magnetic susceptibility with a thermal hysteresis loop is observed for the complex with $n = 3$. This anomaly is not observed in the case of the complex with $n = 5$. The origin of this anomaly has been successfully determined to be the dynamic process of electron transfer between Fe^{II} and Fe^{III} , and its frequency has been estimated from LF- μSR measurements to be about 0.1 MHz. This result is the first observation of a dynamic electron-transfer process in such mixed-valence complexes by μSR measurement.⁴⁾ On the basis of these observations for $(n\text{-C}_n\text{H}_{2n+1})_4\text{N}[\text{Fe}^{\text{II}}\text{Fe}^{\text{III}}(\text{dto})_3]$, the dynamic process of the CTPT for the complex with $n = 5$ under high pressure can be studied using μSR measurements. Since total magnetization was observed in the magnetic-susceptibility measurement, it is difficult to distinguish the spin states of each iron site. Till date no microscopic magnetic investigation has been performed under high pressure for

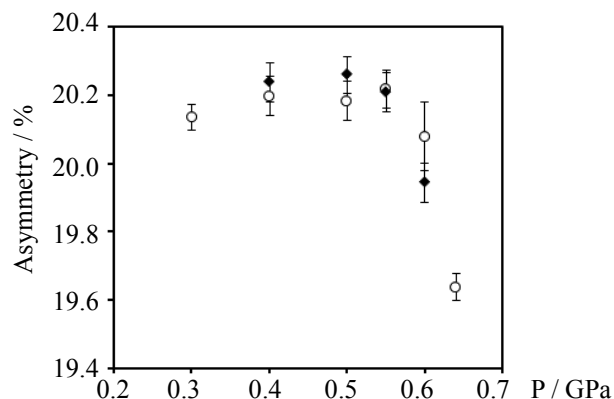


Fig. 1 Pressure dependence of the asymmetry change

the complex with $n = 5$ to study the changes in the magnetic state. Such investigation is particularly important for understanding the dynamic properties of the CTPT. The μSR technique is suitable for distinguishing the static and dynamic magnetic states.

In order to investigate the pressure-induced CTPT for the complex with $n = 5$, we have carried out μSR measurement for the complex with $n = 5$ at 150 K under high pressures ranging from 0.3 to 0.64 GPa using ^4He -gas-operated pressure device at the RIKEN-RAL Muon Facility of the Rutherford Appleton Laboratory. The gas-operated system has the advantage of that the correct pressure is applied to the sample over the whole measurement temperature range. As shown in Fig. 1, the asymmetry for the sample with $n = 5$, which includes the signal from Cu-Be pressure cell, remains almost constant up to 0.55 GPa, while it rapidly decreases with increasing pressure above 0.6 GPa. In this experiment, pressure hysteresis has been ignored. Further, applying pressure induces CTPT, which causes spin fluctuation. This spin fluctuation leads to a decrease in the asymmetry. The pressure dependence of the asymmetry change is consistent with the result of magnetic-susceptibility measurement under high pressure in a liquid medium.

References

- 1) N. Kojima, W. Aoki, M. Itoi, Y. Ono, M. Seto, Y. Kobayashi, and Yu. Maeda: *Solid State Commun.* **120**, 165 (2001).
- 2) M. Itoi, Y. Ono, N. Kojima, K. Kato, K. Osaka, and M. Takata: *Eur. J. Inorg. Chem.*, 1198 (2006).
- 3) Y. Kobayashi, M. Itoi, N. Kojima, and K. Asai: *J. Magn. Magn. Matter.*, **272-276**, 1091 (2004).
- 4) (a) N. Kida, M. Enomoto, I. Watanabe, T. Suzuki, and N. Kojima: *Phys. Rev. B* **77**, 144427 (2008). (b) M. Enomoto, N. Kida, I. Watanabe, T. Suzuki, and N. Kojima: *Physica B* **404**, 642 (2009).

^{*1} Graduate School of Arts and Sciences, The University of Tokyo

^{*2} Advanced Meson Science Laboratory, RIKEN

Investigating the role of protons in the unusual muon-spin relaxation of single molecule magnets[†]

T. Lancaster,^{*1} S.J. Blundell,^{*1} F.L. Pratt,^{*2} I. Franke,^{*1} A.J. Steele,^{*1} P.J. Baker,^{*2} Z. Salman,^{*3} C. Baines,^{*3} I. Watanabe,^{*4} S. Carretta,^{*5} G.A. Timco,^{*6} and R.E.P. Winpenny,^{*6}

[Molecular magnet, muon-spin relaxation]

Molecular nanomagnets (MNM)¹⁾ comprise clusters of exchange-coupled transition metal ions which often have a negative anisotropy constant favoring a ground state with a large eigenvalue of the electronic spin component S_z . MNMs have been successfully probed using techniques such as magnetization, heat capacity, neutron scattering and electron spin resonance. In contrast, measurements made using muon spin relaxation (μ^+ SR) have proven difficult to interpret. In order to address the question of what the muon probes in MNM systems we have made identical μ^+ SR measurements on protonated and deuterated samples of Cr_7Mn ($S = 1$) and Cr_8 ($S = 0$) (structure shown in Fig. 1).

To compare the Cr_7Mn and Cr_8 systems, measurements were made over the temperature range $2 \leq T \leq 100$ K. In this regime the spectra for $S = 1$ Cr_7Mn (Fig. 1(a)) were found to be described by the relaxation function $A(t) = A_1 \exp(-\sqrt{\lambda t}) + A_{\text{bg}}$, where A_{bg}

accounts for any background contribution from muons that stop in the sample holder or cryostat tails. This behavior is typical of that observed previously in MNM materials and arises because of the complex dynamic distribution of local fields within the material sampled by the muon ensemble.

The spectra measured for the $S = 0$ Cr_8 samples are quite different (Fig 1(b)). In this case the relaxation rate is far smaller and resembles a Kubo-Toyabe (KT) function $f_{\text{KT}}(\Delta t)$ with $\Delta = \gamma_\mu \langle B^2 \rangle$ where $\gamma = 2\pi \times 135.5$ MHz T^{-1} is the muon gyromagnetic ratio and B is the local magnetic field at a muon site. Our conclusion from these measurements is that the muon is sensitive to the disordered nuclear moments in Cr_8 . This is confirmed by the application of a small longitudinal magnetic field which quenches the relaxation. Most importantly, the dramatic difference between the measured spectra and relaxation rates for $S = 0$ Cr_8 and $S = 1$ Cr_7Mn samples (Fig. 1) strongly suggests that the muon response in MNM systems with $S \neq 0$ stems from dynamic fluctuations of the *electronic* spin. In the absence of an electron spin in Cr_8 , the muon spin is relaxed by quasistatic disordered nuclear moments.

The temperature dependence of the relaxation rate λ for the protonated (λ^{h}) and deuterated (λ^{d}) Cr_7Mn samples was measured. On cooling below $T \sim 50$ K, the relaxation rate λ increases before saturating below ~ 10 K. with the onset of the increase and the saturation occurring at similar values of T for both materials. This T -dependence is common to nearly all MNM systems that have been previously measured with μ^+ SR. At high T we see that $\lambda^{\text{d}} > \lambda^{\text{h}}$. It is likely that at these high temperatures the electronic spins are fluctuating very fast and are at least partially motionally narrowed from the spectra. Upon cooling the increase in λ is greater for the deuterated sample, with λ^{d} becoming greater than λ^{h} below ≈ 15 K. Most significantly the saturation of the relaxation at $T < 10$ K occurs with $\lambda^{\text{d}} > \lambda^{\text{h}}$. The T -dependence of the ratio $\lambda^{\text{d}}/\lambda^{\text{h}}$ increases on cooling.

A full account of this work may be found in Ref.¹⁾.

References

- 1) T. Lancaster *et al.*, Phys. Rev. B **81**, 140409(R) (2010).

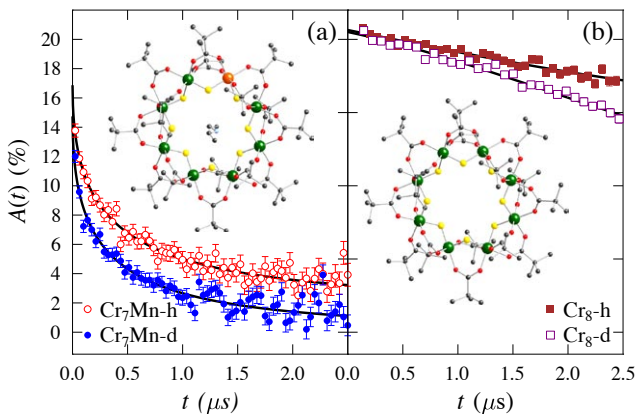


Fig. 1. μ^+ SR spectra for protonated and deuterated (a) Cr_7Mn and (b) Cr_8 materials, measured at $T = 4.5$ K. Inset: structures of the molecules.

[†] Condensed from Phys. Rev. B **81**, 140409(R) (2010)

^{*1} Clarendon Laboratory, Oxford University Department of Physics, Parks Road, Oxford, OX1 3PU, UK

^{*2} ISIS Facility, Rutherford Appleton Laboratory, Chilton, Oxfordshire OX11 0QX, UK

^{*3} Laboratory for Muon-Spin Spectroscopy, Paul Scherrer Institut, Villigen, CH

^{*4} Muon Science Laboratory, RIKEN, 2-1 Hirosawa, Wako, Saitama 351-0198, Japan

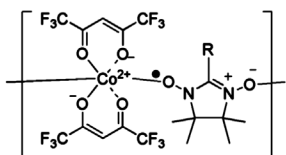
^{*5} Dipartimento di Fisica, Università di Parma, I-43100 Parma, Italy

^{*6} Department of Chemistry, University of Manchester, Oxford Road, Manchester, M13 9PL, UK

Muon-spin rotation and relaxation on the one-dimensional coordination polymer magnet [Co(hfac)₂•HNN] (HNN = hydro nitronyl nitroxide)

Takayuki Ishida,^{*1} Yoshitomo Okamura,^{*1} Yasuyuki Ishii, and Isao Watanabe

The first single-chain magnet [Co(hfac)₂•AnNN] was discovered by Gatteschi et al.¹⁾ (see below for the molecular structure, with R = *p*-CH₃O-C₆H₄). The single-chain magnet nature is identified with magnetic hysteresis from a single-chain origin without any interchain interaction. On the other hand, we reported the highest coercivity ($H_C = 52$ kOe at 6 K) for [Co(hfac)₂•BPNN] (R = *p-n*-C₄H₉O-C₆H₄)²⁾ and clarified its long-range ordered state below 40 K in the μ SR study.³⁾ The smallest radical species (HNN; R = H) is also available for paramagnetic bridges, and α -[Co(hfac)₂•HNN] (CoHNN) was earlier characterized as a single-chain magnet.⁴⁾ We reexamined whether CoHNN behaves as a bulk magnet.



The μ SR measurements on CoHNN were carried out at the RIKEN-RAL Muon Facility in the UK. We investigated detailed zero-field muon-spin relaxation over a wide temperature range (Fig. 1a). We obtained a superposition of slow- and fast-relaxation curves. The time spectra were analyzed using a double exponential equation with modification of the Kubo-Toyabe function. The relaxation rate constant (λ_{slow}) and the total initial asymmetry $A(0)$ are plotted as a function of temperature (Fig. 1b). A sharp peak of λ was observed at 27 K, and a plateau of $A(0)$ was observed below 27 K. Extremely slow depolarization and a constant $A(0)$ are indicative of completely frozen systems such as magnetically ordered systems. The temperature at which λ diverges is usually defined as a magnetic phase-transition temperature.

Below 22 K, wiggling spectra were recorded (Fig. 2a). The oscillation due to the muon Larmor precession clearly indicates the presence of an appreciable internal magnetic field attributed to spontaneous magnetization. The coherency of the rotation implies the presence of a magnetically ordered state. The small amplitude of the oscillation may be related to the size of the magnetic domain. The frequency and amplitude are almost constant up to 22 K; in other words, on warming, the long-range ordered state disappears suddenly around 22 K without any decrease of the internal field (ca. 200 G; Fig. 2b).

Taking into account the present μ SR results together with the results of our previous experiments,⁴⁾ the magnetically ordered state of CoHNN can be interpreted as follows. On cooling from 27 K, which can be defined as an intrinsic T_N ,

CoHNN enters into the quasistatic magnetically ordered state. The appearance of the quasistatic long-range ordered state below 22 K is sensed by muons. The dynamics observed from ac susceptibility measurements below T_N can be attributed to the freezing of domain-wall motion, as in the case of [Co(hfac)₂•BPNN].³⁾

In conclusion, the one-dimensional magnet CoHNN undergoes a magnetic phase transition at 27 K, and the domain-wall motion freezes below 22 K at the timescale of μ SR.

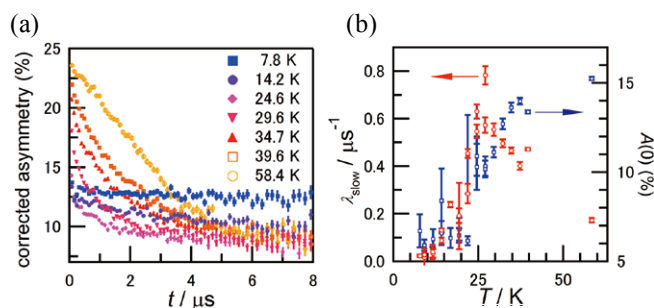


Fig. 1. (a) ZF-muon spin relaxation observed for CoHNN. (b) Temperature dependence of the depolarization rate constant (λ_{slow}) and corrected initial asymmetry ($A(0)$).

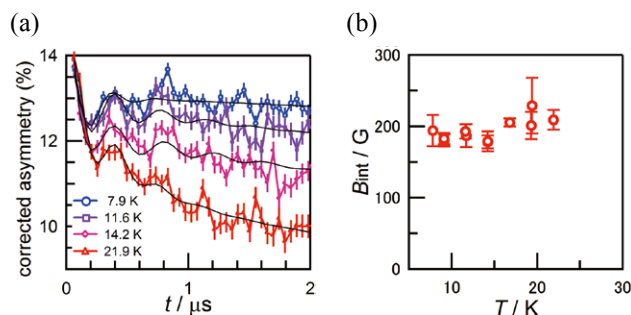


Fig. 2. (a) ZF-muon spin rotation observed for CoHNN. Solid lines represent best-fit curves. (b) Internal field (from the oscillation frequency) as a function of temperature.

References

- 1) A. Caneschi, D. Gatteschi, N. Lalioti, C. Sangregorio, R. Sessoli, G. Venturi, A. Vindigni, A. Rettori, M. G. Pini, and M. A. Novak: *Angew. Chem. Int. Ed. Engl.* **40**, 1760 (2001).
- 2) N. Ishii, Y. Okamura, S. Chiba, T. Nogami, and T. Ishida: *J. Am. Chem. Soc.* **130**, 24 (2008).
- 3) T. Ishida, Y. Okamura, and I. Watanabe: *Inorg. Chem.* **48**, 7012 (2009).
- 4) N. Ishii, T. Ishida, and T. Nogami: *Inorg. Chem.* **45**, 3837 (2006).

^{*1} Department of Engineering Science, The University of Electro-Communications

Zero-Field and Longitudinal-Field μ SR Studies of Quasi-One-Dimensional Organic Conductor, $\text{TMTTF}_2\text{PF}_6$

Y. Ishii, M. Nagasawa*¹, I. Watanabe, T. Suzuki, T. Matsuzaki, H. M. Yamamoto, and R. Kato

After the discovery of the first organic pressure-induced superconductor, $(\text{TMTSF})_2\text{PF}_6$ (TMTSF = tetramethyltetrathiofulvalene) at 12 kbar in 1980¹⁾, a family of quasi-one-dimensional (Q1D) organic conductors, $(\text{TMTSF})_2X$ and $(\text{TMTTF})_2X$ (TMTTF = tetramethyltetraselenafulvalene, X = monovalent anion), has been investigated extensively. A wide variety of ground states such as the spin-Peierls (sP) state, antiferromagnetic (AF) state, spin-density wave (SDW) state and superconducting (SC) state appear depending on the pressure or choice of anion X . The spin-Peierls transition is one of the unique phenomena in Q1D antiferromagnetic spin chain systems. However, there are only a few materials that undergo the sP state. This is because antiferromagnetic chains often enter a three-dimensional magnetic ordered state, such as AF and SDW state, because of interchain coupling. In this study, we aim to investigate the magnetic properties of the sP state of the PF_6 salt.

Single crystals used in this study were synthesized by the standard electrochemical method. ZF- and LF- μ SR experiments were carried out using the ARGUS spectrometer installed at port 2 of the RIKEN-RAL Muon Facility in the U. K.^{2,3)}. The facility provides a intense pulsed muon beam. Randomly oriented crystals with a total weight of 120 mg were wrapped in a silver foil, and the wrapped sample was formed to a disk-like shape. The sample was cooled to 0.26 K using a ^3He cryostat.

Figure 1 shows the ZF- μ SR time spectra at temperature above and below T_{sP} . Above T_{sP} , the ZF- μ SR time spectra are almost unchanged and the spectra show exponential-like relaxation. Below T_{sP} , the relaxation rate is significantly enhanced and the μ SR time spectra do not show simple exponential relaxation as the temperature decreases. Moreover, below 1 K, a strange change in the μ SR time spectrum is observed when a field is applied. Figure 2 shows the low-temperature muon time spectra obtained for $\mu_0 H_{\text{LF}} = 0.1$ mT. The spectrum correspond to 0.26 K can be fitted to the function $A(t) = A_S \exp(-\lambda t) \times \cos(\omega t + \theta)$. The internal field at the muon site, B_{int} , can be calculated as $B_{\text{int}} \simeq 10$ G by using the relation $B_{\text{int}} = \gamma_\mu / \omega$, where $\gamma_\mu = 2\pi \times 13.5534$ kHz/G is a gyromagnetic ratio of the muon spin. Interestingly, under zero-field conditions, no significant change was observed in the μ SR time spectra between 1.5 K and 0.26 K. This suggests that some kind of unconventional magnetic ordering may appear at low temperatures. Further investigations are necessary to clarify this unconventional be-

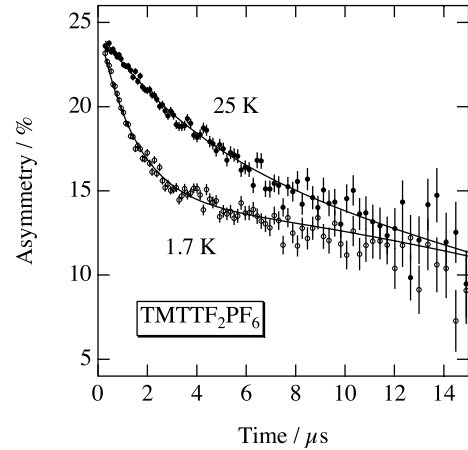


Fig. 1. ZF- μ SR time spectra of $\text{TMTTF}_2\text{PF}_6$ at temperature above and below $T_{\text{sP}} = 18$ K.

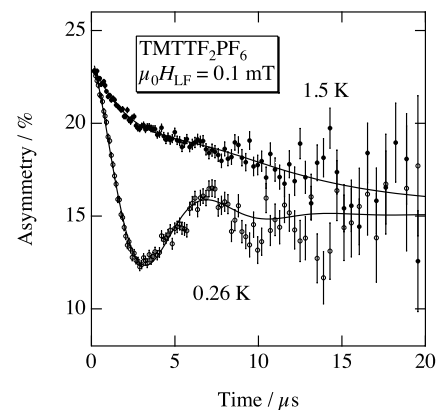


Fig. 2. Low-temperature μ SR time spectra of $\text{TMTTF}_2\text{PF}_6$ at $\mu_0 H_{\text{LF}} = 0.1$ mT.

havior.

References

- 1) D. Jérôme, A. Mazaud, M. Ribault and K. Bechgaard, *J. Phys. Lett. France* 41(1980) L95.
- 2) T. Matsuzaki, K. Nagamine, M. Tanase, M. Kato, K. Kurosawa, H. Sugai, K. Ishida, S. N. Nakamura, I. Watanabe and G. H. Eaton, *Nucl. Instr and Meth. A* 480 (2002) 814.
- 3) K. Nagamine, T. Matsuzaki, K. Ishida, I. Watanabe, R. Kadono, G. H. Eaton, H. J. Jones, G. Thomas and W. G. Williams, *Hyperfine Interact.* 87 (1994) 1091.
- 4) S J Blundell, F L Pratt, P A Pattenden, M Kurmoo, K H Chow, S Takagi, Th Jestädt and W Hayes, *J. Phys.: Condens. Matter* f9 (1997) L119.

*¹ Department of Physics, Tokyo Denki University

High-Pressure μ SR Study of an Organic Spin-Peierls Material MEM-[TCNQ]₂

Y. Ishii, H. Komatsu*¹, Y. Manabe*¹, A. Taniguchi*¹, H. Taniguchi*¹, K. Satoh*¹, I. Watanabe
and T. Matsuzaki

Long-range magnetic order cannot be induced in ideal one-dimensional spin system. The spin-Peierls (sP) transition, which is a unique phenomenon in quasi one-dimensional antiferromagnetic spin chain systems, gives rise to a gap in the magnetic excitation spectrum. The driving force for the sP transition is the magnetoelectric coupling between the one-dimensional spin structure and three-dimensional lattice vibrations. Very few materials exhibit sP transition. This is because antiferromagnetic chains often become three-dimensional magnetic ordered state because of interchain interaction.

MEM-[TCNQ]₂ (N-Methyl-N-ethyl-morpholinium-[7,7',8,8'-tetracyanoquinodimethane]₂) forms one dimensional stacking structure of TCNQ molecules. This compound exhibits spin-Peierls transition at transition temperature $T_{sP} = 18$ K¹). We carried out μ SR measurement of MEM-[TCNQ]₂ under high-pressure since it is expected that sP state is destabilized by applying pressure because the inter-chain coupling should increase with pressure.

Single crystals of MEM-[TCNQ]₂ were grown from an acetonitrile solution, which contained TCNQ and MEMiodine, by a slow diffusion method. The product was obtained as fine black needles with a typical length of 1 mm. High-pressure μ SR experiments were carried out using the ARGUS spectrometer that is installed at the RIKEN-RAL Muon Facility in the UK²⁻⁴). The facility can provide a high-momentum muon beam that can pass through the window of a high-pressure cell.

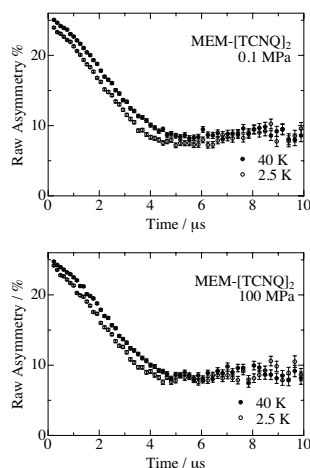


Fig. 1. μ SR time spectra of MEM-[TCNQ]₂ for 0 and 100 MPa.

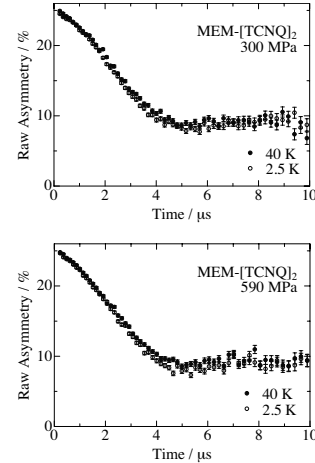


Fig. 2. μ SR time spectra of MEM-[TCNQ]₂ for 300 and 590 MPa.

μ SR time spectra obtained below 100 MPa are shown in fig. 1. At 2.5 K, an exponential-like fast-damping component of small magnitude is observed at both 0 and 100 MPa. This component should be a characteristic feature of the spin-Peierls ground state⁵). However, it is difficult to find out this exponential component analytically, because in the obtained μ SR time spectra, a paramagnetic component from the pressure cell is dominant. Detailed analyses are underway. On the other hand, there are no signs of a spin-gap or of magnetic ordering above 300 MPa even at the base temperature. This suggests that the ground state above 300 MPa is a paramagnetic one. This result is quantitatively inconsistent with previous high-pressure magnetic measurements^{6,7}).

References

- 1) S. Huizinga et al.: Phys. Rev. **B 19**, 4723 (1979).
- 2) T. Matsuzaki et al.: Nucl. Instr and Meth. **A 480**, 814 (2002).
- 3) K. Nagamine et al.: Hyperfine Interact. **87**, 1091 (1994).
- 4) I. Watanabe et al.: Physica **B In Press**.
- 5) S J Blundell et al.: J. Phys.: Condens. Matter **9**, L119 (1997).
- 6) D. Bloch et al.: Physica **119 B**, 43 (1983)
- 7) S. Takagi et al.: Mol. Cryst. Liq. Cryst. **376**, 377 (2002).

*¹ Department of Physics, Saitama University

μ SR study on the spin-singlet state in cluster magnet GaNb_4S_8 †Y. Tabata,^{*1} Y. Kajinami,^{*1} T. Waki,^{*1} I. Watanabe, H. Nakamura^{*1}

A mixed-valent magnetic cluster system, in which atoms in the cluster share unpaired electrons, is very attractive as an intermediate system between a localized spin system and an itinerant electron magnet. As a category of such materials, the ternary chalcogenides AB_4X_8 ($A = \text{Ga, Al, Ge}$; $B = \text{V, Mo, Nb, Ta}$; $X = \text{S, Se}$), having cubic GaMo_4S_8 structure (space group $F\bar{4}3m$), are of particular interest¹⁻⁴. In the compounds, the cubic $(\text{B}_4\text{X}_4)^{n+}$ and the tetrahedral $(\text{AX}_4)^{n-}$ ions are weakly coupled in the NaCl manner, resulting in hopping conduction between the clusters. These compounds are generally semiconducting with a narrow bandgap. In the $(\text{B}_4\text{X}_4)^{n+}$ ion, one can find a tetrahedral cluster (tetramer) of magnetic B-atoms in which d electrons form cluster orbitals. Intracuster and intercluster interactions result in a wide variety of magnetic properties.

GaNb_4S_8 has attracted attention as a Mott insulator in which 4d electrons are localized in Nb_4 clusters due to electron correlations and also as one of pressure-induced superconductors¹. In the compound, the Nb_4 tetramers have a local moment with $S = 1/2$. The magnetic susceptibility of the compound obeys the Curie-Weiss law with the effective moment (μ_{eff}) of $1.73 \mu_{\text{B}}/\text{f.u.}$ and the Weiss constant (θ) of -298K ¹. The large negative Weiss constant suggests that the antiferromagnetic (AF) coupling exists between the clusters. The compound exhibits a structural phase transition from the high-temperature cubic state to the tetragonal state ($P4_21m$) at a temperature (T_s) of 32K ². This phase transition is possibly due to the Jahn-Teller instability of the degenerate molecular orbital of the the Nb_4 tetramers. Our zero-field (ZF) and longitudinal-field (LF) μ SR studies⁵ indicate that the magnetic ground state in GaNb_4S_8 is a non-magnetic spin-singlet state. The details are provided below. From the lattice symmetry², it is suggested that the spin-singlet state is formed because of formation of the Nb_8 octamer from two Nb_4 tetramers.

The ZF and the LF μ SR experiments on GaNb_4S_8 were conducted at the RIKEN-RAL Muon Facility at the Rutherford-Appleton Laboratory in the UK in the temperature (T) range of $4.5\text{--}100\text{K}$ in a LF of $0\text{--}3950\text{G}$. All experiments were performed using polycrystalline samples obtained from the solid-state reaction of pure elements sealed in evacuated quartz tubes.

Even at the lowest temperature, the ZF μ SR spectra, shown in Fig. 1, exhibit no oscillation due to the muon precession caused by the static internal field. This clearly indicates the absence of a magnetic long-

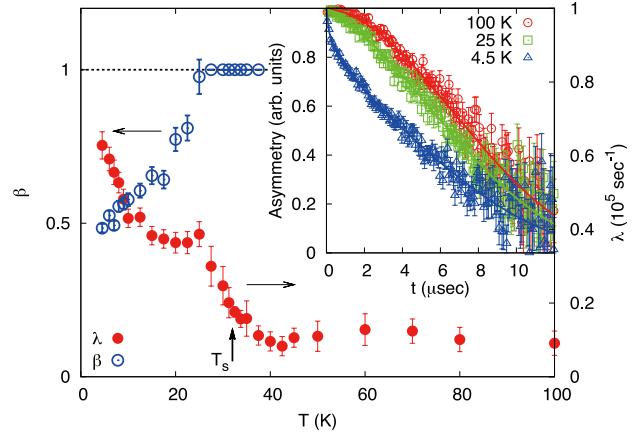


Fig. 1. T -dependence of λ and β . Above 27.5K , the value of β is fixed at 1. Inset: Typical Examples of ZF- μ SR spectra at $T = 4.5, 25,$ and 100K . The solid curves represent the fit by the damped KT function described in the text. Below T_s , the spectra are fit with a phenomenological stretched exponential function.

range order at temperatures below T_s . The relaxation curve can be fitted by a phenomenological damped Kubo-Toyabe (KT) function with a stretched exponential function given by $P_\mu(t) = \exp[-(\lambda t)^\beta] G_z^{\text{KT}}(\Delta, t)$, where $G_z^{\text{KT}}(\Delta, t) = \frac{1}{3} + \frac{2}{3}(1 - \Delta^2 t^2) \exp(-\frac{1}{2}\Delta^2 t^2)$. The KT relaxation rate Δ is almost independent of temperature and the damping rate λ exhibits a gradual increase with a decrease of temperature below 40K . The exponent β is considered a free fitting parameter at low temperatures, and above 27.5K , its value is fixed at 1 because λ is too small to determine β precisely by fitting the data. Thus, the cusp-like anomaly of λ at around 25K may be an artifact of the curve-fitting. The stretched exponential relaxation is not decoupled by an applying LF up to 3950G ; this clearly indicates that the increase in λ below T_s mainly due to the dynamic internal field resulting from fluctuating electronic spins. These results can be considered as sporadic dynamics of spin fluctuations in the spin-singlet sea⁶, and they also indicate that the spin-singlet state of GaNb_4S_8 is formed because of the formation of Nb_8 octamers from two Nb_4 tetramers.

References

- 1) R. Pocha R et al.: J. Am. Chem. Soc. **127**, 8732 (2005).
- 2) S. Jakob et al.: J. Mater. Chem. **17**, 3833 (2007).
- 3) R. Pocha R et al.: Chem. Mater. **12**, 2882 (2000).
- 4) H. Nakamura et al.: J. Phys.: Conf. Series **145**, 012077 (2009).
- 5) T. Waki et al.: Phys. Rev. **B 81**, 020401(R) (2010).
- 6) Y. J. Uemura et al.: Phys. Rev. Lett. **73**, 3306 (1994).

^{*1} Department of Materials Science and Engineering, Kyoto University

Magnetic order of the frustrated triangular lattice antiferromagnet HCrO_2^\dagger

H. Kikuchi,^{*1} Y. Fujii,^{*2} I. Watanabe,^{*3} T. Suzuki,^{*3} and T. Kawamata^{*3}

[Spin frustration, antiferromagnet, magnetic order]

Geometrically frustrated magnets have attracted much interest recently because their high degeneracy generates new phenomena such as spin liquid state. A triangular lattice antiferromagnet (TAF) is a typical frustrated magnet and has been studied extensively. HCrO_2 is a model compound of the TAF. Edge-sharing CrO_6 octahedra form a layer in the c plane, and Cr^{3+} ions ($S = 3/2$) form the triangular lattice. The Weiss temperature of HCrO_2 has been estimated to be -276 K from magnetic susceptibility measurements above 77 K [1]. About two decades ago, Y. Ajiro *et al.* [2] measured the X-band ESR (electron spin resonance) spectra of HCrO_2 and discussed the temperature dependence of the ESR linewidth in terms of the Z_2 vortex excitation, which is a topological defect predicted for the Heisenberg triangular-lattice antiferromagnet [3]. They observed that the ESR linewidth of polycrystalline HCrO_2 diverged at around 20 K, which agrees with the predicted temperature for the Z_2 vortex phase transition. No magnetic study of HCrO_2 has been performed since the study in [2]. We measured the μSR spectra of HCrO_2 and DCrO_2 to investigate the magnetic properties of these frustrated magnets. Powder samples were synthesized using a hydrothermal method.

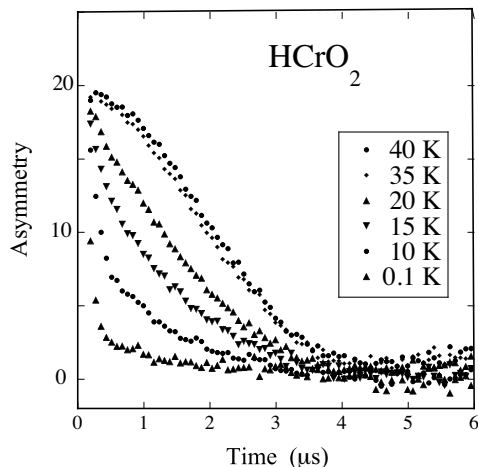


Fig. 1. Temperature dependence of the time spectra of HCrO_2 .

^{*1} Department of Applied Physics, University of Fukui

^{*2} Research Center for Development of Far-Infrared Region, University of Fukui

^{*3} Advanced Meson Science Laboratory, RIKEN Nishina Center

Zero-field (ZF) and longitudinal-field (LF) μSR spectra were measured at the RIKEN-RAL Muon Facility at temperatures down to 0.1 K and for fields up to 3950 Oe. Figure 1 shows temperature dependence of the ZF- μSR time spectra of HCrO_2 . At high temperatures the spectra can be fitted with Gaussian curve. Below about 20 K, a fast relaxing component rapidly develops so that exponential decay becomes prominent at lower temperatures. The observation clearly indicates that a magnetic transition occurs at around 20 K. However, since no spin rotation was observed even at the lowest temperature of 0.1 K, it is suggested that the magnetic phase below 20 K is characterized not by a long-range order, but a short-range order. Figure 2 shows the LF dependence of the time spectra of HCrO_2 measured at 0.1 K. Almost no change is observed when the magnetic field is increased to 1000 Oe. At the highest magnetic field of 3950 Oe, decoupling of the muon relaxation is still insufficient, suggesting that the magnetic moments are dynamic even at 0.1 K.

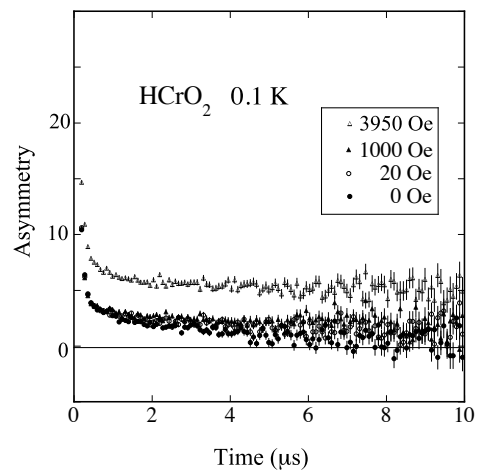


Fig. 2. LF dependence of the time spectra of HCrO_2 at 0.1 K up to 3950 Oe.

References

- 1) R. G. Meisenheimer and J. D. Swalen: Phys. Rev. **123**, 831 (1961).
- 2) Y. Ajiro *et al.*: J. Phys. Soc. Jpn. **57**, 2268 (1988).
- 3) H. Kawamura and S. Miyashita: J. Phys. Soc. Jpn. **53**, 4138 (1984).

μ SR Study of Ordered Phases in Triangular Ising-like Antiferromagnets CsCoCl₃ and CsCoBr₃

T. Kawamata, Y. Nishiwaki,^{*1} T. Kato,^{*2} T. Nakamura,^{*3} Y. Tanabe^{*4} and I. Watanabe

[μ SR, frustration system]

Recently, cooperative phenomena with different degrees of freedom in a frustration system have attracted interest. In particular, RbCoBr₃ is a unique frustration compound with spin and lattice frustration, as suggested by a new spin-lattice model,¹⁾ which is introduced in the frustration of not only spin systems but also lattice systems, say “lattice frustration”. RbCoBr₃ has been classified as an ABX_3 -type compound. The ABX_3 -type compounds are well-known frustrated magnets, which have chains formed by face-sharing BX_6 octahedra. This model shows that the spins of the Co²⁺ ions and those of the lattice chains change their alignments cooperatively to minimize the energy for releasing the frustrations.

RbCoBr₃ undergoes several magnetic and structural phase transitions. It has been suggested by neutron scattering measurements²⁾ that a partial disordered (PD) phase appears below $T_{N1} = 37$ K and that a three-sublattice ferromagnetic (3FR) phase appears below $T_{N2} = 32$ K, with a decreasing in temperature. However, our previous μ SR result³⁾ suggested that the 3FR phase appears at temperatures between T_{N1} and T_{N2} . The two frequency components, ~ 4 MHz and ~ 8 MHz, observed between T_{N1} and T_{N2} during μ SR measurements are consistent with those determined by our dipole field calculations on the 3FR phase, while the calculations on the PD phase indicate the existence of only one frequency component. Furthermore, the spin-lattice model predicts that the 3FR phase in RbCoBr₃ appears in a very small temperature regime at around T_{N1} .¹⁾ Therefore, there is a possibility of the 3FR phase appearing between T_{N1} and T_{N2} . In order to determine the exact number of frequency components in the PD phase, we carried out μ SR experiments on CsCoCl₃ and CsCoBr₃, in which the PD phase is known to be established at low temperatures.

CsCoCl₃ and CsCoBr₃ are ABX_3 -type compounds, and hence, in these compounds, magnetic phase transitions occur at $T_{N1} = 21$ K, $T_{N2} = 9$ K and $T_{N1} = 28$ K, $T_{N2} = 13$ K, respectively. The PD phase of CsCoCl₃ and CsCoBr₃ is observed between T_{N1} and T_{N2} . μ SR measurements have been carried out in the past on CsCoCl₃ using pulsed muon beam at KEK and dc beam at TRIUMF. The results suggested the existence of only one component of the muon-spin ro-

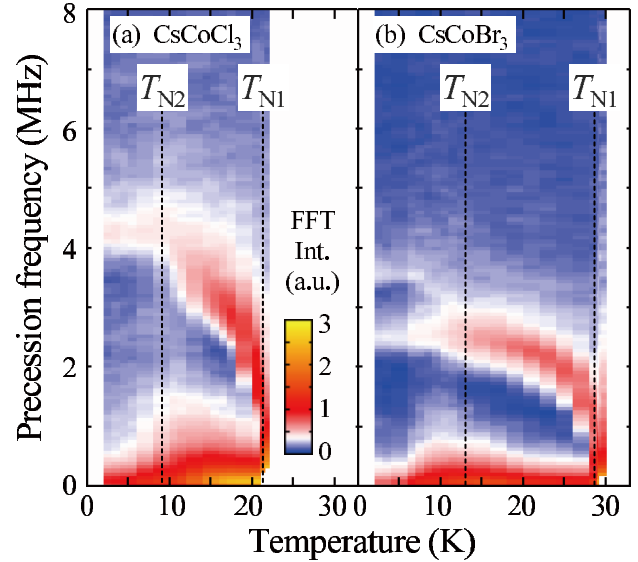


Fig. 1. Temperature dependence of precession frequency obtained by Fourier analysis of (a) CsCoCl₃ and (b) CsCoBr₃.

tation at ~ 4 MHz.⁴⁾ We must carry out experiments on CsCoCl₃ again because there is a possibility of the high-frequency component remaining undetected owing to the low statistics of the data obtained in the previous experiments. The present μ SR measurements on CsCoCl₃ and CsCoBr₃ are performed at the RIKEN-RAL Muon Facility.

Clear muon spin rotation is observed below $T_{N1} \sim 21$ K and ~ 28 K in the μ SR spectra of CsCoCl₃ and CsCoBr₃, respectively. Figure 1 shows the temperature dependence of the precession frequency of CsCoCl₃ and CsCoBr₃ obtained by Fourier analysis of the spectra. Only one broad component is observed in the PD phase between T_{N1} and T_{N2} in both compounds. This result suggests that there is only one broad component in the PD phase in an ABX_3 system. Accordingly, it is likely that the magnetically ordered state between T_{N1} and T_{N2} in RbCoBr₃ is the 3FR phase, which contradicts with the results suggested by the neutron scattering experiment²⁾.

References

- 1) T. Nakamura and Y. Nishiwaki: Phys. Rev. B **78**, 104422 (2008).
- 2) Y. Nishiwaki et al.: J. Phys. Soc. Jpn. **77**, 104703 (2008).
- 3) T. Kawamata et al.: RIKEN Accel. Prog. Rep **42**, 243 (2009).
- 4) M. Mekata et al.: J. Magn. Magn. Mater. **104–107**, 825 (1992).

^{*1} Dept. of Physics, Tokyo Women’s Medical University

^{*2} Faculty of Education, Chiba University

^{*3} Faculty of Engineering, Shibaura Institute of Technology

^{*4} Dept. of Applied Physics, Tohoku University

μ SR Studies of the 2D Triangular-lattice Spin-liquid System κ -ET₂Cu₂(CN)₃

F.L. Pratt^{*1}, S. Kawamura^{*2}, T. Lancaster^{*3}, S.J. Blundell^{*3}, P.J. Baker^{*1}, Y. Shimizu^{*4}, K. Kanoda^{*5} and I. Watanabe^{*6}

[Spin liquid, magnetism]

The S=1/2 triangular-lattice antiferromagnet (AF) with nearest neighbour Heisenberg interactions was one of the first candidates to be considered for a spin-liquid (SL) ground state in the resonating-valence-bond (RVB) picture¹. Although subsequent studies indicated that non-collinear three-sublattice AF ordering is the ground state (Fig.1a), the SL state may be recovered when higher order interactions are taken into account (Fig.1b)^{2,3}. These interactions are significant in strongly-correlated electronic systems just on the insulating side of a Mott transition^{4,5}, such as the organic system κ -ET₂Cu₂(CN)₃ studied here⁶, which shows SL properties down to at least 20 mK⁷.

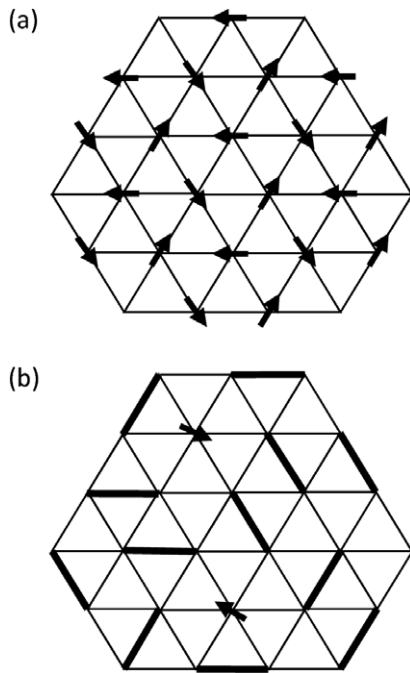


Fig. 1. (a) The three-sublattice ground state of S=1/2 spins on a triangular lattice with simple nearest-neighbour Heisenberg interactions. (b) Higher order interactions can stabilise the RVB SL phase and one of the many degenerate configurations is shown here. Thick lines represent valence bonds and two mobile spinon excitations are also shown.

^{*1} ISIS Facility, Rutherford Appleton Laboratory, UK
^{*2} JPARC, Tokai

^{*3} Department of Physics, University of Oxford, UK

^{*4} Department of Physics, University of Nagoya

^{*5} Department of Physics, University of Tokyo

^{*6} RIKEN

In the RVB SL phase, the spinon excitations are expected to be mobile and implanted muons may be used to study their dynamical properties. An example of the field dependent muon spin relaxation resulting from unpaired electronic spins in κ -ET₂Cu₂(CN)₃ is shown in Fig.2. The field dependence can be represented by the sum of two contributions, the first term dominates at low fields and has the form of a Lorentzian that reflects localised spin fluctuations with a single dominant relaxation time. The second term has the characteristic logarithmic dependence of a 2D diffusion process and is assigned to relaxation of the muon by the mobile spinons present in the SL phase.

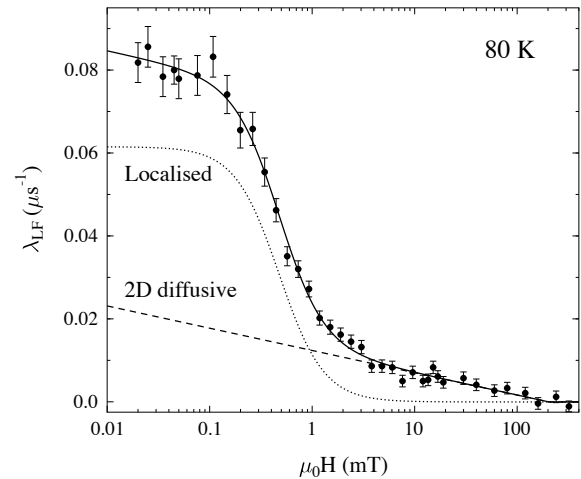


Fig. 2. Electronic contribution to the longitudinal muon spin relaxation in κ -ET₂Cu₂(CN)₃ measured at 80 K. The field dependence can be represented by the sum (solid line) of contributions from localised and diffusing spin excitations, with the mobile excitations dominating the relaxation for fields above 2 mT.

References

- 1) P. W. Anderson, *Mat. Res. Bull.* **8**, 153 (1973).
- 2) G. Misguich *et al*, *Phys. Rev. B* **60**, 1064 (1999); W. LiMing *et al*, *Phys. Rev. B* **62**, 2372 (2000).
- 3) O.I. Motrunich, *Phys. Rev. B* **72**, 045105 (2005).
- 4) H. Morita, S. Watanabe and M. Imada, *J. Phys. Soc. Jpn.* **71**, 2109 (2002).
- 5) B.J. Powell and R.H. McKenzie, *J. Phys.: Condens. Matter* **18**, R827 (2006).
- 6) Y. Shimizu *et al*, *Phys. Rev. Lett.* **91**, 107001 (2003); *Phys. Rev. B* **73**, 140407 (2006).
- 7) S. Ohira *et al*, *J. Low. Temp. Phys.* **142**, 153 (2006).

μ SR study around a quantum critical point in heavy-fermion compounds $\text{Ce}_2\text{RhIn}_{8-x}\text{Sn}_x$ [†]

K. Ohishi, T. Suzuki, R. H. Heffner,^{*1,*2} T. U. Ito,^{*1} W. Higemoto,^{*1} and E. D. Bauer^{*2}

One of the most exciting topics in modern condensed matter physics is the interplay between different electronic ground states near a quantum critical point (QCP)¹. In *f*-electron compounds, a quantum critical phase transition appears due to the competition between magnetic ordering (via RKKY interactions) and paramagnetic phase (via Kondo singlet formation). It is observed that unconventional superconductivity and/or non-Fermi-liquid behavior is often exhibited in the vicinity of a QCP, where the Curie or Neel temperature of a magnetically ordered state approaches 0 K. Recently, it has been found that Ce_2RhIn_8 has two different QCPs; this was observed when pressure was applied²) and when chemical substitution of Sn for In was carried out³). In order to study the difference between the magnetic properties of the two QCPs, we first performed μ SR measurements of the $\text{Ce}_2\text{RhIn}_{8-x}\text{Sn}_x$ before performing the measurements of the Ce_2RhIn_8 under pressure. The μ SR measurements were carried out at the RIKEN-RAL Muon Facility in the U.K. Single crystalline samples of $\text{Ce}_2\text{RhIn}_{8-x}\text{Sn}_x$ ($x = 0.0, 0.1, 0.5, 0.7$) were mounted on a high-purity silver plate such that their *c*-axes were parallel to the initial muon spin polarization.

Figure 1(a) shows the ZF- μ SR time spectra of Ce_2RhIn_8 . At temperatures above T_N , the time spectra consist of two components; the first component shows the slow relaxation due to random local fields from nuclear magnetic moments, and the other component shows that the relaxation is independent of time. More specifically, we have $A(t) = AP_z(t) + A_{\text{Ag}}$, where A and A_{Ag} are the initial μ -e decay asymmetries of the sample and the silver backing plate, respectively. $P_z(t) = \exp(-\Delta^2 t^2)$, where Δ/γ_μ is the rms value of the random local field. [Here, $\gamma_\mu (= 2\pi \times 135.54 \text{ MHz/T})$ is the muon gyromagnetic ratio.] Note that the second component is a constant because the relaxation rate of the silver backing plate is negligible (~ 0). The time spectra were reproduced well by the above formula with $\Delta = 0.214(5) \mu\text{s}^{-1}$. For $T < T_N$, we found that the spectra can be described well by $A(t) = A_1 \exp(-\sigma_1^2 t^2) \cos(2\pi f t + \phi) + A_2 \exp(-\sigma_2^2 t^2) + A_{\text{Ag}}$, where σ_1 and σ_2 are the relaxation rates, f is the muon-spin precession frequency under a local field H_{loc} , and ϕ is the initial phase. As shown in Fig. 1(a), a clear precession signal was observed and T_N is estimated to be 2.8 K. A fitting procedure similar to that for the par-

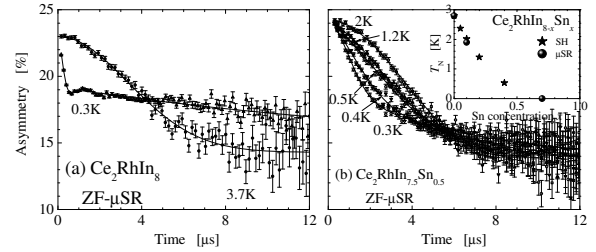


Fig. 1. ZF- μ SR time spectra of (a) Ce_2RhIn_8 and (b) $\text{Ce}_2\text{RhIn}_{7.5}\text{Sn}_{0.5}$. Inset shows T_N vs. Sn concentration.

ent compound was used for the $\text{Ce}_2\text{RhIn}_{7.9}\text{Sn}_{0.1}$ data, and T_N was estimated to be 1.8 K.

Figure 1(b) shows the ZF- μ SR time spectra of $\text{Ce}_2\text{RhIn}_{7.5}\text{Sn}_{0.5}$. While the relaxation rate above 2 K is almost independent of temperature, there is a gradual increase in the relaxation rate with decreasing temperature. Muon-spin precession signal was not observed at the lowest temperature; this indicates that there is no magnetic ordering at this temperature. The time spectra were described by $A(t) = AP_z(t) + A_{\text{Ag}}$ using the stretched exponential function $P_z(t) = \exp[-(\lambda t)^\beta]$, where λ is the relaxation rate and β is the power of the exponent. The change from Gaussian ($\beta = 2$) to single exponential decay ($\beta = 1$) that occurs with decrease in temperature can be seen in the figure. The rate λ is almost independent of temperature above 0.5 K, and starts to increase rapidly with a decrease in temperature below 0.5 K. Such fast relaxation without any detectable oscillation is a common signature of disordered magnetism that is either static or dynamically fluctuating. Application of longitudinal fields showed that these magnetic signals were completely decoupled between 100–200 mT at 0.3 K; this observation is consistent with a static distribution of local fields. This suggests a spin-glass-like phase, which has been observed in isostructural material Ce_2IrIn_8 ⁴). Muon-spin precession was not observed in the sample of $x = 0.7$ and λ was approximately constant at $\sim 0.29 \mu\text{s}^{-1}$.

As a summary of our results, the magnetic phase diagram of $\text{Ce}_2\text{RhIn}_{8-x}\text{Sn}_x$ as a function of x is shown in the inset of Fig. 1(b). Next, we intend performing μ SR measurements in Ce_2RhIn_8 under pressure.

References

- 1) P. Coleman and A. Schofield; *Nature* **433**, 226 (2005).
- 2) M. Nicklas et al.; *Phys. Rev. B* **67**, 020506(R) (2003).
- 3) E. D. Bauer: Unpublished results.
- 4) G. D. Morris et al.; *Phys. Rev. B* **69**, 214415 (2004).

[†] Condensed from an article submitted to *J. Phys.: Conf. Series*

^{*1} ASRC, Japan Atomic Energy Agency

^{*2} Los Alamos National Laboratory, USA

Precise investigation and re-examination of magnetism and superconductivity of high-quality Fe-based superconductor, $\text{LaFeAsO}_{1-x}\text{F}_x$

H. Fukazawa,^{*1,*5} T. Saito,^{*1} Y. Kohori,^{*1,*5} K. Ohishi,^{*2,*5} Y. Ishii,^{*2,*5} I. Watanabe,^{*2,*5} K. Miyazawa,^{*3,*4} N. Takeshita,^{*3,*5} P. M. Shirage,^{*3} K. Kihou,^{*3,*5} C.-H. Lee,^{*3,*5} H. Kito,^{*3,*5} A. Iyo,^{*3,*5} and H. Eisaki^{*3,*5}

[Iron-based superconductors, μSR , magnetic fluctuation, multiple-gap superconductivity]

Much attention has been paid after the discovery of superconductivity in F-doped LaFeAsO with a superconducting transition temperature $T_c = 26$ K.¹⁾ In over electron-doped iron-pnictide superconductors, pseudo-gap like behavior was observed in normal state.²⁾ Contrary to high- T_c cuprate, theoretical explanation for this phenomenon is not entirely of the magnetic origin but of specific band structure origin.³⁾ From the viewpoint of ZF μSR , we examined the existence of magnetic fluctuation in over electron-doped iron-pnictide superconductors.

In Fig. 1, we show the muon time spectra of $\text{LaFeAsO}_{1-x}\text{F}_x$ with $T_c = 19$ K, which is confirmed to locates in over-doped region from a -axis lattice parameter. The muon time spectra remain the same at all the measurement temperatures. This result clearly revealed that the origin of the pseudo-gap like behavior is not magnetic one. We also examined sample dependence of this temperature behavior of muon time spectra and found that there is no sign of magnetic fluctuation for all the measured samples ($T_c = 27, 23$, and 19 K).

K-doped (hole-doped) BaFe_2As_2 is the firstly reported oxygen-free iron-pnictide superconductor with $T_c = 38$ K.⁴⁾ We reported the ^{75}As nuclear magnetic resonance (NMR) measurement of this hole-doped superconductor $\text{Ba}_{1-x}\text{K}_x\text{Fe}_2\text{As}_2$ with different lattice parameters and different superconducting volume fractions ($T_c \sim 38$ K).⁵⁾ ^{75}As -NMR spectra revealed that the magnetically ordered and superconducting phases are microscopically separated. In our samples synthesized by high pressure method, antiferromagnetic (AFM) ordered state remains up to $x = 0.4$. The internal magnetic field evaluated by zero-field ^{75}As -NMR is suppressed by the substitution x . However, it is also robust with x . This tendency is quite similar to the pressure dependence of the internal magnetic field in the parent material BaFe_2As_2 .⁶⁾ This reflects the first-order nature of this phase transition.

Recent experiments on iron-pnictide superconductors

revealed that the superconductivity in this series of compounds basically possesses multiple superconducting gap nature. Indeed, we clarified that two superconducting gap of distinct sizes realizes in KFe_2As_2 ($T_c = 3.5$ K).⁷⁾ In our previous NQR (nuclear quadrupole resonance) and specific heat measurements, we utilized ^3He refrigerator: we could perform experiments only down to about 0.3 K. Therefore, we are planning to perform zero-field (ZF) μSR measurements on KFe_2As_2 down to about 50 mK in next R383 proposed experiments. Temperature dependence of relaxation rate derived from muon time spectra may clarify the superconducting gap symmetry and sizes of gaps in detail.

References

- 1) K. Kamihara et al., J. Am. Chem. Soc. **130**, 3296 (2008).
- 2) Y. Nakai et al., Phys. Rev. B **79**, 212506 (2009).
- 3) H. Ikeda, J. Phys. Soc. Jpn. **77**, 123707 (2008).
- 4) M. Rotter et al., Angew. Chem. Int. Ed. **47**, 7949 (2008).
- 5) H. Fukazawa et al., J. Phys. Soc. Jpn. **78**, 033704 (2009).
- 6) H. Fukazawa et al., J. Phys. Soc. Jpn. **77**, 105004 (2008).
- 7) H. Fukazawa et al., J. Phys. Soc. Jpn. **78**, 083712 (2009).

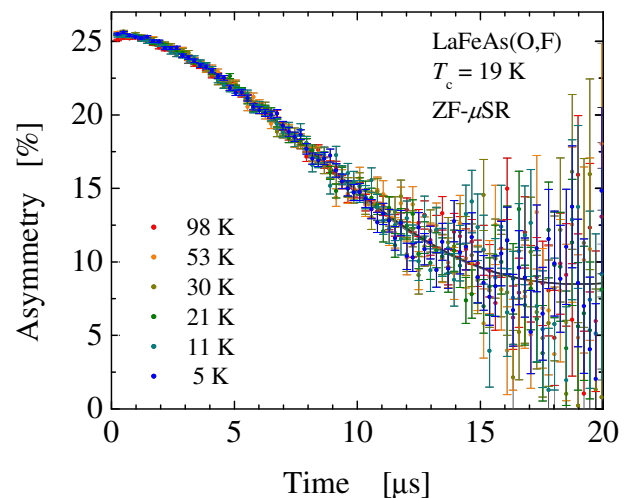


Fig. 1. Muon time spectra of $\text{LaFeAsO}_{1-x}\text{F}_x$ ($T_c = 19$ K).

*1 Department of Physics, Chiba University

*2 Advanced Meson Science Laboratory, RIKEN Nishina Center

*3 National Institute of Advanced Industrial Science and Technology

*4 Department of Applied Electronics, Tokyo University of Science

*5 JST, TRIP

Effect of Pressure on the Stripe Dynamics in $\text{La}_{2-x}\text{Sr}_x\text{Cu}_{1-y}\text{Zn}_y\text{O}_4$ with $x = 0.13$

I. Watanabe, Y. Ishii, T. Kawamata, T. Suzuki, T. Adachi¹⁾, Y. Tanabe^{1,2)}, Y. Koike¹⁾, R. Khasanov³⁾, and D. Andreica⁴⁾

The main purpose of the experiment in this paper is to investigate the effect of pressure on the stabilization of the stripes of spins and holes in high- T_c superconducting oxides [1]. The high- T_c superconductivity is strongly correlated with the stabilization and destabilization of Cu spins for a hole concentration of approximately 1/8 per Cu atom for which the dynamically fluctuating stripes are considered to be stabilized hence, controlling the stripe dynamics is important to determine the point of superconductivity. It has been reported that the stabilization of stripes can be controlled by applying a small pressure of 0.2 GPa [2]. However, recently, it has been pointed out that the electronic state of stripes does not change considerably by even under a pressure higher than 0.2 GPa [3]. Thus, the effect of pressure on stripe dynamics is still a controversial subject.

In order to clarify the effect of pressure on stripe dynamics, we chose $\text{La}_{2-x}\text{Sr}_x\text{Cu}_{1-y}\text{Zn}_y\text{O}_4$ (LSCZO) with $x = 0.13$ as the target material for our study. In this system, the static stabilization of stripes is clearly observed at low temperature and at a specific hole concentration of around $x = 0.115$ even when $y = 0$. The stripes are completely destabilized at $x = 0.13$, and fluctuating outside the μSR characteristic time-window [4-6]. In addition to this, our group has clarified that the dynamics of stripes at $x = 0.13$ can be easily controlled by substituting Cu with the nonmagnetic atom Zn [6]. It is expected that at $x = 0.13$, the stripes are at the border between stabilized and destabilized states. We speculate that if stripe dynamics can be controlled by applying pressure, we will be able to detect a change in stripe dynamics by applying pressure on samples that contain a small amount of Zn. This means that when we apply pressure to a Zn-substituted sample, in which the dynamic stripes appear to be stabilized, we can detect the disappearance of the signs of the stabilized states of Cu spins.

We have already carried out high-pressure μSR measurements on a sample with $x = 0.13$ and $y = 0.0025$ by applying pressure of 0.81 GPa. We carried out the measurements at Paul Scherrer Institute (PSI) in Switzerland and reported the result in the APR report of 2008. From these measurements, we did not observe any effect of pressure on the stabilized stripes. In the present study, we applied high pressure up to a maximum of 1.2 GPa to a sample with $x = 0.13$ and $y = 0.005$; for this sample, the stabilization of stripes is observed appears below 10 K [6]. The high-pressure measurement was carried out at the GPD at PSI in Switzerland, as before.

Figure 1 shows the temperature dependence of the muon-spin-precession amplitude in $\text{TF} = 20$ G of LSCZO with $x = 0.13$ and $y = 0.005$. The top panel shows the data obtained ambient pressure, and the bottom panel shows the data measured at 1.24 GPa. Both panels show that the muon-spin-precession decreases with decreasing temperature. This indicates the appearance of the stabilized state of the stripes. Using a broadened Fermi function, the magnetic transition temperature was estimated to be approximately 6.7 K at ambient pressure and 6.0 K at 1.24 GPa. The effect pressure is quite small, and the difference in the magnetic transition temperature is approximately 10%. Thus, it can be stated that statically stabilized stripes cannot be destabilized by applying a low pressure of 0.2 GPa [2].

At present, we are planning to determine the superconducting states under pressure for the same samples that were used PSI. By comparing the effect of pressure on stripe dynamics of samples in superconducting state, we expect to understand the relationship between the pressure and stripe dynamics.

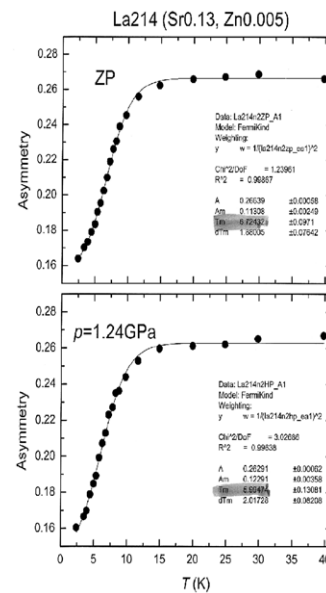


Figure 1: Temperature dependence of the amplitude of the muon-spin precession in $\text{TF} = 20$ G for the sample with $x = 0.13$ and $y = 0.005$. The top panel shows the result of μSR measurement and the bottom panel shows the result of μSR measurement at a high-pressure of 1.2 GPa.

References

- [1] J.M. Tranquada *et al.*, *Nature* (London) **375**, 561 (1995).
- [2] S. Arumugam *et al.*, *Phys. Rev. Lett.* **88**, 247001 (2002).
- [3] J.M. Tranquada *et al.*, in press.
- [4] I. Watanabe *et al.*, *J. Phys. Soc. Jpn.* **61**, 3058 (1992).
- [5] I. Watanabe *et al.*, *Phys. Rev. B* **65**, R180516 (2002)
- [6] T. Adachi *et al.*, *Phys. Rev. B* **69**, 184507 (2004).

*1 Department of Applied Physics, Tohoku University, Japan.

*2 WPI-AIMR, Tohoku University

*3 Bulk Muon Group, PSI, Switzerland.

*4 Department of Physics, Babes-Bolyai University, Rumania,

μ SR study of iron-substitution effects on the Cu-spin dynamics in the overdoped regime of $\text{La}_{2-x}\text{Sr}_x\text{Cu}_{1-y}\text{Fe}_y\text{O}_4$

T. Adachi,^{*1} Y. Tanabe,^{*1*2} K. Suzuki,^{*1} H. Sato,^{*1} T. Suzuki,^{*3} T. Kawamata,^{*3} I. Watanabe,^{*3} and Y. Koike^{*1}

Since the early stage of the research of the high- T_c superconductivity, much attention has been paid to the physics in the overdoped regime. In particular, around $x = 0.22$ in the overdoped regime of $\text{La}_{2-x}\text{Sr}_x\text{CuO}_4$ (LSCO), significant anomalies have been observed so far; a slight depression of the superconducting (SC) transition temperature, T_c ,^{1,2)} a development of the Cu-spin correlation at low temperatures.³⁾ These are suggestive of a possible development of the so-called stripe correlations of holes and spins⁴⁾ around $x = 0.22$, because these are analogous to those observed around $x = 1/8$ where the stripe correlations are much developed.

Recently, Fujita *et al.* have revealed from the elastic neutron-scattering experiment that incommensurate magnetic and nuclear peaks are observed through the partial substitution of Fe with a large magnetic moment (Fe^{3+} : the spin quantum number $S = 5/2$) for Cu in LSCO around the hole concentration per Cu, p , $= 1/8$.⁵⁾ As the superconductivity is strongly suppressed through the Fe substitution around $p = 1/8$,⁶⁾ it is suggested that the Fe substitution is effective for the stabilization of the charge-spin stripe order around $p = 1/8$.

Based on the above results, we have investigated Fe-substitution effects on the electronic properties around $x = 0.22$ in the overdoped regime of $\text{La}_{2-x}\text{Sr}_x\text{Cu}_{1-y}\text{Fe}_y\text{O}_4$ (LSCFO) from measurements of the electrical resistivity, ρ , and magnetic susceptibility.⁷⁾ It has been found around $x = 0.22$ that ρ exhibits a pronounced upturn at low temperatures and that T_c is anomalously depressed. These results suggest that the dynamical stripe correlations are stabilized by Fe, leading to the marked suppression of superconductivity around $x = 0.22$ in LSCFO. This is, however, a very circumstantial conclusion deduced from only the electronic properties. Therefore, in order to find out a direct evidence for the Fe-induced stripe order from the study of the Cu-spin dynamics, we have performed zero-field (ZF) μ SR measurements in the overdoped LSCFO. Polycrystalline samples of LSCFO were prepared by the ordinary solid-state reaction method. The ZF- μ SR measurements were carried out at temperatures down to ~ 2 K at RIKEN-RAL.

Figure 1 shows ZF- μ SR time spectra of LSCFO with $x = 0.225$ and $y = 0.01$ where the superconductivity

is anomalously suppressed. Above 20 K, the spectrum shows Gaussian-like depolarization due to the randomly oriented nuclear spins. On the other hand, fast depolarization of muon spins is observed below 20 K, followed by marked missing of the initial asymmetry at 1.9 K. The change of the spectra indicates the development of the magnetic correlation at low temperatures. Moreover, this result suggests a strong effect of the Fe substitution on the Cu-spin dynamics as well as at $p \sim 1/8$.⁵⁾ The next step is to investigate the p dependence of the spectra around $x = 0.22$.

In summary, we have found from ZF- μ SR measurements fast depolarization of muon spins at low temperatures below 20 K for $x = 0.225$ and $y = 0.01$ in LSCFO where the superconductivity is anomalously suppressed. This suggests the development of the stripe correlations through the Fe substitution in LSCFO around $x = 0.22$. Therefore, there exists an intimate relation between the stripe correlations and superconductivity in the overdoped LSCO.

References

- 1) N. Kakinuma *et al.*: Phys. Rev. B **59**, 1491 (1999).
- 2) T. Kawamata *et al.*: Phys. Rev. B **62**, R11981 (2000).
- 3) I. Watanabe *et al.*: Phys. Rev. B **62**, R11985 (2000).
- 4) J. M. Tranquada *et al.*: Nature **375**, 561 (1995).
- 5) M. Fujita *et al.*: J. Phys. Chem. Solids **69**, 3167 (2008).
- 6) J. Arai *et al.*: J. Phys. Soc. Jpn. **66**, 2875 (1997).
- 7) T. Adachi *et al.*: J. Phys. Soc. Jpn. **78**, 025002 (2009).

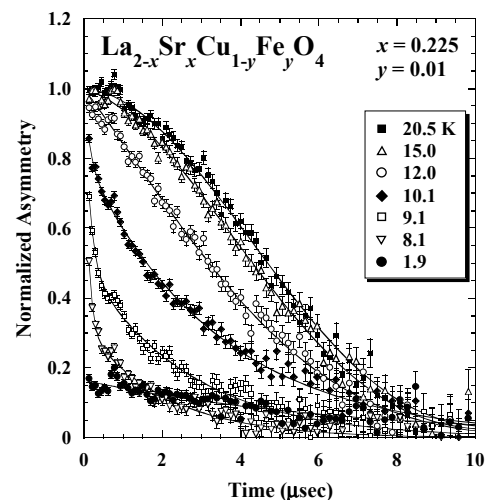


Fig. 1. Zero-field μ SR time spectra at various temperatures for $\text{La}_{2-x}\text{Sr}_x\text{Cu}_{1-y}\text{Fe}_y\text{O}_4$ with $x = 0.225$ and $y = 0.01$.

^{*1} Department of Applied Physics, Tohoku University

^{*2} WPI-AIMR, Tohoku University

^{*3} Advanced Meson Science Laboratory, RIKEN Nishina Center

μ SR study of the impurity-induced development of magnetic correlation in the Bi-2201 high- T_c superconductor

T. Adachi,^{*1} Y. Tanabe,^{*1*2} K. Suzuki,^{*1} T. Suzuki,^{*3} T. Kawamata,^{*3} I. Watanabe,^{*3} and Y. Koike^{*1}

In the history of the high- T_c physics, the relationship between the magnetism and superconductivity has been a central issue. In especial, the so-called dynamical stripe correlations of spins and holes have attracted considerable attention both experimentally and theoretically.¹⁾

Since 2001, we have performed systematic zero-field (ZF) μ SR measurements in the whole superconducting (SC) regime of Zn-substituted La-214 cuprate $\text{La}_{2-x}\text{Sr}_x\text{Cu}_{1-y}\text{Zn}_y\text{O}_4$ (LSCZO) and have found out an intimate relation between the stripe correlations and superconductivity.^{2,3)} However, one may doubt the universality of this relation in various high- T_c cuprates due to predominant effects of the stripe correlations and the possible effect of disorder in the CuO_2 plane through the Sr substitution on various physical properties in $\text{La}_{2-x}\text{Sr}_x\text{CuO}_4$.

The Zn-substituted monolayer Bi-2201 cuprate $(\text{Bi,Pb})_2\text{Sr}_2\text{Cu}_{1-y}\text{Zn}_y\text{O}_{6+\delta}$ (BPSCZO) is one of the best high- T_c systems showing almost all characteristics of the high- T_c superconductivity, i.e., the so-called pseudo-gap, quantum critical point and inhomogeneous SC state. Moreover, this is another high- T_c system in which the hole concentration can be changed widely from the insulating lightly doped to non-SC heavily overdoped regime controlling the excess oxygen content, δ , without large effects of disorder.⁴⁾ In the Zn-substituted double-layer Bi-2212 cuprate $\text{Bi}_2\text{Sr}_2\text{CaCu}_{2-2y}\text{Zn}_{2y}\text{O}_{8+\delta}$, on the other hand, it has been suggested that Zn-induced development of the magnetic correlation is observed but weaker than that in the La-214 cuprate,⁵⁾ suggesting that effects of the stripe correlations are weaker in the Bi-2212 than in the La-214 cuprate. These results encourage us to study the impurity-induced development of magnetic correlation in BPSCZO.

Therefore, we have investigated Zn-substitution effects from μ SR measurements in a wide range of hole concentration per Cu, p , of BPSCZO. Polycrystalline samples of BPSCZO with $y = 0 - 0.03$ were prepared by the ordinary solid-state reaction method. The μ SR measurements were carried out at temperatures down to ~ 0.3 K at RIKEN-RAL.

Figure 1 shows ZF- μ SR time spectra of the underdoped BPSCZO with $p = 0.077$ and $y = 0.03$. Above 2 K, the spectrum shows Gaussian-like depolarization due to the randomly oriented nuclear spins.

Below 2 K, on the other hand, the spectrum changes to exponential-like behavior and fast depolarization of muon spins is observed at 0.27 K. This change of the spectra indicates the development of the magnetic correlation at low temperatures. Moreover, this change is quite similar to that observed in Zn-substituted LSCZO,^{2,3)} suggesting the possible development of the stripe correlations also in Zn-substituted BPSCZO. As for the p dependence, it is found that the fast depolarization is observed in the whole SC regime, though it becomes weak gradually with increasing p . This suggests that the stripe correlations exist throughout the SC regime.

In summary, we have found in ZF- μ SR measurements fast depolarization of muon spins at low temperatures below 2 K in BPSCZO with $y = 0.03$ in a wide range of p where the superconductivity appears. This suggests the development of the stripe correlations in the monolayer Bi-2201 cuprate as well as in the La-214 cuprate. Accordingly, the intimate relation between the stripe correlations and superconductivity might be concluded to be universal in various high- T_c cuprates.

References

- 1) S. A. Kivelson et al.: Rev. Mod. Phys. **75**, 1201 (2003).
- 2) T. Adachi et al.: Phys. Rev. B **69**, 184507 (2004).
- 3) Risdiana et al.: Phys. Rev. B **77**, 054516 (2008).
- 4) K. Kudo et al.: J. Phys. Soc. Jpn. **75**, 124710 (2006).
- 5) I. Watanabe et al.: Phys. Rev. B **60**, R9955 (1999).

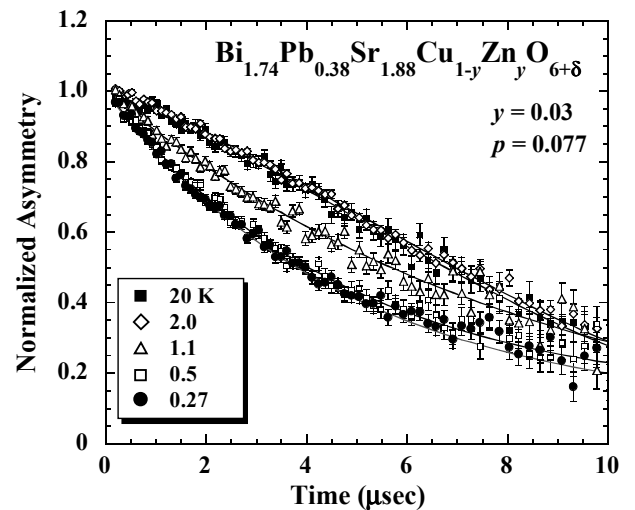


Fig. 1. Zero-field μ SR time spectra of $(\text{Bi,Pb})_2\text{Sr}_2\text{Cu}_{1-y}\text{Zn}_y\text{O}_{6+\delta}$ with $p = 0.077$ and $y = 0.03$ at various temperatures down to 0.27 K.

^{*1} Department of Applied Physics, Tohoku University

^{*2} WPI-AIMR, Tohoku University

^{*3} Advanced Meson Science Laboratory, RIKEN Nishina Center

μ SR study of the vortex state above T_c in high- T_c superconductors

T. Adachi,^{*1} Y. Tanabe,^{*1*2} K. Suzuki,^{*1} M. Akoshima,^{*1} T. Suzuki,^{*3} I. Watanabe,^{*3} and Y. Koike^{*1}

There have been an increasing number of studies on the electronic state in high- T_c cuprates. Among them, the so-called electronic inhomogeneity in the CuO₂ plane has been one of recent interests in high- T_c physics. In the underdoped regime, microscopic inhomogeneity of the superconductivity has been suggested from the scanning tunneling spectroscopy (STS),¹⁾ magnetic susceptibility, χ , and specific heat, C .²⁾ Moreover, a pseudo-gap state has been observed from various kinds of measurements at high temperatures above the superconducting (SC) transition temperature, T_c . One interpretation of these phenomena is that strong-coupling superconductivity with a very short coherence length is realized so that the SC fluctuation is very large, leading to the pseudo-gap state above T_c and the inhomogeneous SC state below T_c .

In the overdoped regime, on the other hand, the superconductivity was regarded as a homogeneous weak-coupling one as in the case of BCS-like conventional superconductors. Recently, however, it has been suggested from χ ^{3,4)} and C ⁵⁾ measurements in the overdoped regime of La_{2-x}Sr_xCuO₄ (LSCO) that a microscopic phase separation into SC and normal-state regions takes place. When the separated two phases in the overdoped regime consist of a hole-rich normal Fermi-liquid state region and a hole-poor strong-coupling SC one, a large SC fluctuation is expected to be observed above T_c even in the overdoped regime.

Although the existence of SC vortices above T_c due to the large SC fluctuation has been pointed out from the observation of a large Nernst effect under magnetic field,⁶⁾ the details have not yet been clarified, because the large Nernst effect do not give a direct evidence for the existence of SC vortices. On the other hand, μ SR measurements may be one of conclusive ways confirming the existence of SC vortices, because μ SR spectra are sensitive to the inhomogeneity of the local magnetic field in a sample caused by SC vortices. Therefore, we have investigated the possible existence of the SC vortices above T_c in LSCO and Bi₂Sr₂Ca_{1-x}Y_xCu₂O_{8+ δ} (BSCYCO) from the underdoped to overdoped regime. Polycrystalline samples of LSCO and BSCYCO were prepared by the ordinary solid-state reaction method. The μ SR measurements were performed at temperatures below 300 K under zero field, longitudinal field (LF) and transverse field conditions at RIKEN-RAL.

Figure 1 shows the temperature dependence of the distribution width of local fields at the muon site, Δ , estimated from the best fit of LF- μ SR spectra using

the analysis function of $A(t) = A_0 G_Z(\Delta, t)$ for the optimally doped BSCYCO with $x = 0.2$. The $G_Z(\Delta, t)$ is the static Kubo-Toyabe function. With decreasing temperature below 150 K, it is found that Δ increases gradually, followed by a steep increase below T_c . The steep increase in Δ below T_c is due to the large inhomogeneity of the local magnetic field inside a sample caused by SC vortices. On the other hand, the gradual increase below 150 K is possibly due to the creation of SC vortices and/or SC islands showing diamagnetism⁷⁾ in the SC fluctuation state, which is consistent with the result of STS in BSCYCO.⁸⁾ Therefore, it appears that SC vortices and/or SC islands exist even above T_c in the optimally doped BSCYCO.

In summary, we have found from LF- μ SR measurements of the optimally doped BSCYCO that the local field at the muon site becomes inhomogeneous below 150 K far above T_c . This suggests the existence of SC vortices and/or SC islands above T_c in high- T_c cuprates.

References

- 1) S. H. Pan et al.: Nature **413**, 282 (2001).
- 2) T. Adachi et al.: J. Phys. Soc. Jpn. **78**, 114707 (2009).
- 3) Y. Tanabe et al.: J. Phys. Soc. Jpn. **74**, 2893 (2005).
- 4) Y. Tanabe et al.: J. Phys. Soc. Jpn. **76**, 113706 (2007).
- 5) Y. Wang et al.: Phys. Rev. B **76**, 064512 (2007).
- 6) Z. A. Xu et al.: Nature **406**, 486 (2000).
- 7) J. E. Sonier et al.: Phys. Rev. Lett. **101**, 117001 (2008).
- 8) K. K. Gomes et al.: Nature **447**, 569 (2007).

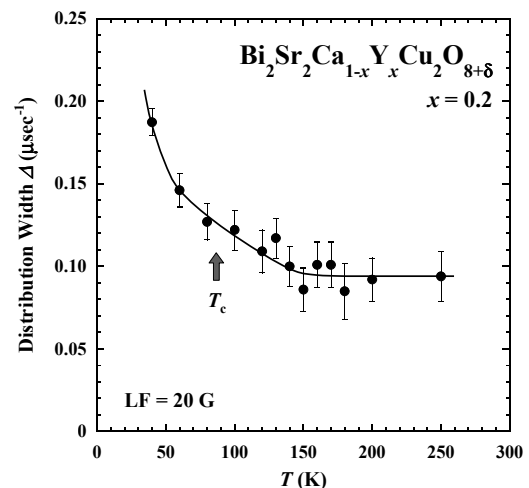


Fig. 1. Temperature dependence of the distribution width of local fields at the muon site, Δ , estimated from LF- μ SR spectra using the function of $A(t) = A_0 G_Z(\Delta, t)$ for the optimally doped Bi₂Sr₂Ca_{1-x}Y_xCu₂O_{8+ δ} with $x = 0.2$.

*1 Department of Applied Physics, Tohoku University

*2 WPI-AIMR, Tohoku University

*3 Advanced Meson Science Laboratory, RIKEN Nishina Center

μ SR study of the Heusler compound $\text{Ru}_{1.9}\text{Fe}_{0.1}\text{CrSi}$

M. Hiroi,^{*1} T. Hisamatsu,^{*1} T. Suzuki, K. Oishi, Y. Ishii, and I. Watanabe

Recently, magnetic properties of the Heusler compounds $\text{Ru}_{2-x}\text{Fe}_x\text{CrSi}$ were studied.¹⁾ It was found that the Fe-rich compounds are ferromagnetic. On the other hand, it was observed that Ru-rich compounds with $x = 0.1$ are not ferromagnetic, but show a peak in magnetic susceptibility at 30 K; this peak probably indicates an antiferromagnetic transition. Meanwhile, in resistivity and specific heat, anomalies that indicate phase transitions were not found. Below ~ 15 K the difference between the magnetic susceptibilities observed in a zero-field-cooling process and field-cooling process increases.²⁾ This observation suggests the formation of a spin-glass state. In our previous study involving zero-field (ZF) μ SR measurements, the peak of the relaxation rate was observed at ~ 15 K, and this suggested the onset of magnetic freezing at this temperature. In order to investigate whether a static internal field is present below this temperature, longitudinal-field (LF) μ SR measurements have been performed for polycrystalline $\text{Ru}_{1.9}\text{Fe}_{0.1}\text{CrSi}$. The measurements were carried out at the RIKEN-RAL Muon Facility using a spin-polarized single-pulse positive surface muon beam. LF- μ SR time spectra were measured at 0.26 K for longitudinal magnetic fields (H_{LF}) up to 3950 Oe.

Figure 1 shows the μ SR time spectra of $\text{Ru}_{1.9}\text{Fe}_{0.1}\text{CrSi}$ for different values of the longitudinal magnetic field. The spectra consist of two components, and $A(t)$ can

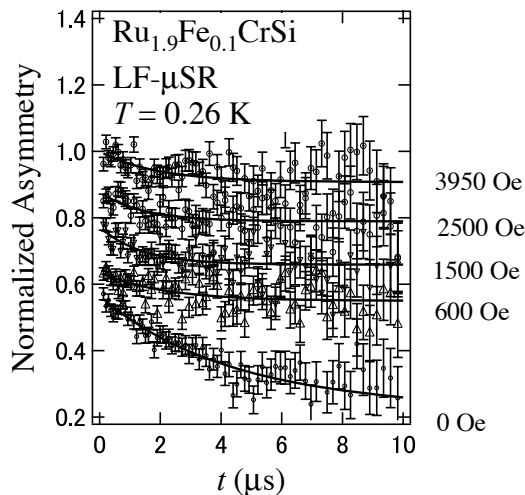


Fig. 1. LF- μ SR spectra of $\text{Ru}_{1.9}\text{Fe}_{0.1}\text{CrSi}$ at various longitudinal magnetic fields at 0.26 K. Solid lines are the fit of $A_1 \exp(-\lambda_1 t) + A_2 \exp(-\lambda_2 t)$.

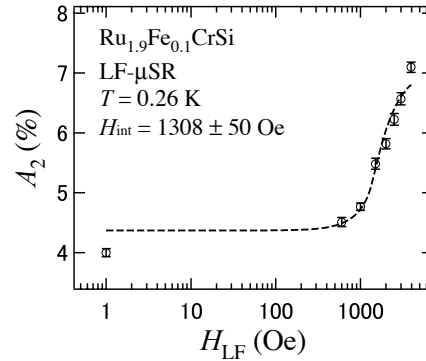


Fig. 2. Dependence of A_2 on the longitudinal field H_{LF} at 0.26 K. The best fit obtained using formula (2) is shown by the solid line.

be expressed as

$$A(t) = A_1 \exp(-\lambda_1 t) + A_2 \exp(-\lambda_2 t), \quad (1)$$

where A_i and λ_i ($\lambda_1 > \lambda_2$) are the initial asymmetry and muon spin relaxation rate, respectively, for each component. As shown in Fig. 1, the time spectra are fitted well by Eq. (1). The tails of the spectra increase with increasing H_{LF} . These results imply that the observed depolarization of muon spins is caused by a static internal magnetic field, H_{int} .

Figure 2 shows the H_{LF} dependence of A_2 at 0.26 K. This represents the decoupling of muon spins from H_{int} due to H_{LF} . Under the assumption that the internal field at each muon site has a unique magnitude but a random direction, H_{int} was estimated by using the following formula:

$$A_2 = \frac{3}{4} - \frac{1}{4x^2} + \frac{(x^2 - 1)^2}{16x^3} \ln \frac{(x + 1)^2}{(x - 1)^2}, \quad (2)$$

where $x = H_{\text{LF}}/H_{\text{int}}$. The solid line shown in Fig. 2 is the best fit obtained using Eq. (2). The value of H_{int} was evaluated to be approximately 1308 ± 50 Oe.

The present results show the existence of a static internal field in $\text{Ru}_{1.9}\text{Fe}_{0.1}\text{CrSi}$ at low temperatures. When considered together with the results of studies on magnetic susceptibility and specific heat, the present results show that spin-glass-like freezing occurs below ~ 15 K, even though long-range order is not realized.

References

- 1) M. Hiroi, K. Matsuda, and T. Rokkaku: Phys. Rev. B. **76** 132401 (2007).
- 2) M. Hiroi et al.: Phys. Rev. B. **79** 224423 (2009).

^{*1} Department of Physics and Astronomy, Kagoshima University

ALC- μ SR Investigation of Model Porphyrins

I. Watanabe, A. Kikuchi, T. Suzuki, T. Kawamata, A. Stoykov, ^{*1} and R. Scheuermann ^{*1}

The main purpose of this study is to clarify the relationship between local structures around the central metal ion, Fe, and functions of hemeproteins because the functions of hemeproteins vary with by not only their 3D-structures but also the electronic state around the Fe ion in hemeproteins. Samples of model-porphyrins Fe(TPP)X ($X = (\text{Imidazole})_2, \text{Cl}$) and Fe(por)X ($X = (\text{Imidazole})_2, \text{Cl}$) were prepared. It should be noted that the latter contained protoporphyrin IX, which is identical to the moiety of hemeproteins. The valence of Fe ion in all samples are 3+. This means that these models are suitable for investigating the “oxidized state” of hemeproteins.

In 2009, our main goal was to obtain information about the location of muons in model porphyrins. Before considering the dynamics of Fe spins in model porphyrins, it is important to answer the following question; where are muons located in porphyrin? If this problem is not addressed, it would be futile to carry out studies to determine the spin dynamics because the muon-spin depolarization behavior is determined by the magnitude and the fluctuation frequency of the internal field at the muon site. In particular, the former depends on the distance between the muon and Fe spin. If the position of the muon is different in each sample, it would be difficult to discuss the internal field from the Fe spin.

In order to satisfy this requirement, we studied an Avoided Level Crossing (ALC) resonance measured at PSI in Switzerland using a continuous muon beam. The injected muons stop at the potential minimum position in the sample and sometimes form a characteristic bound state with surrounding electrons. In such a case, the surrounding electrons induce hyperfine fields at the muon site. These hyperfine fields affect resonance positions of the muon spin when external magnetic fields are applied. Thus, when such resonance signals are observed in fields, the chemical states of muons in materials can be discussed.

The measurement has been performed only at room temperature at the ALC area using a superconducting magnet from zero to about 3 T. Figure 1 shows ALC resonance signals of TPP model porphyrin, which does not have Fe spin at the center of the porphyrin ring. We have clearly observed four resonances in this sample. This result means that there are at least four muon stopping-positions that have different chemical states in TPP. The depth of the signal is approximately corresponds to the fraction of each muon state. Thus, most of muons form similar chemical states with the signal main ALC resonance obtained at 0.75 T. In order to estimate the muon-stopping position, calculation of electric potential is required.

Unfortunately, we did not observe any clear ALC resonance signal in other samples that contained the Fe spin at the center of the porphyrin ring. In these samples, strong depolarization behavior is observed. We argue that the absence of the ALC signal would be due to the strong depolarization behavior of the muon spin caused by the strong fluctuation of Fe spins. Thus, it was impossible to estimate the muon-stopping positions in those samples.

In order to avoid this problem, we are planning to prepare samples that will have the same structure as the measured model porphyrins but no Fe spin at the center position. Since core structures of model porphyrins are not very different from each other, we expect similar ALC signals for all samples. Consequently, we can assume that the locations of muons in all model porphyrin samples would be the same. If this is the case, we would be able to directly compare the fluctuation frequencies of the fluctuating internal field at the muon site.

We plan to carry out ALC- μ SR measurement of the samples in 2010 at PSI using the same experimental apparatus. In addition to this experiment at PSI, we plan to measure the Fe-spin dynamics at the ISIS to determine the fluctuation frequency of each sample. We expect that the results of these experiments would clarify the relationship between local structures of heme and the functions of heme proteins.

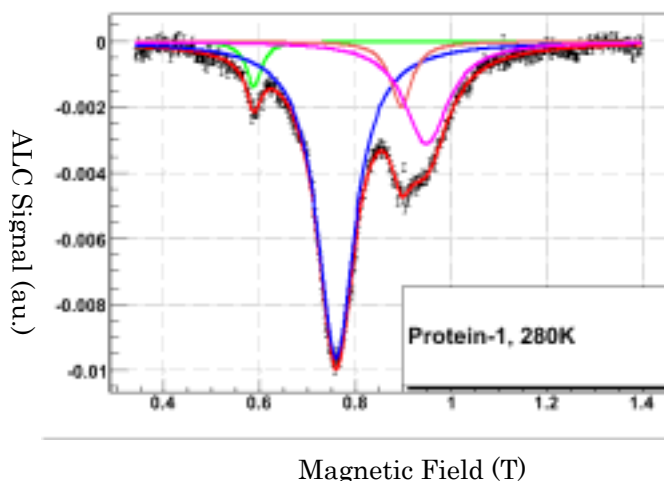


Figure 1: ALC resonances of TPP at the room temperature.

^{*1} Bulk Muon Group, PSI, Villigen, Switzerland.

μ SR study of structure-dependent electron radical dynamics in polythiophene and its derivatives[†]

Risdiana,^{*1} Fitrilawati,^{*1} R. E. Siregar,^{*1} R. Hidayat,^{*2} A. A. Nugroho,^{*2} M. O. Tjia,^{*2} and I. Watanabe

Among the various conducting polymers available, polythiophene (PT) and its derivatives have been studied extensively because of their chemical and thermal stability, as well as their existing and emerging applications in various fields. In particular, extensive studies have been carried out on the PT derivative poly(3-alkylthiophene) (P3AT) because the physical and chemical properties of this derivative can be effectively modified by varying the alkyl-side-chain length. Transport measurements performed on P3AT have revealed a strong dependence of the conductivity of P3AT on its molecular structure such as regioregularity (regioregular (RR) and regiorandom (Rdm)).

Previously, we studied the microscopic charge-transport processes in RR-poly(3-hexylthiophene-2,5-diyl) (RR-P3HT) by performing longitudinal-field (LF) μ SR measurements¹. Herein, we report the temperature-dependent spin diffusion dynamics of the charge-carrying polarons in Rdm-poly(3-hexylthiophene-2,5-diyl) (Rdm-P3HT) and RR-poly(3-octylthiophene-2,5-diyl) (RR-P3OT) observed along the alkyl chain and in the direction perpendicular to the alkyl chain. The diffusion dynamics were studied by the LF- μ SR method for the purpose of determining the relative contributions of intrachain hopping and interchain coupling to the charge-transport process in these polymers. All the time spectra could be well fitted by the two-component function below:

$$A(t) = A_1 \exp(-\lambda_1 t) + A_2 \exp(-\lambda_2 t), \quad (1)$$

where A_1 and A_2 are the initial asymmetries, and λ_1 and λ_2 are the depolarization rates for fast and slow components, respectively. The LF dependence of λ reflects the dimensionality of the diffusion of the spin-excited state. That is, λ is proportional to $H^{-0.5}$ for one-dimensional (1D) intrachain diffusion and $C \cdot H^{0.5}$ for three-dimensional (3D) interchain diffusion².

Figure 1 shows the LF dependence of λ_1 in Rdm-P3HT and RR-P3OT. For comparison, the results obtained for RR-P3HT are also displayed. In the lower panels, λ_1 indicates the $H^{-0.5}$ field-dependent characteristics of 1D intrachain diffusion, implying that the charge transport is dominated by the mobility of the charge carriers along the polymer chain. With an increase in temperature, the charge carriers, which initially follow 1D intrachain diffusion, move by 3D interchain diffusion, as characterized by the field dependence of λ_1 , which could be well fitted by the $C \cdot H^{0.5}$ curve, as shown in the upper panels. The initial change in the carrier mobility appeared to have occurred at

around 25 K to 50 K, 50 K to 75 K, and 50 K to 75 K, in RR-P3HT, Rdm-P3HT, and RR-P3OT, respectively. A similar behavior was observed in the LF-dependent variation of λ_2 . However, the values of λ_2 were two orders of magnitude smaller than those of λ_1 . The present results revealed a remarkable shift in the relative dominance between the intra and interchain charge transport, which depends on the regioregularity and side-chain length of the polymers. Comparison between regioregular and regiorandom in P3HT revealed that interchain diffusion is facilitated at high temperatures for regiorandom polymer system. While a thorough explanation of this difference cannot be given on the basis of the current experimental results, this difference is thought to be related to the difference in the bandgaps between regioregular and regiorandom P3HT. A regioregular structure is known to have a small bandgap (1.7 eV), which is 0.4 eV smaller than that of a regiorandom structure³. Because of the small bandgap, the thermal excitation energy required to support the interchain charge transport is supposedly smaller, and hence, crossover observations can be carried out at a low temperature for regioregular structures. Comparison of the difference in the side-chain lengths of RR-P3HT and RR-P3OT showed that the interchain polaron diffusion process in RR-P3OT is favored at high temperatures. This high-temperature dependence may be related to the difference in the interchain distance between RR-P3HT and RR-P3OT. Clearly, a longer side-chain results in a longer interchain distance, which in turn indicates the need for a high thermal energy to support interchain hopping.

References

- 1) Risdiana *et al.*: RIKEN Accel. Prog. Rev. **42** (2009) 256.
- 2) M. A. Butler *et al.*: J. Chem. Phys. **64** (1976) 3592.
- 3) T. Chen *et al.*: J. Am. Chem. Soc. **117** (1995) 233.

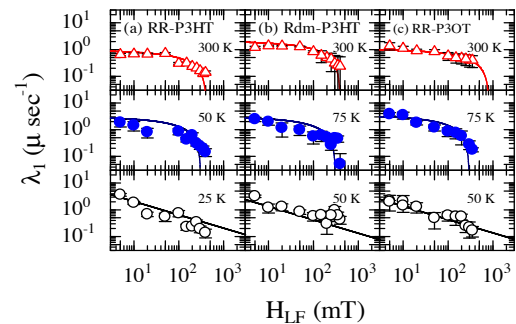


Fig. 1. Longitudinal-field dependence of λ_1 in RR-P3HT (a), Rdm-P3HT (b), and RR-P3OT (c).

^{*1} Department of Physics, Padjadjaran University, Indonesia

^{*2} FMIPA, Bandung Institute of Technology, Indonesia

Study of dynamics of amorphous polymer by performing μ SR measurements

T. Kanaya,*¹ R. Inoue,*¹ I. Watanabe, and T. Matsuzaki,

In order to understand the unresolved problem of glass transition and related dynamics, we have studied the dynamics of a glass-forming polymer using μ SR. We used polybutadiene (PB) with molecular weight M_w of 2.8×10^5 and molecular weight distribution (M_w/M_n) = 1.15. Its glass-transition temperature (T_g) was 170 K. The μ SR measurements were performed at RIKEN-RAL, and the focus was mainly on the dynamic properties of PB. Hence, we performed longitudinal field (LF) measurements with a 100-G magnetic field at temperatures ranging from 10 K to 300 K, which included T_g . In order to evaluate the accurate relaxation rate, we also performed careful dead-time correction of the obtained time-dependence results. Figure 1 shows the decay of the asymmetry for PB at 10 K, 180 K (which was quite close to T_g), and 300 K. With increasing temperature, we can observe a

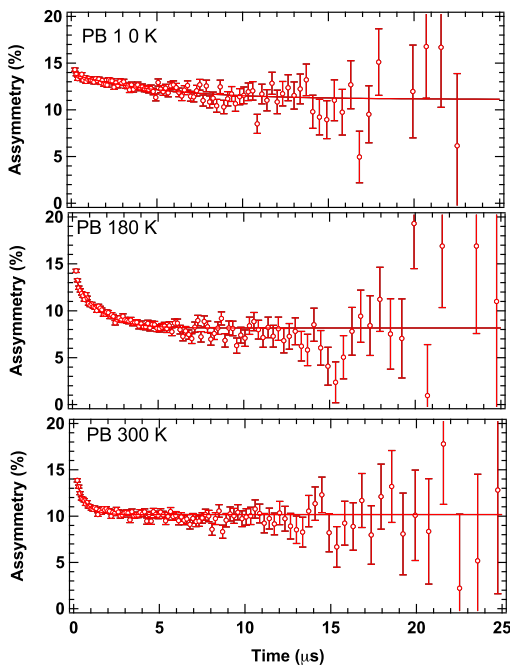


Fig. 1. Time dependence of the decay of asymmetry for PB at 10 K, 180 K, and 300 K under a LF of 100 G.

very clear increase in the relaxation rate very clearly, suggesting the acceleration of dynamics with temperature. In order to analyze the relaxation rate, we fitted the obtained time-dependence data with a single exponential function. It appears that a single exponential function can describe the experimental results reasonably at temperatures below and above T_g . The temper-

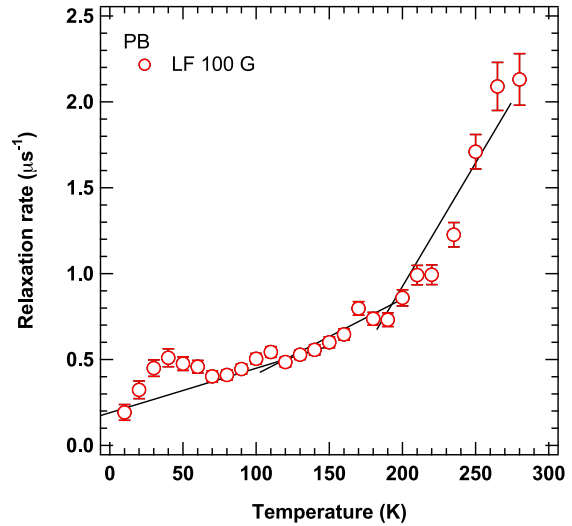


Fig. 2. Temperature dependence of the decay rate for PB. Lines are shown in order to clearly observe the onset of relaxation.

ature dependence of the decay rate is shown in Figure 2. At present, we don't know the physical significance of the small peak observed at around 50 K; apart from this peak, the relaxation rate increased with temperature monotonically. We can observe a steep increase in the relaxation rate above 180 K (which is near to T_g), suggesting that glass transition was detected by μ SR. In addition to the detection of glass transition, we also observe a small increase in the relaxation rate at around 120 K. This temperature corresponds to the onset temperature of the local motion of a so-called fast process. In principle, the time scale of this fast process is about picosecond (ps); hence, it is quite surprising that μ SR can successfully detect such a local motion as well. The temperature dependence of the relaxation rate is quite similar to that of the mean square displacement $\langle u^2 \rangle$ that is evaluated from inelastic neutron scattering. By studying the results of μ SR and inelastic neutron scattering, we can obtain a better understanding of the dynamics of amorphous polymer on a wide-time scale. We are currently trying to evaluate the temperature dependence of heterogeneous relaxation time and rates by fitting a stretched exponential curve to the spectrum. Further analysis is in progress.

*¹ Institute for Chemical Research, Kyoto University

Diffusion of muon in hydrogen tungsten bronze

M. Mihara,^{*1} K. Shimomura,^{*2} I. Watanabe, D. Nishimura,^{*1} J. Komurasaki,^{*1} T. Suzuki, Y. Ishii, T. Kawamata, W. Sato,^{*3} T. Nakano,^{*1} K. Nishiyama,^{*2} R. Kadono,^{*2} S. Takai,^{*4} M. K. Kubo,^{*5} and H. Matsue^{*6}

Hydrogen tungsten bronze H_xWO_3 has important applications in electrochromic (EC) devices in which the dark-blue colored ($x > 0$) and bleached ($x \approx 0$) states of the devices are reversibly controlled by applying an electric field. In order to use a WO_3 -based EC device in thin film displays, a short response time of the EC device must be achieved¹⁾ and the basic property of hydrogen diffusion in H_xWO_3 must be understood. We performed the positive muon spin relaxation (μ SR) measurements, which are potentially useful for the study of hydrogen diffusion; we considered a muon to be a light isotope of proton.

Figure 1 shows the typical ZF- μ SR spectra of H_xWO_3 measured at the RIKEN-RAL muon facility. The hydrogen content $x = 0.4-0.5$ was estimated by a neutron-induced prompt γ -ray analysis (PGA)²⁾ of a test sample that was prepared by following the same procedure as the one for preparing the sample used in the present μ SR experiment. The spectra of H_xWO_3 are characterized by a Gaussian damping, which is in contrast to the exponential-like relaxation observed for pure WO_3 ³⁾. The relaxation curves obtained at $T < 350$ K were well-reproduced by a static Kubo-Toyabe (KT) function that was multiplied by an exponential relaxation factor $\sim KT(\Delta, t)e^{-\lambda t}$. The Gaussian distribution width Δ was nearly constant at around $0.09 \mu s^{-1}$ at temperatures between 10 and 350 K, though the value of λ , which is about $0.03 \mu s^{-1}$ at $T < 100$

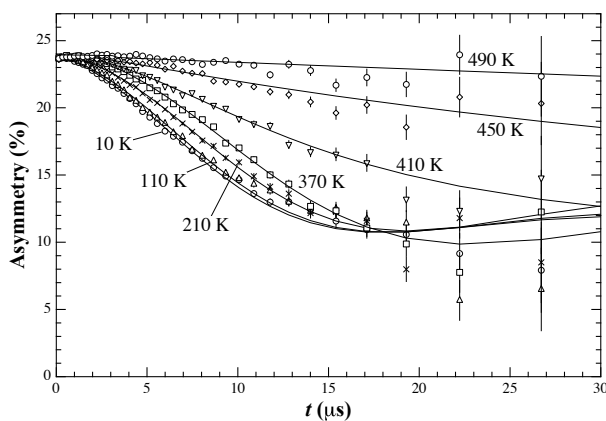


Fig. 1. Typical ZF- μ SR spectra in H_xWO_3 .

*1 Department of Physics, Osaka University
 *2 Institute of Materials Structure Science, KEK
 *3 Department of Chemistry, Kanazawa University
 *4 Department of Materials Science, Tottori University
 *5 The College of Liberal Arts, ICU
 *6 Quantum Beam Science Directorate, JAEA

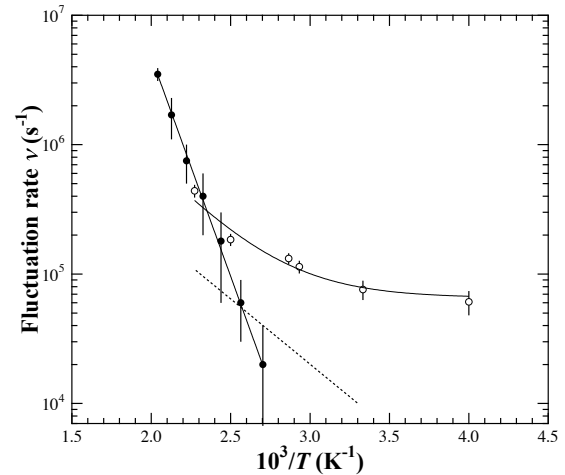


Fig. 2. Fluctuation rate for muons in H_xWO_3 , as deduced from the ZF- μ SR data. The solid circles denote the present results ($x = 0.4-0.5$) and the open circles represent the previous results for $H_{0.22}WO_3$ ³⁾. The dotted line represents the proton NMR results for $H_{0.39}WO_3$ ⁴⁾.

K, decreases with increasing temperature and becomes almost 0 at around 300 K. The value of Δ is almost consistent with that estimated by taking into consideration the nuclear dipolar field of the protons in H_xWO_3 . Motional narrowing effect occurred at $T > 350$ K since the relaxation rate rapidly reduced with increasing temperature. This is considered to be due to the dynamic behavior of muons.

The dynamic properties of muons in H_xWO_3 was determined from the data obtained at $T > 350$ K. The fluctuation rate of the internal field ν , which is considered to be the muon hop rate, was deduced by the χ^2 fitting procedure using a dynamic KT function $KT(\Delta, t, \nu)$ with Δ fixed at $0.09 \mu s^{-1}$. The deduced preliminary result for the fluctuation rate ν is shown in Fig. 2; the results of the previous ZF- μ SR measurements for $H_{0.22}WO_3$ ³⁾ and the proton NMR line widths of $H_{0.39}WO_3$ ⁴⁾ are also shown in this figure.

References

- 1) H. Yoshimura et al.: Jpn. J. Appl. Phys. **45**, 3479 (2006).
- 2) H. Matsue and C. Yonezawa: BUNSEKI KAGAKU **53**, 249 (2004).
- 3) M. Mihara et al.: Physica **B 404**, 801 (2009).
- 4) P.G.Dickens et al.: J. Solid State Chem. **6**, 370 (1973).

Measurement of the Mössbauer γ -rays from exotic Fe atoms produced by μ^- -capture reactions

Y. Kobayashi, M. K. Kubo,^{*1} K. Ninomiya,^{*2} K. Ishida, and M. Iwasaki

Products of nuclear reactions and radioactive decays have been extensively studied for several decades. The large amount of energy available to the atom following a nuclear event induces exotic chemical and physical changes that cannot be achieved by ordinary thermal, electric, mechanical, or electromagnetic excitations. The formation of anomalous chemical species by hot-atom reactions in gas and liquid phases has been extensively studied and clarified. However, the characteristics of the unstable species produced in solid-state hot-atom reactions are not yet completely understood. Therefore, the development of non-destructive characterization methods is necessary to clarify the anomalous chemical states of an atom created by the nuclear events.

Emission Mössbauer spectroscopy has a high sensitivity and can be used to characterize extremely small amounts of any species formed during or after nuclear events; it does not require any chemical treatment of the sample. In particular, the in-beam Mössbauer spectra can be measured simultaneously while inducing the excited states by nuclear reaction or by implantation of nuclear probes. We have successfully measured the neutron in-beam Mössbauer spectra of Fe compounds. The obtained results suggested that thermally unstable and exotic Fe chemical species are formed immediately after the completion of a neutron-capture reaction¹⁾.

It is well known that exotic atoms are produced following negative muon (μ^-) capture or neutron capture in hot-atom reaction. Backenstoss et al. evaluated the distribution of the excited nuclei formed after μ^- -capture process and determined the probabilities of the evaporation of neutrons by identifying the γ -rays emitted in the excited states²⁾. They reported that excited states of $^{57}\text{Fe}^*$ are obtained in the reaction $^{59}\text{Co}(\mu^-, 2n)^{57}\text{Fe}^*$ Co metal target. It is expected that the nuclear probes formed by μ^- -capture possess the large amount of energy associated with neutron recoil. It is important to use the in-beam Mössbauer technique to understand the chemical states of $^{57}\text{Fe}^*$ that results from the μ^- -capture process. As per our knowledge, the formation of excited nuclei after μ^- capture has not been used in Mössbauer studies or other materials science studies. In this experiment, the μ^- -capture process has been used in the study of hot-atom chemistry for the first time.

The experiment was performed at Port-1 in the RIKEN-RAL muon facility. A Co foil with a thickness of 200 μm was set at the target position in the beamline. The γ -rays and muonic X-rays emitted as a result of μ^- capture

were detected by Si(Li) and pure Ge detectors. First, it was determined whether negative muon (30 MeV/c) stopped in the Co target. γ -peaks were observed at 285 keV, 1341 keV (from μCo), and 810 keV (from ^{58}Fe) using the Ge detector. Next, the momentum dependence of 122-keV γ -transition intensity in a thinner Co foil was measured. The 122-keV γ -transition is a precursor of Mössbauer γ -ray, and it is necessary to reduce the thickness of the target because of the low energy of the 14.4-keV Mössbauer γ -ray. Figure 1 shows the energy spectra of the Co metal target foil that captured μ^- with a momentum of 20.4 MeV/c. Although the peak intensities were not sufficient, it was consistent with the intensity ratio of the 14.4-keV transition to the 122-keV transition considering that the internal conversion coefficient is 8.2. The μ^- -beam intensity and the configuration of thin Co target will be optimized further for improved in-beam Mössbauer measurements.

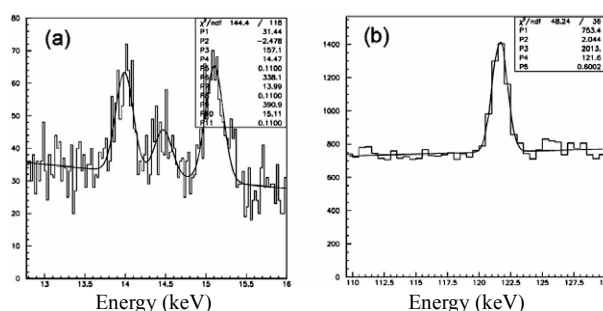


Fig. 1. Energy spectra of Co that captured negative muon with the momentum of 20.4 MeV/c. The Co foil was sandwiched between two Al degraders with a thickness of 30 μm (upstream) and 45 μm (downstream), respectively. (a) 14.4-keV Mössbauer γ -transition and (b) 122-keV transition resulting from the formation of the excited states $^{57}\text{Fe}^*$.

References

- 1) Y. Kobayashi et al.: Hyp. Int. **187**, 49 (2008).
- 2) G. Backenstoss et al.: Nucl. Phys. A **162**, 541 (1971).

^{*1} Division of Natural Science, International Christian University

^{*2} Japan Atomic Energy Agency

Muon Transfer Studies in Solid D₂ with Implanted Rare-Earth Ions

P. Strasser,^{*1} A. Taniguchi,^{*2} S. Ohya,^{*3} T. Matsuzaki, K. Ishida, Y. Matsuda,^{*4} M. Iwasaki, and K. Nagamine^{*5}

[Muonic atom spectroscopy, solid hydrogen film, ion implantation]

The cold hydrogen film method¹⁾ was proposed to apply muonic atom spectroscopy to nuclear beams, including radioactive isotope (RI) beams, with the aim of producing muonic radioactive atoms in the future. This would enable RI studies by the muonic X-ray method at facilities in which both intense μ^- and RI beams will be available. The basic idea is to simultaneously stop both μ^- and nuclear beams in a solid hydrogen film, followed by the direct muon transfer reaction to higher Z nuclei to form muonic radioactive atoms. An experimental program to perform muon spectroscopy with stable ions implanted in a solid D₂ film is in progress at the RIKEN-RAL muon facility. A new surface ion source was installed on the μA^* apparatus with the goal of using RI in the future. Ions from alkali and alkaline-earth elements can be produced very efficiently. Results have already been reported²⁾ from transfer experiments performed with isotopically separated ^{88,87,86}Sr ions. ^{138,137}Ba were also measured.

The new surface ion source can also produce ions from rare-earth elements that ideal candidates for an experiment to study very high Z nuclei with deformation properties. For instance, samarium isotopes show very abrupt changes in their nuclear characteristics from spherical to highly deformed nuclei. ¹⁴⁴Sm is magic in neutrons and displays the characteristics of stiff spherical nuclei, which are very hard to excite, whereas ¹⁵²Sm and ¹⁵⁴Sm reveal low energy levels characteristic of highly deformed nuclei whose muonic X-ray spectra show a 2p hyperfine structure (hfs). The latest measurements were performed with isotopically separated Sm ions utilizing the same procedure as that followed previously to implant Sr and Ba ions²⁾. Figure 1 shows the delayed energy spectra measured by the Ge detector with 1-mm-thick pure D₂ and about 1 ppm of ¹⁴⁸Sm and ¹⁵²Sm ions implanted non-uniformly. This experiment was performed using natural samarium oxide (Sm₂O₃) in the ion source, and only about 6×10^{16} Sm ions in the D₂ film. The measured isotope shift is consistent with that observed in previous experiments performed using enriched Sm isotopes^{3,4)}. ¹⁴⁸Sm still has a spherical nucleus, while ¹⁵²Sm clearly shows the 2p hfs characteristic of highly deformed nuclei.

At present, the experimental accuracy is limited essentially for statistical reasons related to the relatively

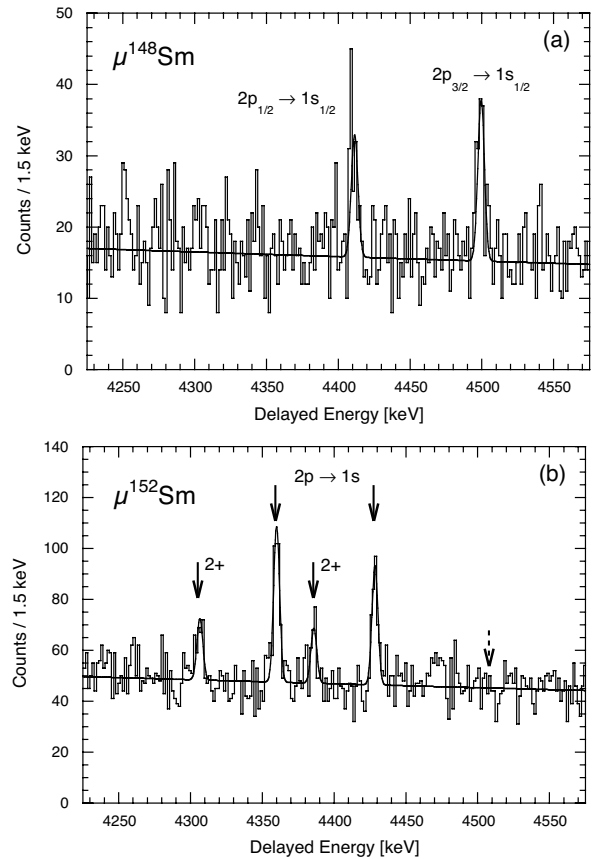


Fig. 1. Delayed spectrum of the 2p \rightarrow 1s muonic transitions in Samarium measured with 1-mm-thick pure D₂ and about 1 ppm of (a) ¹⁴⁸Sm and (b) ¹⁵²Sm ions implanted non-uniformly. The arrows show the most intense lines. The transitions where the ¹⁵²Sm nucleus was excited to the 2⁺ level as the muon reached the 1s state are shown.

low μ^- beam intensity at 27 MeV/c, making the comparison with other measurements involving enriched stable isotopes in very large quantities difficult. Future intense muon facilities with higher muon flux would improve the statistics and also require fewer implanted ions. The advantages of this method with stable isotopes are that the isotope separation can be achieved during the implantation and that high-purity isotopes can be measured. Further, it is free from the chemical composition of the element if it can be fully ionized.

References

- 1) P. Strasser et al.: AIP Conf. Proc. **793**, 242 (2005).
- 2) P. Strasser et al.: RIKEN Acc. Prog. Rep. **41** (2007); RIKEN Acc. Prog. Rep. **42** (2008).
- 3) D. Hitlin et al.: Phys. Rev. **C 1**, 1184 (1970).
- 4) R.J. Powers et al.: Nucl. Phys. **A 316**, 295 (1979).

*1 Muon Science Laboratory, IMSS, KEK

*2 Research Reactor Institute, Kyoto University

*3 Department of Physics, Niigata University

*4 Graduate School of Arts and Sciences, University of Tokyo

*5 University of California Riverside, CA, USA

Progress in the analysis of muon beam density enhancement effect observed when using tapered tubes

D. Tomono, T.M. Kojima, T. Ikeda, K. Ishida, Y. Iwai, M. Iwasaki*¹, Y. Kanazawa*², Y. Matsuda*³, T. Matsuzaki, M. Tokuda*¹ and Y. Yamazaki*³

Generation of highly intense muon beams is currently an important issue in μ SR studies and high-density muonium formation for slow-muon generation at RIKEN-RAL. Since the sample or target used in these studies is usually very small when compared to the beam size (approximately 40 mm), a number of muons are stopped by the collimator at the end of the beamline. By optimizing inner shape of the collimator, the number of muons available can be increased, as in a capillary technique: charged particles can be effectively focused by a tapered glass tube, which deflects them at the inner wall surface and guides them to the outlet. A previous experiment at RIKEN-RAL¹⁾ showed that when a tapered glass tube is coaxially aligned with the muon beam, the 54-MeV/ c pulsed muon beam is partly scattered at the inner wall surface and muons are directed to the outlet by a Coulomb force; as a result, the number of available muons is almost twice that in the case of using a normal beam collimator. In addition, after the upgrade of the proton accelerator, muon beams that are 1.5 times more intense have been generated. By combining this technique and upgrade, we can obtain beams that are at least three times as intense as the previously generated beams. In order to understand muons scattering at the inner wall for practical applications, a new experiment was started using the continuous beam at the M9B beamline, TRIUMF, Canada. In-flight-decay muons whose momentum ranged from 30 MeV/ c to 50 MeV/ c were employed. The experimental setup and detector details have been included in a previous report²⁾. The purpose of this study is to determine the energy and angular distribution of the outgoing muons by identifying each incoming muon with the continuous beam. In addition, density enhancement effect is expected to depend on the material of the tapered tube; this effect is more pronounced when heavy metals such as copper and gold are used instead of glass, probably because of the large Coulomb scattering coefficient in the former case. For simplicity, metal and glass capillary plates were prepared instead of capillary tubes. This article includes the preliminary results of the energy distribution in the case of copper plates observed by lithium-drifted silicon detector (SSD, ORTEC TL-045-200-5).

Figure 1 shows a photograph of the outlet of the

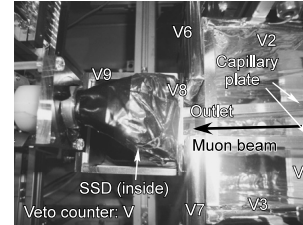


Fig. 1. Photograph of the setup around the outlet of the plates and the SSD detector.

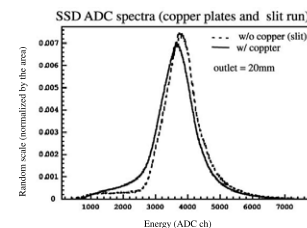


Fig. 2. Muon energy distributions at the outlet of the capillary plates (line) and of the slit (dashed line) for reference.

plates and the SSD (thickness: 5 mm; detection area: 16 mm²). Although the plate material, plate outlet width, SSD position, and array counter position could be varied during the measurements under the present conditions, the SSD was positioned 10 mm downstream of the 20-mm-wide plate outlet. Further, a slit was inserted instead of a plate as a reference for comparison with the case where there was no density enhancement. The muon beam was first identified by a start counter (T1) placed upstream of the plates. Since other particles entering the same time window of 15 μ s could distort the energy spectra because of pile-up signals or accidental background hits, only one muon injection was guaranteed to reject background particles along with the beam under naive analysis conditions; event at the initial time of muon injection and a single hit event to the T1 counter were chosen in the time window.

Figure 2 shows the preliminary results of the energy distribution in the SSD at the 20-mm-wide outlet of the copper plates and slit for 40-MeV/ c muons; the results are normalized by the number of events in the SSD. The obtained results suggest that the scattered muons have lower energy than the initial muons and thus result in a low-energy tail. This might provide information about the stopping range distribution for practical μ SR studies. Presently, all recorded data are being analyzed for a quantitative understanding of the plates and experimental conditions.

References

- 1) T.M. Kojima et al.: J. Phys. Soc. Jpn. **76**, 093501(2007).
- 2) D. Tomono et. al.: RIKEN Accel. Rep. **43**, 261(2009).

*1 RIKEN and Tokyo Institute of Technology

*2 Department of Physics, Sophia University

*3 Graduate School of Arts and Sciences, University of Tokyo

*4 RIKEN and Graduate School of Arts and Sciences, University of Tokyo

3. Radiochemistry and Nuclear Chemistry

Production of an isomeric state of ^{261}Rf by the $^{248}\text{Cm}(^{18}\text{O},5n)^{261}\text{Rf}$ reaction

H. Haba, D. Kaji, Y. Kasamatsu, H. Kikunaga,^{*1} Y. Komori,^{*1} Y. Kudou, K. Morimoto, K. Morita, K. Ooe,^{*1} K. Ozeki, A. Shinohara,^{*1} T. Sumita,^{*2} and A. Yoneda

Previous studies of the $^{208}\text{Pb}(^{70}\text{Zn},n)^{277}\text{112}^{1,2)}$ and $^{248}\text{Cm}(^{26}\text{Mg},5n)^{269}\text{Hs}^{3)}$ reactions have shown the existence of an isomeric state $^{261}\text{Rf}^b$ (half-life $T_{1/2} = 3$ s, α energy $E_\alpha = 8.51$ MeV, Spontaneous Fission branch $b_{\text{SF}} = 0.91$) of ^{261}Rf ($^{261}\text{Rf}^a$: $T_{1/2} = 68$ s, $E_\alpha = 8.28$ MeV, $b_{\text{SF}} < 0.11$).⁴⁾ However, so far, $^{261}\text{Rf}^b$ has not been directly observed as an evaporation residue. Recently, Gorshkov et al.⁵⁾ successfully produced $^{261}\text{Rf}^b$ by the $^{244}\text{Pu}(^{22}\text{Ne},5n)$ reaction at GSI Helmholtzzentrum für Schwerionenforschung GmbH. The Rf atoms were separated with TASCA (TransActinide Separator and Chemistry Apparatus) and transported to ROMA (Rotating wheel On-line Multidetector Analyzer) by a He/KCl gas-jet system. A total of eleven SFs were assigned to $^{261}\text{Rf}^b$ on the basis of the measured $T_{1/2}$ of $2.2^{+0.9}_{-0.5}$ s, though no 8.51-MeV α was observed. In RIKEN, we have been developing a gas-jet transport system coupled to RIKEN GARIS (GAs-filled Recoil Ion Separator) for use in experimental studies in the field of superheavy element chemistry. Recently, $^{261}\text{Rf}^a$ was produced by the $^{248}\text{Cm}(^{18}\text{O},5n)$ reaction and was extracted by the gas-jet to a chemistry laboratory after physical separation by GARIS.⁶⁾ Alpha particles of $^{261}\text{Rf}^a$ were clearly identified using the rotating wheel system MANON for α spectrometry under extremely low background conditions. In this work, we investigated the production and decay properties of $^{261}\text{Rf}^b$ using the GARIS/gas-jet system.

A $^{248}\text{Cm}_2\text{O}_3$ target with a thickness of $230 \mu\text{g cm}^{-2}$ was prepared by electrodeposition onto a Ti foil with a thickness of 0.91 mg cm^{-2} . An $^{18}\text{O}^{5+}$ ion beam was extracted from the RIKEN Linear Accelerator, RILAC. The beam energy was 95.1 MeV at the center of the target, and the average beam intensity was $7 \mu\text{A}$. The reaction products of interest were separated in-flight from the beam and the majority of the nuclear transfer products by GARIS and then guided into the gas-jet chamber through a Mylar window of $0.5 \mu\text{m}$ thickness, which was supported by a honeycomb grid with 84% transparency. GARIS was filled with He gas at 33 Pa and its magnetic rigidity was set at 1.72 Tm. The transmission of GARIS was 8% for $^{261}\text{Rf}^a$.⁶⁾ The reaction products were then transported by the He/KCl gas-jet to MANON in the chemistry laboratory with an efficiency of $\sim 50\%$.⁶⁾ In MANON, the KCl aerosols were deposited on 200-position Mylar foils of $0.5 \mu\text{m}$ thickness placed at the periphery of a wheel with a diameter of 420 mm. The wheel was stepped at 1.67-s intervals to position the foils between seven pairs of Si PIN photodiodes (Hamamatsu S3204-09).

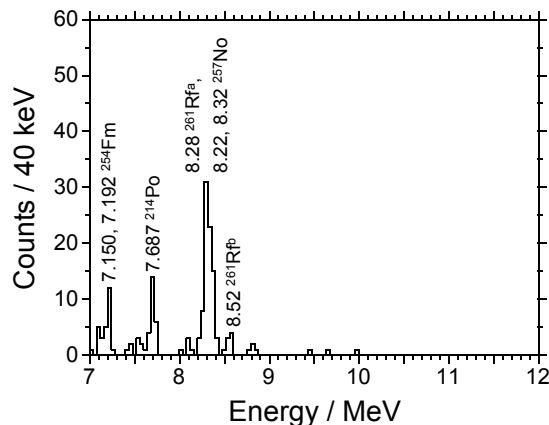


Fig. 1. Sum of α -particle spectra measured in the seven top detectors of MANON.

Figure 1 shows the sum of α -particle spectra measured in the seven top detectors of MANON. A beam dose of 3.2×10^{18} was accumulated. It is to be noted that an α -peak is clearly observed at 8.52 MeV together with those of $^{261}\text{Rf}^a$ and its daughter ^{257}No (24.5 s, 8.22 and 8.32 MeV)⁴⁾ at 8.00–8.43 MeV. Totally, twenty-one 8.52-MeV α -events were registered, and the half-life was determined to be 1.6 ± 0.6 s. Six time-correlated α -events on the 8.52-MeV α were found in the energy window ≥ 7.90 MeV and in the time window ≤ 250 s. The energies of the correlated α ranged from 8.18 MeV to 8.31 MeV, and the half-life deduced from the decay times was 22^{+14}_{-6} s. These decay properties agree well with those of ^{257}No . In addition, sixty SF events with $T_{1/2} = 2.1 \pm 0.6$ s were also registered. In this work, the isomeric state of $^{261}\text{Rf}^a$, $^{261}\text{Rf}^b$, was successfully confirmed directly in the $^{248}\text{Cm}(^{18}\text{O},5n)$ reaction. The α -energy and half-life of $^{261}\text{Rf}^b$ are determined to be 8.52 ± 0.03 MeV and 1.9 ± 0.4 s, respectively. This half-life agrees well with that ($2.2^{+0.9}_{-0.5}$ s) reported in Ref.⁵⁾ The b_{SF} of $^{261}\text{Rf}^b$ is 0.74 ± 0.06 . The cross section (σ) of $^{261}\text{Rf}^b$ was evaluated to be 11 ± 2 nb by assuming the cross section of $^{261}\text{Rf}^a$ to be $12 \text{ nb}^{7)}$ and the gas-jet transport time to be 2.7 s. The σ ratio of $^{261}\text{Rf}^a$ to $^{261}\text{Rf}^b$ (1.1 ± 0.2) is smaller by a factor of two than that (~ 2.5) in the $^{244}\text{Pu}(^{22}\text{Ne},5n)$ reaction.⁵⁾

References

- 1) S. Hofmann et al.: Eur. Phys. J. A **14**, 147 (2002).
- 2) K. Morita: J. Phys. Soc. Jpn. **76**, 043201 (2007).
- 3) J. Dvorak et al.: Phys. Rev. Lett. **100**, 132503 (2008).
- 4) C. E. Düllmann and A. Türler: Phys. Rev. C **77**, 064320 (2008).
- 5) Gorshkov et al.: GSI Sci. Rep. 2008, 140 (2009).
- 6) H. Haba et al.: Chem. Lett. **38**, 426 (2009).
- 7) Y. Nagame et al.: J. Nucl. Radiochem. Sci. **3**, 85 (2002).

^{*1} Graduate School of Science, Osaka University

^{*2} Graduate School of Science, Tokyo University of Science

Experiment on electrochemical oxidation of nobelium using a microchannel-electrode chip

K. Ooe,^{*1} Y. Komori,^{*1} H. Fujisawa,^{*1} A. Kuriyama,^{*1} R. Takayama,^{*1} Y. Kikutani,^{*1} H. Kikunaga,^{*1} T. Yoshimura,^{*1} N. Takahashi,^{*1} H. Haba, Y. Kasamatsu, Y. Kudou, Y. Ezaki, and A. Shinohara.^{*1}

Redox studies of heavy elements with atomic numbers greater than 100 are interesting because the redox potential clearly corresponds to the energy level of the valence state, which is significantly influenced by strong relativistic effects. Recently, the oxidation of element 102, nobelium (No), by an electrochemical approach has been reported by Toyoshima et al.¹⁾ In their experiments, an electrochemical apparatus was combined with ion exchange column chromatography, and No^{2+} was successfully oxidized to No^{3+} . As another method for studying the electrochemistry of the heavy elements, we employed a microchip integrated with electrodes (hereafter referred to as a microchannel-electrode chip). Because various chemical processes can be integrated on a microchip, it is expected that the redox operation can be carried out along with solvent extraction by using a microchannel-electrode chip. In the present study, as a first step towards carrying out an on-chip redox reaction along with solvent extraction, we performed electrochemical oxidation of No^{2+} using a microchannel-electrode chip.

The layout of the glass-substrate microchannel-electrode chip (custom-made by the Institute of Microchemical Technology) is shown in Fig. 1. The dimensions of the microchannel are 2 mm (width) \times 15 μm (depth) \times 60 mm (length). The Pt/Ti electrodes were used as working and counter electrodes. The lengths of the working and counter electrodes are 50 mm and 4 mm, respectively. A thin Ag layer electrodeposited onto the Pt/Ti electrode was used as a pseudo-reference electrode.²⁾ Although this chip has two identical microchannels, only one side of the microchannel was used in the following experiments.

The experiment on No oxidation was performed using the RIKEN K70 AVF Cyclotron. The isotopes ^{255}No ($T_{1/2} = 3.1$ min) and ^{163}Yb ($T_{1/2} = 11.05$ min) were simultaneously produced via the $^{248}\text{Cm}(^{12}\text{C},5n)$ and $^{\text{nat}}\text{Gd}(^{12}\text{C},xn)$ reactions, respectively. The reaction products recoiling out of the target were transported by a He/KCl gas-jet transport system to a chemistry laboratory. The transported products were collected on a Naflon sheet for 5 min and were then dissolved in 1 μL of 0.1 M HNO_3 . The solution was drawn up by a syringe and fed into the microchannel-electrode chip at a flow rate of 3.5 $\mu\text{L}/\text{min}$. The potential applied to the working electrode was 500 or 1250 mV with respect to the Ag pseudo-reference electrode. The effluent from the microchannel-electrode chip was collected in a polypropylene tube for 140 s, and 43 μL of 0.1 M HNO_3

was added to the effluent. The solution was mixed with 50 μL of 0.5 M di(2-ethylhexyl) phosphoric acid in CCl_4 solution and the mixture was shaken for 1 min at 30 $^\circ\text{C}$ to separate No^{3+} from No^{2+} . After centrifugation, 40- μL aliquots of the aqueous and organic phases were separated and evaporated to dryness on Ta discs. These samples were subjected to α -spectrometry for 10 min using Si PIN photodiode detectors. Ytterbium-163 was used to monitor the chemical behavior of the trivalent ion. The extraction behavior of No^{2+} and Yb^{3+} was also investigated in separate experiments carried out using a batch extraction method.

In the batch extraction experiments, the extraction efficiency of No^{2+} was about 7%, while that of Yb^{3+} was more than 99%. Therefore, this extraction system can effectively separate No^{3+} from No^{2+} . In the oxidation experiment at an applied potential of 1250 mV, four α -events in the case of ^{255}No in the aqueous phase and six α -events in the organic phase were observed. On the other hand, at an applied potential of 500 mV, 14 α -events in the case of ^{255}No in the aqueous phase and 1 α -event in the organic phase were detected. Thus, No^{2+} was successfully oxidized to No^{3+} at an applied potential of 1250 mV. In this experimental condition, 1250 mV with respect to the Ag pseudo-reference electrode corresponds to approximately 1600 mV with respect to the normal hydrogen electrode (NHE). The redox potential of No was reported as 1.4–1.5 V with respect to the NHE by Silva et al.³⁾ The present result is consistent with their result. In the future, the dependence of the oxidation efficiency of No^{2+} on the applied potential will be investigated for the determining the redox potential of $\text{No}^{2+}/\text{No}^{3+}$ in 0.1 M HNO_3 .

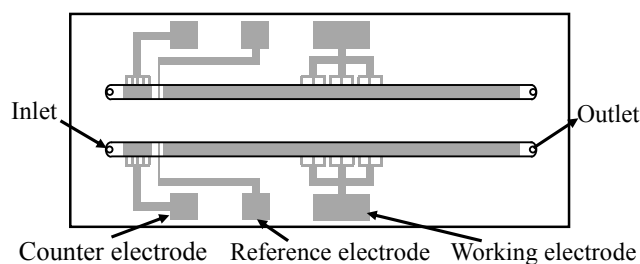


Fig. 1. Structural layout of the glass-substrate microchannel-electrode chip.

References

- 1) A. Toyoshima et al.: J. Am. Chem. Soc. **131**, 9180 (2009).
- 2) C. D. T. Bratten et al.: Anal. Chem. **69**, 253 (1997).
- 3) R. J. Silva et al.: J. Inorg. Nucl. Chem. **31**, 3405 (1969).

^{*1} Department of Chemistry, Osaka University

Liquid scintillation counting of ^{261}Rf produced in $^{248}\text{Cm}(^{18}\text{O},\text{xn})$ reaction and pre-separated using RIKEN GARIS/gas-jet system

Y. Komori,^{*1} K. Ooe,^{*1} H. Fujisawa,^{*1} R. Takayama,^{*1} H. Kikunaga,^{*1} T. Yoshimura,^{*1} N. Takahashi,^{*1}
H. Haba, Y. Kudou, Y. Kasamatsu, and A. Shinohara^{*1}

In order to perform chemical experiments involving superheavy elements (SHEs), a rapid and efficient chemistry apparatus is required because of the short half-lives and low production rates of SHEs.

Liquid scintillation (LS) counting has been used for the detection of α particles in studies of aqueous chemistry of SHEs because it has high detection efficiency and does not require time-consuming evaporation steps for sample preparation.¹⁾ However, LS counting is also sensitive to β particles and γ rays in addition to α particles. Further, the energy resolution is not sufficient to identify α events of SHEs from the large amount of α , β , and γ radiations originating from by-products. In order to remove these by-products, which are unwanted, a technique has been developed for the physical pre-separation for SHE atoms.^{1,2)} In the RIKEN linear accelerator (RILAC) facility, a gas-jet system has been installed behind the gas-filled recoil ion separator (GARIS) to transport pre-separated SHE atoms to the chemistry laboratory.^{3,4)}

We are planning to develop a liquid-liquid extraction system with LS counters coupled with the preseparator GARIS/gas-jet system. In this work, we evaluate the applicability of the LS counting system to the identification of ^{261}Rf on the basis of the observation of a time-correlated α pairs originating from ^{261}Rf and from its daughter ^{257}No , which are reaction products pre-separated and transported by the GARIS/gas-jet system; the α pairs are measured by the LS counter.

^{261}Rf , the most used nuclide for studying Rf chemistry, was produced in the $^{248}\text{Cm}(^{18}\text{O}, 5n)$ reaction. The $^{18}\text{O}^{5+}$ ion beam was extracted from RILAC. The beam energy was 95.1 MeV at the center of a $^{248}\text{Cm}_2\text{O}_3$ target. The reaction products that were pre-separated by GARIS were attached to KCl aerosol particles and then transported through a Teflon capillary in the gas-jet system to the chemistry laboratory.⁴⁾ Samples for LS counting were prepared as follows. The aerosol particles were deposited on a polyethylene terephthalate film for 2 min and were then dissolved in 100 μL of dilute HCl solution (pH 3.1). The HCl solution was mixed with 900 μL of a water-miscible scintillation cocktail in a 10 mm ϕ \times 75 mm Pyrex culture tube. A blank sample for use in LS counting was also prepared by mixing 100 μL of radioactivity-free HCl solution with 900 μL of the scintillation cocktail.

These samples were measured using a PERALS[®] spectrometer (ORDELA, Inc), which is capable of performing pulse shape discrimination (PSD) to distinguish between α and β events. The energy resolution was approximately 550 keV FWHM for ^{241}Am . During the experiment, polyethylene blocks were used to shield the spectrometer from fast neutrons because fast neutron events overlap with α -particle events in a pulse shape spectrum. The aerosol particles were deposited on a glass filter for 5 min and then subjected to γ -ray spectrometry using a Ge detector.

In the LS α spectrometry, the counting rate of β particles in the sample was comparable to that in the blank sample. A total of 12 counts in 14 run, 7495 s of measurement time, were observed in the region where the ^{261}Rf events were expected. These α counts are considered to originate from ^{261}Rf and ^{257}No , other α emitters in the transported products, fast neutrons, or noise of the LS spectrometer. In order to identify time-correlated α pairs from ^{261}Rf and ^{257}No , successively observed events in a time interval of 125 s, which is five times the half-life of ^{257}No , were identified. As a result, four decay sequences were attributed to the time-correlated α pairs from ^{261}Rf and ^{257}No . The mean lifetime of the 2nd α decay is 27 s. The background count rate for α events under the present conditions was determined by excluding the α pairs of ^{261}Rf and ^{257}No from the observed α counting rate and was found to be $(5.3 \pm 2.7) \times 10^{-4}$ cps. The probability of the random correlation evaluated from the background count rate for α events is evaluated to be 0.01%. In the γ spectra, only prompt γ rays from neutron-capture reactions were observed. This observation indicates that no γ -emitting nuclides were transported with the aerosol particles. These results show that LS counting can be used to identify the time-correlated α pairs from ^{261}Rf and ^{257}No by using the GARIS/gas-jet system.

References

- 1) J. P. Omtvedt et al.: J. Nucl. Radiochem. Sci. **3**, 121 (2002).
- 2) C. E. Düllman et al.: Eur. Phys. J. D **45**, 75 (2007).
- 3) H. Haba et al.: J. Nucl. Radiochem. Sci. **9**, 27 (2008).
- 4) H. Haba et al.: Chem. Lett. **38**, 426 (2009).

^{*1} Department of Chemistry, Graduate School of Science, Osaka University

Anionic fluoro complex of element 105, Db†

Y. Kasamatsu, A. Toyoshima,^{*1} M. Asai,^{*1} K. Tsukada,^{*1} Z. Li,^{*1} Y. Ishii,^{*1} H. Toume,^{*1} T. K. Sato,^{*1} T. Kikuchi,^{*1}
 I. Nishinaka,^{*1} Y. Nagame,^{*1} H. Haba, H. Kikunaga, Y. Kudou, Y. Oura,^{*2} K. Akiyama,^{*2} W. Sato,^{*3} K. Ooe,^{*3}
 H. Fujisawa,^{*3} A. Shinohara,^{*3} S. Goto,^{*4} T. Hasegawa,^{*4} H. Kudo,^{*4} T. Nanri,^{*5} M. Araki,^{*5} N. Kinoshita,^{*5}
 A. Yokoyama,^{*6} F. Fan,^{*7} Z. Qin,^{*7} C. E. Düllmann,^{*8} M. Schädel,^{*8} and J. V. Kratz^{*9}

Transactinide elements with $Z \geq 104$ are produced at accelerators using heavy-ion-induced nuclear reactions. Because of their low production rates and short half-lives, chemical experiments with these elements must be performed on a one-atom-at-a-time scale. In the past, the chemical behavior of element 105 (Db), a group 5 element, in aqueous phases has been investigated by comparing it with the behavior of each of the lighter homologues Nb and Ta, and also with the behavior of the pseudo-homologue Pa. Little is however known about the chemical properties of Db because of the constraints of one-atom-at-a-time experiments.

In our previous work,¹⁾ we investigated the anion-exchange behavior of Db in 13.9 M HF and found that the distribution coefficient (K_d) of Db is smaller than those of Nb and Ta, which presumably form $[\text{MF}_6]^-$ and/or $[\text{MF}_7]^{2-}$ ($M = \text{Nb}$ and Ta). In solutions with a lower fluoride ion concentration $[\text{F}^-]$, Nb is known to form oxo-fluoro complexes, whereas Ta forms fluoro complexes. In fact, we have ascertained a significant difference in the anion-exchange behavior between Nb and Ta in HF/ HNO_3 solution ($[\text{F}^-] \leq 0.01 \text{ M}$);²⁾ see Fig. 1. It is therefore of great interest to examine how Db behaves in anion-exchange

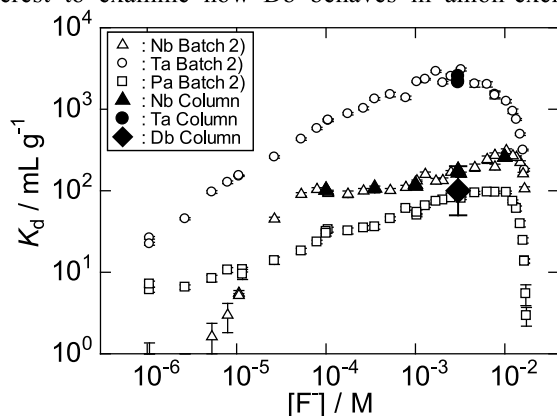


Fig. 1. The K_d values of Nb, Ta, Pa, and Db on the anion-exchange resin in HF/ HNO_3 solutions.

† Condensed from the article in Chem. Lett. **38**, 1084 (2009).

- *1 Japan Atomic Energy Agency
- *2 Department of Chemistry, Tokyo Metropolitan University
- *3 Department of Chemistry, Osaka University
- *4 Department of Chemistry, Niigata University
- *5 Department of Natural Science, Kanazawa University
- *6 Faculty of Chemistry, Kanazawa University
- *7 Institute of Modern Physics, Chinese Academy of Science, China
- *8 GSI Helmholtzzentrum für Schwerionenforschung GmbH, Germany
- *9 Institut für Kernchemie Universität Mainz, Germany

chromatography in a lower $[\text{F}^-]$ solution. In this report, we present a successful measurement of the K_d value of Db in 0.31 M HF/0.10 M HNO_3 solution ($[\text{F}^-] = 0.003 \text{ M}$), where Nb and Ta form $[\text{NbOF}_4]^-$ and $[\text{TaF}_6]^-$, respectively.²⁾

Dubnium-262 was produced in the $^{248}\text{Cm}(^{19}\text{F}, 5n)$ reaction at the JAEA tandem accelerator. The beam energy ranged from 102.1 to 103.8 MeV in the ^{248}Cm target (1.4 mg/cm^2) and the average beam current was 440 particle nA. The reaction products were continuously transported by a He/KF gas-jet system to the collection site of a newly developed rapid ion-exchange apparatus. After collection for 83.4 s, the products were dissolved in 300 μL of 0.31 M HF/0.10 M HNO_3 and subsequently fed to a micro-column (1.0 mm i.d. \times 3.5 mm length) filled with the anion-exchange resin MCI GEL CA08Y at a flow rate of 1.2 mL/min. The eluate was collected as Fraction 1 on a 15 mm \times 300 mm tantalum sheet that was continuously moving toward an α -particle detection chamber at 2.0 cm/s. The sample on the sheet was automatically evaporated to dryness with a halogen heat lamp and then subjected to the α -particle measurement for 75 s in the chamber equipped with an array of 12 Si PIN photodetectors. The remaining products on the resin were stripped with 290 μL of 0.015 M HF/6.0 M HNO_3 . The eluate was collected on another Ta sheet as Fraction 2 followed by the above-mentioned procedures for sample preparation and measurement. The above procedure was repeated 1222 times.

Totally, 26 α events were registered in the energy range of interest for ^{262}Db and its daughter nuclide ^{258}Lr (8.1–8.7 MeV). After subtracting the background count rate of 7.5×10^{-7} counts/s for each detector, the number of α events ascribed to the decays of ^{262}Db and ^{258}Lr was 9.7 for Fraction 1 and 7.6 for Fraction 2. The adsorption probability ($\%ads$) of Db on the resin was determined to be $56^{+16}_{-13}\%$ from the α -decay counts. The K_d value of Db plotted in Fig. 1 was evaluated from the $\%ads$ value in the same way as described in ref. 3. It was found that the adsorption of Db on the resin is considerably weaker than that of Ta and is similar to that of Nb and Pa. The present result suggests that Db would form an oxo-fluoro complex $[\text{DbOF}_4]^-$ like Nb, but not $[\text{DbF}_6]^-$ like Ta.

References

- 1) K. Tsukada et al.: Radiochim. Acta **97**, 83 (2009).
- 2) Y. Kasamatsu et al.: J. Radioanal. Nucl. Chem. **279**, 371 (2009).
- 3) A. Toyoshima et al.: Radiochim. Acta **96**, 125 (2008).

Electrochemical reduction of Europium on a tracer scale as a model experiment for the reduction of Mendeleevium

A. Toyoshima,^{*1} K. Tsukada,^{*1} M. Asai,^{*1} T. K. Sato,^{*1} Z. Li,^{*1} N. Sato,^{*1} T. Kikuchi,^{*1} Y. Kitatsuji,^{*1} Y. Nagame,^{*1} K. Ooe,^{*2}
A. Shinohara,^{*2} Y. Kasamatsu, H. Haba, and J. Even,^{*3,*4}

It is interesting and challenging to study the redox (oxidation - reduction) properties of the heaviest elements. Since redox properties depend largely on the structure of valence electron orbitals, redox studies of the heaviest elements will provide unique information on the influence of relativistic effects on their valence electron orbitals. The heaviest elements (atomic numbers (Z) ≥ 101) are produced in heavy-ion induced nuclear reactions and are available as short-lived isotopes in quantities of a few atoms at a time. Electrochemical experiments of the elements are conducted with single atoms. We had previously developed an electrochemical apparatus for a chromatographic technique for single atoms.¹⁾ Carbon fibers covered with Nafion were packed into a porous glass tube that was employed as a working electrode as well as a cation exchanger to identify the oxidation states of single atoms on the basis of its elution behavior. The oxidation of divalent nobelium ($Z = 102$) to its trivalent state was successfully performed using the apparatus.²⁾

The purpose of the present study is the measurement of the reduction potential for $\text{Eu}^{3+} + \text{e}^- \rightarrow \text{Eu}^{2+}$ reaction on a tracer scale; this reaction is considered as a model experiment for the following reaction involving mendeleevium (Md , $Z = 101$): $\text{Md}^{3+} + \text{e}^- \rightarrow \text{Md}^{2+}$. Hulet et al. performed the reduction of Md by extraction chromatography with some reducing agents and showed that the stable trivalent ion of Md is reduced to the divalent state.³⁾ They also reported that the redox potential of Md is -0.2 V vs. a standard hydrogen electrode (SHE).³⁾ The reported value, however, is fairly doubtful because the experimental conditions were considerably different among the employed reducing agents due to their slow kinetics, and the redox potential value was tentatively estimated on the basis of only one datum despite the fact that the data measured under the various conditions varied considerably. Therefore, accurate determination of the reduction potential of Md by an electrochemical method is necessary.

The radioisotopes ^{139}Ce , ^{146}Gd , ^{169}Yb , ^{85}Sr , and ^{146}Eu present in RIKEN Multitracer (MT) were used to investigate the reduction of Eu by comparing its elution behavior with those of typical divalent (Sr^{2+}) and trivalent (Ce^{3+} , Gd^{3+} , Yb^{3+}) ions on a tracer scale. The delivered MT solution was evaporated to dryness and then stored in 0.1 M HCl. After injection of 20 μL of the stored solution into the

Nafion electrode, 0.1 M HCl solution which was electrolyzed before use to remove dissolved oxygen was subsequently flowed. The effluent from the electrode was collected in eight plastic vials. The ions adsorbed on the electrode were then stripped using 3.0 M HCl. The effluent was collected in two vials. The effluent samples were then subjected to γ -spectrometry using a Ge detector. Elution behavior was examined at applied potentials between 0.4 V and -0.8 V vs. an SHE electrode.

Figure 1 shows the elution behavior at the applied potentials of (a) 0.4 V and (b) -0.8 V. At the potential of 0.4 V, ^{146}Eu was not eluted with 0.1 M HCl and was stripped by 3.0 M HCl. This behavior is almost the same as that of Ce^{3+} , Gd^{3+} , and Yb^{3+} , which indicates that Eu remains in its stable trivalent state. At the lower potential of -0.8 V, on the other hand, ^{146}Eu and ^{85}Sr are eluted with 0.1 M HCl, which indicates that ^{146}Eu is successfully reduced to divalent state. The reduction probability of Eu was varied at around -0.5 V; this observation was in agreement with the result of separately conducted cyclic-voltammetry with 0.001 M Eu in 0.1 M HCl. Thus, the reduction potential of Eu on a tracer scale was successfully determined. The electrochemical reduction of Md will be performed in the near future.

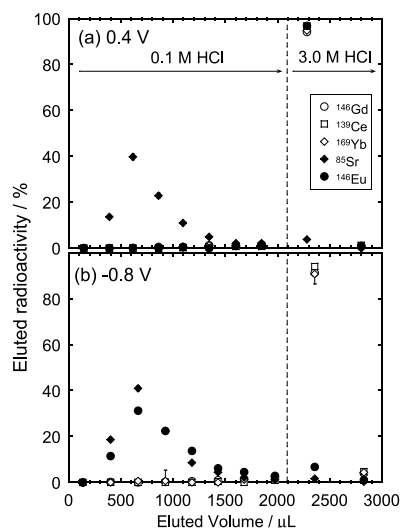


Fig. 1. Elution behavior of ^{139}Ce , ^{146}Gd , ^{169}Yb , ^{85}Sr , and ^{146}Eu at applied potentials of (a) 0.4 V and (b) -0.8 V.

References

- 1) A. Toyoshima et al.: *Radiochim. Acta* **96**, 323 (2008).
- 2) A. Toyoshima et al.: *J. Am. Chem. Soc.* **131**, 9180 (2009).
- 3) E. K. Hulet et al.: *Science* **158**, 486 (1967).

^{*1} Japan Atomic Energy Agency

^{*2} Department of Chemistry, Osaka University

^{*3} Institut für Kernchemie, Universität Mainz, Germany

^{*4} Gesellschaft für Schwerionenforschung Germany

Hydroxide coprecipitation of Zr and Hf with Sm: Model experiment for the chemical study of Rf

Y. Kasamatsu, H. Haba, Y. Ezaki, Y. Kudou and K. Morita

Chemical studies on transactinide elements with atomic numbers $Z \geq 104$ are currently at the frontier in inorganic and nuclear chemistry. Transactinide elements must be produced at accelerators using heavy-ion-induced nuclear reactions. Chemical studies of these elements are conducted on a one-atom-at-a-time basis by rapid chemical separation techniques because of the low production rates and short half-lives ($T_{1/2} \leq 1$ min) of these elements. For unambiguous identifications of these elements existing as one atom at a time, it is necessary to detect α or spontaneous fission decays and to measure the half-lives of these elements. Thus, chemical characterization of transactinide elements is not only fascinating but also challenging. Thus far, mainly from the results of gas-phase and aqueous-phase chromatographic experiments, it has been found that these transactinide elements with atomic numbers up to 108 belong to the set of transition metal elements (d -orbital) in the 7th period. However, the chemical properties of these elements have not been clarified in detail.

Recently, the anion- and cation-exchange behaviors of rutherfordium (Rf, $Z = 104$) in HF and HF/HNO₃ solutions were successfully investigated in detail at the Japan Atomic Energy Agency Tandem Facility, and the behavior of Rf was reported to be clearly different from that of the homologues Zr and Hf.¹⁾ Detailed studies on Rf in various chemical systems must be carried out for a deeper understanding of its chemical properties. The purpose of the present study is to establish a new experimental method for investigating the formation of the hydroxide complex of ²⁶¹Rf ($T_{1/2} = 68$ s). Since Rf can be treated as only one atom at a time, we must study the coprecipitation behavior of Rf with a carrier element. Coprecipitated samples with samarium hydroxide, which facilitated the α spectrometry with a high energy resolution, were prepared by Kikunaga et al.²⁾ using alumina-membrane filters. Therefore, by using this method, we investigated the hydroxide coprecipitation behavior of Zr and Hf with Sm in order to carry out the Rf experiment.

We produced carrier-free radiotracers ⁸⁸Zr ($T_{1/2} = 83.4$ d) and ¹⁷⁵Hf ($T_{1/2} = 70.0$ d) in the ⁸⁹Y/^{nat}Lu(p, xn) reactions in the RIKEN K 70 AVF cyclotron. The radiotracers were chemically purified by an anion-exchange method and finally dissolved in 6 M HCl solution. The hydroxide coprecipitates of Zr and Hf with Sm were prepared by adding 20 μ g of Sm and basic solutions with various compositions (conc. NH₃ water, 0.1, 1, and 6 M NaOH solutions) to the hydrochloric solutions, which contained trace amounts of Zr and Hf (10^8 – 10^9 atoms), until the solution was alkalified (the concentrations of the basic solutions obtained were about 3 M NH₃ water, 0.08, 0.8,

and 3 M NaOH, respectively). The precipitates were soon filtered with the alumina filters, and the preparations were completed within 1 min. Then, the samples were dried at 100 °C using a heater and were subjected to γ -ray measurement with a Ge detector. On the other hand, the reference radioactivity of the radiotracers was also determined by the γ -ray measurement. From the ratio of the measured radioactivities of the precipitates to the reference radioactivity, the yield of each precipitate was determined. The dependence of the yields on the compositions of the basic solutions is depicted in Fig. 1.

It was found that almost the entire amounts of Zr and Hf are coprecipitated with Sm when NH₃ water and 0.1 M NaOH are used. This shows the well-known property of Zr and Hf, i.e., formation of a neutral hydroxide complex and precipitation in basic solutions. The results suggest that the formation of hydroxide complexes of Zr and Hf is sufficiently rapid and that precipitation is complete within 1 min. For more concentrated NaOH solutions, however, the yields decrease as the concentration increases. This is probably because the formation of hydroxide complexes of Zr and Hf proceeds further in the concentrated NaOH solutions; Zr and Hf form anionic hydroxide complexes. For all samples, the yields of Sm were $\sim 100\%$ as determined by the α -particle measurement. As a result, the behaviors of Zr and Hf were observed to be similar under all conditions. It is very interesting to study how Rf behaves under the present experimental conditions.

We are planning to prepare the first hydroxide precipitate of Rf and to investigate the formation of the ammine complexes and the hydroxide complexes of Rf.

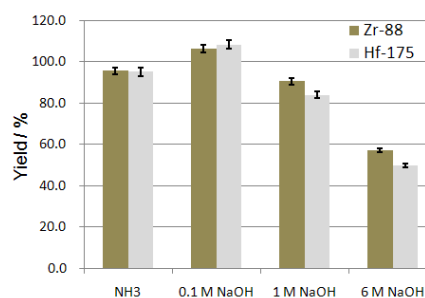


Fig. 1. Variation of the yields of the hydroxide coprecipitation of Zr and Hf according to the compositions of the basic solutions.

References

- 1) Y. Ishii et al.: Chem. Lett. **37**, 288 (2008), and references therein.
- 2) H. Kikunaga et al.: Appl. Radiat. Isot. **67**, 539 (2008).

Study of the reversed-phase chromatography of element 104, rutherfordium (Rf) with TIOA or TTA extractant

M. Araki,^{*1} T. Nanri,^{*1} Y. Takeda,^{*1} M. Nishio,^{*1} M. Nishikawa,^{*1}
Y. Kasamatsu, Y. Ezaki, Y. Kudou, H. Haba, and A. Yokoyama^{*2}

In order to investigate a chemical property of Rf, which is a superheavy element of group 4, we have studied the distribution ratios (D) in liquid-liquid systems for column chromatography under static conditions with resin containing TTA (2-thenoyltrifluoroacetone) or TIOA (Tri-iso-octylamine) extractant, which may clarify the relevant chemical species and provide the complex formation constants. Introduction of this chemical system for the Rf experiment with AIDA (Automated Ion exchange separation apparatus coupled with the Detection system for Alpha spectroscopy) is discussed in this study.

A TTA support material Kel-F (42–80 mesh), which is a polychlorotrifluoroethylene copolymer, was used to prepare a TTA resin for performing reversed-phase chromatography. Batch experiments were carried out to determine the D values for Zr and Hf in chemical equilibrium with TTA resin. The resin with 30-wt% TTA (30–50 mg) and 3 mL of 10^{-4} – 10^{-1} M HF/0.1 M HNO₃ containing 50 μ L of ⁸⁸Zr and ¹⁷⁵Hf carrier-free tracer solution were mixed and allowed to attain equilibrium in a polypropylene tube for 15 min at 20 °C. After centrifugation, 2 mL of the aqueous layer was pipetted into another polyethylene tube and subjected to γ -ray spectrometry using a Ge detector.

Off-line reversed-phase extraction chromatography of ⁸⁸Zr and ¹⁷⁵Hf was performed with a teflon tube column (1.6 mm ϕ) or a microcolumn (1.6 mm ϕ \times 7 mm). The 30-wt% TTA-resin was filled into the column. The radiotracers of ⁸⁸Zr and ¹⁷⁵Hf were deposited on a collection site. Then, the tracers were dissolved in the mixed HF/HNO₃ solutions and fed into the column at a flow rate of 0.5 mL min⁻¹. The effluent was collected in 7–15 polypropylene tubes in order to obtain their elution curves. The remaining Zr and Hf in the column were finally stripped with 0.1 M HF/0.1 M HNO₃ at a flow rate of 0.5 mL min⁻¹. The effluent was collected in two polypropylene tubes. These fractions were assayed by γ -ray spectrometry using a Ge detector.

On-line reversed-phase extraction chromatography of ^{89m}Zr and ¹⁷⁵Hf was performed with a teflon tube or a micro-column. The nuclides of ^{89m}Zr and ¹⁷⁵Hf were simultaneously produced in the ⁸⁹Y(p, n) and ¹⁷⁵Lu(p, n) reactions, respectively, at the RIKEN K70 AVF Cyclotron. The reaction products were transported by a He/KCl gas-jet system, and collected for 300 s. The subsequent procedures are the same as those of off-line reversed-phase chromato-

graphy.

Figure 1 shows typical elution curves of Zr, Hf, and Y in 0.0029 M HF/0.1 M HNO₃ solutions obtained by using the 1.6 mm ϕ teflon tube. The separation of Zr, Hf, or Y from the others achieved is as shown in Fig.1. Distribution ratios were derived from the curves on the basis of a formula developed by Glöckauf for chromatography.

Figure 2 shows the variation of D of Zr and Hf obtained by the batch method and the column chromatography as a function of the equilibrated concentration of F⁻ ($[F]_{eq}$). The dependence of the variation of D on $[F]_{eq}$ observed using the column method corresponds well to that observed using the batch method as well as its magnitude relation between the elements. This demonstrates that the chemical systems of this study are more suitable to be applied to the Rf experiment for investigating the strength of F⁻ complexation compared to that of the other group-4 elements.

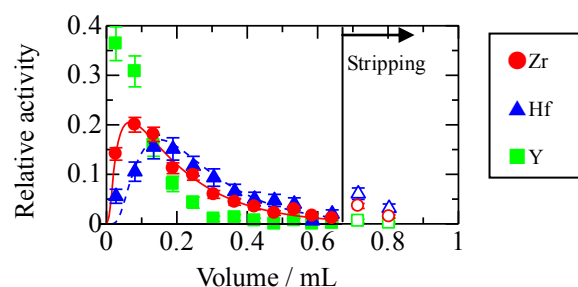


Fig. 1. Typical elution curves for Zr, Hf, and Y with TTA-resin.

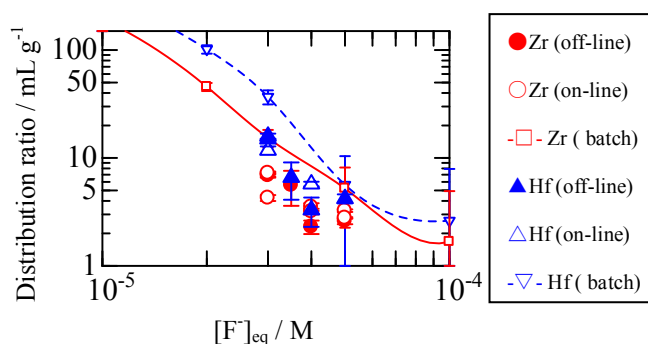


Fig. 2. Variation of the distribution ratios (D) of Zr and Hf for column chromatography under static conditions as a function of the equilibrated concentration of F⁻ ($[F]_{eq}$). The lines drawn joining the batch data are eye guides.

^{*1} Faculty of Science and Graduate School of Natural Science and Technology, Kanazawa University

^{*2} Institute of Science and Engineering, Kanazawa University

Use of solvent-extraction apparatus with microchemical chip in heavy-element chemistry

H. Fujisawa,^{*1} K. Ooe,^{*1} Y. Komori,^{*1} A. Kuriyama,^{*1} R. Takayama,^{*1} Y. Kikutani,^{*1} H. Kikunaga,^{*1} T. Yoshimura,^{*1} N. Takahashi,^{*1} H. Haba, Y. Kasamatsu, Y. Kudou, Y. Ezaki, and A. Shinohara^{*1}

Studies of the chemical properties of superheavy elements and heavy actinides with atomic numbers greater than 100 require rapid analytical techniques with repeatability because of the low production rates and short lifetimes of these nuclides. Thus far, we have so far developed a solvent-extraction technique involving the use of a microchemical chip (MCC), and we have successfully applied this technique in an online experiment¹⁾. In this study, we have automated an apparatus with MCC and use it in solvent-extraction experiment for nobelium.

Figure 1 shows a schematic diagram of the developed solvent extraction apparatus. Nuclear reaction products are transported to the chemistry laboratory by a He/KCl gas-jet transport system. The transported products are deposited on the collection site of a polychlorotrifluoroethylene slider, are dissolved in aqueous solution, and are then subsequently fed into an MCC (ICC-DY15, Institute of Microchemical Technology Co., Ltd.). An organic solution is fed from the other inlet of the MCC. The aqueous and organic effluents from the MCC are separately collected on Ta discs. After the samples are evaporated, they are subjected to α -spectrometry using Si detectors. The series of the operations is automated by using a LabView system (National Instruments Co.).

Off-line tests of this apparatus were carried out using multitracers produced at the RIKEN Ring Cyclotron and single radiotracers produced at the RCNP AVF Cyclotron in Osaka University. The radiotracers were stored in acetic acid/ammonium acetate solutions with a pH of approximately 5.8. Batch experiments were performed as follows. Hundred microliters of the aqueous solution with various pH values and 100 μ L of 0.01 M di(2-ethylhexyl) phosphoric acid- CCl_4 solution were mixed in a test tube. The mixture was shaken for 10 min using a vortex mixer and was then centrifuged for 2 min. After phase separation, each phase was assayed for γ -radioactivity. In the off-line extractions performed by utilizing the apparatus, the same solutions as those in batch experiments were used. Aqueous and organic solutions were fed into the MCC at a flow rate of 5 μ L/min. Each phase from the MCC was separately collected in test tubes and was assayed for γ -radioactivity.

The distribution ratio D is obtained from the equation $D = V_{aq}A_{org}/V_{org}A_{aq}$, where V represents volume and A represents radioactivity. In the case of the

MCC, V is replaced by the flow rate. In Fig. 2, the values of $\log D$ for strontium, which is a divalent cation like nobelium, are plotted as a function of pH in the aqueous phase. The D values obtained by using the apparatus were consistent with those obtained in the batch experiments.

The online experiment involving the extraction of nobelium was performed using the apparatus described above. The ^{255}No ($T_{1/2} = 3.1$ min) isotope was produced in the $^{248}\text{Cm}(^{12}\text{C}, 5n)$ reaction at the RIKEN AVF Cyclotron. In this experiment, the AIDA system²⁾ was used for α -detection. The time elapsed between from the dissolution of the reaction products and the start of the measurement was approximately 4 min. Thus, we have obtained the D value of nobelium in the extraction system, although thorough corrections such as those for cross-contamination between aqueous and organic phases are required. To perform chemical experiments on superheavy elements with atomic numbers greater than 104, we will further improve the present apparatus for carrying out rapid chemical experiments.

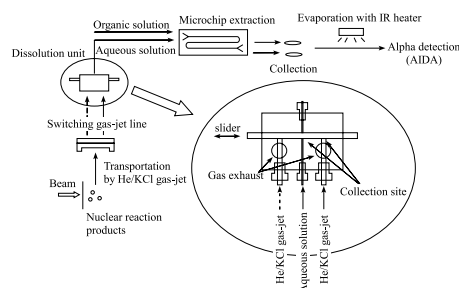


Fig. 1. Schematic diagram of the automated solvent-extraction apparatus.

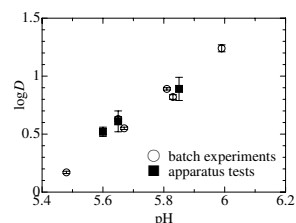


Fig. 2. Plot of $\log D$ vs. pH for strontium with 0.01 M di(2-ethylhexyl) phosphoric acid.

References

- 1) K. Ooe et al.: J. Nucl. Radiochem. Sci. **8**, 59 (2007).
- 2) H. Haba et al.: J. Nucl. Radiochem. Sci. **3**, 143 (2002).

^{*1} Department of Chemistry, Graduate School of Science, Osaka University

Basic study of solvent extraction system with FIA for superheavy element chemistry

Y. Kudou, Y. Ezaki, H. Haba, Y. Kasamatsu, and K. Morita

Chemical investigation of superheavy elements (SHEs, atomic numbers $Z \geq 104$) is of considerable interest because their chemical properties are strongly influenced by relativistic effects.¹⁾ The solvent extraction method is commonly used to investigate the chemical properties of SHEs, especially the complexation equilibrium constants, which are indicative of the chemical-bonding nature, so that these relativistic effects can be well understood. However, since SHEs have short half-lives and very low production rates, ordinary solvent extraction methods should be improved on a one-atom-at-a-time basis. Flow-injection analysis (FIA) makes it possible to perform a series of analytical operations in a continuous flow, such as pretreatment, separation, and detection. FIA is a suitable candidate for a solvent extraction system that facilitates rapid reactions for the SHE chemistry. Itabashi et al.²⁾ succeeded in developing an FIA system for accelerating the extraction process, by using a polytetrafluoroethylene (PTFE) tube packed with PTFE chips as an extraction coil; the PTFE chips help increasing the specific interfacial area and shortening the diffusion length. In this paper, we report the performance and applicability of this FIA system and its applicability to the SHE chemistry.

Using this system, we examined the solvent extraction behaviors of ^{88}Zr and ^{175}Hf (homologues of Rf ($Z = 104$)) in a test experiment performed on Rf. Radiotracers ^{88}Zr ($t_{1/2} = 83.4$ d) and ^{175}Hf ($t_{1/2} = 70.0$ d) were produced in the ^{89}Y ($p, 2n$) ^{88}Zr and ^{nat}Lu (p, xn) ^{175}Hf reactions, respectively; these reactions were carried out in the RIKEN K70 AVF cyclotron. 11.5 M, 10.0 M, and 7.0 M solutions of these tracers in HCl were prepared and stored polypropylene containers. The HCl solutions were used as the aqueous phase, while a toluene of tributyl phosphate (TBP; 50 wt%) was used as the organic phase for solvent extraction. A schematic diagram of the solvent extraction system is shown in Fig. 1.

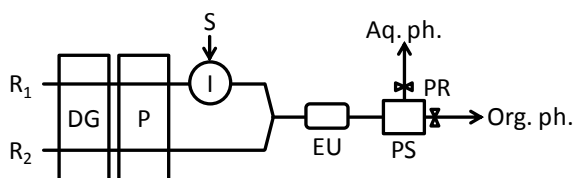


Fig. 1. Schematic diagram of the solvent extraction / FIA system. R₁: HCl solution (11.5 M, 10.0 M, and 7.0 M), R₂: toluene solution containing 50 wt% TBP, S: tracer solution, EU: extraction unit packed with PTFE chips (i. d.: ϕ 2 mm, length: 10 cm), DG: degasser, P: double plunger pump (flow rate: $0.5 \text{ cm}^3 \text{ min}^{-1}$), I: six-way valve that acts as a sample injector, PS: phase separator using a PTFE membrane filter, PR: pressure regulator, Aq. ph.: aqueous phase, Org. ph.: organic phase.

The HCl solution and the toluene solution were propelled by the double plunger pump (P). A solution containing ^{88}Zr and ^{175}Hf was introduced into the aqueous phase by switching the flow channel with the six-way valve (I). The solutions were mixed by using a T-connector and introduced into the extraction unit (EU) packed with PTFE chips ($ca. 1.0 \times 1.0 \times 0.5$ mm), which were obtained by cutting a PTFE tube into pieces of the desired dimensions. The phases were separated by the phase separator via a PTFE membrane filter (pore size: $0.8 \mu\text{m}$). Pressure regulators (PR) were newly installed downstream of both the phases in order to achieve efficient phase separation. After the separation, the aqueous and organic effluents were separately collected in polyethylene tubes and analyzed by γ -ray spectrometry.

The extraction percentage E was calculated by using the following equation:

$$E(\%) = \frac{100 A_{org}}{A_{aq} + A_{org}}, \quad (1)$$

where A_{aq} and A_{org} are the radioactivities in the aqueous and organic phases, respectively. In Fig. 2, the extraction percentages obtained by a batch method and the FIA system are shown for (a) ^{88}Zr and (b) ^{175}Hf as a function of HCl concentration. The extraction percentages obtained using the FIA system agree well with those obtained by the batch method for the 11.5 M and 10.0 M solutions; however, in the case of the 7.0 M solutions, the extraction percentage obtained using the FIA system is less than that obtained by the batch method. In separate experiments, it is found that the percentages obtained by using the FIA system for the 7.0 M solution becomes close to that obtained by the batch method when the flow rate is decreased and the extraction unit is elongated. The total time taken for the online experiments is approximately 1 min. Therefore, this system can be applied to ^{261}Rf , which has a half-life of 74 s. The system proposed in this paper is considered to be feasible for SHE experiments after adequate optimization of the experimental conditions.

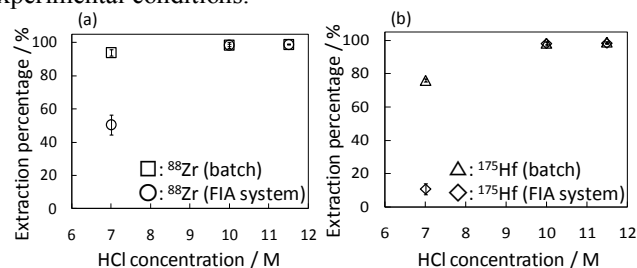


Fig. 2. Difference in the extraction percentages obtained by the batch method and the FIA system for (a) ^{88}Zr and (b) ^{175}Hf as a function of HCl concentration ($n = 3$).

References

- 1) M. Schädel: *Angew. Chem. Int. Ed.* **45**, 368 (2006).
- 2) H. Itabashi and Y. Mesuda: *J. Flow Injection Anal.* **20**, 193 (2003).

Mutual separation of short-lived lanthanides by capillary electrophoresis

H. Kikunaga,^{*1} T. Yoshimura,^{*1} T. Kuribayashi,^{*1} Y. Kitamoto,^{*1} N. Takahashi,^{*1} H. Haba, Y. Ezaki, S. Enomoto,^{*2} T. Mitsugashira,^{*3} and A. Shinohara^{*1}

For studying of the chemical properties of heavy actinides with atomic numbers greater than or equal to ≥ 100 , rapid analysis techniques with high-resolution are required because of the low production rates and short lifetimes of these nuclides. We have successfully applied capillary electrophoresis to ^{152}Dy ($T_{1/2} = 2.37$ h) produced in the $^{nat}\text{Ce}(^{16}\text{O}, \text{xn})$ reactions¹⁾ for the rapid isolation of the element. In this study, we have applied this method for the mutual separation of lanthanides with lifetimes shorter than that of ^{152}Dy , namely, $^{150\text{m}}\text{Tb}$ ($T_{1/2} = 5.8$ min), ^{154}Ho ($T_{1/2} = 11.8$ min), and ^{157}Er ($T_{1/2} = 18.7$ min).

A lanthanide-multitracer solution was prepared as follows. Radiotracers were produced in the $^{197}\text{Au}(^{14}\text{N}, \text{X})$ reactions at the RIKEN Ring Cyclotron. The Au target was dissolved in aqua regia and then heated to dryness. The residue was dissolved in 2 M HCl and passed through an anion exchange resin column (Dowex 1 \times 8, 200-400 mesh) to eliminate the Au target material from the lanthanide fraction. The anion exchange procedure was repeated using a fresh column. The lanthanide fraction was heated to dryness and adjusted to pH 3.

The isotopes $^{150\text{m}}\text{Tb}$, ^{152}Dy , ^{154}Ho , and ^{157}Er were produced in nuclear reactions that involved a 120 MeV ^{16}O beam supplied from the AVF cyclotron at the RCNP in Osaka University. A target that was a mixture of La, Ce, Pr, and Nd was prepared by electrodeposition onto titanium backing foil. The reaction products recoiling from the targets were continuously transported to a chemistry laboratory by using a He/KCl gas-jet transport system. The reaction products were deposited on a polyethylene terephthalate film and dissolved in 2 μL of the lanthanide-multitracer solution. The solution was injected into the anode side of a fused silica capillary, which was filled with an electrolyte solution (12 mM 2-hydroxyisobutyric acid, 350 mM acetic acid, and 10 mM creatinine). A voltage of +30 kV was applied across the capillary with platinum electrodes at room temperature. The separated lanthanides were fractionated by a tailor-made apparatus and assayed for radioactivity by γ -ray spectrometry.

Figure 1 shows electrophoretogram of yttrium and trivalent lanthanides. These elements were derived

from the lanthanide multitracer, except for Tb, Dy, Ho, and Er. The lanthanides moved in ascending order of the atomic number. Figure 2 shows the electrophoretic mobility as a function of the reciprocal ionic radius (coordination number (CN) = 8). The solid line in Fig. 2 is the electrophoretic mobility simulated on the basis of the stability constants for the complexes of lanthanides with 2-hydroxyisobutyrate and acetate²⁾. The mobility of lanthanides is in good agreement with the simulated value. Although there is still room for improving the chemical yield, the present system will be used to study the properties of heavy actinides.

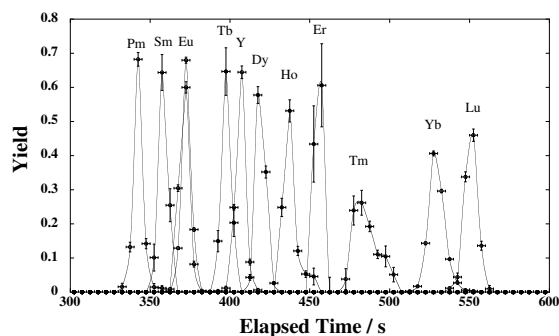


Fig. 1. Electrophoretogram of yttrium and trivalent lanthanides.

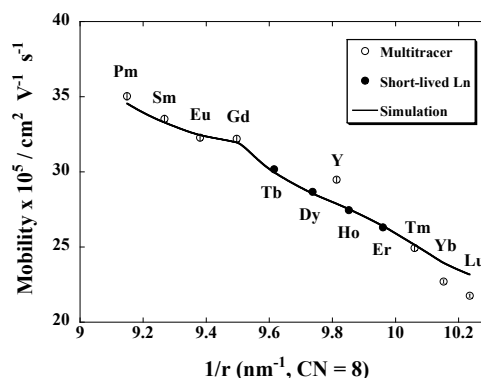


Fig. 2. Electrophoretic mobility as a function of the reciprocal ionic radius (CN = 8).

^{*1} Department of Chemistry, Graduate School of Science, Osaka University

^{*2} Graduate School of Medicine, Dentistry and Pharmaceutical Science, Okayama University

^{*3} International Research Center for Nuclear Materials Science, Institute for Materials Research, Tohoku University

References

- 1) T. Kuribayashi et al.: RIKEN Accel. Prog. Rep. **41**, 213 (2007).
- 2) T. Hirokawa et al.: J. Chromatogr. **312**, 11 (1984).

4. Radiation Chemistry and Biology

The effects of trichostatin A on DNA damage response after X-ray irradiation in human cells

M. Izumi

In eukaryotes, DNA is packaged into nucleosomes that are in turn arranged in various high-order structures to form chromatin. The chromatin structure is regulated by chromatin-associated factors and histone modifications such as acetylation, methylation, and phosphorylation. The chromatin structure influences many aspects of DNA metabolism including replication, recombination, and transcription. However, it is not fully understood how chromatin structure influences DNA double-strand break (DSB) repair and how chromatin structure is altered in response to DNA damage.

The clinical trials for evaluating histone deacetylase (HDAC) inhibitors as anticancer drugs are in progress.¹⁾ HDAC inhibitors exhibit anticancer effects by causing the accumulation of acetylated histones, which relaxes the chromatin structure and activates tumor suppressor genes. In addition to their intrinsic anticancer activity, HDAC inhibitors are synergistic with radiotherapy,^{2,3)} although the mechanism by which HDAC inhibitors enhance the radiation sensitivity of human cells remains unknown.

To examine the roles of chromatin structure in DNA repair and investigate the potential of HDAC inhibitors in combination with heavy-ion radiotherapy, I have been investigating the damage response initiated after treatment of cells with the HDAC inhibitor trichostatin A (TSA). In the previous study, I have examined the effect of TSA on the phosphorylation of histone H2AX⁴⁾. Histone H2AX is a histone variant and is rapidly phosphorylated at the sites of DSBs by ionizing radiation.⁵⁾ I have found that the pretreatment of normal human fibroblast NB1-RGB cells with 0.1 μM TSA for 5 h increased the amount of phosphorylated histone H2AX ($\gamma\text{-H2AX}$) by 2.5-fold at 1 h after irradiation. This result suggests that the relaxed chromatin structure facilitates the repair response by improving damage recognition or changing the susceptibility of DNA to radiation.

Herein, I have investigated the effect of low (0.1 μM) and high (1 μM) concentrations of TSA in HeLa cells. The pretreatment with TSA did not increase the $\gamma\text{-H2AX}$ levels before irradiation (data not shown). At 1 h after irradiation, the amount of $\gamma\text{-H2AX}$ was elevated by 1.8-fold at 0.1 μM and 2.3-fold at 1 μM respectively (Fig. 1). This result indicates that the effect of TSA was dose dependent. Next, HeLa cells were pretreated with TSA and immunostained with anti- $\gamma\text{-H2AX}$ antibody at 1 h after irradiation (Fig. 2). The intensity of immunofluorescence of individual $\gamma\text{-H2AX}$ foci in TSA-treated cells was much higher than that in the control cells. On the other hand, the number of foci in TSA-treated cells was similar to that in the control cells. Therefore, the increase of $\gamma\text{-H2AX}$ level was mainly due to the facilitated damage response and not due to the increase in DSB.

Now, I am investigating whether TSA affects the mutation rate and survival of HeLa cells after irradiation. Further, I am investigating whether TSA has the same effect on the damage response after heavy-ion irradiation.

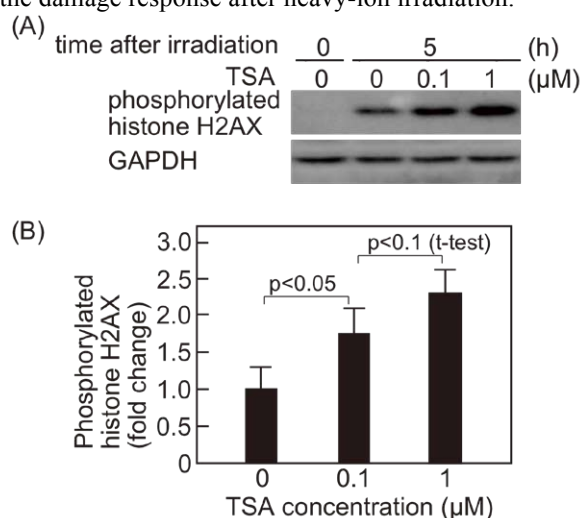


Fig. 1 The effect of TSA at different concentrations. A, HeLa cells were treated with 0.1 or 1 μM of TSA for 5 h and then irradiated with 10 Gy of X-ray using Radioflex. Whole cell extracts were prepared at the indicated time points after irradiation and subjected to immunoblotting. Glyceraldehyde-3-phospho dehydrogenase (GAPDH) was detected as the loading control. B, the intensity of each band was measured using luminoimage analyzer LAS3000 (Fuji Film) and normalized against the amount of GAPDH. Bar graphs represent mean \pm SD of 4 independent experiments.

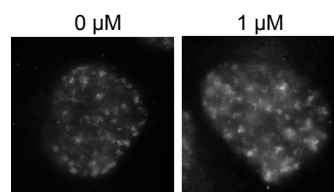


Fig. 2 The pretreatment with TSA increased the intensity of immunofluorescence of $\gamma\text{-H2AX}$ foci. HeLa cells were treated with 1 μM TSA for 5 h and then irradiated with 5 Gy of X-ray. After 1 h, the cells were fixed with ethanol/acetic acid, and $\gamma\text{-H2AX}$ was detected by indirect fluorescent staining.

References

- 1) R. L. Piekarz et al.: *Blood* **103**, 4636 (2004).
- 2) Y. Zhang, et al.: *Radiat. Res.* **161**, 667 (2004).
- 3) K. Camphausen et al.: *Clin. Cancer Res.* **10**, 6066 (2004).
- 4) M. Izumi: *RIKEN Accel. Prog. Rep.* **42**, 249 (2009).
- 5) C. Thiriet and J. J. Hayes: *Mol. Cell* **18**, 617 (2005).

Cell-killing effect of low dose of high-LET heavy ions (III)

M. Tomita,^{*1} T. Tsukada, and M. Izumi

The radiation-induced bystander response is defined as a response in cells that have not been directly targeted by radiation but that are in the neighborhood of cells that have been directly exposed.¹⁾ In space, astronauts are exposed to low fluencies of high-LET (linear energy transfer) radiation. In heavy-ion cancer therapy, normal cells surrounding a tumor are also exposed to heavy ions. Therefore, the bystander responses induced by low doses of high-LET radiation are an important problem in radiation biology. In our study, we aim to clarify the molecular mechanisms and biological implications of bystander responses induced by low doses of high-LET radiation. Previously, we had reported that normal human fibroblasts that were irradiated with low doses of high-LET Fe ions showed low-dose hyper-radiosensitivity (HRS), suggesting that bystander cell killing was induced.^{2,3)} In order to enable a functioning bystander response, at least two signaling pathways should be functional: one pathway is through direct physical interaction between cells such as in the case of gap-junction intercellular communication (GJIC), and the other is through the interaction between the cells and the culture medium.⁴⁾ In addition, it was suggested that reactive nitrogen species (RNS) and reactive oxygen species (ROS) are molecules that play an important role in bystander signaling.⁴⁾ Recently, we reported that the bystander cell killing induced by synchrotron X-ray microbeam irradiation was mainly mediated by nitric oxide (NO).⁵⁾ Now, we are studying the role of NO in the HRS induced by low doses of high-LET Fe ions.

Figure 1 shows the clonogenic survival curve of normal human lung embryonic fibroblast WI-38 cells irradiated with 90 MeV/u Fe ions at 1000 keV/ μm . WI-38 cells were plated in a 25-cm² cell-culture flask for one week before irradiation in order to form confluent monolayers. Carboxy-PTIO (c-PTIO; (2-(4-Carboxyphenyl)-4,4,5,5-tetramethylimidazole-1-oxyl-3-oxide))⁶⁾ is a scavenger of NO. The c-PTIO solution was diluted before the start of the experiments in order to obtain the desired culture medium with a final c-PTIO concentration of 20 μM 2 h before irradiation. The surviving fraction was determined by a colony formation assay. As previously reported,^{2,3)} HRS was observed in the cells irradiated with low doses of Fe ions. The surviving fractions of the cells that were pretreated with c-PTIO at doses of over 1 Gy were not significantly different from those of the cells that were not pretreated with c-PTIO. The decrease in the cell survival at low doses of under 1 Gy was partly suppressed by the pretreatment

with c-PTIO. These results suggest that NO-mediated bystander responses are involved in the process of HRS induced by low doses of Fe ions. The incomplete suppression of the HRS by c-PTIO indicates that other molecules are involved in bystander signaling. Next, we will examine the effect of the inhibitor of GJIS and the scavenger of ROS on the HRS induced by low doses of high-LET Fe ions.

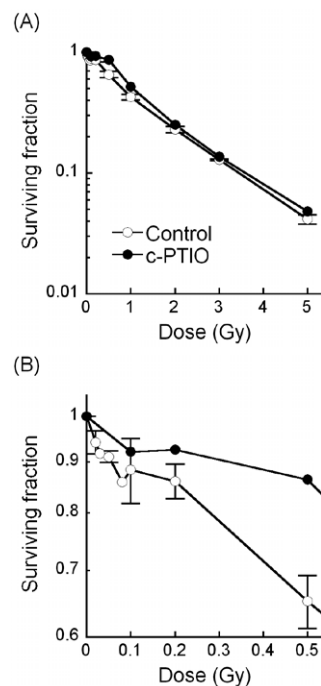


Fig. 1. Cell-survival curves of WI-38 cells. Confluent monolayers of WI-38 cells were irradiated with 90 MeV/u Fe ions (1000 keV/ μm) and were pretreated with c-PTIO with a concentration of 20 μM or not pretreated. The cells were harvested and plated 24 h after irradiation. Surviving fractions (*SFs*) were normalized to those for non-irradiated controls. Panel A shows all *SFs* obtained in this study. Panel B shows *SFs* for doses under 0.5 Gy. The error bars of the *SFs* represent the standard errors of the means (SEMs).

References

- 1) K. M. Prise et al.: *Radiat. Prot. Dosimetry* **99**, 223 (2002).
- 2) M. Tomita et al.: *RIKEN Accel. Prog. Rep.* **41**, 220 (2008).
- 3) M. Tomita et al.: *RIKEN Accel. Prog. Rep.* **42**, 276 (2009).
- 4) H. Matsumoto et al.: *J. Radiat. Res.* **50**, A67 (2009).
- 5) M. Tomita et al.: *Radiat. Res.*, in press.
- 6) T. Akaike et al.: *Biochemistry* **32**, 827 (1993).

^{*1} Central Research Institute of Electric Power Industry

Comparison of mutations of *Neurospora crassa* DSB repair-deficient mutants induced by carbon-ion beam

L. Q. Ma,* S. Tanaka,* H. Inoue,* Y. Kazama, K. Nishihara, T. Hirano, T. Abe, and S. Hatakeyama*

Ion beams are known to cause severe damages to various cellular components. In particular, exposure to ion beams can cause DNA double-strand breaks (DSBs). DSBs are generally repaired by either of the following two DSB repair systems: nonhomologous end-joining (NHEJ) or homologous recombination (HR). If DSBs are allowed to persist or are improperly repaired, mutations will occur. In this study, we determined the types of mutations induced in carbon-ion irradiated wild-type strains and DSB repair-deficient mutant strains.

A carbon-ion beam ($^{12}\text{C}^{6+}$; energy: 135 MeV/u, LET: 30 keV/ μm) was used to irradiate the conidia of the filamentous fungus *Neurospora crassa* at a dose of 25 to 200 Gy. For our experiments, we used the *mus-52* (*YKU80* homologue, NHEJ deficient) and *mei-3* (*RAD51* homologue, HR deficient) mutant strains, as well as 74OR-28a, which was a wild-type control strain. The forward-mutation frequency was determined by calculating the occurrence of genetic alteration at the *ad-3* loci (*ad-3A* or *ad-3B*), which causes the accumulation of a purple metabolic intermediate of the adenine biochemical pathway and thus results in purple colonies. At a dose of 100 Gy, the mutation frequency of the *mus-52* strain was approximately 2.8 times lower than that of the wild-type strain (3.3×10^{-5} /conidia). Conversely, the frequency of mutation of the *mei-3* strain was about 3.0 times that of the wild-type.

Single colony isolates obtained from purple colonies arising in jug cultures were subjected to genetic complementation tests to determine whether mutations had been introduced in *ad-3A* (924 bp) or *ad-3B* (2501 bp) genes. Sequence analysis of DNA fragments obtained by PCR amplification of the *ad-3A* (or *ad-3B*) gene from genomic DNA isolated from each mutant was then carried out. The types of mutations observed in the *ad-3A* and *ad-3B* genes of each strain are shown in Fig. 1 and Fig. 2, respectively. In three independent experiments using the *mus-52* mutant, we observed no mutations in the *ad-3A* gene and a total of 16 mutations in the *ad-3B* gene; this indicates that *mus-52* has a relatively low mutation frequency. It was observed that deletions were the most common type of mutation in the wild-type strain and in *mei-3*, while transversions were predominant in *mus-52*.

According to the mutational analysis performed by Y. Matuo, single base substitutions, especially GC \rightarrow TA transversions, are most commonly induced by the carbon-ion beam irradiation of wild-type *Saccharomyces cerevisiae* (Y. Matuo et al., Mutat.

Res. 2006, 602: 7-13). This is similar to the trend that was observed in the *mus-52* mutant of *N. crassa*, which is deficient in NHEJ and therefore, must use HR. Since *S. cerevisiae* has an extremely high frequency of HR compared to other eukaryotic organisms, one could speculate that in cells where HR is highly active, single base substitutions are more likely to occur. Additionally, as is the case in *N. crassa*, the occurrence of HR is also low in plants, and thus, it is possible that mutational analyses conducted for *N. crassa* can also be used in plant-breeding studies that involve ion-beam irradiation.

We could not determine whether the mutation occurred in the *ad-3A* or the *ad-3B* gene in some of the *ad-3* mutants generated in this study. It is possible that in addition to the *ad-3* mutation, these strains are deficient in an essential gene. In this case, we suspect that some of these strains carry a large deletion mutation that removes *ad-3A* and/or *ad-3B* as well as a neighboring essential gene. To confirm this hypothesis, we are developing tester strains that may help us identify such large deletions.

*Laboratory of Genetics, Saitama University

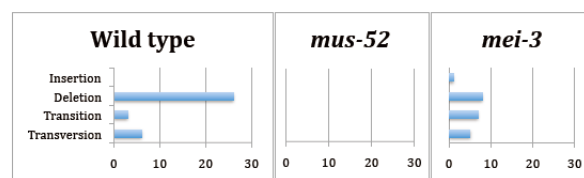


Fig. 1. The type of mutation at the *ad-3A* locus of wild-type, *mus-52* and *mei-3* strains

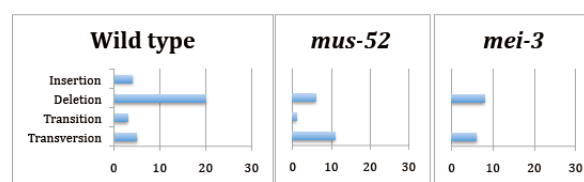


Fig. 2. The type of mutation at the *ad-3B* locus of wild-type, *mus-52* and *mei-3* strains

Chronic effects of ion-beam irradiation on protonemal cells in the moss *Funaria hygrometrica*

M. Itouga*¹, Y. Komatsu-Kato*¹, S. Kawakami*², Y. Kazama, H. Ichida, Y. Hayashi, T. Abe, and H. Sakakibara*¹

Ash-tolerance moss *Funaria hygrometrica* Hedw. grows on waste area (e.g. final landfill, smelter) in field. It also prefers burned areas or campfire sites, where the fire has released large amounts of nutrients. In our previous works, we obtained the cultured cells from the plant growing on a waste area (Omuta city, Fukuoka Pref., Japan) and we demonstrated that the *Funaria* cells have very large capacities with an adsorption of lead from water¹⁾. We are now developing on the bio-sorption systems of water contaminated with heavy- and/or rare-metals using a novel mutant cells which created by ion-beam irradiation technology. In this report, we describe the effects of ion-beam irradiation on protonemal cells in this moss.

Protonemal cells were cultured on agar plate seated with cellophane. Their cells were irradiated by ¹²C⁶⁺(LET 23 keV/μm), ²⁰Ne¹⁰⁺(LET 63 keV/μm), ⁴⁰Ar¹⁷⁺(LET 280 keV/μm) and ⁵⁶Fe²⁴⁺(LET 640 keV/μm) with a dose range of 0 to 400Gy. Each ion was accelerated to 135, 135, 95 and 90 MeV/nucleon by RRC. Then, their cells were collected with cellophane to inoculate on a new agar plate and each plate was incubated under a same condition for 40 days. We checked the growth rate of protonemal cells at 10 days after inoculation and counted the number of leafy gametophytes per a colony at 24 days after inoculation. Length of shoot and number of leaf in 30 samples of leafy gametophytes were also examined at 40 days after inoculation.

Changes in growth rate were caused by ion-beam irradiation (Fig.1). Leaf gametophytes development was induced at lower dose irradiation with high growth rate (Fig.1, 2). For example, Fe-ions obviously induced leafy gametophytes development (Fig.3). Fe-ion treatment with 150Gy achieved the peak value, suggesting that higher mutagenic potential may occur at 150Gy (Fig.2, 3). Similarly, each specific peak value for C, Ne, and Ar was also observed (i.e. 200-225Gy for C, 200Gy for Ne, 75Gy for Ar) (Fig.3). These results show that specific peak values

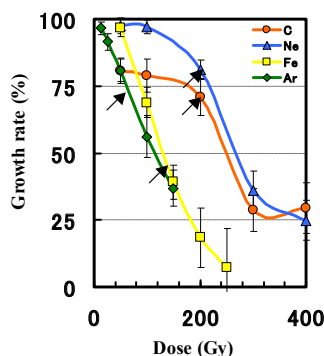


Fig. 1. Changes in growth rates of protonemal cells at 10 days after inoculation. Bars show standard error (n=30). Arrows show a point with strong induction of and leafy gametophytes development.

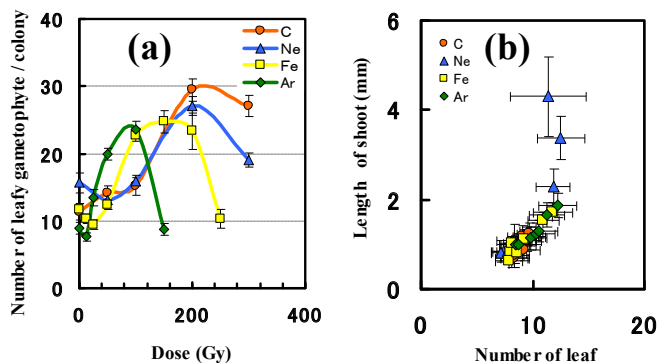


Fig. 2. Chronic effects of heavy-ion irradiation on leafy gametophytes development form protonemal cells. (a) Dose response changes in mean number of leafy gametophytes per colony at 24 days after inoculation. Bars show standard deviation (n=30). (b) Relationship between leaf number and shoot length at 40 days. Bars show standard error (n=30).

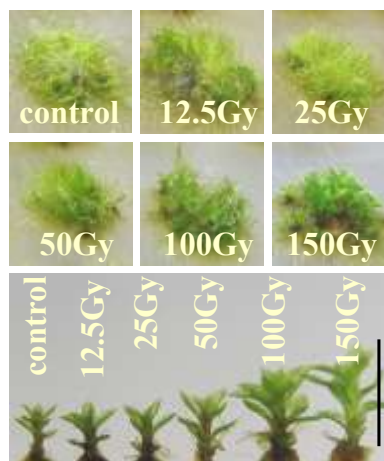


Fig. 3. Effect of ⁵⁶Fe ion irradiation on protonemal cells. Typical colony and leafy gametophytes are shown as optical images. Bar = 2.0 mm.

for heavy-ions are our optimum condition for *Funaria* mutation breeding, however these chronic effects are associated to several biological changes by stress response such as accumulation of reactive oxygen species (ROS) to heavy ion irradiation²⁾.

In our future works, we should confirm these effects are not depended on transient responses to heavy ions.

References

- 1) M. Itouga et al. PCT/JP2008/053142.
- 2) L. Zhang et al.: Nuclear Science and Techniques **19**, 138 (2008).

*¹ RIKEN, Plant Science Center

*² DOWA ECO-SYSTEM CO., LTD., Environmental Protection Lab.

Seed hypoplasia induced by heavy-ion beam irradiation of pollen grains in dioecious plant *Silene latifolia*

K. Ishii^{*1}, W. Aonuma^{*1}, C. Torii^{*1}, N. Fujita^{*1}, Y. Kazama, T. Abe, and S. Kawano^{*1}

We have previously conducted carbon-ion-beam irradiation of dry seeds of the dioecious plant *Silene latifolia* and obtained sex-reversal mutants.¹⁾ However, the mutant derived from the irradiated seeds exhibited chimeric phenotypes. Fixation of the mutant gene was quite difficult. Therefore, to obtain mutants without chimeric mutations, carbon-ion irradiation of the pollen grains was performed, and this was followed by artificial pollination. Further, we investigated the hypoplasia that was observed in the seeds derived from pollen grains irradiated with the heavy-ion beam.

Mature anthers of an inbred line (K line) of *S. latifolia* were irradiated with a $^{12}\text{C}^{6+}$ beam (135 MeV/nucleon) at a dose of 0–200 Gy; the LET of the ions was 23 keV/ μm . The ratio of the number of pollen grains that showed pollen-tube growth without any rupture to the total number of pollen grains was calculated at 24 h after sowing in the germination medium (Fig. 1A). In the case of the pollen grains irradiated at doses of up to 10 Gy, the germination rate of the pollen grains was 100%. On the other hand, at doses of over 20 Gy, the number of pollen grains showing pollen-tube growth gradually decreased as the absorbed dose increased.

The irradiated pollen grains were used to fertilize female plants of the K line. After one month, seeds were collected and sown in pots. The germination rates were measured three weeks after sowing (Fig. 1B). The germination rate of the seeds derived from 5-Gy-irradiated pollen grains was 55% and that of the seeds derived from 60-Gy-irradiated pollen grains was 0%. The 50% inhibitory dose (I50) for the irradiated seeds and that for the seeds derived from the irradiated pollen grains were approximately 150 Gy and 30 Gy, respectively.

Two types of seeds were derived from the irradiated pollen grains. Seeds of type A showed normal morphology, and their short axes were more than 1 mm in length (Fig. 2A). Seeds of type B exhibited aberrant morphology and their short axes were less than 1 mm in length (Fig. 2B). These two types of seeds coexisted in the same capsule. The ratio of the number of type-A seeds to the total number of seeds decreased as the absorbed dose increased (Fig. 3A, black circles). The germination rates of both types of seeds were measured three weeks after sowing (Fig. 3B). The germination rate of type-A seeds derived from the 40-Gy-irradiated pollen grains was 81%, while that of the type-A seeds derived from the 60-Gy-irradiated pollen grains was 0%. On the other hand, the germination rate of type-B seeds derived from the pollen grains irradiated at doses of up to 20 Gy was 17%, while that of the type-B seeds derived from the 40-Gy-irradiated pollen grains was

0%. Thus, we can obtain plants in which abnormality during embryogenesis would not be observed, by sowing only type-A seeds.

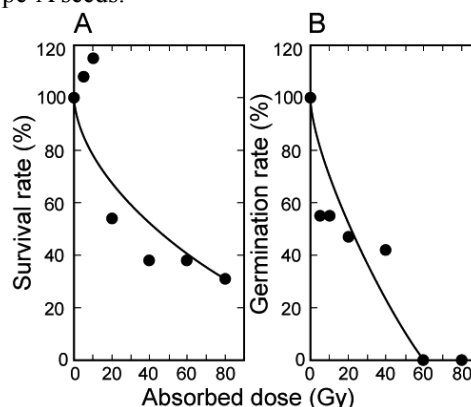


Fig. 1. Effects of carbon-ion-beam irradiation. (A) Survival rate of irradiated pollen grains. (B) Germination rate of seeds derived from the irradiated pollen grains. The relative rates for 0-Gy-irradiation are defined as a survival rate or a germination rate of 100%.

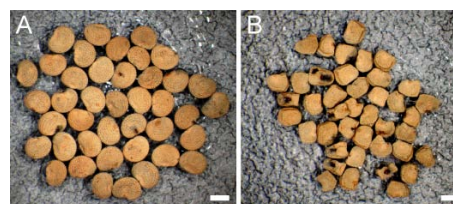


Fig. 2. Seeds obtained from irradiated pollen grains. (A) Type-A seeds. (B) Type-B seeds. Bars = 1 mm.

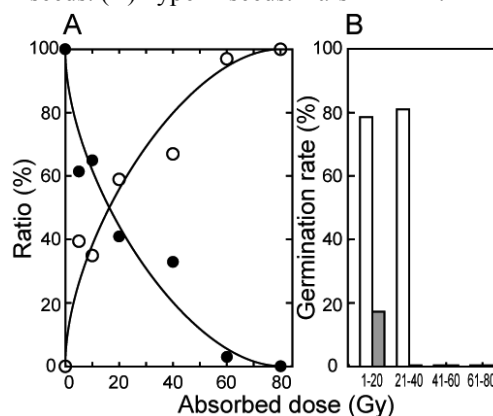


Fig. 3. Difference between the two types of seeds. (A) Ratios of the number of type-A seeds (black circles) and the number of type-B seeds (white circles) to the total number of seeds in each capsule. (B) Germination rates of type-A (white bars) and type-B (gray bars) seeds. The relative rate for 0-Gy irradiation is defined as a germination rate of 100%.

References

1) K. Ishii et al.: RIKEN Accel. Prog. Rep. 41, 226 (2008).

^{*1} Department of Integrated Biosciences, Graduate School of Frontier Sciences, The University of Tokyo

Effect of X-ray irradiation on the expression of DNA repair related genes in rice

T. Shibukawa, Y. Hayashi, T. Hirano, Y. Kazama, M. Izumi, T. Abe

Rice is the most important food crop, and several approaches have been adopted for rice breeding. Several types of radiation have been used for breeding; we performed heavy-ion irradiation, which is used for mutational breeding.¹ To help improve the efficiency of breeding by heavy-ion irradiation, in this study, we aim to elucidate the relationship between the optimum dose of heavy-ion irradiation and the expression of DNA-repair-related genes in rice. As the first step of this study, we investigated the effect of x-ray irradiation on the expression of DNA-repair-related genes in rice.

First, to decide under lethal condition 50% (LD_{50}) value as optimum condition, we measured the survival rates of water-imbibed rice seeds after x-ray irradiation. After 3 days of imbibition, the seeds were irradiated using an x-ray source (Radioflex 250 CG (Rigaku)). The irradiation dose range from 0 to 80 Gy, and the dose rate was 3 Gy per min. The seeds were sown, and the survival rates were measured 3 weeks after sowing. The survival rate started to decrease in 40 Gy, and the survival rate of seeds irradiated with 50 Gy x-rays was 48% (Fig. 1). Therefore, we used 50 Gy irradiation as LD_{50} for water-imbibed rice seeds.

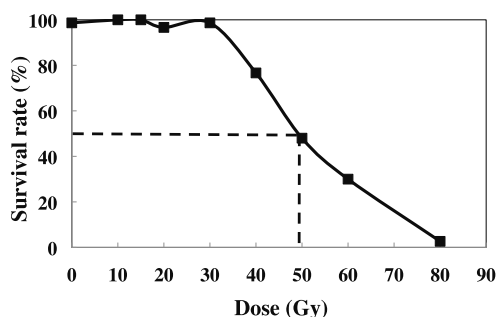


Fig. 1. Survival curve of rice seeds after x-ray irradiation.

Many DNA-repair-related genes have been identified in rice.² DMC1 and Rad51 proteins are types of RecA recombinase, which is required for homologous recombination and DNA repair. *OsDMC1* and *OsRad51* are homologues in rice. *OsRPA70a* encodes the homologue of the replication protein A, which is involved in nucleotide excision repair. We analyzed the expression of DNA-repair-related genes such as *OsDMC1*, *OsRad51*, and *OsRPA70a* by real-time PCR in embryos without seed coats and endosperms; these embryos had earlier been subjected to imbibition and x-ray irradiation at 50 Gy. These genes had different patterns of expression (Fig. 2). There was no difference between the expression levels of *OsDMC1* in the irradiated and nonirradiated (control) embryos at 0 h after

irradiation (Fig. 2A). The expression level increased gradually and reached its peak 3 h after irradiation, and then the level decreased with time. In the case of *OsRad51*, a high level of the gene expression was induced immediately after irradiation (0_1 h), and the level decreased after 3 h (Fig. 2B). There was no change in the expression level of *OsRPA70a* during the time course of this study (Fig. 2C).

These results indicate that the DNA repair systems correlated with *OsDMC1* and *OsRad51* in water-imbibed seeds respond rapidly to x-ray irradiation. Therefore, the period until 1 h after irradiation is speculated to be suitable for comparing the expression of DNA-repair-related genes after heavy-ion beam and x-ray irradiation.

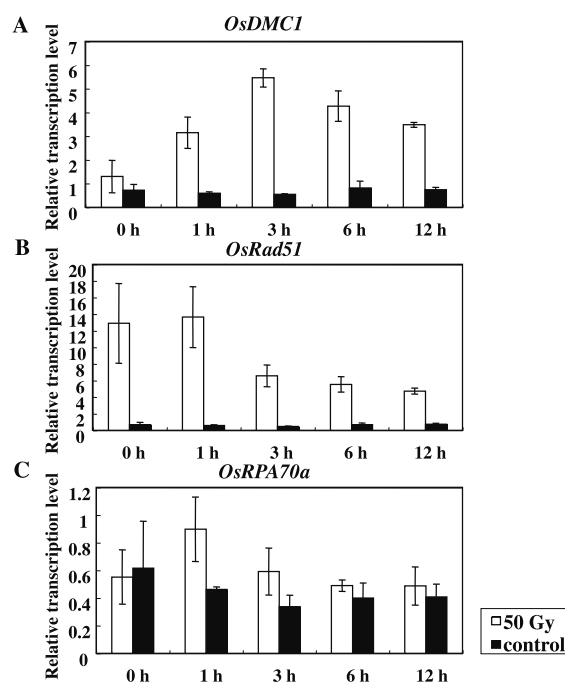


Fig. 2. Expression of DNA repair related genes by real-time PCR. Samples with irradiation (50 Gy) or not (control) were collected at several times after irradiation. Expressions of *OsDMC1* (A), *OsRad51* (B), and *OsRPA70a* were normalized by *OsEF1a* expression. Each experiment was repeated three times: the average value is shown with the SD.

References

- 1) Y. Hayashi et al.: Pro. 18th int. Conf. Cyclotrons and Their Applications (Cyclotrons 2007), 237 (2008)
- 2) S. Kimura and K. Sakaguchi: Chem. Rev. 106, 753 (2006).

Characterization of temperature-sensitive chlorotic mutant induced by ion beam irradiation

M. Nakagawa, H. Takehisa,^{*1} Y. Hayashi, H. Tokairin, T. Sato,^{*2} and T. Abe

Mutants have a very important role in the breeding and development of new cultivars. Heavy-ion beam irradiation is an effective technique used in mutation breeding to produce new cultivars. Rice is an important staple food and a model monocot plant, especially among cereal species. To evaluate the effect of heavy-ion beam irradiation on mutation induction in rice (*Oryza sativa* L. cv. Nipponbare), we have examined the frequency of chlorophyll-deficient mutants. Line 22-4Y was one of the chlorotic mutants with semi-dwarf phenotype isolated from M₂ populations that were irradiated with a C-ion beam (LET:22.5 keV/mm; 20 Gy).¹⁾ In the early seedling stages, the 22-4Y mutant plants produced chlorotic leaves only the first four leaves and during the later stages in a paddy field, the plant produced mostly green leaves. In addition, when the 22-4Y plants were grown at 25°C, chlorophyll deficiency was observed, but the plants produced green leaves when grown at 30°C. These plants exhibiting conditional chlorosis are called "virescent." The previously reported virescent rice mutants, *virescent-1*, *virescent-2*, and *virescent-3*, also have the temperature-dependent chlorosis phenotype.²⁾

To characterize the temperature-dependent chlorosis phenotype, we analyzed temperature-shift experiments. In the experiment with a temperature shift from the restrictive temperature (25°C) to the permissive temperature (30°C) after imbibition in darkness for four days, the 22-4Y plants were almost green, and chlorophyll deficiency was observed only on the toward edge of the second leaf, which had emerged before the temperature shift. In the experiment with a temperature shift from 30°C to 25°C, the 22-4Y produced chlorotic leaves, no chlorosis was observed on edge of the blade and sheath of the second leaf. These results indicate that the virescent phenotype of 22-4Y is irreversibly determined by the temperature at the developmental stage of the leaf.

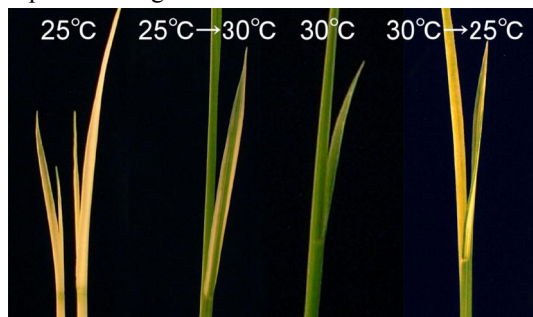


Fig. 1. Comparison of the phenotype of 22-4Y plants grown under different temperature conditions five days after germination.

^{*1} NIAS, Genome Resource Center

^{*2} Graduate School of Life Science, Tohoku University

To determine the number of genes controlling chlorosis in 22-4Y, F₂ plants that were obtained by crossing the 22-4Y and wild-type strains were subjected to genetic analysis. Seventy mutants and 295 wild-type individuals in the F₂ populations had a segregation ratio of 3:1 ($\chi^2 = 0.01$) < ($\chi^2_{0.05} = 3.84$). From the results of the genetic analysis, it was inferred that 22-4Y was a single recessive mutant.

Genetic mapping of the mutation locus of 22-4Y was performed using F₂ plants that were obtained by crossing 22-4Y mutant (var. *japonica*) and Kasalath (var. *indica*). Using 36 STS markers and 4 CAPS markers, the 22-4Y locus was located between 75 cM and 80.4 cM on chromosome 5. Furthermore, thirteen SSR markers were selected to generate a fine physical map. 22-4Y was mapped within the 422-kb region between the STS marker E10886 and the SSR marker RM18690 on the long arm of chromosome 5 (Fig. 2).

A classical phenotypic marker, *virescent-10*, has been mapped previously in this region, but the gene responsible for the virescent phenotype has not been isolated.²⁾ We suggest that the mutation in 22-4Y is caused by the same genes that cause mutation in *virescent-10*.

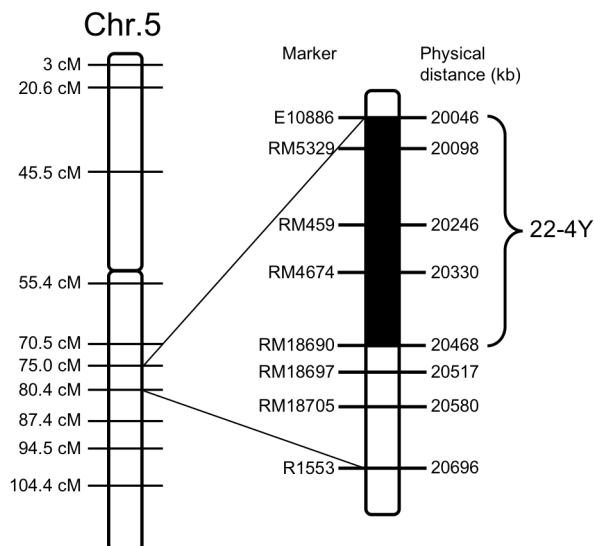


Fig. 2. Genetic mapping of 22-4Y on chromosome 5. The figure on the left shows the genetic linkage map while that on the right shows the physical map. The black box indicates the candidate region for the 22-4Y locus.

References

- 1) Y. Hayashi, et al.: Proc. 18th Int. Conf. Cyclotrons and Their Applications (Cyclotrons 2007), 2008, p.#237.
- 2) A. Yoshimura et al.: Plant Mol. Biol. **35**, 49 (1997).

Identification of mutated gene induced by heavy ion beam irradiation in rice

Y. Hayashi, H. Takehisa^{*1}, Y. Kazama, S. Ohbu, N. Fukunishi, H. Tokairin, T. Sato^{*2}, and T. Abe

Heavy-ion beams have been recognized as an effective mutagen. We have investigated the effect of heavy-ion beam irradiation on mutation induction in rice. The high effectiveness of ion-beams was indicated by the high frequency of chlorophyll-deficient mutants in M₂ progenies with low dose of irradiation¹. This is one of the characteristic features of mutation induction by heavy-ion beam irradiations. Accelerated particles of ions with high linear energy transfer (LET) are thought to be capable of causing local DNA damage. As a result, it is possible to obtain mutants without involving undesirable characters. In previous studies, we isolated various mutants such as dwarf, salt tolerant, necrosis, bronzing and staygreen (Table 1). Most of these mutants were fixed in the M₂ or M₃ generation, and this is another feature of mutation induction by heavy-ion beam irradiation. Furthermore, it is possible to clarify the characteristics of mutation induced by heavy-ion beams by identifying the mutation sites of these mutants. In this paper, we report the identification of the mutated region of a dwarf mutant induced by heavy-ion beam irradiation in rice.

We obtained the dwarf mutant (6-66) by irradiating imbibed seeds of rice (*Oryza sativa* L. cv. Nipponbare) with Ne-ion beam (15 Gy, 63 keV/μm). 6-66 showed the typical phenotype of rice gibberellin (GA) related mutants, severe dwarf with wide leaf blades and dark green leaves (Fig.1). In addition, 6-66 showed no response to GA₃ treatment. In the GA signaling pathway, GID1 is a receptor for GA²) and GID2 is a positive regulator of GA³). Both these proteins are necessary for GA action. PCR analyses of mutant and wild type were performed using specific primers to *GID1* and *GID2* genes. Sequence analysis revealed that 6-66 contained 4-bps deletion in *GID2*, which caused frameshift mutation (Fig.2). No mutation was detected in *GID1*. It is necessary to detect more mutated regions of rice mutants and characterize the mutations induced by heavy-ion beam irradiation. Furthermore, detection of

mutated genes may lead to the discovery of unknown genes or new functions of known genes in rice. Analyses of mutations in some other mutants of rice shown in Table1 are in progress.

Table 1. Isolated mutants by heavy-ion beam irradiation

Line	Ion	Dose (Gy)	LET (keV/μm)	Phenotype
6-99L	C	40	23	Salt tolerant
19-74	C	20	23	Salt tolerant
7-3B	Ne	10	63	Bronzing
11-29	C	20	23	Bronzing
22-70	C	20	60	Necrosis
40-S	C	40	23	Crinkled dwarf
22-4Y	C	20	23	Chlorosis
11-26	C	20	23	Staygreen
5-106	C	20	30	Waxy
3-58	C	15	50	Semi-dwarf
6-66	Ne	15	63	Dwarf

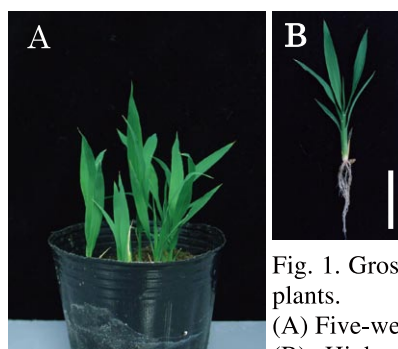


Fig. 1. Gross morphology of 6-66 plants. (A) Five-weeks-old seedlings. (B) Higher magnification of a 6-66 plant. Bar=5cm.

Reference

- 1) Y. Hayashi et al.: RIKEN Accel. Prog. Rep. **42**, 285 (2009).
- 2) M. Ueguchi-Tanaka et al.: Nature **437**, 693 (2005).
- 3) A. Sakai et al.: Science **299**, 1896 (2003).

```

WT 1  MKFRSDSSGGDEPRAPAAGDGGGGDEPAKRQRTDPSSSSSQGEASSSSQPPPOQQEEQ
6-66 1  MKFRSDSSGGDEPRAPAAGDGGGGDEPAKRQRTDPSSSSSQGEASSSSQPPPOQQEEQ

WT 61  PPEADAGEGEGQPRVVDLGEDLVFEVLRRAEARTLAAAACVSRGWQLAEDERLWEAACVRE
6-66 61  PPEADAGEGEGQPRVVDLGEDLVFEVLRRAEARTLAAAACVSRGWQLAEDERLWEAACVRE

WT 121  WANLGFSEERQLRAVVLSLGGFRRLHAVYIRPLOWRGAIVPROQERRQPPVRLGRDQVQLS
6-66 121  WANLGFSEERQLRAVVLSLGSAGSTLSTSAPCSGVAPACPGNRGGSSRR-----

WT 181  LSLFSIGFFQNMPCPKKDKGNSDKNGGGQCG
6-66 147  -----
    
```

Fig. 2. Comparison of amino acid sequences of *GID2* between wild type and dwarf mutant (6-66). The *GID2* gene consists of one exon. Identical amino acids are represented by white-on-black letters.

^{*1} National Institute of Agrobiological Sciences
^{*2} Graduate School of Life Sciences, Tohoku University

Identification of heavy-ion-beam induced DNA mutation by genetic mapping in *Arabidopsis* mutant

Y. Kazama, S. Ohbu, Y. Hayashi and T. Abe

Heavy-ion-beam irradiation can efficiently induce mutations. We are studying the type of mutation induced by heavy-ion beam irradiation. Previously, we had reported a 985-bp deletion in an *Arabidopsis* mutant and a deletion of more than 3 kb in a tobacco mutant, both of which were caused by $^{12}\text{C}^{6+}$ -ion irradiation.^{1), 2)} In this study, we determined two mutations occurring in *Arabidopsis* mutants to gain further insight into mutations induced by heavy-ion beam.

Two mutants, C-48-as1 and Ar-28-pg1, were isolated by screening the M₂ generation obtained by irradiation of wild-type dry seeds (col-0) with $^{12}\text{C}^{6+}$ ions (250 Gy, 22.5 keV/ μm) and $^{40}\text{Ar}^{17+}$ ions (50 Gy, 290 keV/ μm), respectively. Phenotypes of these mutants are shown in Fig. 1. Ar-28-pg1 developed yellow-green leaves (Fig. 1). In a mature Ar-28-pg1 plant, a strong chlorosis was observed in the leaves (data not shown). C-48-as1 showed increased leaf growth and an altered pattern of leaf emergence (Fig. 1). The number of leaves observed in C-48-as1 20 days after sowing was about twice that in the wild-type plant. Pollens from these mutants were used to pollinate a wild-type (col-0). All of their progenies showed wild-type like leaves, indicating that both mutants have a recessive mutation.

The method for identifying the responsible mutation in each mutant is summarized in Table 1. To determine the responsible loci of the mutants, genetic mapping was carried out as described previously.³⁾ A total of 151 and 114 homozygous F₂ plants were used for mapping of C-48-as1 and Ar-28-pg1, respectively. Rough mapping results showed that the responsible loci of the C-48-as1 and Ar-28-pg1 mutants are located in a 2.6-Mb region near the telomere of chromosome 3 and a 3-Mb region near the centromere of chromosome 5.

From the results of phenotype analysis and genetic mapping, their responsible genes were predicted. Database search (TAIR, <http://www.arabidopsis.org/>) indicated that the putative responsible genes for C-48-as1 and Ar-28-pg1 were *ALTERD MERISTEM PROGRAM (AMP) 1* and *ETHYLENE-DEPENDENT GRAVITROPISM-DEFICIENT AND YELLOW-GREEN (EGY) 1*, respectively.^{4),5)} *AMP1* encodes a putative glutamate carboxypeptase,

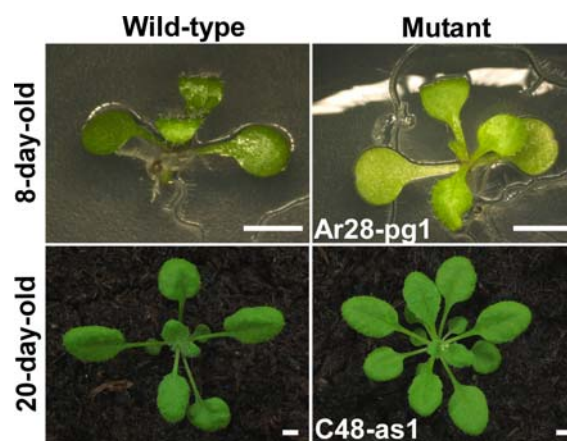


Fig. 1 Phenotypes of isolated mutants. Bars = 2 mm.

passively involved in peptide signaling.⁶⁾ *EGY1* encodes a membrane-associated metalloprotease.⁴⁾ Genomic fragments containing *AMP1* and *EGY1* in C-48-as1 and Ar-28-pg1, respectively, were sequenced. In C-48-as1, a single A-to-T transversion at 2384-bp downstream of the initiation codon was observed in *AMP1*. This base substitution caused a stop codon resulting in the production of 3'-truncated protein. In Ar-28-pg1, a 5-bp deletion (from nucleotide 1410-1414) with five base substitutions (one transition and four transversions) was observed in *EGY1*. The 5-bp deletion created a frameshift. It was observed that the phenotypes of C-48-as1 and Ar-28-pg1 are quite similar to those of the original null mutants, respectively, indicating that both mutants might be null.

Accumulating of these mutation data will help us understand the characteristics of heavy-ion-induced mutation.

References

- 1) Y. Kazama et al.: Bioci. Biotech. Biochem. **71**, 2864 (2007).
- 2) Y. Kazama et al.: RIKEN Accel. Prog. Rep. **42**, 280 (2009).
- 3) G. Jander et al.: Plant Physiol. **129**, 440 (2002).
- 4) G. Chen et al.: Plant J. **41**, 364 (2005).
- 5) A. Chaudhury et al.: Plant J. **4**, 907 (1993).
- 6) C.A. Helliwell et al.: Plant Cell **13**, 2115 (2001).

Table 1 Summary of detection of mutation by genetic mapping

Analysis technique	Genetic mapping		Database search	Sequencing
	Chromosome	Region	Gene	Mutation type
C-48-as1	3	2.6 Mb near telomere	<i>AMP1</i>	BS
Ar-28-pg1	5	3.0 Mb near centromere	<i>EGY1</i>	Del (5 bp) + BS

BS: Base substitution, Del: Deletion

LET-dependent effect of heavy-ion-beam mutagenesis on deletion size

Y. Kazama, T. Hirano, Y. Liu,*¹ K. Nishihara, S. Ohbu, Y. Hayashi and T. Abe

A heavy-ion beam is a high-Linear Energy Transfer (LET) radiation compared with X-ray and γ -ray. Previously, we have reported that LET affects the mutation rate and that an LET of 30 keV/ μ m is most effective in inducing mutation in dry seeds of *Arabidopsis thaliana*.¹⁾ Thus, LET is considered to important factor for mutation induction by heavy-ion beam. In *Mesorhizobium loti*, irradiation by iron ions (640 keV/ μ m) induced larger deletions compared to those induced by carbon ions (23 keV/ μ m).²⁾ From this result, we postulate that LET may also influence the deletion size in the mutated genes. To date, there is no known mutagen that can control the deletion size. In the present study, therefore, we aimed to develop a novel method for deletion-size-controlled mutagenesis by heavy-ion-beam irradiation with different LETs. As the first step toward controlling deletion size, we irradiated the seeds of *A. thaliana* with heavy-ion beams having four different LETs ranging from 30.0 to 640 keV/ μ m and analyzed the deletion size in mutated genes.

Dry seeds of *A. thaliana* (Col-0) were packed in a plastic bag to obtain a monolayer of seeds. They were irradiated with $^{12}\text{C}^{6+}$ (22.5 keV/ μ m, 30 keV/ μ m, or 290 keV/ μ m), $^{40}\text{Ar}^{17+}$ (290 keV/ μ m), or $^{56}\text{Fe}^{24+}$ (640 keV/ μ m) ions using the E5 beam line at the RIBF. These ions were accelerated up to 1.62, 3.80, and 5.04 GeV. The LET of $^{12}\text{C}^{6+}$ were varied by passing the ions through a combination of absorbers. The irradiation doses were selected on the basis of the results of previous research.¹⁾ The irradiated M_1 seeds were surface-sterilized and incubated on a 0.7% agar-containing MS medium supplemented with MS vitamins and 3% sucrose at 4°C in the dark for four days to induce vernalization. Then, they were grown at 22°C under long-day condition (16 h light and 8 h of darkness). Seedlings that developed true leaves were transplanted on plastic trays (13 \times 9 cm) containing soil. Eleven seedlings were planted in each tray and cultured at 22°C under long-day condition in a greenhouse. M_2 seeds were collected from each tray and they were considered as one batch. From the M_2 generation, *elongated hypocotyl* (*hy*) and *globrous* (*gl*) mutants, were screened by growing the M_2 seeds on an MS agar medium. DNAs of the collected mutants were purified using DNeasy plant mini kit (QIAGEN). Then, they were subjected to PCR and sequencing by using specific primers for the putative responsible genes (*HY1*, *HY2*, *HY3*, and *HY4* for the *hy* mutants; *GL1*, *GL2*, and *TTG1* for the *gl* mutants). M_3 seeds of the mutants were harvested and the phenotype of the M_3 plants was analyzed to confirm whether the phenotype of the mutants was inherited.

In total, 89,794 of M_2 plants were screened, and 36

mutants were collected (Table 1). The highest mutation rate was observed 30-keV/ μ m irradiation; this observation was in agreement with a previous result according to which the 30-keV/ μ m irradiation is most effective in inducing albino mutants.¹⁾ Since the mutants isolated from the same batch were considered to have originated from the same M_1 plants, mutants of the same batch that exhibited the same phenotype were characterized as a single mutation event. After determining the DNA mutation, all of the mutants from the same having the same phenotype were analyzed by PCR and sequencing.

Twenty-one mutations were identified in the genes of the mutants (Table 2). The mutations included fifteen deletions, two translocations with a deletion, two base substitutions, one insertion, and one translocation. This result indicates that the heavy-ion-beam irradiation predominantly induces deletion mutation. Base substitution was observed only in the case of 22.5-keV/ μ m irradiation. When the sizes of the deletions induced by radiations with different LETs were compared, smaller deletions were observed in the case of lower-LET irradiation. In contrast, with 290- and 640-keV/ μ m irradiations, large deletions of over 1,000 bp were detected.

Table 1. Screening results for *hy* and *gl* mutants.

LET (keV/ μ m)	Ion species	Dose (Gy)	No. of M_1	No. of M_2	No. of mutants*
22.5	$^{12}\text{C}^{6+}$	250	2,024	11,662	5
22.5	$^{12}\text{C}^{6+}$	450	1,710	16,103	7
30.0	$^{12}\text{C}^{6+}$	400	1,419	13,485	14
290	$^{12}\text{C}^{6+}$	50	1,452	15,140	1
290	$^{40}\text{Ar}^{17+}$	50	1,100	7,229	4
640	$^{56}\text{Fe}^{24+}$	50	2,893	26,175	5

*Total number of isolated *hy* and *gl* mutants.

Table 2. Classification of mutations induced by heavy-ion beams with different LETs.

LET (keV/ μ m)	Base substitution	Deletion			Others
		10 bp \geq	1000 bp \geq	1000 bp <	
22.5	2	3	2	0	0
30.0	0	4	1	0	1
290	0	1	2	1	0
640	0	1	0	2	1

References

- 1) Y. Kazama et al.: Plant Biotech. **25**, 115 (2008).
- 2) H. Ichida et al.: Mutation Res. **639**, 101 (2008).

* ¹ Institute of Modern Physics, Chinese Academy of Science

C-ion-induced DNA mutations in variegated mutant *Arabidopsis*

K. Nishihara, Y. Kazama, M. Nakagawa, T. Hirano, S. Ohbu, S. Kawano,* and T. Abe

Since high Linear-Energy-Transfer (LET) heavy-ion beams effectively induce DNA double-strand-breaks¹⁾, they induce high-frequency mutations. LET affects mutation rate when dry *Arabidopsis* seeds are irradiated with heavy-ion beams²⁾. To study LET-dependency of DNA mutations, we studied DNA mutations induced by irradiation with heavy-ion beams. We report two DNA mutations induced by C-ion irradiation with LET of 50 keV/ μ m in *Arabidopsis thaliana*.

We focused on variegated mutants, some of which were well characterized, and identified the genes that had mutations causing the variegated phenotype. The *var1* (*yellow variegated 1*) mutant had normal cotyledons and green- and white-sectored rosette leaves³⁾. The *var2* mutant had normal cotyledons and white/yellow sectors in the normally green parts of the plant³⁾. The *var3* mutant had green cotyledons and yellow variegated rosette leaves⁴⁾. The cotyledons of the *immutans* (*im*) mutant appeared white under high-intensity light, and *im* had green- and white-sectored leaves⁵⁾. The *thylakoid formation 1* (*thf1*) mutant had plastids in the white/yellow sectors, the plastids were composed of accumulated vesicles and lacked organized lamellar structures⁶⁾. DNA mutations were detected by screening variegated mutants and sequencing the genes responsible for the mutations.

Dry *Arabidopsis* seeds were irradiated with C-ions (135 MeV/nucleon) at a dose of 200 Gy with LET of 50 keV/ μ m. The irradiated M₁ seeds were incubated on 1/2 Murashige and Skoog agar medium for 3 days at 4°C in the dark for vernalization and then at 23°C under 16-h light/8-h dark conditions for germination. Three weeks after germination, 484 well-grown plants were selected for transplantation into pots. Eleven seedlings were transplanted into each pot. M₂ seeds were collected from 476 M₁ plants. Thirteen days after germination, the variegated mutants were screened from among 19,124 M₂ seedlings.

We found three variegated mutants (C-11-var1, C-11-var2, and C-35-var1) (Fig. 1). Among them,



Fig. 1. Photographs of variegated *Arabidopsis thaliana* with mutations induced by C-ion irradiation with LET of 50 keV/ μ m. Bar = 1 cm.

C-11-var1 and C-11-var2 were obtained from the same pot. The phenotypes of C-11-var1 and C-35-var1 were similar to those of *im* and *var2* mutants, respectively. However, we could not determine the genes responsible for these phenotypes only by phenotypic characterization. Therefore, we sequenced all genes in these mutants (Table 1).

Sequencing analysis revealed that the C-11-var1 mutant had a 2-bp deletion in the *IM* gene sequence (Fig. 2). The deletion was located in the first exon of the *IM* gene, and caused a frameshift mutation. Sequencing of the *IM* gene in the C-11-var2 mutant revealed that this mutant had the same deletion as C-11-var1, thereby indicating that these two mutants may have originated from a single M₁ plant. The C-35-var1 mutant had a 46-bp deletion in the *VAR2* gene (Fig. 2). This deletion occurred at the last 4 bp of the first exon and the first 42 bp of the following intron. Therefore, this deletion may have caused a shift in the splice site.

Gathering data on mutations induced by C-ion irradiation will help us to understand the mutagenesis ability of C-ion irradiation.

Table 1. Sequencing results for genes responsible for mutations in variegated mutants

Gene name	C-11-var1	C-35-var1
<i>VARI</i>	No mutation	No mutation
<i>VAR2</i>	No mutation	46-bp deletion
<i>VAR3</i>	No mutation	No mutation
<i>IM</i>	2-bp deletion	-
<i>THF1</i>	No mutation	-

IM gene of C11var1 mutant

```

63                               142
WT TCGACGCTGTAGAGCCGCGTTTCGTACAGCTCCTCTGACCGATTGCTTCATCATCTTCCCTCTCTCTCTGCTGCTGCTG
C11var1 TCGACGCTGTAGAGCCGCGTTTCGTACAGCTCCTG-ACCGATTGCTTCATCATCTTCCCTCTCTCTGCTGCTGCTGCTG

```

2-bp deletion

VAR2 gene of C35var1 mutant

```

1155                               1234
WT AGGACGCTTTGACCCGCGAGTACTATCTGATATTACACATTGATGTTTTGTAATCCTGTACTACTCTAGAGCTTGT
C35var1 AGGACGCTTTGACCG-----TACTACTCTAGAGCTTGT

```

46-bp deletion

Fig. 2. Deletions detected in variegated mutants. The numbers indicate the nucleotide position from the initiation codon.

References

- 1) D. T. Goodhead: Int. J. Radiat. Biol. **65**, 7 (1994).
- 2) Y. Kazama et al.: Plant Biotech. **25**, 113 (2008).
- 3) J. M. Martínez-Zapater et al.: J. Hered. **84**, 138 (1993).
- 4) H. Næsted et al.: J. Cell Sci. **117**, 4807 (2004).
- 5) C. M. Wetzel et al.: Plant J. **6**, 161 (1994).
- 6) Q. Wang et al.: Plant Physiol. **136**, 3594 (2004).

* Graduate School of Frontier Sciences, The University of Tokyo.

Early-flowering mutants developed by heavy-ion-beam irradiation in soybean

H. Kuribara*¹, Y. Sadamura*¹, H. Watanuki*¹, T. Hirano, Y. Hayashi, T. Abe

The soybean cultivar ‘Oojirodaizu’ is known as a local food that tastes good; it is cultivated in Katashina-mura, Gunma prefecture. In order to increase the demand for ‘Oojirodaizu’, its use as green soybean has been proposed. However, the flowering time of ‘Oojirodaizu’ is too late to produce green soybean during summer in order to increase demand. Therefore, in the present study, we attempted to develop early-flowering mutants by heavy-ion-beam irradiation in ‘Oojirodaizu’, as a step toward efficient usage of local germplasm.

Seeds of soybean (*Glycine max* (L.) Merr. ‘Oojirodaizu’) were irradiated with a C-ion beam (22.5 keV/μm) at doses between 10 and 200 Gy. The irradiated seeds were sowed in the field for raising seedlings, and then, their germination and survival rates were measured. The seedlings that survived were transplanted to the field, and a yield survey was carried out. For screening of the early-flowering mutants in the M₂ generation, the flowering time and seed pod maturity were measured from July to August and in October, respectively. Then, progeny tests were performed in each line of early-flowering mutants.

The germination rate of M₁ seeds did not decrease relative to that of the untreated control (0 Gy), irrespective of the dose range (Fig. 1). In contrast, the survival rate of the seeds decreased from 92% at 100 Gy to 10% at 200 Gy. The results of the yield survey showed a similar trend in the survival rate, and the total number and weight of seeds per plant started to decrease at 100 Gy. These results suggest that the effective dose for mutant screening is not greater than 100 Gy.

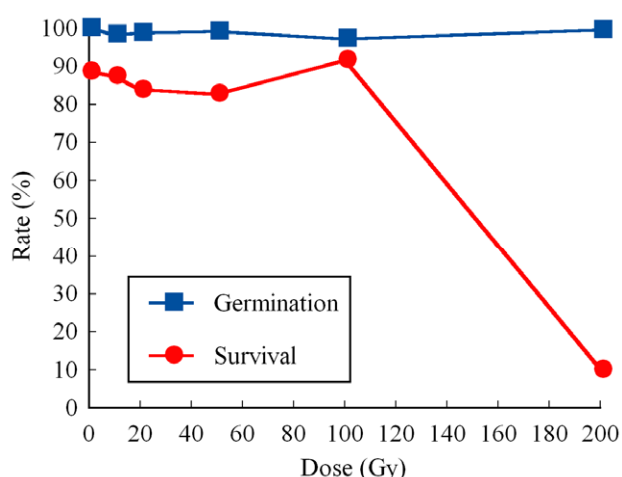


Fig. 1 Germination and survival of soybean seeds rate after irradiation with a C-ion beam. These data were obtained in a single experiment.

When early-flowering mutants were screened from M₂ plants, we obtained two lines (C-10-47 and C-10-55; Fig. 2) derived from seeds irradiated at 10 Gy and one line (C-100-32) derived from seeds irradiated at 100 Gy. In the progeny test, it was confirmed that the flowering times of C-10-47 and C-10-55 were about 20 and 15 days earlier than that of the wild type, respectively. However, the seed yields of the two lines were lower than that of the wild type, and C-10-47 showed a marked decrease in the seed yield (Table 1). Therefore, it is thought that the mutant line of C-10-55, which did not show a severe decrease in seed yield, can be used as a breeding parent.

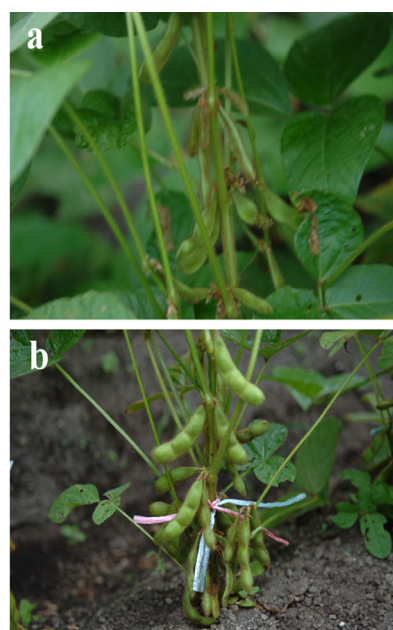


Fig. 2 Phenotype of early-flowering mutant developed by irradiation with a C-ion beam. Photographs were taken on the same date (August 26th) for the wild type (a) and the mutant line of C-10-47 (b).

Table 1 Comparison of seed yield in early-flowering mutants.

Line	Number of seed pods	Number of seeds	Single-seed weight (g)
Wild type	99.8	159.7	0.38
C-10-47	6.0	9.0	0.33
C-10-55	53.0	93.0	0.38

These data are the values averaged over the values for all plants.

*¹ Gunma Pref., Seta-Norin High school.

Induction of high-formaldehyde-absorption mutant by heavy-ion-beam irradiation in *Murraya paniculata*

T. Hirano, R. Mukai^{*1}, S. Yoshida, Y. Hayashi, T. Abe

Phytoremediation, or the use of plants for removing pollutants, is an attractive method for the control of air, water, and soil pollution; this is because this method is inexpensive and environment friendly. Formaldehyde is one of the volatile toxic substances that cause the sick house syndrome and is a suspected carcinogen. The aim of this study is to develop an ornamental foliage plant with novel functions. We attempted to enhance the formaldehyde-absorption ability of Orange jasmine (*Murraya paniculata*), which is an ornamental shrub with dense foliage and fragrant flowers, by heavy-ion-beam irradiation.

The linear energy transfer of the C ion beam used in this study was 22.5 keV/ μm . Dry and imbibed seeds of *M. paniculata* were irradiated with the C ion beam at a dose of 10–40 Gy and 5–30 Gy, respectively. The survival rate of the M₁ plants obtained from the irradiated dry seeds did not decrease, irrespective of the used dose range. On the other hand, in the case of the plants obtained from the irradiated imbibed seeds, the survival rate decreased from 78% to 49% when the irradiation dose was increased from 5 Gy to 10 Gy. We also used cuttings for mutation induction; the cuttings were irradiated by a C ion beam at a dose of 5–100 Gy. The survival rate of the axillary buds in the irradiated cuttings decreased drastically from 85% to 33% when the dose was increased from 50 Gy to 60 Gy.

The mutation rate in the M₂ generation derived from the irradiated seeds was calculated on the basis of morphological mutations such as leaf variegation, leaf serration, flower shape mutation, and weeping. The highest mutation rate was 1.7% in dry seeds irradiated at 30 Gy and 9.4% in the imbibed seeds irradiated at 10 Gy. In the regenerated plants obtained from the irradiated axillary buds, the mutation rate was high (5.1–6.7%) when the dose was varied between 40 Gy and 50 Gy.

We analyzed the formaldehyde-absorption ability of the M₂ plants derived from irradiated seeds and that of the plants regenerated from irradiated the axillary buds. The experiments were carried out in a 210-L chamber. After placing the plant in the chamber, 5 μl of 4% formaldehyde solution was injected into the filter in the fan unit and evaporated in the chamber. After the plants were exposed to formaldehyde for 30 min, the concentration of formaldehyde in the chamber (C : ppm) and the temperature in the chamber (t : °C) were measured. Then, the total leaf area (S : dm²) of each plant used in the experiment was also measured. The residual volume of formaldehyde in the

chamber (Q : μg) is calculated by using eq. (1). The velocity of formaldehyde absorption per unit leaf area (V : $\mu\text{g}/\text{dm}^2/\text{h}$) is calculated using eq. (2), and it is assumed that the entire amount of injected formaldehyde is evaporated in the chamber.

$$Q = \frac{7.68 \times 10^4 \times C}{273.15 + t} \quad (1)$$

$$V = \frac{2 \times (200 - Q)}{S} \quad (2)$$

For the wild type, the average and maximum values of V were 31.5 and 97.0 $\mu\text{g}/\text{dm}^2/\text{h}$, respectively (Table 1). The maximum value obtained for the wild type was used as the criterion value for the screening of high-ability mutants. The plants derived from the irradiated materials were screened; 58 plants were selected as candidates with enhanced formaldehyde-absorbing ability (Table 1). The highest value of V was 183.0 $\mu\text{g}/\text{dm}^2/\text{h}$ for the plants obtained from the irradiated imbibed seeds and 237.0 $\mu\text{g}/\text{dm}^2/\text{h}$ for the plants obtained from the irradiated axillary buds; the ability of the candidates was 1.9–2.4 times higher than the criterion value. These results demonstrate that mutation breeding by heavy-ion-beam irradiation is a promising method for the development of suitable plants that can be used in phytoremediation.

Table 1 Evaluation of velocity of formaldehyde absorption in M₂ plants derived from irradiated seeds and plants derived from axillary buds after ion beam irradiation.

Irradiated material	Dose (Gy)	No. of plants	Max value of V ($\mu\text{g}/\text{dm}^2/\text{h}$)	No. of mutant candidates*
Wild type	0	236	97.0	-
Dry seed	30	160	139.0	23
Imbibed seed	5	80	131.4	12
	10	49	183.0	5
Axillary bud	30	25	237.0	5
	40	74	131.0	6
	50	45	136.5	7

*Mutants showed V values of more than 97.0 $\mu\text{g}/\text{dm}^2/\text{h}$.

^{*1}Environmental Affairs Dept., Tokyo Gas

Development of early-flowering mutant of strawberry cultivar "Satsumaotome" by C-ion irradiation

Y. Takenoshita,* T. Nagatani,* M. Ooe,* H. Saito and T. Abe

In Japan, the demand for strawberries increases at the end of the year. Although the strawberry cultivar "Satsumaotome" developed in Kagoshima prefecture is large and has fruits of good quality, it is classified as a late-harvesting cultivar and is not suitable for harvesting in seasons during which prices are high. Therefore, we aimed to develop early-flowering mutants derived from "Satsumaotome" by ion beam breeding. We estimated suitable doses of C-ion beams for irradiation of multiple shoot cultures¹⁾, and we selected an early-flowering mutant line B0518²⁾. In this study, we found genetic uniformity and stability in early-flowering characteristics of B0518, and we also found that the quality of B0518 is as good as that of the original cultivar.

To examine the uniformity and stability of the early-flowering, we formed seven lines (B0518-1to7) by clone propagation from seven individual stocks, which were propagated from the original B0518 stock. Each line was planted in a plastic greenhouse on September 26, 2008, and the cultivation was carried out by using the standard method for "Satsumaotome" in Kagoshima prefecture.

The date of flower bud initiation of B0518 was eight days earlier than that of "Satsumaotome" (Table 1). Because strawberries were planted in the field just after the flower bud initiation, this result shows that B0518 can be planted and harvested than "Satsumaotome". The terminal inflorescence of B0518 flowered on November 2 and November 3, and the primary axillary inflorescence flowered from December 24 to 29 (Table 1). The range of flowering dates of the seven lines was very small. The harvest date of the terminal inflorescence of B0518 was December 1 which is 14 days earlier than that of "Satsumaotome" (Table 1). On the basis of these results, we concluded that there is genetic uniformity and stability in the early-flowering of B0518.

In terms of the shape of the fruit, color of the peel, and color of the flesh, B0518 was identical to "Satsumaotome" (data not shown). These results indicate that the unexpected change in fruit quality was negligible in the case of B0518.

As for the harvest until December 31, 2008, the number of fruits of B0518 was about 2.2 times that of "Satsumaotome", and the fruit yield was about 1.7 times the yield of "Satsumaotome" (Table 2).

From the results of this study, we confirmed that B0518 was a fixed and early-flowering line whose fruits retain the excellent characteristics of the fruits of "Satsumaotome". We also confirmed that B0518 was a high-yielding line compared to the original cultivar "Satsumaotome". We are

planning to further investigate the characteristics of B0518 for commercial production.

Table 1 Flowering and harvest of B0518 in 2008

Line Cultivar	Flower bud	Terminal inflorescence		Primary axillary inflorescence
	Initiation date	Flowering date	Harvest date	Flowering date
B0518-1		Nov.3	Dec.4	Dec.29
B0518-2		Nov.2	Dec.1	Dec.25
B0518-3		Nov.2	Dec.1	Dec.24
B0518-4		Nov.2	Dec.4	Dec.28
B0518-5		Nov.2	Dec.1	Dec.24
B0518-6		Nov.2	Dec.4	Dec.24
B0518-7		Nov.2	Dec.8	Dec.25
B0518 (average)	Sep.18	Nov.2	Dec.1	Dec.26
Satsumaotome	Sep.26	Nov.12	Dec.15	Jan.12

Table 2 Total number of fruits and fruit yield for B0518. The fruits were harvested until December 31, 2008

Line Cultivar	Number of fruits	Fruit yield
	(fruits/a)	(kg/a)
B0518-1	3,446	73
B0518-2	3,877	80
B0518-3	4,156	83
B0518-4	3,752	73
B0518-5	4,002	80
B0518-6	3,573	76
B0518-7	3,797	74
B0518 (average)	3,800	77
Satsumaotome	1,734	46

References

- 1) M.Ooe et al.:RIKEN Accel.Prog.Rep.42, 286 (2009)
- 2) Y.Takenoshita et al.:RIKEN Accel.Prog.Rep.42, 287 (2009)

* Kagoshima Biotechnology Institute

IV. OPERATION RECORDS

1. Operation of RIBF

Operations of RIBF ring cyclotrons

M. Kase, N. Fukunishi, E. Ikezawa, T. Nakagawa, H. Okuno, N. Sakamoto, M. Fujimaki, H. Hasebe, Y. Higurashi, T. Kageyama, M. Kidera, M. Kobayashi-Komiyama, H. Kuboki, K. Kumagai, T. Maie, M. Nagase, J. Ohnishi, Y. Ohshiro,^{*1} K. Suda, T. Watanabe, K. Yamada, S. Yokouchi, T. Ohki,^{*2} N. Tsukiori,^{*2} T. Aihara,^{*2} S. Fukuzawa,^{*2} M. Hamanaka,^{*2} S. Ishikawa,^{*2} K. Kobayashi,^{*2} Y. Kotaka,^{*2} R. Koyama,^{*2} M. Nishimura,^{*2} T. Nakamura,^{*2} M. Nishida,^{*2} K. Oyamada,^{*2} J. Shibata,^{*2} M. Tamura,^{*2} A. Uchiyama,^{*2} K. Yadomi,^{*2} H. Yamauchi,^{*2} A. Goto, O. Kamigaito, and Y. Yano

^{*1} Center for Nuclear Study, the University of Tokyo

^{*2} SHI Accelerator Service Ltd.

In 2009, the operation of four ring cyclotrons (RRC, fRC, IRC, and SRC) along with two injectors (AVF and RILAC) in the RIBF accelerator complex was satisfactory. Although there are various acceleration modes (corresponding to the combinations of these ring cyclotrons), the RRC works as the first booster ring cyclotron in every acceleration mode. The annual operation time of the RRC reached 5140 h in 2009, which was by 30% more than that in 2008. The operation statistics of RIBF accelerators are summarized in Table 1.

In 2009, the range of ion mass in the beam in the RIBF accelerators extended toward lighter masses; on the other hands in 2007 and 2008 the heavy ion beams such as ⁴⁸Ca and ²³⁸U beams were used. In March, the new acceleration mode of AVF-RRC-SRC was tested for the first time. In order to skip the IRC, the recently completed bypass beam line was used. A ¹⁴N beam with an energy of 250 MeV/u was successfully accelerated in the new mode, and it was used for the commissioning of the SHARAQ (the newly completed spectrometer that is promoted by CNS, the University of Tokyo).

In April, a polarized deuteron beam with an energy of 250 MeV/u was accelerated in the same acceleration mode. After each cyclotron was tuned precisely in order to achieve single turn extractions, the polarized deuteron beam could be supplied to the experiments for three days. In early May, a ¹⁴N beam with an energy of 250 MeV/u was accelerated again and used for carrying out the further performance test on the SHARAQ, a beam optics research, and for a preliminary testing of the Kappa magnet.

Experiments involving the use of α beam with an energy of 320 MeV/u were scheduled in autumn. Initially, we intended to produce this beam in the AVF-RRC-SRC mode as well by changing the acceleration frequency. However, during the frequency tuning of the SRC amplifiers, we met with the difficulties in using the new frequency (around 32 MHz) in the SRC, as the result of which a vacuum tube in the final stage amplifier for one of the SRC resonators (RES1) was damaged. Therefore the other mode of RILAC-RRC-IRC-SRC was chosen in order to avoid using this frequency. From October to early November, 320 MeV α beam was accelerated successfully and used for

Injector	Beam	Cyclotrons	Energy (MeV/u)	Beam Course	Beam Tuning (hours)	Duration	
AVF	¹⁴ N	RRC – SRC	250	MS	38.0 h	70.0 h	
				SHARAQ	282.0 h	316.0 h	
				BigRIPS	11.5 h	57.0 h	
		d	RRC – SRC	250	BigRIPS	147.0 h	66.5 h
RILAC	²³⁸ U	RRC – (D – E5)	10.75	MS	26.5 h	163.5 h	
		RRC – fRC	10.75	MS	98.0 h	64 h	
		RRC – fRC – IRC – SRC	345	BgRIPS	378.5 h	230 h	
	¹³⁶ Xe	RRC – fRC	10.75	MS	25.5 h	115 h	
		RRC – fRC – IRC – SRC	345	BigRIPS	24.0 h	144 h	
		⁴⁸ Ca	RRC – IRC – SRC	345	BigRIPS	208.5 h	89 h
		⁴ He ²⁺	RRC – fRC – IRC – SRC	320	SHARAQ	132 h	280.5 h

the first SHARAQ experiment after it were converged into a triton beam in the BigRIPS.

At the end of 2009 between November and December, the campaign of heavy-ion beam time was arranged. ^{238}U and ^{48}Ca beams with an energy of 345 MeV/u were accelerated as well as in 2008.

In order to produce $^{238}\text{U}^{35+}$ ions, a new superconducting ECR ion source was used in November 2009, which had been designed for a new injector (RILAC2) and installed on the 100kV stage for a test to be performed since summer 2009. The beam from the ECR ion source was accelerated by a dc voltage of 100 kV and transported to the first cavity of RILAC via a temporary beam line (MEBT) bypassing the commonly used RFQ linac. Although the $^{238}\text{U}^{35+}$ beam at the ion source was much more intense than before, the obtained ^{238}U beam at the exit of SRC was 0.7 pA at maximum, being around two times. The matching between the ring cyclotrons was probably poor.

In December, the ^{48}Ca beam with 345 MeV/n was accelerated by using the ordinary 18GHz ECR and the RFQ linac. Just before the beam tuning, a serious vacuum leak was detected in the main tuner of the SRC resonator (RES2), and the operation was performed with acceleration without RES2 and with other three cavities in the SRC. In the final stage of the beam tuning, there was significant instability in the extracted beam of the SRC, which was later attributed to a poor connection of high voltage line of the SRC deflector

(EDC). The ^{48}Ca beam sent to the BigRIPS was limited to around several tens of pA.

About half the RRC operation time was devoted to ordinary experiments in the Nishina Building, as listed in Table 2. A total of 1070 h were spent on eight kinds of RIPS experiments, including those on the development of ion-trapping technology. The experiments related to the biological research were so extensive that a total of 113 h were devoted to them; in these experiments the four kinds of beams, namely, ^{12}C , ^{14}N , ^{40}Ar and ^{56}Fe ions were used, 25 iterations were carried out on a regular basis in the E5 target room. In the E3 target room, the RI productions for multi-tracer was carried out using an intense ^{14}N -135MeV/n beam, and the simulation of single event in electronic devices against irradiation of cosmic ray was performed, using the low energy Kr beam.

In June and July 2009, during the summer shutdown period, cooling water leaked into the vacuum chamber of the SRC, because a water pipe of the beam buffer burst; the buffer was located at the entrance of the superconducting magnet (SBM) in the central region of the SRC. Since the leakage was not noticed for two months, a large amount of water estimated at more than 20 tons flowed into the SRC beam chamber. It took around two months to repair the SRC; recovery was performed by replacing the damaged vacuum components and cleaning the interior of the vacuum chamber.

	Beam Course	No. of Allocation	Beam & Energy	Tuning Hours	Supply Hours	Proportion
RINAC		2	^{23}Na -63 MeV/u	67	167	
			^{58}Fe -63 MeV/u			
AVF	E6(RIPS)	13	H^{2+} -100 MeV/u	782	904	1071
			^{13}C -100 MeV/u			
			^{13}C -115 MeV/u			
			^{18}O -100 MeV/u			
			^{24}Mg -100 MeV/u			
			^{40}Ar -95 MeV/u			
	E5b	25	^{12}C -135 MeV/u		113	8.5%
			^{13}C -100 MeV/u			
			^{14}N -135 MeV/u			
			^{40}Ar -95 MeV/u			
	E3a	1	^{84}Kr -70 MeV/u		30	2.3%
	E3b	2	^{14}N -135 MeV/u		109	8.2%
Total				1323	100%	

RILAC operation

Eiji Ikezawa, Ohki Tomonori,* Kase Masayuki, Takahide Nakagawa, Naruhiko Sakamoto,
 Hiroki Okuno, Nobuhisa Fukunishi, Masaki Fujimaki, Makoto Nagase, Tadashi Kageyama, Shigeru Yokouchi,
 Misaki Kobayashi-Komiyama, Masanori Kidera, Yoshihide Higurashi, Tamaki Watanabe, Kazunari Yamada,
 Takeshi Maie, Hiroo Hasebe, Hironori Kuboki, Kenji Suda, Yutaka Watanabe, Toshimitsu Aihara,*
 Hiromoto Yamauchi,* Akito Uchiyama,* Kazuyuki Oyamada,* Masashi Tamura,*
 Akira Goto, Osamu Kamigaito, and Yasushige Yano

* SHI Accelerator Service Ltd.

The RIKEN heavy-ion linac (RILAC) has been in steady operation throughout the reporting period and has supplied various ion beams in various experiments, in beam acceleration tests, and in beam commissioning. Some statistics on the RILAC operation from January 1 to December 31, 2009 are summarized in Table 1. The total beam service time of the RILAC accounted for 87.0% of the operation time of the RILAC. The percentages of the stand-alone RILAC and the injection into the RIKEN Ring Cyclotron (RRC) were 44.2% and 55.8% of the total beam service time of the RILAC, respectively.

For the beam commissioning and experiments of the RI Beam Factory (RIBF), 0.67-MeV/nucleon ^{238}U , 0.67-MeV/nucleon ^{136}Xe , 2.68-MeV/nucleon ^{48}Ca , and 2.66-MeV/nucleon ^4He ion beams accelerated by the RILAC were injected into the RRC seven times between February and December 2009.

For installation, as described below, the regular RILAC

Table 1. Statistics on RILAC operation from January 1 to December 31, 2009.

Operation time of RILAC	4152.0 h
Mechanical trouble	63.0 h
Stand-alone RILAC	1596.5 h
Injection into RRC	2017.5 h
Total beam service time of RILAC	3614.0 h

Table 2. Beam service time of the stand-alone RILAC allotted to each beam course in target rooms No. 1 and No. 2 of RILAC in 2009.

Beam course	Total time (h)	%
e2	59.5	3.7
e3	1520.0	95.2
e6	17.0	1.1
Total	1596.5	100.0

operation was put on hold between March 12 and March 27, 2009, and between April 13 and June 5, 2009.

The beam time schedule was affected by problems in the water-cooling circuit of an electrical motor and of a valve, as described below. Other machine troubles did not affect the beam time schedule significantly.

Table 2 summarizes the beam service time of the stand-alone RILAC allotted to each beam course in the RILAC target rooms in 2009. The e3 beam course in target room No. 1 was used in the research experiments on the heaviest elements and in the study of the physical and chemical properties of these elements using a gas-filled recoil isotope separator (GARIS). The e2 beam course in target room No. 1 and the e6 beam course in target room No. 2 were used in the study of radiation chemistry and in the study of accelerator mass spectrometry, respectively.

This year, research experiments on the heaviest elements were carried out for 57 days in January and February, 4 days in June, and 4 days in July.

Table 3. Operation statistics on two ion sources (18G-ECRIS and 28G-SCECRIS) in 2009; the statistics include preliminary work time. The durations for which the 28G-SCECRIS was in operation are indicated in parentheses.

Ion	Mass	Charge state	Total time (h)
He	4	1	440.0 (0.0)
O	16	2	61.5 (0.0)
O	18	5	109.5 (0.0)
Ne	22	6	129.5 (0.0)
Na	23	7	1454.0 (0.0)
Ar	40	11	244.0 (0.0)
Ca	48	10	340.0 (0.0)
Fe	58	13	365.0 (0.0)
Xe	136	20, 27, (20)	388.0 (56.0)
U	238	35, (35)	404.5 (711.0)
Total			3936.0 (767.0)

Statistics on the operation times for the year 2009 of an 18-GHz ECR ion source (18G-ECRIS) and a new 28-GHz superconducting ECR ion source (28G-SCECRIS) that use an existing 18-GHz microwave power source are listed in Table 3. The ion beams of 10 elements were used in various experiments, in beam acceleration tests, and in beam commissioning.

In order to increase in the intensity of the ^{238}U ion beam for the RIBF, we carried out the following installation tasks and beam tests during this reporting period:

- 1) The 28G-SCECRIS on the high-voltage terminal of the Cockcroft-Walton pre-injector (HV-Terminal) was incorporated in all devices. In May 2009, the plasma of the 28G-SCECRIS was successfully generated using an existing 18-GHz microwave power source.
- 2) The low-energy beam transport (LEBT) line on the HV-Terminal and the medium-energy beam transport (MEBT) line were installed. These beam transport lines are connected to a new acceleration tube. The ion beam extracted from the 28G-SCECRIS can be directly injected to the RILAC through the LEBT and MEBT lines. The installation of these lines was successfully completed in July 2009.
- 3) The beam acceleration test at RILAC was started in July 2009. At first, we used the $^{136}\text{Xe}^{20+}$ beam, which was extracted from the 28G-SCECRIS.
- 4) Tests on the production of Au ions and U ions at the 28G-SCECRIS were carried out from October to November 2009.
- 5) As a result, we started supplying the $^{238}\text{U}^{35+}$ beam for experiments at the RIBF from November 2009.

We carried out the following improvements and overhauls during this reporting period:

- 1) In the rf system for rf power amplifiers No. 1, No. 3, and No. 4, rf pickup probes of the cavities and auto gain controllers, were improved.
- 2) In the rf systems, power supplies at the final stages and the intermediate stages were subjected to annual inspection. In addition, major components of mechanical parts were subjected to a simple inspection.
- 3) The installation of new power supplies for dipole magnets (DMe1, DMe3, DMe4, and DMe5) was completed in March 2009. The power supplies for DMe3, DMe4, and DMe5 were replaced with new ones. We are temporarily using the power supply for DMe1 to excite an analyzing dipole magnet on the HV-Terminal.
- 4) A turbomolecular pump of the RILAC cavity No. 2 was replaced with cryogenic pumps. The other vacuum pumps were subjected to annual inspection.
- 5) All the water pumps of each water-cooling system were subjected to a simple inspection. Two heat exchangers for the ordinary water-cooling circuit and the deionized water-cooling circuit for RILAC were overhauled. All cooling towers were subjected to a monthly inspection and annual cleaning.

- 6) A decelerator of the Charge-State Multiplier system (CSM-D1) was removed from the beam transport line in target room No. 2 in May 2009 and was converted to the drift tube linac No. 3 (DTL3) cavity of a new injector linac (RILAC2). The empty section was connected by an aluminum tube for vacuum plumbing.
- 7) In the e2 beam course, magnets of a new gas-filled recoil isotope separator were installed in May 2009. Therefore, the existing experimental devices belonging to two users were removed. The experimental devices belonging to one of the users were reinstalled in the e6 beam course in June 2009. The devices belonging to the other user will be reinstalled in a different beam course.

We experienced the following mechanical problems during this reporting period:

- 1) Water splashed on a magnet power supply for the millercoil for the 18G-ECRIS because of leakage from a drain valve of the magnets on an upper floor; we repaired the valve.
- 2) Water splashed on a high-voltage DC power supply for the 28G-SCECRIS because of leakage from a water joint for the sputtering electrode; we repaired the joint.
- 3) A re-buncher was damaged in an accident during the installation of the MEBT line. Fortunately, the damage was rectified.
- 4) Water splashed on an rf power amplifier system of the FC-RFQ because of leakage from a water joint of the cryogenic pump on an upper floor; we repaired the joint.
- 5) There were problems in the rf power amplifier systems, DC power supplies, low-level controllers, wide-band amplifiers, and a programmable logic controller; we replaced each component with spare components.
- 6) The bellows and pipe of a vacuum chamber in target room No. 1 were damaged in an accident during the reinstallation of the dipole magnet (DMe2); we repaired these components.
- 7) An electrical motor of the ordinary water pump for the RILAC cavities and magnets broke down because of the insulation failure in a coil phase. It was replaced immediately with an inactive electrical motor of the other water circuit, in accordance with specifications.
- 8) A thermostatically controlled valve of the deionized water circuit for the CSM suffered from a problem caused by the deterioration failure of the gasket material; we repaired the valve.
- 9) An air-cooling fan of the cooling tower circuit for RILAC suffered from a problem caused by the breakage of the bearing assembly; we repaired the fan.

AVF cyclotron operation

M. Kase, T. Kageyama, N. Tsukiori,^{*2} Y. Ohshiro,^{*1} N. Fukunishi, T. Nakagawa, H. Okuno, N. Sakamoto, M. Fujimaki, M. Kidera, M. Komiyama, Y. Higurashi, M. Nagase, S. Yokouchi, K. Yamada, H. Hasebe, K. Suda, H. Kuboki, T. Maie, K. Kobayashi,^{*2} M. Nishida,^{*2} Y. Kotaka,^{*2} S. Fukuzawa,^{*2} T. Nakamura,^{*2} R. Koyama,^{*2} K. Yadomi,^{*2} S. Ishikawa,^{*2} M. Hamanaka,^{*2} M. Nishimura,^{*2} J. Shibata,^{*2} A. Goto, O. Kamigaito, and Y. Yano

^{*1} CNS: Center of Nuclear Study, Graduate School of Science, the University of Tokyo

^{*2} SHI Accelerator Service Ltd.

Table 1 shows the operation statistics of the RIKEN K70-MeV AVF cyclotron (hereafter denoted as AVF) for 2009 together with those for the preceding years. The total operation time of 3870 h in 2009 is greater than that in 2008 by 8% and is equal to that in 2006, when regular RIBF operation had not started.

In 2009, RIBF experiments involving the use of relatively light ion beams were performed for the first time. For these experiments, the AVF was operated as an injector and the acceleration mode of AVF-RRC-SRC was operated for 550 h. In spring 2009, a nitrogen beam and a polarized deuteron beam were accelerated and injected into the RRC-SRC-BigRIPS; the final energy of the beam was 250 MeV/u. In April, the polarized deuteron beam was produced in the PIS after a long time and accelerated by the AVF. A single-turn extraction for the deuteron beam could be done well, which is significant for the experiment.

The AVF injection mode for the RIPS experiments which requires high-intensity beams of solid ions were changed to the RILAC injection mode in order to examine the ion source performance. Eventually, the operation time of AVF-RRC decreased by 33% compared to that in the previous year.

In standalone operations of the AVF, a total of 817 h was dedicated in 2009 to the CRIB experiments, which has been managed by CNS, the University of Tokyo. This value is smaller than that in 2008 by 30%. This decrease is partly due to the fact that the CRIB experiments have been efficiently performed in the previous years and the number of experiments on the backlog list is small. However, some of the CRIB experiments involving the use of Li ion beam were cancelled in 2009. Intense and stable beams

were not delivered due to certain problems with the RF transmitter of the Hyper-ECR ion source. In December 2009, a cooling water leakage occurred at AVF RF amplifier #1, and the CRIB experiment by the Korean group could not be performed well.

As an annual university curriculum, four sets of one-day experiments were conducted by students belonging to the University of Tokyo in autumn 2009. Elastic scattering experiments involving the use of 6 MeV/u α -beam were performed in the vacuum chamber on the way of the CRIB course in E7.

The E7b beam line was used frequently in 2009 for general purposes. Experiments on the electrochemistry of seaborgium and on α fine structure spectroscopy were conducted frequently. In September, a well-defined single-bunch Ar beam with an energy of 4 MeV/u was used to the Mossbauer experiment. The parallel-plate chopper was used in an ion-source beam line with a voltage of 1 kV and a repetition rate of 1 MHz; the resultant beam intensity is approximately 10 pA. Mixing of adjacent bunch to the single bunch was reduced to less than 0.1%.

It is third year since the RI productions for charged distribution began in 2007. The C03 target station has been used frequently for this purpose. Radio-nuclides of ⁶⁵Zn and ¹⁰⁹Cd were produced using a 14-MeV proton beam and delivered to facilities outside RIKEN by the Japan Radioisotope Association.

In summer 2009, a new hot laboratory was completed in the ion-source room just above the C03 target station. Its location permits a quick transportation of RI product the target. The efficient treatments of the RI product are expected in the new hot laboratory. In order to make a

space for the new laboratory, the old 10-GHz ECR ion source, which is relatively large, was replaced by the super-conducting ECR ion source in 2008. The new SCECRIS, which is jointly operated by RIKEN, CNS and

Tsukuba University, began to produce ions in spring 2009; it mainly produces the gaseous ions. The alternate use of the two ion sources, the Hyper ECR ion source and the super conducting ECR source, became possible.

Table1. Statistical data on AVF operation in 2006–2009					
	Year	2006	2007	2008	2009
Total operation time		3963 h	3669 h	3648 h	3870 h
Beam tuning		853 h (22%)	767 h (21%)	686 h (19%)	701 h (18%)
Injection to RRC		1051 h (27%)	1235 h (34%)	1165 h (32%)	782 h (20%)
Injection to RRC + SRC		0 h	0 h	0 h	547 h (14%)
AVF standalone		2059 h (52%)	1667 h (45%)	1797 h (49%)	1894 h (48%)
Baem course (AVF standalone)					
E7a (CRIB)		1275 h (62%)	1289 h (77%)	1119 h (62%)	817 h (43%)
E7b		257 h (12%)	0 h (0%)	228 h (13%)	302 h (16%)
C03		527 h (26%)	378 h (23%)	450 h (25%)	622 h (33%)
Machine study					153 h (8%)

Beam time statistics for user experiments

T. Suda, M. Kase, and T. Fujinawa

The operation of the RIBF for FY2009 was planned according to the approved budget for the fiscal year, plans for machine commissioning and construction, and beam-time requests from experimenters who have the PAC approved experimental proposals.

In this report, beam-time related statistics are presented. Figure 1 shows the number of experiments and developments performed and their duration in 2009. The experiments are categorized on the basis of accelerator-operation modes, namely, experiments involving the stand-alone operation of the AVF cyclotron, the stand-alone operation of RILAC, the use of the RRC, and the use of new accelerator complex named RIBF.

Figure 2 shows the total electric consumption profile for facility operation of Nishina Center for FY2009 categorized into those from TEPCO (Tokyo Electric Power Company) and those generated using our CGS (Co-generation system).

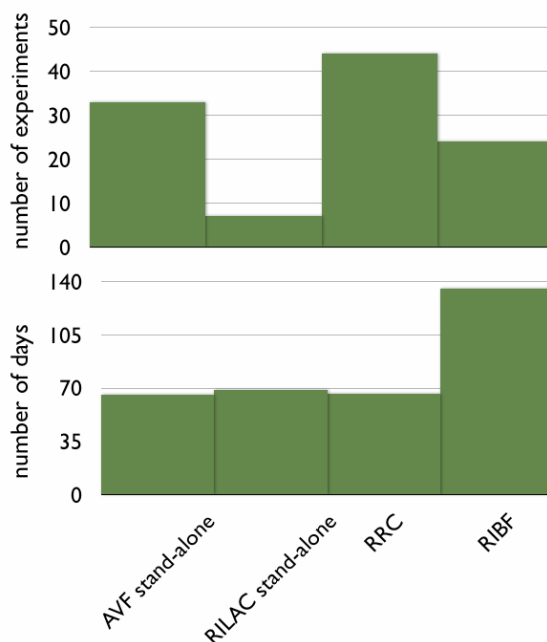


Fig. 1 Statistics of the number of experiments and developments performed and their duration in the year 2009.

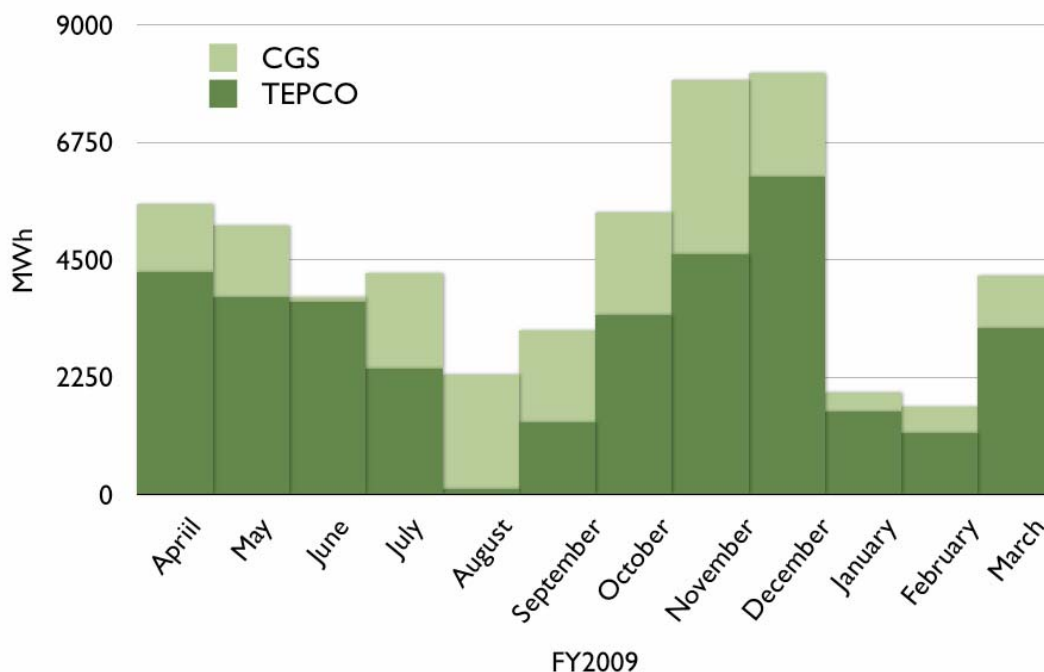


Fig. 2 The total electric consumption profile for facility operation of Nishina Center.

PAC Meetings for Nuclear Physics, and Material and Life Science

T. Suda, K. Ishida, and Y. Kobayashi

Two Program Advisory Committees (PACs) are responsible for reviewing submitted proposals in the fields of nuclear physics (NP) and material and life science (ML). Each PAC holds meetings twice a year and reviews the proposals.

The NP-PAC is co-organized by RIKEN Nishina Center and CNS, Univ. of Tokyo. The ML-PAC reviews experimental programs at RAL and RIBF.

NP-PAC

The NP-PAC meetings were held on June 18-19 and on Dec. 2-4 this year¹⁾. The statics of the meetings are shown in Table 1.

ML-PAC

This year, the ML-PAC meeting was held only once on September 3-4²⁾. Due to the long shutdown period of RAL in the latter half of FY2009, the 6th PAC meeting has been postponed to FY2010. The statics of the meeting are shown in Table 2.

PAC members

NP-PAC : *W. F. Henning (ANL, the chair), M. Huysse (K.U.Leuven), M. Lewitowicz (GANIL), K. Langanke (GSI), R. Tribble (Texas A&M), T. Glasmacher (MSU), W. Liu (CIAE), A. A. Ogloblin (Kurchatov), B. Fulton (Univ. of York), A. Ono (Tohoku Univ.), K. Yabana (Univ. of Tsukuba), I. Hamamoto (Lund Univ.), T. Kishimoto (RCNP), T. Noro (Kyushu Univ.), T. Nakamura (Tokyo Inst. Of Technology), T. Shimoda (Osaka Univ.), H. Sakai (Univ. of Tokyo)*

ML-PAC : *J. M. Poutissou (TRIUMF, the chair), A. Amato (PSI), B. A. Beer (Univ. of Victoria), F. Hanaoka (Gakushuuin Univ.), R. Kato (RIKEN), K. Komaki (National Center for Univ. Entrance Exam.), K. Kubo (ICU), D. E. MacLaughlin (UC, Riverside), S. Maekawa (Tohoku Univ.), K. Nagamine (UC, Riverside), N. Nishida (Tokyo Inst. Of Technology), K. Nishiyama (KEK), F. L. Pratt (RAL), I. Yamaguchi (Food Angri. Mat. Inspection), J. Zmeskal (Stefan Meyer Inst.)*

	5th (June 18-19, 2009)				6th (Dec. 3-4, 2009)			
	Proposals		Days		Proposals		Days	
	requested	approved	requested	approved	requested	approved	requested	approved
GARIS	1	1	19	19	0	0	0	0
CRIB	3	2	23	15	1	1	10	7
RIPS	0	0	0	0	1	1	9	9
BigRIPS/ZD/S	10	9	87.5	35	9	7	81	34
HARAQ								
Construction	2	2			2	2		
TOTAL	16	14	129.5	69	13	11	100	50

Table 1. Statistics of the NP-PAC meetings held this year.

	5th (Sep. 3-4, 2009)			
	Proposals		Days	
	requested	approved	requested	approved
RAL	18	17	105	60
RIBF	2	2	4	4
TOTAL	20	19	109	64

Table 2. Statistics of the ML-PAC meeting held this year.

References

- 1) <http://www.nishina.riken.jp/UsersGuide/NP-PAC>
- 2) <http://www.nishina.riken.jp/UsersGuide/ML-PAC/>

Radiation Safety Management at RIBF

Y. Uwamino, H. Sakamoto, R. Hirunuma Higurashi, H. Mukai^{*1}, A. Akashio, H. Fukuda, S. Fujita, T. Yamaki, K. Igarashi, K. Nakano and S. Iizuka

Residual radioactivity in cyclotron deflectors was measured, and variations in the dose rates since 1986 are shown in Fig. 1. Since 2006, intense beam has been used at AVF cyclotron for radioisotope production; this has been accompanied by a high of the residual radiation. RRC was operated with a 0.4- μ A 135-MeV/u 14 N beam until two days before the measurement in 2009, and the dose rate was found to be extremely high, 100 mSv/h. The dose rate of the residual radiation in the deflector of SRC was first measured 28 days after the operation with a 50-pnA 250-MeV/u 14 N beam.

The residual radioactivity was measured along beam lines after almost every experiment. Spots 1–32, marked with solid circles in Fig. 2, are the points where high dose rates were observed. Table 1 shows these dose rates along with the measurement dates, beam conditions, and decay periods after the end of the operation. The maximum dose rate was found to be 2.0 mSv/h at point 25, which is the surface of the G01 Faraday cup placed after SRC.

We continuously monitor the radiation in and around the RIBF facility by using neutron and gamma-ray area monitors. Measurement of dose rates outside the radiation-controlled area is difficult due to the presence of natural radiation. No accelerator was operated between August 11 and September 4 in 2009, and the dose rates during this period were assumed to be the natural background dose rate. The net accumulated dose, i.e., the dose obtained after subtracting the background dose, at the site boundary was lower than the detection limit, which was assumed to be 9 μ Sv/y for gamma-rays and 2 μ Sv/y for neutrons. In any case, the annual dose at the site boundary was considerably lower than the legally permissible limit (1 mSv/y).

Three monitors are placed at the boundary of the radiation-controlled area. One is in the computer room of the Nishina building and two are on the roofs of the IRC and BigRIPS vaults. The highest value was observed in the computer room, which is on the ground floor immediately

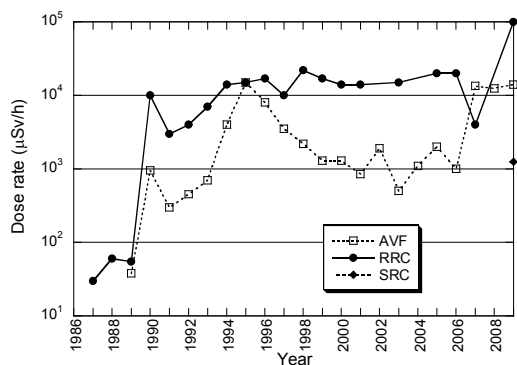


Fig. 1. Dose rate at the deflectors of RRC, AVF, and SRC since 1986.

above a bending magnet that guides the beam from the RRC vault to the distribution corridor. The neutron dose was 5.3 ± 3.3 μ Sv/y, and the gamma dose was below the detection limit of 4 μ Sv/y. The annual neutron dose in the computer room since 1999 is shown in Fig. 3.

The water from the closed cooling systems at BigRIPS was sampled after the operation by using a 320-MeV/u 4 He beam, which had an intensity of approximately 1 μ A, in November 2009, and radionuclide concentrations were measured by using a liquid-scintillation counter and a Ge detector. The results are shown in Table 2. The radionuclide concentration was highest in the cooling water at the side-wall beam dump, but the sum of ratios of the concentrations to the legal limits for the drain water over all the radionuclides was still considerably lower than unity. The range of the 4 He beam was long, and the cooling water was directly irradiated by the primary beam. This 4 He beam increased the 3 H concentration in the cooling water at the side-wall beam dump from 0.36 Bq/cm³ to 1.0 Bq/cm³.

Table 1. Dose rates measured along beam lines in 2009. Points 1–32 indicate the measurement locations shown in Fig. 2.

Point	Dose rate (μ Sv/h)	Date (M/D)	Particle	Energy (MeV/u)	Intensity (pnA)	Decay period (h)
1	400	8/17	40 Ar	3.97	12	130
2	1000	8/17	40 Ar	3.97	12	130
3	400	8/17	40 Ar	3.97	12	130
4	1000	8/17	13 C	100	550	176
5	35	8/17	13 C	100	550	176
6	38	5/22	84 Kr	70	20	97
7	20	5/22	84 Kr	70	20	97
8	35	8/17	13 C	100	550	176
9	35	8/17	13 C	100	550	176
10	23	5/22	84 Kr	70	20	98
11	160	8/17	13 C	100	550	176
12	1700	8/17	13 C	100	550	176
13	1600	8/17	13 C	100	550	176
14	1000	8/17	13 C	100	550	176
15	130	5/22	84 Kr	70	20	98
16	55	8/17	13 C	100	550	176
17	85	6/25	14 N	135	429	314
18	33	6/25	14 N	135	429	314
19	400	6/25	14 N	135	429	314
20	45	6/25	14 N	135	429	314
21	10	5/22	14 N	109	100	169
22	58	5/22	14 N	109	100	169
23	14	5/22	14 N	250	1	243
24	100	3/31	14 N	250	50	20
25	2000	3/31	14 N	250	50	20
26	16	5/22	14 N	250	1	243
27	50	5/22	14 N	250	1	243
28	35	5/22	14 N	250	1	243
29	12	5/22	14 N	250	1	246
30	180	5/22	14 N	250	1	246
31	110	5/22	14 N	250	1	246
32	900	2/26	48 Ca	345	160	1620

^{*1} Japan Environment Research Corp.

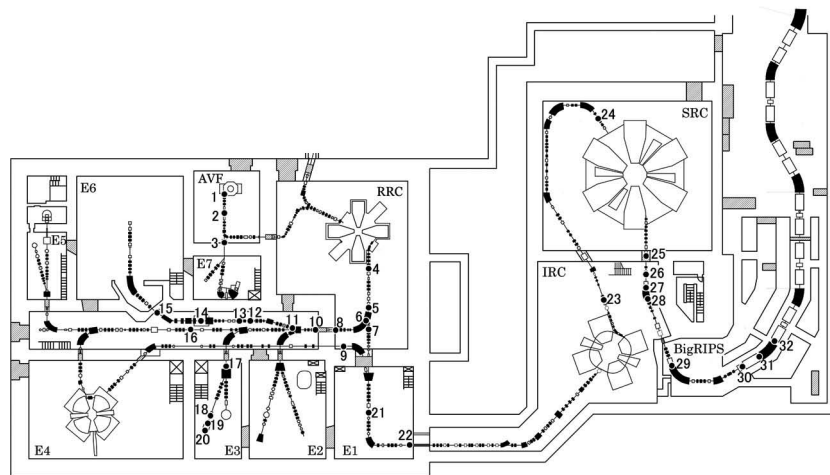


Fig. 2. Layout of beam lines at RIBF. Locations where a high dose rate was observed are indicated by solid circles, 1–32.

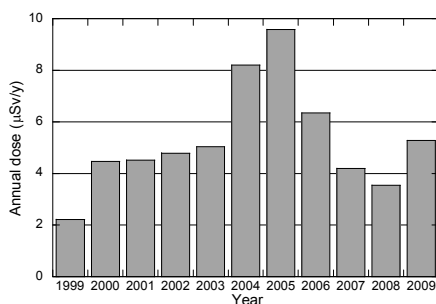


Fig. 3. Annual dose of the leakage radiation in the computer room of Nishina building since 1999.

Table 2. Radionuclide concentration in the cooling water of BigRIPS on November 16, 2009, the legally permissible limits for radionuclides concentration in the drain water, and the ratio of the concentration to the limit.

cooling water	nuclide	concentration (Bq/cm ³)	limit	ratio to limit
F0 target	³ H	4.1e-2 ¹⁾	60	6.8e-4
Exit beam dump	³ H	1.0e-1	60	1.7e-3
Side-wall beam dump	³ H	1.04	60	1.7e-2
	⁷ Be	2.0e-1	30	6.7e-3
	sum			2.4e-2

1) read as 4.1×10^{-2}

The radiation safety interlock system of Nishina building was replaced in February 2009. A conceptual block diagram of the new system is shown in Fig. 4. The main programmable logic controller (PLC) reads the status of the shield doors, safety keys, emergency stop buttons, and radiation monitors. On the basis of the status and the control commands given by the accelerator operators or the radiation safety staffs, the main PLC controls the beam stoppers, radiation shutters, electric power to the shield doors, exhaust dampers, warning sirens, and beam status indicators. The control commands are entered on the control PCs, and the commands are transferred to the PLC by the database server.

The access-control system is a part of the safety system. It consists of access controllers at the boundaries of the

radiation-controlled area and at the entrances of the accelerator rooms and experimental rooms, and personal contamination monitors.

The access controller reads the barcode on the personal dosimeters, and records the entry of people into the radiation-controlled area and rooms. When the system recognizes the existence of persons in a room, it inhibits beam transport to the room. The system does not permit a person to leave the area, until the personal contamination monitor confirms the absence of contamination.

To avoid interruption of the accelerator operation by problems in the database server or the LAN, a switch box is available. It is connected to the main PLC, and an accelerator operator can directly control the main PLC through the key box to continue the experiment. The safety interlock system has shown good reliability since February 2009.

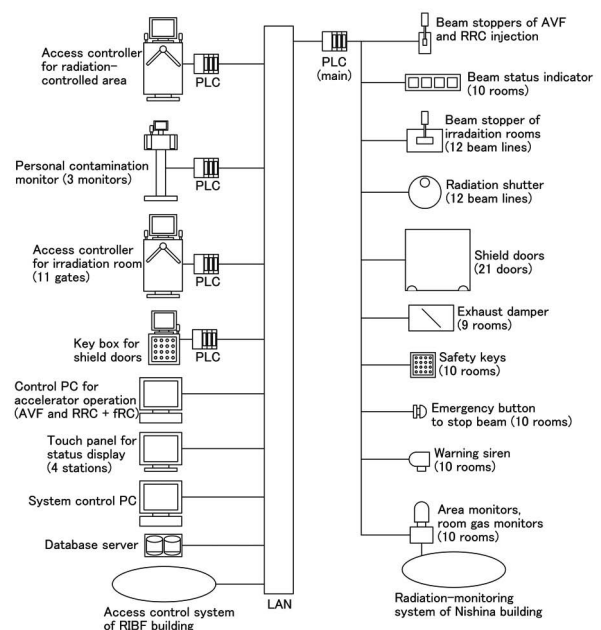


Fig. 4. Conceptual block diagram of the new radiation-safety interlock system of Nishina building.

Fee-based distribution of radioisotopes produced at AVF cyclotron

T. Kambara, H. Haba, Y. Ezaki, K. Takahashi, and H. Miyamoto

Since October 2007, RIKEN Nishina Center has been involved with fee-based distribution of radioisotopes (RIs) ^{65}Zn ($T_{1/2} = 244$ days) and ^{109}Cd ($T_{1/2} = 463$ days) among the general public in collaboration with the Japan Radioisotope Association¹⁾ (JRIA), which is an organization of RI users and research workers and regulates the process from supply to disposal of RIs in Japan. According to a Material Transfer Agreement (MTA) between JRIA and RIKEN,²⁾ JRIA receives orders from users, sends them to RIKEN, and distributes the produced RIs from RIKEN to the users. In 2009, we accepted four orders for ^{109}Cd and distributed total radioactivity of 30 MBq; and we also accepted twelve orders for ^{65}Zn and distributed total radioactivity of 51.1 MBq. Compared with 2008 when we distributed 33 MBq of ^{109}Cd and 34.7 MBq of ^{65}Zn , the distribution of ^{109}Cd showed a decrease of about 9% and that of ^{65}Zn showed an increase of about 47%. These RIs were supplied to universities and research institutes in Japan.

The ^{65}Zn and ^{109}Cd are produced by the $^{65}\text{Cu}(p,n)^{65}\text{Zn}$ and $^{109}\text{Ag}(p,n)^{109}\text{Cd}$ reaction respectively with a 14-MeV proton beam from the AVF cyclotron at the C03 beam line dedicated to RI production. After irradiation, the RIs are separated by an ion-exchange method to obtain ^{65}Zn and by precipitation and ion-exchange methods to obtain ^{109}Cd .

Recently, we have established techniques for the production and separation of a nuclide ^{88}Y ($T_{1/2} = 107$ days), and it is now ready to join the list of RIs available for fee-based distribution. ^{88}Y was produced by the $^{88}\text{Sr}(p,n)^{88}\text{Y}$ reaction. The target was a pellet of strontium oxide (SrO) with a diameter of 10 mm and a thickness of 200 mg/cm², and SrO was prepared from SrCO₃ with a chemical purity of 99.99% and a natural isotopic composition of 82.6% ^{88}Sr . A proton beam from the AVF cyclotron having a maximum intensity of 4.9 μA irradiated the target for 0.55 hours during which the target placed on a target holder was cooled by He gas and water. After the irradiation, 1.61 MBq of ^{88}Y was separated using Eichrom Ln resin. The chemical yield was 99.4%. We estimated the specific activity of ^{88}Y to be 1.09 MBq/ng using ICP-MS.

In December 2009, the MTA was amended to add the ^{88}Y to the list of nuclides available for distribution. Those who order the ^{88}Y can select its chemical form among solutions in hydrochloric acid, acetic acid, and nitric acid with a concentration of 0.1 mol/L or 1 mol/L. The maximum radioactivity of one package is 1 MBq. Details can be found on the on-line ordering system J-RAM³⁾ of JRIA.

Orders for RIs can be sent from any place in

Japan to JRIA by Fax (03-5395-8055) or E-mail (gyomu1@jrias.or.jp). Normally, the RIs are delivered within 16 days from the acceptance of the order.

References

- 1) <http://www.jrias.or.jp/index.cfm/1,html> (Japanese), <http://www.jrias.or.jp/index.cfm/11,html> (English).
- 2) T. Kambara, H. Haba, Y. Ezaki, K. Takahashi, and H. Miyamoto: RIKEN Accel. Prog. Rep. **42**, 295 (2009).
- 3) <https://www.j-ram.net/jram/DispatchTopPage.do> (Japanese).

Operation of SRC cryogenic system

H. Okuno, T. Dantsuka, M. Kase, Y. Mori,^{*1}, I. Tajima,^{*1}, M. Ohshima,^{*1}, K. Iwasaki,^{*1}, T. Suzuki,^{*1}, K. Yamamoto,^{*1} and S. Watanabe^{*1}

[Superconducting ring cyclotron, cryogenic, helium refrigerator]

The SRC cryogenic system, which consists of three compressors, a He refrigerator, and four He buffer tanks, was operated for around 9 months in 2009, with a 3-month maintenance shutdown in summer (June–August). The most serious problem encountered during the operation was water leakage, in addition to other minor issues. These problems indicated that safe long-term operation of the cryogenics system was difficult.

The long-term operation lasted from October 2008 to June 4, 2009, as shown in Fig. 1. The total operation period was around 230 days, during which period oil contamination in the He refrigerator, which was a major problem in 2008, was solved.

The first step in the shutdown of the cryogenic system was the recovery of 5000 L of liquid He from the superconducting magnets to the buffer tanks. In the recovery process, the TMP (Turbo Molecular Pump)s for thermal insulation vacuum had to be switched on to evacuate the outgas from the cold mass whose temperature arise. Unfortunately, the above mentioned process however was delayed by 1-2 days owing to human error. Figure 2 shows the trend in the thermal insulation vacuum and cold-mass temperature. This deterioration caused cooling of the beam duct surrounded by the vacuum. The cooled beam duct caused the water in the copper pipe attached to the beam duct to freeze and this led to rupture of the copper pipe, as shown in Fig. 3. As a consequence, water entered the vacuum for until we could detect the leak. However,

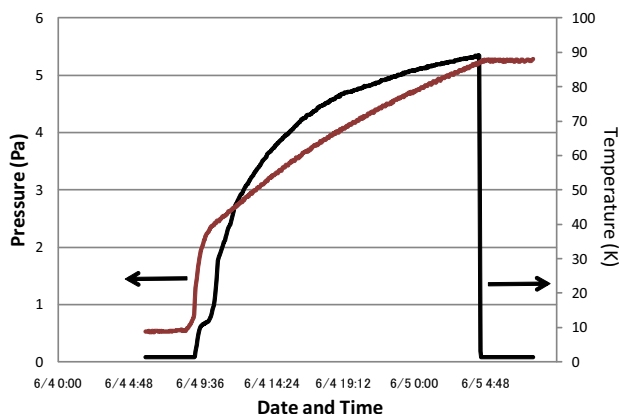


Fig. 2. Trend in the vacuum for thermal insulation and temperature for SBM cold mass after recovery was started.

by this time, almost 30 tons of water had entered the SRC. It was very difficult to remove the water and dry the vacuum chamber and rf cavity. Nevertheless, we successfully overcame this problem by autumn. Improvements had to be made the operation manual and alarm system in order to prevent the above mentioned problem from recurring.

Operation of the compressors was started on August 29, 2009, after regular maintenance. The cryogenic system was maintained in the normal operation

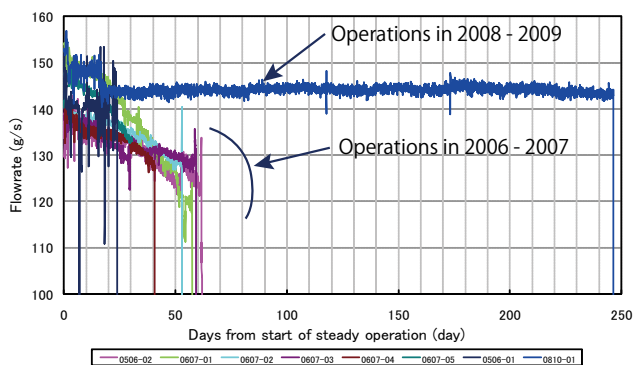


Fig. 1. Flow-rate trend in the He refrigerator during the 2008–2009 operation and that during the 2006–2007 operation, which lasted for approximately 60 days.

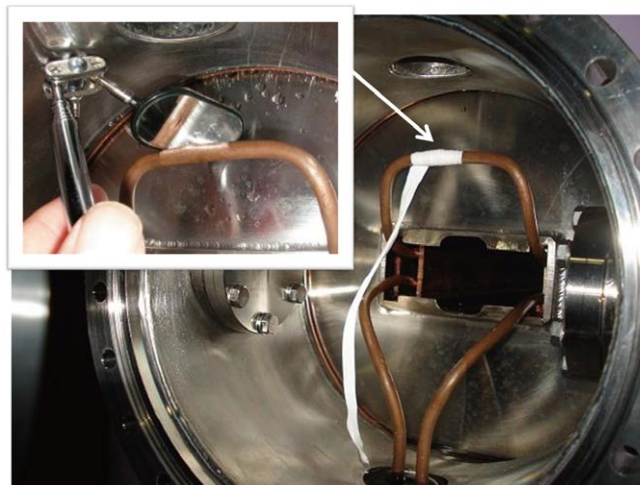


Fig. 3. Broken copper pipe attached to the beam duct in the SBM.

^{*1} Nippon Kucho Service Co., Ltd

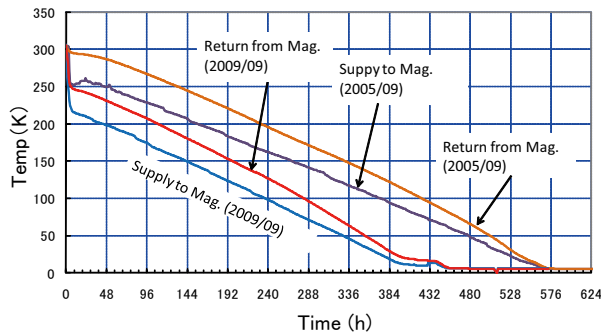


Fig. 4. Trend observed in the temperature of the supply and return gas to/from the magnet in September 2009. Trend observed in 2005 is also shown.

mode from October 12, 2009 to January 6, 2010; the following minor problems were encountered during this period. A purification process had to be carried out for stable long-term operation before the superconducting magnets were cooled. The compressors stopped working suddenly during the purification process because of the failure of the 24-V power supply that was necessary for the DI/DO VME board. Although the compressor could be restarted after replacing the old power supply with a new one, we learnt from this experience that a dual power supply should be used for such important devices.

After purification, we started the cooldown operation. Figure 4 shows the trend in the temperature of the supply and return gas used for the He refrigerator; previously recorded data are also shown for comparison. The temperature of the supply gas never decreased below 12 K at the final stage of the cooldown process. We found that the main supply valve of CV5190 did not open even when the control display showed its status as "OPEN"; this was because the valve for supplying compressed air to the pneumatic control of CV5190 was closed. We realized that the operator had forgotten to open the valve after the regular maintenance.

After cooldown, the vessels for the superconducting magnets were filled with 5000 L of liquid He on October 19, 2009. We maintained the operation steady until January 6, 2010. During the steady operation, we encountered a new problem. At 9:59 AM on October 11, 2009, the slide valve in compressor A started to close by few 5 %. The trend observed for the pressure control valve suggested that operation was not stable and that there was a very high risk of the operation being interrupted, as shown in Fig. 5. We discussed this unusual phenomenon with our colleagues. We decided that control of the slide valve is very important for protection against external factors. However, we

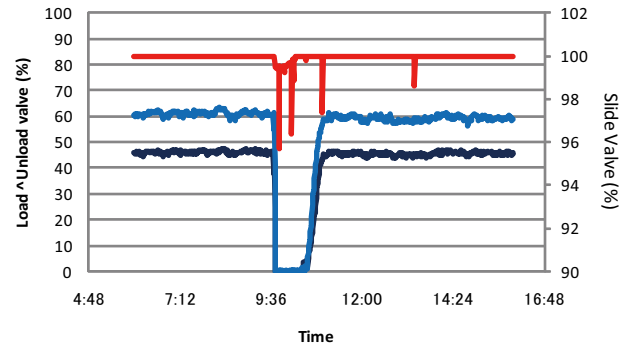


Fig. 5. Trend in CV values observed for the slide valve in compressor A and valves used to control the suction and output pressure of the compressor.

could not identify the reason for automatic closing of the control. We speculated that this was due to the failure of the PLC programs and stopped the automated control of the slide valve.

Present status of the BigRIPS cryogenic plant

K. Kusaka, M. Ohtake, T. Kubo, K. Yoshida, A. Yoshida, T. Ohnishi, Y. Yanagisawa, N. Fukuda, Y. Yano,
M. Nobutoki,^{*1} H. Ito,^{*2} T. Sasaki,^{*2} N. Kakutani,^{*2} T. Tsuchihashi,^{*2} and K. Sato^{*2}

The five superconducting triplet quadrupoles (STQ1–STQ5) in the first stage of the BigRIPS separator are cooled by a large liquid-helium cryogenic plant, whose main components are a Linde-TCF50S refrigerator (cold box) and a Mayekawa 315-kW compressor unit.¹⁾ The whole cryogenic system, including the STQs, was fabricated by Toshiba Corporation and Taiyo Nippon Sanso Corporation and installed in the RIBF building in early 2004.

Regular operation of the BigRIPS cryogenic plant started in October 2006 after test operation was performed from March 2004 to June 2006.^{2,3)} The cryogenic plant typically operates according to the following thermal cycle: purification of helium gas, precooling of the magnets, liquefaction, steady-state operation in the refrigerator mode, and warm-up. Until July 2007, we repeated four thermal cycles in which the periods of the steady-state operation in the refrigerator mode were 53, 59, 39, and 34 days. The cooling capacity decreased gradually in each operation cycle, and we had to warm the cold box to recover the cooling capacity.

In February 2008, when the cryogenic valve at the entrance of the 80-K adsorber (ADS) was removed for maintenance, a small amount of oil was found on the valve sheet. The oil contamination in the cold box was investigated, and it was found that the heat exchangers and internal high-pressure lines in the cold box were contaminated. We concluded that the oil contamination in the heat exchangers caused the decrease in the cooling capacity. The oil-removal module of the compressor unit was then improved, and the heat exchangers of the cold box and the contaminated high-pressure lines were cleaned from April to August 2008.⁴⁾

Our main compressor is a two-stage oil-flooded screw-type with a flow rate of 73.5 g/s and a discharge pressure of 1.60 MPaG. The improved five-stage oil-removal module comprises an oil vessel with a demister as a bulk oil separator (1SP), three coalescer vessels (2SP, 3SP, and 3.5SP), and two adsorbent vessels (4SP and 5SP) that contain activated charcoal and molecular sieves. The design of the improved compressor unit is schematically shown in Fig. 1. The newly introduced third coalescer vessel (3.5SP) is identical to the two original coalescer vessels (2SP and 3SP), and the design of the final charcoal vessel (5SP) is based on the oil-removal unit in the RIKEN-RAL Muon facility. The compressor lubricant injected in the screws is separated from the discharged helium gas by using the five-stage oil-removal module, and the oil contamination is expected to be 0.008–0.02 ppm.

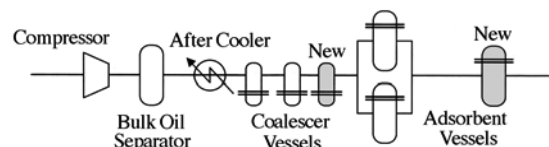


Fig. 1. Schematic diagram of the improved compressor unit.

Continuous operation of the BigRIPS cryogenic plant started on September 11, 2008. After one week of carrying out the purification operation, STQ1–STQ5 were cooled from room temperature to 4 K in 18 days, and cryostats were filled with liquid helium in 3 days. Steady-state operation in the refrigerator mode started on October 7, 2008, and ended on July 1, 2009. The plant was operated in the steady state in the refrigerator mode for 237 days, and the total operation time of the compressor after the improvement was approximately 6500 h.

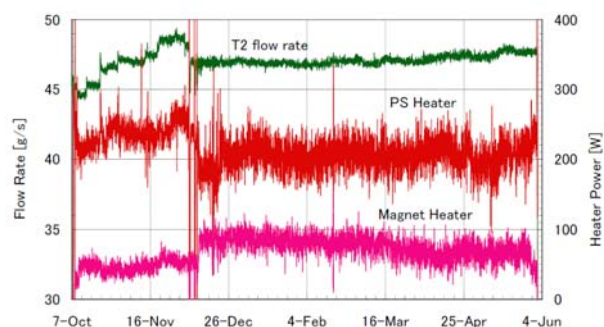


Fig. 2. T2 turbine flow rate and heater power in the period of steady-state operation.

Figure 2 shows the flow rate of the T2 turbine and the heater power during the steady-state operation in the refrigerator mode. From October 7 to early December, we manually increased the inlet pressure of turbines to optimize the cooling capacity so as to increase the T2 flow rate. After December 6, we set the inlet pressure of turbines at a constant value (1.23 MPaG) so as to maintain a constant T2 flow rate. In the operations before July 2007, the T2 flow rate decreased gradually even though the inlet pressure was increased due to the oil contaminations.

The power of the magnet heater, shown in Fig. 2, is the sum of the heater power of the cryostats containing STQ1–STQ5. The heater power of each cryostat is automatically controlled such that the liquid helium level in the cryostat remains constant. The power of the heater installed in the phase separator (PS) in the cold box is also shown in Fig. 2. The sum of the two curves of heater power indicates that the excess cooling capacity of the cryogenic system is approximately 300 W at 4 K; this

^{*1} Taiyo Nippon Sanso Corporation

^{*2} Toshiba Corporation

observation is consistent with the results of the test operation in 2005.^{2,3)}

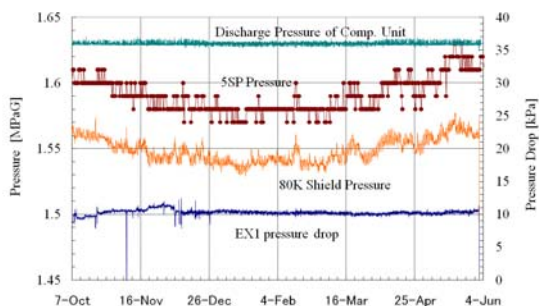


Fig. 3. Pressures at the exits of the compressor unit and the last adsorbent vessel (5SP) and the supply pressure to the 80-K shield. The pressure drop across the heat exchanger EX1 is also shown.

Figure 3 shows the variation in pressure in the high-pressure part of the system. The discharge pressure of the compressor unit is measured by a pressure transducer, and the load and unload valves are operated such that the discharge pressure is constant. When we cleaned the cold box in 2008, we introduced differential pressure transmitters in the cold box; these transmitters measure the pressure drop across the high-pressure line of the first heat exchanger (EX1). After we fixed the inlet pressure of turbines on December 6, the measured differential pressure was constant (~10 kPa), as shown in Fig. 3. We conclude that the heat exchanger was not contaminated.

Figure 3 shows that the pressure at the exit of the 5SP, which is measured by a Bourdon gauge, and the supply pressure of the 80-K shield line as functions of the pressure drop. Unlike the discharge pressure of the compressor unit, the 5SP pressure and shield pressure decrease between October 2008 and February 2009 and subsequently increase. However, the difference between the 5SP pressure and shield pressure is almost constant; hence, we consider that the decrease in the 5SP pressure and shield pressure is not caused by the contamination of the high-pressure line. The temperature-drift of the pressure transducer may be the cause of the decrease in pressure.

In addition to the cold-box data, we adopted different methods to study the oil contamination of the discharge helium gas. The typical value of oil contamination measured downstream of the coalescer vessels is 0.75–50 weight ppm. An “oil check kit” is used to measure this level of oil contamination. A fixed volume of gas is sprayed through a controlled orifice onto a treated slide, and the size of the oil spot on the slide is compared with that of spots on a standard slide. We repeatedly measure the oil contamination at the exit of the coalescer vessels by using the oil check kit. Figure 4 shows the measurement at the exit of the 3SP, as an example of the results obtained using the kit. An estimate of the oil drain from the 3.5SP is also shown in Fig. 4. In our compressor unit, after sensing the oil level in the vessel, the drain oil in the coalescer vessels is exhausted to the compressor via a drain line with solenoid valves. By counting the number of times the solenoid

valve is operated or by manually measuring the amount of the drain oil, we can estimate the level of oil contamination. Both plots in Fig. 4 show gradual increase in the oil contamination.

To measure oil contamination in the range 0.008–0.15 weight ppm, which is expected to be contamination level at the exit of the adsorbent vessels, we used two different methods. One method involves the use of an apparatus called the pyrolyzer with multicomponent detector based on optical emission spectrometry. We used Linde’s apparatus and measured the oil contamination at the exit of 5SP for two weeks in December 2008 and for three weeks in March 2009. The results for both periods indicate an oil contamination of 0 ppb.

Another method to measure oil contamination in the range 0.008–0.15 weight ppm is a trap method in which helium gas passes through a stainless steel sampler tube containing glass beads and contaminant (oil) sticks on the surface of the beads and/or the sampler tube. The contaminant trapped in the sampler tube is then extracted using a solvent, and the amount of the oil contaminant is measured by Fourier transform infrared (FTIR) spectroscopy analysis. By introducing the sampler tube in a liquid-nitrogen Dewar, the trapping efficiency is improved; we call this method as the “cold trap” (CT) method.

The CT method was applied to measure the oil contamination at the exits of 5SP, 4SP, and 3.5SP. In all three cases, results indicate that the oil contamination is below the limits of 10, 41, and 10 weight ppb, respectively. The room-temperature trap method was also applied to measure the oil contamination at the exit of 3.5SP, and the oil contamination was evaluated to be less than 40 weight ppb.

After the maintenance in summer 2009, continuous operation of the cryogenic plant started on September 17, 2009. Steady-state operation in the refrigerator mode started on October 9, 2009, and we are planning to carry out the continuous operation till the end of June 2010.

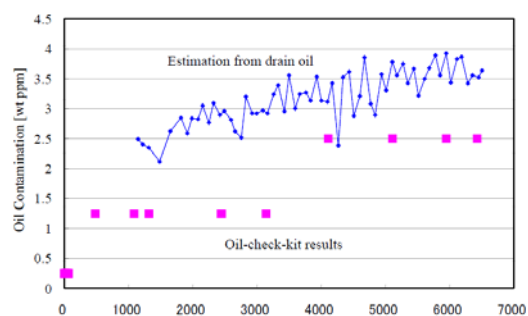


Fig. 4. Oil contamination at the exit of the second coalescer vessel (3SP)

References

- 1) T. Kubo et al.: RIKEN Accel. Prog. Rep. **36**, 316 (2003).
- 2) T. Kubo et al.: RIKEN Accel. Prog. Rep. **38**, 289 (2005).
- 3) K. Kusaka et al.: RIKEN Accel. Prog. Rep. **41**, 244 (2008).
- 4) K. Kusaka et al.: RIKEN Accel. Prog. Rep. **42**, 309 (2009).

Present Status of Liquid-Helium Supply and Recovery System

T. Dantsuka, H. Okuno, Y. Odashima, M. Nakamura, T. Maie, K. Kato, K. Ikegami, M. Kase

M. Ohshima*, I. Tajima*, R. Ise* Nippon Air Conditioning Service K.K*

The liquid-helium supply and recovery system¹⁾, which can generate liquid helium at a rate of 200 L/h from pure helium gas, has been stably operated since the beginning of April 2001. The volumes of liquid helium that were supplied each year are listed in Table 1 and also shown in Fig. 2. The volume of liquid helium supplied has gradually increased since the supply was started. The Exploratory Materials Team began using liquid-helium for the first time in March 2008, the while the Laboratory for Human Brain Dynamics at the Brain Science Institute (BSI) stopped using liquid-helium by the end of September 2008.

We extended the recovery pipe at two places. First, at the end of January 2010, a new recovery pipe was connected from the south side of the Laser Science Laboratory to the recovery station behind the building on the east at the BSI. Next, new recovery pipes will be connected to the existing pipe in the Nishina Memorial Building from E6 and J8; this will be done by the middle of August.

The control system of the compressor for liquefying helium gas tripped several times between December 2009 and February 2010. The cause for this is unknown and is currently being investigated.

The purity of the helium gas recovered from laboratories improved gradually once the construction of the system was completed. The volume of the helium gas recovered from each building in the Wako campus and transported to the liquid-helium supply and recovery system was measured. The recovery efficiency, which is defined as the ratio of the recovered helium gas to the supplied liquid helium, was

calculated. The recovery efficiency for the building on the south side of the Wako campus-such as the Cooperation Center building of the Advanced Device Laboratory, the Chemistry and Material Physics building, and the Nanoscience Joint Laboratory building-increased to over 90%. Recovery efficiencies of the main research building and the Laser Science Laboratory were 7.8%. The average recovery efficiency from January 2008 to December 2009 is shown in Fig. 1. It has increased to over 90%.

References

- 1) K. Ikegami et al.: RIKEN Accel. Prog. Rep. 34, 349 (2001).

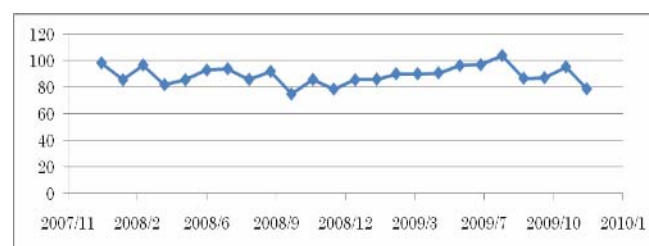


Fig1. Average recovery efficiency measured from January 2008 to December 2009

Fiscal Year	2001	2002	2003	2004	2005	2006	2007	2008
Laboratory & institute	Amount of supplied liquid helium (ℓ)							
Magnetic materials laboratory	3392	7024	7713	11829	15672	16512	23282	20899
Low-temperature physics laboratory	1270	3090	6966	9515	34713	29520	39855	48756
Advanced device laboratory	9977	10849	9726	7401	11264	15017	14733	12554.5
Condensed molecular materials laboratory	1939	1615	3079	5353	5912	7772	5331	5459.5
Surface chemistry laboratory	1146	1676	4533	5007	5370	5486	3636	4080.5
Brain science institute	6277	8144	5055	6292	7285	6956	6480	3226
Exploratory materials team							624.5	9853.5
Other laboratories	3535	7730	14476	9487	15717	14767	14628.5	9862.5
Total	27536	40182	51530	54884	95933	96030	109194	114691.5

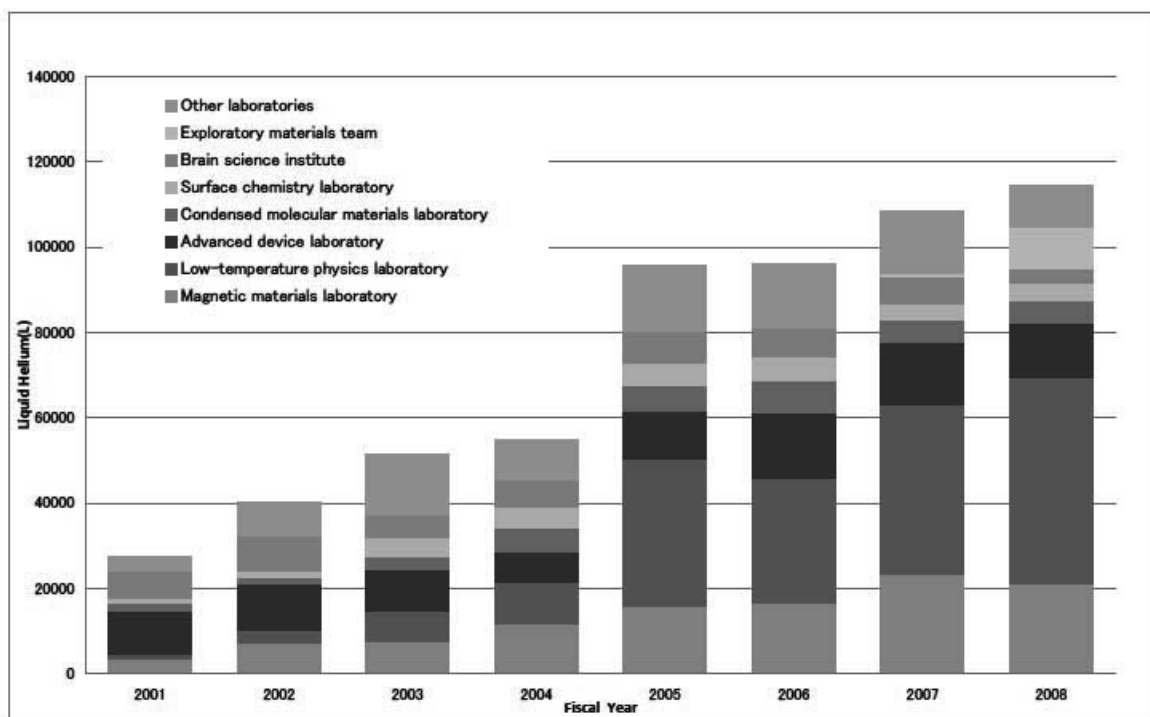


Fig2. Volumes of liquid helium supplied to laboratories per year from fiscal 2001 to 2008

Improvement made to couplers used for liquid-helium supply and recovery lines (1)

Y. Odashima, H. Okuno, M. Kase, T. Dantsuka, I. Tajima,^{*1}, M. Ohshima,^{*1}, R. Ise,^{*1} and K. Kato

[liquid helium, cryogenic system]

Workers at the liquid-helium plant transfer liquid helium from a 7000-L Dewar to containers (100 L, 250 L) through a supply pipe. The users use this helium in their laboratories for various experiments, connecting the containers with recovery lines to the liquid helium plant. We believe that it is important to establish a liquid-helium-handling system that can be safely handled by users and suppliers. For this purpose, we are in the process of developing the process of new couplers for liquid-helium supply and recovery lines, by taking into account the suggestions given by the suppliers and users. These couplers are expected to help overcome the difficulties faced when handling liquid helium.

First, we describe the improvements made to the coupler used for the liquid-helium-supplying line. Previously, the users employed Wilson seals for transferring helium to the experimental devices in the laboratory; on the other hand, a simple dynamic seal was used when liquid helium was transferred to the container in the liquid-helium plant, as shown in Fig. 1. The workers in the plant had to remove the Wilson seal before pouring helium and then remove the frozen Teflon tube to re-attach the Wilson seal. This process was time-consuming, and there was a risk of losing the parts of the Wilson seal. Hence, we asked the users to replace the Wilson seal with the dynamical-seal so that the aforementioned process could be avoid. Fig. 2 shows the structure of a Teflon dynamic seal for the users. A ditch was fabricated on the O-ring to prevent the leakage of helium.

Next, we describe the improvements made to the coupler used for the helium-recovery lines. Before the improvement, a conventional rubber hose was used. The disadvantage of the rubber hose is the possible leakage of helium; further, the hose may become rigid when used for liquid-helium transfer and may have to be warmed with a heat gun fro easy detachments. We developed a cryogenic coupler by adding a check valve to a conventional coupler. We replaced the O-ring and thin Teflon plate with a thick packing, as shown in Fig. 3. In this case, no leakage was observed ever at low temperatures such as around 30K, and the pipe for recovery from the container could be easily detached at lower temperatures when the pressure in the container decreased to 0 bar. Figure 4 shows a photograph of the coupler connecting the container the recovery line.

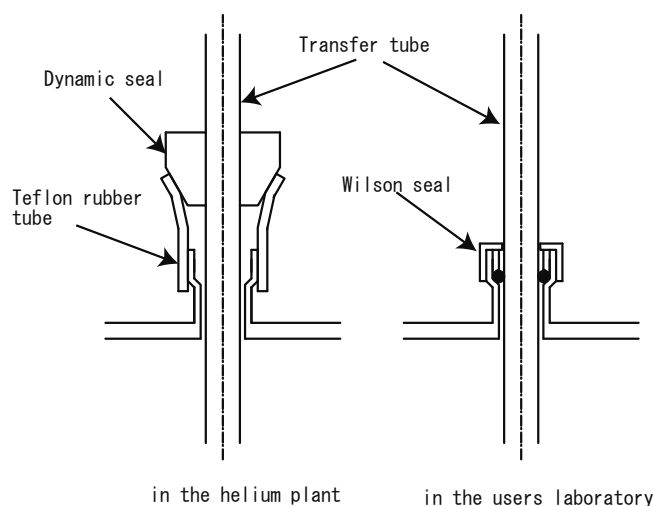


Fig. 1. The sealing structure when a transfer tube is added to a port of the container in the helium plant and the in the user's laboratory.

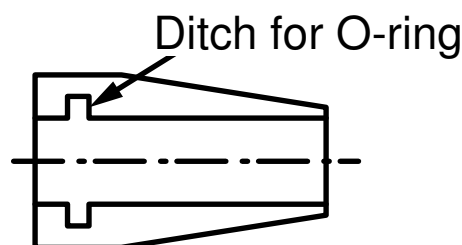


Fig. 2. A drawing of the dynamic seal newly developed for the users.

^{*1} Nippon Kucho Service Co., Ltd



Fig. 3. Modified coupler with a thick packing developed for the recovery line.



Fig. 4. The container is connected to the recovery line using the newly developed cryogenic coupler.

**V. RECORDS OF LABORATORIES,
GROUPS, AND TEAMS
(Activities and Members)**

Events of Nishina Center & CNS from Jan. 2009 to Mar. 2010

2009

- 13-14,Jan. ML-PAC
- 15-17,Jan. Nishina Center Advisory Council (NCAC)
- Dec.-Mar. ^{266}Bh production experiment
- Mar. SHARAQ(Spectroscopy of Hadronic Systems with Radioactive Quantum Beam) Commissioning
- 17,Mar. Laboratory assessment (periodical review) for Radiation Laboratory
- 24,Mar. Laboratory assessment for Heavy Ion Nuclear Physics Laboratory
- 18,Apr. RIKEN Wako Institute Open Campus Day
- 18,May Joint ISIS/RIKEN Muon Facility Development Symposium at Abingdon, Oxford, England
- 2,Jun. RBRC Management and Steering Committee on videoconference
- 18-19,Jun. NP-PAC
- 30,Jun SHARAQ Ceremony of its completion
- 3,Jul. Scientific Policy Committee of Nishina Center
- 7,Jul. The signing ceremony of the Memorandum of Understanding promoting research collaboration between Nishina Center and TRIUMF
- 15,Jul. Press Release "Strongest beam in the world enables scientists to explore laws governing all matter in the universe"
- 26,Aug.-2,Sep. CNS-EFES Summer School (CNS-EFES09)
- 3-4,Sep. ML-PAC
- 29,Sep.-8,Oct. Nishina School
- 3-4,Dec. NP-PAC
- 22,Dec. Press Release "Neon isotope reveals new type of neutron halo"
- 24,Dec. The microtron for the SCRIT facility has successfully produced electron beam of 150MeV
- Dec. Application for trademark registration of breeds for "Nishina Otome" to Ministry of Agriculture, Forestry and Fishery of Japan

2010

- 14,Jan. Press Release "New cherry blossom tree blooms in all four seasons"
- 20-21,Jan. RIKEN Symposium "Muon Science at the RIKEN-RAL Muon Facility 2009"
- 15,Feb. Press Release "'Perfect' Liquid Hot Enough to be Quark Soup"---Protons, neutrons melt to produce 'quark-gluon plasma' at RHIC---

**Theoretical Research Division
Theoretical Physics Laboratory**

1. Abstract

The aim of this laboratory is to reveal the laws of nature ranging from elementary particles to the universe. More precisely, the following three issues are pursued with their mutual relations emphasized: (1) Understanding the microscopic fundamental law of nature. In particular, trying to give a consistent definition of superstring and derive all the fundamental laws from one principle. (2) Understanding many-body systems. Both of the following two aspects are considered. One is the universal laws such as thermodynamics and the universality of spin systems, and the other is specific properties of individual systems such as hadrons, condensed matter, and the universe. (3) Computational science. Besides numerical analyses as an important tool for the above mentioned (1) and (2), aspects of fundamental mathematics are also pursued.

2. Major Research Subjects

- (1) Constructive Definition of String Theory as Fundamental law of Physics
- (2) Fundamental aspects of Quantum Field Theory and its applications
- (3) High precision inspection of experimental and observational data

3. Summary of Research Activity

The ability to understand nature at its most profound level is a basic human desire. Science is founded on accumulated and tremendous efforts driven by that aspiration. The objective of our laboratory is to participate in the endeavor to better understand nature by adding our contributions to theoretical physics. The present seems to be a particularly exciting time for this as many developments appear to be about to converge and allow formation of the ultimate theory of everything.

We organize our research activities into three segments: the pursuit of the microscopic fundamental laws of physics, the study of many-body systems, and the science and technology of computation. These three aspects have an inseparable interrelation and are investigated in an integrated manner throughout the research conducted within this laboratory.

- (1) Understanding the fundamental law of nature through string theory.

1) Scale transformation and AdS/CFT correspondence

A scale transformation in the world sheet description of D3-branes in Type IIB theory was studied. It was shown that this transformation is a real stringy symmetry in a region near D3-branes. By using this symmetry, Wilson loops in $N = 4$ supersymmetric Yang-Mills theory are explicitly related to minimal surfaces in the AdS space, and the AdS/CFT correspondence follows naturally as a consequence of this symmetry. This argument was generalized to the correspondence for high energy scattering amplitudes of $N = 4$ super-Yang-Mills theory and to the AdS/CFT correspondence at finite temperature. It turned out that various forms of the AdS/CFT correspondence can be understood in a unified manner as a consequence of this stringy scale transformation.

2) Matrix models and curved space-time

Incorporating curved space time into matrix models is pursued. In particular, a method in which larger additional degrees of freedom is introduced to represent space-time symmetry, is proposed.

3) Domain Wall in string theory

We investigate a global structure of the moduli space of the BPS domain wall system. In particular, we are interested in the case where the dimensions of the moduli space is greater than those expected from the index theorem. We also study the T-duality between the vortices and domain walls from a string theoretical point of view. We explicitly construct a vortex solution in the Higgs phase of supersymmetric gauge theory and find an exact correspondence between the solution and D-brane configuration in the domain wall side.

4) Non BPS branes and supergravity

We investigate the correspondences between a class of classical solutions of Type II supergravity (the three-parameter solution) and D-branes in the superstring theory. In addition to the mass, the RR-charge, the solution also carries the so-called dilaton charge, whose physical meaning was unclear. We find that the appearance of the dilaton charge is a consequence of deformations of the boundary condition from that of the boundary state for BPS D-branes. We also show that such deformed boundary states are realized as tachyonic and/or massive excitations of the open strings on D-brane systems.

5) Application of string theory to Nuclear physics

Holographic QCD, which is the application of the AdS/CFT correspondence to QCD, turns out to be a very fruitful arena of research in string theory. Using holographic QCD technique, various quantities which are difficult to calculate by perturbative QCD, lattice QCD and conventional nuclear physics approach are investigated. For example, the decay rate of $f_0(1500)$ is calculated suggesting its connection to much sought glueballs.

(2) Quantum field theory and physics of many body systems

1) Lattice formulation of supersymmetric gauge theory

We proposed a lattice formulation of low dimensional supersymmetric gauge theories, aiming at practical implementation for numerical simulations.

2) Lattice formulation of fermions coupled to gravity

We formulated lattice Dirac operator of the overlap-type that describes the propagation of a Dirac fermion in a gravitational field. We also analyzed global gauge anomalies associated with Majorana fermions in $8k$ and $8k+1$ dimensions.

3) Mathematical aspects of 2-dimensional gauge theories and string.

We investigate a non-perturbative correction to the $N=2$ supersymmetric Yang-Mills theory from the discrete matrix model point of view. We utilize the D-brane picture in superstring theory and localization theorem in order to derive the discrete matrix model from 2-dimensional Yang-Mills theory on a compact 2-cycles in the ALE space. We also find the relationship to the Dijkgraaf-Vafa theory in the continuum limit.

4) Quantum field theory over the deformed commutation relation

A quantum theory of free scalar field based on the deformed Heisenberg algebra which is the correction of stringy physics is constructed.

(3) High precision calculation of field theory and computational science

1) High precision calculation of QED

We have announced the final result of our calculation of the electron anomalous magnetic moment. It contains up to the eighth-order of the perturbation theory of QED. The very reliable result was obtained by using high precision calculation on RIKEN's supercomputer system (RSCC).

We also succeeded in automating the calculation of the tenth-order of the perturbation theory, particularly in constructing the ultra-violet subtraction terms. This is an important step to accelerate our calculation of the entire tenth-order contribution.

The dominant contribution from the tenth order to the muon anomalous magnetic moment was also announced by us. In contrast to the electron, some specific Feynman diagrams give rise to the large contributions to the muon anomaly. We explicitly evaluated about 2000 Feynman diagrams which are possible to give the leading and next-to-leading contributions.

2) Improved perturbation method and its applications

We apply improved perturbation method which is one of the variational schemes to Ising model in two-dimensions. It enables us to evaluate free energy and magnetization at strong coupling regions from weak coupling expansion even in the presence of the phase transition.

We determine approximated transition point in this scheme. In the presence of external magnetic field we can see not only stable physical states but metastable one. This research motivated by availability of this method to IIB matrix model which is expected to show a phase transition from 10-dimensional universe to 4-dimensional universe.

Head

Hikaru KAWAI

Members

Hiroshi SUZUKI

Koji HASHIMOTO

Tsukasa TADA

Postdoctoral Researchers

Isao KISHIMOTO

Daisuke KADOH

Ta-sheng TAI

Koichi MURAKAMI

Yutaka SAKAMURA

Yutaka BABA

Minoru ETO

Yasuyuki HATSUDA

Contract Researchers

Makiko MATSUKAWA

Visiting Scientists

Hajime AOKI (Fac. of Sci. and Eng., Saga Univ.)
Jiro ARAFUNE (National Inst. for Academic Degrees and Univ. Evaluation)
ZyunF. EZAWA (Grad. Sch. of Sci., Tohoku Univ.)
Kazuo FUJIKAWA (College of Sci. and Tech., Nihon Univ.)
Masashi HAYAKAWA (Grad. Sch. of Sci., Nagoya Univ.)
Takeo INAMI (Fac. of Sci. and Eng., Chuo Univ.)
Nobuyuki ISHIBASI (Grad. Sch. of Pure and Applied Sci., Univ. of Tsukuba,)
Satoshi ISO (High Energy Accelerator Res. Organization)
Hiroshi ITOYAMA (Grad. Sch. of Sci., Osaka City Univ.)
Toichiro KINOSHITA (Cornell Univ., USA)
Yoshihisa KITAZAWA (High Energy Accelerator Res. Organization)
Ivan KOSTOV (Service de Physique Theorique, CNRS, FRANCE)
Didina SERBAN (Service de Physique Theorique, CE-Saclay, FRANCE)
Dhar AVINASH (Tata Institute of Fundamental Research)
Jnanadeva MAHARANA (Inst. of Phys., INDIA)
Jun NISHIMURA (High Energy Accelerator Res. Organization)
Fumihiko SUGINO (Okayama Inst. for Quantum Phys.)
Asato TSUCHIYA (Fac. Of Sci., Shizuoka Univ.)
Tatsumi AOYAMA (High Energy Accelerator Res. Organization)
Shoichi MIDORIKAWA (Aomori Univ.)
Masanori HANADA (Weizmann Inst.)
Issaku KANAMORI (Univ. of Torino)
Yuuichirou SHIBUSA (Nagasaki Institute of Applied Science)
Kazutoshi OHTA (Meiji Gakuin Univ.)
Muneto NITTA (Keio Univ.)
Norisuke Sakai (Tokyo Woman's Christian University)

Research Consultants

Keiji IGI
Hironari MIYAZAWA
Yoshio YAMAGUCHI
Masao NINOMIYA

Junior Research Associate

Secretary

Yumi KURAMITSU
Yoko SAGIYA

Theoretical Research Division Theoretical Nuclear Physics Laboratory

1. Abstract

Nuclei are finite many-particle systems composed of protons and neutrons. They are self-bound in femto-scale (10^{-15} m) by the strong interaction (nuclear force) whose study was pioneered by Hideki Yukawa. Uncommon properties of the nuclear force (repulsive core, spin-isospin dependence, tensor force, etc.) prevent complete microscopic studies of nuclear structure. There exist number of unsolved problems even at present. In addition, radioactive beam facilities reveal novel aspects of unstable nuclei. We are tackling these old problems and new issues in theoretical nuclear physics, developing new models and pursuing large-scale calculations of quantum many-body systems. We are also strongly involved in research on other quantum many-body systems, to resolve mysteries in the quantum physics

2. Major Research Subjects

- (1) Nuclear structure and quantum reaction theories
- (2) First-principle calculations with the density functional theory for many Fermion systems
- (3) Computational nuclear physics

3. Summary of Research Activity

- (1) Finite amplitude method for nuclear response calculations

We are performing a systematic calculation of nuclear photoabsorption cross section for light nuclei. The calculation is fully self-consistent and is based on the time-dependent density-functional theory with the Skyrme functional. This is achieved using the finite amplitude method we have recently developed. The key feature of the method is to obtain the matrix elements of the random-phase approximation (RPA) in a simple way avoiding explicit calculation of induced residual fields. The method is called "Finite amplitude method" (FAM). So far, even-even nuclei up to mass number $A=100$ have been studied.

We have also been developing a new theoretical tool to apply the finite amplitude method to nuclei with superfluidity. Then, we have been involved in the implementation of the FAM on an existing spherically symmetric Hartree-Fock-Bogoliubov code (HFBRAD) which is currently being turned into a quasi-particle-random-phase approximation (QRPA) code.

- (2) Many-body green's function approaches to nuclear structure

Green's functions theory using modern realistic nuclear interactions was applied to study ^{56}Ni and ^{48}Ca . This allowed us to investigate the role of different types of correlations on the problem of quenching of the spectroscopic factors. Based on this success, the dependence of nuclear correlations on proton-neutron asymmetry is being investigated. The "state of the art" Green's function theory was also benchmarked on the ground state energy of ^4He , where accuracies of 100-200 keV or less were found. This shows the feasibility of ab-initio studies with this method. Analogous calculations have been performed for electronic systems (atoms) to aid in developments of density functional theory.

- (3) Low-lying collective modes in deformed neutron-rich nuclei

Low-frequency negative-parity excitations in deformed neutron-rich nuclei have been studied with the self-consistent Hartree-Fock-Bogoliubov and the QRPA. The Skyrme energy density functional together with the pairing energy density functional is adopted. We found a significant coupling effect between the dipole and the octupole excitations for the pygmy resonance in neutron-rich Mg isotopes.

(4) Spectroscopic study of odd-mass nuclei

The quasi-particle-vibration-coupling Hamiltonian has been derived in a framework of the nuclear density functional method to describe the low-lying properties of odd-mass nuclei in a microscopic way. We applied it to the electric-quadrupole moments of neutron-rich Al isotopes around $N=20$, and showed an important role of neutron pairing correlations implying a weakening of the $N=20$ shell gap. The results show a reasonable agreement with recent experimental data.

(5) Linear response calculation using the canonical-basis TDHFB with a schematic pairing functional

Aiming at constructing a theoretical framework that is able to analyze and predict properties of unknown nuclei, we proposed the Canonical-basis time-dependent Hartree-Fock-Bogoliubov (Cb-TDHFB) approach in the three-dimensional coordinate-space representation. In this approach, we assume that the time evolution can be described by the time-dependent canonical basis with the time-dependent (u,v) factors. We have shown that this can be achieved only when we use a special pairing functional. The computer program with the Skyrme functional has been developed and applied to E1 and E2 nuclear response.

(6) Microscopic description of large-amplitude quadrupole collective dynamics in low-lying states

We have proposed a microscopic method to calculate the vibrational and rotational inertial functions, which includes the time-odd contribution of the mean-field, in the Bohr-Mottelson collective Hamiltonian for large-amplitude quadrupole collective dynamics. The method is composed of constrained HFB and the local QRPA equations, which are derived from the adiabatic self-consistent collective coordinate method. The method is applied to shape coexistence and anharmonic vibrations in Se isotopes, and we have shown that the time-odd mean field increases the collective inertial functions and lowers the excitation energies.

(7) Phenomenological analysis of the oblate-prolate symmetry breaking in triaxial deformation dynamics

In this study, we have analyzed the effects of the oblate-prolate symmetry breaking on dynamics of triaxial deformation in oblate-prolate shape coexistence phenomena using a simple model based on the well-known quadrupole collective Hamiltonian. We have obtained a number of interesting suggestions through the numerical solutions of this model: (i) The relative energy of the excited 0^+ state can be a signature of the potential shape along the γ direction. (ii) Specific E2 transition probabilities are sensitive to the breaking of the oblate-prolate symmetry. (iii) Nuclear rotation may induce the localization of collective wave functions in the quadrupole deformation space if the oblate-prolate symmetry in the moments of inertia is broken.

(8) Structures of superdeformed states in ^{28}Si and ^{40}Ar

Structures in ^{28}Si and ^{40}Ar have been studied using the antisymmetrized molecular dynamics (AMD) method. The oblate-prolate shape coexistence is reproduced and existence of superdeformed (SD) band is predicted for ^{28}Si . The SD states contain alpha- ^{24}Mg cluster structure components. For ^{40}Ar , the SD band is reproduced, which were experimentally identified very recently. The calculation suggests that the SD states form triaxial shapes, and the $K^\pi = 2+$ side band exists.

(9) Nuclear “pasta” in supernova

We aim to bridge between astrophysics and nuclear and atomic physics by solving astrophysical problems using nuclear/atomic physics and by providing interesting nuclear/atomic physics problems in astrophysical systems. This year, we have solved a long-standing problem about the formation of rod-like and slab-like nuclei referred to as "pasta" nuclei in collapsing supernova cores. In the field of cold atom physics, we have studied the critical velocity of unitary Fermi superfluids flowing in a periodic potential. Unitary Fermi gases resemble the low density dripped neutron gases in neutron stars and this work also provides useful information to study neutron star crusts and the related phenomena.

(10) Study of vortex lattices in cold Fermi gases

We are developing a theoretical framework to describe both the vortex structure in rotating condensates and the band-structure of Fermi superfluids in a periodic potential. This year, we have developed a new efficient scheme to create a Schrodinger cat-like maximally entangled state in a two-state Bose system.

(11) Phenomenological formulae for nuclear reaction cross sections

We examine the mass-number dependence of the cross section formula based on the black-sphere picture of nucleus. We find analytically that, in contrast to other formulae, our formula includes $A^{1/6}$ -dependence in addition to $A^{2/3}$ -dependence. The $A^{1/6}$ -dependence, which comes from the optical depth of target nucleus, is one of the characteristic features of our formula.

We study the scaling properties of proton-nucleus total reaction cross sections for stable nuclei, and propose an approximate expression just in proportion to $Z^{2/3}\sigma_{pp}^{total} + N^{2/3}\sigma_{pn}^{total}$. Based on this expression, we can derive a relation that enables us to predict a total reaction cross section for any stable nucleus within at most 10% uncertainty, using the empirical value of the total reaction cross section of a given nucleus.

Head

Takashi NAKATSUKASA

Members

Akihisa KOHAMA

Special Postdoctoral Researchers

Yasutaka TANIGUCHI
Nobuo HINOHARA
Kenichi YOSHIDA
Gentaro WATANABE

Foreign Postdoctoral Researcher

Carlo BARBIERI

Contract Researcher

Paolo AVOGADORO

Senior Visiting Scientist

Kenichi MATSUYANAGI

Research Consultants

Kiyomi IKEDA
Syuhei YAMAJI
Kosai TANABE

Visiting Scientists

Yasuhisa ABE (RCNP)
Anatolijs AFANASJEVS (Mississippi State Univ.)
Shigeyoshi AOYAMA (Niigata Univ.)
Yoshihiro ARITOMO (JINR)
Simone BARONI (Univ. of Washington)
Carlos BERTULIANI (Texas A&M Univ.)
Satoshi CHIBA (Japan Atomic Energy Agency.)
TiebKhoa DAO (Inst. Nucl. Scie. Tech.)
Elisabeth ELSTER (Ohio Univ.)
Yoshiko ENYO (Yukawa Inst. Theoretical Phys.)
Hubert FLOCARD (INP-Orsay)
Yasuro FNAKI (Univ. Tsukuba)
Koichi HAGINO (Tohoku Univ.)
Ikuko HAMAMOTO (Lund Univ.)
Koji HIGASHIYAMA (Chiba Institute of Technology)
Nobuo HINOHARA (Yukawa Inst. Theoretical Phys.)
Michio HONMA (Aizu Univ.)
Takatoshi HORIBATA (Aomori Univ.)
Munetake ICHIMURA (The Open Univ of Japan)
Kei IIDA (Kochi Univ.)
Akitsu IKEDA (Shizuoka Inst. Scie. Tech.)
Tsunenori INAKURA (Grad. Sch. of Pure and Applied Sci., Univ. Tsukuba)

Naoyuki ITAGAKI (Univ of Tokyo)
Akira IWAMOTO (Japan Atomic Energy Agency)
Meng JIE (Peking Univ.)
Kiyoshi KATO (Hokkaido Univ.)
Toshitaka KAZINO (NAOJ)
Masaaki KIMURA (Hokkaido Univ.)
Wenhui LONG (Peking Univ.)
Masayuki MATSUO (Tohoku Univ.)
Takuma MATSUMOTO (Hokkaido Univ.)
Bradley MEYER (Clemson Univ.)
Kazuo MUTO (Tokyo Institute of Technology)
Takayuki MYO (Osaka Univ.)
Kazusuke OGATA (Kyushu Univ.)
Makito OI (Univ of Surrey.)
Akira ONO (Tohoku Univ.)
Masahisa OTA (Konan Univ.)
Kazuhiro OYAMATSU (Aichi Shukutoku Univ.)
Hiroyuki SAGAWA (Aizu Univ.)
Badawy SARHAN (Cairo Univ.)
Ryoichi SEKI (California Univ.)
Noritaka SHIMIZU (Univ of Tokyo)
Yoshihumi SHIMIZU (Kyushu Univ.)
Kosuke SUMIYOSHI (Numazu National College of Technology)
Akihiro SUZUKI (Suzuki Corporation)
Yasuyuki SUZUKI (Niigata Univ.)
Toshio SUZUKI (Fukui Univ.)
Naoki TAJIMA (Univ of Fukui)
Masatoshi TAKANO (Waseda Univ.)
Masaaki TAKASHINA (RCNP)
Kazuo TAKAYANAGI (Sophia Univ.)
Noboru TAKIGAWA (Tohoku Univ.)
Kazuko TANABE (Otsuma Women's Univ.)
Jun TERASAKI (Univ. North Carolina)
Yutaka UTSUNO (Japan Atomic Energy Agency.)
Takahiro WADA (Kansai Univ.)
Kazuhiro YABANA (Grad. Sch. of Pure and Applied Sci., Univ. Tsukuba)
Taiichi YAMADA (Kanto Gakuin Univ.)
Masayuki YAMAGAMI (Aizu Univ.)
Naotaka YOSHINAGA (Saitama Univ.)
Yumin ZHAO (Shanghai Jiao Tong Univ.)

Students

Junior Research Associates

Shuichiro EBATA (Grad. Sch. of Pure and Applied Sci., Univ. Tsukuba)
Koichi SATO (Dept. Phys., Kyoto Univ.)

Intern

Fabien LAINE (Pari-Sud 11 Univ.)
Hakim TAKLANTI (Pari-Sud 12 Univ.)

Student Trainees

Wataru HORIUCHI (Niigata Univ.)

Secretary

Shinko ODAI

**Theoretical Research Division
Strangeness Nuclear Physics Laboratory**

1. Abstract

We proposed accurate few-body calculational method called “Infinitesimally shifted Gaussian lobe method”. Recently, we developed this method to four-body systems and five-body systems. This method is applicable for various three- and four-body systems. For example, we applied it to hypernuclear physics and clarified what is important and impressed. In fact, we applied this method to three kinds of hypernuclear experiments (KEK-E419, BNL-E930, and -E929) in the past, and we contributed to these experiments by discussing with experimentalists, analyzing the data, and interpreting the data.

2. Major Research Subjects

- (1) Hypernuclear structure from the view point of few-body problem
- (2) Structure of exotic hadron system
- (3) Baryon-baryon interaction based on lattice QCD
- (4) Neutron-rich Λ hypernuclei from shell model approach

3. Summary of Research Activity

- (1) The structure of the T=1 isotriplet hypernuclei, ${}^7\text{He}_\Lambda$, ${}^7\text{Li}_\Lambda$, ${}^7\text{Be}_\Lambda$ within the framework of an $\alpha+\Lambda+N+N$ four-body cluster model is studied. The Λ binding energy of the ground state in ${}^7\text{He}_\Lambda$ which is under analysis at JLAB by $(e,e'K^+)$ reaction is predicted to be 5.16 (5.36) MeV with (without) the CSB interaction.
- (2) A theoretical approach based on the shell model is presented to calculate effective charge of electric quadrupole transitions. The shell-model calculation with single-particle $2h$ -bar ω excitations in the first order perturbation qualitatively reproduces existing B(E2) values for carbon isotopes with neutron number $5 \leq N \leq 16$ and shows a sudden change of the isovector effective charge beyond $N=8$.

Head

Emiko HIYAMA

Contract Researchers

Atsushi UMEYA

Visiting Scientists

Yasuo YAMAMOTO (Tsuru University)

Taiichi YAMADA (Kanto Gakuin University)

Tetsuo HYODO (Tokyo Institute of Technology)

Makoto OKA (Tokyo Institute of Technology)

Tomokazu FUKUDA (Osaka Electro-Communication University)

Daisuke JIDO (YITP, Kyoto University)

Yoichi IKEDA (University of Tokyo)

Hidekatsu NEMURA (Tohoku University)
Soichi ISHIKAWA (Hosei University)
Takenori FURUMOTO (Osaka City University)
Atsushi HOSAKA (RCNP, Osaka University)
Shoji SHINMURA (Gifu University)
Akinobu DOTE (HIGH ENERGY ACCELERATOR RESEARCH ORGANIZATION,
KEK)
Thomas RIJKEN (Radboud University Nijmegen)
Kazuma NAKAZAWA (Gifu University)

Research Consultants

Masayasu KAMIMURA
Kiyomi IKEDA

Student Trainees

Kaori HORII (RCNP, Osaka University)

JRA

Hitomi NODA (Tokyo Institute of Technology)

Secretary

Makiko OHISHI

Sub Nuclear System Research Division Radiation Laboratory

1. Abstract

Nucleons, such as protons and neutrons, are a bound state of constituent quarks glued together with gluons. The detail structure of nucleons, however, is not well understood yet. Especially the mechanism to build up the spin of proton, which is $1/2$, is a major problem in physics of the strong force. The research goal of Radiation Laboratory is to solve this fundamental question using the first polarized-proton collider, realized at RHIC, Brookhaven National Laboratory (BNL) in USA. RHIC stands for Relativistic Heavy Ion Collider, aiming also to create Quark Gluon Plasma, the state of Universe just after the Big Bang. RIKEN-BNL Research Center (RBRC) directed by N. Samios carries our core team at BNL for those exciting researches. Recent data analysis has shown that the proton spin carried by gluons is indeed small, which is a very striking finding beyond our expectations. We have been doing other pioneering researches at the domestic accelerators at SPring-8 and High Energy Accelerator Research Organization (KEK) which is now preceded to the new experiment at J-PARC. We are also performing technical developments such as novel ion sources, fine pitch pixel detectors and neutron optical devices.

2. Major Research subjects

- 1) Spin physics with relativistic polarized-proton collisions at RHIC
- 2) Study of nuclear matter at high temperature and/or at high density
- 3) Technical developments on radiation detectors and accelerators

3. Summary of Research Activity

- (1) Experimental study of spin structure of proton using RHIC polarized proton collider
[See: RIKEN-BNL Research Center Experimental Group]
- (2) Experimental study of quark-gluon plasma using RHIC heavy ion collider
[See: RIKEN-BNL Research Center Experimental Group]
- (3) Study of properties of mesons and exotic hadrons with domestic accelerators

Hadrons with more than three quarks are of great interest and have been looked for over the past 30 years. The Θ^+ is a genuine exotic baryon with the minimum quark configuration of u, u, d, d and anti- s . After the first report on the evidence of the Θ^+ at SPring-8/LEPS in 2002, evidence and counterevidence have been reported from all over the world, but its existence is not conclusive yet. We have made effort to establish the Θ^+ since our first report. In 2009, we reported again the observation of the Θ^+ with clean and high statistics data at SPring-8/LEPS [Phys.Rev.C 79, 025210 (2009)].

In addition, we are searching for Θ^+ with three times higher statistics. The results will be open soon. The spin and parity of Θ^+ is quite important to understand the internal structure of Θ^+ . The mechanism of Θ^+ production with vector meson, $K^*(890)$, is sensitive to parity of Θ^+ . The analysis aiming for the measurement of (Θ^+ , $K^*(890)$) production is underway. In order to establish the Θ^+ and explore the world of multi-quark hadrons, R & D work is underway to construct LEPS-II, which is a new beam line and detectors at SPring-8.

Preparation of the experiment E16 at J-PARC 50-GeV PS is ongoing to obtain the full approval by PAC. The experiment aims to perform the systematic study of the mass modification of low-mass vector mesons in nuclei to explore the chiral symmetry in nuclear matter. GEM tracker and hadron-blind Cherenkov counter (HBD) are being developed for the experiment. In the beam tests,

incident-angle dependence of the position resolution was studied for the tracker . At the same time, several photoelectrons were successfully observed by the HBD and improvement the prototype detector is underway.

(4) Detector development for PHENIX experiment

We have been developing the silicon vertex tracker (VTX) in order to enhance physics capability of the PHENIX detector at RHIC. It consists of two inner layers of pixel detectors and two outer layers of strip detectors. Radiation Laboratory group is responsible for the ladder fabrication of the pixel detector. The production of the ladder has been started. Seven of the ladders are assembled and tested with production version of readout electronics.

We also have been developing the momentum-sensitive trigger system for the PHENIX muon arms under the collaboration with KEK, Kyoto and Rikkyo University. All additional electronics which generate fast trigger signal were installed on the muon arm and has been commissioned.

(5) Neutron optics

Cold or thermal neutron beam is a high-sensitivity probe to study not only the structure of condensed matter, but also nuclear and particle physics. However, its realistic applications are still limited since the numbers of available neutron sources are small and their intensities are low. This project aims to enhance the efficiency in using those precious neutron beams by improving the neutron beam optics, in order to maximize scientific outputs within a short period of time. Base on the developed technologies, devices are fabricated and distributed to other laboratories and universities by "Riken Venture Company", Japan Neutron Optics Inc.

We stay with the fundamental physics research in a new beam line at 1MW Pulse Spallation Neutron Source in J-PARC. This beam line was designed by applying our knowledge and technique of neutron optics. We also succeed to observe interference signals of cold neutrons using the Si crystal interferometer at JRR-3M. There, we are developing a new type of instrument for phase-difference imaging with use of the gratings developed by us. We are also planning to study neutron Electron Dipole Moment using a perfect crystal at the J-PARC beam line.

The fact that permeability of the neutron beam for metals whose atomic number is large and thick cement attracts attention to various engineering fields.

This year the vision to develop so small neutron source that in some day we use it outside as a portable neutron source instruments is becoming more and more a reality.

In this project, the various ways of imaging using neutron beam are trial survey and under the development, including not only neutron radiography but phase differential imaging, CT-imaging using special technique which is founded in VCAD project in RIKEN. We are now collaborating with VCAD project program team to realize small neutron source.

(6) Theoretical study of hadron physics

Nuclear matter at finite temperature and density has been studied in lattice simulations of quantum chromodynamics (QCD) which is the first principle to describe the interactions of quarks and gluons. Several properties of QCD phase transition from hadronic matter to quark-gluon plasma have been investigated with calculations of Polyakov-loop correlations and quark number susceptibilities. A new approach to calculate the equation of state have also been derived and developed in the full-QCD simulations which include dynamical quarks of up, down and strange flavors. Study of hadron and chiral properties in finite temperature and density is going on.

In continuation of the studies on the fragmentation functions based on the Nambu-Jona-Lasinio model, the effect of pion multiple production processes is taken into account in a modified version of the quark-jet model originally proposed by Field and Feynman. The effect is found to be crucial and the calculated fragmentation function for the pion qualitatively reproduces the experimental one.

In connection with the Unruh effect, the hydrogen-like system in a uniformly accelerated frame is studied using the analogy with the Stark effect. The energy shift as well as the decay width is calculated by the WKB method.

The tetraquark is studied in quenched lattice QCD simulation to see whether the state exists or not from the first principle calculation of QCD. By performing the diagonalization, the energy eigenvalues are obtained for isospin zero and $J^P=1^\pm$ channels. The volume dependence of the energy eigenvalues are checked to distinguish between bound or resonance state and scattering state. As a result, no evidence of existence of the tetraquark is obtained within our calculation.

Head

Hideto EN'YO

Members

Yasuyuki AKIBA

Yuji GOTO

Itaru NAKAGAWA

Yoshie OTAKE

Atsushi TAKETANI

Yasushi WATANABE

Satoshi YOKKAICHI

Special Postdoctoral Researchers

Masayuki NIIYAMA

Kazuya AOKI

Tomohiro NISHITANI

Foreign Postdoctoral Researcher

Stephen BAUMGART

Contract Researchers

Yoshinori FUKAO

Hideaki IIDA

Maki KUROSAWA

Kenichi NAKANO

Tomoaki NAKAMURA

Yu MAESAWA

Contract Technical Scientist

Yohei NAKATSUGAWA

Research Consultant

Katsuya HIROTA

Senior Visiting Scientists

Ken-ichi IMAI (Grad. Sch. of Sci., Kyoto Univ.)
Toshiaki SHIBATA (Grad. Sch. of Sci. and Eng., Tokyo Inst. of Tech. Sch. of Sci.)
Hirohiko SHIMIZU (Inst. of Materials Structure Sci., KEK)
Ken-ichi AOKI (Grad. Sch. of Sci., Kanazawa Univ.)
Koichi YAZAKI (Tokyo Woman's Christian Univ.)
Takashi NAKANO (RCNP, Osaka Univ.)

Visiting Scientists

Tomohiro ADACHI (DAI-ICHI KIDEN CO.,LTD)
ChristineA. AIDALA (Univ. Massachusetts, Amherst, USA)
Alexander BAZILEVSKY (BNL, USA)
Wolfgang BENTZ (Tokai Univ.)
Mickey CHIU (Univ. of Illinois at Urbana, USA)
Ondrej CHVALA (Univ. of California at Riverside)
Takumi DOI (University of Kentucky)
Dipanwita DUTTA (Nuclear Physics Division, Bhabha Atomic Research Centre)
Hirotugu FUJII (Grad. Sch. /College of Arts and Sciences, Univ. of Tokyo)
Kenji FUKUSHIMA (YITP, Kyoto Univ.)
Haruhiko FUNAHASHI (Grad. Sch. of Sci., Kyoto Univ.)
Takashi HACHIYA (Private Company)
Yuji HASEGAWA (Wien Inst. Tech.)
Tetsuo HATSUDA (Grad. Sch. of Sci., Univ. of Tokyo)
Toshiyuki HATTORI (Res. Lab. for Nuclear Reactors, Tokyo Inst. of Tech. Sch. of Sci.)
Masanori HIRAI (Grad. Sch. of Sci. and Eng., Tokyo Inst. of Tech.)
Kensuke HONMA (Grad. Sch. of Sci., Hiroshima Univ.)
Takuma HORAGUCHI (Grad. Sch. of Sci., Hiroshima Univ.)
Ryo ICHIMIYA (KEK)
Katsuya ISHIGURO (Grad. Sch. of Natural Sci. & Tech., Kanazawa Univ.)
Noriyoshi ISHII (Grad. Sch. of Pure and Applied Sci., Univ. of Tsukuba)
Hirokazu ISHINO (Tokyo Inst.Tech.)
Robert JAMESON (Goethe Universitat Frankfurt, Germany)
Takeshi KANESUE (Kyushu Univ.)
Hirotugu KASHIWAGI (Takasaki Advanced Radiation Res. Inst., JAEA)
Hiroyuki KAWAMURA (The Univ.of Liverpool)
Akio KIYOMICHI (KEK)
Yuji KOIKE (Grad. Sch. of Sci. & Tech., Niigata Univ.)
Yoshiaki KOMA (Numazu National College of Technology)
Kotaro KONDO (Grad. Sch. of Sci. and Eng., Tokyo Inst. of Tech.)
Dmitiri KOTCHETKOV (Univ. New Mexico, USA)
Shunzo KUMANO (Inst. of Particle and Nuclear Studies, KEK)
Teiji KUNIHIRO (Yukawa Inst. for Theoretical Phys., Kyoto Univ.)
Han LIU (Phys. Dept., New Mexico State Univ.)
Yoshikazu MAEDA (RCNP, Osaka Univ.)

Yajun MAO (Peking Univ., China)
Tsutomu MIBE (KEK)
Liu MING (LANL)
Kenji MISHIMA (KEK)
Yoshiyuki MIYACHI (Tokyo Inst. Tech.)
Yoshihiro MORI (Grad. Sch. of Sci., Kanazawa Univ.)
Norihito MURAMATSU (RCNP, Osaka Univ.)
Ryotaro MUTO (KEK)
Katsuro NAKAMURA (Grad. Sch. of Sci., Kyoto Univ.)
Yoshifumi NAKAMURA (DESY, Germany)
Atsushi NAKAMURA (Information Media Center, Hiroshima Univ.)
Megumi NARUKI (KEK)
Munehisa OHTANI (Inst. fuer Theoretische Physik, Universitact Regensburg, Germany)
Hiromi OKADA (KEK)
Masahiro OKAMURA (BNL, USA)
Kyoichiro OZAWA (Grad. Sch. of Sci., Univ. of Tokyo)
Petra RIEDLER (CERN, Switzerland)
Naohito SAITO (J-PARC, KEK)
Murad SARSOOR (Georgia State University)
Shoichi SASAKI (Grad. Sch. of Sci., Univ. of Tokyo)
Shin-ya SAWADA (Inst. of Particle and Nuclear Studies, KEK)
Michiko SEKIMOTO (Inst. of Particle and Nuclear Studies, KEK)
Kenta SHIGAKI (Grad. Sch. of Sci., Hiroshima Univ.)
Prashant SHUKLA (Nuclear Physics Division, Bhabha Atomic Research Centre)
Kazutaka SUDO (Inst. of Particle and Nuclear Studies, KEK)
Toru SUGITATE (Grad. Sch. of Sci., Hiroshima Univ.)
Mizuki SUMIHAMA (RCNP , Osaka Univ.)
Kazutaka SUMISAWA (KEK)
Tsuneo SUZUKI (Grad. Sch. of Sci., Kanazawa Univ.)
Taneja SWADHIN (SUNY at Stony Brook)
Junpei TAKANO (KEK)
Kiyoshi TANIDA (Grad. Sch. of Sci., Kyoto Univ.)
Hisayuki TORII (Grad. Sch. of Sci., Hiroshima Univ.)
Xiaorong WANG (New Mexico State University)
Shizui WATANABE (Tokyo Metropolitan College of Aeronautical Engineering)
Imuran YOUNUS (Univ. of New Mexico, USA)

Visiting Researcher

Yoshichika SEKI (Fac. of Sci., Kyoto Univ.)

Students

Junior Research Associate

Yoki ARAMAKI (CNS, Univ. Tokyo)

Kimiaki HASHIMOTO (Fac. of Sci., Rikkyo Univ.)

Kenichi KARATSU (Fac. of Sci., Kyoto Univ.)
Miki KASAI (Fac. of Sci., Rikkyo Univ.)
Misaki OUCHIDA (Facul. Science, Facul. Sci. Hiroshima Univ.)
Dosatsu SAKATA (Univ. Tsukuba)
Satoshi SANO (CNS , Univ.Tokyo)
Jun TAMURA (Grad. Sch. at Nagatsuta, Tokyo Inst.Technol.)
Yorito YAMAGUCHI (CNS, Univ. Tokyo)

International Program Associate

Ryu Sunyoung (RCNP, Osaka Univ.)

Intern

Kohei SHOJI (Grad. Sch. of Sci., Kyoto Univ.)
Seishi DAIRAKU (Grad. Sch. of Sci., Kyoto Univ.)
Rei SAMESHIMA (Faculty of Science , Kyoto University)
Yudai ICHIKAWA (Faculty of Science , Kyoto University)
Shinichi MASUMOTO (Fac. Sci. , Univ. Tokyo)
Yusuke KOMATSU (Fac. Sci. , Univ. Tokyo)
Yosuke WATANABE (Fac. Sci. , Univ. Tokyo)
Kazuki UTSUNOMIYA (Fac. Sci. , Univ. Tokyo)

Student Trainees

Satoshi ADACHI (Faculty of Science , Kyoto University)
Hidemitsu ASANO (Grad. Sch. of Sci. & Eng., Saitama Univ.)
Yosuke HAKI (Fac. of Sci., Rikkyo Univ.)
Masayasu HASEGAWA (Grad. Sch. of Sci., Kanazawa Univ.)
Taku HUSHOUYANG (China Inst. Atom. Energy)
Yuki IKEDA (Coll.Sci. , Rikkyo Univ.)
Yuuji KATOU (RCNP , Osaka Univ.)
Kotaro KIJIMA (Grad. Sch. of Sci., Hiroshima Univ.)
Toshiya KIMURA (SOKENDAI)
Paul KLINE (Dept. of Physics , SUNY at Stony Brook)
Yuki KOBAYASHI (Tokyo Inst.Technol.)
Andrew MANION (Dept. of Physics , SUNY at Stony Brook)
Shunsuke MASUIKE (Tokyo Inst.Technol.)
Nathan MEANS (Dept. of Physics, SUNY at Stony Brook)
Shinji MOTOKI (Grad. Sch. of Biosphere Sci., Hiroshima Univ.)
Keiko MURANO (Inst. Phys. , Univ.Tsukuba)
Yoshihide NAKAMIYA (Grad. Sch. of Sci., Hiroshima Univ.)
Masaya NIHASHI (Facul. Science , Facul. Sci. Hiroshima Univ.)
Atsushi OKAMURA (Facul.Sci. , Kyoto Univ.)
Yuta SADA (Facul.Sci. , Kyoto Univ.)

Tamotsu SATO (Fac. Sci. , Univ. Tokyo)
Takahiro SAWADA (RCNP, Osaka Univ.)
Satoru UEDA (Grad. Sch. of Pure and Applied Sciences, Univ. of Tsukuba)

Technical Staff

Junpei KANAYA

Secretaries

Noriko KIYAMA
Yoko SAKUMA

Sub Nuclear System Research Division Advanced Meson Science Laboratory

1. Abstract

Particles like muons, pions, and kaons have finite life times, so they do not exist in natural nuclei or matters. Implanting these particles into nuclei/matters, exotic phenomena in varieties of objects can be studied from a new point of view.

Kaon is the second lightest meson which has strange-quark as a constituent quark. It is expected that if one embed a kaon into nuclei, the sizes of the nuclei become smaller and forms a high density object beyond the normal nuclear density. Study of this object could lead to better understanding of the origin of the mass of the matter, and may reveal the quark degree of freedom beyond the quark-confinement. Those properties can be studied by precise heavy pionic atom research in different angle. The other example is the weak interaction in nuclear matter. It can only be studied by the weak decay of hypernuclei, which have Lambda particle in the nuclei,

Muon provides even wider variety of study from nuclear reaction to magnetism in matter. For instance, stopping positively charged muon in a material, we obtain information on the magnetic properties or the local field at the trapped site. Injecting negatively charged muon to mixture of deuterium and tritium, muon attracts surrounding atoms and is known to cause d-t fusions.

As is already clear, in our research we introduce different kind of impurities into nuclei/matters, and study new states of matter, new phenomena, or the object properties.

2. Major Research Subjects

- (1) Study of meson property and interaction in nuclei
- (2) Origin of matter mass / quark degree of freedom in nuclei
- (3) Condensed matter and material studies with muon
- (4) Nuclear and particle physics studies via muon catalyzed fusion and ultra cold muon beam
- (5) Materials science using Mössbauer spectroscopy

3. Summary of Research Activity

Hadron physics at J-PARC and RIKEN-RIBF

Kaon and pion will shed a new insight to the nuclear physics. The recent discovery of deeply bound pionic atom enables us to investigate the properties of mesons in nuclear matter. At RIKEN-RIBF, we are preparing precise experimental study of the pionic atom. We are intensively preparing another next generation kaon experiments (E15 and E17) at J-PARC as day-one experiments. In these experiments, we are aiming at precise determination of the KN interaction, and clarify the nature of kaon in nuclei. By these experiments, we aim to be a world-leading scientific research group using these light meta-stable particles.

1) Deeply bound kaonic nuclei

We have performed experimental exploration of theoretically predicted deeply bound kaonic nuclear states in ^3He nucleus $K^-\text{ppn}$ and $K^-\text{pnn}$. Akaishi and Yamazaki first

calculated large binding energy and narrow width for the K^-ppn state. One of the most interesting features of the kaonic nucleus is that the strong attraction of the kaon is expected to contract the surrounding nucleons resulting in extremely high density of several times larger than normal nuclear density. Measurement of the kaon properties at such high energy density will provide precious information on the origin of hadron masses and the chiral symmetry breaking and its partial restoration.

The experimental principle adopted uses stopped K^- on superfluid helium target, and we focus on emitted nucleon momenta measurement by Time-of-Flight (TOF) method. The last orbit of kaonic ${}^4\text{He}$ atom is $2p$ and the branching ratio from the last orbit to the nuclear kaon bound state accompanied with a nucleon emission was estimated to be 1 % at minimum.

The exploration was performed from 2002/September till 2005/December as series of experiments at the KEK-PS (E471, E549, E570) with almost common experimental setup. The obtained spectral shape was rather smooth and elaborate analysis showed upper limit of the kaonic nucleus formation for both K^-ppn and K^-pnn states.

After the completion of above series of experiments, the KEK-PS was shut down to switch to a new facility J-PARC. Presently, we are preparing for an experiment to search for K^-pp nuclear system at the K1.8BR beamline of the J-PARC.

2) Deeply bound pionic atoms

We have made precision spectroscopy of pionic lead and tin atoms, and extracted information on the in-medium interaction between pion and nucleus, which leads to the exclusive quantitative evaluation of the chiral symmetry restoration in the nuclear matter.

Our collaboration which mainly consists of the RIKEN and the University of Tokyo group conducted throughout the experiments starting from R&D of pionic atom formation in nuclear reactions to its application to the precision spectroscopy.

The experiment was carried out in GSI, Darmstadt. Our first discovery was pionic $2p$ state in the lead ${}_{207}\text{Pb}$ nucleus where the negative pion is accommodated in a delicate balance between the Coulomb attraction and the strong repulsion.

Following the discovery, we have performed experiments to measure $1s$ pionic lead ${}_{205}\text{Pb}$ and tin ${}_{115}\text{Sn}$, ${}_{119}\text{Sn}$, and ${}_{123}\text{Sn}$ isotopes.

We have analyzed the experimental spectra elaborately and extracted in-medium isovector interaction between pion and nucleus. In combination with experimental information on the pionic hydrogen and deuterium which gives the interaction in vacuum, we have accomplished evaluation of the in-medium interaction modification. The modification is originating in the partial restoration of the chiral symmetry in the nucleus, and we have quantitatively evaluated for the first time the reduction of the chiral order parameter in the nuclear matter to be 33 %, which is consistent with theoretical prediction of 30 %.

Presently, we have been preparing for a sophisticated experimental setup of the pionic atom spectroscopy at the RIBF in the RIKEN. We expect about twice better experimental resolution with much smaller systematic errors.

3) Precision X-ray measurement of kaonic atom

Simultaneously with the above experiment (1), we have performed an X-ray spectroscopy of atomic $3d \rightarrow 2p$ transition of negatively charged K^- mesons captured by helium atoms. Many Kaonic atoms are known to be measured with various elements, however, there are

very large deviations in the measured energy levels for the helium (and the oxygen) from the systematic expectations. The deviation originates in technical issues in old experiments, and new and high precision data have been long awaited for. Also, wave functions of the Kaonic atoms are expected to reflect the information on the existence of the inner structure, namely deeply bound Kaonic states. As a result of the experiment, we have succeeded in performing the spectroscopy and achieved the shift of $2 \pm 2(\text{stat.}) \pm 2(\text{syst.})$ eV. The obtained results reject older data beyond any doubt, and the above deviation is dissolved. Presently, aiming at the determination of the level width and yield, we are analyzing the data. To clarify the KN interaction strength, we are preparing another x-ray measurement of the kaonic helium-3 atom, which is another day-one experiment at J-PARC.

Muon science at RIKEN-RAL branch

The research area ranges over particle physics to condensed matter studies and life science. Our core activities are based on the RIKEN-RAL Muon Facility located at the Rutherford Appleton Laboratory (UK), which provides the most intense pulsed muon beam. We have variety of important research activities such as muon-catalyzed fusion (μCF) and condensed matter physics by muon spin rotation / relaxation / resonance (μSR).

(A) Condensed matter/materials studies with μSR

The world-first gas pressurized μSR setup has been established and its applications for material sciences have been started. The maximum pressure of the system is 6.4 kbar and the temperature range is from 2 K to 300 K. The strong advantage of the system is to achieve the homogeneous pressure in all temperature range and the pressure can be changed quickly without removing samples from the spectrometer.

A new spectrometer named CHRONUS has been installed in Port-4 and commissioning works are going on in order to optimize the performance of the new spectrometer. The spectrometer has more than 600 detectors to minimize the counting loss and maximize the performance to measure tiny samples less than 20 mg. A platform of the Port-4 area is now being designed and the installation will be done within 2010. After the completion of the Port-4 area, parallel experiment at both Port-2 and Port-4 will be planned.

There are three topics of material sciences studied by the muon-spin relaxation method at the RIKEN-RAL Muon facility in 2009.

- 1) The Li-diffusion behavior in Li-based batteries has been investigated. On the basis of some assumptions concerning the hopping behavior of the Li atom in batteries, the diffusion constant of the Li atom has been obtained. This value seems to be closer to the realistic value rather than those previously obtained by other experimental techniques.
- 2) A co-existing relationship between a magnetically ordered state and the superconducting state in a newly found Fe-based superconducting oxide has been clarified. A competing relationship between the magnetically ordered state of Fe spins and the superconducting state has been suggested.
- 3) A three-dimensional coherent magnetic ordered state of radical spins in a one-dimensional Co(II) molecular magnet has been detected. This is the second example which show a long-range magnetic ordered state of radical spins in the family of the one-dimensional molecular magnet. An important role of the magnetic interaction between one-dimensional magnetic chains to the magnetism of the one-dimensional magnetic chain has been suggested.

(B) Nuclear and particle physics studies via muon catalyzed fusion and ultra cold muon beam

1) Muon catalyzed fusion (μ CF)

We are studying the muon catalyzed fusion (μ CF) processes in a wide range of hydrogen target conditions such as isotope mixtures and temperatures. This year we constructed a test high pressure target, which will enable us to keep D_2 target in solid state up to 30 K, thus we will be able to study μ CF in high density and high temperature solid target, where the μ CF is expected to occur much faster than in liquid.

2) Generation of ultra slow positive muon beam

Low energy muon beam, whose kinetic energy is variable from a few keV to a few tens of keV, will extend the scope of μ SR technique from a bulk material to surfaces and multi-layered materials. It is also expected that a very sharp beam of low energy muon may enable a new way of precision measurement of muon's anomalous gyro-magnetic ratio ($g-2$). Following the successful generation of slow muon beam by laser ionization of thermally emitted muonium in vacuum, we plan to increase the slow muon beam intensity by more than 100 times. For this purpose, we have started works such as construction of a new intense laser system, search of materials for efficient muonium emission at room temperature, and design of new slow muon microscope optics. The first part of the new laser system was manufactured. We are preparing for a precise measurement of the muonium emission from material surface such as silica powder and silica aerogel in collaboration with TRIUMF.

Mössbauer spectroscopy at RIKEN-RIBF, HIMAC and CERN-ISOLDE

^{57}Fe Mössbauer spectroscopy following ion implantation of radioactive ^{57}Mn ($T_{1/2} = 1.45$ min) has been applied to investigate the atomic jump processes of Fe impurity in Si semiconductor in RIKEN-RIBF. ^{57}Mn is one of the useful nuclear probes to study the dynamic behavior and chemical states of dilute Fe atoms in solid. Iron impurities are known to degrade seriously electronic properties of silicon-based devices as well as solar cells. Generally, Fe atoms are thought to occupy only on interstitial sites in Si leading to a fast diffusion. In addition, substitutional Fe atoms were not found experimentally by standard evaluation techniques. Our investigation is to clarify the impurity diffusion of Fe atoms and the formation processes of “*substitutional Fe atoms*” in Si at high temperatures.

^{57}Mn implantation Mössbauer spectra from 800 K to 1200 K can be analyzed only by a broad singlet. The area intensities decreased with increasing temperatures, as explained by Debye model. The intensities suddenly decreased at 1000 K, but recovered again at 1100 K.

The relaxation behaviors observed in the present experiment can be interpreted in terms of a diffusion-reaction process of interstitial Fe atoms with vacancies within the time scale of 100 ns, leading to the formation of substitutional Fe atoms in the Si matrix. The process must be related to the recovery processes from non-equilibrium to the equilibrium states of the Si lattice around the ^{57}Fe nuclear probes.

^{57}Mn implantation Mössbauer studies were performed to study the defect formations induced by Fe/Mn implantation in ZnO, Al_2O_3 , and MgO. These are attracting attention as dilute magnetic oxides. In the case of ZnO, the formation of Fe^{3+} -vacancy complexes is found to depend strongly on the implanted dose and to be faster and more efficient at higher temperatures. The results at these temperatures suggest the mobility of the Zn vacancy,

together with vacancy trapping at the substitutional Mn/Fe impurities are responsible for the formation of Fe-V_{Zn} complexes. These experiments were carried out at CERN-ISOLDE and HIMAC.

The detection system for ⁵⁷Mn implantation Mössbauer studies was improved by using an anticoincidence method where a thin plastic scintillation counter was set between the detector and a sample in order to reject the β -rays from ⁵⁷Mn. The Mössbauer spectrum with sufficient signal-to-noise (S/N) ratio that is about 20 times higher than that in previous measurements was successfully obtained.

Head

Masahiko IWASAKI

Members

Katsuhiko ISHIDA

Kenta ITAHASHI

Yoshio KOBAYASHI

Teiichiro MATSUZAKI

Hiroaki OHNISHI

Haruhiko OUTA

Fuminori SAKUMA

Isao WATANABE

Special Postdoctoral Researchers

Masami IIO

Kazuki OHISHI

Foreign Postdoctoral Researcher

Risdiana

Special Contract Researchers

Kyo TSUKADA

Contract Researchers

Yasuyuki ISHII

Takayuki KAWAMATA

Takahisa KOIKE

Katsuya MIZUNO

Takao SUZUKI

Dai TOMONO

Koji YOKOYAMA

Visiting Scientists

Tadashi ADACHI (Grad. Sch. Eng., Tohoku Univ.)
Jun AKIMITSU (Coll. Sci. Eng., Aoyama Gakuin Univ.)
Shingo ARAKI (Grad. Sch. Sci., Osaka Univ.)
Kunio AWAGA (Grad. Sch. Sci., Nagoya Univ.)
Pavel BAKULE (RAL, UK)
George BEER (Univ. of Victoria, Canada)
HyoungChan BHANG (Seoul National Univ., Korea)
N. Ludmila BOGDANOVA (ITEP, Russia)
Catalina CURCEANU (INFN, Italy)
Prasad Tara DAS (SUNY Albany, USA)
Irwan DHARMAWAN (UNPAD, Indonesia)
Truong DUAN (Grad. Sch. Sci., Osaka Univ.)
Yasuaki EINAGA (Fac. Sci & Tech., Keio. Univ.)
Donald FLEMING (Univ. of British Columbia/TRIUMF)
Masaya ENOMOTO (Grad. Sch. Arts and Sci., Univ. of Tokyo)
Mark FAYFMAN (Kurchatov Inst., Russia)
Yutaka FUJII (Fac. Eng., Fukui Univ.)
Hiroyuki FUJIOKA (Grad. Sch. Sci., Kyoto Univ.)
Masaki FUJITA (IMR, Tohoku Univ.)
Hideto FUKAZAWA (Grad. Sch. Sci., Chiba Univ.)
Takayuki GOTO (Fac. Sci. & Tech., Sophia Univ.)
Makoto HAGIWARA (Fac. Eng. Design, Kyoto Inst. Tech.)
Kazuo HAYAKAWA (Fac of Sci. & Tech., Shizuoka Inst. Sci. & Tech.)
Ryugo S. HAYANO (Grad. Sch. Sci., Univ. of Tokyo)
Wataru HIGEMOTO (Advanced Sci. Res. Center, JAEA)
Masahiro HIRANO (JST)
Kazuto HIRATA (NIMS)
Satoru HIRENZAKI (Fac. Sci., Nara Women's Univ.)
Masahiko HIROI (Fac. Sci., Kagoshima Univ.)
Susumu IKEDA (IMSS, KEK)
Yutaka IKEDO (IMSS, KEK)
Rintaro INOUE (ICR, Kyoto Univ.)
Takayuki ISHIDA (Fac. Elect. Commu., Univ. Elect. Commu.)
Fumihiko ISHIKAWA (Grad. Sch. Sci. & Tech., Niigata Univ.)
Shigeru ISHIMOTO (IPNS, KEK)
Tomoichi ISHIWATARI (SMI, Austria)
Ryosuke KADONO (IMSS, KEK)
Yoichi KAMIHARA (JST)
Toshiji KANAYA (ICR, Kyoto Univ.)
Motomi KATADA (Grad. Sch. Sci. & Eng., Tokyo Met. Univ.)

Mineo KATO (IMSS, KEK)
Roland KAWAKAMI (UC Riverside, USA)
Naritoshi KAWAMURA (IMSS, KEK)
Seiko KAWAMURA (J-PARC, JAEA)
Hikomitsu KIKUCHI (Grad. Sch. Eng., Univ. of Fukui)
Jungho KIM (KRISS, Korea)
Yasushi KINO (Fac. Sci., Tohoku Univ.)
Akihiro KODA (IMSS, KEK)
Yoh KOHORI (Fac. Sci., Chiba Univ.)
Yoji KOIKE (Grad. Sch. Eng., Tohoku Univ.)
Norimichi KOJIMA (Grad. Sch. Arts and Sci., Univ of Tokyo)
Kenya KUBO (Coll. Liberal Arts, ICU)
Yoshitaka KUNO (Grad. Sch. Sci., Osaka Univ.)
Takuya KURAHASHI (IMS)
Haruhiko KUROE (Fac. Sci. & Tech., Sophia Univ.)
Guido LANGOUCHE (Univ. of Leuven, Belgium)
Chow LEE (UCF, USA)
Shunsuke MAKIMURA (IMSS, KEK)
Goro MARUTA (Grad. Sch. Sci., Hokkaido Univ.)
Yasuyuki MTSUDA (Grad. Sch. Arts and Sci., Univ of Tokyo)
Satoru MATSUIISHI (FCRC, Tokyo Tech.)
Yasuhiro MIYAKE (IMSS, KEK)
Hitoshi MIYASAKA (Grad. Sch. Sci., Tohoku Univ.)
Jun MIYAZAKI (Fac. Sci. Div., Nihon Univ.)
Soichiro MIZUSAKI (Coll.Sci. & Eng., Aoyama Gakuin Univ.)
Tomoyuki MOCHIDA (Grad. Sch. Sci., Kobe Univ.)
Kazuhiko MUKAI (Toyota Central R&D Labs.)
Yujiro NAGATA (Coll. Sci. Eng., Aoyama Gakuin Univ.)
Takashi NAGATOMO (Coll. Liberal Arts, ICU)
Hiroyuki NAKAMURA (Grad. Sch. Eng., Kyoto Univ.)
Jin NAKAMURA (Fac. Elect. Commu., Univ. Elect. Commu.)
Kazutaka NAKAHARA (Univ. of Maryland, USA)
Satoshi NAKAMURA (Grad. Sch. Sci., Tohoku Univ.)
Takashi NAKAMURA (Grad. Sch. Sci. & Eng., Tokyo Tech.)
Takayoshi NAKAMURA (RIES, Hokkaido Univ.)
Takehito NAKANO (Grad. Sch. Sci., Osaka Univ.)
Saburou NASU (Grad, Sch. Eng. & Sci., Osaka Univ.)
Kazuhiko NINOMIYA (Advanced Sci. Res. Center, JAEA)
Nobuhiko NISHIDA (Fac. Sci., Tokyo Tech.)
Yoichi NISHIWAKI (Sch. Medi., TWMU)
Kusuo NISHIYAMA (IMSS, KEK)

Hiroshi NOZAKI (Toyota Central R&D Labs.)
Yasuo NOZUE (Grad. Sch. Sci., Osaka Univ.)
Agung NUGROHO (ITB, Indonesia)
Masaaki OHBA (Grad. Sch. Eng., Kyoto Univ.)
Yoshitaka OHKUBO (KURRI, Kyoto Univ.)
Susumu OHYA (Fac. Sci., Niigata Univ.)
Shinji OKADA (INFN, Italy)
Vassili PEREVOZCHIKO (VNIIEF, Russia)
Leonid PONOMAREV (Kurchatov Institute, Russia)
Francis PRATT (RAL, UK)
Shin-ichi SAKAMOTO (J-PARC, JAEA)
Naohito SAITO (IPNS, KEK)
Kazuhiko SATO (Grad. Sch. Sci. & Eng., Saitama Univ.)
Masaharu SATO (Grad. Sch. Sci., Univ. of Tokyo)
Ralph SCHEICHER (Michigan Tech. Univ., USA)
Ryoichi SEKI (California State Univ. , Northridge, USA)
Kouichirou SHIMOMURA (IMSS, KEK)
Ichiro SHIRAKI (Grad. Sch. Medi. & Eng. Sci., Univ. of Yamanashi)
Vyacheslav STORCHAK (VNIIEF, Russia)
Patrick STRASSER (IMSS, KEK)
Hiroyuki SUGAI (Advanced Sci. Res. Center, JAEA)
Jun SUGIYAMA (Toyota Central R&D Labs.)
Ken SUZUKI (SMI, Austria)
Haruhiko SUZUKI (Grad. Sch. Nat. Sic. & Tech., Kanazawa Univ.)
Hiroyuki SUZUKI (NIMS)
Soh SUZUKI (CRC, KEK)
Takatoshi SUZUKI (Grad. Sch. Sci., Univ. of Tokyo)
Yoshikazu TABATA (Grad. Sch. Eng. & Sci., Kyoto Univ.)
Shigeru TAKAGI (Grad. Sch. Sci., Tohoku Univ.)
Kazuyuki TAKAI (Grad. Sch. Sci. & Eng., Tokyo Tech.)
Keiji TAKEDA (ISSP, Univ. of Tokyo)
Nao TAKESHITA (NeRI, AIST)
Hiroyuki TAKEYA (NIMS)
Yoichi TANABE (WPI, Tohoku Univ.)
Manobu TANAKA (IPNS, KEK)
Akihiro TANIGUCHI (KURRI, Kyoto Univ.)
Harry TOM (UC Riverside, USA)
Eiko TORIKAI (Grad. Sch. Medi. & Eng. Sci., Univ. of Yamanashi)
Akihisa TOYODA (IPNS, KEK)
Satoshi TSUTSUI (JASRI)
Kazuo UEDA (ISSP, Univ. of Tokyo)

Yun XUE (Grad. Sch. Nat. Sic. & Tech., Kanazawa Univ.)
Eiichi YAGI (Fac. Sci. & Eng., Waseda Univ.)
Kazuyoshi YAMADA (IMR, Tohoku Univ.)
Yasuhiro YAMADA (Fac. Sci., Tokyo Univ. of Sci.)
Yutaka YOSHIDA (Fac of Sci. & Tech., Shizuoka Inst. Sci. & Tech.)
Arkady YUKHINCHUK (VNIIEF, Russia)
Johann ZMESKAL (SMI, Austria)

Visiting Technician

Shinji KAI (Tanaka Kikinzoku Kogyo K.K.)
Kunihiro SHIMA (Tanaka Kikinzoku Kogyo K.K.)

Research Consultants

Yoshinori AKAISHI
Masayasu KAMIMURA
Atsuko ITO
Toshimitsu YAMAZAKI

Students

Junior Reserch Associates

Yuya FUJIWARA (Grad. Sch. Sci., Univ. of Tokyo)
Toshihiko HIRAIWA (Grad. Sch. Sci., Kyoto Univ.)
Satoshi ITOH (Grad. Sch. Sci., Univ. of Tokyo)

Intern

Makoto TOKUDA (Grad. Sch. Sci. & Eng., Tokyo Tech.)

Student Trainees

Takashi AKAHORI (Grad. Sch.Sci. & Eng., Shizuoka Inst. Sci. & Tech.)
Yuki AKIYAMA (Grad. Sch.Sci. & Eng., Shizuoka Inst. Sci. & Tech.)
Mika DOIZOE (Grad. Sch. Sci., Tokyo Univ. Sci.)
Shun ENOMOTO (Grad, Sch. Sci., Osaka Univ.)
Jafar ESMAILI (Isfahan Univ. Tech., Iran)
Yusuke GOTO (Fac. Sci., Univ. of Tokyo)
Ryuta HANAZAWA (Grad. Sch. Sci. & Eng., Shizuoka Inst. Sci. & Tech.)
Masatoshi HIRAISHI (Sch. High Enegy Acce. Sci.,Sokendai)
Toru HISAMATSU (Grad. Sch. Sci. & Eng., Kagoshima Univ.)
Tadashi HASHIMOTO (Grad. Sch. Sci., Univ. of Tokyo)
Masahiro ICHINO (Grad. Sch.Sci. & Eng., Shizuoka Inst. Sci. & Tech.)
Naho IINUMA (Grad. Sch. Sci., Tokyo Univ. Sci.)
Asae ITO (Fac. Sci., Tokyo Univ. Sci.)

Naoki KASE (Grad. Sch. Sci.& Eng., Aoyama Gakuin Univ.)
Yu KAWAHARA (Grad. Sch. Sci., Tokyo Univ. Sci.)
Takumi KOBAYASHI (Grad. Sch. Sci., Univ. of Tokyo)
Naoyuki KONNO (Grad. Sch. Sci., Tokyo Univ. Sci.)
Hiroshi KOU (Grad. Sch. Sci. & Eng., Tokyo Tech.)
Hiroto KUMABE (Grad. Sch.Sci. & Eng., Shizuoka Inst. Sci. & Tech.)
Yoko MANABE (Grad. Sch. Sci. & Eng., Saitama Univ.)
Masanori MIYAZAKI (Sch. Phys. Sci.,Sokendai)
Kiichi MIYAZAWA (Grad. Sch. Indus. Sci. & Tech., Tokyo Univ. Sci.)
Saori NAKAJIMA (Grad. Sch. Sci. & Tech., Sophia Univ.)
Takahiro NISHI (Fac. Sci., Univ. of Tokyo)
Kumiko OKAMURA (Fac. Sci., Tokyo Univ. Sci.)
ROGER PINK (SUNY at Albany, USA)
Manami SATAKE (Grad. Sch. Sci. & Eng., Tokyo Tech.)
Ryuichi SUEHIRO (Grad. Sch. Sci., Osaka Univ.)
Kensuke SUZUKI (Grad. Sch. Eng., Tohoku Univ.)
Tomonori TAKAHASHI (Grad. Sch. Sci., Univ. of Tokyo)
Arisa TANIGUCHI (Grad. Sch. Sci. & Eng., Saitama Univ.)
Hideyuki TATSUNO (Grad. Sch. Sci., Univ. of Tokyo)
Koichi TODOROKI (Grad. Sch. Sci., Univ. of Tokyo)
Maai UCHIKAWA (Grad. Sch. Sci., Univ. of Tokyo)
Shin UEGAKI (Grad. Sch. Sci., Tokyo Univ. Sci.)
Ryo USUI (Fac. Sci., Tokyo Univ. Sci.)
Heejoong YIM (Seoul National Univ., Korea)

Secretaries

Yoko FUJITA
Junko SATO

**Sub Nuclear System Research Division
RIKEN-BNL Research Center
Theory Group**

1. Abstract

The RIKEN BNL Research Center (RBRC) was established in April 1997 at Brookhaven National Laboratory in New York, USA. The Center is dedicated to study of strong interactions, including hard QCD/spin physics, lattice QCD and RHIC physics through nurturing of a new generation of young physicists. The Theory Group activities are closely and intimately related to those of the Nuclear Theory, High Energy Theory and Lattice Gauge Theory Groups at BNL. The RBRC theory group carries out research in three areas: numerical lattice QCD, perturbative QCD and phenomenological QCD. It pioneered the use of the domain-wall fermion method in lattice QCD and has investigated various aspects of hadron physics including the calculation of neutral Kaon CP-violations that is relevant for checking the Cabibbo-Kobayashi-Maskawa theory. The perturbative QCD effort has developed various new methods required for studying hadron structures, especially in spin physics research. The group has pioneered phenomenological QCD researches of color superconductivity, isospin density, and small-x phenomena in extreme hadronic matters.

2. Major Research Subjects

- (1) Perturbative QCD
- (2) Lattice QCD numerical research
- (3) Phenomenological QCD

3. Summary of Research Activity

The RIKENBNL Research Center (RBRC) was established in 1997 to support the RIKEN activities at RHIC in BNL, and also to promote theoretical studies related to RHIC, i.e. theories of strong interaction. The center's first director was T. D. Lee (Columbia University), and in October 2003, the former director of BNL, N. P. Samios, succeeded to the post of director. H. En'yo, Chief scientist of RIKEN in Wako, is also associate director of RBRC. The center consists of a theory group lead by L. McLerran (BNL) and an experimental group lead by Y. Akiba of RIKEN, currently resident at BNL.

Research in the RBRC theory group focuses on a wide variety of phenomena caused by the strong interaction, one of the four fundamental interactions in nature. The strong interaction is described theoretically by Quantum Chromodynamics (QCD), and the research projects in the RBRC theory group aim to elucidate various phenomena brought about by the strong interaction from the principles of QCD. Major subjects of our research include studies (a) based on lattice QCD, (b) on spin physics based on perturbative QCD, and (c) on QCD in extreme conditions such as high temperature, high density or high energy. RBRC offers RHIC Physics Fellowships, allowing joint appointments with universities. These Fellowships enable a talented researcher to maintain a tenure track position at his/her university as well as a Fellow position at RBRC for a certain period of time. This system was established in order to increase the research potential of RBRC and to disseminate its research activities and results. At present, RBRC has cooperative agreements with Arizona State University, the City University of New York, Iowa State University,

Purdue University, Pennsylvania State University, the State University of New York at Stony Brook, Texas A&M University, the University of Tsukuba, as well as with BNL and with Lawrence Berkeley National Laboratory.

(1) Lattice QCD

QCDOC (QCD on chip), a second-generation lattice-QCD computer, was developed in the collaboration amongst the RBRC group, Columbia University and IBM. Three units of such a machine with 10 teraflops computing power are in operation since 2005; two in BNL (RBRC and DOE) and one in Edinburgh (UK-QCD), and formed a world-wide strong collaboration for the lattice QCD studies. Such computing power enables us to perform precise calculations with 3 quark flavors with proper handling on the chiral symmetry breaking. Several projects are ongoing: flavor physics for Kaon and B-meson, electro-magnetic properties of hadrons, proton decay, the nuclear force, nucleon form factors which relates to the proton spin problem, and QCD thermodynamics in finite temperature/density systems as is produced in RHIC heavy-ion collisions. R and D for a next generation RBRC lattice supercomputer, QCDCQ is finalized. The initial 1/2 rack QCDCQ will be installed in fall 2010, and larger volume machines are under consideration of installation in 2011.

(2) Perturbative QCD and spin physics

The ongoing RHIC spin experiments have motivated much of the parallel theoretical developments at RBRC. In the area of transverse spin physics, novel predictions have been obtained for the single transverse-spin asymmetry in open charm production in pp collisions at RHIC. This asymmetry probes three gluon correlations in polarized proton. In addition, radiative QCD corrections to single-spin observables were investigated, providing the relevant evolution equations. Further work focused on hyperon production at RHIC, and on azimuthal asymmetries in the Drell-Yan process.

(3) Phenomenological QCD -- QCD under extreme conditions --

To establish a detailed picture of relativistic heavy ion collisions, QCD-based theoretical approaches are in progress. Especially the idea of “color glass condensation (CGC)” can be a key to understand the initial condition of the heavy ion collision. Other phenomenological approaches are in progress to understand the characteristics of strongly interacting quark gluon plasma. A recent effort has been initiated to understand heavy ion elliptic flow in terms of viscous hydrodynamics. A new finite temperature effective field theory is being developed for the strongly interacting quark gluon plasma to explain the suppression of shear viscosity in the region of the phase transition.

Group Leader

Larry McLERRAN

Deputy Group Leader

AnthonyJ. BALTZ

Members

Yasumichi AOKI *1
Denes MOLNAR *2
Kirill TUCHIN *2
Rainer FRIES *2
Tomomi ISHIKAWA *3
Feng YUAN *2
Toru KOJO *4
Peter PETRECZKY *2
Taku IZUBUCHI *1
Sinya AOKI *5
Derek TEANEY *2
Adrian DUMITRU *2
Cecilia LUNARDINI *2
Anna STASTO *2
Zhongbo Kang *3

Visiting Members

Miklos GYULASSY (Columbia Univ., USA)
RobertL. JAFFE (Massachusetts Inst. Technol., USA)
Robert MAWHINNEY (Columbia Univ., USA)
Edward SHURYAK (State Univ. New York, Stony Brook, USA)
Testufumi HIRANO (U. Tokyo)
Shigemi OHTA (KEK)

Secretarial Staff

Doris RUEGER (Secretary to Director N. P. Samios)
Pamela ESPOSITO (Theory Group Secretary)
Taeko ITO (Assistant to Account Manager for Administration)
Susan FOSTER (Experimental Group Secretary)

Administrative Staff / RIKEN Japan

Minoru Fujiki, Deputy Director, Nishina Center Research Promotion Office
Emiko ADACHI (RBRC Account Manager for Administration)
Keiko SUSUKI (Japan)

*1 RIKEN BNL Fellow *2 RHIC Physics Fellow,
*3 Research Associate, *4 Special Postdoctoral Researcher,
*5 RHIC visiting Fellow

Sub Nuclear System Research Division
RIKEN-BNL Research Center
Experimental Group

1. Abstract

RIKEN BNL Research Center (RBRC) Experimental Group studies the strong interactions (QCD) using RHIC accelerator at Brookhaven National Laboratory, the world first heavy ion collider and polarized p+p collider. We have three major activities: Spin Physics at RHIC, Heavy ion physics at RHIC, and detector upgrades of PHENIX experiment at RHIC. We study the spin structure of the proton using the polarized proton-proton collisions at RHIC. This program has been promoted by RIKEN's leadership. The first focus of the research is to measure the gluon spin contribution to the proton spin. Our recent data analysis has shown that the proton spin carried by the gluons is small, which is a very striking finding beyond our expectations. The aim of Heavy ion physics at RHIC is to re-create Quark Gluon Plasma (QGP), the state of Universe just after the Big Bang. Two important discoveries, jet quenching effect and strong elliptic flows, have established that new state of dense matter is indeed produced in heavy ion collisions at RHIC. We are proceeding to understand the nature of the matter. Recently, we have measured direct photons in Au+Au collisions for $1 < p_T < 3$ GeV/c, where thermal radiation from hot QGP is expected to dominate. The comparison between the data and theory calculations indicates that the initial temperature of 300 MeV to 600 MeV is achieved. These values are well above the transition temperature to QGP, which is calculated to be approximately 170 MeV by lattice QCD calculations.

We have major roles in detector upgrades of PHENIX experiment, namely, the silicon vertex tracker (VTX) and muon trigger upgrades.

2. Major Research Subjects

- (1) Experimental Studies of the Spin Structure of the Nucleon
- (2) Study of Quark-Gluon Plasma at RHIC
- (3) PHENIX detector upgrades

3. Summary of Research Activity

The RIKEN-BNL Research Center was established in 1997 to support the RIKEN activities at RHIC in BNL, and also to promote theoretical studies related to RHIC, i.e. theories of strong interaction. The center's first director was T. D. Lee (Columbia University), and in October 2003, the former director of BNL, N.P. Samios, succeeded to the post of the director. The center consists of a theory group lead by L. McLerran (BNL) and an experimental group lead by Y. Akiba, a vice chief scientist of RIKEN in Wako.

We study the strong interactions (QCD) using the RHIC accelerator at Brookhaven National Laboratory, the world first heavy ion collider and polarized p+p collider. We have three major activities: Spin Physics at RHIC, Heavy ion physics at RHIC, and detector upgrades of PHENIX experiment.

(1) Experimental study of spin structure of proton using RHIC polarized proton collider

How is the spin of proton formed with 3 quarks and gluons? This is a very fundamental question in Quantum Chromodynamics (QCD), the theory of the strong nuclear forces. The

RHIC Spin Project has been established as an international collaboration between RIKEN and Brookhaven National Laboratory (BNL) to solve this problem by colliding two polarized protons for the first time in history. This project also has extended the physics capabilities of RHIC.

The first goal of the RHIC spin physics program is to elucidate a contribution of the gluon spin in the proton spin. We have measured double-helicity asymmetries of neutral pions to study gluon polarization in proton. The most recent data from 2006 run have shown that the gluon polarization in the proton is small, and only about half of proton spin can be accounted by gluon spin in the measured region of gluon momentum in proton. The remaining part must be carried by gluons in lower momentum region where the measurement is not sensitive, and/or reside in the orbital-angular momentum of quarks and gluons.

To finalize the smallness of the gluon-spin contribution, we need to measure double helicity asymmetry in direct photon production. This process is dominated by a single and the simplest process, gluon Compton scattering, in perturbative QCD, and is the golden channel to determine the gluon density and the gluon polarization in the proton. We published a paper on direct photon cross section in p+p collisions at RHIC. Preliminary results on double-helicity asymmetry of direct photon from the 2006 run have been obtained.

We have also accumulating transversely-polarized proton collision data to measure single transverse-spin asymmetries of processes which are predicted to be sensitive to the orbital-angular momentum of quarks and gluons. In 2006 and 2008, PHENIX recorded 2.7/pb and 4.5/pb, respectively, of transversely-polarized proton collisions data at 200 GeV to investigate single transverse-spin asymmetries. Several transverse spin analysis of these high statistics data are on going.

The 2009 run of RHIC is a major spin run. We had the first 500 GeV p+p run and a long p+p run at 200 GeV. The main purpose of the 500 GeV run is to measure anti-quark polarization from the single longitudinal asymmetry A_L in the W boson production. The 500 GeV part of RUN9 is an engineering run. The polarization is lower (~40%) than the 200 GeV run and the luminosity in the 5 weeks of data taking period is rather limited, at about 14/pb recorded in PHENIX. Yet we have observed the first signal of $W \rightarrow e$ decays in p+p collisions in PHENIX central arm. The group is working on the cross section analysis and the A_L measurement analysis. In the 200 GeV part of RUN9, PHENIX recorded approximately twice as much longitudinal polarized p+p data as the 2006 RUN.

In addition to the study of polarized p+p collisions at RHIC, we study quark fragmentation function. With collaboration with the BELLE experiment at High Energy Accelerator Research Organization (KEK), we discovered that the spin direction of a quark can be determined from its hadronic fragments. Precise data of the quark fragmentation function can be used to understand the cross sections and the spin dependences of particle production in polarized p+p collisions at RHIC. We continue the study of the quark fragmentation function at BELLE.

(2) Experimental study of Quark-Gluon Plasma using RHIC heavy-ion collider

The goal of high energy heavy ion physics at RHIC is study of QCD in extreme conditions i.e. at very high temperature and at very high energy density. Experimental results from RHIC have established that dense partonic matter is formed in Au+Au collisions at RHIC. The matter is very dense and opaque, and it has almost no viscosity and behaves like a perfect fluid. These conclusions are primarily based on the following two discoveries:

- Strong suppression of high transverse momentum hadrons in central Au+Au collisions

(jet quenching)

- Strong elliptic flow

The focus of the research in heavy ion physics at RHIC is now to investigate the properties of the matter. RBRC have played the leading roles in some of the most important results from PHENIX in the study of the matter properties. These include (1) measurements of heavy quark production from the single electrons from heavy flavor decay (2) measurements of J/Psi production (3) measurements of di-electron continuum and (4) measurements of direct photons.

The most important recent result is the measurement of direct photons for $1 < p_T < 5$ GeV/c in p+p and Au+Au through their internal conversion to e+e- pairs. If the dense partonic matter formed at RHIC is thermalized, it should emit thermal photons. Observation of thermal photon is direct evidence of early thermalization, and we can determine the initial temperature of the matter. It is predicted that thermal photons from QGP phase is the dominant source of direct photons for $1 < p_T < 3$ GeV/c at the RHIC energy. We measured the direct photon in this p_T region from measurements of quasi-real virtual photons that decays into low-mass e+e- pairs. Strong enhancement of direct photon yield in Au+Au over the scaled p+p data has been observed. Several hydrodynamical models can reproduce the central Au+A data within a factor of two. These models assume formation of a hot system with initial temperature of $T_{init} = 300$ MeV to 600 MeV. This is the first measurement of initial temperature of quark gluon plasma formed at RHIC.

(3) PHENIX detector upgrade

The group has major roles in several PHENIX detector upgrades, namely, the silicon vertex tracker (VTX) and muon trigger upgrades.

VTX is 4 layers of silicon tracker, jointly funded by RIKEN and the US DOE. The inner two layers are silicon pixel detectors and the outer two layers are silicon strip detectors. The detector will be completed in 2010.

Muon trigger upgrades are needed for $W \rightarrow \mu$ measurement at 500 GeV. New trigger electronics (Muon Trigger FEE) have been installed in one of muon arms and they will be commissioned in the 2009 run. After the 2009 run, the rest of the Muon Trigger FEE will be installed in PHENIX. Prototype of muon trigger detectors using MRPC technology have been installed for test during the 2009 run.

Group Leader

Yasuyuki AKIBA

Deputy Group Leader

Abhay DESHPANDE

Members

Yuji GOTO

Itaru NAKAGAWA

Takashi ICHIHARA

Atsushi TAKETANI
Yasushi WATANABE
Satoru YOKKAICHI
Kensuke OKADA *1
Ralf-Christian SEIDL *1
Stefan BATHE *1
David KAWALL *2
Kieran BOYLE *3
Manabu Togawa *4
Jun TAMURA (T.I.Tech)*5
Yorito YAMAGUCHI (CNS-U-Tokyo)*5
Misaki OUCHIDA (Hiroshima Univ)*5
Kenichi KARATSU (Kyoto Univ)*5
Yoki ARAMAKI (CNS-U-Tokyo)*5
Akihisa TAKAHARA (CNS-U-Tokyo)*5
Miki KASAI (Rikkyo)*5

Visiting Members

Naohito SAITO (KEK)
Zheng LEE (BNL)
Kiyoshi TANIDA (Kyoto Univ.)
Akio OGAWA (BNL)
Masahiro OKAMURA (BNL)
Rachid NOUICER (BNL)
Kotaro KONDO (T.I.Tech)*8
Kohei SHOJI (Kyoto Univ.)*7
Seishi DAIRAKU (Kyoto Univ.)*7
Katsuro NAKAMURA (Kyoto Univ.)*6
Takeshi KANESUE (Kyusyu Univ.)*7

*1RIKEN BNL Fellow, *2 RHIC Physics Fellow,
*3 Research Associate, *4 Special Postdoctoral Researcher,
*5 Junior Research Associate, *6 JSPS Student, *7 Student trainee
*8 *JSPS Postdoc*

RIBF Research Division Heavy Ion Nuclear Physics Laboratory

1 Abstract

With fast RI beams provided by the RIBF cyclotron complex and the in-flight RI separators RIPS and BigRIPS, we study exotic behavior of nuclei far from the stability line, explosive nuclear burning in stars and early universe, and nuclear reactions related to solar neutrino production. For that purpose, we develop various experimental methods utilizing intermediate-energy inelastic scattering including Coulomb excitation, Coulomb dissociation, transfer- and fragmentation-reactions coupled with gamma- and particle-decay measurements. We perform also study of the three-nucleon forces by precise measurements of elastic scattering and breakup reactions of few-nucleon systems. A new laser-spectroscopy technique for exotic nuclei is also developed. Technical developments of radiation measurements such as semiconductor detectors and scintillation detectors, data processing methods, and construction of experimental equipment are also made. Theoretical studies on nuclear structure and nuclear reaction are performed.

2 Major Research Subjects

- (1) Spectroscopy of unstable nuclei with direct reactions
- (2) Study of astrophysical nuclear reactions with fast beams of unstable nuclei
- (3) Three nucleon forces studied by intermediate-energy p+d scattering
- (4) Development of high performance radiation detector systems
- (5) Development of laser spectroscopy for studying unstable nuclei
- (6) Theoretical studies on nuclear structure and nuclear reactions

3 Summary of Research Activity

3.1. Spectroscopy using direct reactions with γ -ray measurements

The evolution of shell structure, development of collectivity, and possible decoupling of proton- and neutron-motion in neutron- and proton-rich nuclei are studied by direct reactions with γ -ray measurements. In order to extract different quantities, various reactions were used such as proton inelastic scattering, Coulomb excitation, nucleon removal reactions.

- (1) ^{32}Ne , ^{32}Mg , ^{34}Si – in island of inversion around $N=20$

In order to clarify the nature of the “islands of inversion” around $N=20$, the structures of low-lying levels in ^{32}Mg and ^{34}Si were studied through the proton inelastic scattering. The 4^+ state as well as several other excited states were found in ^{32}Mg . The location of the 3^- state indicates disappearance of the sd-pf shell gap in ^{32}Mg . The anomalously hindered $B(E2)$ value for the $0^+ - 2^+$ transition in ^{34}Si was compared with the neutron-transition quadrupole matrix element extracted from the $^{34}\text{Si}(p,p')$ result. The very neutron rich nucleus ^{32}Ne was studied by the Coulomb excitation at the new facility of RIBF. The result indicates that this nucleus is in the island of inversion.

- (2) $^{17,18}\text{C}$ – new method with transverse momentum measurement

The spins and parities of the low-lying levels in ^{17}C and ^{18}C were determined by the transverse momentum distributions of fragments produced in the one neutron removal reactions of ^{18}C and ^{19}C beams with a hydrogen target. The final states were identified by detecting their de-excitation γ -rays. The result indicates the usefulness of the transverse-momentum associated with proton induced nucleon removal processes for the spin-assignment with the help of new approach for the reaction process, *i.e.* CDCC.

- (3) $^{62,64}\text{Cr}$ – behavior of neutron-rich nuclei around $N=40$

The development of deformation in ^{62}Cr was observed by the large deformation length and the

$4^+ - 2^+$ energy ratio obtained in the proton inelastic scattering experiment performed at RIPS. This confirms the new region of deformation emerging in the neutron-rich $N \sim 40$ region despite of the fact that $N=40$ is a magic number for the harmonic oscillator potential

(4) ^{20}Mg – role of four protons around the ^{16}O core

The collectivity of the proton-rich nucleus ^{20}Mg was studied by the Coulomb excitation. The $B(E2)$ value for the 2^+ excitation was compared with that for the mirror nucleus ^{20}O . The large ratio between the neutron- and proton-matrix elements is consistent with the known core polarization effect induced by the valence nucleons, showing that the anomalous decoupling phenomena observed in ^{16}O is not observed in ^{20}O and ^{20}Mg .

3.2. Spectroscopy of unbound states using breakup and other reactions

(1) Halo structure of ^{31}Ne

The structure of the very neutron-rich nucleus ^{31}Ne was studied at RIBF via Coulomb breakup reaction. The obtained inclusive cross section shows an abnormal enhancement, which indicates the neutron halo structure in this nucleus.

(1) Invariant mass spectroscopy of nuclei in the vicinity of the neutron drip line

(a) Study of unbound states in ^{13}Be and ^{14}Be

The first 2^+ state of ^{14}Be at $E_x=1.55$ MeV was measured in the proton inelastic scattering. From the cross section, deformation length was obtained, which shows a small value as compared with that of ^{12}Be . The unbound states in ^{13}Be were identified at around $E_{xx}=0.5$ MeV and 2 MeV in the invariant mass spectrum observed in the one-neutron removal reaction. The former has a d -wave property, while the latter is of p -wave nature which indicates obliteration of the $N=8$ shell gap.

(b) Invariant mass spectra were obtained by the breakup and inelastic scattering of ^6He , ^{17}C , and ^{19}C on proton targets. New peaks were found for neutron-rich carbon isotopes.

(2) Invariant mass spectroscopy of proton-rich nuclei

Coulomb dissociation of proton-rich nuclei ^{23}Al , ^{27}P , and ^{31}Cl on ^{208}Pb were measured to obtain the radiative proton capture cross section of ^{22}Mg , ^{26}Si , and ^{30}S . These reactions are relevant in the explosive nucleosynthesis in novae and X-ray bursts and thus their cross sections are indispensable for the astrophysical network calculation.

(3) Missing mass spectroscopy of very neutron-rich light nuclei

Experimental search for the ^7H system with largest N/Z ratio ever known was performed in the $d(^8\text{He}, ^3\text{He})^7\text{H}$ reaction using missing mass method. The excitation spectrum shows the peculiarity at ~ 2 MeV that can not be reproduced by a reasonable phase space distributions and might indicate the existence of the ^7H state at low excitation energy. Simultaneously, the strong peaks that corresponds to ^7He and ^{11}Li ground states were observed in the $d(^8\text{He}, t)$ and $d(^{12}\text{Be}, ^3\text{He})$ reaction channels.

3.3. Experimental studies on the three nucleon forces

(1) Necessity of the three-nucleon-force is shown to reproduce the deuteron-proton elastic scattering cross section. To further investigate the three-nucleon-force, spin transfer coefficients for deuteron-proton breakup reactions were measured. The study has been extended using the new RIBF facility to higher energies at 250 MeV/nucleon, where the effect of the three-nucleon-force is expected to be more pronounced.

(2) We tested Bell's inequality in the proton-neutron system by measuring the spin-correlation between the proton-neutron pair in 1S_0 -state which was produced by the $^2\text{H}(d, pn)$ reaction.

Among many other experiments performed thus far, this is the first case using the proton and neutron pair.

3.4. “OROCHI” (Optical RI atom Observation in Condensed Helium as Ion-catcher) development

A novel nuclear laser spectroscopy technique for exotic nuclei trapped in superfluid helium, named as OROCHI (Optical RI-atom Observation in Condensed Helium as Ion-catcher), is being developed. We have carried out high precision measurement of Zeeman and hyperfine splitting of $^{85,87}\text{Rb}$ and ^{133}Cs atoms in superfluid helium, and successfully demonstrated that the nuclear spins and moments of unknown nuclei can be deduced by comparing their Zeeman and hyperfine splitting energies with those of known nuclei. We have also succeeded in optical pumping of non-alkali atoms such as Ag, which opens the door to the versatility of the OROCHI method. We are now ready to measure unknown spins and moments of exotic nuclei.

3.5. SCRIT development

SCRIT (Self-Confining RI Target) is a novel experimental scheme to enable the study of the internal structure of exotic nuclei by electron scattering. We have shown the feasibility of this scheme by using a prototype installed at the electron storage ring, KSR, of Kyoto University. Aiming at the future experiment using SCRIT with unstable nuclear beams, the construction of the SR2 (SCRIT-equipped RIKEN Storage RING) has been started at RIBF. We have achieved the accumulation of the electron beam with the energy of 700MeV.

3.6. SAMURAI

SAMURAI (Superconducting Analyzer for Multi-particle from Radio Isotope Beams) is a large-acceptance multi-particle spectrometer we will construct at RIBF. Its major part is of a large-gap superconducting magnet with 7 Tm of bending power. SAMURAI enables momentum analysis of heavy projectile fragments and projectile-rapidity protons with large angular and momentum acceptance. SAMURAI also affords projectile-rapidity neutron measurements with large angular acceptance in coincidence with heavy projectile fragments.

The construction budget has been approved, and is funded in four years from fiscal year 2008. The budget covers the superconducting dipole magnet and most part of detectors for heavy ions, neutrons, and protons. Our lab is, in particular, in charge of silicon strip detectors for protons and heavy ions and readout circuits requiring capability of broad dynamic range and high density signal processing. Our lab also partly takes care of the total arrangements of the SAMURAI collaboration group constituted by members from several institutes, each of which has unique physics interest.

Detailed design of the superconducting dipole magnet has been almost complete. The magnet construction in RIBF will start in the summer of 2010, and will complete early in 2011. The detectors are constructed in parallel. It is planned that the first SAMURAI experiment is performed in summer 2011.

3.7. Theoretical studies of nuclear physics

Studies on nuclear structure at finite temperature are in progress: A self-consistent formulation of quasiparticle RPA including the effects of quantal and thermal fluctuations to study the properties of finite systems with pairing at finite temperature and angular momentum.

Head

Tohru MOTOBAYASHI

Member

Yukari MATSUO
Yoshiyuki YANAGISAWA
Nori AOI
Ken-ichiro YONEDA
Yasushi WATANABE
Toshimi SUDA
Akihisa KOHAMA

Contract Researchers

NguyenDinh DANG
Kimiko SEKIGUCHI(SAKAGUCHI)

Senior Visiting Scientists

Kengo OGAWA (Yamazaki Lab. In Riken)
Wolfgang MITTIG (GANIL)
Hisashi HORIUCHI (Osaka Univ.Nuclear Physics Center)
Hiroyuki SAKURAGI (Grad. Sch. of Sci., Osaka City Univ.)

Research Consultants

Yasuo AOKI (univ. of Tsukuba)
Hiroyuki MURAKAMI (Rikkyo Univ.)
Toshimitsu YAMAZAKI (Nishina Foundation)

Special Postdoctoral Researchers

Yasuhiro TOGANO (Rikkyo Univ.)

Junior Research Associates

Kenjiro MIKI (Univ. of Tokyo)
Masafumi MATSUSHITA (Rikkyo Univ.)

Nishina Fellow Ship

NguyenQuang HUNG (Hanoi Univ. of science)

International Program Associates

He WANG (Peking Univ., China)

Visiting Scientists

Mototsugu MIHARA (Osaka Univ.)

Takuji IZUMIKAWA (Niigata Univ.)
Tomotsugu WAKASA (Kyushu Univ.)
Kyoichiro OZAWA (Univ. of Tokyo)
Didier BEAUMEL (Pris-XI Univ.)
Shinichiro FUJII (Kyushu Univ.)
Yasuo MIAKE (Tsukuba Univ.)
Mitsuo SAKAI (Univ. of Tokyo)
Peter MOLLER (Los Alamos)
Nasser KALANTAR (Univ. of Groningen)
Michael FAMIANO (Michigan State Univ.)
Kikuo KIMURA (Nagasaki Institute of Applied Science)
Kensaku MATSUTA (Osaka Univ.)
Yasuo WAKABAYASHI (Univ. of Tokyo)
Yosuke KONDO (Tokyo Institute of Technology)
Zoltan ELEKES (ATOMKI)
Gabor KALINKA (ATOMKI)
Takashi OHTSUBO (Niigata Univ.)
Jianjun HE (Chinese Academy of Science)
Takahiro KAWABATA (Kyoto Univ.)
Ben MOTTELSON (NORDITA)
Kazushige MAEDA (Tohoku Univ.)
Hiroshi SUZUKI (Tsukuba Univ.)
KevinInsik HAHN (Ewha Woman's Univ)
PeterVon BRENTANO (Univ. of Cologne)
Atsushi HATAKEYAMA (Tokyo Univ. of Agriculture and Technology)
Yanlin YE (Peking Univ.)
Julien GIBELIN (CEAN)
Dorottya SOHLER (ATOMKI)
JunYoung MOON (Chung-Ang Univ.)
Yorick BLUMENFELD (Paris-XI Univ.)
Bo CEDERWALL (Royal Institute of Technology)
Takashi KIKUCHI (Nagaoka Univ. of Technology)
Tetsuro KOMATSUBARA (Tsukuba Univ.)
Hironobu ISIYAMA (KEK)
Rubens LICHTENTHALER (The Univ. of Sao Paulo)
Valdir GUIMARAES (The Univ. of Sao Paulo)
Jingbin LU
Johannes MESSCHENDORP
Akos HORVATH (Budapest)
Takeshi KOIKE (Tohoku Univ.)
Kimikazu SASA (Tsukuba Univ.)
Xiangzhou CAI (SINAP)
Alessandra GUGLIELMETTI (Univ. of Milano)

Marco MAZZOCCO (Univ. of Padova)
Mauro ROMOLI (INFN)
Sunchan JEONG (KEK)
Betty TSANG (Michigan State Univ.)
Franck DELAUNAY (CEAN)
Andreas STOLZ (Michigan State Univ.)
Zhihong LI (China Institute of Atomic Energy)
Shoji SUZUKI (KEK)
Silvio CHERUBINI (Univ. of Catania)
MarcoLa COGNATA (Univ. of Catania)
Gianluca PIZZONE (Univ. of Catania)
YoungKwan KWON (Chung-Ang Univ.)
Ken-Ichi FUSHIMI (Tokushima Univ.)
Ichiro ARAI (Tsukuba Univ.)
Tadaaki TAMAE (Tohoku Univ.)
Jonathan PEARSON
Alan CHEN (McMaster Univ.)
Masatoshi ITOH (Tohoku Univ.)
Daniel BEMMERER
Adam KISS (Eotvos Lorand Univ.)
Georg BERG (Univ. of Notre Dame)
Henning ESBENSEN (Argonne National Laboratory)
Weiping LIU (China Institute of Atomic Energy)
Wei GUO
Patricia ROUSSEL-CHOMAZ (GANIL)
Chen LI (Inst. of Modern Physics, Chinese Academy of Sciences (IMP, CAS))
David HINDE (Australian National University)
Renju THOMAS
Mahananda DASGUPTA
Stefano ROMANO (Univ. of Catania)
Wendong TIAN (Chinese Academy of Science)
Tomokazu SUZUKI (Osaka Univ.)
Richard BOYD (Ohio State Univ.)
Yang SUN (Shanghai Jiao Tong University)
NicolasDe SEREVILLE (IPN-Orsay)
Alian COC (C.N.R.S)
David DEAN (Oak Ridge National Univ.)
Thomas PAPENBROCK (Univ. of Tennessee)
Alinka LEPINE (The Univ. of Sao Paulo)
Zhendong WU (China Institute of Atomic Energy)
Chengjian LIN (China Institute of Atomic Energy)
Takashi ABE (Univ. of Tokyo)
MarcoLa COMMARA (Univ. of Napoli)

Claudio SPITALERI (Catania Univ.)
Livius TRACHE (Texas A&M Univ.)
Aurora TUMINO (Catania Univ.)
Alexander MURPHY (Univ. of Edinburgh)
Fairouz HAMMACHE (IPN-Orsay)
Philip WOODS (Univ. of Edinburgh)
Jiansong WANG (Inst. of Modern Physics, Chinese Academy of Sciences (IMP, CAS))
Hongwei WANG (SINAP)
Rudrajyoti PALIT (Tata Institute of Fundamental Research)
Bing GUO (China Institute of Atomic Energy)
Youbao WANG (China Institute of Atomic Energy)
Zhengguo HU (Chinese Academy of Science)
Meng WANG (Chinese Academy of Science)
Jingen CHEN (Chinese Academy of Science)
Nigel ORR (CEAN)
Roman GERNHAUSER (Technische Universität München, TUM)
Shengquan YAN (China Institute of Atomic Energy)
MarquesMiguel MORENO (CEAN)
Changbum MOON (Hoseo Univ.)
Remco ZEGERS (Michigan State Univ.)
Se-Hwan PARK (KAERI)
David JENKINS (The Univ. of York)
Setepane GREVY (GANIL)
Lucia CACERES (GANIL)
F.A. BECK
Alexey KORSHENINNIKOV (Kurchatov Institute)
Masahiro NOTANI
Kazuyoshi KURITA (Rikkyo Univ.)
Naohito IWASA (Tohoku Univ.)
Yoshiteru SATO (Seoul National Univ.)
Takayuki YAMAGUCHI (Saitama Univ.)
Yutaka WATANABE (KEK)
Chongcheoul YUN (Jyungang Univ.)
Tadanori MINAMISONO (Fukui University of Tech.)
Yasuki NAGAI (JAEA)
Hiroyuki OKAMURA (RCNP Osaka Univ.)
Kichiji HATANAKA (Osaka Univ.)
Yoshiro TAGISHI
Hideyuki SAKAI (Tokyo Univ.)
Yoshitaka FUJITA (Osaka Univ.)
Hiroari MIYATAKE (KEK)
Zsolt FULOP (Hungarian Academy of Science)

Sadao MOMOTA (Kouchi Univ. of Technology)
Takeshi SUZUKI (Saitama Univ.)
Jun HASEGAWA (Tokyo Institute of Technology)
Tadayuki TAKAHASHI
Yoshihide FUCHI (KEK)
Kazuo IEKI (Rikkyo Univ.)
Shintaro NAKAYAMA (Tokushima Univ.)
Tsuneyasu MORIKAWA (Kyusyu Univ.)
Harutaka SAKAGUCHI (Miyazaki Univ.)
Seigo KATO (Yamagata Univ.)
Mitsunori FUKUDA (Osaka Univ.)
Masahiko TANAKA (KEK)
Takashi NAKAMURA (Tokyo Institute of Technology)
Atsuko ODAHARA (Osaka Univ.)
Alberto MENGONI (JAXA)
Atsushi TAMII (Osaka Univ.)
Takashi TERANISHI (Kyusyu Univ.)
Tetsuro ISHII (JAEA)
Dombradi DOMBRADI (ATOMKI)
Takashi MIYASHI
Takao SAKAGUCHI (Brookhaven National Laboratory)
HongKhiem HONG (VAST)
Evgueni KUZMIN (Kurchatov Institute)
Evgueni NIKOLSKI (Kurchatov Institute)
Alexey OGLOBLIN (Kurchatov Institute)
GurgenTer AKOPYAN (Joint Institute for Nuclear Research)
Shigeru ISHIMOTO (KEK)
Dimitra PIERROUTSAKOU (INFN)
Shuwei XU
Cosimo SIGNORINI (Padova Univ.)
Takashi WAKUI (Tohoku Univ.)
Tomoko MIYAGISHI (National Cancer Center)
Nobuaki IMAI (KEK)
Yukie MAEDA (Miyazaki Univ.)
Kentaro YAKO (Tokyo Univ.)
Tao ZHENG (Peking Univ.)

Student Trainees

Keisuke ITOH (Saitama Univ.)
Ryohei MATSUMIYA (Osaka Univ.)
Kim ARAM (Ewaha Woman's Univ.)
Syumpei NOJI (Tokyo Univ.)
Tomomi KAWAHARA (Toho Univ.)

Livio LAMIA (Univ. of Catania)
Maria SERGI (Univ. of Catania)
Vincenzo CRUCILLA (Univ. of Catania)
Chen JUN (Mc Master Univ.)
Kunihiko TAJIRI (Osaka Univ.)
Hyo-Soon JUNG (Chung-Ang Univ.)
Kiana SETOODEHN (Mc Master Univ.)
Yoshiaki NAKAYAMA (Tokyo Institute of Technology)
Daiki NISHIMURA (Osaka Univ.)
Ayako SASAKI (Tohoku Univ.)
Kana TANAKA (Tokyo Institute of Technology)
Nobuyuki KOBAYASHI (Tokyo Institute of Technology)
Kousuki NAMIHIRA (Saitama Univ.)
Isao HACHIUMA (Saitama Univ.)
Sebastiana PUGLIA (Univ. of Catania)
Gabor KISS (University of Debrecen & ATOMIKI)
Takashige HONDA (Rikkyo Univ.)
Masayuki KAZATO (Osaka Univ.)
Mi-Hee NAN (Ewaha Woman's Univ.)
Nam-Hee LEE (Ewaha Woman's Univ.)
Anna TAKASHIMA (Osaka Univ.)
Masaki SUGA (Osaka Univ.)
Yosuke KAWADA (Tokyo Institute of Technology)
Naoki TANAKA (Tokyo Institute of Technology)
Shigeki DEGUCHI (Tokyo Institute of Technology)
Naoto KUME (Tohoku Univ.)
Yuta HARA (Rikkyo Univ.)
Yuichi MATSUURA (Meiji Univ.)
Sayaka IZUMI (Tohoku Univ.)
Hiroyuki OUCHI (Tohoku Univ.)
Tomonori SUZUKI (Tohoku Univ.)
Kensuke UCHIDA (Tohoku Univ.)
Yuichi NAMIKI (Niigata Univ.)
Yuki OHKUMA (Niigata Univ.)
Shinji SUZUKI (Niigata Univ.)
Ngyuen THO (Graduate School, OP, VAST)
Kyoko YAMAGUCHI (Osaka Univ.)
Kanao YAMAGUCHI (Tsukuba Univ.)
Toru SAITO (Miyazaki Univ.)
Yosuki ITO (Osaka Univ.)
Yo KENMOKU (Osaka Univ.)
Masaaki TACHI (Rikkyo Univ.)
Kensuki TANAKA (Rikkyo Univ.)

Anna SHIBUYA (Toho Univ.)
Sotaro OSHIMA
Yunju LI (Institute of Modern Pysics)
Jun SU (Institute of Modern Pysics)
Shiwei XU (Institute of Modern Pysics)
Jun HU (Institute of Modern Pysics)
Masayuki NAGASHIMA (Niigata Univ.)
Yuta MIURA (Tohoku Univ.)
Yuki KATO (Meiji Univ.)
Koutaro TAKAHASHI (Tokyo Institute of Technology)
Takayuki SAKO (Tokyo Institute of Technology)
Riyato KAMBAYASHI (Rikkyo Univ.)
Takahiro NISHIGUTI (Aoyama Gakuin Univ.)
Yudai ICHIKAWA (Kyoto Univ.)
John CAPPINO (Mc Master Univ.)
Duy NGUYEN (Vietnamese Academy of Science and Technology)
Keishun YAMAMURA (Fukui Univ. of Technology)

Visiting Technician

HenriPatrice GANGNANT
PatriceJean-Francois LIBIN
VincentCharles SPITAEELS

Secretary

Emiko ISOGAI

RIBF Research Division Radioactive Isotope Physics Laboratory

1. Abstract

This laboratory explores exotic nuclear structures and dynamics in exotic nuclei that have never been investigated before, such as those with largely imbalanced proton and neutron numbers. Our aim is to develop new experimental techniques utilizing fast RI beams to discover new phenomena and properties in exotic nuclei. Another important subject is the equation-of-state in asymmetric nuclear matter, and its association with the origin of elements and with neutron stars. For instance, we are making attempts to the better understand underlying mechanism for exotic stability-enhancements of very neutron-rich fluorine isotopes, the large deformation of the nucleus ^{34}Mg with $N=22$ in spite of its vicinity to the $N=20$ magic neutron number and anomalous collectivity in ^{16}C . We are further extending these studies to medium- and heavy-mass regions by developing facilities, detectors and unique methods at RIBF, thereby leading on the challenging task to find new exotic phenomena. We also perform numerical simulations of nucleosynthesis under the environment of core-collapse supernovae, and moreover quest for footprints of supernovae and solar activities in the past, embedded in Antarctic ice core.

2. Major Research Subjects

- (1) Study of structure and dynamics of exotic nuclei through developments of new tools in terms of reaction- and technique-based methodology
- (2) Research on EOS in asymmetric nuclear matter via heavy-ion induced reactions
- (3) Promotion of nuclear astrophysics in an interdisciplinary organization
- (4) Detector developments for spectroscopy and reaction studies

3. Summary of Research Activity

(1) Missing mass method

Missing mass technique is promising for future radioactive isotope programs at RIBF. Detection of recoil particles from target is essential in excitation energy determination of particle unbound states without any assumption of particle- and gamma-decay processes, and also giving us transfer angular momentum from the angular distribution measurement. We have developed a solid hydrogen target as well as a detector system called ESPRI for proton-(in)elastic scattering. In 2009, the ESPRI system was exported to GSI to perform an experiment. In addition, we prepared a first missing mass experiment at RIBF, where the start-of-art detector MUST2 will be invited from France. A result obtained from spectroscopy on ^{12}O with MUST2 at GANIL was published in PRL.

(2) In-beam gamma spectroscopy

In the medium and heavy mass region explored at RIBF, collective natures of nuclei are one of important subjects, which are obtained through production and observation of high excited and high spin states. To populate such states, heavy-ion induced reactions such as fragmentation, fission are useful. So far, we have developed two-step fragmentation method as an efficient method to identify and populate excited states, and lifetime measurements to deduce transition strength. At the end of 2008, the first spectroscopy on nuclei island-of-inversion region was performed and the result on the first excited state in ^{32}Ne was published in PRL in 2009. At the end of 2009, the second campaign of in-beam gamma spectroscopy was organized and

backgrounds originating from atomic processes in heavy target were investigated.

(3) Decay spectroscopy

Beta- and isomer-spectroscopy is an efficient method for studying nuclear structure, especially for non-yrast levels. We had accumulated experimental techniques at the RIPS facility to investigate nuclear structure in light mass region via beta-gamma and beta-p coincidence. Concerning the medium and heavy mass region available at RIBF, we have developed two position-sensitive active-stoppers to achieve low-background via position correlation; strip-silicon detectors and a cylindrical active stopper called CAITEN. At the end of 2009, the first decay spectroscopy on neutron-rich nuclei with $A \sim 100$ was performed at the new facility of RIBF. At the same time, the CAITEN detector was successfully tested with fragments produced with a ^{48}Ca beam.

(4) Equation-of-state via heavy-ion central collisions

Equation-of-state in asymmetric nuclear matter is one of major subjects in physics of exotic nuclei. Concerning RIBF programs, a detector for pions produced in heavy-ion collisions is being tested at the HIMAC. In addition, a TPC for the SAMURAI spectrometer is being designed.

(5) Interdisciplinary study for nuclear astrophysics

To understand the origin of elements beyond iron, interdisciplinary works are important in linking data from nuclear physics program. We are promoting simulation of nucleosynthesis in the r-process path, and investigation of Antarctic ice core to search for footprints of supernovae as well as solar activity in the past via mass spectrometer, to link data obtained from nuclear physics program.

Head

Hiroyoshi SAKURAI

Members

Takashi ICHIHARA

Takashi KISHIDA

Yoichi NAKAI

Shunji NISHIMURA

Hideaki OTSU

Heiko SCHEIT

Nishina Center Researcher

Yuko MOTIZUKI

Research Associate

Hiroshi WATANABE

Satoshi TAKEUCHI

Mizuki NISHIMURA

Special Postdoctoral Researcher

Maya TAKECHI
Satoshi SAKAGUCHI

Foreign Postdoctoral Researcher

David STEPPENBECK
Zhihuan LI

Senior Visiting Scientist

Wolfgang MITTIG (Michigan State University, USA)

Visiting Scientists

Sachiko AMARI (Washington Univ., USA)
Koichiro ASAHI (Tokyo Institute of Technology)
Sudhee BANERJEE (Variable Energy Cyclotron Center, India)
Xiangzhou CAI (Shanghai Inst. Applied Physics, China)
Junsei CHIBA (Tokyo University of Science)
Alfred DEWALD (Univ. Cologne Insti. Nucl. Phys.)
Deqing FANG (Shanghai Inst. Applied Physics, China)
Adrian GELBERG (Univ. zu Koeln Inst. Fur Kern Physik, Germany)
Wei GUO (Shanghai Inst. Applied Physics, China)
Kaoru HARA (University of Tsukuba)
Steven KARATAGLIDIS (Rhodes Univ., South Africa)
Hiroyuki KOURA (JAEA)
Yugang MA (Shanghai Inst. Applied Physics, China)
Hideki MADOKORO (Mitsubishi Heavy Industries, Ltd)
Masayuki MATSUO (Grad. Sch. of Sci. and Tech., Niigata Univ.)
Tetsuya MURAKAMI (Kyoto Univ.)
Jiro MURATA (Rikkyo Univ.)
Tetsuo NORO (Kyusyu Univ. Fac. of Sci.)
Akira ONO (Tohoku Univ.)
Naohiko OTSUKA (International Atomic Energy Agency, Austria)
YURI PENIONZHKEVICH (Flerov Lab. Nucl. Reactions, JINR, Russia)
Simona SCHEIT (Univ. of Tokyo)
Toshiyuki SUMIKAMA (Tokyo University of Science)
Takahiro TACHIBANA (Waseda High Sch., Waseda Univ.)
Kohji TAKAHASHI (Universite Libre de Bruxelles, Belgium)
Noboru TAKIGAWA (Fac. of Sci., Tohoku Univ.)
Oleg TARASOV (MSU, NSCL, USA)
Ryouichi WADA (Texas A&M Univ., USA)
Juzo ZENIHIRO (Grad. Sch. of Sci., Kyoto Univ.)
Shuangquan ZHANG (Peking Univ., China)
Yumin ZHAO (Shanghai Jiao Tong Univ.)

Contract Researcher

Yasuyuki GONO

Students

Junior Research Associate

Takamasa KUBOKI

Student Trainees

Shoichiro EBESU (Kyoto Univ.)

Yuhei HASHIZUME (Tsukuba Univ.)

Maki HATA (Rikkyo Univ.)

Chihiro ISHII (Tokyo University of Science)

Yoshihiko IWAO (Kyoto Univ.)

Hiroaki MATSUMOTO (Kyoto Univ.)

Minori NIITA (Rikkyo Univ.)

Ken-ichiro OGAWA (Tsukuba Univ.)

Kensuke OKADA (Rikkyo Univ.)

Akio SHIRAKI (Tokyo Univ.)

Daisuke SUZUKI (Tokyo Univ.)

Hirotake TAKAHASHI (Shinsyu Univ.)

Nobuya UEMATSU (Tokyo University of Science)

Hideakira YOSHII (Tokyo University of Science)

Kenta YOSHINAGA (Tokyo University of Science)

IPA

Kuoang LI (Peking Univ., China)

Visiting Researcher

Pieter DOORNENBAL (JSPS Fellow)

Mattias LANTZ (JSPS Fellow)

Secretary

Tomoko FUJII (Temporary staff)

RIBF Research Division Superheavy Element Laboratory

1 Abstract

The elements with their atomic number $Z > 103$ are called as trans-actinide or superheavy elements. The chemical properties of those elements have not yet been studied in detail. Those elements does not exist in nature therefore, they must be produced artificially for scientific studies. In our laboratory, we have been studying the physical and chemical properties of the superheavy elements utilizing the accelerators in RIKEN and various methods of efficient production for the superheavy elements.

2 Major Research Subjects

- (1) Search for new superheavy elements
- (2) Decay spectroscopy of the heaviest nuclei
- (3) Study of the chemical properties of the heaviest elements
- (4) Study of the reaction mechanism of the fusion process (theory)

3 Summary of Research Activity

- (1) Searching for new elements

To expand the periodic table of elements and the nuclear chart, we will search for new elements.

- (2) Spectroscopic study of the nucleus of heavy elements

Using the high sensitivity system for detecting the heaviest element, we plan to perform a spectroscopic study of nuclei of the heavy elements.

- (3) Chemistry of superheavy elements

Study of chemistry of the trans-actinide (superheavy element) has just started world-wide, making it a new frontier in the field of chemistry. Relativistic effects in chemical property are predicted by many theoretical studies. We will try to develop this new field.

- (4) Study of a reaction mechanism for fusion process

Superheavy elements have been produced by complete fusion reaction of two heavy nuclei. However, the reaction mechanism of the fusion process is still not well understood theoretically. When we design an experiment to synthesize nuclei of the superheavy elements, we need to determine a beam-target combination and the most appropriate reaction energy. This is when the theory becomes important. We will try to develop a reaction theory useful in designing an experiment by collaborating with the theorists.

Head

Kosuke MORITA

Members

Hiromitsu HABA

Kouji MORIMOTO

Nishina Center Researcher

Daiya KAJI

Research Associate

Yoshitaka KASAMATU

Special Postdoctoral Researcher

Kazutaka OZEKI

Yuki KUDOU

Contract Technical Scientist

Akira YONEDA

Visiting Scientists

Kazuhiko AKIYAMA (Tokyo Metropolitan Univ.)

Masato ASAI (Japan Atomic Energy Agency)

Shin-ichi GOTO (Niigata Univ.)

Kouichi HAGINO (Tohoku Univ.)

Kentaro HIROSE (Tohoku Univ.)

Hidetoshi KIKUNAGA (Osaka Univ.)

Hisaaki KUDO (Fac. Sci., Niigata Univ.)

Yuichiro NAGAME (Japan Atomic Energy Agency)

Tetsuya MURAKAMI (Grad. Sch. Sci., Kyoto Univ.)

Minoru SAKAMA (Tokushima Univ.)

Tsutomu Ohtsuki (Tohoku Univ.)

Atsushi SHINOHARA (Osaka Univ.)

Nozomi SATO (Japan Atomic Energy Agency)

Tetsuya SATO (Japan Atomic Energy Agency)

Keisuke SUEKI (Grad. Sch. Pure Appl. Sci., Univ. Tsukuba)

Fuyuki TOKANAI (Dept. Phys., Yamagata Univ.)

Atsushi TOYOSHIMA (Japan Atomic Energy Agency)

Kazuaki TSUKADA (Japan Atomic Energy Agency)

Akihiko YOKOYAMA (Dept. Chemi., Kanazawa Univ.)

Takashi YOSHIMURA (Osaka Univ.)

Research Consultants

Takashi INAMURA

Kenji KATORI

Toru NOMURA

Students

Junior Research Associate

Student Trainees

Takayuki SUMITA (Tokyo Univ. of Science)
Mikio ARAKI (Dept. Chem., Kanazawa Univ.)
Kazuhiro OOE (Osaka Univ.)
Yukiko KOMORI (Osaka Univ.)
Ai KURIYAMA (Osaka Univ.)
Yuki KIKUTANI (Osaka Univ.)
Hideki KAIYA (Kanazawa Univ.)
Yuki TAKEDA (Kanazawa Univ.)
Reona TAKAYAMA (Osaka Univ.)
Hiroyuki FUJISAWA (Osaka Univ.)
Ryutaro SAKAI (Saitama Univ.)
Keita MAYAMA (Yamagata Univ.)
Mirei TAKEYAMA (Yamagata Univ.)
Saori NAMAI (Yamagata Univ.)

RIBF Research Division

Accelerator Group (Group Director : Osamu KAMIGAITO)

Accelerator R&D Team

1. Abstract

We are developing the key hardware in upgrading the RIBF accelerator complex. Firstly we are developing the challenging superconducting coils for the new 28 GHz ECR ion source which is being developed in order to increase the intensity of uranium beam. We are designing LEBT (Low Energy Beam Transport) which transport the high power beam from the ion source to the next injector linac. Correct estimations of neutralization of space charge forces are hard task. Finally we are developing long-lived charge stripper foils which are installed to breed the ion charges for reduction of their magnetic rigidities. We are also developing gas or window-less liquid lithium strippers.

2. Major Research Subjects

- (1) Development of superconducting technology in acceleration system.
- (2) Development of the LEBT(Low Energy Beam Transport) and the new injector for the high power beams.
- (3) Development of charge strippers for high power beams (foil, gas, liquid)

3. Summary of Research Activity

- (1) Development of superconducting technology in acceleration system.

Ohnishi, J.

We are developing the challenging superconducting magnets for the 28GHz ECR ion source. We just started to study the possibility of the superconducting cavity in the RIBF accelerator complex.

- (2) Development of the LEBT (Low Energy Beam Transport) and the new injector for the high power beams.

Sato, Y., Okuno, H.,

We are developing the LEBT for the ion beams from the new 28GHz ion source. We are also studying space charge effects in the new injector for the RIBF accelerator complex.

- (3)Development of charge strippers for high power beams (foil, gas, liquid)

Hasebe, H., Kuboki, H., Yokouchi, S., Okuno, H.,

We are developing the long lived charge stripper for high power ion beams. Foils, gas and liquid for the strippers are being studied in parallel.

Team Leader

Hiroki OKUNO

Members

Jun-ichi OHNISHI

Nishina center engineer

Hiroo HASEBE

Contract Researcher

Hironori KUBOKI

Yoichi SATO

Visiting Scientists

Noriyosu HAYASHIZAKI (Tokyo Institute of Technology)

Mitsuhiro FUKUDA (RCNP, Osaka Univ.)

Andreas ADELMANN (PSI, Switzerland)

Research Consultants

Yoshiaki CHIBA

Hiroshi FUJISAWA

Shigeru YOKOUCHI

Students

Student trainees

Hiroaki MATSUBARA (Grad Sch. Sci., Osaka Univ.)

RIBF Research Division

Accelerator Group (Group Director : Osamu KAMIGAITO)

Ion Source Team

1. Abstract

Our aim is to operate and develop the ECR ion sources for the accelerator-complex system of the RI Beam Factory. We focus on further upgrading the performance of the RI Beam Factory through the design and fabrication of a superconducting ECR heavy-ion source for production of high-intensity uranium ions.

2. Major Research Subjects

- (1) Operation and development of the ECR ion sources
- (2) Development of a superconducting ECR heavy-ion source for production of high-intensity uranium ions

3. Summary of Research Activity

- (1) Operation and development of ECR ion sources

T. Nakagawa, M. Kidera, Y. Higurashi, H. Haba, T. Kageyama and A. Goto

We routinely produce and supply various kinds of heavy ions such as zinc and neon ions for the super-heavy element search experiment as well as uranium ions for RIBF experiments. We also perform R&D's to meet the requirements for stable supply of high-intensity heavy ion beams.

- (2) Development of a superconducting ECR ion source for use in production of a high-intensity uranium beam

T. Nakagawa, J. Ohnishi, M. Kidera, Y. Higurashi, H. Haba and A. Goto

The RIBF is required to supply uranium beams with very high intensity so as to produce RI's. We have designed and are fabricating an ECR ion source with high magnetic field and high microwave-frequency, since the existing ECR ion sources have their limits in beam intensity. The coils of this ion source are designed to be superconducting for the production of high magnetic field. We are also designing the low-energy beam transport line of the superconducting ECR ion source.

Team Leader

Takahide Nakagawa

Members

Hiromitsu HABA

Tadashi KAGEYAMA

Contract Researcher

Yoshihide HIGURASHI

Masanori KIDERA

Visiting Scientists

Takehiro MATSUSE (Fac. Text. Sci. Technol., Shinshu Univ.)

RIBF Research Division

Accelerator Group (Group Director : Osamu KAMIGAITO)

RILAC Team

1. Abstract

The operation and maintenance of the RIKEN Heavy-ion Linac (RILAC) have been carried out. There are the two modes, the standalone mode, in which the beam is delivered directly to the low-energy beam user in the RILAC, and the injection mode, in which the RILAC beam is injected to the RIKEN Ring Cyclotron (RRC). The RILAC is composed of two ion sources, the frequency-variable RFQ linac, six frequency-variable cavities, and six energy booster cavities (CSM). The maintenance of these devices is important to keep the long-term stability of RILAC beams.

2. Major Research Subjects

- (1) The long term stability of the RILAC operation.
- (2) Improvement of efficiency of the RILAC operation.

3. Summary of Research Activity

The RIKEN Heavy-ion Linac (RILAC) is a frequency-tunable linac. The RILAC is composed of two Heavy-ion ECR ion sources, RFQ linac, six main cavities, and six energy booster cavities. Thousands hours are spent in a year for delivering many kinds of heavy-ion beams to various experiments.

The RILAC has two operation modes: the stand-alone operation delivering low-energy beams directly to experiments and the injection mode operation supplying beams into the RIKEN Ring Cyclotron (RRC). In the first mode, the RILAC supplies very important beam to the nuclear physics experiment of “the research of super heavy elements”. In the second mode, the RILAC plays very important role as upstream end of the RIBF accelerators.

The maintenance is very important in order to keep the high quality performance of the RILAC. Improvements are always carried out for the purpose of more efficient operation.

Team Leader

Eiji IKEZAWA

Member

Yutaka WATANABE

Shigeaki ARAI

Research Consultants

Toshiya CHIBA

Masatake HEMMI

Yoshitoshi MIYAZAWA

RIBF Research Division

Accelerator Group (Group Director : Osamu KAMIGAITO)

Cyclotron Team

1. Abstract

Together with other teams of Nishina Center accelerator division, maintaining and improving the RIBF cyclotron complex. The accelerator provides high intensity heavy ions. Our mission is to have stable operation of cyclotrons for high power beam operation. Recently stabilization of the rf system is a key issue to provide 10 kW heavy ion beam.

2. Major Research Subjects

- (1) RF technology for Cyclotrons
- (2) Beam-RF correlation analysis
- (4) Maintenance and improvement of RIBF cyclotrons and linacs.
- (5) Design and construction of new injector linac.
- (6) Single turn operation for polarized deuteron beams.

3. Summary of Research Activity

Development of the rf system for a stable operation.

Improvement and maintenance of rf devices.

Correlation analysis between rf and beam.

Team Leader

Naruhiko SAKAMOTO

Members

Research Associate

Kenji SUDA

RIBF Research Division

Accelerator Group (Group Director : Osamu KAMIGAITO)

Beam Dynamics and Diagnostics Team

1. Abstract

In order to realize stable and efficient operations of RIBF accelerator complex, various improvements including beam diagnosis, computer control, power supplies have been performed. Our final goal is to establish simulation-based operation of RIBF accelerator complex.

2. Major Research Subjects

- (1) Improvement on the beam transmission along the multi-stage accelerator system.
- (2) Development of beam diagnosis.
- (3) Development of computer control.
- (4) Establishment of long-term stabilities of magnet and magnet power supplies.

3. Summary of Research Activity

- (1) Development of the beam diagnostic technology

We have improved existing beam intensity monitors (Faraday cup) for precise measurements of heavy ions like uranium. In addition, non-destructive beam intensity monitor using SQUID have been developed. These modifications resulted in a great improvement of beam transmission efficiency.

- (2) Development of the computer control system of accelerator

EPICS-based control system and a home-made beam interlock system have been stably operated. We also applied embedded EPICS system on F3RP61-2L to our new injector system RILAC2.

- (3) Stability tests of old power supplies

We tested long-term stabilities of old power supplies used for more than twenty years to realize stable operation of accelerator complex.

- (4) New injector system RILAC2

Team Leader

Nobuhisa FUKUNISHI

Members

Masaki FUJIMAKI

Sachiko ITO

Keiko KUMAGAI

Tamaki WATANABE

Contract Technical Scientist

Misaki KOBAYASHI-KOMIYAMA

Kazunari YAMADA

Hiroshi WATANABE

Makoto NAGASE

Visiting Scientists

Hikomichi RYUTO (Photonics and Electronics Science and Engineering Center,
Kyoto Univ.)

Jun-ichi ODAGIRI

Yuichiro SASAKI

Research Consultants

Jiro FUJITA

RIBF Research Division

Accelerator Group (Group Director : Osamu KAMIGAITO)

Cryogenic Technology Team

1. Abstract

We are operating the cryogenic system for the superconducting ring cyclotron in RIBF. We are operating the helium cryogenic system in the south area of RIKEN Wako campus and delivering the liquid helium to users in RIKEN. We are trying to collect efficiently gas helium after usage of liquid helium.

2. Major Research Subjects

- (1) Operation of the cryogenic system for the superconducting ring cyclotron in RIBF
- (2) Operation of the helium cryogenic plant in the south area of Wako campus and delivering the liquid helium to users in Wako campus.

3. Summary of Research Activity

- (1) Operation of the cryogenic system for the superconducting ring cyclotron in RIBF
Okuno, H., Dantsuka, T., Maie, T.
- (2) Operation of the helium cryogenic plant in the south area of Wako campus and delivering the liquid helium to users in Wako campus.
Dantsuka, T., Odashima, Y., Nakamura, M., Maie, T., Ikegami, K., Okuno., H.

Team Leader

Hiroki OKUNO

Members

Masato NAKAMURA

Nishina Center Engineer

Takeshi MAIE

Technical Staff-I

Tomoyuki DANTSUKA

Research Consultant

Kumio IKEGAMI

Yutaka ODAJIMA

Ken-ici KATO

RIBF Research Division

Instrumentation Development Group (Group Director : Masanori WAKASUGI)

SLOWRI Team

1. Abstract

A next-generation slow radioactive nuclear ion beam facility (SLOWRI) which provides slow, high-purity and small emittance ion beams of all elements is being build as one of the principal facilities at the RIKEN RI-beam factory (RIBF). High energy radioactive ion beams from the projectile fragment separator BigRIPS are thermalized in a large gas catcher cell. The thermalized ions in the gas cell are guided and extracted to a vacuum environment by a combination of dc electric fields and inhomogeneous rf fields (rf carpet ion guide). From there the slow ion beam is delivered via a mass separator and a switchyard to various devices: such as an ion trap, a collinear fast beam apparatus, and a multi-reflection time of flight mass spectrometer. In the R&D works at the present RIKEN facility, an overall efficiency of 5% for a 100A MeV ^8Li ion beam from the present projectile fragment separator RIPS was achieved and the dependence of the efficiency on the ion beam intensity was investigated.

First spectroscopy experiment at the prototype SLOWRI was performed on Be isotopes. Energetic ions of $^{7,10,11}\text{Be}$ from the RIPS were trapped and laser cooled in a linear rf trap and precision spectroscopy was performed. The evaluated ion temperature of <10 mK demonstrates that a reduction of more than 15 orders of magnitude for the kinetic energy of radioactive Be was achieved online. Precise investigation of the hyperfine structure will confirm the anomalous mean radius of the valence neutron of the so called neutron halo nucleus.

Other spectroscopy experiments using the slow RI-beams are also under progress in off-line setups. A collinear fast beam apparatus for nuclear charge radii measurements was build and tested with stable Ar⁺ ion beams. A multi-reflection time-of-flight mass spectrograph was build for precise and fast measurements of short-lived radioactive nuclei. A high mass resolving power of 200,000 has been achieved with a 5 ms measurement period.

An advanced SLOWRI facility is also proposed. The expected number of nuclides which can be investigated at SLOWRI is more than 3000, however, the realistic beam time for each experiment would be very limited. The advanced facility will parasitically provide slow RI-beams everyday as long as the fragment separator BigRIPS is operated. The parasitic beam can be produced from those nuclei dumped at the first focal plane slits of BigRIPS by placing a compact gas catcher cell. The thermalized and neutralized RI in the cell can be re-ionized at the exit of the cell by resonance laser ionization. Development the new scheme, named PALIS, is underway.

2. Major Research Subjects

- (1) Development and construction of the next-generation slow RI-beam facility
- (2) Precision hyperfine spectroscopy of trapped ions for magnetization distribution in a halo nucleus
- (3) Nuclear charge radii measurements using ion trap and collinear fast beam apparatus
- (4) Precision mass measurements of short-lived nuclei using a multi-reflection TOF mass spectrograph
- (5) Development of deceleration and cooling devices for energetic beams using gas cell and rf fields.

- (6) Atomic physics and fundamental symmetry research investigating nuclear decay of an isolated atom
- (7) Development of parasitic slow RI-beam production method using resonance laser ionization.

3. Summary of Research Activity

- (1) Development of universal slow RI-beam facility

WADA, Michiharu, TAKAMINE, Aiko, SCHURY Peter, SONODA, Tetsu, OKADA, Kunihiro, KANAI, Yasuyuki, YOSHIDA, Atsushi, KUBO, Toshiyuki, YAMAZAKI, Yasunori, WOLLNIK, Hermann, SCHUESSLER, Hans, NODA, Koji, OHTANI, Shunsuke, KATAYAMA Ichiro

A next-generation slow radioactive nuclear ion beam facility (SLOWRI) which provides slow, high-purity and small emittance ion beams of all elements is being build as one of the principal facilities at the RIKEN RI-beam factory (RIBF). High energy radioactive ion beams from the projectile fragment separator BigRIPS are thermalized in a large gas catcher cell. The thermalized ions in the gas cell are guided and extracted to a vacuum environment by a combination of dc electric fields and inhomogeneous rf fields (rf carpet ion guide). From there the slow ion beam is delivered via a mass separator and a switchyard to various devices: such as an ion trap, a collinear fast beam apparatus, and a multi-reflection time of flight mass spectrometer. In the R&D works at the present RIKEN facility, an overall efficiency of 5% for a 100A MeV ^8Li ion beam from the present projectile fragment separator RIPS was achieved and the dependence of the efficiency on the ion beam intensity was investigated. An advanced gas cell with cryogenic cooler and an additional rf carpet at the wall of the cell is under development.

- (2) Laser spectroscopy of trapped radioactive beryllium isotope ions

WADA, Michiharu, TAKAMINE, Aiko, SCHURY Peter, SONODA Tetsu, OKADA, Kunihiro, KANAI, Yasuyuki, YOSHIDA, Atsushi, KUBO, Toshiyuki, YAMAZAKI, Yasunori, WOLLNIK, Hermann, SCHUESSLER, Hans, NODA, Koji, OHTANI, Shunsuke, KATAYAMA Ichiro

As a first application of the prototype SLOWRI setup, we are applying hyperfine structure spectroscopy to the beryllium isotopes to determine in particular the anomalous radius of the valence neutron of the neutron halo nucleus ^{11}Be , and to determine the charge radii of these beryllium isotopes through laser-laser double resonance spectroscopy of laser-cooled ions. Laser cooling is an essential prerequisite for these planned experiments. However, the exact resonance frequencies of the cooling transitions for radioactive beryllium isotopes are not known. In such light elements, the isotope shifts in the atomic transitions are larger than several 10 GHz and their dominant parts are due to complicated multi-electron correlations. Some theoretical works on the isotope shifts of the beryllium ion exist, however the values contradict each other at the level of accuracy needed.

The first laser spectroscopy experiments for beryllium isotopes were performed to measure the resonance frequencies of $2s\ ^2S_{1/2} - 2p\ ^2P_{3/2}$ transition of $^7\text{Be}^+$, $^9\text{Be}^+$, $^{10}\text{Be}^+$ and $^{10}\text{Be}^+$ ions and the nuclear charge radii of these Be isotopes were determined. The hyperfine structure of $^{11}\text{Be}^+$ and $^7\text{Be}^+$ ions using the laser-microwave double resonance spectroscopy were also performed and

$A(^7\text{Be}^+) = -742.7723(4)$ MHz and $A(^{11}\text{Be}^+) = -2677.308(2)$ MHz were determined for the first time. Precision measurements of the nuclear magnetic moments of these Be isotopes are under preparation.

(3) Development of a multi-reflection TOF mass spectrograph

WADA, Michiharu, SCHURY Peter, TAKAMINE, Aiko, SONODA Tetsu, OKADA, Kunihiro, WOLLNIK, Hermann,

The atomic mass is one of the most important quantity of a nucleus and has been studied in various methods since the early days of physics. Among many methods we chose a multi-reflection time-of-flight (MR-TOF) mass spectrometer. Slow RI beams extracted from the RF ion-guide are bunch injected into the spectrometer with a repetition rate of ~ 500 Hz. The spectrometer consists of two electrostatic mirrors between which the ions travel back and forth repeatedly. These mirrors are designed such that energy-isochronicity in the flight time is guaranteed during the multiple reflections while the flight time varies with the masses of ions. A mass-resolving power of $>200,000$ has been obtained with about 500 reflections in a 30 cm length spectrometer. This mass-resolving power should allow us to determine ion masses with an accuracy of 10^{-7} . The advantages of the MR-TOF spectrometer are: 1) short measurement periods, typically 2 ms, which allows all neutron rich nuclei to be investigated, 2) the device is compact and its operation is simple, especially, it is independent from the all upstream devices, accelerators and fragment separators, 3) ions of more than isobars can be measured simultaneously, so that mass reference can easily be established in the mass spectra. In total, the number of measurable nuclides within a limited beam time would be larger than that can be achieved by other methods. It should be noted here also that this method can be used even during a low-duty parasite beam time. An on-line MR-TOF mass spectrograph with 80 cm length having an expected mass resolving power of 1,000,000 is under fabrication.

(4) Development of collinear fast beam apparatus for nuclear charge radii measurements

WADA, Michiharu, SCHUESSLER, Hans, IIMURA, Hideki, SONODA, Tetsu, SCHURY, Peter, TAKAMINE, Aiko, OKADA, Kunihiro, WOLLNIK, Hermann,

The root-mean-square charge radii of unstable nuclei have been determined exclusively by isotope shift measurements of the optical transitions of singly-charged ions or neutral atoms by laser spectroscopy. Many isotopes of alkaline, alkaline-earth, noble-gases and several other elements have been measured by collinear laser spectroscopy since these ions have all good optical transitions and are available at conventional ISOL facilities. However, isotopes of other elements especially refractory and short-lived ones have not been investigated so far.

In SLOWRI, isotopes of all atomic elements will be provided as well collimated mono-energetic beams. This should expand the range of applicable nuclides of laser spectroscopy. In the first years of the RIBF project, Ni and its vicinities, such as Ni, Co, Fe, Cr, Cu, Ga, Ge are planned to be investigated. They all have possible optical transitions in the ground states of neutral atoms with presently available laser systems. Some of them have so called recycle transitions which enhance the detection probabilities noticeably. Also the multistep resonance ionization (RIS) method can be applied to the isotopes of Ni as well as those of some other elements. The required minimum intensity for this method can be as low as 10 atoms per second.

We have built an off-line mass separator and a collinear fast beam apparatus with a large

solid-angle fluorescence detector. A 617 nm transition of the metastable Ar⁺ ion at 20 keV was measured with both collinear and anti-collinear geometry that allowed us to determine the absolute resonant frequency of the transition at rest with more than 10⁻⁸ accuracy. Such high accuracy measurements for Ti and Ni isotopes are in progress.

- (5) Development of parasitic slow RI-beam production scheme using resonance laser ionization
WADA, Michiharu, SONODA Tetsu, TAKAMINE, Aiko, OKADA, Kunihiro, MATSUO Yukari, FURUKAWA, Takeshi, KOBAYASHI T., MIYATAKE Hiroari, JEONG Sun Chan, ISHIYAMA, H., IMAI, N., HIRAYAMA Y., KATAYAMA I., TOMITA, H., IIMURA, H., SHINOZUKA T., WAKUI, T., HUYSE, M., VAN DUPPEN, P., KUDRYAVTSEV, Yu., SCHUESSLER, H., WOLLNIK, H.

More than 99.9% of RI ions produced in projectile fission or fragmentation are simply dumped in the first dipole magnet and the slits. A new scheme, named PALIS, to rescue such dumped precious RI using a compact gas catcher cell and resonance laser ionization was proposed. The thermalized RI ions in a cell filled with Ar gas can be quickly neutralized and transported to the exit of the cell by gas flow. Irradiation of resonance lasers at the exit ionizes neutral RI atoms efficiently and selectively. The ionized RI ions can be further selected by a magnetic mass separator and transported to SLOWRI experimental area for spectroscopy experiment. The resonance ionization scheme itself can also be a useful method to perform precision optical spectroscopy of RI of many elements.

An off-line setup for resonance ionization in gas cell is under construction. Several pulsed dye lasers pumped by two excimer lasers are prepared. A gas cell test bench is also under design.

Head

Michiharu WADA

Members

Aiko TAKAMINE

Tetsu SONODA

Peter SCHURY

Kunihiro OKADA

Ichou KATAYAMA

Hideki IIMURA

Hans SCHUESSLER

Hermann WOLLNIK

RIBF Research Division

Instrumentation Development Group (Group Director : Masanori WAKASUGI)

Polarized RI Beam Team

1. Abstract

The team conducts the research and development on the production of spin-oriented radioactive-isotope beams (RIBs), and applies it to the research on nuclear physics, fundamental physics, and material science. The microscopic investigation of physical and chemical processes is performed based on nuclear techniques which takes the advantage of intrinsic nuclear properties and phenomena (spins, electromagnetic moments, decay modes etc.). In particular, the precession/resonance of a polarized/aligned nuclear spin under an external field is observed through a change in the angular distribution of radiation, for the study of nuclear structures via nuclear moments. The experimental methods and devices for fundamental physics research with polarized nuclei have been also developed. The same method, as well as the Mössbauer technique, are used for the investigation of condensed matter such as semiconductor, ferromagnets, fullerenes, systems with dilute magnetic impurities etc. by capitalizing radioactive nuclei as microscopic probes into them. All these research activities are to be extended to wide variety of unstable nuclei which RI Beam Factory (RIBF) provides. A method to produce beams of highly polarized radioactive nuclei, taking full advantage of RIBF, is being developed.

2. Major Research Subjects

- (1) Nuclear-moment measurements of unstable nuclei
- (2) RIPS upgrade and the development of highly polarized slow RI beams
- (3) Fundamental physics: Study of symmetry
- (4) Condensed matter studies using radioactive nuclear probes

3. Summary of Research Activity

- (1) Nuclear-moment measurements of unstable nuclei

It has been revealed in our earlier work that spin-oriented RIBs can be obtained as a function of their outgoing momentum in the projectile-fragmentation reaction. With the obtained spin-polarized nuclei, ground- and excited-state nuclear moments can be determined by means of the β -NMR and TDPAD methods, respectively. Based on these technique, we have recently been conducted the nuclear-moments measurement of neutron-rich *sd*-shell around the neutron magic number $N=20$. It has been proposed in this region that an inversion of amplitudes between the *sd* normal and the *pf* intruder configurations would lead to deformation of the ground states. Thus, the region of nuclei is called the *island of inversion*. The measured nuclear moments are expected to provide microscopic properties for those nuclei of interest. The sub-themes are the following:

- Studies of shell evolution through nuclear-moment measurements of neutron-rich nuclei. The targets are:
 - the neutron-rich aluminum isotopes $^{30-34}\text{Al}$ for the study of the *island of inversion* phenomena around $N=20$,
 - neutron-rich S, P, and Si isotopes for the magicity of $N=28$, and
 - $N\sim 40$ nuclei $^{54\text{m}}\text{Ni}$ and $^{69\text{m}}\text{Cu}$ for the study of isospin symmetry and the magicity.
- Development of a new method to produce highly spin-aligned RIBs through the two-step

fragmentation reaction and its application to the isomeric-state magnetic-moment measurements.

- The ground-state electric quadrupole moment measurement of ^{23}Al for the study of the $T=3/2$ mirror symmetry.

(2) RIPS upgrade and the development of highly polarized slow RI beams

The upgrade of RIPS has been proposed in the phase-II programs. In the cyclotron-cascade acceleration scheme, beams are accelerated up to the energy of $E = 115 A$ MeV with IRC. In this upgrade, the former fragment separator RIPS is equipped with a new beam line that delivers beams of $115 A$ MeV heavy ions from the IRC cyclotron. RI beams produced by the primary beams at such an intermediate energy are high enough to produce RIBs via projectile-fragmentation reactions and suitably low in energy to be stopped in a sample material of limited thicknesses. Compared with the production yield of RIBs in the present AVF-RRC acceleration scheme, they are drastically increased. The design study of the upgrade program is in progress in our team. We noted that RIBs produced at $E = 115 A$ MeV can be spin-oriented so that the nuclear-moment measurements will be further conducted. Also, combining a new atomic-beam resonance method to combine with fragmentation-based RI beams, which is under development, to this program, highly spin-polarized RI beams will be produced in a low beam-energy region. Then, they could be useful not only for nuclear-moment measurements but also for spin-related subjects in nuclear physics, fundamental physics, and material sciences.

(3) Fundamental physics: Study of symmetry

Nuclear spins of stable and unstable isotopes sometimes play important roles in fundamental physics research. New experimental methods and devices have been developed for studies on the violation of time reversal symmetry (T -violation) using spin-polarized nuclei. These experiments aim detection of small frequency shift of the spin precession or measurement of the T -odd angular correlation in β -decay as T -violating signals arising from new mechanisms beyond the “Standard Model”. Sub-themes are the following:

- Precision measurement of spin-precession frequency with a new type of the nuclear spin maser for atomic EDM (Electric Dipole Moment) search.
- Development of a new Mott polarimeter for T -violation experiment using β -decay of polarized unstable nuclei.

(4) Condensed matter studies using radioactive nuclear probes

Utilizing RI beams as a probe, online Mössbauer spectroscopy and online perturbed angular correlation experiments have been carried out through the γ -ray measurements. The microscopic structures, dynamics in ferromagnets, and properties of semiconductors have been investigated from the deduced internal local fields and the spin relaxation of the probe in materials. The β -NMR/NQR method is also utilized for these condensed matter studies. The methods and apparatus have been developed. Also, basic studies on the probe nuclei have been carried out. Sub-themes are the following:

- Study of “exotic” chemical states and the fast atomic-jump processes in solid with the online Mössbauer spectroscopy of implanted ^{57}Fe
- Development of the on-line perturbed angular-correlation method with ^{19}O beams as a new probe
- Study of the diffusion and segregation of Fe impurity atoms in Si through in-beam

Mössbauer experiment with a Coulomb excited, recoil implanted ^{57}Fe nuclei.

- Study of the fast diffusion of Cu impurity atoms in Si through β -NMR/NQR with implanted ^{58}Cu .

Team Leader

Hideki UENO

Members

Akihiro YOSHIMI

Yuichi ICHIKAWA

Yoshio KOBAYASHI

RIBF Research Division

Instrumentation Development Group (Group Director : Masanori WAKASUGI)

Rare RI-ring Team

1. Abstract

We are developing the isochronous storage ring to measure the mass for rare radioactive isotopes (Rare RI ring). It is assumed that uranium is synthesized by neutron capture process after the supernovae explosion (r-process). To prove r-process, mass measurements for the rare RI are indispensable. To deduce the mass, we measure the circulation time (cyclotron frequency) for the rare RI inside the ring. RI beams produce in RIBF have some energy spread. To compensate the spread, isochronicity inside the ring is indispensable (isochronous storage ring). We will inject the rare RI one by one to the ring (individual injection) to identify the RI event-by-event.

2. Major Research Subjects

Developments of isochronous storage ring to measure mass of rare RI.

3. Summary of Research Activity

Developments of isochronous storage ring to measure mass of rare RI.

The conceptual design for an isochronous storage ring has been finalized in this year. To minimize construction cost, we plan to use the SHARQA beam line as an injection beam transport line for the isochronous ring and re-use TARN-II bending magnets, which have been moved from KEK, as main components of the ring. R&D study of quick activated kicker magnet system required for one by one injection has been started, and the feasibility will be demonstrated in next year. Another important item in the ring is schottki beam monitor, which observes single ion circulating the ring. It is now under designing, and it will be manufactured in next year and installed in the HIMAC for test experiment.

Team Leader

Masanori WAKASUGI

Research Associate

Yoshitaka YAMAGUCHI

JRA

Shinpei NAKAJIMA (Saitama University)

Tetsuaki MORIGUCHI (University of Tsukuba)

Visiting Scientists

Akira OZAWA (Inst. Phys., Univ. of Tsukuba)

Yusuke YASUDA (Inst. Phys., Univ. of Tsukuba)

Ichiro ARAI (Inst. Phys., Univ. of Tsukuba)

Takeshi SUZUKI (Saitama University)

Takayuki YAMAGUCHI (Saitama University)
Takashi KIKUCHI (Nagaoka University of Technology)
Daisuke NAGAE (Inst. Phys., Univ. of Tsukuba)

RIBF Research Division

Instrumentation Development Group (Group Director : Masanori WAKASUGI)

SCRIT Team

1. Abstract

We aim at the investigation of internal nuclear structure of short-lived radioactive nuclei (RI) by means of electron scattering. Electron scattering for RI's has never been performed due to inability to make target of these nuclei. An electron-RI collider system, which requires a huge accelerator complex, has so far been unique solution to overcome the difficulty. We have developed a novel internal target system named SCRIT (Self-Confining RI Ion Target) in an electron storage ring to make the experiment easier with much compact experimental system. An electron accelerator system required in this experiment has been constructed in this year, and it is under commissioning. The SCRIT device, which will be installed in the accelerator, has also been manufactured.

2. Major Research Subjects

Development of the SCRIT technology and electron scattering for unstable nuclei.

3. Summary of Research Activity

Development of a novel internal target of unstable nuclei (SCRIT) in an electron storage ring for electron scattering experiment.

(Wakasugi, Miyashita, Kurita, Suda, Tamae, Hori, Hara)

We have constructed an electron accelerator system, which consists of an injector microtron (RTM) and a storage ring (SR2). The commissioning and machine study is now in progress. The SCRIT (Self-Confining Radioactive Ion Target) device was manufactured in this year and we are now making the preparation for installing to the SR2. In this electron scattering facility, we will construct the U photo-fission ion source for RI production and an ISOL system for RI injection into the SCRIT device. They are now under designing. Detector system for scattered electrons from the SCRIT is also under designing and it will be manufactured in next year. We plan to start the electron scattering experiment for unstable nuclei from the beginning of 2012.

Team Leader

Masanori WAKASUGI

Members

Takashi EMOTO

Special Postdoctoral Researcher

Yuji MIYASHITA

Research Consultant

Shin-ichi ICHIKAWA

Masahiro HARA

Toshitada HORI

Visiting Scientists

Toshimi SUDA (Research Center of Electron Photon Science, Tohoku Univ.)

Tadaaki TAMAE (Research Center of Electron Photon Science, Tohoku Univ.)

Kazuyoshi KURITA (Inst. Phys., Rikkyo Univ.)

RIBF Research Division

Research Instruments Group (Group Director : Toshiyuki KUBO)

GARIS Team

1 Abstract

Development and maintenance of devices related to study of the superheavy elements.

2 Major Research Subjects

- (1) Maintenance and development of recoil separators GARIS and GARIS-II.
- (2) Maintenance and development of a focal-plane detector system and rapid chemistry devices.

3 Summary of Research Activity

- (1) Maintenance and development of recoil separator

A gas-filled recoil separator has been used as a main experimental device for the study of superheavy elements. We will develop and maintain the related devices. We will also offer user-support if a researcher wishes to use the devices for his/her own research program.

- (3) Maintenance and development of focal-plane detectors and devices for fast chemistry

We will develop and maintain the focal-plane detector system for the study of the superheavy elements. We do research and development of devices for fast chemistry of superheavy elements. We also offer user-support for potential users.

Team Leader

Kouji MORIMOTO

Special Postdoctoral Researcher

Daiya KAJI

Contract Technical Scientist

Akira YONEDA

RIBF Research Division

Research Instruments Group (Group Director : Toshiyuki KUBO)

BigRIPS Team

1. Abstract

This team is in charge of design, construction, development and operation of BigRIPS in-flight separator and its related research instruments at RI beam factory (RIBF). They are employed not only for the production of RI beams but also the experimental studies using RI beams.

2. Major Research Subjects

Design, construction, development and operation of BigRIPS in-flight separator, RI-beam transport lines, and their related research instruments

3. Summary of Research Activity

This team is in charge of design, construction, development and operation of BigRIPS in-flight separator, RI-beam transport lines, and their related research instruments such as ZeroDegree spectrometer at RI beam factory (RIBF). They are employed not only for the production of RI beams but also various kinds of experimental studies using RI beams.

The research subjects may be summarized as follows:

- (1) General studies on RI-beam production using in-flight scheme.
- (2) Studies on ion-optics of in-flight separators, including particle identification of RI beams
- (3) Simulation and optimization of RI-beam production.
- (4) Development of beam-line detectors and their data acquisition system.
- (5) Experimental studies on production reactions and unstable nuclei.
- (6) Experimental studies of the limits of nuclear binding.
- (7) Development of superconducting magnets and their helium cryogenic systems.
- (8) Development of a high-power production target system.
- (9) Development of a high-power beam dump system.
- (10) Development of a remote maintenance and remote handling systems.
- (11) Operation, maintenance and improvement of BigRIPS separator system, RI-beam transport lines, and their related research instruments such as Zero Degree spectrometer and so on.
- (12) Experimental research using RI beams.

Team Leader

Toshiyuki KUBO

Members

Naohito INABE

Atsushi YOSHIDA

Koichi YOSHIDA

Masao OHTAKE

Yoshiyuki YANAGISAWA

Contract Researchers

Kensuke KUSAKA
Tetsuya OHNISHI
Naoki FUKUDA
Hiroyuki TAKEDA

Research Associates

Daisuke KAMEDA
Kanenobu TANAKA

Part-time Staff

Hidekazu KUMAGAI

Visiting Scientist

Bradly SHERRILL (NSCL, Michigan State Univ., USA)
Daniel BAZIN (NSCL, Michigan State Univ., USA)
Anthony NETTLETON (NSCL, Michigan State Univ., USA)
Hans GEISSEL (GSI, Germany)
Martin WINKLER (GSI, Germany)
Michael FAMIANO (Western Michigan Univ., USA)
Shashikant MANIKONDA (Argonne National Lab., USA)
Yutaka MIZOI (Osaka Electro-Communication Univ.)
Khiem LEHONG (IOP, Vietnamese Academy for Science and Technology)
Cuong PHANVIET (IOP, Vietnamese Academy for Science and Technology)

RIBF Research Division

Research Instruments Group (Group Director : Toshiyuki KUBO)

SAMURAI Team

1. Abstract

This team is in charge of design, development and construction of the SAMURAI spectrometer that will be used for reaction experiments using RI beams at RI Beam Factory. SAMURAI consists of a large superconducting dipole magnet and a variety of detectors to detect charged particles and neutrons.

2. Major Research Subjects

Design, development and construction of the SAMURAI spectrometer at RI Beam Factory and its related research instruments.

3. Summary of Research Activity

This team is in charge of design, development and construction of the SAMURAI spectrometer at RI Beam Factory. Consisting of a large superconducting dipole magnet and a variety of detectors to detect charged particles and neutrons, SAMURAI will be used for various reaction studies with RI beams.

The research subjects may be summarized as follows:

- (1) Design, development and construction of a large superconducting dipole magnet that will be the main component of the SAMURAI spectrometer.
- (2) Design, development and construction of various detectors that are used for nuclear reaction experiments using the SAMURAI spectrometer.

Team Leader

Toshiyuki KUBO

Members

Hiromi SATO

Ken-ichiro YONEDA

Yohei SIMIZU

Senior Visiting Scientist

Toshio KOBAYASHI (Tohoku University)

RIBF Research Division

Research Instruments Group (Group Director : Toshiyuki KUBO)

Computing and Network Team

1. Abstract

The Computing and Network team is in charge of the development, management, and operation of the computing and networking environment, mail and information servers, and data acquisition system; the team is also responsible for information security management at RIKEN Nishina Center.

2. Major Research Subjects

- (1) Development, management, and operation of general computing servers
- (2) Development, management, and operation of mail and information servers
- (3) Development, management, and operation of the data acquisition system
- (4) Development, management, and operation of the network environment
- (5) Information security management

3. Summary of Research Activity

This team is in charge of the development, management, and operation of the computing and networking environment, mail and information servers, and data acquisition system; further, the team is responsible for information security management. Details of the research activities will be provided later in this progress report.

- (1) Development, management, and operation of general computing servers

We are operating the Linux/Unix NIS/NFS cluster system for analysis of the experimental data and general computing. This cluster system consists of eight computing servers with 28 CPU cores and a 20 TB RAID comprising highly reliable fiber channels (HDD). Approximately 500 user accounts are registered on this cluster system. We have adopted Scientific Linux, which has been developed at Fermi National Laboratory, as the primary operating system. Scientific Linux is widely used by the nuclear physics and high-energy physics communities, as well as in accelerator research facilities worldwide.

The SSH login server is RIBF00.RIKEN.JP. Public-key authentication is used for SSH login to improve information security.

- (2) Development, management, and operation of mail and information servers

We are operating the RIBF.RIKEN.JP mail server. Postfix is used as the mail transport software, and Dovecot is used for IMAP and POP services. These software packages enable secure and reliable mail delivery. Front-end mail servers (RIBFSMTP1/RIBFSMTP2) are used for tagging spam mails and isolating virus-infected mails. Sophos Email Security and Control (PMX) was installed on these servers in March 2008, and since then, it has been functioning satisfactorily and serving the intended purposes. Almost 99% of the spam mails are identified by PMX.

We are operating several information servers such as WWW servers, Wiki servers, indico server, twitter server, Groupware servers, Windows Media streaming servers, and QuickTime streaming servers.

An anonymous ftp server, FTP.RIKEN.JP, is managed and operated at RIKEN Nishina Center. This server has a speed of 10 Gbps and is connected to the Local Area Network (LAN) via a dual-port 10GbE NIC with a PCI Express interface. This server has an average network transfer rate of approximately 50 MBps, and it is one of the most heavily loaded servers at RIKEN. A 26 TB SATA RAID system with a quad-port 8-Gbps fiber channel interface has been added to this server. Major Linux distributions, which include Scientific Linux, CentOS, Ubuntu, Fedora, Debian, OpenSUSE, Mandrake, Slackware, and Vine, are mirrored daily at the ftp server for facilitating high-speed access by the users. The archived data on the server can be accessed by using anonymous ftp, http, and rsync protocols.

(3) Development, management, and operation of the data acquisition system

We are developing a data acquisition system for the RIBF. The functions of this system are network-distributed data processing, hierarchical event building, and parallel readout, which are achieved using the newly developed software and commodity hardware. This system is both versatile and scalable and hence meets the various requirements for RIBF experiments. The system has a maximum data processing capability of around 40 MB/s. We are also developing a time-stamping system with a precision of 10 ns for the RIBF experiments.

(4) Development, management, and operation of the network environment

We have been managing the network environment in collaboration with Advanced Center for Computing and Communications (ACCC). All the Ethernet ports of the information wall sockets are capable achieving Gigabit Ethernet connection (10/100/1000BT). Many (approximately 60) wireless LAN access points have been installed to cover almost the entire area of Nishina Center.

(5) Information security management

It is essential to adopt proper information security measures for information assets. The most important safety measures include (1) protection of information from virus attacks, (2) detection of virus attacks, and (3) recovering information in the event of a virus attack. We are currently involved in information security management at Nishina Center, in collaboration with ACCC.

Team Leader

Takashi ICHIHARA

Member

Yasushi WATANABE

Hidetada BABA

RIBF Research Division

Research Instruments Group (Group Director : Toshiyuki KUBO)

Detector Team

1. Abstract

This team is in charge of development, fabrication, and operation of various detector for nuclear physics experiment in RIKEN Nishina center. Also the team organizes collaboration work for detector technology among related research groups in order to improve mutual share of knowledge and experience with both in the RIKEN and outside RIKEN.

2. Major Research Subjects

- (1) Development of silicon pixel detector.
- (2). Development of high dynamic range preamplifier for silicon strip detector
- (3) Development of readout electronics for time projection chamber
- (4) Muon detector development for high energy hadron reaction experiment.

3. Summary of Research Activity

This team is presently focusing on developments of detectors for RHIC PHENIX experiments and RIBF nuclear experiments.

- (1) Development of silicon pixel detector.

RIKEN, Rikkyo, Kyoto, CNS and KEK group is responsible for the pixel ladder fabrications for the RHIC PHENIX detector upgrade. The ladder is a module which is composed of pixel sensor modules, support frame, and readout bus. These ladders will be installed in 2010 fall and will generate physics data with 100 micron meter resolution for heavy flavor decay vertex identification.

- (2) Development of high dynamic range preamplifier

Coulomb break up experiment at RIBF needs high dynamic range silicon strip detector in order to identify the charged particle from proton to Sn. We propose to use both high gain and low gain preamplifiers. Dual hybrid preamplifiers with discrete devices were developed and proofed the principal. Then an application specific integrated circuit was designed and fabricated by collaboration with KEK and CNS. Also We collaborate Washington University for readout.

- (3) Development of readout electronics for time projection chamber

A time projection chamber will be used for SAMURAI spectrometer. RIKEN and Kyoto group is in charge of the readout electronics. We started the conceptual design.

- (4) Development of the detector with high position resolution and high counting rate

RIBF experiment must have high rate capability to explore low cross section events. We would like to develop such detector by using MICROMEGAS or GEM technology.

- (5) Muon detector development for high energy hadron reaction experiment

Muon detector at the RHIC PHENIX experiments has been upgrading to detecting weak boson in order to explore spin structure of the proton. KEK, RIKEN and Kyoto group is in charge of the electronics for the fast trigger electronics to pick up high momentum muon from W decay and optical alignment system for geometrical alignment.

Team Leader

Toshiyuki KUBO (until June 2009)

Atsushi Taketani (since July 2009)

Members

Ken-ichiro YONEDA

Contract Researcher

Meiko UESAKA

Internship

Yoshiyuki Aoki (Tokyo Metropolitan college of Aeronautical Engineering)

Masataka Masuyama (Tokyo Metropolitan college of Aeronautical Engineering)

RIBF Research Division

Accelerator Applications Research Group (Group Director : Tadashi KAMBARA)

Radiation Biology Team

1. Abstract

Radiation biology team studies various biological effects of fast heavy ions. It also develops new technique to breed plants by heavy-ion irradiations. Fast heavy ions can produce dense and localized ionizations in matters along their tracks, in contrast to photons (X rays and gamma rays) which produce randomly distributed isolated ionizations. These localized and dense ionization can cause double-strand breaks of DNA in cells which are not easily repaired and result in mutation more effectively than single-strand breaks. A unique feature of our experimental facility at the RIKEN Ring Cyclotron (RRC) is that we can irradiate living bodies in atmosphere or in bottles since the delivered heavy-ion beams have energies high enough to penetrate deep in matter. This team utilizes a dedicated beam line (E5B) of the RRC to irradiate cultivated cells, plants and animals with beams ranging from carbon to iron. Its research subjects cover physiological study of DNA repair, genome analyses of mutation, and development of mutation breeding of plants by heavy-ion irradiation. Some new cultivars have already been brought to the market.

2. Major Research Subjects

- (1) Study on the biological effects by heavy-ion irradiation
- (2) Studies on ion-beam breeding and genome analysis
- (3) New medical application of heavy-ion beams

3. Summary of Research Activity

We study biological effects of fast heavy ions from the RIKEN Ring Cyclotron using 135 MeV/N C, N, Ne ions, 95 MeV/N Ar ions and 90 MeV/N Fe ions. We also develop breeding technology of plants. Main subjects are:

- (1) Study and application of heavy-ion induced plant mutation

In contrast to X rays and gamma rays, fast heavy ions are found to be useful for plant breeding since they only cause localized damage on DNA and can induce mutations more effectively with lower dosage. Our team utilizes beams of fast heavy ions from the RIKEN Ring Cyclotron to develop heavy-ion breeding techniques. Genome analyses are performed to reveal the relation between genotype and phenotype.

- (2) Study of heavy ion-induced damage of DNA and its repair processes

We study the double-strand break of DNA induced by heavy-ion irradiation and its repair processes. DNA double strand break (DSB) is characteristic to heavy-ion irradiation and considered to be the characteristic lesion responsible for its biological effects. Cells have two pathways to repair DSB, non-homologous end-joining

(NHEJ) and homologous recombination (HR), and it is unknown how the two pathways are involved in repairing the damage caused by heavy-ion irradiation. To elucidate it, we irradiate higher vertebrate cells lacking DNA repair proteins with C, Ar, or Fe ions and analyze them with colony formation assay and molecular biology methods.

Team Leader

Tomoko ABE

Members

Tomonari HIRANO
Masako IZUMI
Yusuke KAZAMA
Mayu NAKAGAWA
Teruyo TSUKADA

Part-time Staff I

Hideo TOKAIRIN

Technical Staff I

Yoriko HAYASHI

Technical Staff II

Sumie OHBU
Tomiko SHIBUKAWA

Visiting Scientists

Ryutaro AIDA (Natl. Inst. Floricult. Sci.)
Mari AMINO (Tokai University Hospital)
Chang-Hyu BAE (Sunchon Natl. Univ., Korea)
Yasuhiro CHIMI (JAEA)
Hiroyuki DAIMON (Osaka Pref. Univ.)
Ali FERJANI (Tokyo Gakugei Univ.)
Makoto FUJIWARA (Grad. Sch., Col. Arts Sci., Univ. of Tokyo)
Eitaro FUKATSU (Forest tree breeding Cet.)
Koji FURUKAWA (Mukoyama Orchids Co., Ltd.)
Yoshiya FURUSAWA (Natl. Inst. Radiol. Sci.)
Toshinari GODO (Botanic Gardens Toyama)
Misako HAMATANI (Hiroshima City Agric. Forest. Promot. Cen.)
Yasuhide HARA (Kanagawa Inst. Agric. Sci.)
Masanori HATASHITA (Wakasa Wan Energy Res. Cen.)
Atsushi HIGASHITANI (Grad. Sch. Life Sci., Tohoku Univ.)
Ryoichi HIRAYAMA (Natl. Inst. Radiol. Sci.)
Akiko HOKURA (Tokyo Denki Univ.)
Ichiro HONDA (Natl. Agric. Res. Cen.)
Mitsugu HORITA (Hokuren Agri. Res. Inst.)
Hiroyuki ICHIDA (Meiji Univ.)
Yuji ITO (Natl. Agric. Res. Cen., Hokkaido Region)
Akihiro IWASE (Grad. Sch. Engin., Osaka Pref. Univ.)
Hiroshi KAGAMI (Shizuoka Citrus Exp. Station)
Kensuke KAGEYAMA (Fac. Engin., Saitama Univ.)
Takeshi KANAYA (Suntory Flowers, Ltd.)

Si-Yong KANG (Dep. Rad. Plant Breed. Genet., KAERI, Korea)
Tomojirou KOIDE (Riken Vitamin Co., Ltd.)
Tsutomu KUBOYAMA (Ibaraki Univ.)
Norihiko MISHIMA (Fukuda Denshi Co., Ltd.)
Yutaka MIYAZAWA (Grad. Sch. Life Sci., Tohoku Univ.)
Kazumitsu MIYOSHI (Fac. Bioresour. Sci., Akita Pref. Univ.)
Toshikazu MORISHITA (Inst. Rad. Breeding, Natl. Inst. Agric. Res.)
Koji MURAI (Fukui Pref. Univ.)
Francesco MUSUMECI (Catania Univ.)
Daisuke NAKADA (Ela Medical Japan Co. Ltd.)
Koichiro NISHIKAWA (FLORSAIKA CIA. LTDA.)
Ishikawa NORITO (JAEA)
Mio OHNUMA (Inst. Mol. Cell. Biosci., Univ. Tokyo)
Norihiro OHTSUBO (Natl. Inst. Floricult. Sci.)
Fumihisa ONO (Grad. Sch. Natural Sci. & Tech., Okayama Univ.)
Tomo OOMIYA (Hokkaido Ornamental Plants Veg. Res. Cen.)
Kenji OSAWA (Nagano Agric. Res. Cen.)
Masaya SAKAI (Fukuda Denshi Co., Ltd.)
Kouichi SAKAMOTO (YUKIGUNI AGURI Co.,Ltd.)
Tadashi SATO (Grad. Sch. Life Sci., Tohoku Univ.)
Yoichi SATO (Riken Food Co., Ltd.)
Hiroaki SERIZAWA (Nagano Veg. Ornamental Crops Exp. Station)
Takiko SHIMADA (Res. Inst. Agric. Resour., Ishikawa Agric. Coll.)
Fumio SUGAWARA (Tokyo Univ. of Sci.)
Masao SUGIYAMA (Hokko Chem. Ind. Co., Ltd.)
Keita SUGIYAMA (Nat. Inst. Veg. Tea Sci.)
Ryuji SUGIYAMA (Ajinomoto, Co., INC.)
Kazunori SUZUKI (Plant Biotech. Inst. Ibaraki Agric. Cen.)
Masao SUZUKI (Natl. Inst. Radiol. Sci.)
Kenichi SUZUKI (Suntory Flowers, Ltd.)
Kunio SUZUKI (Technoflora, Co., Ltd.)
Hinako TAKEHISA (Natl. Inst. Agric. Sci.)
Sachie TANAKA (Tokai University)
Teruhiko TERAOKA (Hokko Chem. Ind. Co., Ltd.)
Ken TOKUHARA (Dogashima Orchid Cen.)
Masanori TOMITA (CRIEPI)
Hisashi TSUJIMOTO (Fac. Agri., Tottori Univ.)
Kozo TSUKADA (Nippon Veterinary and Life-sci. Univ.)
Masao WATANABE (Fac. Agri., Tohoku Univ.)
Takuji YOSHIDA (Takii Seed Co., Ltd.)
Koichiro YOSHIOKA (Tokai University Hospital)

Research Fellows

Hideki ASAUMI (Ehime Agricultural Experiment Station)
Masataka CHAYA (Nagasaki Agr. Forest. Exp. Station)
Fumiko HIDAKA (Kagoshima Pref. Inst. for Agric. Dev.)
Hiroaki KISAKA (Ajinomoto, Co., INC.)
Tadanori MINO (Wadamari Cho Agr. Exp. Station)
Miyuki NISHI (Saga Agricultural Experiment Station)
Kyouzuke NIWA (Hyogo Pref. Res. Inst.)
Tadahito OOTUBO (Wadamari Cho Agr. Exp. Station)
Eikou OYABU (Saga Pref. Agr. Res. Cen.)
Takenori SAITO (Shizuoka Tea Exp. Station)
Tsukasa SHIRAO (Kagoshima Biotechnology Inst.)
Keiichi TAKAGI (Wakasa-wan Energy Research Center)
Kei-ichiro UENO (Kagoshima Biotechnology Inst.)
Naoji WAKITA (Wadamari Cho Agr. Exp. Station)
Yoshihide SAKITA (Wadamari Cho Agr. Exp. Station)

Consultant

Hiroyuki SAITO

Students

Junior Research Associate

Kiyoshi NISHIHARA (Grad. Sch. Frontier Sci., Univ. of Tokyo)

Student trainees

Kotaro ISHII (Grad. Sch. Frontier Sci., Univ. of Tokyo)
Liqiu MA (Grad. Sch. Sci. & Engin., Saitama Univ.)
Nobuhiro MAEDA (Grad. Sch. Eng., Osaka Pref. Univ.)
Yoshitaka MATSUMOTO (Grad. Sch. Medicine & Sch., Chiba Univ.)
Tomomi MORISHIMA (Tokyo Denki Univ.)
Saori TAKADA (Fac. Sci., Tokyo Univ. of Sci.)
Hiroki TAOKA (Fac. Sci., Tokyo Univ. of Sci.)
Wakiko YAMAOKA (Fac. Sci., Tokyo Univ. of Sci.)
Yuichi YOSHII (Fac. Sci., Tokyo Univ. of Sci.)

RIBF Research Division

Accelerator Applications Research Group (Group Director : Tadashi KAMBARA)

RI Applications Team

1. Abstract

RI Applications Team performs following researches at the heavy ion accelerators of RIBF: (1) With 14-MeV protons from the RIKEN AVF Cyclotron, we produce radioisotopes (RIs) for research of chemistry, biology, medicine, pharmaceutical and environmental sciences. The nuclides Zn-65, Cd-109 and Y-88 are delivered to Japan Radioisotope Association for charged distribution to the general public in Japan. We also study the production and application of short-lived RIs. (2) We develop new technologies of mass spectrometry for the trace-element analyses using accelerator technology and apply them to the scientific research fields, such as cosmochemistry, environmental science, archaeology and so on.

2. Major Research Subjects

- (1) Production of radioisotopes Zn-65, Cd-109 and Y-88 for charged distribution,
- (2) Research and development for new RI production at AVF cyclotron,
- (3) The development of trace element analysis, using the accelerator techniques, and its application to geoscience and environmental science.

3. Summary of Research Activity

RI applications team utilizes RIBF heavy-ion accelerators for following research subjects:

(1) Production of radioisotopes

Using a 14-MeV proton beam from the RIKEN AVF Cyclotron, we develop techniques of production and application of various radio-isotopes (RIs) for research in chemistry, biology, medicine, pharmaceutical and environmental sciences. We can produce RIs with wide range of lifetimes as short as seconds. Long-life (> a few days) RIs are produced in a target which is cooled by water and He gas, and short-life RIs are produced at a gas-jet system where RI atoms are recoiled out of thin foil targets, captured by KCl aerosols and transported to a hot lab by a flow of He carrier gas. These systems are in the same chamber in series and can operate simultaneously with the same beam. Among the long-life RIs, Zn-65 ($T_{1/2}=244$ days) and Cd-109 ($T_{1/2}=463$ days) have been delivered to Japan Radioisotope Association since October 2007 for charged distribution to the general public in Japan. In addition, we started to deliver Y-88 ($T_{1/2}=107$ days) in February 2010.

(2) R/D for RI production

We work to improve production procedure of the present Zn-65, Cd-109 and Y-88 for stable supply and better quality. We also develop production techniques for other RI species like Ce-139 ($T_{1/2}=138$ days) which are demanded but lack supply sources. For the production of short-life RIs, the collection efficiency of gas-jet system has been optimized for Zr-89m ($T_{1/2}=4.16$ m), Nb-90m ($T_{1/2}=18.8$ s) and Nd-141m ($T_{1/2}=62$ s) nuclides.

(3) Trace element analyses with accelerator technologies

We have developed two new technologies of mass spectrometry for the trace-element analyses as an application of accelerator technology to various fields such as cosmochemistry, environmental science, archaeology and so on. One is a new type Accelerator Mass Spectrometry

(AMS) at the RILAC equipped with an ECR ion source. This system is available for the measurements of trace-elements (10^{-14} - 10^{-15} level), and is expected to be especially effective for the measurements of low electron-affinity elements such as ^{26}Al , ^{41}Ca , ^{53}Mn and so on. As a preliminary study, the ECR ion source system has been evaluated and the basic data have been obtained for the detection and quantitative analysis of trace nuclides in archaeological samples (cinnabar) and functional metals. As another technology, we have attempted to customize a mass spectrometer equipped with a stand-alone ECR ion source for analyses of elemental and isotopic abundances.

Team Leader

Tadashi KAMBARA

Members

Hiromitsu HABA

Kazuya TAKAHASHI

Shuichi ENOMOTO

Temporary Staff

Yutaka EZAKI

Visiting Scientists

Hiroshi HIDAKA (Fac. Sci., Hiroshima Univ.)

Hiroshi SHIMIZU (Fac. Sci., Hiroshima Univ.)

Miho TAKAHASHI (Tokyo Univ. Marine Sci. and Tech.)

Shigekazu YONEDA (Natl. Sci. Museum)

Tokuko WATANABE (Aoyama Gakuin Women's Junior College)

Masayoshi TODA (Tokyo Univ. Marine Sci. and Tech.)

Research Consultants

Kuniko MAEDA

Part-time Staffs

Tatsuya URABE (Tokyo Univ. Marine Sci. and Tech.)

Tomohiro OIKAWA (Tokyo Univ. Marine Sci. and Tech.)

RIBF Research Division

User Liaison and Industrial Cooperation Group (Group Director : Tohru MOTOBAYASHI)

User Support Office

1. Abstract

The RIKEN RI Beam Factory is the world preeminent facility providing the greatest opportunities for scientific researches. The facility, completed its construction in 2007, has started its full-scale operation in the end of the year 2008. It is our important mission to serve for a broad range of application of a large variety of researchers so that we bring out the best performance of the RI Beam Factory. We manage to facilitate the use of RI Beam Factory to the researchers both inside and outside of RIKEN, to support experiments using the accelerator complex, to exploit industrial application researches, and to promote the RI Beam Factory to interested researchers

2. Major Research Subjects

- (1) Facilitation of the use of the RI Beam Factory
- (2) Support of experiments in the RI Beam Factory
- (3) Promotion of the RI Beam Factory to interested researchers

3. Summary of Research Activity

In order to facilitate the use of RI Beam Factory to the researchers both inside and outside of RIKEN, we have organized international Program Advisory Committee, consisting of world leading scientists, to review proposals, purely based on their scientific merit and feasibility, in the fields of nuclear physics (NP) and material-and-life science (ML). The NP- and ML-PAC meetings are organized twice a year.

Another important activity is beam-time coordination of the PAC approved experiments and other development activities. The operation schedule of the RIBF accelerator complex is managed by our team taking into account strong demand of user's experiments.

Team Leader

Toshimi SUDA

Members

Mieko KOGURE

Technical Staff I

Narumasa MIYAUCHI

Assistant

Tomoko IWANAMI

Yuri TSUBURAI

RIBF Research Division

User Liaison and Industrial Cooperation Group (Group Director : Tohru MOTOBAYASHI)
Industrial Cooperation Team

1. Abstract

The scope of the industrial cooperation team includes industrial application of RIBF facility and research and development for industrial application of accelerator associated technologies.

2. Major Research Subjects

Distribution of radioisotopes Zn-65, Cd-109 and Y-88 produced at RIKEN AVF Cyclotron and investigation of novel industrial applications of the accelerator beam and its related technologies

3. Summary of Research Activity

(1) Charged distribution of radioisotopes

At RIBF, various specific radioisotopes for research have been produced with the cyclotrons and used for various research projects. Since October 2007, we have distributed radioisotopes Zn-65 and Cd-109, which are produced by the RI application team at the AVF cyclotron, to nonaffiliated users under a Material Transfer Agreement between Japan Radioisotope Association and RIKEN. In 2009, we distributed total amount of 51.1MBq of Zn-65 and 30MBq of Cd-109. In addition, we started distribution of Y-88 in February 2010.

(2) Feasibility study of RI-beam application in industries

To study feasibility of application of RI beam to industrial fields, research collaboration is being arranged with a private company.

Team Leader

Tadashi KAMBARA

Members

Tomoko ABE

Hiroshige TAKEICHI

Visiting Scientists

Akira NAGANO (S. H. I. Examination & Inspection, LTD.)

Ryuji UEMOTO (S. H. I. Examination & Inspection, LTD.)

Hiroyuki UNO (S. H. I. Examination & Inspection, LTD.)

RIBF Research Division Safety Management Group

1. Abstract

The Nishina Center for Accelerator-Based Science possesses one of the biggest accelerator facilities in the world which consists of a heavy-ion linear accelerator and 5 cyclotrons. Uranium ions are accelerated here only in Japan. Electron accelerators of microtron and synchrotron-storage-ring also exist. Our function is to keep the radiation level in and around the facility below the allowable limit and to control the exposure on the workers as low as reasonably achievable. We are also involved in the safety management of the Radioisotope Center where many types of experiments are performed with sealed and unsealed radioisotopes.

2. Major Research Subjects

- (1) Safety management at radiation facilities of Nishina Center for Accelerator-Based Science
- (2) Safety management at Radioisotope Center
- (3) Radiation shielding design and development of accelerator safety systems

3. Summary of Research Activity

Our most important task is to keep the personnel exposure as low as reasonably achievable, and to prevent an accident. Therefore, we daily patrol the facility, measure the ambient dose rates, maintain the survey meters, shield doors and facilities of exhaust air and wastewater, replenish the protective supplies, and manage the radioactive waste. Advice, supervision and assistance at major accelerator maintenance works are also our task.

A new accelerator interlock system was installed at RIBF building for the newly built electron machines. We extend the radiation safety interlock system (HIS) for heavy-ion accelerators to meet the change of experiment area at RIBF building where new detectors are installed. The suffocation-safety interlock system is working at the BigRIPS tunnel of RIBF accelerator building where huge amount of liquid He is used for superconducting magnets. Since a new injector linac, RILAC2, is installed in the AVF vault, the radiation safety interlock system for Nishina building is also modified.

Head

Yoshitomo UWAMINO

Members

Hisao SAKAMOTO

Rieko HIGURASHI (HIRUNUMA)

Technical Staff I

Atsuko AKASHIO

Assistant

Tomomi OKAYASU

Contract Officer

Hiroki MUKAI

Satoshi HASHIGUCHI

Hiroyuki FUKUDA

Special Temporary Employee

Shin FUJITA

Visiting Scientists

Koji OHISHI

Secretary

Tsutomu YAMAKI

Kazushiro NAKANO

Kimie IGARASHI

Satomi IIZUKA

Hiroko AISO

Center for Nuclear Study, Graduate School of Science, University of Tokyo.

1. Abstract

The Center for Nuclear Study (CNS) aims to elucidate the nature of nuclear system by producing the characteristic states where the Isospin, Spin and Quark degrees of freedom play central roles. These researches in CNS lead to the understanding of the matter based on common natures of many-body systems in various phases. We also aim at elucidating the explosion phenomena and the evolution of the universe by the direct measurements simulating nuclear reactions in the universe. In order to advance the nuclear science with heavy-ion reactions, we develop AVF upgrade, CRIB and SHARAQ facilities in the large-scale accelerators laboratories RIBF. We promote collaboration programs at RIBF as well as RHIC-PHENIX and ALICE-LHC with scientists in the world, and host international meetings and conferences. We also provide educational opportunities to young scientists in the heavy-ion science through the graduate course as a member of the department of physics in the University of Tokyo and through hosting the international summer school.

2. Major Research Subjects

- (1) Accelerator Physics
- (2) Nuclear Astrophysics
- (3) Nuclear spectroscopy of exotic nuclei
- (4) Quark physics
- (5) Spin Physics
- (6) Nuclear Theory
- (7) SHARAQ project

3. Summary of Research Activity

- (1) Accelerator Physics

One of the Major tasks of the accelerator group is the AVF upgrade project which includes development of ion sources, upgrading the AVF cyclotron of RIKEN and the beam line to CRIB. A new heavy ion ECR source of CNS that use super-conducting magnet was successfully installed to the AVF cyclotron, and has been used to provide a variety heavy ion beams. Two CNS ECR sources now provide all the beams for the AVF cyclotron and support not only CRIB experiments but also a large number of RIBF experiments. A charge-breeding ECR source is also under development.

Two major works were advanced for upgrading the AVF cyclotron. One is the detailed design study of the central region of the cyclotron, which remedies insufficiencies for the transmission of the heavy ion beams through the cyclotron. A new central module will be made following the design. The second is a successful acceleration of heavy ion beams up to 11 MeV/u which was about 9.5 MeV/u before. Following the detailed simulation studies of the heavy ion beams through the cyclotron, beam acceleration tests were successfully performed for ^{16}O and ^6Li beams. These beams will be provided to new experimental projects at CRIB.

A non-destructive beam monitor was also successfully developed and installed just in front of the CRIB production target. It showed a sensitivity of about a few nA. This new beam monitor will become a powerful tool for all the RIBF facility.

- (2) Nuclear Astrophysics

Major activity of the nuclear astrophysics group is to investigate experimentally nucleosynthesis

of the universe, specifically of explosive phenomena in the universe such as novae and supernovae. High-intensity RI beams of light nuclei from the CNS low-energy RI beam separator CRIB provides a good opportunity to study stellar nuclear reactions under explosive conditions both by the direct method as well as by indirect methods. The research programs include investigations of α -induced stellar reactions on ${}^7\text{Li}$, ${}^{14}\text{O}$ and ${}^{21}\text{Na}$. The beta decay of ${}^{46}\text{Cr}$ was also studied to learn the Gamow-Teller Transitions. Some beam developments were made for new RI beams, and an active target was also designed for studies of stellar reactions with low-cross sections.

Some technological development for the beam line as well as for the Wienfilter of CRIB were made in the past year.

(3) Nuclear structure of exotic nuclei

The NUSPEQ (NUclear SPectroscopy for Extreme Quantum system) group studies exotic structures in high-isospin and/or high-spin states in nuclei. The CNS GRAPE (Gamma-Ray detector Array with Position and Energy sensitivity) is a major apparatus for high-resolution in-beam gamma-ray spectroscopy. In 2009, the following progress has been made.

Neutron-rich nuclei around island-of-inversion have been studied by using nucleon transfer and inelastic scattering where the final states are identified by measuring de-excited gamma-rays. Several candidates of cluster states in ${}^{12}\text{Be}$ was found especially for odd-spin states suggesting asymmetric cluster configuration.

New high-spin states in ${}^{49-51}\text{Ti}$ populated by fusion reactions of an RI beam have been found, which gives information on the $N=28$ shell gap and the single particle energies in the fp-shell.. High-spin states in $A \sim 40$ mass region were studied via ${}^{18}\text{O}+{}^{26}\text{Mg}$ fusion evaporation reactions. A superdeformed rotational band up to 12^+ state was observed in ${}^{40}\text{Ar}$. This finding indicates the presences of the $N=22$ and $Z=18$ superdeformed shell structure in this region. High-spin states of ${}^{107}\text{In}$ was studied via ${}^{58}\text{Ni}({}^{52}\text{Cr},3p)$ reaction. A rotational cascade consisting ten gamma-ray transitions was observed. The band exhibits the features typical for smooth terminating bands in $A \sim 100$ mass region.

Upgrade of the readout system of the CNS GRAPE has started, where digital pulse data taken by sampling ADCs are analyzed by FPGAs on boards.

(4) Quark Physics

Main goal of the quark physics group is to understand the properties of hot and dense nuclear matter created by colliding heavy nuclei at relativistic energies. The group has been involved in the PHENIX experiment at Relativistic Heavy Ion Collider (RHIC) at Brookhaven National Laboratory, and in the ALICE experiment at Large Hadron Collider (LHC) at CERN. In 2009, LHC finally started making collisions.

As for PHENIX, the group has been concentrating on the physics analysis with leptons and photons, which include direct photon yield at low transverse momentum using the virtual-gamma method, neutral pion yield at high transverse momentum as a function of azimuthal angle from the reaction plane in Au+Au collisions, J/ψ production in ultra-peripheral Au+Au collisions.

As for ALICE, the group has been committing the commissioning of the Transition Radiation Detector (TRD), and calibration and performance study of Time Projection Chamber (TPC). The group has been leading development of forward calorimeter for a possible future upgrade.

R&D of gas electron multiplier (GEM) and related techniques has been continuing. Time

projection chamber, to be used as an active target at RIBF experiments, was developed. Resistive GEM, which utilizes resistive anodes, has been developed.

(6) Nuclear Theory

The nuclear theory group has been promoting the RIKEN-CNS collaboration project on large-scale nuclear structure calculations since 2001 and maintaining its parallel computing cluster. In 2009, we developed the effective interactions of various mass region based on the large-scale shell model calculation technique and discussed the "shell evolution" and the role of tensor force quantitatively in exotic nuclei, such as ^{17}C , ^{48}Ca , $N=50$ isotones, Sm isotopes and so on.

(7) SHARAQ project

Construction of the SHARAQ spectrometer and the dedicated high-resolution beamline are coming to the final phase. The magnetic field distribution in dipole magnets, D1 and D2, were precisely measured with the search coil method. A major part of the beamline has been constructed. Cathode readout drift chambers for tracking detectors at the SHARAQ focal plane have been fabricated in GANIL and installed to SHARAQ in December 2008. It was also found that Low-pressure multiwire drift chambers (LP-MWDC) developed for beamline tracking detectors works well under pressure as low as 10 kPa with an isobutane gas.

Director

Takaharu OTSUKA

Scientific Staff

Susumu SHIMOURA (Professor)

Shigeru KUBONO (Professor)

Hideki HAMAGAKI (Associate Professor)

Tomohiro UESAKA (Associate Professor)

Eiji IDEGUCHI (Lecturer)

Takahiro KAWABATA (Research Associate (- Jan. 31, 2009))

Hidetoshi YAMAGUCHI (Research Associate)

Shin'ichiro MICHIMASA (Research Associate)

Taku GUNJI (Research Associate)

Shinsuke OTA (Research Associate)

Guest Scientists

Toshio SUZUKI (Guest Professor, Nihon Univ.)

Toshinori MITSUMOTO (Guest Associate Professor, Sumitomo Heavy Industries, Ltd.)

Technical Staff

Yukimitsu OHSHIRO

Norio YAMAZAKI

Technical Assistants

Shin-ichi WATANABE
Hiroshi KUREI
Hideaki NINOMIYA
Akira YOSHINO
Shoichi YAMAKA

Post Doctoral Associates

Shinsuke OTA (-Mar. 31, 2009)
Takashi ABE (-Mar. 31, 2009)
Yohei SHIMIZU (-Dec. 31, 2010)
Kosuke NAKANISHI (-June 30, 2009)
Takashi HASHIMOTO
Yasuo WAKABAYASHI (-Mar. 31, 2009)
Yuji TSUCHIMOTO (Mar. 25, 2009 -)
Akito SAITO
Toru YOSHIDA (April 1, 2009 -)
Megumi NIIKURA (-April 30, 2009)

Graduate Students

Megumi NIIKURA (-Mar. 31, 2009)
Yuhei MORINO (-Mar. 31, 2009)
Satoshi SAKAGUCHI (-Mar. 31, 2009)
Yoshiko SASAMOTO
Yorito YAMAGUCHI
Yoki ARAMAKI
Nguyen Binh DAM
Satoshi SANO
Seiya HAYAKAWA
David. M KAHL
Akihisa TAKAHARA
Yuzo KURIHARA (-Mar. 31, 2009)
Hiroyuki MIYA
Ryoji AKIMOTO
Yasuto HORI
Kenshi OKADA (-Mar. 31, 2009)
Hiroshi TOKIEDA
Tomoya TSUJI
Shintaro GO
Shoichiro KAWASE

Administration Staff

Midori HIRANO

Ikuko YAMAMOTO

Takako ENDO

Yukino KISHI

Toshiko ITAGAKI

Yuko SOMA

TORIJIN (Todai-RIKEN Joint International Program for Nuclear Physics) Term

1. Abstract

University of Tokyo and RIKEN agreed to cooperate with each other in the field of nuclear physics and established Todai-RIKEN Joint International Program for Nuclear Physics (TORIJIN) in June 2006. The aim of this organization is to promote the international collaborations, such as JUSTIPEN (Japan-US Theory Institute for Physics with Exotic Nuclei) and EFES (International Research Network for Exotic Femto Systems). JUSTIPEN was launched in June 2006 in order to facilitate collaborations between U.S. and Japanese scientists whose main research thrust is in the area of the physics of exotic nuclei. More than 40 nuclear scientists in U.S. have visited Japan in three years, and many collaborations are established. EFES was selected as one of the Core-to-Core Programs of Japan Society for the Promotion of Science (JSPS). This is the program to send Japanese nuclear scientists to U.S., Germany, France, Italy, Norway, and Finland and to promote the international collaborations in the field of nuclear study. Many joint workshops were held with the partner countries.

2. Main activities

Promote the international collaborations of both theoretical and experimental nuclear physicists under JUSTIPEN and EFES programs.

3. Summary of Research Activity

Under the JUSTIPEN program, many nuclear scientists visited in this fiscal year and collaborations are established. Under the EFES program, we have carried out four types of activities: initiating the collaboration projects, organizing seminars with partner countries, sending researchers abroad, and sending/inviting young scientists to the summer schools. Regarding the collaborative works, we have carried out seven projects. Many experimentalists and theoreticians have been sent abroad. As for the joint workshops, we have organized six workshops and all of them were quite fruitful. Also, young scientists have been sent to partner countries for educational purpose and starting collaborations. As for the summer school, Japanese graduate students have been sent to the summer schools in Germany, Italy, and USA, and we have invited students to CNS-EFES summer school from the partner countries.

Leader

Takaharu OTSUKA (University of Tokyo)

Vice leader

Tohru MOTOBAYASHI (RIKEN)

Members

Susumu SHIMOURA (University of Tokyo),

Hiroyoshi SAKURAI (RIKEN),

Takashi NAKATSUKASA (RIKEN),

Tomohiro UESAKA (University of Tokyo),

Naoyuki ITAGAKI (University of Tokyo)

**VI. LIST OF PUBLICATIONS
& PRESENTATION**

Publications

Journal

(Original Papers) *Subject to Peer Review

- Adare A., Akiba Y., Aoki K., Asai J., Bazilevsky A. V., Bunce G. M., Deshpande A., Enyo H., Fields D. E., Fox B., Fujiwara K., Fukao Y., Goto Y., Gross P. M., Hasuko K., Heuser J. M., Horaguchi T., Ichihara T., Imai K., Inoue Y., Ishihara M., Jinnouchi O., Kamihara N., Kaneta M., Kanoh H., Kawall D., Kiyomichi A., Kobayashi H., Kurita K., Mao Y., Murata J., Nakagawa I., Nakano K., Onishi H., Okada H., Okada K., Rykov V. L., Saito N., Sato H., Shibata T., Shoji K., Tabaru T., Taketani A., Tanida K., Togawa M., Tojo J., Torii H., Wagner M. M., Watanabe Y., Xie W., and Yokkaichi S.: “Cold Nuclear Matter Effects on J/ψ Production as Constrained by Deuteron-Gold Measurements at $\sqrt{s_{NN}} = 200$ GeV”, Phys. Rev. C **77**, 024912-1–024912-15 (2008). *
- Adare A., Akiba Y., Aoki K., Asai J., Bunce G. M., Deshpande A., Enyo H., Fields D. E., Fujiwara K., Fukao Y., Goto Y., Gross P. M., Hachiya T., Hasuko K., Heuser J. M., Horaguchi T., Ichihara T., Imai K., Inoue Y., Ishihara M., Jinnouchi O., Kajihara F., Kamihara N., Kaneta M., Kanoh H., Kawall D., Kiyomichi A., Kurita K., Mao Y., Murata J., Nakagawa I., Nakano K., Onishi H., Okada H., Okada K., Rykov V. L., Saito N., Sato H., Shibata T., Shoji K., Tabaru T., Taketani A., Tanida K., Togawa M., Tojo J., Torii H., Tsuchimoto Y., Wagner M. M., Watanabe Y., Xie W., and Yokkaichi S.: “Quantitative Constraints on the Transport Properties of Hot Partonic Matter from Semi-Inclusive Single High Transverse Momentum Pion Suppression in Au+Au Collisions at $\sqrt{s_{NN}} = 200$ GeV”, Phys. Rev. C **77**, 064907-1–064907-12 (2008). *
- Adare A., Akiba Y., Aoki K., Asai J., Bunce G. M., Deshpande A., Enyo H., Fields D. E., Fujiwara K., Fukao Y., Goto Y., Gross P. M., Hachiya T., Hasuko K., Heuser J. M., Horaguchi T., Ichihara T., Imai K., Inoue Y., Ishihara M., Jinnouchi O., Kajihara F., Kamihara N., Kaneta M., Kanoh H., Kawall D., Kiyomichi A., Kurita K., Mao Y., Murata J., Nakagawa I., Nakano K., Onishi H., Okada H., Okada K., Rykov V. L., Saito N., Sato H., Shibata T., Shoji K., Tabaru T., Taketani A., Tanida K., Togawa M., Tojo J., Torii H., Tsuchimoto Y., Wagner M. M., Watanabe Y., Xie W., and Yokkaichi S.: “Dihadron azimuthal correlations in Au+Au collisions at $\sqrt{s_{NN}} = 200$ GeV”, Phys. Rev. C **78**, 014901-1–014901-42 (2008). *
- Adare A., Akiba Y., Aoki K., Asai J., Bazilevsky A. V., Bunce G. M., Deshpande A., Enyo H., Fields D. E., Fox B., Fujiwara K., Fukao Y., Goto Y., Gross P. M., Hachiya T., Hasuko K., Heuser J. M., Horaguchi T., Ichihara T., Imai K., Inoue Y., Ishihara M., Jinnouchi O., Kametani S., Kamihara N., Kaneta M., Kanoh H., Kawall D., Kiyomichi A., Kurita K., Kurosawa M., Li Z., Mao Y., Murata J., Nakagawa I., O., Kajihara F., Kamihara N., Kaneta M., Kanoh H., Kawall D., Kiyomichi A., Kobayashi H., Kurita K., Mao Y., Murata J., Nakagawa I., Nakano K., Onishi H., Okada H., Okada K., Rykov V. L., Saito N., Sato H., Shibata T., Shoji K., Tabaru T., Taketani A., Tanida K., Togawa M., Tojo J., Torii H., Tsuchimoto Y., Wagner M. M., Watanabe Y., Xie W., and Yokkaichi S.: “Charged hadron multiplicity fluctuations in Au+Au and Cu+Cu collisions from $\sqrt{s_{NN}} = 22.5$ to 200 GeV”, Phys. Rev. C **78**, 044902-1–044902-15 (2008). *
- Afanasiev S., Akiba Y., Aoki K., Bunce G. M., Deshpande A., Enyo H., Fields D. E., Fukao Y., Goto Y., Gross P. M., Hachiya T., Hasuko K., Heuser J. M., Horaguchi T., Ichihara T., Imai K., Ishihara M., Jinnouchi O., Kajihara F., Kamihara N., Kaneta M., Kiyomichi A., Kurita K., Murata J., Onishi H., Okada H., Okada K., Rykov V. L., Saito N., Sato H., Shibata T., Shoji K., Tabaru T., Taketani A., Tanida K., Togawa M., Tojo J., Torii H., Tsuchimoto Y., Wagner M. M., Watanabe Y., Xie W., and Yokkaichi S.: “Source breakup dynamics in Au+Au Collisions at $\sqrt{s_{NN}}=200$ GeV via three-dimensional two-pion source imaging”, Phys. Rev. Lett. **100**, 232301-1–232301-6 (2008). *
- Afanasiev S., Akiba Y., Aoki K., Bunce G. M., Deshpande A., Enyo H., Fields D. E., Fukao Y., Goto Y., Gross P. M., Hachiya T., Hasuko K., Heuser J. M., Horaguchi T., Ichihara T., Imai K., Ishihara M., Jinnouchi O., Kajihara F., Kamihara N., Kaneta M., Kiyomichi A., Kurita K., Murata J., Onishi H., Okada H., Okada K., Rykov V. L., Saito N., Sato H., Shibata T., Shoji K., Tabaru T., Taketani A., Tanida K., Togawa M., Tojo J., Torii H., Tsuchimoto Y., Wagner M. M., Watanabe Y., Xie W., and Yokkaichi S.: “Particle-species dependent modification of jet-induced correlations in Au+Au collisions at $\sqrt{s_{NN}} = 200$ GeV”, Phys. Rev. Lett. **101**, 082301-1–082301-6 (2008). *
- Adare A., Akiba Y., Aoki K., Asai J., Bunce G. M., Deshpande A., Enyo H., Fields D. E., Fujiwara K., Fukao Y., Goto Y., Gross P. M., Horaguchi T., Ichihara T., Imai K., Inoue Y., Ishihara M., Jinnouchi O., Kamihara N., Kaneta M., Kanoh H., Kawall D., Kiyomichi A., Kurita K., Mao Y., Murata J., Nakagawa I., Nakano K., Onishi H., Okada H., Okada K., Rykov V. L., Saito N., Shibata T., Shoji K., Tabaru T., Taketani A., Tanida K., Togawa M., Tojo J., Torii H., Wagner M. M., Watanabe Y., Xie W., and Yokkaichi S.: “ J/ψ Production in $\sqrt{s_{NN}} = 200$ GeV Cu+Cu Collisions”, Phys. Rev. Lett. **101**, 122301-1–122301-6 (2008). *
- Adare A., Akiba Y., Aoki K., Asai J., Bunce G. M., Dairaku S., Deshpande A., Enyo H., Fields D. E., Fujiwara K., Fukao Y., Goto Y., Gross P. M., Horaguchi T., Ichihara T., Ichimiya R., Imai K., Inoue Y., Ishihara M., Jinnouchi O., Kametani S., Kamihara N., Kaneta M., Kanoh H., Kawall D., Kiyomichi A., Kurita K., Kurosawa M., Li Z., Mao Y., Murata J., Nakagawa I.,

- Nakano K., Onishi H., Okada H., Okada K., Onuki Y., Rykov V. L., Saito N., Sakashita K., Shibata T., Shoji K., Tabaru T., Taketani A., Tanida K., Togawa M., Tojo J., Torii H., Wagner M. M., Watanabe Y., Xie W., and Yokkaichi S.: “Onset of π^0 suppression studied in Cu+Cu collisions at $\sqrt{s_{NN}} = 22.4, 62.4,$ and 200 GeV”, Phys. Rev. Lett. **101**, 162301-1–162301-6 (2008). *
- Adare A., Akiba Y., Aoki K., Asai J., Bunce G. M., Deshpande A., Enyo H., Fields D. E., Fujiwara K., Fukao Y., Goto Y., Gross P. M., Hachiya T., Hasuko K., Heuser J. M., Horaguchi T., Ichihara T., Imai K., Inoue Y., Ishihara M., Jinnouchi O., Kajihara F., Kamihara N., Kaneta M., Kanoh H., Kawall D., Kiyomichi A., Kurita K., Mao Y., Murata J., Nakagawa I., Nakano K., Onishi H., Okada H., Okada K., Rykov V. L., Saito N., Sato H., Shibata T., Shoji K., Tabaru T., Taketani A., Tanida K., Togawa M., Tojo J., Torii H., Tsuchimoto Y., Wagner M. M., Watanabe Y., Xie W., and Yokkaichi S.: “Suppression pattern of neutral pions at high transverse momentum in Au+Au collisions at $\sqrt{s_{NN}} = 200$ GeV and constraints on medium transport coefficients”, Phys. Rev. Lett. **101**, 232301-1–232301-7 (2008). *
- Asahi K., Ueno H., Shimada K., Nagatomo T., Yoshimi A., Nagae D., Kameda D., Uchida M., Inoue T., Hatakeyama N., Kagami S., Hasama Y., Suzuki K., Murata J., Kawamura H., Narita K., and Ishihara M.: “Nuclear Structure Studies with Polarized Radioactive Beams”, AIP Conf. Proc. **1149**, 90–99 (2009). *
- Adare A., Akiba Y., Aoki K., Asai J., Bunce G. M., Deshpande A., Enyo H., Fields D. E., Fujiwara K., Fukao Y., Goto Y., Gross P. M., Horaguchi T., Ichihara T., Imai K., Inoue Y., Ishihara M., Jinnouchi O., Kamihara N., Kaneta M., Kanoh H., Kawall D., Kiyomichi A., Kurita K., Mao Y., Murata J., Nakagawa I., Nakano K., Onishi H., Okada H., Okada K., Rykov V. L., Saito N., Shibata T., Shoji K., Tabaru T., Taketani A., Tanida K., Togawa M., Tojo J., Torii H., Wagner M. M., Watanabe Y., Xie W., and Yokkaichi S.: “Dilepton mass spectra in p+p collisions at $\sqrt{s} = 200$ GeV and the contribution from open charm”, Phys. Lett. B **670**, 313–320 (2009). *
- Adare A., Akiba Y., Aoki K., Asai J., Bunce G. M., Dairaku S., Deshpande A., Enyo H., Fields D. E., Fujiwara K., Fukao Y., Goto Y., Gross P. M., Horaguchi T., Ichihara T., Ichimiya R., Imai K., Ishihara M., Kametani S., Kamihara N., Kawall D., Kurita K., Kurosawa M., Li Z., Mao Y., Murata J., Nakagawa I., Nakano K., Okada H., Okada K., Onuki Y., Rykov V. L., Saito N., Sakashita K., Shibata T., Shoji K., Taketani A., Tanida K., Togawa M., Torii H., Watanabe Y., Xie W., and Yokkaichi S.: “Inclusive cross section and double helicity asymmetry for π^0 production in p + p collisions at $\sqrt{s} = 62.4$ GeV”, Phys. Rev. D **79**, 012003-1–012003-11 (2009). *
- Suda T., Wakasugi M., Emoto T., Ito S., Kurita K., Tamae T., Wang S., and Yano Y.: “First demonstration of electron scattering using a novel target developed for short-lived nuclei”, Phys. Rev. Lett. **102**, No. 10, pp. 102501-1–102501-4 (2009). *
- Book • Proceedings**
(Others)
- Fukunishi N., Fujimaki M., Watanabe T., Kumagai K., Komiyama M., Watanabe H., Goto A., Hasebe H., Higurashi Y., Ikezawa E., Kageyama T., Kamigaito O., Kase M., Kuboki H., Kidera M., Nagase M., Maie T., Nakagawa T., Ohnishi J., Okuno H., Sakamoto N., Sekiguchi K., Suda K., Suzuki H., Wakasugi M., Watanabe Y., Yokouchi S., Yano Y., and Yamada K.: “Operating experience with the RIKEN Radioactive Isotope Beam Factory”, Proceedings of the 2009 Particle Accelerator Conference (PAC09), Vancouver, Canada, 2009–5, PAC09 Editor, Vancouver, pp. MO3GRI0-1–MO3GRI0-5 (2009).
- Oral Presentations**
(International Conference etc.)
- Takeuchi S., Shimoura S., Motobayashi T., Akiyoshi H., Ando Y., Aoi N., Fulop Z., Gomi T., Higurashi Y., Hirai M., Iwasa N., Iwasaki H., Iwata Y., Kobayashi H., Kurokawa M., Liu Z., Minemura T., Ozawa S., Sakurai H., Serata M., Teranishi T., Yamada K., Yanagisawa Y., and Ishihara M.: “Isobaric analog state of ^{14}Be ”, RIKEN-CNS RIBF International Workshop “Correlation and Condensation: New Features in Loosely Bound and Unbound Nuclear States”, Wako, Dec. (2005).
- Fukunishi N., Fujimaki M., Watanabe T., Kumagai K., Komiyama M., Watanabe H., Goto A., Hasebe H., Higurashi Y., Ikezawa E., Kageyama T., Kamigaito O., Kase M., Kuboki H., Kidera M., Nagase M., Maie T., Nakagawa T., Ohnishi J., Okuno H., Sakamoto N., Sekiguchi K., Suda K., Suzuki H., Wakasugi M., Watanabe Y., Yokouchi S., Yano Y., and Yamada K.: “Operating experience with the RIKEN Radioactive Isotope Beam Factory”, 23rd Particle Accelerator Conference (PAC09), Vancouver, Canada, May (2009).
- Motizuki Y., Takahashi K., Nakai Y., Makishima K., Bamba A., Yano Y., Igarashi M., Motoyama H., Kamiyama K., Suzuki K., and Imamura T.: “A Dome Fuji ice core recording both supernovae and solar cycles”, 2nd International Symposium on Dome Fuji Ice Core and Related Topics, (National Institute of Polar Research), Tachikawa, Nov. (2009).
- (Domestic Conference)
- 福西暢尚, 藤巻正樹, 込山美咲, 長瀬誠, 渡邊環, 山田一成, 熊谷桂子, 後藤彰, 長谷部裕雄, 日暮祥英, 池沢英二, 影山正, 加瀬昌之, 木寺正憲, 久保木浩功, 眞家武士, 中川孝秀, 大西純一, 奥野広樹, 龍頭啓充, 坂本成彦, 若杉昌徳, 横内茂, 上垣外修一, 矢野安重, 小山亮, 須田健嗣. “RI ビームファクトリーにおけるウランビーム加速試験”, 第5回日本加速器学会年会/第33回リニアック技術研究会, (日本加速

器学会、リニアック技術研究会), 東広島, 8月(2008).
望月優子, 高橋和也, 牧島一夫, 馬場彩, 中井陽一; 矢野安重,
五十嵐誠, 本山秀明, 神山孝吉, 鈴木啓助, 今村隆史: “南極
氷床コアからさぐる超新星の痕跡と太陽活動周期”, 日本地
球惑星科学連合2009年大会, 千葉, 5月(2009).
渡邊環, 福西暢尚, 佐々木雄一朗, 加瀬昌之, 矢野安重: “高温
超伝導電流センサーとSQUIDを用いたビーム電流モニ
ターの実用化”, 第6回日本加速器学会年会, (日本加速器学
会), 茨城県東海村, 8月(2009).

Theoretical Physics Laboratory

Publications

Journal

- (Original Papers) *Subject to Peer Review
- Ishida M. and Igi K.: “Test of the universal rise of hadronic total cross sections at super-high energies”, *Eur. Phys. J. C* **52**, 357–362 (2007). *
- Takimi T.: “Relationship between various supersymmetric lattice models”, *J. High Energy Phys.* **0707**, 010-1–010-25 (2007). *
- Loaiza-Brito O. and Oda K.: “Effects of brane-flux transition on black holes in string theory”, *J. High Energy Phys.* **0708**, 002-1–002-22 (2007). *
- Hanada M. and Nishioka T.: “Cascade of Gregory-Laflamme Transitions and U(1) Breakdown in Super Yang-Mills”, *J. High Energy Phys.* **0709**, 012-1–012-14 (2007). *
- Kawamura Y., Kinami T., and Oda K.: “Orbifold family unification”, *Phys. Rev. D* **76**, 035001-1–035001-11 (2007). *
- Hanada M., Nishimura J., and Takeuchi S.: “Nonlattice simulation for supersymmetric gauge theories in one dimension”, *Phys. Rev. Lett.* **99**, 161602-1–161602-4 (2007). *
- Ohta K. and Takimi T.: “Lattice formulation of a two-dimensional topological field theory”, *Prog. Theor. Phys.* **117**, No. 2, pp. 317–345 (2007). *
- Damgaard P. and Fukaya H.: “Partially quenched chiral perturbation theory in the epsilon-regime”, *Nucl. Phys. B* **793**, 160–191 (2008). *
- Aoki S., Chiu T., Fukaya H., Hashimoto S., Hsieh T., Kaneko T., Matsufuru H., Noaki J., Ogawa K., Onogi T., and Yamada N.: “Topological susceptibility in two-flavor lattice QCD with exact chiral symmetry”, *Phys. Lett. B* **665**, 294–297 (2008). *
- Hanada M., Anagnostopoulos K., Nishimura J., and Takeuchi S.: “Monte Carlo studies of supersymmetric matrix quantum mechanics with sixteen supercharges at finite temperature”, *Phys. Rev. Lett.* **100**, 021601-1–021601-4 (2008). *
- Baba Y., Ishibashi N., and Murakami K.: “Light-cone gauge superstring field theory and dimensional regularization”, *J. High Energy Phys.* **10**, 035-1–035-17 (2009). *
- Baba Y., Ishibashi N., and Murakami K.: “Light-cone gauge string field theory in noncritical dimensions”, *J. High Energy Phys.* **12**, 010-1–010-24 (2009). *
- Gibbons G. W., Hashimoto K., and Hirano S.: “Gravitational Dual of Tachyon Condensation”, *J. High Energy Phys.* **0909**, 100-1–100-7 (2009). *
- Hashimoto K.: “Holographic Nuclei: supersymmetric examples”, *J. High Energy Phys.* **0912**, 065-1–065-9 (2009). *
- Kadoh D., Sugino F., and Suzuki H.: “Lattice formulation of 2D $\mathcal{N} = (2, 2)$ SQCD based on the B model twist”, *Nucl. Phys. B* **820**, No. 1-2, pp. 99–115 (2009). *
- Ishida M. and Igi K.: “Universal Rise of Hadronic Total Cross Sections based on Forward pi p and anti-p p(pp) Scatterings”, *Phys. Lett. B* **670**, 395–398 (2009). *
- Igi K. and Ishida M.: “Test of Universal Rise of Hadronic Total Cross Sections based on pi p, Kp and anti-p p,pp Scatterings”, *Phys. Rev. D* **79**, 096003-1–096003-15 (2009). *
- Hanada M. and Kanamori I.: “Lattice study of two-dimensional $\mathcal{N} = (2, 2)$ super Yang-Mills theory at large N ”, *Phys. Rev. D* **80**, 065014-1–065014-12 (2009). *
- Kishimoto I. and Takahashi T.: “Numerical evaluation of gauge invariants for a-gauge solutions in open string field theory”, *Prog. Theor. Phys.* **121**, No. 4, pp. 695–710 (2009). *
- Kishimoto I. and Takahashi T.: “Vacuum structure around identity-based solutions”, *Prog. Theor. Phys.* **122**, No. 2, pp. 385–399 (2009). *
- Hashimoto K., Sakai T., and Sugimoto S.: “Nuclear Force from String Theory”, *Prog. Theor. Phys.* **122**, No. 2, pp. 427–476 (2009). *
- Baba Y., Ishibashi N., and Murakami K.: “Light-cone gauge NSR strings in noncritical dimensions”, *J. High Energy Phys.* **1001**, 119-1–119-19 (2010). *
- Kadoh D. and Suzuki H.: “SUSY WT identity in a lattice formulation of 2D $\mathcal{N} = (2, 2)$ SYM”, *Phys. Lett. B* **682**, 466–471 (2010). *
- Kadoh D. and Suzuki H.: “Supersymmetric nonperturbative formulation of the WZ model in lower dimensions”, *Phys. Lett. B* **684**, No. 2-3, pp. 167–172 (2010). *
- (Review)
- Ezawa Z. and Tsitsishvili G.: “Quantum Hall ferromagnets”, *Rep. Prog. Phys.* **72**, 086502-1–086502-32 (2009).

Oral Presentations

(International Conference etc.)

- Kishimoto I. and Takahashi T.: “Numerical evaluation of gauge invariants for a-gauge solutions in open string field theory”, 2nd International Conference on String Field Theory and Related Aspects, (Steklov Mathematical Institute), Moscow, Russia, Apr. (2009).

- Kishimoto I. and Takahashi T.: “On identity based solutions in open string field theory”, APCTP Focus Program on Current Trends in String Field Theory, Pohang, Korea, Dec. (2009).

(Domestic Conference)

- 橋本幸士: “Gravity dual of tachyon condensation”, 日本物理学会第 64 回年次大会, (日本物理学会), 東京, 3 月 (2009).
- 戴大盛, 橋本幸士, 寺嶋靖治: 日本物理学会 2009 年春季大会, (日本物理学会), 東京, 3 月 (2009).
- 岸本功, 高橋智彦: “Numerical evaluation of gauge invariants for a-gauge solutions in open string field theory”, KEK 理論研究会 2009, つくば, 3 月 (2009).

- 岸本 功, 高橋 智彦: “Vacuum structure around identity based solutions”, 基研研究会「場の理論と弦理論」, (京都大学基礎物理学研究所), 京都, 7月(2009).
- 衛藤 稔: “高密度QCDにおけるカラー超伝導ボーズクス”, 基研研究会「場の理論と弦理論」, (京都大学基礎物理学研究所), 京都, 7月(2009).
- 橋本幸士: “Holographic QCD and Nuclear Force”, KEK理論センター研究会「原子核・ハドロン物理」, つくば, 8月(2009).
- 橋本幸士: “Gravity Dual of Nuclei”, 日本物理学会2009年秋季大会, 神戸, 9月(2009).
- 馬場裕, 石橋延幸, 村上公一: “非臨界次元における light-cone gauge 弦の場の理論”, 日本物理学会2009年秋季大会, 神戸, 9月(2009).
- 馬場裕, 石橋延幸, 村上公一: “light-cone gauge 超弦の場の理論と次元正則化”, 日本物理学会2009年秋季大会, 神戸, 9月(2009).
- 岸本功, 高橋智彦: “単位弦場に基づく解のまわりの開弦の場の理論の真空構造”, 日本物理学会2009年秋季大会, 神戸, 9月(2009).
- 橋本幸士: “超弦理論の応用と重力解”, 基研研究会「高次元ブラックホール研究最前線」, (京都大学), 京都, 12月(2009).

Theoretical Nuclear Physics Laboratory

Publications

Journal

(Original Papers) *Subject to Peer Review

- Yabana K., Nakatsukasa T., and Ito M.: “Time-dependent description for nuclear reaction dynamics in the continuum”, *Few Body Syst.* **43**, 247–253 (2008). *
- Barbieri C. and Van Neck D.: “Ab-initio Green’s Functions Calculations of Atoms”, *AIP Conf. Proc.* **1120**, 104–108 (2009). *
- Yoshida K.: “Monopole Modes of Excitation in Deformed Neutron-rich Mg Isotopes”, *AIP Conf. Proc.* **1165**, 162–164 (2009).
- Nakatsukasa T., Inakura T., and Yabana K.: “Finite amplitude method and systematic studies of photoresponse in deformed nuclei”, *AIP Conf. Proc.* **1165**, 173–176 (2009). *
- Yoshida K.: “Skyrme-QRPA calculations for low-lying excitation modes in deformed neutron-rich nuclei”, *Eur. Phys. J. A* **42**, No. 3, pp. 583–590 (2009). *
- Inakura T., Nakatsukasa T., and Yabana K.: “Systematic study of electric dipole excitations with fully self-consistent Skyrme HF plus RPA from light to medium-mass deformed nuclei”, *Eur. Phys. J. A* **42**, 591–594 (2009). *
- Middleton D., Annard J. R., Barbieri C., Giusti C., Grabmayr P., Hehl T., MacGregor I. J., Martin I., MacGeorge J. C., Moschini F., Pacati F. D., Schwamb M., and Watts D.: “Knockout of proton-neutron pairs from ^{16}O with electromagnetic probes”, *Eur. Phys. J. A* **43**, 137–143 (2009). *
- Nakatsukasa T., Inakura T., and Yabana K.: “TDDFT approach to photoabsorption in even-even nuclei”, *Int. J. Mod. Phys. A* **24**, 2159–2167 (2009). *
- Inakura T., Nakatsukasa T., and Yabana K.: “Response functions in the continuum of deformed nuclei studied with the time-dependent density-functional calculations”, *Int. J. Mod. Phys. E* **18**, No. 10, pp. 2088–2092 (2009). *
- De Rydt M., Neyens G., Asahi K., Balabanski D. L., Daugas J., Depuydt M., Gaodefroy L., Grevy S., Hasama Y., Ichikawa Y., Morel P., Nagatomo T., Ohtsuka T., Perrot L., Shimada K., Stoedel C., Thomas J., Ueno H., Utsuno Y., Wannes V., Vermeulen N., Vingerhoets P., and Yoshimi A.: “Precision measurement of the electric quadrupole moment of ^{31}Al and determination of the effective proton charge in the sd-shell”, *Phys. Lett. B* **678**, 344–349 (2009). *
- Long W., Nakatsukasa T., Sagawa H., Meng J., Nakada H., and Zhang Y.: “Non-local mean field effect on nuclei near $Z = 64$ sub-shell”, *Phys. Lett. B* **680**, 428–431 (2009). *
- Watanabe G., Dalfovo F., Piazza F., Pitaevskii L. P., and Stringari S.: “Critical velocity of superfluid flow through single-barrier and periodic potentials”, *Phys. Rev. A* **80**, No. 5, pp. 053602-1–053602-9 (2009). *
- Yoshida K.: “Core polarization for the electric quadrupole moment of neutron rich aluminum isotopes”, *Phys. Rev. C* **79**, No. 5, pp. 054303-1–054303-6 (2009). *
- Enyo Y., Hinohara N., Suhara T., and Schuck P.: “Dineutron correlations in quasi-two-dimensional systems in a simplified model, and possible relation to neutron-rich nuclei”, *Phys. Rev. C* **79**, No. 5, pp. 054305-1–054305-14 (2009). *
- Takeuchi S., Aoi N., Motobayashi T., Ota S., Takeshita E., Suzuki H., Baba H., Fukui T., Hashimoto Y., Ieki K., Imai N., Iwasaki H., Kanno S., Kondo Y., Kubo T., Kurita K., Minemura T., Nakamura T., Okumura T., Onishi T., Sakurai H., Shimoura S., Sugou R., Suzuki D., Suzuki M., Takashina M., Tamaki M., Tanaka K., Togano Y., and Yamada K.: “Low-lying States in ^{32}Mg studied by proton inelastic scattering”, *Phys. Rev. C* **79**, No. 5, pp. 054319-1–054319-11 (2009). *
- Barbieri C. and Hjorth-Jensen M.: “Quasiparticle and quasihole states of nuclei around ^{56}Ni ”, *Phys. Rev. C* **79**, 064313-1–064313-12 (2009). *
- Hinohara N., Nakatsukasa T., Matsuo M., and Matuyanagi K.: “Microscopic description of oblate-prolate shape mixing in proton-rich Se isotopes”, *Phys. Rev. C* **80**, No. 1, pp. 014305-1–014305-11 (2009). *
- Taniguchi Y., Enyo Y., and Kimura M.: “Cluster structures and superdeformation in ^{28}Si ”, *Phys. Rev. C* **80**, No. 4, pp. 044316-1–044316-9 (2009). *
- Yoshida K.: “Pygmy dipole mode in deformed neutron-rich Mg isotopes close to the drip line”, *Phys. Rev. C* **80**, No. 4, pp. 044324-1–044324-8 (2009). *
- Inakura T., Nakatsukasa T., and Yabana K.: “Self-consistent calculation of nuclear photoabsorption cross sections: Finite amplitude method with Skyrme functionals in the three-dimensional real space”, *Phys. Rev. C* **80**, 044301-1–044301-11 (2009). *
- Yamagami M., Shimizu Y., and Nakatsukasa T.: “Optimal pair density functional for description of nuclei with large neutron excess”, *Phys. Rev. C* **80**, 064301-1–064301-10 (2009). *
- Want X., Janssens R., Carpenter M. P., Zhu S., Wiedenhover I., Garg U., Frauendorf S., Nakatsukasa T., Ahmad I., Bernstein A., Diefenderfer E., Freeman S. J., Greene J. P., Khoo T., Kondev F. G., Larabee A., Lauritsen T., Lister C. J., Meredith B., Seweryniak D., Teal C., and Wilson P.: “Structure of ^{240}Pu : Evidence for octupole phonon condensation?”, *Phys. Rev. Lett.* **102**, 122501-1–122501-4 (2009). *
- Watanabe G., Sonoda H., Maruyama T., Katsuhiko S., Yasuoka K., and Ebisuzaki T.: “Formation of nuclear “pasta” in supernovae”, *Phys. Rev. Lett.* **103**, No. 12, pp. 121101-1–121101-4 (2009). *
- Barbieri C.: “Role of Long-Range Correlations in the

- Quenching of Spectroscopic Factors”, *Phys. Rev. Lett.* **103**, 202502-1–202502-4 (2009). *
- Ogasawara H., Yoshida K., Yamagami M., Mizutori S., and Matuyanagi K.: “Rotational Frequency Dependence of Octupole Vibrations on Superdeformed States in ^{40}Ca ”, *Prog. Theor. Phys.* **121**, No. 2, pp. 357–374 (2009). *
- Watanabe G.: “Efficient creation of maximally entangled states by modulation of tunneling rates”, *Phys. Rev. A* **81**, No. 2, pp. 021604-1–021604-4 (2010). *
- Sato K., Hinohara N., Nakatsukasa T., Matsuo M., and Matuyanagi K.: “A Model Analysis of Triaxial Deformation Dynamics in Oblate-Prolate Shape Coexistence Phenomena”, *Prog. Theor. Phys.* **123**, No. 1, pp. 129–155 (2010). *
- (Review)
- Yoshida K.: “Low-lying excitation modes in deformed neutron-rich nuclei”, *Int. J. Mod. Phys. E* **17**, No. Supplement 1, pp. 272–285 (2008).
- Barbieri C. and Dickhoff W. H.: “Spectroscopic Factors in ^{16}O and Nucleon Asymmetry”, *Int. J. Mod. Phys. A* **24**, No. 11, pp. 2060–2068 (2009).
- 中務孝: “原子核の変形, 対称性の破れ, 殻構造”, *原子核研究* **53**, 132–141 (2009).
- (Others)
- Hinohara N., Nakatsukasa T., Matsuo M., and Matuyanagi K.: “Collective path and inertial mass of large-amplitude collective dynamics: Application to shape coexistence”, *AIP Conf. Proc.* **1175**, 49–56 (2009).
- Barbieri C., Charity R. J., Dickhoff W. H., and Sobotka L. G.: “Toward a Global Dispersive Optical Model for the Driplines”, *Nucl. Phys. A* **834**, No. 1/4, pp. 788c–791c (2010).
- Book • Proceedings**
- (Review)
- Barbieri C.: “Toward an Ab-initio Description of Quasiparticle Properties”, *Proceedings of the 12th International Conference on Nuclear Reaction Mechanisms, Varenna, Italy, 2009–6*, CERN-Proceedings-2010-001, CERN, pp. 137–144 (2010).
- (その他)
- Enyo Y., Hinohara N., Suhara T., and Schuck P.: “Dineutron correlations in nuclear surface”, *Proceedings of the 12th International Conference on Nuclear Reaction Mechanisms, Varenna, Italy, 2009–6*, CERN, Geneva, pp. 291–298 (2010).
- Oral Presentations**
- (International Conference etc.)
- Yoshida K.: “Skyrme QRPA calculations for collective modes of excitation in deformed neutron-rich nuclei”, 3rd LACM-EFES-JUSTIPEN Workshop, Oak Ridge, USA, Feb. (2009).
- Yoshida K.: “Low-lying monopole and quadrupole modes in deformed neutron-rich nuclei”, LIA-EFES Workshop “Low-energy collective excitations in exotic nuclei”, Caen, France, Mar. (2009).
- Avogadro P. and Nakatsukasa T.: “Does the finite amplitude method allow to obtain easily the QRPA matrix?”, Arctic FIDIPRO-EFES Workshop, (University of Jyvaskyla), Saariselka, Finland, Apr. (2009).
- Nakatsukasa T.: “Finite amplitude method and systematic studies of photoresponse in deformed nuclei”, Arctic FIDIPRO-EFES Workshop, (University of Jyvaskyla), Saariselka, Finland, Apr. (2009).
- Hinohara N., Nakatsukasa T., Matsuo M., and Matuyanagi K.: “Collective path and inertial mass of large-amplitude collective dynamics: application to shape coexistence”, 4th International Workshop on Nuclear Fission and Fission-Product Spectroscopy (FISSION 2009), (CEA), Saint-Paul-lez-Durance, France, May (2009).
- Watanabe G., Orso G., Dalfovo F., Pitaevskii L. P., and Stringari S.: “Properties of superfluid unitary Fermi gases in an optical lattice”, *Conference on Research Frontiers in Ultra-Cold Atoms*, (ICTP), Trieste, Italy, May (2009).
- Nakatsukasa T.: “Finite amplitude method and systematic studies of photoresponse in deformed nuclei”, *International Conference on Nuclear Structure and Dynamics (NSD09)*, (University of Zagreb), Dubrovnik, Croatia, May (2009).
- Yoshida K.: “Monopole modes of excitation in deformed neutron-rich Mg isotopes”, *International Conference on Nuclear Structure and Dynamics (NSD09)*, (University of Zagreb), Dubrovnik, Croatia, May (2009).
- Yoshida K.: “Collective modes of excitation in deformed neutron-rich nuclei”, *Workshop on Importance of continuum coupling for nuclei close to the drip-lines*, (CEA Saclay), Saclay, France, May (2009).
- Hinohara N.: “Oblate-prolate shape mixing in proton-rich Se isotopes as large-amplitude collective motion”, *Workshop on Importance of continuum coupling for nuclei close to the drip-lines*, (CEA/SPhN), Saclay, France, May (2009).
- Taniguchi Y., Enyo Y., and Kimura M.: “Clustering and shape coexistence in ^{28}Si ”, *YITP International Workshop on Development of nuclear structure models from the viewpoint of nuclear force*, (Yukawa Institute for Theoretical Physics, Kyoto University), Kyoto, May (2009).
- Barbieri C.: “Green’s Functions Calculations of Quasiparticle States”, *YITP International Workshop on Development of nuclear structure models from the viewpoint of nuclear force*, (Yukawa Institute for Theoretical Physics), Kyoto, May (2009).
- Nakatsukasa T.: “Recent activities in RIKEN RI Beam Factory: Experiments and theories”, *12th International Conference on Nuclear Reaction Mechanisms*, (Univer-

- sity of Milano), Varenna, Italy, June (2009).
- Barbieri C.: “Toward an Ab-initio Description of Quasi-particle Properties”, 12th International Conference on Nuclear Reaction Mechanisms, Varenna, Italy, June (2009).
- Yoshida K.: “Giant monopole resonance and soft monopole mode in neutron-rich Mg isotopes”, 3rd International Conference on Collective Motion in Nuclei under Extreme Conditions (COMEX3), (National Superconducting Cyclotron Laboratory (NSCL) at Michigan State University), Mackinac Island, USA, June (2009).
- Nakatsukasa T.: “Finite amplitude method and canonical-basis TDHFB”, Annual UNEDF Collaboration Meetings, (University of Washington), Pack Forest, USA, June (2009).
- Watanabe G.: “Efficient scheme for creating NOON state in a double-well potential”, Cold Atoms and Molecules: Collisions, Field-effects, and Applications, (Kyoto University), Kyoto, June (2009).
- Barbieri C.: “Toward an ab-initio description of single-particle properties”, ECT International Workshop on Confrontation and Convergence in Nuclear Theory, Trento, Italy, July (2009).
- Barbieri C.: “Applicazioni delle funzioni di green agli stati di quasiparticella in atomi e nuclei”, Seminar at the University of Pavia, (University of Pavia), Pavia, Italy, July (2009).
- Barbieri C.: “Applications of many-body theory to derive accurate global optical potentials and predictions at the driplines”, 10th International Conference on Nucleus-Nucleus collisions (NN2009), Beijing, China, Aug. (2009).
- Watanabe G.: “Efficient scheme for creating NOON state in a double-well potential”, Telluride Workshop on Quantum Chemistry and Quantum Computational Physics in the Theory of Ultra-cold Gasses, Telluride, USA, Aug. (2009).
- Taniguchi Y., Enyo Y., and Kimura M.: “ α clustering and superdeformation of ^{28}Si ”, 19th International IUPAP Conference on Few-Body Problems in Physics, Bonn, Germany, Aug.-Sept. (2009).
- Hinohara N.: “Large-amplitude collective dynamics in proton-rich Se isotopes”, 8th CNS-EFES International Summer School (CNS-EFES 09), Wako, Aug.-Sept. (2009).
- Watanabe G.: “Nuclear “pasta”: its formation and consequences”, Conference on Neutron stars: The crust and beyond, (NORDITA), Stockholm, Sweden, Sept. (2009).
- Watanabe G.: “Efficient scheme for creating maximally entangled state in a double-well potential”, International Conference on Quantum Information Processing and Communication (QIPC 2009), (QUROPE and the Sapienza Università di Roma), Rome, Italy, Sept. (2009).
- Avogadro P. and Nakatsukasa T.: “A method to compute the QRPA”, 3rd Joint Meeting of the APS Division of Nuclear Physics and the Physical Society of Japan (HAW 09), (APS, JPS), Waikoloa, USA, Oct. (2009).
- Kohama A., Iida K., and Oyamatsu K.: “Constructing formula for total reaction cross sections without adjustable energy-dependent parameters”, 3rd Joint Meeting of the Nuclear Physics Divisions of the APS and JPS (Hawaii 2009), Hawaii, USA, Oct. (2009).
- Barbieri C.: “Large-Scale Calculations of Single-Particle Properties”, 3rd Joint Meeting of the Nuclear Physics Divisions of the APS and JPS (Hawaii 2009), Hawaii, USA, Oct. (2009).
- Nakatsukasa T., Hinohara N., Sato K., Matsuo M., and Matuyanagi K.: “Microscopic analysis of large amplitude collective dynamics in triaxial nuclear shapes”, 3rd Joint Meeting of the Nuclear Physics Divisions of the APS and JPS (Hawaii 2009), Hawaii, USA, Oct. (2009).
- Nakatsukasa T.: “Photoneuclear reactions studied with the time-dependent density-functional theory”, 3rd Joint Meeting of the Nuclear Physics Divisions of the APS and JPS (Hawaii 2009), Hawaii, USA, Oct. (2009).
- Hinohara N., Sato K., Nakatsukasa T., Matsuo M., and Matuyanagi K.: “Microscopic derivation of five-dimensional collective Hamiltonian of large-amplitude quadrupole motion: application to shape coexistence in proton-rich Se isotopes”, 7th Japan-China Joint Nuclear Physics Symposium, (Univ. of Tsukuba), Tsukuba, Nov. (2009).
- Hinohara N., Sato K., Nakatsukasa T., Matsuo M., and Matuyanagi K.: “Large-amplitude quadrupole collective dynamics in Se and Kr isotopes”, Hadron and Nuclear Physics (HNP09), (RCNP, Osaka Univ.), Suita, Nov. (2009).
- Watanabe G.: “Study of matter in ultradense and ultradilute environments: towards bridging astrophysics and cold atom physics”, Symposium on Fields of Special Interests in Theoretical Physics, (Asia Pacific Center for Theoretical Physics), Pohang, Korea, Nov. (2009).
- Hinohara N., Sato K., Nakatsukasa T., Matsuo M., and Matuyanagi K.: “Large-amplitude quadrupole collective dynamics of shape coexistence phenomena in proton-rich Se and Kr isotopes”, Tours Symposium on Nuclear Physics and Astrophysics VII (TOURS 2009), (Konan Univ.), Kobe, Nov. (2009).
- Hinohara N.: “Five-dimensional collective Hamiltonian with Thouless-Valatin inertial functions”, JUSTIPEN-EFES Workshop on Unstable Nuclei, Wako, Dec. (2009).
- Barbieri C.: “Ground states and single particle energies from Green’s function theory”, JUSTIPEN-EFES Workshop on Unstable Nuclei, Wako, Dec. (2009).
- Taniguchi Y., Kimura M., Enyo Y., Ikeda K., Horiuchi H., and Ideguchi E.: “Triaxial superdeformation in ^{40}Ar ”, JUSTIPEN-EFES Workshop on Unstable Nuclei, Wako, Dec. (2009).

- Watanabe G.: "Formation of nuclear "pasta" in supernovae", RIKEN-TRIUMF Nuclear Theory Meeting, (TRIUMF and RIKEN), Vancouver, Canada, Dec. (2009).
- Nakatsukasa T.: "Global fitting of the pairing functional", RIKEN-TRIUMF Nuclear Theory Meeting, Vancouver, Canada, Dec. (2009).
- Watanabe G.: "Formation of nuclear pasta in supernovae", Mini Symposium on Nuclear Astrophysics in "New Frontiers in QCD 2010", (Yukawa Institute for Theoretical Physics), Kyoto, Jan. (2010).
- Hinohara N.: "Beyond mean-field description of low-lying states of nuclei", ICHOR-EFES International Symposium on New Facet of Spin-Isospin Responses (SIR2010), (University of Tokyo), Tokyo, Feb. (2010).
- Barbieri C.: "Pygmy dipole response of proton-rich argon nuclei in random-phase approximation and no-core shell model", ICHOR-EFES International Symposium on New Facet of Spin-Isospin Responses (SIR2010), (Tokyo University/CNS), Tokyo, Feb. (2010).
- Yoshida K.: "Pygmy mode in deformed neutron-rich nuclei", ICHOR-EFES International Symposium on New Facet of Spin-Isospin Responses (SIR2010), Tokyo, Feb. (2010).
- Barbieri C.: "Ground and Single-Particle States from Green's Function Theory", International Symposium on Forefronts of Researches in Exotic Nuclear Structures (Niigata2010), (Niigata University), Tokamachi, Niigata Pref., Mar. (2010).
- Sato K., Hinohara N., Nakatsukasa T., Matsuo M., and Matuyanagi K.: "Microscopic analysis of shape mixing in low-lying states of proton-rich Kr isotopes", International Symposium on Forefronts of Researches in Exotic Nuclear Structures (Niigata2010), (Niigata University), Tokamachi, Niigata Pref., Mar. (2010).
- Hinohara N., Sato K., Nakatsukasa T., Matsuo M., and Matuyanagi K.: "Microscopic approach to adiabatic large-amplitude quadrupole collective dynamics in Se isotopes", International Symposium on Forefronts of Researches in Exotic Nuclear Structures (Niigata2010), (Niigata Univ.), Tokamachi, Niigata Pref., Mar. (2010).
- Sato K., Hinohara N., Nakatsukasa T., Matsuo M., and Matuyanagi K.: "Phenomenological analysis of the oblate-prolate symmetry breaking in triaxial deformation dynamics", International Symposium on Forefronts of Researches in Exotic Nuclear Structures (Niigata2010), (Niigata University), Tokamachi, Niigata Pref., Mar. (2010).
- Taniguchi Y.: "Triaxial superdeformation in ^{40}Ar ", International Symposium on Forefronts of Researches in Exotic Nuclear Structures (Niigata2010), (Niigata University), Tokamachi, Niigata Pref., Mar. (2010).
- Avogadro P. and Nakatsukasa T.: "Finite amplitude method for the QRPA", International Symposium on Forefronts of Researches in Exotic Nuclear Structures (Niigata2010), (Niigata University), Tokamachi, Niigata Pref., Mar. (2010).
- (Domestic Conference)
- Barbieri C.: "Green's Functions Calculations of Spectroscopic Factors", 日本物理学会第 64 回年次大会, 東京, 3 月 (2009).
- 吉田賢市: "Low-frequency vibrational modes in neutron-rich Mg isotopes close to the drip line", 日本物理学会第 64 回年次大会, 東京, 3 月 (2009).
- 小濱洋央, 飯田圭, 親松和浩: "くろたま断面積の質量数依存性", 日本物理学会第 64 回年次大会, 東京, 3 月 (2009).
- 小笠原弘道, 吉田賢市, 水島正二郎, 山上雅之, 松柳研: "超変形 ^{40}Ca の高スピン状態に於ける負パリティ励起モードに対する RPA 計算", 日本物理学会第 64 回年次大会, 東京, 3 月 (2009).
- 中務孝: "密度汎関数理論による計算核データ", Numazu Workshop 2009 「クオーク力学・原子核構造に基づく爆発的天体現象と元素合成」, (沼津高等専門学校), 沼津, 3 月 (2009).
- 小濱洋央: "高エネルギー核反応データ収集への期待: データベースユーザの立場から", RIBF ミニワークショップ「核データと核理論」, 和光, 3 月 (2009).
- 中務孝: "計算核データ構築に向けて", RIBF ミニワークショップ「核データと核理論」, 和光, 3 月 (2009).
- 中務孝: "有限振幅法による中重領域核の光吸収断面積", 第 5 回「計算科学による新たな知の発見・統合・創出」シンポジウム, (筑波大学), つくば, 5 月 (2009).
- 小濱洋央: "Purpose of this WS and the overview: how to deduce charge densities", RIBF ミニワークショップ "Electron Scattering data needed for the charge-density determination of unstable nuclei", 和光, 5 月 (2009).
- 小濱洋央: "Systematic analyses of total reaction cross sections using the black-sphere picture of nuclei", RIBF ミニワークショップ "One goal, different approaches - how to predict total reaction cross sections", 和光, 5 月 (2009).
- 中務孝: "密度汎関数理論の最近の発展", 宇宙核物理連絡協議会主催第 2 回研究戦略ワークショップ「日本の核データ〜天と地の核エネルギー」, (宇宙核物理連絡協議会), 和光, 7 月 (2009).
- Barbieri C.: "Toward an "ab-initio" Description of Single-Particle Properties", 千葉大学自然科学研究科原子核理論セミナー, (Chiba university), Chiba university, 7 月 (2009).
- 吉田賢市: "Collectivity in nuclei at around and beyond the island of inversion", 東京工業大学理学部物理学科セミナー, 東京, 7 月 (2009).
- 渡辺元太郎: "Efficient scheme for creating NOON state in a double-well potential", Workshop on Quantum Foundations for Young Researchers: From Mathematical Physics to Experimental Physics, (量子に関する関東 Student Chapter), 東京, 7 月 (2009).
- 川野原伸生: "原子核の低励起状態における大振幅集団ダイナミクス", KEK 理論センター研究会「原子核・ハドロン物理」, つくば, 8 月 (2009).

- 江幡修一郎, 中務孝, 稲倉恒法, 橋本幸男, 矢花 浩: “Skyrme-TDHF+“BCS”を用いた線形応答計算”, KEK 理論センター研究会「原子核・ハドロン物理」, (高エネルギー加速器研究機構, 素粒子原子核研究所), つくば, 8月(2009).
- 中務孝: “密度汎関数理論による核構造と核反応”, KEK 理論センター研究会「原子核・ハドロン物理」, (KEK), つくば, 8月(2009).
- 吉田賢市: “Pygmy mode in deformed neutron-rich Mg isotopes close to the drip line”, RCNP ミニワークショップ「原子核の E1, M1 励起モードの探究と今後の戦略」, (大阪大学核物理研究センター), 茨木, 8月(2009).
- 日野原伸生: “原子核低励起状態における大振幅集団運動”, 筑波大学原子核理論セミナー, つくば, 9月(2009).
- 渡辺 元太郎: “Efficient scheme for creating NOON state in a double-well potential: assisted higher-order cotunneling”, 筑波大学原子核理論研究室セミナー, (筑波大学), 筑波, 9月(2009).
- 渡辺元太郎: “分子動力学法でせまる原子核の Pasta 相: 超新星コアにおける Pasta 相の形成”, 早稲田大学 山田・前田研合同セミナー, (早稲田大学), 東京, 11月(2009).
- Avogadro P., 中務孝: “A tool to solve the QRPA problem fully self-consistently and with no symmetry restriction”, JUSTIPEN Workshop, 和光, 12月(2009).
- 渡辺元太郎: “超新星爆発における Pasta 相の形成”, 日本学術振興会科学研究費基盤研究 S2010「超新星の爆発機構とガンマ線バースト源エンジンの統一的理解」, (日本学術振興会, 国立天文台, 明星大学), 東京, 1月(2010).
- Barbieri C.: “Toward an accurate understanding of optical models and single-particle states in exotic nuclei”, RIBF 核物理セミナー, Wako, 1月(2010).
- 渡辺元太郎: “時間変調トンネル確率による NOON 状態の効率的な生成”, 日本物理学会第 65 回年次大会, (日本物理学会), 岡山, 3月(2010).
- 佐藤弘 一, 日野原伸生: “5 次元四重極集団 Hamiltonian を用いた Kr 同位体における変形共存の微視的解析”, 日本物理学会第 65 回年次大会, 岡山, 3月(2010).
- 日野原伸生, 佐藤弘 一, 中務孝, 松尾正之, 松柳研 一: “四重極集団 Hamiltonian による Se 同位体の低励起状態の系統的記述”, 日本物理学会第 65 回年次大会, 岡山, 3月(2010).
- 江幡修一郎, 中務孝, 稲倉恒法, 橋本幸男, 矢花 浩: “中重核に対する Skyrme-TDHF+“BCS”のアプローチ”, 日本物理学会第 65 回年次大会, 岡山, 3月(2010).
- 谷口億宇: “ ^{40}Ar の非軸対称超変形状態”, 日本物理学会第 65 回年次大会, 岡山, 3月(2010).

Strangeness Nuclear Physics Laboratory

Publications

Journal

(Original Papers) *Subject to Peer Review

- Nemura H.: “A New Three-Baryon-Force in $\Lambda\Lambda$ Hypernuclei”, AIP Conf. Proc. **1011**, 129–134 (2008). *
- Hatsuda T., Aoki S., Ishii N., and Nemura H.: “From Lattice QCD to Nuclear Force”, Mod. Phys. Lett. A **23**, 2265–2272 (2008). *
- Nemura H., Ishii N., Aoki S., and Hatsuda T.: “Lattice QCD Simulation of Hyperon-Nucleon Potential”, Mod. Phys. Lett. A **23**, 2285–2288 (2008). *
- Nemura H.: “ $\Lambda\Lambda$ - $N\Xi$ - $\Lambda\Sigma$ - $\Sigma\Sigma$ Coupled Channel Calculations of Doubly Strange Hypernuclei”, Nucl. Phys. A **805**, 191–193 (2008). *
- Aoki S., Balog J., Hatsuda T., Ishii N., Murano K., Nemura H., and Weisz P.: “Energy Dependence of Nucleon-Nucleon Potentials”, Proceedings of Science **LATTICE 2008**, No. 152, pp. 1–7 (2008). *
- Nemura H., Ishii N., Aoki S., and Hatsuda T.: “Lambda-nucleon force from lattice QCD”, Proceedings of Science **LATTICE 2008**, No. 156, pp. 1–7 (2008). *
- Umeya A., Kaneko G., and Muto K.: “Shell-model calculation of E2 effective charges: Application to carbon isotopes”, Nucl. Phys. A **829**, 13–30 (2009). *
- Nemura H., Ishii N., Aoki S., and Hatsuda T.: “Hyperon-nucleon force from lattice QCD”, Phys. Lett. B **673**, 136–141 (2009). *
- Hiyama E., Yamamoto Y., Motoba T., and Kamimura M.: “Structure of A=7 Iso-Triplet Λ Hypernuclei Studied with the Four-Body Cluster Model”, Phys. Rev. C **80**, 054321-1–054321-12 (2009). *

(Review)

- Hiyama E. and Yamada T.: “Structure of Light Hypernuclei”, Prog. Part. Nucl. Phys. **63**, No. 2, pp. 339–395 (2009).

Oral Presentations

(International Conference etc.)

- Nemura H., Ishii N., Aoki S., and Hatsuda T.: “Lambda-nucleon force from lattice QCD”, Lattice 2008, 26th International Symposium on Lattice Field Theory, (College of Williams and Mary), Virginia, USA, July (2008).
- Nemura H., Ishii N., Aoki S., and Hatsuda T.: “Hyperon-nucleon force calculated from lattice QCD”, KGU Yokohama Autumn School of Nuclear Physics, (KGU), Yokohama, Oct. (2008).
- Nemura H., Ishii N., Aoki S., and Hatsuda T.: “Study of hyperon-nucleon potential from lattice QCD”, Sendai International Symposium on Strangeness in Nuclear and Hadronic Systems (SENDAI08), (Tohoku University), Sendai, Dec. (2008).
- Hiyama E.: “Structure of Three- and Four-Body Light Hypernuclei”, International Summer School on Sub-

atomic Physics / 5th course: Some New Facets in Nuclear Physics, (Peking University), Beijing, China, Aug. (2009).

- Ikeda Y., Aoki S., Hatsuda T., Ishii N., Nemura H., Inoue T., Doi T., Sasaki K., and Murano K.: “Kaon-nucleon potential from lattice QCD”, 19th International IUPAP Conference on Few-Body Problems in Physics, (University of Bonn), Bonn, Germany, Aug.–Sept. (2009).
- Hiyama E.: “Recent Progress in Hypernuclear Physics”, 19th International IUPAP Conference on Few-Body Problems in Physics, (University of Bonn), Bonn, Germany, Aug.–Sept. (2009).
- Umeya A. and Harada T.: “Sigma-admixture in neutron-rich lithium Lambda hypernuclei in a microscopic shell-model calculation”, 19th International IUPAP Conference on Few-Body Problems in Physics, (University of Bonn), Bonn, Germany, Aug.–Sept. (2009).
- Hiyama E.: “Few Body Systems with S=-1,-2”, 10th International Conference on Hypernuclear and Strange Particle Physics (Hyp-X), (Kyoto university, the Global COE Program), Tokai-mura, Ibaraki Pref., Sept. (2009).
- Ikeda Y., Sato T., and Kamano H.: “On the resonance energy of the $K\bar{K}NN$ - π YN system”, 10th International Conference on Hypernuclear and Strange Particle Physics (Hyp-X), Tokai-mura, Ibaraki Pref., Sept. (2009).
- Umeya A. and Harada T.: “Shell-model study on Sigma-mixing in neutron-rich lithium Lambda hypernuclei”, 10th International Conference on Hypernuclear and Strange Particle Physics (Hyp-X), (Kyoto university), Tokai-mura, Ibaraki Pref., Sept. (2009).
- Rijken T. A.: “Status of Our Understanding on the YN Interaction”, 10th International Conference on Hypernuclear and Strange Particle Physics (Hyp-X), (Kyoto university, the Global COE Program), Tokai-mura, Ibaraki Pref., Sept. (2009).
- Hiyama E., Kamimura M., and Yamamoto Y.: “Five-Body Structure of Double Λ Hypernuclei”, 3rd Joint Meeting of the APS Division of Nuclear Physics and the Physical Society of Japan (HAW 09), Hawaii, USA, Oct. (2009).
- Umeya A., Motoba T., and Harada T.: “Shell model study of typical sd-shell hypernuclei”, 3rd Joint Meeting of the Nuclear Physics Divisions of the APS and JPS (Hawaii 2009), (APS Division of Nuclear Physics, The Physical Society of Japan), Hawaii, USA, Oct. (2009).
- Ikeda Y., Aoki S., Doi T., Hatsuda T., Inoue T., Ishii N., Nemura H., Sasaki K., and Murano K.: “NK potential in full QCD lattice simulation”, US-Japan Joint Workshop on Meson Production Reaction at Jefferson Lab and J-PARC, Hawaii, USA, Oct. (2009).
- Hiyama E.: “Light Ξ Hypernuclei in Four-Body Cluster Models”, Hadron and Nuclear Physics (HNP09), (RCNP), Osaka, Nov. (2009).
- Umeya A., Motoba T., and Harada T.: “Shell-model cal-

- culations for typical sd-shell hypernuclei”, Hadron and Nuclear Physics (HNP09), (Osaka University, RCNP), Osaka, Nov. (2009).
- Rijken T. A.: “Strange and Non-Strange Baryon-Baryon Interactions Recent Nijmegen Extended-Soft-Core Models”, Hadron and Nuclear Physics (HNP09), (RCNP), Osaka, Nov. (2009).
- Hiyama E.: “Theory of Light Hypernuclear Structure Cluster Model Approach”, 2nd JSPS Core-to-core Seminar on Strangeness Nuclear Physics by Electron Beams, Rome, Italy, Dec. (2009).
- Ikeda Y., Aoki S., Doi T., Hatsuda T., Inoue T., Ishii N., Murano K., Nemura H., and Sasaki K.: “K-N potential and Theta+ in lattice QCD”, New Frontiers in QCD 2010, (YITP), Kyoto, Jan.-Mar. (2010). (Domestic Conference)
- 飯尾雅実, 板橋健太, 岩崎雅彦, 應田治彦, 大西宏明, 岡田信一, 佐久間史典, 鈴木隆敏, 友野大, 松田恭幸, 山崎敏光, 石元茂, 鈴木祥二, 関本美知子, 豊田晃久, 永江知文, 石川隆, 竜野秀行, 早野龍五, 藤岡宏之, 味村周平, 阪口篤志, 佐藤将春, 福田芳之, 千葉順成, 花木俊生, 福田共和, 溝井浩, Beer G. A., 方享燦, Choi S., 林熙重, 石渡智一, Buehler P., Hirtl A., Cargnelli M., Kienle P., Marton J., Widmann E., Zmeskal J., Curceanu C. O., Guaraldo C., Iliescu M., Pietreanu D., Sirghi D., Sirghi F., Faso D., Busso L., Morra O.: “K 中間子原子核探索実験のための液体ヘリウム 3 標的の開発”, 日本物理学会 2007 年春季大会, 八王子, 3 月 (2007).
- 根村英克, 石井理修, 青木慎也, 初田哲男: “格子 QCD によるハイペロンポテンシャルの研究”, 文科省科研費補助金特定領域研究「サマースクールエキゾチック原子核実践講座-あなたも計算できる-」, (京都大学), 和光, 8 月 (2008).
- 飯尾雅実, 板橋健太, 岩崎雅彦, 應田治彦, 大西宏明, 佐久間史典, 佐藤将春, 塚田暁, 友野大, 藤岡宏之, 山崎敏光, 石元茂, 岩井正明, 鈴木祥二, 関本美知子, 豊田晃久, 石川隆, 竜野秀行, 鈴木隆敏, 早野龍五, 松田恭幸, 永江知文, 平岩聡彦, 味村周平, 野海博之, 阪口篤志, 藤原裕也, 徳田真, 千葉順成, 福田共和, 溝井浩, Beer G. A., 方享燦, Choi S., 林熙重, 石渡智一, Buehler P., Cargnelli M., Hirtl A., Kienle P., Marton J., Widmann E., Zmeskal J., 岡田信一, Curceanu C. O., Guaraldo C., Iliescu M., Pietreanu D., Sirghi D., Sirghi F., Faso D., Morra O., Busso L.: “K 中間子原子核探索実験のための液体ヘリウム 3 標的の開発 III”, 日本物理学会 2008 年秋季大会, 山形, 9 月 (2008).
- 根村英克: “格子 QCD と J-PARC のハイペロン相互作用方面”, 「J-PARC ハドロン物理の将来研究計画を考える」研究会, 和光, 9 月 (2008).
- 根村英克, 石井理修, 青木慎也, 初田哲男: “格子 QCD によるハイペロン核子相互作用の研究”, 文科省科研費補助金特定領域研究「ストレンジネスで探るクォーク多体系」研究会 2008, 加賀, 10 月 (2008).
- 根村英克, 石井理修, 青木慎也, 初田哲男: “Hyperon Potentials from Lattice QCD”, Aizu meeting 2009 on Spin Excitations and Exotic Degree of Freedom in Nuclei and Nuclear Matter, 会津若松, 2 月 (2009).
- 根村英克, 石井理修, 青木慎也, 初田哲男: “格子 QCD によるハイペロン核子相互作用の研究”, 文科省科研費補助金特定領域研究「ストレンジネスで探るクォーク多体系」理論班主催「ストレンジネスを含むクォーク多体系分野の理論的将来を考える」研究会, 熱海, 2 月 (2009).
- 根村英克, 石井理修, 青木慎也, 初田哲男: “格子 QCD による ΛN ポテンシャル”, 日本物理学会第 64 回年次大会, (日本物理学会), 東京, 3 月 (2009).
- 根村英克, 石井理修, 青木慎也, 初田哲男: “格子 QCD によるハイペロンポテンシャル”, 文科省科研費補助金新学術領域研究「素粒子融合による計算科学に基づいた重層の物質構造の解明」A02 班主催「ハイパー核研究と中性子星研究の連携の可能性を探る」研究会, 和光, 3 月 (2009).
- 肥山詠美子: “テンサー力とハイパー核”, RCNP ワークショップ「テンサー力と原子核物理」, (大阪大学核物理研究センター), 大阪, 4 月 (2009).
- 肥山詠美子: “ハイパー核から決めるバリオン間力”, 「バリオン間相互作用に基づく核物質の構造」研究会, 盛岡, 6 月 (2009).
- 梅谷篤史, 原田融: “中性子過剰ハイパー核におけるラムダ・シグマ結合”, KEK 理論センター研究会「原子核・ハドロン物理」, (高エネルギー加速器研究機構), つくば, 8 月 (2009).
- 肥山詠美子: “理系はおもしろい! どうしたら研究者になれるの?: ストレンジネスをもつ原子核 (ハイパー核) の研究を通して”, 文科省科研費補助金特定領域研究「ストレンジネスで探るクォーク多体系」高校生のための講演会, (京都大学), 京都, 8 月 (2009).
- 肥山詠美子: “Few-Body Structure of S=-2 Systems”, Workshop on Flavor Nuclear Physics in HIDA, 高山, 11 月 (2009).
- 梅谷篤史, 原田融: “中性子過剰ハイパー核の殻模型研究”, 科研費特定領域と新学術領域による研究会「ストレンジネスから新ハドロンへ」, (大阪大学 RCNP), 吹田, 12 月 (2009).
- 肥山詠美子: “特定領域の成果まとめ I ハイパー核の構造”, 科研費特定領域と新学術領域による研究会「ストレンジネスから新ハドロンへ」, 吹田, 12 月 (2009).
- 肥山詠美子: “量子力学的 3 体・4 体問題計算法の確立と原子核分野への応用”, 第 22 回北海道原子核理論グループ研究会, 札幌, 1 月 (2010).
- 肥山詠美子: “ハイパー核構造の今後の展望-少数粒子系理論物理的観点から-”, 第 7 回原子核ハドロン物理セミナー, (日本原子力研究開発機構), 茨城県東海村, 3 月 (2010).

Radiation Laboratory

Publications

Journal

(Original Papers) *Subject to Peer Review

- Hatsuda T., Aoki S., Ishii N., and Nemura H.: “From Lattice QCD to Nuclear Force”, *Mod. Phys. Lett. A* **23**, 2265–2272 (2008). *
- Nemura H., Ishii N., Aoki S., and Hatsuda T.: “Lattice QCD Simulation of Hyperon-Nucleon Potential”, *Mod. Phys. Lett. A* **23**, 2285–2288 (2008). *
- Adare A., Akiba Y., Aoki K., Asai J., Bazilevsky A. V., Bunce G. M., Deshpande A., Enyo H., Fields D. E., Fox B., Fujiwara K., Fukao Y., Goto Y., Gross P. M., Hasuko K., Heuser J. M., Horaguchi T., Ichihara T., Imai K., Inoue Y., Ishihara M., Jinnouchi O., Kamihara N., Kaneta M., Kanoh H., Kawall D., Kiyomichi A., Kobayashi H., Kurita K., Mao Y., Murata J., Nakagawa I., Nakano K., Onishi H., Okada H., Okada K., Rykov V. L., Saito N., Sato H., Shibata T., Shoji K., Tabaru T., Taketani A., Tanida K., Togawa M., Tojo J., Torii H., Wagner M. M., Watanabe Y., Xie W., and Yokkaichi S.: “Cold Nuclear Matter Effects on J/ψ Production as Constrained by Deuteron-Gold Measurements at $\sqrt{s_{NN}} = 200$ GeV”, *Phys. Rev. C* **77**, 024912-1–024912-15 (2008). *
- Adare A., Akiba Y., Aoki K., Asai J., Bunce G. M., Deshpande A., Enyo H., Fields D. E., Fujiwara K., Fukao Y., Goto Y., Gross P. M., Hachiya T., Hasuko K., Heuser J. M., Horaguchi T., Ichihara T., Imai K., Inoue Y., Ishihara M., Jinnouchi O., Kajihara F., Kamihara N., Kaneta M., Kanoh H., Kawall D., Kiyomichi A., Kurita K., Mao Y., Murata J., Nakagawa I., Nakano K., Onishi H., Okada H., Okada K., Rykov V. L., Saito N., Sato H., Shibata T., Shoji K., Tabaru T., Taketani A., Tanida K., Togawa M., Tojo J., Torii H., Tsuchimoto Y., Wagner M. M., Watanabe Y., Xie W., and Yokkaichi S.: “Quantitative Constraints on the Transport Properties of Hot Partonic Matter from Semi-Inclusive Single High Transverse Momentum Pion Suppression in Au+Au Collisions at $\sqrt{s_{NN}} = 200$ GeV”, *Phys. Rev. C* **77**, 064907-1–064907-12 (2008). *
- Adare A., Akiba Y., Aoki K., Asai J., Bunce G. M., Deshpande A., Enyo H., Fields D. E., Fujiwara K., Fukao Y., Goto Y., Gross P. M., Hachiya T., Hasuko K., Heuser J. M., Horaguchi T., Ichihara T., Imai K., Inoue Y., Ishihara M., Jinnouchi O., Kajihara F., Kamihara N., Kaneta M., Kanoh H., Kawall D., Kiyomichi A., Kurita K., Mao Y., Murata J., Nakagawa I., Nakano K., Onishi H., Okada H., Okada K., Rykov V. L., Saito N., Sato H., Shibata T., Shoji K., Tabaru T., Taketani A., Tanida K., Togawa M., Tojo J., Torii H., Tsuchimoto Y., Wagner M. M., Watanabe Y., Xie W., and Yokkaichi S.: “Dihadron azimuthal correlations in Au+Au collisions at $\sqrt{s_{NN}} = 200$ GeV”, *Phys. Rev. C* **78**, 014901-1–014901-42 (2008). *
- Adare A., Akiba Y., Aoki K., Asai J., Bazilevsky A. V., Bunce G. M., Deshpande A., Enyo H., Fields D. E., Fox B., Fujiwara K., Fukao Y., Goto Y., Gross P. M., Hachiya T., Hasuko K., Heuser J. M., Horaguchi T., Ichihara T., Imai K., Inoue Y., Ishihara M., Jinnouchi O., Kajihara F., Kamihara N., Kaneta M., Kanoh H., Kawall D., Kiyomichi A., Kobayashi H., Kurita K., Mao Y., Murata J., Nakagawa I., Nakano K., Onishi H., Okada H., Okada K., Rykov V. L., Saito N., Sato H., Shibata T., Shoji K., Tabaru T., Taketani A., Tanida K., Togawa M., Tojo J., Torii H., Tsuchimoto Y., Wagner M. M., Watanabe Y., Xie W., and Yokkaichi S.: “Charged hadron multiplicity fluctuations in Au+Au and Cu+Cu collisions from $\sqrt{s_{NN}} = 22.5$ to 200 GeV”, *Phys. Rev. C* **78**, 044902-1–044902-15 (2008). *
- Afanasiev S., Akiba Y., Aoki K., Bunce G. M., Deshpande A., Enyo H., Fields D. E., Fukao Y., Goto Y., Gross P. M., Hachiya T., Hasuko K., Heuser J. M., Horaguchi T., Ichihara T., Imai K., Ishihara M., Jinnouchi O., Kajihara F., Kamihara N., Kaneta M., Kiyomichi A., Kurita K., Murata J., Onishi H., Okada H., Okada K., Rykov V. L., Saito N., Sato H., Shibata T., Shoji K., Tabaru T., Taketani A., Tanida K., Togawa M., Tojo J., Torii H., Tsuchimoto Y., Wagner M. M., Watanabe Y., Xie W., and Yokkaichi S.: “Source breakup dynamics in Au+Au Collisions at $\sqrt{s_{NN}}=200$ GeV via three-dimensional two-pion source imaging”, *Phys. Rev. Lett.* **100**, 232301-1–232301-6 (2008). *
- Afanasiev S., Akiba Y., Aoki K., Bunce G. M., Deshpande A., Enyo H., Fields D. E., Fukao Y., Goto Y., Gross P. M., Hachiya T., Hasuko K., Heuser J. M., Horaguchi T., Ichihara T., Imai K., Ishihara M., Jinnouchi O., Kajihara F., Kamihara N., Kaneta M., Kiyomichi A., Kurita K., Murata J., Onishi H., Okada H., Okada K., Rykov V. L., Saito N., Sato H., Shibata T., Shoji K., Tabaru T., Taketani A., Tanida K., Togawa M., Tojo J., Torii H., Tsuchimoto Y., Wagner M. M., Watanabe Y., Xie W., and Yokkaichi S.: “Particle-species dependent modification of jet-induced correlations in Au+Au collisions at $\sqrt{s_{NN}} = 200$ GeV”, *Phys. Rev. Lett.* **101**, 082301-1–082301-6 (2008). *
- Adare A., Akiba Y., Aoki K., Asai J., Bunce G. M., Deshpande A., Enyo H., Fields D. E., Fujiwara K., Fukao Y., Goto Y., Gross P. M., Horaguchi T., Ichihara T., Imai K., Inoue Y., Ishihara M., Jinnouchi O., Kamihara N., Kaneta M., Kanoh H., Kawall D., Kiyomichi A., Kurita K., Mao Y., Murata J., Nakagawa I., Nakano K., Onishi H., Okada H., Okada K., Rykov V. L., Saito N., Shibata T., Shoji K., Tabaru T., Taketani A., Tanida K., Togawa M., Tojo J., Torii H., Wagner M. M., Watanabe Y., Xie W., and Yokkaichi S.: “ J/ψ Production in $\sqrt{s_{NN}} = 200$ GeV Cu+Cu Collisions”, *Phys. Rev. Lett.* **101**, 122301-1–122301-6 (2008). *
- Adare A., Akiba Y., Aoki K., Asai J., Bunce G. M.,

- Dairaku S., Deshpande A., Enyo H., Fields D. E., Fujiwara K., Fukao Y., Goto Y., Gross P. M., Horaguchi T., Ichihara T., Ichimiya R., Imai K., Inoue Y., Ishihara M., Jinnouchi O., Kametani S., Kamihara N., Kaneta M., Kanoh H., Kawall D., Kiyomichi A., Kurita K., Kurosawa M., Li Z., Mao Y., Murata J., Nakagawa I., Nakano K., Onishi H., Okada H., Okada K., Onuki Y., Rykov V. L., Saito N., Sakashita K., Shibata T., Shoji K., Tabaru T., Taketani A., Tanida K., Togawa M., Tojo J., Torii H., Wagner M. M., Watanabe Y., Xie W., and Yokkaichi S.: “Onset of π^0 suppression studied in Cu+Cu collisions at $\sqrt{s_{NN}} = 22.4, 62.4,$ and 200 GeV”, *Phys. Rev. Lett.* **101**, 162301-1–162301-6 (2008). *
- Adare A., Akiba Y., Aoki K., Asai J., Bunce G. M., Deshpande A., Enyo H., Fields D. E., Fujiwara K., Fukao Y., Goto Y., Gross P. M., Hachiyu T., Hasuko K., Heuser J. M., Horaguchi T., Ichihara T., Imai K., Inoue Y., Ishihara M., Jinnouchi O., Kajihara F., Kamihara N., Kaneta M., Kanoh H., Kawall D., Kiyomichi A., Kurita K., Mao Y., Murata J., Nakagawa I., Nakano K., Onishi H., Okada H., Okada K., Rykov V. L., Saito N., Sato H., Shibata T., Shoji K., Tabaru T., Taketani A., Tanida K., Togawa M., Tojo J., Torii H., Tsuchimoto Y., Wagner M. M., Watanabe Y., Xie W., and Yokkaichi S.: “Suppression pattern of neutral pions at high transverse momentum in Au+Au collisions at $\sqrt{s_{NN}} = 200$ GeV and constraints on medium transport coefficients”, *Phys. Rev. Lett.* **101**, 232301-1–232301-7 (2008). *
- Aoki S., Balog J., Hatsuda T., Ishii N., Murano K., Nemura H., and Weisz P.: “Energy Dependence of Nucleon-Nucleon Potentials”, *Proceedings of Science LATTICE 2008*, No. 152, pp. 1–7 (2008). *
- Nemura H., Ishii N., Aoki S., and Hatsuda T.: “Lambda-nucleon force from lattice QCD”, *Proceedings of Science LATTICE 2008*, No. 156, pp. 1–7 (2008). *
- Hata M., Akiyama T., Ikeda Y., Kawamura H., Narota K., Ninomiya K., Ogawa N., Sato T., Seitaibashi E., Sekiguchi Y., Tsutsui R., Yazawa K., and Murata J.: “Recent results on short-range gravity experiment”, *J. Phys.: Con. Ser.* **189**, 012019-01–012019-10 (2009). *
- Ninomiya K., Akiyama T., Hata M., Ikeda Y., Kawamura H., Narota K., Ogawa N., Sato T., Seitaibashi E., Sekiguchi Y., Tsutsui R., Yazawa K., and Murata J.: “New experimental technique for short-range gravity measurement”, *J. Phys.: Con. Ser.* **189**, 012026-1–012026-7 (2009). *
- Akiba Y.: “Dilepton radiation measured in PHENIX probing the strongly interacting matter created at RHIC”, *Nucl. Phys. A* **830**, 567–570 (2009). *
- Adare A., Akiba Y., Aoki K., Asai J., Bunce G. M., Deshpande A., Enyo H., Fields D. E., Fujiwara K., Fukao Y., Goto Y., Gross P. M., Horaguchi T., Ichihara T., Imai K., Inoue Y., Ishihara M., Jinnouchi O., Kamihara N., Kaneta M., Kanoh H., Kawall D., Kiyomichi A., Kurita K., Mao Y., Murata J., Nakagawa I., Nakano K., Onishi H., Okada H., Okada K., Rykov V. L., Saito N., Sakashita K., Shibata T., Shoji K., Tabaru T., Taketani A., Tanida K., Togawa M., Tojo J., Torii H., Wagner M. M., Watanabe Y., Xie W., and Yokkaichi S.: “Dilepton mass spectra in p+p collisions at $\sqrt{s} = 200$ GeV and the contribution from open charm”, *Phys. Lett. B* **670**, 313–320 (2009). *
- Nemura H., Ishii N., Aoki S., and Hatsuda T.: “Hyperon-nucleon force from lattice QCD”, *Phys. Lett. B* **673**, 136–141 (2009). *
- Adare A., Akiba Y., Aoki K., Asai J., Bunce G. M., Dairaku S., Deshpande A., Enyo H., Fields D. E., Fujiwara K., Fukao Y., Goto Y., Gross P. M., Horaguchi T., Ichihara T., Ichimiya R., Imai K., Ishihara M., Kametani S., Kamihara N., Kawall D., Kurita K., Kurosawa M., Li Z., Mao Y., Murata J., Nakagawa I., Nakano K., Okada H., Okada K., Onuki Y., Rykov V. L., Saito N., Sakashita K., Shibata T., Shoji K., Taketani A., Tanida K., Togawa M., Torii H., Watanabe Y., Xie W., and Yokkaichi S.: “Inclusive cross section and double helicity asymmetry for π^0 production in $p + p$ collisions at $\sqrt{s} = 62.4$ GeV”, *Phys. Rev. D* **79**, 012003-1–012003-11 (2009). *
- (Others)
- Murata J., Akiyama T., Hata M., Hirayama Y., Ikeda Y., Ishii T., Kameda D., Kawamura H., Mitsuoka S., Miyatake H., Nagae D., Ninomiya K., Nitta M., Seitaibashi E., and Toyoda T.: “Test of time reversal symmetry using polarized nuclei”, *JAEA-Review* **2009-036**, 62–63 (2009).
- Book • Proceedings**
- (Review)
- Yokkaichi S.: “In-medium mass modification of vector mesons”, *Particle and Nuclear Physics at J-PARC (Lecture Notes in Physics 781)*, Springer, Heidelberg, pp. 161–193 (2009).
- Akiba Y.: “Heavy Ion Physics at RHIC”, *Proceedings of the 6th Japan-Italy symposium on Heavy-Ion Physics, Tokai-mura, Ibaraki Pref., 2008–11*, American Institute of Physics, New York, pp. 157–162 (2009).
- Oral Presentations**
- (International Conference etc.)
- Takeuchi S., Shimoura S., Motobayashi T., Akiyoshi H., Ando Y., Aoi N., Fulop Z., Gomi T., Higurashi Y., Hirai M., Iwasa N., Iwasaki H., Iwata Y., Kobayashi H., Kurokawa M., Liu Z., Minemura T., Ozawa S., Sakurai H., Serata M., Teranishi T., Yamada K., Yanagisawa Y., and Ishihara M.: “Isobaric analog state of ^{14}Be ”, *RIKEN-CNS RIBF International Workshop “Correlation and Condensation: New Features in Loosely Bound and Unbound Nuclear States”*, Wako, Dec. (2005).
- Nemura H., Ishii N., Aoki S., and Hatsuda T.: “Lambda-nucleon force from lattice QCD”, *Lattice 2008, 26th International Symposium on Lattice Field Theory*, (Col-

- lege of Williams and Mary), Virginia, USA, July (2008).
- Nemura H., Ishii N., Aoki S., and Hatsuda T.: “Hyperon-nucleon force calculated from lattice QCD”, KGU Yokohama Autumn School of Nuclear Physics, (KGU), Yokohama, Oct. (2008).
- Nemura H., Ishii N., Aoki S., and Hatsuda T.: “Study of hyperon-nucleon potential from lattice QCD”, Sendai International Symposium on Strangeness in Nuclear and Hadronic Systems (SENDAI08), (Tohoku University), Sendai, Dec. (2008).
- Enyo H.: “RIKEN Activity at J-PARC”, International Workshop on Physics and Upgrade of the J-PARC Hadron Facility, (RCNP, Osaka University, RIKEN), Tokai-mura, Ibaraki Pref., Sept. (2009).
- Enyo H.: “Experimental Quest for Proton Spin Structure: Past, Present and Future”, 3rd Joint Meeting of the Nuclear Physics Divisions of the APS and JPS (Hawaii 2009), (The Physical Society of Japan, American Physical Society), Hawaii, USA, Oct. (2009).
- Baba H., Ichihara T., Ohnishi T., Takeuchi S., Yoshida K., Watanabe Y., Ota S., and Shimoura S.: “The New DAQ System in RIKEN RIBF”, 3rd Joint Meeting of the Nuclear Physics Divisions of the APS and JPS (Hawaii 2009), Hawaii, USA, Oct. (2009).
- Akiba Y.: “Enhanced production of direct photons in Au+Au collisions at $\sqrt{s_{NN}}=200$ GeV and implications for the initial temperature”, APS April Meeting 2010, (American Physical Society), Washington DC, USA, Feb. (2010).
- (Domestic Conference)
- 飯尾雅実, 板橋健太, 岩崎雅彦, 應田治彦, 大西宏明, 岡田信一, 佐久間史典, 鈴木隆敏, 友野大, 松田恭幸, 山崎敏光, 石元茂, 鈴木祥二, 関本美知子, 豊田晃久, 永江知文, 石川隆, 竜野秀行, 早野龍五, 藤岡宏之, 味村周平, 阪口篤志, 佐藤将春, 福田芳之, 千葉順成, 花木俊生, 福田共和, 溝井浩, Beer G. A., 方享燦, Choi S., 林熙重, 石渡智一, Buehler P., Hirtl A., Cargnelli M., Kienle P., Marton J., Widmann E., Zmeskal J., Curceanu C. O., Guaraldo C., Iliescu M., Pietreanu D., Sirghi D., Sirghi F., Faso D., Busso L., Morra O.: “K 中間子原子核探索実験のための液体ヘリウム 3 標的の開発”, 日本物理学会 2007 年春季大会, 八王子, 3 月 (2007).
- 根村英克, 石井理修, 青木慎也, 初田哲男: “格子 QCD によるハイペロンポテンシャルの研究”, 文科省科研費補助金特定領域研究「サマースクールエキゾチック原子核実践講座-あなたも計算できる-」, (京都大学), 和光, 8 月 (2008).
- 飯尾雅実, 板橋健太, 岩崎雅彦, 應田治彦, 大西宏明, 佐久間史典, 佐藤将春, 塚田暁, 友野大, 藤岡宏之, 山崎敏光, 石元茂, 岩井正明, 鈴木祥二, 関本美知子, 豊田晃久, 石川隆, 竜野秀行, 鈴木隆敏, 早野龍五, 松田恭幸, 永江知文, 平岩聡彦, 味村周平, 野海博之, 阪口篤志, 藤原裕也, 徳田真, 千葉順成, 福田共和, 溝井浩, Beer G. A., 方享燦, Choi S., 林熙重, 石渡智一, Buehler P., Cargnelli M., Hirtl A., Kienle P., Marton J., Widmann E., Zmeskal J., 岡田信一, Curceanu C. O., Guaraldo C., Iliescu M., Pietreanu D., Sirghi D., Sirghi F., Faso D., Morra O., Busso L.: “K 中間子原子核探索実験のための液体ヘリウム 3 標的の開発 III”, 日本物理学会 2008 年秋季大会, 山形, 9 月 (2008).
- 根村英克, 石井理修, 青木慎也, 初田哲男: “格子 QCD によるハイペロン核子相互作用の研究”, 文科省科研費補助金特定領域研究「ストレンジネスで探るクォーク多体系」研究会 2008, 加賀, 10 月 (2008).
- 根村英克, 石井理修, 青木慎也, 初田哲男: “Hyperon Potentials from Lattice QCD”, Aizu meeting 2009 on Spin Excitations and Exotic Degree of Freedom in Nuclei and Nuclear Matter, 会津若松, 2 月 (2009).
- 根村英克, 石井理修, 青木慎也, 初田哲男: “格子 QCD によるハイペロン核子相互作用の研究”, 文科省科研費補助金特定領域研究「ストレンジネスで探るクォーク多体系」理論班主催「ストレンジネスを含むクォーク多体系分野の理論的将来を考える」研究会, 熱海, 2 月 (2009).
- 延與秀人: “Mesons in dense matter”, 日本物理学会第 64 回年次大会, (日本物理学会), 東京, 3 月 (2009).
- 根村英克, 石井理修, 青木慎也, 初田哲男: “格子 QCD による ΛN ポテンシャル”, 日本物理学会第 64 回年次大会, (日本物理学会), 東京, 3 月 (2009).
- 四川市悟: “Experimental study of vector-meson modification in nuclei”, Workshop “Photons and Leptons in Hot/Dense QCD”, (名古屋大学), 名古屋, 3 月 (2009).
- 根村英克, 石井理修, 青木慎也, 初田哲男: “格子 QCD によるハイペロンポテンシャル”, 文科省科研費補助金新学術領域研究「素粒子宇宙融合による計算科学に基づいた重層的物質構造の解明」A02 班主催「ハイパー核研究と中性子星研究の連携の可能性を探る」研究会, 和光, 3 月 (2009).
- 西谷智博, 田淵雅夫, 鈴木祐史, 元木和也, 竹田美和: “負電子親和力表面を持つ半導体を用いた 30keV フォトカソード電子銃の開発”, 日本顕微鏡学会第 65 回学術講演会, (日本顕微鏡学会), 仙台, 5 月 (2009).
- 四川市悟: “J-PARC E16: 電子対測定実験の物理と実験計画”, 新学術領域キックオフ研究会 “多彩なフレーバーで探る新しいハドロン存在形態の包括的研究”, (新学術領域研究「多彩なフレーバーで探る新しいハドロン存在形態の包括的研究」総括班), 名古屋大学, 11 月 (2009).
- 森田晋也, 山形豊, 見原俊介, 須長秀行, 広田克也: “JRR-3 MUSASI を用いた中性子ラジオグラフィによる工業製品内部欠陥観察”, 日本中性子科学会第 8 回年会, 名古屋, 12 月 (2009).
- 四川市悟: “核物質中の中間子質量測定とカイラル対称性”, GCOE シンポジウム「対称性の破れと量子現象」, (京都大学 大学院理学研究科), 京都, 2 月 (2010).
- 川村広和, 秋山岳伸, 秦麻記, 平山賀一, 池田友樹, 石井哲朗, 亀田大輔, 光岡慎一, 宮原直亮, 宮武宇也, 村田次郎, 中谷祐輔, 長江大輔, 二宮一史, 新田稔, 大西潤一, 聖代橋悦子, 豊田健司, 塚田和司, 渡辺裕: “KEK-TRIAC における偏極 ^8Li を用いた時間反転対称性研究”, 日本物理学会第 65 回年次大会, 岡山, 3 月 (2010).
- 川村広和, 秋山岳伸, Behr J. A., 秦麻記, 平山賀一, 池田友樹, 石井哲朗, 亀田大輔, Levy P., 宮原直亮, 宮武宇也, 光岡真一, 村田次郎, 長江大輔, 中谷祐輔, 二宮一史, 新田稔, 小川就也, 大西潤一, Pearson M., 聖代橋悦子, 豊田健司,

塚田和司, 渡辺裕: “偏極 ^8Li のベータ崩壊における時間反転対称性の破れの探索”, 第 6 回停止・低速不安定核ビームを用いた核分光研究会, 東京, 3 月 (2010).

Publications

Journal

(Original Papers) *Subject to Peer Review

- Nagae D., Asahi K., Ueno H., Kameda D., Takemura M., Takase T., Yoshimi A., Sugimoto T., Nagatomo T., Kobayashi Y., Uchida M., Shimada K., Arai T., Inoue T., Kagami S., and Hatakeyama N.: “Measurement of Electric Quadrupole Moments for ^{31}Al Using Spin Polarized RI Beams”, AIP Conf. Proc. **915**, 853–856 (2007). *
- Shimada K., Nagae D., Asahi K., Arai T., Takemura M., Inoue T., Takase T., Kagami S., Hatakeyama N., Kobayashi Y., Ueno H., Yoshimi A., Kameda D., Nagatomo T., Sugimoto T., Kubono S., Yamaguchi H., Wakabayashi Y., Amadio G., Hayakawa S., Murata J., and Kawamura H.: “Production of Polarized Radioactive Beams via The Inverse-kinematics Reactions and Their Applications”, AIP Conf. Proc. **915**, 857–860 (2007). *
- Adare A., Akiba Y., Aoki K., Asai J., Bazilevsky A. V., Bunce G. M., Deshpande A., Enyo H., Fields D. E., Fox B., Fujiwara K., Fukao Y., Goto Y., Gross P. M., Hasuko K., Heuser J. M., Horaguchi T., Ichihara T., Imai K., Inoue Y., Ishihara M., Jinnouchi O., Kamihara N., Kaneta M., Kanoh H., Kawall D., Kiyomichi A., Kobayashi H., Kurita K., Mao Y., Murata J., Nakagawa I., Nakano K., Onishi H., Okada H., Okada K., Rykov V. L., Saito N., Sato H., Shibata T., Shoji K., Tabaru T., Taketani A., Tanida K., Togawa M., Tojo J., Torii H., Wagner M. M., Watanabe Y., Xie W., and Yokkaichi S.: “Cold Nuclear Matter Effects on J/ψ Production as Constrained by Deuteron-Gold Measurements at $\sqrt{s_{NN}} = 200$ GeV”, Phys. Rev. C **77**, 024912-1–024912-15 (2008). *
- Adare A., Akiba Y., Aoki K., Asai J., Bunce G. M., Deshpande A., Enyo H., Fields D. E., Fujiwara K., Fukao Y., Goto Y., Gross P. M., Hachiya T., Hasuko K., Heuser J. M., Horaguchi T., Ichihara T., Imai K., Inoue Y., Ishihara M., Jinnouchi O., Kajihara F., Kamihara N., Kaneta M., Kanoh H., Kawall D., Kiyomichi A., Kurita K., Mao Y., Murata J., Nakagawa I., Nakano K., Onishi H., Okada H., Okada K., Rykov V. L., Saito N., Sato H., Shibata T., Shoji K., Tabaru T., Taketani A., Tanida K., Togawa M., Tojo J., Torii H., Tsuchimoto Y., Wagner M. M., Watanabe Y., Xie W., and Yokkaichi S.: “Quantitative Constraints on the Transport Properties of Hot Partonic Matter from Semi-Inclusive Single High Transverse Momentum Pion Suppression in Au+Au Collisions at $\sqrt{s_{NN}} = 200$ GeV”, Phys. Rev. C **77**, 064907-1–064907-12 (2008). *
- Adare A., Akiba Y., Aoki K., Asai J., Bunce G. M., Deshpande A., Enyo H., Fields D. E., Fujiwara K., Fukao Y., Goto Y., Gross P. M., Hachiya T., Hasuko K., Heuser J. M., Horaguchi T., Ichihara T., Imai K., Inoue Y., Ishihara M., Jinnouchi O., Kajihara F., Kamihara N., Kaneta M., Kanoh H., Kawall D., Kiyomichi A., Kurita K., Mao Y., Murata J., Nakagawa I., Nakano K., Onishi H., Okada H., Okada K., Rykov V. L., Saito N., Sato H., Shibata T., Shoji K., Tabaru T., Taketani A., Tanida K., Togawa M., Tojo J., Torii H., Tsuchimoto Y., Wagner M. M., Watanabe Y., Xie W., and Yokkaichi S.: “Charged hadron multiplicity fluctuations in Au+Au and Cu+Cu collisions from $\sqrt{s_{NN}} = 22.5$ to 200 GeV”, Phys. Rev. C **78**, 044902-1–044902-15 (2008). *
- Afanasiev S., Akiba Y., Aoki K., Bunce G. M., Deshpande A., Enyo H., Fields D. E., Fukao Y., Goto Y., Gross P. M., Hachiya T., Hasuko K., Heuser J. M., Horaguchi T., Ichihara T., Imai K., Ishihara M., Jinnouchi O., Kajihara F., Kamihara N., Kaneta M., Kiyomichi A., Kurita K., Murata J., Onishi H., Okada H., Okada K., Rykov V. L., Saito N., Sato H., Shibata T., Shoji K., Tabaru T., Taketani A., Tanida K., Togawa M., Tojo J., Torii H., Tsuchimoto Y., Wagner M. M., Watanabe Y., Xie W., and Yokkaichi S.: “Source breakup dynamics in Au+Au Collisions at $\sqrt{s_{NN}}=200$ GeV via three-dimensional two-pion source imaging”, Phys. Rev. Lett. **100**, 232301-1–232301-6 (2008). *
- Afanasiev S., Akiba Y., Aoki K., Bunce G. M., Deshpande A., Enyo H., Fields D. E., Fukao Y., Goto Y., Gross P. M., Hachiya T., Hasuko K., Heuser J. M., Horaguchi T., Ichihara T., Imai K., Ishihara M., Jinnouchi O., Kajihara F., Kamihara N., Kaneta M., Kiyomichi A., Kurita K., Murata J., Onishi H., Okada H., Okada K., Rykov V. L., Saito N., Sato H., Shibata T., Shoji K., Tabaru T., Taketani A., Tanida K., Togawa M., Tojo J., Torii H., Tsuchimoto Y., Wagner M. M., Watanabe Y., Xie W., and Yokkaichi S.: “Particle-species dependent modification of jet-induced correlations in Au+Au collisions at $\sqrt{s_{NN}} = 200$ GeV”, Phys. Rev. Lett. **101**, 082301-1–082301-6 (2008). *
- Adare A., Akiba Y., Aoki K., Asai J., Bunce G. M., Deshpande A., Enyo H., Fields D. E., Fujiwara K., Fukao Y., Goto Y., Gross P. M., Horaguchi T., Ichihara T.,

- Imai K., Inoue Y., Ishihara M., Jinnouchi O., Kamihara N., Kaneta M., Kanoh H., Kawall D., Kiyomichi A., Kurita K., Mao Y., Murata J., Nakagawa I., Nakano K., Onishi H., Okada H., Okada K., Rykov V. L., Saito N., Shibata T., Shoji K., Tabaru T., Taketani A., Tanida K., Togawa M., Tojo J., Torii H., Wagner M. M., Watanabe Y., Xie W., and Yokkaichi S.: “ J/ψ Production in $\sqrt{s_{NN}} = 200$ GeV Cu+Cu Collisions”, Phys. Rev. Lett. **101**, 122301-1–122301-6 (2008). *
- Adare A., Akiba Y., Aoki K., Asai J., Bunce G. M., Dairaku S., Deshpande A., Enyo H., Fields D. E., Fujiwara K., Fukao Y., Goto Y., Gross P. M., Horaguchi T., Ichihara T., Ichimiya R., Imai K., Inoue Y., Ishihara M., Jinnouchi O., Kametani S., Kamihara N., Kaneta M., Kanoh H., Kawall D., Kiyomichi A., Kurita K., Kurosawa M., Li Z., Mao Y., Murata J., Nakagawa I., Nakano K., Onishi H., Okada H., Okada K., Onuki Y., Rykov V. L., Saito N., Sakashita K., Shibata T., Shoji K., Tabaru T., Taketani A., Tanida K., Togawa M., Tojo J., Torii H., Wagner M. M., Watanabe Y., Xie W., and Yokkaichi S.: “Onset of π^0 suppression studied in Cu+Cu collisions at $\sqrt{s_{NN}} = 22.4, 62.4,$ and 200 GeV”, Phys. Rev. Lett. **101**, 162301-1–162301-6 (2008). *
- Adare A., Akiba Y., Aoki K., Asai J., Bunce G. M., Deshpande A., Enyo H., Fields D. E., Fujiwara K., Fukao Y., Goto Y., Gross P. M., Hachiya T., Hasuko K., Heuser J. M., Horaguchi T., Ichihara T., Imai K., Inoue Y., Ishihara M., Jinnouchi O., Kajihara F., Kamihara N., Kaneta M., Kanoh H., Kawall D., Kiyomichi A., Kurita K., Mao Y., Murata J., Nakagawa I., Nakano K., Onishi H., Okada H., Okada K., Rykov V. L., Saito N., Sato H., Shibata T., Shoji K., Tabaru T., Taketani A., Tanida K., Togawa M., Tojo J., Torii H., Tsuchimoto Y., Wagner M. M., Watanabe Y., Xie W., and Yokkaichi S.: “Suppression pattern of neutral pions at high transverse momentum in Au+Au collisions at $\sqrt{s_{NN}} = 200$ GeV and constraints on medium transport coefficients”, Phys. Rev. Lett. **101**, 232301-1–232301-7 (2008). *
- Asahi K., Ueno H., Shimada K., Nagatomo T., Yoshimi A., Nagae D., Kameda D., Uchida M., Inoue T., Hatakeyama N., Kagami S., Hasama Y., Suzuki K., Murata J., Kawamura H., Narita K., and Ishihara M.: “Nuclear Structure Studies with Polarized Radioactive Beams”, AIP Conf. Proc. **1149**, 90–99 (2009). *
- Nagatomo T., Shimada K., Asahi K., Balabanski D. L., Daugas J., Depuydt M., De Rydt M., Gaudefroy L., Grevy S., Hasama Y., Ichikawa Y., Kameda D., Morel P., Perrot L., Stodel C., Thomas J. C., Vanderheijden W., Vermeulen N., Vingerhoets P., Yoshimi A., Neyens G., and Ueno H.: “Electric quadrupole moment of the neutron-rich ^{33}Al ”, Eur. Phys. J. A **42**, No. 3, pp. 383–385 (2009). *
- Imao H., Ishida K., Kawamura N., Matsuzaki T., Matsuda Y., Toyoda A., Strasser P., Iwasaki M., and Nagamine K.: “Density effect in d-d muon-catalyzed fusion with ortho- and para-enriched deuterium”, Hyperfine Interact. **193**, No. 1-3, pp. 159–163 (2009). *
- Koike T. and Harada T.: “The $\bar{K}N \rightarrow \pi\Sigma$ decay threshold effect in $^3\text{He}(\text{in-flight } K^-, n)$ reaction spectrum”, Hyperfine Interact. **193**, 221–227 (2009). *
- Imao H., Hassan T. A., Michishio K., Enomoto Y., Shimoyama T., Kanai Y., Kuroda N., Mohri A., Higaki H., Saitoh H., Torii H., Nagata Y., Toyoda H., Matsuda Y., Nagashima Y., and Yamazaki Y.: “ASACUSA MUSASHI: New progress with intense ultra slow antiproton beam”, Hyperfine Interact. **194**, No. 1-3, pp. 71–76 (2009). *
- Koike T. and Harada T.: “FORMATION OF DEEPLY-BOUND K^-pp STATE IN $^3\text{He}(\text{IN-FLIGHT } K^-, n)$ REACTION SPECTRUM”, Int. J. Mod. Phys. A **24**, No. 11, pp. 2126–2133 (2009). *
- Kawamata T., Sugawara N., Uesaka M., Kaneko N., Kajiwara T., Yamane H., Koyama K., Kudo K., Kobayashi N., and Koike Y.: “Single-Crystal Growth of $\text{Pb}_2\text{V}_3\text{O}_9$ and the Bose-Einstein Condensed State of Triplons Studied by Thermal Conductivity, Specific Heat and Magnetization Measurements”, J. Phys.: Con. Ser. **150**, 042087-1–042087-4 (2009). *
- Adachi T., Haidar S. M., Kawamata T., Sugawara N., Kaneko N., Uesaka M., Sato H., Tanabe Y., Noji T., Kudo K., Kobayashi N., and Koike Y.: “Thermal-conductivity study on the electronic state in the overdoped regime of $\text{La}_{2-x}\text{Sr}_x\text{CuO}_4$: Phase separation and anomaly at $x \sim 0.21$ ”, J. Phys.: Con. Ser. **150**, 052115-1–052115-4 (2009). *
- Oosawa A., Suzuki T., Kanada K., Kojima S., Goto T., and Manaka H.: “ $^1\text{H-NMR}$ Spin-Lattice Relaxation Rate of the Quantum Spin System $(\text{CH}_3)_2\text{CHNH}_3\text{Cu}(\text{Cl}_x\text{Br}_{1-x})_3$ with $x = 0$ and 0.35 ”, J. Phys. Soc. Jpn. **78**, No. 5, pp. 053702-1–053702-4 (2009). *
- Yagi E., Yoshii M., Okada Y., Matsuba H., Miyahara K., Koike S., Sugawara T., Shishido T., and Ogiwara K.: “Site change of hydrogen in niobium on alloying with oversized Ta atoms”, J. Phys. Soc. Jpn. **78**, No. 6, pp. 064601-1–064601-8 (2009). *
- Suzuki T., Yamada F., Watanabe I., Matsuzaki T., Goto T., Oosawa A., and Tanaka H.: “Spin fluctuations in the ground state of doped quantum spin system $\text{TlCu}_{1-x}\text{Mg}_x\text{Cl}_3$ with $x = 0.0047$ probed by muon-spin-relaxation technique”, J. Phys. Soc. Jpn. **78**, No. 7, pp. 074705-1–074705-5 (2009). *
- Koike T. and Harada T.: “ $^3\text{He}(K^-, n)$ REACTION SPECTRUM NEAR THE $\bar{K}N \rightarrow \pi\Sigma$ DECAY THRESHOLD AND THE DEEPLY-BOUND K^-pp STATE”, Mod. Phys. Lett. A **24**, No. 11/13, pp. 911–914 (2009). *
- Adare A., Akiba Y., Aoki K., Asai J., Bunce G. M., Deshpande A., Enyo H., Fields D. E., Fujiwara K., Fukao Y., Goto Y., Gross P. M., Horaguchi T., Ichihara T.,

- Imai K., Inoue Y., Ishihara M., Jinnouchi O., Kamihara N., Kaneta M., Kanoh H., Kawall D., Kiyomichi A., Kurita K., Mao Y., Murata J., Nakagawa I., Nakano K., Onishi H., Okada H., Okada K., Rykov V. L., Saito N., Shibata T., Shoji K., Tabaru T., Taketani A., Tanida K., Togawa M., Tojo J., Torii H., Wagner M. M., Watanabe Y., Xie W., and Yokkaichi S.: “Dilepton mass spectra in p+p collisions at $\sqrt{s} = 200$ GeV and the contribution from open charm”, *Phys. Lett. B* **670**, 313–320 (2009). *
- De Rydt M., Neyens G., Asahi K., Balabanski D. L., Daugas J., Depuydt M., Gaudefroy L., Grevy S., Hasama Y., Ichikawa Y., Morel P., Nagatomo T., Ohtsuka T., Perrot L., Shimada K., Stedel C., Thomas J., Ueno H., Utsuno Y., Wannes V., Vermeulen N., Vingerhoets P., and Yoshimi A.: “Precision measurement of the electric quadrupole moment of ^{31}Al and determination of the effective proton charge in the sd-shell”, *Phys. Lett. B* **678**, 344–349 (2009). *
- Andresen G. B., Bertsche W., Bray C. C., Butler E., Cesar C. L., Chapman S., Charlton M., Fajans J., Fujiwara M., Gill D. R., Hardy W. N., Hayano R., Hayden M. E., Humphries A. J., Hydromako R., Jorgensen L. V., Kerrigan S. J., Keller J., Kurchaninov L., Lamb R., Madsen N., Nolan P., Olchansk K., Olin A., Povilus A., Pusa P., Robicheaux F., Sarid E., Seif El Nasr S., Silveira D. M., Storey J. W., Thompson R. I., van der Werf D. P., Wurtele J. S., and Yamazaki Y.: “Magnetic multipole induced zero-rotation frequency bounce-resonant loss in a Penning-Malmberg trap used for antihydrogen trapping”, *Phys. Plasmas* **16**, No. 10, pp. 100702-1–100702-4 (2009). *
- Suzuki T., Yamada F., Kawamata T., Watanabe I., Goto T., and Tanaka H.: “Quantum critical behavior in highly random system $\text{Tl}_{1-x}\text{K}_x\text{CuCl}_3$ probed by zero- and longitudinal-field muon-spin-relaxation measurements”, *Phys. Rev. B* **79**, 104409-1–104409-5 (2009). *
- Inoue H., Tani S., Hosoya S., Inokuchi K., Fujiwara T., Saito T., Suzuki T., Oosawa A., Goto T., Fujisawa M., Tanaka H., Sasaki T., Awaji S., Watanabe K., and Kobayashi N.: “ $^{63/65}\text{Cu}$ - and $^{35/37}\text{Cl}$ -NMR Studies of Triplet Localization in the Quantum Spin System NH_4CuCl_3 ”, *Phys. Rev. B* **79**, 174418-1–174418-7 (2009). *
- Suzuki T., Watanabe I., Yamada F., Ishii Y., Ohishi K., Risdiana ., Goto T., and Tanaka H.: “Evidence for continuous change of spin states between impurity-induced order and pressure-induced order in $\text{TlCu}_{0.985}\text{Mg}_{0.015}\text{Cl}_3$ probed via muon spin rotation”, *Phys. Rev. B* **80**, 064407-1–064407-5 (2009). *
- Ohishi K., Heffner R. H., Ito T. U., Higemoto W., Morris G. D., Hur H., Bauer E. D., Sarrao J. L., Thompson J. D., MacLaughlin D. E., and Shu L.: “Development of the heavy-fermion state in Ce_2IrIn_8 and the effects of Ce dilution in $(\text{Ce}_{1-x}\text{La}_x)_2\text{IrIn}_8$ ”, *Phys. Rev. B* **80**, 125104-1–125104-7 (2009). *
- Koike T. and Harada T.: “Deeply bound K^-pp state in the ^3He (in-flight K^-, n) spectrum, and its moving pole near the $\pi\Sigma N$ threshold”, *Phys. Rev. C* **80**, 055208-1–055208-14 (2009). *
- Ito T. U., Higemoto W., Ohishi K., Nishida N., Heffner R. H., Yuji A., Amato A., Onimaru T., and Suzuki H. S.: “Quantized Hyperfine Field at an Implanted μ^+ in PrPb_3 : Interplay between Localized f electrons and Interstitial Charged Particle”, *Phys. Rev. Lett.* **102**, 096403-1–096403-4 (2009). *
- Yokoyama K., Nagamine K., Simomura K., Tom H. W., Roland K. K., Bakule P., Matsuda Y., Pratt F. L., and Torikai E.: “Muons for spintronics: photo-induced conduction electron polarization in n-type GaAs observed by the muonium method”, *Physica B* **404**, No. 5-7, pp. 856–858 (2009). *
- Satoh K., Fujita H., Katayama K., Taniguchi H., Ito T. U., Ohishi K., and Higemoto W.: “ μSR study of an layered organic superconductor κ -(BEDT-TTF) $_4\text{Hg}_{2.89}\text{Br}_8$ ”, *Physica B* **404**, 597–599 (2009). *
- Satoh K., Sato K., Yoshida T., Taniguchi H., Goko T., Ito T. U., Ohishi K., and Higemoto W.: “ μSR study of organic antiferromagnet β' -(BEDT-TTF) $_2\text{Icl}_2$ under high pressure”, *Physica B* **404**, 600–602 (2009). *
- Ohishi K., Heffner R. H., Spehling J., MacDougall G. J., Ito T. U., Higemoto W., Amato A., Andreica D., Nieuwenhuys G., Klauss H. H., Luke G. M., Thompson J. D., Bianchi A. D., and Fisk Z.: “Magnetism and superconductivity in heavy fermion superconductor $\text{CeCo}(\text{In}_{0.97}\text{Cd}_{0.03})_5$ ”, *Physica B* **404**, 754–756 (2009). *
- Yuji A., Higemoto W., Tsunashima Y., Yonezawa Y., Satoh K., Koda A., Ito T. U., Ohishi K., Heffner R. H., Kikuchi D., and Sato H.: “Weak ferromagnetic ordering in the anomalous field-insensitive heavy-fermion state in $\text{SmOs}_4\text{Sb}_{12}$ ”, *Physica B* **404**, 757–760 (2009). *
- Ito T. U., Higemoto W., Ohishi K., Heffner R. H., Nishida N., Satoh K., Sugawara H., Yuji A., Kikuchi D., and Sato H.: “Possible low-energy excitations of multipoles in $\text{SmRu}_4\text{P}_{12}$ probed by muon spin relaxation”, *Physica B* **404**, 761–764 (2009). *
- (Review)
大隅寛幸, 高阪勇輔, 秋光純: “円偏光 X 線による構造研究: 結晶とスピン配列のヘリシティ”, *固体物理* **44**, 719–725 (2009).
- Book • Proceedings**
(Original Papers) *Subject to Peer Review
Ishida K., Matsuzaki T., Imao H., Matsuda Y., Iwasaki M., Nagamine K., Kawamura N., Kato M., Sugai H., and Eaton G. H.: “Muon Catalyzed d-t Fusion in Non-equilibrated Mixtures of T2 with Normal, Ortho and Para-rich D2”, International Conference on Muon Cat-

alyzed Fusion and Related topics Proceedings (μ CF-07), Dubna, Russia, 2007–6, Joint Institute for Nuclear Research, Dubna, pp. 99–104 (2008). *

Oral Presentations

(International Conference etc.)

- Inoue H., Tani S., Hosoya S., Suzuki T., Goto T., Tanaka H., Sasaki T., and Kobayashi N.: “ ^2D , $^{35/37}\text{Cl}$, $^{63/65}\text{Cu}$ -NMR study on quantum spin system NH_4CuCl_3 ”, 24th International Conference on Low Temperature Physics (LT24), Orlando, USA, Aug. (2005).
- Tonishi J., Suzuki T., and Goto T.: “Anomalous change of Hall coefficient in overdoped $\text{La}_{2-x}\text{Sr}_x\text{Cu}_{1-y}\text{Zn}_y\text{O}_4$ around $x = 0.2$ ”, 24th International Conference on Low Temperature Physics (LT24), Orlando, USA, Aug. (2005).
- Goto T., Ueda M., Sumikawa H., Suzuki T., Fujita M., Yamada K., Koike Y., and Adachi T.: “Backling of the CuO_2 plane in single crystals of La-based high- T_c cuprates observed by NMR”, 24th International Conference on Low Temperature Physics (LT24), Orlando, USA, Aug. (2005).
- Kanada K., Saito T., Oosawa A., Goto T., Suzuki T., and Manaka H.: “Magnetic order in the solid solution of two spin-gap systems $(\text{CH}_3)_2\text{CHNH}_3\text{Cu}(\text{Cl}_{1-x}\text{Br}_x)_3$ ”, ICM2006 Satellite Conference: 1st International Symposium of Quantum Beam Science Directorate of JAEA, Advances in Neutron, Synchrotron Radiation, μ SR and NMR Researches (QuBS2006), Tokai-mura, Ibaraki Pref., Aug. (2006).
- Fujiwara T., Oosawa A., Tsunoda R., Goto T., Suzuki T., Shindo Y., Tanaka H., Sasaki T., Kobayashi N., Awaji S., and Watanabe K.: “Cu-NMR Study on disordered dimer system $(\text{Tl}_{1-x}\text{K}_x)\text{CuCl}_3$ with the Bose-glass ground state”, Yamada Conference LX on Research in High Magnetic Fields (RHMF2006), Sendai, Aug. (2006).
- Tonishi J., Ueda M., Suzuki T., Oosawa A., Goto T., Adachi T., Koike Y., Fujita M., and Yamada K.: “Local structure in single crystals of La-based High T_c Cuprates”, Yamada Conference LX on Research in High Magnetic Fields (RHMF2006), Sendai, Aug. (2006).
- Oosawa A., Suzuki T., Watanabe I., Goto T., and Manaka H.: “ μ SR-detected Softmode toward a Possible Phase Transition in disordered spin gap system $(\text{CH}_3)_2\text{CHNH}_3\text{-Cu}(\text{Cl}_x\text{Br}_{1-x})_3$ ”, 11th International Conference on Muon Spin Rotation, Relaxation and Resonance (μ SR2008), Tsukuba, July (2008).
- Yokoyama K., Nagamine K., Simomura K., Tom H. W., Roland K. K., Bakule P., Matsuda Y., Pratt F. L., and Torikai E.: “Muons for spintronics: Polarized conduction electrons in GaAs observed by spin exchange scattering of muonium”, 11th International Conference on Muon Spin Rotation, Relaxation and Resonance (μ SR2008), (International Society for MuSR Spectroscopy), Tsukuba, July (2008).
- Kousaka Y., Ohsumi H., Komesu T., Arima T., Sakai S., Akita M., Inoue K., Yokobori T., Nakao Y., Kaya E., and Akimitsu J.: “Crystallographic Chirality in CsCuCl_3 Investigated by Resonant Circularly-polarized X-ray Scattering”, 2nd International Symposium on Anomalous Quantum Materials (ISAQM2008) and the 7th Asia-Pacific Workshop, (Invention of Anomalous Quantum Materials), Tokyo, Nov. (2008).
- Ishida K.: “Ultra slow muon source for new g-2 experiment”, 11th International Workshop on Neutrino Factories, Superbeams and Beta Beams (NuFact09), (Illinois Institute of Technology), Chicago, USA, July (2009).
- Ishida K., Miller J., and Nicolo D.: “WG4 Summary”, 11th International Workshop on Neutrino Factories, Superbeams and Beta Beams (NuFact09), (Illinois Institute of Technology), Chicago, USA, July (2009).
- Yamazaki Y., Enomoto Y., Kuroda N., Mohri A., Matsuda Y., Higaki H., Kira K., Kanai Y., Imao H., Shimoyama T., Michishio K., Torii H., Nagata Y., Nagashima Y., and saito H.: “Developments of the cusp trap to synthesize antihydrogen atoms for high precision spectroscopy of ground state hyperfine splitting”, 26th International Conference on Photonic, Electronic, and Atomic Collisions (ICPEAC 2009), (Western Michigan University), Kalamazoo, USA, July (2009).
- Nakajima S., Goto T., Suzuki T., Watanabe I., and Manaka H.: “ μ SR and NMR Study on Quantum Critical Point in Quantum Spin Ladder $(\text{CH}_3)_2\text{CHNH}_3\text{Cu}(\text{Cl}_x\text{Br}_{1-x})_3$ ”, International Conference on Magnetism (ICM 2009), Karlsruhe, Germany, July (2009).
- Goto T., Suzuki T., Nakajima S., Kanada K., Saito T., Watanabe I., Luetkens H., and Amato A.: “ μ SR study on the ground state of bond-disordered spin gap system $(\text{CH}_3)_2\text{CHNH}_3\text{Cu}(\text{Cl}_{1-x}\text{Br}_x)_3$ ($x = 0.95, 0.88$)”, International Conference on Magnetism (ICM 2009), Karlsruhe, Germany, July (2009).
- Kawamata T., Kaneko N., Uesaka M., Sato M., and Koike Y.: “Enhancement of Thermal Conductivity due to Spinons in the One-Dimensional Spin System SrCuO_2 ”, International Conference on Magnetism (ICM 2009), (Universitat Karlsruhe), Karlsruhe, Germany, July (2009).
- Suzuki T., Watanabe I., Yamada F., Ishii Y., Ohishi K., Risdiana ., Goto T., and Tanaka H.: “Pressure effect on magnetic ground states in $\text{Tl}(\text{Cu}_{1-x}\text{Mg}_x)\text{Cl}_3$ probed by muon-spin-rotation”, International Conference on Magnetism (ICM 2009), Karlsruhe, Germany, July (2009).
- Uesaka M., Kawamata T., Kaneko N., Sato M., Kudo K., Kobayashi N., and Koike Y.: “Quasi One-Dimensional Spin System Thermal Conductivity of the $\text{Sr}_2\text{V}_3\text{O}_9$ ”, International Conference on Magnetism (ICM 2009), (Universitat Karlsruhe), Karlsruhe, Germany, July (2009).
- Sato M., Kawamata T., Sugawara N., Kaneko N., Uesaka

- M., Kudo K., Kobayashi N., and Koike Y.: “Thermal Conductivity in the Bose-Einstein Condensed State of Triplons in the Bond-Alternating Spin-Chain System $\text{Pb}_2\text{V}_3\text{O}_9$ ”, International Conference on Magnetism (ICM 2009), (Universitat Karlsruhe), Karlsruhe, Germany, July (2009).
- Koike T. and Harada T.: “ ^3He (in-flight K^-, n) spectrum and moving pole of a deeply-bound K^-pp state in complex energy plane”, 10th International Conference on Hypernuclear and Strange Particle Physics (Hyp-X), (Kyoto university, the Global COE Program), Tokaimura, Ibaraki Pref., Sept. (2009).
- Ohishi K., Ito T. U., Higemoto W., Uehara A., Kozawa K., Yamazaki T., Kimishima Y., and Uehara M.: “Quasi-particle Excitations in Newly Discovered Antiperovskite Superconductor ZnNi_3 ”, 9th International Conference on Materials and Mechanisms of Superconductivity (M2S-IX), Tokyo, Sept. (2009).
- Sakuma F.: “Double anti-kaon production in nucleus by Stopped Anti-proton Annihilation”, International Workshop on Physics and Upgrade of the J-PARC Hadron Facility, (RCNP), Tokaimura, Ibaraki Pref., Sept. (2009).
- Sakuma F.: “Development of the Cylindrical Detector System for an experimental search for kaonic nuclei at J-PARC”, 3rd Joint Meeting of the Nuclear Physics Divisions of the APS and JPS (Hawaii 2009), Hawaii, USA, Oct. (2009).
- Ohishi K., Suzuki T., Heffner R. H., Ito T. U., Higemoto W., Bauer E. D., and Thompson J. D.: “Magnetism and muon Knight shift measurements in heavy fermion compound $\text{Ce}_2\text{Rh}(\text{In}, \text{Sn})_8$ ”, Advanced Science Research Symposium 2009 (ASR2009): Positron, Muon and other exotic particle beams for materials and atomic/molecular sciences, (Japan Atomic Energy Agency), Tokaimura, Nov. (2009).
- Imao H., Michishio K., Kanai Y., Kuroda N., Enomoto Y., Higaki H., Kira K., Mohri A., Torii H., Nagata Y., Kim C., Matsuda Y., Nagashima Y., and Yamazaki Y.: “Positron Accumulation and Manipulation for Antihydrogen Synthesis”, Advanced Science Research Symposium 2009 (ASR2009): Positron, Muon and other exotic particle beams for materials and atomic/molecular sciences, (Japan Atomic Energy Agency), Tokaimura, Nov. (2009).
- Ishii Y., Watanabe I., Ito M., Matsuo T., Kobayashi Y., Matsuzaki T., and Tamao K.: “ μSR studies of linear two-coordinate iron complexes”, RIKEN Symposium on Molecular Ensemble 2009, Wako, Dec. (2009).
- Risdiana ., Fitrilawati ..., Siregar R., Hidayat R., Nugroho A. A., Tjia M., Ishii Y., and Watanabe I.: “Muon-spin-relaxation study of spin dynamics in poly(3-alkylthiophene)”, RIKEN Symposium on Molecular Ensemble 2009, Wako, Dec. (2009).
- (Domestic Conference)
- 岡田信二, Beer G. A., 方亨燦, Cargnelli M., 千葉順成, Choi S., Curceanu C. O., 福田芳之, 花木俊生, 早野龍五, 飯尾雅美, 石川隆, 石元茂, 石渡智 ; 板橋健太, 岩井正明, 岩崎雅彦, Juhasz B., Kienle P., Marton J., 松田恭幸, 大西宏明, 應田 治彦, Schmid P., 佐藤 将春, 鈴木 祥仁, 鈴木隆敏, 竜野秀行, 友野大, Widmann E., 山崎敏光, 林熙重, Zmeskal J.: 理研ワークショップ「放射線検出器と電子回路の課題と展望-光子検出器を中心に」, 和光市, 5月(2005).
- 井上絢亨, 黒江晴彦, 鈴木栄男, 大沢明, 後藤貴行, 関根智幸, 佐々木孝彦, 小林典男, 淡路智, 渡辺和雄: “F-AF 交替鎖系 $(\text{CH}_3)\text{CHNH}_3\text{CuCl}_3$ の Cl-NMR”, 日本物理学会 2005 年秋季大会, 京田辺, 9月(2005).
- 藤原崇雄, 角田玲子, 大沢明, 後藤貴行, 神藤陽介, 田中秀数, 鈴木栄男: “ボースグラス相を示す乱れを含んだ量子スピン磁性体の NMR III”, 日本物理学会 2005 年秋季大会, 京田辺, 9月(2005).
- 後藤貴行, 知久宏之, 浦野萌美, 鈴木栄男, 佐々木孝彦, 小林典男, 淡路智, 渡辺和雄: “有機超伝導体 κ -(BEDT-TTF) $_2\text{Cu}(\text{NCS})_2$ における格子の量子融解”, 日本物理学会 2005 年秋季大会, 京田辺, 9月(2005).
- 佐藤将春, 飯尾雅美, 板橋健太, 岩崎雅彦, 應田治彦, 大西宏明, 岡田信二, 鈴木隆敏, 友野大, 松田恭幸, 山崎敏光, 福田芳之, 石川隆, 早野龍五, 石元茂, 岩井正明, 鈴木祥仁, 千葉順成, 花木俊生, Bhang H., Choi S., Kim J., Yim H., 石渡智 ; Widmann E., Kienle P.: “ $^4\text{He}(\text{K}_{\text{stopped}}^-, \text{N})$ 反応を用いたストレンジライバリオンの実験的研究 (1)”, 日本物理学会第 61 回年次大会, (日本物理学会), 松山, 3月(2006).
- 岡田信二, Beer G. A., 方亨燦, Cargnelli M., 千葉順成, Choi S., Curceanu C. O., 福田芳之, 花木俊生, 早野龍五, 飯尾雅美, 石川隆, 石元茂, 石渡智 ; 板橋健太, 岩井正明, 岩崎雅彦, Juhasz B., Kienle P., Marton J., 松田恭幸, 大西宏明, 應田 治彦, Schmid P., 佐藤 将春, 鈴木 祥仁, 鈴木隆敏, 竜野秀行, 友野大, Widmann E., 山崎敏光, 林熙重, Zmeskal J.: “K 中間子ヘリウム 4 原子 $3d \rightarrow 2p$ X 線の精密測定”, 日本物理学会第 61 回年次大会, 松山, 3月(2006).
- 飯尾雅美, 板橋健太, 岩崎雅彦, 應田治彦, 大西宏明, 岡田信二, 鈴木隆敏, 友野大, 松田恭幸, 山崎敏光, 石川隆, 竜野秀行, 早野龍五, 石元茂, 鈴木祥仁, 佐藤将春, 福田芳之, 千葉順成, 花木俊生, 方亨燦, Choi S., 林熙重, 石渡智 ; Cargnelli M., Juhasz B., Kienle P., Marton J., Widmann E., Zmeskal J., Schmid P., Beer G. A., Curceanu C. O.: “K 中間子ヘリウム原子 X 線測定実験のための検出器系 I”, 日本物理学会第 61 回年次大会, 松山, 3月(2006).
- 遠西淳, 上田真徳, 鈴木栄男, 後藤貴行, 大沢明, 藤田全基, 山田和芳, 足立匡, 小池洋二: “La 系高温超伝導体における局所構造”, 日本物理学会第 61 回年次大会, 松山, 3月(2006).
- 佐藤将春, 飯尾雅美, 板橋健太, 岩崎雅彦, 應田治彦, 大西宏明, 岡田信二, 鈴木隆敏, 友野大, 松田恭幸, 山崎敏光, 福田芳之, 石川隆, 早野龍五, 石元茂, 岩井正明, 鈴木祥仁, 千葉順成, 花木俊生, Bhang H., Choi S., Kim J., Yim H., 石渡智 ; Widmann E., Kienle P.: “ $^4\text{He}(\text{K}_{\text{stopped}}^-, \text{N})$ 反応を用いたストレンジライバリオンの実験的研究 (4)”, 日本物理学会 2006 年秋季大会, (日本物理学会), 奈良, 9月(2006).
- 遠西淳, 上田真徳, 鈴木栄男, 後藤貴行, 大沢明, 藤田全基, 山田和芳, 足立匡, 小池洋二: “ $\text{La}_{2-x}\text{Sr}_x\text{CuO}_4$ のストライ

- ブ相における局所構造の磁場効果”, 日本物理学会 2006 年秋季大会, 千葉, 9 月 (2006).
- 齊藤健浩, 遠西淳, 大沢明, 後藤貴行, 鈴木栄男, 佐々木孝彦, 小林典男, 淡路智, 渡辺和雄: “複合ハルデン鎖 IPA-CuCl₃ の磁気格子相関”, 日本物理学会 2006 年秋季大会, 千葉, 9 月 (2006).
- 齊藤健浩, 金田圭史, 大沢明, 後藤貴行, 鈴木栄男, 田中秀数: “量子スピン系 IPACu(Cl_xBr_{1-x})₃ の μ SR”, 日本物理学会 2006 年秋季大会, 千葉, 9 月 (2006).
- 飯尾雅美, 石元茂: “K 中間子原子核探索実験のための液体ヘリウム 3 標的”, 文科省科研費補助金特定領域研究「ストレンジネスで探るクォーク多体系」研究会 2006, 熱海, 12 月 (2006).
- 岡田信二, Beer G. A., 方亨燦, Buehler P., Cargnelli M., 千葉順成, Choi S., Curceanu C. O., 福田芳之, Guaraldo C., 花木俊生, 早野龍五, Hirtl A., 飯尾雅美, Iliescu M., 石川隆, 石元茂, 石渡智, 板橋健太, 岩井正明, 岩崎雅彦, Kienle P., Marton J., 松田恭幸, 大西宏明, 應田治彦, Pietreanu D., Sirghi D., Sirghi F., 佐藤将春, 鈴木隆敏, 竜野秀行, 友野大, Widmann E., 山崎敏光, 林熙重, Zmeskal J.: “Precision spectroscopy of Kaonic Helium-3 3d \rightarrow 2p X-rays (J-PARC E17 実験)”, 文科省科研費補助金特定領域研究「ストレンジネスで探るクォーク多体系」研究会 2006, 熱海, 12 月 (2006).
- 大西宏明: “Dilepton measurement at CERN/SPS”, 日本物理学会 2007 年春季大会, (日本物理学会), 八王子, 3 月 (2007).
- 佐藤将春, 飯尾雅美, 板橋健太, 岩崎雅彦, 應田治彦, 大西宏明, 岡田信二, 鈴木隆敏, 友野大, 松田恭幸, 山崎敏光, 福田芳之, 石川隆, 早野龍五, 石元茂, 岩井正明, 鈴木祥仁, 千葉順成, 花木俊生, Bhang H., Choi S., Kim J., Yim H., 石渡智, Widmann E., Kienle P.: “⁴He(K⁻_{stopped}, N) 反応を用いたストレンジトライブリオンの実験的研究 (6)”, 日本物理学会 2007 年春季大会, (日本物理学会), 八王子, 3 月 (2007).
- 大西宏明: 日本物理学会 2007 年春季大会, (日本物理学会), 八王子, 3 月 (2007).
- 飯尾雅美, 板橋健太, 岩崎雅彦, 應田治彦, 大西宏明, 岡田信二, 佐久間史典, 鈴木隆敏, 友野大, 松田恭幸, 山崎敏光, 石元茂, 鈴木祥仁, 関本美知子, 豊田晃久, 永江知文, 石川隆, 竜野秀行, 早野龍五, 藤岡宏之, 味村周平, 阪口篤志, 佐藤将春, 福田芳之, 千葉順成, 花木俊生, 福田共和, 溝井浩, Beer G. A., 方亨燦, Choi S., 林熙重, 石渡智, Buehler P., Hirtl A., Cargnelli M., Kienle P., Marton J., Widmann E., Zmeskal J., Curceanu C. O., Guaraldo C., Iliescu M., Pietreanu D., Sirghi D., Sirghi F., Faso D., Busso L., Morra O.: “K 中間子原子核探索実験のための液体ヘリウム 3 標的の開発”, 日本物理学会 2007 年春季大会, 八王子, 3 月 (2007).
- 遠西淳, 上田真徳, 鈴木栄男, 後藤貴行, 大沢明, 藤田全基, 山田和芳, 足立匡, 小池洋二: “NMR でみたランタン系高温超伝導体におけるインコヒーレント構造”, 日本物理学会 2007 年春季大会, 鹿児島, 3 月 (2007).
- 齊藤健浩, 金田圭史, 足立知彌, 大沢明, 後藤貴行, 鈴木栄男, 渡邊功雄: “量子スピン系 IPA-Cu(Cl_xBr_{1-x})₃ の異常量子臨界”, 日本物理学会 2007 年春季大会, 鹿児島, 3 月 (2007).
- 岡田信二, Beer G. A., 方亨燦, Cargnelli M., 千葉順成, Choi S., Curceanu C. O., 福田芳之, 花木俊生, 早野龍五, 飯尾雅美, 石川隆, 石元茂, 石渡智, 板橋健太, 岩井正明, 岩崎雅彦, Juhasz B., Kienle P., Marton J., 松田恭幸, 大西宏明, 應田治彦, Schmid P., 佐藤将春, 鈴木祥仁, 鈴木隆敏, 竜野秀行, 友野大, Widmann E., 山崎敏光, 林熙重, Zmeskal J.: 日本物理学会第 62 回年次大会, 札幌, 9 月 (2007).
- 大沢明, 齊藤健浩, 佐々木孝彦, 鈴木栄男, 後藤貴行, 淡路智, 渡辺和雄, 小林典男: “強磁場トルク測定によるスピングャップ磁性体 IPACuCl₃ の磁場誘起相転移”, 日本物理学会第 62 回年次大会, 札幌, 9 月 (2007).
- 後藤貴行, 金田圭史, 齊藤健浩, 大沢明, 鈴木栄男, 渡邊功雄, 真中浩貴: “乱れを含んだ量子スピン磁性体 IPA-Cu(Cl_{0.35}Br_{0.65})₃ の μ SR”, 日本物理学会第 62 回年次大会, 札幌, 9 月 (2007).
- 岡田信二, Beer G. A., 方亨燦, Buehler P., Cargnelli M., 千葉順成, Choi S., Curceanu C. O., 福田芳之, Guaraldo C., 花木俊生, 早野龍五, Hirtl A., 飯尾雅美, Iliescu M., 石川隆, 石元茂, 石渡智, 板橋健太, 岩井正明, 岩崎雅彦, Kienle P., Marton J., 松田恭幸, 大西宏明, 應田治彦, Pietreanu D., Sirghi D., Sirghi F., 佐藤将春, 鈴木隆敏, 竜野秀行, 友野大, Widmann E., 山崎敏光, 林熙重, Zmeskal J.: “J-PARC における K 中間子ヘリウム 3 原子 X 線分光実験 J-PARC E17 の現状”, 文部科学省科学研究費補助金特定領域研究特定領域研究「ストレンジネスで探るクォーク多体系」第 3 回総括班主催研究会 (2007), 仙台, 11 月 (2007).
- 小林義男: “不安定核で見る化学反応と原子の振る舞い”, 東京工業大学大学院理工学研究科理学研究流動機構シンポジウム「元素の個性: どう見るか, どうつくるか, どう使うか」, (東京工業大学大学院理工学研究科理学研究流動機構), 東京, 11 月 (2007).
- 大西宏明: “ Φ 中間子原子核探索実験”, RCNP ワークショップ「J-PARC ハドロン実験施設のビームライン設備拡充に向けて」, (大阪大学核物理研究センター), 大阪, 11 月 (2007).
- 鈴木隆敏, 飯尾雅美, 板橋健太, 岩崎雅彦, 應田治彦, 大西宏明, 岡田信二, 佐藤将春, 友野大, 松田恭幸, 山崎敏光, 福田芳之, 石川隆, 早野龍五, 石元茂, 岩井正明, 鈴木祥仁, 千葉順成, 花木俊生, Bhang H., Choi S., Kim J., Yim H., 石渡智, Widmann E., Kienle P.: “⁴He 上の静止 K⁻ 反応に於ける重陽子測定によるストレンジマルチバリオン状態の探索 (1)”, 日本物理学会第 63 回年次大会, (日本物理学会), 東大阪, 3 月 (2008).
- 藤原裕也, 岩崎雅彦, 板橋健太, 應田治彦, 大西宏明, 岡田信二, 佐久間史典: “J-PARC E15 実験のための K 中間子崩壊事象 veto カウンターの開発”, 日本物理学会第 63 回年次大会, (日本物理学会), 東大阪, 3 月 (2008).
- 後藤貴行, 金田圭史, 齊藤健浩, 大沢明, 鈴木栄男, 渡邊功雄: “スピンラダー固溶系 IPA-Cu(Cl_xBr_{1-x})₃ の Cl-rich 相 (x > 0.87) における μ SR 及び ¹H-NMR”, 日本物理学会第 63 回年次大会, 東大阪, 3 月 (2008).
- 金田圭史, 大沢明, 後藤貴行, 鈴木栄男, 真中浩貴: “乱れを含んだ量子スピン磁性体 IPA-Cu(Cl_{0.35}Br_{0.65})₃ の NMR”,

- 日本物理学会第 63 回年次大会, 東大阪, 3 月 (2008).
- 飯尾雅実, 板橋健太, 岩崎雅彦, 應田治彦, 大西宏明, 佐久間史典, 佐藤将春, 塚田暁, 友野大, 藤岡宏之, 山崎敏光, 石元茂, 岩井正明, 鈴木祥二, 関本美知子, 豊田晃久, 石川隆, 竜野秀行, 鈴木隆敏, 早野龍五, 松田恭幸, 永江知文, 平岩聡彦, 味村周平, 野海博之, 阪口篤志, 藤原裕也, 徳田真, 千葉順成, 福田共和, 溝井浩, Beer G. A., 方亨燦, Choi S., 林熙重, 石渡智一, Buehler P., Cargnelli M., Hirtl A., Kienle P., Marton J., Widmann E., Zmeskal J., 岡田信一, Curceanu C. O., Guaraldo C., Iliescu M., Pietreanu D., Sirghi D., Sirghi F., Faso D., Morra O., Busso L.: “K 中間子原子核探索実験のための液体ヘリウム 3 標的の開発 III”, 日本物理学会 2008 年秋季大会, 山形, 9 月 (2008).
- 後藤貴行, 鈴木栄男, 真中浩貴, 金田圭史, 中島紗織, 大沢明, 渡邊功雄: “乱れを含んだ量子スピラダー IPA-Cu(Cl, Br)₃ の量子臨界近傍における μ SR”, 日本物理学会 2008 年秋季大会, 盛岡, 9 月 (2008).
- 大西宏明: “反陽子ビームを用いた Φ 中間子原子核探索実験”, 「J-PARC ハドロン物理の将来研究計画を考える」研究会, 和光, 9 月 (2008).
- 大石一城, 石井康之, 渡邊功雄, 齊藤拓, 深澤英人, 小堀洋, 木方邦宏, 李哲虎, 宮沢喜一, 伊豫彰, 嶋谷幸佑, 山田和芳, 永崎洋: “ μ SR から眺めた鉄ヒ素系超伝導体の常伝導状態及び超伝導状態の研究”, JST-TRIP 新規材料による高温超伝導基盤技術 第 3 回領域会議, (科学技術振興機構), 東京, 12 月 (2008).
- 鈴木栄男, 川股隆行, 渡邊功雄, 後藤貴行, 山田文子, 田中秀数: “量子スピン系 $Tl_{1-x}K_xCuCl_3$ ($x = 0.51, 0.60$) におけるミュオンスピン緩和 (μ SR) とソフトモード”, 日本物理学会第 64 回年次大会, 東京, 3 月 (2009).
- 大石一城, 山田幾也, 幸田章宏, 門野良典, Saha S. R., 髭本亘, 小嶋健児, 東正樹, 高野幹夫: “頂点塩素を有する銅酸化物超伝導体 $Ca_{2-x}Na_xCuO_2Cl_2$ における磁場誘起磁性 II”, 日本物理学会第 64 回年次大会, (日本物理学会), 東京, 3 月 (2009).
- 中島紗織, 鈴木栄男, 渡邊功雄, 真中浩貴, 後藤貴行, Alex A.: “乱れを含んだ量子スピラダー $IPACu(Cl_xBr_{1-x})_3$ の量子臨界点近傍における μ SR II”, 日本物理学会第 64 回年次大会, 東京, 3 月 (2009).
- 佐久間史典: “Nuclear astrophysics at J-PARC with a search for deeply-bound kaonic nuclear states”, 2008 年度国立天文台研究集会「R プロセス元素組成の統合的理解: 宇宙の中の不安定核物理, (筑波大学物理学系原子核実験グループ, 国立天文台), つくば, 3 月 (2009).
- 大石一城, Heffner R. H., 髭本亘, 伊藤孝, Bauer E. D., Graf M. J., Zhu J. -, Morales L. A., Sarrao J. L., Morris G. D., Fluss M. J., MacLaughlin D. E., Shu L.: “Muon spin rotation measurements of the superfluid density in fresh and aged superconducting $PuCoGa_5$ ”, Workshop on Issues on Magnetic Penetration Depth Measurements in Superconductors, (日本原子力研究開発機構), 茨城県東海村, 4 月 (2009).
- 長友傑, 小林義男, 久保謙哉, 山田康洋, 三原基嗣, 佐藤渉, 宮崎淳, 佐藤眞二, 北川敦志: “プラスチックシンチレーション検出器を用いた ^{57}Mn インビームメスバウアー分光における S/N 比の向上”, 2009 日本放射化学学会年会・第 53 回放射化学討論会, (日本放射化学学会), 東京, 9 月 (2009).
- 長友傑, 小林義男, 久保謙哉, 山田康洋, 三原基嗣, 佐藤渉, 宮崎淳, 佐藤眞二, 北川敦志: “酸化アルミニウム固体中の ^{57}Mn インビーム・メスバウアー分光実験”, 2009 日本放射化学学会年会・第 53 回放射化学討論会, (日本放射化学学会), 東京, 9 月 (2009).
- 長友傑, 小林義男, 久保謙哉, 山田康洋, 三原基嗣, 佐藤渉, 宮崎淳, 佐藤眞二, 北川敦志: “酸化マグネシウム固体中の ^{57}Mn インビーム・メスバウアー分光実験”, 2009 日本放射化学学会年会・第 53 回放射化学討論会, (日本放射化学学会), 東京, 9 月 (2009).
- Risdiana.: “ μ SR study of structure dependent electron radical dynamics in polythiophene and its derivative”, 5th Program Advisory Committee Meeting for Materials and Life Science experiments at RIKEN Nishina Center, 和光, 9 月 (2009).
- 鈴木栄男, 石井康之, 大石一城, Risdiana., 渡邊功雄, 後藤貴行, 山田文子, 山田基樹, 田中秀数: “量子スピン系 $Tl(Cu_{1-x}Mg_x)Cl_3$ ($x = 0.015$) における圧力下ミュオン実験”, 日本物理学会 2009 年秋季大会, 熊本, 9 月 (2009).
- 大石一城, 伊藤孝, 髭本亘, 上原啓, 小沢克也, 山崎敬大, 君嶋義英, 上原政智: “ μ SR から眺めたアンチペロブスカイト型伝導体 $ZnNiNi_3$ の準粒子励起”, 日本物理学会 2009 年秋季大会, (日本物理学会), 熊本, 9 月 (2009).
- 本堂英, 益田隆嗣, 川股隆行, 佐藤光秀, 小池洋二: “ $S = 1/2$ スピン・ギャップ物質 $Pb_2V_3O_9$ の磁気励起”, 日本物理学会 2009 年秋季大会, 熊本, 9 月 (2009).
- 廣井政彦, 久松徹, 伊藤昌和, 鈴木栄男, 大石一城, 石井康之, 渡邊功雄: “ホイスラー化合物 $Ru_{1.9}Fe_{0.1}CrSi$ の μ SR”, 日本物理学会 2009 年秋季大会, 熊本, 9 月 (2009).
- 大久保晋, 近藤健太, 日野俊一, 藤澤真士, 櫻井敬博, 太田仁, 菅原直樹, 川股隆行, 小池洋二: “ボンド交替系 $Pb_2V_3O_9$ 単結晶試料の強磁場 ESR 測定 II”, 日本物理学会 2009 年秋季大会, 熊本, 9 月 (2009).
- 佐藤光秀, 川股隆行, 上坂正憲, 工藤一貴, 小林典男, 小池洋二: “一次元ボンド交替鎖を持つ $Pb_2V_3O_9$ におけるトリプロンのポーズ・アインシュタイン凝縮転移と熱伝導”, 日本物理学会 2009 年秋季大会, 熊本, 9 月 (2009).
- 中島紗織, 鈴木栄男, 渡邊功雄, 真中浩貴, 後藤貴行, Alex A.: “量子スピラダー磁性体 $IPACu(Cl_xBr_{1-x})_3$ の磁気秩序相における μ SR-NMR”, 日本物理学会 2009 年秋季大会, 熊本, 9 月 (2009).
- 長友傑, 小林義男, 三原基嗣, 久保謙哉, 山田康洋, 佐藤渉, 宮崎淳, 佐藤眞二, 北川敦志: “プラスチック検出器を用いた ^{57}Mn インビームメスバウアー分光の S/N 比の向上”, 平成 21 年度京都大学原子炉実験所専門研究会「短寿命核および放射線を用いた物性研究 (II)」研究会, 大阪府熊取町, 12 月 (2009).
- 徳田哲久, 大隅寛幸, 竹下聡史, 高橋功, 有馬孝尚, 高田昌樹, 鈴木基寛, 河村直己, 高阪勇輔, 中尾裕也, 横堀利夫, 松井秀樹, 秋光純: “ラセミ双晶観察のための円偏光マイクロビーム共鳴 X 線回折顕微測定”, 日本結晶学会年会 2009 年度年会, 西宮, 12 月 (2009).
- 徳田哲久, 大隅寛幸, 竹下聡史, 高橋功, 有馬孝尚, 高田昌樹,

- 高阪勇輔, 中尾裕也, 横堀利夫, 松井秀樹, 秋光純: “門偏光マイクロビーム共鳴 X 線回折による CsCuCl₃ ラセミ双晶顕微観察”, 第 23 回日本放射光学会年会・放射光科学合同シンポジウム, 姫路, 1 月 (2010).
- Bakule P., 石田勝彦, Fleming D. G.: “Measurement of the Chemical Reaction Rate of Muonium with Stimulated-Raman-Pumped H₂*($v=1$) in the Gas”, 理研シンポジウム「理研-RAL 支所ミュオン施設におけるミュオン科学研究 2009」, 和光, 1 月 (2010).
- 石田勝彦: “水素分子状態制御下の μCF ”, 理研シンポジウム「理研-RAL 支所ミュオン施設におけるミュオン科学研究 2009」, 和光, 1 月 (2010).
- 大石 城, 鈴木栄男, 髭本亘, 伊藤孝, Heffner R. H., Bauer E. D.: “R330,349: μSR Study around a Quantum Critical Point in Heavy Fermion Compounds”, 理研シンポジウム「理研-RAL 支所ミュオン施設におけるミュオン科学研究 2009」, 和光, 1 月 (2010).
- 石田勝彦: “室温ミュオニウムジェネレータ”, 理研シンポジウム「理研-RAL 支所ミュオン施設におけるミュオン科学研究 2009」, 和光, 1 月 (2010).
- 石田勝彦: “g-2 実験用低速ミュオン源開発”, RCNP 研究会「第 2 回ミュオン科学と加速器研究」, (大阪大学核物理研究センター), 吹田, 2 月 (2010).
- 黒田直史, 毛利明博, 永田祐吾, 鳥居寛之, 柴田政宏, 今尾浩士, 榎本嘉範, 金井保之, 檜垣浩之, 松田恭幸, 山崎泰規: “多重電極トラップ中の電子プラズマへの反陽子ビーム入射による静電振動モードのシフト”, 日本物理学会第 65 回年次大会, (日本物理学会), 岡山, 3 月 (2010).
- 山崎泰規, 榎本嘉範, 黒田直史, 今尾浩士, 金燦鉉, 鳥居寛之, 松田恭幸, 永田祐吾, 金井保之, 吉良健太郎, 満汐孝治, 長嶋泰之, 齋藤晴彦, Rizzini L. E., Venturelli L., Zurlo N., Mascagna V.: “反水素合成実験 I: カスプトラップ中における反陽子と陽電子の混合”, 日本物理学会第 65 回年次大会, (日本物理学会), 岡山, 3 月 (2010).
- 今尾浩士, 満汐孝治, 金井保之, 黒田直史, 榎本嘉範, 檜垣浩之, 吉良健太郎, 金燦鉉, 鳥居寛之, 永田祐吾, 齋藤晴彦, 松田恭幸, 長嶋泰之, 毛利明博, 山崎泰規: “反水素捕獲用カスプ磁場における高密度陽電子プラズマの生成”, 日本物理学会第 65 回年次大会, (社団法人日本物理学会), 岡山, 3 月 (2010).
- 大石 城, 石井康之, 深澤英人, 宮沢喜一, 渡邊功雄, Shirage P. M., 鬼頭聖, 伊豫彰, 永崎洋: “ μSR から眺めた鉄ヒ素系超伝導体 LaFeAs(O,H) の磁性と超伝導”, 日本物理学会第 65 回年次大会, (日本物理学会), 岡山, 3 月 (2010).
- 大石 城, 石井康之, 深澤英人, 宮沢喜一, 渡邊功雄, 齋藤拓, 小堀洋, 木方邦宏, 李哲虎, 伊豫彰, 嶋谷幸佑, 山田和芳, 永崎洋: “ μSR から眺めた鉄ヒ素系超伝導体 (Ba,K)Fe₂As₂ 及び Ba(Fe,Co)₂As₂ の磁性と超伝導”, 日本物理学会第 65 回年次大会, (日本物理学会), 岡山, 3 月 (2010).
- 檜垣浩之, 黒田直史, 今尾浩士, 永田祐吾, 榎本嘉範, 満汐孝治, 吉良健太郎, 金燦鉉, 金井保之, 毛利明博, 長嶋泰之, 鳥居寛之, 松田恭幸, 山崎泰規: “MUSASHI トラップにおけるタンク回路を用いた反陽子ビーム計測”, 日本物理学会第 65 回年次大会, (日本物理学会), 岡山, 3 月 (2010).
- 金燦鉉, 黒田直史, 榎本嘉範, 金井保之, 吉良健太郎, 今尾浩士, 満汐孝治, 長嶋泰之, 永田祐吾, 齋藤晴彦, 毛利明博, 鳥居寛之, 松田恭幸, 山崎泰規, Rizzini L. E., Venturelli L., Zurlo N., Mascagna V.: “カスプトラップにおける反水素合成実験”, 日本物理学会第 65 回年次大会, (日本物理学会), 岡山, 3 月 (2010).
- 鳥養映子, 松尾由賀利, 有光直子, 中島美帆, 松島房和, 笹尾真実子, 前田京剛, 柴田純, 中野公世, 高橋春美, 興治文子, 石井恭子: “女子中高生夏の学校における物理学会の活動”, 日本物理学会第 65 回年次大会, 岡山, 3 月 (2010).
- 長友傑, 小林義男, 久保謙哉, 山田康洋, 三原基嗣, 佐藤渉, 宮崎淳, 佐藤真一, 北川敦志: “不安定核 ⁵⁷Mn ビームを用いたインビーム・メスバウアー分光の現状”, 第 11 回メスバウアー分光研究会シンポジウム, 豊中, 3 月 (2010).

Publications

Journal

(Original Papers) *Subject to Peer Review

- Adare A., Akiba Y., Aoki K., Asai J., Bazilevsky A. V., Bunce G. M., Deshpande A., Enyo H., Fields D. E., Fox B., Fujiwara K., Fukao Y., Goto Y., Gross P. M., Hasuko K., Heuser J. M., Horaguchi T., Ichihara T., Imai K., Inoue Y., Ishihara M., Jinnouchi O., Kamihara N., Kaneta M., Kanoh H., Kawall D., Kiyomichi A., Kobayashi H., Kurita K., Mao Y., Murata J., Nakagawa I., Nakano K., Onishi H., Okada H., Okada K., Rykov V. L., Saito N., Sato H., Shibata T., Shoji K., Tabaru T., Taketani A., Tanida K., Togawa M., Tojo J., Torii H., Wagner M. M., Watanabe Y., Xie W., and Yokkaichi S.: “Cold Nuclear Matter Effects on J/ψ Production as Constrained by Deuteron-Gold Measurements at $\sqrt{s_{NN}} = 200$ GeV”, Phys. Rev. C **77**, 024912-1–024912-15 (2008). *
- Adare A., Akiba Y., Aoki K., Asai J., Bunce G. M., Deshpande A., Enyo H., Fields D. E., Fujiwara K., Fukao Y., Goto Y., Gross P. M., Hachiya T., Hasuko K., Heuser J. M., Horaguchi T., Ichihara T., Imai K., Inoue Y., Ishihara M., Jinnouchi O., Kajihara F., Kamihara N., Kaneta M., Kanoh H., Kawall D., Kiyomichi A., Kurita K., Mao Y., Murata J., Nakagawa I., Nakano K., Onishi H., Okada H., Okada K., Rykov V. L., Saito N., Sato H., Shibata T., Shoji K., Tabaru T., Taketani A., Tanida K., Togawa M., Tojo J., Torii H., Tsuchimoto Y., Wagner M. M., Watanabe Y., Xie W., and Yokkaichi S.: “Quantitative Constraints on the Transport Properties of Hot Partonic Matter from Semi-Inclusive Single High Transverse Momentum Pion Suppression in Au+Au Collisions at $\sqrt{s_{NN}} = 200$ GeV”, Phys. Rev. C **77**, 064907-1–064907-12 (2008). *
- Adare A., Akiba Y., Aoki K., Asai J., Bunce G. M., Deshpande A., Enyo H., Fields D. E., Fujiwara K., Fukao Y., Goto Y., Gross P. M., Hachiya T., Hasuko K., Heuser J. M., Horaguchi T., Ichihara T., Imai K., Inoue Y., Ishihara M., Jinnouchi O., Kajihara F., Kamihara N., Kaneta M., Kanoh H., Kawall D., Kiyomichi A., Kurita K., Mao Y., Murata J., Nakagawa I., Nakano K., Onishi H., Okada H., Okada K., Rykov V. L., Saito N., Sato H., Shibata T., Shoji K., Tabaru T., Taketani A., Tanida K., Togawa M., Tojo J., Torii H., Tsuchimoto Y., Wagner M. M., Watanabe Y., Xie W., and Yokkaichi S.: “Dihadron azimuthal correlations in Au+Au collisions at $\sqrt{s_{NN}} = 200$ GeV”, Phys. Rev. C **78**, 014901-1–014901-42 (2008). *
- Adare A., Akiba Y., Aoki K., Asai J., Bazilevsky A. V., Bunce G. M., Deshpande A., Enyo H., Fields D. E., Fox B., Fujiwara K., Fukao Y., Goto Y., Gross P. M., Hachiya T., Hasuko K., Heuser J. M., Horaguchi T., Ichihara T., Imai K., Inoue Y., Ishihara M., Jinnouchi O., Kametani S., Kamihara N., Kaneta M., Kanoh H., Kawall D., Kiyomichi A., Kurita K., Kurosawa M., Li Z., Mao Y., Murata J., Nakagawa I., O., Kajihara F., Kamihara N., Kaneta M., Kanoh H., Kawall D., Kiyomichi A., Kobayashi H., Kurita K., Mao Y., Murata J., Nakagawa I., Nakano K., Onishi H., Okada H., Okada K., Rykov V. L., Saito N., Sato H., Shibata T., Shoji K., Tabaru T., Taketani A., Tanida K., Togawa M., Tojo J., Torii H., Tsuchimoto Y., Wagner M. M., Watanabe Y., Xie W., and Yokkaichi S.: “Charged hadron multiplicity fluctuations in Au+Au and Cu+Cu collisions from $\sqrt{s_{NN}} = 22.5$ to 200 GeV”, Phys. Rev. C **78**, 044902-1–044902-15 (2008). *
- Afanasiev S., Akiba Y., Aoki K., Bunce G. M., Deshpande A., Enyo H., Fields D. E., Fukao Y., Goto Y., Gross P. M., Hachiya T., Hasuko K., Heuser J. M., Horaguchi T., Ichihara T., Imai K., Ishihara M., Jinnouchi O., Kajihara F., Kamihara N., Kaneta M., Kiyomichi A., Kurita K., Murata J., Onishi H., Okada H., Okada K., Rykov V. L., Saito N., Sato H., Shibata T., Shoji K., Tabaru T., Taketani A., Tanida K., Togawa M., Tojo J., Torii H., Tsuchimoto Y., Wagner M. M., Watanabe Y., Xie W., and Yokkaichi S.: “Source breakup dynamics in Au+Au Collisions at $\sqrt{s_{NN}}=200$ GeV via three-dimensional two-pion source imaging”, Phys. Rev. Lett. **100**, 232301-1–232301-6 (2008). *
- Afanasiev S., Akiba Y., Aoki K., Bunce G. M., Deshpande A., Enyo H., Fields D. E., Fukao Y., Goto Y., Gross P. M., Hachiya T., Hasuko K., Heuser J. M., Horaguchi T., Ichihara T., Imai K., Ishihara M., Jinnouchi O., Kajihara F., Kamihara N., Kaneta M., Kiyomichi A., Kurita K., Murata J., Onishi H., Okada H., Okada K., Rykov V. L., Saito N., Sato H., Shibata T., Shoji K., Tabaru T., Taketani A., Tanida K., Togawa M., Tojo J., Torii H., Tsuchimoto Y., Wagner M. M., Watanabe Y., Xie W., and Yokkaichi S.: “Particle-species dependent modification of jet-induced correlations in Au+Au collisions at $\sqrt{s_{NN}} = 200$ GeV”, Phys. Rev. Lett. **101**, 082301-1–082301-6 (2008). *
- Adare A., Akiba Y., Aoki K., Asai J., Bunce G. M., Deshpande A., Enyo H., Fields D. E., Fujiwara K., Fukao Y., Goto Y., Gross P. M., Horaguchi T., Ichihara T., Imai K., Inoue Y., Ishihara M., Jinnouchi O., Kamihara N., Kaneta M., Kanoh H., Kawall D., Kiyomichi A., Kurita K., Mao Y., Murata J., Nakagawa I., Nakano K., Onishi H., Okada H., Okada K., Rykov V. L., Saito N., Shibata T., Shoji K., Tabaru T., Taketani A., Tanida K., Togawa M., Tojo J., Torii H., Wagner M. M., Watanabe Y., Xie W., and Yokkaichi S.: “ J/ψ Production in $\sqrt{s_{NN}} = 200$ GeV Cu+Cu Collisions”, Phys. Rev. Lett. **101**, 122301-1–122301-6 (2008). *
- Adare A., Akiba Y., Aoki K., Asai J., Bunce G. M., Dairaku S., Deshpande A., Enyo H., Fields D. E., Fujiwara K., Fukao Y., Goto Y., Gross P. M., Horaguchi T., Ichihara T., Ichimiya R., Imai K., Inoue Y., Ishihara M., Jinnouchi O., Kametani S., Kamihara N., Kaneta M., Kanoh H., Kawall D., Kiyomichi A., Kurita K., Kurosawa M., Li Z., Mao Y., Murata J., Nakagawa I.,

- Nakano K., Onishi H., Okada H., Okada K., Onuki Y., Rykov V. L., Saito N., Sakashita K., Shibata T., Shoji K., Tabaru T., Taketani A., Tanida K., Togawa M., Tojo J., Torii H., Wagner M. M., Watanabe Y., Xie W., and Yokkaichi S.: “Onset of π^0 suppression studied in Cu+Cu collisions at $\sqrt{s_{NN}} = 22.4, 62.4,$ and 200 GeV”, Phys. Rev. Lett. **101**, 162301-1–162301-6 (2008). *
- Adare A., Akiba Y., Aoki K., Asai J., Bunce G. M., Deshpande A., Enyo H., Fields D. E., Fujiwara K., Fukao Y., Goto Y., Gross P. M., Hachiya T., Hasuko K., Heuser J. M., Horaguchi T., Ichihara T., Imai K., Inoue Y., Ishihara M., Jinnouchi O., Kajihara F., Kamihara N., Kaneta M., Kanoh H., Kawall D., Kiyomichi A., Kurita K., Mao Y., Murata J., Nakagawa I., Nakano K., Onishi H., Okada H., Okada K., Rykov V. L., Saito N., Sato H., Shibata T., Shoji K., Tabaru T., Taketani A., Tanida K., Togawa M., Tojo J., Torii H., Tsuchimoto Y., Wagner M. M., Watanabe Y., Xie W., and Yokkaichi S.: “Suppression pattern of neutral pions at high transverse momentum in Au+Au collisions at $\sqrt{s_{NN}} = 200$ GeV and constraints on medium transport coefficients”, Phys. Rev. Lett. **101**, 232301-1–232301-7 (2008). *
- Adare A., Akiba Y., Aoki K., Asai J., Bunce G. M., Deshpande A., Enyo H., Fields D. E., Fujiwara K., Fukao Y., Goto Y., Gross P. M., Horaguchi T., Ichihara T., Imai K., Inoue Y., Ishihara M., Jinnouchi O., Kamihara N., Kaneta M., Kanoh H., Kawall D., Kiyomichi A., Kurita K., Mao Y., Murata J., Nakagawa I., Nakano K., Onishi H., Okada H., Okada K., Rykov V. L., Saito N., Shibata T., Shoji K., Tabaru T., Taketani A., Tanida K., Togawa M., Tojo J., Torii H., Wagner M. M., Watanabe Y., Xie W., and Yokkaichi S.: “Dilepton mass spectra in p+p collisions at $\sqrt{s} = 200$ GeV and the contribution from open charm”, Phys. Lett. B **670**, 313–320 (2009). *
- Adare A., Akiba Y., Aoki K., Asai J., Bunce G. M., Dairaku S., Deshpande A., Enyo H., Fields D. E., Fujiwara K., Fukao Y., Goto Y., Gross P. M., Horaguchi T., Ichihara T., Ichimiya R., Imai K., Ishihara M., Kametani S., Kamihara N., Kawall D., Kurita K., Kurosawa M., Li Z., Mao Y., Murata J., Nakagawa I., Nakano K., Okada H., Okada K., Onuki Y., Rykov V. L., Saito N., Sakashita K., Shibata T., Shoji K., Taketani A., Tanida K., Togawa M., Torii H., Watanabe Y., Xie W., and Yokkaichi S.: “Inclusive cross section and double helicity asymmetry for π^0 production in $p + p$ collisions at $\sqrt{s} = 62.4$ GeV”, Phys. Rev. D **79**, 012003-1–012003-11 (2009). *

Theory Group

Publications

Journal

(Original Papers) *Subject to Peer Review

- Cheng M., Christ N. H., Jung C., Karsch F., Mawhinney R. D., Petreczky P., and Petrov K.: “Flavor symmetry breaking and scaling for improved staggered actions in quenched QCD”, *Eur. Phys. J. C* **51**, No. 4, pp. 875–881 (2007). *
- Cheng M., Christ N., Clark M. A., van der Heide J., Jung C., Karsch F., Kaczmarek O., Laermann E., Mawhinney R. D., Miao C., Petreczky P., Petrov K., Schmidt C., Soeldner W., and Umeda T.: “Study of the finite temperature transition in 3-flavor QCD”, *Phys. Rev. D* **75**, No. 3, pp. 034506-1–034506-11 (2007). *
- Mocsy A. and Petreczky P.: “Quarkonium-signal of deconfinement”, *J. Phys. G* **35**, No. 4, pp. 044038-1–044038-6 (2008). *
- Datta S. and Petreczky P.: “Zero mode contribution in quarkonium correlators and in-medium properties of heavy quarks”, *J. Phys. G* **35**, No. 10, pp. 104114-1–104114-4 (2008). *
- Mocsy A. and Petreczky P.: “Quarkonium melting above deconfinement”, *J. Phys. G* **35**, No. 10, pp. 104154-1–104154-4 (2008). *
- Hatsuda T., Aoki S., Ishii N., and Nemura H.: “From Lattice QCD to Nuclear Force”, *Mod. Phys. Lett. A* **23**, 2265–2272 (2008). *
- Nemura H., Ishii N., Aoki S., and Hatsuda T.: “Lattice QCD Simulation of Hyperon-Nucleon Potential”, *Mod. Phys. Lett. A* **23**, 2285–2288 (2008). *
- Cheng M., Christ N. H., Datta S., van der Heide J., Jung C., Karsch F., Kaczmarek O., Laermann E., Mawhinney R. D., Miao C., Petreczky P., Petrov K., Schmidt C., Soeldner W., and Umeda T.: “QCD equation of state with almost physical quark masses”, *Phys. Rev. D* **77**, No. 1, pp. 014511-1–014511-20 (2008). *
- Brambilla N., Ghiglieri J., Vairo A., and Petreczky P.: “Static quark-antiquark pairs at finite temperature”, *Phys. Rev. D* **78**, No. 1, pp. 014017-1–014017-21 (2008). *
- Bazavov A., Petreczky P., and Velytsky A.: “Static quark-antiquark pair in SU(2) gauge theory”, *Phys. Rev. D* **78**, No. 11, pp. 114026-1–114026-12 (2008). *
- Aoki S., Balog J., Hatsuda T., Ishii N., Murano K., Nemura H., and Weisz P.: “Energy Dependence of Nucleon-Nucleon Potentials”, *Proceedings of Science LATTICE 2008*, No. 152, pp. 1–7 (2008). *
- Nemura H., Ishii N., Aoki S., and Hatsuda T.: “Lambda-nucleon force from lattice QCD”, *Proceedings of Science LATTICE 2008*, No. 156, pp. 1–7 (2008). *
- Petreczky P.: “On the temperature dependence of quarkonium correlators”, *Eur. Phys. J. C*, pp. 1–9 (2009). *
- Aoki Y., Borsanyi S., Durr S., Fodor Z., Katz S. D., Szabo K. K., and Krieg S.: “The QCD transition temperature: results with physical masses in the continuum limit II”, *J. High Energy Phys.* **0906**, 088-0–088-17 (2009). *
- Dumitru A.: “Quarkonium in a viscous QGP”, *Nucl. Phys. A* **830**, 323c–326c (2009). *
- Aoki Y., Borsanyi S., Durr S., Fodor Z., Katz S. D., Krieg S., and Szabo K. K.: “QCD transition temperature: Approaching the continuum on the lattice”, *Nucl. Phys. A* **830**, 805c–808c (2009). *
- Nemura H., Ishii N., Aoki S., and Hatsuda T.: “Hyperon-nucleon force from lattice QCD”, *Phys. Lett. B* **673**, 136–141 (2009). *
- Schenke B., Strickland M., Dumitru A., Nara Y., and Greiner C.: “Transverse momentum diffusion and collisional jet energy loss in non-Abelian plasmas”, *Phys. Rev. C* **79**, 034903-1–034903-10 (2009). *
- Dumitru A., Guo Y., Mocsy A., and Strickland M.: “Quarkonium states in an anisotropic QCD plasma”, *Phys. Rev. D* **79**, 054019-1–054019-10 (2009). *
- Dumitru A., Guo Y., and Strickland M.: “Imaginary part of the static gluon propagator in an anisotropic (viscous) QCD plasma”, *Phys. Rev. D* **79**, 114003-1–114003-7 (2009). *
- Yamazaki T., Aoki Y., Blum T., Lin H., Ohta S., Sasaki S., Tweedie R. J., and Zanotti J. M.: “Nucleon form factors with 2+1 flavor dynamical domain-wall fermions”, *Phys. Rev. D* **79**, 114505-1–114505-20 (2009). *
- Noronha J. and Dumitru A.: “Heavy quark potential as a function of shear viscosity at strong coupling”, *Phys. Rev. D* **80**, 014007-1–014007-8 (2009). *
- Sturm C., Aoki Y., Christ N. H., Izubuchi T., Sachrajda C. T., and Soni A.: “Renormalization of quark bilinear operators in a momentum-subtraction scheme with a nonexceptional subtraction point”, *Phys. Rev. D* **80**, 014501-1–014501-11 (2009). *
- Noronha J. and Dumitru A.: “Thermal Width of the Υ at Large 't Hooft Coupling”, *Phys. Rev. Lett.* **103**, 152304-1–152304-4 (2009). *
- Ishikawa T., Aoki Y., and Izubuchi T.: “Improving chiral property of domain-wall fermions by reweighting method”, *Proceedings of Science LAT2009*, No. 035, pp. 1–7 (2010).
- Ohta S.: “Nucleon structure functions from dynamical (2+1)-flavor domain wall fermions”, *Proceedings of Science LAT2009*, No. 131, pp. 1–7 (2010). *
- (Review)
- Petreczky P.: “Lattice QCD at finite temperature”, *Nucl. Phys. A* **785**, No. 1, pp. 10c–17c (2007).

Oral Presentations

(International Conference etc.)

- Nemura H., Ishii N., Aoki S., and Hatsuda T.: “Lambda-nucleon force from lattice QCD”, *Lattice 2008, 26th International Symposium on Lattice Field Theory*, (College of Williams and Mary), Virginia, USA, July (2008).

- Nemura H., Ishii N., Aoki S., and Hatsuda T.: “Hyperon-nucleon force calculated from lattice QCD”, KGU Yokohama Autumn School of Nuclear Physics, (KGU), Yokohama, Oct. (2008).
- Nemura H., Ishii N., Aoki S., and Hatsuda T.: “Study of hyperon-nucleon potential from lattice QCD”, Sendai International Symposium on Strangeness in Nuclear and Hadronic Systems (SENDAI08), (Tohoku University), Sendai, Dec. (2008).
- Dumitru A.: “Quarkonium states in an anisotropic (viscous) QGP”, 21st International Conference on Ultrarelativistic Nucleus-Nucleus Collisions (Quark Matter 2009), Knoxville, USA, Mar.–Apr. (2009).
- Aoki Y.: “BNL Non-perturbative renormalization”, 27th International Symposium on Lattice Field Theory (Lattice 2009), Beijing, China, July (2009).
- Ishikawa T.: “Improving chiral property of domain-wall fermions by reweighting method”, 27th International Symposium on Lattice Field Theory (Lattice 2009), (University of Beijing), Beijing, China, July (2009).
- Aoki Y.: “Hadronic matrix elements of proton decay from lattice QCD”, 2009 Workshop on Lepton and Baryon Number Violation (LBV09), (University of Wisconsin-Madison), Madison, USA, Sept. (2009).
- Aoki Y.: “Nucleon properties from chirally symmetric lattice QCD”, 3rd Joint Meeting of the Nuclear Physics Divisions of the APS and JPS (Hawaii 2009), Hawaii, USA, Oct. (2009).
- Aoki Y.: “Lattice QCD Perspective”, RBRC Symposium, Upton, USA, Dec. (2009).
- Dumitru A.: “Snapshot of the Glasma from RHIC: the Ridge”, RBRC Symposium, Upton, USA, Dec. (2009).
- (Domestic Conference)
- 根村英克, 石井理修, 青木慎也, 初田哲男: “格子 QCD によるハイペロンポテンシャルの研究”, 文科省科研費補助金特定領域研究「サマースクールエキゾチック原子核実践講座-あなたも計算できる-」, (京都大学), 和光, 8 月 (2008).
- 根村英克, 石井理修, 青木慎也, 初田哲男: “格子 QCD によるハイペロン核子相互作用の研究”, 文科省科研費補助金特定領域研究「ストレンジネスで探るクォーク多体系」研究会 2008, 加賀, 10 月 (2008).
- 根村英克, 石井理修, 青木慎也, 初田哲男: “Hyperon Potentials from Lattice QCD”, Aizu meeting 2009 on Spin Excitations and Exotic Degree of Freedom in Nuclei and Nuclear Matter, 会津若松, 2 月 (2009).
- 根村英克, 石井理修, 青木慎也, 初田哲男: “格子 QCD によるハイペロン核子相互作用の研究”, 文科省科研費補助金特定領域研究「ストレンジネスで探るクォーク多体系」理論班主催「ストレンジネスを含むクォーク多体系分野の理論的将来を考える」研究会, 熱海, 2 月 (2009).
- 根村英克, 石井理修, 青木慎也, 初田哲男: “格子 QCD による ΛN ポテンシャル”, 日本物理学会第 64 回年次大会, (日本物理学会), 東京, 3 月 (2009).
- 根村英克, 石井理修, 青木慎也, 初田哲男: “格子 QCD によるハイペロンポテンシャル”, 文科省科研費補助金新学術領域研究「素核宇宙融合による計算科学に基づいた重層的物质構造の解明」A02 班主催「ハイパー核研究と中性子星研究の連携の可能性を探る」研究会, 和光, 3 月 (2009).
- 青木保道: “格子 QCD と標準模型”, 理研・格子 QCD 研究会, 和光, 12 月 (2009).

Experimental Group

Publications

Journal

(Original Papers) *Subject to Peer Review

- Adare A., Akiba Y., Aoki K., Asai J., Bazilevsky A. V., Bunce G. M., Deshpande A., Enyo H., Fields D. E., Fox B., Fujiwara K., Fukao Y., Goto Y., Gross P. M., Hasuko K., Heuser J. M., Horaguchi T., Ichihara T., Imai K., Inoue Y., Ishihara M., Jinnouchi O., Kamihara N., Kaneta M., Kanoh H., Kawall D., Kiyomichi A., Kobayashi H., Kurita K., Mao Y., Murata J., Nakagawa I., Nakano K., Onishi H., Okada H., Okada K., Rykov V. L., Saito N., Sato H., Shibata T., Shoji K., Tabaru T., Taketani A., Tanida K., Togawa M., Tojo J., Torii H., Wagner M. M., Watanabe Y., Xie W., and Yokkaichi S.: “Cold Nuclear Matter Effects on J/ψ Production as Constrained by Deuteron-Gold Measurements at $\sqrt{s_{NN}} = 200$ GeV”, Phys. Rev. C **77**, 024912-1–024912-15 (2008). *
- Adare A., Akiba Y., Aoki K., Asai J., Bunce G. M., Deshpande A., Enyo H., Fields D. E., Fujiwara K., Fukao Y., Goto Y., Gross P. M., Hachiya T., Hasuko K., Heuser J. M., Horaguchi T., Ichihara T., Imai K., Inoue Y., Ishihara M., Jinnouchi O., Kajihara F., Kamihara N., Kaneta M., Kanoh H., Kawall D., Kiyomichi A., Kurita K., Mao Y., Murata J., Nakagawa I., Nakano K., Onishi H., Okada H., Okada K., Rykov V. L., Saito N., Sato H., Shibata T., Shoji K., Tabaru T., Taketani A., Tanida K., Togawa M., Tojo J., Torii H., Tsuchimoto Y., Wagner M. M., Watanabe Y., Xie W., and Yokkaichi S.: “Quantitative Constraints on the Transport Properties of Hot Partonic Matter from Semi-Inclusive Single High Transverse Momentum Pion Suppression in Au+Au Collisions at $\sqrt{s_{NN}} = 200$ GeV”, Phys. Rev. C **77**, 064907-1–064907-12 (2008). *
- Adare A., Akiba Y., Aoki K., Asai J., Bunce G. M., Deshpande A., Enyo H., Fields D. E., Fujiwara K., Fukao Y., Goto Y., Gross P. M., Hachiya T., Hasuko K., Heuser J. M., Horaguchi T., Ichihara T., Imai K., Inoue Y., Ishihara M., Jinnouchi O., Kajihara F., Kamihara N., Kaneta M., Kanoh H., Kawall D., Kiyomichi A., Kurita K., Mao Y., Murata J., Nakagawa I., Nakano K., Onishi H., Okada H., Okada K., Rykov V. L., Saito N., Sato H., Shibata T., Shoji K., Tabaru T., Taketani A., Tanida K., Togawa M., Tojo J., Torii H., Tsuchimoto Y., Wagner M. M., Watanabe Y., Xie W., and Yokkaichi S.: “Dihadron azimuthal correlations in Au+Au collisions at $\sqrt{s_{NN}} = 200$ GeV”, Phys. Rev. C **78**, 014901-1–014901-42 (2008). *
- Adare A., Akiba Y., Aoki K., Asai J., Bazilevsky A. V., Bunce G. M., Deshpande A., Enyo H., Fields D. E., Fox B., Fujiwara K., Fukao Y., Goto Y., Gross P. M., Hachiya T., Hasuko K., Heuser J. M., Horaguchi T., Ichihara T., Imai K., Inoue Y., Ishihara M., Jinnouchi O., Kametani S., Kamihara N., Kaneta M., Kanoh H., Kawall D., Kiyomichi A., Kurita K., Kurosawa M., Li Z., Mao Y., Murata J., Nakagawa I., O., Kajihara F., Kamihara N., Kaneta M., Kanoh H., Kawall D., Kiyomichi A., Kobayashi H., Kurita K., Mao Y., Murata J., Nakagawa I., Nakano K., Onishi H., Okada H., Okada K., Rykov V. L., Saito N., Sato H., Shibata T., Shoji K., Tabaru T., Taketani A., Tanida K., Togawa M., Tojo J., Torii H., Tsuchimoto Y., Wagner M. M., Watanabe Y., Xie W., and Yokkaichi S.: “Charged hadron multiplicity fluctuations in Au+Au and Cu+Cu collisions from $\sqrt{s_{NN}} = 22.5$ to 200 GeV”, Phys. Rev. C **78**, 044902-1–044902-15 (2008). *
- Afanasiev S., Akiba Y., Aoki K., Bunce G. M., Deshpande A., Enyo H., Fields D. E., Fukao Y., Goto Y., Gross P. M., Hachiya T., Hasuko K., Heuser J. M., Horaguchi T., Ichihara T., Imai K., Ishihara M., Jinnouchi O., Kajihara F., Kamihara N., Kaneta M., Kiyomichi A., Kurita K., Murata J., Onishi H., Okada H., Okada K., Rykov V. L., Saito N., Sato H., Shibata T., Shoji K., Tabaru T., Taketani A., Tanida K., Togawa M., Tojo J., Torii H., Tsuchimoto Y., Wagner M. M., Watanabe Y., Xie W., and Yokkaichi S.: “Source breakup dynamics in Au+Au Collisions at $\sqrt{s_{NN}}=200$ GeV via three-dimensional two-pion source imaging”, Phys. Rev. Lett. **100**, 232301-1–232301-6 (2008). *
- Afanasiev S., Akiba Y., Aoki K., Bunce G. M., Deshpande A., Enyo H., Fields D. E., Fukao Y., Goto Y., Gross P. M., Hachiya T., Hasuko K., Heuser J. M., Horaguchi T., Ichihara T., Imai K., Ishihara M., Jinnouchi O., Kajihara F., Kamihara N., Kaneta M., Kiyomichi A., Kurita K., Murata J., Onishi H., Okada H., Okada K., Rykov V. L., Saito N., Sato H., Shibata T., Shoji K., Tabaru T., Taketani A., Tanida K., Togawa M., Tojo J., Torii H., Tsuchimoto Y., Wagner M. M., Watanabe Y., Xie W., and Yokkaichi S.: “Particle-species dependent modification of jet-induced correlations in Au+Au collisions at $\sqrt{s_{NN}} = 200$ GeV”, Phys. Rev. Lett. **101**, 082301-1–082301-6 (2008). *
- Adare A., Akiba Y., Aoki K., Asai J., Bunce G. M., Deshpande A., Enyo H., Fields D. E., Fujiwara K., Fukao Y., Goto Y., Gross P. M., Horaguchi T., Ichihara T., Imai K., Inoue Y., Ishihara M., Jinnouchi O., Kamihara N., Kaneta M., Kanoh H., Kawall D., Kiyomichi A., Kurita K., Mao Y., Murata J., Nakagawa I., Nakano K., Onishi H., Okada H., Okada K., Rykov V. L., Saito N., Shibata T., Shoji K., Tabaru T., Taketani A., Tanida K., Togawa M., Tojo J., Torii H., Wagner M. M., Watanabe Y., Xie W., and Yokkaichi S.: “ J/ψ Production in $\sqrt{s_{NN}} = 200$ GeV Cu+Cu Collisions”, Phys. Rev. Lett. **101**, 122301-1–122301-6 (2008). *
- Adare A., Akiba Y., Aoki K., Asai J., Bunce G. M., Dairaku S., Deshpande A., Enyo H., Fields D. E., Fujiwara K., Fukao Y., Goto Y., Gross P. M., Horaguchi T., Ichihara T., Ichimiya R., Imai K., Inoue Y., Ishihara M., Jinnouchi O., Kametani S., Kamihara N., Kaneta M., Kanoh H., Kawall D., Kiyomichi A., Kurita K., Kurosawa M., Li Z., Mao Y., Murata J., Nakagawa I.,

- Nakano K., Onishi H., Okada H., Okada K., Onuki Y., Rykov V. L., Saito N., Sakashita K., Shibata T., Shoji K., Tabaru T., Taketani A., Tanida K., Togawa M., Tojo J., Torii H., Wagner M. M., Watanabe Y., Xie W., and Yokkaichi S.: “Onset of π^0 suppression studied in Cu+Cu collisions at $\sqrt{s_{NN}} = 22.4, 62.4,$ and 200 GeV”, Phys. Rev. Lett. **101**, 162301-1–162301-6 (2008). *
- Adare A., Akiba Y., Aoki K., Asai J., Bunce G. M., Deshpande A., Enyo H., Fields D. E., Fujiwara K., Fukao Y., Goto Y., Gross P. M., Hachiya T., Hasuko K., Heuser J. M., Horaguchi T., Ichihara T., Imai K., Inoue Y., Ishihara M., Jinnouchi O., Kajihara F., Kamihara N., Kaneta M., Kanoh H., Kawall D., Kiyomichi A., Kurita K., Mao Y., Murata J., Nakagawa I., Nakano K., Onishi H., Okada H., Okada K., Rykov V. L., Saito N., Sato H., Shibata T., Shoji K., Tabaru T., Taketani A., Tanida K., Togawa M., Tojo J., Torii H., Tsuchimoto Y., Wagner M. M., Watanabe Y., Xie W., and Yokkaichi S.: “Suppression pattern of neutral pions at high transverse momentum in Au+Au collisions at $\sqrt{s_{NN}} = 200$ GeV and constraints on medium transport coefficients”, Phys. Rev. Lett. **101**, 232301-1–232301-7 (2008). *
- Adare A., Akiba Y., Aoki K., Asai J., Bunce G. M., Deshpande A., Enyo H., Fields D. E., Fujiwara K., Fukao Y., Goto Y., Gross P. M., Horaguchi T., Ichihara T., Imai K., Inoue Y., Ishihara M., Jinnouchi O., Kamihara N., Kaneta M., Kanoh H., Kawall D., Kiyomichi A., Kurita K., Mao Y., Murata J., Nakagawa I., Nakano K., Onishi H., Okada H., Okada K., Rykov V. L., Saito N., Shibata T., Shoji K., Tabaru T., Taketani A., Tanida K., Togawa M., Tojo J., Torii H., Wagner M. M., Watanabe Y., Xie W., and Yokkaichi S.: “Dilepton mass spectra in p+p collisions at $\sqrt{s} = 200$ GeV and the contribution from open charm”, Phys. Lett. B **670**, 313–320 (2009). *
- Adare A., Akiba Y., Aoki K., Asai J., Bunce G. M., Dairaku S., Deshpande A., Enyo H., Fields D. E., Fujiwara K., Fukao Y., Goto Y., Gross P. M., Horaguchi T., Ichihara T., Ichimiya R., Imai K., Ishihara M., Kametani S., Kamihara N., Kawall D., Kurita K., Kurosawa M., Li Z., Mao Y., Murata J., Nakagawa I., Nakano K., Okada H., Okada K., Onuki Y., Rykov V. L., Saito N., Sakashita K., Shibata T., Shoji K., Taketani A., Tanida K., Togawa M., Torii H., Watanabe Y., Xie W., and Yokkaichi S.: “Inclusive cross section and double helicity asymmetry for π^0 production in $p + p$ collisions at $\sqrt{s} = 62.4$ GeV”, Phys. Rev. D **79**, 012003-1–012003-11 (2009). *

RIKEN Facility Office at RAL

Publications

Journal

(Original Papers) *Subject to Peer Review

Imao H., Ishida K., Kawamura N., Matsuzaki T., Matsuda Y., Toyoda A., Strasser P., Iwasaki M., and Nagamine K.: "Density effect in d-d muon-catalyzed fusion with ortho- and para-enriched deuterium", *Hyperfine Interact.* **193**, No. 1-3, pp. 159-163 (2009). *

Oral Presentations

(International Conference etc.)

Matsuzaki T.: "Developments of Extreme Conditioned μ SR setups", RIKEN Symposium on Molecular Ensemble 2009, Wako, Dec. (2009).

(Domestic Conference)

菊地晶裕, 渡邊功雄, 城直嗣: " μ SR 法による鉄ポルフィリンの微視的観測- μ SR 法によるヘムタンパク質の解明を目指して", 第 59 回錯体化学討論会, 長崎, 9 月 (2009).

松崎禎市郎: "高圧固体 D2 標的システム", 理研シンポジウム「理研-RAL 支所ミュオン施設におけるミュオン科学研究 2009」, (J-PARC/MLF 利用者懇談会), 和光, 1 月 (2010).

松崎禎市郎: "理研-RAL 支所ミュオン施設の現状と将来計画", 理研シンポジウム「理研-RAL 支所ミュオン施設におけるミュオン科学研究 2009」, (J-PARC/MLF 利用者懇談会), 和光, 1 月 (2010).

Publications

Journal

(Original Papers) *Subject to Peer Review

- Tatsumi K., Mitani Y., Watanabe J., Takakura H., Hoshi K., Kawai Y., Kikuchi T., Kougo Y., Katayama A., Tomaru Y., Kanamori H., Usui K., Itoh M., Cizdziel P. E., Lejava A., Ueda M., Ichikawa Y., Endo I., Togo S., Shimada H., and Hayashizaki Y.: “Rapid screening assay for KRAS mutations by the modified SMart Amplification Process”, *J. Mol. Diagn.* **10**, No. 6, pp. 520–526 (2008). *
- Ohnishi T., Kubo T., Kusaka K., Yoshida A., Yoshida K., Fukuda N., Ohtake M., Yanagisawa Y., Takeda H., Kameda D., Yamaguchi Y., Aoi N., Yoneda K., Otsu H., Takeuchi S., Sugimoto T., Kondo Y., Scheit H., Gono Y., Sakurai H., Motobayashi T., Suzuki H., Nakao T., Kimura H., Mizoi Y., Matsushita M., Ieki K., Kuboki T., Yamaguchi T., Suzuki T., Ozawa A., Moriguchi T., Yasuda Y., Nakamura T., Nannichi T., Shimamura T., Nakayama Y., Geissel H., Weick H., Nolen J. A., Tarasov O. B., Nettleton A. S., Bazin D. P., Sherrill B. M., Morrissey D. J., and Mittig W.: “Identification of New Isotopes ^{125}Pd and ^{126}Pd Produced by In-Flight Fission of 345 MeV/nucleon ^{238}U : First Results from the RIKEN RI Beam Factory”, *J. Phys. Soc. Jpn.* **77**, No. 8, pp. 083201-1–083201-4 (2008). *
- Moriwaki Y., Matsuo Y., Fukuyama Y., and Morita N.: “Fine structure changing cross section of Ba^+ ions in collisions with He atoms”, *Jpn. J. Appl. Phys.* **47**, 1757–1759 (2008). *
- Nakajima T., Matsuo Y., and Kobayashi T.: “All-optical control and direct detection of ultrafast spin polarization in a multi-valence-electron system”, *Phys. Rev. A* **77**, 063404-1–063404-4 (2008). *
- Adare A., Akiba Y., Aoki K., Asai J., Bazilevsky A. V., Bunce G. M., Deshpande A., Enyo H., Fields D. E., Fox B., Fujiwara K., Fukao Y., Goto Y., Gross P. M., Hasuko K., Heuser J. M., Horaguchi T., Ichihara T., Imai K., Inoue Y., Ishihara M., Jinnouchi O., Kamihara N., Kaneta M., Kanoh H., Kawall D., Kiyomichi A., Kobayashi H., Kurita K., Mao Y., Murata J., Nakagawa I., Nakano K., Onishi H., Okada H., Okada K., Rykov V. L., Saito N., Sato H., Shibata T., Shoji K., Tabaru T., Taketani A., Tanida K., Togawa M., Tojo J., Torii H., Tsuchimoto Y., Wagner M. M., Watanabe Y., Xie W., and Yokkaichi S.: “Cold Nuclear Matter Effects on J/ψ Production as Constrained by Deuteron-Gold Measurements at $\sqrt{s_{NN}} = 200$ GeV”, *Phys. Rev. C* **77**, 024912-1–024912-15 (2008). *
- Adare A., Akiba Y., Aoki K., Asai J., Bunce G. M., Deshpande A., Enyo H., Fields D. E., Fujiwara K., Fukao Y., Goto Y., Gross P. M., Hachiya T., Hasuko K., Heuser J. M., Horaguchi T., Ichihara T., Imai K., Inoue Y., Ishihara M., Jinnouchi O., Kamihara N., Kaneta M., Kanoh H., Kawall D., Kiyomichi A., Kobayashi H., Kurita K., Mao Y., Murata J., Nakagawa I., Nakano K., Onishi H., Okada H., Okada K., Rykov V. L., Saito N., Sato H., Shibata T., Shoji K., Tabaru T., Taketani A., Tanida K., Togawa M., Tojo J., Torii H., Tsuchimoto Y., Wagner M. M., Watanabe Y., Xie W., and Yokkaichi S.: “Quantitative Constraints on the Transport Properties of Hot Partonic Matter from Semi-Inclusive Single High Transverse Momentum Pion Suppression in Au+Au Collisions at $\sqrt{s_{NN}} = 200$ GeV”, *Phys. Rev. C* **77**, 064907-1–064907-12 (2008). *
- Adare A., Akiba Y., Aoki K., Asai J., Bunce G. M., Deshpande A., Enyo H., Fields D. E., Fujiwara K., Fukao Y., Goto Y., Gross P. M., Hachiya T., Hasuko K., Heuser J. M., Horaguchi T., Ichihara T., Imai K., Inoue Y., Ishihara M., Jinnouchi O., Kamihara N., Kaneta M., Kanoh H., Kawall D., Kiyomichi A., Kurita K., Mao Y., Murata J., Nakagawa I., Nakano K., Onishi H., Okada H., Okada K., Rykov V. L., Saito N., Sato H., Shibata T., Shoji K., Tabaru T., Taketani A., Tanida K., Togawa M., Tojo J., Torii H., Tsuchimoto Y., Wagner M. M., Watanabe Y., Xie W., and Yokkaichi S.: “Dihadron azimuthal correlations in Au+Au collisions at $\sqrt{s_{NN}} = 200$ GeV”, *Phys. Rev. C* **78**, 014901-1–014901-42 (2008). *
- Adare A., Akiba Y., Aoki K., Asai J., Bazilevsky A. V., Bunce G. M., Deshpande A., Enyo H., Fields D. E., Fox B., Fujiwara K., Fukao Y., Goto Y., Gross P. M., Hachiya T., Hasuko K., Heuser J. M., Horaguchi T., Ichihara T., Imai K., Inoue Y., Ishihara M., Jinnouchi O., Kamihara N., Kaneta M., Kanoh H., Kawall D., Kiyomichi A., Kobayashi H., Kurita K., Mao Y., Murata J., Nakagawa I., Nakano K., Onishi H., Okada H., Okada K., Rykov V. L., Saito N., Sato H., Shibata T., Shoji K., Tabaru T., Taketani A., Tanida K., Togawa M., Tojo J., Torii H., Tsuchimoto Y., Wagner M. M., Watanabe Y., Xie W., and Yokkaichi S.: “Charged hadron multiplicity fluctuations in Au+Au and Cu+Cu collisions from $\sqrt{s_{NN}} = 22.5$ to 200 GeV”, *Phys. Rev. C* **78**, 044902-1–044902-15 (2008). *
- Afanasiev S., Akiba Y., Aoki K., Bunce G. M., Deshpande A., Enyo H., Fields D. E., Fukao Y., Goto Y., Gross P. M., Hachiya T., Hasuko K., Heuser J. M., Horaguchi T., Ichihara T., Imai K., Ishihara M., Jinnouchi O., Kamihara N., Kaneta M., Kiyomichi A., Kurita K., Murata J., Onishi H., Okada H., Okada K., Rykov V. L., Saito N., Sato H., Shibata T., Shoji K., Tabaru T., Taketani A., Tanida K., Togawa M., Tojo J., Torii H., Tsuchimoto Y., Wagner M. M., Watanabe Y., Xie W., and Yokkaichi S.: “Source breakup dynamics in Au+Au Collisions at $\sqrt{s_{NN}}=200$ GeV via three-dimensional two-pion source imaging”, *Phys. Rev. Lett.* **100**, 232301-1–232301-6 (2008). *
- Afanasiev S., Akiba Y., Aoki K., Bunce G. M., Deshpande

- A., Enyo H., Fields D. E., Fukao Y., Goto Y., Gross P. M., Hachiya T., Hasuko K., Heuser J. M., Horaguchi T., Ichihara T., Imai K., Ishihara M., Jinnouchi O., Kajihara F., Kamihara N., Kaneta M., Kiyomichi A., Kurita K., Murata J., Onishi H., Okada H., Okada K., Rykov V. L., Saito N., Sato H., Shibata T., Shoji K., Tabaru T., Taketani A., Tanida K., Togawa M., Tojo J., Torii H., Tsuchimoto Y., Wagner M. M., Watanabe Y., Xie W., and Yokkaichi S.: “Particle-species dependent modification of jet-induced correlations in Au+Au collisions at $\sqrt{s_{NN}} = 200$ GeV”, *Phys. Rev. Lett.* **101**, 082301-1–082301-6 (2008). *
- Adare A., Akiba Y., Aoki K., Asai J., Bunce G. M., Deshpande A., Enyo H., Fields D. E., Fujiwara K., Fukao Y., Goto Y., Gross P. M., Horaguchi T., Ichihara T., Imai K., Inoue Y., Ishihara M., Jinnouchi O., Kamihara N., Kaneta M., Kanoh H., Kawall D., Kiyomichi A., Kurita K., Mao Y., Murata J., Nakagawa I., Nakano K., Onishi H., Okada H., Okada K., Rykov V. L., Saito N., Shibata T., Shoji K., Tabaru T., Taketani A., Tanida K., Togawa M., Tojo J., Torii H., Wagner M. M., Watanabe Y., Xie W., and Yokkaichi S.: “ J/ψ Production in $\sqrt{s_{NN}} = 200$ GeV Cu+Cu Collisions”, *Phys. Rev. Lett.* **101**, 122301-1–122301-6 (2008). *
- Adare A., Akiba Y., Aoki K., Asai J., Bunce G. M., Dairaku S., Deshpande A., Enyo H., Fields D. E., Fujiwara K., Fukao Y., Goto Y., Gross P. M., Horaguchi T., Ichihara T., Ichimiya R., Imai K., Inoue Y., Ishihara M., Jinnouchi O., Kametani S., Kamihara N., Kaneta M., Kanoh H., Kawall D., Kiyomichi A., Kurita K., Kurosawa M., Li Z., Mao Y., Murata J., Nakagawa I., Nakano K., Onishi H., Okada H., Okada K., Onuki Y., Rykov V. L., Saito N., Sakashita K., Shibata T., Shoji K., Tabaru T., Taketani A., Tanida K., Togawa M., Tojo J., Torii H., Wagner M. M., Watanabe Y., Xie W., and Yokkaichi S.: “Onset of π^0 suppression studied in Cu+Cu collisions at $\sqrt{s_{NN}} = 22.4, 62.4,$ and 200 GeV”, *Phys. Rev. Lett.* **101**, 162301-1–162301-6 (2008). *
- Adare A., Akiba Y., Aoki K., Asai J., Bunce G. M., Deshpande A., Enyo H., Fields D. E., Fujiwara K., Fukao Y., Goto Y., Gross P. M., Hachiya T., Hasuko K., Heuser J. M., Horaguchi T., Ichihara T., Imai K., Inoue Y., Ishihara M., Jinnouchi O., Kajihara F., Kamihara N., Kaneta M., Kanoh H., Kawall D., Kiyomichi A., Kurita K., Mao Y., Murata J., Nakagawa I., Nakano K., Onishi H., Okada H., Okada K., Rykov V. L., Saito N., Sato H., Shibata T., Shoji K., Tabaru T., Taketani A., Tanida K., Togawa M., Tojo J., Torii H., Tsuchimoto Y., Wagner M. M., Watanabe Y., Xie W., and Yokkaichi S.: “Suppression pattern of neutral pions at high transverse momentum in Au+Au collisions at $\sqrt{s_{NN}} = 200$ GeV and constraints on medium transport coefficients”, *Phys. Rev. Lett.* **101**, 232301-1–232301-7 (2008). *
- Dang N. D. and Nguyen H. Q.: “Nuclear pairing at finite temperature and angular momentum”, *AIP Conf. Proc.* **1090**, 179–183 (2009). *
- Nakajima T., Matsuo Y., and Kobayashi T.: “First step toward ultrafast nuclear-spin polarization: All-optical control and direct detection of ultrafast electron-spin polarization using femtosecond laser pulses”, *AIP Conf. Proc.* **1149**, 876–879 (2009).
- Ichikawa Y., Onishi T., Suzuki D., Iwasaki H., Naik V., Kubo T., Chakrabarti A., Aoi N., Brown A., Fukuda N., Kubono S., Motobayashi T., Nakabayashi T., Nakao T., Okumura T., Ong H., Suzuki H., Suzuki M., Teranishi T., Yamada K., Yamaguchi H., and Sakurai H.: “Investigation into behavior of weakly-bound proton via $B(GT)$ measurement for the β decay of ^{24}Si ”, *AIP Conf. Proc.* **1165**, 98–101 (2009).
- Kobayashi T., Matsuo Y., Nishimura M., Hayashizaki Y., and Kawai J.: “Hydrogenation of carbon fragments after femtosecond laser ablation of solid C_{60} ”, *Appl. Surf. Sci.* **255**, 9652–9654 (2009). *
- Nishimura M., Kobayashi T., Matsuo Y., Motobayashi T., Hayashizaki Y., and Kawai J.: “Dynamics of Ablation Plasma induced by a Femtosecond Laser Pulse in Electric Fields”, *Appl. Surf. Sci.* **255**, 9729–9733 (2009). *
- Ichikawa Y., Kubo T., Aoi N., Naik V., Chakrabarti A., Fukuda N., Iwasaki H., Kubono S., Motobayashi T., Nakabayashi T., Nakao T., Okumura T., Ong H., Onishi T., Suzuki D., Suzuki H., Suzuki M., Teranishi T., Yamada K., Yamaguchi H., and Sakurai H.: “Beta-decay study of $T_z = -2$ proton-rich nucleus ^{24}Si ”, *Eur. Phys. J. A* **42**, 375–378 (2009). *
- Adare A., Akiba Y., Aoki K., Asai J., Bunce G. M., Deshpande A., Enyo H., Fields D. E., Fujiwara K., Fukao Y., Goto Y., Gross P. M., Horaguchi T., Ichihara T., Imai K., Inoue Y., Ishihara M., Jinnouchi O., Kamihara N., Kaneta M., Kanoh H., Kawall D., Kiyomichi A., Kurita K., Mao Y., Murata J., Nakagawa I., Nakano K., Onishi H., Okada H., Okada K., Rykov V. L., Saito N., Shibata T., Shoji K., Tabaru T., Taketani A., Tanida K., Togawa M., Tojo J., Torii H., Wagner M. M., Watanabe Y., Xie W., and Yokkaichi S.: “Dilepton mass spectra in p+p collisions at $\sqrt{s} = 200$ GeV and the contribution from open charm”, *Phys. Lett. B* **670**, 313–320 (2009). *
- De Rydt M., Neyens G., Asahi K., Balabanski D. L., Daugas J., Depuydt M., Gaudefroy L., Grevy S., Hasama Y., Ichikawa Y., Morel P., Nagatomo T., Ohtsuka T., Perrot L., Shimada K., Stoenel C., Thomas J., Ueno H., Utsuno Y., Wannes V., Vermeulen N., Vingerhoets P., and Yoshimi A.: “Precision measurement of the electric quadrupole moment of ^{31}Al and determination of the effective proton charge in the sd-shell”, *Phys. Lett. B* **678**, 344–349 (2009). *
- Takeuchi S., Aoi N., Motobayashi T., Ota S., Takeshita E., Suzuki H., Baba H., Fukui T., Hashimoto Y., Ieki K., Imai N., Iwasaki H., Kanno S., Kondo Y., Kubo T.,

- Kurita K., Minemura T., Nakamura T., Okumura T., Onishi T., Sakurai H., Shimoura S., Sugou R., Suzuki D., Suzuki M., Takashina M., Tamaki M., Tanaka K., Togano Y., and Yamada K.: “Low-Iying States in ^{32}Mg studied by proton inelastic scattering”, *Phys. Rev. C* **79**, No. 5, pp. 054319-1–054319-11 (2009). *
- Nguyen H. Q. and Dang N. D.: “Exact and Approximate Ensemble Treatments of Thermal Pairing in a Multilevel Model”, *Phys. Rev. C* **79**, No. 5, pp. 054328-1–054328-10 (2009). *
- Ichikawa Y., Onishi T., Suzuki D., Iwasaki H., Naik V., Kubo T., Chakrabarti A., Aoi N., Brown A., Fukuda N., Kubono S., Motobayashi T., Nakabayashi T., Nakao T., Okumura T., Ong H., Suzuki H., Suzuki M., Teranishi T., Yamada K., Yamaguchi H., and Sakurai H.: “Beta decay of the proton-rich nucleus ^{24}Si and its mirror asymmetry”, *Phys. Rev. C* **80**, 044302-1–044302-12 (2009). *
- Adare A., Akiba Y., Aoki K., Asai J., Bunce G. M., Dairaku S., Deshpande A., Enyo H., Fields D. E., Fujiwara K., Fukao Y., Goto Y., Gross P. M., Horaguchi T., Ichihara T., Ichimiya R., Imai K., Ishihara M., Kametani S., Kamihara N., Kawall D., Kurita K., Kurosawa M., Li Z., Mao Y., Murata J., Nakagawa I., Nakano K., Okada H., Okada K., Onuki Y., Rykov V. L., Saito N., Sakashita K., Shibata T., Shoji K., Taketani A., Tanida K., Togawa M., Torii H., Watanabe Y., Xie W., and Yokkaichi S.: “Inclusive cross section and double helicity asymmetry for π^0 production in $p + p$ collisions at $\sqrt{s} = 62.4$ GeV”, *Phys. Rev. D* **79**, 012003-1–012003-11 (2009). *
- (Others)
- Murata J., Akiyama T., Hata M., Hirayama Y., Ikeda Y., Ishii T., Kameda D., Kawamura H., Mitsuoka S., Miyatake H., Nagae D., Ninomiya K., Nitta M., Seitabashi E., and Toyoda T.: “Test of time reversal symmetry using polarized nuclei”, *JAEA-Review* **2009-036**, 62–63 (2009).
- Book • Proceedings**
- (Others)
- Fukunishi N., Fujimaki M., Watanabe T., Kumagai K., Komiyama M., Watanabe H., Goto A., Hasebe H., Higurashi Y., Ikezawa E., Kageyama T., Kamigaito O., Kase M., Kuboki H., Kidera M., Nagase M., Maie T., Nakagawa T., Ohnishi J., Okuno H., Sakamoto N., Sekiguchi K., Suda K., Suzuki H., Wakasugi M., Watanabe Y., Yokouchi S., Yano Y., and Yamada K.: “Operating experience with the RIKEN Radioactive Isotope Beam Factory”, *Proceedings of the 2009 Particle Accelerator Conference (PAC09)*, Vancouver, Canada, 2009–5, PAC09 Editor, Vancouver, pp. MO3GRI0-1–MO3GRI0-5 (2009).
- Takeuchi S.: “Detector array for low intensity radiation”, *CNS-RIKEN Joint Symposium on Frontier of Gamma-Ray Spectroscopy and Its Application*, Wako, Mar. (2004).
- Takeuchi S., Shimoura S., Motobayashi T., Akiyoshi H., Ando Y., Aoi N., Fulop Z., Gomi T., Higurashi Y., Hirai M., Iwasa N., Iwasaki H., Iwata Y., Kobayashi H., Kurokawa M., Liu Z., Minemura T., Ozawa S., Sakurai H., Serata M., Teranishi T., Yamada K., Yanagisawa Y., and Ishihara M.: “Isobaric analog state of ^{14}Be ”, *RIKEN-CNS RIBF International Workshop “Correlation and Condensation: New Features in Loosely Bound and Unbound Nuclear States”*, Wako, Dec. (2005).
- Ohnishi T., Kubo T., Kusaka K., Yoshida A., Yoshida K., Fukuda N., Yanagisawa Y., Ohtake M., Takeda H., and Kameda D.: “BigRIPS Commissioning Experiment”, *Third experts meeting on critical issues of next-generation high-intensity In-flight separators*, (National Superconducting Cyclotron Laboratory, Michigan State University), East Lansing, USA, Mar.–Apr. (2008).
- Fukunishi N., Fujimaki M., Watanabe T., Kumagai K., Komiyama M., Watanabe H., Goto A., Hasebe H., Higurashi Y., Ikezawa E., Kageyama T., Kamigaito O., Kase M., Kuboki H., Kidera M., Nagase M., Maie T., Nakagawa T., Ohnishi J., Okuno H., Sakamoto N., Sekiguchi K., Suda K., Suzuki H., Wakasugi M., Watanabe Y., Yokouchi S., Yano Y., and Yamada K.: “Operating experience with the RIKEN Radioactive Isotope Beam Factory”, *23rd Particle Accelerator Conference (PAC09)*, Vancouver, Canada, May (2009).
- Ichikawa Y., Onishi T., Suzuki D., Iwasaki H., Naik V., Kubo T., Chakrabarti A., Aoi N., Brown A., Fukuda N., Kubono S., Motobayashi T., Nakabayashi T., Nakao T., Okumura T., Ong H., Suzuki H., Suzuki M., Teranishi T., Yamada K., Yamaguchi H., and Sakurai H.: “Investigation into behavior of weakly-bound proton via $B(\text{GT})$ measurement for the β decay of ^{24}Si ”, *International Conference on Nuclear Structure and Dynamics (NSD09)*, (University of Zagreb), Dubrovnik, Croatia, May (2009).
- Furukawa T., Hatakeyama A., Fujikake K., Matsuura Y., Kobayashi T., Shimoda T., and Matsuo Y.: “Precision Laser Spectroscopy of Alkaline and Alkaline-like Atoms in Superfluid Helium”, *19th International Conference on Laser Spectroscopy (ICOLS2009)*, Kussharo, June (2009).
- Matsuo Y.: “Novel nuclear laser spectroscopy of RI atoms in superfluid helium: OROCHI”, *Advanced Studies Institute: Symmetries and Spin (SPIN-Praha-2009)*, Praha, Czech, July–Aug. (2009).
- Ichikawa Y., Onishi T., Suzuki D., Iwasaki H., Naik V., Kubo T., Chakrabarti A., Aoi N., Brown A., Fukuda N., Kubono S., Motobayashi T., Nakabayashi T., Nakao T., Okumura T., Ong H., Suzuki H., Suzuki M., Teranishi T., Yamada K., Yamaguchi H., and Sakurai H.: “Beta

Oral Presentations

(International Conference etc.)

- decay of ^{24}Si and mirror asymmetry of Gamow-Teller transition strength”, 3rd Joint Meeting of the Nuclear Physics Divisions of the APS and JPS (Hawaii 2009), Hawaii, USA, Oct. (2009).
- Sasaki A., Wakui T., Furukawa T., Kazato M., Wada M., Sonoda T., Takamine A., Kobayashi T., Nishimura M., Ueno H., Yoshimi A., Aoi N., Nishimura S., Togano Y., Takechi M., Kondo Y., Hatakeyama A., Matsuura Y., Kato Y., Odahara A., Shimoda T., Asahi K., Shinozuka T., Motobayashi T., and Matsuo Y.: “Fluorescence detection system for nuclear laser spectroscopy of Rb in superfluid helium”, 3rd Joint Meeting of the Nuclear Physics Divisions of the APS and JPS (Hawaii 2009), Hawaii, USA, Oct. (2009).
- Ichikawa Y., Onishi T., Suzuki D., Iwasaki H., Naik V., Kubo T., Chakrabarti A., Aoi N., Brown A., Fukuda N., Kubono S., Motobayashi T., Nakabayashi T., Nakao T., Okumura T., Ong H., Suzuki H., Suzuki M., Teranishi T., Yamada K., Yamaguchi H., and Sakurai H.: “Gamow-Teller transition of proton-rich nucleus ^{24}Si ”, 7th Japan-China Joint Nuclear Physics Symposium, (University of Tsukuba), Tsukuba, Nov. (2009).
- Ichikawa Y., Onishi T., Suzuki D., Iwasaki H., Naik V., Kubo T., Chakrabarti A., Aoi N., Brown A., Fukuda N., Kubono S., Motobayashi T., Nakabayashi T., Nakao T., Okumura T., Ong H., Suzuki H., Suzuki M., Teranishi T., Yamada K., Yamaguchi H., and Sakurai H.: “Mirror asymmetry for $B(\text{GT})$ of ^{24}Si induced by Thomas-Ehrman shift”, Tours Symposium on Nuclear Physics and Astrophysics VII (TOURS 2009), (Konan University), Kobe, Nov. (2009).
- Taniguchi Y., Kimura M., Enyo Y., Ikeda K., Horiuchi H., and Ideguchi E.: “Triaxial superdeformation in ^{40}Ar ”, JUSTIPEN-EFES Workshop on Unstable Nuclei, Wako, Dec. (2009).
- Dang N. D.: “The Selfconsistent Quasiparticle RPA and Its Description of Thermal Pairing Properties in Nuclei”, Multidisciplinary Workshop on the Random Phase Approximation and extensions, (Universite Pierre et Marie Curie (Jussieu campus)), Paris, France, Jan. (2010).
- Ichikawa Y., Onisi T. K., Suzuki D., Iwasaki H., Kubo T., Naik V., Chakrabarti A., Aoi N., Brown A. B., Fukuda N., Kubono S., Motobayashi T., Nakabayashi T., Nakamura T., Nakao T., Okumura T., Ong H., Suzuki H., Suzuki M. K., Teranishi T., Yamaguchi H., and Sakurai H.: “Proton-rich nuclear structure investigated by β decay of ^{24}Si ”, ICHOR-EFES International Symposium on New Facet of Spin-Isospin Responses (SIR2010), (University of Tokyo), Tokyo, Feb. (2010).
- Ichikawa Y., Onisi T. K., Suzuki D., Iwasaki H., Kubo T., Naik V., Chakrabarti A., Aoi N., Brown A. B., Fukuda N., Kubono S., Motobayashi T., Nakabayashi T., Nakamura T., Nakao T., Okumura T., Ong H., Suzuki H., Suzuki M. K., Teranishi T., Yamaguchi H., and Sakurai H.: “Mirror asymmetry investigated by β decay of proton-rich ^{24}Si ”, International Symposium on Frontiers of Researches in Exotic Nuclear Structures (Niigata2010), (Niigata University), Toka-machi, Niigata Pref., Mar. (2010).
- (Domestic Conference)
- 岡田信二, Beer G. A., 方享燦, Cargnelli M., 千葉順成, Choi S., Curceanu C. O., 福田芳之, 花木俊生, 早野龍五, 飯尾雅美, 石川隆, 石元茂, 石渡智一, 板橋健太, 岩井正明, 岩崎雅彦, Juhasz B., Kienle P., Marton J., 松田恭幸, 大西宏明, 應田治彦, Schmid P., 佐藤将春, 鈴木祥仁, 鈴木隆敏, 竜野秀行, 友野大, Widmann E., 山崎敏光, 林熙重, Zmeskal J.: 理研ワークショップ「放射線検出器と電子回路の課題と展望-光子検出器を中心に」, 和光市, 5月(2005).
- 岡田信二, Beer G. A., 方享燦, Cargnelli M., 千葉順成, Choi S., Curceanu C. O., 福田芳之, 花木俊生, 早野龍五, 飯尾雅美, 石川隆, 石元茂, 石渡智一, 板橋健太, 岩井正明, 岩崎雅彦, Juhasz B., Kienle P., Marton J., 松田恭幸, 大西宏明, 應田治彦, Schmid P., 佐藤将春, 鈴木祥仁, 鈴木隆敏, 竜野秀行, 友野大, Widmann E., 山崎敏光, 林熙重, Zmeskal J.: “K 中間子ヘリウム4 原子 $3d \rightarrow 2p$ X 線の精密測定”, 日本物理学会第 61 回年次大会, 松山, 3月(2006).
- 飯尾雅美, 板橋健太, 岩崎雅彦, 應田治彦, 大西宏明, 岡田信二, 鈴木隆敏, 友野大, 松田恭幸, 山崎敏光, 石川隆, 竜野秀行, 早野龍五, 石元茂, 鈴木祥一, 佐藤将春, 福田芳之, 千葉順成, 花木俊生, 方享燦, Choi S., 林熙重, 石渡智一, Cargnelli M., Juhasz B., Kienle P., Marton J., Widmann E., Zmeskal J., Schmid P., Beer G. A., Curceanu C. O.: “K 中間子ヘリウム原子 X 線測定実験のための検出器系 I”, 日本物理学会第 61 回年次大会, 松山, 3月(2006).
- 岡田信二, Beer G. A., 方享燦, Buehler P., Cargnelli M., 千葉順成, Choi S., Curceanu C. O., 福田芳之, Guaraldo C., 花木俊生, 早野龍五, Hirtl A., 飯尾雅美, Iliescu M., 石川隆, 石元茂, 石渡智一, 板橋健太, 岩井正明, 岩崎雅彦, Kienle P., Marton J., 松田恭幸, 大西宏明, 應田治彦, Pietreanu D., Sirghi D., Sirghi F., 佐藤将春, 鈴木隆敏, 竜野秀行, 友野大, Widmann E., 山崎敏光, 林熙重, Zmeskal J.: “Precision spectroscopy of Kaonic Helium-3 $3d \rightarrow 2p$ X-rays (J-PARC E17 実験)”, 文科省科研費補助金特定領域研究「ストレンジネスで探るクォーク多体系」研究会 2006, 熱海, 12月(2006).
- 飯尾雅美, 板橋健太, 岩崎雅彦, 應田治彦, 大西宏明, 岡田信二, 佐久間史典, 鈴木隆敏, 友野大, 松田恭幸, 山崎敏光, 石元茂, 鈴木祥一, 関本美知子, 豊田晃久, 永江知文, 石川隆, 竜野秀行, 早野龍五, 藤岡宏之, 味村周平, 阪口篤志, 佐藤将春, 福田芳之, 千葉順成, 花木俊生, 福田共和, 溝井浩, Beer G. A., 方享燦, Choi S., 林熙重, 石渡智一, Buehler P., Hirtl A., Cargnelli M., Kienle P., Marton J., Widmann E., Zmeskal J., Curceanu C. O., Guaraldo C., Iliescu M., Pietreanu D., Sirghi D., Sirghi F., Faso D., Busso L., Morra O.: “K 中間子原子核探索実験のための液体ヘリウム 3 標的の開発”, 日本物理学会 2007 年春季大会, 八王子, 3月(2007).
- 岡田信二, Beer G. A., 方享燦, Cargnelli M., 千葉順成, Choi S., Curceanu C. O., 福田芳之, 花木俊生, 早野龍五, 飯尾雅美, 石川隆, 石元茂, 石渡智一, 板橋健太, 岩井正明, 岩崎

- 雅彦, Juhasz B., Kienle P., Marton J., 松田恭幸, 大西宏明, 應田治彦, Schmid P., 佐藤将春, 鈴木祥仁, 鈴木隆敏, 竜野秀行, 友野大, Widmann E., 山崎敏光, 林熙重, Zmeskal J.: 日本物理学会第 62 回年次大会, 札幌, 9 月 (2007).
- 岡田信二, Beer G. A., 方亨燦, Buehler P., Cargnelli M., 千葉順成, Choi S., Curceanu C. O., 福田芳之, Guaraldo C., 花木俊生, 早野龍五, Hirtl A., 飯尾雅美, Iliescu M., 石川隆, 石元茂, 石渡智一, 板橋健太, 岩井正明, 岩崎雅彦, Kienle P., Marton J., 松田恭幸, 大西宏明, 應田治彦, Pietreanu D., Sirghi D., Sirghi F., 佐藤将春, 鈴木隆敏, 竜野秀行, 友野大, Widmann E., 山崎敏光, 林熙重, Zmeskal J.: “J-PARC における K 中間子ヘリウム 3 原子 X 線分光実験 J-PARC E17 の現状”, 文部科学省科学研究費補助金特定領域研究特定領域研究「ストレンジネスで探るクォーク多体系」第 3 回総括班主催研究会 (2007), 仙台, 11 月 (2007).
- 飯尾雅美, 板橋健太, 岩崎雅彦, 應田治彦, 大西宏明, 佐久間史典, 佐藤将春, 塚田暁, 友野大, 藤岡宏之, 山崎敏光, 石元茂, 岩井正明, 鈴木祥二, 関本美知子, 豊田晃久, 石川隆, 竜野秀行, 鈴木隆敏, 早野龍五, 松田恭幸, 永江知文, 平岩聡彦, 味村周平, 野海博之, 阪口篤志, 藤原裕也, 徳田真, 千葉順成, 福田共和, 溝井浩, Beer G. A., 方亨燦, Choi S., 林熙重, 石渡智一, Buehler P., Cargnelli M., Hirtl A., Kienle P., Marton J., Widmann E., Zmeskal J., 岡田信二, Curceanu C. O., Guaraldo C., Iliescu M., Pietreanu D., Sirghi D., Sirghi F., Faso D., Morra O., Busso L.: “K 中間子原子核探索実験のための液体ヘリウム 3 標的の開発 III”, 日本物理学会 2008 年秋季大会, 山形, 9 月 (2008).
- 小林徹, 松尾由賀利, 西村美月, 林崎良英, 河合純: “Chemical Reaction at Laser Ablation ; Nanosecond vs. Femtosecond”, 第 8 回エクストリーム研究会 (分子研・理研共催), 蒲郡, 11 月 (2008).
- 安藤 吉成, 西村 美月, 小林 徹, 松尾 由賀利, 外丸 靖浩, Lassmann T., 河合純, 林崎良英: “Application of fs-TOF MS for analyzing DICER function”, 第 31 回日本分子生物学会年会・第 81 回日本生化学会大会合同大会 (BMB2008), 神戸, 12 月 (2008).
- 胡子昇一郎, 酒向正己, 村上哲也, 新田稔, 池田友樹, 中谷祐輔, 川村広和, 豊田健司, 村田次郎, 家城和夫, 中井陽一, 西村俊二, 高田栄一: “中間エネルギー重イオン衝突における荷電パイオン生成 (I)”, 日本物理学会第 64 回年次大会, 東京, 3 月 (2009).
- 酒向正己, 胡子昇一郎, 村上哲也, 新田稔, 池田友樹, 中谷祐輔, 川村広和, 豊田健司, 村田次郎, 家城和夫, 中井陽一, 西村俊二, 高田栄一: “中間エネルギー重イオン衝突における荷電パイオン生成 (II)”, 日本物理学会第 64 回年次大会, 東京, 3 月 (2009).
- 西村美月, 松尾由賀利, 小林徹, 本林透, 林崎良英, 河合純: “電場中におけるフェムト秒レーザーアブレーションプラズマの P-LIF 観測”, 第 56 回応用物理学関係連合講演会, つくば, 3-4 月 (2009).
- 西村美月, 小林徹, 松尾由賀利, 安藤吉成, 林崎良英, 河合純: “フェムト秒レーザーアブレーションによる分子の原子イオン化の利用”, 理研シンポジウム「エクストリームフォトニクスシンポジウム: 光で繋ぐ理研の基礎科学」, 和光, 5 月 (2009).
- 小林徹, 松尾由賀利: “Hydrogenation reaction of the carbon fragments produced by laser ablation of solid C60”, 第 25 回化学反応討論会, (化学反応討論会), さいたま, 6 月 (2009).
- 古川武, 崑山温, 藤掛浩太郎, 松浦佑一, 小林徹, 下田正, 松尾由賀利: “超流動ヘリウム中に植え込まれたアルカリおよびアルカリ様原子の精密レーザー分光と光ポンピング”, 第 6 回 AMO 討論会, 豊中, 6 月 (2009).
- 長友傑, 小林義男, 久保謙哉, 山田康洋, 三原基嗣, 佐藤渉, 宮崎淳, 佐藤真二, 北川敦志: “プラスチックシンチレーション検出器を用いた ^{57}Mn インビームメスバウアー分光における S/N 比の向上”, 2009 日本放射化学学会年会・第 53 回放射化学討論会, (日本放射化学学会), 東京, 9 月 (2009).
- 長友傑, 小林義男, 久保謙哉, 山田康洋, 三原基嗣, 佐藤渉, 宮崎淳, 佐藤真二, 北川敦志: “酸化アルミニウム固体中の ^{57}Mn インビーム・メスバウアー分光実験”, 2009 日本放射化学学会年会・第 53 回放射化学討論会, (日本放射化学学会), 東京, 9 月 (2009).
- 長友傑, 小林義男, 久保謙哉, 山田康洋, 三原基嗣, 佐藤渉, 宮崎淳, 佐藤真二, 北川敦志: “酸化マグネシウム固体中の ^{57}Mn インビーム・メスバウアー分光実験”, 2009 日本放射化学学会年会・第 53 回放射化学討論会, (日本放射化学学会), 東京, 9 月 (2009).
- 松浦佑一, 古川武, 藤掛浩太郎, 崑山温, 小林徹, 立川真樹, 松尾由賀利: “超流動ヘリウム中での光ポンピング法を用いた Au 原子の偏極生成”, 日本物理学会 2009 年秋季大会, 熊本, 9 月 (2009).
- 小林徹, 松尾由賀利: “フェムト秒レーザーアブレーションによる負イオン生成”, 第 10 回エクストリーム・フォトニクス研究会「凝縮系における量子の世界」, 蒲郡, 11 月 (2009).
- 長友傑, 小林義男, 三原基嗣, 久保謙哉, 山田康洋, 佐藤渉, 宮崎淳, 佐藤真二, 北川敦志: “プラスチック検出器を用いた ^{57}Mn インビームメスバウアー分光の S/N 比の向上”, 平成 21 年度京都大学原子炉実験所専門研究会「短寿命核および放射線を用いた物性研究 (II)」研究会, 大阪府熊取町, 12 月 (2009).
- 西村美月, 安藤吉成, 小林徹, 松尾由賀利, 鈴木治和, 林崎良英, 河合純: “フェムト秒レーザーアブレーション飛行時間型質量分析法と安定同位体元素標識を組み合わせた small RNA の配列解析法”, 第 57 回応用物理学関係連合講演会, 平塚, 3 月 (2010).
- 松浦佑一, 古川武, 小林徹, 崑山温, 加藤裕樹, 立川真樹, 松尾由賀利: “Au 原子の光ポンピングに向けた紫外領域光源開発”, 日本物理学会第 65 回年次大会, 岡山, 3 月 (2010).
- 川村広和, 秋山岳伸, 秦麻記, 平山賀一, 池田友樹, 石井哲朗, 亀田大輔, 光岡慎一, 宮原直亮, 宮武宇也, 村田次郎, 中谷祐輔, 長江大輔, 二宮一史, 新田稔, 大西潤一, 聖代橋悦子, 豊田健司, 塚田和司, 渡辺裕: “KEK-TRIAC における偏極 ^8Li を用いた時間反転対称性の研究”, 日本物理学会第 65 回年次大会, 岡山, 3 月 (2010).
- 鳥養映子, 松尾由賀利, 有光直子, 中島美帆, 松島房和, 笹尾真実子, 前田京剛, 柴田純, 中野公世, 高橋春美, 興治文子, 石井恭子: “女子中高生夏の学校における物理学会の活動”,

日本物理学会第 65 回年次大会, 岡山, 3 月 (2010).

川村広和, 秋山岳伸, Behr J. A., 秦麻記, 平山賀一; 池田友樹, 石井哲朗, 亀田大輔, Levy P., 宮原直亮, 宮武宇也, 光岡真一; 村田次郎, 長江大輔, 中谷祐輔, 二宮一史, 新田稔, 小川就也, 大西潤一; Pearson M., 聖代橋悦子, 豊田健司, 塚田和司, 渡辺裕: “偏極 ^8Li のベータ崩壊における時間反転対称性の破れの探索”, 第 6 回停止・低速不安定核ビームを用いた核分光研究会, 東京, 3 月 (2010).

長友傑, 小林義男, 久保謙哉, 山田康洋, 三原基嗣, 佐藤渉, 宮崎淳, 佐藤真一, 北川敦志: “不安定核 ^{57}Mn ビームを用いたインビーム・メスバウアー分光の現状”, 第 11 回メスバウアー分光研究会シンポジウム, 豊中, 3 月 (2010).

Radioactive Isotope Physics Laboratory

Publications

Journal

(Original Papers) *Subject to Peer Review

- Nagae D., Asahi K., Ueno H., Kameda D., Takemura M., Takase T., Yoshimi A., Sugimoto T., Nagatomo T., Kobayashi Y., Uchida M., Shimada K., Arai T., Inoue T., Kagami S., and Hatakeyama N.: "Measurement of Electric Quadrupole Moments for ^{31}Al Using Spin Polarized RI Beams", AIP Conf. Proc. **915**, 853–856 (2007). *
- Shimada K., Nagae D., Asahi K., Arai T., Takemura M., Inoue T., Takase T., Kagami S., Hatakeyama N., Kobayashi Y., Ueno H., Yoshimi A., Kameda D., Nagatomo T., Sugimoto T., Kubono S., Yamaguchi H., Wakabayashi Y., Amadio G., Hayakawa S., Murata J., and Kawamura H.: "Production of Polarized Radioactive Beams via The Inverse-kinematics Reactions and Their Applications", AIP Conf. Proc. **915**, 857–860 (2007). *
- Ohnishi T., Kubo T., Kusaka K., Yoshida A., Yoshida K., Fukuda N., Ohtake M., Yanagisawa Y., Takeda H., Kameda D., Yamaguchi Y., Aoi N., Yoneda K., Otsu H., Takeuchi S., Sugimoto T., Kondo Y., Scheit H., Gono Y., Sakurai H., Motobayashi T., Suzuki H., Nakao T., Kimura H., Mizoi Y., Matsushita M., Ieki K., Kuboki T., Yamaguchi T., Suzuki T., Ozawa A., Moriguchi T., Yasuda Y., Nakamura T., Nannichi T., Shimamura T., Nakayama Y., Geissel H., Weick H., Nolen J. A., Tarasov O. B., Nettleton A. S., Bazin D. P., Sherrill B. M., Morrissey D. J., and Mittig W.: "Identification of New Isotopes ^{125}Pd and ^{126}Pd Produced by In-Flight Fission of $345\text{ MeV/nucleon }^{238}\text{U}$: First Results from the RIKEN RI Beam Factory", J. Phys. Soc. Jpn. **77**, No. 8, pp. 083201-1–083201-4 (2008). *
- Adare A., Akiba Y., Aoki K., Asai J., Bazilevsky A. V., Bunce G. M., Deshpande A., Enyo H., Fields D. E., Fox B., Fujiwara K., Fukao Y., Goto Y., Gross P. M., Hasuko K., Heuser J. M., Horaguchi T., Ichihara T., Imai K., Inoue Y., Ishihara M., Jinnouchi O., Kamihara N., Kaneta M., Kanoh H., Kawall D., Kiyomichi A., Kobayashi H., Kurita K., Mao Y., Murata J., Nakagawa I., Nakano K., Onishi H., Okada H., Okada K., Rykov V. L., Saito N., Sato H., Shibata T., Shoji K., Tabaru T., Taketani A., Tanida K., Togawa M., Tojo J., Torii H., Tsuchimoto Y., Wagner M. M., Watanabe Y., Xie W., and Yokkaichi S.: "Cold Nuclear Matter Effects on J/ψ Production as Constrained by Deuteron-Gold Measurements at $\sqrt{s_{NN}} = 200\text{ GeV}$ ", Phys. Rev. C **77**, 024912-1–024912-15 (2008). *
- Adare A., Akiba Y., Aoki K., Asai J., Bunce G. M., Deshpande A., Enyo H., Fields D. E., Fujiwara K., Fukao Y., Goto Y., Gross P. M., Hachiya T., Hasuko K., Heuser J. M., Horaguchi T., Ichihara T., Imai K., Inoue Y., Ishihara M., Jinnouchi O., Kamihara N., Kaneta M., Kanoh H., Kawall D., Kiyomichi A., Kobayashi H., Kurita K., Mao Y., Murata J., Nakagawa I., Nakano K., Onishi H., Okada H., Okada K., Rykov V. L., Saito N., Sato H., Shibata T., Shoji K., Tabaru T., Taketani A., Tanida K., Togawa M., Tojo J., Torii H., Tsuchimoto Y., Wagner M. M., Watanabe Y., Xie W., and Yokkaichi S.: "Quantitative Constraints on the Transport Properties of Hot Partonic Matter from Semi-Inclusive Single High Transverse Momentum Pion Suppression in Au+Au Collisions at $\sqrt{s_{NN}} = 200\text{ GeV}$ ", Phys. Rev. C **77**, 064907-1–064907-12 (2008). *
- Adare A., Akiba Y., Aoki K., Asai J., Bunce G. M., Deshpande A., Enyo H., Fields D. E., Fujiwara K., Fukao Y., Goto Y., Gross P. M., Hachiya T., Hasuko K., Heuser J. M., Horaguchi T., Ichihara T., Imai K., Inoue Y., Ishihara M., Jinnouchi O., Kamihara N., Kaneta M., Kanoh H., Kawall D., Kiyomichi A., Kurita K., Mao Y., Murata J., Nakagawa I., Nakano K., Onishi H., Okada H., Okada K., Rykov V. L., Saito N., Sato H., Shibata T., Shoji K., Tabaru T., Taketani A., Tanida K., Togawa M., Tojo J., Torii H., Tsuchimoto Y., Wagner M. M., Watanabe Y., Xie W., and Yokkaichi S.: "Dihadron azimuthal correlations in Au+Au collisions at $\sqrt{s_{NN}} = 200\text{ GeV}$ ", Phys. Rev. C **78**, 014901-1–014901-42 (2008). *
- Adare A., Akiba Y., Aoki K., Asai J., Bazilevsky A. V., Bunce G. M., Deshpande A., Enyo H., Fields D. E., Fox B., Fujiwara K., Fukao Y., Goto Y., Gross P. M., Hachiya T., Hasuko K., Heuser J. M., Horaguchi T., Ichihara T., Imai K., Inoue Y., Ishihara M., Jinnouchi O., Kamihara N., Kaneta M., Kanoh H., Kawall D., Kiyomichi A., Kobayashi H., Kurita K., Mao Y., Murata J., Nakagawa I., Nakano K., Onishi H., Okada H., Okada K., Rykov V. L., Saito N., Sato H., Shibata T., Shoji K., Tabaru T., Taketani A., Tanida K., Togawa M., Tojo J., Torii H., Tsuchimoto Y., Wagner M. M., Watanabe Y., Xie W., and Yokkaichi S.: "Charged hadron multiplicity fluctuations in Au+Au and Cu+Cu collisions from $\sqrt{s_{NN}} = 22.5\text{ to }200\text{ GeV}$ ", Phys. Rev. C **78**, 044902-1–044902-15 (2008). *
- Afanasiev S., Akiba Y., Aoki K., Bunce G. M., Deshpande A., Enyo H., Fields D. E., Fukao Y., Goto Y., Gross P. M., Hachiya T., Hasuko K., Heuser J. M., Horaguchi T., Ichihara T., Imai K., Ishihara M., Jinnouchi O., Kajihara F., Kamihara N., Kaneta M., Kiyomichi A., Kurita K., Murata J., Onishi H., Okada H., Okada K., Rykov V. L., Saito N., Sato H., Shibata T., Shoji K., Tabaru T., Taketani A., Tanida K., Togawa M., Tojo J., Torii H., Tsuchimoto Y., Wagner M. M., Watanabe Y., Xie W., and Yokkaichi S.: "Source breakup dynamics in Au+Au Collisions at $\sqrt{s_{NN}}=200\text{ GeV}$ via three-dimensional two-pion source imaging", Phys. Rev. Lett. **100**, 232301-1–232301-6 (2008). *
- Afanasiev S., Akiba Y., Aoki K., Bunce G. M., Deshpande

- A., Enyo H., Fields D. E., Fukao Y., Goto Y., Gross P. M., Hachiya T., Hasuko K., Heuser J. M., Horaguchi T., Ichihara T., Imai K., Ishihara M., Jinnouchi O., Kajihara F., Kamihara N., Kaneta M., Kiyomichi A., Kurita K., Murata J., Onishi H., Okada H., Okada K., Rykov V. L., Saito N., Sato H., Shibata T., Shoji K., Tabaru T., Taketani A., Tanida K., Togawa M., Tojo J., Torii H., Tsuchimoto Y., Wagner M. M., Watanabe Y., Xie W., and Yokkaichi S.: “Particle-species dependent modification of jet-induced correlations in Au+Au collisions at $\sqrt{s_{NN}} = 200$ GeV”, *Phys. Rev. Lett.* **101**, 082301-1–082301-6 (2008). *
- Adare A., Akiba Y., Aoki K., Asai J., Bunce G. M., Deshpande A., Enyo H., Fields D. E., Fujiwara K., Fukao Y., Goto Y., Gross P. M., Horaguchi T., Ichihara T., Imai K., Inoue Y., Ishihara M., Jinnouchi O., Kamihara N., Kaneta M., Kanoh H., Kawall D., Kiyomichi A., Kurita K., Mao Y., Murata J., Nakagawa I., Nakano K., Onishi H., Okada H., Okada K., Rykov V. L., Saito N., Shibata T., Shoji K., Tabaru T., Taketani A., Tanida K., Togawa M., Tojo J., Torii H., Wagner M. M., Watanabe Y., Xie W., and Yokkaichi S.: “ J/ψ Production in $\sqrt{s_{NN}} = 200$ GeV Cu+Cu Collisions”, *Phys. Rev. Lett.* **101**, 122301-1–122301-6 (2008). *
- Adare A., Akiba Y., Aoki K., Asai J., Bunce G. M., Dairaku S., Deshpande A., Enyo H., Fields D. E., Fujiwara K., Fukao Y., Goto Y., Gross P. M., Horaguchi T., Ichihara T., Ichimiya R., Imai K., Inoue Y., Ishihara M., Jinnouchi O., Kametani S., Kamihara N., Kaneta M., Kanoh H., Kawall D., Kiyomichi A., Kurita K., Kurosawa M., Li Z., Mao Y., Murata J., Nakagawa I., Nakano K., Onishi H., Okada H., Okada K., Onuki Y., Rykov V. L., Saito N., Sakashita K., Shibata T., Shoji K., Tabaru T., Taketani A., Tanida K., Togawa M., Tojo J., Torii H., Wagner M. M., Watanabe Y., Xie W., and Yokkaichi S.: “Onset of π^0 suppression studied in Cu+Cu collisions at $\sqrt{s_{NN}} = 22.4, 62.4,$ and 200 GeV”, *Phys. Rev. Lett.* **101**, 162301-1–162301-6 (2008). *
- Adare A., Akiba Y., Aoki K., Asai J., Bunce G. M., Deshpande A., Enyo H., Fields D. E., Fujiwara K., Fukao Y., Goto Y., Gross P. M., Hachiya T., Hasuko K., Heuser J. M., Horaguchi T., Ichihara T., Imai K., Inoue Y., Ishihara M., Jinnouchi O., Kajihara F., Kamihara N., Kaneta M., Kanoh H., Kawall D., Kiyomichi A., Kurita K., Mao Y., Murata J., Nakagawa I., Nakano K., Onishi H., Okada H., Okada K., Rykov V. L., Saito N., Sato H., Shibata T., Shoji K., Tabaru T., Taketani A., Tanida K., Togawa M., Tojo J., Torii H., Tsuchimoto Y., Wagner M. M., Watanabe Y., Xie W., and Yokkaichi S.: “Suppression pattern of neutral pions at high transverse momentum in Au+Au collisions at $\sqrt{s_{NN}} = 200$ GeV and constraints on medium transport coefficients”, *Phys. Rev. Lett.* **101**, 232301-1–232301-7 (2008). *
- Asahi K., Ueno H., Shimada K., Nagatomo T., Yoshimi A., Nagae D., Kameda D., Uchida M., Inoue T., Hatakeyama N., Kagami S., Hasama Y., Suzuki K., Murata J., Kawamura H., Narita K., and Ishihara M.: “Nuclear Structure Studies with Polarized Radioactive Beams”, *AIP Conf. Proc.* **1149**, 90–99 (2009). *
- Yoshimi A., Asahi K., Inoue T., Uchida M., Hatakeyama N., Tsuchiya M., and Kagami S.: “Nuclear Spin Maser at Highly Stabilized Low Magnetic Field and Search for Atomic EDM”, *AIP Conf. Proc.* **1149**, 249–252 (2009). *
- Ichikawa Y., Onishi T., Suzuki D., Iwasaki H., Naik V., Kubo T., Chakrabarti A., Aoi N., Brown A., Fukuda N., Kubono S., Motobayashi T., Nakabayashi T., Nakao T., Okumura T., Ong H., Suzuki H., Suzuki M., Teranishi T., Yamada K., Yamaguchi H., and Sakurai H.: “Investigation into behavior of weakly-bound proton via $B(GT)$ measurement for the β decay of ^{24}Si ”, *AIP Conf. Proc.* **1165**, 98–101 (2009).
- Kobayashi T., Matsuo Y., Nishimura M., Hayashizaki Y., and Kawai J.: “Hydrogenation of carbon fragments after femtosecond laser ablation of solid C_{60} ”, *Appl. Surf. Sci.* **255**, 9652–9654 (2009). *
- Nishimura M., Kobayashi T., Matsuo Y., Motobayashi T., Hayashizaki Y., and Kawai J.: “Dynamics of Ablation Plasma induced by a Femtosecond Laser Pulse in Electric Fields”, *Appl. Surf. Sci.* **255**, 9729–9733 (2009). *
- Nagatomo T., Shimada K., Asahi K., Balabanski D. L., Daugas J., Depuydt M., De Rydt M., Gaudefroy L., Grevy S., Hasama Y., Ichikawa Y., Kameda D., Morel P., Perrot L., Stodel C., Thomas J. C., Vanderheijden W., Vermeulen N., Vingerhoets P., Yoshimi A., Neyens G., and Ueno H.: “Electric quadrupole moment of the neutron-rich ^{33}Al ”, *Eur. Phys. J. A* **42**, No. 3, pp. 383–385 (2009). *
- Ichikawa Y., Kubo T., Aoi N., Naik V., Chakrabarti A., Fukuda N., Iwasaki H., Kubono S., Motobayashi T., Nakabayashi T., Nakao T., Okumura T., Ong H., Onishi T., Suzuki D., Suzuki H., Suzuki M., Teranishi T., Yamada K., Yamaguchi H., and Sakurai H.: “Beta-decay study of $T_z = -2$ proton-rich nucleus ^{24}Si ”, *Eur. Phys. J. A* **42**, 375–378 (2009). *
- Mizuno T., Yamada T., Tsuchida H., Nakai Y., and Itoh A.: “Structure deformation dynamics of acetylene molecules following electron loss and capture collisions of 6 MeV O^{4+} ions”, *J. Phys.: Con. Ser.* **163**, 012039-1–012039-4 (2009). *
- Hata M., Akiyama T., Ikeda Y., Kawamura H., Narota K., Ninomiya K., Ogawa N., Sato T., Seitabashi E., Sekiguchi Y., Tsutsui R., Yazawa K., and Murata J.: “Recent results on short-range gravity experiment”, *J. Phys.: Con. Ser.* **189**, 012019-01–012019-10 (2009). *
- Ninomiya K., Akiyama T., Hata M., Ikeda Y., Kawamura H., Narota K., Ogawa N., Sato T., Seitabashi E., Sekiguchi Y., Tsutsui R., Yazawa K., and Murata J.: “New experimental technique for short-range gravity

- measurement”, *J. Phys.: Con. Ser.* **189**, 012026-1–012026-7 (2009). *
- Adare A., Akiba Y., Aoki K., Asai J., Bunce G. M., Deshpande A., Enyo H., Fields D. E., Fujiwara K., Fukao Y., Goto Y., Gross P. M., Horaguchi T., Ichihara T., Imai K., Inoue Y., Ishihara M., Jinnouchi O., Kamihara N., Kaneta M., Kanoh H., Kawall D., Kiyomichi A., Kurita K., Mao Y., Murata J., Nakagawa I., Nakano K., Onishi H., Okada H., Okada K., Rykov V. L., Saito N., Shibata T., Shoji K., Tabaru T., Taketani A., Tanida K., Togawa M., Tojo J., Torii H., Wagner M. M., Watanabe Y., Xie W., and Yokkaichi S.: “Dilepton mass spectra in p+p collisions at $\sqrt{s} = 200$ GeV and the contribution from open charm”, *Phys. Lett. B* **670**, 313–320 (2009). *
- De Rydt M., Neyens G., Asahi K., Balabanski D. L., Daugas J., Depuydt M., Gaudefroy L., Grevy S., Hasama Y., Ichikawa Y., Morel P., Nagatomo T., Ohtsuka T., Perrot L., Shimada K., Stodel C., Thomas J., Ueno H., Utsuno Y., Wannes V., Vermeulen N., Vingerhoets P., and Yoshimi A.: “Precision measurement of the electric quadrupole moment of ^{31}Al and determination of the effective proton charge in the sd-shell”, *Phys. Lett. B* **678**, 344–349 (2009). *
- Takeuchi S., Aoi N., Motobayashi T., Ota S., Takeshita E., Suzuki H., Baba H., Fukui T., Hashimoto Y., Ieki K., Imai N., Iwasaki H., Kanno S., Kondo Y., Kubo T., Kurita K., Minemura T., Nakamura T., Okumura T., Onishi T., Sakurai H., Shimoura S., Sugou R., Suzuki D., Suzuki M., Takashina M., Tamaki M., Tanaka K., Togano Y., and Yamada K.: “Low-Iying States in ^{32}Mg studied by proton inelastic scattering”, *Phys. Rev. C* **79**, No. 5, pp. 054319-1–054319-11 (2009). *
- Zhu S., Janssens R. V., Fornal B., Freeman S. J., Honma M., Broda R., Carpenter M. P., Deacon A. N., Jackson E., Kay B. P., Lauritsen T., Lister C. J., Mantica P. F., Otsuka T., Seweryniak D., Smith J. F., Steppenbeck D., and Wang X.: “High-lying, non-yrast shell structure in ^{52}Ti ”, *Phys. Rev. C* **80**, 024318-1–024318-11 (2009). *
- Ichikawa Y., Onishi T., Suzuki D., Iwasaki H., Naik V., Kubo T., Chakrabarti A., Aoi N., Brown A., Fukuda N., Kubono S., Motobayashi T., Nakabayashi T., Nakao T., Okumura T., Ong H., Suzuki H., Suzuki M., Teranishi T., Yamada K., Yamaguchi H., and Sakurai H.: “Beta decay of the proton-rich nucleus ^{24}Si and its mirror asymmetry”, *Phys. Rev. C* **80**, 044302-1–044302-12 (2009). *
- Adare A., Akiba Y., Aoki K., Asai J., Bunce G. M., Dairaku S., Deshpande A., Enyo H., Fields D. E., Fujiwara K., Fukao Y., Goto Y., Gross P. M., Horaguchi T., Ichihara T., Ichimiya R., Imai K., Ishihara M., Kametani S., Kamihara N., Kawall D., Kurita K., Kurosawa M., Li Z., Mao Y., Murata J., Nakagawa I., Nakano K., Okada H., Okada K., Onuki Y., Rykov V. L., Saito N., Sakashita K., Shibata T., Shoji K., Taketani A., Tanida K., Togawa M., Torii H., Watanabe Y., Xie W., and Yokkaichi S.: “Inclusive cross section and double helicity asymmetry for π^0 production in $p + p$ collisions at $\sqrt{s} = 62.4$ GeV”, *Phys. Rev. D* **79**, 012003-1–012003-11 (2009). *
- Nakano Y., Kondo C., Hatakeyama A., Nakai Y., Azuma T., Komaki K., Yamazaki Y., Takada E., and Murakami T.: “Polarization control in three-dimensional resonant coherent excitation”, *Phys. Rev. Lett.* **102**, 085502-1–085502-4 (2009). *
- Mizuno T., Yamada T., Tsuchida H., Nakai Y., and Itoh A.: “Measurement of kinetic energy release in CO fragmentation by charge-changing collisions of fast heavy ions”, *Phys. Rev. A* **81**, 012704-1–012704-6 (2010). *
- Steppenbeck D., Deacon A. N., Freeman S. J., Janssens R. V., Zhu S., Carpenter M. P., Chowdhury P., Honma M., Lauritsen T., Lister C. J., Seweryniak D., Smith J. F., Tabor S. L., and Varley B. J.: “High-spin structures in the neutron-rich isotopes $^{57-60}\text{Mn}$ ”, *Phys. Rev. C* **81**, No. 1, pp. 014305-1–014305-21 (2010). *
- (Others)
- Murata J., Akiyama T., Hata M., Hirayama Y., Ikeda Y., Ishii T., Kameda D., Kawamura H., Mitsuoka S., Miyatake H., Nagae D., Ninomiya K., Nitta M., Seitabashi E., and Toyoda T.: “Test of time reversal symmetry using polarized nuclei”, *JAEA-Review* **2009-036**, 62–63 (2009).

Oral Presentations

(International Conference etc.)

- Takeuchi S., Shimoura S., Motobayashi T., Akiyoshi H., Ando Y., Aoi N., Fulop Z., Gomi T., Higurashi Y., Hirai M., Iwasa N., Iwasaki H., Iwata Y., Kobayashi H., Kurokawa M., Liu Z., Minemura T., Ozawa S., Sakurai H., Serata M., Teranishi T., Yamada K., Yanagisawa Y., and Ishihara M.: “Isobaric analog state of ^{14}Be ”, RIKEN-CNS RIBF International Workshop “Correlation and Condensation: New Features in Loosely Bound and Unbound Nuclear States”, Wako, Dec. (2005).
- Motizuki Y.: “A prospect of theoretical and interdisciplinary r-process studies around RIBF”, RIBF users meeting 2008, Wako, Nov. (2008).
- Ichikawa Y., Onishi T., Suzuki D., Iwasaki H., Naik V., Kubo T., Chakrabarti A., Aoi N., Brown A., Fukuda N., Kubono S., Motobayashi T., Nakabayashi T., Nakao T., Okumura T., Ong H., Suzuki H., Suzuki M., Teranishi T., Yamada K., Yamaguchi H., and Sakurai H.: “Investigation into behavior of weakly-bound proton via $B(\text{GT})$ measurement for the β decay of ^{24}Si ”, International Conference on Nuclear Structure and Dynamics (NSD09), (University of Zagreb), Dubrovnik, Croatia, May (2009).
- Motizuki Y. and Dome-F g. c.: “Solar cycles and supernovae embedded in a Dome F ice core”, International Astronomical Union 27th General Assembly, (Intern-

- tional Astronomical Union), Rio de Janeiro, Brazil, Aug. (2009).
- Ichikawa Y., Onishi T., Suzuki D., Iwasaki H., Naik V., Kubo T., Chakrabarti A., Aoi N., Brown A., Fukuda N., Kubono S., Motobayashi T., Nakabayashi T., Nakao T., Okumura T., Ong H., Suzuki H., Suzuki M., Teranishi T., Yamada K., Yamaguchi H., and Sakurai H.: “Beta decay of ^{24}Si and mirror asymmetry of Gamow-Teller transition strength”, 3rd Joint Meeting of the Nuclear Physics Divisions of the APS and JPS (Hawaii 2009), Hawaii, USA, Oct. (2009).
- Sasaki A., Wakui T., Furukawa T., Kazato M., Wada M., Sonoda T., Takamine A., Kobayashi T., Nishimura M., Ueno H., Yoshimi A., Aoi N., Nishimura S., Togano Y., Takechi M., Kondo Y., Hatakeyama A., Matsuura Y., Kato Y., Odahara A., Shimoda T., Asahi K., Shinozuka T., Motobayashi T., and Matsuo Y.: “Fluorescence detection system for nuclear laser spectroscopy of Rb in superfluid helium”, 3rd Joint Meeting of the Nuclear Physics Divisions of the APS and JPS (Hawaii 2009), Hawaii, USA, Oct. (2009).
- Ueno H., Yoshimi A., and Asahi K.: “RIPS upgrade and physics programs”, 3rd Joint Meeting of the Nuclear Physics Divisions of the APS and JPS (Hawaii 2009), Hawaii, USA, Oct. (2009).
- Baba H., Ichihara T., Ohnishi T., Takeuchi S., Yoshida K., Watanabe Y., Ota S., and Shimoura S.: “The New DAQ System in RIKEN RIBF”, 3rd Joint Meeting of the Nuclear Physics Divisions of the APS and JPS (Hawaii 2009), Hawaii, USA, Oct. (2009).
- Motizuki Y., Takahashi K., Nakai Y., Makishima K., Bamba A., Yano Y., Igarashi M., Motoyama H., Kamiyama K., Suzuki K., and Imamura T.: “A Dome Fuji ice core recording both supernovae and solar cycles”, 2nd International Symposium on Dome Fuji Ice Core and Related Topics, (National Institute of Polar Research), Tachikawa, Nov. (2009).
- Ichikawa Y., Onishi T., Suzuki D., Iwasaki H., Naik V., Kubo T., Chakrabarti A., Aoi N., Brown A., Fukuda N., Kubono S., Motobayashi T., Nakabayashi T., Nakao T., Okumura T., Ong H., Suzuki H., Suzuki M., Teranishi T., Yamada K., Yamaguchi H., and Sakurai H.: “Gamow-Teller transition of proton-rich nucleus ^{24}Si ”, 7th Japan-China Joint Nuclear Physics Symposium, (University of Tsukuba), Tsukuba, Nov. (2009).
- Ichikawa Y., Onishi T., Suzuki D., Iwasaki H., Naik V., Kubo T., Chakrabarti A., Aoi N., Brown A., Fukuda N., Kubono S., Motobayashi T., Nakabayashi T., Nakao T., Okumura T., Ong H., Suzuki H., Suzuki M., Teranishi T., Yamada K., Yamaguchi H., and Sakurai H.: “Mirror asymmetry for $B(\text{GT})$ of ^{24}Si induced by Thomas-Ehrman shift”, Tours Symposium on Nuclear Physics and Astrophysics VII (TOURS 2009), (Konan University), Kobe, Nov. (2009).
- Ichikawa Y., Onisi T. K., Suzuki D., Iwasaki H., Kubo T., Naik V., Chakrabarti A., Aoi N., Brown A. B., Fukuda N., Kubono S., Motobayashi T., Nakabayashi T., Nakamura T., Nakao T., Okumura T., Ong H., Suzuki H., Suzuki M. K., Teranishi T., Yamaguchi H., and Sakurai H.: “Proton-rich nuclear structure investigated by β decay of ^{24}Si ”, ICHOR-EFES International Symposium on New Facet of Spin-Isospin Responses (SIR2010), (University of Tokyo), Tokyo, Feb. (2010).
- Ichikawa Y., Onisi T. K., Suzuki D., Iwasaki H., Kubo T., Naik V., Chakrabarti A., Aoi N., Brown A. B., Fukuda N., Kubono S., Motobayashi T., Nakabayashi T., Nakamura T., Nakao T., Okumura T., Ong H., Suzuki H., Suzuki M. K., Teranishi T., Yamaguchi H., and Sakurai H.: “Mirror asymmetry investigated by β decay of proton-rich ^{24}Si ”, International Symposium on Forefronts of Researches in Exotic Nuclear Structures (Niigata2010), (Niigata University), Toka-machi, Niigata Pref., Mar. (2010).
- (Domestic Conference)
- 岡田信二, Beer G. A., 方享燦, Cargnelli M., 千葉順成, Choi S., Curceanu C. O., 福田芳之, 花木俊生, 早野龍五, 飯尾雅美, 石川隆, 石元茂, 石渡智一, 板橋健太, 岩井正明, 岩崎雅彦, Juhasz B., Kienle P., Marton J., 松田恭幸, 大西宏明, 應田治彦, Schmid P., 佐藤将春, 鈴木祥仁, 鈴木隆敏, 竜野秀行, 友野大, Widmann E., 山崎敏光, 林熙重, Zmeskal J.: 理研ワークショップ「放射線検出器と電子回路の課題と展望-光子検出器を中心に」, 和光市, 5月(2005).
- 佐藤将春, 飯尾雅美, 板橋健太, 岩崎雅彦, 應田治彦, 大西宏明, 岡田信二, 鈴木隆敏, 友野大, 松田恭幸, 山崎敏光, 福田芳之, 石川隆, 早野龍五, 石元茂, 岩井正明, 鈴木祥仁, 千葉順成, 花木俊生, Bhang H., Choi S., Kim J., Yim H., 石渡智一, Widmann E., Kienle P.: “ $^4\text{He}(\text{K}_{\text{stopped}}^-, \text{N})$ 反応を用いたストレンジトライブリオンの実験的研究(1)”, 日本物理学会第61回年次大会, (日本物理学会), 松山, 3月(2006).
- 岡田信二, Beer G. A., 方享燦, Cargnelli M., 千葉順成, Choi S., Curceanu C. O., 福田芳之, 花木俊生, 早野龍五, 飯尾雅美, 石川隆, 石元茂, 石渡智一, 板橋健太, 岩井正明, 岩崎雅彦, Juhasz B., Kienle P., Marton J., 松田恭幸, 大西宏明, 應田治彦, Schmid P., 佐藤将春, 鈴木祥仁, 鈴木隆敏, 竜野秀行, 友野大, Widmann E., 山崎敏光, 林熙重, Zmeskal J.: “K中間子ヘリウム4原子 $3d \rightarrow 2p$ X線の精密測定”, 日本物理学会第61回年次大会, 松山, 3月(2006).
- 飯尾雅美, 板橋健太, 岩崎雅彦, 應田治彦, 大西宏明, 岡田信二, 鈴木隆敏, 友野大, 松田恭幸, 山崎敏光, 石川隆, 竜野秀行, 早野龍五, 石元茂, 鈴木祥仁, 佐藤将春, 福田芳之, 千葉順成, 花木俊生, 方享燦, Choi S., 林熙重, 石渡智一, Cargnelli M., Juhasz B., Kienle P., Marton J., Widmann E., Zmeskal J., Schmid P., Beer G. A., Curceanu C. O.: “K中間子ヘリウム原子 X線測定実験のための検出器系I”, 日本物理学会第61回年次大会, 松山, 3月(2006).
- 佐藤将春, 飯尾雅美, 板橋健太, 岩崎雅彦, 應田治彦, 大西宏明, 岡田信二, 鈴木隆敏, 友野大, 松田恭幸, 山崎敏光, 福田芳之, 石川隆, 早野龍五, 石元茂, 岩井正明, 鈴木祥仁, 千葉順成, 花木俊生, Bhang H., Choi S., Kim J., Yim H., 石渡智一, Widmann E., Kienle P.: “ $^4\text{He}(\text{K}_{\text{stopped}}^-, \text{N})$ 反応を用いた

- ストレンジトライブリオンの実験的研究(4)”, 日本物理学会 2006 年秋季大会, (日本物理学会), 奈良, 9 月 (2006).
- 岡田信二, Beer G. A., 方享燦, Buehler P., Cargnelli M., 千葉順成, Choi S., Curceanu C. O., 福田芳之, Guaraldo C., 花本俊生, 早野龍五, Hirtl A., 飯尾雅美, Iliescu M., 石川隆, 石元茂, 石渡智一, 板橋健太, 岩井正明, 岩崎雅彦, Kienle P., Marton J., 松田恭幸, 大西宏明, 應田治彦, Pietreanu D., Sirghi D., Sirghi F., 佐藤将春, 鈴木隆敏, 竜野秀行, 友野大, Widmann E., 山崎敏光, 林熙重, Zmeskal J.: “Precision spectroscopy of Kaonic Helium-3 $3d \rightarrow 2p$ X-rays (J-PARC E17 実験)”, 文科省科研費補助金特定領域研究「ストレンジネスで探るクォーク多体系」研究会 2006, 熱海, 12 月 (2006).
- 佐藤将春, 飯尾雅美, 板橋健太, 岩崎雅彦, 應田治彦, 大西宏明, 岡田信二, 鈴木隆敏, 友野大, 松田恭幸, 山崎敏光, 福田芳之, 石川隆, 早野龍五, 石元茂, 岩井正明, 鈴木祥仁, 千葉順成, 花本俊生, Bhang H., Choi S., Kim J., Yim H., 石渡智一, Widmann E., Kienle P.: “ $^4\text{He}(K_{\text{stopped}}^-, N)$ 反応を用いたストレンジトライブリオンの実験的研究(6)”, 日本物理学会 2007 年春季大会, (日本物理学会), 八王子, 3 月 (2007).
- 飯尾雅美, 板橋健太, 岩崎雅彦, 應田治彦, 大西宏明, 岡田信二, 佐久間史典, 鈴木隆敏, 友野大, 松田恭幸, 山崎敏光, 石元茂, 鈴木祥仁, 関本美知子, 豊田晃久, 永江知文, 石川隆, 竜野秀行, 早野龍五, 藤岡宏之, 味村周平, 阪口篤志, 佐藤将春, 福田芳之, 千葉順成, 花本俊生, 福田共和, 溝井浩, Beer G. A., 方享燦, Choi S., 林熙重, 石渡智一, Buehler P., Hirtl A., Cargnelli M., Kienle P., Marton J., Widmann E., Zmeskal J., Curceanu C. O., Guaraldo C., Iliescu M., Pietreanu D., Sirghi D., Sirghi F., Faso D., Busso L., Morra O.: “K 中間子原子核探索実験のための液体ヘリウム 3 標的の開発”, 日本物理学会 2007 年春季大会, 八王子, 3 月 (2007).
- 岡田信二, Beer G. A., 方享燦, Cargnelli M., 千葉順成, Choi S., Curceanu C. O., 福田芳之, 花本俊生, 早野龍五, 飯尾雅美, 石川隆, 石元茂, 石渡智一, 板橋健太, 岩井正明, 岩崎雅彦, Juhasz B., Kienle P., Marton J., 松田恭幸, 大西宏明, 應田治彦, Schmid P., 佐藤将春, 鈴木祥仁, 鈴木隆敏, 竜野秀行, 友野大, Widmann E., 山崎敏光, 林熙重, Zmeskal J.: 日本物理学会第 62 回年次大会, 札幌, 9 月 (2007).
- 岡田信二, Beer G. A., 方享燦, Buehler P., Cargnelli M., 千葉順成, Choi S., Curceanu C. O., 福田芳之, Guaraldo C., 花本俊生, 早野龍五, Hirtl A., 飯尾雅美, Iliescu M., 石川隆, 石元茂, 石渡智一, 板橋健太, 岩井正明, 岩崎雅彦, Kienle P., Marton J., 松田恭幸, 大西宏明, 應田治彦, Pietreanu D., Sirghi D., Sirghi F., 佐藤将春, 鈴木隆敏, 竜野秀行, 友野大, Widmann E., 山崎敏光, 林熙重, Zmeskal J.: “J-PARC における K 中間子ヘリウム 3 原子 X 線分光実験 J-PARC E17 の現状”, 文部科学省科学研究費補助金特定領域研究特定領域研究「ストレンジネスで探るクォーク多体系」第 3 回総括班主催研究会 (2007), 仙台, 11 月 (2007).
- 鈴木隆敏, 飯尾雅美, 板橋健太, 岩崎雅彦, 應田治彦, 大西宏明, 岡田信二, 佐藤将春, 友野大, 松田恭幸, 山崎敏光, 福田芳之, 石川隆, 早野龍五, 石元茂, 岩井正明, 鈴木祥仁, 千葉順成, 花本俊生, Bhang H., Choi S., Kim J., Yim H., 石渡智一, Widmann E., Kienle P.: “ ^4He 上の静止 K^- 反応に於ける重陽子測定によるストレンジマルチバリオン状態の探索(1)”, 日本物理学会第 63 回年次大会, (日本物理学会), 東大阪, 3 月 (2008).
- 中野祐司, 日時健一, 井上岳史, 東俊行, 高野靖史, 崑山温, 小牧研一郎, 中井陽一, 山崎泰規, 高田栄一, 村上健: “コヒーレント共鳴励起による中空原子イオンの生成”, 日本物理学会第 63 回年次大会, 東大阪, 3 月 (2008).
- 東俊行, 日時健一, 井上岳史, 中野祐司, 高野靖史, 崑山温, 小牧研一郎, 中井陽一, 山崎泰規, 高田栄一, 村上健: “様々な結晶面配列を用いた 3 次元コヒーレント共鳴励起の観測”, 日本物理学会第 63 回年次大会, 東大阪, 3 月 (2008).
- 日時健一, 中野祐司, 東俊行, 高野靖史, 崑山温, 中井陽一, 小牧研一郎, 山崎泰規, 高田栄一, 村上健: “3 次元コヒーレント共鳴励起(3D-RCE)による Fe^{24+} イオンの 2 重共鳴”, 日本物理学会 2008 年秋季大会, 盛岡, 9 月 (2008).
- 飯尾雅美, 板橋健太, 岩崎雅彦, 應田治彦, 大西宏明, 佐久間史典, 佐藤将春, 塚田暁, 友野大, 藤岡宏之, 山崎敏光, 石元茂, 岩井正明, 鈴木祥仁, 関本美知子, 豊田晃久, 石川隆, 竜野秀行, 鈴木隆敏, 早野龍五, 松田恭幸, 永江知文, 平岩聡彦, 味村周平, 野海博之, 阪口篤志, 藤原裕也, 徳田真, 千葉順成, 福田共和, 溝井浩, Beer G. A., 方享燦, Choi S., 林熙重, 石渡智一, Buehler P., Cargnelli M., Hirtl A., Kienle P., Marton J., Widmann E., Zmeskal J., 岡田信二, Curceanu C. O., Guaraldo C., Iliescu M., Pietreanu D., Sirghi D., Sirghi F., Faso D., Morra O., Busso L.: “K 中間子原子核探索実験のための液体ヘリウム 3 標的の開発 III”, 日本物理学会 2008 年秋季大会, 山形, 9 月 (2008).
- 胡子昇一郎, 酒向正己, 村上哲也, 新田稔, 池田友樹, 中谷祐輔, 川村広和, 豊田健司, 村田次郎, 家城和夫, 中井陽一, 西村俊一, 高田栄一: “中間エネルギー重イオン衝突における荷電パイオン生成 (I)”, 日本物理学会第 64 回年次大会, 東京, 3 月 (2009).
- 酒向正己, 胡子昇一郎, 村上哲也, 新田稔, 池田友樹, 中谷祐輔, 川村広和, 豊田健司, 村田次郎, 家城和夫, 中井陽一, 西村俊一, 高田栄一: “中間エネルギー重イオン衝突における荷電パイオン生成 (II)”, 日本物理学会第 64 回年次大会, 東京, 3 月 (2009).
- 日時健一, 中野祐司, 寺田正裕, 高野靖史, 崑山温, 中井陽一, 東俊行, 小牧研一郎, 山崎泰規, 高田栄一, 村上健: “コンポジット電子による 3 次元コヒーレント共鳴励起の観測”, 日本物理学会第 64 回年次大会, 東京, 3 月 (2009).
- 黒田武彦, 林左絵子, 富田晃彦, 望月優子, 木村かおる, 田代信: “一緒に宇宙探検をしよう: 男女共同参画委員会の取り組み”, 日本天文学会 2009 年春季年会, 堺, 3 月 (2009).
- 西村美月, 松尾由賀利, 小林徹, 本林透, 林崎良英, 河合純: “電場中におけるフェムト秒レーザーアブレーションプラズマの P-LIF 観測”, 第 56 回応用物理学関係連合講演会, つくば, 3-4 月 (2009).
- 望月優子, 高橋和也, 牧島一夫, 馬場彩, 中井陽一, 矢野安重, 五十嵐誠, 本山秀明, 神山孝吉, 鈴木啓助, 今村隆史: “南極氷床コアからさぐる超新星の痕跡と太陽活動周期”, 日本地球惑星科学連合 2009 年大会, 千葉, 5 月 (2009).
- 西村美月, 小林徹, 松尾由賀利, 安藤吉成, 林崎良英, 河合純:

- “フェムト秒レーザーアブレーションによる分子の原子イオン化の利用”, 理研シンポジウム「エクストリームフォトリクスシンポジウム: 光で繋ぐ理研の基礎科学」, 和光, 5月(2009).
- 望月優子: “宇宙と生命とのつながり: 生命と元素, 星, 宇宙のリズム”, 兵庫県立大学皆既日食観測公開アカデミックツーリズム, 小笠原, 7月(2009).
- 望月優子: “南極氷床コアから超新星の痕跡と太陽周期をさぐる”, 東京大学大学院総合文化研究科宇宙地球グループセミナー, 東京, 7月(2009).
- 望月優子: “南極氷床コアからさぐる超新星の痕跡と太陽活動周期”, 東京大学大学院理学研究科地球惑星システム科学セミナー, 東京, 10月(2009).
- 望月優子: “南極氷床コアからさぐる過去の超新星爆発と太陽活動周期”, 青山学院大学理工学部物理・数理学科コロキウム, 相模原, 11月(2009).
- 望月優子, 中井陽一, 高橋和也, 本山秀明: “ドームふじ浅層コアの酸素同位体比と太陽活動長周期”, 第32回極域気水圏シンポジウム, (国立極地研), 立川, 11月(2009).
- 中井陽一, 望月優子, 高橋和也, 五十嵐誠, 本山秀明, 鈴木啓助: “ドームふじの浅層氷床コアにおける硝酸イオン濃度の年代プロファイル: 12世紀~19世紀”, 第32回極域気水圏シンポジウム, (国立極地研究所), 立川, 11月(2009).
- 望月優子: “南極氷床コアからさぐる過去の超新星爆発と太陽周期”, 東京大学大学院理学系研究科天文学教室談話会, 東京, 12月(2009).
- 望月優子: “南極氷床コアからさぐる過去の太陽活動周期とSEP イベントの痕跡に関する考察”, 太陽圏シンポジウム: STE 研究集会, 名古屋, 1月(2010).
- 望月優子: “元素誕生の宇宙史~わかっていること、わかっていないこと~”, JSR 一般教養セミナー, 四日市, 2月(2010).
- 黒田武彦, 木村かおる, 田代信, 富田晃彦, 林左絵子, 望月優子: “日本天文学会男女共同参画委員会による理系進路選択支援事業”, 日本天文学会2010年春季年会, 広島, 3月(2010).
- 西村美月, 安藤吉成, 小林徹, 松尾由賀利, 鈴木治和, 林崎良英, 河合純: “フェムト秒レーザーアブレーション飛行時間型質量分析法と安定同位体元素標識を組み合わせた small RNA の配列解析法”, 第57回応用物理学関係連合講演会, 平塚, 3月(2010).
- 聖代橋悦子, Behr J. A., 平山賀一, 川村広和, Levy P., 二宮一史, 小川就也, 大西潤一, Pearson M., 豊田健司, 村田次郎: “TRIUMF-ISACにおける偏極 ^8Li を用いた時間反転対称性の破れ探索実験”, 日本物理学会第65回年次大会, 岡山, 3月(2010).
- 川村広和, 秋山岳伸, 秦麻記, 平山賀一, 池田友樹, 石井哲朗, 亀田大輔, 光岡慎一, 宮原直亮, 宮武宇也, 村田次郎, 中谷祐輔, 長江大輔, 二宮一史, 新田稔, 大西潤一, 聖代橋悦子, 豊田健司, 塚田和司, 渡辺裕: “KEK-TRIACにおける偏極 ^8Li を用いた時間反転対称性の研究”, 日本物理学会第65回年次大会, 岡山, 3月(2010).
- 二宮一史, 秋山岳伸, 小川就也, 川村広和, 関口雄太, 西尾悠法, 秦麻記, 渡邊健太郎, 村田次郎: “ピコ精度画像処理型変位計を用いた近距離重力実験2”, 日本物理学会第65回年次大会, 岡山, 3月(2010).
- 川村広和, 秋山岳伸, Behr J. A., 秦麻記, 平山賀一, 池田友樹, 石井哲朗, 亀田大輔, Levy P., 宮原直亮, 宮武宇也, 光岡真一, 村田次郎, 長江大輔, 中谷祐輔, 二宮一史, 新田稔, 小川就也, 大西潤一, Pearson M., 聖代橋悦子, 豊田健司, 塚田和司, 渡辺裕: “偏極 ^8Li のベータ崩壊における時間反転対称性の破れの探索”, 第6回停止・低速不安定核ビームを用いた核分光研究会, 東京, 3月(2010).
- 西村美月, 安藤吉成, 小林徹, 鈴木治和, 河合純: “フェムト秒レーザーアブレーション飛行時間型質量分析法と安定同位体元素標識を組み合わせた small RNA の配列解析法”, 応用物理学関係連合講演会, (応用物理学関係連合講演会), 平塚, 3月(2010).

Superheavy Element Laboratory

Publications

Journal

(Original Papers) *Subject to Peer Review

Haba H., Akiyama K., Tsukada K., Asai M., Toyoshima A., Yaita T., Hirata M., Sueki K., and Nagame Y.: "Chloride Complexation of Zr and Hf in HCl Investigated by Extended X-ray Absorption Fine Structure Spectroscopy: Toward Characterization of Chloride Complexation of Element 104, Rutherfordium (Rf)", *Bull. Chem. Soc. Jpn.* **82**, No. 6, pp. 698–703 (2009). *

Haba H., Kaji D., Komori Y., Kudou Y., Morimoto K., Morita K., Ooe K., Ohzeki K., Sato N., Shinohara A., and Yoneda A.: "RIKEN Gas-filled Recoil Ion Separator (GARIS) as a promising interface for superheavy element chemistry : Production of element 104, 261Rf, using the GARIS/gas-jet system", *Chem. Lett.* **38**, No. 5, pp. 426–427 (2009). *

Kasamatsu Y., Toyoshima A., Asai M., Tsukada K., Li Z., Ishii Y., Toume H., Sato T., Kikuchi T., Nishinaka I., Nagame Y., Haba H., Kikunaga H., Kudou Y., Oura Y., Akiyama K., Sato W., Ooe K., Fujisawa H., Shinohara A., Goto S., Hasegawa Taichi ., Kudo H., Nanri T., Araki M., Kinoshita N., Yokoyama A., Fan F., Qin Z., Duellman C. E., Schaedel M., and Kratz J. V.: "Anionic Fluoro Complex of Element 105, Db", *Chem. Lett.* **38**, No. 11, pp. 1084–1085 (2009). *

Toyoshima A., Kasamatsu Y., Tsukada K., Asai M., Kitatsuji Y., Ishii Y., Toume H., Nishinaka I., Haba H., Ooe K., Sato W., Shinohara A., Akiyama K., and Nagame Y.: "Oxidation of element 102, nobelium, with flow electrolytic column chromatography on an atom-at-a-time scale", *J. Am. Chem. Soc.* **131**, 9180–9181 (2009). *

Akiyama K., Haba H., Tsukada K., Asai M., Toyoshima A., Sueki K., Nagame Y., and Katada M.: "A metallofullerene that encapsulates 225Ac", *J. Radioanal. Nucl. Chem.* **280**, No. 2, pp. 329–331 (2009). *

Inamura T. and Haba H.: "Search for a "3.5-eV isomer" in ²²⁹Th in a hollow-cathode electric discharge", *Phys. Rev. C* **79**, No. 3, pp. 034313-1–034313-10 (2009). *

(Others)

Asai M., Tsukada K., Kasamatsu Y., Sato T., Toyoshima A., Ishii Y., Takahashi R., Nagame Y., Ishii T., Nishinaka I., Kaji D., Morimoto K., and Kojima Y.: "Alpha-gamma spectroscopy of ²⁵⁹Rf produced by using a mixed Cf target", *JAEA-Review* **2009**, No. 036, pp. 37–38 (2009).

Nishinaka I., Kasamatsu Y., Tanikawa M., Goto S., and Asai M.: "Sub-barrier fusion hindrance in ¹⁹F + ²⁰⁹Bi reaction", *JAEA-Review* **2009**, No. 036, pp. 60–61 (2009).

Kasamatsu Y., Toyoshima A., Asai M., Tsukada K., Li

Z., Ishii Y., Sato T., Nishinaka I., Kikuchi T., Haba H., Kudou Y., Sato N., Oura Y., Akiyama K., Ooe K., Fujisawa H., Shinohara A., Goto S., Kudo H., Araki M., Nishikawa M., Yokoyama A., and Nagame Y.: "Anion-exchange experiment of Db with 0.31 M HF/0.10 M HNO₃ solution", *JAEA-Review* **2009**, No. 036, pp. 67–68 (2009).

Oral Presentations

(International Conference etc.)

Ooe K., Yahagi W., Komori Y., Fujisawa H., Kikunaga H., Yoshimura T., Sato W., Takahashi N., Takahisa K., Haba H., Kudou Y., Ezaki Y., and Shinohara A.: "Studies of Extraction Behavior of Tungsten toward Solution Chemistry of Seaborgium (Element 106)", International Workshop on Molecular Information and Dynamics 2008, (Osaka University Global COE Program), Taipei, Taiwan, Nov. (2008).

Kasamatsu Y., Toyoshima A., Asai M., Tsukada K., Li Z., Ishii Y., Sato T., Nishinaka I., Kikuchi T., Nagame Y., Haba H., Kikunaga H., Kudou Y., Sato N., Oura Y., Akiyama K., Sato W., Ooe K., Fujisawa H., Shinohara A., Goto S., Kudo H., Araki M., Kinoshita N., Nishikawa M., Yokoyama A., Fan F., Qin Z., and Duellmann C. E.: "Anion-exchange experiment of Db with AIDA-II", 7th Workshop on the Chemistry of the Heaviest Elements, (Johannes Gutenberg - Universitaet Mainz), Mainz, Germany, Oct. (2009).

Ooe K., Yahagi W., Komori Y., Fujisawa H., Takayama R., Kikunaga H., Yoshimura T., Takahashi N., Haba H., Kudou Y., Ezaki Y., Takahisa K., and Shinohara A.: "Solvent Extraction Studies of Molybdenum and Tungsten as Homologues of Seaborgium (Element 106)", 7th Workshop on the Chemistry of the Heaviest Elements, (Mainz University), Mainz, Germany, Oct. (2009).

(Technical Document)

塚田和明, 笠松良崇, 浅井雅人, 豊嶋厚史, 石井康雄, Li Z., 佐藤哲也, 西中一朗, 永日諭一郎, 菊池貴宏, 後藤真一, 長谷川太一, 工藤久昭, 藤沢弘幸, 大江一弘, 矢作亘, 佐藤涉, 篠原厚, 南里朋洋, 荒木幹生, 横山明彦, Fan F., 工藤祐生, 大浦泰嗣: "新実験システムを利用した 105 番元素 (Db) の HF/HNO₃ 水溶液中での陰イオン交換挙動", 日本化学会第 89 春季年会, (日本化学会), 船橋, 3 月 (2009).

佐藤哲也, 浅井雅人, 塚田和明, 豊嶋厚史, 笠松良崇, Li Z., 石井康雄, 羽場宏光, 後藤真一, 工藤久昭, 永日諭一郎: "106 番元素 Sg のためのオンライン気相化学分離装置の開発", 日本化学会第 89 春季年会, (日本化学会), 船橋, 3 月 (2009).

菊池貴宏, 豊嶋厚史, Li Z., 塚田和明, 浅井雅人, 佐藤哲也, 佐藤望, 永日諭一郎, 笠松良崇, Fan F.: "Rf を模擬した同族元素 Zr ならびに Hf の α-HiB 錯形成", 2009 日本放射化学会年会・第 53 回放射化学討論会, (日本放射化学会), 東京, 9 月 (2009).

笠松良崇, 豊嶋厚史, 浅井雅人, 塚田和明, Li Z., 石井康雄, 佐藤哲也, 西中一朗, 菊池貴宏, 羽場宏光, 工藤祐生, 佐藤望, 大浦泰嗣, 秋山和彦, 大江一弘, 藤沢弘幸, 篠原厚, 後藤

- 真一, 工藤久昭, 荒木幹生, 西川恵, 横山明彦, 永日諭一郎: “HF/HNO₃ 水溶液系における 105 番元素 Db の陰イオン交換挙動”, 2009 日本放射化学会年会・第 53 回放射化学討論会, (日本放射化学会), 東京, 9 月 (2009).
- 笠松良崇, 羽場宏光, 江崎豊: “超重元素化学実験に向けたサマリウム共沈 α 線源作成法の開発”, 2009 日本放射化学会年会・第 53 回放射化学討論会, (日本放射化学会), 東京, 9 月 (2009).
- 大江一弘, 矢作亘, 小森有希子, 藤沢弘幸, 山玲央奈, 菊永英寿, 吉村崇, 高橋成人, 羽場宏光, 工藤祐生, 江崎豊, 高久圭二, 篠原厚: “106 番元素シーボーギウムの同族元素モリブデンの溶媒抽出挙動”, 2009 日本放射化学会年会・第 53 回放射化学討論会, (日本放射化学会), 東京, 9 月 (2009).
- 佐藤哲也, 塚田和明, 浅井雅人, 豊嶋厚史, 笠松良崇, Li Z., 佐藤望, 菊池貴宏, 永日諭一郎: “Db を模擬した 5 族元素 Nb ならびに Ta のオンライン等温ガスクロマトグラフ挙動”, 2009 日本放射化学会年会・第 53 回放射化学討論会, (日本放射化学会), 東京, 9 月 (2009).
- 浅井雅人, 塚田和明, 笠松良崇, 佐藤哲也, 豊嶋厚史, 永日諭一郎: “Cf 標的を用いた長寿命 Fm, Es トレーサーの製造と核分光”, 2009 日本放射化学会年会・第 53 回放射化学討論会, (日本放射化学会), 東京, 9 月 (2009).
- 江崎豊, 笠松良崇, 羽場宏光: “^{nat}Hf 標的を用いた希土類元素マルチトレーサーの製造”, 2009 日本放射化学会年会・第 53 回放射化学討論会, (日本放射化学会), 東京, 9 月 (2009).
- 豊嶋厚史, 塚田和明, 浅井雅人, 佐藤哲也, Li Z., 佐藤望, 菊池貴宏, 北辻章浩, 永日諭一郎, 大江一弘, 篠原厚, 笠松良崇, 羽場宏光: “電気化学的手法による 101 番元素メンデレビウムの還元”, 2009 日本放射化学会年会・第 53 回放射化学討論会, (日本放射化学会), 東京, 9 月 (2009).
- 西中一朗, 笠松良崇, 谷川勝至, 後藤真一, 浅井雅人: “¹⁹F + ²⁰⁹Bi 反応におけるサブバリアー融合阻害”, 2009 日本放射化学会年会・第 53 回放射化学討論会, (日本放射化学会), 東京, 9 月 (2009).
- 笠松良崇: “Development of the rapid α detection apparatus for aqueous chemistry of superheavy elements at RIKEN”, 理研超重元素化学ワークショップ 2010, 和光, 2 月 (2010).

Accelerator Group

Publications

Book • Proceedings

(Others)

Fukunishi N., Fujimaki M., Watanabe T., Kumagai K., Komiyama M., Watanabe H., Goto A., Hasebe H., Higurashi Y., Ikezawa E., Kageyama T., Kamigaito O., Kase M., Kuboki H., Kidera M., Nagase M., Maie T., Nakagawa T., Ohnishi J., Okuno H., Sakamoto N., Sekiguchi K., Suda K., Suzuki H., Wakasugi M., Watanabe Y., Yokouchi S., Yano Y., and Yamada K.: “Operating experience with the RIKEN Radioactive Isotope Beam Factory”, Proceedings of the 2009 Particle Accelerator Conference (PAC09), Vancouver, Canada, 2009-5, PAC09 Editor, Vancouver, pp. MO3GRI0-1-MO3GRI0-5 (2009).

Oral Presentations

(International Conference etc.)

Fukunishi N., Fujimaki M., Watanabe T., Kumagai K., Komiyama M., Watanabe H., Goto A., Hasebe H., Higurashi Y., Ikezawa E., Kageyama T., Kamigaito O., Kase M., Kuboki H., Kidera M., Nagase M., Maie T., Nakagawa T., Ohnishi J., Okuno H., Sakamoto N., Sekiguchi K., Suda K., Suzuki H., Wakasugi M., Watanabe Y., Yokouchi S., Yano Y., and Yamada K.: “Operating experience with the RIKEN Radioactive Isotope Beam Factory”, 23rd Particle Accelerator Conference (PAC09), Vancouver, Canada, May (2009).

(Domestic Conference)

Vorozhtsov S., Perepelkin E., Vorozhtsov A., 渡邊伸 ; 久保野 茂, 後藤 彰: “Beam simulations in computer-modelled 3D fields for RIKEN AVF cyclotron upgrade”, 第6回日本加速器学会年会, (日本加速器学会), 茨城県東海村, 8月(2009).

渡邊裕, 池沢英二, 佐藤洋 ; 奥野広樹, 中川孝秀, 日暮祥英, 大西純 ; 藤巻正樹, 福西暢尚, 横内茂, 熊谷桂子, 込山美咲, 渡辺博, 加瀬昌之, 後藤彰, 上垣外修 ; “理研リニアック(RILAC)新入射BT系建設状”, 第6回日本加速器学会年会, (日本加速器学会), 茨城県東海村, 8月(2009).

山田一成, 須田健嗣, 坂本成彦, 新井重昭, 藤澤博, 奥野広樹, 池沢英二, 加瀬昌之, 上垣外修 ; “理研RIBF新入射器RILAC2の加速空洞の設計および改造”, 第6回日本加速器学会年会, 茨城県東海村, 8月(2009).

渡邊環, 福西暢尚, 佐々木雄一朗, 加瀬昌之, 矢野安重: “高温超伝導電流センサーとSQUIDを用いたビーム電流モニターの実用化”, 第6回日本加速器学会年会, (日本加速器学会), 茨城県東海村, 8月(2009).

福西暢尚, 段塚知志, 藤巻正樹, 後藤彰, 上垣外修 ; 加瀬昌之, 長谷部裕雄, 久保木浩功, 大西純 ; 奥野広樹, 横内茂, 坂本成彦, 須田健嗣, 日暮祥英, 影山正, 木寺正憲, 中川孝秀, 池沢英二, 渡邊裕, 眞家武士, 込山美咲, 熊谷桂子, 長瀬誠, 山田一成, 渡邊環, 渡辺博: “RIビームファクトリー加速器系の現状”, 第6回日本加速器学会年会, 茨城県東海村, 8

月(2009).

池沢英二, 加瀬昌之, 渡邊裕, 大木智則, 藍原利光, 山内啓資, 内山暁仁, 小山田和幸, 田村匡史: “理研重イオンリニアックの現状報告”, 第6回日本加速器学会年会, (日本加速器学会), 茨城県東海村, 8月(2009).

須田健嗣, 藤巻正樹, 福西暢尚, 逸見政武, 上垣外修 ; 加瀬昌之, 小山亮, 熊谷桂子, 坂本成彦, 渡邊環, 山田一成: “理研RIBFにおける高周波系およびビームの安定度”, 第6回日本加速器学会年会, (日本加速器学会), 茨城県東海村, 8月(2009).

坂本成彦, 須田健嗣, 藤巻正樹, 後藤彰, 上垣外修 ; 加瀬昌之, 小山亮, 山田一成, 横内茂: “理研RIBF高周波系の現状”, 第6回日本加速器学会年会, (日本加速器学会), 茨城県東海村, 8月(2009).

Accelerator R&D Team

Publications

Book • Proceedings

(Others)

Fukunishi N., Fujimaki M., Watanabe T., Kumagai K., Komiyama M., Watanabe H., Goto A., Hasebe H., Higurashi Y., Ikezawa E., Kageyama T., Kamigaito O., Kase M., Kuboki H., Kidera M., Nagase M., Maie T., Nakagawa T., Ohnishi J., Okuno H., Sakamoto N., Sekiguchi K., Suda K., Suzuki H., Wakasugi M., Watanabe Y., Yokouchi S., Yano Y., and Yamada K.: “Operating experience with the RIKEN Radioactive Isotope Beam Factory”, Proceedings of the 2009 Particle Accelerator Conference (PAC09), Vancouver, Canada, 2009-5, PAC09 Editor, Vancouver, pp. MO3GRI0-1-MO3GRI0-5 (2009).

Oral Presentations

(International Conference etc.)

Fukunishi N., Fujimaki M., Watanabe T., Kumagai K., Komiyama M., Watanabe H., Goto A., Hasebe H., Higurashi Y., Ikezawa E., Kageyama T., Kamigaito O., Kase M., Kuboki H., Kidera M., Nagase M., Maie T., Nakagawa T., Ohnishi J., Okuno H., Sakamoto N., Sekiguchi K., Suda K., Suzuki H., Wakasugi M., Watanabe Y., Yokouchi S., Yano Y., and Yamada K.: “Operating experience with the RIKEN Radioactive Isotope Beam Factory”, 23rd Particle Accelerator Conference (PAC09), Vancouver, Canada, May (2009).

(Domestic Conference)

福西暢尚, 藤巻正樹, 込山美咲, 長瀬誠, 渡邊環, 山田一成, 熊谷桂子, 後藤彰, 長谷部裕雄, 日暮祥英, 池沢英二, 影山正, 加瀬昌之, 木寺正憲, 久保木浩功, 眞家武士, 中川孝秀, 大西純一, 奥野広樹, 龍頭啓充, 坂本成彦, 若杉昌徳, 横内茂, 上垣外修一, 矢野安重, 小山亮, 須田健嗣: “RI ビームファクトリーにおけるウランビーム加速試験”, 第5回日本加速器学会年会/第33回リニアック技術研究会, (日本加速器学会、リニアック技術研究会), 東広島, 8月(2008).

渡邊裕, 池沢英二, 佐藤洋一, 奥野広樹, 中川孝秀, 日暮祥英, 大西純一, 藤巻正樹, 福西暢尚, 横内茂, 熊谷桂子, 込山美咲, 渡辺博, 加瀬昌之, 後藤彰, 上垣外修一: “理研リニアック(RILAC)新入射BT系建設状”, 第6回日本加速器学会年会, (日本加速器学会), 茨城県東海村, 8月(2009).

山田一成, 須田健嗣, 坂本成彦, 新井重昭, 藤澤博, 奥野広樹, 池沢英二, 加瀬昌之, 上垣外修一: “理研RIBF新入射器RILAC2の加速空洞の設計および改造”, 第6回日本加速器学会年会, 茨城県東海村, 8月(2009).

福西暢尚, 段塚知志, 藤巻正樹, 後藤彰, 上垣外修一, 加瀬昌之, 長谷部裕雄, 久保木浩功, 大西純一, 奥野広樹, 横内茂, 坂本成彦, 須田健嗣, 日暮祥英, 影山正, 木寺正憲, 中川孝秀, 池沢英二, 渡邊裕, 眞家武士, 込山美咲, 熊谷桂子, 長瀬誠, 山田一成, 渡邊環, 渡辺博: “RI ビームファクトリー加速器系の現状”, 第6回日本加速器学会年会, 茨城県東海村, 8月(2009).

坂本成彦, 須田健嗣, 藤巻正樹, 後藤彰, 上垣外修一, 加瀬昌之, 小山亮, 山田一成, 横内茂: “理研RIBF高周波系の現状”, 第6回日本加速器学会年会, (日本加速器学会), 茨城県東海村, 8月(2009).

Ion Source Team

Publications

Book • Proceedings

(Others)

Fukunishi N., Fujimaki M., Watanabe T., Kumagai K., Komiyama M., Watanabe H., Goto A., Hasebe H., Higurashi Y., Ikezawa E., Kageyama T., Kamigaito O., Kase M., Kuboki H., Kidera M., Nagase M., Maie T., Nakagawa T., Ohnishi J., Okuno H., Sakamoto N., Sekiguchi K., Suda K., Suzuki H., Wakasugi M., Watanabe Y., Yokouchi S., Yano Y., and Yamada K.: “Operating experience with the RIKEN Radioactive Isotope Beam Factory”, Proceedings of the 2009 Particle Accelerator Conference (PAC09), Vancouver, Canada, 2009-5, PAC09 Editor, Vancouver, pp. MO3GRI0-1–MO3GRI0-5 (2009).

Oral Presentations

(International Conference etc.)

Fukunishi N., Fujimaki M., Watanabe T., Kumagai K., Komiyama M., Watanabe H., Goto A., Hasebe H., Higurashi Y., Ikezawa E., Kageyama T., Kamigaito O., Kase M., Kuboki H., Kidera M., Nagase M., Maie T., Nakagawa T., Ohnishi J., Okuno H., Sakamoto N., Sekiguchi K., Suda K., Suzuki H., Wakasugi M., Watanabe Y., Yokouchi S., Yano Y., and Yamada K.: “Operating experience with the RIKEN Radioactive Isotope Beam Factory”, 23rd Particle Accelerator Conference (PAC09), Vancouver, Canada, May (2009).

Seto Y., Kishi S., Ohmori T., Kanamori M., Tsuge K., Okumura A., Takada Y., Ezawa N., Watanabe S., Hashimoto H., Kidera M., and Takahashi K.: “On-site detection of chemical warfare agents by mass spectrometry and ion mobility spectrometry”, 57th ASMS Conference on Mass Spectrometry and Allied Topics, (ASMS), Philadelphia, USA, May–June (2009).

(Domestic Conference)

福西暢尚, 藤巻正樹, 込山美咲, 長瀬誠, 渡邊環, 山田一成, 熊谷桂子, 後藤彰, 長谷部裕雄, 日暮祥英, 池沢英二, 影山正, 加瀬昌之, 木寺正憲, 久保木浩功, 眞家武士, 中川孝秀, 大西純一, 奥野広樹, 龍頭啓充, 坂本成彦, 若杉昌徳, 横内茂, 上垣外修一, 矢野安重, 小山亮, 須田健嗣: “RI ビームファクトリーにおけるウランビーム加速試験”, 第5回日本加速器学会年会/第33回リニアック技術研究会, (日本加速器学会, リニアック技術研究会), 東広島, 8月(2008).

渡邊裕, 池沢英二, 佐藤洋一, 奥野広樹, 中川孝秀, 日暮祥英, 大西純一, 藤巻正樹, 福西暢尚, 横内茂, 熊谷桂子, 込山美咲, 渡辺博, 加瀬昌之, 後藤彰, 上垣外修一: “理研リニアック(RILAC)新入射BT系建設状”, 第6回日本加速器学会年会, (日本加速器学会), 茨城県東海村, 8月(2009).

福西暢尚, 段塚知志, 藤巻正樹, 後藤彰, 上垣外修一, 加瀬昌之, 長谷部裕雄, 久保木浩功, 大西純一, 奥野広樹, 横内茂, 坂本成彦, 須田健嗣, 日暮祥英, 影山正, 木寺正憲, 中川孝秀, 池沢英二, 渡邊裕, 眞家武士, 込山美咲, 熊谷桂子, 長瀬誠,

山田一成, 渡邊環, 渡辺博: “RI ビームファクトリー加速器系の現状”, 第6回日本加速器学会年会, 茨城県東海村, 8月(2009).

木寺正憲: “ECR イオン源と重イオン加速器(RILAC)を用いた極微量多元素同時質量分析法”, 2009日本放射化学学会年会・第53回放射化学討論会, (日本放射化学学会), 東京, 9月(2009).

RILAC Team

Publications

Journal

(Original Papers) *Subject to Peer Review

Kasuga H., Ohmori H., Mishima T., Watanabe Y., and Lin W.: "Investigation on mirror surface grinding characteristics of SiC materials", *J. Ceram. Process. Res.* **10**, No. 3, pp. 351–354 (2009). *

Kasuga H., Ohmori H., Lin W., Watanabe Y., Mishima T., and Doi T.: "Efficient and smooth grinding characteristics of monocrystalline 4H-SiC wafer", *J. Vac. Sci. Technol. B* **27**, No. 3, pp. 1578–1582 (2009). *

Kasuga H., Ohmori H., Watanabe Y., and Mishima T.: "Surface characteristics of efficient-ground alumina and zirconia ceramics for dental applications", *Key Eng. Mater.* **404**, 69–75 (2009). *

Kasuga H., Ohmori H., Lin W., Watanabe Y., Mishima T., and Doi T.: "Efficient super-smooth finishing characteristics of sic materials through the use of fine-grinding", *Key Eng. Mater.* **404**, 137–141 (2009). *

Book • Proceedings

(Others)

Fukunishi N., Fujimaki M., Watanabe T., Kumagai K., Komiyama M., Watanabe H., Goto A., Hasebe H., Higurashi Y., Ikezawa E., Kageyama T., Kamigaito O., Kase M., Kuboki H., Kidera M., Nagase M., Maie T., Nakagawa T., Ohnishi J., Okuno H., Sakamoto N., Sekiguchi K., Suda K., Suzuki H., Wakasugi M., Watanabe Y., Yokouchi S., Yano Y., and Yamada K.: "Operating experience with the RIKEN Radioactive Isotope Beam Factory", *Proceedings of the 2009 Particle Accelerator Conference (PAC09)*, Vancouver, Canada, 2009–5, PAC09 Editor, Vancouver, pp. MO3GRI0-1–MO3GRI0-5 (2009).

Oral Presentations

(International Conference etc.)

Fukunishi N., Fujimaki M., Watanabe T., Kumagai K., Komiyama M., Watanabe H., Goto A., Hasebe H., Higurashi Y., Ikezawa E., Kageyama T., Kamigaito O., Kase M., Kuboki H., Kidera M., Nagase M., Maie T., Nakagawa T., Ohnishi J., Okuno H., Sakamoto N., Sekiguchi K., Suda K., Suzuki H., Wakasugi M., Watanabe Y., Yokouchi S., Yano Y., and Yamada K.: "Operating experience with the RIKEN Radioactive Isotope Beam Factory", *23rd Particle Accelerator Conference (PAC09)*, Vancouver, Canada, May (2009).

Kasuga H., Ohmori H., Katahira K., Watanabe Y., and Mishima T.: "Efficient and precise grinding of silicon nitride (Si₃N₄) ceramics", *42nd CIRP Conference on Manufacturing Systems*, Grenoble, France, June (2009).

Kasuga H., Ohmori H., Watanabe Y., and Mishima T.: "Grinding characteristics of optical glass for surface roughness reduction", *5th International Conference on*

Leading Edge Manufacturing in 21st Century (LEM21), (Japan Society of Mechanical Engineers), Osaka, Dec. (2009).

(Domestic Conference)

福西暢尚, 藤巻正樹, 込山美咲, 長瀬誠, 渡邊環, 山田一成, 熊谷桂子, 後藤彰, 長谷部裕雄, 日暮祥英, 池沢英二, 影山正, 加瀬昌之, 木寺正憲, 久保木浩功, 眞家武士, 中川孝秀, 大西純一, 奥野広樹, 龍頭啓充, 坂本成彦, 若杉昌徳, 横内茂, 上垣外修一, 矢野安重, 小山亮, 須田健嗣: "RI ビームファクトリーにおけるウランビーム加速試験", 第5回日本加速器学会年会/第33回リニアック技術研究会, (日本加速器学会, リニアック技術研究会), 東広島, 8月(2008).

春日博, 三島健稔, 片平和俊, 渡邊裕, 大森整: "Si₃N₄における高能率・高精度加工の検討", 日本セラミックス協会2009年年会, (日本セラミックス協会), 野田, 3月(2009).

渡邊裕, 池沢英二, 佐藤洋一, 奥野広樹, 中川孝秀, 日暮祥英, 大西純一, 藤巻正樹, 福西暢尚, 横内茂, 熊谷桂子, 込山美咲, 渡辺博, 加瀬昌之, 後藤彰, 上垣外修一: "理研リニアック(RILAC)新入射BT系建設状", 第6回日本加速器学会年会, (日本加速器学会), 茨城県東海村, 8月(2009).

山田一成, 須田健嗣, 坂本成彦, 新井重昭, 藤澤博, 奥野広樹, 池沢英二, 加瀬昌之, 上垣外修一: "理研RIBF新入射器RILAC2の加速空洞の設計および改造", 第6回日本加速器学会年会, 茨城県東海村, 8月(2009).

福西暢尚, 段塚知志, 藤巻正樹, 後藤彰, 上垣外修一, 加瀬昌之, 長谷部裕雄, 久保木浩功, 大西純一, 奥野広樹, 横内茂, 坂本成彦, 須田健嗣, 日暮祥英, 影山正, 木寺正憲, 中川孝秀, 池沢英二, 渡邊裕, 眞家武士, 込山美咲, 熊谷桂子, 長瀬誠, 山田一成, 渡邊環, 渡辺博: "RIビームファクトリー加速器系の現状", 第6回日本加速器学会年会, 茨城県東海村, 8月(2009).

池沢英二, 加瀬昌之, 渡邊裕, 大木智則, 藍原利光, 山内啓資, 内山曉仁, 小山田和幸, 田村匡史: "理研重イオンリニアックの現状報告", 第6回日本加速器学会年会, (日本加速器学会), 茨城県東海村, 8月(2009).

須田健嗣, 藤巻正樹, 福西暢尚, 逸見政武, 上垣外修一, 加瀬昌之, 小山亮, 熊谷桂子, 坂本成彦, 渡邊環, 山田一成: "理研RIBFにおける高周波系およびビームの安定度", 第6回日本加速器学会年会, (日本加速器学会), 茨城県東海村, 8月(2009).

込山美咲, 藤巻正樹, 福西暢尚, 内山曉仁, 小田切淳一: "組み込みEPICSを用いた理研RIビームファクトリー新入射器制御系の開発", 第6回日本加速器学会年会, (日本加速器学会), 茨城県東海村, 8月(2009).

春日博, 渡邊裕, 三島健稔, 大森整: "精密モールドレンズ用光学ガラスの研削特性", 2009年度精密工学会秋季大会学術講演会, (精密工学会), 神戸, 9月(2009).

Cyclotron Team

Publications

Book • Proceedings

(Others)

Fukunishi N., Fujimaki M., Watanabe T., Kumagai K., Komiyama M., Watanabe H., Goto A., Hasebe H., Higurashi Y., Ikezawa E., Kageyama T., Kamigaito O., Kase M., Kuboki H., Kidera M., Nagase M., Maie T., Nakagawa T., Ohnishi J., Okuno H., Sakamoto N., Sekiguchi K., Suda K., Suzuki H., Wakasugi M., Watanabe Y., Yokouchi S., Yano Y., and Yamada K.: “Operating experience with the RIKEN Radioactive Isotope Beam Factory”, Proceedings of the 2009 Particle Accelerator Conference (PAC09), Vancouver, Canada, 2009–5, PAC09 Editor, Vancouver, pp. MO3GRI0-1–MO3GRI0-5 (2009).

Oral Presentations

(International Conference etc.)

Fukunishi N., Fujimaki M., Watanabe T., Kumagai K., Komiyama M., Watanabe H., Goto A., Hasebe H., Higurashi Y., Ikezawa E., Kageyama T., Kamigaito O., Kase M., Kuboki H., Kidera M., Nagase M., Maie T., Nakagawa T., Ohnishi J., Okuno H., Sakamoto N., Sekiguchi K., Suda K., Suzuki H., Wakasugi M., Watanabe Y., Yokouchi S., Yano Y., and Yamada K.: “Operating experience with the RIKEN Radioactive Isotope Beam Factory”, 23rd Particle Accelerator Conference (PAC09), Vancouver, Canada, May (2009).

(Domestic Conference)

福西暢尚, 藤巻正樹, 込山美咲, 長瀬誠, 渡邊環, 山田一成, 熊谷桂子, 後藤彰, 長谷部裕雄, 日暮祥英, 池沢英二, 影山正, 加瀬昌之, 木寺正憲, 久保木浩功, 眞冢武士, 中川孝秀, 大西純一, 奥野広樹, 龍頭啓充, 坂本成彦, 若杉昌徳, 横内茂, 上垣外修一, 矢野安重, 小山亮, 須田健嗣: “RI ビームファクトリーにおけるウランビーム加速試験”, 第5回日本加速器学会年会/第33回リニアック技術研究会, (日本加速器学会、リニアック技術研究会), 東広島, 8月(2008).

山田一成, 須田健嗣, 坂本成彦, 新井重昭, 藤澤博, 奥野広樹, 池沢英二, 加瀬昌之, 上垣外修一: “理研 RIBF 新入射器 RILAC2 の加速空洞の設計および改造”, 第6回日本加速器学会年会, 茨城県東海村, 8月(2009).

福西暢尚, 段塚知志, 藤巻正樹, 後藤彰, 上垣外修一, 加瀬昌之, 長谷部裕雄, 久保木浩功, 大西純一, 奥野広樹, 横内茂, 坂本成彦, 須田健嗣, 日暮祥英, 影山正, 木寺正憲, 中川孝秀, 池沢英二, 渡邊裕, 眞冢武士, 込山美咲, 熊谷桂子, 長瀬誠, 山田一成, 渡邊環, 渡辺博: “RI ビームファクトリー加速器系の現状”, 第6回日本加速器学会年会, 茨城県東海村, 8月(2009).

須田健嗣, 藤巻正樹, 福西暢尚, 逸見政武, 上垣外修一, 加瀬昌之, 小山亮, 熊谷桂子, 坂本成彦, 渡邊環, 山田一成: “理研 RIBF における高周波系およびビームの安定度”, 第6回日本加速器学会年会, (日本加速器学会), 茨城県東海村, 8月(2009).

坂本成彦, 須田健嗣, 藤巻正樹, 後藤彰, 上垣外修一, 加瀬昌之, 小山亮, 山田一成, 横内茂: “理研 RIBF 高周波系の現状”, 第6回日本加速器学会年会, (日本加速器学会), 茨城県東海村, 8月(2009).

Beam Dynamics & Diagnostics Team

Publications

Journal

(Original Papers) *Subject to Peer Review

Ichikawa Y., Onishi T., Suzuki D., Iwasaki H., Naik V., Kubo T., Chakrabarti A., Aoi N., Brown A., Fukuda N., Kubono S., Motobayashi T., Nakabayashi T., Nakao T., Okumura T., Ong H., Suzuki H., Suzuki M., Teranishi T., Yamada K., Yamaguchi H., and Sakurai H.: “Investigation into behavior of weakly-bound proton via $B(GT)$ measurement for the β decay of ^{24}Si ”, AIP Conf. Proc. **1165**, 98–101 (2009).

Ichikawa Y., Kubo T., Aoi N., Naik V., Chakrabarti A., Fukuda N., Iwasaki H., Kubono S., Motobayashi T., Nakabayashi T., Nakao T., Okumura T., Ong H., Onishi T., Suzuki D., Suzuki H., Suzuki M., Teranishi T., Yamada K., Yamaguchi H., and Sakurai H.: “Beta-decay study of $T_z = -2$ proton-rich nucleus ^{24}Si ”, Eur. Phys. J. A **42**, 375–378 (2009). *

Kikuchi S., Saito Y., Ryuto H., Fukunishi N., Abe T., Tanaka H., and Tsujimoto H.: “Effects of heavy-ion beams on chromosomes of common wheat, *Triticum aestivum*”, Muta. Res./Fund. Mol. Mech. Mutagen. **669**, 63–66 (2009). *

Takeuchi S., Aoi N., Motobayashi T., Ota S., Takeshita E., Suzuki H., Baba H., Fukui T., Hashimoto Y., Ieki K., Imai N., Iwasaki H., Kanno S., Kondo Y., Kubo T., Kurita K., Minemura T., Nakamura T., Okumura T., Onishi T., Sakurai H., Shimoura S., Sugou R., Suzuki D., Suzuki M., Takashina M., Tamaki M., Tanaka K., Togano Y., and Yamada K.: “Low-Iying States in ^{32}Mg studied by proton inelastic scattering”, Phys. Rev. C **79**, No. 5, pp. 054319-1–054319-11 (2009). *

Ichikawa Y., Onishi T., Suzuki D., Iwasaki H., Naik V., Kubo T., Chakrabarti A., Aoi N., Brown A., Fukuda N., Kubono S., Motobayashi T., Nakabayashi T., Nakao T., Okumura T., Ong H., Suzuki H., Suzuki M., Teranishi T., Yamada K., Yamaguchi H., and Sakurai H.: “Beta decay of the proton-rich nucleus ^{24}Si and its mirror asymmetry”, Phys. Rev. C **80**, 044302-1–044302-12 (2009). *

仲條真介, 長谷川聡, 吉田宏, 漆原昌二, 阿部陽, 阿部知子, 福西暢尚, 龍頭啓充, 大清水保見: “低アミロース短稈ヒエ新品種「ヒエ岩手1号」, 「ヒエ岩手2号」, 「ヒエ岩手3号」の育成”, 雑穀研究, No. 24, pp. 12–19 (2009). *

Book • Proceedings

(Review)

阿部知子, 林依子, 風間裕介, 竹久妃奈子, 龍頭啓充, 福西暢尚: “重イオンビーム育種技術の開発と実用化”, 荷電粒子ビームの工業への応用と第132委員会 第188回研究会資料, 東京, 2009–11, 日本学術振興会, 東京, pp. 27–34 (2009).

(Others)

Fukunishi N., Fujimaki M., Watanabe T., Kumagai K., Komiyama M., Watanabe H., Goto A., Hasebe H.,

Higurashi Y., Ikezawa E., Kageyama T., Kamigaito O., Kase M., Kuboki H., Kidera M., Nagase M., Maie T., Nakagawa T., Ohnishi J., Okuno H., Sakamoto N., Sekiguchi K., Suda K., Suzuki H., Wakasugi M., Watanabe Y., Yokouchi S., Yano Y., and Yamada K.: “Operating experience with the RIKEN Radioactive Isotope Beam Factory”, Proceedings of the 2009 Particle Accelerator Conference (PAC09), Vancouver, Canada, 2009–5, PAC09 Editor, Vancouver, pp. MO3GRI0-1–MO3GRI0-5 (2009).

Oral Presentations

(International Conference etc.)

Fukunishi N., Fujimaki M., Watanabe T., Kumagai K., Komiyama M., Watanabe H., Goto A., Hasebe H., Higurashi Y., Ikezawa E., Kageyama T., Kamigaito O., Kase M., Kuboki H., Kidera M., Nagase M., Maie T., Nakagawa T., Ohnishi J., Okuno H., Sakamoto N., Sekiguchi K., Suda K., Suzuki H., Wakasugi M., Watanabe Y., Yokouchi S., Yano Y., and Yamada K.: “Operating experience with the RIKEN Radioactive Isotope Beam Factory”, 23rd Particle Accelerator Conference (PAC09), Vancouver, Canada, May (2009).

Ichikawa Y., Onishi T., Suzuki D., Iwasaki H., Naik V., Kubo T., Chakrabarti A., Aoi N., Brown A., Fukuda N., Kubono S., Motobayashi T., Nakabayashi T., Nakao T., Okumura T., Ong H., Suzuki H., Suzuki M., Teranishi T., Yamada K., Yamaguchi H., and Sakurai H.: “Investigation into behavior of weakly-bound proton via $B(GT)$ measurement for the β decay of ^{24}Si ”, International Conference on Nuclear Structure and Dynamics (NSD09), (University of Zagreb), Dubrovnik, Croatia, May (2009).

Ichikawa Y., Onishi T., Suzuki D., Iwasaki H., Naik V., Kubo T., Chakrabarti A., Aoi N., Brown A., Fukuda N., Kubono S., Motobayashi T., Nakabayashi T., Nakao T., Okumura T., Ong H., Suzuki H., Suzuki M., Teranishi T., Yamada K., Yamaguchi H., and Sakurai H.: “Beta decay of ^{24}Si and mirror asymmetry of Gamow-Teller transition strength”, 3rd Joint Meeting of the Nuclear Physics Divisions of the APS and JPS (Hawaii 2009), Hawaii, USA, Oct. (2009).

Ichikawa Y., Onishi T., Suzuki D., Iwasaki H., Naik V., Kubo T., Chakrabarti A., Aoi N., Brown A., Fukuda N., Kubono S., Motobayashi T., Nakabayashi T., Nakao T., Okumura T., Ong H., Suzuki H., Suzuki M., Teranishi T., Yamada K., Yamaguchi H., and Sakurai H.: “Gamow-Teller transition of proton-rich nucleus ^{24}Si ”, 7th Japan-China Joint Nuclear Physics Symposium, (University of Tsukuba), Tsukuba, Nov. (2009).

Ichikawa Y., Onishi T., Suzuki D., Iwasaki H., Naik V., Kubo T., Chakrabarti A., Aoi N., Brown A., Fukuda N., Kubono S., Motobayashi T., Nakabayashi T., Nakao T., Okumura T., Ong H., Suzuki H., Suzuki M., Teranishi T., Yamada K., Yamaguchi H., and Sakurai H.: “Mir-

ror asymmetry for $B(GT)$ of ^{24}Si induced by Thomas-Ehrman shift”, Tours Symposium on Nuclear Physics and Astrophysics VII (TOURS 2009), (Konan University), Kobe, Nov. (2009).

(Domestic Conference)

福西暢尚, 藤巻正樹, 込山美咲, 長瀬誠, 渡邊環, 山田一成, 熊谷桂子, 後藤彰, 長谷部裕雄, 日暮祥英, 池沢英二, 影山正, 加瀬昌之, 木寺正憲, 久保木浩功, 眞冢武士, 中川孝秀, 大西純一, 奥野広樹, 籠頭啓充, 坂本成彦, 若杉昌徳, 横内茂, 上垣外修一, 矢野安重, 小山亮, 須田健嗣: “RI ビームファクトリーにおけるウランビーム加速試験”, 第5回日本加速器学会年会/第33回リニアック技術研究会, (日本加速器学会, リニアック技術研究会), 東広島, 8月(2008).

渡邊裕, 池沢英二, 佐藤洋一, 奥野広樹, 中川孝秀, 日暮祥英, 大西純一, 藤巻正樹, 福西暢尚, 横内茂, 熊谷桂子, 込山美咲, 渡辺博, 加瀬昌之, 後藤彰, 上垣外修一: “理研リニアック(RILAC)新入射BT系建設状”, 第6回日本加速器学会年会, (日本加速器学会), 茨城県東海村, 8月(2009).

山田一成, 須田健嗣, 坂本成彦, 新井重昭, 藤澤博, 奥野広樹, 池沢英二, 加瀬昌之, 上垣外修一: “理研 RIBF 新入射器 RILAC2 の加速空洞の設計および改造”, 第6回日本加速器学会年会, 茨城県東海村, 8月(2009).

渡邊環, 福西暢尚, 佐々木雄一朗, 加瀬昌之, 矢野安重: “高温超伝導電流センサーと SQUID を用いたビーム電流モニターの実用化”, 第6回日本加速器学会年会, (日本加速器学会), 茨城県東海村, 8月(2009).

福西暢尚, 段塚知志, 藤巻正樹, 後藤彰, 上垣外修一, 加瀬昌之, 長谷部裕雄, 久保木浩功, 大西純一, 奥野広樹, 横内茂, 坂本成彦, 須田健嗣, 日暮祥英, 影山正, 木寺正憲, 中川孝秀, 池沢英二, 渡邊裕, 眞冢武士, 込山美咲, 熊谷桂子, 長瀬誠, 山田一成, 渡邊環, 渡辺博: “RI ビームファクトリー加速器系の現状”, 第6回日本加速器学会年会, 茨城県東海村, 8月(2009).

須田健嗣, 藤巻正樹, 福西暢尚, 逸見政武, 上垣外修一, 加瀬昌之, 小山亮, 熊谷桂子, 坂本成彦, 渡邊環, 山田一成: “理研 RIBF における高周波系およびビームの安定度”, 第6回日本加速器学会年会, (日本加速器学会), 茨城県東海村, 8月(2009).

坂本成彦, 須田健嗣, 藤巻正樹, 後藤彰, 上垣外修一, 加瀬昌之, 小山亮, 山田一成, 横内茂: “理研 RIBF 高周波系の現状”, 第6回日本加速器学会年会, (日本加速器学会), 茨城県東海村, 8月(2009).

込山美咲, 藤巻正樹, 福西暢尚, 内山曉仁, 小田切淳一: “組み込み EPICS を用いた理研 RI ビームファクトリー新入射器制御系の開発”, 第6回日本加速器学会年会, (日本加速器学会), 茨城県東海村, 8月(2009).

Cryogenic Technology Team

Publications

Book • Proceedings

(Others)

Fukunishi N., Fujimaki M., Watanabe T., Kumagai K., Komiyama M., Watanabe H., Goto A., Hasebe H., Higurashi Y., Ikezawa E., Kageyama T., Kamigaito O., Kase M., Kuboki H., Kidera M., Nagase M., Maie T., Nakagawa T., Ohnishi J., Okuno H., Sakamoto N., Sekiguchi K., Suda K., Suzuki H., Wakasugi M., Watanabe Y., Yokouchi S., Yano Y., and Yamada K.: “Operating experience with the RIKEN Radioactive Isotope Beam Factory”, Proceedings of the 2009 Particle Accelerator Conference (PAC09), Vancouver, Canada, 2009–5, PAC09 Editor, Vancouver, pp. MO3GRI0-1–MO3GRI0-5 (2009).

Oral Presentations

(International Conference etc.)

Fukunishi N., Fujimaki M., Watanabe T., Kumagai K., Komiyama M., Watanabe H., Goto A., Hasebe H., Higurashi Y., Ikezawa E., Kageyama T., Kamigaito O., Kase M., Kuboki H., Kidera M., Nagase M., Maie T., Nakagawa T., Ohnishi J., Okuno H., Sakamoto N., Sekiguchi K., Suda K., Suzuki H., Wakasugi M., Watanabe Y., Yokouchi S., Yano Y., and Yamada K.: “Operating experience with the RIKEN Radioactive Isotope Beam Factory”, 23rd Particle Accelerator Conference (PAC09), Vancouver, Canada, May (2009).

(Domestic Conference)

福西暢尚, 藤巻正樹, 込山美咲, 長瀬誠, 渡邊環, 山田一成, 熊谷桂子, 後藤彰, 長谷部裕雄, 日暮祥英, 池沢英二, 影山正, 加瀬昌之, 木寺正憲, 久保木浩功, 眞家武士, 中川孝秀, 大西純一, 奥野広樹, 龍頭啓充, 坂本成彦, 若杉昌徳, 横内茂, 上垣外修一, 矢野安重, 小山亮, 須田健嗣: “RI ビームファクトリーにおけるウランビーム加速試験”, 第5回日本加速器学会年会/第33回リニアック技術研究会, (日本加速器学会、リニアック技術研究会), 東広島, 8月(2008).

福西暢尚, 段塚知志, 藤巻正樹, 後藤彰, 上垣外修一, 加瀬昌之, 長谷部裕雄, 久保木浩功, 大西純一, 奥野広樹, 横内茂, 坂本成彦, 須田健嗣, 日暮祥英, 影山正, 木寺正憲, 中川孝秀, 池沢英二, 渡邊裕, 眞家武士, 込山美咲, 熊谷桂子, 長瀬誠, 山田一成, 渡邊環, 渡辺博: “RI ビームファクトリー加速器系の現状”, 第6回日本加速器学会年会, 茨城県東海村, 8月(2009).

Instrumentation Development Group

Publications

Journal

(Original Papers) *Subject to Peer Review

Nagae D., Asahi K., Ueno H., Kameda D., Takemura M., Takase T., Yoshimi A., Sugimoto T., Nagatomo T., Kobayashi Y., Uchida M., Shimada K., Arai T., Inoue T., Kagami S., and Hatakeyama N.: "Measurement of Electric Quadrupole Moments for ^{31}Al Using Spin Polarized RI Beams", AIP Conf. Proc. **915**, 853–856 (2007). *

Shimada K., Nagae D., Asahi K., Arai T., Takemura M., Inoue T., Takase T., Kagami S., Hatakeyama N., Kobayashi Y., Ueno H., Yoshimi A., Kameda D., Nagatomo T., Sugimoto T., Kubono S., Yamaguchi H., Wakabayashi Y., Amadio G., Hayakawa S., Murata J., and Kawamura H.: "Production of Polarized Radioactive Beams via The Inverse-kinematics Reactions and Their Applications", AIP Conf. Proc. **915**, 857–860 (2007). *

Asahi K., Ueno H., Shimada K., Nagatomo T., Yoshimi A., Nagae D., Kameda D., Uchida M., Inoue T., Hatakeyama N., Kagami S., Hasama Y., Suzuki K., Murata J., Kawamura H., Narita K., and Ishihara M.: "Nuclear Structure Studies with Polarized Radioactive Beams", AIP Conf. Proc. **1149**, 90–99 (2009). *

Nagatomo T., Shimada K., Asahi K., Balabanski D. L., Daugas J., Depuydt M., De Rydt M., Gaodefroy L., Grevy S., Hasama Y., Ichikawa Y., Kameda D., Morel P., Perrot L., Stodel C., Thomas J. C., Vanderheijden W., Vermeulen N., Vingerhoets P., Yoshimi A., Neyens G., and Ueno H.: "Electric quadrupole moment of the neutron-rich ^{33}Al ", Eur. Phys. J. A **42**, No. 3, pp. 383–385 (2009). *

De Rydt M., Neyens G., Asahi K., Balabanski D. L., Daugas J., Depuydt M., Gaodefroy L., Grevy S., Hasama Y., Ichikawa Y., Morel P., Nagatomo T., Ohtsuka T., Perrot L., Shimada K., Stodel C., Thomas J., Ueno H., Utsuno Y., Wannes V., Vermeulen N., Vingerhoets P., and Yoshimi A.: "Precision measurement of the electric quadrupole moment of ^{31}Al and determination of the effective proton charge in the sd-shell", Phys. Lett. B **678**, 344–349 (2009). *

De Rydt M., Balabanski D. L., Daugas J., Himpe P., Kameda D., Lozeva R., Morel P., Perrot L., Shimada K., Stodel C., Sugimoto T., Thomas J. C., Ueno H., Vermeulen N., Vingerhoets P., Yoshimi A., and Neyens G.: "*g* factors of ^{17}N and ^{18}N remeasured", Phys. Rev. C **80**, No. 3, pp. 037306-1–037306-4 (2009). *

Book • Proceedings

(Others)

Fukunishi N., Fujimaki M., Watanabe T., Kumagai K., Komiyama M., Watanabe H., Goto A., Hasebe H., Higurashi Y., Ikezawa E., Kageyama T., Kamigaito

O., Kase M., Kuboki H., Kidera M., Nagase M., Maie T., Nakagawa T., Ohnishi J., Okuno H., Sakamoto N., Sekiguchi K., Suda K., Suzuki H., Wakasugi M., Watanabe Y., Yokouchi S., Yano Y., and Yamada K.: "Operating experience with the RIKEN Radioactive Isotope Beam Factory", Proceedings of the 2009 Particle Accelerator Conference (PAC09), Vancouver, Canada, 2009–5, PAC09 Editor, Vancouver, pp. MO3GRI0-1–MO3GRI0-5 (2009).

Oral Presentations

(International Conference etc.)

Fukunishi N., Fujimaki M., Watanabe T., Kumagai K., Komiyama M., Watanabe H., Goto A., Hasebe H., Higurashi Y., Ikezawa E., Kageyama T., Kamigaito O., Kase M., Kuboki H., Kidera M., Nagase M., Maie T., Nakagawa T., Ohnishi J., Okuno H., Sakamoto N., Sekiguchi K., Suda K., Suzuki H., Wakasugi M., Watanabe Y., Yokouchi S., Yano Y., and Yamada K.: "Operating experience with the RIKEN Radioactive Isotope Beam Factory", 23rd Particle Accelerator Conference (PAC09), Vancouver, Canada, May (2009).

Ichikawa Y., Onisi T. K., Suzuki D., Iwasaki H., Kubo T., Naik V., Chakrabarti A., Aoi N., Brown A. B., Fukuda N., Kubono S., Motobayashi T., Nakabayashi T., Nakamura T., Nakao T., Okumura T., Ong H., Suzuki H., Suzuki M. K., Teranishi T., Yamaguchi H., and Sakurai H.: "Proton-rich nuclear structure investigated by β decay of ^{24}Si ", ICHOR-EFES International Symposium on New Facet of Spin-Isospin Responses (SIR2010), (University of Tokyo), Tokyo, Feb. (2010).

Ichikawa Y., Onisi T. K., Suzuki D., Iwasaki H., Kubo T., Naik V., Chakrabarti A., Aoi N., Brown A. B., Fukuda N., Kubono S., Motobayashi T., Nakabayashi T., Nakamura T., Nakao T., Okumura T., Ong H., Suzuki H., Suzuki M. K., Teranishi T., Yamaguchi H., and Sakurai H.: "Mirror asymmetry investigated by β decay of proton-rich ^{24}Si ", International Symposium on Frontiers of Researches in Exotic Nuclear Structures (Niigata2010), (Niigata University), Toka-machi, Niigata Pref., Mar. (2010).

SLOWRI Team

Publications

Journal

(Original Papers) *Subject to Peer Review

Takamine A., Wada M., Okada K., Nakamura T., Sonoda T., Lioubimov V., Iimura H., Yamazaki Y., Kanai Y., Kojima T., Yoshida A., Kubo T., Katayama I., Ohtani S., Wollnik H., and Hans A. S.: "Isotope shift measurements of $^{11,9,7}\text{Be}^+$ ", Eur. Phys. J. A, pp. 1-5 (2009).

*

Oral Presentations

(International Conference etc.)

Wada M.: "Precision laser spectroscopy of radioactive Be isotopes and prospects for SLOWRI facility at RIKEN", 8th International Workshop on APPLICATION OF LASERS AND STORAGE DEVICES IN ATOMIC NUCLEI RESEARCH, (FLNR), Poznan, Poland, June (2009).

Sasaki A., Wakui T., Furukawa T., Kazato M., Wada M., Sonoda T., Takamine A., Kobayashi T., Nishimura M., Ueno H., Yoshimi A., Aoi N., Nishimura S., Togano Y., Takechi M., Kondo Y., Hatakeyama A., Matsuura Y., Kato Y., Odahara A., Shimoda T., Asahi K., Shinozuka T., Motobayashi T., and Matsuo Y.: "Fluorescence detection system for nuclear laser spectroscopy of Rb in superfluid helium", 3rd Joint Meeting of the Nuclear Physics Divisions of the APS and JPS (Hawaii 2009), Hawaii, USA, Oct. (2009).

(Domestic Conference)

高峰愛子: "Be 同位体の荷電半径測定に向けて", 第4回「停止・低速不安定核を用いた核分光研究」研究会, (「停止・低速不安定核を用いた核分光研究」研究会), 仙台, 12月 (2007).

Polarized RI Beam Team

Publications

Journal

(Original Papers) *Subject to Peer Review

- Nagae D., Asahi K., Ueno H., Kameda D., Takemura M., Takase T., Yoshimi A., Sugimoto T., Nagatomo T., Kobayashi Y., Uchida M., Shimada K., Arai T., Inoue T., Kagami S., and Hatakeyama N.: “Measurement of Electric Quadrupole Moments for ^{31}Al Using Spin Polarized RI Beams”, AIP Conf. Proc. **915**, 853–856 (2007). *
- Shimada K., Nagae D., Asahi K., Arai T., Takemura M., Inoue T., Takase T., Kagami S., Hatakeyama N., Kobayashi Y., Ueno H., Yoshimi A., Kameda D., Nagatomo T., Sugimoto T., Kubono S., Yamaguchi H., Wakabayashi Y., Amadio G., Hayakawa S., Murata J., and Kawamura H.: “Production of Polarized Radioactive Beams via The Inverse-kinematics Reactions and Their Applications”, AIP Conf. Proc. **915**, 857–860 (2007). *
- Ohnishi T., Kubo T., Kusaka K., Yoshida A., Yoshida K., Fukuda N., Ohtake M., Yanagisawa Y., Takeda H., Kameda D., Yamaguchi Y., Aoi N., Yoneda K., Otsu H., Takeuchi S., Sugimoto T., Kondo Y., Scheit H., Gono Y., Sakurai H., Motobayashi T., Suzuki H., Nakao T., Kimura H., Mizoi Y., Matsushita M., Ieki K., Kuboki T., Yamaguchi T., Suzuki T., Ozawa A., Moriguchi T., Yasuda Y., Nakamura T., Nannichi T., Shimamura T., Nakayama Y., Geissel H., Weick H., Nolen J. A., Tarasov O. B., Nettleton A. S., Bazin D. P., Sherrill B. M., Morrissey D. J., and Mittig W.: “Identification of New Isotopes ^{125}Pd and ^{126}Pd Produced by In-Flight Fission of $345\text{ MeV/nucleon }^{238}\text{U}$: First Results from the RIKEN RI Beam Factory”, J. Phys. Soc. Jpn. **77**, No. 8, pp. 083201-1–083201-4 (2008). *
- Asahi K., Ueno H., Shimada K., Nagatomo T., Yoshimi A., Nagae D., Kameda D., Uchida M., Inoue T., Hatakeyama N., Kagami S., Hasama Y., Suzuki K., Murata J., Kawamura H., Narita K., and Ishihara M.: “Nuclear Structure Studies with Polarized Radioactive Beams”, AIP Conf. Proc. **1149**, 90–99 (2009). *
- Yoshimi A., Asahi K., Inoue T., Uchida M., Hatakeyama N., Tsuchiya M., and Kagami S.: “Nuclear Spin Maser at Highly Stabilized Low Magnetic Field and Search for Atomic EDM”, AIP Conf. Proc. **1149**, 249–252 (2009). *
- Ichikawa Y., Onishi T., Suzuki D., Iwasaki H., Naik V., Kubo T., Chakrabarti A., Aoi N., Brown A., Fukuda N., Kubono S., Motobayashi T., Nakabayashi T., Nakao T., Okumura T., Ong H., Suzuki H., Suzuki M., Teranishi T., Yamada K., Yamaguchi H., and Sakurai H.: “Investigation into behavior of weakly-bound proton via $B(\text{GT})$ measurement for the β decay of ^{24}Si ”, AIP Conf. Proc. **1165**, 98–101 (2009).
- Nagatomo T., Shimada K., Asahi K., Balabanski D. L., Daugas J., Depuydt M., De Rydt M., Gaudefroy L., Grevy S., Hasama Y., Ichikawa Y., Kameda D., Morel P., Perrot L., Stodel C., Thomas J. C., Vanderheijden W., Vermeulen N., Vingerhoets P., Yoshimi A., Neyens G., and Ueno H.: “Electric quadrupole moment of the neutron-rich ^{33}Al ”, Eur. Phys. J. A **42**, No. 3, pp. 383–385 (2009). *
- Ichikawa Y., Kubo T., Aoi N., Naik V., Chakrabarti A., Fukuda N., Iwasaki H., Kubono S., Motobayashi T., Nakabayashi T., Nakao T., Okumura T., Ong H., Onishi T., Suzuki D., Suzuki H., Suzuki M., Teranishi T., Yamada K., Yamaguchi H., and Sakurai H.: “Beta-decay study of $T_z = -2$ proton-rich nucleus ^{24}Si ”, Eur. Phys. J. A **42**, 375–378 (2009). *
- Hata M., Akiyama T., Ikeda Y., Kawamura H., Narota K., Ninomiya K., Ogawa N., Sato T., Seitabashi E., Sekiguchi Y., Tsutsui R., Yazawa K., and Murata J.: “Recent results on short-range gravity experiment”, J. Phys.: Con. Ser. **189**, 012019-01–012019-10 (2009). *
- Ninomiya K., Akiyama T., Hata M., Ikeda Y., Kawamura H., Narota K., Ogawa N., Sato T., Seitabashi E., Sekiguchi Y., Tsutsui R., Yazawa K., and Murata J.: “New experimental technique for short-range gravity measurement”, J. Phys.: Con. Ser. **189**, 012026-1–012026-7 (2009). *
- De Rydt M., Neyens G., Asahi K., Balabanski D. L., Daugas J., Depuydt M., Gaudefroy L., Grevy S., Hasama Y., Ichikawa Y., Morel P., Nagatomo T., Ohtsuka T., Perrot L., Shimada K., Stodel C., Thomas J., Ueno H., Utsuno Y., Wannes V., Vermeulen N., Vingerhoets P., and Yoshimi A.: “Precision measurement of the electric quadrupole moment of ^{31}Al and determination of the effective proton charge in the sd-shell”, Phys. Lett. B **678**, 344–349 (2009). *
- De Rydt M., Balabanski D. L., Daugas J., Himpe P., Kameda D., Lozeva R., Morel P., Perrot L., Shimada K., Stodel C., Sugimoto T., Thomas J. C., Ueno H., Vermeulen N., Vingerhoets P., Yoshimi A., and Neyens G.: “ g factors of ^{17}N and ^{18}N remeasured”, Phys. Rev. C **80**, No. 3, pp. 037306-1–037306-4 (2009). *
- Ichikawa Y., Onishi T., Suzuki D., Iwasaki H., Naik V., Kubo T., Chakrabarti A., Aoi N., Brown A., Fukuda N., Kubono S., Motobayashi T., Nakabayashi T., Nakao T., Okumura T., Ong H., Suzuki H., Suzuki M., Teranishi T., Yamada K., Yamaguchi H., and Sakurai H.: “Beta decay of the proton-rich nucleus ^{24}Si and its mirror asymmetry”, Phys. Rev. C **80**, 044302-1–044302-12 (2009). *
- Katayama N., Uchida M., Hashizume D., Niitaka S., Matsuno J., Matsumura D., Nishihata Y., Mizuki J., Takeshita N., Guazzi A., Nohara M., and Takagi H.: “Anomalous Metallic State in the Vicinity of Metal to Valence-Bond Solid Insulator Transition in LiVS_2 ”, Phys. Rev. Lett. **103**, 146405-1–146405-4 (2009). *

(Others)

Murata J., Akiyama T., Hata M., Hirayama Y., Ikeda Y., Ishii T., Kameda D., Kawamura H., Mitsuoka S., Miyatake H., Nagae D., Ninomiya K., Nitta M., Seitabashi E., and Toyoda T.: “Test of time reversal symmetry using polarized nuclei”, JAEA-Review **2009-036**, 62–63 (2009).

Oral Presentations

(International Conference etc.)

Ooe K., Yahagi W., Komori Y., Fujisawa H., Kikunaga H., Yoshimura T., Sato W., Takahashi N., Takahisa K., Haba H., Kudou Y., Ezaki Y., and Shinohara A.: “Studies of Extraction Behavior of Tungsten toward Solution Chemistry of Seaborgium (Element 106)”, International Workshop on Molecular Information and Dynamics 2008, (Osaka University Global COE Program), Taipei, Taiwan, Nov. (2008).

Ichikawa Y., Onishi T., Suzuki D., Iwasaki H., Naik V., Kubo T., Chakrabarti A., Aoi N., Brown A., Fukuda N., Kubono S., Motobayashi T., Nakabayashi T., Nakao T., Okumura T., Ong H., Suzuki H., Suzuki M., Teranishi T., Yamada K., Yamaguchi H., and Sakurai H.: “Investigation into behavior of weakly-bound proton via $B(GT)$ measurement for the β decay of ^{24}Si ”, International Conference on Nuclear Structure and Dynamics (NSD09), (University of Zagreb), Dubrovnik, Croatia, May (2009).

Furukawa T., Hatakeyama A., Fujikake K., Matsuura Y., Kobayashi T., Shimoda T., and Matsuo Y.: “Precision Laser Spectroscopy of Alkaline and Alkaline-like Atoms in Superfluid Helium”, 19th International Conference on Laser Spectroscopy (ICOLS2009), Kussharo, June (2009).

Ueno H.: “Nuclear moments of neutron-rich aluminium isotopes”, Gordon Research Conference on Nuclear Chemistry, New London, USA, June–June (2009).

Ueno H.: “Electromagnetic moments of exotic nuclei”, Advanced Studies Institute: Symmetries and Spin (SPIN-Praha-2009), (Charles University in Prague), Prague, Czech, July–Aug. (2009).

Inoue T.: “A ^{129}Xe active spin maser with digitalized feedback”, 3rd Joint Meeting of the Nuclear Physics Divisions of the APS and JPS (Hawaii 2009), Hawaii, USA, Oct. (2009).

Ichikawa Y., Onishi T., Suzuki D., Iwasaki H., Naik V., Kubo T., Chakrabarti A., Aoi N., Brown A., Fukuda N., Kubono S., Motobayashi T., Nakabayashi T., Nakao T., Okumura T., Ong H., Suzuki H., Suzuki M., Teranishi T., Yamada K., Yamaguchi H., and Sakurai H.: “Beta decay of ^{24}Si and mirror asymmetry of Gamow-Teller transition strength”, 3rd Joint Meeting of the Nuclear Physics Divisions of the APS and JPS (Hawaii 2009), Hawaii, USA, Oct. (2009).

Yoshimi A.: “Development of Rb atomic magnetometer

for EDM experiment with ^{129}Xe spin maser”, 3rd Joint Meeting of the Nuclear Physics Divisions of the APS and JPS (Hawaii 2009), Hawaii, USA, Oct. (2009).

Sasaki A., Wakui T., Furukawa T., Kazato M., Wada M., Sonoda T., Takamine A., Kobayashi T., Nishimura M., Ueno H., Yoshimi A., Aoi N., Nishimura S., Togano Y., Takechi M., Kondo Y., Hatakeyama A., Matsuura Y., Kato Y., Odahara A., Shimoda T., Asahi K., Shinozuka T., Motobayashi T., and Matsuo Y.: “Fluorescence detection system for nuclear laser spectroscopy of Rb in superfluid helium”, 3rd Joint Meeting of the Nuclear Physics Divisions of the APS and JPS (Hawaii 2009), Hawaii, USA, Oct. (2009).

Suzuki K.: “Observation of stress effect on iron diffusion in Si by Mössbauer spectroscopy”, 3rd Joint Meeting of the Nuclear Physics Divisions of the APS and JPS (Hawaii 2009), Hawaii, USA, Oct. (2009).

Ueno H., Yoshimi A., and Asahi K.: “RIPS upgrade and physics programs”, 3rd Joint Meeting of the Nuclear Physics Divisions of the APS and JPS (Hawaii 2009), Hawaii, USA, Oct. (2009).

Ichikawa Y., Onishi T., Suzuki D., Iwasaki H., Naik V., Kubo T., Chakrabarti A., Aoi N., Brown A., Fukuda N., Kubono S., Motobayashi T., Nakabayashi T., Nakao T., Okumura T., Ong H., Suzuki H., Suzuki M., Teranishi T., Yamada K., Yamaguchi H., and Sakurai H.: “Gamow-Teller transition of proton-rich nucleus ^{24}Si ”, 7th Japan-China Joint Nuclear Physics Symposium, (University of Tsukuba), Tsukuba, Nov. (2009).

Ichikawa Y., Onishi T., Suzuki D., Iwasaki H., Naik V., Kubo T., Chakrabarti A., Aoi N., Brown A., Fukuda N., Kubono S., Motobayashi T., Nakabayashi T., Nakao T., Okumura T., Ong H., Suzuki H., Suzuki M., Teranishi T., Yamada K., Yamaguchi H., and Sakurai H.: “Mirror asymmetry for $B(GT)$ of ^{24}Si induced by Thomas-Ehrman shift”, Tours Symposium on Nuclear Physics and Astrophysics VII (TOURS 2009), (Konan University), Kobe, Nov. (2009).

Yoshimi A.: “Structures of neutron-rich Si, S and P isotopes studied from electromagnetic moments”, International Workshop on Physics of Nuclei at Extreme, (Tokyo Institute of Technology), Tokyo, Jan. (2010).

Inoue T.: “Ultrahigh precision observation of nuclear spin precession and application to EDM measurement”, International Workshop on Physics of Nuclei at Extreme, (Tokyo Institute of Technology), Tokyo, Jan. (2010).

(Domestic Conference)

佐藤 渉, 田中 稔久, 吉田 泰彦, 岩田 忠久: “ポリ [(R)-3-ヒドロキシブチレート] の平面ジグザグ構造 (β 構造) の結晶構造解析”, 第8回グリーン・サステイナブルケミストリーシンポジウム (GSC シンポジウム), (グリーン・サステイナブルケミストリーネットワーク), 東京, 3月 (2008).

胡子昇 郎, 酒向正己, 村上哲也, 新田稔, 池田友樹, 中谷祐輔, 川村広和, 豊田健司, 村田次郎, 冢城和夫, 中井陽 一, 西村 俊一, 高田 栄 一: “中間エネルギー重イオン衝突における荷

- 電パイオン生成 (I)”, 日本物理学会第 64 回年次大会, 東京, 3 月 (2009).
- 酒向正己, 胡子昇一郎, 村上哲也, 新田稔, 池田友樹, 中谷祐輔, 川村広和, 豊田健司, 村田次郎, 家城和夫, 中井陽一, 西村俊一, 高田栄一: “中間エネルギー重イオン衝突における荷電パイオン生成 (II)”, 日本物理学会第 64 回年次大会, 東京, 3 月 (2009).
- 古川武, 畠山温, 藤掛浩太郎, 松浦佑一, 小林徹, 下田正, 松尾由賀利: “超流動ヘリウム中に植え込まれたアルカリおよびアルカリ様原子の精密レーザー分光と光ポンピング”, 第 6 回 AMO 討論会, 豊中, 6 月 (2009).
- 井上壯志: “ ^{129}Xe 原子 EDM 測定のためのスピンメーザー開発”, 東京工業大学研究会「Fundamental Physics Using Atoms」, (東京工業大学), 東京, 8 月 (2009).
- 長友傑, 小林義男, 久保謙哉, 山田康洋, 三原基嗣, 佐藤涉, 宮崎淳, 佐藤眞一, 北川敦志: “プラスチックシンチレーション検出器を用いた ^{57}Mn インビームメスbauer分光における S/N 比の向上”, 2009 日本放射化学学会年会・第 53 回放射化学討論会, (日本放射化学会), 東京, 9 月 (2009).
- 長友傑, 小林義男, 久保謙哉, 山田康洋, 三原基嗣, 佐藤涉, 宮崎淳, 佐藤眞一, 北川敦志: “酸化アルミニウム固体中の ^{57}Mn インビーム・メスbauer分光実験”, 2009 日本放射化学学会年会・第 53 回放射化学討論会, (日本放射化学会), 東京, 9 月 (2009).
- 長友傑, 小林義男, 久保謙哉, 山田康洋, 三原基嗣, 佐藤涉, 宮崎淳, 佐藤眞一, 北川敦志: “酸化マグネシウム固体中の ^{57}Mn インビーム・メスbauer分光実験”, 2009 日本放射化学学会年会・第 53 回放射化学討論会, (日本放射化学会), 東京, 9 月 (2009).
- 松浦佑一, 古川武, 藤掛浩太郎, 畠山温, 小林徹, 立川真樹, 松尾由賀利: “超流動ヘリウム中での光ポンピング法を用いた Au 原子の偏極生成”, 日本物理学会 2009 年秋季大会, 熊本, 9 月 (2009).
- 長友傑, 小林義男, 三原基嗣, 久保謙哉, 山田康洋, 佐藤涉, 宮崎淳, 佐藤眞一, 北川敦志: “プラスチック検出器を用いた ^{57}Mn インビームメスbauer分光の S/N 比の向上”, 平成 21 年度京都大学原子炉実験所専門研究会「短寿命核および放射線を用いた物性研究 (II)」研究会, 大阪府熊取町, 12 月 (2009).
- 上野秀樹: “RIKEN nuclear-moment measurements: Current researches and perspectives”, Workshop on exotic nuclei and modern shell models, (東京工業大学), 東京, 2 月 (2010).
- 松浦佑一, 古川武, 小林徹, 畠山温, 加藤裕樹, 立川真樹, 松尾由賀利: “Au 原子の光ポンピングに向けた紫外領域光源開発”, 日本物理学会第 65 回年次大会, 岡山, 3 月 (2010).
- 聖代橋悦子, Behr J. A., 平山賀一, 川村広和, Levy P., 二宮一史, 小川就也, 大西潤一, Pearson M., 豊田健司, 村田次郎: “TRIUMF-ISAC における偏極 ^8Li を用いた時間反転対称性の破れ探索実験”, 日本物理学会第 65 回年次大会, 岡山, 3 月 (2010).
- 川村広和, 秋山岳伸, Behr J. A., 秦麻記, 平山賀一, 池田友樹, 石井哲朗, 亀田大輔, Levy P., 宮原直亮, 宮武宇也, 村田次郎, 中谷祐輔, 長江大輔, 二宮一史, 新田稔, 大西潤一, 聖代橋悦子, 豊田健司, 塚田和司, 渡辺裕: “KEK-TRIAC における偏極 ^8Li を用いた時間反転対称性の研究”, 日本物理学会第 65 回年次大会, 岡山, 3 月 (2010).
- 二宮一史, 秋山岳伸, 小川就也, 川村広和, 関口雄太, 西尾悠法, 秦麻記, 渡邊健太郎, 村田次郎: “ピコ精度画像処理型変位計を用いた近距離重力実験 2”, 日本物理学会第 65 回年次大会, 岡山, 3 月 (2010).
- 川村広和, 秋山岳伸, Behr J. A., 秦麻記, 平山賀一, 池田友樹, 石井哲朗, 亀田大輔, Levy P., 宮原直亮, 宮武宇也, 光岡真一, 村田次郎, 長江大輔, 中谷祐輔, 二宮一史, 新田稔, 小川就也, 大西潤一, Pearson M., 聖代橋悦子, 豊田健司, 塚田和司, 渡辺裕: “偏極 ^8Li のベータ崩壊における時間反転対称性の破れの探索”, 第 6 回停止・低速不安定核ビームを用いた核分光研究会, 東京, 3 月 (2010).
- 長友傑, 小林義男, 久保謙哉, 山田康洋, 三原基嗣, 佐藤涉, 宮崎淳, 佐藤眞一, 北川敦志: “不安定核 ^{57}Mn ビームを用いたインビーム・メスbauer分光の現状”, 第 11 回メスbauer分光研究会シンポジウム, 豊中, 3 月 (2010).

Rare RI-ring Team

Publications

Journal

(Original Papers) *Subject to Peer Review

Nagae D., Asahi K., Ueno H., Kameda D., Takemura M., Takase T., Yoshimi A., Sugimoto T., Nagatomo T., Kobayashi Y., Uchida M., Shimada K., Arai T., Inoue T., Kagami S., and Hatakeyama N.: "Measurement of Electric Quadrupole Moments for ^{31}Al Using Spin Polarized RI Beams", AIP Conf. Proc. **915**, 853–856 (2007). *

Shimada K., Nagae D., Asahi K., Arai T., Takemura M., Inoue T., Takase T., Kagami S., Hatakeyama N., Kobayashi Y., Ueno H., Yoshimi A., Kameda D., Nagatomo T., Sugimoto T., Kubono S., Yamaguchi H., Wakabayashi Y., Amadio G., Hayakawa S., Murata J., and Kawamura H.: "Production of Polarized Radioactive Beams via The Inverse-kinematics Reactions and Their Applications", AIP Conf. Proc. **915**, 857–860 (2007). *

Ohnishi T., Kubo T., Kusaka K., Yoshida A., Yoshida K., Fukuda N., Ohtake M., Yanagisawa Y., Takeda H., Kameda D., Yamaguchi Y., Aoi N., Yoneda K., Otsu H., Takeuchi S., Sugimoto T., Kondo Y., Scheit H., Gono Y., Sakurai H., Motobayashi T., Suzuki H., Nakao T., Kimura H., Mizoi Y., Matsushita M., Ieki K., Kuboki T., Yamaguchi T., Suzuki T., Ozawa A., Moriguchi T., Yasuda Y., Nakamura T., Nannichi T., Shimamura T., Nakayama Y., Geissel H., Weick H., Nolen J. A., Tarasov O. B., Nettleton A. S., Bazin D. P., Sherrill B. M., Morrissey D. J., and Mittag W.: "Identification of New Isotopes ^{125}Pd and ^{126}Pd Produced by In-Flight Fission of 345 MeV/nucleon ^{238}U : First Results from the RIKEN RI Beam Factory", J. Phys. Soc. Jpn. **77**, No. 8, pp. 083201-1–083201-4 (2008). *

SCRIT Team

Publications

Journal

(Original Papers) *Subject to Peer Review

Suda T., Wakasugi M., Emoto T., Ito S., Kurita K., Tamae T., Wang S., and Yano Y.: "First demonstration of electron scattering using a novel target developed for short-lived nuclei", Phys. Rev. Lett. **102**, No. 10, pp. 102501-1-102501-4 (2009). *

Research Instruments Group

Publications

Journal

(Original Papers) *Subject to Peer Review

Ichikawa Y., Onishi T., Suzuki D., Iwasaki H., Naik V., Kubo T., Chakrabarti A., Aoi N., Brown A., Fukuda N., Kubono S., Motobayashi T., Nakabayashi T., Nakao T., Okumura T., Ong H., Suzuki H., Suzuki M., Teranishi T., Yamada K., Yamaguchi H., and Sakurai H.: “Investigation into behavior of weakly-bound proton via $B(GT)$ measurement for the β decay of ^{24}Si ”, AIP Conf. Proc. **1165**, 98–101 (2009).

Ichikawa Y., Kubo T., Aoi N., Naik V., Chakrabarti A., Fukuda N., Iwasaki H., Kubono S., Motobayashi T., Nakabayashi T., Nakao T., Okumura T., Ong H., Onishi T., Suzuki D., Suzuki H., Suzuki M., Teranishi T., Yamada K., Yamaguchi H., and Sakurai H.: “Beta-decay study of $T_z = -2$ proton-rich nucleus ^{24}Si ”, Eur. Phys. J. A **42**, 375–378 (2009). *

Takeuchi S., Aoi N., Motobayashi T., Ota S., Takeshita E., Suzuki H., Baba H., Fukui T., Hashimoto Y., Ieki K., Imai N., Iwasaki H., Kanno S., Kondo Y., Kubo T., Kurita K., Minemura T., Nakamura T., Okumura T., Onishi T., Sakurai H., Shimoura S., Sugou R., Suzuki D., Suzuki M., Takashina M., Tamaki M., Tanaka K., Togano Y., and Yamada K.: “Low-Iying States in ^{32}Mg studied by proton inelastic scattering”, Phys. Rev. C **79**, No. 5, pp. 054319-1–054319-11 (2009). *

Ichikawa Y., Onishi T., Suzuki D., Iwasaki H., Naik V., Kubo T., Chakrabarti A., Aoi N., Brown A., Fukuda N., Kubono S., Motobayashi T., Nakabayashi T., Nakao T., Okumura T., Ong H., Suzuki H., Suzuki M., Teranishi T., Yamada K., Yamaguchi H., and Sakurai H.: “Beta decay of the proton-rich nucleus ^{24}Si and its mirror asymmetry”, Phys. Rev. C **80**, 044302-1–044302-12 (2009). *

Oral Presentations

(International Conference etc.)

Ichikawa Y., Onishi T., Suzuki D., Iwasaki H., Naik V., Kubo T., Chakrabarti A., Aoi N., Brown A., Fukuda N., Kubono S., Motobayashi T., Nakabayashi T., Nakao T., Okumura T., Ong H., Suzuki H., Suzuki M., Teranishi T., Yamada K., Yamaguchi H., and Sakurai H.: “Investigation into behavior of weakly-bound proton via $B(GT)$ measurement for the β decay of ^{24}Si ”, International Conference on Nuclear Structure and Dynamics (NSD09), (University of Zagreb), Dubrovnik, Croatia, May (2009).

Ichikawa Y., Onishi T., Suzuki D., Iwasaki H., Naik V., Kubo T., Chakrabarti A., Aoi N., Brown A., Fukuda N., Kubono S., Motobayashi T., Nakabayashi T., Nakao T., Okumura T., Ong H., Suzuki H., Suzuki M., Teranishi T., Yamada K., Yamaguchi H., and Sakurai H.: “Beta

decay of ^{24}Si and mirror asymmetry of Gamow-Teller transition strength”, 3rd Joint Meeting of the Nuclear Physics Divisions of the APS and JPS (Hawaii 2009), Hawaii, USA, Oct. (2009).

Ichikawa Y., Onishi T., Suzuki D., Iwasaki H., Naik V., Kubo T., Chakrabarti A., Aoi N., Brown A., Fukuda N., Kubono S., Motobayashi T., Nakabayashi T., Nakao T., Okumura T., Ong H., Suzuki H., Suzuki M., Teranishi T., Yamada K., Yamaguchi H., and Sakurai H.: “Gamow-Teller transition of proton-rich nucleus ^{24}Si ”, 7th Japan-China Joint Nuclear Physics Symposium, (University of Tsukuba), Tsukuba, Nov. (2009).

Ichikawa Y., Onishi T., Suzuki D., Iwasaki H., Naik V., Kubo T., Chakrabarti A., Aoi N., Brown A., Fukuda N., Kubono S., Motobayashi T., Nakabayashi T., Nakao T., Okumura T., Ong H., Suzuki H., Suzuki M., Teranishi T., Yamada K., Yamaguchi H., and Sakurai H.: “Mirror asymmetry for $B(GT)$ of ^{24}Si induced by Thomas-Ehrman shift”, Tours Symposium on Nuclear Physics and Astrophysics VII (TOURS 2009), (Konan University), Kobe, Nov. (2009).

GARIS Team

Publications

Journal

(Original Papers) *Subject to Peer Review

Haba H., Kaji D., Komori Y., Kudou Y., Morimoto K., Morita K., Ooe K., Ohzeki K., Sato N., Shinohara A., and Yoneda A.: “RIKEN Gas-filled Recoil Ion Separator (GARIS) as a promising interface for superheavy element chemistry : Production of element 104, ^{261}Rf , using the GARIS/gas-jet system”, Chem. Lett. **38**, No. 5, pp. 426–427 (2009). *

(Others)

Asai M., Tsukada K., Kasamatsu Y., Sato T., Toyoshima A., Ishii Y., Takahashi R., Nagame Y., Ishii T., Nishinaka I., Kaji D., Morimoto K., and Kojima Y.: “Alpha-gamma spectroscopy of ^{259}Rf produced by using a mixed Cf target”, JAEA-Review **2009**, No. 036, pp. 37–38 (2009).

BigRIPS Team

Publications

Journal

(Original Papers) *Subject to Peer Review

Ariyoshi S., Taino T., Dobroiu A., Sato H., Matsuo H., and Otani C.: “Terahertz Detector based on a Superconducting Tunnel Junction Coupled to a Thin Superconductor Film”, *Appl. Phys. Lett.* **95**, No. 19, pp. 193504-1–193504-3 (2009). *

Book • Proceedings

(Original Papers) *Subject to Peer Review

Ariyoshi S., Taino T., Dobroiu A., Sato H., Matsuo H., and Otani C.: “Design of a Terahertz Detector based on a Superconducting Tunnel Junction Coupled to a Thin Superconductor Film”, *Proceedings of the 34th International Conference on Infrared, Millimeter, and Terahertz Wave (IRMMW-THz 2009)*, Busan, Korea, 2009–9, IRMMW-THz 2009, Busan, p. T5E06.0372 (2009).

(Others)

Ariyoshi S., Otani C., Dobroiu A., Sato H., Taino T., Matsuo H., and Shimizu H.: “Two-dimensional Superconducting Detector Array for Terahertz Imaging Applications”, *Extended Abstracts of 12th International Superconductive Electronics Conference, Fukuoka, 2009–6, ISEC 2009, Fukuoka*, pp. MD-P35-1–MD-P35-2 (2009).

Oral Presentations

(International Conference etc.)

Ariyoshi S., Otani C., Dobroiu A., Sato H., Taino T., Matsuo H., and Shimizu H.: “Two-dimensional Superconducting Detector Array for Terahertz Imaging Applications”, *International Superconductive Electronics Conference (ISEC 2009)*, Fukuoka, June (2009).

Ariyoshi S., Taino T., Dobroiu A., Sato H., Matsuo H., and Otani C.: “Design of a Terahertz Detector based on a Superconducting Tunnel Junction Coupled to a Thin Superconductor Film”, *34th International Conference on Infrared, Millimeter, and Terahertz Waves (IRMMW-THz 2009)*, Busan, Korea, Sept. (2009).

Ariyoshi S., Taino T., Dobroiu A., Sato H., Matsuo H., and Otani C.: “Evaluation of a Terahertz-wave Detector with a Superconducting Tunnel Junction Coupled to a Thin Superconductor Film”, *2009 East Asia Symposium on Superconductor Electronics (EASSE2009)*, Nanjing, China, Oct. (2009).

SAMURAI Team

Publications

Journal

(Original Papers) *Subject to Peer Review

- Nagae D., Asahi K., Ueno H., Kameda D., Takemura M., Takase T., Yoshimi A., Sugimoto T., Nagatomo T., Kobayashi Y., Uchida M., Shimada K., Arai T., Inoue T., Kagami S., and Hatakeyama N.: “Measurement of Electric Quadrupole Moments for ^{31}Al Using Spin Polarized RI Beams”, AIP Conf. Proc. **915**, 853–856 (2007). *
- Shimada K., Nagae D., Asahi K., Arai T., Takemura M., Inoue T., Takase T., Kagami S., Hatakeyama N., Kobayashi Y., Ueno H., Yoshimi A., Kameda D., Nagatomo T., Sugimoto T., Kubono S., Yamaguchi H., Wakabayashi Y., Amadio G., Hayakawa S., Murata J., and Kawamura H.: “Production of Polarized Radioactive Beams via The Inverse-kinematics Reactions and Their Applications”, AIP Conf. Proc. **915**, 857–860 (2007). *
- Ohnishi T., Kubo T., Kusaka K., Yoshida A., Yoshida K., Fukuda N., Ohtake M., Yanagisawa Y., Takeda H., Kameda D., Yamaguchi Y., Aoi N., Yoneda K., Otsu H., Takeuchi S., Sugimoto T., Kondo Y., Scheit H., Gono Y., Sakurai H., Motobayashi T., Suzuki H., Nakao T., Kimura H., Mizoi Y., Matsushita M., Ieki K., Kuboki T., Yamaguchi T., Suzuki T., Ozawa A., Moriguchi T., Yasuda Y., Nakamura T., Nannichi T., Shimamura T., Nakayama Y., Geissel H., Weick H., Nolen J. A., Tarasov O. B., Nettleton A. S., Bazin D. P., Sherrill B. M., Morrissey D. J., and Mittig W.: “Identification of New Isotopes ^{125}Pd and ^{126}Pd Produced by In-Flight Fission of ^{238}U : First Results from the RIKEN RI Beam Factory”, J. Phys. Soc. Jpn. **77**, No. 8, pp. 083201-1–083201-4 (2008). *
- Asahi K., Ueno H., Shimada K., Nagatomo T., Yoshimi A., Nagae D., Kameda D., Uchida M., Inoue T., Hatakeyama N., Kagami S., Hasama Y., Suzuki K., Murata J., Kawamura H., Narita K., and Ishihara M.: “Nuclear Structure Studies with Polarized Radioactive Beams”, AIP Conf. Proc. **1149**, 90–99 (2009). *
- Ichikawa Y., Onishi T., Suzuki D., Iwasaki H., Naik V., Kubo T., Chakrabarti A., Aoi N., Brown A., Fukuda N., Kubono S., Motobayashi T., Nakabayashi T., Nakao T., Okumura T., Ong H., Suzuki H., Suzuki M., Teranishi T., Yamada K., Yamaguchi H., and Sakurai H.: “Investigation into behavior of weakly-bound proton via $B(\text{GT})$ measurement for the β decay of ^{24}Si ”, AIP Conf. Proc. **1165**, 98–101 (2009).
- Nagatomo T., Shimada K., Asahi K., Balabanski D. L., Daugas J., Depuydt M., De Rydt M., Gaodefroy L., Grevy S., Hasama Y., Ichikawa Y., Kameda D., Morel P., Perrot L., Stodel C., Thomas J. C., Vanderheijden W., Vermeulen N., Vingerhoets P., Yoshimi A., Neyens G., and Ueno H.: “Electric quadrupole moment of the neutron-rich ^{33}Al ”, Eur. Phys. J. A **42**, No. 3, pp. 383–385 (2009). *
- Ichikawa Y., Kubo T., Aoi N., Naik V., Chakrabarti A., Fukuda N., Iwasaki H., Kubono S., Motobayashi T., Nakabayashi T., Nakao T., Okumura T., Ong H., Onishi T., Suzuki D., Suzuki H., Suzuki M., Teranishi T., Yamada K., Yamaguchi H., and Sakurai H.: “Beta-decay study of $T_z = -2$ proton-rich nucleus ^{24}Si ”, Eur. Phys. J. A **42**, 375–378 (2009). *
- Takamine A., Wada M., Okada K., Nakamura T., Sonoda T., Lioubimov V., Iimura H., Yamazaki Y., Kanai Y., Kojima T., Yoshida A., Kubo T., Katayama I., Ohtani S., Wollnik H., and Hans A. S.: “Isotope shift measurements of $^{11,9,7}\text{Be}^+$ ”, Eur. Phys. J. A, pp. 1–5 (2009). *
- Takeuchi S., Aoi N., Motobayashi T., Ota S., Takeshita E., Suzuki H., Baba H., Fukui T., Hashimoto Y., Ieki K., Imai N., Iwasaki H., Kanno S., Kondo Y., Kubo T., Kurita K., Minemura T., Nakamura T., Okumura T., Onishi T., Sakurai H., Shimoura S., Sugou R., Suzuki D., Suzuki M., Takashina M., Tamaki M., Tanaka K., Togano Y., and Yamada K.: “Low-Iying States in ^{32}Mg studied by proton inelastic scattering”, Phys. Rev. C **79**, No. 5, pp. 054319-1–054319-11 (2009). *
- De Rydt M., Balabanski D. L., Daugas J., Himpe P., Kameda D., Lozeva R., Morel P., Perrot L., Shimada K., Stoedel C., Sugimoto T., Thomas J. C., Ueno H., Vermeulen N., Vingerhoets P., Yoshimi A., and Neyens G.: “ g factors of ^{17}N and ^{18}N remeasured”, Phys. Rev. C **80**, No. 3, pp. 037306-1–037306-4 (2009). *
- Ichikawa Y., Onishi T., Suzuki D., Iwasaki H., Naik V., Kubo T., Chakrabarti A., Aoi N., Brown A., Fukuda N., Kubono S., Motobayashi T., Nakabayashi T., Nakao T., Okumura T., Ong H., Suzuki H., Suzuki M., Teranishi T., Yamada K., Yamaguchi H., and Sakurai H.: “Beta decay of the proton-rich nucleus ^{24}Si and its mirror asymmetry”, Phys. Rev. C **80**, 044302-1–044302-12 (2009). *

(Others)

- Murata J., Akiyama T., Hata M., Hirayama Y., Ikeda Y., Ishii T., Kameda D., Kawamura H., Mitsuoka S., Miyatake H., Nagae D., Ninomiya K., Nitta M., Seitabashi E., and Toyoda T.: “Test of time reversal symmetry using polarized nuclei”, JAEA-Review **2009-036**, 62–63 (2009).

Oral Presentations

(International Conference etc.)

- Ohnishi T., Kubo T., Kusaka K., Yoshida A., Yoshida K., Fukuda N., Yanagisawa Y., Ohtake M., Takeda H., and Kameda D.: “BigRIPS Commissioning Experiment”, Third experts meeting on critical issues of next-generation high-intensity In-flight separators, (National Superconducting Cyclotron Laboratory, Michigan State

- University), East Lansing, USA, Mar.–Apr. (2008).
- Yoshida A.: “BigRIPS target system”, Third experts meeting on critical issues of next-generation high-intensity In-flight separators, (MSU, NSCL), East Lansing, USA, Mar.–Apr. (2008).
- Ichikawa Y., Onishi T., Suzuki D., Iwasaki H., Naik V., Kubo T., Chakrabarti A., Aoi N., Brown A., Fukuda N., Kubono S., Motobayashi T., Nakabayashi T., Nakao T., Okumura T., Ong H., Suzuki H., Suzuki M., Teranishi T., Yamada K., Yamaguchi H., and Sakurai H.: “Investigation into behavior of weakly-bound proton via $B(GT)$ measurement for the β decay of ^{24}Si ”, International Conference on Nuclear Structure and Dynamics (NSD09), (University of Zagreb), Dubrovnik, Croatia, May (2009).
- Uwamino Y., Mukai H., Higurashi R., Akashio A., Fukuda H., Sakamoto H., Yoshida A., and Yoshida K.: “Dosimetry around BigRIPS at RIKEN RIBF”, 11th Neutron and Ion Dosimetry Symposium, (iThemba Laboratory for Accelerator-Based Sciences), Cape Town, South Africa, Oct. (2009).
- Ichikawa Y., Onishi T., Suzuki D., Iwasaki H., Naik V., Kubo T., Chakrabarti A., Aoi N., Brown A., Fukuda N., Kubono S., Motobayashi T., Nakabayashi T., Nakao T., Okumura T., Ong H., Suzuki H., Suzuki M., Teranishi T., Yamada K., Yamaguchi H., and Sakurai H.: “Beta decay of ^{24}Si and mirror asymmetry of Gamow-Teller transition strength”, 3rd Joint Meeting of the Nuclear Physics Divisions of the APS and JPS (Hawaii 2009), Hawaii, USA, Oct. (2009).
- Baba H., Ichihara T., Ohnishi T., Takeuchi S., Yoshida K., Watanabe Y., Ota S., and Shimoura S.: “The New DAQ System in RIKEN RIBF”, 3rd Joint Meeting of the Nuclear Physics Divisions of the APS and JPS (Hawaii 2009), Hawaii, USA, Oct. (2009).
- Ichikawa Y., Onishi T., Suzuki D., Iwasaki H., Naik V., Kubo T., Chakrabarti A., Aoi N., Brown A., Fukuda N., Kubono S., Motobayashi T., Nakabayashi T., Nakao T., Okumura T., Ong H., Suzuki H., Suzuki M., Teranishi T., Yamada K., Yamaguchi H., and Sakurai H.: “Gamow-Teller transition of proton-rich nucleus ^{24}Si ”, 7th Japan-China Joint Nuclear Physics Symposium, (University of Tsukuba), Tsukuba, Nov. (2009).
- Ichikawa Y., Onishi T., Suzuki D., Iwasaki H., Naik V., Kubo T., Chakrabarti A., Aoi N., Brown A., Fukuda N., Kubono S., Motobayashi T., Nakabayashi T., Nakao T., Okumura T., Ong H., Suzuki H., Suzuki M., Teranishi T., Yamada K., Yamaguchi H., and Sakurai H.: “Mirror asymmetry for $B(GT)$ of ^{24}Si induced by Thomas-Ehrman shift”, Tours Symposium on Nuclear Physics and Astrophysics VII (TOURS 2009), (Konan University), Kobe, Nov. (2009).
- Ichikawa Y., Onisi T. K., Suzuki D., Iwasaki H., Kubo T., Naik V., Chakrabarti A., Aoi N., Brown A. B., Fukuda N., Kubono S., Motobayashi T., Nakabayashi T., Nakamura T., Nakao T., Okumura T., Ong H., Suzuki H., Suzuki M. K., Teranishi T., Yamaguchi H., and Sakurai H.: “Proton-rich nuclear structure investigated by β decay of ^{24}Si ”, ICHOR-EFES International Symposium on New Facet of Spin-Isospin Responses (SIR2010), (University of Tokyo), Tokyo, Feb. (2010).
- Ichikawa Y., Onisi T. K., Suzuki D., Iwasaki H., Kubo T., Naik V., Chakrabarti A., Aoi N., Brown A. B., Fukuda N., Kubono S., Motobayashi T., Nakabayashi T., Nakamura T., Nakao T., Okumura T., Ong H., Suzuki H., Suzuki M. K., Teranishi T., Yamaguchi H., and Sakurai H.: “Mirror asymmetry investigated by β decay of proton-rich ^{24}Si ”, International Symposium on Frontiers of Researches in Exotic Nuclear Structures (Niigata2010), (Niigata University), Toka-machi, Niigata Pref., Mar. (2010).
- (Domestic Conference)
- 飯尾雅実, 板橋健太, 岩崎雅彦, 應田治彦, 大西宏明, 岡田信二, 佐久間史典, 鈴木隆敏, 友野大, 松田恭幸, 山崎敏光, 石元茂, 鈴木祥二, 関本美知子, 豊田晃久, 永江知文, 石川隆, 竜野秀行, 早野龍五, 藤岡宏之, 味村周平, 阪口篤志, 佐藤将春, 福田芳之, 千葉順成, 花木俊生, 福田共和, 溝井浩, Beer G. A., 方享燦, Choi S., 林熙重, 石渡智 ; Buehler P., Hirtl A., Cargnelli M., Kienle P., Marton J., Widmann E., Zmeskal J., Curceanu C. O., Guaraldo C., Iliescu M., Pietreanu D., Sirghi D., Sirghi F., Faso D., Busso L., Morra O.: “K 中間子原子核探索実験のための液体ヘリウム 3 標的の開発”, 日本物理学会 2007 年春季大会, 八王子, 3 月 (2007).
- 高峰愛子, 和田道治, 中村貴志, 岡田邦宏, 園田哲, 飯村秀紀, Schury P. H., Lioubimov V., 山崎泰規, 金井保之, 小島隆夫, 吉田敦, 久保敏幸, 大谷俊介, 片山 一郎, Wollnik H., Hans A. S.: “超精密レーザー分光による Be 同位体の荷電半径の系統的測定”, 日本物理学会 2008 年秋季大会, 山形, 9 月 (2008).
- 飯尾雅実, 板橋健太, 岩崎雅彦, 應田治彦, 大西宏明, 佐久間史典, 佐藤将春, 塚田暁, 友野大, 藤岡宏之, 山崎敏光, 石元茂, 岩井正明, 鈴木祥二, 関本美知子, 豊田晃久, 石川隆, 竜野秀行, 鈴木隆敏, 早野龍五, 松田恭幸, 永江知文, 平岩聡彦, 味村周平, 野海博之, 阪口篤志, 藤原裕也, 徳田真, 千葉順成, 福田共和, 溝井浩, Beer G. A., 方享燦, Choi S., 林熙重, 石渡智 ; Buehler P., Cargnelli M., Hirtl A., Kienle P., Marton J., Widmann E., Zmeskal J., 岡田信二, Curceanu C. O., Guaraldo C., Iliescu M., Pietreanu D., Sirghi D., Sirghi F., Faso D., Morra O., Busso L.: “K 中間子原子核探索実験のための液体ヘリウム 3 標的の開発 III”, 日本物理学会 2008 年秋季大会, 山形, 9 月 (2008).
- 川村広和, 秋山岳伸, 秦麻記, 平山賀 ; 池田友樹, 石井哲朗, 亀田大輔, 光岡慎 ; 宮原直亮, 宮武宇也, 村田次郎, 中谷祐輔, 長江大輔, 二宮 一史, 新田稔, 大西潤 ; 聖代橋悦子, 豊田健司, 塚田和司, 渡辺裕: “KEK-TRIAC における偏極 ^8Li を用いた時間反転対称性の研究”, 日本物理学会第 65 回年次大会, 岡山, 3 月 (2010).
- 川村広和, 秋山岳伸, Behr J. A., 秦麻記, 平山賀 ; 池田友樹, 石井哲朗, 亀田大輔, Levy P., 宮原直亮, 宮武宇也, 光岡

真一; 村田次郎, 長江大輔, 中谷祐輔, 二宮一史, 新田稔,
小川就也, 大西潤一; Pearson M., 聖代橋悦子, 豊田健司,
塚田和司, 渡辺裕: “偏極 ^8Li のベータ崩壊における時間反
転対称性の破れの探索”, 第 6 回停止・低速不安定核ビーム
を用いた核分光研究会, 東京, 3 月 (2010).

Computing and Network Team

Publications

Journal

(Original Papers) *Subject to Peer Review

Takeuchi S., Aoi N., Motobayashi T., Ota S., Takeshita E., Suzuki H., Baba H., Fukui T., Hashimoto Y., Ieki K., Imai N., Iwasaki H., Kanno S., Kondo Y., Kubo T., Kurita K., Minemura T., Nakamura T., Okumura T., Onishi T., Sakurai H., Shimoura S., Sugou R., Suzuki D., Suzuki M., Takashina M., Tamaki M., Tanaka K., Togano Y., and Yamada K.: “Low-Iying States in 32Mg studied by proton inelastic scattering”, Phys. Rev. C **79**, No. 5, pp. 054319-1–054319-11 (2009). *

Oral Presentations

(International Conference etc.)

Baba H., Ichihara T., Ohnishi T., Takeuchi S., Yoshida K., Watanabe Y., Ota S., and Shimoura S.: “The New DAQ System in RIKEN RIBF”, 3rd Joint Meeting of the Nuclear Physics Divisions of the APS and JPS (Hawaii 2009), Hawaii, USA, Oct. (2009).

Accelerator Applications Research Group

Publications

Journal

(Original Papers) *Subject to Peer Review

Ishii K., Sugiyama R., Onuki M., Kazama Y., Matsunaga S., and Kawano S.: "The Y chromosome-specific STS marker MS2 and its peripheral regions on the Y chromosome of the dioecious plant *Silene latifolia*", Genome **51**, No. 4, pp. 251–260 (2008). *

Kazama Y., Fujiwara M., Koizumi A., Nishihara K., Kifune E., Abe T., and Kawano S.: "A *SUPERMAN*-like gene is exclusively expressed in female flowers of the dioecious plant *Silene latifolia*", Plant Cell Physiol. **50**, No. 6, pp. 1127–1141 (2009). *

(Review)

風間裕介, 河野重行: "ヒロハノマンテマの性染色体構造と性発現", Plant. Morphol. **21**, No. 1, pp. 71–77 (2009).

風間裕介, 河野重行: "雌雄異株性一性染色体ならびに雄蕊(♂)と雌蕊(♀)の選択的発達制御", 生物の科学 遺伝 **63**, No. 3, pp. 42–47 (2009).

Oral Presentations

(International Conference etc.)

Kazama Y., Liu Y., Hirano T., Ohbu S., Hayashi Y., Matsuyama T., and Abe T.: "The powerful technology for inducing deletion mutations in *Arabidopsis thaliana*", Plant Biology 2009: Joint Annual Meetings of the American Society of Plant Biologists and the Phycological Society of America, (American Society of Plant Biologist), Honolulu, USA, July (2009).

(Domestic Conference)

小泉綾子, 山中香, 石井公太郎, 鳥居千尋, 西原潔, 風間裕介, 阿部知子, 河野重行: "ヒロハノマンテマ両性花変異体と無性花変異体における雌雄花芽メリステムの発達と抑制", 第50回日本植物生理学会年会, 名古屋, 3月(2009).

石井公太郎, 鳥居千尋, 風間裕介, 阿部知子, 河野重行: "雌雄異株植物ヒロハノマンテマの重イオンビームによるY染色体部分欠損変異体", 第6回イオンビーム育種研究会大会, 和光, 5月(2009).

風間裕介, 石井公太郎, 鳥居千尋, 青沼航, 河野重行, 阿部知子: "重イオンビーム照射による雌雄異株植物ヒロハノマンテマY染色体欠失ライブラリーの構築", 日本育種学会第116回講演会, 札幌, 9月(2009).

石井公太郎, 藤田尚子, 鳥居千尋, 青沼航, 風間裕介, 阿部知子, 河野重行: "雌雄異株植物ヒロハノマンテマの重イオンビーム照射によるY染色体欠失変異体の網羅的解析", 日本植物学会第73回大会, 山形, 9月(2009).

西原潔, 風間裕介, 平野智也, 大部澄江, 松山知樹, 河野重行, 阿部知子: "鉄イオンビーム照射により誘導されたシロイヌナズナDNA突然変異", 日本遺伝学会第81回大会, (日本遺伝学会), 松本, 9月(2009).

Radiation Biology Team

Publications

Journal

(Original Papers) *Subject to Peer Review

Ichida H., Yoneyama K., Koba T., and Abe T.: "Epigenetic modification of rhizobial genome is essential for efficient nodulation", *Biochem. Biophys. Res. Commun.* **389**, 301–304 (2009). *

Fujiwara M., Dongliang L., Kazama Y., Abe T., Uno T., Yamagata H., Kanamaru K., and Itoh R. D.: "Further evaluation of the localization and functionality of hemagglutinin epitope- and fluorescent protein-tagged AtMinD1 in *Arabidopsis thaliana*", *Biosci. Biotechnol. Biochem.* **73**, No. 7, pp. 1693–1697 (2009). *

Kikuchi S., Saito Y., Ryuto H., Fukunishi N., Abe T., Tanaka H., and Tsujimoto H.: "Effects of heavy-ion beams on chromosomes of common wheat, *Triticum aestivum*", *Muta. Res./Fund. Mol. Mech. Mutagen.* **669**, 63–66 (2009). *

Niwa K., Hayashi Y., Abe T., and Aruga Y.: "Induction and isolation of pigmentation mutants of *Porphyra yezoensis* (Bangiales, Rhodophyta) by heavy-ion beam irradiation", *Phycol. Res.* **57**, No. 3, pp. 194–202 (2009). *

Kazama Y., Fujiwara M., Koizumi A., Nishihara K., Kifune E., Abe T., and Kawano S.: "A *SUPERMAN*-like gene is exclusively expressed in female flowers of the dioecious plant *Silene latifolia*", *Plant Cell Physiol.* **50**, No. 6, pp. 1127–1141 (2009). *

Shimada S., Ogawa T., Kitagawa S., Suzuki T., Ikari C., Shitsukawa N., Abe T., Kawahigashi H., Kikuchi R., Handa H., and Murai K.: "A genetic network of flowering-time genes in wheat leaves, in which an *APETALA1/FRUITFULL*-like gene, *VRN1*, is upstream of *FLOWERING LOCUS T*", *Plant J.* **58**, 668–681 (2009). *

河津哲, 土居智仁, 阿部知子: "遺伝子組替えユーカリの吃用かに向けた不着花個体の開発", *Cellulose Communications* **16**, No. 2, pp. 54–57 (2009). *

三尾咲紀子, 柏原輝彦, 保倉明子, 北島信行, 後藤文之, 吉原利一, 阿部知子, 中井泉: "放射光マイクロビーム蛍光 X 線分析を用いたシダ植物ヘビネゴザの Pb と Cu の蓄積機構に関する研究", *X 線分析の進歩* **40**, 183–193 (2009). *
仲條真介, 長谷川聡, 吉田宏, 漆原昌二, 阿部陽, 阿部知子, 福西暢尚, 龍頭啓充, 大清水保見: "低アミロース短稈ヒエ新品種「ヒエ岩手1号」, 「ヒエ岩手2号」, 「ヒエ岩手3号」の育成", *雑穀研究*, No. 24, pp. 12–19 (2009). *

(Review)

大坪憲弘, 鳴海貴子, 阿部知子, 高木優, 間竜太郎: "遺伝子組換えを基盤とした新形質花きの作出", *農業技術* **63**, 551–558 (2008).

竹久妃奈子, 林依子, 阿部知子, 佐藤雅志: "重イオンビーム育種技術による耐塩性イネの育成", *放射線と産業*, No. 121, pp. 22–26 (2009).

Book • Proceedings

(Review)

白尾吏, 松山知樹: "秋輪ギク無側枝性系統の DNA マーク開発", *DNA 多型 Vol.17*, 日本 DNA 多型学会, 東京, pp. 118–120 (2009).

阿部知子, 林依子, 風間裕介, 竹久妃奈子, 龍頭啓充, 福西暢尚: "重イオンビーム育種技術の開発と実用化", 荷電粒子ビームの工業への応用と第 132 委員会 第 188 回研究会資料, 東京, 2009–11, 日本学術振興会, 東京, pp. 27–34 (2009).

平野智也, 星野洋一郎: "植物は 2 度受精する: 雄性配偶子の花粉管内ダイナミクス", 第 2 回智のシンポジウム: 文明・文化と科学技術 論文集, 東京, 2009–11, 「智のシンポジウム」組織委員会, 八王子, pp. 29–32 (2009).

風間裕介, 河野重行, 阿部知子: "巨大 Y 染色体との格闘: 世界初の植物性決定遺伝子を求めて", 第 2 回智のシンポジウム: 文明・文化と科学技術 論文集, 東京, 2009–11, 「智のシンポジウム」組織委員会, 東京, pp. 33–36 (2009).

阿部知子, 林依子, 風間裕介, 平野智也: "重イオンビームの生物効果と育種利用", 平成 21 年度常緑果樹研究会資料「カンキツの消費拡大のために」, 静岡, 2010–1, 果樹研究所, つくば, pp. 91–94 (2010).

Oral Presentations

(International Conference etc.)

Takada S., Kitajima N., Tarada Y., Abe T., Hokura A., and Nakai I.: "Study on Cd storage and detoxication mechanism of tobacco by micro-XRF-XAFS analysis using high-energy synchrotron radiation", International Symposium on Metallomics (ISM 2009), Cincinnati, USA, June (2009).

Niwa K. and Abe T.: "Occurrence of chimeras with mosaic patterns in archeospore germlings of the marine crop *Porphyra yezoensis* Ueda (Bangiales, Phodophyta)", Plant Biology 2009: Joint Annual Meetings of the American Society of Plant Biologists and the Phycological Society of America, Honolulu, USA, July (2009).

Kazama Y., Liu Y., Hirano T., Ohbu S., Hayashi Y., Matsuyama T., and Abe T.: "The powerful technology for inducing deletion mutations in *Arabidopsis thaliana*", Plant Biology 2009: Joint Annual Meetings of the American Society of Plant Biologists and the Phycological Society of America, (American Society of Plant Biologist), Honolulu, USA, July (2009).

Kazama Y., Takehisa H., Fujiwara M., Ohbu S., Hayashi Y., and Abe T.: "A DFR-deficient white flower mutant induced by heavy-ion beam irradiation in *Nicotiana tabacum*", 5th International Workshop on Anthocyanins (IWA 2009), Nagoya, Sept. (2009).

Abe T., Hayashi Y., Kazama Y., Nishihara K., Hirano T., Nakagawa M., Ohbu S., Kanaya T., Miyazaki K., and Suzuki K.: "New flower cultivar produced by heavy-ion beam irradiation in RIBF", 5th International Workshop on Anthocyanins (IWA 2009), Nagoya, Sept. (2009).

Murakami K., Yamamoto T., Fujimoto K., Okabe K.,

- Masuda M., Abe T., and Maeda K.: "Low-Pungent Sweet Pepper Selected under Continuous Fluorescent illumination", 6th International Symposium Light in Horticulture, (The International Society for Horticultural Science), Tsukuba, Nov. (2009).
- (Domestic Conference)
- 風間裕介, 阿部知子: "植物突然変異誘発における LET 効果の解析", 長浜バイオ大学植物環境分子生理学研究室ラボセミナー, (長浜バイオ大学), 長浜, 5月(2008).
- 市田裕之: "微生物における重イオンビーム誘発突然変異の解析", 長浜バイオ大学植物環境分子生理学研究室ラボセミナー, (長浜バイオ大学植物環境分子生理学研究室), 長浜, 5月(2008).
- 林依子, 竹久妃奈子, 風間裕介, 市田裕之, 大部澄江, 東海林英夫, 宮本咲紀子, 高田沙織, 半澤栄子, 保倉明子, 中井泉, 佐藤雅志, 阿部知子: "炭素イオンビーム照射によって作出した耐塩性イネ突然変異系統の特性", 日本育種学会第115回講演会, (日本育種学会), つくば, 3月(2009).
- 齋藤隆範, 鈴木康孝, 西川博, 風間裕介, 林依子, 阿部知子: "チャの種子及び挿し穂に対する重イオンビーム照射の影響", 日本育種学会第115回講演会, (日本育種学会), つくば, 3月(2009).
- 古川浩二, 岩澤洋樹, 阿部知子, 松山知樹: "DNA マーキングによるシンビジウムの品種内識別", 園芸学会平成21年度春季大会, (園芸学会), 東京, 3月(2009).
- Kim H., 保坂ふみ子, 寺上伸吾, 西谷千佳子, 澤村豊, 高田教臣, 阿部知子, 松山知樹, 山本俊哉: "DNA マーキングによるナシの品種・産地判別技術の開発 3. ニホンナシにおけるレトロトランスポゾンの解析", 園芸学会平成21年度春季大会, (園芸学会), 東京, 3月(2009).
- 小泉綾子, 山中香, 石井公太郎, 鳥居千尋, 西原潔, 風間裕介, 阿部知子, 河野重行: "ヒロハノマンテマ両性花変異体と無性花変異体における雌雄花芽メリステムの発達と抑制", 第50回日本植物生理学会年会, 名古屋, 3月(2009).
- 阿部知子: "重イオンビームを用いて新しい植物・微生物を創る", 第14回理事長ファンダワークショップ「持続可能な社会を構築するための科学は何か」-環境・エネルギー・食糧分野の研究推進のための未来予想図を描く-, 葉山, 3月(2009).
- 阿部知子: "先端量子ビームを用いた生命科学の新しい展開", 先端量子ビームとナノ応用技術調査専門委員会, 東京, 3月(2009).
- 石井公太郎, 鳥居千尋, 風間裕介, 阿部知子, 河野重行: "雌雄異株植物ヒロハノマンテマの重イオンビームによる Y 染色体部分欠損変異体", 第6回イオンビーム育種研究会大会, 和光, 5月(2009).
- 阿部知子: "理研加速器を用いた植物科学研究", 京都大学育種学教室セミナー, 京都, 6月(2009).
- 佐々木克友, 山口博康, 間竜太郎, 四方雅仁, 小松拓真, 阿部知子, 大坪憲弘: "第2ウオールが専化したトレンニア変異体の原因遺伝子の解析", 第27回日本植物細胞分子生物学会大会・シンポジウム, 藤沢, 7月(2009).
- 大坪憲弘, 阿部知子, 高木優, 高根健一: "遺伝子組換え花き樹脂封入標本の教材化", 第27回日本植物細胞分子生物学会大会・シンポジウム, 藤沢, 7月(2009).
- 古川浩二, 岩澤洋樹, 阿部知子, 松山知樹: "DNA マーキングによるシンビジウムの品種内識別 (第2報)", 園芸学会平成21年度秋季大会, (園芸学会), 秋田, 9月(2009).
- 寺岡毅, 澤野郁夫, 中島輝子, 加々美裕, 神尾章子, 林依子, 龍頭啓充, 福西暢尚, 阿部知子: "重イオンビーム照射により誘発されるウンシュウミカンの形態変異", 園芸学会平成21年度秋季大会, 秋田, 9月(2009).
- 林依子, 風間裕介, 竹久妃奈子, 大部澄江, 東海林英夫, 佐藤雅志, 阿部知子: "重イオンビーム照射によって誘発したイネ突然変異体の解析", 日本育種学会第116回講演会, (日本育種学会), 札幌, 9月(2009).
- 神川典子, 繁木雄一, 権藤崇裕, 阿部知子, 明石良: "重イオンビーム照射により見いだされた「わい性チガヤ」の特性と大量増殖", 日本育種学会第116回講演会, 札幌, 9月(2009).
- 風間裕介, 石井公太郎, 鳥居千尋, 青沼航, 河野重行, 阿部知子: "重イオンビーム照射による雌雄異株植物ヒロハノマンテマ Y 染色体欠失ライブラリーの構築", 日本育種学会第116回講演会, 札幌, 9月(2009).
- 平野智也, 風間裕介, Liu Y., 大部澄江, 林祐子, 林依子, 松山知樹, 阿部知子: "重イオンビームの異核種間 LET 照射における DNA 変異の比較", 日本育種学会第116回講演会, (日本育種学会), 札幌, 9月(2009).
- 石井公太郎, 天内康人, 風間裕介, 河野重行: "染色体末端特異的サテライトの FISH で明らかにされたヒロハノマンテマ異型性染色体の起源", 日本植物形態学会第21回総会・大会, 山形, 9月(2009).
- 石井公太郎, 藤田尚子, 鳥居千尋, 青沼航, 風間裕介, 阿部知子, 河野重行: "雌雄異株植物ヒロハノマンテマの重イオンビーム照射による Y 染色体欠失変異体の網羅的解析", 日本植物学会第73回大会, 山形, 9月(2009).
- 阿部知子: "重イオンビーム育種技術の概略", 平成21年度第1回育種研究所 生物工学関係ゼミナール, (千葉県農林総合研究センター), 千葉, 9月(2009).
- 馬立秋, 田中秀逸, 井上弘一, 風間裕介, 市田裕之, 阿部知子, 崑山晋: "イオンビーム照射による DNA 損傷の修復様式の解析", 日本遺伝学会第81回大会, 松本, 9月(2009).
- 西原潔, 風間裕介, 平野智也, 大部澄江, 松山知樹, 河野重行, 阿部知子: "鉄イオンビーム照射により誘導されたシロイヌナズナ DNA 突然変異", 日本遺伝学会第81回大会, (日本遺伝学会), 松本, 9月(2009).
- 阿部知子, 林依子, 風間裕介, 平野智也, 竹久妃奈子, 龍頭啓充, 福西暢尚: "重イオンビーム育種技術の開発と実用化", 日本学術振興会132委員会第188回研究会, 東京, 11月(2009).
- 平野智也, 星野洋一郎: "植物は2度受精する: 雄性配偶子の花粉管内ダイナミクス", 第2回智のシンポジウム: 文明・文化と科学技術, (第2回 智のシンポジウム-文明・文化と科学技術-組織委員会), 東京, 11月(2009).
- 風間裕介, 河野重行, 阿部知子: "巨大 Y 染色体との格闘: 世界初の植物性決定遺伝子を求めて", 第2回智のシンポジウム: 文明・文化と科学技術, 東京, 11月(2009).
- 水野武, 泉雅子, 花岡文雄, 今本尚子: "マウス DNA ポリメラーゼ α の品質管理機構: 核内分解系と細胞質係留系による品質管理機構", 第20回 DNA 複製・組換え・修復ワークショップ, 彦根, 11月(2009).
- 古川浩二, 岩澤洋樹, 阿部知子, 松山知樹: "DNA マーキング

- によるシンビジウムの品種内判別”, 日本 DNA 多型学会第 18 回学術集会, (日本 DNA 多型学会), 久留米, 11 月 (2009).
- 白尾吏, 松山知樹: “秋輪ギク品種内識別における DNA マーキングの利用”, 日本 DNA 多型学会第 18 回学術集会, (日本 DNA 多型学会), 久留米, 11 月 (2009).
- 吉井雄一, 保倉明子, 中井泉, 阿部知子, 井藤賢操, 榊原均: “金属蓄積植物ホンモンジゴケにおける重金属元素マッピングと化学形態分析”, 第 45 回 X 線分析討論会, (日本分析化学会), 大阪, 11 月 (2009).
- 水野武, Eichinger C. S., 水野恵子, 泉雅子, 三宅康之, 柳憲一郎, 花岡文雄, 今本尚子: “異常な DNA ポリメラーゼ α は核移行阻害及び核内分解により核より排除される”, 第 32 回日本分子生物学会年会, 横浜, 12 月 (2009).
- 泉雅子, 柳憲一郎, 水野武, 杉村和人, 今本尚子, 奥村克純, 花岡文雄: “Analysis on the functional domains of Mcm10 in mammalian cells”, 第 32 回日本分子生物学会年会, (日本分子生物学会), 横浜, 12 月 (2009).
- 白尾吏, 松山知樹: “DNA マーキングを利用した秋輪ギクの品種内識別”, DNA 鑑定学会第 2 回大会, (DNA 鑑定学会), 横浜, 12 月 (2009).
- 高田沙織, 保倉明子, 中井泉, 寺田靖子, 阿部知子: “タバコの植物種における Cd の蓄積挙動の高エネルギー放射光蛍光 X 線分析による研究”, 第 23 回日本放射光学会年会・放射光科学合同シンポジウム, 姫路, 1 月 (2010).
- 阿部知子, 林依子, 風間裕介, 平野智也: “重イオンビームの生物効果と育種利用”, 平成 21 年度常緑果樹研究会, (農業・食品産業技術総合研究機構果樹研究所), 静岡, 1 月 (2010).
- 井藤賢操, 川上智, 阿部知子, 榊原均: “蘚類ヒョウタンゴケの原糸体細胞を用いた水環境中の金属資源回収技術”, 第 147 回生存圏シンポジウム Metal hyperaccumulator —植物の金属集積機構の解明とその応用に向けて—, (京大大学生存圏研究所), 京都, 1 月 (2010).
- 井藤賢操, 川上智, 阿部知子, 榊原均: “蘚類(コケ植物)の育種によるレアメタル回収技術の開発”, 理研シンポジウム「重イオンビーム育種技術の実用化 10 年」, 和光, 1 月 (2010).
- 林依子, 渡川登美子, 風間裕介, 平野智也, 大部澄江, 東海林英夫, 佐藤雅志, 阿部知子: “イネの突然変異誘発に対する重イオンビームの LET 効果”, 日本育種学会第 117 回講演会, (日本育種学会), 京都, 3 月 (2010).
- 森下敏和, 六笠裕治, 鈴木達郎, 清水明美, 山口博康, 出花幸之介, 相井城太郎, 長谷純宏, 鹿園直哉, 田中淳, 宮沢豊, 林依子, 阿部知子: “ガンマ線およびイオンビーム照射によって得られたダツタンソバ半矮性系統の遺伝および農業特性”, 日本育種学会第 117 回講演会, 京都, 3 月 (2010).
- 風間裕介, 平野智也, 西原潔, Liu Y., 大部澄江, 林祐子, 林依子, 松山知樹, 阿部知子: “シロイヌナズナを用いた DNA 突然変異への LET 効果の解析 (1)”, 日本育種学会第 117 回講演会, 京都, 3 月 (2010).
- 平野智也, 渡川登美子, Arner E. A., 市田裕之, 竹久妃奈子, 林依子, 眞鍋理一郎, 河合純, 佐藤雅志, 阿部知子: “重イオンビーム照射により得られた耐塩性イネ突然変異系統の全ゲノム解析”, 日本育種学会第 117 回講演会, (日本育種学会), 京都, 3 月 (2010).
- 藤原誠, Li D., 風間裕介, 阿部知子, 宇野知秀, 山形裕士, 金丸研吾, 伊藤竜一: “HA エピトープ及び蛍光タンパク質を付加したシロイヌナズナ AtMinD1 タンパク質の局在性と機能性に関する評価”, 日本農芸化学会 2010 年度大会, 東京, 3 月 (2010).
- 平野智也, 星野洋一郎: “キルタンサスにおける花粉管伸長過程での精細胞の異型化”, 園芸学会平成 22 年度春季大会, (園芸学会), 藤沢, 3 月 (2010).
- 中川繭, 竹久妃奈子, 林依子, 東海林英夫, 佐藤雅志, 長村吉晃, 阿部知子: “イネ温度感受性緑変白苗突然変異体の変異解析”, 第 51 回日本植物生理学会年会, 熊本, 3 月 (2010).
- 大坪憲弘, 高根健一, 中澤美紀, 菊崎綾子, 黒田浩文, 阿部知子, 高木優, 間竜太郎: “遺伝子組換え花き樹脂封入標本の教材としての利用”, 第 51 回日本植物生理学会年会, 熊本, 3 月 (2010).
- 藤原誠, 関根康介, 山本義治, 阿部知子, 佐藤直樹, 伊藤竜一: “シロイヌナズナ MinE 過剰発現体及び変異体における葉緑体 FtsZ1-GFP タンパク質のライブ観察”, 第 51 回日本植物生理学会年会, 熊本, 3 月 (2010).

RI Applications Team

Oral Presentations

(International Conference etc.)

Ooe K., Yahagi W., Komori Y., Fujisawa H., Takayama R., Kikunaga H., Yoshimura T., Takahashi N., Haba H., Kudou Y., Ezaki Y., Takahisa K., and Shinohara A.: "Solvent Extraction Studies of Molybdenum and Tungsten as Homologues of Seaborgium (Element 106)", 7th Workshop on the Chemistry of the Heaviest Elements, (Mainz University), Mainz, Germany, Oct. (2009).

(Domestic Conference)

笠松良崇, 羽場宏光, 江崎豊: "超重元素化学実験に向けたサマリウム共沈 α 線源作成法の開発", 2009 日本放射化学学会年会・第53回放射化学討論会, (日本放射化学学会), 東京, 9月 (2009).

大江 弘, 矢作亘, 小森有希子, 藤沢弘幸, 三山玲央奈, 菊永英寿, 吉村崇, 高橋成人, 羽場宏光, 工藤祐生, 江崎豊, 高久圭二, 篠原厚: "106番元素シーボーギウムの同族元素モリブデンの溶媒抽出挙動", 2009 日本放射化学学会年会・第53回放射化学討論会, (日本放射化学学会), 東京, 9月 (2009).

江崎豊, 笠松良崇, 羽場宏光: " ^{nat}Hf 標的を用いた希土類元素マルチレーザーの製造", 2009 日本放射化学学会年会・第53回放射化学討論会, (日本放射化学学会), 東京, 9月 (2009).

中井陽一, 望月優子, 高橋和也, 五十嵐誠, 本川秀明, 鈴木啓助: "ドームふじの浅層氷床コアにおける硝酸イオン濃度の年代プロファイル: 12世紀~19世紀", 第32回極域気水圏シンポジウム, (国立極地研究所), 立川, 11月 (2009).

User Liaison and Industrial Cooperation Group

Publications

Journal

(Original Papers) *Subject to Peer Review

Takeuchi S., Aoi N., Motobayashi T., Ota S., Takeshita E., Suzuki H., Baba H., Fukui T., Hashimoto Y., Ieki K., Imai N., Iwasaki H., Kanno S., Kondo Y., Kubo T., Kurita K., Minemura T., Nakamura T., Okumura T., Onishi T., Sakurai H., Shimoura S., Sugou R., Suzuki D., Suzuki M., Takashina M., Tamaki M., Tanaka K., Togano Y., and Yamada K.: "Low-Iying States in ^{32}Mg studied by proton inelastic scattering", Phys. Rev. C **79**, No. 5, pp. 054319-1–054319-11 (2009). *

Industrial Cooperation Team

Publications

Journal

(Original Papers) *Subject to Peer Review

Mitsudo T., Nakajima Y., Remijn G. B., Takeichi H., Goto Y., and Tobimatsu S.: "Electrophysiological Evidence of Auditory Temporal Perception Related to the Assimilation Between Two Neighboring Time Intervals", *NeuroQuantology* **7**, No. 1, pp. 114-127 (2009). *

井上康之, 小川昭利, 荒井宏太, 松本秀彦, 松崎直幸, 小川幸子, 豊巻敦人, 大森隆司, 諸冨隆, 竹市博臣, 北崎充晃: "聴覚事象関連電位への神経デコーディングの適用: 統計的識別手法の比較と脳波分析方法としての評価", *基礎心理学研究* **28**, No. 1, pp. 44-58 (2009). *

Oral Presentations

(Domestic Conference)

竹市博臣: "談話理解の計測: 劣化音声に対する脳波応答の判別分析", 日本神経回路学会第19回全国大会 (JNNS2009), 仙台, 9月 (2009).

竹市博臣: "神経情報場の理論の可能性", 日本理論心理学会第55回大会, 京都, 11月 (2009).

Safety Management Group

Publications

Journal

(Review)

辻井博彦, 赤城卓, 赤羽恵一, 上袁義朋, 大野達也, 金井達明, 河野良介, 榮武二, 清水勝一, 浦壁恵理子, 中山隆, 中村尚司, 西尾禎治, 西澤かな枝, 西澤邦秀, 福田茂一, 松藤成弘, 山下晴男, 米内俊祐: “Research on Radiation Protection in the Application of New Technologies for Proton and Heavy Ion Radiotherapy”, 医学物理 **28**, No. 4, pp. 172–206 (2009).

Oral Presentations

(International Conference etc.)

Uwamino Y., Mukai H., Higurashi R., Akashio A., Fukuda H., Sakamoto H., Yoshida A., and Yoshida K.: “Dosimetry around BigRIPS at RIKEN RIBF”, 11th Neutron and Ion Dosimetry Symposium, (iThemba Laboratory for Accelerator-Based Sciences), Cape Town, South Africa, Oct. (2009).

Publications

Journal

(Original Papers) *Subject to Peer Review

- Aamodt K. *et al* for the ALICE Collaboration: “First proton+proton collisions at the LHC as observed with the ALICE detector-Measurement of the charged-particle pseudorapidity density at $\sqrt{s} = 900$ GeV”, *Eur. Phys. J. C* **65**, 111-125, 2010,*
- Aamodt K. *et al* for the ALICE Collaboration: “Alignment of the ALICE Inner Tracking System with cosmic-ray tracks”, *JINST*, 5, PO3003, 2010,*
- Adare A. *et al* for the PHENIX Collaboration: “Enhanced production of direct photons in Au+Au collisions at $\sqrt{s_{NN}} = 200$ GeV and implications for the initial temperature”, *Phys. Rev. Lett.* 104, 132301, 2010,*
- Adare A. *et al* for the PHENIX Collaboration: “Detailed measurement of the e^+e^- pair continuum in $p+p$ and Au+Au collisions at $\sqrt{s_{NN}} = 200$ -GeV and implications for direct photon production”, *Phys. Rev. C* 81, 034911, 2010,*
- Adare A. *et al* for the PHENIX Collaboration: “Double Helicity Dependence of Jet Properties from Dihadrons in Longitudinally Polarized $p+p$ Collisions at $\sqrt{s} = 200$ -GeV”, *Phys. Rev. D* 81, 012002, 2010,*
- Adanasiev S. *et al* for the PHENIX Collaboration: “Systematic Studies of Elliptic Flow Measurements in Au+Au Collisions at $\sqrt{s_{NN}} = 200$ -GeV”, *Phys. Rev. C* 80, 024909, 2009,*
- Adanasiev S. *et al* for the PHENIX Collaboration: “High- p_T π^0 Production with Respect to the Reaction Plane in Au + Au Collisions at $\sqrt{s_{NN}} = 200$ -GeV”, *Phys. Rev. C* 80, 054907, 2009,*
- Adanasiev S. *et al* for the PHENIX Collaboration: “Kaon interferometric probes of space-time evolution in Au+Au collisions at $\sqrt{s_{NN}} = 200$ -GeV”, *Phys. Rev. Lett.* 103, 142301, 2009,*
- Adare A. *et al* for the PHENIX Collaboration: “Measurement of Bottom versus Charm as a Function of Transverse Momentum with Electron-Hadron Correlations in $p+p$ Collisions at $\sqrt{s} = 200$ GeV”, *Phys. Rev. Lett.* 103, 082002, 2009,*
- Adare A. *et al* for the PHENIX Collaboration: “Photon-Hadron Jet Correlations in $p+p$ and Au+Au Collisions at $\sqrt{s} = 200$ -GeV”, *Phys. Rev. C* 80, 024908, 2009,*
- Adanasiev S. *et al* for the PHENIX Collaboration: “Photoproduction of J/ψ and of high mass e^+e^- in ultra-peripheral Au+Au collisions at $\sqrt{s_{NN}} = 200$ -GeV”, *Phys. Lett. B* 679, 321-329, 2009,*
- Adare A. *et al* for the PHENIX Collaboration: “The Polarized gluon contribution to the proton spin from the double helicity asymmetry in inclusive π^0 production in polarized $p+p$ collisions at $\sqrt{s} = 200$ -GeV”, *Phys. Rev. Lett.* 103, 012003, 2009,*
- Tamagawa T., Hayato A., Asami F., Abe K., Iwamoto S., Nakamura S., Harayama A., Iwahashi T., Konami S., Hamagaki H., Yamaguchi Y.L., Tawara H., Makishima K., “Development of Thick-foil and Fine-pitch GEMs with a Laser Etching Technique”, *Nucl. Instrum. Meth. in Physics Research A* **608** (2009) 390 – 396.,*
- He J. J., Kubono S., Teranishi T., Hu J., Notani M., Baba H., Nishimura S., Moon J. Y., Nishimura M., Iwasaki H., Yanagisawa Y., Hokoikiwa N., Kibe M., Lee J. H., Kato S., Gono Y., and Lee C. S.: “Investigation of excited states in 22Mg via resonant elastic scattering of 21Na+p and its astrophysical implications”, *Phys. Rev. C* **80** (2009) 015801-6,*
- Ichikawa Y., Onishi T.K., Suzuki D., Iwasaki H., Kubo T., Naik V., Chakrabarti A., Aoi N., Brown B.A., Fukuda N., Kubono S., Motobayashi T., Nakabayashi T., Nakamura T., Nakao T., Okumura T., Ong H.J., Suzuki H., Suzuki M.K., Teranishi T., Yamada K.N., Yamaguchi H., Sakurai H., “ β decay of the proton-rich nucleus 24Si and its mirror asymmetry”, *Phys. Rev. C* **80**, 044302 (2009),*
- Doornenbal P., Scheit H., Aoi N., Takeuchi S., Li K., Takeshita E., Wang H., Baba H., Deguchi S., Fukuda N., Geissel H., Gernhauser R., Gibelin J., Hachiuma I., Hara Y., Hinke C., Inabe N., Itahashi K., Itoh S., Kameda D., Kanno S., Kawada Y., Kobayashi N., Kondo Y., Krucken R., Kubo T., Kuboki T., Kusaka K., Lantz M., Michimasa S., Motobayashi T., Nakamura T., Nakao T., Namihira K., Nishimura S., Ohnishi T., Ohtake M., Orr N.A., Otsu H., Ozeki K., Satou Y., Shimoura S., Sumikama T., Takechi M., Takeda H., N. K., Tanaka K., Togano Y., Winkler M., Yanagisawa Y., Yoneda K., Yoshida A., Yoshida K., Sakurai H., “Spectroscopy of ^{32}Ne and the Island of Inversion”, *Phys. Rev. Lett.* **103**, (2009) 032501, *
- Hagino K., Sagawa H., Nakamura T., Shimoura S., “Two-particle correlations in continuum dipole transitions in Borromean nuclei”, *Phys. Rev. C* **80**, (2009) 031301,*
- Imai N., Aoi N., J. H., Sakurai H., Demichi K., Kawasaki H., Baba H., Dombrádi Zs., Elekes Z., Fukuda N., Fülöp Zs., Gelberg A., Gomi T., Hasegawa H., Ishikawa K., Ishihara M., Iwasaki H., Kaneko E., Kanno S., Kishida T., Kondo Y., Kubo T., Kurita K., Michimasa S., Minemura T., Miura M., Motobayashi T., Nakamura T., Notani M., K. T., Saito A., Shimoura S., Sugimoto T., K. M., Takeshita E., Takeuchi S., Tamaki M., Watanabe H., Yoneda K., “First lifetime measurement of 2_1^+ state in ^{12}Be ”, *Phys. Lett. B* **673**, (2009) 179 – 182,*
- Kondo Y., Nakamura T., Satou Y., Matsumoto T., Aoi N., Endo N., Fukuda N., Gomi T., Hashimoto Y., Ishihara M., Kawai S., Kitayama M., Kobayashi T., Matsuda Y., Matsui N., Motobayashi T., Nakabayashi T., Ogata K., Okumura T., Ong H.J., Onishi T.K., Otsu H., Sakurai H., Shimoura S., Shinohara M., Sugimoto T., Takeuchi S., Tamaki M., Togano Y., Yanagisawa Y.,

- “One-neutron removal reactions of ^{18}C and ^{19}C on a proton target”, *Phys. Rev. C* **79**, (2009) 014602, *
- Nakamura T., Kobayashi N., Kondo Y., Satou Y., Aoi N., Baba H., Deguchi S., Fukuda N., Gibelin J., Inabe N., Ishihara M., Kameda D., Kawada Y., Kubo T., Kusaka K., Mengoni A., Motobayashi T., Ohnishi T., Ohtake M., Orr N.A., Otsu H., Otsuka T., Saito A., Sakurai H., Shimoura S., Sumikama T., Takeda H., Takeshita E., Takechi M., Takeuchi S., Tanaka K., N. K., Tanaka N., Togano Y., Utsuno Y., Yoneda K., Yoshida A., Yoshida K., “ Halo Structure of the Island of Inversion Nucleus ^{31}Ne ”, *Phys. Rev. Lett.* **103**, (2009) 262501, *
- Takeuchi S., Aoi N., Motobayashi T., Ota S., Takeshita E., Suzuki H., Baba H., Fukui T., Hashimoto Y., Ieki K., Imai N., Iwasaki H., Kanno S., Kondo Y., Kubo T., Kurita K., Minemura T., Nakabayashi T., Nakamura T., Okumura T., K. T., Sakurai H., Shimoura S., Sugou R., Suzuki D., K. M., Takashina M., Tamaki M., Tanaka K., Togano Y., Yamada K., “ Low-lying states in ^{32}Mg studied by proton inelastic scattering”, *Phys. Rev. C* **79**, (2009) 054319, *
- Ideguchi E., Cederwall B., Ganioglu E., Hadinia B., Lagergren K., Bäck T., Johnson A., Wyss R., Eeckhauudt S., Grahn T., Greenlees P., Julin R., Juutinen S., Kettunen H., Leino M., Leppanen A.-P., Nieminen P., Nyman M., Pakarinen J., Rahkila P., Scholey C., Uusitalo J., Joss D.T., Paul E.S., Wiseman D.R., Wadsworth R., Afanasjev A.V., Ragnarsson I., “High-spin intruder band in ^{107}In ”, *Phys. Rev. C* **81**, (2010) 034303, *
- Scholey C., Andgren K., Bianco L., Cederwall B., G. I., Eeckhauudt S., Ertürk S., GomezHornillos M.B., Grahn T., T. P., Hadinia B., Ideguchi E., Jones P., T. D., Julin R., Juutinen S., Ketelhut S., Leino M., Leppänen A.-P., Nieminen P., Niikura M., Nyman M., O'Donnell D., D. R., Pakarinen J., Rahkila P., Sarén J., Sandzelius M., Simpson J., Sorri J., Thomson J., Uusitalo J., Venhart M., “Isomeric and ground-state properties of ^{171}Pt , ^{167}Os , and ^{163}W ”, *Phys. Rev. C* **81**, (2010) 014306, *
- Hadinia B., Cederwall B., D. R., Sandzelius M., Scholey C., Andgren K., Bäck T., Ganioglu E., Gómez M.B., Hornillos , Grahn T., T. P., Ideguchi E., Jakobsson U., Johnson A., M. P., Julin R., Juutinen J., Ketelhut S., Khaplanov A., Leino M., Niikura M., Nyman M., Özgür I., S. E., Peura P., Rahkila P., Sarén J., Sorri J., Uusitalo J., Wyss R., “Identification of gamma rays from ^{172}Au and alpha decays of ^{172}Au , ^{168}Ir , and ^{164}Re ”, *Phys. Rev. C* **80**, (2009) 064310, *
- Morita K., Morimoto K., Kaji D., Haba H., Ozeki K., Kudou Y., Sato N., Sumita T., Yoneda A., Ichikawa T., Fujimori Y., Goto S., Ideguchi E., Kasamatsu Y., Katori K., Komori Y., Koura H., Kudo H., Ooe K., Ozawa A., Tokanai F., Tsukada K., Yamaguchi T., Yoshida A., “Decay Properties of ^{266}Bh and ^{262}Db Produced in the $^{248}\text{Cm} + ^{23}\text{Na}$ Reaction”, *J. Phys. Soc. Jpn.* **78**, (2009) 064201, *
- Tanaka K., Yamaguchi T., Suzuki T., Ohtsubo T., Fukuda M., Nishimura D., Takechi M., Ogata K., Ozawa A., Izumikawa T., Aiba T., Aoi N., Baba H., Hashizume Y., Inafuku K., Iwasa N., Kobayashi K., Komuro M., Kondo Y., Kubo T., Kurokawa M., Matsuyama T., Michimasa S., Motobayashi T., Nakabayashi T., Nakajima S., Nakamura T., Sakurai H., Shinoda R., Shinohara M., Suzuki H., Takeshita E., Takeuchi S., Togano Y., Yamada K., Yasuno T., Yoshitake M., “Observation of a Large Reaction Cross Section in the Drip-Line Nucleus ^{22}C ”, *Phys. Rev. Lett.* **104**, (2010) 062701, *
- Suzuki D., Iwasaki H., Beaumel D., Nalpas L., Pollacco E., Assié M., Baba H., Blumenfeld Y., De N., Séréville , Drouart A., Franchoo S., Gillibert A., Guillot J., Hammache F., Keeley N., Lapoux V., Maréchal F., Michimasa S., Mougeot X., Mukha I., Okamura H., Otsu H., Ramus A., Roussel-Chomaz P., Sakurai H., Scarpaci J.A., Sorlin O., Stefan I., Takechi M., “Breakdown of the $Z = 8$ Shell Closure in Unbound ^{12}O and its Mirror Symmetry ”, *Phys. Rev. Lett.* **103**, (2009) 152503, *
- Ideguchi E., Ota S., Morikawa T., Oshima M., Koizumi M., Toh Y., Kimura A., Harada H., Furutaka K., Nakamura S., Kitatani F., Hatsukawa Y., Shizuma T., Sugawara M., Miyatake H., X. Y., Hirayama Y., Oi M., “Superdeformation in asymmetric $N > Z$ nucleus ^{40}Ar ”, *Phys. Lett. B* **686** (2010) 18–22, *
- Sekiguchi K., Sakai H., Witala H., Glockle W., Golak J., Itoh K., Kamada H., Kawabata T., Kuboki H., Maeda Y., Nogga A., Okamura H., Sakaguchi S., Sakamoto N., Sasamoto Y., Sasano M., Skibiński R., Suda K., Takahashi Y., Uesaka T., Wakasa T., Yako K., “Three-nucleon force effects in the $^1\text{H}(\bar{d}, \bar{p}p)n$ reaction at 135 MeV/nucleon”, *Phys. Rev. C* **79** (2009) 054008, *
- Yako K., Sasano M., Miki K., Sakai H., Dozono M., Frekers D., B. M., Hatanaka K., Ihara E., Kato M., Kawabata T., Kuboki H., Maeda Y., Matsubara H., Muto K., Noji S., Okamura H., H. T., Sakaguchi S., Sakemi Y., Sasamoto Y., Sekiguchi K., Shimizu Y., Suda K., Tameshige Y., Tamii A., Uesaka T., Wakasa T., Zheng H., “Gamow-Teller Strength Distributions in ^{48}Sc by the $^{48}\text{Ca}(p, n)$ and $^{48}\text{Ti}(n, p)$ Reactions and Two-Neutrino Double- β Decay Nuclear Matrix Elements”, *Physical Review Letters* **103** (2009) 012503, *
- Tamii A., Fujita Y., Matsubara H., Adachi T., Carter J., Dozono M., Fujita H., Fujita K., Hashimoto H., Hatanaka K., Itahashi T., Itoh M., Kawabata T., Nakanishi K., Ninomiya S., Perez-Cerdan A.B., Popescu L., Rubio B., Saito T., Sakaguchi H., Sakemi Y., Sasamoto Y., Shimbara Y., Shimizu Y., Smit F.D., Tameshige Y., Yosoi M., Zenihiro J., “Measurement of high energy resolution inelastic proton scattering at and close to zero degrees”, *Nucl.Instrum.Methods Phys.Res.*

- A605, 326 (2009),*
- Suzuki T., Honma M., Higashiyama K., Yoshida T., Kajino T., Otsuka T., Umeda H., Nomoto K., “Neutrino-induced reactions on ^{56}Fe and ^{56}Ni , and production of ^{55}Mn in population III stars”, *Phys. Rev. C* **79** (2009) 061603(R)/1-4,*
- Otsuka T., Suzuki T., Honma M., Utsuno Y., Tsunoda N., Tsukiyama K., Hjorth-Jensen M., “Novel features of nuclear forces and shell evolutions in exotic nuclei”, *Phys. Rev. Lett.* **104** (2010) 012501/1-4,*
- Suzuki T., Otsuka T., “Exotic Electromagnetic Transitions in Neutron-rich Carbon Isotopes”, *Int. Journal of Modern Physics* **E18** (2009) 1992–1996,*
- Book • Proceedings**
(Original Papers) *Subject to Peer Review
- Gunji T.: “Quarkonia production in high-energy heavy-ion collisions at the RHIC”. Proc. of the International Conference on Strangeness in Quark Matter 2008, Oct. 6-10, 2008, Tsinghua University, Beijing, China *J. Phys. G* **36**, -64015, 2009,*
- Tsujimoto Y. for the PHENIX Collaboration: “In-Medium Modifications of Low-Mass Vector Mesons in PHENIX at RHIC”, Proc. of the 21st International Conference on Ultra-Relativistic Nucleus-Nucleus Collisions (QM2009), Mar. 30–Apr. 4, 2009, Knoxville, USA, *Nucl. Phys. A* **830** (2009) 487c–490c,*
- Yamaguchi Y.L. for the PHENIX collaboration: “Measurements of Soft and Intermediate pT Photons from Hot and Dense Matter at RHIC-PHENIX”, Proc. of the 21st International Conference on Ultra-Relativistic Nucleus Nucleus Collisions (Quark Matter 2009), Mar. 30–Apr. 5, 2009, Knoxville, Tennessee, USA, *Nucl. Phys. A* **830** (2009) 575c–578c,*
- Aramaki Y., for the PHENIX Collaboration: “Reaction plane dependence of neutral pion production in center-of-mass energy of 200 GeV Au+Au collisions at RHIC-PHENIX”, Proc. of the eighteenth Particles and Nuclei International Conference - PANIC08, November 9–14, 2008, Eilat, Israel, Conference record, (2009) pp. 570–572.
- Aramaki Y., for the PHENIX Collaboration: “Study of QGP with probes associated with photon at RHIC-PHENIX”, Proc. of the XLIVth Rencontres de Moriond, March 14–21, 2009, La Thuile, Italy, Conference record, (2009) pp. 291–294.
- Akimoto R., Hamagaki H., Gunji T., Yamaguchi Y.L., Hori Y., “Measurement of the basic features of Thick-GEM and Resistive GEM”, Proc. of the 1st International conference on Micro Pattern Gaseous Detectors, Jun. 12–15, 2009, Crete, Greece, *Journal of Instrumentation*, **5** (2010)
- Cherubini S., Crucilla V., Gulino M., Kiss G., La Cognata M., Li C., Munhoz M.G., Kroha V., Kubono S., Somoryai E., Szanto de Toledo A., Liguori Neto R., De M.M., Moura , Pizzone R.G., Rapisarda G.G., Sergi M.L., Souza F.A., Suaide A.A.P., Szanto E., Tabacaru G., Tudisco S., Tumino A., Wakabayashi Y., Wen Q., and , Yamaguchi H., “New results on the Trojan Horse Method applied to the $^{10,11}\text{B}+p$ reactions”, Proceedings of the 6th Japan-Italy Symposium on Heavy-Ion Physics, AIP Conf. Proc. 1120 (2009) 171 - 176,*
- Cherubini S., Spitaleri C., Crucilla V., Gulino M., La M., Cognata , Lamia L., Pizzone R.G., Romano S., Kubono S., Yamaguchi H., Wakabayashi Y., Hayakawa S., Iwasa N., Kato S., Komatsubara H., Teranishi T., Coc A., De N., Sereville , and , Hammache F., “The study of $^{18}\text{F}+p$ reaction at astrophysical energies”, Proceedings of the 6th Japan-Italy Symposium on Heavy-Ion Physics, AIP Conf. Proc. 1120 (2009) 294 - 297,*
- Kubono S., Binh D.N., Hayakawa S., Hashimoto H., M. D., Wakabayashi Y., Yamaguchi H., Teranishi T., Iwasa N., Komatsubara T., Kato S., Khiem L.H., “Nuclear Clusters in Astrophysics”, Proc. of the 10th International Conference on Nucleus-Nucleus Collisions (NN2009), August 16-21, 2009, Beijing, China *Nucl. Phys. A* **834** (2010) 647c – 650c,*
- Kubono S., Binh D.N., Hayakawa S., Hashimoto T., Kahl D.M., Yamaguchi H., Wakabayashi Y., Teranishi T., Iwasa N., Komatsubara T., Kato S., and , Khiem L.H., “Nuclear Astrophysics Programs with Low-Energy RI Beams at CRIB”, Proc. of the International Symposium on Exotic Nuclei (EXON), Sochi, Russia, October, 2009, AIP Conf. Proc. vol. 1224 (2010) 475 - 481 (2010),*
- Kubono S., “Nuclear Cluster Aspects in Astrophysics”, Proc. of the 5th European Summer School on Nuclear Astrophysics, Sept. 20 - 27, 2009, Santa Tecla, Italy, AIP Conf. Proc. vol. 1213 (2010) 107 - 111,*
- Yamaguchi H., Wakabayashi Y., Hayakawa S., Binh D.N., Kahl D., Kurihara Y., Kubono S., Teranishi T., He J.J., Kwon Y.K., Nishimura S., Togano Y., Iwasa N., Niikura M., and , Khiem L.H., “Nuclear Astrophysical Studies Using Low-Energy RI Beams at CRIB”, Perspective in Nuclear Physics, AIP conference proceeding **1120** (2009) 189–193,*
- Chen J., Chen A.A., Schatz H., Kubono S., Reyes A.B., Smith A., Wales B., Ouellet C., Kahl D., Redondo D.G., Lorusso G., LeNestour J., Conca J.P., Smith K., Amthor M., Matos M., Yamaguchi H., Iwasa N., Hayakawa S., Michimasa S., Teranishi T., Kurihara Y., and , Wakabayashi Y., “Study of astrophysically important states in ^{26}Si with the $p(^{27}\text{Si},^{26}\text{Si}^*)d$ reaction and the $p(^{25}\text{Al},p)^{25}\text{Al}$ elastic scattering”, *Nucl. Phys. A* **834** (2010) 667c–669c,*
- Niikura M., Ideguchi E., Aoi N., Baba H., Fukuchi T., Ichikawa Y., Iwasaki H., Kubo T., Kurokawa M., Liu M., Michimasa S., Ohnishi T., Onishi T.K., Ota S., Shimoura S., Suzuki H., Suzuki D., Wakabayashi Y., Yoshida K., Zheng Y., “Yrast spectroscopy in $^{49-51}\text{Ti}$ via fusion-evaporation reaction induced by a radioactive beam”, Proceedings of the Fifth International Confer-

- ence on Exotic Nuclei and Atomic Masses (ENAM'08), Sept. 7 – 13, 2008, Ryn, Poland, Eur. Phys. J. A **42** (2009) 471–475,*
- Shimoura S., “High-resolution spectroscopy using RI-beams — SHARAQ project”, Proceedings of the Franco-Japanese symposium “New Paradigms in Nuclear Physics”, Sept. 29 – Oct. 2, 2008, Paris, France, Int. J. Mod. Phys. E **18**, (2009) 2011–2014,*
- Takeuchi S., Aoi N., Baba H., Kubo T., Motobayashi T., Tanaka K., Yamada K., Fukui T., Ota S., Hashimoto Y., Kondo Y., Nakabayashi T., Nakamura T., Okumura T., Ieki K., Kanno S., Kurita K., Sugou R., Takeshita E., Togano Y., Imai N., Minemura T., Iwasaki H., Onishi T.K., Sakurai H., Suzuki D., Suzuki H., Suzuki M.K., Shimoura S., Tamaki M., “Study of low-lying states in ^{32}Mg ”, Proceedings of the Franco-Japanese symposium “New Paradigms in Nuclear Physics”, Sept. 29 – Oct. 2, 2008, Paris, France, Int. J. Mod. Phys. E **18**, (2009) 2025–2029,*
- Satou Y., Nakamura T., Fukuda N., Sugimoto T., Kondo Y., Matsui N., Hashimoto Y., Nakabayashi T., Okumura Y., Shinohara M., Motobayashi T., Yanagisawa Y., Aoi N., Takeuchi S., Gomi T., Togano Y., Kawai S., Sakurai H., Ong H.J., Onishi T.K., Shimoura S., Tamaki M., Kobayashi T., Otsu H., Endo N., Kitayama M., Ishihara M., “Invariant mass spectroscopy of $^{19,17}\text{C}$ and ^{14}B using proton inelastic and charge-exchange reactions”, Proc. the 10th International Conference on Nucleus-Nucleus Collisions (NN2009), Beijing, China, 16–21 August 2009, Nucl. Phys. A **834** (2010) 404c–407c,*
- Doornenbal P., Scheit H., Aoi N., Takeuchi S., Li K., Takeshita E., Wang H., Baba H., Deguchi S., Fukuda N., Geissel H., Gernhäuser R., Gibelin J., Hachiuma I., Hara Y., Hinke C., Inabe N., Itahashi K., Itoh S., Kameda D., Kanno S., Kawada Y., Kobayashi N., Kondo Y., Krücken R., Kubo T., Kuboki T., Kusaka K., Lantz M., Michimasa S., Motobayashi T., Nakamura T., Nakao T., Namihira K., Nishimura S., Ohnishi T., Ohtake M., Orr N.A., Otsu H., Ozeki K., Satou Y., Shimoura S., Sumikama T., Takeuchi M., Takeda H., Tanaka K.N., Tanaka K., Togano Y., Winkler M., Yanagisawa Y., Yoneda K., Yoshida A., Yoshida K., Sakurai H., “Exploring the Southern Boundaries of the “Island of Inversion” at the RIBF”, Proc. Int. Conf. on Nuclear Structure and Dynamics '09, Dubrovnik, Croatia, 4–8 May 2009, AIP Conf. Proc. **1165** (2009) 82–85,*
- Imai N., Aoi N., Ong H.J., Sakurai H., Demichi K., Kawasaki H., Baba H., Dombrádi Zs., Elekes Z., Fukuda N., Fülöp Zs., Gelberg A., Gomi T., Hasegawa H., Ishikawa K., Ishihara M., Iwasaki H., Kaneko E., Kanno S., Kishida T., Kondo Y., Kubo T., Kurita K., Michimasa S., Minemura T., Miura M., Motobayashi T., Nakamura T., Notani M., Ohnishi T.K., Saito A., Shimoura S., Sugimoto T., Suzuki M.K., Takeshita E., Takeuchi S., Tamaki M., Watanabe H., Yoneda K., “Ap-
plication of Doppler-shift attenuation method to the de-excitation γ rays from the in-flight ^{12}Be beam”, Proc. of the 6th Japan-Italy Symposium on Heavy-Ion Physics, Tokai, Japan, 11–15 November 2008, AIP Conf. Proc. **1120** (2009) 265–269,*
- Shimoura S., “High-resolution spectroscopy using direct reactions of RI beams”, Proc. of the 6th Japan-Italy Symposium on Heavy-Ion Physics, Tokai, Japan, 11–15 November 2008, AIP Conf. Proc. **1120** (2009) 59–63,*
- von Neumann-Cosel P., Adachi T., Bertulani C.A., Carter J., Dozono M., Fujita H., Fujita K., Fujita Y., Hashimoto H., Hatanaka K., Itoh M., Kalmykov Y., Kato K., Kawabata T., Matsubara H., Nakanishi K., Neveling R., Okamura H., Poltoratska I., Ponomarev V.Yu., Richter A., Rubio B., Sakaguchi H., Sakemi Y., Sasamoto Y., Shimbara Y., Shimizu Y., Smit F.D., Tameshige Y., Tamii A., Wambach J., Yosoi M., “Complete dipole response in ^{208}Pb from high-resolution polarized proton scattering at 0 degrees”, Proc. 13th Intern. Symposium on Capture Gamma-Ray Spectroscopy and Related Topics, Cologne, Germany, 25–29 Aug. 2008, J. Jolie, A. Zilges, N. Warr, A. Blazhev, Eds., p.404, AIP Conf. Proc. 1090 (2009),*
- Suzuki S., Otsuka T., “Structure of Light Neutron-rich Nuclei and Important Roles of Tensor Interaction”, Proc. of the International Conference on Nuclear Structure and Dynamics, May. 4-8, 2009, Dubrovnik, Croatia, AIP Conf. Proc. **1165** (2009) 54–56,*

Oral Presentations

(International Conference etc.)

- Gunji T., “Practice n GRID/CAF”, at the Workshop on ALICE Analysis Workshop for Asian Communities, Jan. 21–23, Hiroshima, Japan
- Gunji T., “Forward Physics at LHC energy”, at the Workshop on ALICE upgrades in Asian countries, Nov. 11–15, Yonsei University, Korea
- Gunji T., “Heavy Quarkonia Production in High Energy Heavy Ion Collisions at RHIC and Perspectives for the LHC”, at the Workshop on the Expanding Future of High Energy Nuclear Physics at LHC and RHIC, Oct. 13, 2009, Waikoloa, Hawaii, USA.
- Gunji T., “Heavy Quarks and Quarkonia Production at RHIC as a Probe of hot and dense QCD medium”, at the International Symposium on Multiparticle Dynamics, Sept. 05-09, Gold Sands, Gomel, Belarus
- Gunji T., “Quarkonia Melting in expanding hot and dense medium at RHIC”, at the workshop on Heavy Quarkonium Production in Heavy Ion Collisions, May 25–29, ECT*, Trento, Italy
- Yamaguchi Y.L. for the PHENIX Collaboration, “Measurements of low pT direct photons in PHENIX”, at the Workshop on the Expanding Future of High Energy Nuclear Physics at LHC and RHIC, Oct. 13, 2009, Waikoloa, Hawaii, USA.

- Akimoto R., Hamagaki H., Gunji T., Yamaguchi Y.L., Hori Y., “Measurement of the basic features of Thick-GEM and Resistive GEM” at the 1st International conference on Micro Pattern Gaseous Detectors, Jun. 12–15, 2009, Orthodox Academy of Crete Conference Center, Crete, Greece.
- Hori Y., “A simulation study for a Forward Calorimeter upgrade plan in ALICE at LHC”, at the Workshop on ALICE upgrades in Asian countries, Nov. 11–15, Yonsei University, Korea
- Saito A., “The ${}^6\text{He}+{}^6\text{He}$ and $\alpha+{}^8\text{He}$ cluster states in ${}^{12}\text{Be}$ via inelastic scattering”, International Symposium on Forefronts of Researches in Exotic Nuclear Structures (Niigata2010), March 1–4, 2010, Tokamachi, Niigata, Japan.
- Shimoura S., “Recent developments of radiation detector systems for RIBF experiments”, Workshop On Developments of new Scintillator Detectors for Gamma Spectroscopy and Imaging, November 16–17, 2009, Milano, Italy.
- Ota S., Shimoura S., Aoi N., Takeshita E., Takeuchi S., Suzuki H., Baba H., Fukuchi T., Fukui T., Hashimoto Y., Ideguchi E., Ieki K., Iwasa N., Iwasaki H., Kanno S., Kondo Y., Nakabayashi T., Nakamura T., Niikura M., Okumura T., Onishi T.K., Sakurai H., Shinohara M., Suzuki D., K. M., Tamaki M., Tanaka K., Togano Y., Wakabayashi Y., Yamada K., “High Resolution In-beam Spectroscopy of island-of-inversion nuclei via alpha induced reaction”, International Workshop on Direct Reactions with Exotic Beams (DREB2009), December 16–19, 2009, Tallahassee, Florida, USA.
- Michimasa S., “SHARAQ Overview and Scientific Programs”, Sept. 9–10, 2009, JUSEIPEN Workshop.
- Uesaka T., “Polarized Solid Proton Target in Low Magnetic Field and at High Temperature”, 13th International Workshop on Polarized Sources, Targets and Polarimetry, Sept. 7–11, 2009, Ferrara, Italy.
- Kawahara T., Uesaka T., Shimizu Y., Sakaguchi S., Wakui T., “Pulse structure dependence of the proton spin polarization rate”, 13th International Workshop on Polarized Sources, Targets and Polarimetry Sep. 07–11, 2009, Camera di Commercio, Ferrara, Italy.
- Uesaka T., “SHARAQ Spectrometer —Current status and future experimental plans—”, International Symposium of Exotic Nuclei 2009, Sep. 28–Oct. 2, 2009, Sochi, Russia
- Uesaka T., “Current status and future experimental program of the SHARAQ Spectrometer”, 7th Japan-China Joint Nuclear Physics Symposium, Nov. 9–13, 2009, University of Tsukuba, Ibaraki, Japan
- Uesaka T., “The SHARAQ Spectrometer”, ICHOR-EFES International Symposium on New Facet of Spin-Isospin Responses 2010, Feb. 18–21, 2010, University of Tokyo, Tokyo, Japan
- Shimizu Y., “Spin dependent momentum distribution of proton in ${}^3\text{He}$ studied via proton induced exclusive knockout reaction”, 19th International IUPAP Conference on Few-Body Problems in Physics, FB19, Aug. 31–Sep. 5, University of Bonn, Bonn, Germany.
- Sasamoto Y., Uesaka T., Sakai H., Shimoura S., Noji S., Yako K., Michimasa S., Ota S., Saito A., Miki K., Tokieda H., Miya H., Kawase S., Kubo T., Yoshida K., Ohnishi T., Yanagisawa Y., Fukuda N., Takeda H., Kameda D., Aoi N., Takeuchi S., Ichihara T., Baba H., Sakaguchi S., Shimizu Y., Schiet H., Doornembal P., Kawabata T., Itoh K., Kawahara T., Maeda Y., Saitoh T., Itoh M., Zegers R.G.T., Sasano M., Roussel-Chomaz P., Berg G.P.A., “The super-allowed Fermi type charge exchange reaction for studies of isovector non-spin-flip monopole resonance”, ICHOR-EFES International Symposium on New Facet of Spin-Isospin Responses (SIR2010), Feb. 18–21, 2010, Koshiba Hall, University of Tokyo, Japan.
- Ota S., “High-resolution in-beam spectroscopy of island-of-inversion nuclei via alpha induced reactions”, Direct Reactions with Exotic Beams (DREB) 2009, Dec. 16–19, 2009, Florida State University, Tallahassee, Florida, USA.
- Ota S., “Active Target in CNS, UT”, Instrumentation discussion session, Direct Reactions with Exotic Beams (DREB) 2009, Dec. 16, 2009, Florida State University, Tallahassee, Florida, USA.
- Ota S., “Active Target Development in CNS”, GET-ACTAR General Meeting, Jan. 11–15, 2010, Ferme de la Rançonnière, Crepon, France.
- Ota S., “Study of giant resonances in unstable nuclei with CNS Active Target”, ICHOR-EFES International Symposium on New Facet of Spin-Isospin Responses (SIR2010), Feb. 18–21, 2010, Koshiba Hall, University of Tokyo, Japan.
- Miki K., Sakai H., Uesaka T., Baba H., Berg G.P.A., Fukuda N., Kameda D., Kawabata T., Kawase S., Kubo T., Kusaka K., Michimasa S., Miya H., Noji S., Ohnishi T., Ota S., Saito A., Sasamoto Y., Sasano M., Shimoura S., Takeda H., Tokieda H., Yako K., Yanagisawa Y., Yoshida A., Yoshida K., and , Zegers R.G.T., “Search for the Isovector Spin Monopole Resonance via the ${}^{208}\text{Pb}, {}^{90}\text{Zr}(t, {}^3\text{He})$ Reactions at 300 MeV/u”, The 4th LACM-EFES-JUSTIPEN Workshop, Mar. 15–17, 2010, Oak Ridge National Laboratory, Tennessee, USA
- Miki K., Sakai H., Uesaka T., Baba H., Berg G.P.A., Fukuda N., Kameda D., Kawabata T., Kawase S., Kubo T., Kusaka K., Michimasa S., Miya H., Noji S., Ohnishi T., Ota S., Saito A., Sasamoto Y., Sasano M., Shimoura S., Takeda H., Tokieda H., Yako K., Yanagisawa Y., Yoshida A., Yoshida K., and , Zegers R.G.T., “Measurement of the ${}^{208}\text{Pb}$ and ${}^{90}\text{Zr}(t, {}^3\text{He})$ reactions at 300 MeV/u – the first physics measurement with SHARAQ –”, ICHOR-EFES International Symposium on New Facet of Spin-Isospin Responses (SIR2010),

- Feb. 18–21, 2010, University of Tokyo, Tokyo, Japan
- Yamaguchi H., Hashimoto T., Hayakawa S., Binh D.N., Kahl D., Kubono S., “Nuclear astrophysics and structure studies using low-energy RI beams at CRIB”, 7th Japan-China Joint Nuclear Physics Symposium, November 9–13, 2009, Tsukuba University, Ibaraki, Japan.
- Yamaguchi H., Hashimoto T., Hayakawa S., Binh D.N., Kahl D., Kubono S., “Status of the studies on nuclear reactions and structures at CRIB”, The 6th International Workshop on “Physics with Stopped and Slow Radioisotope Beams (SSRI)”, Mar 1–2, 2010, Tokyo Institute of Technology, Tokyo, Japan.
- Yamaguchi H., Hashimoto T., Hayakawa S., Binh D.N., Kahl D., Kubono S., “Studies for alpha-induced astrophysical reactions at CRIB”, The 10th. International Symposium on. Origin of Matter and Evolution of the Galaxies (OMEG10), March 8–10, 2010, RCNP, Osaka University, Osaka, Japan.
- Suzuki T., Otsuka T., “Structure of Light Neutron-rich Nuclei and Important Roles of Tensor Interaction”, International Conference on Nuclear Structure and Dynamics, May 2009, Dubrovnik, Croatia
- Suzuki T., “Structure of Light Exotic Nuclei”, International Conference on Nuclear Structure and Related Topics, June 2009, Dubna, Russia
- Suzuki T., “Neutrino-induced Reactions on Nuclei and Nucleosynthesis in Stars”, Neutrinos and Dark Matter 2009, Sept. 2009, Wisconsin University, U.S.A.
- T. Suzuki, M. Honma, K. Higashiyama, T. Yoshida, T. Kajino, T. Otsuka, H. Umeda and K. Nomoto (Oral): “Neutrino-induced Reactions on Ni and Fe Isotopes and Nucleo- synthesis in Stars”, 3rd Joint Meeting of the APS-DNP and Physical Society of Japan, Oct. 2009, Hawaii, U.S.A.
- Suzuki T., “Spin Responses in Nuclei, Neutrino-induced Reactions and Nucleo- synthesis in Stars”, 7th Japan-China Joint Nuclear Physics Symposium, Nov. 2009, Univ. of Tsukuba, Japan
- Suzuki T., “Gamow-Teller Transitions in Astrophysical Processes”, EFES- JUSTIPEN workshop, Dec. 2009, RIKEN, Wako, Japan
- Suzuki T., “Shell Model Study of Spin Modes in Ni and Ca Isotopes”, EFES-NSCLWorkshop on Perspectives on the Modern Shell Model and Related Experimental Topics, Feb. 2010, Michigan State University, U.S.A.
- Suzuki T., “Nuclear Weak Processes and Nucleosynthesis in Stars”, ICOR-EFES International Symposium on New Facet of Spin-isospin Responses (SIR2010), Feb. 2010, Koshiha Hall, Univ. of Tokyo, Japan
- Suzuki T., Yoshida T., Utsuno Y., “Half-lives of N=126 Isotones and the r-Process”, 10th International Symposium on Origin of Matter and Evolution of the Galaxies (OMEG10), Mar. 2010, RCNP, Osaka, Japan
- Suzuki T., “GT and FF Transitions in Astrophysical Processes”, The 4th LACM- EFES-JUSTIPEN Workshop, Mar. 2010, Oak Ridge, USA
- Yoshida T., Kato K., “Algebraic N alpha model (applications for ^{12}C)”, Hadron and Nuclear Physics (HNP09), Nov. 16-19, 2009, RCNP, Osaka, Japan.
- Gunji T., “Quarkonia Melting in expanding hot and dense medium at RHIC”, at the 3rd Joint Meeting of the APS Division of Nuclear Physics and Physical Society of Japan, Oct. 14–17, 2009, Hilton Waikoloa Village, Hawaii, USA.
- Tsuchimoto Y., for the PHENIX Collaboration: “Measurement of Low-Mass Vector Mesons (LVM) in PHENIX at RHIC”, at the 3rd Joint Meeting of the APS Division of Nuclear Physics and Physical Society of Japan, Oct. 14–17, 2009, Hilton Waikoloa Village, Hawaii, USA.
- Aramaki Y., for the PHENIX Collaboration: “Neutral pion production with respect to the reaction plane in $\sqrt{s_{NN}} = 200$ GeV Au+Au collisions at PHENIX”, 3rd Joint Meeting of the Nuclear Physics Divisions of the APS and The Physical Society of Japan, October 13–17, 2009, Waikoloa, Hawaii, USA.
- Akimoto R., Ota S., Michimasa S., Gunji T., Yamaguchi H., Hashimoto T., Tokieda H., Hamagaki H., Uesaka T., Kubono S., “Simulation study of performance of active target GEM TPC”, at the 3rd Joint Meeting of the APS Division of Nuclear Physics and Physical Society of Japan, Oct. 14–17, 2009, Hilton Waikoloa Village, Hawaii, USA.
- Ideguchi E., “Lifetime measurements of RI beam and high-spin studies with degraded beams”, Workshop on Physics Opportunities with GRETINA, Third Joint Meeting of the Nuclear Physics Divisions of the APS and JPS, October 13, 2009, Hawaii, USA.
- Miya H., Shimoura S., Saito A., Miki K., Sasano M., Itoh S., Itahashi K., Kawabata T., Shimbara Y., Yako K., Shimizu Y., Baba H., Kurei H., Michimasa S., Nakanishi K., Noji S., Ota S., Sasamoto Y., Tokieda H., Uesaka T., Sakai H., “Performance evaluation of Low Pressure Multi-Wire Drift Chamber for RI beam” Third Joint Meeting of the Nuclear Physics Divisions of the APS and JPS, October 13–17, 2009, Hawaii, USA.
- Go S., Shimoura S., Ideguchi E., Ota S., Miya H., Baba H., “New method of digital pulse shape analysis of signals for segmented Ge detectors”, Third Joint Meeting of the Nuclear Physics Divisions of the APS and the JPS, October 13–17, 2009, Hawaii, USA.
- Tokieda H., Michimasa S., Ota S., Shimoura S., Uesaka T., Noji S., Sakai H., Roussel-Chomaz P., Libin J-F., Gangnant P., Spitaels C., “Performance of Focal-Plane Tracking Detector CRDC for SHARAQ”, Third Joint Meeting of the Nuclear Physics Divisions of the APS and the JPS, Oct. 13–17, 2009, Hawaii, USA.
- Uesaka T., Nakanishi K., Kurei H., Ota S., Michimasa S., Saito A., Sasamoto Y., Miya H., Tokieda H., Shimoura S., Miki K., Noji S., Sakai H., “Field mapping measurement of SHARAQ dipole magnets”, Third Joint Meeting

- of the Nuclear Physics Divisions of the APS and the JPS, Oct. 13–17, 2009, Hawaii, USA.
- Sasamoto Y., Uesaka T., Kawabata T., Berg G.P.A., Nakanishi K., Noji S., Takeda H., Shimoura S., Sakai H., “Ion optical studies in the high resolution beam line and the SHARAQ spectrometer”, 3rd Joint Meeting of the Nuclear Physics Divisions of the APS and JPS, Oct. 13–17, 2009, Hilton Waikooa Village, Hawaii, USA.
- Yamaguchi H., Hashimoto T., Hayakawa S., Binh D.N., Kahl D., Kubono S., “Study on astrophysical reactions using low-energy RI beams”, Workshop on Frontiers in Nuclear Astrophysics I, Third Joint Meeting of the Nuclear Physics Divisions of the APS and JPS, October 13–17, 2009, Hilton Waikoloa Village, Hawaii, USA.
- Wakabayashi Y., Yamaguchi H., Hashimoto T., Hayakawa S., Kurihara Y., Binh D.N., Kahl D., Kubono S., Nishimura S., Gono Y., Suga M., Fujita Y., “Beta-decay measurement of ^{46}Cr ”, at third joint meeting of the APS and the JPS, Oct. 13–17, 2009, Waikoloa, Hawaii
- Hayakawa S., Yamaguchi H., Hashimoto T., Wakabayashi Y., Binh D.N., Kahl D.M., Kubono S., Iwasa N., Kume N., Miura Y., Teranishi T., He J.J., Kwon Y.K., Komatsubara T., Kato S., Wanajo S., “Direct measurement of the $^{11}\text{C}(\alpha, p)^{14}\text{N}$ stellar reaction”, at 3rd Joint Meeting of the APS Division of Nuclear Physics and the Physical Society of Japan, Oct. 13–17, 2009, Hawaii, USA.
- Yoshida T., Kato K., “Algebraic N alpha model (applications for ^{12}C)”, at the APS and JPS meeting, Oct. 13–17, 2009, Waikoloa, Hawaii, US.
- (Domestic Conference)
- Hamagaki H., “A Critical Review of the Recent Results from Electro-Magnetic Measurements”, 12th Heavy Ion Cafe, at the University of Tokyo, Tokyo, May 9, 2009.
- Hamagaki H., “Discoveries of Hydro-Dynamical Behavior in High-Energy Heavy-Ion Collisions”, 13th Heavy Ion Cafe, at the University of Tokyo, Tokyo, Nov. 11, 2009.
- Gunji T., “Development of W+Si Tracking Calorimeter and readout for LHC-ALICE”, at the Detector workshop for RIBF experiments, Dec. 21–22, 2009, RIKEN, Wako, Japan.
- Gunji T., “東大 CNS における GEM 開発と Active Target GEM-TPC の開発”, at the 6th Workshop on Micor Pattern Gas Detector, Dec. 11–12, Kobe University, Japan
- Akimoto R., Ota S., Michimasa S., Gunji T., Yamaguchi H., Hashimoto T., Tokieda H., Tsuji T., Kawase S., Hamagaki H., Uesaka T., Kubono S., Isobe T., Kawabata T., Ozawa A., Suzuki H., Nagae D., Moriguchi T., Ito Y., Ishibashi Y., Ooishi H., Abe Y., “Design and performance of CNS active target TPC” at the Detector workshop for RIBF experiments, Dec. 21–22, 2009, RIKEN, Wako, Japan.
- Uesaka T., Akimoto R., Ota S., Michimasa S., Gunji T., Yamaguchi H., Hashimoto T., Tokieda H., Tsuji T., Kawase S., Hamagaki H., Kubono S., Kawabata T., Isobe T., Ozawa A., Suzuki H., Nagae D., Moriguchi T., Ito Y., Ishibashi Y., Oishi H., Abe Y., Kamiguchi N., “CNS active targets for Missing Mass Spectroscopy with RI beams”, Detector Workshop for RIBF Experiments, Dec. 21–22, 2010, RIKEN, Saitama, Japan
- Gunji T., “ J/ψ Production in High energy heavy ion collisions at RHIC”, at the JPS Spring meeting, Mar. 20–23, 2010, Okayama University, Okayama, Japan.
- Sano S., for the ALICE Collaboration: “LHC-ALICE 実験における粒子多重度測定” at the JPS Spring meeting, Mar. 20–23, 2010, Okayama University, Okayama, Japan.
- Takahara A., for the PHENIX Collaboration: “Study of J/ψ photoproduction in ultra-peripheral Au+Au collisions at the PHENIX experiment”, at the JPS Spring meeting, Mar. 20–23, 2010, Okayama University, Okayama, Japan.
- Akimoto R., Ota S., Michimasa S., Gunji T., Yamaguchi H., Hashimoto T., Tokieda H., Tsuji T., Kawase S., Hamagaki H., Uesaka T., Kubono S., Isobe T., Kawabata T., Ozawa A., Suzuki H., Nagae D., Moriguchi T., Ito Y., Ishibashi Y., Ooishi H., Abe Y., “Performance evaluation of active target GEM-TPC” at the JPS Spring meeting, Mar. 20–23, 2010, Okayama University, Okayama, Japan.
- Tsuji T., Hamagaki H., Gunji T., Hori Y., Kistenev E., Chiu M., Sukhanov A., Seto R., “Study of basic properties of the Forward Calorimeter for PHENIX upgrade”, at the JPS Spring meeting, Mar. 20–23, 2010, Okayama University, Okayama, Japan.
- Go S., Shimoura S., Ideguchi E., Ota S., Miya H., Baba H., “New method of digital pulse shape analysis of signals from segmented Ge detectors by using moments”, JPS Spring Meeting, March 20-23, 2010, Okayama University, Okayama, Japan.
- Michimasa S., Tokieda H., Noji S., Ota S., Shimoura S., Uesaka T., Sakai H., Roussel-Chomaz P., Libin J-F., Gangnant P., Spetaels C., “Performance of Detectors Installed at SHARAQ Final Focal Plane”, JPS Spring Meeting, March 20-23, 2010, Okayama University, Okayama, Japan.
- Kawase S., Ota S., Baba H., Shimoura S., Uesaka T., “Performance Evaluation of Charge-to-Time-Converter (QTC)”, the 65th JPS Annual Meeting, Mar. 20–23, 2010, Okayama University, Okayama, Japan.
- Ota S., Shimoura S., Aoi N., Takeshita E., Takeuchi S., Suzuki H., Baba H., Fukuchi T., Fukui T., Hashimoto Y., Ideguchi E., Ieki K., Iwasa N., Iwasaki H., Kanno S., Kondo Y., Kubo T., Kurita K., Minemura T., Michimasa S., Motobayashi T., Murakami T., Nakabayashi T., Nakamura T., Niikura M., Okumura T., Onishi T.K., Sakurai H., Shinohara M., Suzuki D., Suzuki M., Tamaki M., Tanaka K., Togano Y., Wakabayashi Y., Yamada K., “High Resolution Gamma-ray Spectroscopy of N=20 Neutron-rich Nuclei via Direct Reactions”, the 65th JPS Annual Meeting, Mar.

20–23, 2010, Okayama University, Okayama, Japan.

Miki K., Sakai H., Uesaka T., Baba H., Berg G.P.A., Fukuda N., Kameda D., Kawabata T., Kawase S., Kubo T., Kusaka K., Michimasa S., Miya H., Noji S., Ohnishi T., Ota S., Saito A., Sasamoto Y., Sasano M., Shimoura S., Takeda H., Tokieda H., Yako K., Yanagisawa Y., Yoshida A., Yoshida K., and , Zegers R.G.T., “Measurement of the the isovector spin monopole resonance via the $^{208}\text{Pb}, ^{90}\text{Zr}(t, ^3\text{He})$ reactions at 300 MeV/u”, at the JPS Spring meeting, Mar. 20–23, 2010, Okayama University, Okayama, Japan.

Suzuki T., “Beta decay modes of nuclei in the third peak region of the r-process”, at the 65th JPS Annual meeting, Mar. 20–23, 2010, Okayama University, Okayama, Japan

Yoshida T., Kato K., Study of ^{12}C structure based on Sp(2,R) algebra”, at the JPS meeting, Mar. 20-23, 2010, Okayama University, Okayama, Japan.

TORIJIN

(Todai-RIKEN Joint International Program for Nuclear Physics)

Publications

[Journal]

(Original papers) *Subject to Peer Review

- S. Aoyama and N. Itagaki, “Di-neutron correlations in ${}^7\text{H}$ ” *Phys. Rev. C* **80** rapid communication 021304 1-5 (2009).
- T. Yoshida, N. Itagaki, and T. Otsuka, “Appearance of cluster states in ${}^{13}\text{C}$ ” *Phys. Rev. C* **79** 034308 1-6 (2009).
- N. Itagaki and M. Kimura, “Cluster structure stabilized by s^2 neutrons in light neutron-rich nuclei” *Phys. Rev. C* **79** 034312 1-4 (2009).
- Y. Iwata, T. Otsuka, J.A. Maruhn, and N. Itagaki, “Synthesis of exotic nuclei in heavy-ion collisions at higher energies” *Eur. Phys. J. A* **42** 613-621 (2009).

[Book Proceedings]

(Original papers) *Subject to Peer Review

- M. Ito and N. Itagaki, “Covalent, ionic, and atomic structures in ${}^{12}\text{Be}$ ”, *Int. J. Modern Physics Letters A* **24** Issue: 11 1005-1008 (2009).
- Makoto Ito and Naoyuki Itagaki, “Unified studies of the exotic structures in ${}^{12}\text{Be}$ and $\alpha+{}^8\text{He}$ scattering”, *AIP Conf. Proc.* **1098** 231-236 (2009).
- N. Itagaki, M. Kimura, M. Ito, S. Aoyama, and Y. Hirata “Application of THSR wave function using Monte Carlo technique” *Int. J. Modern Physics Letters A* **24** Issue: 11 2019-2026 (2009).
- Y. Iwata, T. Otsuka, J. A. Maruhn, and N. Itagaki “Reduced charge equilibration in heavy-ion collisions at higher energies” *AIP Conf. Proc.* **1098** 308-312 (2009).

Oral Presentations

(International Conference etc.)

- N. Itagaki, “Multi cluster correlations studied with UCOM-like treatment”, First EMMI-EFES workshop on neutron-rich exotic nuclei “Realistic effective nuclear forces for neutron-rich nuclei” 9-11 Feb., GSI, Germany
- N. Itagaki, “Cluster-like correlations in light nuclei”, The 3rd LACM-EFES-JUSTIPEN workshop, 23-25 Feb., Oak Ridge National Lab., USA
- N. Itagaki, “Nuclear structure studies in JUSTIPEN and EFES activities”, The 3rd APS-JPS meeting, 13 Oct., Big Island, Hawaii, USA
- (Domestic Conference)
- N. Itagaki, “Exotic structure in the excited states of neutron-rich nuclei”, 64-th Japan Physical Society Meeting, Tokyo, Mar. 2009

VII. LIST OF PREPRINTS

(2009 January ~ 2010 March)

1. M. Yamagami, and Y. R. Shimizu, and T. Nakatsukasa “Optimal pair density functional for description of nuclei with large neutron excess” January, 2009
2. J. Gibelin, D. Beaumel, T. Motobayashi, Y. Blumenfeld, N. Aoi, H. Baba, Z. Elekes, S. Fortier, N. Frascaria, N. Fukuda, T. Gomi, K. Ishikawa, Y. Kondo, T. Kudo, V. Lima, T. Nakamura, A. Saito, Y. Satou, J. -A. Scarpaci, E. Takeshita, S. Takeuchi, T. Teranishi, Y. Togano, A. M. Vinodkumar, Y. Yanagisawa, and K. Yoshida “Decay Pattern of Pygmy States Observed in neutron-Rich ^{26}Ne ” January, 2009
3. T. Suda, M. Wakasugi, T. Emoto, K. Ishii, S. Ito, K. Kurita, A. Kuwajima, A. Noda, T. Shirai, T. Tamae, H. Tongu, S. Wang, and Y. Yano “First Demonstration of Electron Scattering using a Novel Target Developed for Short-Lived Nuclei” February, 2009
4. N. Imai, N. Aoi, H. J. Ong, H. Sakurai, K. Demich, H. Kawasaki, H. Baba, Zs. Dombradi, Z. Elekes, N. Fukuda, Zs. Fulop, A. Gelberg, T. Gomi, H. Hasegawa, K. Ishikawa, M. Ishihara, H. Iwasaki, E. Kaneko, S. Kanno, T. Kishida, Y. Kondo, T. Kubo, K. Kurita, S. Michimasa, T. Minemura, M. Miura, T. Motobayashi, T. Nakamura, M. Notani, T. K. Ohnishi, A. Saito, S. Shimoura, T. Sugimoto, M. K. Suzuki, E. Takeshita, S. Takeuchi, M. Tamaki, H. Watanabe, and K. Yoneda “First lifetime measurement of $2+1$ state in ^{12}Be ” February, 2009
5. S. Taakeuchi, N. Aoi, T. Motobayashi, S. Ota, E. Takeshita, H. Suzuki, H. Baba, T. Fukui, Y. Hashimoto, K. Ieki, N. Imai, H. Iwasaki, S. Kanno, Y. Kondo, T. Kubo, K. Kurita, T. Minemura, T. nakabayashi, T. Nakamura, T. Okumura, T. K. Onishi, H. sakurai, S. Shimoura, R. Sugou, D. Suzuki, M. K. Suzuki, M. Takashina, M. Tamaki, K. Tanaka, Y. Togano, and K. Yamada “Low-lying states in ^{23}Mg studied by proton inelastic scattering” May, 2009
6. N. Hinohara, T. Nakatsukasa, M. Matsuo, and K. Matsuyanagi “Microscopic description of oblate-prolate shape mixing in proton-rich Se isotopes” June, 2009
7. P. Doornenbal, H. Scheit, N. Aoi, S. Takeuchi, K. li, E. Takeshita, H. wang, H. Baba, S. deguchi, N. Fukuda, H. Geissel, R. Gernhauser, J. gibelin, I. Hachiuma, Y. Hara, C. Hinke, N. Inabe, K. Itahashi, S. Itoh, D. Kameda, S. Kannno, Y. kawada, N. Kobayashi, Y. Kondo, R. Krucken, T. Kubo, T. Kuboki, K. Kusaka, M. Lantz, S. Michimasa, T. Motabayashi, T. Nakamura, T. Nakao, K. Namihira, S. Nishimura, T. Ohnishi, M. Ohtake, N. A. Orr, H. Otsu, K. Ozeki, Y. satou, S. Shimoura, T. Sumikama, M. takechi, H. Takeda, K. N. Tanaka, K. Tanaka, Y. togano, M. Winkler, Y. Yanagisawa, K. Yoneda, A. Yoshida, K. Yoshida, and H. Sakurai “Spectroscopy of ^{32}Ne and the “Island of Inversion” June, 2009
8. Y. Ichikawa, T. K. Ohnishi, D. Suzuki, H. Iwasaki, T. Kubo, V. Banerjee, A. Chakrabarti, N. Aoi, B. A. Brown, N. Fukuda, S. Kubono, T. Motobayashi, T. Nakabayashi, T. Nakamura,

- T. Nakao, T. Okumura, H. J. Ong, H. Suzuki, M. K. Suzuki, T. Teranishi, K. N. Yamada, H. Yamaguchi, and H. Sakurai “Beta decay of proton-rich nucleus ^{24}Si and its mirror asymmetry” July, 2009
9. T. Inakura, T. Nakatsukasa, and K. Yabana “Self-consistent calculation of nuclear photoabsorption cross section: Finite amplitude method with Skyrme functionals in the three-dimensional real space” July, 2009
 10. G. Watanabe, H. Sonoda, T. Maruyama, K. Sato, K. Yasuoka, and T. Ebisuzaki “Formation of Nuclear "Pasta" in Supernovae” July, 2009
 11. G. Watanabe “Efficient scheme for creating a maximally entangled state in a double-well potential” July, 2009
 12. G. Watanabe, F. Dalfovo, F. Piazza, L. P. Pitaevskii, and S. Stringari “Critical velocity of superfluid flow through single barrier and periodic potentials” July, 2009
 13. K. Matsuyanagi, M. Matsuo, T. Nakatsukasa, N. Hinohara, and K. Sato “Open problems in microscopic theory of large-amplitude collective motion” January, 2010
 14. K. sato, N. Hinohara, T. Nakatsukasa, M. Matsuo, and K. Matsuyanagi “A Model Analysis of Triaxial Deformation Dynamics in Oblate-Prolate Shape Coexistence Phenomena” January, 2010
 15. M. Matsuo and T. Nakatsukasa “Open problems in nuclear structure near drip lines” January, 2010

CNS-REP

1. Deuteron beam polarimeter in the Nuclotron ring and analyzing power for the d-p elastic scattering at 880 MeV, T.Uesaka, K.Suda, P.K.Kurilkin, V.P.Ladygin, Yu.V.Gurchin, A.Yu.Isupov, K.Itoh, M.Janek, J.-T.Karachuk, T.Kawabata, A.N.Khrenov, A.S.Kiselev, V.A.Kizka, J.Kliman, V.A.Krasnov, A.N.Livanov, Y.Maeda, A.I.Malakhov, V.Matousek, M.Morhach,, S.M.Piyadin, S.G.Reznikov, S.Sakaguchi, H.Sakai, Y.Sasamoto, K.Sekiguchi, I.Turzo, T.A.Vasiliev, CNS-REP 79, May, 2009
2. CNS Annual Report 2007, Edited by E. Ideguchi, CNS-REP 80, Aug. 2009
3. Computer Modelling of Electromagnetic Fields for RIKEN AVF Cyclotron, A. S. Vorozhtsov, S. B. Vorozhtsov, JINR, Dubna, Russia, S. Watanabe, S. Kubono, CNS, University of Tokyo, Japan, A. Goto, RIKEN Nishina Center, RIKEN, Wako, Japan, CNS-REP 82, June, 20
4. CNS Annual Report 2008, Edited by S. Mitimasa, CNS-REP 83, Feb. 2010

VIII. LIST OF SYMPOSIA

(2009 April ~ 2010 March)

1. Arctic FIDIPRO-EFES workshop, Apr.20-24 2, Saariselka, Finland, University of Jyvaskyla, TORIJIN
2. Mini Workshop 「KbarN and its Few-Baryon Derivatives」 May.11 Advanced Meson Science Laboratory
3. RIBF Mini Workshop 「Electron scattering data needed for the charge-distribution determination of unstable nuclei」 M a y .14 RIBF Research Division
4. RIBF Mini Workshop 「One goal, different approaches - how to predict total reaction cross sections」 M a y .15 RIBF Research Division
5. RIKEN Workshop 「Mysteries of plant sexual differentiation」 Jun.11 Radiation Biology Team
6. Joint Theory / Experimental Workshop 「LHC@BNL」 Jun.20 Joint Theory/Experimental
7. "The 2nd Research Strategy Workshop 「Nuclear data base in Japan -the nuclear energies in the universe and the earth」 Jul.27-29 J.F.N.A."
8. Joint Theory / Experimental Workshop 「Early Physics at the LHC」 Sep.2 Joint Theory/ Experimental Workshop
9. EFES Ab initio workshop, Oct.12 , Big Island Hawaii, USA, JUSTIPEN, TORIJIN
10. JUSTIPEN-EFES workshop on unstable nuclei, Dec. 7-9, RIKEN , JUSTIPEN, TORIJIN
11. "RIKEN Workshop 「Studies on mutagenic effect of heavy-ion beam using model organisms II」 Dec.11 Radiation Biology Team & The Wakasa Wan Energy Research Center "
12. Joint CATHIE/TECHQM RIKEN Workshop 15-19 Dec. RIKEN/CATHIE/TECHQM
13. Detector Workshop for RIBF experiments Dec.21-22 Detector Team
14. RIKEN Lattice QCD Workshop Dec.22 Radiation Laboratory
15. RIKEN-TRIUMF collaborative workshop on nuclear theory, Dec.15-16 RIKEN Nishina Center & TRIUMF
16. RIKEN Symposium 「Muon Science at the RIKEN-RAL Muon Facility 2009 」 Jan.20-21 Advanced Meson Science Laboratory
17. Mini Workshop 「Study of the Superheavy Element at RIKEN」 Jan.21 RIBF Research Division
18. The decade of ion-beam breeding in RIKEN Jan.21-22 Radiation Biology Team
19. RIKEN Workshop on 「Superheavy Element Chemistry」 Feb.2 Superheavy Element Laboratory
20. First EMMI-EFES workshop on neutron-rich exotic nuclei ``Realistic effective nuclear forces for neutron-rich nuclei" Feb.9-11, GSI, Germany, EMMI, GSI, EFES
21. Workshop for Orbital Angular Momentum (OAM) of nucleon Feb.12 Radiation Laboratory
22. Workshop on Kaonic Nuclear Clusters Feb.16 Advanced Meson Science Laboratory

23. First EMMI-EFES workshop on neutron-rich exotic nuclei “Realistic effective nuclear forces for neutron-rich nuclei” Feb.9-11, GSI, Germany, EMMI, GSI, EFES
24. The 3rd LACM-EFES-JUSTIPEN workshop, Feb.23-25, Oak Ridge National Lab., USA, EFES, JUSTIPEN, Oak Ridge National Lab.
25. Japanese-French Workshop 「EFES-LIA workshop on the Nuclear Energy Density Functional Method」 Feb.26-27 EFES-LIA
26. CNS Workshop 「EFES-LIA workshop on the Nuclear Energy Density Functional Method」 Feb. 26
27. First LIA-EFES workshop “Low-energy collective motion of exotic nuclei”, Mar.2-4, GANIL, France, LIA, EFES, GANIL

IX. LIST OF SEMINAR

(2009 April ~ 2010 March)

Theoretical Research Division

- 1 Elias Kiritsis (Physics Department, University of Crete, GR-71003, Heraklion,(REECE) Apr.3 「A holographic approach to QCD」
- 2 Hidenori Sonoda (Graduate School of Science, Kobe University) Apr.10 「Quadratic divergences in the Wess-Zumino model, revisited」
- 3 T. Nakatsukasa(RIKEN Nishina Center) Apr.15 Colloquium 「Symmetry breaking and phase transition in nuclei」
- 4 Takuya Kanazawa (Department of Physics, Graduate School of Science, The University of Tokyo) May.8 「Dense QCD in a finite volume」
- 5 Hideo Matsufuru (Computing Research Center, High Energy Accelerator Research Organization) May.15 「Lattice QCD simulation with dynamical overlap fermion」
- 6 Tooru Yoshida (CNS, Univ. of Tokyo) May.27 13th Nuclear Theory Seminar 「Appearance of cluster states in ^{13}C 」
- 7 Satoshi Yamaguchi (Seoul National University) May.29 「Surface operators and AdS/CFT correspondence」
- 8 Hans Feldmeier (GSI, YITP) Jun.8 14th Nuclear Theory Seminar 「Shells, clusters, and halos - Concepts to solve the nuclear many-body problem」
- 9 Shotaro Shiba (Department of Physics, Faculty of Science, University of Tokyo) Jun.12 「Dp-branes and U-duality from BLG model」
- 10 Atsushi Mochizuki(RIKEN) Jun.17 Colloquium 「Structure of regulatory networks and dynamics of bio-molecules」
- 11 Shinya Aoki (Univ. of Tsukuba) and others Jun.25-27 「Structure of Nuclear Matter and Baryon-Baryon Interaction」
- 12 Makiko Nio (RIKEN Nishina Center) Jul.8 15th Nuclear Theory Seminar 「Anomalous magnetic moments of the lepton」
- 13 So Matsuura (Department of Physics, Hiyoshi Campus, Keio University) Jul.13 「Instanton Counting and Dielectric Branes」
- 14 Norihiro Iizuka (Kavli Inst. for Theoretical Physics, Univ. of California, Santa Barbara, USA) Jul.17 「Matrix Quantum Mechanics for the Black Hole Information Problem」
- 15 Takenori Furumoto (Osaka City Univ.) Jul.22 16th Nuclear Theory Seminar 「Optical potential based on complex G-matrix folding model - Important role of three-body force effect -」
- 16 In Yong Park (Philander Smith College) Jul.24 「Open string induced D-brane geometry: Two loop analysis」
- 17 Takeshi KOIKE (Department of Physics, Graduate School of Science, Tohoku University. Jul.24 「gamma-ray spectroscopy of well deformed sd-shell hypernuclei」
- 18 Kazuhito Mizuyama (Univ. of Jyvaskyla) Aug.3 17th Nuclear Theory Seminar 「Microscopic description of the two-body correlation density in the ground state and in the excited states of nuclei」
- 19 Makoto Oka(TITECH) and others Aug.3-6 「Summer School on Exotic Nuclei」
- 20 Mitsutoshi Fujita (Department of Physics, Kyoto University) Aug.7 「Eschenburg space as gravity dual of flavored $N=4$ Chern-Simons-matter theory」
- 21 Cristina Manuel (Instituto de Ciencias del Espacio (CSIC)) Aug.15 「Cold Relativistic Superfluids: Transport Phenomena and Applications」
- 22 Oleg Andreev (TU Munich and Landau Moscow) Aug.15 「Searching for a mean string theory description of the pure gauge theory in the IR」
- 23 "Hiroataka Hayashi (School of Science, the University of Tokyo) Aug.21 「Codimension-3 Singularities and Yukawa Couplings in F-theory」 "
- 24 Edmond Iancu (IPhT, CEA Saclay) Aug.22 「AdS/CFT and Heavy Ion Collisions」
- 25 Kazuhiro Sakai (Hiyoshi Department of Physics, Keio University) Sep.4 「Entanglement through conformal interfaces」

- 26 Shinji Ejiri (Brookhaven National Laboratory, USA) Sep.7 「Study of the critical point in finite density lattice QCD」
- 27 Hitoshi Nakada (Chiba Univ.) Sep.16 18th Nuclear Theory Seminar 「Self-consistent mean-field and RPA calculations with semi-realistic NN interactions」
- 28 Takashi Okamura (Department of Physics, School of Science and Technology, Kwansei Gakuin University) Sep.25 「Superfluidity of holographic superconductor models」
- 29 Simone Baroni (INT, Univ. of Washington and TRIUMF, JUSTIPEN guest) Oct.8 19th Nuclear Theory Seminar「Odd-even mass staggering and nuclear superfluidity」
- 30 Jun Goryo (Department of Physics, Nagoya University) Oct.9 「Chiral p-wave superconductivity」
- 31 Wen Wen-Yu (National Taiwan University, Taiwan) Oct.16 「Greybody factor in warped AdS3 black hole and its CFT interpretation」
- 32 Hyun Seok Yang (KIAS) Oct.19 「Anatomy of Spacetime」
- 33 Jnanadeva Maharana (Inst. Phys., Bhubaneswar) Oct.20 「Toroidal Compactification of Type IIB Theory with Fluxes」
- 34 Robert Dijkgraaf (Amsterdam Univ.) Oct.27 「Superconformal gauge theories, Liouville theory and matrix models」
- 35 Yutaka Okochi (Perimeter Institute for Theoretical Physics, Canada) Oct.27 「On Confinement Index」
- 36 Katsushi Ito (Tokyo Institute of Technology, Department of Physics) Oct.27 「Supersymmetric Gauge theories and Instantons IX」
- 37 Robert Dijkgraaf (Amsterdam Univ.) Oct.27 「Superconformal gauge theories, Liouville theory and matrix models」
- 38 Jnanadeva Maharana (Inst. Phys., Bhubaneswar) Oct.27 「Toroidal Compactification of Type IIB Theory with Fluxes」
- 39 Goro Ishiki (CQeST(Center for Quantum SpaceTime), Sogang University, Korea) Oct.3 「A novel large N reduction for gauge theories on 3-sphere」
- 40 Norihiro Iizuka (CERN, Switzerland) Oct.30 「Exploring N-body Nuclear Force in Holographic QCD」
- 41 Yutaka Ohkochi (Perimeter Institute for Theoretical Physics) Oct.30 「On Confinement Index」
- 42 Nick Stephen Manton (Cambridge Univ.) Nov.2 「Nuclei as quantized skyrmions」
- 43 Dominik Smith (Frankfurt Univ.) Nov.6 「Lattice simulation of a three dimensional effective theory for SU(2) Yang Mills」
- 44 Yuri Aisaka (Instituto Fisica Teorica, Sao Paulo State University, Brazil) Nov.13 「Some Recent Developments in Pure Spinor Formalism」
- 45 Hiroshi Suzuki (RIKEN Nishina Center) Nov.18 Colloquium 「Spontaneous breaking of supersymmetry 」
- 46 Toshio Nakatsu (Department of Mathematics and Physics, Setsunan University) Nov.20 「Melting crystal, quantum torus and supersymmetric Yang-Mills」
- 47 Ken'ichiro Nakazato (Kyoto Univ.) Nov.25 20th Nuclear Theory Seminar 「Gyroid Phase in Nuclear Pasta」
- 48 Ryuichiro Kitano (Department of Physics, Tohoku University) Nov.30 「Higgsinoless Supersymmetry and Hidden Gravity」
- 49 Raffaele Mollo (University of Trento) Dec.3 「Vacuum polarization and Strong CP-violation: from macroscopic effects to microscopic dynamics」
- 50 C.S. Lim (Department of Physics, Kobe University) Dec.5 「CP Violation in Higher Dimensional Gauge Theories」
- 51 Tatsuo Kobayashi (Graduate School of Science, Kyoto University) Dec.5 「Extra dimensional models with magnetic fluxes」
- 52 Yutaka Hosotani (Graduate School of Science, Osaka University) Dec.5 「Stable Higgs bosons as cold dark matter in the realistic gauge-Higgs unification」
- 53 Yutaka Sakamura (Theoretical Physics Laboratory, RIKEN) Dec.5 「Radius stabilization in gauge-Higgs unification」

- 54 C.S. Lim (Kobe Univ.) Dec.5 「CP Violation in Higher Dimensional Gauge」
- 55 Masatoshi TAKANO (Waseda University) Dec.21 「Variational calculations for the nuclear equation of state」
- 56 M. Takano (Waseda University) Dec.21 「Variational calculations for the nuclear equation of state」
- 57 Hidenori Sonoda(Kobe University) Jan.12 「A simple proof of the non-renormalization theorem for the Wess-Zumino model」
- 58 Toshikazu Ebisuzaki(Riken) Jan.20 Colloquium 「Gamma-ray Signal from Earth-mass Dark Matter Microhalos」
- 59 Masaya Kohda (Graduate School of Science and Engineering, Saitama University) Jan.29 「The strongly coupled fourth family and a first-order electroweak phase transition」
- 60 Tetsuya Sakurai (Dept. of Computer Science, Univ. of Tsukuba) Feb.10 21st Nuclear Theory Seminar 「A Parallel Eigensolver using Contour Integration for Large-Scale Scientific Computing」
- 61 Junya Yagi(Rutgers University) Feb.12 「Chiral algebras of (0,2) models: Beyond perturbation theory」
- 62 " Shinji Hirano (Niels Bohr Institute, Denmark)
(Niels Bohr Institute) Feb.17 「Anomalous Charge Shifts in AdS(4)/CFT(3)」 "
- 63 Pascal Naidon (The University of Tokyo) Mar.18 「Efimov physics in cold atoms」
- 64 B. R. Barrett (Univ. of Arizona) Mar.26 22st Nuclear Theory Seminar Using the Concavity of Thermodynamical Functions to Predict Nuclear Binding Energies (not open to the public)
- 65 "Takenori Furumoto (Osaka City Univ.) Jul.22 The 16th Nuclear Theory Seminar 「Optical potential based on complex G-matrix folding model- Important role of three-body force effect」 "
- 66 Kazuhito Mizuyama (Univ. of Jyvaskyla) Aug.3 The 17th Nuclear Theory seminar 「Microscopic description of the two-body correlation density in the ground state and in the excited states of nuclei」
- 67 Hitoshi Nakada (Chiba Univ.) Sep.16The 18th Nuclear Theory Seminar 「Measurement of Low-mass Vector Mesons in Hot-Medium created by Relativistic Heavy-Ion Collisions」

Sub Nuclear System Research Division

- 1 Julius Kuti (University of California, San Diego) Apr.9 「Nearly Conformal Gauge Theories and Compositeness at the LHC」
- 2 Stefano Profumo (SCIPP, University of California, Santa Cruz) Apr.10 「Fundamental Physics from the Sky」
- 3 Mark Trodden (University of Pennsylvania) Apr.16 「Constraining Interactions in Cosmology's Dark Sector」
- 4 Eugene Levin (Tel Aviv University) Apr.17 「Glauber-Gribov approach for DIS on nuclei in N=4 SYM」
- 5 Saul Cohen (JLab) Apr.30 「Electromagnetic Neutral-Meson Decays on the Lattice」
- 6 Urs Heller (APS/BNL) May.1 「Center Vortices, Confinement and Chiral Symmetry Breaking」
- 7 Ian Low (Argonne National Laboratory/Northwestern University) May.7 「Implications of the Higgs Discovery in MS
- 8 Ayako Yamamoto (Magnetic Materials Laboratory,RIKEN) May.7 「Variation of magnetic properties in metal complex oxides with pyrochlore-type structure」
- 9 Matthias Burkardt (New Mexico State University) May.8 「Transverse (Spin) Structure of Hadrons」
- 10 Amarjit Soni (BNL) May.9 「"4th generation" and B-CP anomalies」
- 11 Matthew Reece (Princeton Center for Theoretical Science) May.21 「The AdS/QCD Correspondence: Still Undelivered」
- 12 Adrian Dumitru (Baruch College) May.28 「Gluon propagator and quarkonium decay width in a viscous QGP」
- 13 Eduardo Fraga (Rio de Janeiro Federal University) Jun.5 「Chiral symmetry restoration and strong CP violation in a strong magnetic background」

- 14 D. A. Bryman (TRIUMF/University of British Columbia, Canada) Jun.5 「Rare opportunities: Seeking new physics with rare decays of light particles」
- 15 Douglas Bryman (TRIUMF) Jun.5 「Rare opportunities: Seeking new physics with rare decays of light particles」
- 16 Nasser Demir (Duke University) Jun.6 「Eta/s of a relativistic hadron gas from a hadronic cascade」
- 17 Miura Kohtaroh (Yukawa Institute for Theoretical Physics, Kyoto University) Jun.9 「Strong coupling lattice study in QCD phase diagram and dense matter」
- 18 Marco Stratmann (Regensburg University) Jun.10 「The story behind a half - from current probes to future avenues」
- 19 Antonio Masiero (INFN/PADUA) Jun.12 「Flavor and SUSY: between frustration and hope」
- 20 Tim Tait (Argonne National Laboratory) Jun.18 「Academic Lectures, Top Quark Physics」
- 21 Giovanni Chirilli (Old Dominion University & JLAB) Jun.23 「Small-x Evolution of Structure Functions in the Next-to-Leading Order」
- 22 Sebastian Klein (DESY) Jun.25 「Moments of the 3-loop corrections to the heavy flavor contribution to $F_2(x, Q^2)$ for $Q^2 \gg m^2$ 」
- 23 Harutaka SAKAGUCHI (RCNP) Jul.3 「Neutron skin in 208Pb」
- 24 Gilad Perez (Weizman) Jul.8 「The inside and outside of top jets」
- 25 Thomas McElmurry (Madison) Jul.9 「Colored Scalars at the LHC」
- 26 Yasumichi Aoki (RBRC) Jul.10 「Non-perturbative renormalization in lattice QCD」
- 27 Chris Jackson (ANL) Jul.11 「The WIMP Forest」
- 28 Kirill Tuchin (Iowa State University) Jul.17 「Coherence at high energies and J/Psi production」
- 29 Anastasios Taliotis (Ohio State University) Jul.18 「Applications of AdS/CFT in DIS」
- 30 Seung Lee (Weizman) Jul.23 「Anti-Matter Signals from Matter Stability (DM from RS-GUT @ Galactic Cosmic Rays and LHC)」
- 31 LAURA REINA (FSU) Jul.25 「W/Z+b jets at hadron colliders: a challenging background」
- 32 Eduardo Ponton (Columbia University) Aug.6 「MSSM Higgs extensions: a model-independent approach」
- 33 Hye-Sung Lee (UC Riverside) Aug.8 「U(1)' instead of R-parity」
- 34 Shaouly Bar-Shalom (Technion, Haifa) Aug.13 「Flavor Physics with Friedberg-Lee hidden symmetries & the case for the Standard Model with 4 families」
- 35 Bowen Xiao (Lawrence Berkeley National Lab.) Aug.19 「Polarized DIS and Spin Puzzle in AdS/CFT」
- 36 Jian Zhou (LBL, Berkeley & Shandong U) Aug.21 「Azimuthal Ssymmetry in the Polarized Drell-Yan Process」
- 37 Emil Mottola (Los Alamos National Lab.) Aug.28 「Systematics of High Temperature Perturbation Theory」
- 38 Kai Wang (University of Tokyo) Sep.17 「Probing B/L Violation in the Extended Scalar Models at the LHC」
- 39 Gustavo Burdman (Sao Paulo/FNAL) Sep.24 「Fourth Generation and Electroweak Symmetry Breaking」
- 40 Jens Braun (TRIUMF) Sep.25 「Extreme limits of QCD: On QCD with many flavors or many colors」
- 41 Zhongbo Kang (RIKEN/BNL) Oct.2 「Some recent progress on single transverse spin asymmetry」
- 42 Sakai Nobuhiko(University of Hyogo) Oct.5 「3D Momentum Density Distribution of Spins of Magnetic Electrons in Ferromagnetic Fe and Ni」
- 43 Sergey Syritsyn (MIT) Oct.7 「Electromagnetic Form Factors of a Nucleon in Full Lattice QCD」
- 44 Sean Fleming (University of Arizona) Oct.22 「Top Jets & Precision Measurements of the Top Quark Mass」
- 45 Lev Lipatov Oct.29 「Integrability of high energy scattering amplitudes in multi-color QCD and N=4 SUSY」
- 46 Cecilia Lunardini (Arizona State University / RBRC) Oct.30 「Neutrinos from collapsing stars and future neutrino telescopes」

- 47 Jorge Noronha (Columbia Univ.) Nov.13 「Connecting Polyakov Loops to the Thermodynamics of $SSU(N_c)$ 」
- 48 Aleksandr Azatov (University of Maryland) Nov.14 「Flavor physics of the scalar sector of the models with warped extra dimension」
- 49 Aaron Pierce (University of Michigan) Nov.19 「Non-minimal Dark Matter--Nucleon Scattering」
- 50 Cai-Dian Lu (IHEP, Beijing) Dec.12 「Study of light scalar meson: four quark states and glueball possibility」
- 51 Kathryn Zurek (University of Michigan) Jan.7 「Dark Matter from the Baryon Asymmetry」
- 52 Ying-chuan Li (Univ. of Wisconsin, Madison) Jan.22 「EDM's & Baryogenesis」
- 53 N. Arkani-Hamed (Institute for Advanced Study) Jan.28 「 $N=4$ SYM and the Grassmannian」 N. Arkani-Hamed (Institute for Advanced Study)」
- 54 Jay Hubisz (Syracuse University) Feb.4 「Revealing Randall-Sundrum Hidden Valleys」
- 55 Yoshimasa Hidaka (Kyoto University) Feb.5 「Novel Diagrammatic Method for Computing Transport Coefficients」
- 56 Lance Dixon (SLAC) Feb.10 「NLO QCD Predictions for Vector Bosons Plus Jets at the LHC」
- 57 Catalina Oana Curceanu (LNF-INFN, Italy) Feb.12 「Exotic Atoms and Nuclei search at the DAFNE collider in Frascati」
- 58 Brent Nelson (Northeastern University) Feb.18 「Nonuniversal Gaugino Masses, Dark Matter and the LHC」
- 59 Jan Pawłowski (University of Heidelberg) Feb.19 「The QCD phase diagram: Results and challenges」
- 60 Andrea Ferroglia (Mainz University) Feb.25 「Top-Quark Pair Production Beyond Next-To-Leading Order」
- 61 Sanjay Reddy (LANL) Feb.27 「Transport and Screening in the Magnetized Neutron Star Crusts」
- 62 Jamie Gainer (Northwestern University and Argonne National Lab) Mar.4 「Supersymmetry without Prejudice」
- 63 Yamazaki Toshimitsu (RIKEN Nishina Center) Mar.5 「DDR (High Density Deuterium Reaction) Project」
- 64 Antonio Delgado (University of Notre Dame) Mar.11 「Unitarity applied to hidden sector processes」
- 65 Masanobu Yahiro (Faculty of Sciences, Kyushu University) Mar.16 「Microscopic approach to reaction of unstable nuclei (not open to the public)」
- 66 Jesse Thaler (MIT) Mar.25 「Goldstini」
- 67 Yasushi Nara (Akita International University) Mar.26 「Eccentricity fluctuations and CGC」

RIBF Research Division

- 1 "Yoichi Momozaki (Argonne National Laboratory) Apr. 27
RIBF accelerator seminar 「Proper handling and safety of liquid lithium」 "
- 2 "Kimitoshi Kono (RIKEN) RIBF Accelerator Seminar Apr.21 「Free surface of superfluid 3He 」 "
- 3 Hideyuki Sakai (Faculty of Science & Graduate School of Science, The University) May.19 Colloquium 「--EPR paradox and Bell's inequality test by pairs of two protons -- Einstein was wrong? --」
- 4 Shunsuke Imanishi (National Institute of Vegetable and Tea Science, National Agriculture and Food Research Organization) May.21 Radiation Biology Seminar 「Isolation of heavy-ion induced mutant in M1 plant generation」
- 5 Morita Kosuke (RIKEN Nishina Center) May. 26 Nuclear Physics Seminar 「Decay Properties of ^{266}Bh and ^{262}Db Produced in the $^{248}\text{Cm} + ^{23}\text{Na}$ Reaction」
- 6 "Toru Tamagawa (RIKEN) Jun.9
RIBF Nuclear Physics seminar 「Observations of Supernova Remnants with the Suzaku X-ray satellite」 "
- 7 Akira MIZUTA (Center for Frontier Science, Chiba University) Jun.16 「Nuclear Physics Seminar 「Gamma-Ray-Burst Jet from Collapsars」」
- 8 Satoshi Sakaguchi (RIKEN) Jun.23 Nuclear Physics Seminar 「Spin-orbit potential in neutron-rich helium isotopes」

- 9 Yoshitaka KASAMATSU (RIKEN) Jun.23 Nuclear Physics Seminar 「Fluoro Complex of Element 105, Db」
- 10 Toshimi Suda(RIKEN) Jun.30 Nuclear Physics Seminar 「First demonstration of electron scattering using a novel target developed for short-lived nuclei- towards Hofstadter's experiments for short-lived nuclei -」
- 11 Markus Friedl (Inst. of High Energy Physics,Austrian Academy of Sciences) Jul.10 「The Silicon Vertex Detector upgrade for Belle II」
- 12 Kaori Otsuki (Hokkaido Univ. Graduate School of Science, School of Science) Jul.14 Nuclear Physics Seminar 「In quest of the Origin of r-process elements
- 13 Erik Arner (RIKEN, Omics Science Center) Jul.17 Radiation Biology Seminar 「Rice mutant re-sequencing mate pair analysis」
- 14 Sasano Masaaki (Heavy Ion Nuclear Physics Laboratory) Jul.21 Nuclear Physics Seminar「Study of Gamow-Teller transition strengths in the intermediate nucleus of the ^{116}Cd double-beta decay by the $^{116}\text{Cd}(p,n)$ and $^{116}\text{Sn}(n,p)$ reactions at 300 MeV 」
- 15 Satoshi Chiba (Advanced Science Research Center, Japan Atomic Energy Agency) Jul.28 Nuclear Physics Seminar「Nuclear data research for nuclear energy and possible cooperations with nuclear and cosmo-nuclear physics」
- 16 Wayne M. Itano (National Institute of Standards and Technology, Boulder, CO USA) Aug.25 Nuclear Physics Seminar 「Diamagnetic Shift of the Hyperfine Interaction in $^9\text{Be}^+$ - Experiment and Theory 」
- 17 Gentaro Watanabe (RIKEN) Sep.8 Nuclear Physics Seminar 「Formation of nuclear "pasta" in supernovae」
- 18 Umeya Atsushi (RIKEN) Sep.29 Nuclear Physics Seminar 「Shell-model study on Lambda-Sigma coupling effect in neutron-rich lithium hypernuclei」
- 19 Hara (RIKEN) Oct.7 RIBF Accelerator Seminar 「Calculation of Emittance in Aurora Storage Ring」
- 20 Thomas Schilcher(Paul Scherrer Institute (PSI)) Oct.16 RIBF Accelerator Seminar 「Status of PSI Accelerators」
- 21 M. Broennimann (PSI) Oct.16 RIBF Accelerator Seminar 「Status about RF activities at the PSI accelerator facilities」
- 22 A. Caruso (LNS/INFN) Oct.23 RIBF Accelerator Seminar 「The radiofrequency system at INFN-LNS」
- 23 Christian Smorra (Mainz University, Germany) Oct.27 「TRIGA-TRAP: A double Penning trap mass spectrometer at the research reactor TRIGA MAINZ」
- 24 "Yoshiyuki Aoki and Masataka Masuyama (Department of Monozukuri Engineering Aerospace engineering course Tokyo Metropolitan College of Industrial Technology) Oct.27 Detector Team Informal Seminar 「Development and evaluation of the wide dynamic range preamplifier for silicon sensor」 "
- 25 Naoto Nagaosa (Univ. of Tokyo) Oct.28 Colloquium 「Symmetry and topology in multiferroics」
- 26 E. Donets (Dubna, Russia) Nov.5 RIBF Accelerator Seminar 「ELECTRON STRING ION SOURCES APLIED FOR FORMATION OF HIGLY CHARGED AND PRIMARY RADIOACTIVE ION BEAMS」
- 27 T. Hirano, Y. Kazama (RIKEN) Nov.9 Radiation biology seminar 「Frontiers of plant reproduction research」
- 28 Avraham Lalazar (Inst. of Plant Sciences) Nov.12 「DET1 gene - good and bad aspects of pleiotropism」
- 29 "Tomoko. Abe(RIKEN), Yoshiaki Nagamura (NIAS) Nov.24 Radiation biology seminar 「Advancement of mutation breeding technology in rice」 "
- 30 H. Hosotani (Graduate School of Science, Osaka Univ.) Nov.24 Colloquium 「What the Higgs boson really is like -from symmetry breaking to extra dimensions 」
- 31 Ken'ichiro Nakazato (Kyoto Univ.) Nov.25 Nuclear Theory Seminar 「Gyroid Phase in Nuclear Pasta」
- 32 Hans Geissel (GSI) Nov.26 Nuclear Physics Seminar 「Present and Future Experiments with Exotic Nuclei at GS」
- 33 " Andreas Adelmann (PSI) Nov.27 RIBF Accelerator Seminar 「The Object Oriented Parallel Accelerator Library (OPAL), Design, Implementation and Application」 "

- 34 "Hiromi Okamoto (Graduate School of Advanced Science Matter, Hiroshima Univ.) Nov.30 RIBF Accelerator Seminar 「Beam Cooling and Coulomb Crystallization」, 「Space-Charge Effects in Intense Particle Beams」 and 「Phase-Space Manipulation by Means of Coupling Resonance」
- 35 "Hiromi Okamoto (Graduate School of Advanced Science Matter, Hiroshima Univ.) RIBF Accelerator Seminar 「Non-neutral plasma and its experimental applications to beam dynamics studies」 "
- 36 Alexei A. Ogloblin (RRC Kurchatov Institute, Russia) Dec.7 Nuclear Physics Seminar 「Measuring the radii of particle unstable nuclear states and search for the signatures of alpha condensation in light nuclei」
- 37 Tatsuyuki Takatsuka (Iwate University) Dec.14 Colloquium 「New nuclear-physics-problems addressed by neutron stars」
- 38 "Richard F. Casten (Yale U./JUSTIPEN Guest) Jan.6 RNC Lecture Series on Nuclear Physics Course VIII 「Shell Model and Collective Models in Nuclei: experimental and theoretical perspectives」 "
- 39 "Tomonari Hirano, Yusuke Kazama (Riken), Yuko Odaira (Fukushima Pref. Soma High School) Jan.8 Radiation biology seminar 「Educational materials for genetics using Arabidopsis mutants II」 "
- 40 Bikash Sinha (VECC, SINP Former Director) Jan.15 「Accelerator based activities at VECC & SINP」
- 41 T. Kubo (RIKEN) Jan.19 Nuclear Physics Seminar 「Overview of BigRIPS In-flight Separator at RIBF: Production and Identification of RI Beams Using In-Flight Fission of a 345 MeV/u ^{238}U Beam」
- 42 Heiko Scheitt (RIKEN) Jan.19 Nuclear Physics Seminar 「Spectroscopy of ^{32}Ne and the "Island of Inversion"」
- 43 Toshio Takeyumi (National Institute of Agrobiological Sciences) Jan.19 「Evaluation of radiosensitivity (irradiation with gamma rays) in soybean」
- 44 Carlo Barbieri (RIKEN) Jan.26 Nuclear Physics Seminar 「Toward an accurate understanding of optical models and single-particle states in exotic nuclei」
- 45 LIU Yong (IMP, Chinese Academy of Sciences) Feb.4 RIBF Accelerator Seminar 「HIRFL-CSR STATUS AND ACTIVITIES FOR FUTURE UPGRADES」
- 46 HE Yuan (IMP, Chinese Academy of Sciences) Feb.4 RIBF Accelerator Seminar 「Design of New LINAC Injector for SSC of HIRFL」
- 47 C.Reed (ANL) Feb.8 RIBF Accelerator Seminar 「Development of the Liquid Lithium Thin Film Stripper and its Electron Beam Film Thickness Monitor for FRIB」
- 48 Nobuo Hinohara (Theoretical Nuclear Physics Lab, Nishina Center) Feb.9 Nuclear Physics Seminar 「Microscopic approach to large-amplitude collective dynamics in Se isotopes」
- 49 Yasutaka Taniguchi (RIKEN) Feb.9 Nuclear Physics Seminar 「Triaxiality of excited states in sd-shell nuclei」
- 50 C.Reed (ANL) Feb.9 RIBF Accelerator Seminar 「Options for Beam-on-Film Testing of the FRIB Liquid Lithium Stripper」
- 51 N. Hinohara (RIKEN) Feb.9 RIBF Nuclear Physics Seminar 「Microscopic approach to large-amplitude collective dynamics in Se isotopes」
- 52 Y.Taniguchi (RIKEN) Feb.9 RIBF Nuclear Physics Seminar 「Triaxiality of excited states in sd-shell nuclei」
- 53 XU Zhe (IMP, Chinese Academy of Sciences) RIBF Accelerator Seminar 「RF system in the institute of modern physics」
- 54 Nakamura Takashi (Department of Physics, Tokyo Institute of Technology) Feb.23 Nuclear Physics Seminar 「Halo structure and shell evolution studied by breakup reactions」
- 55 Giuseppe Verde (INFN, Catania) Mar.8 Heavy Ion Nuclear Physics Lab. Seminar 「Correlation measurements in heavy-ion collisions: probing dynamics and spectroscopy with unbound systems」

- 56 N. Inabe (RIKEN) Mar.9 Nuclear Physics Seminar 「Discovery of 42 new isotopes and 13 new isomer using 345 MeV/u U beam with BigRIPS」
- 57 Maya Takechi (RIKEN) Mar.9 Nuclear Physics Seminar 「Measurements of Interaction cross sections towards neutron rich Ne isotopes at RIBF」
- 58 Tohru Motobayashi (RIKEN) Mar.30 Special Colloquium 「Study of unstable nuclei with direct reactions」

CNS

- 1 "S. Ota (CNS, University of Tokyo), Jul.21 CNS Seminar, 「Low-lying Proton Intruder State in ^{13}B 」 "
- 2 "Y.~Tsuchimoto (CNS, University of Tokyo), Sep.8
CNS Seminar, 「Measurement of Low-mass Vector Mesons in Hot-Medium created by Relativistic Heavy-Ion Collisions」 "
- 3 "S.~Romano (University of Catania), Dec. 17 CNS Seminar, 「Recent results on the $^{10}\text{B}(p,\alpha)^7\text{Be}$ and $^{11}\text{B}(p,\alpha)^8\text{Be}$ reactions studied by means of the THM」 "
- 4 "G.~Pizzone (INFN-LAS), Dec.17 CNS Seminar, 「Effects of distortion of the intercluster motion in light nuclei」 "
- 5 "S. Cherubini (University of Catania), Dec.17 CNS Seminar, 「Nuclear Astrophysics at Catania」 "
- 6 "S.~Amari (Washington University, St. Louis, USA), Mar.12 CNS Seminar, 「Presolar grains from meteorites: a new window to stars」 "
- 7 "D. N.~Bihm (CNS, University of Tokyo), Mar.30 CNS Seminar, 「The measurement of $^{21}\text{Na}+\alpha$ in inverse kinematics and the $^{21}\text{Na}(\alpha,p)$ stellar reaction rate」 "

AUTHOP INDEX

- ABE Takashi 阿部喬 46
ABE Yasushi 阿部康志 23
ABE Tomoko 阿部知子 vii, 277, 278, 279, 280,
281, 282, 283, 284, 285,
287, 288
ADACHI Tadashi 足立匡 253, 254, 255, 256
ADELMAN Andreas 129
AIBA Takeshi 相場健 13
AIHARA Toshimitsu 藍原利光 114, 116, 117, 289,
291
AKASHIO Atsuko 赤塩敦子 297
AKIBA Yasuyuki 秋葉康之 65, 201, 202, 204
206, 208, 210
AKIYAMA Takashi 秋山岳伸 27
AKIYAMA Kazuhiko 秋山和彦 268
AKOSHIMA Megumi 阿子島めぐみ 256
ANDO Ryosuke 安藤良祐 34, 35
ANDREICA Daniel 253
AOI Nori 青井考 x, 4, 8, 10, 11, 12, 13, 14, 17,
18, 19
AOKI Yoshiyuki 青木義幸 182
AOKI Sinya 青木慎也 xiii
AOKI Yasumichi 青木保道 86
AOKI Yasuo 青木保夫 22
AOKI Kazuya 青木和也 217
AONUMA Wataru 青沼航 279
AOYAMA Tatsumi 青山龍美 91
ARAI Ryoichi 荒井亮一 88
ARAI Ichiro 新井一郎 184, 186
ARAI Shigeaki 新井重昭 105, 107, 109, 112
ARAKI Mikio 荒木幹生 268
ARAMAKI Yoki 荒巻陽紀 66
ARIMA Akito 有馬朗人 56
ASAHI Koichiro 旭耕一郎 231, 16
ASAI Masato 浅井雅人 ix, 268, 269
ASANO Katsuyuki 浅野克行 91
ASANO Tomomasa 浅野大雅 62
ASSIÉ Marlène 9
AVOGADRO Paolo 52
BABA Hidetada 馬場秀忠 x, 5, 6, 7, 8, 9, 12, 13,
15, 17, 18, 169, 191, 192,
199, 221, 222, 224,
BABA Yutaka 馬場裕 97, 98, 99, 100
BAINES Christopher 243
BAKER Peter 243, 250
BAKULE Pavel xx, 240, 241
BARBIERI Carlo 41
BAUER Eric 251
BAUMGART Stephen 201, 206, 208, 210
BAZIN Daniel 169
BEAUMEL Didier 9
BEHR John 27
BEMMERER Daniel 13, 15
BENTZ Wolfgang 84
BERG Georg 7, 169, 172, 191
BHANG Hyoung-Chan 10
BINH Dam 30
BISHOP Shawn 17, 18
BLAU Dmitry 70
BLUMENFELD Yorick 9
BLUNDELL Stephen 243, 250
BOYLE Kieran 63, 72, 78
BROWN Alex 11, 13, 15, 44
CAI XiangZhou 蔡翔舟 12, 17, 18, 19
CAO Z 10
CARRETTA Stefano 243
CARTER Biggs 204
CASSANO Nicole 201
CHAKRABARTI Alok 11
CHARLES Pancake 208
CHEN JinGen 12, 19,
CHEN RuiJiu 3
CHEN Alan 30
CHEN Jun 30
CHIBA Yoshiaki 千葉好明 109
CHIBA Junsei 千葉順成 5, 6
CHOI Seonho 崔善浩 10
CHOLLET Simon 202
CHUCK Pancake 204
CIANCIOLO Vince 201
CLOET Ian 84
DAIRAKU Seishi 大樂誠司 64, 69
DALFOVO Franco 61
DAM Binh 29, 31
DANTSUKA Tomoyuki 段塚知志 300, 304, 306
DESÉREVILLE Nicolas 9
DEGUCHI Shigeki 出口茂樹 x, 5, 6, 10
DELAUNAY Franck 10
DENIKIN Andrey 8
DESHPANDE Abhay 72, 201
DINHANG Nguyen 54
DOI Takumi 土井琢身 xiii
DOMBRÁDI Zsolt 13, 15
DOORNENBAL Pieter x, 4, 17, 18

- DOZONO Masanori 堂園昌伯 xi
 DRAPIER Oliver 201, 202
 DRESS Axel 201, 202
 DROUART Antoine 9
 DÜLLMANN Christoph 268
 DUMITRU Adrian 89
 DUPPEN Piet 190
 EBATA Shuichiro 江幡修一郎 51
 EBISUZAKI Toshikazu 戎崎俊一 iii
 EISAKI Hiroshi 永崎洋 252
 ELEKES Zoltán 13, 15
 EMOTO Takashi 江本隆 24
 EN' YO Hideto 延與秀人 1, 167, 201, 202, 204,
 206, 208, 210
 ENOMOTO Shuichi 榎本秀一 274
 ENOMOTO Masaya 榎本真哉 242
 ERIC Mannel 204
 ETO Minoru 衛藤稔 92
 EUGENE Shafto 204, 208
 EVEN Julia 269
 EZAKI Yutaka 江崎豊 266, 270, 271, 272, 273,
 274, 299
 FAMIANO Michael 5, 6
 FAN Fangli 268
 FANG Deqing xv, 3, 16, 17, 18
 FITRILAWATI 259
 FLEMING Donald 241
 FOMICHEV Andrey 8
 FRANCHOO Serge 9
 FRANCIS Pratt 240
 FRANCISCONI Patricia 73, 78
 FRANKE Isabel 243
 FU Yao 傅瑤 12
 FUJII Yutaka 藤井裕 248
 FUJIKAKE Kotaro 藤掛浩太郎 235
 FUJIMAKI Masaki 藤巻正樹 112, 116, 119, 121,
 123, 133, 135, 136,
 289, 291
 FUJINAWA Tadashi 藤縄雅 112, 142, 184, 186, 295
 FUJISAWA Hiroyuki 藤沢弘幸 266, 267, 268, 272,
 FUJISAWA Hiroshi 藤澤浩 105
 FUJITA Mitsutoshi 藤田充俊 95, 96
 FUJITA Naoko 藤田尚子 279
 FUJITA Shin 藤田新 297
 FUJIWARA Kohei 藤原康平 201, 202, 204, 206,
 208, 210
 FUJIWARA Yuya 藤原裕也 216
 FUKAO Yoshinori 深尾祥紀 75, 76, 80, 228
 FUKAZAWA Hideto 深澤英人 252
 FUKUDA Mitsunori 福田光順 3, 23
 FUKUDA Hiroyuki 福田弘幸 297
 FUKUDA Naoki 福田直樹 x, xvii, 3, 5, 6, 7, 11, 151
 155, 156, 157, 159, 161,
 165, 169, , 302
 FUKUNISHI Nobuhisa 福西暢尚 xii, xv, 112, 119,
 121, 123, 125, 131,
 135, 136, 184, 186,
 191, 282, 289, 291,
 293
 FUKUZAWA Seiji 福澤聖児 293, 289
 FÜLÖP Zsolt 13, 15
 FURUKAWA Takeshi 古川武 16, 18, 17, 190, 231,
 235
 FURUKAWA Melissa 196
 FURUMOTO Takenori 古本猛憲 13, 15
 FURUTACHI Naoya 古立直也 62
 GANGNANT Patrice 174
 GASTALDI Franck 201, 202
 GEISSEL Hans x, 3, 5
 GERNHÄUSER Roman x
 GIBBONS Gary 94
 GIBELIN Julien x, 10
 GILLIBERT Alain 9
 GO Shintaro 郷慎太郎 199
 GOLOVKOV Mikhail 8
 GONO Yasuyuki 郷農靖之 5, 6, 163
 GOTO Takayuki 後藤貴行 xix
 GOTO Akira 後藤彰 xvii, xv, 112, 119, 121, 123,
 125, 127, 136, 184, 186,
 289, 291, , 293
 GOTO Shin-ichi 後藤真一 28, 268
 GOTO Yusuke 後藤裕介 191
 GOTO Yuji 後藤雄二 69, 80, 167, 219
 GROSSE-PERDEKAMP Matthias 73, 77, 78
 GRUBER Bruno 56
 GUILLOT Jacques 9
 GUNJI Taku 郡司卓 82, 65
 GUO Wei 郭威 12, 19
 HABA Hiromitsu 羽場宏光 ix, 28, 230, 265, 266,
 267, 268, 269, 270, 271,
 272, 273, 274, 299,
 HACHIUMA Isao 八馬功 x, 3, 5, 6, 23
 HAGIWARA Shinichi 萩原慎一 233
 HAKI Yosuke 羽木洋介 201, 202, 204, 206, 208, 210
 HAMAGAKI Hideki 浜垣秀樹 65, 82
 HAMANAKA Makoto 濱仲誠 289, 293
 HAMMACHE Fairouz 9
 HARA Masahiro 原雅弘 i, 144, 145

- HARA Yuta 原裕太 x, 12, 17, 19
- HARADA Toru 原田融 39
- HASAMA Yuka 挟間優佳 16, 231
- HASEBE Hiroo 長谷部裕雄 xvii, 125, 289, 291, 293
- HASEGAWA Taichi 長谷川太一 268
- HASHIMOTO Yoshiko 橋本佳子 14
- HASHIMOTO Kimiaki 橋本公瑛 201, 202, 204, 206, 208, 210
- HASHIMOTO Koji 橋本幸士 60, 83, 94
- HASHIMOTO Yukio 橋本幸男 51, 57
- HASHIMOTO Takashi 橋本尚志 29, 30, 31
- HASHIMOTO Tadashi 橋本直 191
- HATA Maki 秦麻記 27
- HATAKEYAMA Shin 畠山晋 277
- HATSUDA Yasuyuki 初田泰之 93, 96
- HATSUDA Tetsuo 初田哲男 xiii
- HATTORI Toshiyuki 服部俊幸 148
- HAYAKAWA Kazuo 早川一生 231
- HAYAKAWA Masashi 早川雅司 91
- HAYAKAWA Seiya 早川勢也 29, 30, 31
- HAYANO Ryugo 早野龍五 191
- HAYASHI Yoriko 林依子 vii, 278, 280, 281, 282, 287
- HAYASHI Hironori 林宏憲 16, 231
- HAYASHI Tatuya 林達也 233
- HAYASHI Yuko 林祐子 284, 283
- HAYASHIZAKI Noriyosu 林崎規託 148
- HEFFNER Robert 251
- HEMMI Masatake 逸見政武 136
- HERMANN Wollnik 20, 21
- HIDAYAT Rahmat 259
- HIGAMI Naota 樋上直太 233
- HIGASHIYAMA Koji 東山幸司 49, 50
- HIGEMOTO Wataru 髭本亘 251
- HIGURASHI Rieko 日暮(蛭沼)利江子 297
- HIGURASHI Yoshihide 日暮祥英 112, 114, 116, 117, 119, 121, 123, 133, 289, 291, 293
- HINKE Christoph x
- HINOHARA Nobuo 日野原伸生 47, 48
- HIRABAYASHI Yoshiharu 平林義治 40
- HIRAIWA Toshihiko 平岩聡彦 216
- HIRANO Shinji 平野真司 94
- HIRANO Tomonari 平野智也 277, 280, 284, 285, 287
- HIRAYAMA Yoshikazu 平山賀一 27, 190
- HIRAYAMA Yuzo 平山雄三 237
- HIROI Masahiko 廣井政彦 257
- HIROTA Seiko 廣田誠子 75
- HISAMATSU Toru 久松徹 257
- HIYAMA Emiko 肥山詠美子 38
- HJORTH-JENSEN Morten 45
- HONDA Takashige 本多崇成 12, 10, 17, 19
- HONMA Michio 本間道雄 44, 45
- HORI Toshitada 堀利匡 i, 144, 145
- HORIBATA Takatoshi 堀端孝俊 57
- HU Zhengguo 12, 19
- HUYSE Mark 190
- HYODO Toshio 兵頭俊夫 232
- ICHIDA Hiroyuki 市田裕之 278
- ICHIHARA Takashi 市原卓 5, 6, 167, 169, 221, 222
- ICHIKAWA Yudai 市川裕大 26, 75
- ICHIKAWA Yuichi 市川雄一 11, 14, 16, 231
- ICHIMIYA Ryo 一宮亮 201, 204, 206, 208
- IDEUCHI Eiji 井手口栄治 5, 6, 199
- IEKI Kazuo 家城和夫 5, 6, 12, 17, 19, 18, 26
- IGARASHI Kimie 五十嵐きみ江 297
- IIDA Kei 飯田圭 59
- IIJIMA Hiroaki 飯島裕章 16, 231
- IIMURA Hideki 飯村秀紀 20, 21
- IIO Masami 飯尾雅実 216
- IIZUKA Satomi 飯塚里美 297
- IKEDA Tokihiro 池田時浩 264
- IKEDA Kiyomi 池田清美 33
- IKEDA Naomi 池田直美 229
- IKEDA Yuki 池田友樹 27, 75
- IKEDA Yoichi 池田陽一 xiii
- IKEGAMI Kumio 池上九三男 304
- IKEGAMI Yuji 池上祐司 204
- IKEZAWA Eiji 池沢英二 105, 107, 112, 116, 119, 121, 123, 140, 291
- IMAI Nobuaki 今井伸明 190
- IMAJO Sohei 今城想平 26
- INABE Naohito 稲辺尚人 x, 5, 6, 151, 155, 156, 159, 161, 163, 165, 169, 191
- INAKURA Tsunenori 稲倉恒法 51
- INOUE Takashi 井上貴史 xiii
- INOUE Hirokazu 井上弘一 277
- INOUE Takeshi 井上壮志 16, 231
- INOUE Rintaro 井上倫太郎 260
- ISE Ryunosuke 伊勢龍之介 300, 304
- ISHIBASHI Nobuyuki 石橋延幸 98, 99, 100
- ISHIBASHI Takuya 石橋拓也 148
- ISHIBASHI Yoko 石橋陽子 3, 12, 16, 19, 23
- ISHIDA Katsuhiko 石田勝彦 xx, 237, 238, 239, 240, 241, 262, 263, 264, 296
- ISHIDA Takayuki 石田尚行 244
- ISHIHARA Masayasu 石原正泰 10
- ISHII Kotaro 石井公太郎 279

- ISHII Yasuyuki 石井康之 xix, 242, 244, 245, 246,
252, 253, 257, 261,
- ISHII Yasuo 石井康雄 268
- ISHII Chihiro 石井千尋 5, 6
- ISHII Tetsuro 石井哲朗 27
- ISHII Yuji 石井祐司 16, 231
- ISHII Noriyoshi 石井理修 xiii
- ISHIKAWA Shigeru 石川盛 289, 293
- ISHIKAWA Tomomi 石川智己 87
- ISHIMOTO Shigeru 石元茂 23
- ISHIYAMA Hironobu 石山博恒 190
- ITAHASHI Kenta 板橋健太 x, 169, 176, 191, 192, 216
- ITO Hiromasa 伊藤寛昌 302
- ITO Takashi 伊藤孝 251
- ITO Makoto 伊藤誠 37
- ITO Takuya 伊藤拓也 84
- ITO Yuta 伊藤由太 3, 12, 19, 23,
- ITOH Masatoshi 伊藤正俊 14
- ITOH Satoshi 伊藤聖 x, 169, 176, 191, 192
- ITOUGA Misao 井藤賀操 278
- IVANOV Marian 82
- IWAI Yoshio 岩井良夫 264
- IWASA Naohito 岩佐直仁 12, 13, 15, 17, 18, 19, 29,
178, 180, 182
- IWASAKI Masahiko 岩崎雅彦 216, 237, 239, 262,
263, 264
- IWASAKI Ken 岩崎健 300
- IWASAKI Hironori 岩崎弘典 9, 11, 14
- IYO Akira 伊豫彰 252
- IZUBUCHI Taku 出淵卓 87
- IZUMI Masako 泉雅子 vii, 275, 276, 280
- JEONG Sunchan 鄭淳讚 190
- JIM LaBounty 204
- KADOH Daisuke 加堂大輔 102, 103
- KADONO Ryosuke 門野良典 261
- KAGEYAMA Tadashi 影山正 140, 289, 291, 293
- KAHL David 29, 30, 31
- KAJI Daiya 加治大哉 28, 30, 224, 265
- KAJINAMI Yoshitomo 梶並佳朋 247
- KAKUTANI Nobukazu 角谷暢一 302
- KAMBARA Tadashi 神原正 229, 230, 232, 299
- KAMEDA Daisuke 亀田大輔 3, 5, 6, 7, 27, 151, 155,
156, 159, 161, 165,
169, 191, 230
- KAMIGAITO Osamu 上垣外修一 xvii, 105, 107, 109,
111, 112, 117, 119,
121, 123, 125, 135,
136, 289, 291, 293
- KAMIMURA Masayasu 上村正康 38
- KANADA-EN' YO Yoshiko 延与佳子 36
- KANAI Yasuyuki 金井保之 20, 21, 201, 204, 206,
208, 210
- KANAYA Toshiji 金谷利治 260
- KANAZAWA Mitsutaka 金澤光隆 25
- KANAZAWA Yuu 金澤悠 264
- KANESUE Takeshi 金末猛 146, 147, 148, 149, 286
- KANNO Shoko 菅野祥子 x, 12, 17, 18, 19
- KANODA Kazushi 鹿野田一司 250
- KARATSU Ken' ichi 唐津謙一 xiv, 75
- KASAI Miki 河西実希 201, 204, 206, 208, 210
- KASAMATSU Yoshitaka 笠松良崇 ix, 28, 265, 266,
267, 268, 269, 270,
271, 272, 273
- KASE Masayuki 加瀬昌之 xvii, 105, 107, 109, 111,
112, 116, 119, 121, 123,
125, 127, 135, 136, 138,
140, 195, 229, 289, 291,
293, 295, 300, 304, 306
- KASHIWAGI Hirotsugu 柏木啓次 147, 148
- KATAYAMA Ichiro 片山一郎 20, 21, 190
- KATO Seigo 加藤静吾 29
- KATO Ken-ichi 加藤賢一 304, 306
- KATO Toshihiro 加藤俊宏 240
- KATO Tetsuya 加藤徹也 249
- KATO Reizo 加藤礼三 245
- KAWABATA Takahiro 川畑貴裕 x, 12, 14, 17, 18,
19, 31, 171, 172,
176, 178, 180, 192
- KAWADA Yosuke 河田鷹介 x, 5, 6, 10
- KAWAHARA Tomomi 河原朋美 14, 197
- KAWAKAMI Satoshi 川上智 278
- KAWAKAMI Roland xx, 240
- KAWALL David 71
- KAWAMATA Takayuki 川股隆行 237, 238, 248, 249
253, 254, 255, 258,
261
- KAWAMURA Seiko 河村聖子 250
- KAWAMURA Hirokazu 川村広和 16, 27
- KAWANO Shigeyuki 河野重行 279, 285
- KAWASE Shoichiro 川瀬頌一郎 7, 169, 172, 176, 192
- KAZAMA Yusuke 風間裕介 vii, 277, 278, 279, 280,
282, 283, 284, 285,
- KEELEY Nicholas 9
- KHASANOV Rustem 253
- KIDA Noriyuki 木田紀行 242
- KIDERA Masanori 木寺正憲 116, 289, 291, 293
- KIENLE Paul 191

KIHOU Kunihiro 木方邦宏 252
 KIKUCHI Yuma 菊地右馬 33, 40
 KIKUCHI Takahiro 菊池貴宏 268, 269
 KIKUCHI Akihiro 菊池晶浩 258
 KIKUCHI Takashi 菊池崇志 184, 186
 KIKUCHI Hikomitsu 菊池彦光 248
 KIKUCHI Yousuke 菊池陽介 3
 KIKUNAGA Hidetoshi 菊永英寿 265, 266, 267,
 268, 272, 274
 KIKUTANI Yuki 菊谷有希 266, 272
 KIM Aram 30
 KIMURA Masaaki 木村真明 62
 KIMURA Hitomi 木村仁美 12, 19
 KINOSHITA Norikazu 木下哲一 268
 KINOSHITA Toichiro 木下東一郎 91
 KISHIDA Takashi 岸田隆 xvii
 KISHIMOTO Isao 岸本功 v, 101
 KISS Ádám 13, 15
 KITAMOTO Yusuke 北本優介 274
 KITATSUJI Yoshihiro 北辻章浩 269
 KITO Hijiri 鬼頭聖 252
 KOBAYASHI Yoshio 小林義男 262, 231, 296
 KOBAYASHI Kei 小林圭 13, 15
 KOBAYASHI Toshio 小林俊雄 10, 25, 178, 180
 KOBAYASHI Takeshi 小林丈士 210
 KOBAYASHI Nobuyuki 小林信之 x, 5, 6, 10, 17, 18
 KOBAYASHI Kiyoshi 小林清志 289, 293
 KOBAYASHI Takumi 小林拓実 191
 KOBAYASHI Tomohiro 小林知洋 232
 KOBAYASHI Toru 小林徹 235
 KOBAYASHI-KOMIYAMA Misaki 小林 - 込山美咲
 112, 116, 123, 133, 289, 291, 293
 KOHAMA Akihisa 小濱洋央 59
 KOHORI Yoh 小堀洋 252
 KOIKE Shigetoshi 小池茂年 233
 KOIKE Yoji 小池洋二 254, 255, 256
 KOJIMA Norimichi 小島憲道 242
 KOJIMA Takao 小島隆夫 20, 21, 264
 KOMATSU Hiroaki 小松宏彰 246
 KOMATSU-KATO Yukari 小松由佳梨 278,
 KOMORI Yukiko 小森有希子 265, 266, 267, 272
 KOMURASAKI Junji 小紫順治 261
 KONDO Kotaro 近藤康太郎 146, 147, 148, 149, 286
 KONDO Takashi 近藤崇 210
 KONDO Yosuke 近藤洋介 x, 4, 5, 6, 8, 10, 12, 13,
 14, 15, 17, 18, 19, 178, 180
 KORSHENINNIKOV Alexey 8
 KOTAKA Yasuteru 小高康熙 289, 293
 KOU Hiroshi 康寛史 216
 KOURA Hiroyuki 小浦寛之 28
 KOYAMA Ryo 小山亮 135, 136, 195, 289, 293
 KRATZ Jens 268
 KRÜCKEN Reiner x
 KRUPKO Sergei 8
 KUBO Kenya 久保謙哉 261, 262
 KUBO Toshiyuki 久保敏幸 x, 3, 5, 6, 7, 11, 20, 21,
 151, 153, 155, 156, 157,
 159, 161, 163, 165, 169,
 171, 172, 178, 180, 190,
 191, 230, 302
 KUBOKI Hironori 久保木浩功 xvii, 14, 125, 135,
 289, 291, 293
 KUBOKI Takamasa 久保木隆正 x, 3, 17, 18, 23
 KUBONO Shigeru 久保野茂 11, 29, 30, 31, 127,
 184, 186
 KUBOYAMA Satoshi 久保山智司 229
 KUDO Hisaaki 工藤久昭 268
 KUDOU Yuki 工藤祐生 28, 265, 266, 267, 268,
 270, 271, 272, 273
 KUDRYAVTSEV Yuri 190
 KUMAGAI Keiko 熊谷桂子 112, 123, 131, 289
 KUME Naoto 久米直人 17, 18, 29
 KURATA-NISHIMURA Mizuki 西村美月 196
 KUREI Hiroshi 樽井博 169, 176, 192
 KURIBAYASHI Takahiro 栗林隆宏 274
 KURIHARA Yuzo 栗原佑蔵 30
 KURITA Kazuyoshi 栗田和好 i, 12, 17, 18, 19, 24,
 201, 204, 206, 208,
 210
 KURIYAMA Ai 栗山亜依 266, 272
 KUROKAWA Meiko 黒川明子 8, 12, 17, 18, 19,
 169, 182
 KUROSAWA Maki 黒澤真城 201, 204, 206, 208, 210
 KUSAKA Kensuke 日下健祐 x, 5, 6, 7, 116, 140, 151,
 153, 155, 156, 157, 169,
 171, 178, 180, 191, 302
 KUZMIN Evgueni 8
 LANCASTER Tom 243, 250
 LANTZ Mattias x, 3, 23
 LAPOUX Valérie 9
 LE Khiem 29
 LEBEDEV Alexander 201
 LEE Chul-Ho 李哲虎 252
 LEE Nam 30
 LEITGAB Martin 73, 78
 LEVY Phil 27
 LI Zijie 李子杰 268, 269
 LI KuoAng 李闊昂 x, 4, 17

- LI Z H 10
- LIBIN Jean-François 174
- LIU Yang 284
- LOUCHEV Oleg 239
- MA LiQiu 馬立秋 277
- MA YuGang 3, 12, 17, 18, 19
- MAEDA Yukie 前田幸重 xi, 14
- MAIE Takeshi 眞家武士 112, 140, 289, 291, 293, 304
- MAKINAGA Ayano 牧永綾乃 62
- MANABE Yoko 眞鍋葉子 246
- MANIKONDA Shashi 5, 6
- MANION Andrew 72
- MANNEL Eric 201
- MANO Daisuke 眞野大輔 232
- MARÉCHAL François 9
- MARQUES F.Miguel 10
- MARTEL Ismael 8
- MARUYAMA Toshiki 丸山敏毅 iii
- MASUYAMA Masataka 増山昌孝 182
- MATSUDA Yasuyuki 松田恭幸 xx, 240, 241, 263, 264
- MATSUDA Yohei 松田洋平 25
- MATSUE Hideaki 松江秀明 261
- MATSUMOTO Takuma 松本琢磨 62
- MATSUO Masayuki 松尾正之 47, 48
- MATSUO Yukari 松尾由賀利 18, 190, 235
- MATSUSHITA Masafumi 松下昌史 5, 6, 10, 17, 18, 26, 157
- MATSUURA Yuichi 松浦佑一 47, 48, 235
- MATSUZAKI Teiichiro 松崎禎市郎 237, 238, 245, 246, 260, 263, 264
- MAYAMA Keita 眞山圭太 28
- MIBE Tsutomu 三部勉 75, 228
- MICHIMASA Shin'ichiro 道正新一郎 x, 9, 17, 30, 169, 172, 174, 176, 192
- MIHARA Mototsugu 三原基嗣 3, 231, 261
- MIKI Kenjiro 三木謙二郎 7, 14, 169, 172, 176, 191, 192
- MITSUMOTO Toshiaki 三頭聰明 274
- MITSUOKA Shinichi 光岡真一 27
- MITTIG Wolfgang 8
- MIYA Hiroyuki 宮裕之 7, 169, 172, 176, 191, 192, 199
- MIYACHI Yoshiyuki 宮地義之 80, 219
- MIYAHARA Naoaki 宮原直亮 27
- MIYAMOTO Hiroshi 宮本寛 299
- MIYASAKA Shou 宮坂翔 80, 219
- MIYASHITA Yuji 宮下裕次 i
- MIYASHITA Yuki 宮下雄樹 5, 10
- MIYATAKE Hiroari 宮武宇也 27, 190
- MIYAZAWA Kiichi 宮澤喜一 252
- MIZOI Yutaka 溝井浩 5
- MIZUGASHIRA Shin'ichi 水頭慎一 80, 219
- MIZUSAKI Takahiro 水崎高浩 44, 45
- MOMOSE Takamasa 百瀬孝昌 241
- MORI Katsuhito 森克仁 233
- MORI Yoshiki 森善樹 300
- MORIGUCHI Tetsuaki 森口哲明 3, 5, 6, 12, 19, 23, 184, 186
- MORIMOTO Kouji 森本幸司 28, 194, 224, 265
- MORITA Kosuke 森田浩介 28, 194, 265, 270, 273
- MOTOKA Toshio 元場俊雄 38
- MOTOBAYASHI Tohru 本林透 x, 4, 5, 6, 8, 10, 11, 12, 13, 15, 17, 18, 19, 22, 178, 180, 182
- MOUGEOT Xavier 9
- MUKAI Hiroki 向井弘樹 297,
- MUKAI Ryuji 向井隆司 287
- MUKHA Ivan 9
- MURAKAMI Koichi 村上公一 98, 99, 100
- MURAKAMI Hiroyuki 村上浩之 12, 17, 18, 19, 182
- MURAKAMI Tetsuya 村上哲也 25, 26, 75, 178, 180
- MURANO Keiko 村野啓子 xiii
- MURATA Jiro 村田次郎 26, 27, 75
- MURAYAMA Hirohumi 村山裕史 28
- MUTOH Hideaki 武藤英明 229
- MYO Takayuki 明孝之 33, 34, 35, 40
- NAGAE Tomofumi 永江知文 80
- NAGAE Daisuke 長江大輔 3, 16, 27, 184, 186,
- NAGAME Yuichiro 永目諭一郎 268, 269
- NAGAMINE Kanetada 永嶺謙忠 xx, 240, 263
- NAGANO Akira 永野章 230
- NAGASAWA Mitsuharu 長澤光晴 245
- NAGASE Makoto 長瀬誠 289, 291, 293
- NAGASHIMA Masayuki 長島正幸 3, 169, 192
- NAGASHIMA Yasuyuki 長嶋泰之 232
- NAGATANI Takeshi 長谷健 288
- NAGATOMO Takashi 長友傑 231
- NAIK Vaishali 11
- NAKABAYASHI Takumi 中林彩 11, 13, 15
- NAKAGAWA Itaru 中川格 75, 228
- NAKAGAWA Takahide 中川孝秀 112, 114, 116, 117, 119, 121, 123, 133, 289, 291, 293
- NAKAGAWA Mayu 中川繭 281, 285

- NAKAI Yoichi 中井陽一 26, 178
- NAKAMURA Takashi 中村貴志 20, 21
- NAKAMURA Katsuro 中村克朗 75, 228,
- NAKAMURA Masato 中村仁音 138, 150, 304
- NAKAMURA Tomoaki 中村智昭 167
- NAKAMURA Tota 中村統太 249
- NAKAMURA Hiroyuki 中村裕之 247
- NAKAMURA Takashi 中村隆司 x, 5, 6, 8, 10, 11, 14,
17, 18, 178, 180
- NAKAMURA Takeshi 仲村武志 289, 293
- NAKANISHI Kohsuke 中西康介 169, 176, 192
- NAKANO Takehito 中野岳仁 261
- NAKANO Kenichi 中野健一 80, 219
- NAKANO Nobuo 中野信夫 232
- NAKANO Kazushiro 中野和城 297
- NAKANO Eiji 仲野英司 92
- NAKAO Taro 中尾太郎 x, 5, 6, 11, 14
- NAKATSUGAWA Yohei 中津川洋平 79
- NAKATSUKASA Takashi 中務孝 47, 48, 51, 52, 58
- NAKAYA Yusuke 中谷裕輔 27
- NAKAYAMA Yoshiaki 中山佳晃 10, 14
- NAKAZATO Hitoshi 中里仁 3
- NALPAS Laurent 9
- NAMAI Saori 生井沙織 28
- NAMIHIRA Kousuke 波平晃佑 x, 3, 23
- NANAO Tsubasa 七尾翼 231
- NANNICHI Takashi 南日卓 13, 15
- NANRI Tomohiro 南里朋洋 268, 271
- NEMURA Hidekatsu 根村英克 xiii
- NETTELETON Anthony 5, 6
- NGUYEN Tho 29
- NICOLE Apadula 202, 204
- NIKURA Megumi 新倉潤 8
- NIKOLSKII Evgenii 8
- NINOMIYA Kazufumi 二宮一史 27, 75
- NINOMIYA Kazuhiko 二宮和彦 262
- NIO Makiko 仁尾真紀子 91
- NISHI Takahiro 西隆博 191
- NISHIDA Minoru 西田稔 289, 293
- NISHIHARA Kiyoshi 西原潔 284, 285, 277
- NISHIKAWA Megumi 西川恵 271
- NISHIMURA Shunji 西村俊二 x, 4, 5, 6, 8, 26, 30
- NISHIMURA Makoto 西村誠 289, 293
- NISHIMURA Daiki 西村太樹 3, 23, 261
- NISHINAKA Ichiro 西中一朗 268
- NISHIO Masaki 西尾正樹 271
- NISHIWAKI Yoichi 西脇洋一 249
- NISHIYAMA Kusuo 西山樟生 261
- NITTA Muneto 新田宗土 92
- NITTA Minoru 新田稔 27
- NOBUTOKI Minoru 信時実 302
- NOJI Shumpei 野地俊平 7, 14, 169, 171, 172, 174,
176, 192
- NOLEN Jerry 5, 6
- NOMIYA Yoshio 野宮芳雄 204
- NOVICER Rachid 201
- NUGROHO Agung 259
- ODASHIMA Yutaka 小田嶋豊 304, 306
- OGAWA Akio 小川暁生 73, 78
- OGAWA Naruya 小川就也 27, 75
- OGILVIE Craig 201
- OGIWARA Kiyoshi 荻原清 233
- OGLOBLIN Alexey 8
- OHBU Sumie 大部澄江 282, 283, 284, 285
- OHISHI Kazuki 大石一城 xx, 240, 251, 252
- OHKI Tomonori 大木智則 289, 291
- OHNISHI Hiroaki 大西宏明 81, 216
- OHNISHI Jun-ichi 大西純一 xv, 112, 114, 116, 117,
119, 121, 123, 178, 180,
289
- OHNISHI Tetsuya 大西哲哉 x, 3, 5, 6, 7, 151, 153,
155, 156, 157, 165, 169,
171, 178, 180, 184, 186,
191, 222, 302
- OHSHIMA Masaya 大島昌也 304
- OHSHIRO Yukimitsu 大城幸光 30, 289, 293
- OHTA Shigemi 太田滋生 85
- OHTAKE Masao 大竹政雄 x, 5, 6, 151, 155, 156,
159, 161, 169, 171, 302
- OHTANI Shunsuke 大谷俊介 20, 21, 234
- OHTSUBO Takashi 大坪隆 3, 5, 6, 23, 184, 186
- OHYA Susumu 大矢進 263
- OHZONO Hironobu 大園浩之 229
- OISHI Hiroto 大石寛人 12, 19
- OKADA Kensuke 岡田健介 12, 17, 18, 19, 70
- OKADA Kunihiro 岡田邦宏 19, 20, 21, 188, 190, 234
- OKAMURA Kei 岡村圭 232
- OKAMURA Hiroyuki 岡村宏之 xi, 9, 14
- OKAMURA Masahiro 岡村昌宏 146, 147, 148, 149,
286
- OKUMURA Toshifumi 奥村俊文 11
- OKUNO Hiroki 奥野広樹 xv, xvii, 105, 107, 112, 116,
119, 121, 123, 125, 129, 138,
140, 150, 178, 180, 289, 291,
293, 300, 304, 306
- ONG Jin 王惠仁 11
- ONISHI Takeo 大西健夫 11
- ONISHI Junichi 大西潤一 27, 75

- ONUKI Yoshiyuki 小貫良行 201, 204, 206, 208, 210
 OOE Kazuhiro 大江一弘 265, 266, 267, 268, 272
 OOE Masakazu 大江正和 288
 OOISHI Hiroto 大石寛人 3, 23
 ORR Nigel x, 10
 OSHIMA Masaya 大島昌也 300,
 OTA Shinsuke 大田晋輔 7, 12, 17, 18, 19, 169, 172,
 174, 176, 192, 199, 222
 OTOMO Hiromitsu 大友洋光 229
 OTSU Hideaki 大津秀暁 x, 5, 6, 8, 9, 10, 25, 178,
 180, 196
 OTSUKA Takaharu 大塚孝治 44, 45, 46
 OTUKA Naohiko 大塚直彦 62
 OUCHIDA Misaki 大内田美沙紀 67
 OURA Yasuji 大浦泰嗣 268
 OUTA Haruhiko 應田治彦 216
 OYAMADA Kazuyuki 小山田和幸 289, 291
 OYAMATSU Kazuhiro 親松和浩 59
 OZAWA Akira 小沢顕 3, 5, 6, 12, 19, 22, 23, 184, 186
 OZEKI Kazutaka 大関和貴 x, 25, 26, 28, 194, 265
 PAK Robert 201
 PANCAKE Charles 201, 206
 PEARSON Matthew 27
 PEREPELKIN Evgeny 127
 PIAZZA Francesco 61
 PITAEVSKII Lev 61
 POLLACCO Emmanuel 9
 PRATT Francis xx, 241, 243, 250
 QIN Zhi 268
 QUANGHUNG Nguyen 21, 54
 RACHID Nouicer 204
 RAMUS Alexis 9
 RIEDLER Petra 201, 208
 RISDIANA 259
 ROUSSEL-CHOMAZ Patricia 8, 9, 169, 174
 SAITO Norihito 斎藤徳人 239
 SAITO Fuminori 斎藤文修 232
 SAITO Hiroyuki 斎藤宏之 288
 SAITO Tohru 斎藤透 xi
 SAITO Akito 齋藤明登 7, 5, 6, 169, 171, 172, 176,
 191, 192
 SAITO Taku 齊藤拓 252
 SAITO Naohito 齊藤直人 75, 228
 SAKA Takashi 坂貴 240,
 SAKAGUCHI Harutaka 坂口治隆 25
 SAKAGUCHI Satoshi 坂口聡志 xi, 14, 197
 SAKAI Hideyuki 酒井英行 xi, 7, 14, 169, 171, 172,
 174, 176, 192
 SAKAI Tadakatsu 酒井忠勝 83
 SAKAKIBARA Hitoshi 榊原均 278
 SAKAMOTO Hisao 坂本久雄 297
 SAKAMOTO Naruhiko 坂本成彦 xi, 105, 107, 109,
 111, 112, 135, 136,
 289, 291, 293,
 SAKO Masami 酒向正己 26
 SAKUMA Kiwamu 佐久間究 233
 SAKUMA Fuminori 佐久間史典 214, 216
 SAKUMA Kazuyuki 佐久間収幸 3
 SAKURAGI Yukinori 櫻木千典 13, 15
 SAKURAI Hiroyoshi 櫻井博儀 x, 4, 5, 6, 9, 10, 11,
 12, 13, 15, 19, 26, 178,
 180, 184, 186, 196
 SALMAN Zaher 243
 SAMEISHIMA Rei 鮫島玲 26, 75
 SANCHEZ-BENITEZ Angel 8
 SANO Satoshi 佐野哲 82
 SASAKI Kenji 佐々木健志 xiii
 SASAKI Tomoyuki 佐々木知之 302
 SASAMOTO Yoshiko 笹本良子 7, 14, 169, 171,
 172, 176, 192
 SASANO Masaki 笹野匡紀 xi, 7, 14, 169, 176, 192
 SATO Kazuhiko 佐藤一彦 246
 SATO Tadashi 佐藤雅志 281, 282
 SATO Yoshiteru 佐藤義輝 x, 5, 6, 8, 10, 14, 17, 18,
 25, 178, 180
 SATO Kiyokazu 佐藤潔和 302
 SATO Hiromi 佐藤広海 157, 178, 180
 SATO Koichi 佐藤弘一 48
 SATO Hidetaka 佐藤秀孝 254
 SATO Katsuhiko 佐藤勝彦 iii
 SATO Wataru 佐藤涉 231, 261, 268
 SATO Tetsuya 佐藤哲也 ix, 269, 268
 SATO Nozomi 佐藤望 ix, 28, 269
 SATO Yoichi 佐藤洋一 xv, 112, 116, 119, 121, 123
 SAWADA Shinya 澤田真也 80, 219
 SCARPACI Jean-Antoine 9
 SCHÄDEL Matthias 268
 SCHEIT Heiko 車糸灰粉 x, 4, 17,
 SCHEUERMANN Robert 258
 SCHUESSLER Hans 20, 21, 234
 SCHURY Peter 20, 21, 188, 190, 226
 SEIDL Ralf 73, 77, 78
 SEITAIBASHI Etsuko 聖代橋悦子 27
 SEKIGUCHI Kimiko 関口仁子 xi, 14, 178, 180
 SEKIMOTO Michiko 関本美知子 201, 204, 206,
 208, 210
 SETOODEHNIA Kiana 30
 SHAFTO Eugene 201, 206

- SHCHEPUNOV Viatslav 188
 SHERRILL Bradley 5, 6
 SHIBATA Junsho 柴田順翔 289, 293
 SHIBATA Toshi-Aki 柴田利明 80, 219
 SHIBUKAWA Tomiko 澁川登美子 280
 SHIGA Yuichiro 志賀雄一朗 232
 SHIMADA Osamu 島田修 229
 SHIMAMURA Tomoyuki 島村智之 14
 SHIMBARA Yoshihiro 新原佳弘 169, 176, 192
 SHIMIZU Yasuhiro 清水康弘 46, 250
 SHIMIZU Yohei 清水陽平 xi, 14, 169, 176, 192, 197
 SHIMIZU Yoshifumi 清水良文 58
 SHIMODA Susumu 霜田進 204
 SHIMOMURA Koichiro 下村浩一郎 xx, 240, 261
 SHIMOURA Susumu 下浦享 x, 10, 12, 17, 18, 19, 169,
 171, 172, 174, 176, 192,
 199, 222
 SHINOHARA Atsushi 篠原厚 265, 266, 267, 268,
 269, 272, 274
 SHINOHARA Mayuko 篠原摩有子 14
 SHINOZUKA Tsutomu 篠塚勉 190
 SHIODA Ryota 塩田良太 12, 17, 18, 19
 SHIRAGE Parasharam 252
 SHIRAISHI Kenichi 白石健一 142
 SHIRAKI Ichiro 白木一郎 xx, 240
 SHIRAKI Yasutsugu 白木恭嗣 5, 6
 SIDORCHUK Sergei 8
 SIREGAR Rustam 259
 SOHLER Dóra 10, 13, 15
 SONDHEIM Walter 201
 SONODA Hidetaka 園田英貴 iii
 SONODA Tetsu 園田哲 20, 21, 188, 190
 SORLIN Olivier 9
 SPITAEELS Charles 174
 STEELE Andrew 243
 STEFAN Iulian 9
 STEPHEN Baumgart 204
 STOYKOV Alexsay 258
 STRASSER Patrick 263
 STRINGARI Sandro 61
 SUDA Kenji 須田健嗣 14, 105, 107, 109, 111, 112,
 135, 289, 291, 293
 SUDA Toshimi 須田利美 i, 3, 8, 23, 24, 295
 SUGAWARA-TANABE Kazuko 田辺和子 55, 56
 SUGIMOTO Shigeki 杉本茂樹 83
 SUGINO Fumihiko 杉野文彦 102
 SUKHORUKOV Oleksandr 241
 SUMIKAMA Toshiyuki 炭竈聰之 x, 5, 6, 10
 SUMITA Takayuki 住田貴之 28, 194, 265
 SUN Xiao-Yan 12
 SUZUKI Takao 鈴木榮男 xix, 242, 245, 248, 251,
 253, 254, 255, 256, 257,
 258, 261
 SUZUKI Yoshiaki 鈴木嘉昭 232
 SUZUKI Takeshi 鈴木健 3, 5, 6, 17, 23, 184, 186
 SUZUKI Ken 鈴木謙 191
 SUZUKI Kensuke 鈴木謙介 254, 255, 256
 SUZUKI Masaru 鈴木賢 11
 SUZUKI Hiroshi 鈴木宏 xi, 3, 8, 11, 23, 184, 186
 SUZUKI Daisuke 鈴木大介 9, 11, 14
 SUZUKI Tatsuo 鈴木達男 300
 SUZUKI Kunifumi 鈴木都文 16, 231
 SUZUKI Hiroshi 鈴木博 102, 103
 TABATA Yoshikazu 田畑吉計 247
 TACHIKAWA Maki 立川真樹 235
 TAI Ta-Sheng 戴大盛 95, 96, 97
 TAJIMA Iwao 田島岩男 300, 304
 TAJIRI Kunihiko 田尻邦彦 16
 TAKADA Eiichi 高田栄一 26
 TAKAGI Keiichi 高城啓一 vii
 TAKAHARA Akihisa 高原明久 68
 TAKAHASHI Hironori 高橋弘範 i
 TAKAHASHI Katsuo 高橋勝緒 232
 TAKAHASHI Naruto 高橋成人 266, 267, 272, 274
 TAKAHASHI Tomohiko 高橋智彦 v, 101
 TAKAHASHI Yoshiyuki 高橋良幸 14
 TAKAHASHI Kazuya 高橋和也 299
 TAKAI Shigeomi 高井茂臣 261
 TAKAMINE Aiko 高峰愛子 20, 21, 188, 190
 TAKASHINA Masaaki 高階正彰 13, 15, 33, 40
 TAKAYAMA Reona 高山玲於奈 266, 267, 272
 TAKAYANAGI Toshinobu 高柳俊暢 234
 TAKECHI Maya 武智麻耶 3, 5, 6, 9, 23
 TAKEDA Hiroyuki 竹田浩之 x, 5, 6, 7, 151, 155, 156,
 157, 165, 169, 191
 TAKEDA Yoshikazu 竹田美和 240
 TAKEDA Yuki 武田勇樹 271
 TAKEDA Hiroyuki 竹田浩之 3
 TAKEHARA Hiroki 竹原広樹 i
 TAKEHISA Hinako 竹久妃奈子 281, 282
 TAKENOSHITA Yoshihisa 竹之下佳久 288
 TAKESHITA Eri 竹下英里 x, 12, 19
 TAKESHITA Nao 竹下直 252
 TAKETANI Atsushi 竹谷篤 80, 182, 201, 202, 204,
 206, 208, 210, 219, 228
 TAKEUCHI Satoshi 武内聡 x, 4, 8, 10, 12, 13, 15,
 17, 18, 19, 222
 TAKEYAMA Mirei 武山美麗 28

- TAMAE Tadaaki 玉江忠明 24
TAMII Atsushi 民井淳 14
TAMURA Masashi 田村匡史 114, 116, 117, 133,
289, 291
TAMURA Jun 田村潤 147, 148, 149
TANABE Kosai 田辺孝哉 55, 56
TANABE Yoichi 田邊洋一 249, 253, 254, 255, 256
TANAKA Kana 田中佳奈 x, 5, 6, 10, 17, 18
TANAKA Shuuitsu 田中秀逸 277
TANAKA Hidekazu 田中秀数 xix
TANAKA Toshiyuki 田中俊行 232
TANAKA Kanenobu 田中鐘信 x, 3, 5, 6, 8, 13, 15, 17,
23, 151, 155, 156, 159,
161, 163, 169
TANAKA Manobu 田中真伸 182
TANAKA Naoki 田中直樹 5, 6, 10
TANAKA Hiroaki 田中裕彬 93
TANEJA Swadhin 63
TANIGUCHI Arisa 谷口亜梨沙 246
TANIGUCHI Yasutaka 谷口億宇 43
TANIGUCHI Hiromi 谷口弘三 246
TANIGUCHI Akihiro 谷口秋洋 263
TATSUNO Hideyuki 竜野秀行 191
TER-AKOPIAN Gurgén 8
TERANISHI Takashi 寺西高 11, 29, 31
TERASHIMA Satoru 寺嶋知 25,
THOMAS Anthony 84
TIAN Wendong 12, 17, 18
TIMCO Grigore 243
TJIA May 259
TODOROKI Koichi 轟孔一 191
TOGANO Yasuhiro 桐野泰宏 x, 4, 8, 10, 12, 13, 15,
17, 18, 19, 178, 180, 182
TOGASAKI Mamoru 戸ヶ崎衛 i
TOGASI Tomoaki 富樫智章 62
TOGAWA Manabu 外川学 69, 80, 201, 204, 206,
208, 210
TOKAIRIN Hideo 東海林英夫 281, 282
TOKANAI Fuyuki 門叶冬樹 28, 224
TOKIEDA Hiroshi 時枝紘史 7, 169, 172, 174, 176, 192
TOKUDA Makoto 徳田真 214, 216, 264
TOM Harry xx, 240
TOMITA Hideo 富田英生 190
TOMITA Masanori 富田雅典 276
TOMONO Dai 友野大 216, 237, 238, 264
TORII Chihiro 鳥居千寛 279
TORIKAI Eiko 鳥養映子 xx, 240
TOUME Hayato 當銘勇人 268
TOYODA Takeshi 豊田健司 27
TOYOSHIMA Atsushi 豊嶋厚史 268, 269
TSHOO KyoungHo 秋庚鎬 10
TSUBAKIHARA Kohsuke 椿原康介 62
TSUCHIHASHI Takahiro 土橋隆博 302
TSUCHIYA Masato 土屋真人 16, 231
TSUKADA Kyo 塚田暁 81, 215, 216
TSUKADA Teruyo 塚田晃代 vii, 276, 284
TSUKADA Kazushi 塚田和司 27
TSUKADA Kazuaki 塚田和明 ix, 268, 269
TSUKIORI Noritoshi 月居憲俊 289, 293
UCHIDA Makoto 内田誠 16
UCHIKOSHI Syoichi 打越祥一 232
UCHIYAMA Akito 内山暁仁 116, 133, 289, 291
UEMATSU Nobuya 植松暢矢 5, 6
UEMOTO Ryuji 上本龍二 230
UENO Hideki 上野秀樹 5, 6, 16, 231
UESAKA Tomohiro 上坂友洋 7, 14, 169, 171, 172, 174,
176, 191, 192, 197
UJIHARA Tooru 宇治原徹 240
UMEYA Atsushi 梅谷篤史 39
UTSUNO Yutaka 宇都野稜 44, 46
UWAMINO Yoshitomo 上菘義朋 297
VOROZHTSOV Alexey 127
VOROZHTSOV Sergey 127
VOSEN Anselm 73, 77, 78
WADA Satoshi 和田智之 239
WADA Michiharu 和田道治 20, 21, 188, 190, 226, 234,
WAKABAYASHI Yasuo 若林泰生 29, 31, 30
WAKASA Tomotsugu 若狭智嗣 xi
WAKASUGI Masanori 若杉昌徳 i, 24, 135, 144, 145,
184, 186
WAKI Takeshi 和氣剛 247
WAKUI Takashi 涌井崇志 14, 190, 197
WANG He 王赫 x, 4
WANG Jian-Song 12, 17, 18, 19
WANG Hong-Wei 12, 17 18, 19
WANG Shuo 24
WANG Meng 12
WATANABE Gentaro 渡辺元太郎 iii, 61
WATANABE Shizui 渡辺静意 210
WATANABE Hiroshi 渡辺博 112, 119, 121, 123,
138, 195
WATANABE Isao 渡辺功雄 xix, 237, 238, 242, 243,
244, 245, 246, 247, 248,
249, 250, 252, 253, 254,
255, 256, 257, 258, 259,
259, 260, 261
WATANABE Yasushi 渡邊康 167, 221, 222
WATANABE Shin-ichi 渡邊伸一 127, 195

- WATANABE Susumu 渡邊進 300
- WATANABE Yutaka 渡邊裕 27, 105, 112, 116, 119,
121, 123, 140, 190, 291
- WATANABE Hiroshi 渡邊寛 5, 6
- WATANABE Tamaki 渡邊環 135, 136, 289, 291
- WATANABE Noriaki 渡邊矩章 91
- WENDONG Tian 19
- WIECHULA Jens 82
- WINKLER Martin x
- WINPENNY Richard 243
- WOLLNIK Hermann 188
- YABANA Kazuhiro 矢花一浩 51
- YADOMI Kazuyoshi 矢富一慎 289, 293
- YAGI Eiichi 八木栄一 233
- YAKO Kentaro 矢向謙太郎 xi, 14, 169, 192
- YAMADA Kazunari 山田一成 8, 11, 12, 13, 15, 17, 18, 19,
105, 107, 109, 111, 112,
135, 136, 289, 291, 293
- YAMADA Motoki 山田基樹 xix
- YAMADA Fumiko 山田文子 xix
- YAMADA Yutaka 山田豊 204
- YAMADA Yusuke 山田雄介 12, 17, 18, 19
- YAMAGAMI Masayuki 山上雅之 58
- YAMAGUCHI Hidetoshi 山口英斉 11, 29, 30, 31
- YAMAGUCHI Takayuki 山口貴之 5, 6, 23, 184, 186
- YAMAGUCHI Mitsutaka 山口充孝 8, 13, 14, 15
- YAMAGUCHI Yoshitaka 山口由高 6, 184, 186
- YAMAGUCHI Yorito 山口頼人 65
- YAMAGUCHI Takayuki 山口貴之 3
- YAMAKA Shoichi 山家捷一 293
- YAMAKI Tsutomu 八巻務 297
- YAMAMOTO Yasuo 山本安夫 38
- YAMAMOTO Hiroshi 山本浩史 245
- YAMAMOTO Kuniyoshi 山本邦儀 300
- YAMANE Isao 山根功 150
- YAMASAWA Hideyuki 山澤秀行 112
- YAMAUCHI Hiromoto 山内啓資 289, 291
- YAMAZAKI Norio 山崎則夫 169
- YAMAZAKI Yasunori 山崎泰規 20, 21, 264
- YAMAZAKI Toshimitsu 山崎敏光 216
- YANAGISAWA Yoshiyuki 柳澤善行 x, 5, 6, 7, 151, 153,
155, 156, 157, 169,
171, 172, 230, 302
- YANG Jianjun 129
- YANO Yasushige 矢野安重 xvii, 24, 125, 184, 186,
289, 291, 293, 302
- YANO Yoshiyuki 矢野善之 229
- YASUDA Yusuke 安田裕介 12, 19
- YASUOKA Kenji 泰岡顕治 iii
- YAZAKI Koichi 矢崎紘一 84
- YOKAYAMA Akihiko 横山明彦 271
- YOKKAICHI Satoshi 四日市悟 167, 212
- YOKOUCHI Shigeru 横内茂 xvii, 112, 119, 121, 123,
289, 291, 293
- YOKOYAMA Koji 横山幸司 xx, 239, 240
- YOKOYAMA Akihiko 横山明彦 268
- YONEDA Ken-ichiro 米田健一郎 x, 4, 8, 10, 12, 13,
15, 17, 18, 19, 25,
178, 180, 182
- YONEDA Akira 米田晃 28, 194, 265
- YOSHIDA Kenichi 吉田賢市 xii, 42
- YOSHIDA Koichi 吉田光一 x, 5, 6, 7, 151, 155, 156,
159, 161, 169, 171,
222, 302
- YOSHIDA Tomohiro 吉田知紘 176
- YOSHIDA Atsushi 吉田敦 x, 5, 6, 7, 151, 153, 155,
156, 169, 230, 302
- YOSHIDA Yutaka 吉田豊 231
- YOSHIDA Shigeo 吉田茂男 287
- YOSHII Hideakira 吉井秀彬 5, 6
- YOSHII Motoyasu 芳井基也寿 233
- YOSHIMI Akihiro 吉見彰洋 5, 6, 16, 231
- YOSHIMURA Takashi 吉村崇 266, 267, 272, 274
- YOSHINAGA Kenta 吉永健太 5, 6, 10
- YOSHINAGA Naotaka 吉永尚孝 49, 50, 88
- YOSHINO Akira 吉野亮 169
- YUKIHIRA Kenichi 行平憲一 231
- ZEGERS Remco 7
- ZENIHIRO Juzo 銭廣十三 25
- ZHANG Guo-Qiang 张国强 12
- ZHENG T 10
- ZHOU Pei 周培 12

RIKEN Accelerator Progress Report vol. 43

独立行政法人理化学研究所加速器年次報告 第43巻 (2010)

印刷 平成22年(2010)9月30日
発行 平成22年(2010)9月30日

発行者 独立行政法人理化学研究所 仁科加速器研究センター

代表者 延 與 秀 人

〒351-0198 埼玉県和光市広沢2番1号
電話 (048) 462-1111

編集者 独立行政法人理化学研究所 仁科加速器研究センター
加速器年次報告編集委員会

印刷所 株式会社デジタル印刷

〒300-4405 茨城県桜川市真壁町桜井307-1
